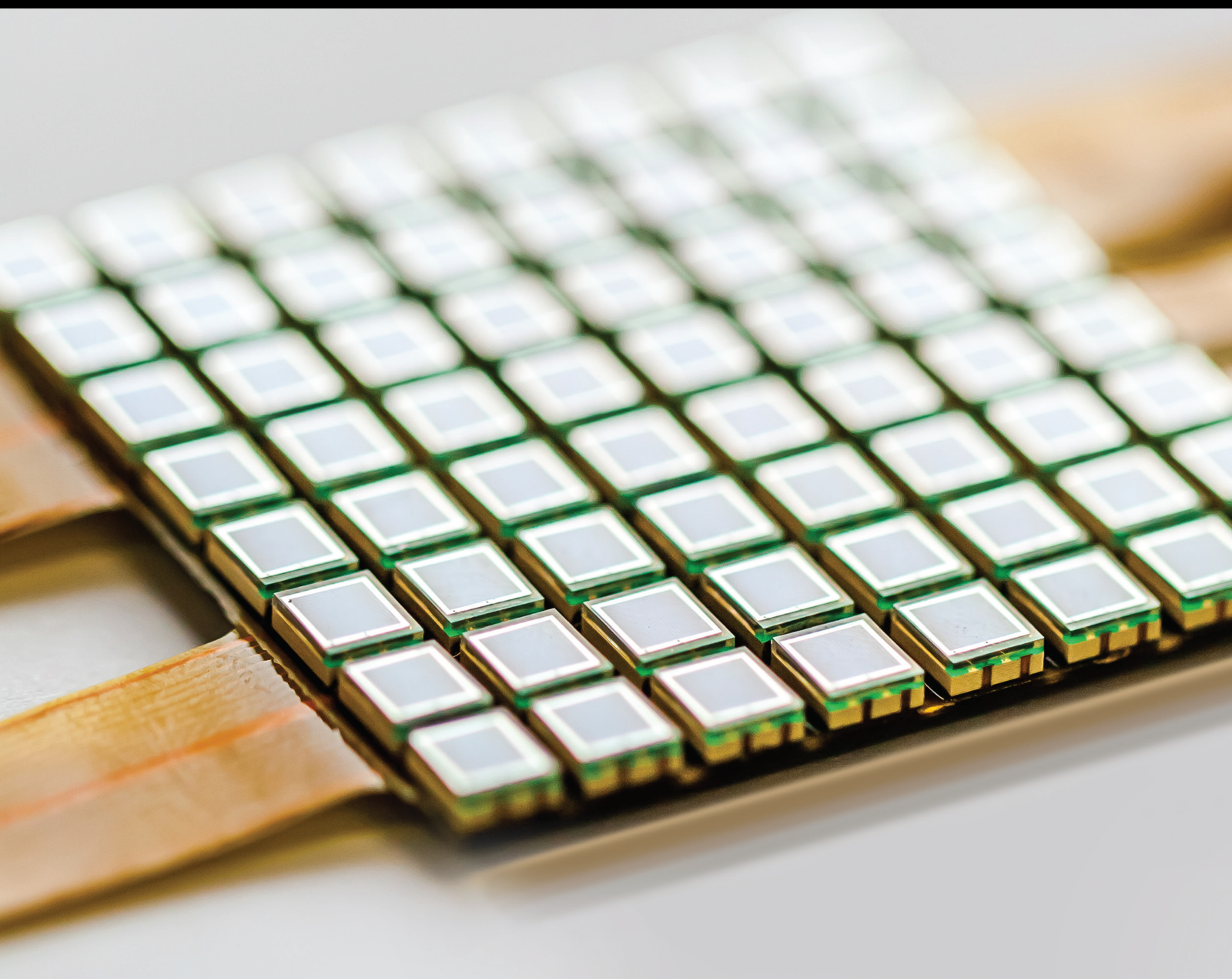# Advanced Sensor Technologies in Agricultural, Environmental, and Ecological Engineering 2021

Lead Guest Editor: Yuan Li
Guest Editors: Jingwei Wang, Liu Hongxiao, and Liang Xu

Advanced Sensor Technologies in Agricultural, Environmental, and Ecological Engineering 2021

Advanced Sensor Technologies in Agricultural, Environmental, and Ecological Engineering 2021

Lead Guest Editor: Yuan Li
Guest Editors: Jingwei Wang, Liu Hongxiao, and Liang Xu

Ehsan Namaziandost (iD), Iran
Heinz C. Neitzert (iD), Italy
Sing Kiong Nguang (iD), New Zealand
Calogero M. Oddo (iD), Italy
Tinghui Ouyang, Japan
SANDEEP KUMAR PALANISWAMY (iD), India
Alberto J. Palma (iD), Spain
Davide Palumbo (iD), Italy
Abinash Panda (iD), India
Roberto Paolesse (iD), Italy
Akhilesh Pathak (iD), Thailand
Giovanni Pau (iD), Italy
Giorgio Pennazza (iD), Italy
Michele Penza (iD), Italy
Sivakumar Poruran, India
Stelios Potirakis (iD), Greece
Biswajeet Pradhan (iD), Malaysia
Giuseppe Quero (iD), Italy
Linesh Raja (iD), India
Maheswar Rajagopal (iD), India
Valerie Renaudin (iD), France
Armando Ricciardi (iD), Italy
Christos Riziotis (iD), Greece
Ruthber Rodriguez Serrezuela (iD), Colombia
Maria Luz Rodriguez-Mendez (iD), Spain
Jerome Rossignol (iD), France
Maheswaran S, India
Ylias Sabri (iD), Australia
Sourabh Sahu (iD), India
José P. Santos (iD), Spain
Sina Sareh, United Kingdom
Isabel Sayago (iD), Spain
Andreas Schütze (iD), Germany
Praveen K. Sekhar (iD), USA
Sandra Sendra, Spain
Sandeep Sharma , India
Sunil Kumar Singh Singh (iD), India
Yadvendra Singh (iD), USA
Afaque Manzoor Soomro (iD), Pakistan
Vincenzo Spagnolo, Italy
Kathiravan Srinivasan (iD), India
Sachin K. Srivastava (iD), India
Stefano Stassi (iD), Italy

Danfeng Sun, China
Ashok Sundramoorthy, India
Salvatore Surdo (iD), Italy
Roshan Thotagamuge (iD), Sri Lanka
Guiyun Tian (iD), United Kingdom
Sri Ramulu Torati (iD), USA
Abdellah Touhafi (iD), Belgium
Hoang Vinh Tran (iD), Vietnam
Aitor Urrutia (iD), Spain
Hana Vaisocherova - Lisalova (iD), Czech Republic
Everardo Vargas-Rodriguez (iD), Mexico
Xavier Vilanova (iD), Spain
Stanislav Vítek (iD), Czech Republic
Luca Vollero (iD), Italy
Tomasz Wandowski (iD), Poland
Bohui Wang, China
Qihao Weng, USA
Penghai Wu (iD), China
Qiang Wu, United Kingdom
Yuedong Xie (iD), China
Chen Yang (iD), China
Jiachen Yang (iD), China
Nitesh Yelve (iD), India
Aijun Yin, China
Chouki Zerrouki (iD), France

Contents

Retracted: Research on Tax Collection and Administration Application and Legal Issues Based on Big Data Analysis
Journal of Sensors
Retraction (1 page), Article ID 9792671, Volume 2024 (2024)

Retracted: Data Collection and Analysis in Sports Practice Teaching Based on Internet of Things Technology
Journal of Sensors
Retraction (1 page), Article ID 9754672, Volume 2024 (2024)

Retracted: Credibility Analysis of Accounting Cloud Service Based on Complex Network
Journal of Sensors
Retraction (1 page), Article ID 9869276, Volume 2023 (2023)

Retracted: Mixture of Gaussian Processes Based on Bayesian Optimization
Journal of Sensors
Retraction (1 page), Article ID 9860286, Volume 2023 (2023)

Retracted: Research on Home Product Design and Intelligent Algorithm Recommendation considering Ergonomics
Journal of Sensors
Retraction (1 page), Article ID 9851829, Volume 2023 (2023)

Retracted: Data Analysis and Optimization of Youth Physical Fitness Training Based on Deep Learning
Journal of Sensors
Retraction (1 page), Article ID 9851520, Volume 2023 (2023)

Retracted: Variation Factors and Dynamic Modeling Analysis of Tennis Players' Competitive Ability Based on Big Data Mining Algorithm
Journal of Sensors
Retraction (1 page), Article ID 9850495, Volume 2023 (2023)

Retracted: Correlation Analysis between Tourism and Economic Growth Based on Computable General Equilibrium Model (CGE)
Journal of Sensors
Retraction (1 page), Article ID 9846046, Volume 2023 (2023)

Retracted: Effects of Different Soil Modifiers on Salt Improvement and Distribution, Crop Growth of the Gully Land Consolidation on Loess Plateau
Journal of Sensors
Retraction (1 page), Article ID 9840685, Volume 2023 (2023)

Retracted: Index Construction and Application of School-Enterprise Collaborative Education Platform Based on AHP Fuzzy Method in Double Creation Education Practice
Journal of Sensors
Retraction (1 page), Article ID 9836060, Volume 2023 (2023)

Contents

Retracted: Development of Ecological Health Tourism Products under the Background of Internet+
Journal of Sensors
Retraction (1 page), Article ID 9878429, Volume 2023 (2023)

Retracted: Research on the Communication Path of Public Opinion in University Ideological and Political Network for Big Data Analysis
Journal of Sensors
Retraction (1 page), Article ID 9845342, Volume 2023 (2023)

Retracted: The Theoretical Topology and Implementation of Enterprise Social Security in the Digital Age Based on Big Data and Artificial Intelligence
Journal of Sensors
Retraction (1 page), Article ID 9823717, Volume 2023 (2023)

Retracted: Construction and Application of Index System for Integration of Red Cultural Resources and Ideological and Political Education Based on Fuzzy Judgment Method
Journal of Sensors
Retraction (1 page), Article ID 9807396, Volume 2023 (2023)

Retracted: Analysis and Application of the Ideological and Political Evaluation System of College Students Based on Text Mining
Journal of Sensors
Retraction (1 page), Article ID 9769201, Volume 2023 (2023)

Retracted: Research on Teaching Quality Evaluation of Ideological Politics Teachers in Colleges and Universities Based on a Structural Equation Model
Journal of Sensors
Retraction (1 page), Article ID 9762501, Volume 2023 (2023)

Analysis of the Evolution of Sea Water Quality in the Spanish Coast from Satellite Images before and during a Confinement Period
Mar Parra, Lorena Parra (iD), Jose M. Jimenez, and Jaime Lloret (iD)
Research Article (20 pages), Article ID 9996626, Volume 2022 (2022)

Broadening the Research Pathways in Smart Agriculture: Predictive Analysis Using Semiautomatic Information Modeling
Komal Sharma, Chetan Sharma, Shamneesh Sharma (iD), and Evans Asenso (iD)
Research Article (19 pages), Article ID 5442865, Volume 2022 (2022)

[Retracted] Analysis and Application of Crosscultural Knowledge System Structure in English Teaching Based on Hierarchical Correlation Analysis
Zhu Jianhong (iD)
Research Article (11 pages), Article ID 3874857, Volume 2022 (2022)

Contents

Contents

Contents

Retraction

Retracted: Evaluation and Analysis of Assisted Instruction and Ability Improvement Based on Artificial Intelligence

Journal of Sensors

This article has been retracted by Hindawi following an investigation undertaken by the publisher [1]. This investigation has uncovered evidence of one or more of the following indicators of systematic manipulation of the publication process:

(1) Discrepancies in scope

(2) Discrepancies in the description of the research reported

(3) Discrepancies between the availability of data and the research described

(4) Inappropriate citations

(5) Incoherent, meaningless and/or irrelevant content included in the article

(6) Manipulated or compromised peer review

The presence of these indicators undermines our confidence in the integrity of the article's content and we cannot, therefore, vouch for its reliability. Please note that this notice is intended solely to alert readers that the content of this article is unreliable. We have not investigated whether authors were aware of or involved in the systematic manipulation of the publication process.

In addition, our investigation has also shown that one or more of the following human-subject reporting requirements has not been met in this article: ethical approval by an Institutional Review Board (IRB) committee or equivalent, patient/participant consent to participate, and/or agreement to publish patient/participant details (where relevant).

Wiley and Hindawi regrets that the usual quality checks did not identify these issues before publication and have since put additional measures in place to safeguard research integrity.

We wish to credit our own Research Integrity and Research Publishing teams and anonymous and named external researchers and research integrity experts for contributing to this investigation.

The corresponding author, as the representative of all authors, has been given the opportunity to register their agreement or disagreement to this retraction. We have kept a record of any response received.

References

[1] Z. Li, Z. Guang, and W. Sun, "Evaluation and Analysis of Assisted Instruction and Ability Improvement Based on Artificial Intelligence," *Journal of Sensors*, vol. 2022, Article ID 9979275, 13 pages, 2022.

Retraction

Retracted: Efficient Management and Application of Human Resources Based on Genetic Ant Colony Algorithm

Journal of Sensors

This article has been retracted by Hindawi following an investigation undertaken by the publisher [1]. This investigation has uncovered evidence of one or more of the following indicators of systematic manipulation of the publication process:

(1) Discrepancies in scope

(2) Discrepancies in the description of the research reported

(3) Discrepancies between the availability of data and the research described

(4) Inappropriate citations

(5) Incoherent, meaningless and/or irrelevant content included in the article

(6) Manipulated or compromised peer review

The presence of these indicators undermines our confidence in the integrity of the article's content and we cannot, therefore, vouch for its reliability. Please note that this notice is intended solely to alert readers that the content of this article is unreliable. We have not investigated whether authors were aware of or involved in the systematic manipulation of the publication process.

Wiley and Hindawi regrets that the usual quality checks did not identify these issues before publication and have since put additional measures in place to safeguard research integrity.

We wish to credit our own Research Integrity and Research Publishing teams and anonymous and named external researchers and research integrity experts for contributing to this investigation.

The corresponding author, as the representative of all authors, has been given the opportunity to register their agreement or disagreement to this retraction. We have kept a record of any response received.

References

[1] C. Cheng, Y. Xu, and G. Daniels, "Efficient Management and Application of Human Resources Based on Genetic Ant Colony Algorithm," *Journal of Sensors*, vol. 2022, Article ID 9903319, 13 pages, 2022.

Hindawi

Retraction

Retracted: Research and Analysis of Combination Forecasting Model in Sports Competition

Journal of Sensors

This article has been retracted by Hindawi following an investigation undertaken by the publisher [1]. This investigation has uncovered evidence of one or more of the following indicators of systematic manipulation of the publication process:

(1) Discrepancies in scope
(2) Discrepancies in the description of the research reported
(3) Discrepancies between the availability of data and the research described
(4) Inappropriate citations
(5) Incoherent, meaningless and/or irrelevant content included in the article
(6) Manipulated or compromised peer review

The presence of these indicators undermines our confidence in the integrity of the article's content and we cannot, therefore, vouch for its reliability. Please note that this notice is intended solely to alert readers that the content of this article is unreliable. We have not investigated whether authors were aware of or involved in the systematic manipulation of the publication process.

In addition, our investigation has also shown that one or more of the following human-subject reporting requirements has not been met in this article: ethical approval by an Institutional Review Board (IRB) committee or equivalent, patient/participant consent to participate, and/or agreement to publish patient/participant details (where relevant).

Wiley and Hindawi regrets that the usual quality checks did not identify these issues before publication and have since put additional measures in place to safeguard research integrity.

We wish to credit our own Research Integrity and Research Publishing teams and anonymous and named external researchers and research integrity experts for contributing to this investigation.

The corresponding author, as the representative of all authors, has been given the opportunity to register their agreement or disagreement to this retraction. We have kept a record of any response received.

References

[1] Z. Miao and Y. Hu, "Research and Analysis of Combination Forecasting Model in Sports Competition," *Journal of Sensors*, vol. 2022, Article ID 5945599, 10 pages, 2022.

Retraction

Retracted: Empirical Study on the Grain Output Based on Regression Analysis

Journal of Sensors

This article has been retracted by Hindawi following an investigation undertaken by the publisher [1]. This investigation has uncovered evidence of one or more of the following indicators of systematic manipulation of the publication process:

(1) Discrepancies in scope

(2) Discrepancies in the description of the research reported

(3) Discrepancies between the availability of data and the research described

(4) Inappropriate citations

(5) Incoherent, meaningless and/or irrelevant content included in the article

(6) Manipulated or compromised peer review

The presence of these indicators undermines our confidence in the integrity of the article's content and we cannot, therefore, vouch for its reliability. Please note that this notice is intended solely to alert readers that the content of this article is unreliable. We have not investigated whether authors were aware of or involved in the systematic manipulation of the publication process.

Wiley and Hindawi regrets that the usual quality checks did not identify these issues before publication and have since put additional measures in place to safeguard research integrity.

We wish to credit our own Research Integrity and Research Publishing teams and anonymous and named external researchers and research integrity experts for contributing to this investigation.

The corresponding author, as the representative of all authors, has been given the opportunity to register their agreement or disagreement to this retraction. We have kept a record of any response received.

References

[1] J. Xu, S. Tang, P. Li, and H. Zhang, "Empirical Study on the Grain Output Based on Regression Analysis," *Journal of Sensors*, vol. 2022, Article ID 2567790, 10 pages, 2022.

Retraction

Retracted: Research on Sustainable Development of Olympic Games Based on Ecological Carrying Capacity Analysis

Journal of Sensors

This article has been retracted by Hindawi following an investigation undertaken by the publisher [1]. This investigation has uncovered evidence of one or more of the following indicators of systematic manipulation of the publication process:

(1) Discrepancies in scope

(2) Discrepancies in the description of the research reported

(3) Discrepancies between the availability of data and the research described

(4) Inappropriate citations

(5) Incoherent, meaningless and/or irrelevant content included in the article

(6) Manipulated or compromised peer review

The presence of these indicators undermines our confidence in the integrity of the article's content and we cannot, therefore, vouch for its reliability. Please note that this notice is intended solely to alert readers that the content of this article is unreliable. We have not investigated whether authors were aware of or involved in the systematic manipulation of the publication process.

Wiley and Hindawi regrets that the usual quality checks did not identify these issues before publication and have since put additional measures in place to safeguard research integrity.

We wish to credit our own Research Integrity and Research Publishing teams and anonymous and named external researchers and research integrity experts for contributing to this investigation.

The corresponding author, as the representative of all authors, has been given the opportunity to register their agreement or disagreement to this retraction. We have kept a record of any response received.

References

[1] B. Zhang and Y. Liu, "Research on Sustainable Development of Olympic Games Based on Ecological Carrying Capacity Analysis," *Journal of Sensors*, vol. 2022, Article ID 4907366, 13 pages, 2022.

Hindawi

Retraction

Retracted: The Influence of Multisensor Fusion Machine Learning on the Controllable Fabrication of MOF (UIO-66)/ZrAl Ceramic Composite Membranes

Journal of Sensors

This article has been retracted by Hindawi following an investigation undertaken by the publisher [1]. This investigation has uncovered evidence of one or more of the following indicators of systematic manipulation of the publication process:

(1) Discrepancies in scope

(2) Discrepancies in the description of the research reported

(3) Discrepancies between the availability of data and the research described

(4) Inappropriate citations

(5) Incoherent, meaningless and/or irrelevant content included in the article

(6) Manipulated or compromised peer review

The presence of these indicators undermines our confidence in the integrity of the article's content and we cannot, therefore, vouch for its reliability. Please note that this notice is intended solely to alert readers that the content of this article is unreliable. We have not investigated whether authors were aware of or involved in the systematic manipulation of the publication process.

Wiley and Hindawi regrets that the usual quality checks did not identify these issues before publication and have since put additional measures in place to safeguard research integrity.

We wish to credit our own Research Integrity and Research Publishing teams and anonymous and named external researchers and research integrity experts for contributing to this investigation.

The corresponding author, as the representative of all authors, has been given the opportunity to register their agreement or disagreement to this retraction. We have kept a record of any response received.

References

[1] X. Xu, X. Yang, S. Shao, C. Zhu, and X. Xu, "The Influence of Multisensor Fusion Machine Learning on the Controllable Fabrication of MOF (UIO-66)/ZrAl Ceramic Composite Membranes," *Journal of Sensors*, vol. 2022, Article ID 3039064, 9 pages, 2022.

Hindawi

Retraction

Retracted: Analysis and Evaluation Research on the Construction of the Music Art Management Curriculum System Based on the Deep Learning Model

Journal of Sensors

This article has been retracted by Hindawi following an investigation undertaken by the publisher [1]. This investigation has uncovered evidence of one or more of the following indicators of systematic manipulation of the publication process:

(1) Discrepancies in scope

(2) Discrepancies in the description of the research reported

(3) Discrepancies between the availability of data and the research described

(4) Inappropriate citations

(5) Incoherent, meaningless and/or irrelevant content included in the article

(6) Manipulated or compromised peer review

The presence of these indicators undermines our confidence in the integrity of the article's content and we cannot, therefore, vouch for its reliability. Please note that this notice is intended solely to alert readers that the content of this article is unreliable. We have not investigated whether authors were aware of or involved in the systematic manipulation of the publication process.

In addition, our investigation has also shown that one or more of the following human-subject reporting requirements has not been met in this article: ethical approval by an Institutional Review Board (IRB) committee or equivalent, patient/participant consent to participate, and/or agreement to publish patient/participant details (where relevant).

Wiley and Hindawi regrets that the usual quality checks did not identify these issues before publication and have since put additional measures in place to safeguard research integrity.

We wish to credit our own Research Integrity and Research Publishing teams and anonymous and named external researchers and research integrity experts for contributing to this investigation.

The corresponding author, as the representative of all authors, has been given the opportunity to register their agreement or disagreement to this retraction. We have kept a record of any response received.

References

[1] S. Hu and L. Yang, "Analysis and Evaluation Research on the Construction of the Music Art Management Curriculum System Based on the Deep Learning Model," *Journal of Sensors*, vol. 2022, Article ID 5873218, 9 pages, 2022.

Hindawi

Retraction

Retracted: Application of Correlation Filter Tracking Algorithm Based on Multiple Color Features in Basketball Motion Capture System

Journal of Sensors

This article has been retracted by Hindawi following an investigation undertaken by the publisher [1]. This investigation has uncovered evidence of one or more of the following indicators of systematic manipulation of the publication process:

(1) Discrepancies in scope

(2) Discrepancies in the description of the research reported

(3) Discrepancies between the availability of data and the research described

(4) Inappropriate citations

(5) Incoherent, meaningless and/or irrelevant content included in the article

(6) Manipulated or compromised peer review

The presence of these indicators undermines our confidence in the integrity of the article's content and we cannot, therefore, vouch for its reliability. Please note that this notice is intended solely to alert readers that the content of this article is unreliable. We have not investigated whether authors were aware of or involved in the systematic manipulation of the publication process.

Wiley and Hindawi regrets that the usual quality checks did not identify these issues before publication and have since put additional measures in place to safeguard research integrity.

We wish to credit our own Research Integrity and Research Publishing teams and anonymous and named external researchers and research integrity experts for contributing to this investigation.

The corresponding author, as the representative of all authors, has been given the opportunity to register their agreement or disagreement to this retraction. We have kept a record of any response received.

References

[1] B. Li and H. Quan, "Application of Correlation Filter Tracking Algorithm Based on Multiple Color Features in Basketball Motion Capture System," *Journal of Sensors*, vol. 2022, Article ID 3190206, 10 pages, 2022.

Hindawi

Retraction

Retracted: Prediction and Analysis of College Sports Test Scores Based on Computational Intelligence

Journal of Sensors

This article has been retracted by Hindawi following an investigation undertaken by the publisher [1]. This investigation has uncovered evidence of one or more of the following indicators of systematic manipulation of the publication process:

(1) Discrepancies in scope

(2) Discrepancies in the description of the research reported

(3) Discrepancies between the availability of data and the research described

(4) Inappropriate citations

(5) Incoherent, meaningless and/or irrelevant content included in the article

(6) Manipulated or compromised peer review

The presence of these indicators undermines our confidence in the integrity of the article's content and we cannot, therefore, vouch for its reliability. Please note that this notice is intended solely to alert readers that the content of this article is unreliable. We have not investigated whether authors were aware of or involved in the systematic manipulation of the publication process.

In addition, our investigation has also shown that one or more of the following human-subject reporting requirements has not been met in this article: ethical approval by an Institutional Review Board (IRB) committee or equivalent, patient/participant consent to participate, and/or agreement to publish patient/participant details (where relevant).

Wiley and Hindawi regrets that the usual quality checks did not identify these issues before publication and have since put additional measures in place to safeguard research integrity.

We wish to credit our own Research Integrity and Research Publishing teams and anonymous and named external researchers and research integrity experts for contributing to this investigation.

The corresponding author, as the representative of all authors, has been given the opportunity to register their agreement or disagreement to this retraction. We have kept a record of any response received.

References

[1] P. Cui, "Prediction and Analysis of College Sports Test Scores Based on Computational Intelligence," *Journal of Sensors*, vol. 2022, Article ID 4070030, 10 pages, 2022.

Retraction

Retracted: Construction and Index Analysis of Whole Chain Linkage Talent Training System Based on Fuzzy AHP Model

Journal of Sensors

This article has been retracted by Hindawi following an investigation undertaken by the publisher [1]. This investigation has uncovered evidence of one or more of the following indicators of systematic manipulation of the publication process:

(1) Discrepancies in scope

(2) Discrepancies in the description of the research reported

(3) Discrepancies between the availability of data and the research described

(4) Inappropriate citations

(5) Incoherent, meaningless and/or irrelevant content included in the article

(6) Manipulated or compromised peer review

The presence of these indicators undermines our confidence in the integrity of the article's content and we cannot, therefore, vouch for its reliability. Please note that this notice is intended solely to alert readers that the content of this article is unreliable. We have not investigated whether authors were aware of or involved in the systematic manipulation of the publication process.

In addition, our investigation has also shown that one or more of the following human-subject reporting requirements has not been met in this article: ethical approval by an Institutional Review Board (IRB) committee or equivalent, patient/participant consent to participate, and/or agreement to publish patient/participant details (where relevant).

Wiley and Hindawi regrets that the usual quality checks did not identify these issues before publication and have since put additional measures in place to safeguard research integrity.

We wish to credit our own Research Integrity and Research Publishing teams and anonymous and named external researchers and research integrity experts for contributing to this investigation.

The corresponding author, as the representative of all authors, has been given the opportunity to register their agreement or disagreement to this retraction. We have kept a record of any response received.

References

[1] L. Yi and S. Yan, "Construction and Index Analysis of Whole Chain Linkage Talent Training System Based on Fuzzy AHP Model," *Journal of Sensors*, vol. 2022, Article ID 7106274, 12 pages, 2022.

Hindawi

Retraction

Retracted: Research on Tax Collection and Administration Application and Legal Issues Based on Big Data Analysis

Journal of Sensors

This article has been retracted by Hindawi following an investigation undertaken by the publisher [1]. This investigation has uncovered evidence of one or more of the following indicators of systematic manipulation of the publication process:

(1) Discrepancies in scope

(2) Discrepancies in the description of the research reported

(3) Discrepancies between the availability of data and the research described

(4) Inappropriate citations

(5) Incoherent, meaningless and/or irrelevant content included in the article

(6) Manipulated or compromised peer review

The presence of these indicators undermines our confidence in the integrity of the article's content and we cannot, therefore, vouch for its reliability. Please note that this notice is intended solely to alert readers that the content of this article is unreliable. We have not investigated whether authors were aware of or involved in the systematic manipulation of the publication process.

In addition, our investigation has also shown that one or more of the following human-subject reporting requirements has not been met in this article: ethical approval by an Institutional Review Board (IRB) committee or equivalent, patient/participant consent to participate, and/or agreement to publish patient/participant details (where relevant).

Wiley and Hindawi regrets that the usual quality checks did not identify these issues before publication and have since put additional measures in place to safeguard research integrity.

We wish to credit our own Research Integrity and Research Publishing teams and anonymous and named external researchers and research integrity experts for contributing to this investigation.

The corresponding author, as the representative of all authors, has been given the opportunity to register their agreement or disagreement to this retraction. We have kept a record of any response received.

References

[1] C. Liuhong, "Research on Tax Collection and Administration Application and Legal Issues Based on Big Data Analysis," *Journal of Sensors*, vol. 2022, Article ID 6578964, 11 pages, 2022.

Retraction

Retracted: Data Collection and Analysis in Sports Practice Teaching Based on Internet of Things Technology

Journal of Sensors

This article has been retracted by Hindawi following an investigation undertaken by the publisher [1]. This investigation has uncovered evidence of one or more of the following indicators of systematic manipulation of the publication process:

(1) Discrepancies in scope

(2) Discrepancies in the description of the research reported

(3) Discrepancies between the availability of data and the research described

(4) Inappropriate citations

(5) Incoherent, meaningless and/or irrelevant content included in the article

(6) Manipulated or compromised peer review

The presence of these indicators undermines our confidence in the integrity of the article's content and we cannot, therefore, vouch for its reliability. Please note that this notice is intended solely to alert readers that the content of this article is unreliable. We have not investigated whether authors were aware of or involved in the systematic manipulation of the publication process.

Wiley and Hindawi regrets that the usual quality checks did not identify these issues before publication and have since put additional measures in place to safeguard research integrity.

We wish to credit our own Research Integrity and Research Publishing teams and anonymous and named external researchers and research integrity experts for contributing to this investigation.

The corresponding author, as the representative of all authors, has been given the opportunity to register their agreement or disagreement to this retraction. We have kept a record of any response received.

References

[1] L. Yang, "Data Collection and Analysis in Sports Practice Teaching Based on Internet of Things Technology," *Journal of Sensors*, vol. 2022, Article ID 2741517, 10 pages, 2022.

Hindawi

Retraction

Retracted: Credibility Analysis of Accounting Cloud Service Based on Complex Network

Journal of Sensors

This article has been retracted by Hindawi following an investigation undertaken by the publisher [1]. This investigation has uncovered evidence of one or more of the following indicators of systematic manipulation of the publication process:

(1) Discrepancies in scope

(2) Discrepancies in the description of the research reported

(3) Discrepancies between the availability of data and the research described

(4) Inappropriate citations

(5) Incoherent, meaningless and/or irrelevant content included in the article

(6) Manipulated or compromised peer review

The presence of these indicators undermines our confidence in the integrity of the article's content and we cannot, therefore, vouch for its reliability. Please note that this notice is intended solely to alert readers that the content of this article is unreliable. We have not investigated whether authors were aware of or involved in the systematic manipulation of the publication process.

Wiley and Hindawi regrets that the usual quality checks did not identify these issues before publication and have since put additional measures in place to safeguard research integrity.

We wish to credit our own Research Integrity and Research Publishing teams and anonymous and named external researchers and research integrity experts for contributing to this investigation.

The corresponding author, as the representative of all authors, has been given the opportunity to register their agreement or disagreement to this retraction. We have kept a record of any response received.

References

[1] X. Chen, C. Guang, and D. Hua, "Credibility Analysis of Accounting Cloud Service Based on Complex Network," *Journal of Sensors*, vol. 2022, Article ID 5420772, 11 pages, 2022.

Hindawi

Retraction

Retracted: Mixture of Gaussian Processes Based on Bayesian Optimization

Journal of Sensors

This article has been retracted by Hindawi following an investigation undertaken by the publisher [1]. This investigation has uncovered evidence of one or more of the following indicators of systematic manipulation of the publication process:

(1) Discrepancies in scope

(2) Discrepancies in the description of the research reported

(3) Discrepancies between the availability of data and the research described

(4) Inappropriate citations

(5) Incoherent, meaningless and/or irrelevant content included in the article

(6) Manipulated or compromised peer review

The presence of these indicators undermines our confidence in the integrity of the article's content and we cannot, therefore, vouch for its reliability. Please note that this notice is intended solely to alert readers that the content of this article is unreliable. We have not investigated whether authors were aware of or involved in the systematic manipulation of the publication process.

Wiley and Hindawi regrets that the usual quality checks did not identify these issues before publication and have since put additional measures in place to safeguard research integrity.

We wish to credit our own Research Integrity and Research Publishing teams and anonymous and named external researchers and research integrity experts for contributing to this investigation.

The corresponding author, as the representative of all authors, has been given the opportunity to register their agreement or disagreement to this retraction. We have kept a record of any response received.

References

[1] R. Mao, C. Cao, J. J. Y. Qian, J. Wang, and Y. Liu, "Mixture of Gaussian Processes Based on Bayesian Optimization," *Journal of Sensors*, vol. 2022, Article ID 7646554, 10 pages, 2022.

Hindawi

Retraction

Retracted: Research on Home Product Design and Intelligent Algorithm Recommendation considering Ergonomics

Journal of Sensors

This article has been retracted by Hindawi following an investigation undertaken by the publisher [1]. This investigation has uncovered evidence of one or more of the following indicators of systematic manipulation of the publication process:

(1) Discrepancies in scope

(2) Discrepancies in the description of the research reported

(3) Discrepancies between the availability of data and the research described

(4) Inappropriate citations

(5) Incoherent, meaningless and/or irrelevant content included in the article

(6) Manipulated or compromised peer review

The presence of these indicators undermines our confidence in the integrity of the article's content and we cannot, therefore, vouch for its reliability. Please note that this notice is intended solely to alert readers that the content of this article is unreliable. We have not investigated whether authors were aware of or involved in the systematic manipulation of the publication process.

Wiley and Hindawi regrets that the usual quality checks did not identify these issues before publication and have since put additional measures in place to safeguard research integrity.

We wish to credit our own Research Integrity and Research Publishing teams and anonymous and named external researchers and research integrity experts for contributing to this investigation.

The corresponding author, as the representative of all authors, has been given the opportunity to register their agreement or disagreement to this retraction. We have kept a record of any response received.

References

[1] X. Wang, "Research on Home Product Design and Intelligent Algorithm Recommendation considering Ergonomics," *Journal of Sensors*, vol. 2022, Article ID 1791269, 10 pages, 2022.

Retraction

Retracted: Data Analysis and Optimization of Youth Physical Fitness Training Based on Deep Learning

Journal of Sensors

This article has been retracted by Hindawi following an investigation undertaken by the publisher [1]. This investigation has uncovered evidence of one or more of the following indicators of systematic manipulation of the publication process:

(1) Discrepancies in scope

(2) Discrepancies in the description of the research reported

(3) Discrepancies between the availability of data and the research described

(4) Inappropriate citations

(5) Incoherent, meaningless and/or irrelevant content included in the article

(6) Manipulated or compromised peer review

The presence of these indicators undermines our confidence in the integrity of the article's content and we cannot, therefore, vouch for its reliability. Please note that this notice is intended solely to alert readers that the content of this article is unreliable. We have not investigated whether authors were aware of or involved in the systematic manipulation of the publication process.

In addition, our investigation has also shown that one or more of the following human-subject reporting requirements has not been met in this article: ethical approval by an Institutional Review Board (IRB) committee or equivalent, patient/participant consent to participate, and/or agreement to publish patient/participant details (where relevant).

Wiley and Hindawi regrets that the usual quality checks did not identify these issues before publication and have since put additional measures in place to safeguard research integrity.

We wish to credit our own Research Integrity and Research Publishing teams and anonymous and named external researchers and research integrity experts for contributing to this investigation.

The corresponding author, as the representative of all authors, has been given the opportunity to register their agreement or disagreement to this retraction. We have kept a record of any response received.

References

[1] J. Pan, "Data Analysis and Optimization of Youth Physical Fitness Training Based on Deep Learning," *Journal of Sensors*, vol. 2022, Article ID 6778882, 9 pages, 2022.

Retraction

Retracted: Variation Factors and Dynamic Modeling Analysis of Tennis Players' Competitive Ability Based on Big Data Mining Algorithm

Journal of Sensors

This article has been retracted by Hindawi following an investigation undertaken by the publisher [1]. This investigation has uncovered evidence of one or more of the following indicators of systematic manipulation of the publication process:

(1) Discrepancies in scope

(2) Discrepancies in the description of the research reported

(3) Discrepancies between the availability of data and the research described

(4) Inappropriate citations

(5) Incoherent, meaningless and/or irrelevant content included in the article

(6) Manipulated or compromised peer review

The presence of these indicators undermines our confidence in the integrity of the article's content and we cannot, therefore, vouch for its reliability. Please note that this notice is intended solely to alert readers that the content of this article is unreliable. We have not investigated whether authors were aware of or involved in the systematic manipulation of the publication process.

Wiley and Hindawi regrets that the usual quality checks did not identify these issues before publication and have since put additional measures in place to safeguard research integrity.

We wish to credit our own Research Integrity and Research Publishing teams and anonymous and named external researchers and research integrity experts for contributing to this investigation.

The corresponding author, as the representative of all authors, has been given the opportunity to register their agreement or disagreement to this retraction. We have kept a record of any response received.

References

[1] Y. Xie, B. Bai, and Y. Zhao, "Variation Factors and Dynamic Modeling Analysis of Tennis Players' Competitive Ability Based on Big Data Mining Algorithm," *Journal of Sensors*, vol. 2022, Article ID 3880527, 8 pages, 2022.

Retraction

Retracted: Correlation Analysis between Tourism and Economic Growth Based on Computable General Equilibrium Model (CGE)

Journal of Sensors

This article has been retracted by Hindawi following an investigation undertaken by the publisher [1]. This investigation has uncovered evidence of one or more of the following indicators of systematic manipulation of the publication process:

(1) Discrepancies in scope

(2) Discrepancies in the description of the research reported

(3) Discrepancies between the availability of data and the research described

(4) Inappropriate citations

(5) Incoherent, meaningless and/or irrelevant content included in the article

(6) Manipulated or compromised peer review

The presence of these indicators undermines our confidence in the integrity of the article's content and we cannot, therefore, vouch for its reliability. Please note that this notice is intended solely to alert readers that the content of this article is unreliable. We have not investigated whether authors were aware of or involved in the systematic manipulation of the publication process.

Wiley and Hindawi regrets that the usual quality checks did not identify these issues before publication and have since put additional measures in place to safeguard research integrity.

We wish to credit our own Research Integrity and Research Publishing teams and anonymous and named external researchers and research integrity experts for contributing to this investigation.

The corresponding author, as the representative of all authors, has been given the opportunity to register their agreement or disagreement to this retraction. We have kept a record of any response received.

References

[1] S. Wang, "Correlation Analysis between Tourism and Economic Growth Based on Computable General Equilibrium Model (CGE)," *Journal of Sensors*, vol. 2022, Article ID 6497125, 8 pages, 2022.

Hindawi

Retraction

Retracted: Effects of Different Soil Modifiers on Salt Improvement and Distribution, Crop Growth of the Gully Land Consolidation on Loess Plateau

Journal of Sensors

This article has been retracted by Hindawi following an investigation undertaken by the publisher [1]. This investigation has uncovered evidence of one or more of the following indicators of systematic manipulation of the publication process:

(1) Discrepancies in scope

(2) Discrepancies in the description of the research reported

(3) Discrepancies between the availability of data and the research described

(4) Inappropriate citations

(5) Incoherent, meaningless and/or irrelevant content included in the article

(6) Manipulated or compromised peer review

The presence of these indicators undermines our confidence in the integrity of the article's content and we cannot, therefore, vouch for its reliability. Please note that this notice is intended solely to alert readers that the content of this article is unreliable. We have not investigated whether authors were aware of or involved in the systematic manipulation of the publication process.

Wiley and Hindawi regrets that the usual quality checks did not identify these issues before publication and have since put additional measures in place to safeguard research integrity.

We wish to credit our own Research Integrity and Research Publishing teams and anonymous and named external researchers and research integrity experts for contributing to this investigation.

The corresponding author, as the representative of all authors, has been given the opportunity to register their agreement or disagreement to this retraction. We have kept a record of any response received.

References

[1] Y. Yang, B. Zhou, and L. Feng, "Effects of Different Soil Modifiers on Salt Improvement and Distribution, Crop Growth of the Gully Land Consolidation on Loess Plateau," *Journal of Sensors*, vol. 2022, Article ID 5282344, 17 pages, 2022.

Hindawi

Retraction

Retracted: Index Construction and Application of School-Enterprise Collaborative Education Platform Based on AHP Fuzzy Method in Double Creation Education Practice

Journal of Sensors

This article has been retracted by Hindawi following an investigation undertaken by the publisher [1]. This investigation has uncovered evidence of one or more of the following indicators of systematic manipulation of the publication process:

(1) Discrepancies in scope

(2) Discrepancies in the description of the research reported

(3) Discrepancies between the availability of data and the research described

(4) Inappropriate citations

(5) Incoherent, meaningless and/or irrelevant content included in the article

(6) Manipulated or compromised peer review

The presence of these indicators undermines our confidence in the integrity of the article's content and we cannot, therefore, vouch for its reliability. Please note that this notice is intended solely to alert readers that the content of this article is unreliable. We have not investigated whether authors were aware of or involved in the systematic manipulation of the publication process.

Wiley and Hindawi regrets that the usual quality checks did not identify these issues before publication and have since put additional measures in place to safeguard research integrity.

We wish to credit our own Research Integrity and Research Publishing teams and anonymous and named external researchers and research integrity experts for contributing to this investigation.

The corresponding author, as the representative of all authors, has been given the opportunity to register their agreement or disagreement to this retraction. We have kept a record of any response received.

References

[1] Z. He and X. Sun, "Index Construction and Application of School-Enterprise Collaborative Education Platform Based on AHP Fuzzy Method in Double Creation Education Practice," *Journal of Sensors*, vol. 2022, Article ID 7707384, 15 pages, 2022.

Retraction

Retracted: Design of Active Display Stand Combing the Pressure Sensor and Kinematics Algorithm

Journal of Sensors

This article has been retracted by Hindawi following an investigation undertaken by the publisher [1]. This investigation has uncovered evidence of one or more of the following indicators of systematic manipulation of the publication process:

(1) Discrepancies in scope

(2) Discrepancies in the description of the research reported

(3) Discrepancies between the availability of data and the research described

(4) Inappropriate citations

(5) Incoherent, meaningless and/or irrelevant content included in the article

(6) Manipulated or compromised peer review

The presence of these indicators undermines our confidence in the integrity of the article's content and we cannot, therefore, vouch for its reliability. Please note that this notice is intended solely to alert readers that the content of this article is unreliable. We have not investigated whether authors were aware of or involved in the systematic manipulation of the publication process.

Wiley and Hindawi regrets that the usual quality checks did not identify these issues before publication and have since put additional measures in place to safeguard research integrity.

We wish to credit our own Research Integrity and Research Publishing teams and anonymous and named external researchers and research integrity experts for contributing to this investigation.

The corresponding author, as the representative of all authors, has been given the opportunity to register their agreement or disagreement to this retraction. We have kept a record of any response received.

References

[1] M. Ma and L. Yong, "Design of Active Display Stand Combing the Pressure Sensor and Kinematics Algorithm," *Journal of Sensors*, vol. 2022, Article ID 9275062, 8 pages, 2022.

Hindawi

Retraction

Retracted: Scene Classification Using Deep Networks Combined with Visual Attention

Journal of Sensors

This article has been retracted by Hindawi following an investigation undertaken by the publisher [1]. This investigation has uncovered evidence of one or more of the following indicators of systematic manipulation of the publication process:

(1) Discrepancies in scope

(2) Discrepancies in the description of the research reported

(3) Discrepancies between the availability of data and the research described

(4) Inappropriate citations

(5) Incoherent, meaningless and/or irrelevant content included in the article

(6) Manipulated or compromised peer review

The presence of these indicators undermines our confidence in the integrity of the article's content and we cannot, therefore, vouch for its reliability. Please note that this notice is intended solely to alert readers that the content of this article is unreliable. We have not investigated whether authors were aware of or involved in the systematic manipulation of the publication process.

Wiley and Hindawi regrets that the usual quality checks did not identify these issues before publication and have since put additional measures in place to safeguard research integrity.

We wish to credit our own Research Integrity and Research Publishing teams and anonymous and named external researchers and research integrity experts for contributing to this investigation.

The corresponding author, as the representative of all authors, has been given the opportunity to register their agreement or disagreement to this retraction. We have kept a record of any response received.

References

[1] J. Shi, H. Zhu, Y. Li, Y. Li, and S. Du, "Scene Classification Using Deep Networks Combined with Visual Attention," *Journal of Sensors*, vol. 2022, Article ID 7191537, 9 pages, 2022.

Hindawi

Retraction

Retracted: Stress Analysis of Concrete Materials Based on Finite Element Analysis

Journal of Sensors

This article has been retracted by Hindawi following an investigation undertaken by the publisher [1]. This investigation has uncovered evidence of one or more of the following indicators of systematic manipulation of the publication process:

(1) Discrepancies in scope

(2) Discrepancies in the description of the research reported

(3) Discrepancies between the availability of data and the research described

(4) Inappropriate citations

(5) Incoherent, meaningless and/or irrelevant content included in the article

(6) Manipulated or compromised peer review

The presence of these indicators undermines our confidence in the integrity of the article's content and we cannot, therefore, vouch for its reliability. Please note that this notice is intended solely to alert readers that the content of this article is unreliable. We have not investigated whether authors were aware of or involved in the systematic manipulation of the publication process.

Wiley and Hindawi regrets that the usual quality checks did not identify these issues before publication and have since put additional measures in place to safeguard research integrity.

We wish to credit our own Research Integrity and Research Publishing teams and anonymous and named external researchers and research integrity experts for contributing to this investigation.

The corresponding author, as the representative of all authors, has been given the opportunity to register their agreement or disagreement to this retraction. We have kept a record of any response received.

References

[1] R. Yang and S. Yuan, "Stress Analysis of Concrete Materials Based on Finite Element Analysis," *Journal of Sensors*, vol. 2022, Article ID 1826598, 11 pages, 2022.

Retraction

Retracted: Evaluation Method of English Talent Training Quality Based on Deep Learning Model

Journal of Sensors

This article has been retracted by Hindawi following an investigation undertaken by the publisher [1]. This investigation has uncovered evidence of one or more of the following indicators of systematic manipulation of the publication process:

(1) Discrepancies in scope

(2) Discrepancies in the description of the research reported

(3) Discrepancies between the availability of data and the research described

(4) Inappropriate citations

(5) Incoherent, meaningless and/or irrelevant content included in the article

(6) Manipulated or compromised peer review

The presence of these indicators undermines our confidence in the integrity of the article's content and we cannot, therefore, vouch for its reliability. Please note that this notice is intended solely to alert readers that the content of this article is unreliable. We have not investigated whether authors were aware of or involved in the systematic manipulation of the publication process.

Wiley and Hindawi regrets that the usual quality checks did not identify these issues before publication and have since put additional measures in place to safeguard research integrity.

We wish to credit our own Research Integrity and Research Publishing teams and anonymous and named external researchers and research integrity experts for contributing to this investigation.

The corresponding author, as the representative of all authors, has been given the opportunity to register their agreement or disagreement to this retraction. We have kept a record of any response received.

References

[1] Q. Fu, "Evaluation Method of English Talent Training Quality Based on Deep Learning Model," *Journal of Sensors*, vol. 2022, Article ID 6726931, 9 pages, 2022.

Retraction

Retracted: Development and Performance Evaluation of Digital Technology and Radio and Television Integration Based on Big Data Model

Journal of Sensors

This article has been retracted by Hindawi following an investigation undertaken by the publisher [1]. This investigation has uncovered evidence of one or more of the following indicators of systematic manipulation of the publication process:

(1) Discrepancies in scope

(2) Discrepancies in the description of the research reported

(3) Discrepancies between the availability of data and the research described

(4) Inappropriate citations

(5) Incoherent, meaningless and/or irrelevant content included in the article

(6) Manipulated or compromised peer review

The presence of these indicators undermines our confidence in the integrity of the article's content and we cannot, therefore, vouch for its reliability. Please note that this notice is intended solely to alert readers that the content of this article is unreliable. We have not investigated whether authors were aware of or involved in the systematic manipulation of the publication process.

Wiley and Hindawi regrets that the usual quality checks did not identify these issues before publication and have since put additional measures in place to safeguard research integrity.

We wish to credit our own Research Integrity and Research Publishing teams and anonymous and named external researchers and research integrity experts for contributing to this investigation.

The corresponding author, as the representative of all authors, has been given the opportunity to register their agreement or disagreement to this retraction. We have kept a record of any response received.

References

[1] J. Lv and Y. Tao, "Development and Performance Evaluation of Digital Technology and Radio and Television Integration Based on Big Data Model," *Journal of Sensors*, vol. 2022, Article ID 1843753, 11 pages, 2022.

Hindawi

Retraction

Retracted: Analysis and Application of Crosscultural Knowledge System Structure in English Teaching Based on Hierarchical Correlation Analysis

Journal of Sensors

This article has been retracted by Hindawi following an investigation undertaken by the publisher [1]. This investigation has uncovered evidence of one or more of the following indicators of systematic manipulation of the publication process:

(1) Discrepancies in scope

(2) Discrepancies in the description of the research reported

(3) Discrepancies between the availability of data and the research described

(4) Inappropriate citations

(5) Incoherent, meaningless and/or irrelevant content included in the article

(6) Manipulated or compromised peer review

The presence of these indicators undermines our confidence in the integrity of the article's content and we cannot, therefore, vouch for its reliability. Please note that this notice is intended solely to alert readers that the content of this article is unreliable. We have not investigated whether authors were aware of or involved in the systematic manipulation of the publication process.

Wiley and Hindawi regrets that the usual quality checks did not identify these issues before publication and have since put additional measures in place to safeguard research integrity.

We wish to credit our own Research Integrity and Research Publishing teams and anonymous and named external researchers and research integrity experts for contributing to this investigation.

The corresponding author, as the representative of all authors, has been given the opportunity to register their agreement or disagreement to this retraction. We have kept a record of any response received.

References

[1] Z. Jianhong, "Analysis and Application of Crosscultural Knowledge System Structure in English Teaching Based on Hierarchical Correlation Analysis," *Journal of Sensors*, vol. 2022, Article ID 3874857, 11 pages, 2022.

Retraction

Retracted: Intelligent Financial Data Analysis and Decision Management Based on Edge Computing

Journal of Sensors

This article has been retracted by Hindawi following an investigation undertaken by the publisher [1]. This investigation has uncovered evidence of one or more of the following indicators of systematic manipulation of the publication process:

(1) Discrepancies in scope

(2) Discrepancies in the description of the research reported

(3) Discrepancies between the availability of data and the research described

(4) Inappropriate citations

(5) Incoherent, meaningless and/or irrelevant content included in the article

(6) Manipulated or compromised peer review

The presence of these indicators undermines our confidence in the integrity of the article's content and we cannot, therefore, vouch for its reliability. Please note that this notice is intended solely to alert readers that the content of this article is unreliable. We have not investigated whether authors were aware of or involved in the systematic manipulation of the publication process.

Wiley and Hindawi regrets that the usual quality checks did not identify these issues before publication and have since put additional measures in place to safeguard research integrity.

We wish to credit our own Research Integrity and Research Publishing teams and anonymous and named external researchers and research integrity experts for contributing to this investigation.

The corresponding author, as the representative of all authors, has been given the opportunity to register their agreement or disagreement to this retraction. We have kept a record of any response received.

References

[1] G. Cheng, "Intelligent Financial Data Analysis and Decision Management Based on Edge Computing," *Journal of Sensors*, vol. 2022, Article ID 1133275, 12 pages, 2022.

Retraction

Retracted: Correlation Analysis between Sports and Antiaging Based on Medical Big Data

Journal of Sensors

This article has been retracted by Hindawi following an investigation undertaken by the publisher [1]. This investigation has uncovered evidence of one or more of the following indicators of systematic manipulation of the publication process:

(1) Discrepancies in scope

(2) Discrepancies in the description of the research reported

(3) Discrepancies between the availability of data and the research described

(4) Inappropriate citations

(5) Incoherent, meaningless and/or irrelevant content included in the article

(6) Manipulated or compromised peer review

The presence of these indicators undermines our confidence in the integrity of the article's content and we cannot, therefore, vouch for its reliability. Please note that this notice is intended solely to alert readers that the content of this article is unreliable. We have not investigated whether authors were aware of or involved in the systematic manipulation of the publication process.

In addition, our investigation has also shown that one or more of the following human-subject reporting requirements has not been met in this article: ethical approval by an Institutional Review Board (IRB) committee or equivalent, patient/participant consent to participate, and/or agreement to publish patient/participant details (where relevant).

Wiley and Hindawi regrets that the usual quality checks did not identify these issues before publication and have since put additional measures in place to safeguard research integrity.

We wish to credit our own Research Integrity and Research Publishing teams and anonymous and named external researchers and research integrity experts for contributing to this investigation.

The corresponding author, as the representative of all authors, has been given the opportunity to register their agreement or disagreement to this retraction. We have kept a record of any response received.

References

[1] Y. Yang, "Correlation Analysis between Sports and Antiaging Based on Medical Big Data," *Journal of Sensors*, vol. 2022, Article ID 3810676, 9 pages, 2022.

Hindawi

Retraction

Retracted: Analysis of Key Factors of College Students' Ideological and Political Education Based on Complex Network

Journal of Sensors

This article has been retracted by Hindawi following an investigation undertaken by the publisher [1]. This investigation has uncovered evidence of one or more of the following indicators of systematic manipulation of the publication process:

(1) Discrepancies in scope

(2) Discrepancies in the description of the research reported

(3) Discrepancies between the availability of data and the research described

(4) Inappropriate citations

(5) Incoherent, meaningless and/or irrelevant content included in the article

(6) Peer-review manipulation

The presence of these indicators undermines our confidence in the integrity of the article's content and we cannot, therefore, vouch for its reliability. Please note that this notice is intended solely to alert readers that the content of this article is unreliable. We have not investigated whether authors were aware of or involved in the systematic manipulation of the publication process.

Wiley and Hindawi regrets that the usual quality checks did not identify these issues before publication and have since put additional measures in place to safeguard research integrity.

We wish to credit our own Research Integrity and Research Publishing teams and anonymous and named external researchers and research integrity experts for contributing to this investigation.

The corresponding author, as the representative of all authors, has been given the opportunity to register their agreement or disagreement to this retraction. We have kept a record of any response received.

References

[1] W. Lu, D. Huo, and S. Jia, "Analysis of Key Factors of College Students' Ideological and Political Education Based on Complex Network," *Journal of Sensors*, vol. 2022, Article ID 6577878, 10 pages, 2022.

Retraction

Retracted: Analysis of College Students' Ideological and Political Dynamics and Communication Path Based on Reinforcement Learning

Journal of Sensors

This article has been retracted by Hindawi following an investigation undertaken by the publisher [1]. This investigation has uncovered evidence of one or more of the following indicators of systematic manipulation of the publication process:

(1) Discrepancies in scope

(2) Discrepancies in the description of the research reported

(3) Discrepancies between the availability of data and the research described

(4) Inappropriate citations

(5) Incoherent, meaningless and/or irrelevant content included in the article

(6) Peer-review manipulation

The presence of these indicators undermines our confidence in the integrity of the article's content and we cannot, therefore, vouch for its reliability. Please note that this notice is intended solely to alert readers that the content of this article is unreliable. We have not investigated whether authors were aware of or involved in the systematic manipulation of the publication process.

In addition, our investigation has also shown that one or more of the following human-subject reporting requirements has not been met in this article: ethical approval by an Institutional Review Board (IRB) committee or equivalent, patient/participant consent to participate, and/or agreement to publish patient/participant details (where relevant).

Wiley and Hindawi regrets that the usual quality checks did not identify these issues before publication and have since put additional measures in place to safeguard research integrity.

We wish to credit our own Research Integrity and Research Publishing teams and anonymous and named external researchers and research integrity experts for contributing to this investigation.

The corresponding author, as the representative of all authors, has been given the opportunity to register their agreement or disagreement to this retraction. We have kept a record of any response received.

References

[1] W. Wu and H. Liu, "Analysis of College Students' Ideological and Political Dynamics and Communication Path Based on Reinforcement Learning," *Journal of Sensors*, vol. 2022, Article ID 9704315, 11 pages, 2022.

Retraction

Retracted: Model Analysis of Applying Computer Monitoring to College Students' Mental Health

Journal of Sensors

This article has been retracted by Hindawi following an investigation undertaken by the publisher [1]. This investigation has uncovered evidence of one or more of the following indicators of systematic manipulation of the publication process:

(1) Discrepancies in scope
(2) Discrepancies in the description of the research reported
(3) Discrepancies between the availability of data and the research described
(4) Inappropriate citations
(5) Incoherent, meaningless and/or irrelevant content included in the article
(6) Peer-review manipulation

The presence of these indicators undermines our confidence in the integrity of the article's content and we cannot, therefore, vouch for its reliability. Please note that this notice is intended solely to alert readers that the content of this article is unreliable. We have not investigated whether authors were aware of or involved in the systematic manipulation of the publication process.

Wiley and Hindawi regrets that the usual quality checks did not identify these issues before publication and have since put additional measures in place to safeguard research integrity.

We wish to credit our own Research Integrity and Research Publishing teams and anonymous and named external researchers and research integrity experts for contributing to this investigation.

The corresponding author, as the representative of all authors, has been given the opportunity to register their agreement or disagreement to this retraction. We have kept a record of any response received.

References

[1] S. Mao and S. Liu, "Model Analysis of Applying Computer Monitoring to College Students' Mental Health," *Journal of Sensors*, vol. 2022, Article ID 4960465, 9 pages, 2022.

Retraction

Retracted: Development of Ecological Health Tourism Products under the Background of Internet+

Journal of Sensors

This article has been retracted by Hindawi following an investigation undertaken by the publisher [1]. This investigation has uncovered evidence of one or more of the following indicators of systematic manipulation of the publication process:

(1) Discrepancies in scope

(2) Discrepancies in the description of the research reported

(3) Discrepancies between the availability of data and the research described

(4) Inappropriate citations

(5) Incoherent, meaningless and/or irrelevant content included in the article

(6) Peer-review manipulation

The presence of these indicators undermines our confidence in the integrity of the article's content and we cannot, therefore, vouch for its reliability. Please note that this notice is intended solely to alert readers that the content of this article is unreliable. We have not investigated whether authors were aware of or involved in the systematic manipulation of the publication process.

Wiley and Hindawi regrets that the usual quality checks did not identify these issues before publication and have since put additional measures in place to safeguard research integrity.

We wish to credit our own Research Integrity and Research Publishing teams and anonymous and named external researchers and research integrity experts for contributing to this investigation.

The corresponding author, as the representative of all authors, has been given the opportunity to register their agreement or disagreement to this retraction. We have kept a record of any response received.

References

[1] X. Wang, "Development of Ecological Health Tourism Products under the Background of Internet+," *Journal of Sensors*, vol. 2022, Article ID 9559606, 9 pages, 2022.

Retraction

Retracted: Research on the Communication Path of Public Opinion in University Ideological and Political Network for Big Data Analysis

Journal of Sensors

This article has been retracted by Hindawi following an investigation undertaken by the publisher [1]. This investigation has uncovered evidence of one or more of the following indicators of systematic manipulation of the publication process:

(1) Discrepancies in scope

(2) Discrepancies in the description of the research reported

(3) Discrepancies between the availability of data and the research described

(4) Inappropriate citations

(5) Incoherent, meaningless and/or irrelevant content included in the article

(6) Peer-review manipulation

The presence of these indicators undermines our confidence in the integrity of the article's content and we cannot, therefore, vouch for its reliability. Please note that this notice is intended solely to alert readers that the content of this article is unreliable. We have not investigated whether authors were aware of or involved in the systematic manipulation of the publication process.

Wiley and Hindawi regrets that the usual quality checks did not identify these issues before publication and have since put additional measures in place to safeguard research integrity.

We wish to credit our own Research Integrity and Research Publishing teams and anonymous and named external researchers and research integrity experts for contributing to this investigation.

The corresponding author, as the representative of all authors, has been given the opportunity to register their agreement or disagreement to this retraction. We have kept a record of any response received.

References

[1] S. Xu, J. Liu, K. Chen, and Y. Yang, "Research on the Communication Path of Public Opinion in University Ideological and Political Network for Big Data Analysis," *Journal of Sensors*, vol. 2022, Article ID 8354909, 9 pages, 2022.

Retraction

Retracted: The Theoretical Topology and Implementation of Enterprise Social Security in the Digital Age Based on Big Data and Artificial Intelligence

Journal of Sensors

This article has been retracted by Hindawi following an investigation undertaken by the publisher [1]. This investigation has uncovered evidence of one or more of the following indicators of systematic manipulation of the publication process:

(1) Discrepancies in scope

(2) Discrepancies in the description of the research reported

(3) Discrepancies between the availability of data and the research described

(4) Inappropriate citations

(5) Incoherent, meaningless and/or irrelevant content included in the article

(6) Peer-review manipulation

The presence of these indicators undermines our confidence in the integrity of the article's content and we cannot, therefore, vouch for its reliability. Please note that this notice is intended solely to alert readers that the content of this article is unreliable. We have not investigated whether authors were aware of or involved in the systematic manipulation of the publication process.

Wiley and Hindawi regrets that the usual quality checks did not identify these issues before publication and have since put additional measures in place to safeguard research integrity.

We wish to credit our own Research Integrity and Research Publishing teams and anonymous and named external researchers and research integrity experts for contributing to this investigation.

The corresponding author, as the representative of all authors, has been given the opportunity to register their agreement or disagreement to this retraction. We have kept a record of any response received.

References

[1] D. Wang, T. Lin, and H. Xu, "The Theoretical Topology and Implementation of Enterprise Social Security in the Digital Age Based on Big Data and Artificial Intelligence," *Journal of Sensors*, vol. 2022, Article ID 7814886, 11 pages, 2022.

Retraction

Retracted: Construction and Application of Index System for Integration of Red Cultural Resources and Ideological and Political Education Based on Fuzzy Judgment Method

Journal of Sensors

This article has been retracted by Hindawi following an investigation undertaken by the publisher [1]. This investigation has uncovered evidence of one or more of the following indicators of systematic manipulation of the publication process:

(1) Discrepancies in scope
(2) Discrepancies in the description of the research reported
(3) Discrepancies between the availability of data and the research described
(4) Inappropriate citations
(5) Incoherent, meaningless and/or irrelevant content included in the article
(6) Peer-review manipulation

The presence of these indicators undermines our confidence in the integrity of the article's content and we cannot, therefore, vouch for its reliability. Please note that this notice is intended solely to alert readers that the content of this article is unreliable. We have not investigated whether authors were aware of or involved in the systematic manipulation of the publication process.

Wiley and Hindawi regrets that the usual quality checks did not identify these issues before publication and have since put additional measures in place to safeguard research integrity.

We wish to credit our own Research Integrity and Research Publishing teams and anonymous and named external researchers and research integrity experts for contributing to this investigation.

The corresponding author, as the representative of all authors, has been given the opportunity to register their agreement or disagreement to this retraction. We have kept a record of any response received.

References

[1] X. Sun and Z. He, "Construction and Application of Index System for Integration of Red Cultural Resources and Ideological and Political Education Based on Fuzzy Judgment Method," *Journal of Sensors*, vol. 2022, Article ID 5103905, 13 pages, 2022.

Hindawi

Retraction

Retracted: Analysis and Application of the Ideological and Political Evaluation System of College Students Based on Text Mining

Journal of Sensors

This article has been retracted by Hindawi following an investigation undertaken by the publisher [1]. This investigation has uncovered evidence of one or more of the following indicators of systematic manipulation of the publication process:

(1) Discrepancies in scope

(2) Discrepancies in the description of the research reported

(3) Discrepancies between the availability of data and the research described

(4) Inappropriate citations

(5) Incoherent, meaningless and/or irrelevant content included in the article

(6) Peer-review manipulation

The presence of these indicators undermines our confidence in the integrity of the article's content and we cannot, therefore, vouch for its reliability. Please note that this notice is intended solely to alert readers that the content of this article is unreliable. We have not investigated whether authors were aware of or involved in the systematic manipulation of the publication process.

Wiley and Hindawi regrets that the usual quality checks did not identify these issues before publication and have since put additional measures in place to safeguard research integrity.

We wish to credit our own Research Integrity and Research Publishing teams and anonymous and named external researchers and research integrity experts for contributing to this investigation.

The corresponding author, as the representative of all authors, has been given the opportunity to register their agreement or disagreement to this retraction. We have kept a record of any response received.

References

[1] J. Geng, T. Wang, and S. Zhang, "Analysis and Application of the Ideological and Political Evaluation System of College Students Based on Text Mining," *Journal of Sensors*, vol. 2022, Article ID 4263974, 14 pages, 2022.

Retraction

Retracted: Research on Teaching Quality Evaluation of Ideological Politics Teachers in Colleges and Universities Based on a Structural Equation Model

Journal of Sensors

This article has been retracted by Hindawi following an investigation undertaken by the publisher [1]. This investigation has uncovered evidence of one or more of the following indicators of systematic manipulation of the publication process:

(1) Discrepancies in scope

(2) Discrepancies in the description of the research reported

(3) Discrepancies between the availability of data and the research described

(4) Inappropriate citations

(5) Incoherent, meaningless and/or irrelevant content included in the article

(6) Peer-review manipulation

The presence of these indicators undermines our confidence in the integrity of the article's content and we cannot, therefore, vouch for its reliability. Please note that this notice is intended solely to alert readers that the content of this article is unreliable. We have not investigated whether authors were aware of or involved in the systematic manipulation of the publication process.

Wiley and Hindawi regrets that the usual quality checks did not identify these issues before publication and have since put additional measures in place to safeguard research integrity.

We wish to credit our own Research Integrity and Research Publishing teams and anonymous and named external researchers and research integrity experts for contributing to this investigation.

The corresponding author, as the representative of all authors, has been given the opportunity to register their agreement or disagreement to this retraction. We have kept a record of any response received.

References

[1] X. Fu and W. Chen, "Research on Teaching Quality Evaluation of Ideological Politics Teachers in Colleges and Universities Based on a Structural Equation Model," *Journal of Sensors*, vol. 2022, Article ID 3047700, 12 pages, 2022.

Research Article

Analysis of the Evolution of Sea Water Quality in the Spanish Coast from Satellite Images before and during a Confinement Period

Mar Parra, Lorena Parra [ID], Jose M. Jimenez, and Jaime Lloret [ID]

Instituto de Investigación para la Gestión Integrada de Zonas Costeras, Universitat Politècnica de València, Spain

Correspondence should be addressed to Jaime Lloret; jlloret@dcom.upv.es

Satellite imaging, a form of remote sensing, can be used to analyse water quality, which must be monitored for proper and sustainable environmental management. This paper studies the effect of a sea traffic reduction in the Alboran Sea (Spain), analysing the changes in water quality before (from February 3rd, 2020) and during (until June 22nd, 2020) a confinement period. This was an unprecedented event in modern times and brought an interesting opportunity to study dynamics when the human impact is reduced. The study of these dynamics and the concentration levels with little human effect is important for environmental conservation purposes. We applied already existing indices using ArcGIS and ACOLITE to determine the following environmental parameters: colored dissolved organic matter (CDOM), suspended particulate matter (SPM), chlorophyll-a (Chl-a), and harmful algal blooms (HABs). Prequarantine concentration levels can reach up to 4 a(CDOM)440 (CDOM), $18 \, g/m^3$ (SPM), and $100 \, \mu g/L$ (Chl-a). Most prequarantine days presented an increment in either concentration level or distribution from the day before. The effects a sudden human impact has on an ecosystem which experimented reduced human influence for months were shown. On the day before the said impact (June 12th), three of the parameters were barely detected with concentration levels of mostly 2 a(CDOM)440 (CDOM), $6 \, g/m^3$ (SPM), and $25 \, \mu g/L$ (Chl-a), and sparse distribution. Afterwards (June 22nd), their levels went up to 4 a(CDOM)440 (CDOM), $14 \, g/m^3$ (SPM), and $1000 \, \mu g/L$ (Chl-a) and were distributed near the ports. The results presented in this study show that the main drivers of change when human impact was reduced were climatologic events (such as storms). Nevertheless, the importance of the human facto can be seen through the CDOM, SPM, and Chl-a plume near port areas observed the day after port activity was reactivated, June 22nd.

1. Introduction

When talking about environmental importance, noncontinental water bodies are essential for life. The oceans and seas serve as a supply of resources and as a key place where important socio-cultural activities are developed. Algae are an important resource in fixing carbon dioxide (CO_2), which can be highly beneficial in stopping and reversing climate change [1]. If we focus on organisms, seas and oceans have very high levels of biodiversity, which must be protected since it is already highly threatened [2]. Tourism is one of the main economic drivers on the coast, especially in areas with warm climates. Furthermore, the oceans are used daily to move goods across the planet, and they offer

many resources, such as fishing and energy. For all these reasons, the adequate protection of the seas and oceans is highly important. Spill pollution, eutrophication, and microplastics are just some of the most pressing problems that plague our waters. Uncontrolled discharges from ships can cause high mortality in a specific functional group or even several of them, as well as eutrophication problems. However, even nutrients can be harmful at high levels since they can generate algal blooms. This increase in microalgae can lead to eutrophication, causing a significant drop in the level of oxygen in an area [3]. The need to follow these problems closely and quantify their effects is clear; nevertheless, the method to do so must be as sustainable as possible. We have to avoid mistakes that have been made in the past, such as inefficient,

high-cost monitoring, and incorrect management [4]. The main problem with the study of marine quality is that the marine environment is aggressive, any instrument used on it is subject to corrosion. Nevertheless, this is not a problem when using satellite imagery. The usefulness of remote sensing to monitor changes in the marine environment has been proved by various authors. It has been applied during the quarantine caused by the virus SARS-CoV-2, the quarantine which prompted this study. Furthermore, remote sensing is a more sustainable alternative than charting a boat to take measures.

Starting in March 2020, Spain went into an emergency state, which reduced and even stopped trafficking [5]. It brought the opportunity to study environmental parameters with a lessened human impact. Some authors [6] have already stated that the first reports from environmental changes during the confinement period were from water and air quality. Yunus et al. [7] observed a 15.9% decrease in suspended particulate matter (SPM) in Vembanad lake, caused by the lockdown, thus proving the effect business activities have on the lake. Another lake (Hussain Sagar) was studied by Wagh et al. [8]. They studied the levels of colored dissolved organic matter (CDOM), chlorophyll-a (Chl-a), and total suspended solids (TSS). The CDOM and Chl-a levels went down during the lockdown. The absence of traffic and the expected decrease in pollutants from rivers (due to the decrease in factory production) is an unprecedented event in recent times. Their impact on the marine environment can be determined by comparing the data before and during the quarantine.

The aim of this paper is the study of the changes which happened on the Mediterranean coast in the Andalusia region (Alboran Sea) during the quarantine caused by SARS-CoV-2. Other authors have already demonstrated the effect a confinement period had on the environment; nevertheless, there is no specific study for this area. The site will be studied before and during the quarantine period. To do so, the dynamics for CDOM, SPM, Chl-a, and harmful algal blooms (HABs), which are water quality indicators, will be studied. Satellite imagery will be used to compare the studied periods. To monitor these parameters from February 2020 to June 2020, a distinctive methodology combining the use of ArcGIS,ESRI [9], and ACOLITE, MUSEUM [10], software will be employed. The imagery for this study will be from the satellite constellation Sentinel-2, more precisely using the Sentinel-2A-treated images. Only one of the two satellites which compose the Sentinel-2 missions will be used to reduce the errors due to possible dissimilarities between them. With this study, areas of interest, which could be more sensitive to changes and interesting for future studies, could be found (for example, close to ports). Moreover, the information derived from this study opens remarkable possibilities for the sustainable monitoring of the oceans. In the recovery and restoration area of environmental sciences, it is very important to specify the state to which the environment should return. One of the possibilities for the standards to which the recovery is to be held is deriving them from areas with reduced human impact. An opportunity to analyze such an area arises with the quarantine; the dynamics and concentration values for the studied parameters could be of use for restoration planning. The data from the months after the beginning of quarantine show what would happen to a marine environment if all human activities stopped. Therefore, the results of this experience could be used for recovery and restoration purposes as well.

This paper summarises the work performed in the thesis degree of the first author published by Parra [11] and is structured as follows. The findings of other research groups and how they can be related to this study are presented in Section 2. Section 3 describes the process through which the results will be obtained. Afterwards, the results are presented in Section 4. In this section, there are subsections for each parameter studied. In Section 5, we present a discussion of the results, breaking them down to better explain them. Finally, Section 6 presents the conclusions, as well as the possibilities for the future on this topic.

2. Related Work

In this section, some cases in which Sentinel imagery has been used to monitor environmental parameters are explained. The focus is on those relative to the sea. All this information is submitted to prove the importance of monitoring sea parameters and the usefulness of remote sensing.

Toming et al. [12] proved the efficiency of Sentinel-2 MSI data to monitor lake water quality at a global and local scale in 2016. They compared in situ measures of CDOM, Chl-a, and dissolved organic carbon (DOC) with band ratio algorithms. They used both Level-1C (pretreated) images and Level-2A images they atmospherically corrected using Sen2Cor. They employed the green to red band ratio to estimate the CDOM, DOC, and water colour. Chl-a concentrations were calculated using the 705 nm peak. They realised the atmospheric correction reduced the band ratio algorithm correlation, thus indicating the need for better atmospheric correction. Nevertheless, the R2 (a parameter which indicates the correlation from 0-no correlation to 1-perfect correlation) values from comparing the in situ results with the calculated results were high for Chl-a, CDOM, and DOC. They concluded that Sentinel-2 MSI data would be the key in developing new water monitoring techniques and research. Moreover, Orlandi et al. [13] used imagery from the Sentinel-2 MSI sensor to map water quality indices. The bands used by them were visible and near-infrared, and they compared the results with in situ data. They measured Chl-a, turbidity, and TSS using fifteen images of the Pescara River estuary on the Adriatic Sea. The Level-1C images were run through two atmospheric correction programs, Sen2Cor and ACOLITE. The R2 for the turbidity model was over 0.95. Although the R2 for Chl-a was ideal, the model presented better results than the standard OC3 algorithm, which is used. They proved the usefulness of Sentinel-2 MSI data for coastal research and monitoring.

Caballero et al. [14] used Sentinel-2 imagery to monitor the southwestern Spanish coast. This experience was conducted during the first year Sentinel-2 imagery was available to the public. They collected in situ samples of TSS in the Cadiz Bay, Guadalquivir estuary, and Conil port. This was

done to later compare the results derived from the model to the empiric results from the samples. They used an algorithm that selected the most sensitive TSS-water reflectance relationship to calculate the concentration. It used the red (664 nm) and near-infrared (865 nm) bands; both models presented high R^2 values. They used atmospheric correction strategies as well, ACOLITE and POLYMER. The latter proved to be quite useful for removing sunglint. In conclusion, Sentinel-2 data turned out to be useful for TSS monitoring in medium to high turbidity waters.

Li et al. [15] calculated SPM concentrations from the last twenty-two years using old imagery and a model created with Sentinel-2. First, they chose between five state-of-art models by comparing their results to 79 in situ datasets from the studied estuary. The models were recalibrated as well to ensure consistency. Then, they applied the chosen model to old Landsat imagery from 1997 to 2019. They were able to determine the SPM fluxes and, among other findings, discover seasonal patterns. Focusing on refining the detection of SPM concentration levels, Liu et al. [16] used in situ measures and Sentinel-2 MSI images to develop a model which could calculate the SPM concentration levels. The sixty-eight hyperspectral measurements they used were from Poyang Lake, China. Half of the samples were used to calibrate the model, whereas the rest were used to validate it. The resulting models were applied to new Sentinel-2 imagery and compared to those from the Terra-Moderate Resolution Imaging Spectroradiometer (MODIS) B01. The models, which used B04 to B8A, explained 77-93% of the SPM concentration variation. The most accurate models were the ones that used B07 for high loadings and B04 for low loadings.

Focusing on HAB detection, Potes et al. [17] tested previous algorithms developed for the ENVISAT-1 with Sentinel-2 data. The study area was the Alqueva reservoir, Portugal. Moreover, they tested the effectiveness of the algorithms for the new MSI instrument for Chl-a, water turbidity, density, and concentration of cyanobacteria. Their results were compared to in situ sampling and the analysis of Chl-a associated with HAB in laboratories. The MSI sensor was able to detect HABs. The study conducted by Khalili and Hasanlou [18] tested up to fifteen different indices for HAB monitoring using Sentinel-2 MSI data. Specifically, the test they performed was aimed at the detection of red tide algal blooms. Different statistical parameters were calculated for each index, such as overall accuracy, type I and II error, area under the curve, and Kappa coefficient. The model that presented the best results considering the statistical parameters was (B04 – B8A)/(B04 + B8A). Following this, Alba et al. [19] used Sentinel-2 imagery to monitor an algal bloom event. This algal bloom event occurred in San Roque lake, Córdoba, Argentina. The bands used to detect the HAB were B04 and B08. Moreover, they used B8A and B09 to discern the algae composition patterns. The results were positive and showed the potential Sentinel-2 MSI data has for monitoring bloom events in eutrophic lakes.

Some authors have studied the effect of the lockdowns from SARS-CoV-2 had on the environment. Focusing specifically on water quality, we find Cecchi [20] who studied the decrease in seawater contaminants in the Lagoon of Venice. They detected that volatile organic compounds (VOCs) as well as microplastics and other pollutants significatively decreased. From the studied compounds, 17 were not detected after the lockdown period, and the ones which were detected were 9 with an input which was not altered by the lockdown or with a stronger persistence. Furthermore, Silva et al. [21] studied both the air and water quality in Spain and Portugal during the lockdown period. The water transparency increased during that time, with a reported reduction in total suspended matter (TSM) of 17% from the month of February to March (when the lockdown started), of 37% from March to April, and of 53% from April to May. It is to be noted that TSM is related to SPM. These studies prove that the lockdowns caused by the SARS-CoV-2 had a relevant effect in seawater quality.

Therefore, all these authors proved the usefulness of Sentinel-2 for monitoring these parameters under normal circumstances. The usefulness of satellite imagery for environmental monitoring has been thoroughly proved. It is especially relevant for areas hard to monitor manually. The sea is one of those areas, which could benefit from the continued monitoring via remote sensing. Nevertheless, the SARS-CoV-2 quarantine presented an unprecedented opportunity to study dynamics and the effect a reduction on human impact could have. Combining remote sensing services and quarantine (which allows for the study of water quality dynamics without human impact in this area) creates an ideal situation for novel research on seawater monitoring. In this paper, the water quality of the Alboran Sea (south-west Mediterranean region) is studied through four parameters: CDOM, SPM, Chl-a, and HABs. The background of the methodology used for each parameter is described in Section 3.4 of Materials and Methods. The study developed by Silva et al. [21] deals with seawater quality in the Iberian Peninsula; nevertheless, they focus on Portuguese waters, whereas this study is centered on the waters between Andalusia and Morocco. A study of the effects on seawater quality caused by the SARS-CoV-2 quarantine has yet to be published for this area.

3. Materials and Methods

Now, we are going to show the background, as well as the technical aspects of this study. To better understand this, the section is divided into four subsections. First, some background is provided in order to show where the data comes from and why it was chosen. Next, the method used to obtain the data is shown. Afterwards, the process the data undergoes before applying the indexes is thoroughly explained. Finally, those indexes are described.

3.1. Background

3.1.1. Spatial and Circumstantial Framework. The quarantine, caused by a virus, began on the 14th of March 2020. That day, many restrictions (most of them on mobility) were issued in Spain. The return to a state similar to the one before quarantine (New Normality) was done gradually

through a process named deescalation. The quarantine was declared officially over on the 21st of June 2020, thus starting the New Normality. It was a state similar to that from before the quarantine, nevertheless, with social distancing and face-masks. We summarised the changes in the marine area brought by every step on the deescalation [22], in Table 1. All the restrictions lifted on every step of the deescalation were forbidden during the period between March 14th and the date indicated on the table. Recreational sailing and cruises were prohibited, and even though commercial transport was still allowed [23], it was slowed due to a reduction in personal and restrictions on other countries.

The study area is situated where the Mediterranean Sea meets the Atlantic Ocean. It is delimited by the Strait of Gibraltar on the west, Andalusia (Spain) on the north, and Morocco and Algeria on the south. It is an exchange area where Atlantic water, less dense, flows on the upper part of the water whilst the Mediterranean waters sink while flowing out [24]. The area, its coordinates, and the surface covered by the study can be seen in Figure 1.

3.1.2. Selected Image Source. The imagery used for this study is obtained from the Sentinel-2 satellite, launched by the European Space Agency (ESA) [25]. It is a mission in conjunction with the Global Monitoring for Environment and Security (GMES) initiative, named "Sentinel." The missions were created within the Copernicus framework, and their objective is to monitor the Earth. The Sentinel-2 mission is comprised of two satellites phased 180°, which offers a high revisit time, and covers latitudes from 84° N to 56° S. The satellites, which weight 1.2 tones, have enough propellant to work for 12 years, although their estimated lifespan is 7 years and 3 months. They are endowed with several instruments, the most remarkable one being the MultiSpectral Instrument (MSI), which works passively by collecting reflected sunlight. The products available to the public are the Level-1C, Level-1B, and Level-2A images. Level-1C images are used in this paper because they have undergone preprocessing (with a <12 m root mean square error) before being accessible to the public [26]. This process includes geometric and radiometric corrections with both spatial registrations and ortho-rectification. The global reference system ensures subpixel accuracy.

The Sentinel-2 products used for this paper are raster images for which the value of the pixel is the reflectance at different wavelengths. The wavelengths, what they depict, and their resolution (pixel size) for the bands used are noted in Table 2.

Although it was not created specifically for marine monitoring like Sentinel-3, the Sentinel-2 mission offers high-resolution optical imagery (which the Sentinel-3 mission does not). This is a crucial factor since, usually, the higher the resolution, the higher the price [27]. Nevertheless, Sentinel-2 offers high-quality imagery for free. Therefore, the images from the satellites belonging to this mission are more suitable for imaging techniques.

3.2. Data Acquisition and Management. The data used for this paper will be extracted from the Copernicus Open Access Hub [28]. In this webpage, data from all over the world can be accessed, from every Sentinel satellite, for free. The areas for each Sentinel-2A image are not big enough to cover the entire Andalusian Mediterranean coast; therefore, we will have to select all the images needed (four images, dividing the coast into four subareas). These areas will be selected to ensure the presence of data from all the Spanish Alboran coastline. The names of the subareas are marked with three letters by Sentinel-2A; the subareas selected are STF, SUF, SVF, and SWF. This area was chosen due to the usually high marine trafficking, which is usually present there. It is the metaphoric door to the Mediterranean Sea, the Strait of Gibraltar. Every ship coming from outside the Mediterranean Sea has to go through it. Therefore, it is a suitable area for the study of possible changes due to a quarantine.

As stated before, there are four subareas, each corresponding to different parts of the Alboran sea. The first day from which we have data is the 3rd of February, and we know Sentinel-2A has a return time of 10 days in this area. Therefore, the last day for which there are data is the 22nd of June, barely a day after quarantine finished. This makes a total of fifteen days, an average of three per month, of data. The subarea SWF has data for more days than those studied; this is since this subarea is in the limit between two runs from the satellite. Therefore, some data from this area will not be used due to the dates not matching.

3.3. Data Treatment. This subsection is divided to understand the process better. Nevertheless, it can be summarised in the scheme presented in Figure 2. This scheme follows the workflow of this study. First images were obtained from the website. Afterwards, they were treated with both ArcGIS, ESRI [9], and ACOLITE, MUSEUM [10]. Finally, the results were displayed using ArcGIS.

3.3.1. Pretreatment. The images obtained from the Sentinel webpage had already been through the pretreatment mentioned in the previous subsection. Nonetheless, they still needed to be further processed before some of the indices were calculated. The Sentinel and Landsat software [10], developed by the Royal Belgian Institute of Natural Sciences, was used for this step. This software was built specifically for marine and inland water bodies monitoring and has been proved to be useful for Sentinel-2 before [29]. It uses the light reflectance from each pixel and applies formulas to the images treating them as if they were matrices. Among the processes it performs, the most important is the atmospheric correction; this is done using the dark spectrum fitting approach by Vanhellemont [30]. Moreover, it can apply indexes and existing formulas to derive parameters with their corresponding values. ACOLITE works with a specific configuration that can be altered by creating .txt files with new settings. Currently, it works with Python 20190326.0.

It is to be noted that part of the main treatment was applied when running the ACOLITE scripts for the pretreatment, specifically for the Chl-a and SPM indices. Nevertheless, this step was just the beginning for the HAB and

TABLE 1: Effects of the deescalation for the marine area.

Phase 0	Phase 1	Phase 2	Phase 3
Quarantine conditions	Exceptions in some autonomic communities for marine transport. 50% occupation with 2 meters between seats, 100% occupation in cabins for people living together	Recreational fishing allowed Recreational sailing only within the territorial unit	Passengers allowed to embark ferries Recreational sailing allowed within the national territory
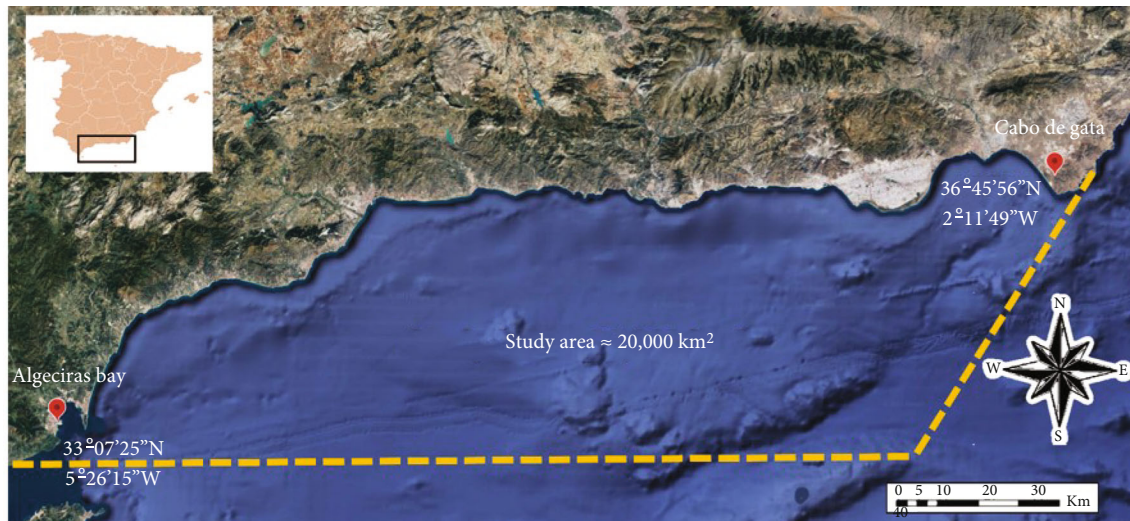
FIGURE 1: Study area, sea delimited by the discontinued line.

TABLE 2: Bands used and their characteristics.

Band name	Wavelength (nm)	Description	Resolution (m)
B03	0.560	Green	10
B04	0.665	Red	10
B06	0.740	Vegetation red edge	20
B08	0.842	Near infrared (NIR)	10
B8A	0.865	Vegetation red edge	20

CDOM indices. It was done to optimise the use of this software instead of running two different scripts, one for the pretreatment and one for the main treatment. Although ACOLITE can represent HAB, the index used in this paper applies a different equation.

The first step for the pretreatment of the images used for the HAB index was to merge the images for B04 and B8A. It was done using the ArcGIS software, ESRI [31], more precisely the "Mosaic To New Raster" tool [32], which can be found in the Data Management Tools. It was done for both B04 and B8A for each day. The images generated are the ones that will be used later for the main treatment for HAB. Said treatment is explained in detail in the next subsection.

3.3.2. Main Treatment. The ACOLITE script for each day was a modification of the default script to which new com-

mands were added and some old commands were modified. The input and output were selected, as well as the 12 w parameters (among them were the indices). Moreover, it was specified for the results to be obtained in .tif format and not to generate .png files. The 12 w parameters chosen were Rrs_560, Rrs_665, spm_nechad2016, and chl_re_moses3b740.

The Rrs_560 and Rrs_665 images were used for the CDOM index, and before calculating it, it was needed to combine them. It was done following the same method as for the HAB images, combining the B03 and B04 images in this case. The main treatment for the Chl-a and SPM was done by ACOLITE, and the files generated by spm_nechad2016 and chl_re_moses3b740 were ready to be analysed. For the main treatment for HAB and CDOM, another ArcGIS Tool was used. In this case, the chosen tool was one that is useful for many remote sensing applications; the "Raster Calculator" [33]. Raster files can be interpreted as large matrices in which each pixel is one number from the matrix. The Raster Calculator applies a specified formula to the matrix represented by the raster. Several indices, explained in the following subsection, were used.

3.4. Used Indices. In this subsection, the indices used to estimate the levels of CDOM, SPM, Chl-a, and HAB are described. This subsection has been divided into four brief parts to ease the understanding thereof. Each of them deals with one of the indices.

3.4.1. CDOM. CDOM [34] is the part of dissolved organic matter which can be detected via optical techniques. It is
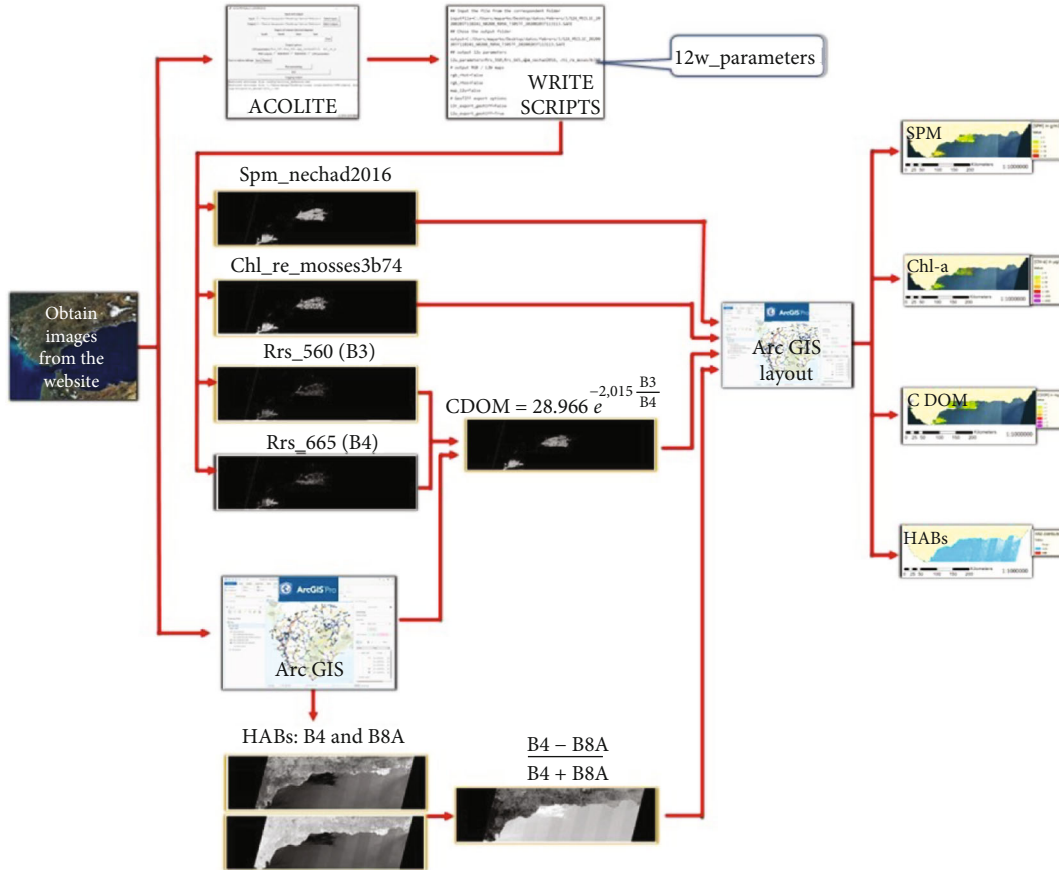
FIGURE 2: Scheme of the methodology.

humic-rich and affects the light levels in the water column, therefore, affecting the entire ecosystem. It peaks naturally during spring and intense weather conditions such as storms and hurricanes. It is due to these events causing massive overland flows. Nonnatural causes for peaks include human activities such as sewage treatment plant discharge and agricultural and farming runoff.

Chen et al. [35] developed several models for the remote sensing of CDOM and Chl-a concentration levels in 2017. They used Sentinel-2 data and calibrated it with data from field measurements. The tests were conducted on Lake Huron, China. Twelve models were developed and tested for CDOM alone, four of them proving to be useful. Later on, in 2020, another study conducted by the same team used one of them, which used B03 and B04 [36]. It is the index used for our CDOM identification, the formula to estimate the CDOM levels using B03 and B04 as seen in

$$\text{CDOM}\,(\text{a(CDOM)}440) = 28.966 \cdot e^{-2.015 \cdot (B3/B4)}. \quad (1)$$

The results from this equation were the CDOM concentration levels in absorbance at 440 nm for each pixel, a(CDOM)440. This is the most used unity for CDOM measurements. It is to be noted that each pixel was 10×10 meters in real life due to both bands used for this index having that resolution.

3.4.2. SPM. SPM [37] is linked to CDOM because both increase with runoffs and both being sediments. It modifies the colour and transparency of water as well. Nevertheless, SPM is associated with bacteria and metallic contaminants. Some human causes for an increase in the SPM levels include offshore wind farms, dams, sand extraction, transport of pollutants… Natural causes for SPM variation include water velocity and hydrological alternation [38].

The SPM levels were derived from the raster files generated by ACOLITE. The program used the formula developed by Nechad et al. [39], seen in its empirical formula in Equation (2). In which T is the turbidity (SPM in g/m^3), A and B are coefficients which depend on the wavelength used (2383.49 and 0, respectively, for 842λ). The R^2 for this method using the selected wavelength is 0.889. The X is the water-leaving reflectance, obtained from the $842\ \lambda$. The equation with the parameters for this case can be seen in Equation (3).

$$T\left(\frac{g}{m^3}\right) = A(\lambda) \cdot X(\lambda) + B(\lambda), \quad (2)$$

$$T\left(\frac{g}{m^3}\right) = 2383.49 \cdot B8 + 0. \quad (3)$$

The formula has been proved useful by Chapalain [40], who used it for a study on SPM dynamics and characteristics

on the French coast. First, the program applied an atmospheric correction to the images; next, using the NIR images, the concentration (in g/m^3) was calculated for each pixel. This step was done when running the script on ACOLITE, and there was no need for ArcGIS to generate this data, only to display it. The equation for this parameter was not introduced; it was applied automatically by ACOLITE. Therefore, it is not noted in this study.

3.4.3. Chl-a. As stated by Pérez-Ruzafa et al. [41], Chl-a indicates the trophic state of waters since it is a proxy for phytoplankton biomass. High Chl-a levels indicate eutrophication, a state for which dissolved oxygen becomes a scarce resource, thus affecting the entire ecosystem. This increase in phytoplankton happens when there is a high nutrient load. The Chl-a levels in the sea are usually lower than in lakes and coastal lagoons; nonetheless, they increase with weather events such as storms since overland flow increases the nutrient load.

In the case of Chl-a, the results were obtained from ACOLITE as well. The formula used was first postulated by Moses et al. [42]. The said formula usually employs the reflection at a wavelength of 708 nm as a reference. Nevertheless, it can be specified for it to use the one at 740 nm (B6), as seen in Equation (4), for which Rx is the remote sensing reflectance for the band at x nm. This equation was chosen because the concentrations were slightly higher when employing the 740 nm band as reference. When determining harmful concentrations, it is better to overestimate them. Moreover, since the objective is to compare the changes between different days, it is better to have higher values; the changes can be more notable.

$$\text{Chl}_a \left(\frac{\mu g}{L} \right) = \left[113.36 \cdot \left\{ \left(R_{B4}^{-1} - R_{B6}^{-1} \right) + R_{B6} \right\} + 16.45 \right]^{1.124}. \tag{4}$$

Many studies have used the equation developed by Moses et al. [42] in 2012. In 2019, Warren et al. [43] used it to monitor Chl-a levels in a comparative study. Moreover, it was used by Phalevan et al. [44] when they retrieved Chl-a from Sentinel-3 and Sentinel-2 imagery using machine learning in 2020. For our study, the concentration levels were calculated for each pixel and were shown in $\mu g/L$. The formula was applied automatically by ACOLITE during the pretreatment. ArcGIS was only used to display the data.

3.4.4. HABs. HABs [45] disrupt the entire marine ecosystem and can cause eutrophication. They can impact the local economy, food security, human health, and tourism. The warming and acidification of the seas, as well as deoxygenation (all caused by climate change), increase the possibility of a HAB. Moreover, they can be caused by high nutrient loads after extreme climatic events such as storms or hurricanes.

For HABs, the formula used was the one determined to be the best for this type of measure by Khalili and Hasanlou [18]. This equation resulted from research with an extensive background; the likes of which include the work developed by Carvalho et al. [46] to detect *Karenia brevis* blooms along the west coast of Florida and the Gulf of Mexico. Moreover, they also applied the results from the research conducted by Matthews et al. [47] in which the HABs were studied through the use of Chl-a levels. The formula developed by them and used in this paper is different from the ones above. It shows the pixels that have a higher difference between Red and Vegetation Red Edge bands. It is to be noted that B8A had a smaller resolution than B04. Therefore, their result had the smallest resolution (20 m). This index was calculated using the Raster Calculator Tool ARCGIS DESKTOP [33] using

$$\text{HABs} = \frac{\text{B4-B8A}}{\text{B4-B8A}}. \tag{5}$$

The results for this index ranged from -1 to +1 due to the nature of its equation; they are dimensionless. For pixels where the value for B04 was significantly bigger than for B8A, the results were close to 1. Whereas for pixels where the value for B8A was significantly bigger than for B04, the resulting pixels were close to -1. In pixels where the values for B04 and B8A were similar, the resulting pixel had a value close to 0. According to Khalili and Hasanlou [18], HAB-laden waters present bigger differences for B04 and B8A than normal seawater. Therefore, values closer to 1 represent HABs, whereas low positive values are water. Clouds are white; therefore, the reflectance for B04 and B8A is similar for them. Therefore, numbers very close to 0 (both positive and negative) are clouds, and low positive values represent water. Since land is of no concern for this study and will be represented using another layer on the map, we do not need to specify another category for discerning land.

4. Results

The results are presented now for each of the parameters monitored in the area and period specified. This section has been divided into five subsections to achieve a clean presentation of the results. The representation of the data is explained in the first one. The second section deals with the changes in CDOM. Next, the evolution in SPM is presented. Moreover, the spatial-temporal changes in Chl-a are shown in the third subsection. Next, the distribution of HAB is presented in the fourth subsection. It is important to note that in this section, the results are presented, and their possible causes are mentioned. The next section (Discussion) details and analyses the causes, drivers, and dynamics and summarises them.

4.1. Data Analysis and Representation. The resulting images have been displayed using ArcGIS. Four results have been obtained per day using their pixel values to colour the images. The CDOM, SPM, and Chl-a images correspond to their concentrations, whereas the HAB images represent their presence or absence. All the images have the "≤0" range to indicate water due to the nature of the equations and to eliminate possible errors (negative values).

For the CDOM, SPM, and Chl-a indexes, the true colour images are represented underneath. These images place the clouds and help interpret the results. In order to make sure it rained whenever clouds are present in the pictures, weather tables are checked [48]. The values do not represent the magnitude of the storm at sea, in any case. Nevertheless, they can assert the presence of rain. The effect rain has on concentration levels has to be taken into account to identify the cause of increasements during the quarantine period. It is important to note that the SPM and Chl-a concentration levels (measured g/m^3 and μg/L, respectively) cannot be considered equivalent due to the Chl-a concentration levels in μg/L presenting a difference in concentration values one thousand times smaller than the SPM ones. The choice in units is due to Chl-a levels being very low at sea.

It is to be noted that the period studied in this paper was very cloudy, which is to be expected from a winter-spring time interval. The quality of the data is not the same for every studied day. Some days are cloudier than others, and the area which can be studied is reduced, which affects the distribution. Not all the weather is visible; some clouds look like water due to them being very low. Nevertheless, the images have been thoroughly studied, and the results derived from them are presented in this section, broken down for an easier understanding. In February, the second day, the 13th, presents a storm covering its sky. There are clouds on all three days; nonetheless, those clouds are small and localised for the first day, the 3rd. For the third day, the 23rd, they only cover the western part of the Alboran Sea. On March, the first day, March 4th, the sky is clear. Nevertheless, on March 14th, clouds cover the western part of the Alboran Sea in a similar way to the image from February 23rd. Finally, for the third day, Mach 24th, the sky is almost fully covered; even though the eastern part of the sea seems visible, it is covered by low clouds, in which the imaging techniques are difficult. When observing April, the large clouds covering the second day, April 14th, can be distinguished. Moreover, on the third day, April 24th, some clouds cover the area. Not only they cover the parts which look white, low clouds were present during this day. The only day with complete data is the first day, April 4th. This day presents some errors since the satellite images used were slightly compromised; it can be seen on the right side of the image. It shows lines in which the values are much lower than expected compared to those around them, which is an error due to the source data (the satellite images) being compromised. It can be seen in most of the images; nonetheless, the effect is more notable in this one. May is the first month in which all three days can be studied without major clouds interfering. The first day, May 4th, has a clear sky, as does the third day, May 24th. The second day, May 14th, presents some clouds on the western part of the Alboran Sea, close to the Strait of Gibraltar. Half of the study area had entered phase 1 on May 14th, and next, for the third day, May 24th, all the area was on phase 1. Finally, June 2nd is hard to study due to the clouds that seem similar to those on April 23rd; nevertheless, small gaps between clouds can be analysed. For June 12th, the situation is similar, although a small area in the west can be seen. The third day, June 22nd, pre-

sents a clear sky. It is important to note that on June 1st, the entire area entered phase 2; on June 8th, it entered phase 3, and on June 21st, it entered the New Normality.

4.2. CDOM. In this subsection, the results concerning the concentrations of CDOM are presented. They can be seen in Figure 3.

The CDOM concentration levels for February are presented in Figures 3(a)–3(c). Most values on February 3rd were lower than 2 a(CDOM)440. Their distribution does not seem to reveal any pattern other than it being slightly more prominent near the clouds. It is important to note that these concentrations correspond to data taken in the middle of winter and before the quarantine started. Natural CDOM peaks usually happen during spring [34]. Next, for February 13th, the results are more difficult to interpret since there were many clouds. Nevertheless, the data shown on the gaps between clouds present higher concentrations of CDOM. The concentrations for those areas, higher than that of the 3rd, can be explained through the storm that can be seen in the weather tables [48] and the port activity. Even though some clouds are present on February 23rd, most of the data can be interpreted. An overall increase respecting the concentrations from February 3rd can be seen. Concentrations from 2 to 4 a(CDOM)440 can be found in the southeastern part of the area.

The CDOM concentration levels for March are presented in Figures 3(d)–3(f). The values from March 4th show concentrations from the 0 a(CDOM)440 to 2 a(CDOM)440 range and from the 2 to 4 a(CDOM)440 range. The distribution shown by them is similar to the one present on February 23rd (Figure 3(c)). This could easily be explained due to the rains experienced the week before, as seen in the weather tables [48], and the port activity. The conditions already present ten days before are maintained; heavy rains hit the peninsula the week before March 14th, the date on which quarantine started. Moreover, some clouds only allow the eastern part of the Alboran Sea and the coastline to be studied on this date. Some parts of the sea present concentration values over 4 a(CDOM)440. Furthermore, there seems to be higher concentrations nearshore which could be caused by the overland flow due to the storm. For March 24th, not much can be analysed since clouds cover most of the sea. The CDOM concentration peaked, reaching values of even 8 a(CDOM)440. This can be explained due to the intense weather conditions that week, which created massive overflows and then the currents pulled the matter together in one direction. Furthermore, spring started, which is the time of the year in which CDOM levels naturally peak [34], possibly explaining that peak.

The CDOM concentrations for April are displayed in Figures 3(g)–3(i). Even though the image error concentration values of 0 to 2 a(CDOM)440 can be seen in almost all the sea. Furthermore, concentration levels of 2 to 4 a(CDOM)440 can be seen in the eastern part of the sea, similar to those in Figures 3(c) and 3(d). The previous week was dominated by heavy storms, as seen in weather tables [48], explaining the high concentrations of nearshore. For April
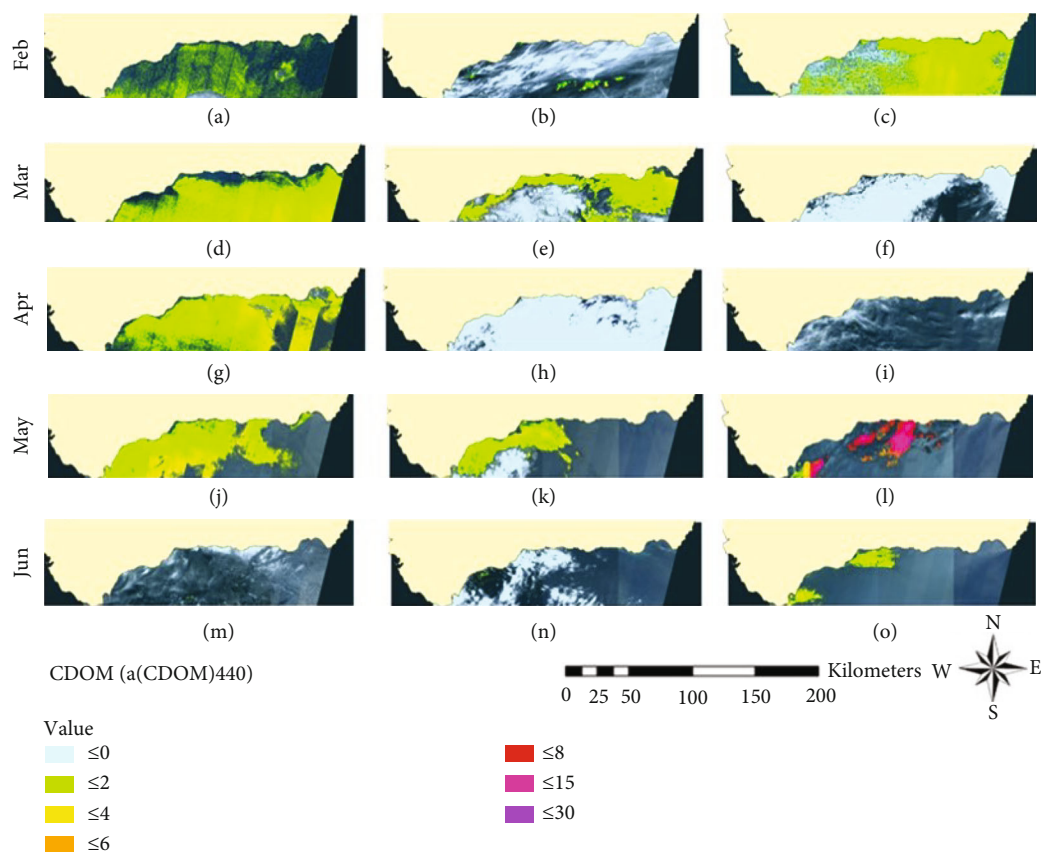
FIGURE 3: CDOM concentrations. Each map represents (a) February 3rd, (b) February 13th (c) February 23rd, (d) March 4th, (e) March 14th, (f) March 24th, (g) April 3rd, (h) April 13th, (i) April 23rd, (j) May 3rd, (k) May 13th and (l) May 23rd, (m) June 2nd, (n) June 12th, and (o) June 22nd.

14th and April 24th, there is not much to be analysed. They both show concentration levels up to 6 a(CDOM)440 in small areas, which could be analysed between clouds. The weather tables [48] show storms throughout the month, explaining the difficulty in obtaining good satellite imagery and the high concentration levels.

For May, the CDOM concentrations are presented in Figures 3(j)–3(l). The concentration levels for May 4th show a distribution close to the coast with higher concentrations at the centre-western offshore waters. It can be explained due to the storms from the week before [48]. Following, for May 14th, it is important to remark the lower presence of storms the week before [48]. Thus, we can see how the CDOM distribution is closer to the coast. This reduction on the week where there were no storms further proves that they are most likely the main cause of peaks on this month and April. In the week previous to the third day this month, May 24th, there were storms again. Moreover, temperatures started to increase [48]. The results presented in Figure 3(l) show the highest CDOM concentrations of all. It is certainly a CDOM peak, which is to be expected around spring [34], and can be caused by the storms combined with the temperature increase. Those parameters can affect the physicochemical properties and its ecosystem, thus making the degradation of CDOM slower.

Finally, the concentrations of CDOM for June are shown in Figures 3(m)–3(o). For June 2nd, only some small gaps between clouds can be analysed. Nevertheless, most of the values for those areas are on the 0 to 2 a(CDOM)440 and 2 to 4 a(CDOM)440 concentration ranges. It means a drastic decrease considering the values for May 24th (Figure 3(l)). Nonetheless, ten mostly dry days went by between both images, and storms are the main drivers of change for these parameters when the human impact is reduced. The impact reduction linked with other parameters such as temperature, wind, and the physicochemical characteristics of the sea may have caused the decrease, which was possible due to the port activity being stopped. The next day, June 12th, shows no CDOM in the eastern part of the Alboran Sea. Moreover, the western side presents very small concentrations in areas where the clouds open and the sea can be studied. After this week, marine transportation was allowed on all the national territory, and passengers were allowed to embark on ferries. Finally, on June 22nd, two very distinctive plumes can be seen heading east. One of them comes from the Algeciras (left) port area, while the other comes from the area around Malaga (centre). Moreover, the concentrations for this date present a more similar distribution of the ranges 0 a(CDOM)440 to 2 a(CDOM)440 and 2 a(CDOM)440 to 4 a(CDOM)440

than any other image. Furthermore, it presents concentration levels up to 14 a(CDOM)440.

4.3. *SPM.* This subsection deals with the results concerning the concentrations of SPM. They can be related to the concentrations of CDOM since their causes are similar [34]. Nevertheless, SPM levels can increase due to other causes. They can be seen in Figure 4.

For February, the concentration levels can be seen in Figures 4(a)–4(c). The SPM levels are low and close to the shore and clouds for February 3rd. This distribution does not correlate to the CDOM distribution, thus indicating the cause for them is different. In comparison to CDOM levels, these are more localised, especially nearshore. Most of the concentration levels for this day are below $6 \, g/m^3$. Even though not much can be analysed for February 13th, the concentration levels for the small areas between clouds certainly present higher values than the previous day, up to $18 \, g/m^3$. It correlates with what happened to CDOM, thus proving they were caused by the same factor. For February 23rd, all the visible water presents concentrations higher than $2 \, g/m^3$. Some parts of the southeastern area present concentrations up to $10 \, g/m^3$. Moreover, areas close to the clouds and close to the coast have SPM levels up to $14 \, g/m^3$ and even $18 \, g/m^3$, which is the highest SPM concentration level for the entire studied period and is presented on two of the three studied days that month.

The next month to be studied is March, during which the quarantine started. The SPM concentration levels for March can be seen in Figures 4(d)–4(f). For March 4th, a distribution similar to the one observed on February 23rd (Figure 4(c)) can be observed. Nevertheless, concentrations seem to peak near Malaga port, with levels up to $18 \, g/m^3$. The port activity is a likely cause of this peak. Concentrations are also high nearshore in Cabo de Gata and Almeria (top right corner). Surprisingly enough, concentrations are not as high in Algeciras port, although the currents can be an important factor. On March 14th, the day quarantine started, the concentrations peaked both in the east and west but lowered at the Malaga port. The areas which can be seen between clouds in the west show concentrations on the 2 to $6 \, g/m^3$ and 6 to $10 \, g/m^3$ ranges. In the east, values peak around Almeria and Cabo de Gata, reaching concentrations up to $14 \, g/m^3$ and even $18 \, g/m^3$. Although they reach the shore near Cabo de Gata, they seem to not due to the effect of clouds. It may be caused by dust transported by wind since the week previous to that day had been dry, and dust being carried offshore is a natural cause for high SPM concentrations at sea [34]. For March 24th, not much can be said. The small gaps between clouds present low concentration levels, unlike CDOM concentrations for this date.

The results from April are presented in Figures 4(g)–4(i). The concentration levels for April 3rd are higher on the eastern side of the Alboran Sea. It is unfortunate since it is the area for which the file was corrupted and could not compute the entire image. Nevertheless, the increased concentration can be seen. Most of the concentration values for that area reach $10 \, g/m^3$. Concentrations are higher nearshore, going

up to $14 \, g/m^3$, reinforcing the possibility of the peaks being due to dust carried through the wind; therefore, not caused by port activity. Concentration levels of CDOM were also higher on the southeastern side for this date, although they were not present nearshore. SPM does seem to be present nearshore for most of the images in which it is detected. For April 13th, some small gaps between clouds can be seen, for which the average concentration seems to be in the 10 to $14 \, g/m^3$. The next studied day, April 23rd, presents lower concentrations, most of them on the 2 to $6 \, g/m^3$ range. Changes for this month may have to do with hydrological conditions caused by the storms on the weeks previous to them [48].

The concentration levels for SPM in May are shown in Figures 4(j)–4(l). The concentration levels for May 3rd seem to be the consequence of those in April still. SPM presence is no longer on the eastern part of the Alboran Sea, and now, the higher values are on the western side. Although most values are on the 2 to $6 \, g/m^3$ range, values from the 6 to $10 \, g/m^3$ and 10 to $14 \, g/m^3$ ranges can be seen offshore. The week previous to this date presents high precipitation levels [48]. CDOM presented high concentration levels on that area for this date, indicating a massive overland flow caused by storms, which has already gone far into the sea and carries SPM. For May 13th, the concentrations seem to have lowered, although they are close to the western side as well. Their distribution is similar to the CDOM distribution for this date, reinforcing the possibility of natural causes. The concentration levels for May 23rd seem to have lowered to mostly values from 2 to $6 \, g/m^3$. Nonetheless, SPM has spread in distribution, covering areas not covered on May 13th, which may have to do with winds. It is important to note that on May 18th, the entirety of the study area entered phase 1. The weather most likely caused all changes for this month.

June (Figures 4(m)–4(o)) is the last month to be studied. Most of the data for June 2nd cannot be analysed due to the clouds covering the sea. Nonetheless, for the small gaps in which the imaging techniques could be run, the values presented are mostly on the 2 to $6 \, g/m^3$ range. On this date, all of Andalusia was already on phase 2. On June 8th, the area of interest entered phase 3. Although data from June 12th cannot be analysed as well as data from other days, it shows low concentration values. Most of them are in the 2 to $6 \, g/m^3$ range and do not cover the full extent of the opening between clouds. Finally, on June 22nd, a day after the end of quarantine, the concentration values peaked. It is interesting to note that their distribution is very similar to the distribution of CDOM for this date. They are higher near the Algeciras port and the Malaga port. Especially on the Algeciras area, for which values on the 10 to $14 \, g/m^3$ range can be seen. On this date, the other concentration levels have values on the 2 to $6 \, g/m^3$ and 6 to $10 \, g/m^3$ ranges.

4.4. *Chlorophyll-a (Chl-a).* In this subsection, the results for the Chl-a levels on the Alboran Sea are presented in Figure 5. High Chl-a levels can be naturally caused by storms and high nutrient loads [38], presenting a correlation with high CDOM and SPM.
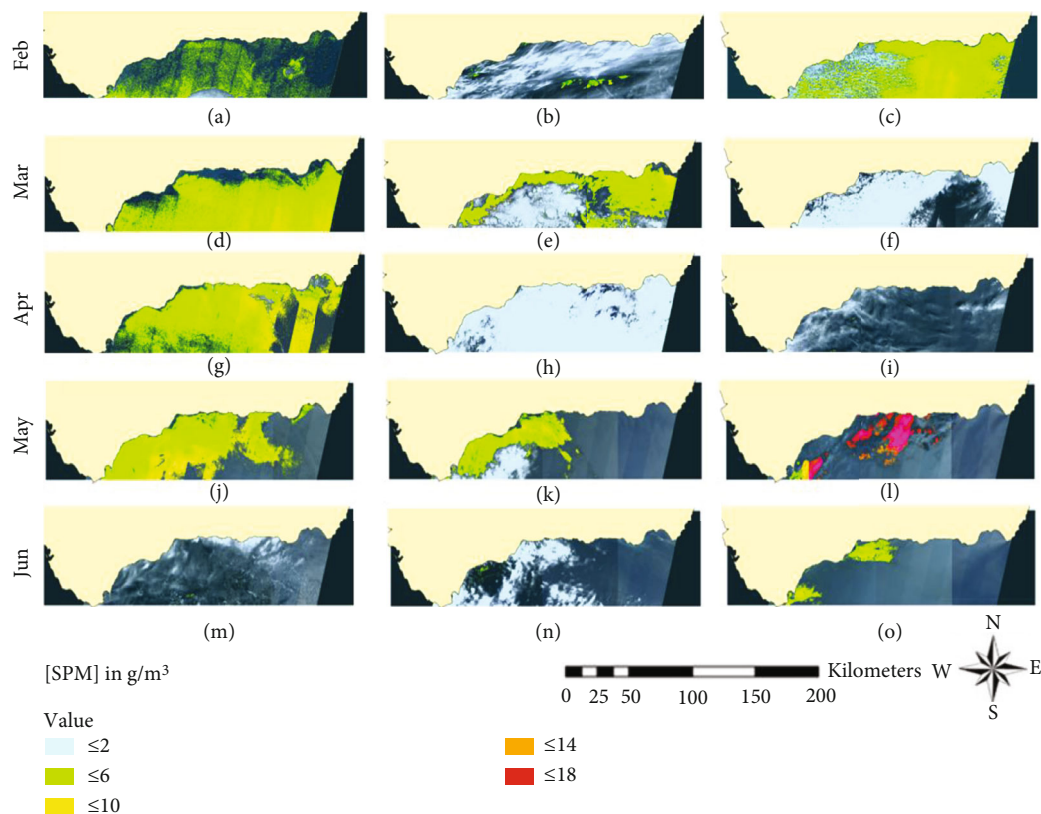
FIGURE 4: SPM concentrations. Each map represents (a) February 3rd, (b) February 13th, (c) February 23rd, (d) March 4th, (e) March 14th, (f) March 24th, (g) April 3rd, (h) April 13th, (i) April 23rd, (j) May 3rd, (k) May 13th, (l) May 23rd, (m) June 2nd, (n) June 12th, and (o) June 22nd.

The concentration levels for February can be seen in Figures 5(a)–5(c). The Chl-a levels for February 3rd present mostly concentrations lower than 50 μg/L. Nonetheless, this date presents higher concentrations near the Malaga port and the Strait of Gibraltar, where the Algeciras port is located. Concentrations present in these areas go up to 100 μg/L. Chl-a is detected in the entirety of the area of study. For February 13th, not much can be studied. Nevertheless, the areas visible through the clouds present concentration levels with most values lower than 25 μg/L. Although concentration levels did not change much, the coverage increased. On February 23rd, both higher concentrations and a larger presence of Chl-a can be seen. Most concentration levels are lower than 50 μg/L. Nonetheless, there seem to be more peaks on the 50 to 75 μg/L and 75 to 100 μg/L ranges than for the first day this month. Since storms those weeks were not intense, the increment was most likely caused by port activity.

For March, the Chl-a concentration levels are shown in Figures 5(d)–5(f). March 4th shows a scenario similar to February 24th (Figure 5(c)), although the Chl-a levels close to the coast seem to have reduced. Most concentration levels present values lower than 50 μg/L for this date. Nevertheless, there are more areas with concentrations up to 100 μg/L than for the previous studied day. For this date, CDOM presented higher concentrations as well. For March 14th, the concentrations seem to have lowered; most of them fall on

the 0 to 25 μg/L range. Nonetheless, their distribution thickens on the eastern side of the sea, which correlates to SPM and CDOM concentration levels increase for this date. It is possible that the dust which could have caused the SPM unusually high levels contained a high proportion of nutrients. It is important to note that this date is the day the quarantine started. Next, March 24th is difficult to interpret. The only data available is from small gaps between clouds, the concentration levels for these gaps present values on the 25 to 50 μg/L range. This is probably caused by the storms which hit Andalusia during this period. CDOM concentrations were high for this date as well.

Next comes April; its Chl-a concentration levels are shown in Figures 5(g)–5(i). For April 3rd, concentration levels mostly on the 0 to 25 μg/L range can be seen throughout the entire area. The said area presents concentration levels on the 25 to 50 μg/L range, although less than for the other range. Similar to SPM and CDOM, the higher concentration levels for this date are on the eastern side of the Alboran Sea. In this case, there are some areas for which the concentration gets to 75 μg/L. The week before this date presented rains; this increase could be caused by those storms. Next, April 13th presents little to no data. The points for which concentrations were calculated between clouds present concentrations on the 0 to 25 μg/L range mostly and some on the 25 to 50 μg/L range. The spatial distribution of the Chl-a cannot be studied for either this date or
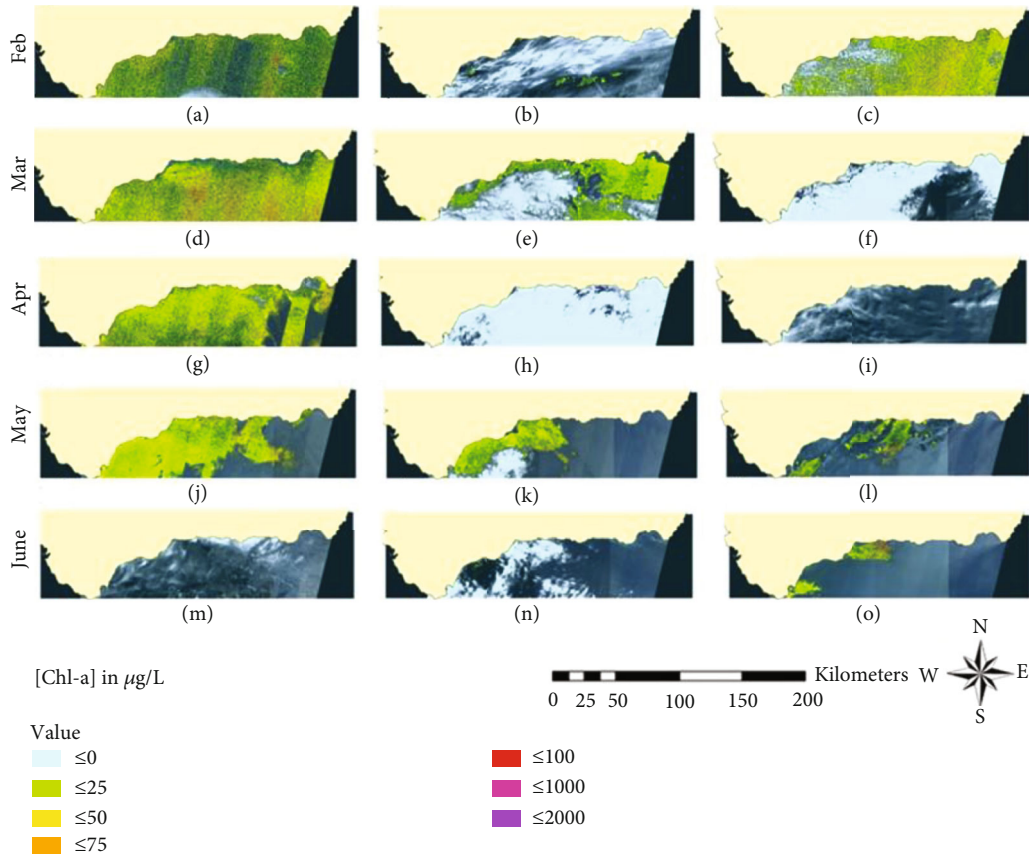
Figure 5: Chl-a concentrations. Each map represents (a) February 3rd, (b) February 13th and (c) February 23rd, (d) March 4th, (e) March 14th, (f) March 24th, (g) April 3rd, (h) April 13th, (i) April 23rd, (j) May 3rd, (k) May 13th, (l) May 23rd, (m) June 2nd, (n) June 12th, and (o) June 22nd.

the next. Then, the concentration levels which can be studied for April 23rd present mostly values on the 0 to 25 μg/L range. Contrary to April 13th, this date presents concentrations higher than 50 μg/L, on the 50 to 75 μg/L range. This sudden increase most likely had to do with the storms, and the massive overland flows caused by them.

Then, the next month analysed is May. The Chl-a concentration values for the said month can be seen in Figures 5(j)–5(l). The first studied day, May 3rd, presents concentration levels mostly on the 0 to 25 μg/L range. Nonetheless, near the Algeciras port, concentration levels increase to the 25 to 50 μg/L range. Furthermore, some values near the coastline on the central and eastern parts of the sea present concentration levels up to 75 μg/L. These levels are not only present there but also on the plume on the east. For May 13th, the concentration levels have mostly reduced both in magnitude and dispersion. During this period, there were fewer storms, which could explain these values. The concentration levels for Chl-a present for this day correlate to CDOM and SPM as well. Increases in concentration levels for all these parameters can be naturally caused by storms. Therefore, this retreating behaviour can be interpreted as the consequence of a storm since it was the main driver of change without human impact. On May 18th, all of Andalusia entered phase 1. The week previous to May 23rd was dominated by heavy rains [48], explaining the higher con-

centration values presented in the central area for this date. These concentrations increased up to 100 μg/L and, on some parts, even 1000 μg/L and 2000 μg/L. It is an unprecedented peak for the period studied for this paper. Moreover, it correlates with the CDOM peak.

Finally, the last month is June. The Chl-a concentration levels for this month can be seen in Figures 5(m)–5(o). The values for June 2nd were taken a day after phase 2 started in Andalusia. It presents concentrations up to 100 μg/L for the small gaps between clouds, which could be caused by precipitations. On June 8th, all of Andalusia entered phase 3. Therefore, the values for June 12th correspond to this period. Recreational fishing was permitted, and recreational sailing was allowed within the territorial unit [22]. Concentration levels and distribution on the gap on the western side of the Alboran Sea are low and sparse. The Chl-a levels show almost no Chl-a compared to the levels before the quarantine (Figure 5(a)). Finally, on June 22nd, barely a day after the instauration of the New Normality, two plumes can be seen. One of them seems to come from the Algeciras port, while the other comes from the Malaga Port. Chl-a concentration levels for the Algeciras port plume are on the 0 to 25 μg/L and 25 to 50 μg/L ranges mostly. In contrast, Chl-a concentration levels for the Malaga port plume reach 1000 μg/L and present many values on the 75 to 100 μg/L range.

4.5. HABs. The analysis of the distribution for HABs throughout the studied period is different from the analysis for CDOM, SPM, and Chl-a. There were only three HAB episodes in the five months studied for this paper. Nevertheless, Figure 6 shows the results for the days which presented HABs.

The first and biggest bloom is on February 3rd (Figure 6(a)). The HAB distribution corresponds with the Chl-a distribution for that date. The values here show a clear HAB, big enough to cover the entire Alboran Sea. The first week of February presents temperatures higher than usual [46], which added to the usually high nutrient content in this season [47] and could have caused the bloom. It happened before the quarantine. The second bloom happened on April 4th (Figure 6(b)), close to the Strait of Gibraltar. It does not match with high Chl-a, CDOM, or SPM levels, which could indicate the algal class [49]. The bloom, nonetheless, seems to come from the strait, probably being caused by a nutrient load entering the Mediterranean Sea. The last noticeable bloom is on May 3rd (Figure 6(c)). It matches up with high Chl-a concentrations as well as the presence of CDOM and SPM. Therefore, it is similar to the bloom on February 3rd. It is most likely due to the high nutrient load present on the sea after the storms which hit Andalusia the week before [48]. Both this HAB and on April 4th happened during phase 0.

5. Discussion

Next, we are going to discuss the results. It has been divided into five subsections to improve the presentation of the observations which have been made. The first one summarises the dynamics observed in the study area and compares the results to those obtained from other studies done in similar areas before the quarantine period. The second subsection deals with the effects of the reactivation of ports. The problem when observing HABs is explained in the third subsection. Localised tendencies are explained in the fourth one. The fifth subsection presents the limitations the technology used has. It is to be noted that this information is key to derive the conclusions for the next section.

5.1. Summary of the Observed Dynamics. The observed dynamics are presented in Figure 7. Increases are shown in colour red, whereas decreases are shown in colour green. The days for which the concentration levels were similar to the days before are shown in yellow. Moreover, the HABs are represented in red. The rains are represented in different shades of blue depending on their intensity (darker for heavier rain). The first day for CDOM, SPM, and Chl-a is marked in red to indicate their presence.

February, a winter month, presents some light to moderate precipitations [48], and an increasing or maintaining trend for CDOM, SPM, and Chl-a. These concentration levels can be explained by the rains. Spring started in March, a month for which the concentrations of Chl-a seem to be a follow-up of the storms in February. SPM presents a peak not related to storms during this month; on the 14th, CDOM does too. Nevertheless, they show different distribu-

tions and may be caused by human factors. March 14th is the day quarantine started.

During the quarantine, the month of April is hard to analyse due to the intense precipitations present in this period. The high CDOM, SPM, and Chl-a values can be explained by those storms. On May 13th, all the concentration levels are lowering; nevertheless, after another intense precipitation event, the CDOM and Chl-a concentration levels rose. Finally, during June, without human activities or storm periods, the CDOM, SPM, and Chl-a concentration levels were lower, although June 22nd, the day after quarantine ended, presents a sudden increase in all three parameters.

It is to be noted that most days that presented increases during the quarantine happened after an intense storm period. Moreover, the quarantine period presents more days with a decreasing trend, especially for May and June, after the rainy season (this season being the last week of March and the month of April). Two out of three HABs correlate with high CDOM, SPM, and Chl-a concentration levels; the outlier may be caused by a nutrient load entering from the Atlantic Ocean. Furthermore, on June 22nd, barely a day after the New Normality was established, an increase can be observed. The data after the quarantine period is not further studied because this study was conducted in June.

Furthermore, to better understand the dynamics, we present three graphics showing the distribution as well as the peak concentration of CDOM, SPM, and Chl-a for each of the studied days. Figures 8–10 present the aforementioned values. For five of the studied days, the distribution cannot be determined due to the high cloud coverage; for those days, it is not represented to avoid misinterpretations since it cannot be stated with accuracy. The days for which was not possible to study the distribution are March 24th, April 13th, April 23rd, June 2nd, and June 12th. The days lockdown started and finished are underlined on the X-axis.

Figure 8 presents the dynamics for CDOM. It can be seen that previous to the lockdown, the highest value was lower; this is due CDOM peaking naturally during spring [34]. The peak on May 23rd comes right after an intense storm period, which is a natural cause for CDOM peaks. What can be observed during the confinement period, though, is the decrease in distribution. Most prelockdown days (except February 2nd) present a high distribution.

When comparing to the results from other authors, Organelli et al. [50] measured the CDOM levels on the NW Mediterranean Sea for two years. For the months studied in this paper, the dynamic observed is an increase in spring and a decrease in June. Later on, El Hourany et al. [51] studied the CDOM levels on the eastern Mediterranean Sea, close to the Nile's mouth. They observed high values from February to April, and they decreased in May and June. Nonetheless, they used a slightly different wavelength (412 nm instead of 440 nm as in this study). Therefore, their results prove the existence of a peak in spring, as has been stated before [34] and as shown in these results. Nevertheless, the numerical data cannot be compared.
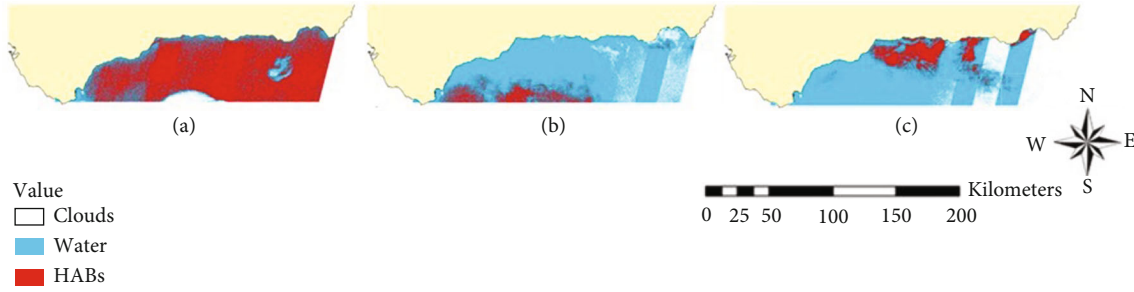
FIGURE 6: HABs during the studied period. Each map represents (a) February 3rd, (b) April 3rd, and (c) May 3rd.
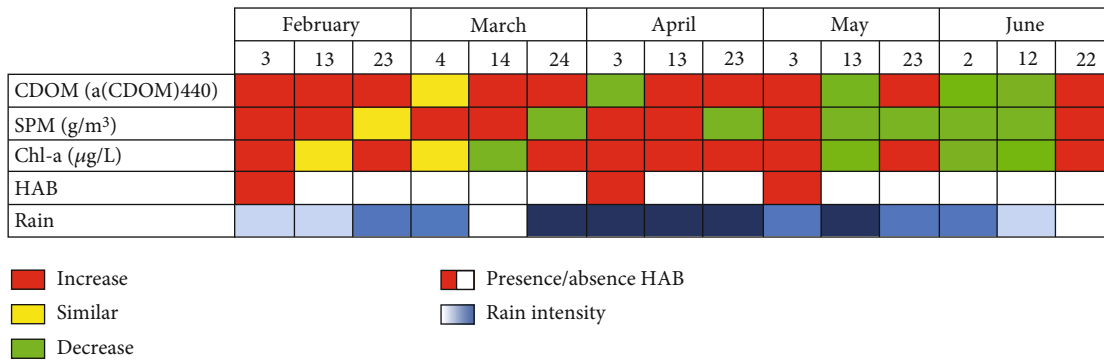
FIGURE 7: Summary of the dynamics and peaks.
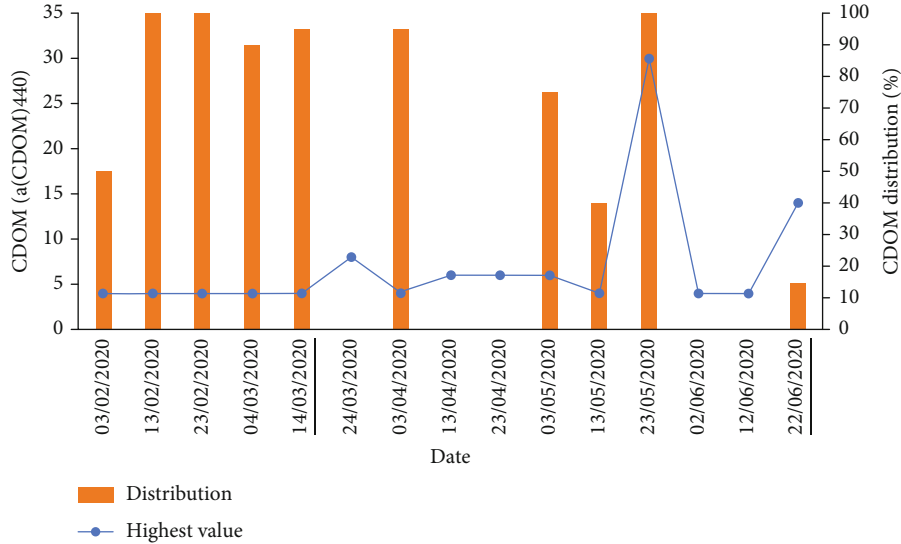
FIGURE 8: CDOM peaks (line) and distribution (columns).

In Figure 9 the evolution of SPM can be observed. This is the parameter which presents the clearest results with both the distribution and its peaks decreasing during the lockdown period. All of the days during lockdown present lower peak values than those from the prelockdown period (except for February 2nd). The distribution decreases for most days as well.

Other authors who have studied SPM values include Cresson et al. [52], who studied the particulate organic mat-ter levels and composition in the Bay of Marseilles, the NW Mediterranean Sea. The units they used (μg/mg) can be con-sidered equivalent to the ones used in our paper (g/m^3), although seawater does not have a density of exactly 1 kg/ 1 dm^3. The values presented are higher than those calculated for the studied period.

Figure 10 shows the evolution of Chl-a distribution and concentration peaks during the studied period. The values decreased at the beginning of quarantine, although they
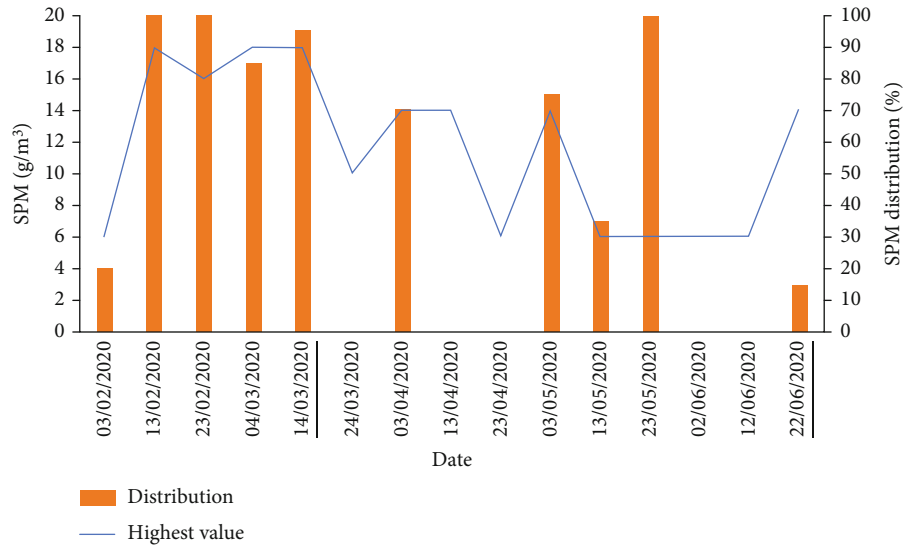
FIGURE 9: SPM peaks (line) and distribution (columns).
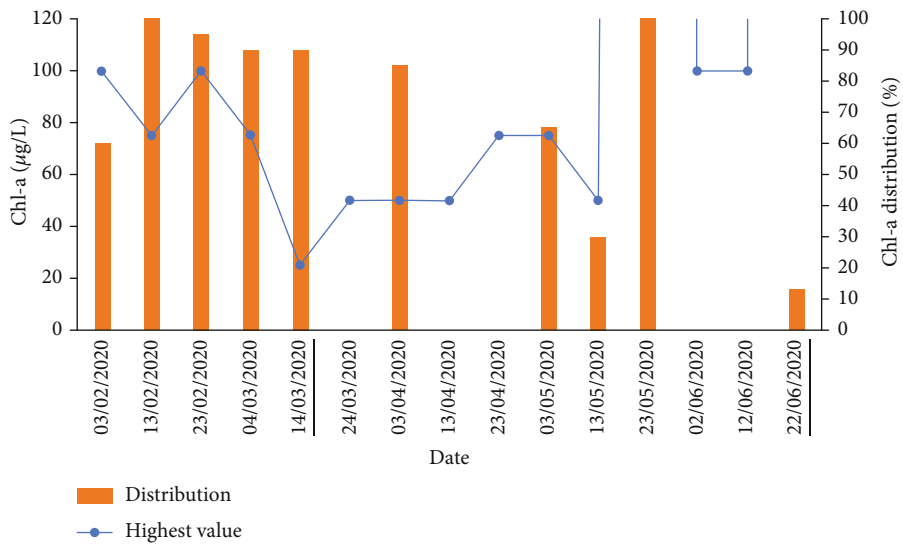
FIGURE 10: Chl-a peaks (line) and distribution (columns).

peaked in spring, as it is natural for Chl-a [41]. The distribution lowered as seen in the days for which it was possible to study it.

To analyse the values of Chl-a, they can be compared to the work conducted by Fabres et al. [53]. As for SPM, the values can be compared, although the density of the water does not make the units completely equivalent. It can be seen that for the days in May, the values on regular years are higher than those for our studied period.

One thing becomes clear when observing Figure 7, the longer the quarantine period had been going on, the lower the concentration levels. Even during spring, for which many of them peak naturally, Slonecker et al. [34], Kang et al. [38, Pérez-Ruzafa et al. [41], and Gobler [45]. Concentration levels before the lockdown are high and not caused by storms since they were lower than those in spring. Nevertheless, the days with high concentration levels during the quarantine period are right after or during storm periods.

5.2. Effects of the Port Reactivation. The quarantine period is characterised by the reduction of port activity. When comparing the March-June period in 2019 and 2020 for the Algeciras Port, Autoridad Portuaria de la Bahía de Algeciras [54], we can observe the shift in dynamics. The passenger traffic decreased an 82.06%, whereas industrial vehicles present a 12.78% reduction. Overall, 42.39% fewer vessels entered the port, and the gross tons shift reaches 13.79%. Furthermore, March et al. [5] showed the rapid port reactivation in Spain in their study.

As shown in Figures 3–5, the concentration levels for CDOM, SPM, and Chl-a increased the day after the

reactivation of port activities. It is important to note that on this date, many restrictions regarding marine transportation had been lifted [22]. Taking this into account and observing both peaks near important ports, it is easy to assert the cause. The plumes are most likely caused by a human factor, the revitalisation of marine transportation. According to Vessel Finder, Historical AIS Data Services [55], the traffic density in the seaport of Algeciras was very high on June 22nd. Although the Malaga port does not seem to present many ships, they were big ships, two of them around 25.000 gross tons [56].

Considering the weather conditions [48], this peak in concentration levels cannot be explained by weather conditions. No storms were present the weeks previous to this date. The most likely explanation is the human impact after the reactivation of port activities. This event generated an anthropogenic impact. As stated before, the plumes seem to have their origin in the two main ports in this area. Although there are more ports in the study area, those two are the most important, with higher trafficaffluence. We see the Algeciras port on the right, while on the left, we see the Malaga port. These are the two most important ports in the area of interest. It is important to note that the plumes have similar behaviour; they drift to the east. It can be explained due to the currents which affect the area; they go from the Atlantic Ocean towards the Mediterranean Sea [57].

Ports are areas with high concentration levels for pollutants [58]. Sipelgas et al. [59] observed the total suspended matter levels on several Estonian harbours for 10 years using MERIS imagery. The behaviour they observed is similar to the one present on the day after the end of quarantine.

5.3. HABs Problematic. The HABs detected in this paper are those associated with high biomass levels. They are dangerous for many reasons, such as eutrophication, gill damage which could kill fish, and food web disruption [60]. They can be caused by toxic or nontoxic species. Nevertheless, it is important to monitor these events due to their negative consequences. Nevertheless, HABs not associated with high biomass cannot be detected with this method. Moreover, HABs are short-spanned phenomena [19], which explains why only three HABs have been observed in this experience. Nonetheless, this does not mean that only three HABs happened during the studied period. The HABs represented in this paper may not be all the blooms that happened during this period. The return time of the images used (10 days) is a problem when monitoring HABs.

It is important to note that even though for June 22nd all concentrations are high near the Algeciras port and the Malaga port, a HAB cannot be seen. Nevertheless, after just one day of marine trafficking, it is to be expected. Ouellette et al. [61] identified, in 2016, the main challenges of remote sensing for marine monitoring purposes. They were reliability, continuity, institutional barriers, knowledge gap, resolution, and coverage. HABs need a high continuity. Later on, in 2018, Burford et al. [62] noted the usefulness of remote sensing for covering large areas and its lack in a high temporal frequency, thus resulting not ideal for HABs monitoring.

Shi et al. [63] included as a challenge the low-time frequency remote sensing presents.

5.4. Localised Tendencies. Several tendencies were observed during the studied period. However, most of them are exposed in Section 4.1. This section deals with those with a more localised extension.

We observe a tendency of higher concentration levels near the Cabo de Gata and Almeria, especially notable for SPM on March 14th (Figure 4(e)). It may be due to the intensive agricultural use of the land in the area [64]. Moreover, this tendency is present during the quarantine, which could be explained since agriculture was not stopped. Pollutants get to the sea through agricultural runoff, a phenomenon that has been studied since the 70s [65]. Like Griffin et al. [66] in 1982, many authors have remarked the impact agricultural runoff has on water quality. Nowadays, the removal of pesticides and pollutants from agricultural runoff is being studied [67].

Furthermore, several days for several parameters present higher concentration levels near the port areas. Besides June 22nd (explained on 4.2.), the most notable one is on March 14th for SPM (Figure 4(e)). It is normal to have high pollution levels near port areas [58], as explained in Section 4.2. Therefore, this peak could be explained by an increase in marine transport activity. The date for these unusually high values near the port is that of the beginning of quarantine, indicating a high activity of the previous days. This activity was caused most likely by many ships returning to the port due to the pandemic.

In addition, the rivers present in this area are either short or wadis. Therefore, it is to be expected not to find a tendency near their river mouths except for when it rains (explained in Section 4.1). Long rivers, with a high flow all year long, carry more pollutants and can affect the sea, as in the Bohai Sea [68].

5.5. Limitations of the Used Technology. The analysis conducted in this paper yields information useful for seawater quality monitoring. Nevertheless, it would be better to be able to have data from more days. Combining Sentinel-2 and Landsat-8 like other researchers have done before would reduce the time between two datasets. Therefore, the monitoring would be more thorough. Statistical analyses could be run (since there are not enough days studied to run a trustworthy t-test to compare results before and during quarantine).

The resolution for some of the bands used is lower than for others, thus creating results with different resolutions. Unfortunately, given the available technology, this cannot be mended. The only option would be to use imagery from other satellite missions. Nonetheless, their cost would be higher than the ideal for this type of study.

There are parameters for which there are not any established indices. ACOLITE only has built-in formulas for SPM, turbidity, Chl-a, HABs, NDVI, particulate backscattering, and temperature. Therefore, other indices cannot be monitored with the proposed system. The obvious solution would be to create those indices, which could be done by

studying the behaviour of those parameters to check which bands would work better and then compare the new indices with real in situ data.

It could be argued that the reliability of remote sensing using satellite imagery is based on contact measures. Nevertheless, the plausible error caused by the calibration is always the same, unlike for contact measures, for which the error changes as the sensor is corroded. Moreover, remote sensing offers periodical results and is less expensive and more sustainable than charting a boat to take contact measures.

6. Conclusions

The study of the water quality has been achieved by analysing satellite imagery using ArcGIS, ESRI [9], and ACOLITE, MUSEUM [10], software to produce indices for a series of environmental parameters. The results (concentration levels) for these parameters have been analysed to study tendencies and possible drivers of change. Furthermore, they have been compared with each other and with weather tables [48].

For several of the days studied, the CDOM, SPM, and Chl-a concentrations peaked simultaneously and showed a similar distribution, presumably due to the storms on the week before each date, causing a massive overland flow. Moreover, the concentrations lowering and dispersing after a storm can be observed in several of the days. Nevertheless, the prequarantine data present more days with high concentrations even though the storms were less intense. The port was reactivated one day after the quarantine was finished, 22nd July. CDOM, SPM, and Chl-a concentrations peaked this day near the Malaga port and the Algeciras port, proving the impact of human activity in an environment that had been undisturbed for several months.

For CDOM, 100% of the days until March 14th present concentration levels higher or similar to those from the previous one. All of them have concentrations on the 0 to 2 a(CDOM)440 and 2 to 4 a(CDOM)440 ranges, covering most of the studied area. Whereas for the quarantine period, a 55% of the days present higher or equal concentration levels than the previous one. For SPM, the contrast is even starker, with 33% of the days during the quarantine presenting increasing tendencies. Meanwhile, all the prequarantine levels (100%) presented an increase. Furthermore, the highest peaks, $18 \, g/m^3$, are presented on February 13th, February 23rd, March 4th, and March 14th. Chl-a levels present a difference that is not as extreme as for SPM; nevertheless, it is higher than for CDOM. An 80% of the studied prequarantine days show higher or similar Chl-a concentrations to the day before (March 14th being the outlier), whilst 67% of the quarantine days present it (although with lower distributions). The Chl-a peak happened during one of the intense storm periods in May. Nonetheless, another peak happened on February 23rd with levels up to $100 \, \mu g/L$.

February 3 presents the biggest HAB and high Chl-a and CDOM concentrations showing a distribution similar to the HAB. It also presents SPM distributed nearshore. The HAB was most likely caused by the high temperatures [48] and the nutrient-rich waters [68] and influenced the Chl-a and CDOM readings. Two more HAB have been observed, one of them, on May 3rd, related to the storms. The other HAB, on April 3rd, does not correlate to the CDOM, SPM, and Chl-a concentration levels or distribution. This HAB is close to the Strait of Gibraltar and could have been caused by nutrient-rich waters entering the Mediterranean Sea. There were only 3 observed HABs during the period. Nevertheless, the most extended one was on February 3rd.

The possible future projects are split into two directions. The first direction would be the continuation of monitoring marine environments. First, other indices could be tested, even some original indices comparing their results to the observed in situ values (from buoys). Moreover, this could be done for other places rather than just the Alboran Sea, and other image sources like Landsat-8 could be used as well. Another future study could be the use of satellite imagery for environmental monitoring during the SARS-CoV-2 quarantine applied to other ecosystems (forests, lakes, wetlands…). It would be interesting to check the effect a prolonged underexposure to human activities could have on these environments. Moreover, it could help us understand their dynamics and processes. Furthermore, wireless sensor networks (WSN) could be employed to improve and verify the data (especially in nonaggressive, hard-to-access environments). By contrasting the data from satellite imagery to that from sensors, the results could be more precise. WSNs have been proved useful for the monitoring of the hydrosphere previously. There are low-cost sensors for monitoring turbidity and SPM, Matos et al. [69]. Areas of interest, like seagrass areas, have already been monitored by multisensory buoys part of a WSN [70] and could benefit from further monitoring.

Data Availability

Publicly available datasets were analysed in this study. This data can be found here: https://scihub.copernicus.eu/dhus/#/home.

Conflicts of Interest

The authors declare no conflict of interest.

Authors' Contributions

All the authors have contributed equally towards the conceptualisation, methodology, development, and conception of the experiments and with reagents/materials/analysis tools. All authors have contributed in writing the paper. All authors have read and agreed to the published version of the manuscript.

Acknowledgments

References

[1] V. Paul, P. C. Shekharaiah, S. Kushwaha, A. Sapre, S. Dasgupta, and D. Sanyal, "Role of algae in CO 2 sequestration addressing climate change: a review," in *Proceedings of Renewable Energy and Climate Change*, pp. 257–265, Maninagar, India, 2019.

[2] C. C. O'Hara, J. C. Villaseñor-Derbez, G. M. Ralph, and B. S. Halpern, "Mapping status and conservation of global at-risk marine biodiversity," *Conservation Letters*, vol. 12, no. 4, p. e12651, 2019.

[3] J. E. van Beusekom, "Eutrophication," in *Handbook on Marine Environment Protection*, M. Salomon and T. Markus, Eds., vol. 1 and 2, pp. 429–445, Springer International Publishing, New York, USA, 2018.

[4] J. D. Nichols and B. K. Williams, "Monitoring for conservation," *Trends in Ecology & Evolution*, vol. 21, no. 12, pp. 668–673, 2006.

[5] D. March, K. Metcalfe, J. Tintoré, and B. J. Godley, "Tracking the global reduction of marine traffic during the COVID-19 pandemic," *Nature Communications*, vol. 12, no. 1, pp. 1–12, 2021.

[6] M. Coll, "Environmental effects of the COVID-19 pandemic from a (marine) ecological perspective," *Ethics in Science and Environmental Politics*, vol. 20, pp. 41–55, 2020.

[7] A. P. Yunus, Y. Masago, and Y. Hijioka, "COVID-19 and surface water quality: improved lake water quality during the lockdown," *Science of the Total Environment*, vol. 731, p. 139012, 2020.

[8] P. Wagh, J. M. Sojan, S. J. Babu, R. Valsala, S. Bhatia, and R. Srivastav, "Indicative lake water quality assessment using remote sensing images-effect of COVID-19 lockdown," *Water*, vol. 13, no. 1, p. 73, 2021.

[9] ArcGIS, ESRI, "ESRI. ArcGIS Pro Website," 2020, https://pro.arcgis.com/es/pro-app/latest/get-started/install-and-sign-in-to-arcgis-pro.html.

[10] Museum Acolite, 2020, https://odnature.naturalsciences.be/remsem/software-and-data/acolite.

[11] M. Parra, "Analysis of the evolution of sea water quality in the Spanish coast from satellite images before and during the quarantine caused by COVID-19, [M.S. thesis]," Universitat Politècnica de València, 2020.

[12] K. Toming, T. Kutser, A. Laas, M. Sepp, B. Paavel, and T. Nõges, "First experiences in mapping lake water quality parameters with Sentinel-2 MSI imagery," *Remote Sensing*, vol. 8, no. 8, p. 640, 2016.

[13] M. Orlandi, F. Silvio Marzano, and D. Cimini, "Remote sensing of water quality indexes from Sentinel-2 imagery: development and validation around Italian river estuaries," in *Proceedings of EGUGA*, p. 19808, Vienna, Austria, 2018.

[14] I. Caballero, F. Steinmetz, and G. Navarro, "Evaluation of the first year of operational Sentinel-2A data for retrieval of suspended solids in medium-to high-turbidity waters," *Remote Sensing*, vol. 10, no. 7, p. 982, 2018.

[15] P. Li, Y. Ke, J. Bai, S. Zhang, M. Chen, and D. Zhou, "Spatiotemporal dynamics of suspended particulate matter in the Yellow River Estuary, China during the past two decades based on time-series Landsat and Sentinel-2 data," *Marine Pollution Bulletin*, vol. 149, p. 110518, 2019.

[16] H. Liu, Q. Li, T. Shi, S. Hu, G. Wu, and Q. Zhou, "Application of sentinel 2 MSI images to retrieve suspended particulate matter concentrations in Poyang Lake," *Remote Sensing*, vol. 9, no. 7, p. 761, 2019.

[17] M. Potes, G. Rodrigues, A. M. Penha et al., "Use of Sentinel 2–MSI for water quality monitoring at Alqueva reservoir," *Proceedings of IAHS*, vol. 380, pp. 73–79, 2018.

[18] M. H. Khalili and M. Hasanlou, "Harmful algal blooms monitoring using SENTINEL-2 satellite images," in *Proceedings of The International Archives of Photogrammetry, Remote Sensing and Spatial Information Sciences*, vol. XLII-4/W18, pp. 609–613, Karaj, Iran, 2019.

[19] G. Alba, F. Anabella, S. Marcelo et al., "Spectral monitoring of algal blooms in an eutrophic lake using Sentinel-2," in *IGARSS 2019 - 2019 IEEE International Geoscience and Remote Sensing Symposium*, pp. 306–309, Yokohama, Japan, 2019.

[20] T. Cecchi, "Analysis of volatiles organic compounds in Venice lagoon water reveals COVID 19 lockdown impact on microplastics and mass tourism related pollutants," *Science of the Total Environment*, vol. 783, no. 20, p. 146951, 2021.

[21] P. Silva, M. Ávila, and M. Gonçalves, "Air and water quality improvement during COVID-19 lockdown," *Proceedings of the 7th International Conference on Geographical Information Systems Theory, Applications and Management*, C. Grueau, R. Laurini, and L. Ragia, Eds., pp. 109–115, 2021.

[22] Orden TMA/419/2020, *Ministerio de Transportes, Movilidad y Agenda Urbana «BOE» núm. 141, de 19 de mayo de 2020 Referencia: BOE-A-2020-5125*, Ministerio de Transportes, Movilidad y Agenda Urbana, Madrid, 2020.

[23] Orden TMA/258/2020, *Ministerio de Transportes, Movilidad y Agenda Urbana «BOE» núm. 76, de 20 de marzo de 2020 Referencia: BOE-A-2020-3894*, Boletín Oficial del Estado 76, Ministerio de Transportes, Movilidad y Agenda Urbana, Madrid, 2020.

[24] T. Oguz, D. Macias, J. Garcia-Lafuente, A. Pascual, and J. Tintore, "Fueling plankton production by a meandering frontal jet: a case study for the Alboran Sea (Western Mediterranean)," *PLoS One*, vol. 9, no. 11, p. e111482, 2014.

[25] Esa sentinel online, "Sentinel-2, Sentinel Products," 2020, https://sentinel.esa.int/web/sentinel/missions/sentinel-2.

[26] Esa sentinel online, "Level-1," 2020, https://sentinel.esa.int/web/sentinel/user-guides/sentinel-2-msi/processing-levels/level-1.

[27] M. Sozzi, F. Marinello, A. Pezzuolo, and L. Sartori, "Benchmark of satellites image services for precision agricultural use," in *Proceedings of the AgEng conference*, pp. 8–11, Wageningen, The Netherlands, 2018.

[28] Copernicus open access hub, "Home," 2020, https://scihub.copernicus.eu/dhus/#/home.

[29] Q. Vanhellemont and K. Ruddick, "Acolite for Sentinel-2: aquatic applications of MSI imagery," *In Proceedings of the 2016 ESA Living Planet Symposium*, L. Ouwehand, Ed., , pp. 9–13, Prague, Czech Republic, 2016.

[30] Q. Vanhellemont, "Adaptation of the dark spectrum fitting atmospheric correction for aquatic applications of the Landsat and Sentinel-2 archives," *Remote Sensing of Environment*, vol. 225, pp. 175–192, 2019.

[31] ESRI ArcGIS Pro, 2020, https://pro.arcgis.com/es/pro-app/get-started/install-and-sign-in-to-arcgis-pro.htm.

[32] ARCGIS Desktop, "Mosaic to new raster," 2020, https://desk top.arcgis.com/en/arcmap/latest/tools/data-management-toolbox/mosaic-to-new-raster.htm.

[33] ARCGIS Desktop, "Raster calculator," 2020, https://desktop.arcgis.com/es/arcmap/latest/tools/spatial-analyst-toolbox/raster-calculator.htm.

[34] E. T. Slonecker, D. K. Jones, and B. A. Pellerin, "The new Landsat 8 potential for remote sensing of colored dissolved organic matter (CDOM)," *Marine Pollution Bulletin*, vol. 107, no. 2, pp. 518–527, 2016.

[35] J. Chen, W. Zhu, Y. Q. Tian, Q. Yu, Y. Zheng, and L. Huang, "Remote estimation of colored dissolved organic matter and chlorophyll-a in Lake Huron using Sentinel-2 measurements," *Journal of Applied Remote Sensing*, vol. 11, no. 3, p. 036007, 2017.

[36] J. Chen, W. Zhu, Y. Q. Tian, and Q. Yu, "Monitoring dissolved organic carbon by combining Landsat-8 and Sentinel-2 satellites: case study in Saginaw River estuary, Lake Huron," *Science of the Total Environment*, vol. 718, p. 137374, 2020.

[37] S. Novoa, D. Doxaran, A. Ody et al., "Atmospheric corrections and multi-conditional algorithm for multi-sensor remote sensing of suspended particulate matter in low-to-high turbidity levels coastal waters," *Remote Sensing*, vol. 9, no. 1, p. 61, 2017.

[38] L. Kang, Y. He, L. Dai et al., "Interactions between suspended particulate matter and algal cells contributed to the reconstruction of phytoplankton communities in turbulent waters," *Water Research*, vol. 149, pp. 251–262, 2019.

[39] B. Nechad, A. Dogliotti, K. Ruddick, and D. Doxaran, "Particulate backscattering retrieval from remotely-sensed turbidity in various coastal and riverine turbid waters," *Proceedings of ESA Living Planet Symposium*, L. Ouwehand, Ed., p. 740, 2016.

[40] M. Chapalain, *Dynamique des matières en suspension en mer côtière: caractérisation, quantification et interactions sédiments/matière organique, [Ph.D. thesis]*, Université de Bretagne Occidentale Brest, 2019.

[41] A. Pérez-Ruzafa, S. Campillo, J. M. Fernández-Palacios et al., "Long-term dynamic in nutrients, chlorophyll a, and water quality parameters in a coastal lagoon during a process of eutrophication for decades, a sudden break and a relatively rapid recovery," *Frontiers in Marine Science*, vol. 6, p. 26, 2019.

[42] W. J. Moses, A. A. Gitelson, S. Berdnikov, V. Saprygin, and V. Povazhnyi, "Operational MERIS-based NIR-red algorithms for estimating chlorophyll-a concentrations in coastal waters – the Azov Sea case study," *Remote Sensing of Environment*, vol. 121, pp. 118–124, 2012.

[43] M. A. Warren, S. G. Simis, V. Martinez-Vicente et al., "Assessment of atmospheric correction algorithms for the Sentinel-2A MultiSpectral imager over coastal and inland waters," *Remote Sensing of Environment*, vol. 225, pp. 267–289, 2019.

[44] N. Pahlevan, B. Smith, J. Schalles et al., "Seamless retrievals of chlorophyll-a from Sentinel-2 (MSI) and Sentinel-3 (OLCI) in inland and coastal waters: a machine-learning approach," *Remote Sensing of Environment*, vol. 240, p. 111604, 2020.

[45] C. J. Gobler, "Climate change and harmful algal blooms: insights and perspective," *Harmful Algae*, vol. 91, p. 101731, 2020.

[46] G. A. Carvalho, P. J. Minnett, V. F. Banzon, W. Baringer, and C. A. Heil, "Long-term evaluation of three satellite ocean color algorithms for identifying harmful algal blooms (Karenia brevis) along the west coast of Florida: a matchup assessment," *Remote Sensing of Environment*, vol. 115, no. 1, pp. 1–18, 2011.

[47] M. W. Matthews, S. Bernard, and L. Robertson, "An algorithm for detecting trophic status (chlorophyll-a), cyanobacterial-dominance, surface scums and floating vegetation in inland and coastal waters," *Remote Sensing of Environment*, vol. 124, pp. 637–652, 2012.

[48] Junta de Andalucia Consejería de Agricultura, Ganaderia, Pesca Y Desarrollo Sostenible, "Temperaturas y precipitaciones semanales AEMET," 2020, https://www.juntadeanda lucia.es/organismos/agriculturaganaderiapescaydesarrollosos tenible/servicios/estadistica-cartografia/estadisticas-agricolas/paginas/estadisticas-aemet.html.

[49] C. E. Binding, A. Zastepa, and C. Zeng, "The impact of phytoplankton community composition on optical properties and satellite observations of the 2017 western Lake Erie algal bloom," *Journal of Great Lakes Research*, vol. 45, no. 3, pp. 573–586, 2019.

[50] E. Organelli, A. Bricaud, D. Antoine, and A. Matsuoka, "Seasonal dynamics of light absorption by chromophoric dissolved organic matter (CDOM) in the NW Mediterranean Sea (BOUSSOLE site)," *Deep Sea Research Part I: Oceanographic Research Papers*, vol. 91, pp. 72–85, 2014.

[51] R. El Hourany, A. Fadel, E. Gemayel, M. Abboud-Abi Saab, and G. Faour, "Spatio-temporal variability of the phytoplankton biomass in the Levantine basin between 2002 and 2015 using MODIS products," *Oceanologia*, vol. 59, no. 2, pp. 153–165, 2017.

[52] P. Cresson, S. Ruitton, M. F. Fontaine, and M. Harmelin-Vivien, "Spatio-temporal variation of suspended and sedimentary organic matter quality in the Bay of Marseilles (NW Mediterranean) assessed by biochemical and isotopic analyses," *Marine Pollution Bulletin*, vol. 64, no. 6, pp. 1112–1121, 2012.

[53] J. Fabres, A. Calafat, A. Sanchez-Vidal, M. Canals, and S. Heussner, "Composition and spatio-temporal variability of particle fluxes in the Western Alboran Gyre, Mediterranean Sea," *Journal of Marine Systems*, vol. 33, pp. 431–456, 2002.

[54] Autoridad Portuaria de la Bahía de Algeciras, "Estadísticas," 2020, https://www.apba.es/estadisticas.

[55] Historical AIS Data Services, 2020, https://www.vesselfinder.com/historical-ais-data#traffic-density.

[56] Puerto de Malaga, "Información de atraques," 2020, https://www.puertomalaga.com/es/informacion-atraques/.

[57] J. Isern-Fontanet, E. García-Ladona, J. A. Jiménez-Madrid et al., "Real-time reconstruction of surface velocities from satellite observations in the Alboran Sea," *Remote Sensing*, vol. 12, no. 4, p. 724, 2020.

[58] A. G. Gómez, P. F. Valdor, B. Ondiviela, J. L. Díaz, and J. A. Juanes, "Mapping the environmental risk assessment of marinas on water quality: the atlas of the Spanish coast," *Marine Pollution Bulletin*, vol. 139, pp. 355–365, 2019.

[59] L. Sipelgas, R. Uiboupin, A. Arikas, and L. Siitam, "Water quality near Estonian harbours in the Baltic Sea as observed from entire MERIS full resolution archive," *Marine Pollution Bulletin*, vol. 126, pp. 565–574, 2018.

[60] R. Kudela, E. Berdalet, and E. Urban, *Harmful Algal Blooms: A Scientific Summary for Policy Makers*, 2015.

[61] W. Ouellette and W. Getinet, "Remote sensing for marine spatial planning and integrated coastal areas management: achievements, challenges, opportunities and future prospects," *Remote Sensing Applications: Society and Environment*, vol. 4, pp. 138–157, 2016.

[62] M. A. Burford, D. P. Hamilton, and S. A. Wood, "Emerging HAB research issues in freshwater environments," in *Global Ecology and Oceanography of Harmful Algal Blooms. Ecological Studies (Analysis and Synthesis)*, P. Glibert, E. Berdalet, M. Burford, G. Pitcher, and M. Zhou, Eds., vol. 232, pp. 381–402, Springer, Cham., Switzerland AG, 2018.

[63] K. Shi, Y. Zhang, B. Qin, and B. Zhou, "Remote sensing of cyanobacterial blooms in inland waters: present knowledge and future challenges," *Science Bulletin*, vol. 64, no. 20, pp. 1540–1556, 2019.

[64] J. L. Caparrós-Martínez, N. Rueda-Lópe, J. Milán-García, and J. de Pablo Valenciano, "Public policies for sustainability and water security: the case of Almeria (Spain)," *Global Ecology and Conservation*, vol. 23, p. e01037, 2020.

[65] D. A. Haith and J. V. Dougherty, "Nonpoint source pollution from agricultural runoff," *Journal of the Environmental Engineering Division*, vol. 102, no. 5, pp. 1055–1069, 1976.

[66] R. C. Griffin and D. W. Bromley, "Agricultural runoff as a nonpoint externality: a theoretical development," *American Journal of Agricultural Economics*, vol. 64, no. 3, pp. 547–552, 1982.

[67] J. Vymazal and T. Březinová, "The use of constructed wetlands for removal of pesticides from agricultural runoff and drainage: a review," *Environment International*, vol. 75, pp. 11–20, 2015.

[68] Q. Li, T. Wang, Z. Zhu et al., "Using hydrodynamic model to predict PFOS and PFOA transport in the Daling River and its tributary, a heavily polluted river into the Bohai Sea, China," *Chemosphere*, vol. 167, pp. 344–352, 2017.

[69] T. Matos, C. L. Faria, M. S. Martins, R. Henriques, P. A. Gomes, and L. M. Goncalves, "Development of a cost-effective optical sensor for continuous monitoring of turbidity and suspended particulate matter in marine environment," *Sensors*, vol. 19, no. 20, p. 4439, 2019.

[70] S. Sendra, L. Parra, J. Lloret, and J. M. Jiménez, "Oceanographic multisensor buoy based on low cost sensors for Posidonia meadows monitoring in Mediterranean Sea," *Journal of Sensors*, vol. 2015, Article ID 920168, 23 pages, 2015.

Research Article

Broadening the Research Pathways in Smart Agriculture: Predictive Analysis Using Semiautomatic Information Modeling

Komal Sharma,[1] **Chetan Sharma,**[2] **Shamneesh Sharma** ![ORCID],[2] **and Evans Asenso** ![ORCID][3]

[1]*Punjabi University, Patiala, India*
[2]*UpGrad Education Private Limited, Mumbai, India*
[3]*Department of Agricultural Engineering, School of Engineering Sciences, University of Ghana, Accra, Ghana*

Correspondence should be addressed to Evans Asenso; easenso@ug.edu.gh

Agriculture has become more industrialized and intensive due to the rising demand for food in quality and quantity. Agricultural modernization will be made possible by the Internet of Things (IoT), a technology with a great promise for revolutionizing the industry. Agricultural products will be in high demand by 2050 due to a 30% increase in the global population, so there is a need to devise new mechanisms for agriculture, and smart agriculture is one of those mechanisms; however, smart agriculture needs to be explored further to realize its potential fully. So, to explore the potential of this field, the researchers have used a corpus that is extracted from the Scopus database from the year 2008 to the year 2022 and applied the LDA technique. A corpus of 4309 articles was selected from the Scopus database to apply the latent Dirichlet analysis (LDA) model to predict research areas for smart agriculture. Using IoT technology, farmers and producers may better manage their resources, such as fertilizer consumption and the number of trips made by farm vehicles, while minimizing waste and maximizing productivity, including water, electricity, and other inputs. This data-driven experimental study identifies smart agriculture research trends by implementing a topic modeling technique previously used in smart agriculture. The authors have created seventeen research themes in smart agriculture based on the LDA topic modeling. This analysis suggests that the indicated areas are in the growth phase and require further research and exploration.

1. Introduction

Digital technologies like the Internet of Things (IoT) are reshaping agriculture. When it comes to farming, what is IoT? The IoT connects "dumb" devices. IoT is all about data [1]. Data is becoming a valuable resource for our world. Farmers may become more intelligent and safe by using data from gadgets to adapt to changing conditions more readily and farm more efficiently [2]. To free up resources, farmers can use the ability to monitor agricultural conditions and infrastructure from afar [3]. Many sectors and industries have adopted IoT to reduce errors and improve performance in manufacturing, energy, health care, and communication [1]. Farm devices can collect and deliver data remotely to their owners using IoT.

Farmers can save time and money using IoT to keep tabs on-farm operations and efficiency, make more informed deci-

sions about boosting productivity, and respond more quickly to changing conditions. In this case, it is putting data ahead of the farmer's intuition [2]. A trough's water supply, the amount of fertilizer to use on a crop, and which ewe to check when lambing are all things a farmer could know about.

Smart agriculture is necessary since 70% of the farming time is spent monitoring and analyzing crop status rather than performing actual field labor [3]. Given the industry's size, it needs various technology and precise solutions to ensure sustainability while reducing environmental damage. Sensors and communication technologies have provided farmers with a remote sight of their fields, allowing them to watch what is happening without leaving home. Wireless sensors make monitoring crops in real-time with greater precision and, more importantly, detecting the early stages of undesirable conditions easier [4]. This is why "smart agriculture uses innovative equipment and kits from seeding to
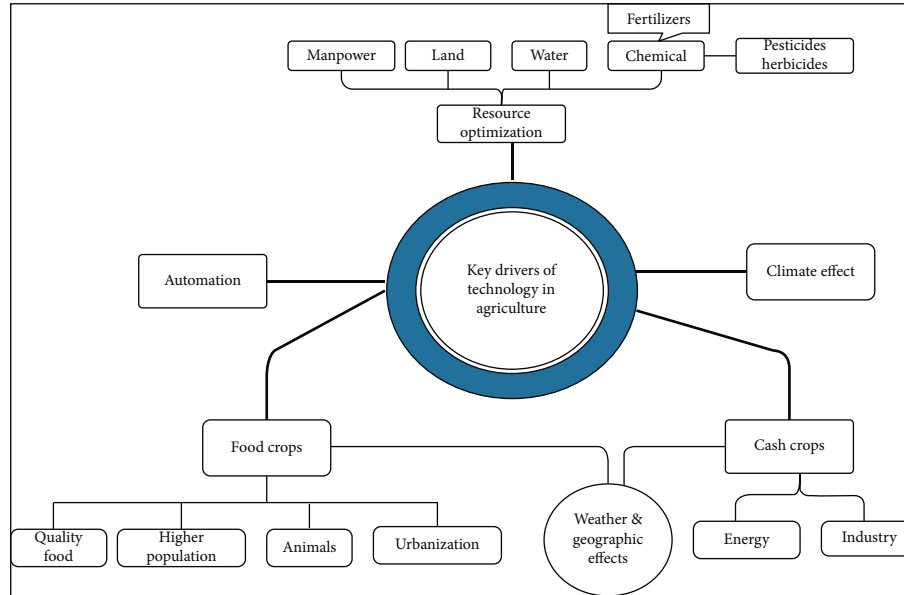
FIGURE 1: Technology's key drivers in the agriculture industry.

crop harvesting, storage, and transportation. The operation is smart and cost-effective due to its accurate monitoring capabilities and prompts reporting using a variety of sensors. Various autonomous tractors, harvesters, robotic weeders, drones, and satellites supplement agriculture equipment [5]. Sensors can be instantly deployed, started collecting data, and made available for further online study. By enabling precise data collection at each area, sensor technology allows crop and site-specific agriculture". IoT and its apps are only scratching the surface of what they can do and have yet to impact people's lives significantly, and everyone can see this. However, given the recent rise in IoT technology in agricultural applications, we can expect it to play a significant role. Figure 1 summarizes the key factors driving agricultural technology.

There are reasonable efforts to emphasize the importance of IoT in agriculture; most published work [6] focuses solely on applications. However, in light of the most recent facts and data, most current publications either give little insight or place a limited emphasis on diverse IoT-based designs, prototypes, advanced approaches, IoT for food quality, and other future issues. The current state of IoT-based agriculture research is examined in this paper. Farmers are either delaying or refusing to change their traditional techniques, which might further depress India's GDP. Recently skilled migrants from all across India who returned to their homelands during the COVID-19 pandemic selected farming as a profession and had no plans to return. These migrants may move closer to smart agricultural systems since it takes less time to persuade them to use them than traditional farmers.

(i) Remote monitoring of agricultural infrastructure and conditions can save farmers time and labor by reducing the frequency of on-site field inspections

(ii) Farmers benefit from data analysis

(iii) Gaining insights from real-time data throughout a value chain allows farmers to respond faster to market requests

(iv) The food manufacturing process should improve efficiency to lower food waste, speed up the time to market, and improve traceability. This will allow us to demonstrate to our consumers that our food is safe and sustainable

(v) Research, development, and adaptation to new technologies ensure continued productivity and innovation

The first objective of this study is to do a meta-analysis of the collected corpus. The second objective is to forecast the present research areas and trends as 2, 5, and 10 topics, as highlighted in Table 1. The third objective is to examine in-depth the current research trends to assist future researchers in determining the correct research directions in the field of smart agriculture.

2. Review of Literature

IoT is revolutionizing agriculture by bringing together various approaches, such as accuracy and conservative farming, to help farmers overcome obstacles in the field. Jayaraman et al. [7] discussed using IoT, cloud computing, mobile computing, and smart agriculture to develop a "phononet" system, an open system of wireless sensors that share information and communicate. For many years, devices presently labeled as IoT have been deployed in agriculture. The Bosch technology corporation provides IoT-based data management strategies to monitor agricultural yield and diseases [8]. A platform based on IoT developed by Intel helps agricultural solutions operate more efficiently by improving the

TABLE 1: Topic labels and high-loading research articles.

Topic ID	Key terms	Topic label	High loading paper	Count of studies	Contribution (%)
2.1	Smart, application, network, agricultural, device, propose, information, provide, communication, security, model, energy, management, service, present, wireless, industry, cloud, design, challenge	Security and privacy in smart agriculture	[34] [35] [36]	2361	99.9 99.85 99.81
2.2	Water, crop, soil, farmer, irrigation, monitor, control, plant, temperature, time, propose, smart, field, monitoring, farm, farming, agricultural, moisture, condition, production	Monitoring and control system in agriculture	[37] [38] [39]	1948	99.82 99.82 99.81
5.1	Machine, model, image, disease, crop, propose, detection, learn, learning, plant, result, time, prediction, deep, accuracy, method, technique, network, classification, neural	Intelligent disease detection models	[40] [41] [42]	464	99.86 99.85 99.80
5.2	Smart, application, device, security, cloud, network, service, provide, compute, propose, architecture, communication, present, challenge, environment, user, information, solution, platform, data	Data security challenges in smart agriculture	[43] [44] [45]	919	99.88 99.84 99.82
5.3	Water, soil, irrigation, crop, farmer, control, monitor, temperature, smart, moisture, field, plant, time, monitoring, humidity, farm, propose, parameter, condition, farming	Smart monitoring system in agriculture	[46] [47] [48]	1373	99.89 99.88 99.84
5.4	Agricultural, food, production, smart, information, farming, development, management, application, product, supply, farm, industry, research, chain, model, study, farmer, process, sector	Production and supply chain management in agriculture	[49] [50] [51]	978	99.87 99.86 99.82
5.5	Network, energy, wireless, node, low, power, application, propose, communication, result, consumption, design, cost, performance, device, monitoring, smart, transmission, range, area	Cost-effective communication system in smart agriculture	[52] [53] [54]	575	99.77 99.73 99.73
10.1	Monitor, temperature, monitoring, time, control, humidity, design, real, environmental, wireless, low, device, application, parameter, greenhouse, cost, develop, network, field, soil	Greenhouse monitoring system	[55] [56] [57]	453	99.89 99.67 99.64
10.2	Application, smart, architecture, platform, model, cloud, propose, service, network, information, provide, solution, device, process, management, present, compute, support, data, precision	Service-based industry for smart agriculture	[58] [59] [60]	440	99.86 99.85 99.82
10.3	Smart, application, device, city, network, challenge, provide, field, industry, make, communication, area, cloud, machine, connect, home, research, compute, present, human	Cloud-based smart applications in agriculture	[61] [62] [63]	442	99.86 99.86 99.85
10.4	Network, energy, wireless, node, power, low, propose, communication, application, consumption, result, device, performance, area, smart, transmission, range, cost, cluster, show	Energy-efficient smart transmission system	[64] [65] [66]	479	99.87 99.85 99.80
10.5	Agricultural, information, intelligent, production, management, product, application, development, improve, control, design, chain, supply, environment, platform, monitoring, problem, greenhouse, layer, modern	Smart solutions for modern farming	[67] [68]	260	99.83 99.80 99.77
10.6	Water, irrigation, soil, moisture, control, crop, smart, plant, monitor, temperature, farmer, field, propose, level, farming, farm, time, humidity, parameter, agricultural	Smart irrigation system for agriculture	[47] [69] [70]	810	99.94 99.93 99.91
10.7	Security, device, blockchain, smart, attack, application, propose, network, secure, privacy, compute, edge, cloud, issue, provide, challenge, communication, authentication, computing, scheme	Blockchain-based security system for agriculture	[71] [72] [73]	218	99.29 98.72 95.35

TABLE 1: Continued.

Topic ID	Key terms	Topic label	High loading paper	Count of studies	Contribution (%)
10.8	Crop, farmer, soil, farming, disease, plant, farm, agricultural, yield, production, field, increase, smart, propose, machine, pest, time, weather, make, growth	Production-based smart system for agriculture	[74] [75] [76]	461	99.90 99.87 99.86
10.9	Food, agricultural, study, research, production, industry, sector, development, supply, farmer, chain, smart, develop, management, farming, farm, sustainable, challenge, digital, business	Industry 4.0 in agriculture	[77] [50] [78]	489	99.94 99.93 99.91
10.10	Model, machine, image, learn, propose, result, detection, learning, method, deep, accuracy, prediction, time, classification, neural, network, technique, feature, algorithm, disease	Image-based classification techniques in intelligent agriculture	[79] [80] [41]	257	99.69 93.38 91.87

interoperability of services [9]. As part of the MIT Media Lab Open Agriculture Initiative, Google has shared its vision for a more sustainable food system [10]. For efficient seed planting, "sensors and vision-based technology" help determine the distance and depth. An autonomous robot named Agribot is being developed to sow seeds using sensors and a vision-based [11]. Technology and economic sustainability go hand in hand. A study was conducted in Pakistan to determine the commercial viability of a proposed crop insurance plan and assess the demand for crop insurance in various flood-prone rural districts of Khyber Pakhtunkhwa Province [12]. Additional research revealed that farm households in the study area faced several barriers to adapting to climate variability, including a lack of labor, an insecure land tenure system, a lack of market access, poverty, a lack of governmental support, a lack of access to assets, a lack of water sources, a lack of credit sources, and a lack of knowledge and information [13]. One study found a link between poverty reduction and natural and social capital for sustainable livelihood. The research provides empirical and quantitative evidence on poverty alleviation, and the conclusions will improve agricultural households' sustainability [14]. A study also uses natural and agricultural resources in Northwestern Pakistan to create a livelihood vulnerability index (LVI), LVI-IPCC, and livelihood effect index [15].

Further, several noncontact sensing methods for determining the seed flow rate are proposed in [16], "where the sensors were equipped with LEDs, infrared, visible light, laser-LED, and a radiation reception element". The output voltage fluctuates depending on how the seeds move through the sensor and band of light rays and how the shades fall on the reception parts [17]. Therefore, the seed flow rate is calculated based on the signal information about the passing seeds. Researchers offer an expert system for evaluating the viability of agricultural land in a 2019 study by combining sensor networks with artificial intelligence systems such as neural networks and multilayer perceptron [18]. The proposed method is intended to assist farmers in categorizing agricultural land for cultivation into the most suitable, suitable, somewhat suitable, and unsuitable categories. In a recent study, researchers used citrus fruits data labeled by a domain expert with four severity levels (high, medium, low, and healthy) to train a deep neural network (DNN) model to detect disease by severity [19]. The model has a 98% likelihood of predicting low severity and a 98% chance of predicting high seriousness. In a subsequent study, the author takes advantage of blockchain's potential benefits, combines it with SDN, and provides justification for worries about energy consumption and security [20]. In the most recent survey, authors applied the same blockchain technology integration technology to different platforms. LDA was used to anticipate blockchain research trends. The researchers have predicted 17 scientific trends that deserve more attention. According to the literature, LDA approaches anticipate smart agriculture research trends [21]. The researcher created a novel routing protocol for IoT networks with a cluster topology using a blockchain-based architecture for the SDN controller. The research concepts of the existing state of the art and its differentiation from the current state are represented in Table 2.

3. Topic Modeling

Data mining is an emerging field to extract data from unstructured formats. Topic modeling is a powerful technique in text mining in natural language processing to explore the relationship between the data and collected documents [22]. This technique is used by various researchers in their native fields, like medical, semantic analysis [23], and engineering [24], to conclude the relationship between the documents and topics. Techniques like latent Dirichlet allocation (LDA), nonnegative matrix factorization (NMF), latent semantic analysis (LSA), parallel latent Dirichlet allocation (PLDA), and Pachinko allocation model (PAM) were used in the topic modeling; among all, LDA is intensively used by researchers. The topic modeling technique is similar to the dimensionality reduction technique used for numerical data. A bag of words (BOW) is created from the dictionary of words, and topic modeling extracts the required features from this BOW. The words contained in the corpus are viewed as a significant feature in NLP.

NLP considers each word as a feature to train the model. This technique helps us find the right content instead of analyzing the accurate data. LDA is used to attain a relationship among the documents in the collected dataset, and results

TABLE 2: Existing and current research differentiation.

Existing research Title of research study	Research concept	Current research
"Knowledge domain and emerging trends of climate-smart agriculture: a bibliometric study"	A bibliometric study of the literature written on the topic of climate-smart agriculture between the years 2010 and 2021	In the current research, the LDA technique has been applied to Scopus dataset from 2008 to 2022
"Privacy and security in smart and precision farming: a bibliometric analysis"	All papers in the ISI Web of Science database totaled around 150 between 2008 and 2018 are considered. Through the use of bibliometric analysis, the number of publications and citations is discussed	The difference lies in the dataset and the technique used for the analysis
"Wireless sensor networks in agriculture: insights from bibliometric analysis"	The current dataset comprising 2444 documents after refining the dataset and subject area is based upon WSN	The final corpus comprises 4309 documents, whereas the subject area defined by the researchers is smart agriculture
"Deep learning for smart agriculture: concepts, tools, applications, and opportunities"	The researchers presented a systematic literature review of all the deep learning techniques used in agriculture	The researchers present a technical perspective of smart agriculture with current research trends
"Latent DIRICHLET allocation (LDA) based information modeling on BLOCKCHAIN technology: a review of trends and research patterns used in the integration"	LDA technique has been applied to blockchain dataset and predicted the current research trends	The researchers have applied the same technique but used a different dataset to predict the current research trends
"Interpreting atomization of agricultural spray image patterns using latent Dirichlet allocation techniques"	The researchers have applied latent Dirichlet allocation (LDA) to discover latent features of spray videos	The researchers have collected and examined 4309 research papers that were published during 2008-2022 using the same technique

are represented statistically and graphically. To develop LDA, variational exception maximization (VEM) algorithm [25] is used to estimate the similarities from the corpus. Usually, the top few words are picked up from the BOW as this approach lacks semantics in the sentence. LDA follows the concept of probabilistic distribution, so each document in the corpus portrays the probabilistic distribution of topics, and each extracted topic depicts the probabilistic distribution of words. It led to concluding a clear vision of the topic connection. LDA is applied to retrieve critical information or analysis from unstructured data. For example, research on social media makes users understandable reactions and conversations among the people connected in social media to conclude the patterns [26].

4. Methodology

The stepwise procedure of whatever tasks have been completed is affectingly explained, which picture quality defines our research methodology to predict the research trends of IoT agriculture. The methods used to conduct this review are depicted in Figure 2, in which three phases are involved. The first phase of research is data collection; in the second phase, collected data is preprocessed; finally, in the third phase, data is analyzed, and results are depicted.

4.1. Corpus. The primary sources of data collection and formation of the research corpus were the various online digital libraries, journals, and conference proceedings available to users through Google Scholar. The search keywords for digital libraries have been selected based on topic selection. The
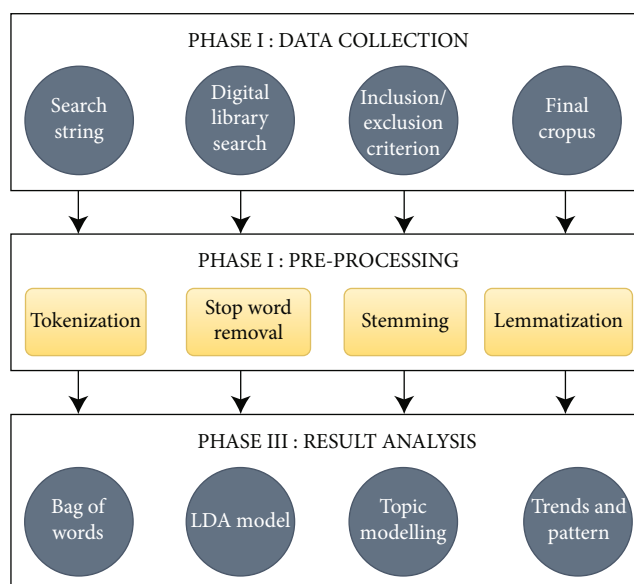
FIGURE 2: Proposed methodology.

research works of Sehra et al. [27] have influenced them to experiment. The search phrases identified were "IoT agriculture". Scopus is considered the most extensive database for published articles globally. The string is run on the Scopus platform, and 4803 articles were extracted from the Scopus database. The specific keywords in the publication's title, abstract, and keywords were collected by searching for them in various databases.

Further processing required inclusion and exclusion criteria to finalize the corpus, so, for inclusion criteria, we considered the research papers published in English only. Then, the studies concerning IoT agriculture were only considered. Under the exclusion procedure, we excluded and removed those studies published in different native languages. In addition, studies having missing information like author, abstract, title, and year were excluded from the corpus. After applying the requirements, 4309 studies were considered for the current research. Figure 3 represents the year-wise growth in article publication in IoT agriculture. It is clear from Figure 3 that after 2015 there has been tremendous growth in publications. The leading publication is in 2021, 26.43% of the total corpus; in 2020, 21.95% of an article was published. In 2022 as per data, there is 0.07% publication, which can be increased by the end of the year.

This area of research is published in various reputed journals. Some top-rated journals or dominating journals in IoT agriculture are shown in Figure 4. Dominating journal analysis shows maximum participation from the *Advances in Intelligent Systems and Computing*, which has 134 articles having 0.031%, and this journal belongs to Springer, having H-Index 48 and 0.66 as its impact factor.

4.2. Preprocessing. It is a preliminary step that processes the dataset or the information collected. The objective of preprocessing is to discard the extraneous information inside the information. Preprocessing removes unwanted words and characters from the accumulated or collected corpus and improves the dataset's quality. As a result, the profile of further processing becomes more accurate and acceptable. In the collected corpus, the author used four types of data for LDA modeling: title of the paper, year of publication, journal of published article, abstract, and keywords of the documents. Further, abstract and keywords are combined under the same column. A sample of the loading corpus is shown in Table 3.

The first step to performing on the uploaded corpus is to token the words so that all the abstracts per title are tokenized into tokens. The generated tokens are then transformed into lowercase letters for each document. In tokenization, the focus is on removing the punctuation marks, single characters, and other special characters like ";", ",", ".", "/", "\", "brackets", "!". Further, any equation or formula used in the abstract was removed. Also, the numerical values were eradicated to get a full-fledge textual token [28]. Finally, after tokenization, the words which have no meaning are removed. The stop words are the commonly used words such as "the", "if", "but", "a", or "an". These words take up space in our corpus and consume valuable processing time. Thus, it becomes crucial to remove these stop removals, and here in our experimentation, we have used Natural Language Toolkit (NLTK). This toolkit has stop words stored in more than sixteen languages. Here, the English-language stop words in the NLTK library and other phrases used to build the corpus were removed from the corpus [29].

Further, stemming is reducing a word to its word stem. Stemming is essential in natural language understanding and natural language processing, endeavoring to extract the root or core word that is usually appended with the English suffixes and prefixes. It erases all the extraneous parts in the word and sources out the accurate, meaningful word. For example, use is the core word that can be extracted by stemming the word useless, useful, and uses. To prepare an adequate corpus, words stem from their original form using the Snowball stemmer algorithm [30], and the resulting base keywords are stored in the cleansed corpus. Finally, the words which were previously stemmed need to be lemmatized. Lemmatization is when the context is considered, and stemmed words are converted into more meaningful base words or lemmas. This phase targets removing inflected words and outputs the dictionary form of a word [31].

5. Latent Dirichlet Allocation

Latent Dirichlet allocation (LDA) is the most popular technique in NLP, so data is fed to the LDA model after preprocessing. Before sending data, bigrams and trigrams are removed from the corpus. Two words that occur together are named bigrams, like human resources, and the three words frequently occurring together in the document are termed trigrams, like human resource management. The LDA model is implemented in python language, where the genism library has been used to remove such phrases. Genism's phrases model can build and identify these bigrams, trigrams, quadgrams, or even n-grams [32]; thus, we can remove and improve the data cleansing process. It is also part of preprocessing, so after completing this stage, data is sent to the LDA model for further analysis [49, 67]. LDA topic modeling is based on three input parameters, one of which is a list of topics, and the other is hyperparameters. Before the distribution of a document's topic content is the magnitude of the Dirichlet. This parameter is regarded as several "pseudowords" equally distributed across the document's topics, regardless of how the document's other words are assigned to topics. β is per-word-weight of Dirichlet prior over topic-word distributions. The α value for this experiment is taken as $1/T$, where T is the desired number of topics [33], and the β has been fixed as 0.01 for all topic solutions. For identifying two, five, and ten topic solutions, as suggested by [26], the number of iterations considered is 1000. Thus, initializing these parameters becomes a concern as the values can define the distribution of high-quality topic results. The bag of words (BOW) extracted is initially processed in LDA topic modeling, where the most frequently and least frequently occurring are removed so the corpus can become absolute. This study removes a word frequency of more than 5000 from BOW. The top 20 frequently occurring words from the corpus with their frequency are shown in Figure 5, as it is clear from the graph that the most occurring keyword is the system, use, sensors, internet, agriculture, and many more.

Hyperparameters are optimized using Python's mallet library, a JAVA-based NLP package. Then, the mallet package extracts the desired topics by training the model using BOW. Unfortunately, no official or proven measure exists

YEAR-WISE ANALYSIS
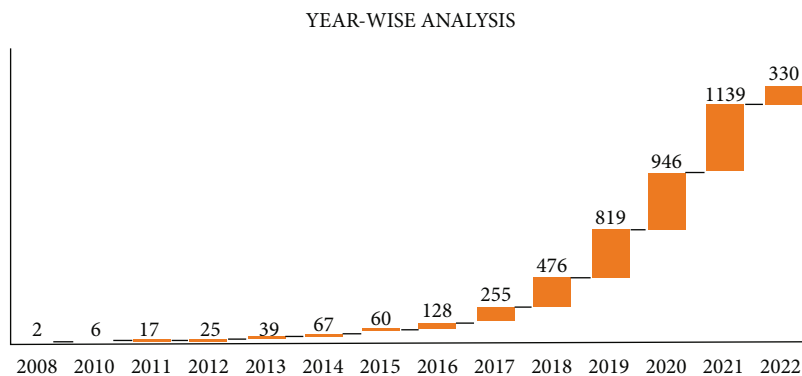
FIGURE 3: Year publication analysis.

Journal wise analysis
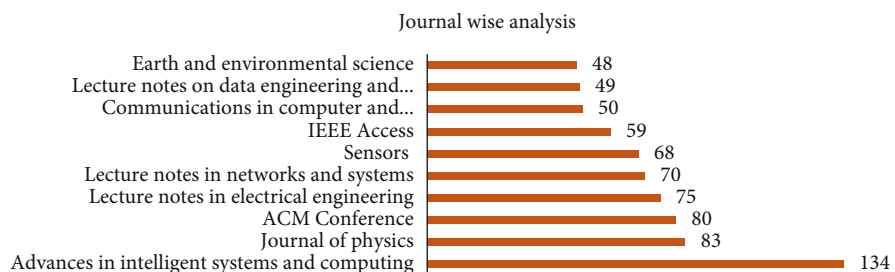
FIGURE 4: Dominating journals analysis.

TABLE 3: Sample of loading dataset.

Index	Title	Year	Journal	Abstract
0	Title 1	2008	Journal 1	The SmartBay initiative (http://www.SmartBay.ca) is led by the School of Ocean Technology, part of the Fisheries and Marine Institute of Memorial University of Newfoundland located in St. John's, Newfoundland.
1	Title 2	2008	Journal 2	The Internet of Things vision introduces the capability of connecting smart sensor/actuators to locally available networks in order to allow the interaction with the real world. The two visions are, thus, perfectly integrated and ideally suited to perform the task of collecting simple information from the surrounding environment.
2	Title 3	2010	Journal 3	Given a set of k-dimensional objects, the SKYCUBE computation returns a skyline cube which consists of skylines of all $2k - 1$ nonempty subspaces. This paper focuses on efficiently balancing the computation cost and update cost of dynamic sky-cube computation in the Internet of Things.
3	Title 4	2010	Journal 4	With the rapid development of new theories and technologies, especially AI, data mining and emerging communication technologies, both data collection and smart data analysis have provided new approaches for the development and improvement of ITS (intelligent transport systems).

to find the optimal number of solutions [27]. Still, some observational parameters are given by Cao and Arun, which helps the researcher decide the optimal number of keys [55, 68]. Furthermore, the choice of the topic solution has been influenced by the heuristics and findings of the studies [55, 61, 68, 69]. Finally, K-mean clustering algorithms are used to find the optimal number of topics from the BOW.

6. Topic Labeling

Once the topics have been extracted with the help of the LDA model, each topic is labeled manually based on the key terms of each topic. As a result, there are 4309 articles in the corpus, and out of all documents, the top five high-loading papers and their contribution to the topic are mentioned in Table 1.

7. Result Analysis

7.1. Parameters of Topic Solutions. The loadings for two, five, and ten topic solutions have been acquired by deploying the LDA model and are presented in Table 1. The selection of two, five, and ten topic solutions is based on a coherence score and is influenced by the previous studies. The
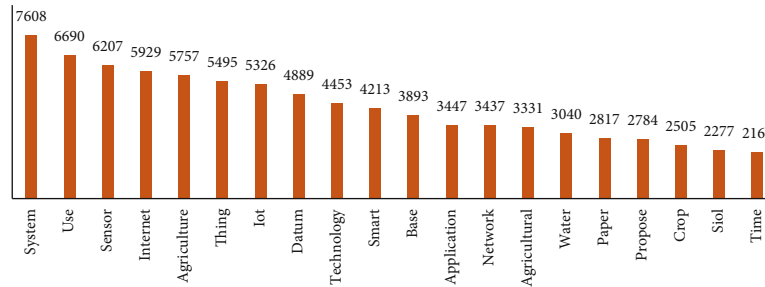
Figure 5: Top 20 words from corpus with frequency.

coherence score plays an essential role in finding the semantic similarity between the key terms in the topic, and ideally, a 0.3 to 0.6 coherence value is considered a good score [81]. In this study, coherence values achieved are good; for two topic solutions, 0.62; for five topics, 0.58; and for ten topic solutions, 0.52 coherence value is reached. Therefore, five topic solutions are considered optimal based on coherence value. The dominance of each topic solution is also supported by the corresponding count of articles it covers. Table 4 summarizes the count of year-wise publications corresponding to each topic solution.

The initial choice of two topics will broadly depict the core research areas that have been widely covered by the researchers in the compiled research literature. Further, in five topic solutions, the researchers have explored the research areas. Therefore, we have depicted in detail the research areas studied in five topic solutions. Further in the hierarchy, the five topic solutions have widened into ten topic solutions, with new areas emerging as the research trends in GHRM.

7.2. Topic Labeling. The core research zones explored and discovered based on the two topic solutions are depicted in topics T-2.1 and T-2.2. Let us discuss how this labeling has been performed. While implementing LDA on two topic solutions, the keywords and their loading has been extracted. The extraction results of LDA depict the high-loading articles per topic and the high-loading terms or keywords per topic. The labeling process is based on the high-loading keywords that have been collected. Thus, in the table, the labeling per topic solution corresponds to the terms extracted under the heads T-2.1, T-2.2, and so on; it goes for five and ten topic solutions.

7.2.1. Core Research Area. The two topic solutions present an abstract view of the literature dataset and divides it into "Security and Privacy in Smart Agriculture" (T-2.1) and "Monitoring and Control System in Agriculture" (T-2.2). These two significant labels depict the research areas the researchers have extensively explored.

(1) T-2.1: Security and Privacy in Smart Agriculture. Agriculture has shaped human civilizations since ancient times. Rapid information and communication growth affects agriculture's structure and operation (ICT) [82]. Despite advances, hazards may be significant, so smart farming must

grasp security and privacy challenges before contemplating cyber attacks. Smart farming uses devices, protocols, and computer ideas to modernize agriculture. Digital farming changes everything and creates effective, efficient, sustainable, and open systems [83]. Mobile devices, precision agronomy, remote sensing, big data, cloud analytics, cyber security, and intelligent systems simplify agricultural technology integration. Incompatibility, heterogeneity, equipment constraints, processing, and data security may threaten smart farming, but recent years have increased usage of ICTs in agriculture [84]. Physical risks and concerns may impede agriculture's deployment, but agriculture 4.0 will be the new agriculture standard [85]. Simultaneous research is also going on in the area to secure smart agriculture. Technology has added to environmental problems—list agriculture's physical threats by category. Population increase, urbanization, aging, and technical developments in food production all affect agriculture and farmers. Agriculture's most significant physical hazard is weather [86]. External factors continually threaten agriculture. In recent decades, technology has reduced its influence. Agriculture apps need stable connections, IoT networks, and cloud computing [87]. External factors continually threaten agriculture. In recent decades, technology has reduced its influence. Agriculture apps need stable connections, IoT networks, and cloud computing. The sensors can malfunction, causing erroneous readings and instructions that could cause a manufacturing failure. Temperature, humidity, obstructions, and human presence can impact Lora WAN, Zigbee, and other agri-wireless networks, causing data loss. Sensors and networking equipment are usually exposed [88].

(2) T-2.2 Monitoring and Control System in Agriculture. New techniques, technology, and approaches have also helped in agriculture. 35% of the world's workforce works in this profession. Agriculture helps many economies to grow [89]. It boosts industrialized nations' economies. India is the second largest country that deals in this profession. Every country has practiced agriculture since ancient times. Businesses and other areas must support agriculture's tech transformation. The future population rise is frightening. Mid-20th century population may have surpassed nine billion counts, so agriculture needs to be strengthened to meet the flooding needs. Agricultural engineering challenges include drainage, irrigation, crop scheduling, and bio-system optimization. The lack of agricultural technology to monitor and manage

TABLE 4: Year-wise publication analysis for 2, 5, and 10 topic solutions.

T-ID	Topic name	<2015	2015	2016	2017	2018	2019	2020	2021	2022	Total
2.1	Security and privacy in smart agriculture	127	43	85	153	237	438	500	588	190	2361
2.2	Monitoring and control system in agriculture	29	17	43	102	239	381	446	551	140	1948
5.1	Intelligent disease detection models	3	6	14	18	42	72	115	146	48	464
5.2	Data security challenges in smart agriculture	33	14	30	74	98	191	181	226	72	919
5.3	Smart monitoring system in agriculture	17	10	31	80	181	291	312	363	88	1373
5.4	Production and supply chain management in agriculture	80	24	33	55	90	159	213	241	83	978
5.5	Cost-effective communication system in smart agriculture	23	6	20	28	65	106	125	163	39	575
10.1	Greenhouse monitoring system	17	11	17	34	53	88	98	111	24	453
10.2	Service-based industry for smart agriculture	23	9	22	42	52	97	85	83	27	440
10.3	Cloud-based smart applications in agriculture	8	7	15	38	52	84	79	111	48	442
10.4	Energy-efficient smart transmission system	11	3	13	17	56	89	118	137	35	479
10.5	Smart solutions for modern farming	77	14	17	14	20	29	29	49	11	260
10.6	Smart irrigation system for agriculture	4	3	15	43	107	174	194	208	62	810
10.7	Blockchain-based security system for agriculture	3	2	4	10	19	36	46	78	20	218
10.8	Production-based smart system for agriculture	3	2	11	19	55	105	101	132	33	461
10.9	Industry 4.0 in agriculture	9	7	10	31	41	79	132	141	39	489
10.10.	Image-based classification techniques in intelligent agriculture	1	2	4	7	21	38	64	89	31	257

systems or machinery likely causes these problems. The report says control approaches increased seedling growth [90].

IoT helps in the process of modernizing the agriculture segment by gathering farming data. IoT-based agricultural monitoring system wirelessly communicates and disseminates the sensor data. Global agriculture uses 70% of available fresh water each year to irrigate 17% of the land [91]. Growing food requirements and global warming reduce irrigated land, a challenge in plague agriculture. FAO predicts global food production must rise by 70% to meet population and urbanization needs. Modern agriculture uses robotics, automation, and computer systems to replace challenging human jobs, so expanding agriculture needs new technologies to be included [92]. Future agricultural technology includes robotics and machine vision. In addition, population growth will increase the demand for resources and products. "Sustainability" is blended into social, economic, and technological problems to address environmental conservation and economic development, and information and control systems will be crucial [93].

7.2.2. Five Topic Solutions: Research Areas

(1) T-5.1: Intelligent Disease Detection Models. India's economy is mainly based on agriculture. Agriculture accounts for 16% of India's GDP and exports. More than 75% of India's population depends on agriculture. Healthy, high-quality agriculture is essential for economic prosperity [94]. Detection of plant disease is critical at an early stage. Plants can become ill while growing. Early illness diagnosis is a challenge in agriculture. Researchers first demonstrated cutting-edge machine learning methods for identifying plant illnesses [95]. Training parameters are used in modern sys-

tems but require powerful computers or lengthy training and prediction durations to work. Convolutional auto encoder (CAE) network prediction features have been reduced while preserving accuracy in this research. Thanks to technological advancements, the world's population of 7 billion people can be fed [96].

Changing climates, declining pollinators, and plant diseases threaten the ability to produce enough food. Plant diseases endanger the livelihoods of smallholder farmers who depend on healthy crops [97]. Despite declining yields, smallholder farmers in developing economies provide more than 80% agricultural output. Methods for preventing disease already exist [98]. Pesticides have been replaced with integrated pest management (IPM). Early diagnosis is essential for successful therapy. Agricultural extension organizations and local plant clinics have long supported disease detection thanks to their computer power, high-resolution displays, and broad accessory sets, such as HD cameras. Smartphone diagnostics are a first-of-its-kind technology. 5-6 billion mobile phones will be in use by 2020. More than two-thirds of the world's people now have access to mobile broadband, a 12-fold increase since 2007 [99].

(2) T-5.2: Data Security Challenges in Smart Agriculture. Technology, equipment, protocols, and computer paradigms are all used to enhance agricultural operations in smart agriculture. Big data, artificial intelligence, the cloud, and edge computing all store and analyze the data in various forms of storage and archiving. As a relatively new field, smart agriculture lacks adequate data security measures [84]. Farming's future relies heavily on the availability and quality of data, which necessitates the need for security. To maintain security in smart agriculture, managing data compatibility, resource constraints, and massive data processing [100].

Agricultural systems may not be well suited to traditional IoT security solutions, resulting in unique demands and possibilities. New agricultural projects have been developed to keep up with population increase and food production. The success of agriculture depends on productivity, era-specific restrictions, and the advancement of science and technology. A lot may go wrong regarding smart agriculture, which is still in its infancy. In the future, farmers will rely heavily on the availability and quality of data to help them; thus, developing secure and stable systems is critical [101]. The growth of the agriculture generation is depicted in Figure 6, in which agriculture 1.0 started in 1784. In the 20th century, agriculture 2.0 came into existence. In 1992 agriculture 3.0 was started, and in 2018 agriculture 4.0 if followed.

Smart agriculture uses IT to increase information perception, quantitative decision-making, intelligent control, suitable investment, and personal service [102]. In addition, current technology boosts agricultural yield and improves security and privacy [103]. There are both advantages and disadvantages to using automation in smart agriculture. Computer-aided farming uses contemporary technology and procedures, so in the future, "digital agriculture" will be more productive, efficient, sustainable, inclusive, transparent, and resilient agriculture. Many different types of agricultural technology may be used in conjunction with one another to increase efficiency and productivity [104].

(3) T-5.3: Smart Monitoring System in Agriculture. Rainfall and temperature fluctuations are very unpredictable. Climate-smart farming is becoming increasingly popular among Indian farmers. IoT enables smart agriculture. It saves water, fertilizer, and agricultural yields. IoT-enabled automated systems and wireless networks are expanding industries. Thus, research into integrated sensor technology and the usage of IoT networks in agriculture is reaching the level [105].

(4) T-5.4: Production and Supply Chain Management in Agriculture. The growth of the supply chain and the movement of information are driven by the gathering of materials, the transformation of products, and the delivery to end-users. Information-driven, "connected supply chains" enable organizations to reduce inventory and expenditures; increase product value; extend resources; expedite time to market; and retain consumers, among other benefits [106]. Supply chain performance determines how healthy activities are linked to maximizing customer value and profitability at each process stage—the end-user benefits from an efficient supply chain. Several agricultural supply chains in India are problematic owing to issues in the agriculture industry [107]. Many factors affect the agri-food supply chain, including small and marginal farmers, disjointed supply chains, a lack of economies of scale, subpar processing, value addition, and fewer marketing options. Supply chain management is expanding into logistics by creating new divisions integrating manufacturing, procurement, transportation, and distribution [108]. Information flow visibility has increased

because of advancements in telecommunications, electronic data interfaces, and other technologies. Animals and plants are used in agriculture to produce products that benefit human health. For example, agribusiness produces textiles and paper. Throughout the supply chain, the needs of customers are met. Organizations in the agricultural supply chain, such as cooperatives, distribute produce, fruits, grains, pulses, and products derived from animals [109]—a network of businesses that make goods and services for the end-user. There are several benefits to establishing a supply chain network, such as shifting risk and profit from one company to another. Quality is ensured by openness and accountability in the process. Quality is dependent on transparent processes and responsibilities at each stage of the process. The price and performance of transfer payments are crucial to the success of process chains.

(5) T-5.5: Cost-Effective Communication System in Smart Agriculture. Low-cost solutions like crop rotation, green manuring, and mulching have cut cultivation expenses while saving soil and water. Legumes, weed control, and increased agricultural diversity are nonmonetary inputs [101]. Climate change, global warming, saltwater intrusion, desertification, and a lack of arable land have increased worldwide worries about food safety and security. Connectivity-of-Things applications require steady internet [110]. In the Mekong Delta and HCMC, climate change threatens food security. Drought and saltwater intrusion in the South and Central Highlands in early 2016 demonstrate the vulnerability and susceptibility of unsustainable agriculture. Agriculture may be more efficient and safer thanks to a new Farming system. Vietnam may become a smart and sustainable farm by modernizing, boosting productivity, and ensuring quality. Businesses in Vietnam have shared their know-how with companies in other countries. Another important factor to consider is the safety of the food being prepared. When deciding which meals are good for you and the environment, most people have no idea where to begin. Concerns about food safety have given rise to new ideas like "city farms" and "growing your veggies at home" [111]. However, the economic sustainability of these models must be thoroughly explored. Researchers are currently focusing on developing an IoT-enabled agriculture system. Increased productivity, quality, and safety may be achieved via this method [82].

7.2.3. Ten Topic Solutions: Research Trends

(1) T-10.1: Greenhouse Monitoring System. Most Indians work in agriculture, contributing to the country's economy—agriculture benefits from technological advancements. However, pesticides are used to grow most fruits and vegetables since contemporary farming methods cannot keep up with demand. As a result, conventional farming practices contend with weather and disease. Although crop yields may be increased by altering agricultural practices [112] because of urbanization and land scarcity, farming must be done in greenhouses. Temperature, humidity, light, water content, pH, and wetness are all shown via LEDs in the greenhouse. The goal is to create an intelligent greenhouse.
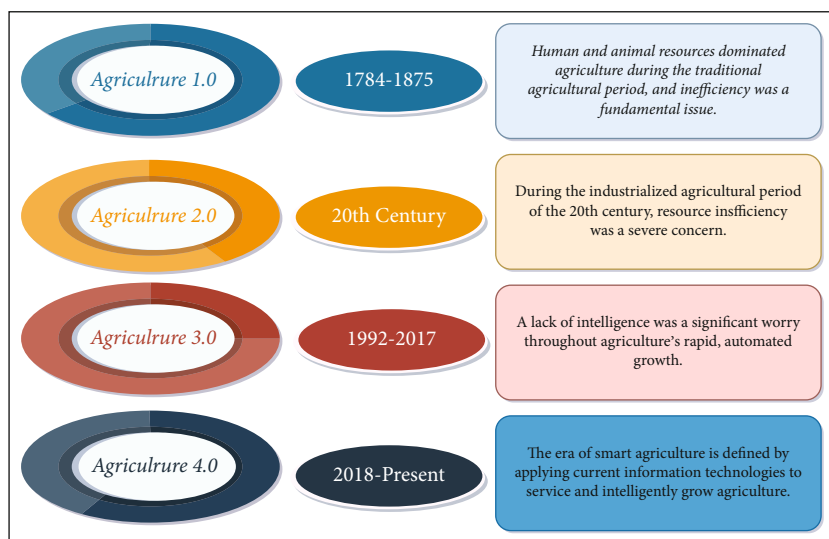
FIGURE 6: Agriculture generation.

Greenhouse temperature and humidity may be adjusted automatically using programmable modules and low-cost and high-efficiency options [113].

Soil water content, light intensity, temperature, and humidity may be adjusted. In greenhouse crop production, the appropriate growth conditions must be changed to achieve high yields, low costs, improved quality, and the lowest environmental impact. To attain these goals, proper heating and ventilation must be maintained. Using a greenhouse is more dependable, but it is also more difficult [114]. Temperature and timing controls had previously improved crop quality. Many control devices and systems lack automation and efficiency in today's dynamic and competitive environment. A variety of complicated models depict the greenhouse effect. Costs increased, plans became more complex, and more control was required. The usage of computers in greenhouses has increased during the last decade. These components are necessary for a control system. Sophisticated microelectronic hybrid circuits boost sensor manufacturing. Advances in product quality and dependability enable commercial competitiveness. Each sensor's performance is determined by its calibration and sensing processes. It will be impossible to automate some jobs even in the far future. Several American businesses have yet to automate fully, maybe due to cost concerns [115].

(2) T-10.2: Service-Based Industry for Smart Agriculture. Technical advancement has been driven by the widespread use of IT and its adaptability in satisfying various requirements. Service-based agriculture (SBA) is widely utilized in multiple industries. Farming systems that make it easier for farmers to do their work. A large-scale service smart agriculture systems link buses to a hotel, hospital, logistics center, restaurant, grocery store, or traditional market. With SBA, material sales partners may easily share information about their products with one other fast. As a result of SBA, Indonesia will see an increase in its economy, as quoted in

one study. Over time, the importance of information technology has grown. The production of farms has increased thanks to the adoption of contemporary technology [116]. Many people are familiar with the predicament of Indonesian farmers. The significance of variables cannot be overstated. Farmers have a fear of technology. Farmers in Indonesia may be able to increase their abilities and produce food for the country's population by utilizing new technologies.

Brokers are often used to resell the produce of Indonesian farmers. Small-scale farmers in Indonesia were hurt by brokers who gambled on the price of agricultural goods [117]. Prices for components are rising. Broker fraud inflated market values. Brokers save agricultural products, giving the impression that the market is oversupplied and driving up the price of food. When chili prices climb and there is a shortage, many brokers refuse to buy from growers. The growing cost of food in Indonesia might harm the country's economy. Farmers must be able to sell their products directly to consumers. The direct distribution offers farmers an easy way to market their products. Wholesalers buy agricultural goods from farmers at inexpensive rates [118]. To get their goods to market, farmers must rent a vehicle. Commodities no longer impact farmers' earnings with a long processing time. Indonesians rely heavily on their smartphones to get information. Technology can help farmers become food wholesalers. Local markets and restaurants might be fed using this method by farmers. The Internet of Things (IoT) and cloud computing support agriculture's food supply and distribution systems [119]. Nowadays, nanotechnology is also used in agriculture to improve yields and reduce waste.

(3) T-10.3: Cloud-Based Smart Applications in Agriculture. Smart farming uses technology to increase production and improve product quality. For example, the Internet of Things-based smart agriculture automates crop inspections and watering. Database traffic and data cannot be handled

by a cloud-based IoT-based system. As a result, there is less lag, the battery lasts longer, and the money and information are better managed [120].

In many cases, the edge for IoT may provide significant advantages, such as removing the need for interval and geometric communications efficiency. High interface automation in IoT activities may achieve reduced latency and faster processing. This simulator replicates the sting, edge, and fog of IoT. IoT-based edge computing is more immediate, cost-effective, and efficient than traditional computer systems [121]. In cities, these strategies are ineffective. Rural locations are where they are most commonly used. Robots should be used in agriculture. The field is navigated using the GPS on the tractor. Agribusiness in the 21st century is anything but digital or computerized. Monitoring crops and animals with sensors, GPS-enabled tractors, image processing, and machine learning is possible. Edge computing reduces the amount of noise in the raw data it analyses which can be cleaned using data mining techniques [122]. On the other hand, Broadband networks are more cumbersome and difficult to standardize. After sensors are installed, data is automatically collected. We can identify if animals or birds are active, inactive, unwell, healthy, submissive, or dominant. We may alter their treatment, living circumstances, medicine, and food to suit their needs [123].

(4) T-10.4: Energy-Efficient Smart Transmission System. An intelligent electrical infrastructure that satisfies society's sustainability and energy efficiency demands is called "smart infrastructure" Customers and utility providers will benefit from the smart grid's ability to monitor their energy use better and link the power grid with micro-networks. As a result, there is a danger to data security and privacy. Economic growth depends on the availability of electricity, which boosts productivity and sustains quality of life. Global economic development and electricity usage are depleting the world's energy resources [124]. The smart grid's core assumption is to minimize resource depletion and promote economic growth through energy efficiency and management technologies. Demand management lowers transmission and distribution system stress and high-demand overhead lines. Several countries have used industrial and commercial demand response strategies to boost their economies. Direct load limiting often reduces peak demand [125]. Direct load management may result in a decrease in customer satisfaction—direct load management. Consumers and utility companies benefit from reduced peak demand when loads are shifted. However, the electrical system's stability and dependability are compromised during periods of high energy demand. The smart grid and load modeling need to limit peak energy use.

Trouble ensues when demand exceeds supply. From 2019 to 2030, India's population and development demands are expected to grow by 50 percent [126]. A transmission system that can endure interruptions and blackouts must meet these criteria. Grid operators must regularly monitor supply and demand to avoid power outages. To fix this prob-

lem, load shedding disconnects specific customers' electricity. Generators must be turned down to prevent blackouts if supply and demand are out of sync. Smart grids can identify problems early on and immediately resolve them. Sensors monitor the grid and manage the flow of current. These are computerized to increase productivity [127].

(5) T-10.5: Smart Solutions for Modern Farming. Sustainable food production is in high demand as the world's population expands and weather patterns shift. Agriculture and development go forward as time goes by. Agricultural technology is advancing rapidly. These new technologies are pretty effective, but they must be constantly improved. Using information and communications technology, planting, watering, and harvesting are all enhanced. Many fields, including agriculture, benefit from technological advancements. The Internet of Things (IoT) in agriculture is referred to as "smart farming" [128]. Produce and livestock will be healthier thanks to IoT-enabled smart farming. Real-time information is provided through wearables and sensors in the field.

Shelter, clothing, and food have been top priorities for humanity since the dawn of civilization. There is a lot of modernity in the house and clothing. According to the UN Food and Agriculture Organization (FAO), humanity's food requirements will rise by 70% by 2050, according to the UN Food and Agriculture Organization (FAO) [129]. IoT can be used to solve problems in business and technology. Tractors are used to plant seeds and gather crops. You can use it for business or yourself. Farming is done with the help of tractors. Farmers can do other things when they use tractors that drive themselves. A Polish company called Agribot makes tractors that can work independently. When they pull weeds, their tractors have sensors that reduce the number of chemicals and pesticides exposed. Agro-IoT devices can meet the needs of farming in the future. Traditional agriculture must become more productive and less risky for the global economy to grow. IoT helps growth. Farmers can keep an eye on their land with the help of the Internet of Things. IoT applications include keeping an eye on climate change, managing water, keeping an eye on land, improving productivity, keeping an eye on farming, and keeping track of pesticides and herbicides [130].

(6) T-10.6: Smart Irrigation System for Agriculture. The most difficult chore in agriculture is watering fields. Water systems consist of drips, nozzles, tubes, and sprinklers, among other things. As a whole, agriculture has a positive impact on economic activity. Watering by hand is required. Gardening and soil deterioration are both covered in rainfall. Agriculture's key objectives are the production of food and livestock. IoT is a network of interconnected devices that can exchange data [131]. When water supplies are limited, automatic irrigation may be necessary.

According on the weather, irrigation might be done continuously or intermittently. As a result, there is less spillage. Almost all of the water comes from drip irrigation or sprinklers. With a wireless gadget, soil moisture and humidity

may be monitored. In agriculture, controllers manage everything from power to intruder detection to pump switching [69]. A pump is used to deliver water to the ground. Water is conserved when drippers are used. Drip irrigation and flood irrigation are both standard irrigation methods. Both all of the sensors, pumps, and controls work as expected. Manual watering may hurt or deplete crops and the environment. Automated irrigation systems can be used to address the difficulties. Farming may benefit from drip irrigation, which saves on water. Automatic irrigation systems for crop management have become widespread during rainstorms, landscaping, and soil erosion. Wi-fi sensors are used to gauge the humidity and moisture content of the soil. In agriculture, controllers keep an eye on the electricity, keep an eye out for intruders, and manage the pumps. Saturating the soil is accomplished with the use of pumps. Using drippers saves water, therefore reducing the amount of water used. Floatation irrigation commonly utilizes electricity, sensors, pumps, and controls [132].

(7) T-10.7: Blockchain-Based Security System for Agriculture. There are nodes in a blockchain, and each node has its own distributed ledger, allowing several nodes to read and amend a single ledger while preserving shared control. Each blockchain node contains a distributed ledger that is safe and accessible to all participants. There are no middlemen to authenticate, track, store or synchronize transactions using blockchain technology. According to several research studies, blockchain has altered technology from centralized to decentralized and distributed networks, a shift that has been well documented. The blockchain helps business networks [133]. Business networks are composed of companies or individuals that trade assets. Products, materials, and equipment are examples of physical assets. A distributed ledger may be used to move assets across the network by anybody who is a member. The most recent ledger is available to all members. Consensus-based distributed ledgers and smart contracts foster network confidence. Assets and transactions are recorded in the distributed ledger. Transactions are possible with a distributed ledger. You cannot remove a transaction after it has been added. An encrypted ledger prevents tampering with transactions. With blockchain, the distributed ledger is transformed into a reliable data source for the network [134]. A distributed ledger of digital commerce is known as a blockchain.

Each node of the network modifies distributed ledgers through cryptography. Components of a blockchain include its block header, timestamp, nonce, and Merkle root hash. Smart apps are being developed for rural agriculture. Agricultural modernization relies on ICT to automate processes and protect personal data. Data from many IoT devices may be sent to a central hub to analyze and manage autonomous farm activities. However, centralized intermediaries are inherent in a single point of failure, data loss risk, and man-in-the-middle attacks. Thanks to smart contracts on the blockchain, decentralized and safe agricultural automations are now possible [135].

(8) T-10.8: Production-Based Smart System for Agriculture. It is possible to increase productivity and quality by using IoT-based agricultural convergence technologies. Predicting demand, managing supply, and ensuring quality are benefits of precision agriculture. The expansion of the economy is mainly fueled by agriculture. The government is responsible for protecting the land [136]. Nothing has changed despite advances in science and technology. There is no shortage of green technologies. Farmers need to reduce the time they spend working and increase the precision they use their resources. Complex statistical methodologies are used by agriculturalists when analyzing historical data and making economic predictions. Farm yields are improved via GPS, sensors, and big data. Real-time data from ICT-based decision support systems can take the role of farmers' knowledge and intuition [137]. Improved decision-making reduces the amount of waste and increases efficiency. Images, GPS, science-based solutions, climate forecasts, technology, and environmental controls play a role in agriculture. As with the terms "smart meters" and "smart cities," "smart farming" refers to any M2M application. Technology advances to aid in harvest forecasting. However, predictions based on statistics are not always accurate. Harvest data and the agricultural environment should be correlated. IoT will provide agricultural data. Complex statistical methodologies are used by agriculturalists when analyzing historical data and making economic predictions. Predicting crop yields is aided by the use of smart systems. In the end, statistical forecasts are not perfect; they are only a starting point. Make a connection between the agricultural environment and harvest data. Crop pattern data will be provided through IoT-based decision support. On IoT, agribusiness utilizes data mining, statistical forecasting, and IoT services [138].

(9) T-10.9: Industry 4.0 in Agriculture. Global agriculture must undergo a paradigm shift in light of evolving environmental conditions, dietary preferences, and a scarcity of critical inputs. It is all about the latest advancements in agriculture. As a result of the adoption of Industry 4.0, businesses may expect to see advances in output, efficiency, and creativity. First, agriculture provides food for the world's population. Second, agriculture 4.0 decreases labor and environmental effects to increase agricultural profitability by reducing greenhouse gas emissions and water use. Third, agriculture is the primary source of income for half of India's population, India's veins and arteries [139]. The fourth stage of industrial development is large-scale agriculture. Among the essential ICTs is the IoT. Flexibility is improved in "smart factories." People, equipment, and software work together to satisfy production demands, which are met through cutting-edge technology such as CPS/IoT/iOS and real-time interaction. The industry benefits from consolidation. However, future manufacturing and commerce will be harmed. This shift is made possible due to the Internet and information technology [140]. Quality control encompasses all aspects of engineering, management, manufacturing, operations, and logistics. Costs, availability, use of resources, and market demand may all be automated. 'The implementation of Industry 4.0 will profoundly impact the agriculture and industrial sectors. All technologies like Big Data, AI, and IoT are part of Industry 4.0. IoT allows agricultural systems

and equipment to connect with one another, making Industry 4.0 a game changer in agriculture [141]. The fourth industrial revolution created networked tractors, farms, and manufacturing equipment [142]. "Industry Revolutions 4.0" refers to three factors:

(1) Digitalization and its integration into simple economical and technical networks

(2) Digitalization of services and products

(3) Market models that have been updated

As economic, economic and business models develop, humans become more distant from the center of production and surveillance of crops. Industry 4.0 is being used by both developed and developing countries. India has a lot of untapped potential for agricultural growth. Robotics, IoT, and e-business are the three pillars of this revolution, aiming to deliver technology to every corner of the globe.

(10) T-10.10: Image-Based Classification Techniques in Intelligent Agriculture. Agriculture originated thirteen thousand years ago between the Tigris and Euphrates rivers north of Iraq. Gathered vegetation included wild wheat and others. Few people needed food. UN estimates that the world's population will reach 10 billion by 2050, impacting farmers. Desertification and urbanization wreak havoc on farmland. COVID-19 is a threat to food security and the nation's economy. To solve this problem, we need to use fewer people to generate more food [143]. In certain parts of India, rainfall is the only irrigation water supply. However, crop destruction can occur in some places due to unpredictability in rainfall, which is a problem. Management of watersheds is critical. Many-variable hydrological modeling is required to predict rainfall and runoff in different basins accurately. Estimates of imperviousness necessitate a terrain categorization, which ultimately categorizes land use and cover [144]. The image classification curve number is used in modeling. Satellite pictures are difficult to classify because of their high resolution and wide range of applications.

Nevertheless, images are a common practice in agriculture and water management. There are a plethora of tools and methods for classifying images. ANN and SVM are used for image classification [145]. Techniques used to organize pictures traditionally are time-consuming and prone to human error. With pattern recognition, alternate ways can reduce time and enhance accuracy. Unlike Bayes' discriminant criteria, SVM multiclassification outperforms.

8. Threats to Validity

This analysis is based on LDA topic modeling and has bounded to the limitations of this topic modeling technique. A sufficient article count has been achieved, yet the risk of missing out is a concern. The bibliographic material has also been inferred. The search string insufficiency has been eradicated appropriately due to the limitations of selected search terms, synonyms, string formulation, and search engines' variedness resulting in imperfect retrieval of literature corpus. Labeling topics is a significant concern due to subjectivity and bias. According to the author, a deep discussion has been conducted to determine the label best to overcome this limitation. Then, based on critical terms, labels have been formulated to draw the best topic labels for researchers and practitioners.

9. Conclusion

Using IoT technology, farmers and producers may better manage their resources, such as fertilizer consumption and the number of trips made by farm vehicles, while minimizing waste and maximizing productivity, including water, electricity, and other inputs. In IoT smart farming systems, sensors monitor the agricultural field and automate the irrigation system. Farmers can monitor their fields from anywhere. This paper concluded the research direction in smart agriculture and farming. Technology has shaped agriculture's history. Historians have identified several agricultural revolutions that changed practice and output. Technological advances have fueled these revolutions. The Industrial Revolution mechanized agriculture, improving farm labor productivity.

Modern mechanized agriculture has replaced numerous farm activities by hand or by oxen, horses, and mules. Weather forecasting and barbed wire were 19[th]century advances. Portable engines and threshing machines became popular after improvements. In the 20[th]century, synthetic fertilizers and insecticides, mass-produced tractors, and agricultural aircraft for aerial pesticide application were developed. Precision farming, disease monitoring, agricultural drones, satellite imagery, and sensors are just ways technology makes farming easier for farmers. Intelligent software analysis for pest and disease prediction and soil management are only a few of the many analytical activities that IoT-based sensor networks may do. New issues in smart farming include the security of the farming data, technical failures, and technical incompetence.

10. Future Work

The LDA model works like a recommender system. The current research is based on extracting keywords from the documents and recommends current and trending research areas based on the correlation of the keywords in the specified field. So, in the real-time scenario, any corpus of any size can be passed to the model to get the relevant keywords, and based on these keywords, suggestions for topics can be depicted. The authors have used this model on smart agriculture in the current research. In contrast, this model can also be implemented in other research fields like smart cities, blockchain, and Wireless Sensor Networks. In this study, the authors analyzed data retrieved from the Scopus database instead of Web of Science, Education Resources Information Center, ScienceDirect, or the Directory of Open Access Journals. However, the authors chose the Scopus database over these other databases because Scopus has more excellent

coverage of publications, demonstrating that it is a comprehensive and dependable data source and so justifying its eligibility for this review.

Data Availability

Data are available upon request from the corresponding author.

Conflicts of Interest

The authors declare that they have no conflicts of interest.

References

[1] L. Zhang, I. K. Dabipi, and W. L. Brown Jr., "Internet of Things applications for agriculture," *Internet of Things A to Z*, pp. 507–528, 2018.

[2] S. Navulur, A. S. C. S. Sastry, and M. N. G. Prasad, "Agricultural management through wireless sensors and Internet of Things," *International Journal of Electrical and Computer Engineering (IJECE)*, vol. 7, no. 6, p. 3492, 2017.

[3] E. Sisinni, A. Saifullah, S. Han, U. Jennehag, and M. Gidlund, "Industrial Internet of Things: challenges, opportunities, and directions," *IEEE Transactions on Industrial Informatics*, vol. 14, no. 11, pp. 4724–4734, 2018.

[4] J. Lin, W. Yu, N. Zhang, X. Yang, H. Zhang, and W. Zhao, "A survey on Internet of Things: architecture, enabling technologies, security and privacy, and applications," *IEEE Internet of Things Journal*, vol. 4, no. 5, pp. 1125–1142, 2017.

[5] X. Shi, X. An, Q. Zhao et al., "State-of-the-art Internet of Things in protected agriculture," *Sensors*, vol. 19, no. 8, p. 1833, 2019.

[6] O. Elijah, T. A. Rahman, I. Orikumhi, C. Y. Leow, and M. H. D. N. Hindia, "An overview of Internet of Things (IoT) and data analytics in agriculture: benefits and challenges," *IEEE Internet of Things Journal*, vol. 5, no. 5, pp. 3758–3773, 2018.

[7] P. P. Jayaraman, D. Palmer, A. Zaslavsky, A. Salehi, and D. Georgakopoulos, "Addressing information processing needs of digital agriculture with OpenIoT platform," in *in Interoperability and Open-Source Solutions for the Internet of Things*, pp. 137–152, Springer, 2015.

[8] Farmbeats, *FarmBeats: AI Edge IoT for Agriculture*, 2022, https://www.microsoft.com/en-us/research/project/farmbeats-iot-agriculture/.

[9] Ibm, *IBMWatson IoT Platform*, 2022, https://www.ibm.com/us-en/marketplace/internet-of-thingscloudlnk=STW_US_STESCH&lnk2=trial_IOTPlat&pexp=def&psrc=none&mhsrc=ibmsearch_a&mhq=iot.

[10] Infiswift, *Infiswift IoT Platform for Agriculture*, 2022, https://www.intel.com/content/www/us/en/internetof-things/infiswift-enterprise-iot-platform-for-agricultural-solution-brief.html?wapkw=infiswift.

[11] G. Cloud, "Open Agriculture Foundation: creating an open-source ecosystem to revolutionize the future of food," 2022, https://cloud.google.com/data-solutions-for-change/open-agriculture/.

[12] S. Fahad and W. Jing, "Evaluation of Pakistani farmers' willingness to pay for crop insurance using contingent valuation method: the case of Khyber Pakhtunkhwa Province," *Land Use Policy*, vol. 72, pp. 570–577, 2018.

[13] S. Fahad and J. Wang, "Farmers' risk perception, vulnerability, and adaptation to climate change in rural Pakistan," *Land Use Policy*, vol. 79, pp. 301–309, 2018.

[14] F. Su, N. Song, N. Ma et al., "An assessment of poverty alleviation measures and sustainable livelihood capability of farm households in rural China: a sustainable livelihood approach," *Agriculture*, vol. 11, no. 12, p. 1230, 2021.

[15] S. Fahad, M. S. Hossain, N. T. L. Huong, A. A. Nassani, M. Haffar, and M. R. Naeem, "An assessment of rural household vulnerability and resilience in natural hazards: evidence from flood prone areas," *Environment, Development and Sustainability*, pp. 1–17, 2022.

[16] P. V. Santhi, N. Kapileswar, V. K. R. Chenchela, and C. H. V. S. Prasad, "Sensor and vision based autonomous AGRIBOT for sowing seeds," in *in 2017 International Conference on Energy, Communication, Data Analytics and Soft Computing (ICECDS)*, pp. 242–245, Chennai, India, 2017.

[17] H. Karimi, H. Navid, B. Besharati, H. Behfar, and I. Eskandari, "A practical approach to comparative design of non-contact sensing techniques for seed flow rate detection," *Computers and Electronics in Agriculture*, vol. 142, pp. 165–172, 2017.

[18] D. R. Vincent, N. Deepa, D. Elavarasan, K. Srinivasan, S. H. Chauhdary, and C. Iwendi, "Sensors driven AI-based agriculture recommendation model for assessing land suitability," *Sensors*, vol. 19, no. 17, p. 3667, 2019.

[19] P. Dhiman, V. Kukreja, P. Manoharan et al., "A novel deep learning model for detection of severity level of the disease in citrus fruits," *Electronics*, vol. 11, no. 3, p. 495, 2022.

[20] S. A. Latif, F. B. X. Wen, C. Iwendi et al., "AI-empowered, blockchain and SDN integrated security architecture for IoT network of cyber physical systems," *Computer Communications*, vol. 181, pp. 274–283, 2022.

[21] C. Sharma, S. Sharma, and Sakshi, "Latent DIRICHLET allocation (LDA) based information modelling on BLOCKCHAIN technology: a review of trends and research patterns used in integration," *Multimedia Tools and Applications*, pp. 1–27, 2022.

[22] D. M. Blei, A. Y. Ng, and M. I. Jordan, "Latent Dirichlet allocation," *Journal of Machine Learning Research*, vol. 3, pp. 993–1022, 2003.

[23] T. K. Landauer, P. W. Foltz, and D. Laham, "An introduction to latent semantic analysis," *Discourse Processes*, vol. 25, no. 2–3, pp. 259–284, 1998.

[24] F. Gurcan and N. E. Cagiltay, "Big data software engineering: analysis of knowledge domains and skill sets using LDA-based topic modeling," *IEEE Access*, vol. 7, pp. 82541–82552, 2019.

[25] C. Reed, *Latent Dirichlet Allocation: Towards a Deeper Understanding*, 2012, http://highenergy.physics.uiowa.edu/.

[26] R. Arun, V. Suresh, C. E. V. Madhavan, and M. N. Murty, "On finding the natural number of topics with latent Dirichlet allocation: some observations," *Lect. Notes Comput. Sci. (including Subser. Lect. Notes Artif. Intell. Lect. Notes Bioinformatics)*, vol. 6118, pp. 391–402, 2010.

[27] S. K. Sehra, Y. S. Brar, N. Kaur, and S. S. Sehra, "Research patterns and trends in software effort estimation," *Information and Software Technology*, vol. 91, pp. 1–21, 2017.

[28] J. J. Webster and C. Kit, *Tokenization as the Initial Phase in NLP*, 1992.

[29] K. V. Ghag and K. Shah, *Comparative Analysis of Effect of Stopwords Removal on Sentiment Classification*, 2016.

[30] M. F. Porter, *Snowball: A Language for Stemming Algorithms*, 2001.

[31] J. Plisson, N. Lavrac, and D. Mladenic, "A rule based approach to word lemmatization," *in Proceedings of IS*, vol. 3, pp. 83–86, 2004.

[32] X. Wang, A. McCallum, and X. Wei, "Topical n-grams: phrase and topic discovery, with an application to information retrieval," *in Seventh IEEE International Conference on Data Mining (ICDM 2007)*, pp. 697–702, Omaha, NE, USA, 2007.

[33] *LDA Hyperparameter*, 2016, https://stackoverflow.com/ questions/39644667/rules-to-set-hyper-parameters-alpha-and-theta-in-lda-model.

[34] J. Li, S. Saide, M. N. Ismail, and R. E. Indrajit, "Exploring IT/ IS proactive and knowledge transfer on enterprise digital business transformation (EDBT): a technology-knowledge perspective," *Journal of Enterprise Information Management*, vol. 35, no. 2, pp. 597–616, 2022.

[35] H. Cui, "Research on agricultural supply chain architecture based on edge computing and efficiency optimization," *IEEE Access*, vol. 10, pp. 4896–4906, 2022.

[36] D. C. Rose and J. Chilvers, "Agriculture 4.0: broadening responsible innovation in an era of smart farming," *Frontiers in Sustainable Food Systems*, vol. 2, p. 87, 2018.

[37] S. Iniyan and R. Jebakumar, "Phenotype based smart mobile application for crop yield prediction and forecasting using machine learning and time series models," *Journal of Mobile Multimedia*, pp. 603–634, 2022.

[38] R. Kumar and V. Singhal, "IoT enabled crop prediction and irrigation automation system using machine learning," *Recent Advances in Computer Science and Communications*, vol. 15, no. 1, pp. 88–97, 2022.

[39] T. V. Nandeesh and H. M. Kalpana, "Smart multipurpose agricultural robot," *in 2021 IEEE International Conference on Electronics, Computing and Communication Technologies (CONECCT)*, pp. 1–6, Bangalore, India, 2021.

[40] G. Chen, Y. Meng, J. Lu, and D. Wang, "Research on color and shape recognition of maize diseases based on HSV and OTSU method," *in International Conference on Computer and Computing Technologies in Agriculture*, pp. 298–309, Springer, Cham, 2019.

[41] M. Waleed, T.-W. Um, T. Kamal, and S. M. Usman, "Classification of agriculture farm machinery using machine learning and Internet of Things," *Symmetry (Basel).*, vol. 13, no. 3, p. 403, 2021.

[42] W. Fang, L. Yue, and C. Dandan, "Classification system study of soybean leaf disease based on deep learning," *in 2020 International Conference on Internet of Things and Intelligent Applications (ITIA)*, pp. 1–5, Zhenjiang, China, 2020.

[43] I. Mistry, S. Tanwar, S. Tyagi, and N. Kumar, "Blockchain for 5G-enabled IoT for industrial automation: a systematic review, solutions, and challenges," *Mechanical Systems and Signal Processing*, vol. 135, article 106382, 2020.

[44] T. Spieldenner, S. Byelozyorov, M. Guldner, and P. Slusallek, "FiVES: an aspect-oriented approach for shared virtual environments in the web," *The Visual Computer*, vol. 34, no. 9, pp. 1269–1282, 2018.

[45] K. M. Abbasi, T. A. Khan, and I. U. Haq, "Hierarchical modeling of complex Internet of Things systems using conceptual modeling approaches," *IEEE Access*, vol. 7, pp. 102772–102791, 2019.

[46] R. Madhumathi, T. Arumuganathan, R. Shruthi, and R. S. Iyer, "Soil nutrient analysis using colorimetry method," *in in 2020 International Conference on Smart Technologies in Computing, Electrical and Electronics (ICSTCEE)*, pp. 252–256, Bengaluru, India, 2020.

[47] G. V. Abishek Prasad, R. S. Sree, S. Meera, and R. A. Kalpana, "Automated irrigation system and detection of nutrient content in the soil," *in in 2020 International Conference on Power, Energy, Control and Transmission Systems (ICPECTS)*, pp. 1–3, Chennai, India, 2020.

[48] Y. Wu, L. Li, M. Li et al., "Remote-control system for greenhouse based on open source hardware," *IFAC-PapersOnLine*, vol. 52, no. 30, pp. 178–183, 2019.

[49] J. Lachman and A. López, "Innovation obstacles in an emerging high tech sector," *Management Research: Journal of the Iberoamerican Academy of Management*, vol. 17, no. 4, pp. 474–493, 2019.

[50] A. Shamin, O. Frolova, V. Makarychev, N. Yashkova, L. Kornilova, and A. Akimov, "Digital transformation of agricultural industry," *in IOP Conference Series: Earth and Environmental Science*, vol. 346, no. 1, p. 012029, 2019.

[51] O. Phuaknok and C. Yuenyong, "Examining categories of students' STEM projects in science class," *Journal of Physics: Conference Series*, vol. 1835, no. 1, p. 012019, 2021.

[52] S. N. Daskalakis, G. Goussetis, and A. Georgiadis, "NFC hybrid harvester for battery-free agricultural sensor nodes," *in in 2019 IEEE International Conference on RFID Technology and Applications (RFID-TA)*, pp. 22–25, Pisa, Italy, 2019.

[53] A. Pandey and S. Kumar, "Smart device localization using femtocell and macro base station based path loss models in IoT networks," *in in 2018 IEEE International Conference on Advanced Networks and Telecommunications Systems (ANTS)*, pp. 1–6, Indore, India, 2018.

[54] S. N. Mishra and S. Chinara, "CA-RPL: a clustered additive approach in RPL for IoT based scalable networks," *in in International Conference on Ubiquitous Communications and Network Computing*, pp. 103–114, Springer, Cham, 2019.

[55] Y.-R. Chien and Y.-X. Chen, "An RFID-based smart nest box: an experimental study of laying performance and behavior of individual hens," *Sensors*, vol. 18, no. 3, p. 859, 2018.

[56] V. D. Bachuwar, A. D. Shligram, and L. P. Deshmukh, "Monitoring the soil parameters using IoT and Android based application for smart agriculture," *in in AIP Conference Proceedings*, Kolkata, India, 2018.

[57] R. Stojanovic, V. Maras, S. Radonjic et al., "A feasible IoT-based system for precision agriculture," *in in 2021 10th Mediterranean Conference on Embedded Computing (MECO)*, pp. 1–4, Budva, Montenegro, 2021.

[58] M. R. Suma and P. Madhumathy, "Acquisition and mining of agricultural data using ubiquitous sensors with Internet of Things," *in in International Conference on Computer Networks and Communication Technologies*, pp. 249–261, Springer, Singapore, 2019.

[59] P. S. Khatoon and M. Ahmed, "Semantic interoperability for IoT agriculture framework with heterogeneous devices," *in in Proceedings of International Conference on Recent Trends in Machine Learning, IoT, Smart Cities and Applications*, pp. 385–395, Springer, Singapore, 2021.

[60] J. V. Pradilla and C. E. Palau, "Micro virtual machines (microVMs) for cloud-assisted cyber-physical systems (CPS)," *in Internet of Things*, pp. 125–142, Elsevier, 2016.

[61] K. Lakhwani, H. Gianey, N. Agarwal, and S. Gupta, "Development of IoT for smart agriculture a review," in *in Emerging Trends in Expert Applications and Security*, pp. 425–432, Springer, 2019.

[62] M. Ashwini and R. V. Ravi, "A detailed investigation on embedded computing systems for IoT applications," in *in 2020 6th International Conference on Advanced Computing and Communication Systems (ICACCS)*, pp. 161–164, Coimbatore, India, 2020.

[63] M. N. Al-Rawahi, T. Sharma, and P. Palanisamy, "Internet of nanothings: challenges & opportunities," in *in 2018 Majan International Conference (MIC)*, pp. 1–5, Muscat, Oman, 2018.

[64] C. Lin, C. Guo, W. Du, J. Deng, L. Wang, and G. Wu, "Maximizing energy efficiency of period-area coverage with UAVs for wireless rechargeable sensor networks," in *in 2019 16th Annual IEEE International Conference on Sensing, Communication, and Networking (SECON)*, pp. 1–9, Boston, MA, USA, 2019.

[65] M. Capuzzo, "PhD Forum: LoRaWAN networks evaluation through extensive ns-3 simulations," in *in 2021 IEEE 22nd International Symposium on a World of Wireless, Mobile and Multimedia Networks (WoWMoM)*, pp. 227-228, Pisa, Italy, 2021.

[66] A. Trotta, M. Di Felice, L. Perilli, E. F. Scarselli, and T. S. Cinotti, "BEE-DRONES: ultra low-power monitoring systems based on unmanned aerial vehicles and wake-up radio ground sensors," *Computer Networks*, vol. 180, article 107425, 2020.

[67] Y. Gu and T. Jing, "The IoT research in supply chain management of fresh agricultural products," in *in 2011 2nd International Conference on Artificial Intelligence, Management Science and Electronic Commerce (AIMSEC)*, pp. 7382–7385, Dengleng, 2011.

[68] W. Feng, L. Wang, J. Zhao, and H. Ruan, "Research on agricultural development based on 'Internet+'," in *in International Conference on Computer and Computing Technologies in Agriculture*, pp. 563–569, Springer, Cham, 2015.

[69] S. Vaishali, S. Suraj, G. Vignesh, S. Dhivya, and S. Udhayakumar, "Mobile integrated smart irrigation management and monitoring system using IoT," in *in 2017 International Conference on Communication and Signal Processing (ICCSP)*, pp. 2164–2167, Chennai, India, 2017.

[70] S. Nuchhi, V. Bagali, and S. Annigeri, "IoT based soil testing instrument for agriculture purpose," in *in 2020 IEEE Bangalore Humanitarian Technology Conference (B-HTC)*, pp. 1–4, Vijiyapur, India, 2020.

[71] K. K. Karmakar, V. Varadharajan, S. Nepal, and U. Tupakula, "SDN-enabled secure IoT architecture," *IEEE Internet of Things Journal*, vol. 8, no. 8, pp. 6549–6564, 2020.

[72] S. Das, B. K. Mohanta, and D. Jena, "A state-of-the-art security and attacks analysis in blockchain applications network," *International Journal of Communication Networks and Distributed Systems*, vol. 28, no. 2, pp. 199–218, 2022.

[73] S. A. Chaudhry, K. Yahya, F. Al-Turjman, and M.-H. Yang, "A secure and reliable device access control scheme for IoT based sensor cloud systems," *IEEE Access*, vol. 8, pp. 139244–139254, 2020.

[74] H. Aafreen Sana, S. Prathibha, P. Pravin Kumar, M. Shabika Fathima, and B. Yashwanth Krishnan, "Design of a comprehensive sensor based soil and crop analysis system model using machine learning algorithms," in *in 2021 4th International Conference on Recent Developments in Control, Automation & Power Engineering (RDCAPE)*, pp. 327–332, Noida, India, 2021.

[75] T. Giri Babu and G. Anjan Babu, "Identification of crop health condition using IoT based automated system," in *in Advances in Data Science and Management*, pp. 421–433, Springer, 2020.

[76] L. Sujihelen, N. N. P. Kumar, P. P. Sai, and G. Nagarajan, "Sentinel-2 images-based intelligent crop type determination," in *in Advances in Data Science and Management*, pp. 555–563, Springer, 2022.

[77] K. Nayal, R. Raut, A. B. L. de Sousa Jabbour, B. E. Narkhede, and V. V. Gedam, "Integrated technologies toward sustainable agriculture supply chains: missing links," *Journal of Enterprise Information Management*, 2021.

[78] H. Ahmad Tarmizi, N. H. Kamarulzaman, A. Abd Rahman, and R. Atan, "Adoption of Internet of Things among Malaysian halal agro-food SMEs and its challenges," *Food Research*, vol. 4, no. S1, pp. 256–265, 2020.

[79] J. Treboux, R. Ingold, and D. Genoud, "Towards retraining of machine learning algorithms: an efficiency analysis applied to smart agriculture," in *in 2020 Global Internet of Things Summit (GIoTS)*, pp. 1–6, Dublin, Ireland, 2020.

[80] J. Zhang, Y. Rao, C. Man, Z. Jiang, and S. Li, "Identification of cucumber leaf diseases using deep learning and small sample size for agricultural Internet of Things," *International Journal of Distributed Sensor Networks*, vol. 17, no. 4, 2021.

[81] *Coherence Score*, 2019, https://stackoverflow.com/questions/54762690/what-is-the-meaning-of-coherence-score-0-4-is-it-good-or-bad.

[82] K. Demestichas, N. Peppes, and T. Alexakis, "Survey on security threats in agricultural IoT and smart farming," *Sensors*, vol. 20, no. 22, p. 6458, 2020.

[83] M. Gupta, M. Abdelsalam, S. Khorsandroo, and S. Mittal, "Security and privacy in smart farming: challenges and opportunities," *IEEE Access*, vol. 8, pp. 34564–34584, 2020.

[84] A. R. de Araujo Zanella, E. da Silva, and L. C. P. Albini, "Security challenges to smart agriculture: current state, key issues, and future directions," *Array*, vol. 8, article 100048, 2020.

[85] O. Calicioglu, A. Flammini, S. Bracco, L. Bellù, and R. Sims, "The future challenges of food and agriculture: an integrated analysis of trends and solutions," *Sustainability*, vol. 11, no. 1, p. 222, 2019.

[86] C. A. Boano, N. Tsiftes, T. Voigt, J. Brown, and U. Roedig, "The impact of temperature on outdoor industrial sensornet applications," *IEEE Transactions on Industrial Informatics*, vol. 6, no. 3, pp. 451–459, 2009.

[87] J. H. Anajemba, T. Yue, C. Iwendi, P. Chatterjee, D. Ngabo, and W. S. Alnumay, "A secure multiuser privacy technique for wireless IoT networks using stochastic privacy optimization," *IEEE Internet of Things Journal*, vol. 9, no. 4, pp. 2566–2577, 2021.

[88] A. Tzounis, N. Katsoulas, T. Bartzanas, and C. Kittas, "Internet of Things in agriculture, recent advances and future challenges," *Biosystems Engineering*, vol. 164, pp. 31–48, 2017.

[89] J. James and P. Manu Maheshwar, "Plant growth monitoring system, with dynamic user-interface," in *in 2016 IEEE Region 10 Humanitarian Technology Conference (R10-HTC)*, pp. 1–5, Agra, India, 2016.

[90] I. A. Lakhiar, G. Jianmin, T. N. Syed, F. A. Chandio, N. A. Buttar, and W. A. Qureshi, "Monitoring and control systems

in agriculture using intelligent sensor techniques: a review of the aeroponic system," *Journal Sensors*, vol. 2018, article 8672769, 18 pages, 2018.

[91] A. Lakshmi, Y. R. Kumar, N. S. Krishna, and G. Manisha, "IoT based agriculture monitoring and controlling system," in *in 2021 6th International Conference on Communication and Electronics Systems (ICCES)*, pp. 609–615, Coimbatre, India, 2021.

[92] M. Lee and H. Yoe, "Analysis of environmental stress factors using an artificial growth system and plant fitness optimization," *BioMed Research International*, vol. 2015, Article ID 292543, 6 pages, 2015.

[93] P. S. Kumar, N. Kumaresh, and M. K. Raj, "Remote based intelligent agriculture monitoring system," *European Journal of Molecular & Clinical Medicine*, vol. 7, no. 2, pp. 5236–5245, 2020.

[94] P. Bedi and P. Gole, "Plant disease detection using hybrid model based on convolutional autoencoder and convolutional neural network," *Artificial Intelligence in Agriculture*, vol. 5, pp. 90–101, 2021.

[95] S. Sanga, V. Mero, D. Machuve, and D. Mwanganda, "Mobile-based deep learning models for banana diseases detection," 2020, arXiv Prepr. arXiv2004.03718.

[96] K. P. Panigrahi, H. Das, A. K. Sahoo, and S. C. Moharana, "Maize leaf disease detection and classification using machine learning algorithms," in *in Progress in Computing, Analytics and Networking*, pp. 659–669, Springer, 2020.

[97] K. Ahmed, T. R. Shahidi, S. M. I. Alam, and S. Momen, "Rice leaf disease detection using machine learning techniques," in *in 2019 International Conference on Sustainable Technologies for Industry 4.0 (STI)*, pp. 1–5, Dhaka, Bangladesh, 2019.

[98] K. Simonyan and A. Zisserman, "Very deep convolutional networks for large-scale image recognition," 2014, arXiv Prepr. arXiv1409.1556.

[99] A. Khamparia, G. Saini, D. Gupta, A. Khanna, S. Tiwari, and V. H. C. de Albuquerque, "Seasonal crops disease prediction and classification using deep convolutional encoder network," *Circuits, Systems, and Signal Processing*, vol. 39, no. 2, pp. 818–836, 2020.

[100] B. Khelifa, D. Amel, B. Amel, C. Mohamed, and B. Tarek, "Smart irrigation using Internet of Things," in *in 2015 Fourth International Conference on Future Generation Communication Technology (FGCT)*, pp. 1–6, Luton, UK, 2015.

[101] Q. T. Minh, T. N. Phan, A. Takahashi et al., "A cost-effective smart farming system with knowledge base," in *in Proceedings of the Eighth International Symposium on Information and Communication Technology*, pp. 309–316, 2017.

[102] A. Goap, D. Sharma, A. K. Shukla, and C. R. Krishna, "An IoT based smart irrigation management system using machine learning and open source technologies," *Computers and Electronics in Agriculture*, vol. 155, pp. 41–49, 2018.

[103] I.-G. Raducu, V.-C. Bojan, F. Pop, M. Mocanu, and V. Cristea, "Real-time alert service for cyber-infrastructure environments," in *in 2015 10th International Conference on P2P, Parallel, Grid, Cloud and Internet Computing (3PGCIC)*, pp. 296–303, Krakow, Poland, 2015.

[104] H. Navarro-Hellín, J. Martínez-del-Rincon, R. Domingo-Miguel, F. Soto-Valles, and R. Torres-Sánchez, "A decision support system for managing irrigation in agriculture," *Computers and Electronics in Agriculture*, vol. 124, pp. 121–131, 2016.

[105] P. L. V. Priya, N. S. Harshith, and N. V. K. Ramesh, "Smart agriculture monitoring system using IoT," *International Journal of Engineering & Technology*, vol. 7, 2018.

[106] R. Gp, *Supply Chain Management in Agriculture*, NAARM, 2019.

[107] J. Blackburn and G. Scudder, "Supply chain strategies for perishable products: the case of fresh produce," *Production and Operations Management*, vol. 18, no. 2, pp. 129–137, 2009.

[108] W. Di, J. Wang, B. Li, and M. Wang, "A location-inventory model for perishable agricultural product distribution centers," in *in 2011 2nd International Conference on Artificial Intelligence, Management Science and Electronic Commerce (AIMSEC)*, pp. 919–922, Dengleng, 2011.

[109] L. P. Catalá, G. A. Durand, A. M. Blanco, and J. A. Bandoni, "Mathematical model for strategic planning optimization in the pome fruit industry," *Agricultural Systems*, vol. 115, pp. 63–71, 2013.

[110] A. Kamilaris, F. Gao, F. X. Prenafeta-Boldu, and M. I. Ali, "Agri-IoT: a semantic framework for Internet of Things-enabled smart farming applications," in *in 2016 IEEE 3rd World Forum on Internet of Things (WF-IoT)*, pp. 442–447, Reston, VA, USA, 2016.

[111] N. Kaewmard and S. Saiyod, "Sensor data collection and irrigation control on vegetable crop using smart phone and wireless sensor networks for smart farm," in *in 2014 IEEE Conference on Wireless Sensors (ICWiSE)*, pp. 106–112, Subang, Malaysia, 2014.

[112] A. Vishwakarma, A. Sahu, N. Sheikh, P. Payasi, S. K. Rajput, and L. Srivastava, "IoT based greenhouse monitoring and controlling system," in *in 2020 IEEE Students Conference on Engineering & Systems (SCES)*, pp. 1–6, Prayagraj, India, 2020.

[113] J. Song, "Greenhouse monitoring and control system based on zigbee wireless senor network," in *in 2010 International Conference on Electrical and Control Engineering*, pp. 2785–2788, Wuhan, China, 2010.

[114] G. Li, W. Zhang, and Y. Zhang, "A design of the IoT gateway for agricultural greenhouse," *Sensors & Transducers*, vol. 172, no. 6, p. 75, 2014.

[115] K. Balakrishna, S. N. Nethravathi, and K. Harshitha, "Real-time soil monitoring system for the application of agriculture," *International Journal of Engineering Science and Computing*, vol. 6, no. 5, 2016.

[116] B. Pratama, S. Sfenrianto, A. N. Fajar, A. Amyus, and R. Nurbadi, "A smart agriculture systems based on service oriented architecture," in *in 2018 3rd International Conference on Information Technology, Information System and Electrical Engineering (ICITISEE)*, pp. 281–286, Yogyakarta, Indonesia, 2018.

[117] R. J. Flor, G. Singleton, M. Casimero et al., "Farmers, institutions and technology in agricultural change processes: outcomes from adaptive research on rice production in Sulawesi, Indonesia," *International Journal of Agricultural Sustainability*, vol. 14, no. 2, pp. 166–186, 2016.

[118] Z. Laliwala, V. Sorathia, and S. Chaudhary, "Semantic and rule based event-driven services-oriented agricultural recommendation system," in *in 26th IEEE International Conference on Distributed Computing Systems Workshops (ICDCSW'06)*, Lisboa, Portugal, 2006.

[119] F. TongKe, "Smart agriculture based on cloud computing and IoT," *Journal of Convergence Information Technology*, vol. 8, no. 2, pp. 210–216, 2013.

[120] S. Nandhini, S. Bhrathi, D. D. Goud, and K. P. Krishna, "Smart agriculture IoT with cloud computing, fog computing and edge computing," *International Journal of Engineering and Advanced Technology*, vol. 9, no. 2, pp. 3578–3582, 2019.

[121] K. A. Patil and N. R. Kale, "A model for smart agriculture using IoT," in *in 2016 International Conference on Global Trends in Signal Processing, Information Computing and Communication (ICGTSPICC)*, pp. 543–545, Jalgaon, 2016.

[122] T. Ojha, S. Misra, and N. S. Raghuwanshi, "Sensing-cloud: leveraging the benefits for agricultural applications," *Computers and Electronics in Agriculture*, vol. 135, pp. 96–107, 2017.

[123] A. Kaloxylos, A. Groumas, V. Sarris et al., "A cloud-based farm management system: architecture and implementation," *Computers and Electronics in Agriculture*, vol. 100, pp. 168–179, 2014.

[124] H. J. Loschi, J. Leon, Y. Iano et al., "Energy efficiency in smart grid: a prospective study on energy management systems," *Smart Grid Renew. Energy*, vol. 6, no. 8, pp. 250–259, 2015.

[125] M. Eissa, *Energy Efficiency: The Innovative Ways for Smart Energy, the Future towards Modern Utilities*, BoD–Books on Demand, 2012.

[126] J. C. Stephens, E. J. Wilson, and T. R. Peterson, *Smart Grid (R) Evolution*, Cambridge University Press, 2014.

[127] K. Park, Y. Kim, S. Kim, K. Kim, W. Lee, and H. Park, "Building energy management system based on smart grid," in *in 2011 IEEE 33rd International Telecommunications Energy Conference (INTELEC)*, pp. 1–4, Amsterdam, Netherlands, 2011.

[128] A. L. Virk, M. A. Noor, S. Fiaz et al., "Smart farming: an overview," *Smart Village Technology*, pp. 191–201, 2020.

[129] T. Wheeler and J. Von Braun, "Climate change impacts on global food security," *Science (80)*, vol. 341, no. 6145, pp. 508–513, 2013.

[130] A. Moon, J. Kim, J. Zhang, and S. W. Son, "Evaluating fidelity of lossy compression on spatiotemporal data from an IoT enabled smart farm," *Computers and Electronics in Agriculture*, vol. 154, pp. 304–313, 2018.

[131] S. P. Vimal, N. Sathish Kumar, M. Kasiselvanathan, and K. B. Gurumoorthy, "Smart irrigation system in agriculture," *Journal of Physics: Conference Series*, vol. 1917, no. 1, p. 012028, 2021.

[132] G. Sivashankar, "A study on smart irrigation systems for agriculture using IoT," *International Journal of Advanced Engineering Science and Information Technology*, vol. 4, no. 4, 2021.

[133] M. Shyamala Devi, R. Suguna, A. S. Joshi, and R. A. Bagate, "Design of IoT blockchain based smart agriculture for enlightening safety and security," in *in International Conference on Emerging Technologies in Computer Engineering*, pp. 7–19, Springer, Singapore, 2019.

[134] O. Novo, "Blockchain meets IoT: an architecture for scalable access management in IoT," *IEEE Internet of Things Journal*, vol. 5, no. 2, pp. 1184–1195, 2018.

[135] Z. Zheng, S. Xie, H. Dai, X. Chen, and H. Wang, "An overview of blockchain technology: architecture, consensus, and future trends," in *in 2017 IEEE International Congress on Big Data (BigData Congress)*, pp. 557–564, Honolulu, HI, USA, 2017.

[136] M. Tech-Student, "A literature study on agricultural production system using IoT as inclusive technology," *Int. J. Innov. Technol. Res*, vol. 4, no. 1, 2016.

[137] K. Moummadi, R. Abidar, and H. Medromi, "Generic model based on constraint programming and multi-agent system for M2M services and agricultural decision support," in *in 2011 International Conference on Multimedia Computing and Systems*, pp. 1–6, Ouarzazate, Morocco, 2011.

[138] S. A. Salunke, S. Y. Chincholikar, and S. P. Kharde, "An overview on wireless sensor technologies for the development of agriculture," *International Journal of Computer Science and Mobile Computing*, vol. 4, no. 6, pp. 416–418, 2015.

[139] T. G. Patil and S. P. Shekhawat, "Industry 4.0 implications on agriculture sector: an overview," *International Journal of Management, Technology and Engineering*, vol. 9, 2019.

[140] N. H. Valente, "Agriculture 4.0-ensuring connectivity of agricultural equipment: challenges and technical solutions for the digital landscape in established farms with mixed or analogue equipment," *365FarmNet Berlin.*, vol. 12p, 2017.

[141] L. Barreto, A. Amaral, and T. Pereira, "Industry 4.0 implications in logistics: an overview," *Procedia Manufacturing*, vol. 13, pp. 1245–1252, 2017.

[142] A. W. Gray and M. Boehlje, *The Industrialization of Agriculture: Implications for Future Policy*, 2007.

[143] A. Bouguettaya, H. Zarzour, A. Kechida, and A. M. Taberkit, "Deep learning techniques to classify agricultural crops through UAV imagery: a review," *Neural Computing and Applications*, vol. 34, no. 12, pp. 9511–9536, 2022.

[144] A. Jámbor, P. Czine, and P. Balogh, "The impact of the coronavirus on agriculture: first evidence based on global newspapers," *Sustainability*, vol. 12, no. 11, p. 4535, 2020.

[145] R. Thakur and V. L. Manekar, "Artificial intelligence-based image classification techniques for hydrologic applications," *Applied Artificial Intelligence*, vol. 36, no. 1, 2022.

Hindawi

Retraction

Retracted: Analysis and Application of Crosscultural Knowledge System Structure in English Teaching Based on Hierarchical Correlation Analysis

Journal of Sensors

This article has been retracted by Hindawi following an investigation undertaken by the publisher [1]. This investigation has uncovered evidence of one or more of the following indicators of systematic manipulation of the publication process:

(1) Discrepancies in scope

(2) Discrepancies in the description of the research reported

(3) Discrepancies between the availability of data and the research described

(4) Inappropriate citations

(5) Incoherent, meaningless and/or irrelevant content included in the article

(6) Manipulated or compromised peer review

The presence of these indicators undermines our confidence in the integrity of the article's content and we cannot, therefore, vouch for its reliability. Please note that this notice is intended solely to alert readers that the content of this article is unreliable. We have not investigated whether authors were aware of or involved in the systematic manipulation of the publication process.

Wiley and Hindawi regrets that the usual quality checks did not identify these issues before publication and have since put additional measures in place to safeguard research integrity.

We wish to credit our own Research Integrity and Research Publishing teams and anonymous and named external researchers and research integrity experts for contributing to this investigation.

The corresponding author, as the representative of all authors, has been given the opportunity to register their agreement or disagreement to this retraction. We have kept a record of any response received.

References

[1] Z. Jianhong, "Analysis and Application of Crosscultural Knowledge System Structure in English Teaching Based on Hierarchical Correlation Analysis," *Journal of Sensors*, vol. 2022, Article ID 3874857, 11 pages, 2022.

Research Article

Analysis and Application of Crosscultural Knowledge System Structure in English Teaching Based on Hierarchical Correlation Analysis

Zhu Jianhong (ORCID)

Hunan Police Academy, Hunan, Changsha 410138, China

Correspondence should be addressed to Zhu Jianhong; 470934098@hnpa.edu.cn

With the prosperity of the economy, China's foreign exchanges are becoming more and more frequent, and English is becoming more and more important as the common language of international communication. For decades, Chinese educators and scholars have achieved great success in teaching English, but there are also some problems, including neglecting the teaching of crosscultural knowledge in English classrooms. And in the crosscultural English teaching based on hierarchical correlation analysis, its specific structure system is not complete, and its application scope is also less. Therefore, this paper analyzes hierarchical correlation analysis, teaching mode, etc., which lays the foundation for subsequent research. In addition, combined with the current research status, this paper analyzes the past crosscultural knowledge system and proposes a new structural model. A large number of experiments have verified the application effect of the improved knowledge architecture model in crosscultural English teaching under the hierarchical correlation analysis. The new model can improve students' crosscultural awareness and crosscultural communication competence and improve the previous teaching system structure. There is a problem that both hierarchical teaching and overall planning cannot be taken into account. This paper studies the crosscultural issues in English teaching and conducts research from the following four aspects: first, it discusses the cultivation of crosscultural communicative competence of college students in English teaching and proposes some feasible solutions to the problem of neglecting the integration of crosscultural knowledge in English teaching. Sexual suggestions cultivate students' crosscultural awareness of English learning and improve the efficiency of English learning. The second is to point out that college school students should pay attention to the differences in cultural communication between China and foreign countries and develop the awareness and ability of crosscultural communication. The third is to explore ways to improve students' crosscultural communicative competence and cultivate all-round English talents for the country and society. The fourth is how to achieve crosscultural communication, so that people with different cultural backgrounds can communicate and learn smoothly. Based on the above problems, this paper adopts the method of case analysis to discuss the problem of imperfect cross-cultural knowledge system in English teaching in China, and the educational structure is incomplete.

1. Introduction

This paper proposes a detection-based three-level hierarchical association method, which is applied to the study of thought reflection of people's cognitive process, and is evaluated on two datasets, cognitive and expressive. Experimental results show that the performance is greatly improved compared to previous methods [1]. We propose a hierarchical association method and train a key trajectory association model with the stimulus algorithm. This method uses a soft max function to relax the overtarget function of traditional instance ranking methods, which provides a tighter upper bound on the empirical error for distinguishing correct and incorrect associations, thereby providing a more accurate trajectory association model for trajectory association problems [2]. This paper proposes a data-oriented data association algorithm that relies on the Hungarian algorithm for the association step, which also treats detection responses

below the detection threshold as evidence associated with high ambiguity [3]. This paper introduces the problem of data mining association rules. We use an iterative approach to gradually increase the size of the itemset and describe the hierarchical algorithm in detail. Finally, an improved algorithm is proposed, which combines the last few iterations and scans the database at a time [4]. In this paper, a system-coupled hierarchical data association scheme is proposed, and a novel teaching model based on depth-invariant parts using RGB-D data is proposed. Our method is verified from several aspects, such as system coupling feature selection scheme, hierarchical data association scheme, and various RGB-D-based modeling schemes for teaching systems, proving its effectiveness and efficiency [5]. Bayesian networks (BN) use probability distributions to build models with the benefits of providing decision-making in complex domains, smooth, consistent, and flexible applicability and association rules based on antecedents and consequences with conditional and decision properties, respectively. We focus on association rules to develop automated data mining techniques, using the association rule binary symmetric matrix of the K2 (ARBSM-K2) technique to generate hierarchical association rules that exhibit more determinism in the hierarchy [6]. This paper shows how this problem can be addressed through corpus-based research, conducted through a study of the idioms most commonly used by students in spoken American English, which includes a close alignment of the idioms used in three contemporary corpora of spoken American English. A search and analysis revealed interesting patterns of English idiom usage [7]. This study investigated mainland Chinese parents' perceptions of their children's participation in English language learning programs outside the classroom. The hypothesis that Chinese parents prefer Westerners to be their children's English teachers has also been tested. The analysis of student perceptions of ELT and the structure of educational institutions in ELT under a cross-cultural system can provide many opportunities for future research in this field [8]. This paper studies college English teachers' decision to adapt teaching materials to adapt to learners' differences. The main purpose of this study is to conduct a descriptive and analytical study of teachers' decisions on the adaptation of English textbooks. This paper begins by describing a review of the college curriculum and English textbooks, analyzing the incremental decision-making model of the curriculum decision-making process and key elements of decision-making, and discussing the relationship between the different levels and elements of future teacher professional development [9]. Through a comprehensive literature review of knowledge management and intercultural competency research, seven thematic competencies of knowledge assimilation were identified. This paper provides a model to improve the crosscultural knowledge architecture to make it more complete [10]. The purpose of this paper is to focus on crosscultural impression management as part of acculturation, examining knowledge gaps by identifying differences between host country norms and domestic cultural norms. These findings tell us about how acculturation begins and are an in-depth qualitative study [11]. This article explores the role of leadership in crosscultural knowledge management (CCKM) and discusses the existing literature on leadership and crosscultural leadership and the relationship between leadership and knowledge management to illustrate the different domains of leadership role in. In order to emphasize the influence of leadership on CCKM, the influence of leadership on different factors in the theoretical model of CCKM was studied, and a multicultural management system was established [12]. This article focuses on the need for intercultural knowledge of people working and living in today's world, recognizing that cultural differences can lead to better employment opportunities. This article describes the benefits of working in multidisciplinary area groups to promote foreign language teaching. The authors highlight the importance of university education in changing and developing mindsets as a long-term way of ensuring stronger education systems [13]. This article discusses end-to-end (ETE) data analysis tools used by educational researchers such as data mining, culminating in the hierarchical knowledge management model (TKMM), which aims to provide a stable structure for organizing a large number of established and nascent technologies, revealing patterns and relationships in data through a high-performance data modeling process, and providing researchers with richer and more unified analytical tools [14]. Starting from the characteristics of English subject, this paper establishes an English model of knowledge structure, analyzes the English knowledge structure of college students, explores the characteristics of students' growth and the differences in the main influencing factors, and finds out the thinking and cognitive development system of college students' English comprehension: an effective way to explore English comprehension [15].

2. Association Function and Crosscultural Knowledge System

2.1. Association Function. The correlation function is a quantitative tool to describe the correlation degree of educational elements. When the educational element value is a specific value and within the range of meeting the requirements, the correlation function represents the change process of quantitative and qualitative change of education. In general, the extended set ρ is expressed in algebraic form to represent the correlation functions to quantitatively express the incompatibility of the contradiction problem, taking the value range as the real number domain $-\infty$, $+\infty$. Association degree is used to describe the relevance of each teaching feature to the proposed rating grade. Teaching characteristics are quantitatively described by the distance between v_i and the limited interval of the corresponding feature vector, recorded as the correlation function and expressed as formula (1):

$$\begin{cases} \rho(v_i, v_{ij}) = \dfrac{1}{2}(a_{ij} - b_{ij}) + \left| v_i - \dfrac{1}{2}(a_{ij} + b_{ij}) \right|, \\ \rho(v_i, v_{im}) = \dfrac{1}{2}(a_{im} - b_{im}) + \left| v_i - \dfrac{1}{2}(a_{im} + b_{im}) \right|. \end{cases} \quad (1)$$

2.2. Determine the Association Degree. Correlation is used to describe the correlation of various educational aspects of the education system with the proposed evaluation grade and can be compared with the concept of membership in obscure English. Scale reflects the level of educational system belonging to a specific classical field, but expanding educational models and differentiated information has richer significance than system concepts. Generally, based on the value of $K_j(v_i)$, when $K_j(v_i) \geq 1.0$, the specific value of the education system exceeds the upper limit of the evaluation score; when $0.0 \leq K_j(v_i) \leq 1.0$, the specific value of the education system reaches the standard range, the closer the median value of $K_j(v_i)$; when $-0.1 \leq K_j(v_i) \leq 0.0$, it shows that although the specific value of the education system is not within the specification, under certain conditions, the specific value can be converted into the standard range, and when the value of $K_j(v_i)$ is larger, the conversion process is about concise; when $K_j(v_i) \leq -0.1$, the specific value of the education system cannot be converted. The characteristics of the instructional system, within the criteria for the level of assessment, are represented by c_i. The correlation of grade j is shown in formula (2):

$$K_j(v_i) = \begin{cases} \dfrac{\rho(v_i, v_{ij})}{\rho(v_i, v_{im}) - \rho(v_i, v_{ij})}, \rho(v_i, v_{im}) \neq \rho(v_i, v_{ij}), \\ -\dfrac{\rho(v_i, v_{ij})}{|v_{ij}|}, \rho(v_i, v_{im}) = \rho(v_i, v_{ij}). \end{cases} \tag{2}$$

In feature $(c_1 c_2, \cdots, c_n)$, the comprehensive correlation of grade j rating is shown in formula (3):

$$\sum_{i=1}^{n} w_i K_j(v_i), \tag{3}$$

where w_i is the weight of the feature c_i.

2.3. Crosscultural Definition. Crosscultural refers to a cultural phenomenon that conflicts with national culture. From the perspective of cultural theory, cultural identity refers to the belonging and acceptance of a group or individual to a specific culture and has a specific cultural value orientation. The so-called "cross-culture" refers to the culture across different national boundaries, which is the interaction between many groups of different cultural backgrounds. In short, "interculture" is the interaction between all people who experience cultural connections through crossing system boundaries and is societies with increased social mobility and racial mixing in globalization. Tradition and the existing culture were combined to create a new culture.

2.4. Construction of Knowledge System. The knowledge system is not a single item of knowledge but a closed loop that a different knowledge content affects each other in a special way and can be used at any time. After the establishment, it is necessary to continuously expand and improve and gradually cultivate from a few saplings into a large forest. The establishment of the knowledge system is a lifelong teacher, and learners must master the ability. However, China's English education overemphasizes the teaching of language skills. Without a complete education system, it is impossible to teach both language skills and compare cultural differences in English classes. In the process of learning English, students can only master vocabulary, sentence forms, grammar, and other language forms, and it is difficult to carry out appropriate and effective crosscultural communication, which undoubtedly deviates from the ultimate goal of English learning. Therefore, English teachers should not only teach English level but also pay attention to improving students' crosscultural awareness. To promote students' crosscultural communication consciousness through college English teaching, it is necessary to organically combine the development of language function and ability with the improvement of cultural literacy and establish a comprehensive English education system with crossculture as the core. It is more necessary to optimize the curriculum system, clarify the teaching concept, and use the teaching methods for the purpose of enhancing the awareness of cultural comparison, so as to realize the tasks and goals of advanced English teacher in the new era.

3. Hierarchical Association Analysis

3.1. Association Rules under Teaching. In educational research, especially for teachers, statistics are very limited, and gray values are very large. Except for human reasons, the data often differ from the normal distribution rules. Therefore, the sequence curve geometry using association analysis is chosen to determine whether it is closely related. The closer the curve is, the greater the correlation between the corresponding sequences, and vice versa. For hierarchical association analysis, first, determine the corresponding attribute sequence and factor sequence, let X_i be the system factor, and the observation data on number k is $x_i(k)$, $k = 1, 2, \cdots, n$; then, $X_i = \{x_i(1), x_i(2), \cdots, x_i(n),\}$ is called the behavioral sequence of factor X_i. Correlation analysis can be performed for either time series data, index row data, or horizontal row data. If the system factor is a dimensionalized quantity, it must be treated correctly, and then the negative correlation factor is converted into a positive correlation factor through the action of the operator. One of the three transformation methods is usually used to reduce the behavioral sequence. The three transformation methods are shown in formulas (4)–(6):

$$\text{Initial value}: x_i(k)d_1 = \frac{x_i(k)}{x_i(1)}, x_i(1) \neq 0, k = 1, 2, \cdots, n, \tag{4}$$

$$\text{equalization}: x_i(k)d_2 = \frac{x_i(k)}{X_i}, \overline{X_i} = \frac{1}{n}\sum_{k=1}^{n} x_i(k), k = 1, 2, \cdots, n, \tag{5}$$

Interval value : $x_i(k)d_3 = \dfrac{x_i(k) - \min_k x_i(k)}{\max_k x_i(k) - \min_k x_i(k)}, k = 1, 2, \cdots, n,$ (6)

where d_1, d_2, d_3, all three operators, can make the dimensionalization and quantitative normalization of the behavior sequence of the system. In general, the three operators cannot be mixed or overlapped. In the system factor analysis, one of them can be selected according to the actual situation, and the transformed value is called the correlation factors.

3.2. Basic Steps of the Association Analysis. The steps of the comprehensive evaluation by using the association method are as follows:

(a) Clarify the assessment purpose, define the index scoring system, collect the index data, determine the data order, and form the formula (7)

$$(X_0, X_1, \cdots, X_n) = \begin{pmatrix} x_{11} & \cdots & x_{1n} \\ \vdots & \ddots & \vdots \\ x_{m1} & \cdots & x_{mn} \end{pmatrix}, \quad (7)$$

where m is the number of indicators $X_i = (x_i(1), x_i(2), \cdots, x_i(m)), i = 0, 1, \cdots, n$. If the k-th index in the data is the reverse indicator and recorded as $x_i(k)$, the reverse indicator must be turned forward as formula (8). Some are indicators that the larger the index value is, the better the evaluation is and are called positive indicators (also known as benefit-type indicators or large-scale indicators, cost-type indicators or small-scale indicators), and some indicators whose value is closer to a certain value, the better, are called moderate indicators. In the comprehensive evaluation, the index must be the same trend first, and generally, the reverse index is converted into a positive index; so, it is also called the forwardization of the reverse index.

$$X_i(k) = \max\{x_i(k)\} - x_i(k), i = 1, 2, \cdots, n. \quad (8)$$

(b) Determine the reference data column X_0, that is, to determine the ideal comparative model according to the purpose of the evaluation (note to formula (9))

$$X_0 = (x_0(1), x_0(2), \cdots, x_0(m)). \quad (9)$$

(c) The index data sequence is preprocessed, such as formula (10)

$$(X_0, X_1, \cdots, X_n) = \begin{pmatrix} x_0(1) & x_1(1) & x_n(1) \\ x_0(2) & x_1(2) & x_n(2) \\ x_0(m) & x_1(m) & x_n(m) \end{pmatrix}. \quad (10)$$

(d) Calculate the absolute difference between the corresponding elements of each index sequence and the reference sequence, as shown in formula (11):

$$|x_0(k) - x_i(k)| \, ; k = 1, \cdots, m \, ; i = 1, \cdots, n. \quad (11)$$

(e) Determine between $\min\limits_{i=1} \min\limits_{k=1} |x_0(k) - x_i(k)|$ and $\max\limits_{i=1} \max\limits_{k=1} |x_0(k) - x_i(k)|$

(f) The correlation coefficient is calculated separately for the corresponding element of each comparison sequence and the reference sequence, as shown in formula (12):

$$\zeta_i(k) = \dfrac{\min\limits_{i=1} \min\limits_{k=1} |x_0(k) - x_i(k)| + \rho * \max\limits_{i=1} \max\limits_{k=1} |x_0(k) - x_i(k)|}{|x_0(k) - x_i(k)| + \rho * \max\limits_{i=1} \max\limits_{k=1} |x_0(k) - x_i(k)|},$$
$$k = 1, \cdots, m. \quad (12)$$

ρ is the resolution coefficient, taking the value within $(0, 1)$, and the smaller ρ, the greater the difference between the correlation coefficients, and the stronger the distinguishing ability.

(g) According to the different importance of each index in the total score, calculate the correlation degree, assign appropriate weights to each index, and calculate the weighted average of the correlation coefficient:

$$r(X_0, X_i) = \dfrac{1}{m} \sum_{k=1}^{m} W_k \zeta_i(k), k = 1, \cdots, m, \quad (13)$$

where W_k is the weight of each indicator.

(h) According to the correlation degree of the observed objects, a comprehensive evaluation result is obtained

3.3. Establish a Hierarchical Structure Model. The construction of hierarchical models is mainly conducted by comparing the influence of various factors at the same level on the corresponding factors. It lets you compare n factors X_1, $X_2, \cdots, X_n$, the influence on the upper layer that is, which determine its proportion in the previous layer. For any two factors X_i and X_j, a_{ij} represents the ratio of X_i and X_j on the previous level, and you can get pairwise comparison structure $A = (a_{ij})_{n \times n}$; when $a_{ij} > 0$, the formula (14) is as follows:

$$a_{ij} = \dfrac{1}{a_{ij}}, a_{ij} = 1, (i, j = 1, 2, \cdots, n). \quad (14)$$

If the elements of structure A are transitional, i.e., satisfy $a_{ik}a_{kj} = a_{ij}$, then A is said to be a consistent structure.

3.4. Conformance Inspection. Method 1: take the arithmetic mean of the normalized column vector of the array list, roughly calculated as the weight, as shown in formula (15):

$$w_i = \frac{1}{n} \sum_{j=1}^{n} \frac{a_{ij}}{\sum_{k=1}^{n} a_{ij}} (i = 1, 2, \cdots, n). \qquad (15)$$

Method 2: the row (or column) vector A is geometrically average normalized and can be approximated as a weight, namely, the formula (16)

$$w_i = \frac{\left(\prod_{j=1}^{n} a_{ij} \right)^{1/n}}{\sum_{k=1}^{n} \left(\prod_{j=1}^{n} a_{ij} \right)^{1/n}}, (i = 1, 2, \cdots, n). \qquad (16)$$

When one array is exactly consistent, all the other eigenvalues are zero. In practice, absolute consistency is not required, but it is usually required to be substantially consistent. The consistency ratio is CR = CI/RI (CI is the consistency index, and RI is the random consistency index); when CR < 0.10, the consistency of the matrix can be considered acceptable. The corresponding attribute vectors can then be used as the weight vector for sorting. At this time, $\lambda_{\max}$ satisfies the formula (17)

$$\lambda_{\max} \approx \sum_{i=1}^{n} \frac{(AW)_i}{nw_i}, \qquad (17)$$

where $(AW)_i$ represents the i-th component of AW. It is now assumed that the weight vector of the n_k element on layer k to the j element on layer $k-1$ is

$$X_j = \left(x_{1j}^{(k)}, x_{2j}^{(k)}, \cdots, x_{nj}^{(k)} \right)^{T}, j = 1, 2, \cdots, n_{k-1}. \qquad (18)$$

The matrix satisfies the formula (19)

$$X^k = \left[X_1^{(K)}, X_2^{(K)}, \cdots, X_{n_{k-1}}^{(K)} \right]. \qquad (19)$$

The elements on the k layer have a total sorting weight vector of the target layer $W^{(k)}$, as shown in formula (20):

$$W^{(k)} = \left(w_1^{(k)}, \cdots, w_{n_k}^{(k)} \right)^{T} = X^{(k)} \cdot W^{(k)}$$
$$= \left[X_1^{(K)}, X_2^{(K)}, \cdots, X_{n_{k-1}}^{(K)} \right] \cdot W^{(k-1)}. \qquad (20)$$

3.5. The Application of the Hierarchical Association Analysis. Hierarchical correlation analysis is an important application of theory teaching, and the main idea is to assess the closeness of relationships through the similarity of the sequence curve geometry. Let $X_i = (x_i(1), x_i(2), \cdots, x_i(n))$ and $X_m = (x_m(1), x_m(2), \cdots, x_m(n))$ be the sequence of correlated fac-

tors. Given the real number $\sum_{k-1}^{n} r(x_0(k), x_i(k))$, if the real number satisfies the formula (21), then

$$r(x_m, x_m) = \frac{1}{n} \sum_{k-1}^{n} r(x_0(k), x_i(k)). \qquad (21)$$

It is said to have standardization, integrity, and dual symmetry, and the representative formula is shown in (22)–(24):

$$0 < r(X_0, X_i) \leq 1, r(X_0, X_i) = 1 \Leftarrow X_0 = X_i, \qquad (22)$$

$$X_j, X_i \in X \{ X_s = s = 0, 1, 2, \cdots, m, m \geq 2 \} r(X_i, X_j) \neq r(X_j, X_i), \qquad (23)$$

$$r(X_i, X_j) = r(X_j, X_i) \Leftrightarrow X = \{ X_i, X_j \} X_j, X_i \in X. \qquad (24)$$

In addition, the smaller $|(x_0(k) - x_0(k)|$ is and the larger $r(X_i, X_j) \neq r(X_j, X_i)$ is in the proximity, then $r(X_0, X_i)$ is called the degree of correlation between X_i and X_0. $r(x_0(k), x_i(k))$ is the correlation coefficient between H and X_i at point X_0. Completeness reflects the influence of the system on the comparison of correlations, which vary from system to system. Therefore, the principle of symmetry is not necessarily satisfied. Pairwise symmetry means that when there are only two sets in the set of correlation factors, the pairwise comparison satisfies the symmetry. Proximity, on the other hand, is a constraint to quantify relatedness. The general hierarchical structure diagram is divided into three layers, of which the highest layer is the goal or ideal result of the problem decision at the target layer, and there is only one element. The middle layer is the criterion layer, which includes all the factors involved in the intermediate links in order to achieve the goal, and each factor is a criterion. The lowest layer is the program layer. The program layer is a variety of measures to choose from to achieve the goal, that is, the decision-making program. Generally speaking, some factors between different levels are related, and some are not necessarily related. The number of factors at each level may not necessarily be the same. In practice, it is determined according to the nature of the problem and the categories of relevant factors.

4. An Empirical Study on the Application of Intercultural Knowledge in English Teaching

4.1. Data Acquisition. Under the guidance and assistance of relevant experts, this study determines the following specific observation aspects: the teaching and development of crosscultural knowledge, the cultivation of crosscultural communication attitude, etc. The nonparticipatory observation method is adopted to understand the state of students' multicultural knowledge in classroom teaching without interfering with teachers' teaching activities and students' normal learning. This paper adopts a questionnaire survey, which consists of three dimensions: crosscultural knowledge teaching, cultivating crosscultural communication attitude, and crosscultural communication development ability. In

Table 1: Sample distribution in the questionnaire survey.

Title	Option	Number of people	Total proportion
Distribution of grades	Freshman	100	35.10%
	Sophomore	92	32.30%
	Senior	93	32.60%
Distribution of sex	Man	119	41.80%
	Woman	166	58.20%
Distribution of English scores	More than 600 points	33	11.50%
	500-600 points are scored	120	42.10%
	425-500 points are scored	97	34%
	Under 425 points	35	12.30%
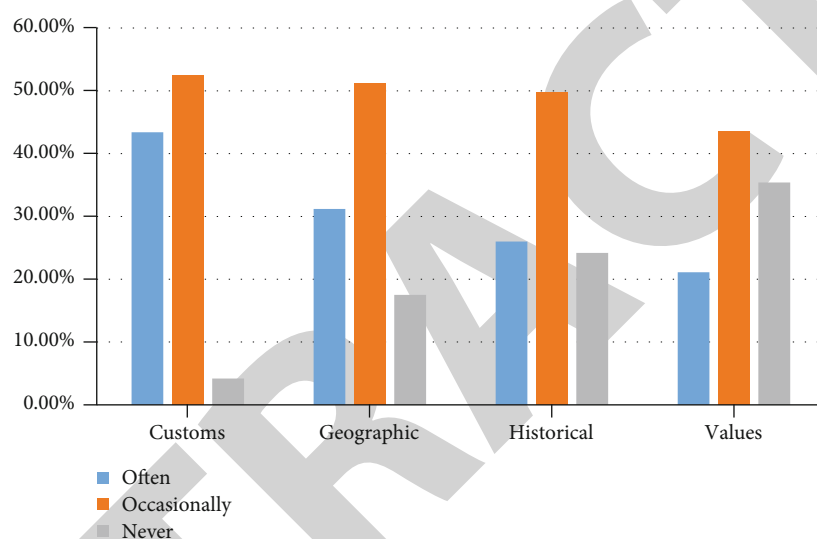
Figure 1: Crosscultural teaching of English teachers.

order to deeply understand the actual situation of crosscultural knowledge training of College English teachers and students, this study is conducted from three aspects: teaching intercultural knowledge, cultivating crosscultural communication attitude, and cultivating intercultural communication attitude. Explore and analyze in English teaching to find out the problems existing in the cultivation. The sample questionnaire was selected from three colleges in J City, Hunan Province. Each college issued 100 votes to students, issued a total of 300 votes, and recovered 285 valid votes, with a valid recovery rate of 95%. The detailed sample distribution of the survey subjects is shown in Table 1.

4.2. Teaching Situation of Crosscultural Knowledge in English Teaching. The formation of any skill should be based on knowledge, so that students should have crosscultural communication competence, and students should have enough crosscultural knowledge. Students' multicultural communication competence is closely related to crosscultural knowledge, and English teaching is the most direct way to acquire crosscultural knowledge. Learning more promotes the development of students' intercultural communicative

competence, but does nothing for the development of skills, and even hinders their subsequent learning. Therefore, this paper examines and analyzes the transfer of foreign cultural knowledge, intercultural language knowledge, and communicative knowledge under the dimension of crosscultural knowledge transfer, so as to show the crosscultural knowledge reserve of college school English teachers. The crosscultural teaching conducted by English teachers is shown in Figure 1.

From the survey results in Figure 1, it is not difficult to see that the overall situation of English teachers teaching students the cultural knowledge from other countries is not very close to the reality, and it is difficult to impress people. However, it is worth confirming that the teachers' understanding of students about foreign customs and Western thoughts is good, and the frequency of lectures is relatively high. The teaching of intercultural language knowledge by college English teachers is shown in Figure 2.

From the survey results in Figure 2, it is not difficult to see that teachers' crosscultural language ability is relatively enough to enable students to understand the culture behind the language from multiple perspectives and clearly realize
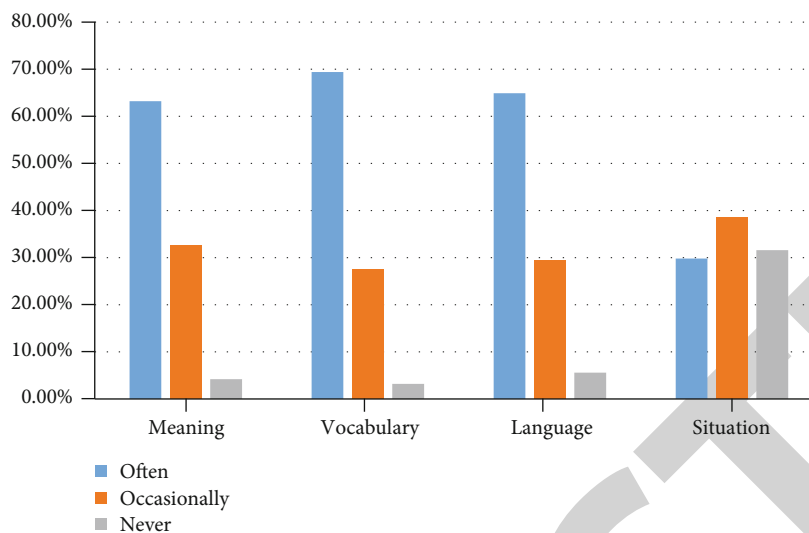
Figure 2: Teachers impart crosscultural language knowledge to students.
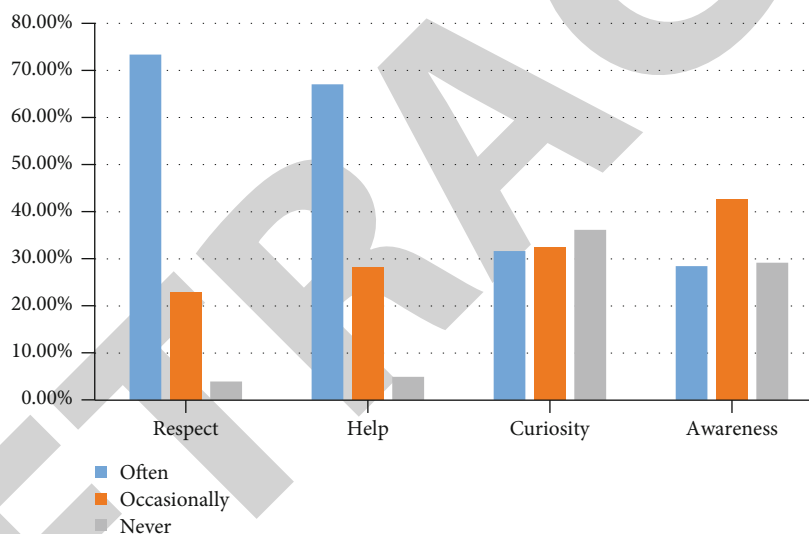
Figure 3: Teachers' cultivation of attitudes towards students' crosscultural communication.

the importance of language ability. However, the existing problems are also more obvious: in language practice, teachers fail to simulate the context and communicative situation.

4.3. Cultivation of Crosscultural Communication Attitude in English Teaching. The main obstacle to students' crosscultural communication is not only the language itself but also the understanding of the sociocultural background and personal attitudes of other countries. Students should be prepared to actively understand foreign cultures, actively explore the similarities and differences between different cultures, respect cultural diversity, and lay the foundation for successful crosscultural exchanges in the future. From the current situation of higher education in China, classroom teaching is not only the main channel for teachers to transfer knowledge but also a platform for students' cognition of the

outside world. The status of English teachers in cultivating students' crosscultural communication attitude is shown in Figure 3.

As can be seen from the data in Figure 3, although teachers are very good at cultivating students' respect and understanding of foreign culture, they still lack the cultivation of communicative attitude, and the importance of cultivating crosscultural communication ability has not been recognized. In addition, many times, people cannot master all the communication knowledge; so, using communication strategies is particularly important. In the process of communication, we will inevitably encounter various difficulties. By choosing appropriate communication strategies, we can effectively avoid silence and embarrassment. The main place for college students to learn intercultural communication is the English classroom. Therefore, whether teachers teach English the necessary communication strategies in class will
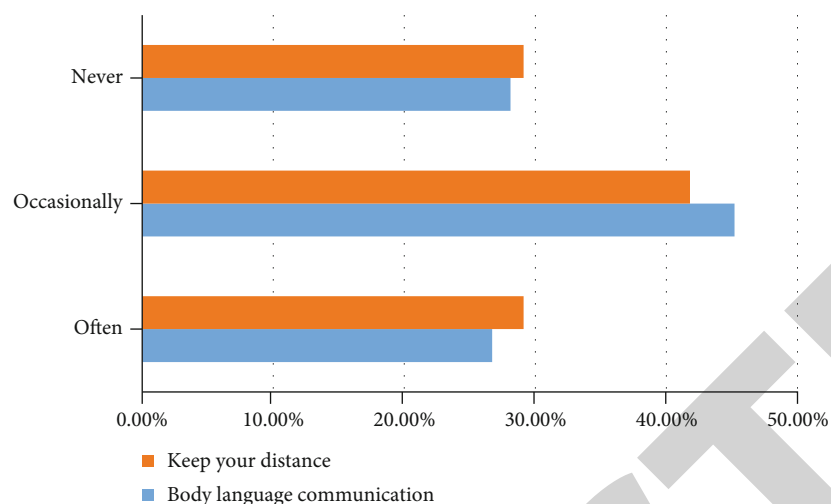
Figure 4: Teachers' cultivation of students' intercultural communication strategies.

Table 2: Scale evaluation score statistics of crosscultural communication competence.

Class	The gift of tongues	Pragmatic ability	Strategy ability	Crosscultural knowledge	Crosscultural attitude
Number of people	43	43	43	43	43
Total points	30	30	30	30	30
Average	13.76	12.83	17.24	15.18	19.69
Scoring average	39.2	42	68.96	65.63	70.9
Standard error	3.24	2.15	2.61	2.37	1.43

be the key to the improvement of students' crosscultural communication ability. The development of intercultural communication strategies by English teachers is shown in Figure 4.

The survey results in Figure 4 show that teachers' cultivation of students' intercultural communication strategies is not enough. Although it is involved, they do not often teach intercultural communication strategies to students. The abscissa is a ratio, which represents a situation in which English teachers maintain distance and communicate with body language when they train students in crosscultural communication, that is, never, occasionally, and often.

4.4. TTPC Strategy Cultivation in the Crosscultural Communication competence of College Students. In order to verify the effect of face-to-face teaching through classroom experiments, we made the following research assumptions before the study: after the implementation of TTPC teaching strategy, the experimental classroom students' crosscultural communication competence was significantly improved. It has improved after the learning test, which means that the application of TTPC learning strategy can enhance students' crosscultural communication skills. Before the start of the experiment, we tested them using the crosscultural communicative competence rating scale and performed a descriptive statistical analysis of the statistics, as shown in Table 2.

Table 2 shows that the scores for the six dimensions of crosscultural communication competence show that the average score of crosscultural attitudes was 19.69, the highest among the five dimensions, indicating one attitude of students'

favorable feelings towards crosscultural teaching. The norm is 1.43 poor compared to those in other countries, indicating that students' long-standing desire for intercultural communication is common. Secondly, due to frequent exchanges and technological progress, students can master some crosscultural basic knowledge and dare to use it boldly in crosscultural communication. On this basis, we performed crosscultural communication ability tests, and a descriptive statistical analysis of the statistics is presented in Table 3.

Table 3 shows that in the crosscultural situation test, the average of students' five dimensions of crosscultural communication competence corresponds to the results of Table 2, and then the average scores and standard deviations of the two classes were compared as shown in Figure 5 (class 1 is the scale evaluation class, and class 2 is the situational test class).

Figure 5 The comparison results show that most of the students can show a positive attitude in the test, willing to actively communicate with foreign teachers and express their ideas and opinions. We should maintain this crosscultural exchange activity.

4.5. t-Test Analysis. After the classroom experiment, the author again used two research tools to evaluate the crosscultural communication competence of experimental classroom students from six dimensions: individual changes and overall classroom differences were analyzed by the SPSS paired t-test sampling method, see also Figures 6 and 7. The M value here refers to a measure of strategic ability,

TABLE 3: Crosscultural communication competence and scores of all dimensions.

Class	The gift of tongues	Pragmatic ability	Strategy ability	Crosscultural knowledge	Crosscultural attitude
Number of people	43	43	43	43	43
Total points	20	20	20	20	20
Average	10.07	10.04	12.02	11.44	14.64
Scoring average	50.85	55.2	45.6	55.65	49.2
Standard error	3.26	2.39	3.11	2.27	2.91
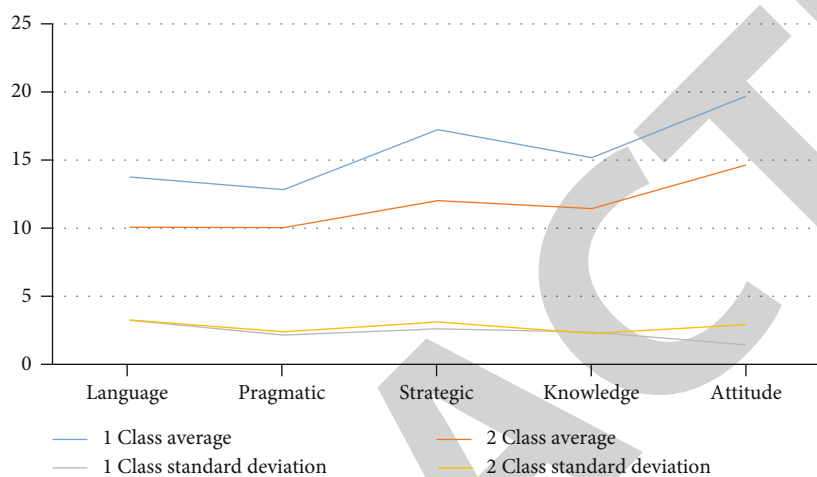
FIGURE 5: Comparison of mean scores and SD between the two classes.
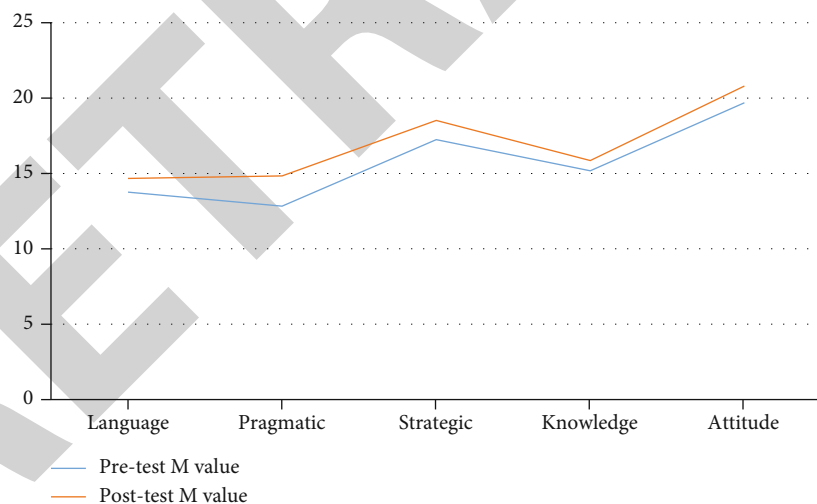
FIGURE 6: Comparison of the t-test results of the paired samples before and after the evaluation of the experimental class scale.

crosscultural attitude, language ability, crosscultural knowledge, and pragmatic ability, and the size of the M value represents the strength of ability.

As can be seen from the comparison of data in Figure 6, there were very significant differences between crosscultural communication competence dimensions before and after the experiment, while there was no significant difference in crosscultural knowledge.

As can be seen from Figure 7, pragmatic abilities and crosscultural attitudes differ significantly before and after the experiment but not in language abilities and cross-cultural knowledge. Compared with the conclusion of Figure 6, it can be seen that the differences and changes in the various dimensions of crosscultural communication competence in Figure 7 are consistent with them in principle. Data on intercultural communication ability are now shown in Table 4.
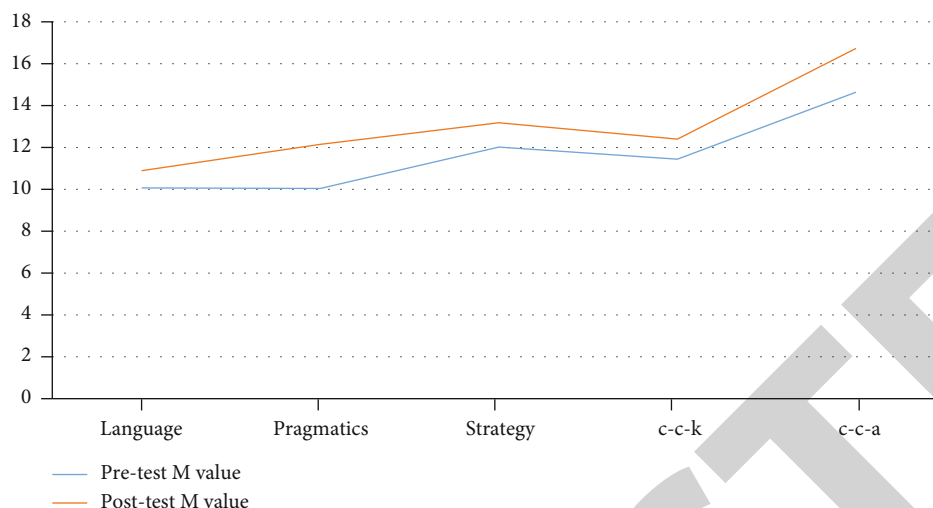
FIGURE 7: Comparison of the *t*-test results of the paired samples before and after the experimental class scenario test.

TABLE 4: Test and comparison of crosscultural communication competence between the two classes.

Group	Average score of pretest	Posttest average score
Scale assessment class	78.7	84.69*
Situational test class	58.21	65.35*

TABLE 5: The factors influencing teacher's curriculum design ability.

Curriculum design ability-school system atmosphere	Correlation (), γ_{oi}
Lesson preparation	0.8542
The number of lectures	0.5610
Training method	0.8889

The results in Table 4 clearly indicate that the intercultural communication ability was measured using the teaching scale, and the situational test was significantly different from the pretest ($P < 0.05$). It can be concluded that through the experimental teaching of TTPC learning strategies, students' crosscultural communication competence is significantly improved. In this article, * means $P < 0.05$; that is, the crosscultural communication competence of the scale is significantly different from the previous one, and the ability has been greatly enhanced.

4.6. Application of Hierarchical Correlation Analysis in Teacher Curriculum. The factors influencing teachers' curriculum design ability are divided into five dimensions: school system atmosphere, teaching materials, teachers' attitude, teachers' knowledge, and teachers' ability to use teaching materials. We conducted a separate study of the College

institutional atmosphere and obtained a total of 3 sets of data, as shown in Table 5.

Table 5 shows that training methods are related to course design skills > degree of lesson preparation to course design skills > number of lectures to course design skills. In addition, hierarchical correlation analysis can also be applied to the correlation degree of the overall curriculum design ability and curriculum resource status, the overall curriculum design ability and teachers' attitude, the overall curriculum design, the overall course design ability and curriculum resource utilization ability, and so on.

5. Conclusion

In today's globalization, international exchanges are increasingly common, and crosscultural exchanges will inevitably encounter cultural differences and potential communication barriers. Therefore, in foreign exchange trading and communication, it is necessary to have certain crosscultural communication skills to ensure smooth and effective communication. Although intercultural communication and college English teaching belong to different fields, the common goal is to cultivate people with both intercultural communication skills. Language teaching eliminates the language barrier of crosscultural communication and lays the foundation for crosscultural communication through the coordinated evolution of language teaching. Crosscultural communication should make full use of foreign language teaching and organically combine crosscultural communication education with foreign language teaching to achieve a profitable situation. In the process of English teaching reform in higher education, we can see the significant changes in the continuous improvement of students' English skills, but we must also objectively solve the problems existing in the current teaching mode. Change teaching methods, pay attention to language knowledge and skills, ignore cultural teaching, and ignore the input and output of local culture, teaching culture imbalance, lack of interoperability, teaching cooperation and communication, and indifferent communication

Hindawi

Retraction

Retracted: Empirical Study on the Grain Output Based on Regression Analysis

Journal of Sensors

This article has been retracted by Hindawi following an investigation undertaken by the publisher [1]. This investigation has uncovered evidence of one or more of the following indicators of systematic manipulation of the publication process:

(1) Discrepancies in scope

(2) Discrepancies in the description of the research reported

(3) Discrepancies between the availability of data and the research described

(4) Inappropriate citations

(5) Incoherent, meaningless and/or irrelevant content included in the article

(6) Manipulated or compromised peer review

The presence of these indicators undermines our confidence in the integrity of the article's content and we cannot, therefore, vouch for its reliability. Please note that this notice is intended solely to alert readers that the content of this article is unreliable. We have not investigated whether authors were aware of or involved in the systematic manipulation of the publication process.

Wiley and Hindawi regrets that the usual quality checks did not identify these issues before publication and have since put additional measures in place to safeguard research integrity.

We wish to credit our own Research Integrity and Research Publishing teams and anonymous and named external researchers and research integrity experts for contributing to this investigation.

The corresponding author, as the representative of all authors, has been given the opportunity to register their agreement or disagreement to this retraction. We have kept a record of any response received.

References

[1] J. Xu, S. Tang, P. Li, and H. Zhang, "Empirical Study on the Grain Output Based on Regression Analysis," *Journal of Sensors*, vol. 2022, Article ID 2567790, 10 pages, 2022.

Hindawi

Research Article

Empirical Study on the Grain Output Based on Regression Analysis

Jiahao Xu ⓘ, Sai Tang ⓘ, Pengyan Li ⓘ, and Hexu Zhang ⓘ

Harbin Institute of Technology, China

Correspondence should be addressed to Sai Tang; tangsai86@126.com

Based on a literature review of influencing factors and forecasting methods for grain production, the empirical analysis of the influencing factors of China's grain output is performed using the full subset regression method, the ridge regression method, and the LASSO regression method. The results show that (1) the increase in the sown area of grain crops is the main reason for the increase in grain output, (2) the use of agricultural fertilizers and the increase in rural electricity consumption are the driving factors for the increase in grain output, (3) the impact of total power of agricultural machinery is limited, and (4) natural disasters have a certain negative impact on food production.

1. Introduction

Food is not only the basis for the people's survival but also the basis for the development of a country. At present, China's economic activities are stable, but the external environment is complex and severe, the economy is facing downward pressure, and risks and difficulties have increased significantly. If there is a problem with the supply of food and important agricultural products, it will not only lead to rising prices, which will cause economic development to fall into a passive situation of downward growth and rising prices, but will also affect social stability. Therefore, it is particularly important to deepen agricultural supply-side reforms and increase grain production capacity. There are some of the key strategies for lowering farm produce production costs, and raising farmer income is to improve agricultural productivity. The level of farmers' income is influenced by their motivation and the safety of the country's food supply. The primary objective of the structural reform of the agricultural supply side, as stated in 2017's No. 1 Central Document, is to raise farmers' incomes and assure an adequate supply. The topic of peasant revenue and reducing the income disparity among urban and rural inhabitants as a "14th Five-Year" period in 2019 and 2021 was discussed in the No. 1 Central Document once more

[1]. Generally, everyone understands that land is where farmers get the majority of their revenue. When grain prices are constant, increasing cost effectiveness and lowering production expenses are practical and efficient strategies to increase farmers' revenue [1, 2].

Since the reform and opening up, especially since the implementation of the household coproduction contract responsibility system, due to the continuous optimization of agricultural-related policies, the continuous improvement of agricultural technology, the deepening of market-oriented reforms, and the dividends released by China's overall macroeconomic development, China's food production has been greatly improved [3]. Taking 2019 as an example, the country's total grain output was 66.384 million tons, achieving "sixteen consecutive harvests." However, due to the influence of uncertain factors such as changes in the industrial structure, increasing restrictions on grain production factors, and fluctuations in the international grain market, the space for further increase in China's grain output has gradually narrowed. Therefore, in order to "ensure basic self-sufficiency of grain and absolute security of rations," it is necessary to clarify important factors affecting grain production, determine effective ways to further increase grain production, continue to do a good job of stabilizing agricultural production and ensuring supply and increasing farmers' income, promote high-quality

agricultural development, and maintain harmony and stability in rural society [4, 5].

Based on the summary of previous research on influencing factors and prediction methods of grain production, this paper uses the full subset regression method, the ridge regression method, and the LASSO regression method to conduct empirical analysis of the main influencing factors of China's grain output from 1991 to 2018.

2. Literature Review

The research on the influencing factors of grain output is mainly carried out from six aspects. First, agricultural resources such as arable land and water are hard constraints on food security. Xiaoshi et al. analyzed the relationship between changes in the quantity and quality of cultivated land and food production and argued that with the economic development and industrialization process, a large amount of agricultural land was deagriculturalized, which had negatively affected food security [1, 6, 7]. Ahmed and Melesse and Han et al. believed that cultivated land resources were the most basic material conditions for agricultural production, and changes in their quantities directly affect food production and food security [7, 8]. Second, population size and population structure will affect food security. Wei et al. and Feng believed that with population growth and consumption expansion, China's future arable land size and per capita arable land area would further decline, and the per capita food consumption level and total food demand would further increase [2, 9]. Yuqiu and Lei believed that the adjustment of China's future population structure would further reduce the growth rate of total food demand [4]. To some extent, changes in population structure have a positive impact on food security. Xiaoshi et al. and Taotao et al. explored the impact of demographic changes on China's food security from the perspective of supply and demand. The results showed that with the advancement of population aging and population urbanization, Xiaoshi et al. were of the opinion that China's food security had suffered a lasting negative impact [1, 10].

Compared with nonhealthy workers, healthy workers have advantages in "rational" choice. On the one hand, as an input factor, healthy human capital participates in labor and forms a reasonable total allocation with other production factors [7]. On the other hand, due to the strong adaptability of labor intensity, it can avoid the unconditional excessive. A study by Xiaoshi et al. and Wei et al. pointed out that the impact of human capital on agricultural production efficiency would change with the scale of cultivated land. However, there are also some literatures that the contribution of human capital in agricultural production is not significant [1, 2]. Jingbo and Yuan and Xiang and Zhong found that the human capital had a positive role in promoting rural economic growth, but the contribution rate was low [3, 11]. Even a few scholars like Sanusi and Singh and Xuejiao and Haifeng have shown that the effect of human capital on rural economic growth was not significant and even sometimes played a negative role. Third, the relationship between urbanization and food security is studied [12, 13]. Wang conducted an empirical study

on the relationship between urbanization and food security using panel data from 31 provinces and cities from 1997 to 2015. The results showed that the development of urbanization had an adverse effect on food security [14]. Cai took Henan Province as the research object and found that rapid urbanization had imposed constraints on food production, and a large number of rural laborers had moved to cities. The expansion of cities and towns had caused large areas of farmland to be converted to nonagricultural land, which had led to increased food security pressure [15]. Fourth is how agricultural technological progress affects food security. Xiaoshi et al. and Du believed that agricultural technological progress had a great impact on food security, and it was necessary to increase investment in agricultural technological progress and increased the use of advanced agricultural technologies to improve the level of food security [1, 16]. Fifth, impact of climate change on food security has been considered. Chen and Xie and Chih-Ming believed that climate disasters would severely affect the balance of food production and food production systems and that an agricultural meteorological disaster defense system needed to be built to improve China's food security level [17, 18]. Chih-Ming and Qiu et al. believed that climate warming would threaten China's food security. It would also change the global food trade pattern and increase factors of instability [18, 19]. In addition to the above factors, the existing literature has also studied from more micro perspectives such as how drought, the use of biomass energy, and genetic modification affect food security.

From the perspective of the main influencing factors, the research mainly focuses on regression and grey correlation analysis. For example, Yin et al. used the data from 1991 to 2005 and 2006 to 2010 to conduct grey prediction and grey correlation analysis. The results showed that the irrigated area, agricultural production materials, agricultural product prices, and grain sown were the main factors which affected grain production [20]; Zai et al. used stepwise regression to perform a regression analysis on 12 factors affecting grain production in Henan Province and determined that the main influencing factors were fertilizer application, pesticide application, and agriculture were the three expenses for fertilizer application, pesticide application and agriculture technology and the planting area [21]; Qiling and Zhang also used gradual regression method to conduct an empirical analysis of six factors that affect China's grain production in 2000-2015. Area was a significant factor affecting grain output [22]. Considering the existence of multicollinearity, many scholars have also used ridge regression to reduce the impact of the collinearity problem on parameter estimation, making the regression results more economically significant. For example, Huang's quantitative analysis of the factors affecting China's food production based on revised CD production function and ridge regression and used the data from 1990 to 2008. The results showed that the increase in machinery input and improvement in irrigation conditions could increase food production, while labor input and chemical fertilizer input were not the driving factors for the increase of food production, and natural disasters still had a strong negative impact on food production, and food production showed increasing returns to scale [23].

From the perspective of food production forecasting, in addition to the above theories and models, time series models, support vector machines, and BP neural networks are the main research hotspots. Zhang et al. used data from 1978 to 2009 and the moving average model ARIMA to analyze and forecast China's total food production. The results showed that the smooth ARIMA model has higher accuracy than the ARIMA model [24]. The filter analysis method separates China's grain production from 1949 to 2008 into a time trend series and a fluctuation series. A polynomial model for the time series was established for the trend series, and a spectrum filtering method was used to estimate and fitted the fluctuation period of the grain output. The above two models were superimposed to predict China's grain output in the next 10 years [25]; Li used the grey correlation analysis of the grain production system to determine the main impact factors in view of the complexity and incompleteness of the grain production system and combined support vector machines to build a prediction model [26]. In addition, many scholars have combined the grey correlation theory or stepwise regression method with BP neural network, the former determines the indicators used, and the latter is used to predict food production [27, 28]. The idea of the LASSO method is that the sum of absolute coefficients cannot be too large. Under this premise, applying the ordinary least squares method, the sum of squares of residuals is the least [28]. In order to ensure the dietary balance of Chinese residents, the influence factors of cereal consumption are valuable to research. They first use the LASSO method to select the main influence factors of cereal consumption, and then, they constructed a partially linear semiparametric model for predicting the cereal consumption of Chinese residents. The results show that the factors affecting per capita consumption of rice, wheat, and maize are different from one another and the three cereals have both common impact factors and differentiated ones; per capita disposable income is the common factor with a linear positive relationship to the consumption of the three cereals; the model constructed in this paper is well fitted and can accurately forecast the consumption of cereals; the average per capita consumption of rice, wheat, and maize is predicted to be 78.56 kg/year, 62.73 kg/year, and 6.64 kg/year, respectively, by 2025, which is excessive and is caused by irrational dietary structure, food wastage, and processing losses [29].

Other models use the whole information generated by spectral measurements, such as ridge regression, which was introduced by Tikhonov and generalized by Hoerl and Kennard [30, 31]. This type of multivariate linear regression includes a contraction of the multivariate model regression coefficients and reduces them to the same degree [25]. Hernandez et al.'s study evaluated the ability of canopy reflectance spectroscopy at the range from 350 to 2500 nm to predict grain yield in a large panel (368 genotypes) of wheat (Triticum aestivum L.) through multivariate ridge regression models. Plants were treated under three water regimes in the Mediterranean conditions of central Chile: severe water stress; mild water stress; and full irrigation with mean grain yields of 1655, 4739, and 7967 kg·ha^{-1}, respectively. Models developed from reflectance data during anthesis and grain filling under all water regimes explained between 77% and 91% of the grain yield variability, with the highest values in severe water stress condition. When individual models were used to predict yield in the rest of the trials assessed, models fitted during anthesis under mild water stress performed best. Combined models using data from different water regimes and each phenological stage were used to predict grain yield, and the coefficients of determination (R^2) increased to 89.9% and 92.0% for anthesis and grain filling, respectively. The model generated during anthesis in mild water stress was the best at predicting yields when it was applied to other conditions. Comparisons against conventional reflectance indices were made, showing lower predictive abilities. It was concluded that a ridge regression model using a data set based on spectral reflectance at anthesis or grain filling represents an effective method to predict grain yield in genotypes under different water regimes [32].

Generally speaking, in the study of the main influencing factors of food production, stepwise regression can only reduce variables without really solving the parameter estimation bias under multicollinearity. Ridge regression has a certain subjectivity in variable selection, which is only suitable for reducing multicollinearity. In the study of food production forecasting methods, the combined model method and models related to machine learning are favored by researchers, but under the premise of a small amount of data, it is easy to produce small training errors and large generalization errors, and its results of multiperiod prediction are inferior to the multiple linear regression method. Therefore, after considering various theories and methods, this paper selects the relevant explanatory variables as fully as possible and uses full subset regression, LASSO regression, and ridge regression analysis to further empirically analyze the selected variables, so as to reduce the impact of collinearity and identify the main influencing factors.

3. Variable Selection

From the perspective of input and output, the main factors affecting China's food production can be divided into four categories: (1) natural conditions, (2) labor input, (3) technology, and (4) policies and other factors [12, 20, 21, 27, 33–35].

The constraints of natural conditions are mainly reflected in three aspects: land, water, and climate. For food production, land is the object of labor and the means of production of people and is the "mother of wealth." Its area and soil type will directly determine the output of food. China has a vast territory and a large north-south span. The geographical and environmental differences cause uneven spatial and temporal distribution of water resources, and the differences in climatic conditions are large. Water resources are relatively scarce in many places, and droughts and floods are endless, which greatly limits food production [21, 27, 34, 35].

The labor input and the technical level need to be considered together. On the one hand, labor input, that is, the actual amount of labor input in the production process, with the socioeconomic level and other factors unchanged, increasing labor input can bring about an increase in food production. On the one hand, the improvement of technology means the

TABLE 1: Variables.

Variables	Variable meaning
y	Grain output (10,000 tons)
x_1	Employment in the primary industry (10,000 people)
x_2	The sown area of food crops (thousand hectares)
x_3	Total power of agricultural machinery (10,000 kilowatts)
x_4	Effective irrigation area (thousand hectares)
x_5	Pure fertilizer application amount (10,000 tons)
x_6	Rural electricity consumption (billion kilowatt hours)
x_7	Consumption of agricultural plastic film (ton)
x_8	Amount of pesticide used (10,000 tons)
x_9	Affected area (thousand hectares)
x_{10}	Disaster area (thousand hectares)

TABLE 2: Descriptive statistics.

Variable	Mean	Maximum	Minimum	Std dev.
y	10.86270817	11.09984221	10.67057107	0.14594216
x_1	10.32984707	10.57382659	9.91630506	0.20978288
x_2	11.61474	11.68881	11.50701	0.04777608
x_3	11.05192624	11.62382325	10.28836212	0.43968355
x_4	10.93997146	11.13124973	10.77524253	0.11156401
x_5	8.43068222	8.70327434	7.93919447	0.23065250
x_6	8.2265766	9.1616143	6.8702611	0.7371465
x_7	14.27251711	14.77239052	13.37256941	0.43000708
x_8	4.92201629	5.19722550	4.33768282	0.25639565
x_9	10.58050597	10.92363367	9.82433611	0.33470965
x_{10}	9.91449979	10.44505574	9.12706745	0.38274362

improvement of labor productivity, the improvement of land utilization rate, or the improvement of resource economic efficiency, so when other factors remain unchanged, greater output is obtained with less labor input [22].

Based on the above analysis and the availability of data, this paper selected 10 variables that affect food production, which are the sown area, the affected area, and the affected area when considering natural conditions. The number of people employed in the primary industry when considering labor input, and effective irrigation area, fertilizer application, rural electricity use, agricultural plastic film use and pesticide use when considering technology. See Tables 1 and 2 for details.

All the research data are from the official website of the National Bureau of Statistics and Data Center, and the time span is from 1991 to 2018. In addition, in order to eliminate the impact of dimensionality and explain the final results, this study also performed logarithmic processing on all data. The descriptive statistics of the data are shown in Table 2.

4. Correlation Analysis

Figure 1 is the scatter plot of the variables selected for the current study. It can be seen from Figure 1 that there is a clear linear relationship between the grain output and the selected variables. In addition to the sown area of grain crops, there are also obvious linear relationships among other variables, indicating that there may be multiple collinearity problems when directly performing regression. It is worth noting that with the increase in the number of employed people in the primary industry, the output of food has shown a downward trend. This does not mean that the decrease in the number of employed people in the primary industry has led to an increase in food production. It means that the improvement of the agricultural industry technology has largely made up for the reduction of labor input, indicating that when analyzing the issue of food production, it is possible to temporarily ignore the explanatory variable of labor input [27]. Further, it can be seen that it is impact of affected area and disaster area which affects the production of the country and has different
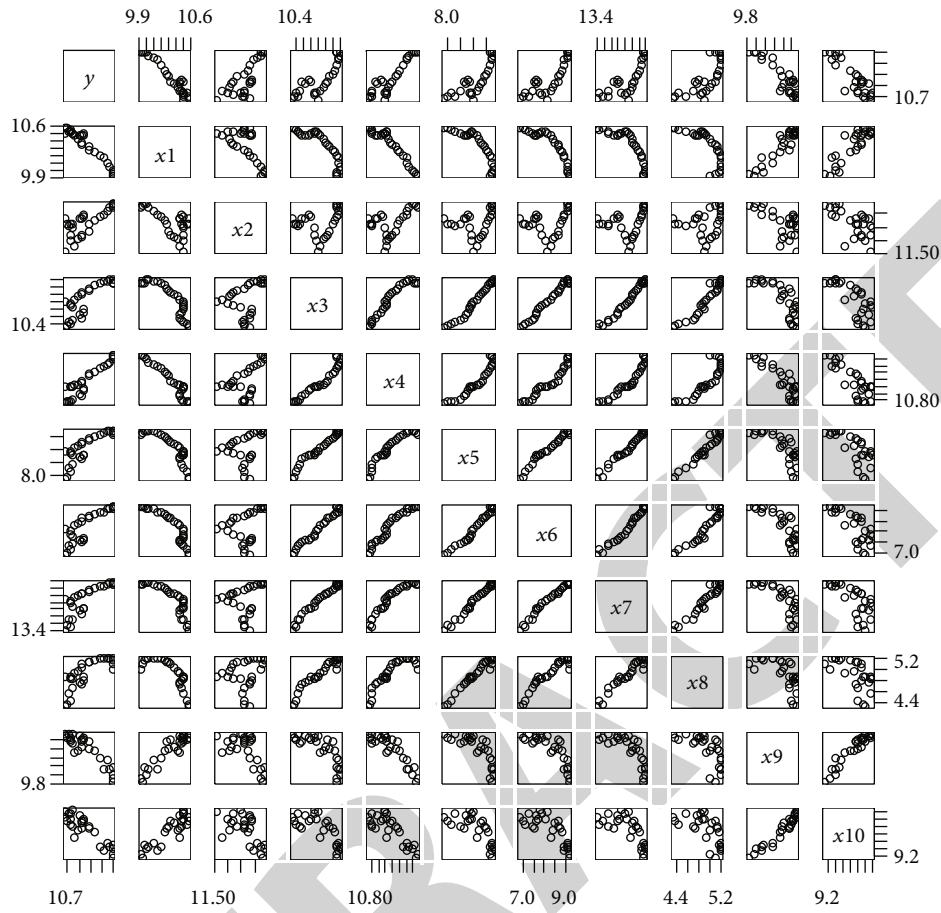
Figure 1: Scatterplot.

	y	$x1$	$x2$	$x3$	$x4$	$x5$	$x6$	$x7$	$x8$	$x9$	$x10$
y	1	−0.97	0.76	0.83	0.92	0.84	0.85	0.81	0.76	−0.91	−0.89
$x1$	−0.97	1	−0.67	−0.86	−0.96	−0.85	−0.89	−0.84	−0.76	0.93	0.89
$x2$	0.76	−0.67	1	0.3	0.5	0.31	0.32	0.26	0.22	−0.61	−0.62
$x3$	0.83	−0.86	0.3	1	0.95	0.99	0.99	0.99	0.96	−0.78	−0.73
$x4$	0.92	−0.96	0.5	0.95	1	0.94	0.96	0.94	0.87	−0.89	−0.83
$x5$	0.84	−0.85	0.31	0.99	0.94	1	0.99	0.99	0.98	−0.76	−0.72
$x6$	0.85	−0.89	0.32	0.99	0.96	0.99	1	0.99	0.95	−0.81	−0.76
$x7$	0.81	−0.84	0.26	0.99	0.94	0.99	0.99	1	0.97	−0.76	−0.7
$x8$	0.76	−0.76	0.22	0.96	0.87	0.98	0.95	0.97	1	−0.65	−0.61
$x9$	−0.91	0.93	−0.61	−0.78	−0.89	−0.76	−0.81	−0.76	−0.65	1	0.96
$x10$	−0.89	0.89	−0.62	−0.73	−0.83	−0.72	−0.76	−0.7	−0.61	0.96	1

Figure 2: Correlation coefficient matrix.

impact on the country's selected variables. And it can also be seen that except affected area and disaster areas, all other variables are having direct relationship between each other. The sown area of food crops shows seasonal relationship to all the selected variables and has seasonal ups and downs.

Figure 2 is the correlation coefficient matrix of the variables. From Figure 2, we can see that (1) the absolute values of the correlation coefficients between the selected independent variable and the dependent variable are larger than 0.7, indicating that the linear relationship is obvious. (2) In addition to the sown area of grain crops, there are also obvious linear correlations between other independent variables, indicating that there may be serious multicollinearity problems when directly performing regression [28].

Regarding the testing of collinearity problems, in addition to using correlation coefficients to assist judgment, there are currently two main methods: (1) judging whether there is a collinearity problem based on the condition number and (2) judging whether a collinearity problem exists based on the variance inflation factor [22].

The mathematical expression of the condition number is as follows:

$$k = \frac{\lambda_{\max}\left(X^T X\right)}{\lambda_{\min}\left(X^T X\right)}, \tag{1}$$

TABLE 3: Variance inflation factor.

Variable	VIF
x_2	6.943401
x_3	111.902358
x_4	119.948846
x_5	495.576474
x_6	146.985565
x_7	195.505956
x_8	204.511600
x_9	25.625410
x_{10}	17.143386

where λ is the eigenvalue and X is the independent variable matrix. Generally speaking, when $k < 100$, the degree of multicollinearity is considered small; when $100 \leq k \leq 1000$, multicollinearity is considered to exist; when $k > 1000$, serious multicollinearity is considered to exist. After removing the independent variable x_1, the condition number of the independent variable matrix composed of the remaining independent variables is 3984.441, which is much greater than 1,000 [7, 8, 34].

The formula for calculating the variance inflation factor is as follows:

$$\text{VIF}_i = \frac{1}{1 - R_i^2}.\tag{2}$$

R_i^2 represents R^2 obtained by linear regression using variable x_i as the dependent variable and the other $k - 1$ variables as independent variables. Generally, we think that there is a multicollinearity problem when the variance inflation factor is greater than 5 or 10. When the variance inflation factor is greater than 100, there is a serious multicollinearity problem [3, 7, 25].

After calculation, the variance inflation factor of various variables is shown in Table 3. From this table, we can clearly see that except for x_2, the variance inflation factor of other variables is all higher than 10, and most of them are higher than 100, which indicates that there is a serious multicollinearity problem between independent variables, and linear regression cannot be performed directly.

5. Empirical Analysis

5.1. Full Subset Regression Analysis. Stepwise regression means that the model will add (or drop) a variable one by one until it reaches a certain stopping criterion. However, in practice, although stepwise regression analysis can find a good model, it cannot guarantee that the model is the best one. Therefore, this paper uses full subset regression analysis to analyze the possible combination of variables [34, 35]. The results are shown in Figure 3.

From Figure 3, we can see that based on the adjusted R-squared, the optimal subset contains five variables, which
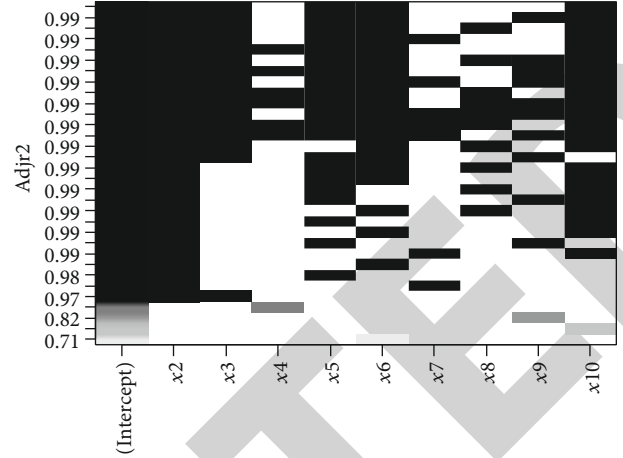
FIGURE 3: Four best models with different subset sizes based on adjusted R-squared.

are x_2, x_3, x_5, x_6, and x_{10}. Based on this, a regression equation is established, and the results are shown in Table 4.

From the table above, we can see that the regression coefficients of the five explanatory variables are all significantly nonzero, but the regression coefficient of the total power of the agricultural machinery represented by the x_3 variable is negative [25, 28]. The main reason for this is the existence of multicollinearity [13, 16].

5.2. LASSO Regression Analysis. LASSO regression is a biased estimation regression method that can be used for collinear data analysis. It differs from ordinary least squares regression in that it adds a 1-norm penalty term in the estimation process [14, 28, 29], which is expressed as a mathematical formula as follows:

$$\widehat{\theta} = \arg_\theta \min ||X\theta - y||_2^2 + C||\theta||_1.\tag{3}$$

Using R 3.6.2 for LASSO regression, the Cp value calculation results are shown in the following table.

Table 5 shows the value of the Cp statistic at each step of variable selection. Among them, it can be seen that the Cp value of step 10 is the smallest, which is 4.6649. The corresponding coefficients of each variable in Table 6 can be seen, only x_2, x_5, x_6, x_9, and x_{10} are not zero, and the coefficients are 1.420427, 0.196403, 0.043928, -0.03694, and -0.0474. It shows that the sown area of food crop has a significant impact on food production, and pure fertilizer application amount, rural electricity consumption, and disaster area can affect grain production as well.

5.3. Ridge Regression Analysis. Ridge regression is also a biased estimation regression method that can be used for collinear data analysis. The regression coefficient is more practical and reliable at the cost of losing some information and reducing accuracy, and it fits a large number of conditions (morbid data) [31, 32]. Other models use the whole information generated by spectral measurements, such as ridge regression, which was introduced by Li and Ren and generalized by Li et al. [27, 28]. This type of multivariate linear regression includes a

TABLE 4: Full subset regression results.

Variable	Coefficients	Std error	T value	P value
Constant	-6.93797	0.84836	-8.178	4.09e-08***
x_2	1.44285	0.06502	22.190	<2e-16***
x_3	-0.11074	0.04638	-2.388	0.02597*
x_5	0.23684	0.07007	3.380	0.00270**
x_6	0.10630	0.02999	3.545	0.00182**
x_{10}	-0.06103	0.01279	-4.770	9.20e-05***
R^2	0.9948	Adjusted R^2	0.9936	
F value	839.1	P value	<2.2e-16	
DW	2.2278			

TABLE 5: Changes in Cp values of the data in LASSO regression.

Step	Df	Rss	Cp
0	1	0.57508	3662.8281
1	2	0.44547	2833.4618
2	3	0.27043	1712.7045
3	4	0.24992	1583.0999
4	5	0.09332	580.5712
5	4	0.04680	280.2289
6	5	0.01993	109.8113
7	6	0.00783	34.2075
8	7	0.00404	11.8952
9	6	0.00362	7.2435
10	7	0.00291	4.6649
11	8	0.00289	6.5284
12	9	0.00286	8.3747
13	10	0.00281	10.0000

TABLE 6: LASSO regression coefficients at each step.

Step	x_2	x_3	x_4	x_5	x_6	x_7	x_8	x_9	x_{10}
1	0	0	0	0	0	0	0	0	0
2	0	0	0.171949	0	0	0	0	0	0
3	0	0	0.316865	0	0	0	0	-0.0483	0
4	0	0	0.339717	0	0	0	0	-0.04577	-0.00753
5	0.45343	0	0.554411	0	0	0	0	0	-0.04692
6	0.672158	0	0.639493	0	0	0	0	0	-0.05293
7	0.938281	0	0.445622	0.112526	0	0	0	0	-0.0617
8	1.153794	0	0.248814	0.211913	0	0	0	-0.02147	-0.05627
9	1.367226	0	0	0.194545	0.043928	0	0	-0.03669	-0.04502
10	1.420427	0	0	0.196403	0.047311	0	0	-0.03094	-0.0474
11	1.422217	-0.08757	0	0.243953	0.086609	0	0	-0.02709	-0.04624
12	1.42105	-0.09139	0	0.262388	0.086814	0	-0.00946	-0.02559	-0.04645
13	1.42738	-0.0914	-0.01892	0.284621	0.087443	0	-0.02325	-0.02566	-0.04562
14	1.473969	-0.09244	-0.1296	0.371263	0.089772	0.018195	-0.09128	-0.02441	-0.04353

TABLE 7: Ridge regression results.

Variable	Regression coefficients	Standardized regression coefficients	Standard error	T value	P value
Intercept	-6.022672				
x_2	1.285106	0.319030	0.017076	18.683	<2e-16***
x_3	0.005408	0.012356	0.021791	0.567	0.570710
x_4	0.125080	0.072509	0.023788	3.048	0.002303**
x_5	0.083995	0.100669	0.013701	7.348	2.01e-13***
x_6	0.023191	0.088829	0.020001	4.441	8.94e-06***
x_7	0.022444	0.050148	0.017251	2.907	0.003650**
x_8	0.059953	0.079874	0.022066	3.620	0.000295***
x_9	-0.043730	-0.076056	0.025652	2.965	0.003028**
x_{10}	-0.052508	-0.104428	0.024886	4.196	2.71e-05***

TABLE 8: Final ridge regression results.

Variable	Regression coefficients	Standardized regression coefficients	Standard error	T value	P value
Intercept	-6.26961				
x_2	1.31299	0.32595	0.01721	18.941	<2e-16***
x_4	0.11369	0.06591	0.02834	2.326	0.020025*
x_5	0.09098	0.10904	0.01537	7.093	1.31e-12***
x_6	0.02624	0.10050	0.02607	3.855	0.000116***
x_7	0.02254	0.05036	0.02100	2.397	0.016516*
x_8	0.05997	0.07989	0.02434	3.282	0.001030**
x_9	-0.04163	-0.07241	0.02957	2.448	0.014348*
x_{10}	-0.05252	-0.10445	0.02747	3.803	0.000143***

contraction of the multivariate model regression coefficients and reduces them to the same degree [25].

Compared with LASSO regression, the ridge regression adds a 2-norm penalty term in the estimation process, which is expressed as a mathematical formula as follows:

$$\widehat{\theta} = \arg_\theta \min ||X\theta - y||_2^2 + C||\theta||_2^2. \qquad (4)$$

Using R 3.6.2 for direct ridge regression, the results are shown in Table 7:

It can be seen from the above table that the variable x_3's coefficient is positive [27], which is in line with economic laws, but the coefficient is not significantly nonzero. Therefore, the x_3 variable is excluded and we perform ridge regression again. The final ridge regression result is shown in Table 8.

The ridge parameter after removing the x_3 variable is 0.03450807. It is relatively small, which indicates that although the estimation is biased, the deviation from the least square estimation result is not large. Comparing the standardized regression coefficients, we can clearly see that the sown area of food crops has a greater positive impact on food production, followed closely by the application of pure agricultural fertilizers and rural power consumption, and the negative impact of disaster area on food production is relatively large, which is basically consistent with LASSO regression results.

6. Conclusion

Considering the results of the previous regression analysis, we can draw the following conclusions:

(1) The increase in the sown area of food crops is the main reason for the increase in food production. After comprehensively analyzing of the regression results of the three regressions, we find that the elasticity coefficient of the variable x_2 is all above 1, indicating that the increase in the sown area can significantly increase the growth of grain output

(2) The use of agricultural fertilizers and the increase in rural electricity consumption are the driving factors for the increase in grain output. From the empirical analysis, we can see that, in addition to the sown area, the amount of fertilizer applied to agriculture and rural electricity consumption are significantly positive in the three models, and the regression coefficient is relatively large than other variables, indicating that they have indeed effectively promoted the increase in food production

(3) The total power of agricultural machinery has a limited impact on grain output. The effects of the total

power of agricultural machinery on grain yield are not the same in the three models. The elasticity coefficient of the total power of agricultural machinery is negative in the full subset regression, and the elastic coefficient is positive in the ridge regression and LASSO regression but not significant. The main reason for this result significance might be due to the suitable variables selecting procedure listed in Figure 3 where to run the full subset regression only 5 variables are selected to show their impact on the dependent variable. Second, it might be the time span of the data is too long, which causes the effect of mechanical inputs on grain output to be not obvious

(4) Natural disasters have a certain negative impact on food production. From the above three regression models, we can see that for each 1% increase in the disaster area, food production will decrease by about 0.05%, indicating that natural disasters still have a certain negative impact on food production. It is still necessary to consolidate the ability of agricultural production to resist natural disasters

Data Availability

All data, models, and code generated or used during the study appear in the submitted article.

Conflicts of Interest

The authors declare that they have no conflicts of interest.

Acknowledgments

References

[1] Z. Xiaoshi, L. Gucheng, L. Cheng, and H. Capital, "Land scale and agricultural production efficiency," *Journal of HZAU(Social Sciences Edition)*, vol. 2, pp. 8–18, 2018.

[2] Y. Wei, Z. Peng, and J. Zhiheng, "Spatial interaction effect of rural education human capital and agricultural total factor productivity in China—empirical analysis based on spatial simultaneous equations," *Journal of China Agricultural University*, vol. 25, no. 3, pp. 192–202, 2020.

[3] L. Jingbo and G. Yuan, "Research on the influence mechanism of China's population aging on labor productivity," *Nankai Economic Studies*, vol. 3, pp. 61–80, 2020.

[4] W. Yuqiu and L. Lei, "The influence of new rural cooperative medical insurance and health human capital on labor participation of rural residents," *Chinese Rural Economy*, vol. 11, pp. 68–81, 2016.

[5] Y. Qiuxia, C. Zhaojiu, and X. Huiting, "Labor allocation efficiency of famer households and its influencing factors: based on the survey data of 637 farmer households in Jiangxi province," *Journal of Hunan Agricultural University(Social Science)*, vol. 19, no. 5, pp. 11–18, 2018.

[6] R. Cerda, C. Allinne, C. Gary et al., "Effects of shade, altitude and management on multiple ecosystem services in coffee agroecosystems," *European Journal of Agronomy*, vol. 82, pp. 308–319, 2017.

[7] M. H. Ahmed and K. A. Melesse, "Impact of off-farm activities on technical efficiency: evidence from maize producers of eastern Ethiopia," *Agricultural and Food Economics*, vol. 6, no. 1, pp. 1–20, 2018.

[8] S. Han, D. Li, and J. Xiong, "Changes in the amount of cultivated land resources in Guangzhou and their impact on food security," *Journal of Agricultural and Forestry Economic Management*, vol. 6, 2016.

[9] Z. Feng, "Food security and cultivated land security for China's future population development," *Population Research*, vol. 2, pp. 17–31, 2007.

[10] T. Taotao, Q. Ma, and G. Li, "Population aging, population urbanization and China's food security: simulation based on China CGE model," *Journal of Zhongnan University of Economics and Law*, vol. 4, 2017.

[11] J. Xiang and F. Zhong, "Impact of demographic transition on food demand in China: 2010-2050," *China Population, Resources and Environment*, vol. 23, no. 6, pp. 117–121, 2013.

[12] S. M. Sanusi and I. P. Singh, "Empirical analysis of economies of scale and cost efficiency of small-scale maize production in Niger state, Nigeria," *Indian Journal of Economics and Development*, vol. 12, no. 1, pp. 55–64, 2016.

[13] W. Xuejiao and X. Haifeng, "Spatial correlation measurement and influence factors of allocation efficiency for maize production in China," *Social Science Journal of Harbin Istitute of Technology*, vol. 18, no. 6, pp. 125–131, 2016.

[14] L. Wang, "Research on the impact of China's population urbanization on food security," Lanzhou University, China, 2019.

[15] X. Cai, "Research on the impact of urbanization development in Henan Province on food security," *Henan Agriculture*, vol. 11, pp. 8-9 + 64, 2015.

[16] X. Du, "Empirical analysis of influencing factors of food security in China," *Anhui Agricultural Science*, vol. 43, no. 5, 2015.

[17] W. Chen and X. Xie, "Research on the impact mechanism of climate disasters on food security," *Issues in Agricultural Economy*, vol. 34, no. 1, pp. 12–19, 2013.

[18] C. Chih-Ming, "Interpretive structural modeling apply to patient safety culture," *International Journal of Medicine and Pharmaceutical Sciences*, vol. 8, no. 4, pp. 21–26, 2018.

[19] J. Qiu, S. Wang, and G. Gao, "Global warming and food security in China——a study based on GTAP model," *Finance Science*, no. 4, pp. 57–67, 2015.

[20] S. Yin, L. Wu, and Y. Zhang, "Empirical analysis of the factors affecting the grain output fluctuation in China," *Systems Engineering Theory & Practice*, vol. 10, pp. 28–34, 2009.

[21] S. Zai, S. Guo, and J. Wen, "Analysis of influencing factors of grain production in Henan Province," *People's Yellow River*, vol. 33, no. 12, pp. 94–96128, 2011.

[22] W. Qiling and K. Zhang, "Analysis of influencing factors of grain output based on regression analysis," *Grain Science and Technology and Economy*, vol. 42, no. 6, 2017.

[23] Z. Huang, "Analysis of influencing factors of China's grain production based on ridge regression analysis of C-D

Research Article

Water Requirement of Naked Oats under Subsurface Drip Irrigation in the North Foot of Yinshan Mountain Based on Single Crop Coefficient Approach

Hu Liu [1,2] **Jian Wang** [1] **Hongfang Li** [1,2] **Jianfeng Liu** [3] **Bo Cheng** [1,2] **Abiyasi** [1,2] **and Nan Ge** [1,2]

[1]*Yinshanbeilu National Field Research Station of Desert Steppe Eco-Hydrological System, China Institute of Water Resources and Hydropower Research, Beijing 100038, China*
[2]*Institute of Water Resources for Pastoral Area, Ministry of Water Resources, Hohhot 010028, China*
[3]*Water Conservancy Science Research Institute of Inner Mongolia, Hohhot 010030, China*

Correspondence should be addressed to Jian Wang; wangjian@iwhr.com

In order to accurately and rapidly calculate the water requirement of naked oats under drip irrigation in the north foot of Yinshan Mountain, the study adopted the K_c and calculation method for potential evapotranspiration recommended in document FAO56 and applied SCCA to calculate the water requirement of crops based on the deficient irrigation experiments. The results indicated that the water requirements of naked oats without drought influence was 383.8 mm, and the maximum daily average water requirement intensity was heading flowering, which was the critical period of crop water requirement, and the mean value of ET_0 in the whole growth period was 3.89 mm/d. After correction, K_C of naked oats in the initial growth stage, crop development growth stage, mid-season growth stage, and late season growth stage was 0.34, 0.94, 1.05, and 0.36. The average K_C of naked oats in the whole growth stage was 0.71. SCCA does not consider the influence of wetting depth in the initial growth period of crops and the correction of local irrigation in the mid-season and late season stage of crops. Therefore, when the irrigation quota of naked oats is 315 mm, the crop water requirement calculated by SCCA is 363.84 mm, which is about 10% different from the measured value. The results show that SCCA can be used to calculate the water requirement of naked oats under drip irrigation at the northern foot of Yinshan Mountain in Inner Mongolia, and the calculation error is within the allowable range. However, it is also necessary to consider the influence of different irrigation forms and plant height of crops on calculation value.

1. Introduction

The calculation methods for crop water requirements generally consist of two categories, including the water requirement of crop growth period measured with water balance method, and actual crop water requirement calculated through the calculation of the water requirement of reference crop. Among them, FAO56 recommended crop coefficient approach has a relatively wide application for the water requirements of crop in current agricultural production activities [1]. The critical process for the application of SCCA recommended by FAO56 in the calculation of the crop water requirement is to calculate out the water requirement ET_0 of reference crop and K_C. K_C reflects the specific value between the crop water requirement Et_c in one certain growth stage and the potential evapotranspiration ET_0 of the reference crop, which is the comprehensive demonstration of the biological characteristics, status of soil, water and fertility, crop type, output, field management level, and other factors of the crop itself toward the crop water requirement. It is an important parameter for the differences between the water requirements of different crops and the water

requirement of the reference crop. On account of different growth and development characteristics, crops in different varieties have quite different characteristics in water requirements in different growth stages [2–8].

The document of FAO56 provides recommended values for K_C of different crops in different growth periods. Considering that the values of K_c in FAO56 are given on the basis of certain climate and plant forms, it is necessary to verify and modify the values according to the actual application environment (variety, climate, water, and fertility conditions) [9–13]. Zhang et al. conducted irrigation experiments for silage corn and alfalfa in Uxin Banner and adopted the measured day-by-day Eta and PM formula of FAO56 to get the day-by-day ET_0 for analysis; K_C of alfalfa on Maowusu sandy land in the growth stage has been calculated [14]. Wang and Xie applied CERES-Wheat model to simulate and calculate out the K_C of north winter wheat in Fufeng County and Chencang District inn Baoji at the initial growing stage, wintering stage, growth peak stage, and final growth stage and compared them with the recommended K_C in FAO56 in terms of relevance and deviation [15]. Wang et al. applied leaf area index LAI and meteorological factors to simulate the crop coefficient and evapotranspiration of corn in the whole growth period. Based on the day-by-day meteorological data of Hebei in nearly 60 years from 1955 to 2014 and the Hebei Soil Data in the China Soil Database, Cao, Li and Zhu adopted SCCA recommended in FAQ to modify the value of K_C, got the spatial and temporal distribution law for the modification of K_C of main crops in the central south region of Hebei, and discussed the main meteorological factors associated with the changes in K_C [16, 17]. Wang et al. perform observation and experiment studies for crop coefficient and laws of rice in Yunnan. The result showed that the spatial differences of K_C did not have any obvious laws [18]. The value in areas with humid and semi-humid climate was relatively high, and the value in areas with wet cool climate was relatively low. Although K_C demonstrated the decline trend along with the ascending of the altitude, the correlation between them was relatively low. Li applied ET_0 and Eta to calculate out K_C on meadow and sand dune and constructed K_C inversion model from multiple vegetation indexes with concurrent consideration of leaf area index and soil moisture content [19]. Zhang et al. applied UAV remote sensing platform with multispectral sensor to implement synchronous observation for crop coefficients of corn in various growth stages under different moisture contents in Dalad Banner and modified the K_C recommended in FAO with dual-crop coefficient approach based on the meteorological data, soil quality, and other external conditions [20]. Based on the recommended method of FAO, Liu made selection for the ET_0 calculation method in Altay Prefecture of Xinjiang and applied actually measured water requirement to modify the K_C value recommended in FAO56 [21]. Ikram elaborated on the global importance of oats and production improvement, showing that oat is a crop that requires a lot of water to increase production, and in order to reduce the water requirement, a new concept is needed to improve productivity [22]. Ejaz indicated that groundwater resources in Pakistan are depleting and conducted groundwater simulations

of different interventions in irrigation and planting practices. The results showed that it is suitable to plant wheat and oats in early spring and cotton in the rainy season; it could maximize the conservation of groundwater resources [23]. Schoot estimated the current and possible future irrigation water consumption of four important irrigated crops in the Rhine River Basin, sugar beet, potato, maize, and oat, and suggested to expand a dynamic crop plan extension model to accurately estimate the water requirement of each sub-basin [24]. Djaman selected 28 oat genotypes suitable for planting in the western United States and conducted a four-year yield evaluation under sprinkler irrigation at the Agricultural Science Center, and the results showed that the oat crop water use efficiency (CWUE) varied by genotype and year [25].

At present, a large number of studies have used SCCA recommended in FAO56 to calculate the water demand of naked oats, alfalfa, cotton, and other crops, but most of the results do not consider the impact of irrigation forms on crop water requirement. Naked oats are one of the main nutritious grains in the alpine regions of northern China. In recent years, due to the increasing shortage of water resources in Northwest China, subsurface drip irrigation and underground drip irrigation are widely used in the naked oats planting area at the northern foot of Yinshan Mountain. Because the underground drip irrigation is located below the ground surface, it directly irrigates the roots of naked oats, reducing the evaporation of water on the soil surface, which is quite different from the traditional cultivation of naked oats. At the same time, FAO56 was published in 1998. Compared with now, there have been obvious changes in crop varieties, especially in plant height. How to quickly and accurately calculate the crop water demand of naked oats in the northern foot of Yinshan Mountain under the condition of carrying out field experiments as little as possible has become one of the important issues of water and soil resources management in the irrigation area.

This paper applied SCCA recommended in FAO to investigate the water requirement of naked oats in the north foot of Yinshan Mountain and verified with the measured value at the fields to study the practical application of SCCA in the calculation of crop water requirements of naked oats under drip irrigation in the north foot of Yinshan Mountain in the actual production and life. The research achievements provide basis for the accurate calculation of the crop water requirements of naked oats under drip irrigation in the north foot of Yinshan Mountain, as well as the formulation of scientific and reasonable irrigation system.

2. Materials and Methods

2.1. Regional Overview. The research area is located at Yinshanbeilu Grassland Eco-Hydrology National Observation and Research Station in Xilamuren Town, Damaoqi, Baotou, Inner Mongolia. With a distance of 80 km from Hohhot City, the research station situates on Wulanchabu grassland at the central position of Inner Mongolia and north foot of Yinshan. The place belongs to continental monsoon climate in warm temperate zone. The climate has the characteristics

of droughty and windy springs and autumns, hot and short summers, and dry and cold winters. The annual mean precipitation is 284 mm, and the annual mean evaporation is 2305.0 mm. The precipitation is mainly concentrated in July and August. The annual mean temperature is 2.5°C, and the frost-free period is 83 days. The predominant wind is westerly wind and northwesterly wind, and the annual mean wind speed is 4.5 m/s. The mountainous area of Yinshan where the research station is located belongs to the transition belt of Inner Mongolian Plateau, which has the average altitude of 1600 m. The area has denudation landforms, as well as alluvial and constructional landforms.

The soil belongs to young soil developed based on base rocks, and the soil on high positions contains limited amount of soil humus. The soil texture is coarse and the distribution area is relatively small. Low places are generally distributed with relatively large area of chestnut soil, with the texture of light loam or sandy loam. With relatively abundant moisture and nutrients, the soil has certain production potential. The thickness of the surface soil layer is only 10 to 15 cm or thinner, and the thickness in low places could reach from 30 to 50 cm. However, the salt content is relatively high.

2.2. Experiment Materials. The varieties of naked oats applied in the experiment are Bayou No. 1 and Yajin No. 7. The initial division of the growth period is shown in Figure 1. The soil for test in the experiment pit is selected from the soil in the research station. The soil is back filled according to the actual volume-weight. The physical and chemical properties of the soil are shown in Table 1.

2.3. Experiment Design. The irrigation form is shallow drip irrigation. The experiment applied deficit irrigation approach, and set four treatment levels, including Without Drought (the moisture content of soil wetting layer is 90% of the field moisture capacity), Slight Drought (the moisture content of soil wetting layer is 80% of the field moisture capacity), Medium Drought (the moisture content of soil wetting layer is 70% of the field moisture capacity), and Severe Drought (the moisture content of soil wetting layer is 60% of the field moisture capacity). Each treatment level repeated for three times, reaching a total of 12 small areas. The experiment for two crops totally had 24 small areas, as shown in Table 2. The irrigation times of various treatments were 10 times, and the irrigation times are May 20, June 1, June 13, June 28, July 10, July 20, August 1, August 13, August 25, and September 5.

From May 5 to 6, the land was ploughed 25 cm deep and then leveled (15 000 kg rotten organic fertilizer was applied per ha as base fertilizer). Before sowing, seeds were mixed with 40% seed dressing double wettable powder according to 0.2% of seed weight to prevent smut. Sowing began on May 14. The seed fertilizer is 175 kg diamine per ha (nitrogen content 18%, phosphorus content 48%). After sowing, the soil must be covered in time to suppress and preserve moisture. The additional fertilizer shall commence from emergence and end in the heading stage. One additional fer-

Sowing -emergence 15/5~25/5 15 cm
Emergence -tillering 26/5~15/6 30 cm
Tillering -jointing 16/6~10/7 30 cm
Heading -blooming 11/7~5/8 45 cm
Filling -milky maturity 6/8~15/9 45 cm
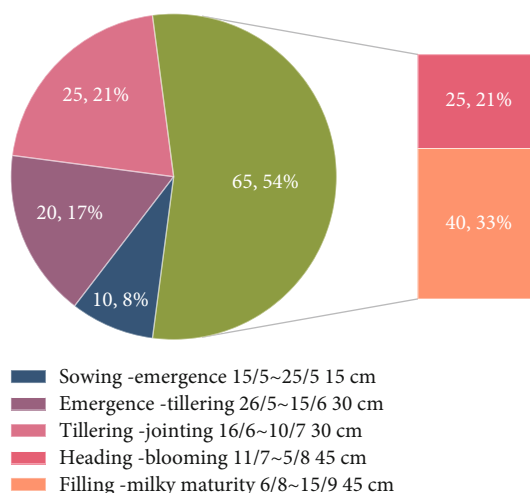
FIGURE 1: Division of the growth stages and soil wetting layer thickness.

TABLE 1: Basic physical and chemical properties of experiment soil.

Experiment pit	Naked oats
Bulk density (g/cm^3)	1.44
Saturated water content (%)	23.7
Field	
Water-holding capacity (%)	19.8
Total nitrogen (%)	0.017
Available nitrogen (mg/kg)	35
Rapid available phosphorus (mg/kg)	9.5
Rapidly available potassium (mg/kg)	195
Organic matter (%)	1.21
Soil texture	Loamy sand
Saltness (%)	0.62
pH value	7.8

tilizer shall be arranged, and 60 kg carbamide is applied for each ha of the land.

2.4. Test Indicator and Method. The observation contents mainly include meteorological data, soil data, and physiological data of crops.

Meteorological data: apply the data from Hobo Meteorological Stations in the site.

Physical indicators of soil: moisture content, saltness, temperature, and soil water potential. The current soil sensor (EM50, Origin, USA) is used to measure the moisture content, saltness, and temperature of the soil. The reading intervals of the sensor may be one reading per hour. Use a laptop to regularly collect the water, salt, and temperature data stored in the sensor. The soil water characteristic curve (SWCC) of the soil samples in the test area was measured by a pressure plate extractor (1500F2, Soil Moisture Equipment Corp., Santa Barbara, CA, USA), and then the van Genuchten (VG) model was constructed by the SWCC. The measured soil moisture data is used to calculate the soil water potential through VG model.

Treatment	No.	Irrigating water quota (mm)	Times	Irrigation quota (mm)
Severe drought	HM1	15	10	150
Medium drought	HM2	18	10	180
Slight drought	HM3	21	10	210
Without drought (CK)	HM4	24	10	240

Chemical indicators of the soil: organic matter, content of nitrogen, phosphorus, and potassium in soil, pH value, etc. Organic matter content was determined by low-temperature external thermal potassium dichromate oxidation colorimetry. The total nitrogen content was determined by alkaline hydrolysis distillation method. The total phosphorus and total potassium contents were determined by sodium hydroxide melting method.

Crop growing status: growth progress, main development indicators, output, etc. Growth progress: commence the daily measurement work from the seeding and record the seeding time, emergence time, emergence rate, entry time of various growth stages, and the final harvest time. Main development indicators: crop height, stem diameter, leaf area indicator; measure once in each ten days. Measure at least 10 plants in each small area, and sample in the shape of plum blossom; arrange at least 3 sampling points in each small area for the leaf area. Output: after the maturity of the naked oats, randomly select typical sampling points in the land plot to measure the output. The area of each sampling point is $1 m^2$.

2.5. *Data Analysis Method.* The crop water requirement of naked oats in the irrigation test is calculated according to the water balance principle, as shown in Formula (1). According to Formula (1), the crop water requirement in the experiment can be calculated through the indicators such as naked oats irrigation amount, irrigation times, rainfall supply amount, and soil moisture.

$$ET_c = P_0 + K + M + W_t + \Delta W, \quad (1)$$

where ET_c is crop water requirement (mm); P_0 is the effective rainfall during the growth period (mm); K is groundwater recharge (mm); M is irrigation water volume during growth period (mm); W_t is the change of soil water content caused by the increase or decrease of the soil wetting layer thickness at the beginning and end of each growth period, and the increase or decrease of soil water storage caused by the increase or decrease of soil wetting layer thickness. Since there is no increase or decrease of the soil wetting layer thickness, this item can be ignored; ΔW is the increase or decrease of soil available water supply caused by the change of soil water content at the beginning and end of each growth period, which is ignored in this study.

The study compared the measured value in experiments with the data calculated out with SCCA and then used SCCA to calculate out the water requirement (Formula (2)) [1].

$$ET_c = ET_0 \cdot K_c, \quad (2)$$

where K_c is the crop coefficient in the whole growth period or in different growth stages of the crop; ET_c is the actual water requirement of the crop in the whole growth period or in different growth stages (the unit is mm); ET_0 is the potential evapotranspiration of the reference crop in the whole growth period or in different growth stages (the unit is mm).

Apply Penman-Monteith formula (Formula (3)) recommended in FAO56 to calculate the potential evapotranspiration ET_0 of the reference crop. Potential evapotranspiration ET_0 of the reference crop (1990): it is the evapotranspiration rate of the reference crop assuming that the crop height is 0.12 m, the fixed surface resistance $y = 70 s/m$, and the reflection rate is $a = 0.23$. Penman-Monteith formula has relatively thorough theoretical basis and high calculation precision. It takes energy balance and water vapor diffusion theories as the basis and considers the aerodynamic parameters and physiological feature of crops.

$$ET_0 = \frac{0.408(R_n - G) + \gamma(900/(T + 273))u_2(e_s - e_a)}{\Delta + \gamma(1 + 0.34u_2)}, \quad (3)$$

where ET_0 is the evapotranspiration of the reference crop (mm/d); R_n represents the net radiation on canopy surface [MJ/(m²•d)]; G is the soil heat flux [MJ/(m²•d)]; T represents average temperature (°C); Δ represents the slope of the vapor pressure-temperature curve for saturated water (kPa/°C); u_2 is the wind speed at the height of 2.0 m (m/s); e_s is the vapor pressure of saturated water (kPa); e_a is the vapor pressure of the actual water (kPa): γ is the constant of the hygrometer (kPa/°C).

SCCA incorporates the influences of crop evapotranspiration and evaporation of soil into the K_C. To coordinate various characteristics of crops and average influence of soil evaporation, SCCA divides the growth period of crop into four growth stage and uses these four growth stages to describe the crop development process and biological and climate characteristics. These four stages are initial growing stage, wintering stage, growth peak stage, and final growth stage. The whole growth period just needs three K_c values (K_{cini}, K_{cmid}, and K_{cend}) to describe and draw the K_c curve.

3. Results and Analysis

3.1. Measured Water Requirements of Naked Oats.

Water requirement characteristics of naked oats were expressed by modulus coefficient and water requirement intensity. The modulus coefficient represents the proportion of water requirement in a certain growth stage to the whole growth stage, and the water requirement intensity represents the average daily water requirement in the growth stage. It could be seen from Table 3 that the water requirements, modulus coefficient, and water requirement intensity of naked oats had the trend from low to high and then from high to low. The plants were relatively small in the seedling stage, and the land coverage was relatively low. Therefore, the surface evaporation took a vital portion in the water consumption. In addition to relatively low temperature and weak illumination, the water requirement model number and intensity in this stage were relatively low. The modulus coefficient is around 20%, and the water requirement intensity was from 2.56 to 3.91 mm/d. After the stage of Tillering-Jointing, the nutrient growing and evapotranspiration accelerated, leading to rapid expansion of the water requirement intensity. Therefore, the stage modulus coefficient was relatively high, which was around 28%. In the stage of Heading-Blooming, the plant height and leaf area of naked oats reached the highest value. In addition, the stage is just the season with the highest temperature in a year; the water requirement intensity reaches the highest level, which is between 3.08 and 4.70 mm/d. The water requirement modulus reaches the highest value of about 31%. This stage is critical for the growth of naked oats. As the gradual descending of the temperature in the stage of Filling-Milky Maturity, the leaves gradually become yellow, the evapotranspiration keeps decreasing, and the water requirement intensity comes across gradual decrease day after day.

3.2. Potential Evapotranspiration of Reference Crop.

It could be seen from Figure 2 that the mean value of the potential evapotranspiration ET_0 in the whole growth period was 3.89 mm/d, which demonstrated the trend of high in the middle and low in the both ends. Due to the decrease in temperature at the stage of emergence, the value of ET_0 was relatively low, and the mean value was only 3.22 mm/d. As the gradual ascending in the temperature and increase in the solar radiation capacity, ET_0 maintained the gradual increase trend after reaching the stage of bud bearing and blossoming. ET_0 reached the highest value of 6.86 mm/d on July 20, and saw the lowest value of 1.82 mm/d on September 23.

3.3. Initial Selection of K_c under SCCA.

In the whole growth period, K_c will change along with changes in the growth and development, ground coverage degree, crop height, and leaf area. According to FAO56 and actual growth performance of crops (Table 4), the growth and development period of the crop could be re-classified into the following stages according to the demands of SCCA.

The initial growth period is determined when about 10% of the soil surface is covered by green.

Crop development growth stage shall refer to the period when the surface coverage reaches about 10%, to the time when the surface is completely covered by green. On account of some physiological features of close crops like naked oats, it is very difficult to determine the effective time of complete shading in a visualized manner. Therefore, for the convenience of observation, the experiment takes the time when the average height of crops reaches about 0.5 meters as the effective time of complete shading.

The mid-season growth stage commences from the time of effective and full shading and ends on the maturity of the crops. The mid-season growth period under the experiment commenced from the time of effective and full shading to the time before harvest.

As annual crops used for grains and oil-bearing materials, naked oats enter into the late season growth stage after filling and would be harvested after become yellow and matured.

In accordance with data provided in No. 24 Document of FAO Irrigation and Drainage, under the conditions of the average sunshine and minimum relatively humidity (RH_{min}) of about 45%, the average wind speed of 2 m/s, the absence of water stress and relatively high management level, the recommended values of naked oats under the three growth stages are $K_{cini} = 0.3$, $K_{cmid} = 1.15$, and $K_{cend} = 0.25$.

3.4. Modification for K_c under SCCA

3.4.1. Calculation and Modification of K_{cini}.

Only one drip irrigation is arranged on May 20 in the initial growth stage of the crops, and the irrigation amount of naked oats is 27 mm. According to the recommended calculation method of FAO, K_{cini} could be estimated and calculated with formula if the average infiltration depth is between 10 mm and 40 mm (Formula (4)).

$$K_{cini} = K_{cini-b} + \frac{(I-10)}{(40-10)} [K_{cini-b} - K_{cini-a}], \qquad (4)$$

where K_{cini-a} represents average K_{cini} as related to the level of ET_0 and the interval between irrigations and/or significant rain during the initial growth stage for all soil types when wetting events are light to medium (3-10 mm per event), and K_{cini-b} represents average K_{cini} as related to the level of ET_0 and the interval between irrigations greater than or equal to 40 mm per wetting event, during the initial growth stage for coarse-textured soils and medium and fine-textured soils [1], and I is the average infiltration depth (mm). According to the relevant data and materials in the figures and table, the value of K_{cini} under drip irrigation condition ascertained from the table is 0.3.

In FAO56, the calculation of K_{cini} still needs the modification for the energy restriction stage and soil moisture restriction stage in the surface evaporation process of the soil. According to the field moisture capacity and moisture rate on wilting point of the soil and the sand content Sa and clay content in the soil in the evaporation layer, K_{cini} for naked oats under drip irrigation is 0.34 when the irrigation quota is 270 mm.

Table 3: Water requirement and water requirement modulus coefficient of naked oats in various growth stages.

Growth stage	Emergence-Tillering			Tillering-Jointing			Heading-Blooming			Filling-Milky maturity		
Indicator	Water requirement	Modulus coefficient	Water requirement intensity	Water requirement	Modulus coefficient	Water requirement intensity	Water requirement	Modulus coefficient	Water requirement intensity	Water requirement	Modulus coefficient	Water requirement intensity
	mm	%	mm/d	mm	%	mm/d	mm	%	mm/d	mm	%	mm/d
YM1	51.18	20.56	2.56	69.17	27.79	2.77	76.97	30.92	3.08	51.58	20.72	1.29
YM2	60.18	20.48	3.01	82.67	28.13	3.31	90.47	30.78	3.62	60.58	20.61	1.51
YM3	69.18	20.41	3.46	96.17	28.38	3.85	103.97	30.68	4.16	69.58	20.53	1.74
YM4	78.16	20.36	3.91	109.64	28.57	4.39	117.44	30.6	4.7	78.56	20.47	1.96
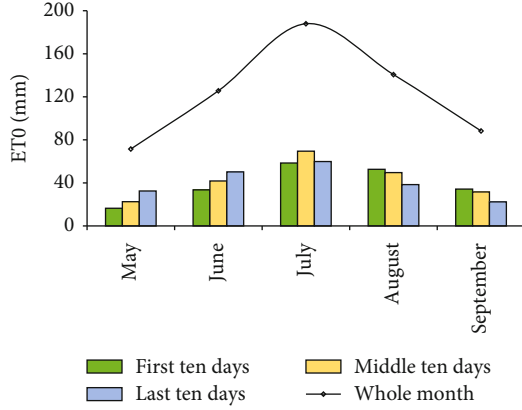
FIGURE 2: Evapotranspiration in growth period.

TABLE 4: Division of the actual growth stages of naked oats.

Growth stage	Date
Initial growth stage	May 5-June 15
Crop development growth stage	June 16-July 10
Mid-season growth stage	July 11-August 5
Late season growth stage	August 6-September 15

3.4.2. Calculation and Modification of K_{cmid}. With dry climate and windy and dusty weather, the north foot of Yinshan Mountain inn Inner Mongolia does not belong to the situations recommended in FAO-56. As for crop coefficient under non-standard situations, FAQ-56 provides the formula of modified K_{cmid} (Formula (5)):

$$K_{cend} = K_{cend(Table)} + [0.04(u_2 - 2) - 0.004(RH_{min} - 45]\left(\frac{h}{3}\right)^{0.3}, \tag{5}$$

where $K_{cmid(T)}$ represents the recommended value of FAO; u_2 represents the average daily wind speed at the positions above 2 m in the growth stage; RH_{min} represents the mean value of the minimum daily relative humidity in the growth stage; h represents the mean height of the crop in the stage. Meteorological data were shown in Table 5. The value of K_{cmid} of naked oats is 1.05.

3.4.3. Calculation and Modification of K_{cend}. Values of K_{cend} of crops recommended in FAO-56 are typical expected values of mean K_{cend} under the standard climate conditions. The value of K_{cend} under drought and strong wind conditions would be higher, while the value of K_{cend} in wet places with relatively low wind speed would be lower. Under the climate conditions that RH_{min} is not equal with 45% or u_2 is higher or lower than 2.0 m/s, it is necessary to make specific calibration for K_{cend}. Formula (6) could be used for

TABLE 5: Days and meteorological factors of naked oats at different growth stages.

	Days/d	u_2/m·s^{-1}	RH_{min}/%	h/m
Initial growth stage	20	3.42	38.95	0.32
Crop development growth stage	25	2.98	31.26	1.17
Mid-season growth stage	25	2.96	35.78	1.42
Late season growth stage	40	3.04	39.22	1.29

the calculation.

$$K_{cend} = K_{cend(Table)} + [0.04(u_2 - 2) - 0.004(RH_{min} - 45]\left(\frac{h}{3}\right)^{0.3}, \tag{6}$$

where $K_{cend\,(table)}$ is the recommended value of 1.15 for K_{cend} in FAO; u_2 is the daily average wind speed (m/s) at the position with the height of 2 m, $1 \leq u_2 \leq 6$ m/s; RH_{min} is the mean value (%) for the minimum daily relative humidity, $20\% \leq RH_{min} \leq 80\%$; h is the mean value of the crop height in the late season growth stage (m), $0.1 \leq h \leq 10$ m. The value of K_{cend} of naked oats is 0.34.

3.5. Crop Water Requirement Calculated with SCCA. In Formula (3), ET_0 and K_c after the modification were used to get the crop water requirements of naked oats in different growth stages, as shown in Figure 3. ET_0 of naked oats at the north foot of Yinshan Mountain in their full growth period in 2021 was 516.01 mm, the water requirements of naked oats under drip irrigation was 363.84 mm, and average K_c in the growth period was 0.71.

4. Discussion

The trend for the water consumption intensity of naked oats was from low to high and to low. The main water consumption of the soil in the seedling stage is mainly from soil evaporation between plants. Therefore, the water requirement is relatively low. Along with the accelerated growth speed and high temperature, the nutrient and reproduction of crops maintain simultaneous growth in the stage of Tillering-Jointing (Tillering-Squaring), and the crops growth rapidly in root, stem, and leaves, leading to strong photosynthesis. Together with high temperature and long sunshine duration, the water consumption comes across accelerated increase. The water requirement intensity of naked oats reached the peak at the Heading-Blooming stage. As the growth speed slows down, the water requirement amount and intensity experience certain decrease.

The water requirements of naked oats in various growth stages calculated out with SCCA were commonly lower than the actual crop water requirements measured at the field, especially that in the initial growth stage, which had certain relationship with the irrigation method of subsurface drip irrigation. In calculating the K_{cini}, the crop coefficient mainly depends on the wetting frequency of the surface soil due to
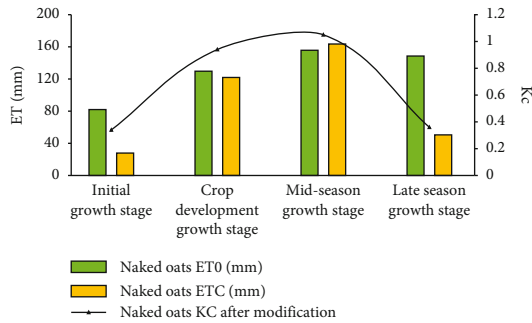
FIGURE 3: Calculation of crop water requirement under SCCA.

the low height and low shading coverage of plants. Under drip irrigation without any film protection, the crops would come across the influence from the supply of underground water due to excessive evaporation amount and relative high level of the underground water. The application of SCCA does not consider the influence of the wetting depth. As a result, the crop water requirement calculated for the initial growth stage of the crop is lower than the actual water requirement measured at the field.

K_c refers to the ratio of crop evapotranspiration and reference evapotranspiration under the standard conditions that crops without pests and diseases, soil fertility, and soil moisture status were good, and the potential maximum production could be obtained with certain climatic conditions. However, the difference in soil fertility, water stress, and management level will affect the value of K_c. Drip irrigation delivers water directly to the roots, reducing the surface water evaporation, but moistening the soil partially, which is quite different from the traditional irrigation form. In initial growth stage of crop, soil surface water evaporates quickly, but the evaporation of soil surface water slows down in the mid-season and late season growth stages. When applying SCCA to calculate K_C, the influence of soil moisture degree on K_C is considered, which plays a positive role in improving the accuracy of K_C calculation. However, because the influence of local irrigation on K_C is ignored, the deviation in the calculation of K_C value in the middle and later period appears.

5. Conclusions

The water requirement of naked oats without drought influence was 383.8 mm, and the respective peaks of the daily water requirement intensity appeared in the stage of Heading-Blooming, with the specific value of 4.70 mm/d. As a critical stage for water requirements of the crops, the water requirements in this stage took 30.60% of the total water requirements in the whole growth period.

The mean value of the potential evapotranspiration ET_0 in the whole growth period of naked oats was 3.89 mm/d; the value reached the peak of 6.86 mm/d in the last third of July and the bottom value of 1.82 mm/d in the last third of September.

After the modification, K_c of naked oats in the initial growth stage, crop development growth stage, mid-season

growth stage, and late season growth stage was 0.34, 0.94, 1.05, and 0.36, respectively, and the mean value of K_c in the whole growth period was 0.71;

Combined with meteorological data, the SCCA can be used to accurately calculate the crop water demand of naked oats under drip irrigation in the northern foot of Yinshan Mountain in Inner Mongolia (the deviation is different under different experimental treatments, generally about 10%). When the irrigation quota of naked oats was 315 mm, the actual crop water requirement of naked oats was 383.8 mm, and the crop water demand calculated by SCCA was 363.84 mm.

Data Availability

After the paper is accepted, the experimental data of this paper will be uploaded to Baidu cloud for other researchers to download and use.

Conflicts of Interest

The authors declare that they have no conflicts of interest.

Acknowledgments

References

[1] R. G. Allen, L. S. Pereira, D. Raes, and M. Smith, "Crop evapotranspiration guidelines for computing water requirements," *FAO Irrigation and Drainage Paper*, vol. 56, pp. 161–173, 1998.

[2] L. Libardi, A. B. R. T. De Faria, D. Dalri, L. F. Glauco, and A. P. Coelho, "Evapotranspiration and crop coefficient (Kc) of presprouted sugarcane plantlets for greenhouse irrigation management," *Agricultural Water Management*, vol. 212, pp. 306–316, 2019.

[3] R. Ragab, J. G. Evans, A. Battilani, and D. Solimando, "Towards accurate estimation of crop water requirement without the crop coefficient K_c: new approach using modern technologies," *Irrigation and Drainage*, vol. 66, no. 4, pp. 35–43, 2017.

[4] L. Gu, Z. Hu, J. Yao, and G. Sun, "Actual and reference evapotranspiration in a cornfield in the Zhangye oasis, northwestern China," *Water*, vol. 9, no. 7, p. 499, 2017.

[5] A. Fifah, M. R. Ismail, E. Puteri, S. Abdullah, and H. Kausar, "Optimum fertigation requirement and crop coefficients of chilli (*Capsicum annuum*) grown in soilless medium in the tropic climate," *International Journal of Agriculture & Biology*, vol. 17, no. 1, pp. 1560–8530, 2015.

[6] M. Abedinpour, "Evaluation of growth-stage-specific crop coefficients of maize using weighing lysimeter," *Soil and Water Research*, vol. 10, no. 2, pp. 99–104, 2015.

[7] W. Silva, J. S. Santana, C. M. D. Silva, and A. A. Nunes, "Crop coefficient regionalization for irrigated agriculture planning in

Maranhão state -Brazil," *Engenharia Agrícola*, vol. 37, no. 5, pp. 953–960, 2017.

[8] D. Carvalho, D. Silva, H. Rocha, W. Almeida, E. Da, and S. Sousa, "Evapotranspiration and crop coefficient for potato in organic farming," *Engenharia Agrícola*, vol. 33, no. 1, pp. 201–211, 2013.

[9] S. K. Dingre and S. D. Gorantiwar, "Determination of the water requirement and crop coefficient values of sugarcane by field water balance method in semiarid region," *Agricultural Water Management*, vol. 232, p. 8, 2020.

[10] L. A. Garcia, A. Elhaddad, J. Altenhofen, and M. Hattendorf, "Developing corn regional crop coefficients using a satellite-based energy balance model (reset-raster) in the South Platte river basin of Colorado," *Journal of Irrigation & Drainage Engineering*, vol. 139, no. 10, pp. 821–832, 2013.

[11] C. E. Maia and E. R. C. De Morais, "Coeficiente de cultura do meloeiro irrigado com água salina estimado por modelo matemático," *Ciencia Rural*, vol. 38, no. 5, pp. 1273–1278, 2008.

[12] A. C. Sanches, D. Souza, F. Jesus, F. C. Mendona, and E. P. Gomes, "Crop coefficients of tropical forage crops, single cropped and overseeded with black oat and ryegrass," *Scientia Agricola*, vol. 76, no. 6, pp. 448–458, 2019.

[13] S. Yilmaz, M. Erayman, H. Gozubenli, and E. Can, "Twin or narrow-row planting patterns versus conventional planting in forage maize production in the Eastern Mediterranean," *Cereal Research Communications*, vol. 36, no. 1, pp. 189–199, 2008.

[14] N. Zhang, Q. U. Zhongyi, K. Guo, W. U. Jiabin, X. U. Bing, and M. Jiang, "Study on crop coefficients for silage maize and alfalfa on Maowusu sandy land," *The Soil*, vol. 48, no. 2, pp. 286–290, 2016.

[15] W. Wang, P. Wang, and Y. Xie, "Estimation of evapotranspiration optimized by crop coefficient based on dynamic simulation," *Transactions of the Chinese Society for Agricultural Machinery*, vol. 46, no. 11, pp. 129–136, 2015.

[16] Y. Wang, X. Zhang, L. Lu et al., "Estimation of crop coefficient and evapotranspiration of summer maize by path analysis combined with BP neural network," *Transactions of the Chinese Society of Agricultural Engineering*, vol. 36, no. 7, pp. 109–116, 2020.

[17] Y. Cao, X. Li, and M. Zhu, "Spatial and temporal distribution characteristics of main crop coefficients in Hebei Province," *Advances in Science and Technology of Water Resources*, vol. 39, no. 2, pp. 37–45, 2019.

[18] S. P. Wang, Q. C. Duan, H. H. Han, and Y. Huang, "Rice crop coefficient and its change rule in typical areas of Yunnan Province," *China Rural Water and Hydropower*, vol. 11, pp. 60–65, 2019.

[19] X. Li, T. Liu, L. Duan, X. Tong, and G. Wang, "Crop coefficient simulation and evapotranspiration estimation of dune and meadow in a semiarid area," *Arid Zone Research*, vol. 37, no. 5, pp. 1246–1255, 2020.

[20] Y. Zhang, L. Zhang, H. Zhang, C. Song, and W. Han, "Crop coefficient estimation method of maize by UAV remote sensing and soil moisture monitoring," *Transactions of the Chinese Society of Agricultural Engineering*, vol. 35, no. 1, pp. 83–89, 2019.

[21] H. Liu, *Water and Fertilizer Response of Forage Crops and Optimal Allocation of Irrigation Water under Different Planting Patterns in Desert Area of Northern Xinjiang*, Inner Mongolia Agricultural University, 2021.

[22] M. Ikram, "Breeding physiology quality fertilization practice productions and improvement. Chapter 7 Oats in a global importance, production and improvement trends," in IKSAD Publishing House, 2021.

[23] F. Ejaz, C. Stefan, A. Fatkhutdinov, and M. Usman, "Integration of raster based irrigation and groundwater for water management in Punjab, Pakistan: a modeling & GIS based approach," *International Journal of Water Resources and Arid Environments*, vol. 9, no. 1, pp. 56–70, 2020.

[24] F. H. E. Schoot, *Estimating Current and Possible Future Irrigation Water Requirements: An Approach for the Rhine Basin during the Growing Season in Periods of Drought*, University of Twente, 2021.

[25] K. Djaman, M. O'Neill, C. Owen, K. Koudahe, and K. Lombard, "Evapotranspiration, grain yield, and water productivity of Spring oat (*Avena sativa L.*) under semiarid climate," *Agricultural Sciences*, vol. 9, no. 9, pp. 1188–1204, 2018.

Hindawi

Research Article

Effect of Coal Water Slurry Gasification Slag on Soil Water Physical Characteristics and Properties in Saline-Alkali Soil Improvement

Chunyan Yin [iD],[1,2] Ju Zhao [iD],[1] Xiaoyu Liu [iD],[1] Zhiguang Yu [iD],[1] and Hu Liu [iD][3]

[1]*Inner Mongolia Academy of Agricultural and Animal Husbandry Sciences, Hohhot 01030, China*
[2]*Inner Mongolia Agricultural University, Hohhot 01020, China*
[3]*National Field Scientific Observation and Research Station of Grassland Ecology and Hydrology at the Northern Foot of Yinshan Mountain in Inner Mongolia, China Institute of Water Resources and Hydropower Research, Hohhot, Inner Mongolia 01020, China*

Correspondence should be addressed to Ju Zhao; zjuren@163.com

To explore the effect of coal water slurry (CWS) gasification slag on the soil water physical characteristics of saline-alkali soil in the Yellow River Basin of Inner Mongolia, CWS gasification coarse slag (GCS) and gasification fine slag (GFS) were used as improvement materials and mixed with saline-alkali soil in different proportions. The influence mechanism of GCS and GFS on saline-alkali soil water holding capacity was investigated by measuring particle size composition, water holding capacity, and the change in the soil water characteristic curve after mixing. The results showed that adding gasification slag improved the particle size composition of saline-alkali soil, with sand content increased by -3.79%~217.31% and clay and silt content decreased by 5.77%~56.50% and -0.38%~41.53%, respectively. Soil bulk density decreased significantly ($P < 0.05$), with a decrease range of 15.17%~45.1%. The soil texture changed from silty loam to sandy loam, and the water retention performance improved, affecting the soil saturated water content, capillary water holding capacity, and field water holding capacity ($P < 0.05$), with increases ranging from 20.75%~86.15%, 7.84%~27.81%, and -1.89%~34.56%, respectively. After adding GCS and GFS, the VG model fit the soil water characteristic curve of saline-alkali soil well, indicating that the addition of gasification slag enhanced soil water retention significantly. In conclusion, CWS gasification slag effectively improved the water physical properties of saline-alkali soil and significantly enhanced the water retention and water holding capabilities.

1. Introduction

Soil salinization is a worldwide issue. China is one of the most severely afflicted countries by salinization. Saline soil covers approximately 36 million hectares, or 3.75% of the total land area. The main distribution areas of saline soil in China are the coast, northwest, northeast, and north. Saline-alkali has damaged 9.2 million hectares of cultivated land, accounting for 6.62% of all cultivated land in the country. In the Inner Mongolia Autonomous Region, saline land is primarily distributed in Bayannaoer, Erdos, Hohhot, Baotou, Tongliao, Chifeng, and other cities, covering 3.55 million hectares with 1.06 million hectares of saline-alkali farmed land and 2.49

million hectares of saline-alkali wasteland [1]. Improving and exploiting saline-alkali land is a vital strategy for the Inner Mongolia Autonomous Region and even the entire country to increase reserve land resources, improve cultivated land quality and production, and ensure food security. China's proven coal reserves account for 12.84% of global reserves, but coal use accounts for half of global consumption. Because of China's resource endowment of "rich coal, less oil, and poor gas," as well as the fact that the Chinese economy is currently in a period of development and peak energy demand, coal will continue to be China's principal energy source for a long time. Coal gasification technology, as one of the main elements of clean coal technology, has

developed rapidly in order to fulfill the aim of "reaching carbon peak by 2030 and carbon neutralization by 2060."

CWS gasification slag is a kind of bulk solid waste produced by the coal chemical industry with huge annual output. Every year, CWS gasification in China produces over ten million tons of gasification slag. This figure is expected to rise as the coal chemical sector develops [2, 3]. According to preliminary experiments, the gasification slag contains a large amount of 0.5~300 μm granular or flaky microparticles [4, 5], which are loose deposits under dry conditions. Longterm stacking under the impact of the monsoon will produce a lot of dust [6, 7], which will substantially impair the air quality. The gasification slag stacking takes up a lot of land as well. Due to the huge amount of gasification slag from CWS every year, the use of CWS gasification slag must be explored and solved promptly. It has important practical significance for the local ecological environment management [8, 9]. Because the CWS gasification residue still includes around 20-30% elemental carbon akin to activated carbon and about 20% aluminum oxide, it has excellent water retention properties. In addition, gasification slag is rich in elements like silica, calcium, and magnesium. And its structural components are comparable to those of soil. As a result, it is recognized as a high-quality raw material for soil improvement [10, 11]. When 20% gasification fine slag is mixed into saline-alkali land where corn and wheat are planted, the soil bulk density is reduced, water retention performance is improved, and crop germination rate is significantly improved [12]. The addition of gasification slag into sandy soil is beneficial to sandy soil improvement and alfalfa growth [13]. The growth of *Arternisia ordosica* is aided by the modified gasification slag [14]. Gasification slag is also a good humic acid storage and release medium [15]. It can be used as a composting addition to extend the high temperature period and make composting more thoroughly harmless [16].

The paper investigates the irrigation areas in Inner Mongolia on both sides of the Yellow River basin, where land salinization is severe, with numerous types of salinization, a vast area, wide distribution, and challenging improvement and application, all of which have a negative impact on and limit the long-term development of local production and economy. Using gasification slag as a novel saline-alkali soil improvement material not only allows for full utilization of the beneficial components in gasification slag, but also reduces the environmental impact of gasification slag stacking. There are currently limited research results on the improvement of saline-alkali soil in Inner Mongolia's Yellow River Basin, particularly in terms of soil water properties. Based on the foregoing analysis, this research mixed saline-alkali soil with CWS gasification slag (including coarse slag and fine slag) in various amounts. Explored the water retention effect of gasification slag on saline-alkali soil through changes in soil water physical properties such as soil particle size composition, water retention performance, and soil water characteristic curve. In order to provide technical support and theoretical basis for the improvement of saline-alkali soil using gasification slag in the Yellow River Basin of Inner Mongolia.

2. Materials and Methods

2.1. Overview of Research Areas. The research experimental site is located at Sandaoqiao Town (106 54′ 35.18 ″E, 40 49′ 34.49″ N) in Hangjinhou Banner, Bayannaoer City, Inner Mongolia. Hangjinhou Banner is located in the central and western region of Bayannaoer City, Inner Mongolia Autonomous Region. It is situated in Hetao Plain, with Linhe District to the east, Wulanbu Desert and Dengkou County to the west, the Yellow River and the Hangjin Banner in Erdos City to the south, and Yinshan Mountain to the north.

Hangjinhou Banner formed an inland faulted basin during the geological neotectonic movement. The lower part is covered by a huge, thick lacustrine sedimentary layer. Due to multiple Yellow River diversions, long-term alluviation of Yellow River water, and a considerable amount of deposition of mountain torrents, the upper half is an alluvial and proluvial plain with high topography and flat surface, at an altitude of 1,032~1,046 meters (As shown in Figure 1(a)).

The annual average temperature in a typical continental climate of the semiarid plateau in the temperate zone is 6.8°C. The annual average precipitation is 245 mm, and 60% of the precipitation falls between July and September in summer. The annual average evaporation is 2720 mm. The relative humidity is 49%, and the dryness is 1.98. The annual average wind speed is 3.0 m/s. The average frost-free period is 155 days, and multiyear soil freezing depth is 1.5 m.

2.2. Test Materials. The saline-alkali soil used in the test was taken from Chengni Village, Sandaoqiao Town, and Hangjinhou Banner. We used a root drill with a diameter of 10 cm to drill 0-50 cm topsoil, then put it into a plastic bag for sealing and mixing. The gasification slag came from Boda Shidi Chemistry Co., Ltd., Wushen County, Erdos City, Inner Mongolia. Table 1 shows the soil basic properties and gasification slag in the soil of the experimental area.

2.3. Experiment Design. The experiment adopted a threefactor orthogonal design with multiple levels and nine treatments, with each treatment being repeated three times. The main characteristics of saline-alkali soil are that the clay content and specific surface area of the soil are large and there are many water-soluble salts or alkaline substances. Salinealkali soil is generally sticky when wet and hard when dry. There are always white salt deposits on the soil surface, and the ventilation and permeability are poor. Therefore, the relative content of clay particles in saline-alkali soil can be reduced by adding gasification slag with relatively coarse particles, which is the basis of the test design. Increasing the amount of gasification coarse slag in the soil may increase pores between particles, weaken capillary action, loosen the soil texture, improve soil permeability, speed up water transport (which follows the water-salt movement rule of "salt is provided with water and salt is removed with water"), and reduce soil salinization. The weight of each sample was 1000 g. The specific treatment scheme is shown in Table 2.

(a) Aerial view of the study area

(b) Test gasification slag

Figure 1: Aerial view of the study area and test gasification slag.

2.4. Experimental Indicators and Methods. The composition of soil particle size is determined by a laser particle size analyzer (BT9300ST, as shown in Figure 2(a)). The soil and gasification residue are dried in a cool area, fully rolled with a wooden roller, and then screened with a 1 mm sieve. Select appropriate suspension and dispersant, mix the sample with the suspension, and allow the sample particles to be fully dispersed in the suspension with the aid of dispersant. Then put the sample into the ultrasonic cleaning machine, make the liquid level in the cleaning tank reach about 1/2 of the total height of the measuring cup, turn on the power supply and let it vibrate for about 2 min (for the sample that is easy to sink, it should be vibrated while stirring with a glass rod). Put the prepared samples into the laser particle size analyzer for measurement, and use the particle size analysis software Talwin to process the data to determine the particle size composition and soil texture [17].

The cutting ring method is used to determine water retention performance. First, weigh the cutting ring containing each treated soil sample. Place it on flat bottom tray and add water to the upper edge of the cutting ring. Weigh it after 24 hours of water absorption. Place the cutting ring on the dry sand and weigh after 2 hours and 24 hours. The cutting ring was then dried at 105°C and weighed once again. Using the weighing data, the saturated water content, capillary water capacity, field water capacity, capillary porosity, and noncapillary porosity of each treatment were calculated [18].

The pressure film instrument (1500F2, as shown in Figure 2(b)) was used to determine the modified soil water characteristic curve. Set the cutting ring filled with each treated soil sample in a flat bottom tray and add water. When the cutting ring is completely saturated, weigh it. Place the cutting ring in a pressure cooker to pressurize. Remove the cutting ring after the water has stopped flowing out and weigh it. Return it back to the pressure cooker, raise the pressure, and pressurize the cutting ring continuously until it reaches equilibrium, then weigh it again. Repeat the process to acquire a series of soil water suction forces and corresponding soil water contents for the soil water characteristic curve.

2.5. Data Analysis Method. The data were statistically analyzed by Excel 2010 and SPSS 19.0 software. LSD method was used for the significance test ($P < 0.05$). Single factor analysis of variance (ANOVA) was used to compare the difference of water retention performance between different treatments, and Duncan method was used to test the significance. The soil water characteristic curve was fitted using RETC software. Principal component analysis was used to assess the improvement effect of each treatment.

3. Results and Analysis

3.1. Effect of Addition of Gasification Slag on Particle Size Composition. The particle size composition of each treatment and CK is shown in Table 3. As the amount of gasification slag increased, the content of soil sand and capillary porosity increased significantly ($P < 0.05$), with increases ranging from -3.79% to 217.31% and from 112.61% to 502.10%, respectively. With reduction ranges of 15.17% ~45.1%, 5.77% ~56.50%, and -0.38% ~41.53%, the soil bulk density, clay, and silt contents all indicated significant decrease trend ($P < 0.05$). Bulk density had significant negative correlation with sand content ($r < 0$, $P < 0.05$) and significant positive correlation ($r > 0$, $P < 0.05$) with silt and clay content.

Capillary porosity had significant positive correlation with sand content ($r > 0$, $P < 0.05$) and significant negative correlation with silt and clay content ($r < 0$, $P < 0.05$). This indicated that as the addition volume of gasification coarse slag and gasification fine slag increased, the bulk density of saline-alkali soil gradually decreased, and the proportion of clay and silt particles decreased continuously, increasing the pores between particles, weakening the capillary effect, improving the disadvantages of poor ventilation and permeability of saline-alkali soil, loosening the soil texture, speeding up water transport, and reducing soil salt content. Moreover, according to the soil texture classification, the soil texture of the reconstructed soil gradually changed from silty loam to sandy loam as the proportion of GCS and GFS increased, improving the soil texture of saline-alkali soil. In the results data, the size grading and soil texture are all

TABLE 1: Physicochemical properties of GCS, GFS and experimental saline-alkali soil.

| Sample name | Bulk density (g/cm^{-3}) | Particle size composition/% | | | Saturated water content (%) | Field water holding capacity (%) | Soil cation exchange capacity (cmol/kg) | Loss on ignition/(%) | Soil texture | pH |
		Sand particle (>50 μm)	Powder particle (2–50 μm)	Cosmid (<2 μm)						
GCS	0.88	81.09	17.18	1.73	65	24	7.81	16	Loamy sand	9.3
GFS	0.36	43.21	51.95	4.85	224	97	3.88	29	Silty loam	8.2
Saline-alkali soil	1.43	16.64	73.13	10.23	32	22	14.07	/	Silty loam	8.5

TABLE 2: Experimental design of improving saline-alkali soil with CWS gasification slag.

Treatment	CK	Treatment 1	Treatment 2	Treatment 3	Treatment 4	Treatment 5	Treatment 6	Treatment 7	Treatment 8
GCS (%)	0	10	20	10	20	30	20	30	40
GFS (%)	0	20	10	40	30	20	50	40	30
Saline-alkali soil (%)	100	70	70	50	50	50	30	30	30

(a) Laser particle size analyzer (BT9300ST)

(b) Pressure film instrument (1500F2)

FIGURE 2: Instruments used in the test.

approaching loam, which is in line with the assumption of the saline-alkali soil improvement scheme.

3.2. Effect of Adding Gasification Slag on Water Retention Performance.

Saturated water content refers to the water content when all pores of soil are filled with water under natural conditions, including capillary pores and noncapillary pores. It represents the maximum water holding capacity of soil, that is, the water content when all pores between soil particles are filled with water. Table 4 showed that following the addition of gasification coarse and fine slag, the water retention performance of saline-alkali soil increased with the continual increase in the addition volume. The saturated water content increased significantly ($P < 0.05$). Treatment 6 had the highest saturated water content, followed by treatment 7, treatment 3, treatment 4, treatment 5, treatment 1, and treatment 2, all of which were higher than the CK. Treatments 1–8 increased by 33.70%, 20.75%, 56.09%, 50.23%, 42.00%, 86.15%, 71.20%, and 71.60%, respectively, as compared to the CK, indicating that the addition of gasification slag improved the water retention capacity of saline-alkali soil.

Capillary water holding capacity refers to the maximum amount of capillary rising water that can be held in the soil. The capillary water holding capacity also showed an upward trend, with treatment 6 being the highest, followed by treatment 3, treatment 1, treatment 8, treatment 4, treatment 5, treatment 7, and treatment 2, all of which were higher than the CK. Treatments 1–8 were 20.36%, 7.84%, 26.05%, 18.57%, 12.03%, 27.81%, 10.69%, and 18.81% higher than CK, respectively.

Field water capacity is the highest soil water content that can be stably maintained by the soil, the maximum amount of suspended water that can be maintained in the soil, and the highest soil water content that is effective for crops. The field water capacity also showed an upward trend, with treatment 3 being the highest, followed by treatment 6, treatment 1, treatment 4, treatment 5, treatment 8, and treatment 2, all of which were higher than the CK, with treatment 7 being the lowest. In comparison to the CK, treatments 1–8 increased 23.38%, 4.47%, 34.56%, 12.19%, 6.84%, 30.22%, 1.89%, and 8.03%, respectively.

Capillary pore refers to the pore with capillary function. Its pore diameter is larger than that of inactive pore. It is the place for water movement and storage. It is the key factor affecting soil permeability and determining surface runoff and runoff time. As Table 4 has shown, the capillary porosity rises with the addition of gasification slag, indicating that it improved the compact texture and few pores of saline-alkali soil. It is a key factor affecting soil permeability and surface runoff and runoff generation time. Compared with CK, the capillary porosity of treatments 1–8 increased by 128.72%, 112.61%, 269.88%, 275.66%, 255.34%, 501.40%, 502.10%, and 447.64%%, respectively.

Noncapillary porosity is the percentage of noncapillary porosity in soil volume. Noncapillary pores are also called macropores. For soil pores with a pore diameter greater than 0.1 mm, macropores are often filled with air and are filled with water only when there is a large amount of gravity water. Noncapillary pores have no water holding capacity, but can make the soil aerated and permeable. As shown in Table 4, the noncapillary porosity shows an upward trend,

TABLE 3: Test results of particle size composition in saline-alkali soil improvement with gasification slag.

Treatment	CK	Treatment 1	Treatment 2	Treatment 3	Treatment 4	Treatment 5	Treatment 6	Treatment 7	Treatment 8
Bulk density/g/cm-3	1.430	1.161	1.213	0.947	0.999	1.051	0.785	0.837	0.889
Sand/%	16.64	16.01	16.95	27.71	24.31	25.82	22.57	25.16	52.8
Clay/%	10.23	10.58	10.82	7.89	8.88	8.2	9.29	8.45	4.45
Particle/%	73.13	73.41	72.24	64.4	66.81	65.98	68.15	66.39	42.76
Capillary porosity/%	5.71	13.06	12.14	21.12	21.45	20.29	34.34	34.38	31.27

Table 4: Test results of water retention performance in saline-alkali soil improvement with gasification slag.

Soil water constant	CK	Treatment 1	Treatment 2	Treatment 3	Treatment 4	Treatment 5	Treatment 6	Treatment 7	Treatment 8
Total porosity/%	40.66	48.94	43.86	51.26	48.22	45.56	51.98	45.02	48.31
Capillary porosity/%	5.71	13.06	12.14	21.12	21.45	20.29	34.34	34.38	31.27
Noncapillary porosity/%	46.37	62.01	56.00	72.39	69.67	65.86	86.32	79.40	79.58
Saturated water content/%	32.43	43.36	39.16	50.62	48.72	46.05	60.37	55.52	55.65
Capillary water holding capacity/%	28.44	34.23	30.67	35.85	33.72	31.86	36.35	31.48	33.79
Field water holding capacity/%	22.80	28.13	23.82	30.68	25.58	24.36	29.69	22.37	24.63

Figure 3: Effect of gasification slag on soil water characteristic curve of saline-alkali soil.

which is represented by CK < treatment, 2 < treatment, 1 < treatment, 5 < treatment, 4 < treatment, 3 < treatment, 7 < treatment, and 8 < treatment 6. Treatment 1–8 was 33.73%, 20.77%, 56.11%, 50.25%, 42.03%, 86.15%, 71.23%, and 71.62% higher than CK, respectively. It can be seen that increasing the amount of gasification slag can improve the water retention performance of saline-alkali soil.

3.3. Effect of Adding Gasification Slag on Soil Water Characteristic Curve.

The soil water characteristic curve is a curve that depicts the changing relationship between soil water suction and content. It can reflect soil water holding capacity and soil water availability as well as the changing relationship between soil water quantity and energy. The soil water characteristic curve of saline-alkali soil under varying proportions of gasified slag is shown in Figure 3. Adding gasified slag to the soil water characteristic curve causes the soil water characteristic curve to shift downward compared to the control, indicating that the soil water content with gasified slag added under the same PF value (soil water suction) is less than that without gasified slag. As the amount of gasified slag addition increases, the soil water content under the same PF value decreases.

The main reason is that adding gasification slag improves the soil pore structure, making it more permeable and accelerated the water transport. Therefore, the CK water content under the same pressure is higher than other treatments. The J-chart showed that in the suction range between PF 0 and 50 kPa, the water content difference between treatment and CK decreased as the PF value increased. In the suction range between PF 50 to 1000 kPa, the soil water content of treatment 1 is higher than the soil water content of CK. While treatments 2~8 are lower than that of the CK under the same PF value. It is clear that the addition of gasification slag had significant impact on the soil water characteristic curve, assisting in the improvement of soil pore

structure, porosity, and permeability and accelerating the soil water transport. The Van Genuchten model was used to further analyze the effect of gasification slag content on the soil water characteristic curve quantitatively.

In Table 5 when the determination coefficient R^2 in the Van Genuchten model ranged from 0.972 to 0.991, the deviation between the VG function-simulated soil saturated water content and the results measured by the experiment is from -3.38% to 4.12%. This indicated that the VG model well simulated the influence of gasification slag content on the soil water characteristic curve. CK had a lower water retention content (θr) than all the other treatments. Value a is the reciprocal of the inflection point suction value when the water characteristic curve is close to saturation. The higher value a is, the poorer the soil water retention capacity. Treatment 1–8 had lower value a than the CK due to the addition of gasification slag (Figure 3). Therefore, adding gasification slag to saline-alkali soil improved the soil water retention performance and enhanced its water holding capacity.

3.4. Principal Component Analysis on Influence of Gasification Slag on Soil Water Retention Performance.

Using the principal component analysis approach, it is possible to screen out many unrelated comprehensive indicators in a complex index system for dimension reduction. These comprehensive indicators can reflect most of the information provided by all the original indicators. Five factors, including saturated water content, capillary water holding capacity, field water holding capacity, capillary porosity, and noncapillary porosity of each treatment were selected. The eigenvalues, eigenvectors, contribution rates, and cumulative contribution rates of the matrix were further calculated using factor analysis in SPSS, as shown in Table 6.

Two principal components were derived using the eigenvalue $\lambda \geq 1$ principle. The variance contribution rates of the two principal components were 63.947% and 32.705%,

TABLE 5: Parameters of Van Genuchten model for saline-alkali soil.

Treatment	θ_r	θ_s	a	n	R^2
CK	0.414	0.336	0.277	1.516	0.972
Treatment 1	0.194	0.437	0.064	2.208	0.981
Treatment 2	0.128	0.389	0.053	2.246	0.987
Treatment 3	0.143	0.489	0.056	2.384	0.991
Treatment 4	0.130	0.475	0.060	2.186	0.991
Treatment 5	0.136	0.447	0.058	2.300	0.982
Treatment 6	0.073	0.580	0.081	1.874	0.984
Treatment 7	0.074	0.545	0.056	2.483	0.989
Treatment 8	0.092	0.537	0.062	2.080	0.987

TABLE 6: Calculated values of principal component analysis on soil water retention performance of saline-alkali soil.

Principal component	Eigenvalue	Contribution rate %	Cumulative contribution rate %	Water retention performance index	Factor load		Score coefficient	
					1	2	1	2
1	3.197	63.947	63.947	Saturated water content	0.928	-0.364	0.450	0.446
2	1.635	32.705	96.652	Capillary water holding capacity	0.925	0.334	0.498	-0.211
3	0.131	2.623	99.275	Field water holding capacity	0.693	0.706	0.399	-0.567
4	0.026	0.528	99.803	Capillary porosity	-0.323	0.930	0.498	-0.212
5	0.010	0.197	100.000	Noncapillary porosity	0.946	-0.170	0.378	0.625

TABLE 7: Comprehensive scores of principal component analysis on water retention performance of saline-alkali soil.

Treatment	CK	Treatment 1	Treatment 2	Treatment 3	Treatment 4	Treatment 5	Treatment 6	Treatment 7	Treatment 8
F_1	-3.54	0.27	-1.94	1.91	0.32	-0.75	2.96	-0.16	0.93
F_2	-0.45	-1.41	-0.28	-1.3	-0.06	0.27	0.11	2.05	1.06
IF value	-2.78	-0.13	-1.54	1.14	0.23	-0.51	2.27	0.36	0.95
Ranking	9	6	8	2	5	7	1	4	3

respectively. The cumulative variance contribution rate was 96.652%, which has reflected the basic information on soil water retention performance. The five components' original data were normalized. And the comprehensive water retention performance score was calculated using principal component score coefficient matrix (Table 6). The water retention performance is reflected in the comprehensive score IFI value. As shown in Table 7, treatment 6 had the highest ranking scores, followed by treatment 3, treatment 8, treatment 7, treatment 4, treatment 1, treatment 5, treatment 2, and CK. Therefore, treatment 6 had the highest water retention capacity, whereas CK had the lowest.

4. Discussion

The gasification slag comprises of coarse slag and fine slag. The gasification coarse slag is slag discharged from the bottom of the gasification furnace through the processes of melting, chilling, condensation, and the like while the gasification furnace is operating at high temperatures and pressures, with particle sizes ranging from 16 to 4 meshes. The gasification coarse slag is characterized by higher sand particle composition ratio and larger sand particle size, which improves the pore structure of the soil, increases internal pores, reduces soil bulk density, and improves soil water retention. Gasification fine slag is slag generated by the airflow from the top of the gasification furnace after being preliminary washed, purified, and precipitated, with particle sizes of fewer than 16 meshes. It is distinguished by high clay-particle ratio, large clay-particle surface area, and strong adsorption effect. When mixed with soil, it could fill the macropores of soil, improving the soil texture and water retention [18].

Due to the large proportion of fine particles such as silt and clay in the saline-alkali soil, the soil is relatively dense, the soil permeability is poor, and there are fewer capillary pores in the total pores. This structure makes the soil water transport difficult, the soil water conductivity is poor, and the soil water and nutrients are difficult to release effectively. The improvement of saline-alkali soil is mainly based on different proportions of gasification coarse slag and fine slag. With the addition of gasification slag, the relatively large

gravel in the gasification slag particles expands the small pores of saline-alkali soil, and the soil texture gradually changes from silty loam to sandy loam, reducing the soil bulk density, improving the soil pore structure, increasing the soil porosity, improving the soil permeability, and making the soil texture loose. The application of gasification slag optimizes the pore structure of saline-alkali soil, thus effectively increasing the proportion of capillary porosity and improving the hydraulic conductivity. At the same time, it follows the water salt movement law of "salt comes with water, and salt goes with water". Therefore, the application of gasification slag also reduces the salt content of soil, weakens the degree of soil salinization, and has obvious improvement effect on saline-alkali soil.

Soil water is one of the most critical elements impacting plant growth in saline-alkali regions. Soil saturated water content, capillary water holding capacity, and field water holding capacity are the most prevalent markers of soil water retention. Previous studies have shown that application of solid additives in the soil, such as fly ash and biochar [19, 20], enhanced the overall porosity of the soil, therefore raising the soil saturated volumetric water content and improving the soil water retention performance significantly. The results of this study suggest that adding gasification slag to saline-alkali soil increased saturated water content, capillary water holding capacity, and field water holding capacity and improved water retention performance, which is consistent with the findings of earlier studies [13, 14]. By studying the effect of different content of gasification slag on soil water characteristic curve of saline-alkali soil, it was found that the water holding capacity and water retention performance of saline-alkali soil were significantly improved with the addition of gasification slag. The reason was that the gasification slag has large specific surface area and porous and uniformed pores [21, 22] due to the high temperature (800–1300°C) and chilling effect of the coal gasification process, allowing it to absorb more water than its own weight; thus improved the soil structure, increased aggregates and other functions and improved soil water holding capacity and water retention performance. Improvements in soil water retention performance not only minimizes water and soil loss and erosion but also promotes crop development.

5. Conclusions

The results demonstrated that adding gasification slag to saline-alkali soil reduced the soil bulk density. With the addition of gasification slag, the texture of saline-alkali soil changed from silty loam to sandy loam. The decrease of soil bulk density and the gasification slag's filling action into macropores lead to the increase of soil pores in saline-alkali soil, which greatly increased the water availability, improved the soil permeability, and solved the problem of poor water holding capacity and water retention performance of saline-alkali soil.

The water retention performance of saline-alkali soil showed an upward trend with the increase of gasification slag dosage. The improvement of water retention performance was related to the addition amount of gasification

slag. With different addition proportions of gasification slag, the saturated water content, capillary water holding capacity, and field water holding capacity of soil were all significantly affected ($P < 0.05$). However, there were no obvious correlations between total porosity, noncapillary porosity of soil and the addition amount of gasification slag.

The Van Genuchten model well fit the soil water characteristic curve of saline-alkali soil after gasification slag addition. The model shows that the addition of gasification slag significantly improved the soil water holding capacity and water retention performance. In the principal component analysis on soil water holding capacity of saline-alkali soil, the higher the addition amount of gasification slag, especially gasification fine slag, the more obvious the improvement of soil water holding capacity and water retention performance.

Data Availability

The data used to support the findings of this study are available from the corresponding author upon request.

Conflicts of Interest

The authors declare that they have no conflicts of interest.

Acknowledgments

References

[1] J. S. Yang, R. J. Yao, X. P. Wang et al., "Research on salt-affected soils in China: history, status quo and prospect," *Acta Pedologica Sinica*, vol. 59, no. 1, pp. 10–27, 2021.

[2] W. D. Ai, *The study on preparation and properties of coal gasification slag/polymer composites*, Jilin University, 2020.

[3] Y. B. Zhao, H. Wu, X. L. Cai et al., "Basic characteristics of coal gasification residual," *Clean Coal Technology*, vol. 21, no. 3, pp. 110–113, 2015.

[4] W. Zhao, J. Zhao, Z. M. Wei, C. Y. Yin, H. Liu, and B. Zhu, "Effect of aeolian sandy soil improved by gasification slag on soil water physical properties," *Research of Soil and Water Conservation*, vol. 29, no. 2, pp. 64–69, 2022.

[5] X. X. Gao, X. L. Guo, and X. Gong, "Characterization of slag from entrained-flow coal gasification," *Journal of East China University of Science and Technology*, vol. 35, no. 5, pp. 677–683, 2009.

[6] S. Li and K. J. Whitty, "Physical phenomena of char–slag transition in pulverized coal gasification," *Fuel Processing Technology*, vol. 95, pp. 127–136, 2012.

[7] P. Borm, "Toxicity and occupational health hazards of coal fly ash (cfa). a review of data and comparison to coal mine dust," *Annals of Occupational Hygiene*, vol. 41, no. 6, pp. 659–676, 1997.

[8] T. Zhang, L. Yu, L. Yu et al., "Characteristic analysis and application discussion of coal water slurry gasifier slag," *Modern chemical research*, vol. 19, pp. 88–90, 2020.

[9] R. F. Ash and R. L. Edmonds, "China's land resources, environment and agricultural production," *China Quarterly*, vol. 156, pp. 836–879, 1998.

[10] C. Y. Yin, J. Zhao, H. Liu et al., "Effects of coal water slurry gasification slag on soil improvement and Jerusalem artichoke growth in mu us Sandy land," *Chinese Journal of Soil Science*, vol. 52, no. 6, pp. 1411–1417, 2021.

[11] N. Liu, Q. Li, L. P. Sun, K. L. Zhang, and F. R. Kang, "Study on the stimulation effect of additional nutrient application on the compound gasification slag-sand soil," *Journal of Yulin College*, vol. 31, no. 2, pp. 28–31, 2021.

[12] D. D. Zhu, S. D. Miao, B. Xue, Y. S. Jiang, and C. D. Wei, "Effect of coal gasification fine slag on the physicochemical properties of soil," *Water, Air, & Soil Pollution*, vol. 230, no. 7, p. ???, 2019.

[13] Q. Li, L. P. Sun, F. R. Kang et al., "Effects of coal gasification slag-sand soil compound on the growth and heavy metal migration of alfalfa in the Mu Us sandy land," in *The 2019 Science and Technology Annual Conference of the Chinese Society for Environmental Sciences-Environmental Engineering Technology Innovation and Application Sub-forum Proceedings*, pp. 590–595, 2019.

[14] Y. L. Xiang, Y. R. Jiao, and L. P. Wang, "The effect of soluble organic matter modified gasification residue on the growth of Artemisia sphaerocephala and the migration and transformation of heavy metals," *Journal of Yulin College*, vol. 29, no. 6, pp. 1–3, 2019.

[15] D. Zhu, J. Zuo, Y. Jiang, J. Zhang, J. Zhang, and C. Wei, "Carbon silica mesoporous composite in situ prepared from coal gasification fine slag by acid leaching method and its application in nitrate removing," *Science of the Total Environment*, vol. 707, no. 136102, pp. 1–10, 2020.

[16] J. C. Feng, "Introduction to waste residue treatment and utilization," *Shandong chemical industry*, vol. 43, no. 1, pp. 148-149, 2014.

[17] X. L. Zheng, *Determination of particle size and particle size distribution of calcium carbonate by laser particle size analyzer*, vol. 1, pp. 13-14, 2018.

[18] Y. J. Sheng, *Study on the Physical and Chemical Properties of Entrained Bed Gasification Ash*, East China University of Science and Technology, 2017.

[19] L. H. Wang, *Effects of Different Modifiers on Acid Soil Properties and Rape Growth*, Shandong Agricultural University, 2014.

[20] N. Cui, *The Physicochemical Characters of the Saline-Alkali Soil Improved with Fly Ash and the Effect of the Soil on the Physiological Characters of Plants*, Beijing University of Technology, 2012.

[21] L. Su, Z. J. Shen, Q. F. Liang, J. L. Xu, and H. F. Liu, "Research on the physical and chemical properties of water chilled solid slag in entrained-flow gasifier," *Chemical Engineering*, vol. 42, no. 5, 2014.

[22] H. F. Yin, Y. Tang, Y. Ren, and J. Z. Zhang, "Study on the characteristic and application of gasification slag from TEXACO gasifier," *Coal conversion*, vol. 32, no. 4, pp. 30–33, 2009.

Hindawi

Retraction

Retracted: Mixture of Gaussian Processes Based on Bayesian Optimization

Journal of Sensors

This article has been retracted by Hindawi following an investigation undertaken by the publisher [1]. This investigation has uncovered evidence of one or more of the following indicators of systematic manipulation of the publication process:

(1) Discrepancies in scope

(2) Discrepancies in the description of the research reported

(3) Discrepancies between the availability of data and the research described

(4) Inappropriate citations

(5) Incoherent, meaningless and/or irrelevant content included in the article

(6) Manipulated or compromised peer review

The presence of these indicators undermines our confidence in the integrity of the article's content and we cannot, therefore, vouch for its reliability. Please note that this notice is intended solely to alert readers that the content of this article is unreliable. We have not investigated whether authors were aware of or involved in the systematic manipulation of the publication process.

Wiley and Hindawi regrets that the usual quality checks did not identify these issues before publication and have since put additional measures in place to safeguard research integrity.

We wish to credit our own Research Integrity and Research Publishing teams and anonymous and named external researchers and research integrity experts for contributing to this investigation.

The corresponding author, as the representative of all authors, has been given the opportunity to register their agreement or disagreement to this retraction. We have kept a record of any response received.

References

[1] R. Mao, C. Cao, J. J. Y. Qian, J. Wang, and Y. Liu, "Mixture of Gaussian Processes Based on Bayesian Optimization," *Journal of Sensors*, vol. 2022, Article ID 7646554, 10 pages, 2022.

Research Article

Mixture of Gaussian Processes Based on Bayesian Optimization

Runjun Mao [ID],[1] Chengdong Cao [ID],[2] James Jing Yue Qian [ID],[3] Jiufan Wang [ID],[4] and Yunpeng Liu [ID][5]

[1]*Imperial College London, London, UK*
[2]*The University of Melbourne, Melbourne, Australia*
[3]*Shanghai High School International Division, Shanghai, China*
[4]*Airport College, Civil Aviation University of China, Chengdu, China*
[5]*Tongji University, Shanghai, China*

Correspondence should be addressed to Runjun Mao; rm522@ic.ac.uk

This paper gives a detailed introduction of implementing mixture of Gaussian process (MGP) model and develops its application for Bayesian optimization (BayesOpt). The paper also develops techniques for MGP in finding its mixture components and introduced an alternative gating network based on the Dirichlet distributions. BayesOpt using the resultant MGP model significantly outperforms the one based on Gaussian process regression in terms of optimization efficiency in the test on tuning the hyperparameters in common machine learning algorithms. This indicates the success of the methods, implying a promising future of wider application for MGP model and the BayesOpt based on it.

1. Introduction

Bayesian optimization (BayesOpt) is a highly effective method for optimizing expensive black-box objective functions. These functions are expensive to evaluate and cannot be accessed analytically due to their complicated structures. They often come along with properties such as being noisy and having multiple local optima. Simple approaches like random search are inappropriate, and derivative-based algorithms like gradient decent are unreliable as well as inefficient due to the noisy and expensive nature of the objective functions. To address these issues, BayesOpt offers a derivative-free approach by building a surrogate that models the objective function and deciding where to evaluate using Bayesian statistics [1–3]. The ability to optimize expensive black-box derivative-free functions brought BayesOpt a wide range of applications since the 1960s [4, 5]. It is extensively used for designing engineering systems in robotics, computer graphics, and sensor networks [6–8], and it has recently become extremely popular for tuning hyperparameters in machine learning algorithms [9, 10].

BayesOpt is a member of the surrogate modelling methods in nature. The central idea behind this more general class of method is to use a well-behaved function that estimates the objective function based on a limited number of sampled data while being cheap to evaluate [11, 12]. The mostly used surrogate in BayesOpt is Gaussian process regression (GPR) [13]. It uses a set of parameters in its covariance function (kernel) to characterize the fluctuation of the objective function and makes regression using Bayes' theorem. When combined with other methods to help finding the parameters in its kernel, GPR provides satisfying result. But it can be further improved by generalizing to the mixture of Gaussian process (MGP) model. The main motivation of this generalization is that the objective function's behaviour is most likely inconsistent throughout the input space; hence, a single GPR with a fixed set of kernel parameters is typically inadequate for modelling the entire objective function. The MGP model overcomes this problem by self-organizing several GPs with different kernel parameters, allowing the kernel to be input-dependent [14].

The MGP model is a variant of the well-known mixture of expert (ME) model of Jacobs et al. [15] and was firstly introduced in Tresp [14]. It is a mixture model consisting of an input-dependent gating network and several GPs as the mixture components. Each GP specializes in a certain region of the input space due to their unique kernel parameters and stands for the local expert in the ME model. The gating network learns the specialization of the experts from the training data and estimates the participation of each expert for a new input. With this mechanism, the MGP model divides up the regression of the entire objective function into several regional subtasks to be executed by each expert, respectively, achieving a better overall result than any individual GPR [14]. By substituting GPR with MGP as the surrogate model, BayesOpt can more accurately estimate the objective function, speeding up its convergence on finding the optimum.

This paper firstly gives a brief review of the BayesOpt using GPR and then provides a detailed description of the MGP model with an alternative gating network modified from Rasmussen and Ghahramani [16] along with the method to find the local experts. Based on the discussions in the previous sections, a clustering-assisted approach to implement the MGP in the BayesOpt is introduced. Finally, the performance of the MGP model and the BayesOpt based on it are tested and discussed.

2. Background Review

2.1. Gaussian Process Regression. Gaussian process regression (GPR) is the most commonly used surrogate regression model in BayesOpt. It uses Gaussian process (GP) to build up the statistical inference, assuming the values of the objective function forming a multivariable Gaussian distribution with a particular mean vector and covariance matrix [17].

$$f(y_1, y_2, \cdots, y_N) = \frac{\exp\left\{-(1/2)\left(\vec{y} - \vec{\mu}\right)^T \Sigma^{-1}\left(\vec{y} - \vec{\mu}\right)\right\}}{(2\pi)^{N/2} \bullet \sqrt{\det(\Sigma)}}. \tag{1}$$

The term $\vec{\mu}$ denotes the mean vector, which is commonly chosen to be a constant value, typically zero or the average of the sampled values. Matrix Σ is the covariance matrix, generated by a covariance function also known as kernel. The kernel models the correlation between each pair of points based on their positions. The mean vector together with kernel completely defines the properties of the GP [18, 19].

Following the fact that points that are closer in the input space typically have stronger correlations, the kernel value is always positive and decreases asymptotically to zero as the spatial distance increases. There are two major two types of kernels. The first type is Gaussian kernel (also called power exponential), where the correlation decreases in the form

of a Gaussian function.

$$k\left(x, x'\right) = \alpha_0 e^{-(1/2)\|x - x'\|^2}. \tag{2}$$

The term α_0 is the variance of the function's values in the prior, and $\|x - x'\|$ is the metric in the input space. Such metric is not necessarily isotropic and Euclidean and typically takes in the form $\sum_{i=1}^{d} (x_i - x_i')^2 / l_i$, where the $l_{1:d}$ in the denominators are called length scales. The second type is called Matérn kernel which takes in the following form [20]:

$$k_v\left(x, x'\right) = \alpha_0 \frac{2^{1-v}}{\Gamma(v)} \left(\sqrt{2v}\|x - x'\|\right)^v K_v\left(\sqrt{2v}\|x - x'\|\right), \tag{3}$$

where Γ is the gamma function and K_v is the modified Bessel function of the second kind. The additional positive parameter v characterizes the smoothness of the regression model as GPs based on Matérn kernel are $\lceil v \rceil - 1$ times differentiable in the mean-square sense [20, 21]. Additionally, in the limit where v tends to infinity, the Matérn kernel converges to Gaussian kernel, which corresponds to the fact that GPs with Gaussian kernel are infinitely differentiable. In practice, Gaussian kernel could overestimate the smoothness of the objective function; hence, Matérn kernel is often used in the cases where the differentiability of the objective function is known or assumed to a certain degree.

In the cases where measurements are noisy, the kernels above still hold for any pairs of points that are distinct (namely, $x \neq x'$) as noises do not contribute to correlation. The variances however are increased by the variance of the noise. Hence, the covariance matrix can be expressed in the following form [20], where σ_n^2 is the variance of the noise.

$$\Sigma = K(x_{1:N}, x_{1:N}) + \sigma_n^2 I. \tag{4}$$

To make regression, GPR firstly combines the sampled points along with the point to evaluate into a GP as the prior distribution. Then, the evaluation is done by finding the posterior distribution of the value to evaluate given the sampled data points according to Bayes' theorem. The resultant posterior distribution can be derived from (1) and is presented below [20, 22]:

$$y(x)\big|\{x_i, y_i\}_{i=1}^N \sim \mathcal{N}\left(\mu_*(x), \sigma_*^2(x)\right), \tag{5}$$

$$\mu_*(x) = \mu(x) + \Sigma(x, x_{1:N})\Sigma^{-1}(x_{1:N}, x_{1:N})\left(\vec{y}_{1:N} - \vec{\mu}(x_{1:N})\right), \tag{6}$$

$$\sigma_*^2(x) = \Sigma(x, x) - \Sigma(x, x_{1:N})\Sigma^{-1}(x_{1:N}, x_{1:N})\Sigma(x_{1:N}, x). \tag{7}$$

2.2. Choosing Kernel Parameters. The parameters in the kernel of GPR, especially the length scales, greatly affect the
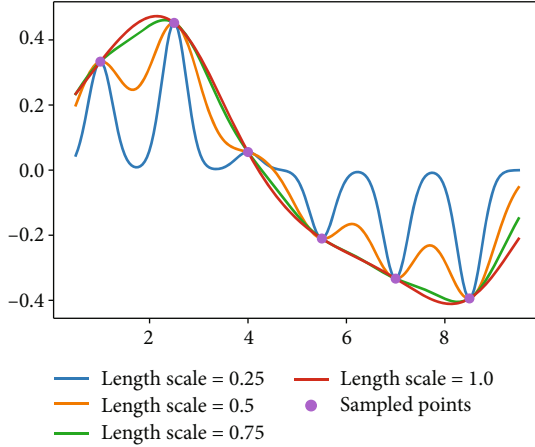
FIGURE 1: The regressions made on the same function using different length scales. The regression value is taken to be the mean of the posterior distribution.

performance of regression. The length scales characterize the inverse speed that the function changes along each axis. A small length scale indicates the function changes rapidly along this axis, while a large length scale assumes the function is flatter and smoother. Based on different assumptions hence different length scales, the regression gives out distinct results as illustrated in Figure 1. If one assumes the actual function is well represented by the sampled points, the length scales can be chosen using maximum likelihood estimation (MLE). In this approach, the length scales are the configuration that maximizes the likelihood of the observations under the prior [23], namely,

$$l_{1:d} = \underset{l_{1:d}>0}{\operatorname{argmax}} \left[p\left(\{x_i, y_i\}_{i=1}^N | l_{1:d} \right) \right]. \qquad (8)$$

The length scales found are anisotropic in general. One can also assume the length scales to be isotropic, meaning that the same length scale is shared for all axes and MLE degenerates to maximizing $p(\{x_i, y_i\}_{i=1}^N | l)$. Such assumption is obviously less comprehensive but more appropriate when there are relatively few sampled points. It is especially the case when the number of sampled points is not significantly larger than the dimension of the input space, since the assumption for the function being well-represented breaks down and MLE could fall into overfitting. Typically, the objective function is randomly sampled a few times before using BayesOpt to meet the minimum requirement for applying GPR. It is also suggested to use isotropic GPR before having enough points to apply the anisotropic GPR.

2.3. Acquisition Function. After finding the posterior distribution of the objective function, BayesOpt uses an acquisition function to evaluate how desirable it is to sample at this position. Two types of most commonly used acquisition functions are the probability of improvement (PI) [24] and the expected improvement (EI) [25]. PI calculates the probability of finding a value better than the current optimum based on the posterior distribution found by GPR. EI mod-

ifies PI by taking into account the scale of the potential improvement but could favour explorative sampling as it does not account for the risk. According to the experiment carried out by Wu et al. [26], EI overall outperforms PI in finding global optimum; hence, it is the acquisition function chosen for this paper. The EI is defined as follows [25]:

$$EI = \int_{y_*}^{\infty} [y - y_*] \bullet f(y) dy, \qquad (9)$$

where y_* denotes the current optimal value and $f(y)$ is the probability density of the posterior distribution given by the surrogate regression model. One may combine this with (5) to evaluate EI in closed form as described in Clark [27]:

$$EI(x) = \sigma_*(x)[\varphi(z) + z \bullet \phi(z)], \qquad (10)$$

where $z = (\mu_*(x) - y_*)/(\sigma_*(x))$ (or $(y_* - \mu_*(x))/(\sigma_*(x))$ if to minimize). The point to sample next is the one that maximizes the acquisition function. After sampling, the GPR and the acquisition function are updated by taking into the new data point. This process is repeated for a certain number of iterations, and the final optimum is the best point among the sampled dataset.

2.4. Mixture of Gaussian Processes. GPR uses a certain configuration of kernel parameters typically optimized via MLE, assuming a global behaviour of the function in each dimension. In most cases, this is inadequate to model the entire objective function, as the function typically has different behaviours in different regions. For example, the objective function could have one local peak that changes quickly on x-axis but slowly on y-axis and another one elsewhere that behaves in reverse, or the objective function could be a single hump surrounded by a vast flat region. The main motivation for replacing GPR by the mixture of Gaussian process (MGP) model is to address these scenarios by permitting input-dependent participation of kernel parameters. The MGP model is a variation of mixture of expert (ME) model and a generalization of GPR. It consists of a set of GPs with different kernel parameters as the experts and a gating network to determine which expert to use for a given input [15]. The gating network and the mixture components are iteratively trained using the expectation maximization (EM) algorithm to maximize the likelihood of the observed data. Compared with the original method introduced in Tresp [14], the MGP model introduced in this paper is slightly modified for better performance.

2.5. Finding the Local Experts. The method for finding the experts is not specified in Tresp [14]. To account for the fact that the function's behaviour is regional, it is desirable to find the local experts that are optimized for certain regions. Here, the modified maximum likelihood estimation approach is introduced to find the experts. For each region $\mathscr{D}$ to optimize, the whole dataset is divided into two groups, the points that are within the region $\{x_i, y_i\}_{i \in \mathscr{D}}$ and the ones that are not $\{x_i, y_i\}_{i \notin \mathscr{D}}$. The kernel parameters for the local GPR are the set that maximizes the probability of finding

the data points within this region conditioned on the rest data points, namely,

$$l_{1:d} = \underset{l_{1:d}>0}{\operatorname{argmax}} \left[p\left(\{x_i, y_i\}_{i \in \mathcal{D}} | l_{1:d}, \{x_i, y_i\}_{i \notin \mathcal{D}} \right) \right], \qquad (11)$$

which is to maximize the likelihood of the regional observations under the posterior. This is a reasonable method as the experts in the MGP model make regressions based on the whole dataset, and the GPR optimized from (11) corresponds to the expert that most accurately predicts the local data. When the region covers the entire dataset, (11) degenerates to (8) and the method becomes MLE.

The regions to generate the local experts are not necessarily mutually exclusive as the gating network will assign the tasks automatically. However, they are expected to be exhaustive since otherwise the regressions in the uncovered area could result badly. A simple approach to fulfill this requirement is to use the GPR optimized via MLE (such GPR will be referred to as global GPR for the rest of this paper) along with the ones optimized for certain regions. Finally, to avoid overfitting, one has to make sure the regions to optimize are well-shaped and contain enough points.

2.6. Iterative Learning Using EM. After finding the GP experts, the model is trained via an iterative learning using the EM algorithm. The EM consists of two steps, the E step for estimation and the M step for maximization. In the E step, based on the current form of the GPs, the latent variables for each data point are estimated using Bayes' theorem:

$$p(z = i | x_k, y_k) = \frac{p(z = i | x_k) \cdot G\left(y_k ; \mu_i(x_k), \sigma_i^2(x_k) \right)}{\sum_{j=1}^{M} p(z = j | x_k) \cdot G\left(y_k ; \mu_j(x_k), \sigma_j^2(x_k) \right)}, \qquad (12)$$

where the discrete variable z denotes the membership of the GPs and notation $G(a ; b, c^2)$ stands for the probability density of a Gaussian distribution with mean b and variance c^2 evaluated at a. A difference from the method in Tresp [14] is that the original paper used another set of GPs to model the variances of the posterior distributions, while (12) uses the variances calculated from (5). The original method has some merit, but (12) is computationally cheaper and theoretically more legitimate. Unlike the EM for the Gaussian mixture model, the prior probability of the latent variable is estimated by the gating network instead of the mixture weights. The term $p(z = i | x_k)$ is the estimated probability of the regression task being assigned to the ith expert evaluated by the gating network at x_k. In the M step, the gating network and the GPs are updated based on the results calculated in the E step to maximize the likelihood. While the procedure to update the gating network will be introduced later, the update of the GPs is done by amplifying the noise variances on the diagonal of the covariance matrix according to the latent variables.

$$\Sigma = K(x_{1:N}, x_{1:N}) + \Psi^i, \qquad (13)$$

where Ψ^i is a diagonal matrix with entries [14]:

$$\Psi_{kk}^i = \frac{\sigma_i^2(x_k)}{p(z = i | x_k, y_k)}. \qquad (14)$$

The M step and the E step are conducted alternately until convergence.

However, there are some problems found during the implementation of the EM. The first one is mentioned in Tresp [14] that calculating the probability density on known data points could lead to serious overtraining. This problem is solved by using all the training data except (x_k, y_k) when calculating (12). However, this leads to the second problem of numerical instability as the predicted value could be tens of standard deviations away from the true value for some GPRs and the probability densities become indistinguishable from zero for the computer. This problem can be solved by using approximations such as the Taylor expansion to provide accurate results for good regressions while keeping it computable for bad regressions. Another problem is that the EM does not guarantee to converge. This is understandable as EM is a maximum likelihood estimation for the mixture model in nature, and it could be oscillating between two points having similar likelihood [28]. To address this problem, one could calculate the logarithm of the posterior density for each EM iteration:

$$\sum_{i=1}^{N} \log \left(\sum_{j=1}^{M} p(z = j | x_i) \cdot G\left(y_i ; \mu_j(x_i), \sigma_j^2(x_i) \right) \right). \qquad (15)$$

If the EM still does not converge after a certain number of iterations, simply choose the iteration step that corresponds to the highest posterior density.

3. Methodology

3.1. Learning the Alternative Gating Network. The gating function in ME model evaluates the expert-membership of a new input by means of regression. In the original paper, this is done using Gaussian process classification [29] (GPC) with a softmax function. This method is found to be not ideal enough. One reason is that GPC requires to label the expert-memberships for each data point, while some points have rather equivalent probabilities for several GPRs, making it inappropriate to label them with any model. Another problem originates from the fact that some data points, inside a region covered by a local GPR through, could fit very well to another GPR optimized for some other region. As a result, the situation that one data point that seemingly belongs to a GPR being surrounded by many data points that favour another GPR is likely a sign of this type of problem. Hence, it may be desirable to take into account the status of the surrounding data. The successful implementation of the original method was on functions that are rather steep, such as the step function in Tresp [14] and the spike-shaped function in Stachniss et al. [30], where the sudden change of label makes sense. However, for most functions, the original method could lead to wrong classification and

Input: Sampled data, the regions to optimize, the term ϕ in the smoother.
1 Sample from the posterior of α using (21) and ARS.
2 Find the global GPR and the local experts using (11).
3 Initialize the gating network (equal probability for all experts is fine).
4 repeat
5   Calculate the probability densities for the data points under each GP.
6   Estimate the latent variables using (12).
7   Update the GPs using (13).
8   Update the gating network using (18).
9   /* The gating network is averaged over the sampled posterior of $\alpha*$/
10   Δ = the root-mean-square deviation of the updated gating network.
11 until Δ < tolerance;
Output: the trained GPs with the gating network.

ALGORITHM 1: Training the MGP model.

(a)

(b)

— Global GPR
— · Local GPR one
- - - Local GPR two

(c)

— Actual curve
— · GPR
- - - MGP

(d)
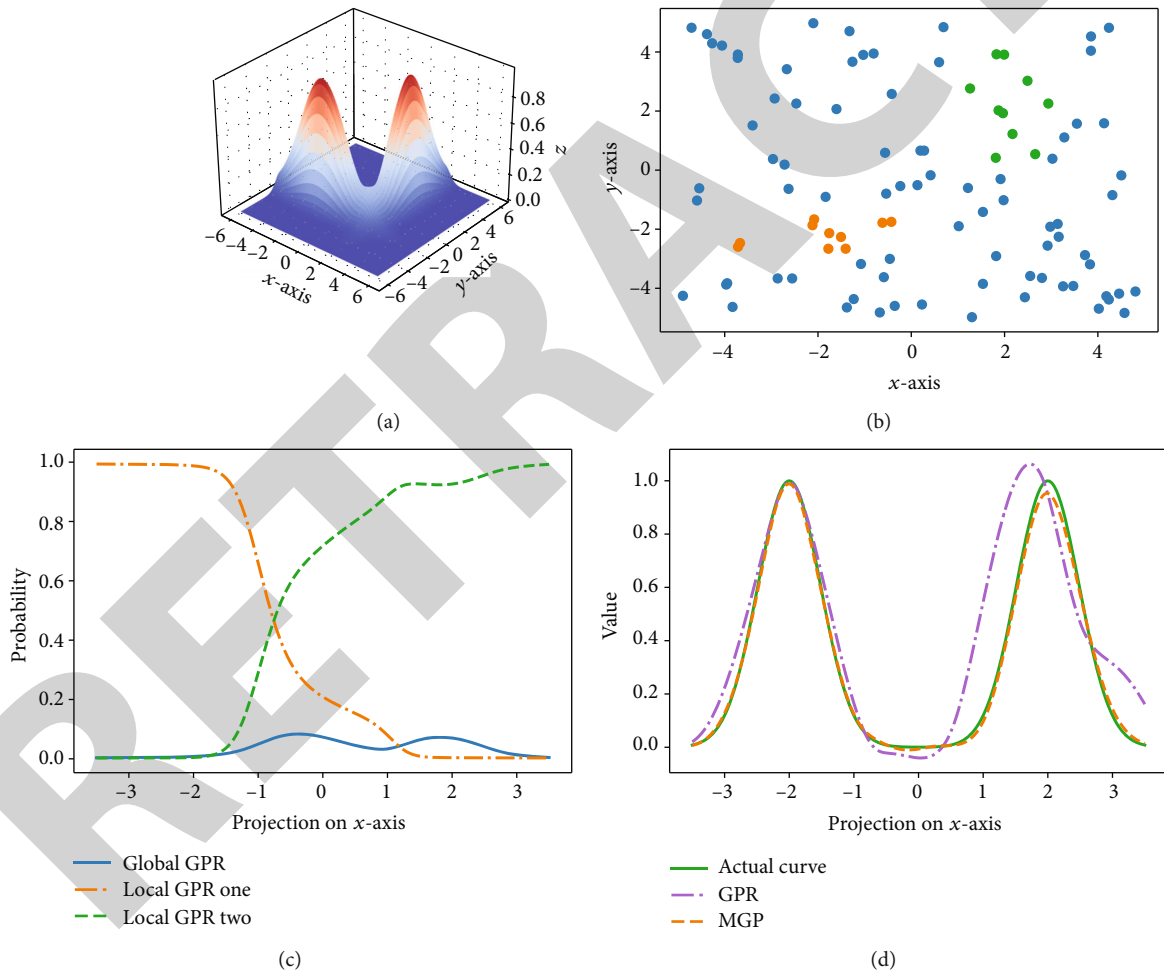
FIGURE 2: (a) The 3D plot of the toy function. The MGP consists of the global GPR and two local experts. (b) The positions of the data points to generate each local expert. (c) The regression results made along the line connecting the two local peaks. (d) The model assignment given by the gating network.

hence is not very ideal. Also, a M-class GPC uses M GPRs to make regressions and is computationally rather expensive.

To address these problems, an alternative gating network modified from Rasmussen and Ghahramani [16] is used. For each data point, the assignment probabilities are assumed to follow a symmetric Dirichlet distribution in the prior:

$$p(\pi_1, \cdots, \pi_M | \alpha) \sim \frac{\Gamma(\alpha)}{\Gamma(\alpha/M)^M} \prod_{j=1}^{M} \pi_j^{\alpha/M-1}, \qquad (16)$$

Input: pre-sampled data, the objective function, the term ϕ in the smoother, the number of iterations N, minimum size of the clusters.
1 for iteration =1 to N: do
2   Standardize the data in the input space.
3   Filter out the data with values below the average.
4   Perform a density-based clustering for the rest data points.
5   Apply k-nearest neighbour classification on unselect data points.
6   Reject the clusters smaller than the minimum size.
7   Use Algorithm 1 to train the MGP.
8   /∗ The regions to optimize are the clusters found ∗/
9   Sample at the position that maximizes the acquisition function (22).
10   Add the sampled point to the data.
11 end for
Output: the value and the coordinates of the best sampled point.

ALGORITHM 2: MGP-based Bayesian optimization.

TABLE 1: The settings for each tested model.

Model	Tuning dimension	Total presampling	Dataset
XGBoost	3	20	Housing [34]
Elastic net	2	10	Diabetes [35]
SVM	2	10	Wine type [36]
MLP	4	30	Artificial

where the α/M is the concentration parameter and the probabilities π_j must be positive and sum to one. The prior probability to find the data points in a certain configuration of assignment can be calculated using the standard Dirichlet integral [31].

$$p(c_1, \cdots, c_N | \alpha) = \frac{\Gamma(\alpha)}{\Gamma(\alpha + N)} \prod_{j=1}^{M} \frac{\Gamma(\alpha/M + N_j)}{\Gamma(\alpha/M)}, \quad (17)$$

where c_i is the expert assignment, also called indicator variable, for the ith data. The term N_j is the occupation number for the jth expert, which is the number of data points assigned to this expert. Using (17), one can calculate the posterior probability distribution for a single indicator variable given the rest.

$$p(c_i = j | c_{-i}, \alpha) = \frac{N_{-i,j} + \alpha/M}{N - 1 + \alpha}, \quad (18)$$

where the subscript $-i$ denotes all indexes except for i. Note that the posterior does not take in any positional information; hence, a local estimation for the occupation number is used to construct the gating network. This is done by using a kernel smoother as in Rasmussen and Ghahramani

[16] to give a higher weight to the neighbouring points.

$$N_{-i,j} = (N-1) \frac{\sum_{i' \neq i} p(c_i = j | x_i, y_i) \cdot K_\phi(x_i, x_{i'})}{\sum_{i' \neq i} K_\phi(x_i, x_{i'})}, \quad (19)$$

$$K_\phi(x_i, x_{i'}) = e^{-1/2 \sum_d (x_{i,d} - x_{i',d})^2 / \phi_d^2}. \quad (20)$$

A modification from Foster et al. [31] is that (19) uses the posterior distribution calculated from (12). This is to integrate the update of the gating network into the EM learning algorithm. This method successfully solves the problems found in the original gating network as it takes in the probabilities of the indicator variable as well as the surrounding data. The length scales ϕ in the kernel smoother characterizes the smoothness of the gating network. Optimizing the ϕ can be difficult as this could fall into overfitting. It is advised to preset an isotropic ϕ and to use the smoother on the data normalized in each dimension.

The α in the concentration parameter controls the prior distribution and hence influences the gating network. To account for the variation of α, one can use a Bayesian approach to find the posterior of α the and sample from this distribution. As the method introduced in Rasmussen [32], the prior of α is assumed to be an inverse gamma and its posterior takes in the following form:

$$P(\alpha | N, M) \propto \alpha^{M-3/2} e^{-1/2\alpha} B(\alpha, N), \quad (21)$$

where $B(\alpha, N)$ denotes the beta function. The sampling of the posterior can be made using the adaptive rejection sampling (ARS) method [33]. Allowing the α to vary makes the gating network more robust. However, the function (21) is not strictly log-concave at the tail end where the probability density is almost zero. One may need to make some approximations to deal with this.

3.2. Complete Algorithm of MGP. To sum up, one can successfully implement the MGP following the steps presented in Algorithm 1.

For any input to evaluate, use (18) to calculate the assignment probabilities and then use (5) to make regressions for each GPR, respectively.

In practice, one may conduct EM until convergence without (13), which is to keep the GPs fixed, before applying the EM with (13). This is because recalculating the probability densities after updating the GPs is the most time-consuming step. Hence, a better gating network to begin with can significantly speed up the training. But above all, one needs to make sure there are enough data points to perform the MGP; otherwise, this can lead to overfitting.

3.3. Clustering-Assisted Method for BayesOpt.
A major drawback of the MGP introduced above is that the local expert can only be designated if the regions to optimize are known. If the behaviour of the function is vaguely known in advance or if there are many sampled data points, one can select the regions manually. But for a general optimization task, this can be hard to do as little is known for the objective function and number of samplings is limited.

By studying general BayesOpt optimizations, one can find that the local experts that the optimizer is mostly interested in are the ones for the local peaks where the sampling density is high. Utilizing this feature, local experts to construct MGP for BayesOpt can be determined using a clustering-assisted approach. One firstly filters out the data with values below the average (or above the average if to minimize) and then applies density-based clustering to the rest points. The clustering step is advised to be conducted on data normalized in each input dimension. Each cluster found corresponds to a group of samplings around a local peak and the local experts can be found using (11). As the later samplings tend to lie around the higher peaks, the average of sampled values increases after each iteration. Thus, the lower peaks are of lesser value and will gradually be filtered out (once the cluster size is too small), leaving only the highest peak standing.

If there is no cluster found, meaning that the BayesOpt has not found any peak or there are not enough points near a peak to fit a local expert, the MGP uses only the global GPR which does not pose any adverse consequences either. The worst case that the clustering approach could lead to is finding a cluster in the filtered data points which turns out to be high value points mixed up with low value ones in the whole dataset. In this case, the GPR calculated via (11) does not reflect any regional behaviour of the function but is simply overlearning this subset of data. This is a rare scenario but is still worthy of attention. A solution addressing this issue is to make a k-nearest neighbour classification of the unselected data for each cluster. This grows each cluster by the data that are potentially filtered out.

3.4. Complete Algorithm of MGP-Based BayesOpt.
The BayesOpt using MGP model combines several GPRs to make regression following the probabilities of participation given by the gating network. Hence, the acquisition function EI for MGP-based BayesOpt becomes the linear combination of the EI given by each GPR:

$$EI(x) = \sum_{j=1}^{M} EI_j(x) \cdot p(z = j|x). \qquad (22)$$

This is equivalent to the marginalized acquisition function and (22) is not limited to EI. If there is no extra local expert found in the clustering step, (22) degenerates to the EI for a single global GPR. The algorithm for MGP-based BayesOpt is summarized and illustrated below.

4. Experiment

4.1. MGP Regression Test.
The first experiment is to test the regression performance of MGP compared with global GPR on a 2D toy function. The toy function consists of two bell-shaped local peaks, where one peak is sensitive on x-axis and the other one is on y-axis. The function is randomly sampled 100 times and the local experts are found by manually selecting the regions of each peak and then applying (11). Although the evaluation of the toy function is accurate, a small noise is assumed for the measurements to perform the update of the GPs. The kernel type used for the MGP is the Matérn kernel with $v = 1.5$, hence at least once differentiable. The regression result of MGP is taken to be the expected value of the posterior [14]:

$$E(y|x) = \sum_{j=1}^{M} p(z = j|x) \cdot \mu_j(x). \qquad (23)$$

It can be seen from Figure 2 that the MGP model trained using Algorithm 1 greatly outperforms the global GPR as the regression curve almost overlaps with the actual curve. Thanks to the gating function that assigns each model to the region where they excel, each peak is assigned to the corresponding local expert, leading to the outstanding regression performance. This recreates the results in Tresp [14] and indicates the success of the method for find local experts and the alternative gating network.

4.2. Test on Hyperparameter Tuning.
The hyperparameter tuning problem in machine learning algorithms is a prime example of optimizing expensive black-box derivative-free functions. The hyperparameters of the machine learning models are specified prior to training and greatly affect the model performance. The training process can be very computationally expensive, and the performance of the trained model is usually noisy as randomness is typically involved during model training and testing.

Based on the successful implementation of the MGP model, Algorithm 2 for applying MGP in BayesOpt is tested on the hyperparameter tuning of four common machine learning algorithms. These algorithms are chosen for being highly tunable with large cross-validated average improvement after optimization [11]. The XGBoost is a boosting tree model, and its regularization is mainly controlled by the shrinkage factor and two penalty terms. The elastic net is a linear model that uses L_1 and L_2 penalties to reduce

(a)

(b)

(c)

(d)
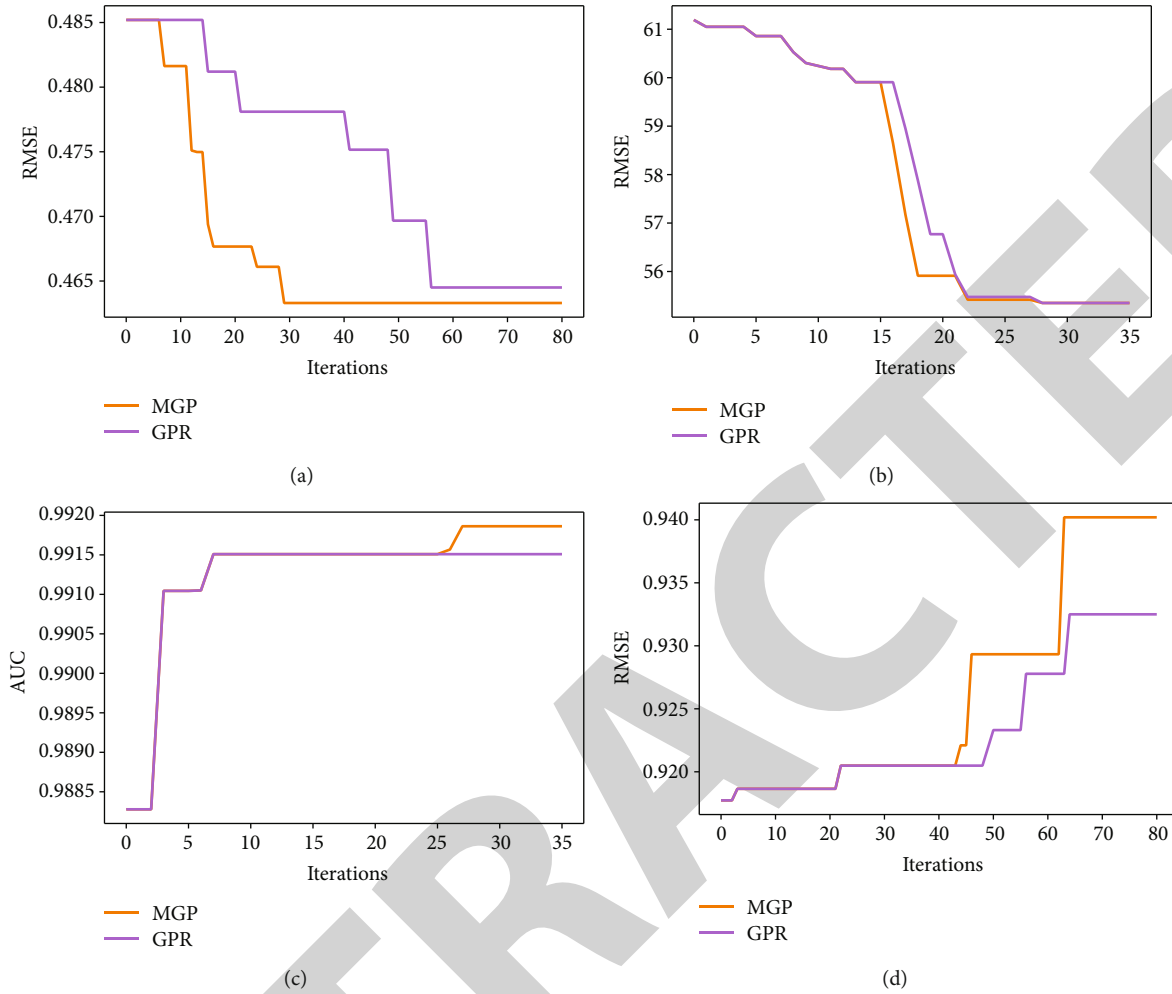
Figure 3: The comparison of tuning efficiency between BayesOpt based on global GPR and that on MGP. The test is conducted on four most common machine learning models. (a) XGBoost, (b) elastic net, (c) SVM, and (d) MLP (with two hidden layers). The model performance is measured by root-mean-square error (RMSE) for regression and area under the ROC curve (AUC) for classification.
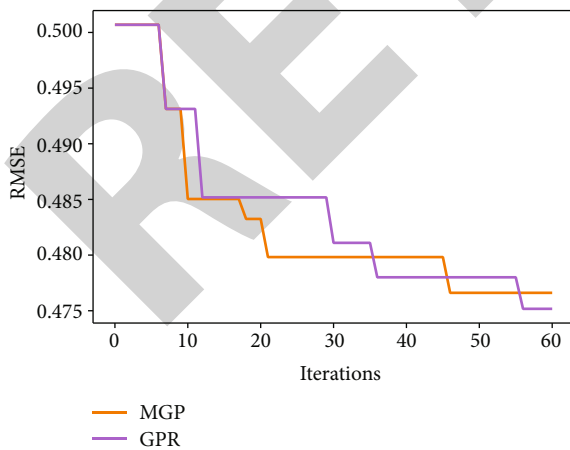
Figure 4: In the test conducted on tuning XGBoost, it is found that MGP-based BayesOpt without any presampling may not always outperform GPR. Compared with Figure 3, MGP with only 5 random samplings is still in the 0.477 local optimum after 50 iterations, while that with additional 15 presampling using GPR has reached the global optimum of 0.463 after 35 iterations.

overfitting. The support vector machine (SVM) is a classifier using kernel trick, where its performance is determined by the regularization parameter and the kernel coefficient. The multilayer perceptron (MLP) is an artificial neural network, where the regularization term, the learning rate, and the hidden-layer sizes together contribute to its performance. The experiment is to test the efficiencies of the MGP-based BayesOpt in optimizing practical back-box derivative-free functions compared with the BayesOpt using GPR. The four algorithms above are trained on different datasets, and the configurations of their hyperparameters are optimized by the two types of Bayesian optimizers, respectively. The values of the current optima found by each optimizer are recorded in each iteration to compare the efficiency of optimization. Considering the MGP needs enough data to find the local experts, both optimizers start from a presampled dataset consisting of 5 random samplings followed by a few iterations of BayesOpt using GPR. The information for each tested model is given in Table 1.

The comparison of tuning efficiency is presented in Figure 3. It can be seen that MGP model outperforms GPR in BayesOpt thanks to the more accurate modelling of the

objective function. It is most significant in the test on XGBoost and MLP where the tuning dimension is relatively higher. This is reasonable as the higher dimension gives more space for tuning, while the other model converges too quickly to their optima even without the use of MGP. Such result marks the success of the clustering assisted method for finding the experts of the peaks. Interestingly, it is observed in the test on XGBoost and MLP that the number of GPs used in each optimizing iteration experienced an increase followed by a decrease. This corresponds to the design that lower peaks will be filtered out for lesser evaluation value.

The presampling before applying MGP is important. It is observed that if the MGP-based BayesOpt is applied without a certain number of presamplings, its performance is not guaranteed to outperform the BayesOpt using GPR (see Figure 4). By examining the optimization processes, it is found that in situations where MGP fails to outperform the GPR, MGP stays in a local optimum (typically the first peak it finds) for longer iterations before moving to the global optimum, which is likely a cause of overfitting to the existing data. The use of MGP is based on the assumption that the behaviour of the objective function is well-represented by the sampled data. This assumption clearly breaks down when MGP is applied to optimize an objective function that is poorly explored. BayesOpt is a trade-off of exploitation and exploration, and MGP favours the former by increasing the complexity of the surrogate model, leading to a higher risk of overfitting and falling into local optima. MGP-based BayesOpt is definitely a good supplement to the GPR-based BayesOpt and may provide more accurate estimations in most cases. But the higher risk of overfitting implies it cannot be a complete replacement for GPR-based BayesOpt, especially when the input space is poorly sampled.

In practical optimization problems, it is advised to take enough samples using GPR before applying MGP to lower the risk of overfitting. One may also combine MGP and GPR together by switching back to GPR as the surrogate model every a few iterations of using MGP-based BayesOpt. This periodically decrease of model complexity makes a more robust optimization approach, having more accurate modelling while reducing the risk of overfitting. In our test where GPR is used every third iteration in the MGP-based BayesOpt, the phenomenon of being trapped in local optima is no longer observed and the combined method always outperforms the GPR-based BayesOpt.

5. Conclusion

This paper explained the motivations for replacing GPR by MGP in BayesOpt and provided a detailed introduction for implementing it. The method for finding the local experts, the alternative gating network, and the clustering-assisted method are proven to be successful by results in the experiment section. The MGP is a powerful candidate for achieving better regression performance than GPR. The BayesOpt based on it significantly outperforms the one using GPR especially for objective functions with larger input dimension. The only drawback of potential overfitting when optimizing with relatively few data can be addressed by more presampling or periodically switching back to GPR, making it an excellent supplement to the GPR-based BayesOpt. Despite the fact that MGP is computationally more expensive than a single GPR, it is still much faster to train than most machine learning algorithms and may significantly boost the efficiency of BayesOpt. Also, many steps in the EM can be trained in parallel, including the evaluation of the probability density for each data point. A fully optimized algorithm of MGP can undoubtedly speed up its implementation, providing a higher application value.

The methods are all explained with details, and the results are clearly illustrated and analysed to be satisfying. Hopefully, future works may be developed on improving the MGP or on finding more applications for it.

Data Availability

All data, models, and code generated or used during the study appear in the submitted article.

Conflicts of Interest

The authors declare that they have no conflicts of interest.

Authors' Contributions

R.M. contributed the central idea and the major part of the software, carried out part of the experiment and analysis, revised the manuscript, and finalized this paper; C.C. provided the data, contributed part of the software, and completed the rest part of the experiment and analysis. The remaining authors equally contributed to refining the idea and designing the experiment. All authors discussed the results and wrote the initial draft of this paper.

References

[1] A. J. Booker, J. E. Dennis Jr., P. D. Frank, D. B. Serafini, V. Torczon, and M. W. Trosset, "A rigorous framework for optimization of expensive functions by surrogates," *Structural Optimization*, vol. 17, no. 1, pp. 1–13, 1999.

[2] P. I. Frazier, "A tutorial on Bayesian optimization," 2018, http://arxiv.org/abs/1807.02811.

[3] R. G. Regis and C. A. Shoemaker, "Parallel radial basis function methods for the global optimization of expensive functions," *European Journal of Operational Research*, vol. 182, no. 2, pp. 514–535, 2007.

[4] D. R. Jones, M. Schonlau, and W. J. Welch, "Efficient global optimization of expensive black-box functions," *Journal of Global Optimization*, vol. 13, no. 4, pp. 455–492, 1998.

[5] J. Mockus, *Bayesian Approach to Global Optimization: Theory and Applications*, vol. 37, Springer Science & Business Media, 2012.

[6] D. J. Lizotte, T. Wang, M. H. Bowling, and D. Schuurmans, "Automatic gait optimization with Gaussian process regression," *International Joint Conference on Artificial Intelligence*, vol. 7, 2007.

Retraction

Retracted: Research on Tax Collection and Administration Application and Legal Issues Based on Big Data Analysis

Journal of Sensors

This article has been retracted by Hindawi following an investigation undertaken by the publisher [1]. This investigation has uncovered evidence of one or more of the following indicators of systematic manipulation of the publication process:

(1) Discrepancies in scope

(2) Discrepancies in the description of the research reported

(3) Discrepancies between the availability of data and the research described

(4) Inappropriate citations

(5) Incoherent, meaningless and/or irrelevant content included in the article

(6) Manipulated or compromised peer review

The presence of these indicators undermines our confidence in the integrity of the article's content and we cannot, therefore, vouch for its reliability. Please note that this notice is intended solely to alert readers that the content of this article is unreliable. We have not investigated whether authors were aware of or involved in the systematic manipulation of the publication process.

In addition, our investigation has also shown that one or more of the following human-subject reporting requirements has not been met in this article: ethical approval by an Institutional Review Board (IRB) committee or equivalent, patient/participant consent to participate, and/or agreement to publish patient/participant details (where relevant).

Wiley and Hindawi regrets that the usual quality checks did not identify these issues before publication and have since put additional measures in place to safeguard research integrity.

We wish to credit our own Research Integrity and Research Publishing teams and anonymous and named external researchers and research integrity experts for contributing to this investigation.

The corresponding author, as the representative of all authors, has been given the opportunity to register their agreement or disagreement to this retraction. We have kept a record of any response received.

References

[1] C. Liuhong, "Research on Tax Collection and Administration Application and Legal Issues Based on Big Data Analysis," *Journal of Sensors*, vol. 2022, Article ID 6578964, 11 pages, 2022.

Research Article

Research on Tax Collection and Administration Application and Legal Issues Based on Big Data Analysis

Chen Liuhong [ID]

Guangzhou Huashang Vocational College, Guangzhou 511300, China

Correspondence should be addressed to Chen Liuhong; clh727926@gzhsvc.edu.cn

In the twenty-first century, in the era of rapid development of big data, people can make some basic problem analysis of the application of tax collection and administration and legal problems through big data. Between taxpayers and the tax collection and management system, the law is used to protect the legitimate rights and interests of taxpayers. Through the improvement and management of the supervision system, it can ensure that taxpayers can clearly know how much tax they should pay when paying taxes. At present, the urgent problem is to adjust the concept of tax, reconstruct the scope of tax, scientifically design the tax rate, and simplify the tax collection and administration procedures. This paper puts forward a more efficient tax process by comparing the tax data, the econometric study of tax, and the secret tax avoidance while the burden of the more poor rural tax class. Through the experiment proved, this paper studies the best tax collection and management mode, so that taxpayers can pay taxes more convenient and fast. The tax collection and administration system have been improved to make taxpayers' information more comprehensive, which is very important for us to improve the efficiency in the twenty-first century, which is also a great breakthrough in the application of tax collection and administration. Due to the limitations of incomplete information, or that the information cannot keep up with the times, the tax collection and management system cannot completely correspond to the complete information of the correct taxpayers. Therefore, for the study of the taxation supervision system, it is necessary to use more algorithms in a more comprehensive way, so as to reduce the number of tax evaders and the number of active taxpayers.

1. Introduction

With the emergence of emerging services such as cloud computing, the Internet of Things, and social networks, the types and quantities of human social data have grown at an alarming rate, and the era of big data has arrived. Data has gone from being a simple transactional object to a fundamental resource. How people better manage and use big data has received a lot of attention [1]. The evolution or revolution of big data database research is a problem. Big data brings new opportunities to modern society and challenges for data scientists. The massive sample size and high dimensionality of big data pose unique computational and statistical challenges, including scalability and storage bottlenecks, noise accumulation, spurious correlations, chance endogeneity, and measurement error. These challenges are prominent and require new computational and statistical paradigms

[2]. In this paper, I use a dynamic general equilibrium framework to assess the quantitative impact of incomplete tax enforcement on aggregate output and productivity. Then, I investigated the effects of improved enforcement. I found that with perfect enforcement, labor productivity and output are 19% higher under perfect competition and 34% higher under monopolistic competition. The source of this benefit is the elimination of distortions caused by incomplete tax enforcement [3]. This article draws inferences about a range of factors that may lead to stubborn taxation by comparing tax data and conducting an extensive econometric study of the main determinants of taxation. We found that the gap between potential and actual targets can be as high as 6% of GDP [4]. In any economic system, the collection of taxes obviously requires the use of resources. How to use reasonable resources is very important. This paper optimizes the method of resource allocation

and proposes a new resource allocation scheme [5]. In this paper, we examine the impact of improving tax administration efficiency on the welfare of the taxpaying public and make plans to optimize the central and even local tax policies [6]. Using any other standard collection scheme used by the government, we identify an optimal tax collection policy that outperforms the taxes paid by calibrated agents. I have found that the design of an optimal audit program depends on three components: income distribution, identification of behavioral patterns, and the number of times an individual is audited [7]. This paper puts forward corresponding countermeasures on the basis of systematically analyzing the current situation and existing problems of tax collection and management in the field of e-commerce in my country. We found that there are problems in my country's e-commerce tax collection and management, such as imperfect legal system, difficulty in tax base measurement, and uncertainty of tax objects [8]. The impact of increased income pressure is derived by a comparative approach. As income pressures increase, the "political value" of jobs granted decreases, and thus the efficiency of paying taxes [9]. Strengthen the training of tax personnel, strengthen the review of taxpayer transactions of affiliated enterprises, strictly monitor the taxpayer's property loss declaration, improve tax reporting, and improve the quality and ability of tax auditing [10]. By comparing the "information flow" and "capital flow" of the two taxation and management models, this paper concludes that my country should transform the taxation model into an e-commerce taxation and management model under the control of "information flow." Capital flow has its rationality and security technology guarantee [11]. An e-tax system is a computerized tax administration system designed to handle general tax administration from registration, assessment, filing, and processing of claims and tax refunds. Therefore, this paper aims to investigate the impact of the electronic tax system on the efficiency of tax collection by the Internal Revenue Service of the Tax Bureau [12]. Regulating the tax collection and management of developing industries is of great significance for improving the tax collection and management system and promoting the establishment of a fair and orderly market competition pattern [13]. In the context of urban-rural integration, reforming the concept of tax collection; reorganizing tax collection areas; designing scientific tax rates; and simplifying tax collection and management procedures are of great significance and have a regulating effect on the unified market of urban and rural construction land in my country [14]. This paper studies the optimization of the tax payment process in terms of taxation, aiming to minimize the taxpayer's tax payment cumbersome process [15].

2. Analysis of Tax Collection and Management and Legal Issues

2.1. Basic Information of Tax Collection and Administration.
Under the impact of the interaction and change of modern information technology, big data has entered more and more into the field of tax collection and administration, and digital tax management and data management have gradually become the development trend of tax collection and administration. Big data and information technology are indispensable forces to improve the ability of tax collection and administration. With the development of big data, there have been many virtual electronic payment and tax forms on the network, and the process is shown in Figures 1 and 2.

The implementation of a fair tax system may lead to the imbalance of different tax burden levels. In the era of big data, when the tax system is more traditional, there will be some tax evasion or even tax avoidance by individual enterprises and individuals. At this time, the protection of the law is needed to carry out normal taxation.

2.2. The Existing Legal Issues in Tax Collection and Administration.
There are many legal problems in China's tax revenue. In recent years, many stars have reported their tax problems, which also reflect the poor supervision of taxpayers in China, the difficulties in the identification of taxable objects under the background of digital economy, and the prominent tax jurisdiction problems and other problems. In the tax law, the meaning and scope of taxpayers are different, which should be made clear in the relevant laws and regulations, and will help to determine the scope of taxation. All citizens in our country must pay taxes according to law. This is the relevant provisions of the Constitution and can be regarded as a constitutional basis, but such provisions are very general and have no more detailed content. The digital economy era has brought more development opportunities, but it also highlights the shortcomings and defects of the current tax law system. Relevant legal systems, whether tax registration or tax management, need to be revised and improved to adapt to the growing market transaction pattern. In fact, under the influence of the rapid development of Internet technology, improving the legal system has become a very urgent and important task.

2.3. Tax Collection and Management System in the Era of Big Data.
The "big data + tax" model has become the main theme of tax research in the Internet era. A relatively perfect set of tax collection and administration and tax service system can better realize the modernization of tax management, improve the efficiency of tax management, and quickly adapt to the development trend of informatics. In the era of big data, we can establish a unified taxpayer identification number and input it into the tax collection and management system according to a special taxpayer identification number, so as to facilitate the subsequent query when needed. As far as possible, the tax supervision system allows all taxpayers' personal information to be input into the system, so that the system becomes more flexible and can timely tell taxpayers, the amount of tax to be paid, and tax time. In the interface of the tax collection and management system, the tax payment information is introduced in detail to analyze and process the information involved in the tax payment, which will more easily facilitate the operation of the subsequent taxpayers. In the era of big data, the relevant information of tax needles is abstracted as a traditional transmission and use process to ensure that their information can be
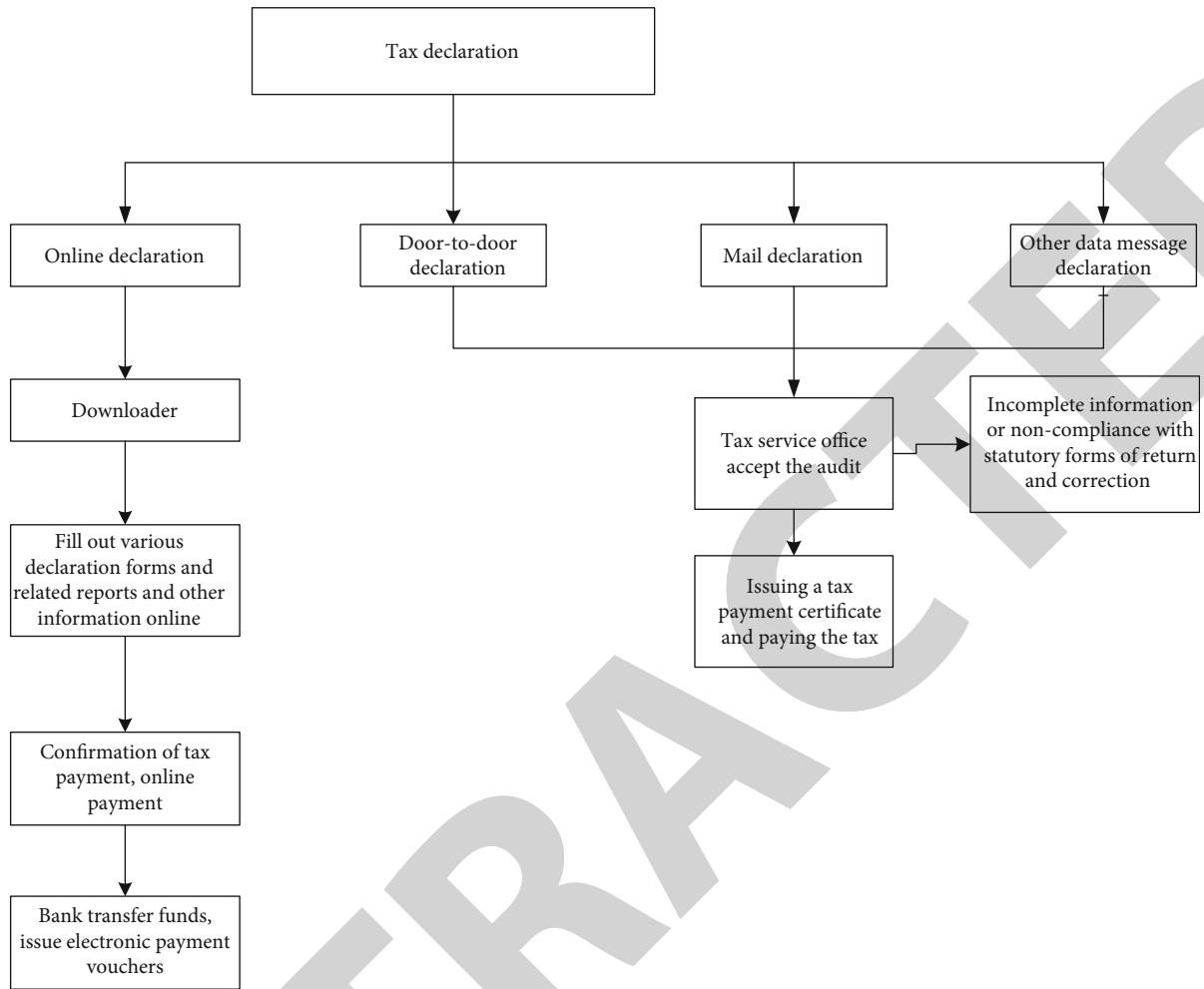
Figure 1: Tax payment process.
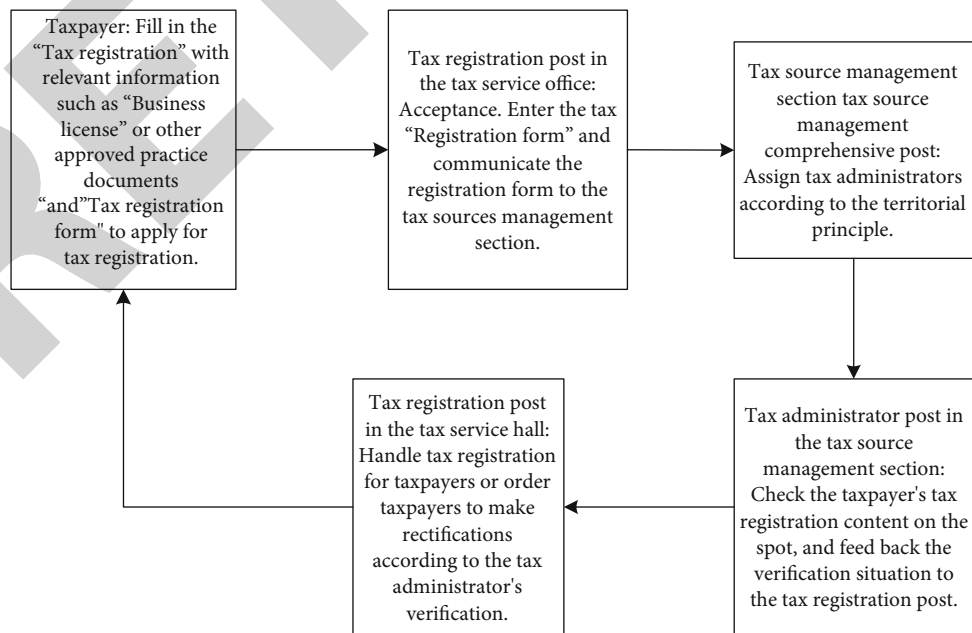
Figure 2: Registration process of tax collection and administration.

conveyed normally and the efficiency of tax collection and management is improved. The tax loss can be reduced through the optimal revenue tax model. The optimal revenue tax model is shown in:

$$\max_{\delta x \longrightarrow 0} \mathrm{E} \int_0^\infty u(\sigma_1 h, y_1(h) - s_1(y_1(h)) - k_1(h), g_t) u(\mathrm{dt}). \quad (1)$$

With some basic information of tax collection and administration and the basic operation methods applicable to taxpayers, the legitimate rights and interests of taxpayers can be protected through law later, and the correct implementation of tax collection and administration can also be guaranteed through law. Under the condition of market equilibrium, the impact of tax policy on economic growth, two main conclusions are drawn: First, when the government implements a stable tax policy, there is a unique optimal capital stock path for consumers, along which the economy can sustained steady and optimal growth; when the tax path given by the government is unstable but can converge to a constant tax rate, there is also a capital stock path that can make the entire economy grow asymptotically and steadily, and eventually converge to the optimal state. Second, the optimal taxation path has the nature of a great road; that is, all optimal taxation paths will converge to the golden rule tax rate (the tax rate that keeps the economy in a stable and optimal growth state), and the government can adjust appropriately according to the golden rule tax rate tax policy, when the value of the tax plan formulated by the government in a certain period is much lower (or much higher) than the tax rate of the golden rule; an appropriate increase (or decrease) of tax at this time is beneficial to economic growth. This article identifies the income tax model most suitable for tax administration for contemporary problems.

2.4. Efficiency of the Tax Collection and Administration System. With the development of information technology, the tax collection and management mode can improve the mode of tax service. However, this cannot fully meet the new needs of new business under the background of big data, especially the deepening of e-commerce market, and the current tax collection and management mode cannot fully meet the needs in management. The advantages and disadvantages will accelerate the speed of tax collection and administration in China, but taxpayers will also show various tax avoidance behaviors through technical means, which makes the work of the tax administration department more difficult. At this stage, information technology can not achieve complex statistical and query operations; taxpayers can not pay taxes directly through the network; tax authorities need to go to the bank to audit data, pay taxes, and deduct taxes; taxpayers can apply for tax payment; and tax authorities themselves do not automatically exchange, which increases the tax process of taxpayers and the workload of tax officials. Tax efficiency can be studied by the variable model. Variable model is shown in

$$\mathrm{DDTBD}_{\mathrm{ijt}} = \partial_0 + \partial_1 \mathrm{TGTP}_{it} + \sum \mathrm{control} + \sum \mathrm{company} + \sum \mathrm{Year} + \varepsilon_{\mathrm{ijt}}. \quad (2)$$

In China, it aims to obtain the maximum tax revenue at the lowest cost, maximize the economic growth, or apply tax rules to reduce the tax barriers to economic growth. It includes two aspects: tax administrative efficiency and tax economic efficiency. By utilizing the following formula:

$$\mathrm{BTD}_{it} = \beta_0 + \beta_1 \mathrm{TACC}_{it} + \theta_i + \varepsilon_{it}. \quad (3)$$

The possibility of subjective tax avoidance can be calculated by using the difference between pre-tax accounting profit and taxable profit to control tax revenue to the maximum extent. The market economy should be made to work efficiently in the most convenient and simple way possible. All the processes have become more streamlined, and some additional costs have been reduced. This is more conducive to the tax between the user and the country, more convenient and easier to operate.

2.5. Legal Principles of Tax Collection and Administration and Network Security Management. As an important part of national e-government, tax informatics has had a profound impact on the reform and renewal of tax management mode, and plays an important role in expanding the field of tax development and implementing tax administration according to law. On March 22, 2004, the state council issued the Communique on Printing and Distributing Comprehensive Incentive Measures for Law-based Administration, requiring local public administrative departments and departments at all levels to establish the party and implement a high level of administrative management. Governing for the people ensures the process of management according to law, reasonable management, reasonable procedures, efficient and convenient, honest and reliable, and consistent powers and responsibilities. It has established the goals and working guidelines for the tax authorities to administer according to law and to provide quality services.

3. Positive Model of Tax Avoidance

3.1. Golden Tax Phase III and Tax Avoidance Construction. Based on realistic theoretical analysis and variable analysis, the model is described as follows

$$\mathrm{DDTBD}_{\mathrm{ijt}} = \partial_0 + \partial_1 \mathrm{TGTP}_{it} + \sum \mathrm{control} + \sum \mathrm{company} + \sum \mathrm{Year} + \varepsilon_{\mathrm{ijt}}, \quad (4)$$

where i represents the i province, j represents the j enterprise, t represents the t year, $\mathrm{DDTBD}_{\mathrm{ijt}}$ represents the degree of enterprise tax evasion, TGTP_{it} represents the virtual variable of the golden tax phase three project (if i province in the t year, the "Golden Tax phase three" project tested on TGTP is designated as 1, if not, set to 0). In this model formula, we mainly focus on the coefficient $\mathrm{DDTBD}_{\mathrm{ijt}}$ and the significance level. If the coefficient is significantly negative, it shows that tax collection and administration inhibit the tax

avoidance activities of enterprises. Tax collection is a compulsory free and relatively fixed distribution of social products by the state in order to meet the public needs of the society. For taxpayers, it is neither repaid directly nor at any cost, which prompts taxpayers to reduce their own taxes. In order to make this wish come true, taxpayers will show different choices. Some people will evade taxes, owe taxes, refuse to pay taxes, avoid taxes and save taxes. Tax avoidance and tax saving are relatively safe or safe methods. Tax evasion is illegal, so everyone will avoid taxes subjectively.

3.2. Tax Avoidance and Nonefficiency Investment Model.
Nonefficiency investment (INEI), excessive investment (OVEREI), and insufficient investment (LESSEI) are taken as the explanatory variables, and the degree of corporate tax avoidance (DDTBD) is taken as the main explanatory variable. Build a mathematical model, as shown in formula M:

$$\text{INEI}_{ijt} = \partial_0 + \text{DDTBD}_{ijt} + \sum \text{control} + \sum \text{company} + \sum \text{Year} + \varepsilon_{ijt}, \tag{5}$$

$$\text{OVEREI}_{ijt} = \partial_0 + D\text{DTBD}_{ijt} + \sum \text{control} + \sum \text{company} + \sum \text{Year} + \varepsilon_{ijt}, \tag{6}$$

$$\text{LESSEI}_{ijt} = \partial_0 + \text{DDTBD}_{ijt} + \sum \text{control} + \sum \text{company} + \sum \text{Year} + \varepsilon_{ijt}, \tag{7}$$

where j represents the j th enterprise and t indicates the year t. Considering the impact of major events at the individual level and year on tax avoidance behavior, this paper controls for the individual effects and time-fixed effects "company" and "year." This paper mainly focuses on the coefficient and significance of the tax avoidance degree DDTBD_{ijt}. If the coefficient is significantly positive, the tax avoidance activity leads to inefficient investment behavior. Tax avoidance can adjust the relationship between nonefficient investments. The promotion of the third phase of the golden tax has improved the taxation authority's collection and management capabilities, strengthened the external control mechanism for enterprises, and indirectly played a role in corporate governance, helping to reduce taxes. Avoid the agency costs brought about by the fund tax avoidance, or the over-investment or under-investment caused by conservative tax avoidance, thereby reducing inefficient investment.

3.3. Difference Model of Tax Avoidance.
This paper therefore adopts the "tax difference" (BTD) to directly reflect the tax burden. It is generally believed that the greater the difference between pre-tax accounting profit and taxable profit, the greater the possibility of subjective tax avoidance. The tax meeting difference (BTD) can be calculated using the following formulas:

$$\text{BTD}_{it} = \beta_0 + \beta_1 \text{TACC}_{it} + \theta_i + \varepsilon_{it}, \tag{8}$$

$$\text{DDBTD}_{it} = \theta_i + \varepsilon_{it}. \tag{9}$$

Through formulas (8) and (9), it is known that the overall accrued income can be used to measure surplus management, and DDBTD is used to measure the true tax avoidance degree of enterprises. The dummy variables and tax avoidance variables of the Golden Tax Phase III Project can be used as dependent variables to construct a regulatory effect model, such as formulas (10), (11), (12):

$$\text{INEI}_{ijt} = \partial_0 + \partial_1 \text{TGTP}_{jt} + \partial_2 \text{DDTBD}_{ijt} + \partial_3 \text{TGTP}_{jt} \\ * \text{DDTBD}_{ijt} + \sum \text{control}_{ijt} + \sum \text{company} + \sum \text{year} + \varepsilon_{ijt}, \tag{10}$$

$$\text{OVEREI}_{ijt} = \partial_0 + \partial_1 \text{TGTP}_{jt} + \partial_2 \text{DDTBD}_{ijt} + \partial_3 \text{TGTP}_{jt} \\ * \text{DDTBD}_{ijt} + \sum \text{control}_{ijt} + \sum \text{company} + \sum \text{year} + \varepsilon_{ijt}, \tag{11}$$

$$\text{LESSEI}_{ijt} = \partial_0 + \partial_1 \text{TGTP}_{jt} + \partial_2 \text{DDTBD}_{ijt} + \partial_3 \text{TGTP}_{jt} \\ * \text{DDTBD}_{ijt} + \sum \text{control}_{ijt} + \sum \text{company} + \sum \text{year} + \varepsilon_{ijt}. \tag{12}$$

3.4. Tax Classification Model.
In order to improve the correct rate of tax, the classification results are used to establish a correct rate model, and the following formula is used to calculate the correct rate.

$$\text{Precision} = \frac{\text{TP} + \text{TN}}{\text{TP} + \text{FP} + \text{FN} + \text{TN}}, \tag{13}$$

$$\text{Accuracy} = \frac{\text{TP}}{\text{TP} + \text{FP}}, \tag{14}$$

$$\text{Recall} = \frac{\text{TP}}{\text{TP} + \text{FN}}, \tag{15}$$

$$F - \text{Measure} = \frac{2 * \text{Precision} * \text{Recall}}{\text{Precision} + \text{Recall}}. \tag{16}$$

3.5. Tax Equilibrium Problem Model.
If the government assumes that it taxes consumer income and invests some of it in consumer goods, consumers will always benefit from the government's public spending. Considering the behavior of these three business representatives, the equilibrium economic problem model is calculated as:

$$k_i(h) = y_i(h) - s_i(y_i(h)) - c_i(h) - k_i(h). \tag{17}$$

Through the optimal revenue tax model,

$$\max_{\delta x \longrightarrow 0} \text{E} \int_0^\infty u(\sigma_1 h, y_1(h) - s_1(y_1(h)) - k_1(h), g_t) u(\text{dt}). \tag{18}$$

We can discuss its more general form with the following formula

$$(y_1(h) - s_1(y_1(h)) - k_1(h), g_t) \in L * M * N * G. \tag{19}$$

This expression is a feasibility constraint.

$$\forall h, h_1 \in H \int_0^\infty u(\sigma_1 h, y_1(h) - s_1(y_1(h)) - k_1(h), g_t) u(\mathrm{dt})$$
$$\geq \int_0^\infty u(\sigma_1 h, y_1(h) - s_1(y_1(h)) - k_1(h), g_t) u(\mathrm{dt}). \tag{20}$$

The formula suggests to maximize the desired utility of a lifetime.

For each variable h, the conditions satisfied are shown in formula (21)

$$E[s_1(y_1(h))] \geq g_i. \tag{21}$$

This is a government budgetary constraint; this means that for a robust tax collection process, the expected tax value for each period will be sufficient to cover the government's spending on supplying goods to the public. When a spatial equilibrium model exists, the equilibrium model can be redefined using the integral form of the probability distribution, as shown in the following formulas:

$$(y_1(h) - s_1(y_1(h)) - k_1(h), g_t) \in L * M * N * G, \tag{22}$$

$$\forall h, h_1 \in H, \Phi(h, y_1(h) - s_1(y_1(h)) - k_1(h), g_t \\ \geq \Phi(h, y_1(h) - s_1(y_1(h)) - k_1(h), g_t, \tag{23}$$

$$\int s(y(h)) d\theta(h) \geq g. \tag{24}$$

For (C, D, g), due to measurable options that meet financial constraints, the best choice problem of the government public sector mechanism can be defined as:

$$\max_{\delta x \longrightarrow 0} \int_\partial \Psi(h, C, D, g) d\partial(h). \tag{25}$$

The model is designed through the economic equilibrium mechanism, and the formula is defined as follows:

$$\max_{\delta x \longrightarrow 0} \int_\partial \Psi(h, k_1(h), y_1(h), s_1(y_1(h)), g) d\partial(h). \tag{26}$$

For the consumer, the objective is to maximize lifetime expected utility under government budget constraints, defined by the formula

$$\max_{\delta x \longrightarrow 0} E \int_\partial \Psi(h, k_1(h), y_1(h), g) \mathrm{dt}. \tag{27}$$

Assuming that the government does not know about the consumer and only evaluates the taxes he must pay based on his income, his budget constraint or equation of state is

$$k_1(h) = y_1(h) - s_i(y_i(h)) - c_i(h) - k_i(h). \tag{28}$$

4. Research on Tax Collection and Administration Mode

4.1. Tax Collection and Management Mode in the Era of Big Data. Since 1950, China's tax collection and management mode have undergone two changes, including three development modes. Two transformations refer to the first transformation: In 1985, China abolished the tax collection and management system, and widely implemented the "administrative system" of separation of management and examination. Tax registration system, tax declaration, and tax inspection are the components of tax collection and management system; in the era of big data, our tax and management system is slowly moving from "management" to "numerical control." The above three kinds of collection management, conventional collection management form is mainly "family budget management system" and "case management system", and data collection management system is "number management system"; compared with "management system,", the "number management system" focuses on using a lot of data to solve the problem of the data inconsistency, it standardizes the flow of information as the main line, data analysis is the key, and it is the combination of manual processing and computer processing. The comparison of tax collection and administration modes in different periods is shown in Table 1:

4.2. Tax Collection and Administration Mode under the Condition of American Informatization. The tax management model in the USA can be summarized as follows: The content of tax service includes taxpayer's self-statement, in-process monitoring, tax-related protection, post-inspection, and tax management. We should scientifically and comprehensively meet the needs of taxpayers; determine development strategies, business rules, and organizational structure; and strengthen performance appraisal.

According to Figure 3, the revenue department e-file usage rate is increasing year by year, indicating the increasingly mature tax collection and administration model in the USA. Part of the reason is that in 1998, the federal taxation bureau reorganized the national tax collection and administration information agencies, relying on the computer network across the country, relying on computer information technology, covering from tax sources, tax authorities, tax authorities, tax returns, tax, tax returns, tax inspection to the whole process of tax inspection, personnel administration.

4.3. Macro Performance of Tax Payment Data under the Tax Collection and Administration Mode. Data analysis is carried out on the taxpayer's tax category statistical table through Figure 4. The table shows the statistical results, the taxpayer's withhold of information tax, or tax evasion. On the premise of a comprehensive and detailed grasp of all tax laws and regulations, we understand the taxpayer's industry and specific transactions. After the general audit procedure, it is impossible to make an accurate judgment on whether the taxpayer has failed to pay the tax. In order to analyze the tax situation of taxpayers, Figure 4 counts the number of

Table 1: Comparison of tax collection and administration modes in different periods.

Stage division	Stage I	Stage II	Phase III	Phase IV
Life period	The planning economy period, 1985	1985-1997	1997-2009	2009-the future
Characteristics of the times	Agricultural era	Industrial age	The internet era	Information age
Collection and management mode	Management household system	Steward system	Steward system	Tube number system
Collection and management procedures	Capital process	Operation flow	Operation flow	Information flow
Collection and management means	Hand operation	Hand operation	Computer + database	Big data technology
Collection and management mode	Tax administrators manage households	Collection, management, inspection and phase separation	"Thirty-four words" Policy	"Thirty-four character" policy + "strengthen management"
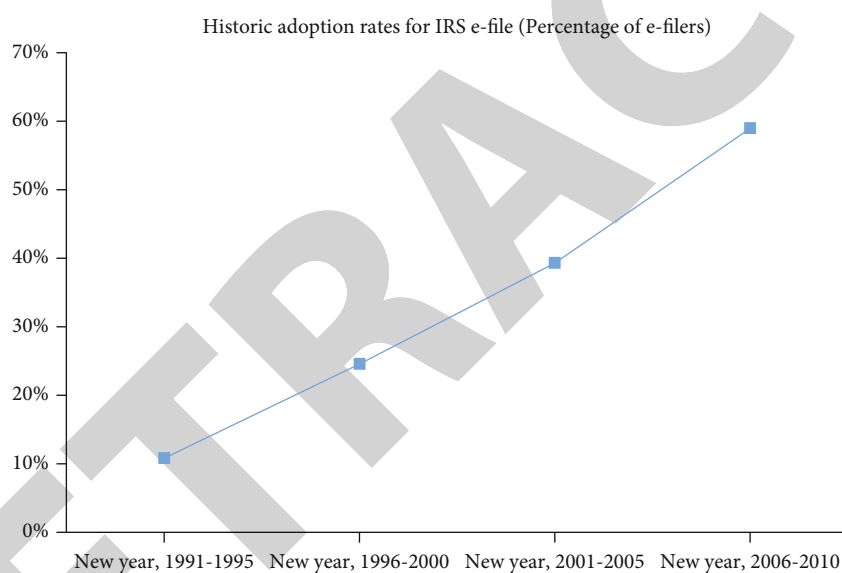
Figure 3: IRS e-file usage ratio history graph.

tax types and the number of people who pay taxes. There is no connection between the two. Taxpayers want to pay taxes and their jobs are related, so it is normal for different people to pay different taxes and different amounts of taxes. The type of taxpayer's tax payment is related to whether the taxpayer has concealed tax returns or tax evasion. The type of tax that the taxpayer needs to pay and the amount of tax to be paid by the taxpayer is related to his work. Therefore, there is no difference between the number of tax types and the number of taxpayers. What is the relationship, so the height of the two is different.

In the audit of tax collection and management, in order to obtain the necessary external data in time (such as industrial and commercial registration data, real estate registration data, engineering construction information data, etc.), auditors need to analyze the reported data itself through the tax collection and management system, and have doubts about the problem, even if a table is self-relevant, they also

need to draw audit conclusions. If we need to get the error problem of storage level, we often need to analyze the data and make some manual judgments. In the face of the deed tax collection audit, it is also facing such a problem. Therefore, from the survey data in the first quarter (Table 2), second quarter (Table 3), and third quarter (Table 4), it can be seen that the taxes paid are basically consistent, and the tax rates and corresponding taxes involved in the deed tax returns are also seen and analyzed.

Compared with the first quarter, deed tax and personal income tax decreased relatively, while vehicle and ship tax increased relatively. Thus, different quarters of the tax paid will have a relatively large change.

In the third quarter, the deed tax had a trend of significant increase, and the vehicle and vessel tax were significantly reduced under the high risk in the second quarter. In different quarters, the tax situation will change due to the personal travel situation.
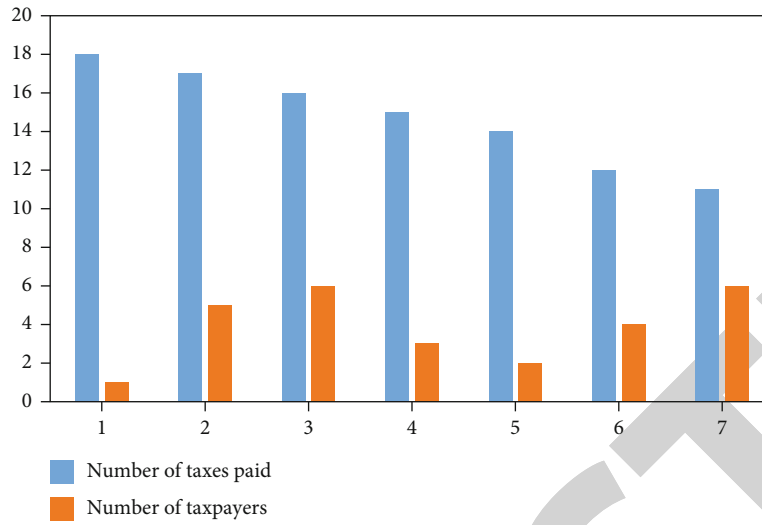
Figure 4: Tax payment data sheet.

Table 2: Tax statistics for the first quarter.

Tax item table	Total tax payment
Contract tax	236, 521
Income tax for individuals	123, 362
Added value tax	213, 233
City planning tax	123, 548
Education fee	34, 265
Stamp duty	52, 451
Building taxes	33, 372
Vehicle and vessel tax	22, 668
Business income taxes	3, 880
Increment tax on land value	162, 662

Table 4: Tax statistics for the third quarter.

Tax item table	Total tax payment
Contract tax	213, 046
Added value tax	63, 251
Building taxes	56, 223
Vehicle and vessel tax	14, 523
Stamp duty	12, 546
Increment tax on land value	15, 426
Additional local education	21, 532
Town land use tax	56, 956
City planning tax	21, 364
Income tax for individuals	15, 426

Table 3: Tax statistics for the second quarter.

Tax item table	Total tax payment
Contract tax	152, 463
Building taxes	54, 231
Business income taxes	24, 621
Income tax for individuals	54, 361
Added value tax	12, 364
Increment tax on land value	23, 233
Town land use tax	12, 433
Stamp duty	456, 123
Vehicle and vessel tax	456, 133
Additional local education	154, 362

Without knowing the relevant rules, the association rule algorithm is the most classic example of shopping cart analysis to find the relationship between item sets in a large number of data, so the VAT, deed tax, consumption tax, enterprise income tax, and personal income tax of the cur-

rent quarter are selected as the key taxes to see the taxpayer's declaration and payment. This is shown in Figure 5.

In the tax collection and management system, because many external data need to be analyzed by auditors through the tax collection and management system to find out the problem in time, so people need to make manual judgments while reanalyzing the data. The data in the machine can only represent the information part of the big data, and when those people actually arrive at the scene, there may be some accidents, which need to be solved manually.

4.4. Analysis of Nonefficient Investment by Tax Avoidance. Secondly, the degree of marketization of state-owned enterprises is relatively low. Since the ultimate controller of state-owned enterprises is the state, the internal proxy problem and the internal and external information asymmetry problem are relatively more serious. Tax collection and administration can not only play the role of corporate governance to restrain nonefficient investment, but also lead to the capital outflow of enterprises to some extent to cause insufficient investment. Therefore, these two opposite effects offset each
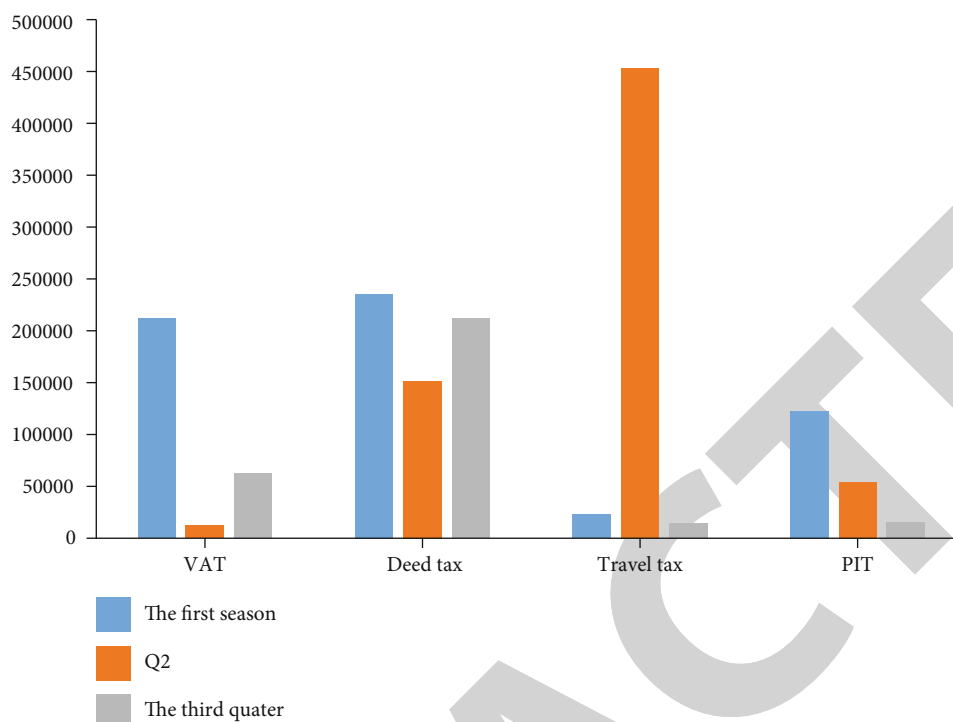
Figure 5: Comparison of tax values in the third quarter.

Table 5: Differences in enterprise nonefficiency investment.

Project	Private enterprises			State-owned enterprise		
Variable name	INEI	OVEREI	LESSEI	INEI	OVEREI	LESSEI
DDBTD	2.671	1.771	-1.785	2.632	3.451	-2.614
Controlled variable	Yes	Yes	Yes	Yes	Yes	Yes
Observations	2.250	1.936	1.842	3.077	1.256	1.888
r-squared	0.113	0.278	0.425	0.232	0.036	0.182
Company PE	Yes	Yes	Yes	Yes	Yes	Yes
Year PE	Yes	Yes	Yes	Yes	Yes	Yes

other, so there is no obvious impact on nonefficient investment. Because of the influence of tax avoidance on unproductive investment, under different financing constraints, there are both "increasing agency cost effect" and "reducing financing pressure effect"; the promotion of tax collection and management strength plays a "corporate governance effect"; for tax avoidance, the "agency cost increase effect" plays a role of mitigation and regulation, and ultimately reduces the level of over-investment and inefficient investment behavior. Therefore, there is reasonable to believe that the impact of tax avoidance on nonefficiency investment will different, as shown in Table 5.

4.5. Tax Circumvention and Legal Risks. Legal risk has a negative inhibitory effect on the tax avoidance activities of enterprises. Enterprises that have litigation violations will be strictly supervised by the administrative regulatory departments, which increases the cost of tax avoidance and increases the tax risks. Legal risk will bring to the enterprise

including reputation loss and financing pressure, standardize the internal tax management, can make the enterprise in the short term to market social responsibility, and play a high marginal benefit; the enterprise risk management culture will promote company management to adopt robust tax policy to deal with the adverse impact of legal risk and reputation risk.

In the regression results of the variables in Table 6, corporate profitability (ROA) and all three tax avoidance indicators are significantly positively correlated at the 1% confidence level; this indicates that the stronger the corporate profitability, the greater the motivation to reduce the tax burden, the higher the tax avoidance. Enterprise solvency (LEV), enterprise size (SIZE), chairman and CEO portfolio (dual), and enterprise value (Tobin Q) and tax avoidance index regression coefficient at 1% confidence level are negative, and this shows that under the legal risk, the stronger the solvency, the larger the asset scale; the executive board independence and enterprise market value development

TABLE 6: The regression table of legal risks and tax avoidance.

Variables	DDBTD		BTD		Rate	
	Coefficient	T price	Coefficient	T price	Coefficient	T price
Litr	-0.003	-3.137	-0.003	-3.201	-0.009	-2.519
LEV	-0.016	-3.082	-0.022	-4.130	-0.052	-2.537
ROA	0.220	14.230	0.274	18.920	0.538	9.417
Size	-0.005	-4.451	-0.066	-5.450	-0.022	-4.632
BM	-0.003	-0.732	-0.003	-0.865	-0.066	-4.365
Dual	-0.003	-2.314	-0.003	-2.043	-0.003	-0.578
Relation	-0.003	-0.124	-0.003	-1.032	0.000	0.033
DA	-0.006	-0.830	0.013	2.531	0.050	2.467
Tobin Q	-0.016	-3.201	-0.002	-3.051	-0.011	-4.528
PPE	0.000	-0.005	-0.007	-0.801	-0.072	-2.255
Constant	0.114	4.465	0.157	5.807	0.573	5.515
Year	Control		Control		Control	
Ind	Control		Control		Control	
N	5.331		5.331		5.331	
R-squared	0.078		0.135		0.061	

prospects will significantly reduce enterprise tax avoidance. In addition, manipulative accrued profit (DA), investment opportunities (BM) and fixed asset density (PPE) will also affect tax aversion to some extent.

5. Conclusion

The massive sample size and high dimensionality of big data bring unique computing and statistical challenges. Now, there are more data stored through the Internet every second than that stored on the whole Internet 20 years ago. People can conduct some basic problem analysis of the application of tax collection and administration and legal issues through big data. An important determinant of irregularity in a country is its tax enforcement capacity, and in this paper, I assess the quantitative impact of incomplete tax enforcement on the total output and productivity. The empirical results show that there is a certain degree of interregional tax competition, and tax centralization increases the effective tax rate and offset the impact of tax. Standardizing tax collection and administration is of great significance to improve the tax collection and administration system and promote the formation of a fair and orderly market competition order. Under the background of urban-rural integration, it is urgent to adjust the tax concept, reconstruct the scope of tax, scientifically design the tax rate, and simplify the tax collection and administration procedures to have a regulating effect on the unified market of urban and rural construction land in China. Over the past decade, some problems have been exposed in the implementation of the tax collection and administration law, which have affected the collection of tax to a certain extent. It is necessary to revise the tax collection and administration law. At the same time, the implementation of the administrative law enforcement law has posed new challenges to tax law enforcement, and it also needs to revise the tax collection and administration law.

This paper discusses some important legal issues of revising the tax collection and administration law and puts forward the corresponding ideas. We study whether tax aggressiveness will reduce the motivation and opportunities for active tax management in the era of big data. Specifically, different institutional settings in China are used to study whether tax aggression in China is affected by the limitations of big data. This paper proves the tax collection and management mode studied in this paper, so that taxpayers can pay taxes more conveniently and quickly, and puts forward the method of improving the tax collection and management system. Although the taxation supervision system can be perfected, it may not be perfect enough to give people the most intuitive answers, so we should consider more humane issues when improving the comprehensiveness of these systems.

Data Availability

The experimental data used to support the findings of this study are available from the corresponding author upon request.

Conflicts of Interest

The authors declared that they have no conflicts of interest regarding this work.

References

[1] X. Meng and X. Ci, "Big data management: concepts, techniques and challenges," *Journal of Computer Research and Development*, vol. 25, no. 2, pp. 96–102, 2013.

[2] J. Fan, F. Han, and H. Liu, "Challenges of big data analysis," *National Science Review*, vol. 1, no. 2, pp. 293–314, 2014.

Retraction

Retracted: Analysis of College Students' Ideological and Political Dynamics and Communication Path Based on Reinforcement Learning

Journal of Sensors

This article has been retracted by Hindawi following an investigation undertaken by the publisher [1]. This investigation has uncovered evidence of one or more of the following indicators of systematic manipulation of the publication process:

(1) Discrepancies in scope

(2) Discrepancies in the description of the research reported

(3) Discrepancies between the availability of data and the research described

(4) Inappropriate citations

(5) Incoherent, meaningless and/or irrelevant content included in the article

(6) Peer-review manipulation

The presence of these indicators undermines our confidence in the integrity of the article's content and we cannot, therefore, vouch for its reliability. Please note that this notice is intended solely to alert readers that the content of this article is unreliable. We have not investigated whether authors were aware of or involved in the systematic manipulation of the publication process.

In addition, our investigation has also shown that one or more of the following human-subject reporting requirements has not been met in this article: ethical approval by an Institutional Review Board (IRB) committee or equivalent, patient/participant consent to participate, and/or agreement to publish patient/participant details (where relevant).

Wiley and Hindawi regrets that the usual quality checks did not identify these issues before publication and have since put additional measures in place to safeguard research integrity.

We wish to credit our own Research Integrity and Research Publishing teams and anonymous and named external researchers and research integrity experts for contributing to this investigation.

The corresponding author, as the representative of all authors, has been given the opportunity to register their agreement or disagreement to this retraction. We have kept a record of any response received.

References

[1] W. Wu and H. Liu, "Analysis of College Students' Ideological and Political Dynamics and Communication Path Based on Reinforcement Learning," *Journal of Sensors*, vol. 2022, Article ID 9704315, 11 pages, 2022.

Research Article

Analysis of College Students' Ideological and Political Dynamics and Communication Path Based on Reinforcement Learning

Wenbin Wu [iD] and Hongwei Liu

Dalian University of Technology, School of Marxism, Liaoning Dalian 116023, China

Correspondence should be addressed to Wenbin Wu; fengjingxian654321@mail.dlut.edu.cn

Contemporary college students are the main force of future national construction. Their ideological political dynamics are related to the development of the party and the country. Some students have some problems with study concepts and study habits. For a long time, the ideological political education of university students has not been paid attention to, resulting in the inability to accurately analyze the ideological political dynamics of university students. Grasping the ideological political dynamics of university students in the new era is the top priority of current educational work and an important guarantee for the development of ideological political education in universities. With the development of the times, communication channels are also constantly updated. The focus of this article is to analyze the ideological political dynamics and communication channels of university students. To some extent, traditional analysis methods cannot satisfy current research. This paper constructs an analysis model of university students' ideological political dynamics and communication paths based on reinforcement learning. The Markov decision process and Monte Carlo method are used to analyze the ideological political dynamics and communication paths of college students. The results show the following: (1) the highest accuracy of reinforcement learning is 99.7%, and the lowest is 96.2%; the highest accuracy is 99.7%, and the lowest is 97.4%; the highest recall is 99.6%, and the lowest is 97.6%. (2) The average accuracy rate of reinforcement learning is 98.16%, the average accuracy rate is 98.75%, and the average recall rate is 98.65%. (3) In the ideological political dynamics of college students, the score of value orientation is 6.975, the score of learning status is 8.025, the score of consumption concept is 7.7, and the score of employment is 7.45. (4) In the communication path analysis, there are 12 people in interpersonal communication, 15 people in organizational communication, 21 people in mass communication, 28 people in network communication, and 24 people in Internet communication.

1. Introduction

As an important part of the youth group, the ideological political dynamics of college students cannot be ignored. Comprehensively analyze the ideological political dynamics and communication channels of university students to improve the effectiveness of ideological and political education for university students. This paper constructs an analysis model of university students' ideological political dynamics and communication paths based on reinforcement learning and analyzes the ideological and political dynamics of university students. This paper provides a lot of support on the basis of previous results. Reinforcement learning is

a popular model for analyzing problems [1]. Analyze behavior through trial-and-error interactions with dynamic environments. Reinforcement learning describes an algorithm similar to Q-learning for finding optimal policies [2]. Popular Q-learning algorithms overestimate action values under certain conditions [3]. A common model for reinforcement learning is the standard Markov decision process [4]. Reinforcement learning is developed from theories such as animal learning and parameter perturbation adaptive control [5]. The goal of reinforcement learning is to dynamically adjust parameters [6]. For maximum signal enhancement, the trend is known as an important content of the ideological political education of university students [7]. It is also an

effective way to carry out ideological political education for university students. Understand the ideological dynamics of college students and apply the Internet to ideological political education [8]. Ideological political education must conform to the changes and trends of the form and keep innovating [9]. At present, ideological political education in universities should be combined with art education [10]. The continuous progress of information technology has broadened the dissemination path of university students' ideological political dynamics [11]. Ideological politics teachers are one of the important ways to optimize the dissemination of ideological political education [12]. Reinforcement learning acquires learning information and updates parameters by receiving action rewards from the environment [13]. Reinforcement learning is mainly manifested in reinforcement signals [14]. Reinforcement learning focuses on online learning [15].

2. Theoretical Bases

2.1. Reinforcement Learning

2.1.1. Overview. Reinforcement learning (RL) [16] is a type of goal-oriented learning. The reinforcement learning process is the continuous interaction between the agent and the environment. In this process, the agent continuously observes the characteristics of the environment state and takes actions on the current environment according to certain policy rules. The environment gives feedback on actions taken in the form of rewards. The agent updates the policy based on the reward value to get a better reward for the next action it takes.

The basic framework of reinforcement learning is shown in Figure 1.

2.1.2. Markov Decision Process. The Markov decision process (MDP) [17] is a mathematical description that can be provided for reinforcement learning, and most reinforcement learning problems can be modeled as an MDP. MDP adds action elements to the transition probability from one state to another state, enriching the Markov feature, and can be expressed as

$$p(s_{i+1}|s_i, a_i, \cdots, s_0, a_0) = p(s_{i+1}|s_i, a_i). \quad (1)$$

For the answer, MDP consists of 5 basic elements, namely, (S, A, R, P, γ). Among them, S is the state space, which can reflect all the state sets of the complete information of the system; s is the current state, $s \in S$; A is the limited action space, which is composed of all possible actions; a is the currently taken action, $a \in A$; $R(s, a)$ is the reward function, which represents the expectation of the reward value that the agent can get from the current state s to the next state s'; $P(s'|s)$ represents the probability of transitioning from state s to state s'; and λ represents the discount factor, which is a random float in the range of 0 to 1. Points can be used to determine whether the total reward is discounted or not.
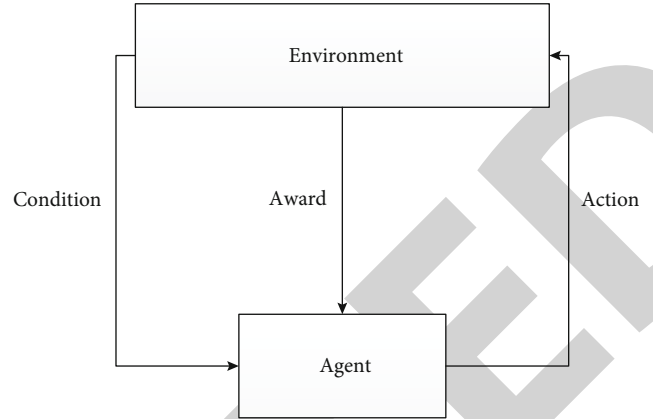
Figure 1: The basic framework of reinforcement learning.

To find the optimal strategy, that is, to find the optimal state, the action value is

$$Q * (s, a) = R(s, a) + \lambda \sum_{s' \in S} P(s'|s) \max_{a \in A} Q(s', a'), \quad (2)$$

where $R(s, a)$ is the average of instant reward $r(s, a)$.

2.1.3. Exploration and Utilization. The purpose of reinforcement learning is to obtain the optimal result; that is, the agent gets the maximum reward. Therefore, during the training process, it is necessary for the agent to perform actions according to the behavior that can obtain the maximum reward value. At the same time, considering that the "trial-and-error" experience experienced by the agent is not necessarily rich, only the local optimal solution can be obtained, so the agent cannot blindly use the existing experience to make actions, but it is necessary to improve the agent's exploration to find new and latest ability to solve. With limited time, we need to rely on strategies to find a balance between exploration and exploitation.

2.1.4. Strategy. Policy refers to the operation policy of the agent in MDP, which is a function that can calculate the output. In reinforcement learning, policies can be defined as deterministic policies and stochastic policies. Deterministic strategy means that in the same state, the action output by the agent is deterministic and unique; on the contrary, in the same state under the stochastic strategy, the output behavior of the agent is not unique but follows a specific probability distribution, but the sum of all possible output behavior probabilities in the same state should be equal to 1.

2.1.5. Value Function. During the interaction between the agent and the environment, actions need to be evaluated to ensure that the final action set can obtain the maximum reward. There are two evaluation mechanisms here, namely, the value function and the Q function. The value function refers to the value function of the state, which measures the pros and cons of the agent's state under the policy. A

value function can be defined as follows:

$$V^{\pi}(s) = E_{\pi}[R_t | s_t = s]. \tag{3}$$

The above formula expresses the expected reward that can be obtained by following policy π in state s. Among them, R_t represents the reward obtained by the agent from the environment at time t, which can be expressed as follows:

$$R_t = r_{t+1} + r_{t+2} + \cdots + r_T. \tag{4}$$

And if it is in a continuous situation, there may be no final state, namely,

$$R_t = r_{t+1} + r_{t+2} + \cdots. \tag{5}$$

A discount factor is required to reward the discount, which can be expressed as

$$R_t = r_{t+1} + \gamma r_{t+2} + \gamma^2 r_{t+3} \cdots,$$
$$R_t = \sum_{k=0}^{\infty} \gamma^k r_{t+k+1}. \tag{6}$$

Among them, if γ is 0, the reward is an immediate reward, and if γ is 1, the reward is mainly reflected in the future reward. Therefore, the value function can be expressed as

$$V^{\pi}(s) = E_{\pi}\left[\sum_{k=0}^{\infty} \gamma r_{t+k+1} | s_t = s \right]. \tag{7}$$

The Q function, also known as the state action value function, is used to measure the pros and cons of the agent following the policy and performing the actions in the state. The Q function can be defined as follows:

$$Q^{\pi}(s, a) = E_{\pi}[R_t | s_t = s, a_t = a]. \tag{8}$$

The above formula represents the expected reward that can be obtained by following policy π and taking action a in state s. This formula can be expressed as

$$Q^{\pi}(s, a) = E_{\pi}\left[\gamma^k r_{t+k+1} | s_t = s, a_t = a \right]. \tag{9}$$

The value function is used to evaluate the state, and the Q function is used to evaluate the action [18]. Further derivation of the value function can be obtained:

$$V^{\pi}(s) = E_{\pi}\left(r_{t+1} + \gamma r_{t+2} + \gamma^2 r_{t+3} + \cdots | s_t = s \right),$$
$$V^{\pi}(s) = E_{\pi}\left(r_{t+1} + \gamma (r_{t+2} + \gamma r_{t+3} + \cdots) | s_t = s \right),$$
$$V^{\pi}(s) = E_{\pi}\left(r_{t+1} + \gamma V^{\pi}(s_{t+1}) | s_t = s \right). \tag{10}$$

Similarly, the Q function can also be derived as

$$Q^{\pi}(s, a) = E_{\pi}\left(r_{t+1} + \gamma Q^{\pi}(s_{t+1}, a_{t+1}) | s_t = s, a_t = a \right). \tag{11}$$

According to the derivation of the above value function and Q function [19]. This can be further extended to the Bellman equations of both:

$$V^{\pi}(s) = \sum_a \pi(a|s) \sum_{s'} p\left(s' | s, a \right) \left[R\left(s' | s, a \right) + \gamma V^{\pi}\left(s' \right) \right],$$
$$Q^{\pi}(s, a) = \sum_{s'} p\left(s' | s, a \right) \left[R\left(s' | s, a \right) + \gamma \sum_{a'} Q^{\pi}\left(s', a' \right) \right]. \tag{12}$$

The value function that produces the maximum value should satisfy

$$V^*(s) = \max_{\pi} V^{\pi}(s). \tag{13}$$

Likewise, the optimal strategy should be better than or equal to any other strategy. The optimal policy can produce the optimal value function [20]. That is, the maximum value of the Q function is the optimal cost function:

$$V^*(s) = \max_a Q^*(s, a). \tag{14}$$

Combining the above formula, the optimal cost equation can be obtained:

$$V^*(s) = \max_a \sum_{s'} p\left(s' | s, a \right) \left[R\left(s' | s, a \right) + \gamma \sum_{a'} Q^{\pi}\left(s', a' \right) \right]. \tag{15}$$

2.2. Commonly Used Reinforcement Learning Algorithms

2.2.1. Monte Carlo Method.
For the Monte Carlo method [21], a very important advantage is that it does not need to know the environment, only needs to get the experience represented by the Markov quadruple interacting with the environment, and then solves the reinforcement learning problem by averaging the returns of the samples. The state value function at this time can be written as

$$Q^{\pi}(s_t, a_t) = \frac{1}{m} \sum_{i=1}^{m} R(\tau_i). \tag{16}$$

Among them, τ_i indicates that in state s_t, action a_t has always used the trajectory data generated by strategy π, and $R(\tau_i)$ indicates the sum of all rewards on this trajectory. When updating the action value function, an incremental method can be used to implement the Monte Carlo method.

2.2.2. Timing Differential Method.
Sutton proposed the temporal difference algorithm, which combines Monte Carlo and dynamic programming methods [22]. It is an important

learning algorithm in reinforcement learning. This method can learn in some continuous state.

The standard temporal difference method is a model-free algorithm that learns directly from experience and estimates the current state value after one or more steps of action. The most basic one-step update is the TD(0) algorithm [23]. When using a table of values, the iterative formula for the TD(0) algorithm is

$$V(s_t) \longleftarrow V(s_t) + \alpha(r_{t+1} + \gamma V(s_{t+1}) - V(s_t)), \qquad (17)$$

where $V(s_t)$ is the value function of state s_t at time t.

The TD method is also called the TD(0) method, because this method updates the value function with the corresponding subsequent state after one step. We can define the general form of step return as

$$G_t^n = R_{t+1} + \lambda R_{t+2} + \lambda^2 R_{t+3} + \cdots + \lambda^{n-1} R_{t+n}. \qquad (18)$$

At this time, the update of the value function becomes

$$V(S_t) \longleftarrow V(S_t) + \alpha(G_T^n - V(S_t)). \qquad (19)$$

2.2.3. Sarsa Learning. The name of the Sarsa algorithm comes from the 5 variables used when the value function is updated, which are the current state s, the action a in the current state, the reward r of the current action, the next state s' reached, and the assumed next state. The action consists of a'.

In the current state s and action a, after the state transitions to another state s', the current action cost function $Q(s, a)$ must be updated. Then, after reaching the next state, update the next action cost function until the end. This cost is updated as follows:

$$Q(s, a) \longleftarrow Q(s, a) + \alpha \left(r + \gamma Q\left(s', s'\right) - Q(s, a) \right), \qquad (20)$$

where α the learning is the rate and γ is the decay factor.

2.2.4. Q-Learning. Q-learning is a temporal difference algorithm under the off-track strategy. The off-track strategy means that the strategy for determining the current behavior is different from the strategy for updating the value function. The agent chooses the action in the current state through a strategy and interacts with the environment, but then, when the value function is updated, it uses another strategy. The action-value function update formula for Q-learning is as follows:

$$Q(s_t, a_t) \longleftarrow Q(s_t, a_t) + \alpha[r_{t+1} + \gamma \max_a Q(s_{t+1}, a) - Q(s_t, a_t)]. \qquad (21)$$

3. Analysis of University Students' Ideological Political Dynamics and Communication Paths

3.1. Dynamic Analysis of University Students' Ideological Politics. Facing the complex and changing social environment, to carry out the ideological political education work in universities and grasp the ideological dynamics of university students, it is necessary to analyze the current ideological political dynamics of university students. It analyzes four aspects: value orientation, learning status, consumption concept, and employment, as shown in Table 1.

3.2. Propagation Path Analysis

3.2.1. Original Propagation Path. The original communication paths of college students' ideological and political dynamics are divided into three categories: interpersonal communication, organizational communication, and mass communication, as shown in Table 2.

3.2.2. New Propagation Paths. Although the original communication path of college students' ideological and political dynamics has its own advantages, its influence on interpersonal communication is not extensive, and it is limited by time and place. At the same time, it is also restricted to a large extent by the quality of the communicator. The scope of organizational communication is still limited to local areas, and it is difficult to solve the problem of timely and effective communication. Mass communication is only one-way communication, not interactive communication [24]. Therefore, in the process of ideological and political dynamic dissemination, while adopting and improving the original dissemination path, a new ideological and political dynamic dissemination path should also be opened up.

(1) Network communication is based on the computer communication network to transmit, exchange, and utilize information, so as to achieve the purpose of social and cultural exchange. On the Internet, people can freely browse almost all the information on the Internet [25]

(2) Opening up the Internet is a new way for college students to exchange ideological and political dynamics. It is not simply to publish some information on the Internet for ideological and political dynamic exchanges. The key is to use the various advantages of the Internet and computers to realize the dynamic exchange of ideological and political dynamics from postevent to preevent through the ideological and political dynamic database and scientifically use this series of databases in practice, from qualitative communication to quantitative communication and edge propagation to multidirectional propagation

3.3. Model Construction. This paper builds an analysis model of college students' ideological political dynamics and propagation path based on reinforcement learning. The model first collects college students' ideological political dynamics

TABLE 1: Dynamic analysis of university students' ideological politics.

Ideological political trends	Detailed analysis
Value orientation	Modern university students strongly support the leadership of the CPC Central Committee with Comrade Xi Jinping as the core, highly identify with the "Chinese dream of the great rejuvenation of the Chinese nation" and "the goal of building a modern socialist country," and are able to understand and grasp the ideas of socialism with Chinese characteristics in the new era. The fundamental core pays close attention to the party's latest strategies and measures.
Learning status	The learning status of contemporary university students presents a positive and good development trend, and their learning initiative is also significantly enhanced. Most of the students have a correct and serious learning attitude, have clear learning goals and plans, and actively expand their knowledge reserves through online courses, lectures, and other methods. When many students encounter difficulties in learning, they will take the initiative to consult relevant materials to solve the problem.
Consumer attitudes	With the rapid development of my country's economy, people's living standards have gradually improved, and the living consumption level of modern college students has also gradually improved. Modern college students already have strong independence and show a strong sense of self in daily consumption. Most of the students do not have the habit of keeping consumption records, and their daily consumption is mainly for meals, shopping for clothes, and class reunions.
Employment	One of the focuses of university students in the new era is employment. Most students have a clear sense of employment and are optimistic about the future. Most of the students showed a positive attitude towards future employment.

TABLE 2: Original propagation path.

Propagation path	Content	Advantages and scope of application
Human-to-human communication	Interpersonal communication, that is, the communicator communicates the ideological and political morality requirements of a certain society to the educational object face to face.	The face-to-face communication between the communicator and the educational object can more accurately understand the current situation of the educational object's ideological and political morality and its formation and development law, so as to effectively carry out the ideological political education dissemination activities.
Organizational communication	Organizational communication means that a certain organization spreads the ideological and political moral requirements of a certain society to members of the organization by holding various meetings with the members of the organization.	The spread of influence is wider than human-to-human transmission and easier to control.
Mass media	Mass communication is the ideological and political education and dissemination carried out by a communication organization to the whole society by means of mass media, such as newspapers, radio, and television.	Spread the widest and timely and effective. For example, television communication also has the advantages of image and intuition.

and then summarizes the ideological political dynamics and propagation paths through call requests. If there is no call request, the call request will continue, until there is a call request. Ideological and political dynamics and propagation paths can only be analyzed after the signal is felt until the end. Similarly, if no signal is sensed, the propagation path analysis will be repeated until a signal is sensed, as shown in Figure 2.

4. Experimental Analysis

4.1. Model Testing. Based on reinforcement learning, this paper constructs an analysis model of university students' ideological political dynamics and communication paths. The model needs to be tested first. 100 college students were

randomly selected as experimental subjects, and 10 groups were divided into 10 groups. Reinforcement learning is compared to deep learning, machine learning, structural equation modeling, and traditional methods. In the model test comparison, this paper uses the most common accuracy rate, precision rate, and recall rate as the comparison indicators. The experimental result data are shown in Tables 3–5.

It can be seen from the data results that reinforcement learning is higher than other models in the comparison of accuracy, precision, and recall, with obvious advantages, indicating that reinforcement learning is more suitable for this study.

The precision of reinforcement learning is 99.7% and 96.2%, which is 37.6% higher than other methods. The highest accuracy was 99.7%, and the lowest was 97.4%.
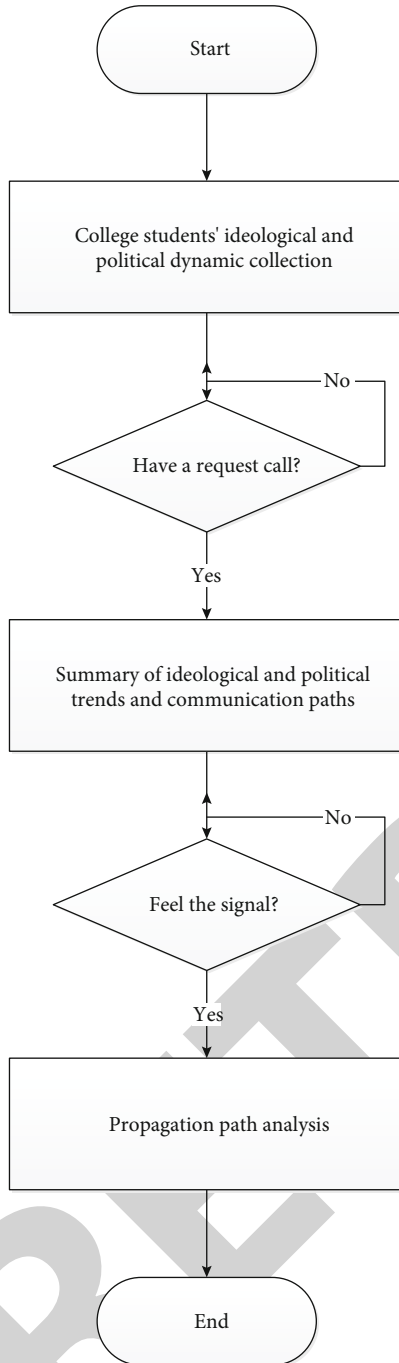
Figure 2: Model construction.

Compared with other methods, it is 37.8% higher than the lowest accuracy. The highest recall rate is 99.6%, and the lowest is 97.6%. Compared with other methods, it is 39.3% higher than the lowest recall. In order to see the advantages of this model more intuitively, it is shown in Figures 3–5.

Through the comprehensive comparison of the accuracy, precision, and recall of the five methods, the average value of each index of the five methods indicates that the reinforcement learning method has more obvious advantages, as shown in Figure 6.

From Figure 6, we know that reinforcement learning has the highest average accuracy, precision, and recall, with an average precision of 98.16%, an average precision of 98.75%, and an average recall of 98.65%. Therefore, this model is most suitable for the research analysis of this article.

4.2. Dynamic Analysis of College Students' Ideology and Politics. After passing the test, the model will be applied to the research of this paper. First, analyze the ideological and political dynamics of college students. Randomly selected 100 college students were divided into four groups: freshmen, sophomores, juniors, and seniors. It analyzes four aspects: value orientation, learning status, consumption concept, and employment. Through the questionnaire survey, students scored four aspects according to their own situation, with a total score of 10 points. The result is shown in Figure 7.

According to Figure 6, the value orientation score in the ideological political dynamics of university students is 6.975, the learning status is 8.025, the consumption concept is 7.7, and the employment aspect is 7.45. Among them, freshman students are more concerned about the state of study, while senior students are most concerned about employment issues and have the highest score among all the scoring results, reaching 10 points.

4.3. Propagation Path Analysis. This article lists five communication paths, interpersonal communication, organizational communication, mass communication, network communication, and the Internet. In order to more accurately analyze the ideological political dynamic communication paths of university students, this experiment made statistics on the ideological political dynamic propagation paths of 100 university students. The results are shown in Figure 8.

The experimental results showed that 12 people communicated through people, 15 people communicated through organizations, 21 people communicated through mass communication, 28 people communicated through the Internet, and 24 people communicated through the Internet. It shows that the communication path of college students' ideological dynamics is mainly based on network communication, and the number of first-year students through interpersonal communication and senior students through organizational communication is only 2.

5. Conclusion

The ideological political trend of university students is related to the future and destiny of the country and the nation, and the communication path is also very important. Based on reinforcement learning, this paper constructs an analysis model of university students' ideological political dynamics and communication paths and improves the accuracy, precision, and recall rate on the basis of traditional methods, which is helpful to analyze the ideological and political dynamics and communication paths of college students.

The findings of this article show that

Table 3: Precision comparison.

Model	1	2	3	4	5	6	7	8	9	10
Reinforcement learning	98.7%	99.4%	97.6%	96.5%	98.3%	99.1%	96.2%	99.7%	97.8%	98.3%
Deep learning	94.1%	89.6%	90.4%	92.4%	90.6%	88.7%	86.4%	89.2%	85.3%	92.6%
Machine learning	85.4%	86.2%	89.3%	90.1%	83.6%	80.5%	79.3%	83.4%	78.4%	80.4%
Structural equation	79.5%	76.1%	80.3%	77.2%	81.3%	70.4%	72.6%	73.4%	76.1%	74.9%
Traditional method	69.4%	65.2%	70.4%	67.8%	69.2%	62.1%	63.8%	65.9%	64.3%	69.1%

Table 4: Accuracy comparison.

Model	1	2	3	4	5	6	7	8	9	10
Reinforcement learning	99.7%	98.9%	97.4%	98.7%	98.3%	99.5%	98.5%	98.6%	98.3%	99.6%
Deep learning	92.4%	87.4%	90.4%	90.8%	91.4%	89.8%	87.3%	87.3%	88.2%	90.5%
Machine learning	86.4%	83.7%	87.6%	87.6%	81.8%	80.3%	78.7%	81.8%	79.1%	83.9%
Structural equation	76.5%	74.8%	81.3%	71.4%	77.4%	71.8%	70.8%	73.7%	75.4%	75.1%
Traditional method	68.4%	66.4%	68.9%	67.3%	68.3%	61.9%	68.9%	63.9%	63.8%	68.9%

Table 5: Comparison of recall rates.

Model	1	2	3	4	5	6	7	8	9	10
Reinforcement learning	97.6%	99.4%	98.6%	99.5%	97.9%	98.4%	99.6%	97.8%	98.8%	98.9%
Deep learning	90.2%	89.2%	91.2%	93.9%	87.6%	87.2%	88.3%	90.7%	86.2%	91.3%
Machine learning	85.8%	80.7%	83.2%	83.8%	80.1%	81.8%	79.8%	87.3%	76.8%	81.5%
Structural equation	79.1%	76.3%	80.8%	74.6%	78.6%	79.1%	73.7%	76.1%	73.2%	78.4%
Traditional method	66.7%	68.7%	69.5%	69.3%	64.3%	60.3%	66.3%	67.4%	61.4%	65.9%
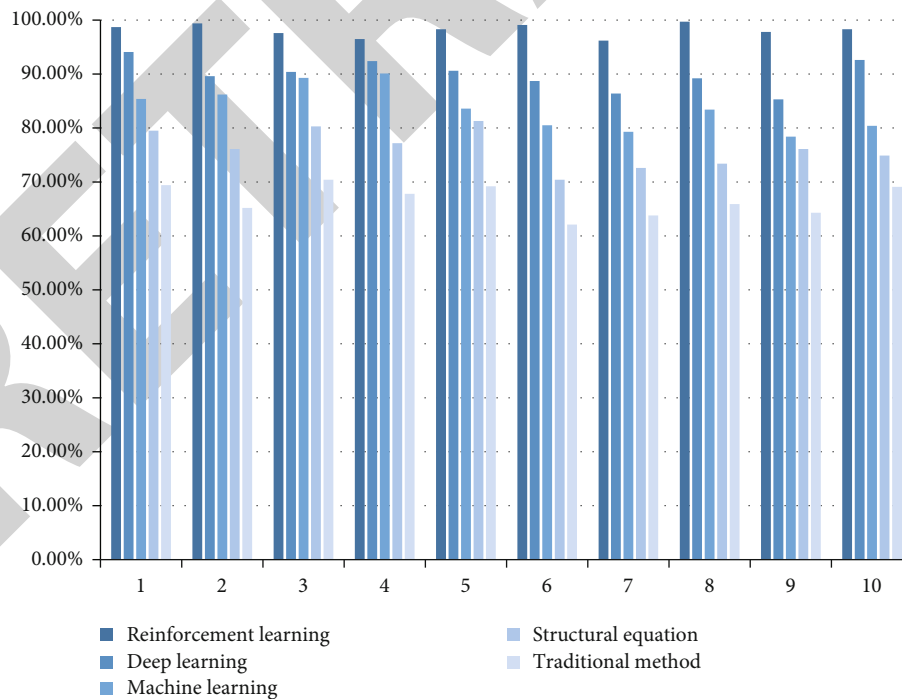
Figure 3: Precision comparison.
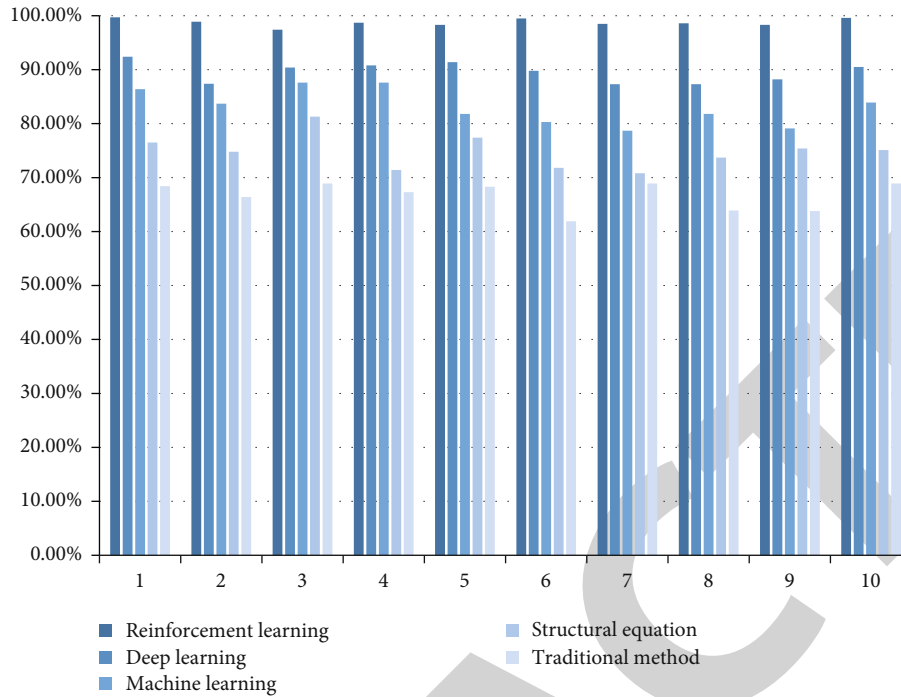
Figure 4: Accuracy comparison.
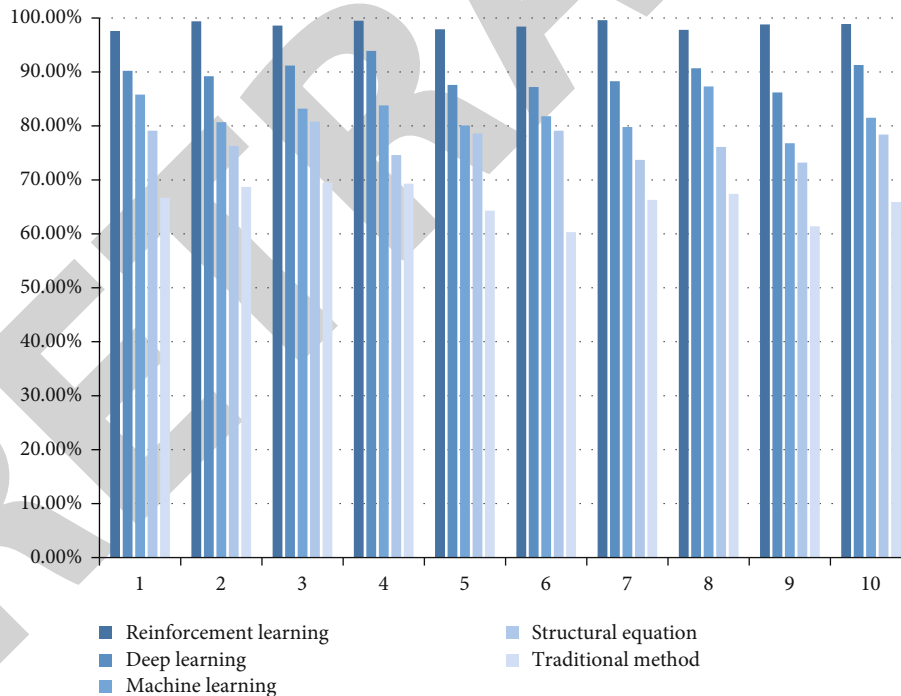
Figure 5: Comparison of recall rates.

(1) by comparing reinforcement learning with deep learning, machine learning, structural equations, and traditional methods, the accuracy of reinforcement learning is 99.7% and 96.2%, respectively, which is 37.6% higher than other methods. The highest accuracy was 99.7%, and the lowest was 97.4%. Compared with other methods, it is 37.8% higher than the lowest accuracy. The highest recall rate is 99.6%, and the lowest is 97.6%. Compared with other methods, it is 39.3% higher than the lowest recall
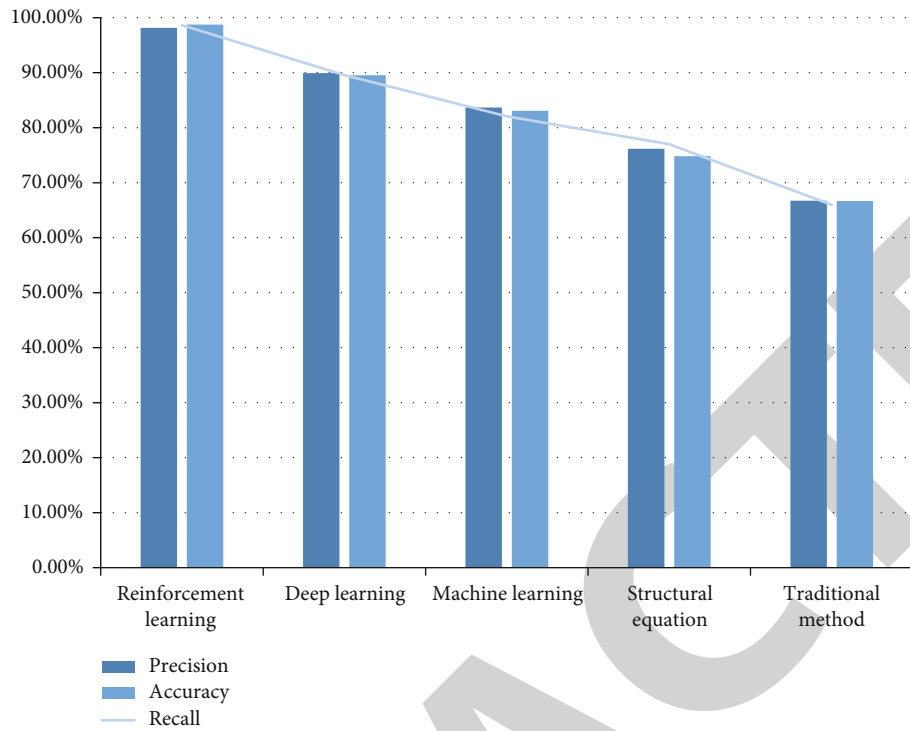
Figure 6: Comprehensive comparison.
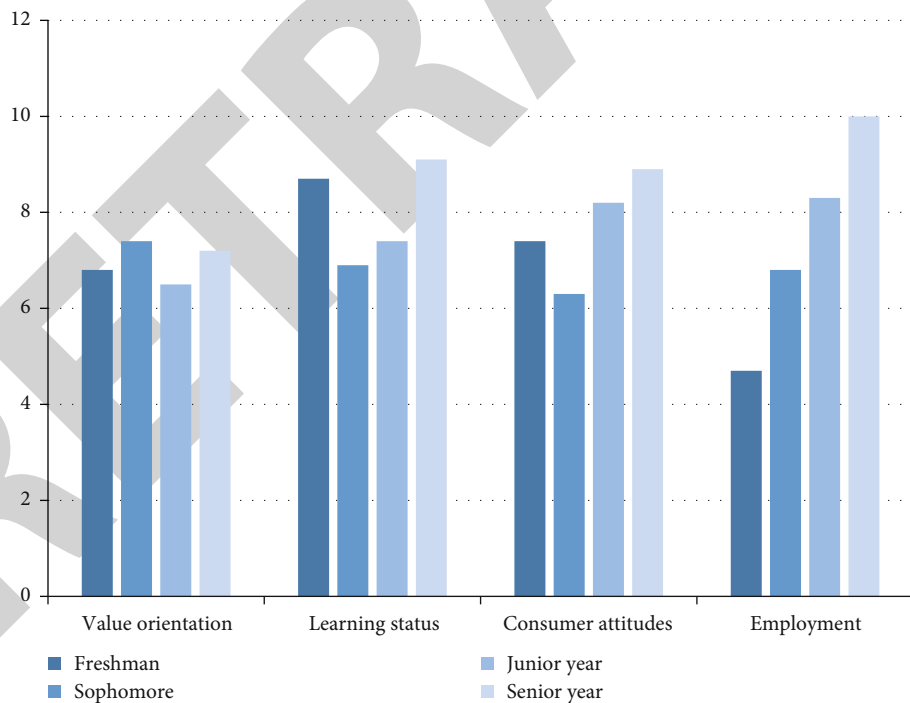
Figure 7: Dynamic analysis of college students' ideology and politics.

(2) reinforcement learning has the highest average accuracy, precision, and recall, with an average accuracy of 98.16%, an average precision of 98.75%, and an average recall of 98.65%

(3) freshman students pay more attention to the state of study, while senior students are most concerned about employment issues, and they have the highest score among all scoring results, reaching 10 points
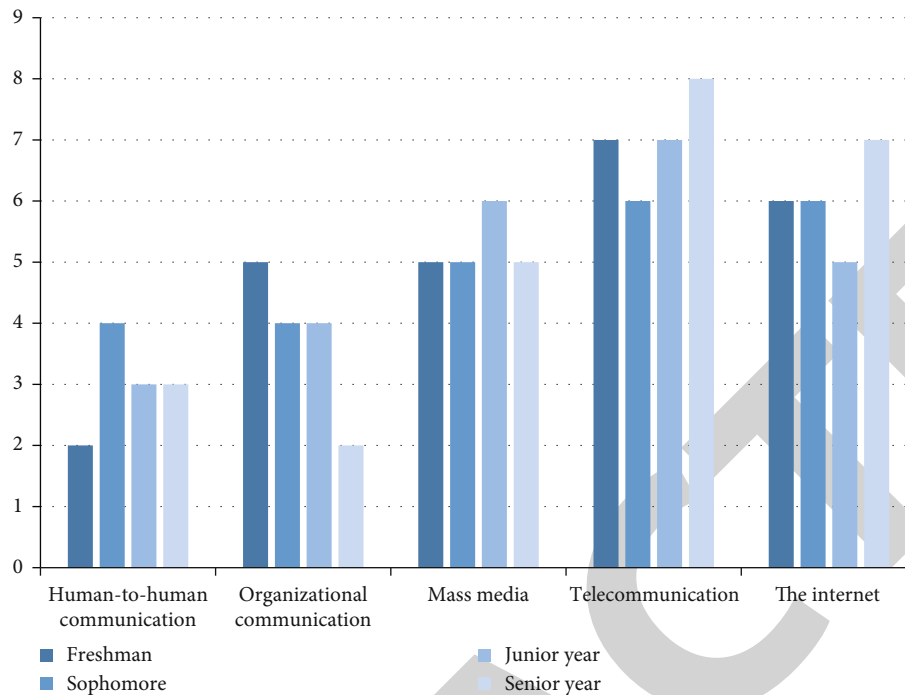
FIGURE 8: Propagation path analysis.

(4) the communication path of college students' ideological dynamics is mainly based on network communication. The number of first-year students through interpersonal communication and the number of senior students through organizational communication is the least, only 2 people, respectively

Based on the analysis of the experimental results, it is concluded that in order to guide the positive development of the ideological political dynamics of university students, (1) increase ideological and political education, (2) improve curriculum and mental health monitoring mechanism, (3) improve school employment guidance, (4) strengthen the management of online public opinion, and (5) strengthen home-school cooperation. Although the model constructed in this article has obvious advantages in terms of accuracy, precision, and recall, it still has certain limitations. This model is limited to the research on the ideological political dynamics of university students. Further research on the generality of the model is needed in the future to increase the generality of the model and enable the model to be applied to a wider range of studies.

Data Availability

The experimental data used to support the findings of this study are available from the corresponding author upon request.

Conflicts of Interest

The authors declared that they have no conflicts of interest regarding this work.

References

[1] S. Mahadevan and J. Connell, "Automatic programming of behavior-based robots using reinforcement learning," *Artificial Intelligence*, vol. 55, no. 2-3, pp. 311–365, 1992.

[2] M. M. Botvinick, Y. Niv, and A. C. Barto, "Hierarchically organized behavior and its neural foundations: a reinforcement learning perspective," *Cognition*, vol. 113, no. 3, pp. 262–280, 2009.

[3] L. Baird, "Residual algorithms: reinforcement learning with function approximation *Proceedings of the Twelfth International Conference on Machine Learning*, pp. 30–37, Tahoe City, California, 1995.

[4] M. J. Frank and E. D. Claus, "Anatomy of a decision: striato-orbitofrontal interactions in reinforcement learning, decision making, and reversal," *Psychological Review*, vol. 113, no. 2, pp. 300–326, 2006.

[5] S. P. Singh and R. S. Sutton, "Reinforcement learning with replacing eligibility traces," *Machine Learning*, vol. 22, no. 1-3, pp. 123–158, 1996.

[6] J. Peters and S. Schaal, "Reinforcement learning of motor skills with policy gradients," *Neural Networks*, vol. 21, no. 4, pp. 682–697, 2008.

[7] B. F. Wan and G. Y. Wang, "Analysis of the status quo of the college students' ideological and political education system,"

Retraction

Retracted: Construction and Application of Index System for Integration of Red Cultural Resources and Ideological and Political Education Based on Fuzzy Judgment Method

Journal of Sensors

This article has been retracted by Hindawi following an investigation undertaken by the publisher [1]. This investigation has uncovered evidence of one or more of the following indicators of systematic manipulation of the publication process:

(1) Discrepancies in scope

(2) Discrepancies in the description of the research reported

(3) Discrepancies between the availability of data and the research described

(4) Inappropriate citations

(5) Incoherent, meaningless and/or irrelevant content included in the article

(6) Peer-review manipulation

The presence of these indicators undermines our confidence in the integrity of the article's content and we cannot, therefore, vouch for its reliability. Please note that this notice is intended solely to alert readers that the content of this article is unreliable. We have not investigated whether authors were aware of or involved in the systematic manipulation of the publication process.

Wiley and Hindawi regrets that the usual quality checks did not identify these issues before publication and have since put additional measures in place to safeguard research integrity.

We wish to credit our own Research Integrity and Research Publishing teams and anonymous and named external researchers and research integrity experts for contributing to this investigation.

The corresponding author, as the representative of all authors, has been given the opportunity to register their agreement or disagreement to this retraction. We have kept a record of any response received.

References

[1] X. Sun and Z. He, "Construction and Application of Index System for Integration of Red Cultural Resources and Ideological and Political Education Based on Fuzzy Judgment Method," *Journal of Sensors*, vol. 2022, Article ID 5103905, 13 pages, 2022.

Research Article

Construction and Application of Index System for Integration of Red Cultural Resources and Ideological and Political Education Based on Fuzzy Judgment Method

Xiuhong Sun [iD] **and Zhenzhen He** [iD]

Baoding University, Hebei Baoding 071000, China

Correspondence should be addressed to Xiuhong Sun; sunxiuhong@bdu.edu.cn

This article states the fuzzy judgment method of the established index system around the history resources and red cultural resources. Firstly, in the second part, it summarizes the system of red culture in ideology and politics and the concepts of various resources of red culture. Then, in the third part, through the construction of the judgment index system, three judgment methods of the index system are put forward, which are the rank sum ratio judgment method, comprehensive index judgment method, and analytic hierarchy process (AHP) judgment method, and the weight judgment calculation of the index system is put forward. Finally, the fourth part puts forward the red cultural resource judgment method of the index system weight, but universities should enhance the cultural heritage of resource system. Besides this theory, the article also analyzes the necessity and effectiveness of the integration of red culture in the new era. This will help to investigate and test the current situation of red culture integrating into the local university foundation. Red culture is the culture formed under the red background, that is, the revolutionary war era. The special background of the times endows red culture with unique vitality, which makes it a unique component of China's advanced culture. Red culture has been finally condensed into a representative culture with Chinese characteristics, which contains endless spiritual wealth.

1. Introduction

An improved method for the tissues was developed. Operational errors, disturbances, and the recovery of the MDA standard and TBARS from tissue samples were studied using the procedure. The recommended judgment method has been satisfactorily applied to evaluate various indexes [1]. The author thinks that in recent years, it is expected to introduce alternative energy sources such as solar energy. However, a sunlight estimation method is needed. Then, the application technology is proposed to use reported data for training. By comparing the prediction ability of computer simulation, the effectiveness of the judgment method is verified [2]. In the paper, the pretreatment and determination of cyanobacteria neurotoxin-methylamino alanine are included. The author proposes a new method to determine BMAA [3]. Religious beliefs and ethnic identity on parental behavior of 40 low-income African-American parents in Ohio and southeastern Michigan are studied. According to the authors of formal structured interviews and questionnaires collected as part of the 1989-1991 Family Study, these data confirm the importance of religion as a sociocultural resource for families of African descent [4]. This study summarizes previous studies on the possibility of tourism utilizing the resources of the Lublin region which are introduced in the field [5]. In this paper, the author studies the effects of sociocultural adversity and cultural resources on the direct influence of this. This study supports the promotion model of cultural resources, in which it is found that there is a negative correlation. Understanding the links between sociocultural adversity and resources and psychological distress can provide information for formulation, which can effectively alleviate the health problems of insufficient research and vulnerable groups [6]. In this paper, the author puts forward a rich view of African-American

young people in cultural resources and explores the concepts of agency and cultural resource elements brought by ethnic minorities and marginalized students in the classroom [7]. In the paper, the special improvement goal and backward enrollment order of vocational colleges determine the political education situation. It advocates students to be taught according to their educational ability. It mainly includes improving students' cognitive ability, eliminating students' antagonistic emotions, enhancing students' self-regulation ability, and improving students' ideology [8]. The paper explains that educators in the context of education are formed on how to treat the individual tendency of the various educated values. Reflecting on the adverse effect education caused by the wrong belittling values held by university educators, and Habermas' communicative action theory, we put forward that educators should establish correct differential values and communication principles [9], mainly that red culture is the only culture for knowledge dissemination and personnel training of education, and the topic is explored and discussed on how to make intrusions into the formation of environmental culture in ideological and political education [10]. It puts forward that in this era, universities should be closely combined with reality, the educational content should be rich, and it should be improved. China's education is developing. As successors, we are the main target group of Chinese dream education. Therefore, higher education should embody the Chinese dream in many aspects [11]. After an overview of the latest benchmarking methodologies for tourism, this paper discusses a critical assessment which was made of the neglect of relevant elements of this approach relating to the production and provision of tourism services. It is then extended conceptually by linking existing benchmarking methodologies [12]: national sustainability assessment, national sustainability assessment and sustainability, technical capability, communication problems, and the relationship between the inherent knowledge gap in the indicator developer community and its theoretical limitations. Drawing on the literature on public policy, this paper outlines a framework for investigating the behavior of the indicator system in the policy process according to utilization [13]. The purpose of this paper is to quantitatively evaluate the land use intensity of different industrial enterprises, so as to put forward relevant suggestions on the adjustment of industrial structure and the improvement of land use intensity to the evaluation of Kunshan. Statistical analysis and the Delphi method are adopted. The conclusion is that the industrial structure should be readjusted according to the comprehensive index system of land use intensity and resource consumption level of different industrial enterprises [14]. The author constructs the evaluation index system of AHP. The system reflects various aspects and can be used in practice. Through this system, interactive development in China in 2000 is evaluated by using the correlation degree of the comprehensive evaluation index. The evaluation results reveal the real situation of the transfer of this factor between urban and rural systems and show the development level of their interaction. The correlation degree is a quantitative study of urban-rural interaction [15]. In the introduction of the paper, the application scenarios of fuzzy decision models are described in detail. However, the above research applies to teaching, personnel training, policy guidance, and resource allocation. It is of great significance to analyze and apply the architecture of red cultural resources. This application scenario has a certain degree of innovation, and only under the condition of characteristics can it be of great value to the study of this scenario.

2. Overview of Red Cultural Resources

2.1. Definition of the Concept of Red Cultural Resources. First of all, red culture is an important part and a main source of Chinese good culture. From this point of view, red culture is driven by Marxism, attracting and integrating advancements, and integrating ancient and modern China. Secondly, from a practical point of view, the new-democratic revolution played an important role in the emergence of red culture and laid a foundation for its birth and development. Thirdly, from the perspective of the role of red culture as a part of progressive culture, it has played a role in developing traditional red culture from each stage of the Chinese socialist revolution, creating solutions and determining culture. To sum up, we can regard red culture as under the guidance of Marxism and the policy of the Communist Party of China to lead culture, learn from the success of foreign advancements, and guide socialist culture with Chinese characteristics which is an advanced culture of social culture with Chinese characteristics.

2.2. Functions of Red Cultural Resources

2.2.1. Incentive Function. The Premier proposed that China is a country full of heroes on the occasion of the 70th anniversary of the Chinese people. We should support heroes, learn from heroes, and gather outstanding strength. "The revolutionary tradition is a mixture of Chinese Marxism and traditional tradition, and it is a different culture developed in the process of creating and transforming the ruling culture." This unique culture not only highlights Chinese characteristics but also encourages all Chinese sons and daughters to go forward and act bravely. The red spirit is the core of the red culture, which was gradually established in the fight against imperialism and other conflicts in order to gain independence, liberate the people, realize national rejuvenation and prosperity, and carry out the revolutionary struggle and practice. These together constitute the center of the red cultural spirit. The red cultural spirit of each era is the great conscience of the Chinese people in different periods. It is the process of changing the times and inspiring the next generation. Starting from the national era, we must inherit the past, seek truth from facts, not be afraid of trouble and danger, and be brave in redemption. These spirits can not only help people establish their ideals and beliefs but also deepen their understanding of the Party and the country and improve their understanding of the existing culture and ideology in Chinese society.

2.2.2. Directional Function. As an important part of Chinese cultural elite, red culture plays an important key value and educational role in China's scientific and cultural practice movement. Therefore, it is applied to the education of ideological and political classes to strengthen Marxist belief and communism. In addition to political-oriented work, there are also ideological functions of red cultural resources. The resources of red culture are the products of a certain era,

which contain rich precious significance and rich spiritual treasures, and can penetrate into the education adapted to values. Leaders of different cultures discuss ideological development, political parties, individuals, and cultures in schools; seek truth and must be pragmatic in schools; and cultivate their values and cultivate trust, which is not ideal patriotism. It provides a good revolutionary spirit for the communist sacrifice spirit and a good foundation for the socialist cause to replace the sacrificial communist spirit.

2.2.3. Demonstration Functionality.

Cultural quality of the student, especially that of advanced culture, influences the student's quality. Red culture criticism inherits Chinese traditional culture, is an advanced and mainstream culture that is gradually formed, and improves national quality. The national spirit and revolutionary spirit carried by the red culture are in line with the fundamental task of the Lideshu people. Ideological and political classes can make red cultural resources to educate students on national self-esteem, cultural awareness, cultural self-confidence, social responsibility, and sense of hardship. By introducing red cultural resources, students can understand the pioneering spirit of revolutionary martyrs who save the motherland from insult and aggression, are not afraid of sacrifice, and are brave in innovation for the prosperity of the motherland. We make full use of the model method, take red stories as teaching materials, take red historical sites as practical teaching bases, and take heroic deeds of revolutionary ancestors as models to stimulate students to learn red culture, feel the red spirit, spread red thoughts, and inherit and carry forward the red quality. In the process of understanding and mastering the red culture, we let students show the responsibilities of teenagers in the new period and try their best to serve, contribute, and give back to the society.

2.3. Embodiment of Red Cultural Resources in Ideological and Political Work

2.3.1. Advantages of Red Culture to Ideological and Political Education.

The culture has finally condensed into a representative culture with Chinese characteristics; the rich spiritual and cultural connotation hidden in the red culture can add vitality to education. Integrating the red culture into teaching in China is conducive to the expansion of classroom cultural content of ideological and political education and the continuation of red culture in China. It sets up students' aspirations, strengthens their cultural confidence, and guides them to go forward bravely for the modernization of our country. As a precious and indispensable educational material, the current red cultural material has been widely used in ideological and political education. First, the red culture creates a strong red cultural atmosphere for the ideological and political classroom. Secondly, there are revolutionary cases in the red culture. Introducing these cases into the classroom enables students to analyze the red spirit and understand the spirit of reform through these red culture education cases, further forming spiritual and cultural resonance, enhancing their mastery of the history of red culture in China, and realizing the inheritance of red culture. Third, he red culture shows rich spiritual ideas. Introducing it realizes the inheritance of advanced culture in

different time and space, helps to inspire contemporary students' ideological and political practice, and improves their ideological cognition with the spirit of red culture.

2.3.2. Historical Remains.

The red cultural resources of historical relics include the old revolutionary base areas. In the exploration of the revolutionary road, Comrade Mao Zedong gradually established the important thought of armed division of workers and peasants, established revolutionary villages near villages and cities, and seized political power by force, which also determined that some rural areas and remote mountainous areas in China became "rich producing areas" of revolutionary base areas in red cultural resources, as shown in Figures 1 and 2. The site refers to the remains of human activities, which belongs to the concept of archaeology and is characterized by incomplete remnants. Being the result of the revolutionary struggle of Chinese people led by the Communist Party of China, therefore, the relics and sites in the red cultural resources are mainly the places where the revolutionary wars, revolutionary events, and activities of great significance took place during the Agrarian Revolution, and the Liberation War after the May Fourth Movement; the door of the new-democratic revolution opened and the Chinese proletariat stepped onto the political stage.

2.3.3. Places of Remembrance.

Memorial places in red material cultural resources include cemeteries, memorial halls, and other memorial places. The memorial hall contains precious cultural relics such as articles used by revolutionary ancestors before their death, manuscripts written, and remains from activities to display major revolutionary historical events. Through sound, light, electricity, pictures, physical sculptures, exhibition boards, and scenes, historical figures and events are vividly reproduced, so that visitors can deeply understand and know the life stories of revolutionary ancestors and revolutionary events of great significance and far-reaching influence. In the red cultural resources, in order to commemorate major historical events and cherish the memory of heroic revolutionary ancestors, besides cemeteries and memorial halls, there are also squares, parks, reliefs, memorial towers, and museums. These memorial places can be transformed into effective sources red culture, as shown in Figures 3 and 4.

3. Construction of Fuzzy Judgment Index System

3.1. Corresponding Relationship between Index System and Judgment Result.

The generalized theory and index system $S = (U, A, V, f)$ are used, so as to reflect the corresponding relationship between the index value of the judging object and the judging result. If by $A - a_i$ for the same number of exponents, the minimum extraction value of the decision function can be calculated, $S = (U, A, V, f)$ is an information system, $R = C \cup D$ is a collection of attributes, a subset $C = \{a_i | i = 1, 2, \cdots, m\}$ and $D = \{d\}$ are conditional attribute sets, and their elements are as follows: element m is a set of all attributes that can distinguish objects i and j, but if i and j belong to the same decision class, the values of elements in the matrix are empty sets. The discernibility matrix is an n
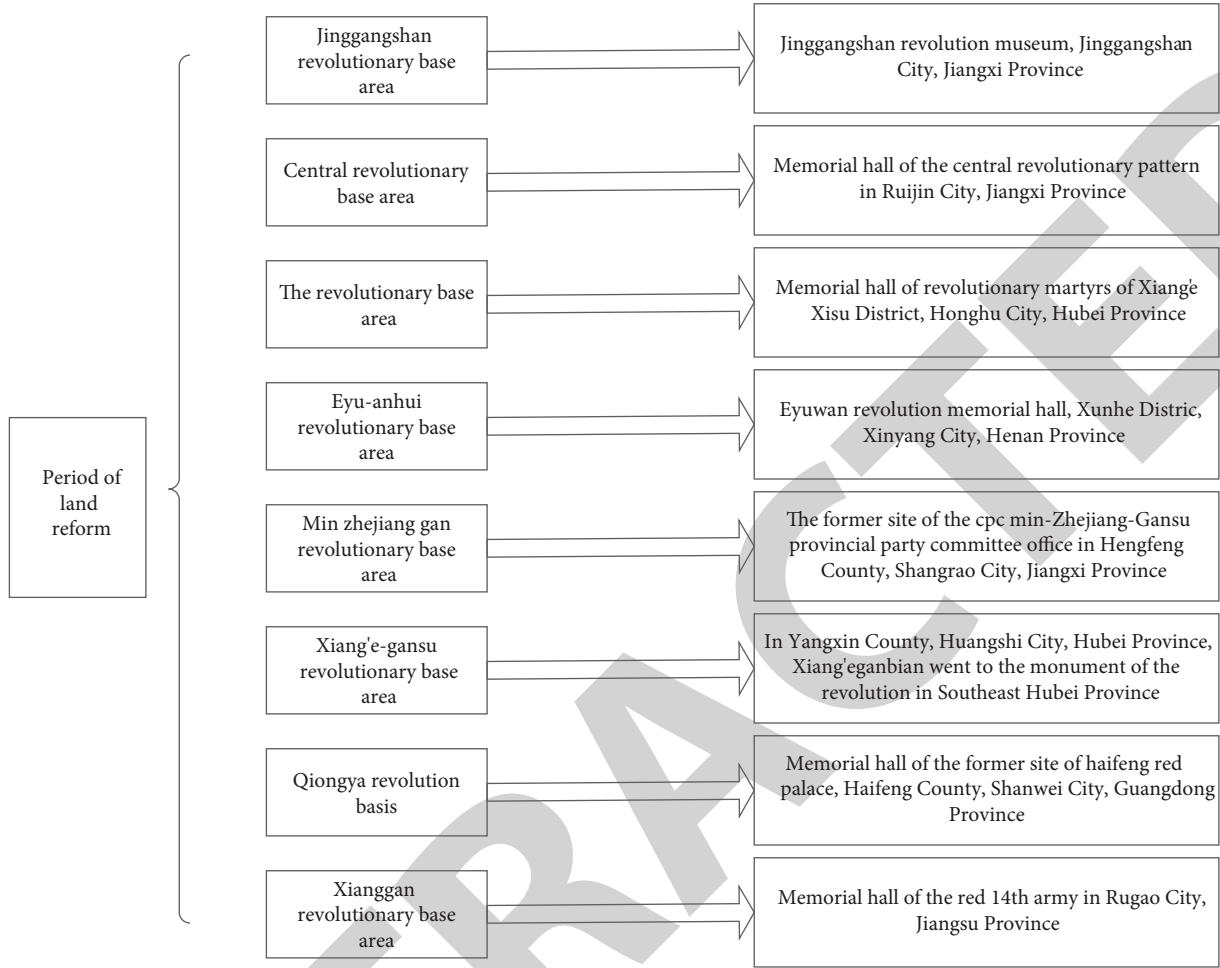
Figure 1: The ruins of the revolutionary base area opened during the revolutionary period.

-order square matrix which is symmetrical according to the main diagonal. When the discernibility matrix is operated, only the upper triangle (or lower triangle) of the discernibility matrix needs to be considered.

$$m_{ij} = \begin{cases} a_k \in C, a_k(x_j) \wedge D(x_i) \neq D(x_j), \\ \varphi, D(x_i) = D(x_j), \end{cases} i, j = 1, 2,. \cdots n.$$

$$(1)$$

3.2. Screening Method for Judging the Positive Index System.
Firstly, the index system is forward, and the forward expression of the inverse index is

$$x_{ij} = \frac{1}{x_{ij}}, \quad i, j = 1, 2, \cdots n. \tag{2}$$

The positive formula of moderate index system is

$$x_{ij} = \frac{1}{|x_{ij} - k|}. \tag{3}$$

Then, the index system is standardized. The value greater than the variogram is represented by 1, and the value less than the variogram is represented by 0. The specific expression is as follows:

$$y = \frac{x_{ij} - \min x_{ij}}{\max x_{ij} - \min x_{ij}}, \quad i, j = 1, 2, \cdots, n. \tag{4}$$

The coefficient of variation formula is

$$v_j = \frac{s_j}{y_j}, \quad j = 1, 2, \cdots, n, \tag{5}$$

where

$$s_j = \sqrt{\frac{1}{n-1} \sum_{i-1}^{n} \left(y_{ij} - \overline{y}_j \right)^2}, \tag{6}$$
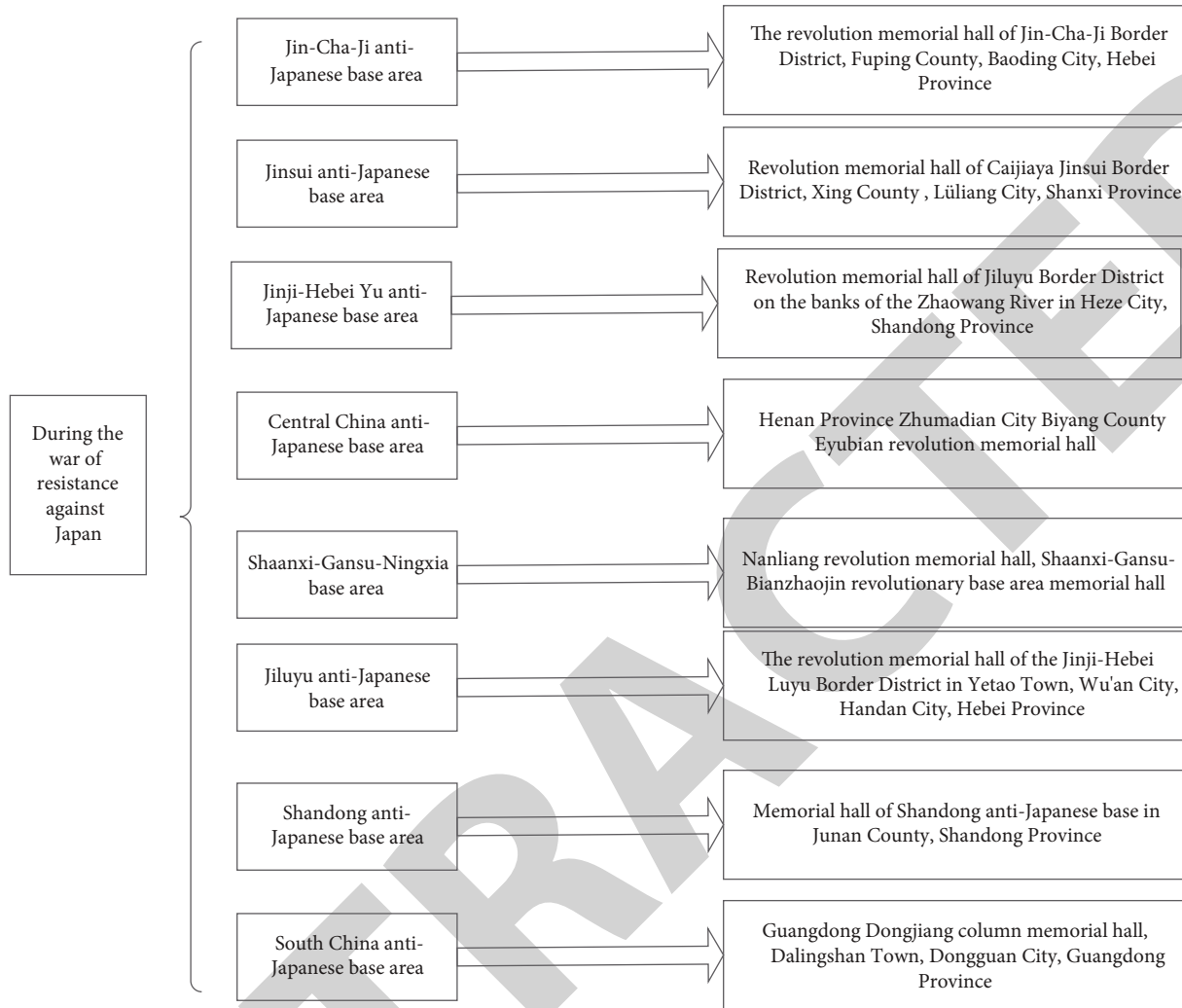
FIGURE 2: The ruins of the revolutionary base area opened during the War of Resistance Against Japan.

$$\bar{y} = \frac{1}{n} \sum_{i-1}^{n} y_{ij}. \tag{7}$$

3.3. Classification of Decision Methods

3.3.1. Rank Sum Ratio Determination Method. The rank sum ratio judgment method is a statistic combining multiple indexes. The RSR judgment value of RSR evaluates the quality of the object directly or in grading order, so as to make a comprehensive evaluation of the object. The importance of each evaluation index in the value is the same. In this paper, because of the different weights of each index, the weighted rank sum ratio is calculated for classification and sorting. First of all, rank should be compiled: it is a combination of multiple indicators and has continuous variables. First, taking M, the determined object of ranking index, as the original data, record N rows of judgments on each index, in which the positive index is the downward index from small to large, and data is equivalent to the average ranking. Because of the different weights of each index, this paper

uses weight and ratio to calculate. The specific formula is

$$WRSR_i = \frac{1}{n} \sum_{j=1}^{m} W_j R_{ij}, \quad i = 1, 2, \cdots n. \tag{8}$$

M is the specific evaluation indexes in the formula, and N is the specific evaluation indexes in the formula. W represents the weight, which is the ranking on the index. Then, the average rank can be obtained through the calculation of the above formula, and the corresponding estimated value can be calculated by transforming it into a linear regression equation, and finally, the ranking is carried out.

3.3.2. Method for Determining the Composite Index. The comprehensive index judgment method is to estimate the index growth scale, the long-term change trend, and the influence degree of various factors to determine the combined index. Calculate the total qualitative index and the single index of each subscript, and the specific formula is
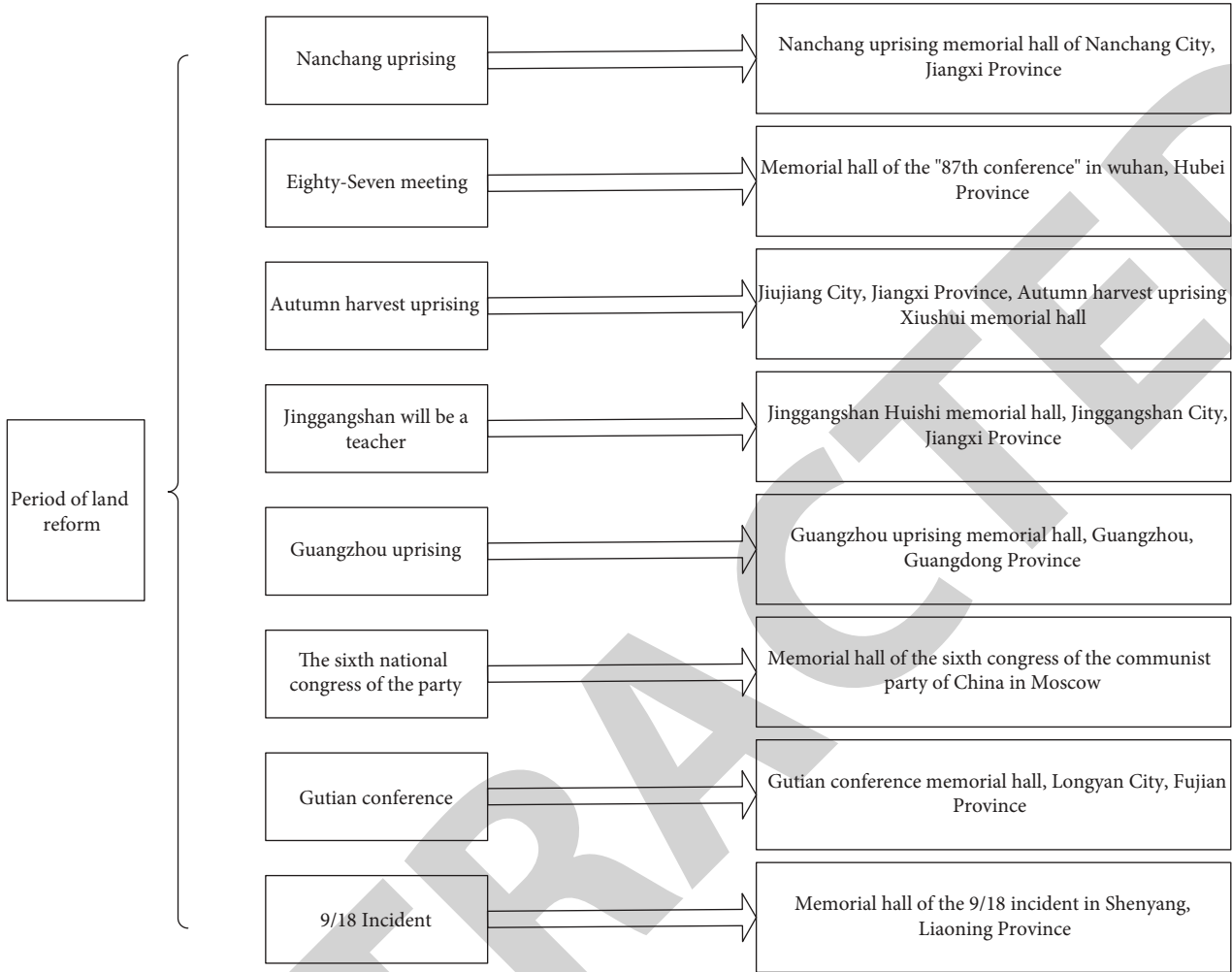
Figure 3: Representative cemeteries and memorial halls during the land reform period.

$$K = \sum_{i=1}^{t} W_{\bar{i}}. \tag{9}$$

The horizontal classification index formula is

$$K_j \frac{\sum_{i=1}^{t_j} W_{\bar{i}}}{\sum_{i=1}^{t_j} W_i}, \tag{10}$$

where T is the indicators, W is each indicator, i is the evaluation value of each indicator, and T is the number of indicators contained in the J-th subsystem. Finally, the total index K is calculated as the total index of high-quality development level, and the classification index K reflects the completion of each subsystem of high-quality development level.

Through the above formula, we calculate the functional relationship between the total index and the classification index. The specific formula is

$$K = \sum_{i=1}^{t} W_i = \sum_{t_j=1}^{v} \sum_{i=1}^{t_j} W_i = \sum_{t_j=1}^{v} \sum_{i=1}^{t_j} W_i \frac{\sum_{i=1}^{t_j} W_i}{\sum_{i=1}^{t_j} W_i} = \sum_{j=1}^{n} \gamma_j K_j. \tag{11}$$

Then, we can get the change relationship between the total index and the classification index. The formula is

$$\Delta K = \sum_n \gamma_j \Delta K_j. \tag{12}$$

Finally, the contribution rate of the classification index to total index can be obtained by dividing the above two formulas. The specific expression formula is

$$\Phi_j = \frac{\gamma_j \Delta K_j}{\Delta K}. \tag{13}$$

3.3.3. Analytic Hierarchy Process. The evaluation index system needs to analyze the importance of each level, and the
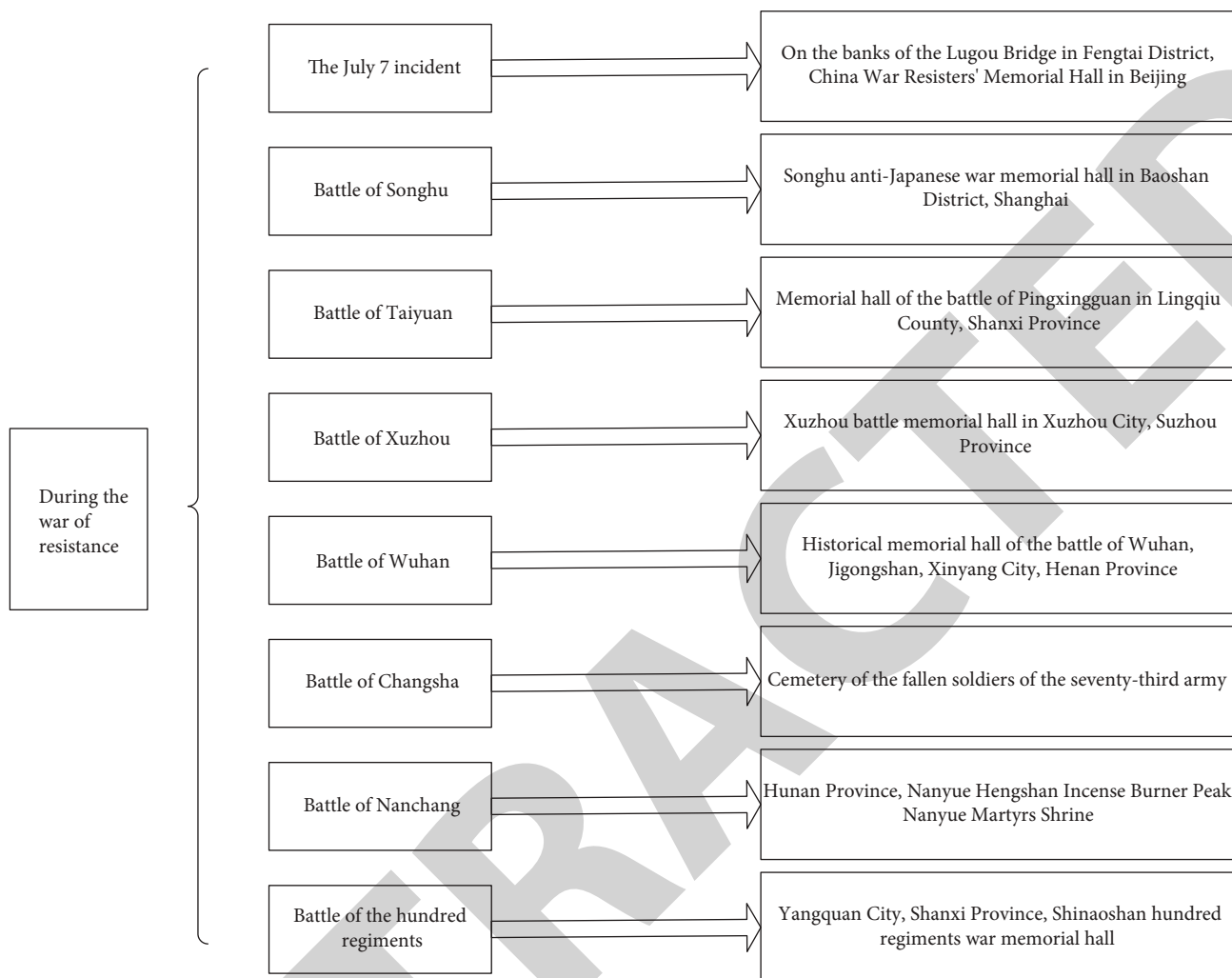
Figure 4: Representative cemeteries and memorial halls during the Anti-Japanese War.

Table 1: Standardized data of the indicator system.

Year	$E(1)$	$E(2)$	$E(3)$	$E(4)$	$E(5)$	$E(6)$	$E(7)$	$E(8)$	$E(9)$	$E(10)$
2000	0.58	0.94	0.75	0.52	0.76	0.34	0.46	0.68	0.65	0.36
2001	0.62	0.93	0.74	0.43	0.73	0.26	0.45	0.72	0.62	0.48
2002	0.78	0.94	0.74	0.47	0.72	0.49	0.55	0.74	0.63	0.41
2003	0.92	1.02	0.73	0.38	0.69	0.42	0.54	0.78	0.68	1.41
2004	0.94	0.94	0.73	0.34	0.67	0.43	0.56	0.82	0.73	2.41
2005	0.96	0.91	0.73	0.35	0.65	0.45	0.59	0.92	0.77	3.41
2006	0.97	0.81	0.62	0.31	0.62	0.45	0.34	0.92	0.83	4.41
2007	0.98	0.78	0.66	0.31	0.59	0.44	0.59	0.97	0.89	5.41
2008	0.99	0.78	0.66	0.28	0.57	0.45	0.59	0.96	0.95	6.41
2009	0.99	0.78	0.71	0.29	0.55	0.46	0.62	0.96	0.97	0.98
2010	0.97	0.73	0.71	0.23	0.68	0.48	0.64	0.97	0.97	0.91

TABLE 2: Data model of the indicator system.

Year	ES(1)	ES(2)	ES(3)	ES(4)	ES(5)	ES(6)	ES(7)	ES(8)	ES(9)
2000	0.36	0.61	0.69	0.48	0.52	0.97	0.59	0.76	0.98
2001	0.49	0.63	0.71	0.52	0.54	0.88	0.52	0.66	0.96
2002	0.44	0.65	0.71	0.54	0.57	0.84	0.56	0.44	0.94
2003	0.49	0.79	0.72	0.57	0.65	0.84	0.65	0.52	0.96
2004	0.55	0.77	0.79	0.65	0.75	0.85	0.75	0.55	0.96
2005	0.59	0.89	0.81	0.75	0.76	0.88	0.77	0.66	0.96
2006	0.67	0.83	0.85	0.76	0.75	0.88	0.81	0.71	0.95
2007	0.77	0.88	0.81	0.89	0.84	0.92	0.84	0.71	0.95
2008	0.89	0.91	0.93	0.84	0.93	0.94	0.88	0.73	0.95
2009	0.89	0.97	0.81	0.93	0.92	0.75	0.92	0.76	0.96
2010	0.97	0.89	0.98	0.98	0.98	0.98	1.02	0.88	0.81

TABLE 3: Correlation coefficients for each indicator.

Year	E(1)	E(2)	E(3)	E(4)	E(5)	E(6)	E(7)
E(1)	1	0.37	0.24	0.21	0.44	0.55	0.14
E(2)	0.29	1	0.66	0.15	0.04	0.41	0.17
E(3)	-0.17	0.21	1	0.66	0.14	0.29	0.34
E(4)	0.11	0.12	-0.32	1	0.25	0.17	0.29
E(5)	0.04	-0.26	0.22	-0.03	1	0.51	0.44
E(6)	0.15	0.03	-0.37	0.06	0.28	1	0.28
E(7)	-0.75	-0.15	-0.09	-0.43	-0.44	0.21	1

specific allocation steps are as follows: The most important thing in the hierarchical model is to determine the hierarchy first. Hierarchy includes goal hierarchy, reference hierarchy, and measurement hierarchy. It can be seen from the above that according to the judgment of each evaluation index, which is specifically expressed as follows:

$$D = \begin{pmatrix} D_{11} & D_{12} & D_{13} \\ D_{21} & D_{22} & D_{23} \\ D_{n1} & D_{n2} & D_{n3} \end{pmatrix}. \tag{14}$$

Among them $D_{ij} > 0$, $D_{ij} = 1$, $D_{ij} = 1/D_{ij}$.

Step 1: it is to calculate the weight of each index of the criterion layer by using the above formula, and the calculation formula is as follows:

$$E_i = \prod_{i=1}^{n} D_{ij}. \tag{15}$$

Step 2: the index vectors are uniformly processed to obtain the weight vectors of each index system, and the calculation formula is as follows:

$$F_i = \sqrt[n]{E_i}. \tag{16}$$

Step 3: the column vectors are normalized to obtain weight vectors G_i, and the formula is

$$G_i = \frac{F_j}{\sum_{j=1}^{n} F_j}. \tag{17}$$

Step 4: the consistency test is obtained by using the judgment method, in which the maximum root can be expressed, and the specific formula is

$$\lambda_{\max} = \frac{1}{n} \sum_{i=1}^{n} \frac{(DG)_i}{G_i}. \tag{18}$$

3.4. Calculation of Weight of Index System. The objective weighting method is mainly the entropy method. The entropy method represents the dispersion of index system data, and coefficient of variation rules mainly use the standard dispersion of index data to determine the importance of the index system. Therefore, the entropy method and method weighting complement each other's advantages and disadvantages to obtain the same weight as the index system. The specific ormula is

$$w_j = \frac{(\delta_j + e_j) \sum_{i=1}^{n} (1 - r_{ij})}{\sum_{j=1}^{m} (\delta_j + e_j) \sum_{i=1}^{n} (1 - r_{ij})}. \tag{19}$$

This is the first step of the index system, then derive each inverse index, and then forward the index to calculate the proportion of the index system. The formula is

$$P_{ij} = \frac{X_{ij}}{\sum_{i=1}^{n} X_{ij}}. \tag{20}$$

Finally, the entropy value of the index of the first item is obtained, and the calculation formula is as follows:

$$e_j = -k \sum_{i=1}^{m} P_{ij \ln} (p_{ij}). \tag{21}$$

TABLE 4: Determination of the weights of each indicator.

Level 1 indicators	Secondary indicators	Secondary indicator synthesis weights	Symbolic representation	Three-level indicators	Three-level indicator synthesis weight
Microscopic level	Quality change	0.09	X1	0.75	0.074
		0.09	X2	0.25	0.027
		0.06	X3	0.36	0.025
	Efficiency change	0.06	X4	0.21	0.012
		0.06	X5	0.15	0.006
		0.06	X6	0.19	0.009
		0.06	X7	0.15	0.015

- ■ Very necessary
- ■ It is necessary
- ■ Not necessarily
- ■ Not necessarily at all
- ■ So so
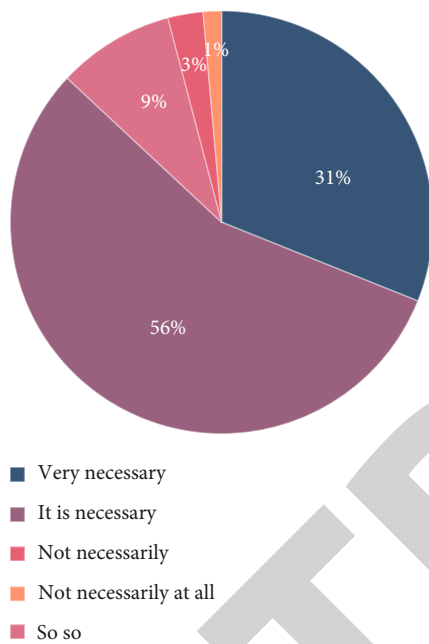
FIGURE 5: Whether red culture is necessary to integrate into ideological education (students).

Among them,

$$\mathrm{cov}\left(X_i, X_j\right) = E((X_i - E(X_i)))\left(\left(X_j - E(X_j)\right)\right). \tag{22}$$

The third step is to calculate the standard deviation of the index system δ_j, and the calculation formula is

$$\delta_j = \sqrt{\frac{1}{n}\sum_{i=1}^{n}\left(x_{ij} - \overline{x_j}\right)^2}, \tag{23}$$

where the weight formula is

$$W = \sum_{j-1}^{i} x_j W_{ij}. \tag{24}$$

4. Construction of Ideological and Political Index System of Red Culture

4.1. Construction of Index System

4.1.1. Standardization of the Determination of the Indicator System. In different fields of ideological and political index system construction, such as red culture, international organizations and institutions have developed framework system models with their own characteristics. Among them, some people put forward the correlation coefficient framework of the index system, divided the middle state module into many sections, and expounded a dynamic and feedback control decision-making approach. On this basis, the ideological and political red cultural indicators are divided into many systems. The data can be substituted into the data standardization formula. In this paper, the subjective and objective weighting methods of actual data are used to determine the coefficient. Although the subjective empowerment method has the advantages of intuition and simplicity, in the process of empowerment, it mainly relies on its own judgment and is divorced from the actual data, which easily leads to subjective preferences; on the contrary, it does not consider the profession. However, it ignores that the actual measurement. Subjective weighting adopts the analytic hierarchy process, and objective weighting adopts the entropy method and method fusion to determine correlation coefficient. and the data standardization results are shown in Tables 1 and 2.

Whether the construction of the evaluation index system is reasonable or not will directly affect the correctness and scientificity of comprehensive evaluation results. Therefore, in order to construct a comprehensive and systematic reflection index system, we must follow the principles of systematicness, scientificity, data availability, quantification, and dynamics in the process of construction. Therefore, we need to design the judgment index system on different bases to make the research conform to the law.

4.1.2. Calculating the Correlation Coefficient of the Indicator System. After the data of correlation system is standardized, the correlation coefficient of the index system is calculated in the unit of the criterion layer. Taking the criterion layer as an example, the correlation coefficient between each index system can be seen from the correlation analysis principle: the absolute value of the correlation coefficient reflects the
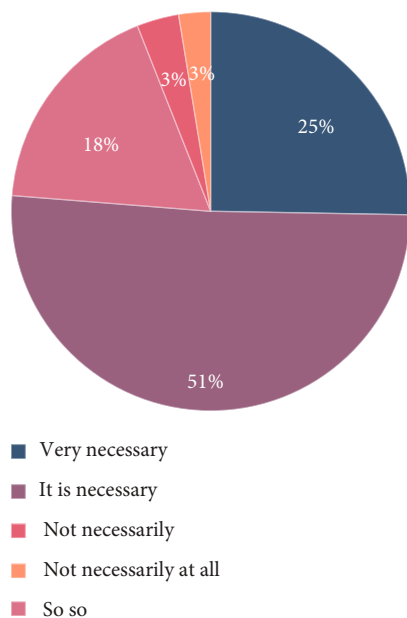
Figure 6: Whether red culture is necessary to integrate into ideological education (teachers).

independence or dependence of the two indexes as shown in Table 3.

4.1.3. Determination of Indicators. According to the number of index samples and the significance level, if the correlation coefficient is greater, the coefficient with the larger correlation coefficient will be removed. On the contrary, it is reserved. Among them, it can be seen from Table 4 that the correlation coefficient between indicators in the criterion layer is higher than that of indicators, which is a high-frequency indicator and can better reflect the situation. Therefore, keep $E(1)$ and delete $E(7)$. The deletion and retention of other criterion layer indicators follow this principle. After correlation analysis, delete the indicators with strong correlation. The importance of each index is different, and it will have different weights, which can accurately reflect the correlation coefficient of indicators in the whole index system. Weight is an important content of judging the index system. Each index will be different in the overall index system; then, we need to use the weight to determine the index system; in the construction of the index system is the need for accurate weight to establish a reasonable index weight, as shown in Table 4.

4.2. The Initiative Consciousness of Integrating Red Culture into Ideological and Political Education Has Been Significantly Enhanced. The important position of ideological and political education in colleges and universities plays an important role in educating people. By insisting on bringing red culture into the survey data of ideological and political education, college students' knowledge and understanding of red culture have been greatly improved. Among the 969 valid questionnaires conducted by people, 77.41% think that red culture has development value. On "Is it necessary for red culture to integrate into ideological education?", college teachers and administrators replied that the proportion is 31.07%, more than 55.89%,

generally 8.95%, and unnecessary 2.69%. It does not need to account for 1.41% at all; 25.28% thought it necessary, and 50.98% thought it necessary. Generally, it is 17.75%, unnecessary 3.41%, and completely redundant 2.56%. It can be seen that due to the promotion of the policies of the state, college teachers and students have greatly improved their understanding and grasp of the integration, as shown in Figures 5 and 6.

4.3. Red Culture Is Gradually Integrated into Ideological and Political Education. Ideological and political work develops with the development of the times and the changes of realistic needs. The material value and spiritual value contained in the rich red culture, whether in the revolutionary period, or in the period of socialism with Chinese characteristics, and even in the future, provide fresh materials for archival education in colleges and universities. Materials are important resources for strengthening ideological and political education. It provides powerful historical materials and bright red stories for the ideals and beliefs of universities and the important contents of hard work. Colleges and universities learn and educate the Party's historical red culture through various ways, improve theoretical literacy, and build teachers' and students' feelings. The results of "Investigation on the Significance of Ideological and Political Education in Colleges and Universities by Using Red Culture" show that college students generally believe that red culture education is conducive to carrying forward patriotism, remembering history, strengthening faith, carrying forward fine traditions, and enhancing personality. Red culture is generally conducive to the education of patriotic ideals and beliefs, hard work spirit, and core values. It shows that in the process of integrating into red culture, colleges and universities should not only tap the rich connotation and value of red culture itself but also keep pace with the times, adapt to the situation, and find red genes based on current practice. At the same time, red culture should be added to ideological and political education to enhance students' patriotic feelings, as shown in Figures 7 and 8.

4.4. Red Culture Is Integrated into Ideological and Political Education. The concept of ideological and political work develops gradually from formation and development to perfection. With the tracking of the times and the deepening of research, the methods of education have also changed from traditional theories to diversification, which makes the red culture more and more diversified and rich into the ways, and promotes the educational reform from the aspects of traditional classroom teaching, practical teaching, student management, and cultural construction. Red cultural resources are the goal of how to implement ideological and political education in the process of integration. The investigation shows that red culture formed multiple channels. Diversified trend, online forum education, and red practice education are becoming more and more popular. Through the questionnaire survey of students, the methods of classroom teaching, special lectures, practical education, party and group activities, network propaganda, extracurricular cultural propaganda, autonomous learning, etc. adopted by universities and desertification schools are made clear, and the specific teaching, practical education, and ideological and cultural integration are made clear. In an
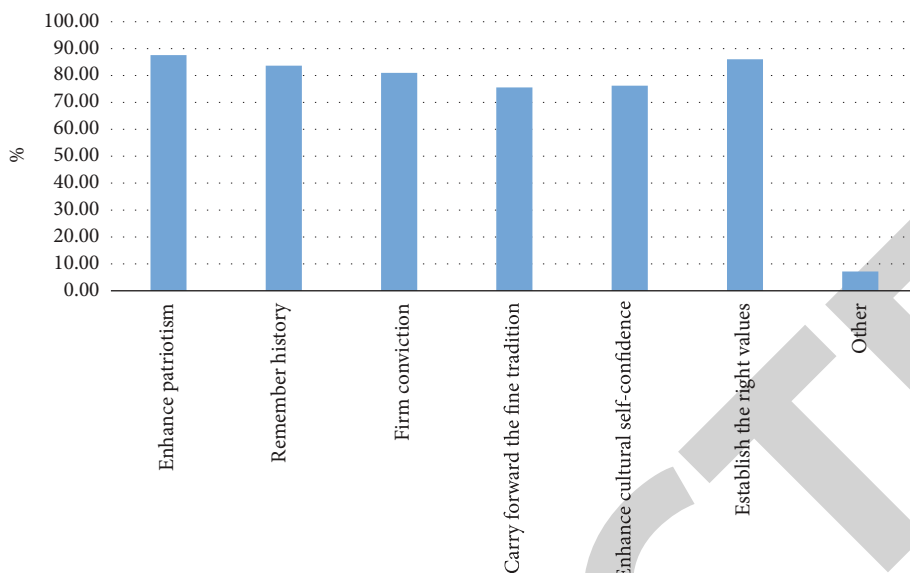
Figure 7: The significance of red culture to ideological and political education in colleges and universities (students).
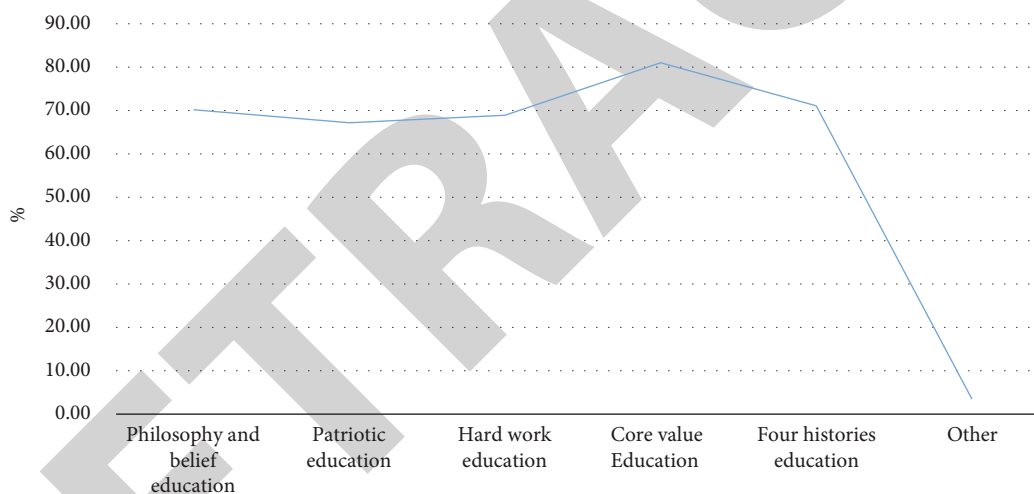
Figure 8: The application of red culture in ideological and political education (faculty).

interview with the school, a group of university teachers said, "At present, the school continues to spread the value and spirit of red culture through ideological and political classes or special lectures, organizes teachers and students to carry out red education bases from time to time, attaches great importance to red culture education, explores organizing campus cultural activities as much as possible, and promotes and actively promotes red positive energy and spirit," as shown in Figure 9.

4.5. The Integration of Red Culture into Ideological and Political Education Is Basically Established. In the ideological and political education in colleges and universities, there are many ideological and political behaviors of working teams, ideological and political educators, counselors, psychological teachers, teachers, students, societies, and college students. Red culture is a high-quality resource of ideological and political education in colleges and universities. Many col-

leges and universities can consciously strengthen the importance of red culture in moral education, set up educational activities in a timely manner, and enrich ideological and political education in colleges and universities. According to the survey data of "whether there is a perfect red culture education model," 25.32% have been established and the effect is good, and 21.48% have been established and the effect is not good. The initial construction was 34.91%, the number of people who did not complete the plan was 15.73%, and the proportion of people who did not plan was 2.56%. The integration of red culture into the system has led to the research on the effect of cultural education. The research on the effect of culture teaching shows that there is more and more network teaching in colleges and universities, forming a recessive teaching mode, which is carried out in terms of educational culture courses, educational goals and ways, etc. In addition, with the rise of the Internet, information network and cyberspace have become
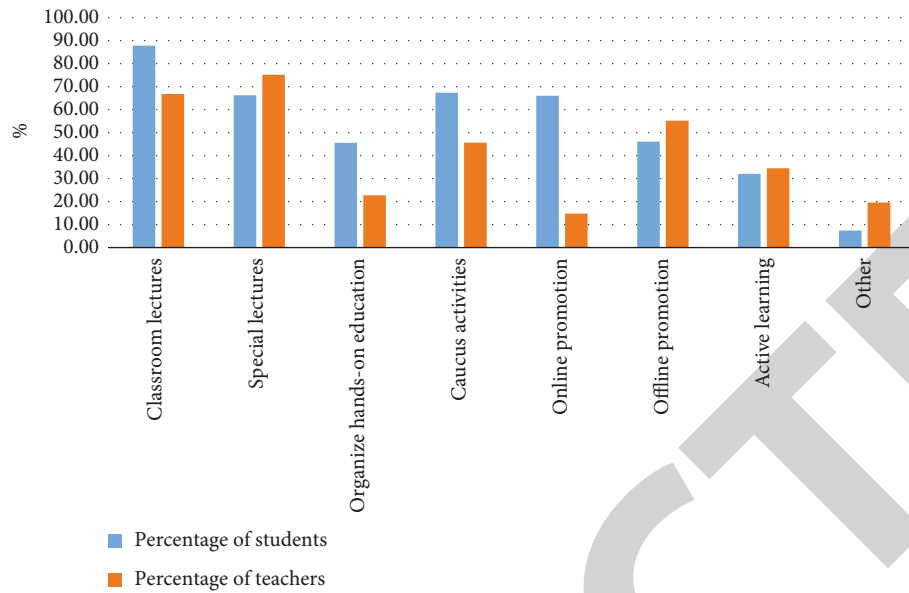
FIGURE 9: Ways for colleges and universities to carry out red culture education.
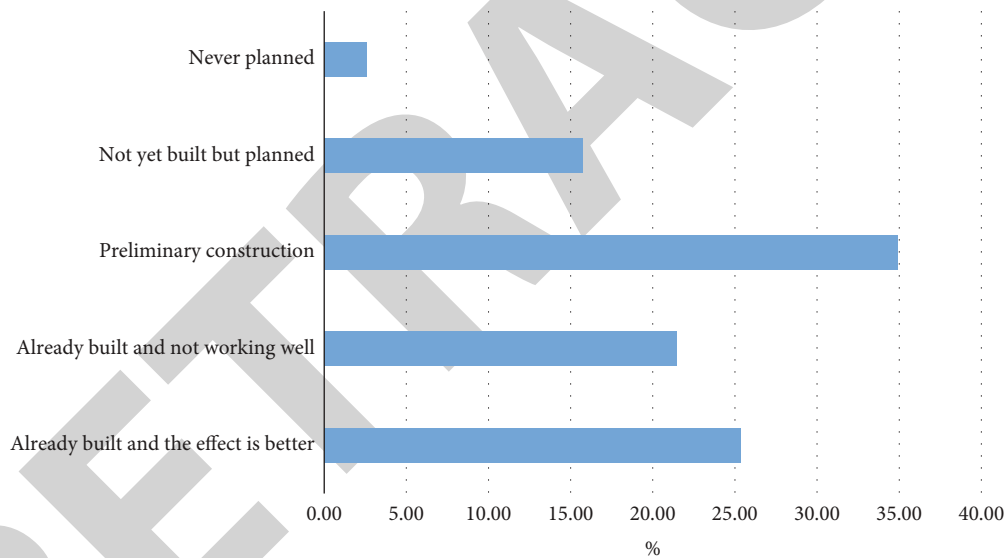
FIGURE 10: Whether there is a perfect red culture education model.

important tools for information collection, and the mode of communication has been developed and continuously expanded in ideological and political education. It is convenient to use, and the new network culture is open to red. The survey results are shown in Figure 10.

5. Concluding Remarks

This paper analyzes the evaluation index system and judgment methods, based on the ideological and political education of red cultural resources, according to its culture as the basis of the index system design principles, research, and use of relevant judgment methods and index system. Through the study of judgment methods and the index system, it is proposed that

red culture is the driving force of cultural development in China. As an important part of construction, its emergence and development are based on social and economic policies. Therefore, we must always keep ideological progress and create red culture while obtaining material satisfaction. At present, the prominent role of cultural soft power makes us put national culture as an important part of construction, and strengthening cultural self-confidence has become inevitable. As a young team of national construction and development, students play a key role in the future. In addition, the progress of society has greatly improved the requirements for the comprehensive quality of college students. It is necessary to strengthen their ideological and political education and improve their comprehensive quality to meet various risks. Starting with the basic

Review Article

WSN Architectures for Environmental Monitoring Applications

Kofi Sarpong Adu-Manu (ID),[1] **Jamal-Deen Abdulai** (ID),[1] **Felicia Engmann** (ID),[2]
Moses Akazue (ID),[1] **Justice Kwame Appati** (ID),[1] **Godwill Enchill Baiden** (ID),[1]
and Godwin Sarfo-Kantanka (ID)[1]

[1]*Department of Computer Science, University of Ghana, Legon, Accra, Ghana*
[2]*School of Technology, Ghana Institute of Management and Public Administration, Accra, Ghana*

Correspondence should be addressed to Kofi Sarpong Adu-Manu; ksadu-manu@ug.edu.gh

Wireless sensor networks (WSNs) have become ubiquitous, permeating every aspect of human life. In environmental monitoring applications (EMAs), WSNs are essential and provide a holistic view of the deployed environment. Physical sensor devices and actuators are connected across a network in environmental monitoring applications to sense vital environmental factors. EMAs bring together the intelligence and autonomy of autonomous systems to make intelligent decisions and communicate them using communication technologies. This paper discusses the various architectures developed for WSNs in environmental monitoring applications and the support for specific design goals, including machine learning in WSNs and its potential in environmental monitoring applications.

1. Introduction

Wireless sensor networks (WSNs) comprise spatially distributed sensor nodes that monitor and record physical environmental conditions [1]. As illustrated in Figure 1, WSNs have practical applications in various domains, including agriculture, water, animal tracking, oceanography, air quality, earthquake/landslide, forest fire, and flood detection. WSNs are self-configuring, infrastructure-free networks that monitor physical or environmental conditions [2]. WSNs can monitor various environmental conditions, including temperature, sound, vibration, acceleration, pressure, motion, humidity, and chemical or pollutant concentrations from the different application domains presented in Figure 1. When deployed in these conditions, WSNs cooperate to transmit data across the network to a central location or sink, from where it can be viewed and analyzed [3]. Wireless sensor nodes can withstand harsh environmental conditions and operate in their deployable environment without human intervention. Wireless sensor nodes can be deployed to cover large geo-

graphical areas, either fixed in place (static deployment) or mobile (dynamic deployment) [4].

EMAs have unique challenges that, if not considered in their deployments, may affect the service quality. For instance, deploying nodes in highly dynamic environments may affect the data collected even for environments with low spatiotemporal variations. Such changes may arise from sudden changes in the weather or close human activities [2, 5]. As such, real-time monitoring of the environment is necessary but without the cost and time needed to achieve even better results when compared to traditional monitoring systems. Conventional monitoring systems use sedimentation, electrostatic sampling, absorption, filtration, and condensation to scan and monitor the soil, air, and water.

Humans, animals, and nonliving things all require a habitat. Human and animal activities harm the environment, lowering people's quality of life. During the last decade, researchers have used wireless sensor devices to automate the monitoring of the environment, ensuring that accurate data is obtained for analysis [4, 6]. For example, sensor nodes monitor air quality to detect and estimate environmental
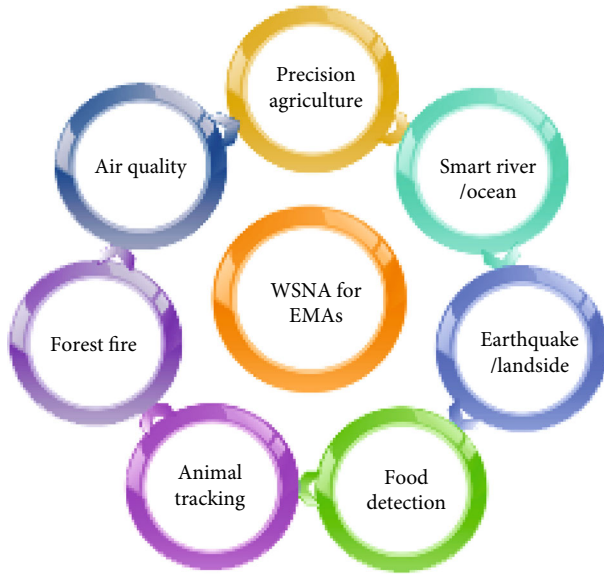
Figure 1: Wireless sensor network application domains.

pollution levels. When soil is observed, it is examined for threats such as biodiversity loss, acidity levels, erosion, and other forms of contamination [7].

Additionally, sensor nodes determine water quality by monitoring physical, chemical, and biological factors [8–10]. Due to WSNs, these monitoring techniques have become practical, simple, and exceptionally reliable. WSNs for EMAs aim to integrate autonomous systems' intelligence and autonomy to make intelligent decisions and communicate them via communication technologies. Hence, some challenges in their implementation include network and communication coverage, energy management and conservation, and data security [11]. Environmental automation allows substantial amounts of data to be collected and transmitted to a central repository via sensor nodes and communication technologies. Water quality monitoring ensures clean and safe water is available for domestic use [11] and clean water bodies for environmental sanitation, disposal, and storage of water [10]. The concept of smart cities powered by green technologies was one of the driving forces behind developing WSN-based EMAs. As a result, it is critical to examine the sensing, network communication, and analysis processes (SNcA). The SNcA operations rely on the underlying WSN architecture's ability to provide the necessary functions, services, and protocols to accomplish the design objectives of the relevant application (R. [12]).

The properties of EMAs that rely on WSNs are depicted in Figure 2. Figure 2 illustrates the communication, deployment, data collection, and energy consumption properties of EMAs. During the operational life of the sensor nodes, the communication group can be classified as broadcast or unicast. WSNs for EMA deployment can occur in either a mobile or static environment. These environments have various characteristics that affect the nodes' lifetime. The environmental data can be collected with high accuracy or with some redundancy. Data collection can also be based on the type of event or traffic generated by the environment. The

energy consumed by sensor node components for sensing, processing, and transmission is significant. WSNs for EMAs have gained popularity in recent years as demand for automation has increased. This growing popularity is because WSNs enable real-time communication, are self-sufficient, and provide intelligent and accurate information. The WSN architecture for EMAs is intended to facilitate the collection, processing, transfer, storage, retrieval, and, in some cases, data management. They provide real-time access to monitoring data, long-term monitoring, and scalability [13]. The type of application that requires WSN affects sensor networks' architecture, scope, and complexity. WSNs used in EMAs are primarily dynamic sensor deployment systems that rely on multi-hop techniques to function correctly. When an environmental application necessitates the deployment of static sensors, point-to-point or single-hop infrastructure is suitable [14].

Additionally, WSNs for EMAs have data collection procedures and energy consumption characteristics. Because data in WSNs is generated from multiple sources, it may be collected accurately or with a certain degree of redundancy. Collecting real-time sensor data enables the accurate representation of current environmental conditions and forecasting of future environmental conditions and threats. Precision agriculture, for example, allows farmers to alter their farming strategies at any time by utilizing real-time data from field-installed sensors. Precision agriculture data will enable farmers to strategize and adjust land management activities accordingly, rather than relying on hypothetical average farmland conditions that may not exist anywhere in real time. In EMAs, data collection depends on either traffic generation or event detection, likely affecting the amount of energy consumed by each sensor node. For example, sensor nodes near a sink rapidly deplete their energy compared to other sensor nodes. Energy is consumed by sensing, processing, and data transmission in WSNs.

When WSN architectures are adopted for deployment in EMAs, they present new opportunities and challenges. For example, introducing machine learning and Internet of Things techniques in WSN for EMAs has associated design challenges requiring new dimensions into algorithm design that impact the network protocol stack. Hence, the researchers must be interested in the sensor node and network architectures, algorithms, and protocol design that support WSNs for EMAs. It is imperative to reconsider the underlying architectures influencing how nodes may be deployed (placement, coverage, and connectivity). Finding novel approaches to maximize the network throughput and lifetime are essential in WSNs for EMAs. It is, therefore, worth considering the various WSN architectures and the environmental characteristics of EMAs in the different application areas.

Given the above, it is essential to specify the architectural requirements for WSNs for EMAs to achieve the design goals and enable continuous environmental monitoring. Hence, this paper presents the state-of-art on wireless sensor networks for environmental monitoring applications. Starting with a description of EMAs, we provide an overview of WSN designs, including hardware and software architectures for EMAs. We
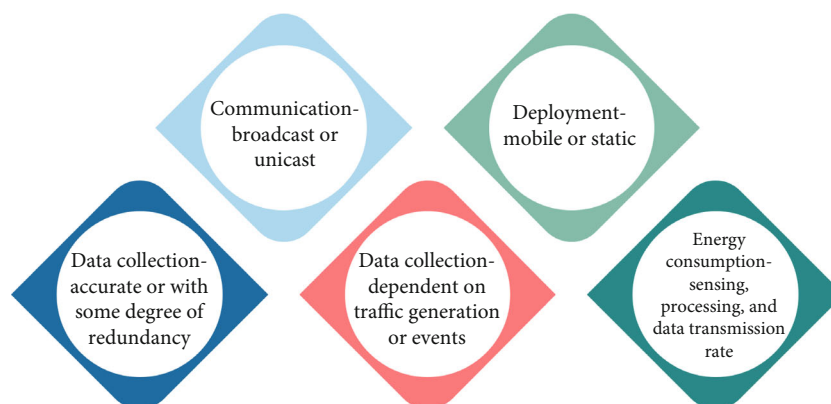
FIGURE 2: Properties of environmental monitoring applications.

then describe the sensor node architecture and present the maximum coverage and connectivity characteristics suitable for the different WSN application environment. In addition, we discuss critical aspects of WSNs for EMAs, including sensor type, sensor node placement, sensor node power consumption, node communication, and remote sensor node control. Finally, the paper discusses current advancements that benefit EMAs, such as machine learning (ML) and the Internet of Things (IoT) and the associated challenges. We present novel approaches for dealing with WSNs for EMAs when monitoring various environmental parameters, considering the different application characteristics. Our work differs from previous review attempts presented in the literature in that it focuses on specific application domains and their underlying algorithms [15–18].

The rest of the paper is organized as follows: Section 2 discusses related works to EMAs. Section 3 presents the wireless sensor node architecture, emphasizing layered and clustered architectures. We describe the suitability of these architectures in EMAs. Section 5 examines sensor node deployment approaches that guarantee EMAs' maximum area coverage and connectivity. Section 5 introduces WSN Applications, concentrating on environmental characteristics and data gathering strategies used in diverse environments. Section 6 discusses current advances in WSNs concerning machine learning and the Internet of Things, relevant simulators, and the underlying operating systems that enable EMA (environmental monitoring applications) architectures. Section 7 concludes the paper by suggesting future research directions.

2. Related Works

EMAs provide a continuous real-time approach to monitoring environmental phenomena using WSNs and IoT (Internet of Things). Traditionally, monitoring the environment involves testing equipment that needs to be checked regularly and reported to a receiving station. However, the monitoring mode is not very efficient due to rapid changes in the weather and other environmental changes that cannot be entirely predicted.

In [10], the authors reviewed the latest works on some implementations of IoT in monitoring water quality param-

eters efficiently and cost-effectively. In their work, an IoT system was developed to test water quality parameters such as pH, conductivity, turbidity, and temperature. The sensor nodes were placed in water, and the ADC and core controller monitored data values read from the cloud. Similar works were done by [19] to measure the pH, conductivity, turbidity, oxidation-reduction, oxygen, and temperature of a moving river in the Greater Accra region of Ghana. The setup included the sensor probes dipped in water connected to a base station placed at a safe place above the water. The base station is connected via a GSM module to cloud storage, from where a web portal visualizes the stream of data produced. In [11], they surveyed current state-of-the-art IoT-enabled WSNs to monitor the water quality parameters for domestic use as safe drinking water. In their paper, they included recommendations for the design of efficient IoT water quality monitoring systems (IoT-WQMS) and a review of contemporary IoT-WQMS.

The authors review current IoT-based water management systems [20]. Their study examined measurement parameters such as pH, turbidity, salinity, and water levels. An architectural design of IoT-based intelligent water management systems with machine learning was proposed but not implemented. Machine learning (ML) tools such as decision trees and support vector machines were implemented as classification algorithms on real data sets obtained from a Tunisian water treatment station [21]. The performance evaluation performed by the authors suggested linear SVM to better classify and detect anomalies in the water distribution network in Tunisia. Other ML classification tools used in water quality applications include the K-nearest neighbor (KNN), single layer, and deep neural networks. Software architectures that combine event processing with remote sensing applications for air quality monitoring using satellite sensors were proposed by [22].

The architecture of the smart water management system considers the controllers and some sensors, and an application is proposed by [20]. Some radios suggested as best for water management systems include LoRa, NB-IoT, Zigbee, and 6lowpan. Hardware and software platforms supporting IoT for EMAs include Arduino, ESP8266, Raspberry Pi, Beagle Bone, Bluetooth, Wi-Fi, RFID, and microcontrollers [9]. Large-scale applications such as unmanned aerial vehicles

(UAVs) and crowdsensing monitoring technologies also use radio and WSN protocols to achieve comprehensive area monitoring [2].

Smart cities have peculiar environmental monitoring concerns such as authentication, data security, device vulnerability, and sustainability. The architecture of smart cities that may support their purposes was considered in these four layers: sensing, transmission, data management, and application [23]. This is similar to our work which considers the WSN architecture of Smart Cities. However, our paper emphasizes the layered and clustered layers in different applications, including smart cities, while [23] view the attributes and possible functions of the layers as mentioned earlier. The layered and clustered architectures highlighted in our paper point to possible EMAs that could be developed under each layer. The work also highlights the general protocols and energy consumption factors these layers and EMAs face. Finally, we discuss the different types of machine learning tools and protocols that can be supported and used in EMAs. To reduce energy consumption in EMAs, our research focuses on potential machine learning tools used in IoTs and the factors influencing their implementation.

3. Wireless Sensor Network Architectures (WSNA)

WSNs enable continuous monitoring of environmental conditions. Sensor nodes comprise WSNs. The sensor node detects and processes the parameters locally or across the network or transfers them to a base station (sink) for processing. For EMAs, the scalability of WSNs is critical. SNA (sensor network architecture) enables the provision of environmental monitoring services. Architecture abstracts physical devices and services from physical manifestations [15]. EMA architectures must be hardware and software agnostic and based on diverse architectures. An animal tracking system may require hardware and software architectures that differ from earthquake monitoring. As a result, the architectures of wireless sensor networks (WSNs) are application-specific (that is, it considers the requirements for the various application domains). When sensor nodes on animals come into contact, pairwise connections allow them to communicate. Static sensor nodes can be installed indoors or outdoors to monitor air quality. The sensor, node, and sensor network architectures are described here. Additionally, the section will discuss OSI-based architectures that are traditional/layered, clustered, and hybrid. Each case is discussed in detail in terms of its EMA suitability.

3.1. Sensor Node Architecture. A wireless sensor network comprises sensor nodes that work together to complete a particular task. Sensor nodes are equipped with components that detect parameters of interest in their immediate environment. Sensing data from a single node can be analyzed and transmitted to another sensor node in the sensor network or a sink. As a result, the sensor node oversees data collection, aggregation, and fusion in a WSN. A wireless sensor node comprises several components: a sensor unit, interface circuitry, a processor, a transceiver system, and a power sup-

ply unit, as depicted in Figure 3. The sensing unit is directly responsible for data collection and environmental interaction, and the computing unit handles data computation, processing, analysis, and storage. The communication unit is in charge of communication between connected sensor nodes and data transmission from sensor nodes to a base station.

The node can communicate with neighboring domains via communication interfaces and wireless links. Additionally, the sensor node's location and positioning information may be provided by a global positioning system (GPS). While it is frequently assumed that all sensor nodes have similar functionality, sensor functionality can be heterogeneous in some cases. The sensor unit is the sensor node architecture component responsible for capturing physical events in the real world. A computing unit handles data processing and aggregation. It comprises an analog to digital converter (which converts analog data to digital), a central processing unit (or microprocessor), memory, protocols, and storage memory.

Additionally, a communication unit comprises a transceiver for data transmission and reception. The transceiver handles the transmission and reception of signals. Finally, a power unit provides power to every component of the sensor node.

3.2. Sensor Network Architecture (SNA). Sensor network architecture (SNA) is used in WSNs. Temperature, humidity, pressure, location, vibration, and sound are all monitored by the wireless SNA nodes. These nodes can perform intelligent detection, neighbor node detection, data processing and storage, data collection, target tracking, monitoring and control, synchronization, node localization, and efficient routing between the base station and nodes in various realtime applications [24]. SNA is developed using the open system interconnection (OSI) model and consists of five layers (physical, data link, network, transport, and application layers). Numerous protocols are being developed to operate at each layer of the SNA. For example, protocols control the transceiver's operation at the physical layer of SNA, and medium access control (MAC) protocols manage channel sharing, timing, and locality at the data link layer. The routing protocols manage networking tasks such as topological and adaptive topology management at the network layer. Transport layer protocols facilitate data dissemination and caching [25]. The sections that follow provide an overview of the layered and clustered architectures. When designing WSNs for EMAs, several design issues must be considered when using the SNA (sensor network architecture). Several of these issues include but are not limited to energy consumption, quality of service (QoS), security, processing, localization, and network design cost. Consumption of energy is critical, as the sensor nodes are battery-powered. Additionally, it is challenging to replace batteries in EMAs.

As a result, the sensor node's sensing, transmission, and computation components must be managed, while the node is operational. Protocols designed efficiently at multiple layers (physical, data link, network, and transport) can significantly reduce the energy consumed by sensor nodes.
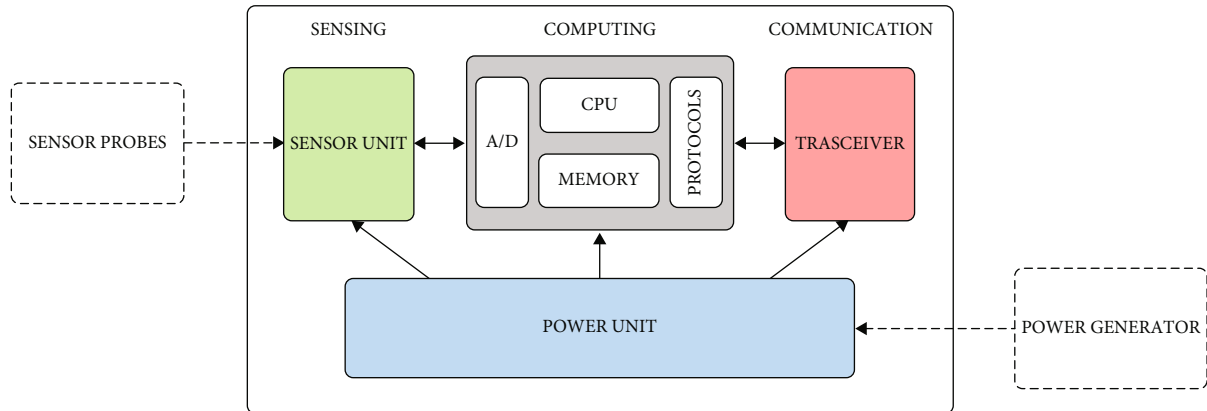
With the quality of service, data is expected to be distributed in real time to enable stakeholders to use it. To effectively detect and report environmental phenomena in EMAs, the nodes should be placed so that they cover a large area within the deployed environment, as illustrated in Figure 4. Sensor nodes in WSNs have a sensing range within which they can detect an event. The sensor node cannot detect events outside of its sensing range. The random placement of nodes may affect coverage and limit sensing of the targeted area. The coverage problem is solved in full sensing coverage because the sensor nodes cover the entire deployable area. This deployment's sensor nodes cover the whole region of interest (see Figure 4(a)). Figure 4(b) shows a similar number of nodes deployed with a sensing limited sensing range that cannot cover most of the deployment area due to the sensor node's shorter sensing range.

Algorithms for coverage have been developed to provide efficient solutions for coverage in WSNs. Three procedures can be modified in SNA to process data sensed by nodes. In-node processing, in-network processing, and data processing at the sink are the data processing techniques. Energy may be consumed in each case. As a result, efficient computational or data processing approaches are required for effective resource utilization. In WSNs, the position of each node is unknown to the others, posing the problem of localization. In most cases, nodes equipped with GPS capabilities can resolve this issue, but the primary challenge associated with GPS implementation is the sensor node's limited energy supply.

3.3. Layered Architectures.

As illustrated in Figure 5, the layered architecture consists of five layers with three cross layers. The LSNA include physical, data link, network, transport, application, power management, mobility, and task management. In a deployable environment, sensor nodes connected to this type of architecture may number in the hundreds [26]. The sensor nodes are connected to a base station, from which the collected data can be sent to the cloud or a central server via a communication architecture. Each sensor node transmits data to neighboring nodes within its sensing range in the layered architecture. As a result, nodes typically consume little power during packet transmission. Table 1 summarizes a detailed description of the layers and cross-plane layers.

3.4. Clustered Architectures.

Thousands of sensor nodes are organized into clusters in a clustered architecture. Each group is assigned a cluster head, which automatically creates clusters and schedules communication according to a predefined schedule, as illustrated in Figure 6. The cluster architecture is based on low energy adaptive clustering hierarchy (LEACH) technique. The clustered architecture is designed so that each node in the cluster can communicate with other nodes via the cluster head. Due to energy consumption constraints, the cluster head may sometimes be rotated. Cluster heads transmit data to the base station or sink node after receiving it from all sensor nodes within their cluster. Clustered architectures are well suited for EMA data fusion in WNS. Self-organizing groups are capable of rotating cluster heads and ensuring network availability.

3.5. Wireless Sensor Network Architectures (WSNA) Challenges.

In this section, we present different challenges that affect the smooth operation of WSNAs (wireless sensor network architectures) for EMAs. These challenges include energy consumption, quality of service (QoS), security, processing and computation, localization, and network design cost. The challenges enumerated in this section indicate significant constraints that must be addressed and resolved before WSN can be used as a supporting technology for EMAs. In what follows, we discuss these challenges about WSNA for EMAs.

3.5.1. Energy Consumption.

Environmental monitoring applications require low-power sensor nodes capable of long-term operation, autonomy, and real-time functionality in a deployable environment (W. [27]). WSN sensor nodes must be energy-efficient for WSNs to perform optimally in their environment and give reliable data. Without energy optimization, the sensor node's battery will only last a few days, negating the long-term design needs of WSNs for EMAs. Alternative ways to extend the battery life of sensor nodes include energy harvesting from various energy sources, particularly solar power, using large capacity batteries, load balancing, and energy neutral operation (ENO) [28]. In some applications, minimizing energy use through energy-efficient protocols has been used to prolong the sensor node and network lifetime [29]. Minimizing energy

(a)

(b)
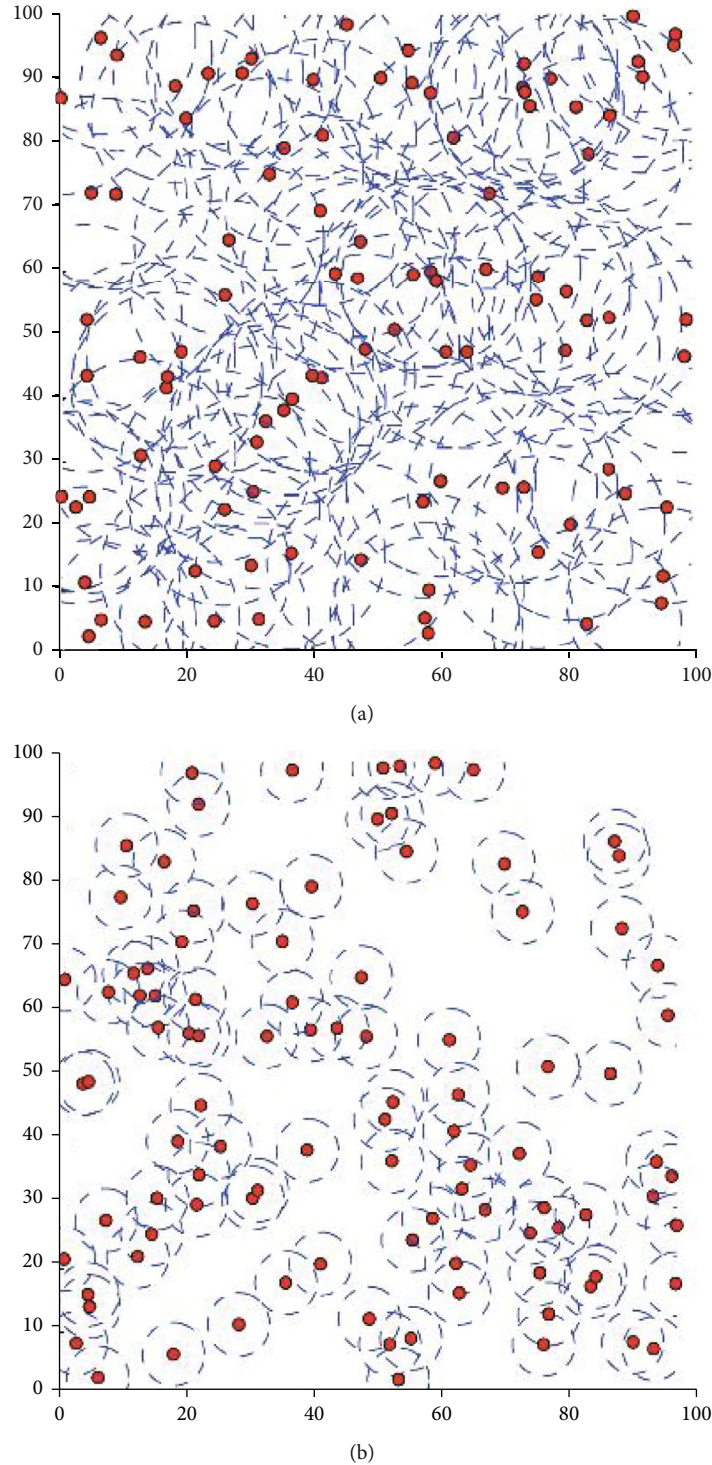
Figure 4: Node sensing range providing (a) full coverage and (b) partial coverage in a deployed environment.

consumption is ideal for the long-term operation of the sensor nodes in challenging application environments such as forests with dense vegetation, oceanography, and animal surveillance.

3.5.2. Quality of Service. Quality of service (QoS), essential in WSNs, has recently received much attention. Achieving a specific performance by measuring various environmental characteristics is necessary for designing, developing, and deploying sensor nodes in WSN for EMAs [30]. It is challenging to improve all QoS parameters at once in WSNs. For instance, reducing latency might result in more energy used by the sensor network. Throughput, packet delivery ratio, end-to-end delay, jitter, and dependability are key performance indicators that may be used in environmental monitoring applications [31]. As a result, maintaining
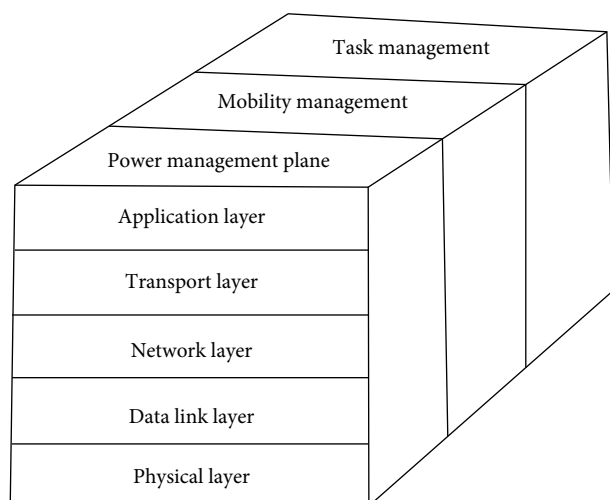
FIGURE 5: Layered sensor network architecture (LSNA).

trade-offs between the performance criteria chosen during the design phases of the specific application domain is necessary. Recently, strategies have been used to enhance service quality while considering the dynamic network and the crucial parameter needed in the application environment to achieve the desired QoS.

3.5.3. Security. WSN advancements enable data collection from various areas of the environment. The data sensed and collected by sensor nodes necessitates extreme care in terms of security. Wireless sensor network security issues are evident in hardware, infrastructure, and software. Identifying all security issues and challenges associated with WSNs and implementing appropriate mitigation measures is critical [32]. Some threats are node replication, selective forwarding, eavesdropping, Sybil, wormhole, signal or radio jamming, and sinkhole [18]. Data integrity and safety, as well as confidentiality and privacy, must be maintained during data transmission. The sensor node should also be safeguarded against theft and vandalism [33]. Physical security measures should be provided when sensor nodes are installed in the field. Other techniques, such as data encryption, should be incorporated in WSNs aimed at EMAs before the sensor nodes are deployed in the environment to improve node efficiency.

3.5.4. Localization. Node localization is critical in WSNs, mainly when WSNs are used in EMAs. Determining the position or location of nodes in WSNs is crucial because it influences the accuracy of the information acquired by sensor nodes [34]. Nonetheless, in WSN for EMAs, it is difficult for nodes to know about other nodes in the deployable environment, making localization an arduous task [35]. Localization presents several challenges, including energy consumption, node dimensionality, node mobility, sensor node security, and global positioning system (GPS) access. Researchers have proposed new methodologies and algorithms to address the inaccuracy in distance and position estimations of unknown sensor node locations. Other

approaches are designed to solve the localization problem by optimizing the selection of reference nodes.

3.5.5. Processing and Computation. WSNs for EMAs are designed to measure various environmental factors to improve our living standards in our immediate surroundings. Several architectures manage data processing and computing when the sensor nodes initiate a sensing operation. In some protocols or architectures, the sensor nodes process and compute data locally or across the network after sensing phenomena before sending the data to a central repository for analysis [31]. In other architectures, the node transmits it to a base station after sensing data, which requires a lot of energy for processing and computation. It then forwards it to a central repository for analysis. Cloud-based architectures have recently been used to analyze and compute data collected from the environment. These cloud-based architectures may visualize processed data through web portals, allowing users to access processed data through their smartphones.

3.5.6. Cost of Network Design. WSNs for EMAs are designed to be alive to meet the application requirements. Some environmental monitoring applications require specialized network design. Animal tracking applications, for example, must be operational at all times to allow users to track the animals' location at any given time. As a result, the type of network architecture improves coverage, connection, robustness, and network lifetime. To meet the goals while staying within budget, sensor network design must be meticulous. Because of the dynamic nature of EMAs, a sensor node deployment plan capable of enhancing coverage and preserving connectivity, while staying under budget is highly recommended for WSNs for EMAs.

4. Sensor Node Deployment Strategies

To ensure maximum area coverage and connectivity, the deployment type must be considered to avoid nodes rapidly depleting their energies in WSNs. The sensor node architecture should be such that nodes within the monitoring area are protected by at least one neighboring node. The coverage of sensor nodes affects how remote network monitoring is administered and the network's lifetime [36]. Nodes may be placed to cover the monitored zone entirely or partially, considering the wireless sensor node's sensing range. Nodes are manually deployed in human-accessible locations where their placement is dangerous.

On the other hand, random deployments occur in hazardous and inaccessible domains that require complete coverage. For instance, battlefield surveillance and open zones for natural life are examples. The primary objectives of researchers studying deployment strategies are to find ways to improve connectivity, maximize coverage, maximize energy efficiency, and maximize network lifetime. Figure 7 illustrates the distinct types of sensor node deployments suitable for EMAs. Details of each deployment strategy are described in the following sections.

TABLE 1: Description of layered sensor network architecture.

Layer/data type	Functions	Related challenges	Recent protocols
Layers of the SNA			
Physical bits	The physical layer is responsible for transmitting bitstreams, frequency selection, carrier frequency generation, modulation, data encryption, and signal detection. The physical layer includes the specification of the transmission medium and the topology of the network (performs encoding and decoding of signals)	Channel-related concerns, radio frequency bands, bandwidth, propagation mode effects, power efficiency, and channel impairments	PL-SKG (physical layer secure key generation) (physical layer secure key generation) IEEE 802.15.4 EAP (energy-aware routing protocol) AKA (authentication and key agreement) (authentication and key agreement) Decode-and-forward protocol
Data link frames	The data link layer is responsible for multiplexing data streams, frame detection, medium access control (MAC), and error control. It is also responsible for ensuring the reliability of point-to-point or multi-point channel access policies, scheduling, and buffer management	Co-channel interference at the MAC layer, multipath fading, and shadowing at the physical layer	MACAW (multiple access with collision avoidance for wireless) (multiple access with collision avoidance for wireless) IEEE 802.11 PAMAS (power-aware multiaccess with signalling) S-MAC (sensor medium access control) (sensor medium access control) T-MAC (timeout MAC) TRAMA (traffic adaptive medium access protocol) DMAC (dynamic *MAC*) IEEE 802.15.4 IEEE 802.15.4e CSMA/CA (carrier-sense multiple access with collision avoidance) CDMA (code division multiple access) ALOHA (ALOHA system) OFDMA (orthogonal frequency-division multiple access)
Network datagrams/ packets	The network layer provides the functionality required to support network configuration, device discovery, security, and topology management. It is also responsible for routing. Routing is responsible for power conservation, buffering, and the ability to be self-organized. The performance of routing protocols depends on the application domain	Limited memory and buffers, power saving, no global ID, and limited communication range	DEEC (distributed energy-efficient clustering) DDEEC (developed distributed energy-efficient clustering) EDEEC (enhanced distributed energy efficient clustering) EDDEEC (enhanced developed distributed energy efficient clustering) BEENISH (balanced energy efficient network integrated super heterogeneous) protocol DSR (dynamic source routing) Open shortest path first Intermediate system to intermediate system protocol AODV (ad hoc on-demand distance vector) RPL (routing protocol for low) (routing protocol for low power and loss network) IP (internet protocol) ICMP (internet control message protocol)

TABLE 1: Continued.

Layer/data type	Functions	Related challenges	Recent protocols
Transport datagrams/ segments	The transport layer is responsible for providing reliability and congestion control or avoidance. Transport layer protocols designed to provide these functionalities use upstream or downstream techniques. Transport layer protocols are grouped into packet-driven and event-driven. The layers rely on the collaborative capabilities of sensor nodes	Limited memory, overhead in avoiding congestion, power constraints, and high traffic events	Sensor transmission control protocol (STCP) Price-oriented reliable transport protocol (PORT) Pump slow fetch quick (PSFQ) OpenFlow Transmission control protocol (TCP) Stream control transmission protocol (SCTP) User datagram protocol (UDP) Cyclic UDP (CUDP) Reliable UDP (RUDP) AppleTalk transaction protocol (ATP) Multipath TCP (MTCP) Transaction control protocol (TCP) Sequenced packet exchange (SPX)
Application user data	The application layer performs management functionalities, including network management, query processing, communication, time synchronization, and localization. The application layer also manages traffic and provides software for various apps that transform data into intelligible formats or send queries to seek specific information	The application-specific nature of EMAs creates many challenges	SMP (simple management protocol) Constrained application protocol HTTP (hypertext transfer protocol) SMTP (simple mail transfer protocol) FTP (file transfer protocol)
Cross layers			
Power management	The power management plane controls the network and ensures the sensor nodes' functionality. The goal is to improve network efficiency. The power plane is responsible for monitoring the power among the sensor node during sensing, data computation, transmission, and reception of data	Network and MAC layer challenges	Energy-efficient distributed schedule-based (EEDS) Fuzzy and ant colony optimization (ACO) based MAC/routing cross-layer protocol (FAMACRO) Distributed energy efficient hierarchical clustering Energy efficient unequal clustering Cross-layer adaptive routing (CLAR) protocol Improved fuzzy unequal clustering protocol Cross-layer energy-efficient protocol (CLEEP) Fuzzy-cross-LEACH protocols
Mobility management	The mobility plane monitors the movement among sensor nodes to improve network efficiency	Quality of services-related challenges, performance metric issues, MAC layer issues, and reliability issues	
Task management	The task plane monitors the task distribution among sensor nodes to improve the network performance. The task plane coordinates with the mobility and power plane to regulate and lower the energy consumption of sensor nodes to prolong the network lifetime	Link quality issues	

4.1. Square and Random Deployments.

For instance, nodes in the deployment area may be arranged in a square pattern to detect events within that region. Due to the environment in which pollution spreads over time, a square deployment model may not be appropriate for river network monitoring. Another method for sensor node deployment is through randomization. It could be uniform or dispersed. Square and random deployments are suitable for stationary freshwater sources with little movement, such as lakes [37]. EMA requires an optimal sensor node deployment strategy that ensures complete coverage of the region of interest within the sensing range to detect events occurring anywhere within the area of interest. Full coverage provides network connectivity, ensuring that sensed data is transmitted to other network nodes and the sink node.

4.2. Grid Deployment.

Grid-based deployments are typically used in static, deterministic applications where the sensor nodes' positions are fixed following a regular grid pattern. Triangular, square, or hexagonal patterns may be used, with
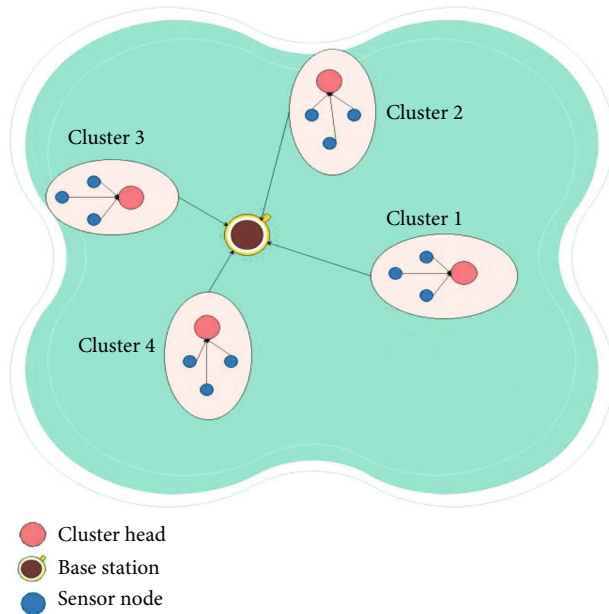
Figure 6: WSN for EMAs—clustered architecture.

the monitoring area divided into smaller grids. As a result, sensor nodes are placed in the grid's center or vertices to maximize connectivity with a small number of nodes. Grid configurations can be triangular, hexagonal, square, or random. Grid deployments are typically two-dimensional or three-dimensional, with some applications in monitoring air pollution [38] and target detection and tracking [39]. According to these deployment applications, the grid is most advantageous for deployments with a limited number of available nodes.

4.3. Mesh Deployment. Nodes are placed in a mesh deployment so that each node serves as a relay to other nodes. In the event of a failure, mesh nodes are fault-tolerant. Recent mesh deployments have rendered the earlier mesh network hubs' single half-duplex radio obsolete. These advancements pave the way for deploying a switched mesh network [40]. Interoperability, energy efficiency, scalability, mobility, and robustness are critical requirements for applications that use mesh in WSNs. Environmental monitoring, home construction, industrial automation and control, and precision agriculture benefit from mesh applications [41]. Earlier mesh topologies such as Zigbee (IEEE.15.4), IEEE 802.15.4e, and Wireless Hart were possible. Newer platforms, such as IEEE 802.15.15, are gradually introduced and integrated into WSN.

4.4. Distributed Deployment. Distributed deployments are critical for establishing an optimal coverage area for WSN systems. In distributed systems, deployment schemes are determined by the sensor node's coordinate information and name (A. [42]). Typically, nodes are homogeneous in terms of their roles and algorithm implementation. Algorithms are based on the base station to allow scattered nodes to be positioned optimally for coverage. Examples of these implementations can be found in the deployment of mobile sensors [43].

4.5. Centralized Deployment. Centralized deployments are used in mobile sensor nodes to improve barrier coverage. Most barrier enhancement strategies involve relocating the sensor nodes. However, their primary challenge is optimizing relocating these sensor nodes' communication and moving costs. Due to the deployment of these centralized nodes, their primary disadvantages are the massive message overheads associated with relocations and their inability to scale. Several examples of centralized implementations are presented in [33, 44].

4.6. Sparse and Dense Deployment. This deployment classification is typically determined by the number of sensor nodes used. While dense deployments involve the placement of many sensor nodes in each area, sparse deployments involve a small number of nodes. When the cost of deploying a substantial number many nodes is prohibitively high, sparse implementations are considered. As a result, sensor nodes are assumed to be static during deployment but reposition themselves to maintain connectivity and coverage. Nodes must remain within their neighbors' communication radius to achieve optimal coverage. Dense deployments are required for applications that require detection of every event, and multiple sensors may act as redundant nodes within a given area [45]. Environmental monitoring applications enable sparse sensor networks across large areas, and robot-based data scavengers collect data from sparse sensor fields.

4.7. Dynamic Deployment. Dynamic deployment entails randomly deploying mobile sensor nodes, moving to optimal locations for coverage and connectivity. The virtual force, force-oriented particles, simulated annealing, and particle swarm optimization algorithms are suitable for such deployments. The critical challenges associated with dynamic deployment are energy efficiency, load balancing, increased throughput, data reliability, and cost reduction. Because the position of the sensor node is unknown in advance, dynamic deployment is applicable in situations where sensor node placement is impractical. Applications such as disaster and battlefield monitoring are examples.

5. WSN Applications

Sensor nodes and base station nodes are used in WSN applications for EMAs. The sensor nodes monitor the parameters (as described in the following sections, depending on the application environment). The parameters sensed or obtained from the environment through a communication infrastructure are transferred from the base station to the central repository, typically a local server or the cloud (GSM, ZigBee, GPRS, Ethernet, RF, and WIFI). When data is stored on a server or in the cloud, it is organized, processed, analyzed, and reported to stakeholders via web portals, SMS gateways, and mobile applications.

The data is presented to stakeholders using data visualization techniques. EMA architectures should be cost-effective, lightweight, reliable, scalable, and self-organizing [46]. There is a guarantee of the environment in WSN applications, which may be static or dynamic/mobile, affecting the
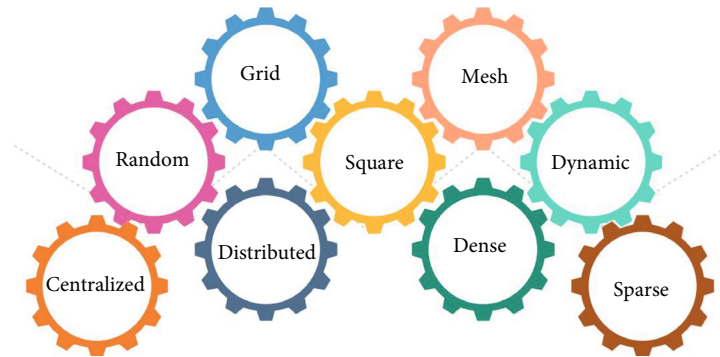
FIGURE 7: Sensor node deployment strategies in environmental monitoring applications.

TABLE 2: Characteristics of WSN applications.

Application	Type of environment	Data gathering approaches
Water monitoring (freshwater/ocean)	Dynamic	Event tasks/periodic
Animal tracking	Dynamic	Tracking event messages
Agriculture	Static	Periodic tasks
Oceanography	Dynamic	Tracking
Earthquake/landslide monitoring	Static	Approximation based
Air quality	Dynamic/static	Event-based/periodic
Forest fire	Static	Event

stability of connections between communicating devices (nodes, sinks, or base stations). Table 2 summarizes the types of applications, the appropriate environment, and the data collection methods.

5.1. Agriculture. Wireless sensor networks can significantly improve a variety of agricultural activities. In agriculture, sensor networks can optimize resource utilization while also increasing the quality and productivity of agricultural products [47]. WSNs enable efficient data collection, transmission, and processing from sensors deployed underground and aboveground in agriculture [48]. WSN has many advantages for farming and agricultural environments. These advantages include monitoring various elements such as microclimates and Phytophthora. This fungal disease spreads rapidly among plants, which is why monitoring water levels and scheduling irrigation based on the temperature of the plant's canopy is critical [49]. WSNs can also be used to monitor and detect microorganisms, antibodies, and other substances in the field, such as soil moisture, temperature, and humidity [50]. Finally, sensor networks can be used for intelligent irrigation, fertilization, pest control, and disease detection in their initial stages [51].

5.2. Animal Tracking. Tracking wild and endangered animals is critical for monitoring them in their natural habitats. There are two ways to track animals with wireless sensor nodes: (1) by attaching devices to the animals or (2) using unmanned aerial vehicles (UAVs) without device attachments. GPS devices may be attached to the animals to ascertain their precise location and movement patterns. Animal health can also be tracked using sensor nodes and sensor

network architectures. WSN application design for animal tracking aims to create architectures that effectively monitor animals in their ecosystem without disturbing or negatively affecting their habitat. Additionally, WSNs will assist rangers in conserving animal sanctuaries and natural areas by recording various sites, rare and protected species migrations, and trend monitoring to ensure that the reserves are well-managed. Collars are worn around animals' necks to collect and transmit location data to sink nodes. Sensor networks have been developed to track zebras (ZebraNet), turtles (TurtleNet), elephants (JumboNet), and red deer (Cervus elaphus) [28]. Using WSNs to track these and other wild animals lays the groundwork for researchers to develop models for adequate wildlife resource protection, sustainable use, and scientific management. imote2, infrared motion detectors, Panasonic AMN41121 sensor, RFID tags, RFID readers, radio signal detectors, actuators, and mobile robots are the hardware architectures used for animal tracking applications. Additionally, animal tracking applications may use communication technologies such as 802.15.4 (ZigBee), GSM, GPS, and clustering architectures.

5.3. Water Monitoring. Water monitoring considers freshwater sources (water quality monitoring) and ocean environment monitoring. The critical difference is that water quality monitoring ensures safe and clean water among freshwater sources. In contrast, marine/ocean monitoring focuses on detecting climate changes or pollution of the marine environment, which affects human and animal habitats. WSNs have proven to be the best alternative to traditional methods when adapted for monitoring freshwater

bodies and marine environments. Research in water environment monitoring classifies the monitoring process into water quality monitoring and ocean/marine environment monitoring [8]. Sensor nodes collect parameters such as water temperature, pH, dissolved oxygen, and others in freshwater sources and measure parameters such as the sea level and marine environment pollution. Sensors may detect climatic changes in the marine environment [19]. The data is transmitted to a base station through a communication architecture. The hardware architectures for water quality monitoring applications are pH, turbidity, temperature, and ammonia concentration.

The marine environment is monitored for different conditions, and uncontrollable human activities affect the health of living organisms. Traditional monitoring approaches are expensive and time-consuming. Hence, the activities require extensive and robust monitoring approaches such as wireless sensor networks to measure the following parameters: pressure, wind direction, water temperature, chlorophyll, wind speed, salinity levels, turbidity, and oxygen density. The data obtained from oceanography or marine monitoring applications are sent from the sensor nodes to base stations using wireless communication infrastructure. An efficient application may be built by employing the following hardware: sensors to measure physical parameters, sink nodes, mobile robots, buoy devices, robot-based sensors, seismic sensors, underwater sensors and transducers, autonomous underwater vehicles, and floating buoys. Some of the communication architectures include ZigBee, WIFI, and WiMAX.

5.4. Air Quality.

Air quality monitoring is critical for human health. Industrialization, urban development, fertilizers, and pesticides are human activities that pollute the atmosphere. Furthermore, the increased use of vehicles has exacerbated air pollution in recent years. Monitoring air pollution is necessary to provide data to authorities to improve livelihood. Traditional methods of collecting data on air pollution are expensive, complex, and time-consuming, necessitating WSNs [52]. Air pollution is monitored using wireless sensor nodes. Carbon monoxide (CO), carbon dioxide (CO_2), and total volatile organic compounds (TVOC) concentrations, as well as ambient temperature, relative humidity, air pressure, moisture content, and luminosity, are all measured [53]. Air quality measurements are reported in real time via a web server that can be accessed via the internet. CCS811 Sensor, MQ Sensor, BME280 Sensor, humidity, temperature, pressure sensors, MQ series sensors, CO Sensor, MQ7 Sensor, MQ135 Sensor, MQ136 Sensor, SO2 Sensor, and NH3 Sensors are among the sensor devices used to measure air pollution levels. These applications ensure that air quality parameters are monitored effectively and efficiently. They created a practical, low-cost air quality monitoring system using sensor nodes and robust communication infrastructure.

5.5. Earthquake and Landslide Monitoring.

Earthquakes are a hazardous type of natural disaster. Earthquakes are the most violent natural disturbances in the earth's crust, significantly affecting the surrounding environment. Earthquakes occur when plate movements exert pressure on the rocks, which causes them to fracture and shift. The sensing element for earthquake detection is a wireless acceleration sensor device [54]. Dissemination of information about the likelihood of an earthquake must occur at the appropriate time [55]. A large mass of rock, rubble, or earth slides down a slope, which is referred to as a landslide. Although gravity is the primary cause of a landslide, numerous other natural (weak materials, weathering, river erosion, rapid snowmelt, and heavy rain) and human-caused factors can affect slope stability (excavations, deforestation, mining, and artificial vibration). Sensors are deployed to monitor various parameters, and an early warning system can be built based on the measured values to minimize losses. Sliding is responsible for the movement of the earth's crust, which can occur anywhere globally. Each incident spreads several kilometers across the continent in a matter of minutes, wreaking havoc on vulnerable structures, dams, and bridges and occasionally resulting in death. Wireless sensor networks are the most efficient method of sensing and detecting the earth's crustal movement.

Additionally, they have been demonstrated to increase earthquake and landslide detection [56]. The deployment of various wireless sensor nodes in the earth's crust enables the detection of earth crust movement more quickly, which can then be transmitted immediately to sinks for preemptive action via communication architectures. WSNs have the potential to significantly enhance the accuracy and efficiency of earthquake and landslide detection [56]. WSNs can collect data from multiple sensors and transmit it to a web server via a GSM cellular network or other communication architecture [57]. In earthquake and landslide monitoring applications, hardware devices such as displacement, angle, and rainfall sensors, geophysical sensors, pore pressure transducers, FBG sensors, microsensors, geophones, soil moisture sensors, strain gauges, optical fiber sensors, temperature, humidity, land movement sensors, slope sensors, tiltmeters, raindrop sensors, microwave radar sensor for motion detection, extender, and rainfall gauges are primarily used. Software applications such as three-dimensional WebGIS, WiSuN, Raman optical time-domain reflectometry, and SLOPEIW are available to operate earthquake and landslide applications. ZigBee protocol, GSM communication between 900 MHz and 1800 MHz, WIFI and satellite terminals, optical remote sensing, RFID technology, LoRa technology, and Bluetooth technology are all examples of communication architectures that support earthquake and landslide applications [54, 56, 58].

5.6. Forest Fire.

Forest fires have become more prevalent in recent years, wreaking havoc on the environment, natural resources, and lives of humans and animals alike. Climate change in most of the world's landmasses may result in forest fires. In countries with scorching and dry weather, fires may rise. Forest fires wreak havoc on the habitats of wild animals and have a detrimental effect on agricultural yields. As a result, it is necessary to develop systems that provide authorities with timely and high-quality information to combat forest fires in the shortest possible time [59]. WSNs can bring a meaningful change in the fight against forest

fires. WSNs can detect forest fires and transmit data to a remote-control center via a communication architecture.

Parameters such as temperature, smoke, oxygen levels, and humidity can be collected to help mitigate forest fires. WSNs are advantageous for the early detection of fires through sensor nodes. WSN architectures are designed to detect forest fires faster than traditional methods and forecast the direction of the fire's flow [60].

Sensor nodes can be used to determine the exact location of the fire and its path of spread. By utilizing WSNs, forest guards can intervene more quickly and ensure that the identification and location of an incident are communicated to relevant stakeholders for immediate action. In detecting forest fires, fire, smoke, and temperature sensors may be distributed randomly throughout the forest or used to regulate a forest region prone to fire [61]. Typically, sensors are configured so that when temperature values exceed a predefined threshold, the nodes activate their radios for data transmission. The sensor nodes continuously monitor the forest environment to ensure temperatures remain within specified ranges [59]. In these application domains, collected data is processed centrally and distributed to appropriate stakeholders via alerts or notifications via a communication architecture. Sensor nodes deployed for forest fire detection made efficient energy use, extending the sensor nodes' lifetime. The power can be distributed evenly among the nodes, and in some areas, energy can be harvested to extend the life of the nodes. Forecasting the direction and speed of forest fire spread is critical for firefighting (Y. H. [62]).

Forest fire detection systems employ a variety of hardware architectures, including temperature sensors, humidity sensors, gas sensors, infrared sensors, pressure sensors, solar radiation sensors, and smoke recognition sensors. Other researchers have detected forest fires using unmanned aerial vehicles, carbon dioxide sensors, GPS devices, and raspberry pi sink nodes. TinyOS, routing (flooding routing, AODV), time synchronization protocols, MAC layer (IEEE 802.15.4, LEACH) protocols, and ad hoc clustering techniques or architectures have all been adopted. To address the application requirements for forest fire detection, clustered hierarchical network architectures and intra- or intercluster architectures may be used.

6. Advances in WSNs

This section presents the advances in WSN architectures with the introduction of machine learning and the Internet of Things.

6.1. WSNs and Machine Learning Architectures. The primary goal of WSN deployments is energy conservation, which results in a more extended network lifetime. Machine learning is used to significantly reduce data communications in typical WSN deployments' distributive environments. Recent research has explored machine learning techniques (supervised, unsupervised, and reinforcement learning) in all layers of the communication stack. Most approaches occur at the routing and medium access layers. These protocols' purpose is to provide current information about the reliability of connections to neighboring nodes. Its properties for reliable networks include its ability to adapt rapidly to changes, energy efficiency, and resistance to short-term aberrations [63].

Q-learning, a reinforcement learning technique, has been applied to WSNs to optimize routing performance and extend network lifetime [64]. Decision trees employ learning trees to forecast output labels based on repeating data. Decision trees have been used in wireless sensor networks to identify link reliability characteristics such as loss rate, restore time, and failure time. Support vector machines (SVM), neural networks, and Bayesian networks are used in environmental monitoring [65]. Additionally, machine learning has been used to design MAC protocols that aid WSNs in adapting to changing environmental monitoring conditions. Q-learning and reinforcement learning techniques have optimized MAC protocols, including Q-learning in Slotted Aloha and RL-MAC.

Smart environmental monitoring applications have benefited from artificial intelligence (AI) and machine learning (ML) by providing precise and optimum control of undesirable effects on the environment. Classifications, clustering, and anomaly detections are some of the many uses of AI and ML in smart monitoring. However, concerns are raised in their implementations due to the pervasion of applications in agriculture, transport, buildings, air quality, water quality, and human and animal tracking and monitoring. Interoperability of the sensors, data structures, standards, and protocols in implementing and controlling smart environmental systems is a significant concern.

Classification and anomaly detection are some tools deployed to mitigate the cost of energy consumption and data deduplication on systems [66, 67]. For a brief survey on anomaly detection systems, the reader may refer to the work by [67]. The authors discuss advances and implementations of ML and AI in smart buildings with strategies in smart vision, architectural design and visualization, progress monitoring and safety, and data storage [66]. ML tools used and implemented in these applications include, but are not limited to, support vector machines (SVM), neural networks (NNs), regression models, deep convolutional neural networks (Deep CNN), Markov chains, and particle swarm optimization (PSO) [66].

Using AI and ML brings innovations in personalized designs, enhances communications and control, and reduces human factor failures.

6.2. WSNs and IoT Architectures. The Internet of Things (IoT) is the network of everyday physical objects embedded with tiny sensors and connected through software and other enabling technologies. IoT networks collect environmental data and transmit it to other connected devices and systems via the internet. By 2025, researchers estimate that there will be over 25 billion connected devices worldwide. Through various standard protocols, domains, and applications, the IoTs connect machines in ways that go beyond machine-to-machine (M2M) communications. Microcontrollers, for example, are frequently used in sensor nodes due to their low cost, ease of connection to other devices, programming

ease, and energy efficiency. The Raspberry Pi, Arduino boards, the Giant board, the XBee module, and the ATMEGA32 series are all examples. In IoTs, communication standards such as Bluetooth, Zigbee, Wi-Fi, and RFIDs are used to implement short-range communication networks that enable IoTs. Radio frequency (RF), optical communication (laser), and infrared are all possible wireless transmission media. The most pertinent mode of communication is radio frequency-based, as it applies to most WSN applications. WSNs communicate at the following license-free frequencies: 173, 433, 868, 915 MHz, and 2.4 GHz.

6.3. Simulators. Most WSN applications are implemented using simulations to evaluate new applications at a lower cost. Simulations enable researchers to experiment with and isolate different network factors by easily tweaking and tuning parameters without regard for cost. As a result, the development of WSN simulators is expanding rapidly. However, simulations are not trivial to implement. Several factors affect the simulation results, including the simulator's suitability and the tools' suitability for implementing the simulation solutions. Network Simulator 2 (NS2), Network Simulator 3 (NS3), TOSSIM (TinyOS Simulator), Castalia OMNeT++, J-SIM, OPNET, and Avrora are all examples of simulators.

NS2 is an IEEE 802.11, IEEE 802.16, and IEEE 802.15.4 discrete event simulator. It is written in two major programming languages, that is, C++ and object-oriented yool command (OTcL), and supports network routing and MAC protocols but only a limited set of energy modelling algorithms. It does not support modelling for nodes greater than 100, which complicates scalability in NS2. Network Simulator 3 was created to address these issues. It is not a replacement for NS2 but an entirely new simulator written in C++ with optional Python bindings, and NS3 provides enhanced energy devices and source support. NS3 has a more advanced WIFI Radio implementation, comparable to IEEE 802.11, the primary networking channel in most WSNs. Castalia is an open-source simulator written in the OMNeT++ programming language. The simulator validates distributed algorithms and protocols by simulating radio models and wireless channels in the real world. It uses real-world node characteristics to simulate the radio's behavior. It includes parameters for sensor bias, clock drift, node energy consumption, memory consumption, CPU energy consumption, CPU time, and the implementation of the MAC and routing protocols.

TOSSIM is not a simulator but a TinyOS emulator. It is a Python-based bit-level discrete event emulator. TOSSIM can be run on Linux or Windows via Cygwin. It can be used to simulate network and radio models and code executions. Power TOSSIM is another TinyOS variant of TOSSIM that simulates each node's energy consumption. TOSSIM-enabled nodes run NesC on TinyOS. TOSSIM's design is limited to the emulation of mote-like nodes. OMNeT++ is also a C++-based discrete event simulator. It provides programmers with a graphical user interface and a framework for sensor node mobility. OMNeT++ includes channel controls, MAC addresses, and a limited number of routing protocols. It only supports a limited amount of information about the energy consumption of individual sensor nodes [28].

6.4. Operating Systems. In WSNs, operating systems must support fundamental power management, portability, scheduling, simulation support, and execution models. Operating systems manage the sensor devices' limited resources and function differently depending on their application domains. Operating systems, on the other hand, are highly communicative. As a result, energy is the primary resource it cannot obtain. Some OS used include TinyOS and Contiki, Mantis [68], Pixie [69], SOS [70], and LiteOS [71]. Contiki and Pixie use a software approach to track the power state in all the system components.

TinyOS is an event-driven, open-source operating system for wireless sensor nodes. It is not an operating system per se but a framework for developing embedded systems tightly coupled with the network embedded system C programming language (NesC). A typical WSN application is approximately 15 kilobytes, with about 400bytes representing the application and approximately 64 kilobytes illustrating the database query system (for example, PostgreSQL). TinyOS primarily comprises a TinyOS simulator (TOSSIM) and a visualiser (the TinyViz).

Pixie is a data-intensive platform for programming sensor networks. It is used in high-data-flow applications requiring extensive in-network processing, such as acoustic and seismic monitoring, acceleration, and water quality monitoring. Pixie's implementation in NesC is backwards compatible with TinyOS. In Pixie, the user must forecast the application's energy requirements and delegate resource management to the operating system. The operating system is aware of and manages the system's resource constraints, which include energy, storage, and bandwidth. It is divided into three primary components: a dataflow programming model, resource tickets, and resource brokers. The data flow model enables the operating system to exert visible control over the application's limited resources. The resource tickets are the abstractions used to manage and discretely allocate available resources. Finally, it includes resource brokers, which implement code modules that have Pixie resource management policies.

The multimodal system for networks of in situ wireless sensors (Mantis) is a multimodal embedded system operating system. Its primary goal is to provide an easy-to-use system that addresses the resource-constrained challenges of developing sensor network applications. Multithreading, time slicing, and pre-emptive scheduling are all features of the Mantis OS architecture, and its core is written in standard C. It includes an implementation of the RC5 security algorithm. Mantis's development enables it to cross-platform and multimodal prototyping of environmental monitoring applications.

7. Future Research Directions and Conclusions

In this section, we present novel research directions from WSNs for EMAs that will require further investigation and provide a conclusion to the paper.

7.1. Future Research Directions

7.1.1. Cloud Computing in WSN for EMAs. The use of cloud computing in WSN for EMAs aims to improve sensor

networks' energy efficiency, processing capability, and node communication. Integration of cloud computing with WSNs for EMAs may be investigated further to leverage the advantages of cloud computing to meet complex application needs and novel architectures for EMAs. In developing virtual sensors in EMAs, using sensor-based cloud computing functions applying virtualization on cloud computing platforms should be investigated. More research on reconfigurable physical, network and MAC layers in the protocol stack should be conducted to improve the protocol design for WSNs for EMAs. Researchers should thoroughly investigate novel ways to employ virtualization in EMAs to satisfy the data gathering approaches (event-based, periodic, and approximation-based) while considering peculiarities of the various application environments (dynamic or static) to meet the needed service requirements.

7.1.2. Integration of Artificial Intelligence and Data Fusion. In recent years, AI has advanced rapidly in wireless networks. AI-based technologies (e.g., machine learning, reinforcement learning, and deep learning) have been used in wireless sensor networks for EMAs. When powerful computational capabilities are introduced for use in WSNs for EMAs, sensor nodes produce more accurate data for use by stakeholders in effective decision-making. As a result, it is time to apply AI-based technologies to EMAs, which opens up new avenues for researchers to obtain more intelligent approaches to enhance data computation going into the future. WSN for EMAs is targeted for the generation of huge tons of data. Exploiting lightweight data fusion approaches to correlate the data gathered from sensor nodes in EMAs is worth researching.

7.1.3. Dynamic Network-Wide Protocol Design. In WSNs for EMAs, it is essential to use the right deployment strategy to optimize the energy utilized in the overall network. By exploiting advanced networking protocols, the sensor nodes will form the required communication paths and establish connectivity for nodes to observe their environment and transmit the phenomena to the base station. Robust network-wide protocols that support dynamic network topology for applications such as animal tracking, freshwater monitoring, oceanography, and air quality monitoring present new challenges to the WSN for the EMAs research community. Considerations for network-wide protocol design for WSNs for EMAs should center on energy-and data-based due to the architectures used in these environments.

7.1.4. Advanced Data Visualization Technologies. One of the essential considerations for EMAs is the measurement, collection, and transmission of enormous amounts of data from nodes to a central repository for processing, analysis, and reporting. Online IoT visualization tools like ThingsBoard have recently been developed to provide real-time data visualization in WSNs to monitor environmental conditions [72]. These technologies could be enhanced further to perform an intelligent assessment of various environmental characteristics obtained from the sensor network. Intelligent monitoring software for EMAs can be designed with a range of real-time visualization techniques to meet the specific requirements of the numerous domains in EMAs.

7.1.5. Novel Approaches for Access Control and Authentication. WSNs for EMAs are susceptible to hacking attacks, particularly with the rise of the Internet of Things technologies used to monitor various environmental conditions. Despite recent research focusing on the Internet of Things security, there are still security problems with IoT implementation in EMAs. As a result, efficient and secure mutual authentication procedures that consider the specific environmental characteristics of EMAs and the architecture developed for use would improve dynamic resource management and performance for modern WSNs for EMAs.

7.2. Conclusions. The sensor network architecture suitable for environmental monitoring applications has been discussed in this paper. The sensor node architecture can be used for a variety of applications. The various components of the sensor node all contribute to the amount of energy expended during the node's operation in each environment. The different strategies presented in this paper must be carefully implemented to coordinate the sensing, data communication, and computation components that consume most of the sensor nodes' energy to implement WSNs for EMAs efficiently. As a result, when designing WSNs for EMAs, the number of sensors, the type of parameters, and the sensor network architecture should all be considered to maintain the wireless sensor network's quality of service and lifetime. Due to the hardware design, addressable communication between sensor nodes in EMAs may be possible. Data collected from sensor nodes deployed in WSNs for EMAs can be transferred to a web server or the cloud and displayed on a web portal for real-time monitoring by stakeholders. The web portal typically includes a dashboard for displaying sensor readings derived from parameters. EMAs benefit from wireless sensor node architectures in energy conservation, hardware reuse, resource management, and real-time performance. This paper also discussed advances in WSNs made possible by machine learning and the Internet of Things (IoT).

Data Availability

There is no data available.

Conflicts of Interest

The authors declare that there is no conflict of interest regarding the publication of this paper.

Acknowledgments

References

[1] D. Kandris, C. Nakas, D. Vomvas, and G. Koulouras, "Applications of wireless sensor networks: an up-to-date survey," *Applied System Innovation*, vol. 3, no. 1, p. 14, 2020.

[2] A. Fascista, "Toward integrated large-scale environmental monitoring using WSN/UAV/Crowdsensing: a review of applications, signal processing, and future perspectives," *Sensors*, vol. 22, no. 5, p. 1824, 2022.

[3] B. Abidi, A. Jilbab, and M. E. Haziti, "Routing protocols for wireless sensor networks: a survey," in *Advances in Ubiquitous Computing*, Academic Press, 2020.

[4] M. Baire, A. Melis, M. B. Lodi et al., "WSN hardware for automotive applications: preliminary results for the case of public transportation," *Electronics*, vol. 8, no. 12, p. 1483, 2019.

[5] F. Engmann, F. A. Katsriku, J.-D. Abdulai, and K. S. Adu-Manu, "Reducing the energy budget in WSN using time series models," *Wireless Communications and Mobile Computing*, vol. 2020, Article ID 8893064, 15 pages, 2020.

[6] A. Mchergui, T. Moulahi, and S. Zeadally, "Survey on artificial intelligence (AI) techniques for vehicular ad-hoc networks (VANETs)," *Vehicular Communications*, vol. 1, article 100403, 2022.

[7] H. Yin, Y. Cao, B. Marelli, X. Zeng, A. J. Mason, and C. Cao, "Soil sensors and plant wearables for smart and precision agriculture," *Advanced Materials*, vol. 33, no. 20, p. e2007764, 2021.

[8] K. S. Adu-Manu, C. Tapparello, W. Heinzelman, F. A. Katsriku, and J.-D. Abdulai, "Water quality monitoring using wireless sensor networks," *ACM Transactions on Sensor Networks (TOSN)*, vol. 13, no. 1, pp. 1–41, 2017.

[9] J. O. Ighalo, A. G. Adeniyi, and G. Marques, "Internet of things for water quality monitoring and assessment: a comprehensive review," *Studies in Computational Intelligence*, vol. 912, pp. 245–259, 2021.

[10] V. Lakshmikantha, A. Hiriyannagowda, A. Manjunath, A. Patted, J. Basavaiah, and A. A. Anthony, "IoT based smart water quality monitoring system," *Global Transitions Proceedings*, vol. 2, no. 2, pp. 181–186, 2021.

[11] F. Jan, N. Min-Allah, and D. Düştegör, "Iot based smart water quality monitoring: recent techniques, trends and challenges for domestic applications," *Water*, vol. 13, no. 13, p. 1729, 2021.

[12] R. Kumar, S. Goel, V. Sharma, L. Garg, K. Srinivasan, and N. Julka, "A multifaceted Vigilare system for intelligent transportation services in smart cities," *IEEE Internet of Things Magazine*, vol. 3, no. 4, pp. 76–80, 2020.

[13] A. Lanzolla and M. Spadavecchia, "Wireless sensor networks for environmental monitoring," *Sensors*, vol. 21, no. 4, pp. 1–3, 2021.

[14] F. Engmann, K. S. Adu-Manu, J.-D. Abdulai, and F. A. Katsriku, "Applications of prediction approaches in wireless sensor networks," in *Wireless Sensor Networks-Design, Deployment and Applications*, Intech Open, 2021.

[15] K. Bajaj, B. Sharma, and R. Singh, "Integration of WSN with iot applications: a vision, architecture, and future challenges," in *EAI/Springer Innovations in Communication and Computing*, pp. 79–102, Springer, Cham, 2020.

[16] H. Chojer, P. T. Branco, F. G. Martins, M. C. Alvim-Ferraz, and S. I. Sousa, "Development of low-cost indoor air quality monitoring devices: recent advancements," *Science of the Total Environment*, vol. 727, article 138385, 2020.

[17] U. B. Iyekekpolo, F. E. Idachaba, S. I. Popoola, A. A. Atayero, and F. Mensah, "Wireless sensor networks: architecture, applications, and challenges," in *Proceedings of the International Conference on Industrial Engineering and Operations Management, 2018 (SEP)*, pp. 1212–1220, Washington, DC, USA, 2018.

[18] O. Olufemi Olakanmi and A. Dada, *Wireless sensor networks (WSNs): security and privacy issues and solutions*, Wireless Mesh Networks-Security, Architectures and Protocols, 2020.

[19] K. S. Adu-Manu, F. A. Katsriku, J.-D. Abdulai, and F. Engmann, "Smart river monitoring using wireless sensor networks," *Wireless Communications and Mobile Computing*, vol. 2020, Article ID 8897126, 19 pages, 2020.

[20] M. Singh and S. Ahmed, "IoT based smart water management systems: a systematic review," *Materials Today: Proceedings*, vol. 46, pp. 5211–5218, 2021.

[21] D. Jalal and T. Ezzedine, "Decision tree and support vector machine for anomaly detection in water distribution networks," in *2020 International Wireless Communications and Mobile Computing (IWCMC)*, pp. 1320–1323, Limassol, Cyprus, 2020.

[22] B. E. B. Semlali, C. AmraniEl, G. Ortiz, J. Boubeta-Puig, and A. Garcia-de-Prado, "SAT-CEP-monitor: an air quality monitoring software architecture combining complex event processing with satellite remote sensing," *Computers and Electrical Engineering*, vol. 93, article 107257, 2021.

[23] A. B. Haque, B. Bhushan, and G. Dhiman, "Conceptualizing smart city applications: requirements, architecture, security issues, and emerging trends," *Expert Systems*, vol. 39, no. 5, pp. 1–23, 2022.

[24] P. O. Kamgueu, E. Nataf, and T. Djotio, "Architecture for an efficient integration of wireless sensor networks to the Internet through Internet of Things gateways," *International Journal of Distributed Sensor Networks*, vol. 13, no. 11, Article ID 1550147717744735, 2017.

[25] K. Sohraby, D. Minoli, and T. Znati, "Basic wireless sensor technology," in *Wireless Sensor Networks*, Wiley Telecom, 2007.

[26] W. Honghui, T. Xianguo, L. Yan et al., "Research of the hardware architecture of the geohazards monitoring and early warning system based on the Iot," *Procedia Computer Science*, vol. 107, no. Icict, pp. 111–116, 2017.

[27] W. Xu, Y. Zhang, Q. Shi, and X. Wang, "Energy management and cross layer optimization for wireless sensor network powered by heterogeneous energy sources," *IEEE Transactions on Wireless Communications*, vol. 14, no. 5, pp. 2814–2826, 2015.

[28] K. S. Adu-Manu, N. Adam, C. Tapparello, H. Ayatollahi, and W. Heinzelman, "Energy-harvesting wireless sensor networks (EH-WSNs)," *ACM Transactions on Sensor Networks (TOSN)*, vol. 14, no. 2, pp. 1–50, 2018.

[29] M. Y. Aalsalem, W. Z. Khan, W. Gharibi, M. K. Khan, and Q. Arshad, "Wireless sensor networks in oil and gas industry: recent advances, taxonomy, requirements, and open challenges," *Journal of Network and Computer Applications*, vol. 113, pp. 87–97, 2018.

[30] K. Jaiswal and V. Anand, "EOMR: an energy-efficient optimal multi-path routing protocol to improve QoS in wireless sensor network for IoT applications," *Wireless Personal Communications*, vol. 111, no. 4, pp. 2493–2515, 2020.

[31] R. P. Meenaakshi Sundhari and K. Jaikumar, "IoT assisted hierarchical computation strategic making (HCSM) and

dynamic stochastic optimization technique (DSOT) for energy optimization in wireless sensor networks for smart city monitoring," *Computer Communications*, vol. 150, pp. 226–234, 2020.

[32] M. Dangana, S. Ansari, Q. H. Abbasi, S. Hussain, and M. A. Imran, "Suitability of nb-IoT for indoor industrial environment: asurvey and insights," *Sensors*, vol. 21, no. 16, p. 5284, 2021.

[33] L. Nguyen, S. Kodagoda, R. Ranasinghe, and G. Dissanayake, "Mobile robotic sensors for environmental monitoring using Gaussian Markov random field," *Robotica*, vol. 39, no. 5, pp. 862–884, 2021.

[34] D. S. Ibrahim, A. F. Mahdi, and Q. M. Yas, "Challenges and issues for wireless sensor networks: A survey," *Journal of global scientific research*, vol. 6, no. 1, pp. 1079–1097, 2021.

[35] A. Coluccia and A. Fascista, "Hybrid TOA/RSS range-based localization with self-calibration in asynchronous wireless networks," *Journal of Sensor and Actuator Networks*, vol. 8, no. 2, p. 31, 2019.

[36] S. Abdollahzadeh and N. J. Navimipour, "Deployment strategies in the wireless sensor network: a comprehensive review," *Computer Communications*, vol. 91-92, pp. 1–16, 2016.

[37] K. Mougou, S. Mahfoudh, P. Minet, and A. Laouiti, "Redeployment of randomly deployed wireless mobile sensor nodes," in *2012 IEEE Vehicular Technology Conference (VTC Fall)*, pp. 1–5, Quebec City, QC, Canada, 2012.

[38] A. Boubrima, W. Bechkit, and H. Rivano, "Optimal WSN deployment models for air pollution monitoring," *IEEE Transactions on Wireless Communications*, vol. 16, no. 5, pp. 2723–2735, 2017.

[39] Y. H. Kim, C. M. Kim, D. S. Yang, Y. J. Oh, and Y. H. Han, "Regular sensor deployment patterns for p-coverage and q-connectivity in wireless sensor networks," in *International Conference on Information Networking*, pp. 290–295, Bali, Indonesia, 2012.

[40] P. Chatterjee, S. C. Ghosh, and N. Das, "Load balanced coverage with graded node deployment in wireless sensor networks," *IEEE Transactions on Multi-Scale Computing Systems*, vol. 3, no. 2, pp. 100–112, 2017.

[41] D. Rodenas-Herraiz, A. J. Garcia-Sanchez, F. Garcia-Sanchez, and J. Garcia-Haro, "Current trends in wireless mesh sensor networks: a review of competing approaches," *Sensors*, vol. 13, no. 5, pp. 5958–5995, 2013.

[42] A. Kumar, V. Sharma, and D. Prasad, "Distributed deployment scheme for homogeneous distribution of randomly deployed mobile sensor nodes in wireless sensor network," *International Journal of Advanced Computer Science and Applications*, vol. 4, no. 4, 2013.

[43] M. Bacco, F. Delmastro, E. Ferro, and A. Gotta, "Environmental monitoring for smart cities," *IEEE Sensors Journal*, vol. 17, no. 23, pp. 7767–7774, 2017.

[44] K. Tzortzakis, K. Papafotis, and P. P. Sotiriadis, "Wireless self powered environmental monitoring system for smart cities based on LoRa," in *2017 Panhellenic Conference on Electronics and Telecommunications (PACET)*, pp. 1–4, Xanthi, Greece, 2017.

[45] V. Tyagi, J. Flusser, and T. Ö. Eds, *24-Multiple Imputation with Spark*, 2018.

[46] S. K. N. El-deen, H. Elborai, H. E. M. Sayour, and A. Yahia, "Wireless sensor network based solution for water quality real-time monitoring," *Egyptian Journal of Solids*, vol. 41, no. 1, pp. 49–62, 2018.

[47] W. Lu, X. Xu, G. Huang et al., "Energy efficiency optimization in SWIPT enabled WSNs for smart agriculture," *IEEE Transactions on Industrial Informatics*, vol. 17, no. 6, pp. 4335–4344, 2021.

[48] M. R. Mohd Kassim, I. Mat, and A. N. Harun, "Wireless sensor network in precision agriculture application," in *2014 international conference on computer, information and telecommunication systems, CITS 2014*, pp. 1–5, Jeju, Korea (South), 2014.

[49] R. Jain, S. Kulkarni, A. Shaikh, and A. Sood, "Automatic irrigation system for agriculture field using wireless sensor network (Wsn)," *International Research Journal of Engineering and Technology*, vol. 3, pp. 1602–1605, 2016.

[50] D. K. Rathinam, D. Surendran, A. Shilpa, A. Santhiya Grace, and J. Sherin, "Modern agriculture using wireless sensor network (WSN)," in *2019 5th International Conference on Advanced Computing and Communication Systems, ICACCS 2019*, pp. 515–519, Coimbatore, India, 2019.

[51] U. Shafi, R. Mumtaz, J. García-Nieto, S. A. Hassan, S. A. R. Zaidi, and N. Iqbal, "Precision agriculture techniques and practices: from considerations to applications," *Sensors*, vol. 19, no. 17, pp. 1–25, 2019.

[52] C. Amuthadevi, J. Sathya Priya, and B. Madhusudhanan, "Validation of multicast routing in cyber physical systems monitoring air quality," *Cluster Computing*, vol. 22, no. S2, pp. 3917–3923, 2019.

[53] Q. A. Al-haija, I. Alfarran, A. Alabdullah, O. Aldhafeeri, and M. Alkhaldi, "Design and on-field testing of wireless sensor network-based air quality monitoring system," *JITCE (Journal of Information Technology and Computer Engineering)*, vol. 3, no. 2, pp. 54–59, 2019.

[54] A. Prof, R. Vinayakumar, A. Prof, and R. Varghese, *An Automated Landslide Detection System*, vol. 9, no. 3, pp. 9–15, 2021.

[55] N. El-Bendary, M. Fouad, R. Ramadan, S. Banerjee, and A. Hassanien, "Smart environmental monitoring using wireless sensor networks," *Wireless Sensor Networks*, pp. 731–754, 2013.

[56] G. Mei, N. Xu, J. Qin, B. Wang, and P. Qi, "A survey of internet of things (IoT) for geohazard prevention: applications, technologies, and challenges," *IEEE Internet of Things Journal*, vol. 7, no. 5, pp. 4371–4386, 2020.

[57] A. Sofwan, M. Ridho, and A. Goni, "Wireless sensor network design for landslide warning system in IoT architecture," in *Proceedings -2017 4th International Conference on Information Technology, Computer, and Electrical Engineering, ICITACEE 2017*, pp. 280–283, Semarang, Indonesia, 2017.

[58] K. S. Bhosale and R. Kulkarni, "Landslide monitoring using wireless sensor networks- a case study," *UGC Care Journal*, vol. 60, pp. 2304–2307, 2020.

[59] V. Vimal and M. Ji Nigam, "Forest fire prevention using WSN assisted IOT," *Engineering & Technology*, vol. 7, p. 1317, 2018.

[60] D. Arjun and A. Hanumanthaiah, "Wireless sensor network framework for early detection and warning of forest fire," in *Proceedings of the 5th International Conference on Inventive Computation Technologies, ICICT 2020*, pp. 186–191, Coimbatore, India, 2020.

[61] B. Kadri, B. Bouyeddou, and D. Moussaoui, "Early fire detection system using wireless sensor networks," in *Proceedings of the 2018 International Conference on Applied Smart Systems, ICASS 2018*, pp. 1–4, Medea, Algeria, 2019.

[62] Y. H. Xu, Q. Y. Sun, and Y. T. Xiao, "An environmentally aware scheme of wireless sensor networks for forest fire

monitoring and detection," *Future Internet*, vol. 10, no. 10, p. 102, 2018.

[63] A. Förster and A. L. Murphy, "Machine learning across the WSN layers," *Emerging Communications for Wireless Sensor Networks*, pp. 165–182, 2011.

[64] H. Sharma, A. Haque, and F. Blaabjerg, "Machine learning in wireless sensor networks for smart cities: a survey," *Electronics*, vol. 10, no. 9, p. 1012, 2021.

[65] A. Sperotto, J. L. Molina, S. Torresan, A. Critto, and A. Marcomini, "Reviewing Bayesian networks potentials for climate change impacts assessment and management: a multi-risk perspective," *Journal of Environmental Management*, vol. 202, Part 1, pp. 320–331, 2017.

[66] S. K. Baduge, S. Thilakarathna, J. S. Perera et al., "Artificial intelligence and smart vision for building and construction 4.0: machine and deep learning methods and applications," *Automation in Construction*, vol. 141, article 104440, 2022.

[67] Y. Himeur, K. Ghanem, A. Alsalemi, F. Bensaali, and A. Amira, "Artificial intelligence based anomaly detection of energy consumption in buildings: a review, current trends and new perspectives," *Applied Energy*, vol. 287, article 116601, 2021.

[68] H. Abrach, S. Bhatti, J. Carlson et al., "MANTIS: system support for multimodal networks of in-situ sensors," in *Proceedings of the Second ACM International Workshop on Wireless Sensor Networks and Applications, WSNA 2003*, pp. 50–59, San Diego, CA, USA, 2003.

[69] K. Lorincz, B. Chen, J. Waterman, G. Werner-allen, and M. Welsh, "Resource aware programming in the pixie OS categories and subject descriptors," in *Proceedings of the 6th ACM conference on Embedded network sensor systems*, pp. 211–224, Raleigh, NC, USA, 2008.

[70] R. Rengaswamy, R. Shea, and E. Kohler, "SOS: A dynamic operating system for sensor networks," in *Proceedings of the third international conference on Mobile systems, applications, and services (Mobisys'05)*, Seattle, WA, USA, 2005.

[71] Q. Cao, T. Abdelzaher, J. Stankovic, and T. He, "The lite OS operating system: towards Unix-like abstractions for wireless sensor networks," in *Proceedings -2008 International Conference on Information Processing in Sensor Networks, IPSN 2008*, pp. 233–244, St. Louis, MO, USA, 2008.

[72] M. Henschke, X. Wei, and X. Zhang, "Data visualization for wireless sensor networks using things board," in *2020 29th Wireless and Optical Communications Conference (WOCC)*, Newark, NJ, USA, 2020.

Hindawi

Retraction

Retracted: Development of Ecological Health Tourism Products under the Background of Internet+

Journal of Sensors

This article has been retracted by Hindawi following an investigation undertaken by the publisher [1]. This investigation has uncovered evidence of one or more of the following indicators of systematic manipulation of the publication process:

(1) Discrepancies in scope

(2) Discrepancies in the description of the research reported

(3) Discrepancies between the availability of data and the research described

(4) Inappropriate citations

(5) Incoherent, meaningless and/or irrelevant content included in the article

(6) Peer-review manipulation

The presence of these indicators undermines our confidence in the integrity of the article's content and we cannot, therefore, vouch for its reliability. Please note that this notice is intended solely to alert readers that the content of this article is unreliable. We have not investigated whether authors were aware of or involved in the systematic manipulation of the publication process.

Wiley and Hindawi regrets that the usual quality checks did not identify these issues before publication and have since put additional measures in place to safeguard research integrity.

We wish to credit our own Research Integrity and Research Publishing teams and anonymous and named external researchers and research integrity experts for contributing to this investigation.

The corresponding author, as the representative of all authors, has been given the opportunity to register their agreement or disagreement to this retraction. We have kept a record of any response received.

References

[1] X. Wang, "Development of Ecological Health Tourism Products under the Background of Internet+," *Journal of Sensors*, vol. 2022, Article ID 9559606, 9 pages, 2022.

Research Article

Development of Ecological Health Tourism Products under the Background of Internet+

Xin Wang [ID]

Department of Culture and Tourism, Taiyuan University, Taiyuan, Shanxi 030032, China

Correspondence should be addressed to Xin Wang; wangxin@tyu.edu.cn

With the development of domestic economy and the improvement of people's living standard, tourism has become more and more popular as a leisure lifestyle. The explosive growth of the mobile Internet has caused the problem of "information overload". The travel recommendation system can help tourists obtain the travel information that users are interested in from the massive data. Ecological health tourism is a special tourism product with ecological environment as the background and leisure health activities as the theme. With the development of China's urbanization and the intensification of population aging, the Chinese people's demand for health tourism products and ecological health tourism market is becoming stronger and stronger, and the development prospect is extremely broad, but there is not much research in this field in the academic circles at present. This paper applies the Collaborative Filtering (CF) to travel recommendation to provide users with accurate travel recommendation services. However, because the traditional CF only relies on a single user's rating data, and has its own defects, it cannot meet the complex needs of users in the tourism industry. This paper improves the traditional CF and designs and implements a tourism recommendation system on this basis. Combine Spark cloud computing platform technology and TC-Personal Rank algorithm to achieve a breakthrough in the algorithm. Through experiments, it can be found that the accuracy of product recommendation can be improved by 75.3% for the algorithm designed in this paper. Overall, the recall rate can reach 65.7%. And it can also achieve good results in recommendation satisfaction and recommendation coverage.

1. Introduction

Ecotourism is one of the hotspots and trends in global tourism development. Ecotourism resources are composed of ecotourism landscape and ecotourism environment. Scientific establishment of ecotravel resources evaluation index system and objective evaluation of ecotravel resources is an important foundation for rational development and utilization of ecotravel resources, tapping its potential, and promoting the healthy development of ecotravel [1, 2]. Therefore, people are enthusiastic about getting rid of diseases, keeping fit, and prolonging life, and there is a more urgent need for health knowledge [3]. With the return of traditional culture in recent years, people gradually understand the main guidance of humanism and tradition for spiritual attribution, and gradually rise the trend of reconstruction of spiritual home. Similarly, in terms of health preservation culture, people find that the essence of traditional culture is the true meaning of health

preservation. Traditional culture is not only people's spiritual home but also directly leads people to a scientific way of health preservation [4].

The development of new tourism products effectively combines our consumers and producers with the power of the Internet, which promotes not only the development of tourism but also the development of the service industry and the tertiary industry, making our new products the structure forms diversified development [5]. Under the conditions of the national macropolicy inclination and the increasing demand for national leisure and vacation, the development of ecotravel has obvious advantages, but it faces multiple obstacles. The arrival of the "Internet plus" era points out a new direction for the development of tourism industry. The high integration of information and tourism can provide new ideas for ecotourism, improve the quality of ecotourism, and promote the development of ecotourism [6, 7]. From the perspective of "Internet+"

ecotourism research and with the social progress, the tourism industry is becoming more and more information-based and gradually developed into the "Internet+ tourism" mode. The following problems are information overload [8]. The so-called information resource overload means that with the development of society, economy, and technology, more and more information is produced, and finally, the total amount of information greatly exceeds people's needs, thus causing difficulties for people to choose and use. In the aspect of theoretical research, it is helpful to enrich the theoretical research system of "Internet plus tourism" and provide new modes and new ideas for the innovative development of ecotravel industry.

At this stage, domestic scholars lack of research on the new development model when studying the innovative development of ecotourism industry [9, 10]. This paper is based on the development model of "Internet+" and "+tourism", and on the basis of in-depth research on the construction of ecotravel network platform, combined with the characteristics of new media such as mobile app, to give full play to the marketing and publicity role of the Internet in the tourism industry, to a certain extent. It is helpful to enrich the theoretical research system of "Internet+tourism" [11]. As the online travel industry is emerging soon, the competition among major travel websites is becoming increasingly fierce, which makes major enterprises finance and integrate one after another, and it is a common problem that travel websites generally lose money by subsidizing and burning money [12, 13]. As a service-oriented tourism website, its core competitiveness is the high quality of its service, increasing the attraction to users and maintaining high loyalty. However, at present, some well-known domestic tourism websites have not provided personalized services to users, and some websites will cooperate with scenic spots and give priority to recommending cooperative scenic spots for users. Such recommendation results do not meet the personal characteristics of users. When building an ecotourism recommendation system, the research and selection of recommendation algorithms are crucial. Today, a single recommendation algorithm technology can no longer meet the needs of tourists for tourism information services, and the combined application of multiple recommendation algorithms has become a new direction of ecotourism recommendation system research [14]. However, the above research has not solved the problem of ecotravel scenic spot recommendation based on the Internet, so this paper puts forward the following innovations on this basis:

(1) Research on the storage, calculation, and analysis of tourism data information. Some existing recommendation algorithms do not consider the problems of tourism data storage and computing analysis. In view of this situation, this paper combines the Spark cloud computing platform technology, which is an excellent technology in the Internet field. The distributed storage platform of Hadoop is used to store tourist information data in a distributed manner, and the Spark distributed computing platform based on memory is used to run the algorithm model of scenic spots recommendation, so as to improve the timeliness of algorithm recommendation

(2) A TC-Personal Rank optimization algorithm with dynamic time weight is proposed [15]. After analyzing the traditional tourism recommendation algorithms, it is found that they often ignore the impact of user travel time on the recommendation results. Therefore, a TC-Personal Rank algorithm based on user consumption model and dynamic time weight is proposed

2. Related Work

Li et al. think that the rapid development of information and communication technology has changed people's traditional way of life, such as communication and consumption. The establishment and development of virtual space not only provide us with more convenient life services but also open a broader vision [16]. Zhu et al. proposed health tourism as an emerging tourism method. Due to its late appearance, theoretical research is still lagging behind other tourism products and systems with more mature markets. There are many aspects of it. A systematic study on it, accurately defining the definition, nature, characteristics, classification of health tourism resources, and development of health tourism products will help clarify its theoretical framework and improve its theory [17]. The research of Liao et al. shows that with the change of the environment and development degree of tourism resources, the quality of tourism resources also show a dynamic change process. However, the original tourism resource evaluation index system focuses more on the evaluation of the current value of resources and less on the development of potential of resources, resulting in the value evaluation of ecotourism resources not being objective and comprehensive, it is difficult to give full play to the potential of ecotourism resources [18]. Cao believes that the rational transformation of tourism resources into economic benefits, how to effectively improve the situation of traditional rural areas, promote rural modernization and improve tourism information services, solve the brain drain in rural areas, lack of motivation for rural construction, etc., are all in the development of rural tourism. It is a common and urgent problem that needs to be solved [19]. Shen believes that the "+" in "Internet plus" determines the integration of the two formats, breaks the isolated relationship between traditional industries, integrates the wisdom of many fields with a more open attitude, advocates "group wisdom", and incorporates the traditional product research and development, production, marketing, publicity, and sales into the new development model [20]. The research of Shang et al. shows that due to their own defects and the complexity of scenic spots and tourism users, the CF cannot fully meet the needs of the users. In view of such characteristics, based on previous studies, it is found that the CF pays attention to user scoring and ignores the self attributes of scenic spots, another important participant of the recommendation system [21]. Chaudhary et al. pointed out that as a service-oriented travel website, its core competitiveness
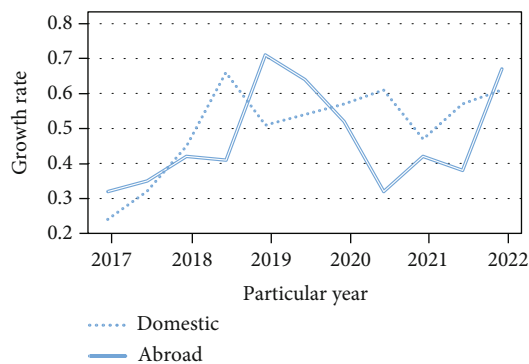
Figure 1: Comparison of growth rate of online tourism at home and abroad in recent years.

is the high quality of its services, increasing its attractiveness to users and keeping them highly loyal. However, at present, some well-known tourism websites in China have not provided personalized services to users, and some websites will cooperate with scenic spots, giving priority to recommending cooperative scenic spots for users. Such recommendation results do not conform to users' personal characteristics. After logging in to the website, users need to look up a lot of travel information by themselves, which makes users who have no clear destination feel confused and tired [22]. Alaei et al. use Bayesian network to build a tourism recommendation system. By obtaining the relevant information of scenic spots from tourism websites, and using Bayesian network to analyze the location, time, and user evaluation of scenic spots, we can provide personalized tourism suggestions for users in unfamiliar scenic spots. The system also provides an interface to display recommendation results and user feedback [23]. Magasic and Gretzel proposed a combined tourism recommendation scheme based on the HSS model and the newly designed MM-VBPR algorithm, which alleviates the sparsity problem of tourism data by utilizing scenic spot images, and can well utilize multiple semantic correlations between image features, and finally, implement combinatorial recommendations based on lists generated from a multimodal and statistical perspective [24]. Son et al. put forward a tourist guidance system W2Go, which uses the attributes of tourist attractions obtained from tourist websites and the automatic landmark ranking algorithm evaluated by users. The system can automatically identify and sort the coordinates of tourist attractions and recommend the results to users [25]. Jiang believes that the model is verified by using dataset acquisition. By searching relevant data, it is summarized that the scenic spots are divided into nine categories: geographical scenic spot, water scenic spot, biological scenic spot, historical relics scenic spot, museum scenic spot, theme park scenic spot, resort, building scenic spot, and national folk custom scenic spot. According to the introduction of scenic spots, key words are extracted to classify all scenic spots in Hebei Province [26]. Qadar et al. believe the gradual promotion of "Internet+" to a strategic level at the national level, especially that government departments actively play the role of advocates and leaders of the "Internet+" model and

deeply explore the potential of the market. With the corresponding and implementation of the slogan of "mass innovation, national innovation", "Internet+" will play a significant social effect and economic value in a certain period of time in the future [27].

On the basis of the above-mentioned research work, this paper determines the positive role of the research field of ecohealth tourism product development under the background of "Internet plus", and constructs a recommendation algorithm model that combines various algorithms, and makes a deep analysis and research on the acquired and collected data by using big data algorithm, so as to make more effective use of the data and mine the valuable hidden behind the data.

3. Methodology

3.1. Research and Analysis of Related Theories

3.1.1. Tourism under the Internet+ Background. Since the reform and opening up, China's tourism industry has developed rapidly with the support of the government and the stimulation of the market, and the number of tourists has been rising. Therefore, tourism is said to be a "sunrise industry". With the emergence of new generation information technologies such as big data, cloud computing, and Internet of Things, the integration of the Internet industry and tourism can bring new vitality to generate. The "Internet+" tourism era is an era of mass entrepreneurship and innovation. "Internet+" not only provides a path for traditional tourism enterprises to transform and upgrade but also attracts more creative entrepreneurs to enter the tourism industry. "Internet+" breaks the limitation of time and region, integrates tourism product production, tourism service, tourism consumption, and tourism management into an organic system, reduces the participation of middlemen, and establishes a borderless and barrier-free communication channel.

From the application of Internet technology in tourism to the transformation of tourism in the "Internet plus" era, the influence of the Internet on tourism has been around for a long time. Ecological health tourism is different from other special tourism. It requires special health activities and strict requirements for the environment. At present, the more popular health preservation tourism projects include forest bath health preservation method, fog bath health preservation method, and ecological warm soup bath method. The emergence of the "Internet+tourism" development model has provided new development ideas for the tourism industry to solve problems such as excess investment and innovative development. In particular, the transformation of infrastructure investment in traditional scenic spots to investment in virtual service fields will help promote the tourism industry. This can optimize the allocation of resources and realize the modern management and development. Figure 1 is a comparison chart of the growth rate of online tourism at home and abroad in recent years.

3.1.2. Development and Trend of Ecological Health Tourism. Health-preserving tourism, as a new way of tourism, not
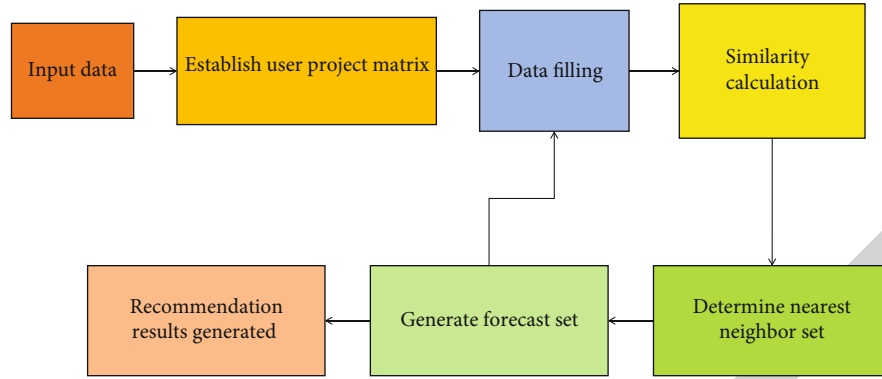
Figure 2: Basic recommendation process of CF.

only has the basic characteristics of tourism, such as consumption, leisure, sociality, aesthetics, and other characteristics, but also has its own characteristics because it highlights the purpose of health-preserving. Health tourism is a healthy, ecological, and green way of tourism. No matter what kind of health tourism product, its consumption process is carried out on the premise of healthy ecological environment. Its goal is also implemented on the premise of maintaining the original ecology and low impact of the environment. Pursuing the sustainability of environment and health is to pursue a kind of original ecological demand. Ecology is the core pursuit of tourism development. It is also one of the core competitiveness of health tourism. With the diversified development trend of tourism demand, tourism content is also enriched. Because health tourism is highly sensitive to the environment, health tourism mostly exists in areas with good ecological environments such as mountains, forests, medical care, and leisure. The health functions are different, and the product content is also different. Eco-travel, as a special form of tourism, emphasizes the nature as the foundation, attaches importance to ecological environmental protection, environmental education, and community participation, and is a sustainable tourism form. Its basic core idea is to maintain the harmony and unity between man and land.

The differences in the understanding of ecotourism resources in tourism academic circles mainly focus on the definition of object attribute category. Strictly speaking, ecotourism resources only refer to pure natural scenery, that is, natural tourism resources with better environment. But at present, more understanding of ecotourism resources is to extend or expand on the basis of strict connotation of ecotourism resources; that is, the generalization of the concept of ecotourism resources is brought about under the background of the phenomenon of "generalization" of ecotourism, believing that ecotourism resources not only refer to nature with "natural beauty" but also include social and cultural landscapes that are in harmony with nature, full of ecological beauty, natural ecology, and human ecology, that is, natural humanistic or natural ten social tourism resources. It is the vitality of characteristic tourism products, and the brand is the business card and pass of tourism products, which often has a good and high image recognition. Charac-

teristic and brand development has become the current trend of tourism product development. Tourists' attention and choice of product features, themes, and product brands have become an important influencing factor of mass tourism consumption.

3.2. Research on Ecotourism Products Based on CF. In an increasingly information-rich world, recommendation systems have become an integral part of people's daily lives, helping individuals quickly and accurately find information about items or services of interest to them in the overwhelming amount of information around them. Especially in the tourism industry, tourism recommendation system plays a vital role in promoting the development of tourism economy. It is a bridge connecting people and things, an advanced business intelligence platform for processing, developing, and applying massive tourism big data, and can provide personalized tourism information services for system users. Generally speaking, recommendation algorithms are divided into three parts: content-based recommendation, knowledge-based recommendation, and association rule-based recommendation. Figure 2 shows the basic recommendation process of CF.

The content-based recommendation is to find the correlation between products, and then analyze the user's historical records to find the products that the user is interested in and recommend them to the user. Its core is to analyze the correlation between commodities and calculate the similarity of different commodities according to their different attributes. Knowledge-based recommendation is suitable for users in the absence of user history and is usually used in infrequent interaction scenarios. Association rules were first proposed in the field of data mining, which refers to the statistics of the relationship between different rules in historical data, that is, the probability that event A and event B will also occur. Support is the probability that a certain set $\{A, B\}$ appears in the total set I. The formula is as follows:

$$\text{Support}(A \longrightarrow B) = \frac{P(A, B)}{P(I)} = \frac{P(A \cup B)}{P(I)}. \tag{1}$$

Confidence refers to the probability of inferring B according to the association rule under the condition that event A occurs. The formula is

$$\text{Confidence}(A \longrightarrow B) = P(B|A) = \frac{P(A, B)}{P(A)} = \frac{P(A \cup B)}{P(A)}. \quad (2)$$

At this time, the promotion degree indicates the ratio of the probability of containing B under the condition of containing A to the probability of containing B under the condition of not containing A. If the final calculation result is greater than 1, it indicates that there is a strong correlation between the two. When buying A, recommending B is better than directly recommending B; 1 indicates that it is irrelevant, and the purchase of A and B is an independent event. If it is less than 1, it means that the effect of recommending B when purchasing A is worse than that of directly recommending B. The formula looks like this:

$$\text{Lift}(A \longrightarrow B) = \frac{P(B|A)}{P(B)}. \quad (3)$$

Evaluation index is an essential element to analyze the tourism competitiveness, which can show the characteristics of scenic spots in detail, and has a gain effect on the similarity calculation results of scenic spots. As a unified index evaluation system has not been formed at present, based on the study of a large number of documents, this paper analyzes and selects those with good quality and high reliability as the theoretical basis for the construction of the evaluation index system of tourist attractions in this paper. The evaluation index system is shown in Table 1.

The method used in this paper to determine the weight of data is AHP, which is a systematic and hierarchical analysis method combining qualitative and quantitative analysis. The determination process is as follows: firstly, the judgment matrix needs to be constructed, and the construction method is as follows: calculate the average value of each analysis item, and then divide by the average value to obtain the judgment matrix. The larger the average value, the higher the importance and the higher the weight. After the result is obtained, calculate the CR value. According to the results, the weights obtained are consistent, and the results are generally shown in Table 2.

Since Hadoop was born, after more than ten years of development, Hadoop has developed into a super ecosystem application system with more than 60 related components. Figure 3 shows the Hadoop big data application ecosystem. Among them, distributed file system HDFS is used as the storage layer of Hadoop, which can be used to store overloaded data information in a distributed way. YARN, as a resource management system of Hadoop, is used for unified management and scheduling of Hadoop cluster resources. MapReduce is a distributed computing system for parallel computing of data. Zookeeper is a distributed collaborative service component, which can solve the problems of data management in distributed environment. Spark is a

Table 1: Evaluation index system.

Primary index	Secondary index	Tertiary indicators
Evaluation index of tourist attractions	Competitiveness B1	Scenic area A1
		Charging standard A2
	Competitiveness B2	Scenic spot heat C1
		Service configuration C2

Table 2: Consistency test results.

Synthesis of consistency test results				
Maximum characteristic root	CI value	RI value	CR value	Consistency test results
12.000	0.000	1.450	0.000	Adopt

memory-based distributed computing framework for improving the real-time performance of massive big data processing. Ambari is a web tool for creating, managing, and monitoring the operation of Hadoop clusters. Figure 3 shows the ecological model diagram of Hadoop big data application.

Compared with Hadoop MapReduce, Spark has a real-time and efficient data processing performance, which overcomes many defects in MapReduce. The advantages of Spark are as follows: strong data processing and analysis ability and Spark will be 100 orders of magnitude faster than Hadoop in data computing level, but actually, it is about 40 orders of magnitude higher. In addition, in terms of ease of use, Spark can use a variety of programming languages, and its shell can be used for interactive programming. For the versatility of application scenarios, Spark technology system includes Spark MLlib for machine learning, Spark Streaming for streaming computing, Spark Graphx for distributed graph computing, and Spark SQL for interactive query operations and batch processing; therefore, Spark can well cope with complex task computing scenarios.

3.3. About the Optimization Scheme in CF. By studying and analyzing the problems of traditional travel recommendation algorithms, this chapter proposes a TC-Personal Rank algorithm based on user consumption model and dynamic time weight. TC-Personal Rank algorithm selects tourism services that meet the user's consumption level and consumption habits for users according to the built user consumption model. At the same time, considering the user's current travel time, give priority to recommending tourism services that meet the user's travel time.

The prediction accuracy is an offline evaluation index, which can measure and predict user behavior. The steps are as follows: first, divide the data into experimental sets and test sets, which are established offline, and then, use the experimental set to analyze the user's behavior and the model of interest to conduct experiments. After the results of the experiment are obtained, the test set data is applied to the model for testing, and the accuracy of the model prediction is calculated according to the results of the experimental set and the test set. There are two main methods of
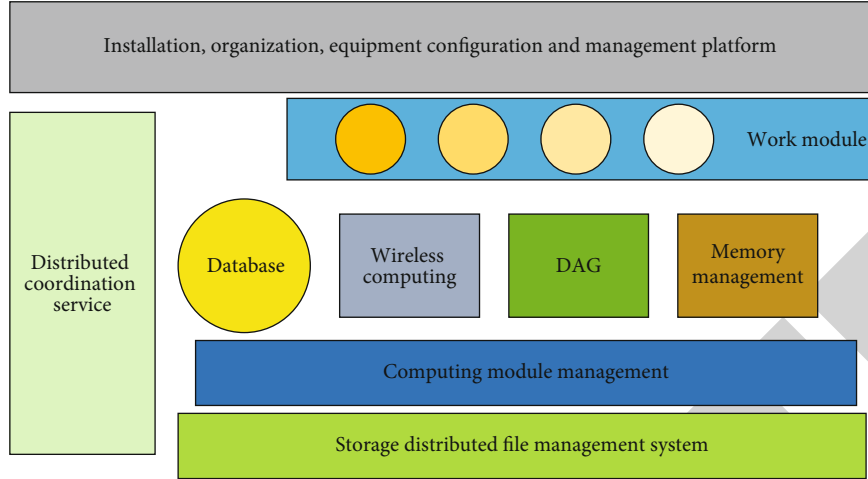
Figure 3: Ecological model diagram of Hadoop big data application.

scoring, one is root mean square error, the other is average absolute error. Defined formula expressions are as follows:

$$\mathrm{RMSE} = \sqrt{\frac{\sum_{u,i \in T} (r_{ui} - \widehat{r}_{ui})^2}{|T|}}, \qquad (4)$$

$$\mathrm{MAE} = \frac{\sum_{u,i \in T} |r_{ui} - \widehat{r}_{ui}|}{|T|}, \qquad (5)$$

where T is the data set used to test the model. The number of element data in T is $|T|$, u is the user, i is the article, is the real score of u on i obtained from the training set, and $\widehat{r}_{ui}$ is the predicted score of u on i obtained from the prediction set.

TOP-N recommendation is as follows: since the recommendation results of many recommendation systems are similar, the user's interest will be lost in the long run. The TOP-N recommendation algorithm can provide users with personalized recommendation list services, and the results of the recommendation list can be judged by the recall rate and accuracy rate (recommended accuracy). The definition formulas are as follows:

$$\mathrm{Recall} = \frac{\sum_{u \in U} |R(u) \cap T(u)|}{\sum_{u \in U} |T(u)|}, \qquad (6)$$

$$\mathrm{Precision} = \frac{\sum_{u \in U} |R(u) \cap T(u)|}{\sum_{u \in U} |T(u)|}. \qquad (7)$$

PageRank algorithm can mark different web pages in grades, and it is an index to measure the importance of web pages. In the web pages in the network, the number of all links pointing to the current web page is called the number of links in the web page. In the search engine, if you want to improve the level of a web page A in the search engine, you often do a lot of pages to point to the web page A. In this way, although the level of the web page is improved, the quality of the web page has not been improved. According to the direct connection relationship of the nodes, start from

the node of $PR \neq 0$, and set the probability to continue along the connected edge, and the probability of $1 - \alpha$ choose not to continue along the edge but stop at the node. Therefore, the formula for calculating PR is as follows:

$$\mathrm{PR}(i) = (1 - \alpha) r + \alpha \sum_{j \in \mathrm{in}(i)} \frac{\mathrm{PR}(j)}{|\mathrm{out}(j)|}, \qquad (8)$$

in which r_i is $i = u$ when $r_i = 1$ and $i \neq u$ when $r_i = 0$.

In the traditional tourism recommendation system, the recommendation algorithm only cares about the relationship between users and scenic spots. However, the travel time of users has an important impact on the results of tourism recommendation. The travel time of the recommended tourist attractions in the recommendation system needs to conform to the travel arrangement of the user. If the travel time of the recommended travel route far exceeds the travel time plan of the user, the user will ignore the recommended data, which will ultimately affect the accuracy of the recommendation result. Therefore, it needs to be solved by weighted time weighting function, and its general calculation formula is as follows:

$$F(u_i) = \log_{0.5} \left(\frac{T_{u_i}}{5} + 1 \right), \qquad (9)$$

where T_{u_i} refers to the travel time length of the user in the current time series. Taking 5 days as a travel unit, when the length of user travel time cannot be judged, $F(u_i) = 0$ indicates that the impact of user travel time on PR calculation is ignored. Then, the PR calculation formula for adding dynamic time weight is as follows:

$$\mathrm{PR}(i) = (1 - \alpha) r_i + \alpha \sum_{j \in \mathrm{in}(i)} \frac{\mathrm{PR}(j)}{|\mathrm{out}(j)|} + \log_{0.5} \left(\frac{T_{u_i}}{5} + 1 \right). \quad (10)$$

In calculating the user's interest in tourist attractions, the recommendation algorithm obtains the user's travel
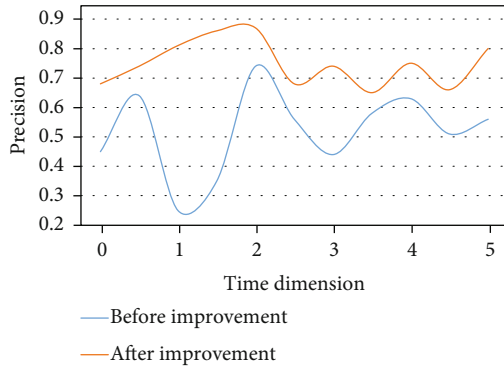
Figure 4: Analysis of the accuracy of the algorithm before and after the improvement.
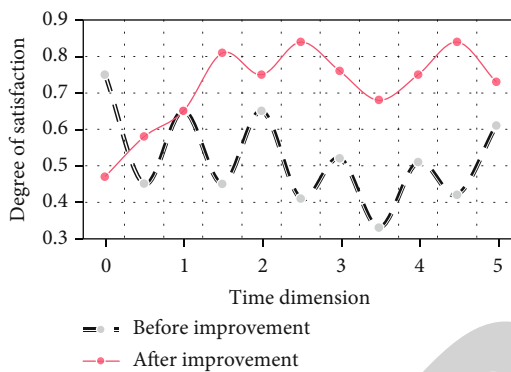
Figure 5: Analysis of algorithm recommendation satisfaction before and after improvement.

schedule according to the current time series of the user. Therefore, when the user's travel schedule time is shorter, the recommendation system will give priority to recommending tourist attractions that are closer; the longer the user's travel time is, the more distant tourist attractions can be recommended, and the user can accept the longer traffic time.

4. Result Analysis and Discussion

Based on the above research and analysis, in order to verify the effectiveness of the improved TC-Personal Rank CF, we choose to test the improved algorithm in the tourism recommendation system. In the experimental test, the improved algorithm is evaluated from the two aspects of accuracy and satisfaction. Among them, the accuracy is tested by root mean square error. Figures 4 and 5 are data analysis diagrams of CFs before and after improvement.

Compared with the traditional CF, the accuracy of the improved CF is greatly improved. With the increase of users' usage time, the recommendation results are more accurate. However, the traditional CF still has the problem of reducing the accuracy when the time increases. Although both are better reflected in the stability, there is a large gap in the accuracy of recommendation. Therefore, the improved algorithm is more powerful in the development of ecological health tourism products. It can be seen from the observation
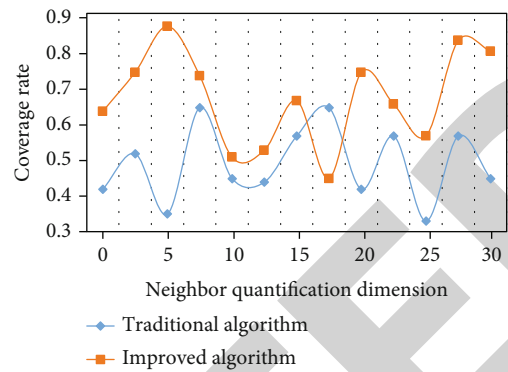
Figure 6: Coverage analysis diagram.
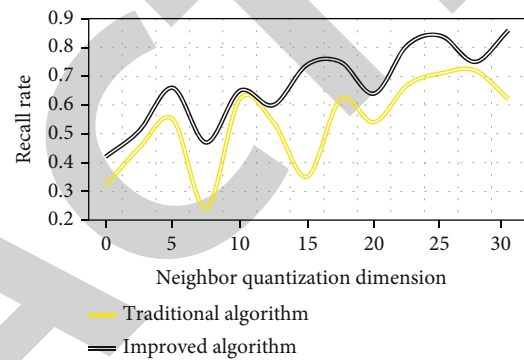
Figure 7: Recall rate analysis diagram.

that the improved algorithm after point 2 basically exhibits stable fluctuation. This is due to the normal fluctuation in the presence of a certain interference term. Since the interference influence needs to be balanced, there will be regular fluctuations to eliminate the influence of the interference term. This improves accuracy. In general, the accuracy of product recommendation is improved by 75.3%. It can be seen from the figure that the satisfaction of TC-Personal Rank algorithm is not very high at the beginning. This is because the training set did not fully understand the characteristics of users' preferences at the beginning, and with the passage of time, the accuracy of the recommendation algorithm increases, which can recommend data more in line with the characteristics of users' travel preferences for users. Finally, it is gradually stable because the user's preference characteristics are relatively stable over a period of time, so the final satisfaction with users will be in a stable stage.

On the basis of the above experimental conclusions, this paper continues to carry out scientific experiments, and then analyzes the coverage rate and recall rate, as shown in Figures 6 and 7.

Coverage is a measure of the integrity and effectiveness of the test. It is verified by calculating the proportion of users who received recommendations in the total number of users. From the figure, it can be seen that the algorithm designed in this paper is better than the traditional algorithm structure as a whole, and it shows better results in actual calculation. Generally speaking, the recall rate is the ratio of the scenic spot recommendation results actually generated for users

to the total scenic spots to be recommended. According to the recommendation list generated for users according to the test data, the results show that compared with the traditional CF, this algorithm model has higher recall rate and more accurate recommendation results. Taken together, the recall rate can reach 65.7%.

5. Conclusions

With the rapid development of information in today's society, with the improvement of people's material living standards and the increasing demand for spiritual civilization, the tourism industry is booming. The vigorous promotion of the state also stimulates the development of local tourism economy. In the face of such a huge potential tourist population, tourism service will also be a factor that cannot be ignored in the fierce competition of tourist attractions and tourism websites. This paper makes an in-depth understanding and exploration of related technologies and methods of tourism big data and related recommendation algorithms. In view of some problems faced by today's tourist attractions recommendation, an optimization scheme of tourist attractions recommendation algorithm based on Spark cloud computing platform technology is proposed, aiming to use big data. Related technologies and related recommendation algorithms are used to provide users with good tourist attractions recommendation information services. At present, the traditional travel recommendation algorithm is studied. Through the research, it is found that the traditional travel recommendation system pays more attention to the relationship between users and tourist attractions but ignores that the consumption level and travel time of users will also have an important impact on the recommendation results. Based on the traditional CF, a TC-Personal Rank algorithm based on user consumption model and dynamic time weight is proposed. Through experiments, it can be found that the accuracy of product recommendation can be improved by 75.3%. Overall, the recall rate can reach 65.7%. And it can also achieve good results in recommendation satisfaction and recommendation coverage.

Data Availability

The labeled datasets used to support the findings of this study are available from the corresponding author upon request.

Conflicts of Interest

The author declares no competing interests.

Acknowledgments

References

[1] L. Li, Z. Zhang, and S. Zhang, "Hybrid algorithm based on content and collaborative filtering in recommendation system optimization and simulation," *Scientific Programming*, vol. 2021, no. 4, 11 pages, 2021.

[2] T. T. Pan, F. Wen, and Q. R. Liu, "Collaborative filtering recommendation algorithm based on rating matrix filling and item predictability," *Zidonghua Xuebao/Acta Automatica Sinica*, vol. 43, no. 9, pp. 1597–1606, 2017.

[3] X. Li and D. Li, "An improved collaborative filtering recommendation algorithm and recommendation strategy," *Mobile Information Systems*, vol. 2019, Article ID 3560968, 11 pages, 2019.

[4] X. Cheng, L. Feng, and Q. Gui, "Collaborative filtering algorithm based on data mixing and filtering," *International Journal of Performability Engineering*, vol. 15, no. 8, p. 2267, 2019.

[5] C. Xiao-Long, D. Bo, S. Guo-Ping, and Y. Yan, "Multi-collaborative filtering algorithm for accurate push of command information system," *Revista de la Facultad de Ingenieria*, vol. 32, no. 7, pp. 165–172, 2017.

[6] S. Ye, "Application of collaborative filtering algorithm in the design of library recommendation system in university library," *Revista de la Facultad de Ingenieria*, vol. 32, no. 14, pp. 348–353, 2017.

[7] G. Luo and W. Ouyang, "A method of forest-fire image recognition based on collaborative filtering algorithm," *Boletin Tecnico/Technical Bulletin*, vol. 55, no. 9, pp. 14–19, 2017.

[8] X. Qian and G. Liu, "Restricted Boltzmann machine collaborative filtering recommendation algorithm based on project tag improvement," *International Journal of Performability Engineering*, vol. 14, no. 6, pp. 1109–1118, 2018.

[9] D. Margaris, D. Spiliotopoulos, G. Karagiorgos, and C. Vassilakis, "An algorithm for density enrichment of sparse collaborative filtering datasets using robust predictions as derived ratings," *Algorithms*, vol. 13, no. 7, p. 174, 2020.

[10] R. Mu and X. Zeng, "Collaborative filtering recommendation algorithm based on knowledge graph," *Mathematical Problems in Engineering*, vol. 2018, no. 4, 11 pages, 2018.

[11] T. Wang and M. Wang, "Distributed collaborative filtering recommendation algorithm based on DHT," *Cluster Computing*, vol. 22, no. S2, pp. 2931–2941, 2019.

[12] W. Tao and M. Wang, "Distributed collaborative filtering recommendation algorithm based on DHT," *Cluster Computing*, vol. 22, no. 1, pp. 1–11, 2019.

[13] M. Alhaj, Q. Y. Shambour, and M. Tahrawi, "A hybrid collaborative filtering recommendation algorithm for requirements elicitation," *International Journal of Computer Applications in Technology*, vol. 63, no. 1-2, p. 135, 2020.

[14] C. Ji, "A heuristic collaborative filtering recommendation algorithm based on book personalized recommendation," *International Journal of Performability Engineering*, vol. 15, no. 11, p. 2936, 2019.

[15] B. Ajma and C. Addab, "Research-supported mobile applications and internet-based technologies to mediate the psychological effects of infertility: a review," *Reproductive Biomedicine Online*, vol. 42, no. 3, pp. 679–685, 2021.

[16] G. Li, Q. Chen, and L. Li, "Collaborative filtering recommendation algorithm based on rating prediction and ranking prediction," *Tien Tzu Hsueh Pao/Acta Electronica Sinica*, vol. 45, no. 12, pp. 3070–3075, 2017.

Research Article

Effect of Forest-Based Health and Wellness on Sleep Quality of Middle-Aged People

Wei Quan [ID],[1,2] **Shaona Yu** [ID],[2] **Lizhi Xia** [ID],[2] **and Miaomiao Ying** [ID][2]

[1]*Zhejiang College of Security Technology, Wenzhou, Zhejiang 325016, China*
[2]*Wenzhou Vocational College of Science and Technology, Wenzhou Key Laboratory of Adding Carbon Sinks and Reducing Carbon Emissions of Agriculture, Forestry and Fishery Ecosystem, Wenzhou, Zhejiang 325006, China*

Correspondence should be addressed to Miaomiao Ying; yingmiaomiao@wzvcst.edu.cn

Academic Editor: Yuan Li

To explore the effect of forest-based health and wellness experiences on sleep quality for middle-aged people, we observed 12 healthy volunteers, aged 35–39 years, for three days and two nights during "forest bathing." Huawei honor-4 bracelets were used to continuously monitor their exercise and sleep patterns. After the forest-based health and wellness experience, the average sleep score of the volunteers increased by 6 points, and the length of night sleep increased by 1.6 hours. The proportion of deep sleep increased by 3%, the proportion of rapid eye movement increased by 1%, and the proportion of shallow sleep decreased by 4%. Overall, sleep quality was improved; however, this was not sustained. The effects of forest-based health and wellness experience on the sleep indicators showed both individual and gender differences; sleep quality generally improved better for females than males.

1. Introduction

The term "forest-based health and wellness" was first coined in China but has not yet been universally adopted or defined. Similar concepts are found in the United States (with the same term), "forest medical treatment" in Germany, and "forest bathing" in Japan. What they have in common is to harness natural resources and environment of the forest to promote the maintenance of physical and mental well-being. In China, it is believed that forest-based health and wellness primarily nourish the body, mind, temperament, wisdom, and morality [1]. With the rapid economic and societal development and the continuous changes in human civilization, the benefit of forest resources and environment on the human health has attracted increasing attention.

The National Bureau of Statistics of China has determined that the standard age range for middle-aged people is 35–60 years. As the dominant workforce age, the quality of sleep of the middle-aged has been shown to be lower than that of other age groups due to social and familial responsibilities [2]. One-third of a person's life is spent sleeping;

therefore, quality of sleep can have a direct impact on human health. Good sleep can regulate physiological functions and maintain nervous system balance [3]. Studies have shown that forest-based health and wellness are effective as human health care and adequate sleep is an important factor in maintaining immune function [4].

Forest experiences can affect sleep. Compared with the pre-trip period, sleeping time during the forest bathing trip has been shown to increase significantly [4]. The effect of forest bathing on improving sleep quality in military pilots was significant and superior to conventional convalescence [5]. After adding forest bathing measures to the traditional recuperation program, the sleep quality index and the satisfaction rate of nursing caregivers were significantly improved [6].

The diet and accommodation for this study were arranged in Yueman forest-based health and wellness base in Wencheng County, which is a demonstration base in Wenzhou City. Through continuous monitoring of exercise, heart rate, and sleep data of the volunteers, the effect of forest-based health and wellness experience activities on sleep changes among middle-aged volunteers was measured. The purpose of this

Sex	Number	Age (year)		Height (cm)		Weight (kg)		BMI index	
		Range	Average	Range	Average	Range	Average	Range	Average
Male	5	37–39	38	169.5–184.5	178.5	61.6–87.0	74.8	19.1–25.6	23.5
Female	7	35–39	37	151.0–172.5	161.4	45.3–72.9	58.0	19.4–24.5	22.3
Average	12	35–39	37	151.0–184.5	168.5	45.3–87.0	65.0	19.1–25.6	22.8

study was to provide a scientific basis for the enhancing the development and rational utilization of forest-based health and wellness resources in Wencheng County and promoting the development of this wellness industry.

2. Research Methods

2.1. Introduction of Volunteers. Five healthy middle-aged men and seven women were selected as volunteers, aged between 35 and 39 years (average 37 years), height range: 151.0–184.5 cm (average 168.5 cm), weight range 45.3–87.0 kg (average 65.0 kg), and BMI range 19.1–25.6 (average 22.8) (Table 1).

2.2. Experimental Design. In Wencheng County, Wenzhou, Zhejiang Province, a 3-day/2-night forest-based health and wellness experience study was conducted. Wencheng County is located in the mountainous area of southern Zhejiang Province of China. Its geographic coordinates are $119°46'$–$120°15'$E, $27°34'$–$57°59'$N. Wencheng County boundary has subtropical marine monsoon climate, forest coverage rate is 71.5%, annual average temperature is 14–18.5°C, and perennial frost-free period is 285 days.

The volunteers used Huawei Glory-4 bracelets to monitor their sleep patterns and daily exercise. A forest walk was arranged on the afternoon of the first day; a forest walk, a lotus watch, a visit to Liu Bowen's hometown, and a forest hot spring bath were arranged on the second day; a forest walk was arranged on the morning of the third day. Commitment and informed consent of family members were obtained from all volunteers. During the experiment period, the volunteers were confirmed healthy without any discomfort and did not take any drugs. To set up the controls and study, the sustainability of forest-based health and wellness experience, all measurements were made one week prior to (30 June–5 July 2019) and after (9–15 July 2019) the experience. The first day of the experiment (6 July 2019) serves as the buffer adaptation stage, and the data were collected from the second day (7 July 2019). This study was approved by the ethics committee of Dian Diagnostic.

2.3. Statistical Analysis. WPS Office 2022 was used for data calculation and mapping. Differences in sleep score, sleep continuity, and sleep ratio at different stages were tested by paired t-test with SPSS Statistics version 17.

3. Results

3.1. Sports Situation

3.1.1. The Influence on the Number of Exercise Steps. During the forest-based health and wellness experience, the number of exercise steps of 12 volunteers increased. There was an average increase of 5444 steps compared with the previous week—a significant difference between before and after the experience ($P < 0.01$). In the week after the experience, the number of exercise steps of the volunteers decreased by an average of 6944, as compared with that of the healthy experiencing activities.

3.1.2. Influence on the Distance. During the forest-based health and wellness experience period, the distance walked by 12 experimenters increased by 4.23 km on average compared with the previous week. The distance walked during forest-based health and wellness experience was significantly different from before to after the experience ($P < 0.01$). One week after the experience, the distance covered by the volunteer decreased by an average of 5.31 km compared with the period of forest-based health and wellness experience.

3.1.3. The Influence of Exercise Calories. During the forest-based health and wellness experience period, the exercise calories of the volunteers increased, and the average exercise calories of volunteers increased by 220 kilocalories compared with the week before recuperation. The exercise calories during forest-based health and wellness experience were significantly different from before to after the experience ($P < 0.01$). One week after the experience, the volunteer's exercise calories were recorded as 264 kilocalories less than that during the recreational experience (Table 2).

3.2. The Effect on the Heart Rate of the Volunteers

3.2.1. The Effect on the Minimum Heart Rate. During the forest-based health and wellness experience period, the minimum heart rate of the volunteers increased by an average of 6.5 beats per minute, compared with the previous week, and 83.33% of their volunteers' minimum heart rate was increased. In the week after the experience, the minimum heart rate of the volunteers' decreased by an average of 6.7 beats per minute. The minimum heart rate during the experience period was significantly different from that before ($P < 0.05$) to after ($P < 0.01$).

3.2.2. The Effect on the Maximum Heart Rate. During the experience period, the maximum heart rate of the volunteers decreased by an average of 8.6 beats per minute compared with the previous week, and 66.67% of the volunteers had a decrease in their maximum heart rate. The maximum heart rate of the volunteers increased by average 6.8 beats per minute in the week after the experience, compared with the period during the experience. There was no significant

TABLE 2: Survey of volunteers' sports.

Sex	Stage	Steps	Distance (km)	Heat (kcal)
	Before	9017.5 ± 2520.2	6.6 ± 2.0	281.8 ± 134.3
Total	During	14462.0 ± 4759.7	10.9 ± 4.2	502.2 ± 342.3
	After	7518.4 ± 2411.7	5.5 ± 1.9	238.4 ± 151.1
	Before	11084.8 ± 918.0	8.4 ± 1.3	410.0 ± 81.5
Male	During	18773.8 ± 5102.4	14.6 ± 5.1	815.5 ± 359.7
	After	9500.6 ± 1650.5	7.2 ± 1.5	367.4 ± 149.4
	Before	7540.9 ± 2231.0	5.3 ± 1.3	190.1 ± 71.7
Female	During	12220.7 ± 2553.8	9.0 ± 1.8	354.9 ± 201.5
	After	6102.6 ± 1798.5	4.3 ± 1.2	146.3 ± 56.4

TABLE 3: Heart rate profile of volunteers.

Sex	Stage	Minimum heart rate	Maximum heart rate	Resting heart rate
	Before	45.0 ± 7.7	145.1 ± 21.3	66.0 ± 4.5
Total	During	51.5 ± 6.1	136.5 ± 14.4	65.7 ± 5.3
	After	44.8 ± 4.7	143.3 ± 16.8	65.8 ± 4.6
	Before	45.0 ± 3.4	137.8 ± 20.1	66.3 ± 4.0
Male	During	47.2 ± 6.9	142.6 ± 19.5	62.6 ± 4.3
	After	43.4 ± 5.9	154.4 ± 20.8	65.4 ± 4.8
	Before	45.0 ± 9.6	149.3 ± 22.3	65.9 ± 5.0
Female	During	54.6 ± 3.3	132.1 ± 8.5	67.9 ± 5.2
	After	45.9 ± 3.8	135.4 ± 7.5	66.0 ± 4.7

difference in the maximum heart rate between stages ($P > 0.05$).

3.2.3. The Effect on Resting Heart Rate. Compared with the previous week, the resting heart rate during forest-based health and wellness experience period increased by 50% and decreased by 50%. There were differences in the effects of forest-based health and wellness on the resting heart rate between different volunteers; however, there was no significant difference in resting heart rate among the three stages ($P > 0.05$) (Table 3).

3.3. Effect on Sleep Patterns of the Volunteers

3.3.1. The Effect on Sleep Score. During the forest-based health and wellness experience period, 83.33% of the volunteers had higher sleep scores than the previous week, while two had lower sleep scores. According to the survey (Figure 1), two volunteers had difficulties during the recreational experience activities, and the decreased mood may have affected their sleep quality of that night. The average sleep score of the volunteers was increased by 6 points, 3 points in males, and 7 points in females. One week after the experience, the sleep score of male and female volunteers was 5 points lower than that during the experience, and 83.33% of the volunteers had lower sleep scores. The sleep scores of the volunteers during the experience were very significantly different from those before and after the experience ($P < 0.01$). There was no significant difference in the sleep scores of the volunteers before and after the experience ($P > 0.05$). The high sleep quality during the experience did not last after the experience, and the improvement of sleep quality was not sustainable.

3.3.2. The Effect on Night Sleep Length. During the forest-based health and wellness experience period, the night sleep length of males increased by 1.4 hours and that of female by 1.8 hours, with an a (Figure 2); the night sleep length increased rate was higher in females than that in males. One week after the experience, the length of sleep at night of all the volunteers was lower than that of the experience period, with a decrease of 1.5 hours in males and 0.9 hours in females. Overall, an average decrease of 1.1 hours was noted for all the volunteers, and the decrease rate of females

FIGURE 1: Comparison of sleep scores among experimental stages by gender.

FIGURE 2: Comparison of night sleep length among experimental stages by gender.

was less than that of the males. The night sleep length of the volunteers in the forest-based health and wellness experience was significantly different from those before and after the experience ($P < 0.01$), but there was no significant difference in the length of night sleep among volunteers before and after the experience ($P > 0.05$). The effect of forest-based health and wellness experience on night sleep length did not persist, and it decreased to the same level as before the experience. However, the effect of forest-based health and

wellness experience on night sleep length of female was better than that of males.

3.3.3. The Effect on Sleep Continuity. During the forest recreation experience period, the sleep continuity average score in males was 2 points lower than that of the previous week, while that in females was 5 points higher. Among them, 50% of the volunteers' sleep continuity scores increased, while that of other 50% decreased, showing significant differences between the individuals. One week after the experience, the sleep continuity score of males increased by average of 2 points, while that of females decreased by 6 points on average. Among them, 66.67% of the volunteers had lower sleep continuity scores while 33.33% of the volunteers had higher sleep continuity scores (Figure 3); forest-based health and wellness experiences have opposite effects on sleep continuity on male and female volunteers. The improvement effect of female sleep continuity was better than among males. Although the scores of sleep continuity in forest-based health and wellness experience were different from those before and after the experience, this difference was not statistically significant ($P > 0.05$).

3.3.4. The Effect on Sleep Ratio. The deep sleep stage is that of fully resting and has a powerful effect to eliminate fatigue (Table 4). Generally speaking, the higher the proportion of deep sleep, the better the quality of sleep. Shallow sleep is also a normal physiological need, but if the proportion of shallow sleep is too high, sleep quality deteriorates. Maintaining normal rapid eye movement (REM) is especially important for mental health, which helps to increase creativity and relieve stress.

In the forest-based health and wellness experience, the proportion of deep sleep of the experiencer increased by an average of 3% in two male and four female volunteers. The proportion of volunteers' REM increased by an average of 1% in four males and five females. The proportion of shallow sleep in the volunteers decreased by an average of 4% in three males and four females.

After the experience, the proportion of deep sleep of the volunteers decreased by an average of 4% in two males and four females. The proportion of volunteers' REM decreased by an average of 2% in three males decreased by two with unchanged patterns, and five females decreased by one with unchanged patterns. The proportion of shallow sleep in the volunteers increased by an average of 6% in three males and six females (Figure 4).

The proportion of deep sleep and REM of the volunteers in the forest-based health and wellness experience showed no significant difference from before to after the experience ($P > 0.05$). During the experience, the proportion of shallow sleep was significantly different from those before and after the experience ($P < 0.05$). However, there was no significant difference in the proportion of shallow sleep before and after experiencing forest bathing ($P > 0.05$). Compared with pre-experience and postexperience, the proportion of deep sleep and REM in forest-based health and wellness experience increased, while the proportion of shallow sleep decreased. Of the three phases (before, during, and after the experi-
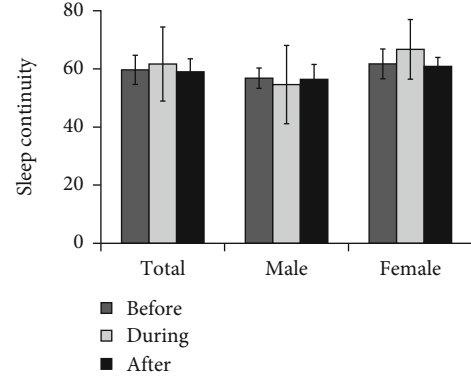
FIGURE 3: Comparison of sleep continuity at different experimental stages by gender.

TABLE 4: Normal reference value of the sleep ratio.

Category	Ratio (%)
Deep sleep	20–60
Shallow sleep	<55
REM	10–30

ence), sleep proportion was best during the experience and played a positive role in improving overall sleep quality. The proportion of shallow sleep in the experience did not last after the experience, and the effect of reducing the proportion of shallow sleep was not sustained.

4. Discussion

Sleep disturbance is a quite common within the general population, particularly as society modernizes. It is important to improve sleep quality among those who complain of sleep difficulties. Concrete and practical methods to improve sleep that are applicable in daily life are increasingly necessary. Forest walking and experiences are thought to contribute to improving sleep quality among such people. Exercise and emotional improvement initiated by walking in forested areas may bring both increased sleeping hours and improved sleep quality [7].

During this forest-based health and wellness experience, the number of exercise steps and energy expenditure increased, which appeared to help improve sleep time. In our study, the length of night sleep time increased by 1.6 hours, which is longer than an earlier study showing an increase by 30 min after forest experience [8]. Sleep time has a weak relationship with exercise [4]. An earlier study showed that a decrease in arm immobilization slows wave activity in subsequent sleep; slow wave activity is thought to reflect sleep needs [9]. Exercise may elevate core body temperature. A steep decline of core body temperature before nocturnal sleep has been reported to induce sleep [10].

A green environment has been reported to have beneficial effects on human health. Forest walking and presence in a natural environment may improve sleep quality because
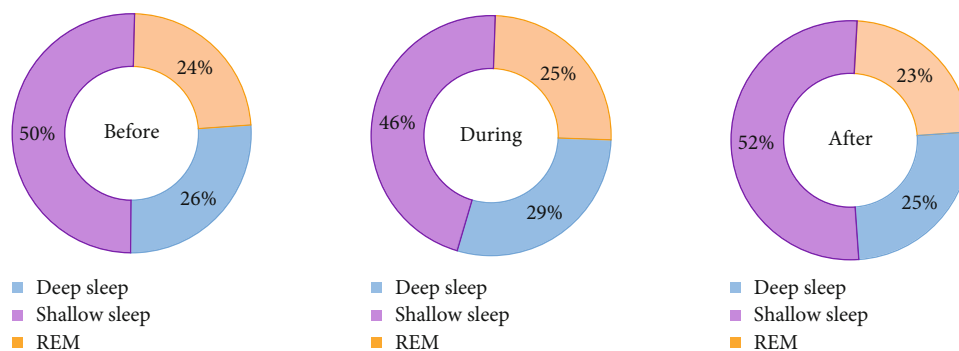
FIGURE 4: Comparison of sleep ratios at different stages of forest experience.

of its benefits on stress reduction and involvement of the physical exercise [7]. Healthy stimulation of the five senses in the forest, forest oils such as phytoncide, circadian-rhythm recovery through a regular sleep–wake cycle, timed exercise, and healthy diet and meals provided during forest therapy could be considered as relevant contributing factors [8]. The negative oxygen ion in air has a regulating effect on autonomic nervous system and high-level central nervous system, thus effectively improving the function of cerebral cortex, eliminating fatigue, and improving the work efficiency. It has a further, positive effect on improving sleep and neurasthenia [11]. There are variable conclusions on the effects of natural killer cells on sleep time [12–16].

During the forest-based health and wellness experience, a hot spring bath can eliminate fatigue and play a role in improving the sleep quality. Two volunteers who had a quarrel had lower sleep quality scores, so sleep improvement may depend on not only exercise but also on psychological factors.

Our study designed in this preliminary investigation had some limitations that could be overcome in future studies. These include a small number of participants, the absence of a control group, and its short duration (three days and two nights). The improvement of sleep quality was the result of multiple, combined factors, and our design prevented us from distinguishing them.

5. Conclusion

By means of the experience, the positive effects of forest-based health and wellness on sleep quality of middle-aged people were further confirmed. The outcomes could be summarized as increasing the length of night sleep, increasing the proportion of deep sleep and REM, improving the sleep score and quality, and reducing the proportion of shallow sleep. The effect of improving the quality of sleep was greater in females than males, so forest bathing showed a beneficial effect on sleep. In order to better understand the internal mechanism, the environmental background such as ambient air quality and plant essence should be taken into account in future research.

Data Availability

The data used to support the findings of this study are available from the corresponding author upon request.

Conflicts of Interest

The authors declare that they have no conflicts of interest.

Acknowledgments

References

[1] H. J. Wu, X. Q. Dan, S. H. Liu et al., "Health rehabilitation and recreation in forests: concept connotation, product type and development route," *Chinese Journal of Ecology*, vol. 37, no. 7, pp. 2159–2169, 2018.

[2] M. L. Liu and J. Chen, "Investigation and analysis on sleep quality status in middle-aged people," *Modem Preventive Medicine*, vol. 35, no. 19, pp. 3735–3737, 2008.

[3] C. Xu, "Good sleep begins with healthy psychology," *Health Guide*, vol. 3, pp. 34-35, 2015.

[4] Q. Li, *Forest Medicine*, Science Press, Beijing, 2013.

[5] B. Li and X. Nie, "Investigation and analysis of the effect of forest bath on sleep quality of military pilots during recuperation period," *Chin J Convalescent Med*, vol. 23, no. 1, pp. 75-76, 2014.

[6] P. Chen and X. Q. Chen, "Effect of forest bath on sleep quality of rehabilitation workers," *Chin J Convalescent Med*, vol. 29, no. 7, pp. 717–719, 2020.

[7] E. Morita, M. Imai, M. Okawa, T. Miyaura, and S. Miyazaki, "A before and after comparison of the effects of forest walking on the sleep of a community-based sample of people with sleep complaints," *BioPsychoSocial medicine*, vol. 5, no. 1, pp. 13–13, 2011.

[8] H. Kim, Y. W. Lee, H. J. Ju, B. J. Jang, and Y. I. Kim, "An exploratory study on the effects of forest therapy on sleep quality in patients with gastrointestinal tract cancers," *International Journal of Environmental Research and Public Health*, vol. 16, no. 14, p. 2449, 2019.

[9] R. Huber, M. F. Ghilardi, M. Massimini et al., "Arm immobilization causes cortical plastic changes and locally decreases sleep slow wave activity," *Nature Neuroscience*, vol. 9, no. 9, pp. 1169–1176, 2006.

[10] K. Kräuchi and A. Wirz-Justice, "Circadian clues to sleep onset mechanisms," *Neuropsychopharmacology*, vol. 25, no. 5, pp. S92–S96, 2001.

[11] L. Yang, C. Qing, and L. Xuan, "The treatment of chronic insomnia convalescents by natural negative oxygen ions," *Chinese Manipulation & Rehabilitation Medicine*, vol. 3, no. 32, pp. 396-397, 2012.

[12] C. Inoue, T. Takeshita, H. Kondo, and K. Morimoto, "Healthy lifestyles are associated with higher lymphokine-activated killer cell activity," *Preventive Medicine*, vol. 25, no. 6, pp. 717–724, 1996.

[13] Y. Kusaka, H. Kondou, and K. Morimoto, "Healthy lifestyles are associated with higher natural killer cell activity," *Preventive Medicine*, vol. 21, no. 5, pp. 602–615, 1992.

[14] Q. Li, K. Morimoto, A. Nakadai et al., "Healthy lifestyles are associated with higher levels of perforin, granulysin and granzymes A/B-expressing cells in peripheral blood lymphocytes," *Preventive Medicine*, vol. 44, no. 2, pp. 117–123, 2007.

[15] H. Moldofsky, F. A. Lue, J. R. Davidson, and R. Gorczynski, "Effects of sleep deprivation on human immune functions," *The FASEB Journal*, vol. 3, no. 8, pp. 1972–1977, 1989.

[16] Y. Matsumoto, K. Mishima, K. Satoh et al., "Total sleep deprivation induces an acute and transient increase in NK cell activity in healthy young volunteers," *Sleep*, vol. 24, no. 7, pp. 804–809, 2001.

Research Article

Analysis of Vegetable Waste Pollution Risk and Resource Potential Based on Geographical Information System and Remote Sensing

Pingheng Li [ID]

Business School, Huanggang Normal University, Huanggang 438000, China

Correspondence should be addressed to Pingheng Li; li_pingheng@outlook.com

Land resources are an important foundation for human survival and development. In recent years, land resources have experienced rapid industrialization and urbanization. With the expansion of urban construction land and the sharp decline of natural and agricultural landscapes, ecological and social problems have gradually surfaced. Based on the intuitive interpretation of LandsatTM/ETM +/OLI image data from 2016 to 2020, this work created an annual land use reference database. The use of resources and the recovery of nutrients from vegetable waste are necessary measures to achieve sustainable and environmentally friendly agriculture. Collecting and analyzing data from the literature are to determine the risk of vegetable waste pollution and the possibility of resource utilization. The amount of vegetable waste produced and the total amount of nitrogen, total phosphorus, and total potassium pollution in the study area are estimated, and ArcGIS is used to characterize TN (total nitrogen) and TP (total phosphorus). The spatial distribution of TK (total potassium) pollution intensity and pollution risk comprehensive index determines the key areas of vegetable waste nonpoint source pollution control in the region and compares the resource utilization potential of vegetable waste based on the demand for fertilizer. This paper combines the research of the subject; takes cultivated land as the research object; clarifies the main pollutants, contaminated area, content, and distribution of cultivated land; uses factor analysis method to conduct a preliminary study on the causes of heavy metal contaminated soil in the study area; and adopts a source-sink balance model, analyze the cumulative characteristics of soil pollution. Based on geographical information system (GIS) and remote sensing technology, this paper investigates the risk assessment of vegetable waste pollution and discusses the analysis of resource potential.

1. Introduction

The surface system is the material basis for human survival, and land use is one of the most direct landscape symbols. As the most direct manifestation of the interaction between human activities and the natural environment, land use land cover (LULC) has become one of the most important way to understand the regional environmental change [1]. At the same time, it has become the main content of the international geosphere biosphere program and the international human program of global environmental change and is the research hotspot in the current academic circles [2]. With the help of dynamic change model, transfer model, and overlay buffer analysis, this paper analyzes the spatial model and regional differences of LUCC in the study area and selects the indicators of ecological security construction based on P.S.R (pressure-state-response) model and obtains the environmental security assessment results through system assessment and GIS remote sensing analysis [3]. Heavy metal pollution is the research focus of agricultural land pollution; and its harm to soil environmental quality, production, and crop quality has aroused widespread concern [4]. Heavy metal pollution of agricultural land in China is mainly concentrated in the current situation of agricultural land pollution and remediation, and the pollution characteristics are not specified [5]. At present, there are few risk assessment methods and indicators for agricultural soil pollution in China, and the assessment results of soil and plant
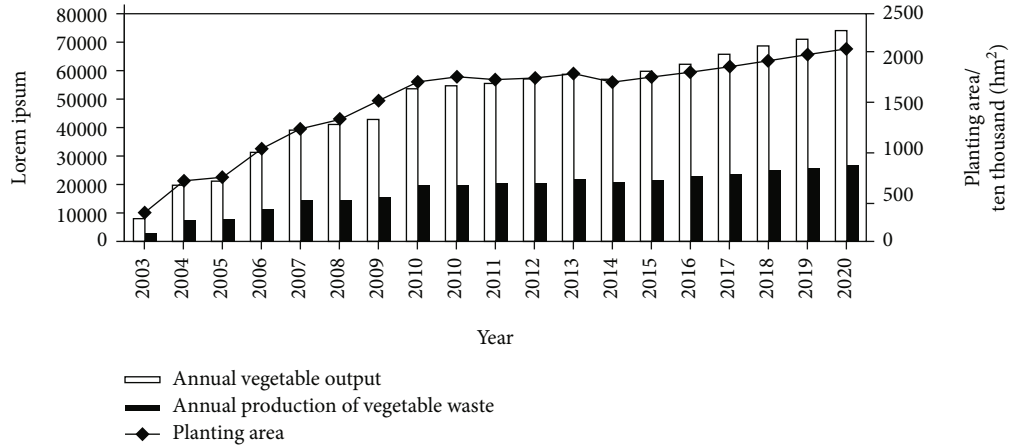
FIGURE 1: The changing trend of vegetable planting area, annual output, and annual output of vegetable waste in China from 1987 to 2020.

pollution are inconsistent [6]. At the same time, China's vegetable planting area and total output continue to grow. In 2020, China's vegetable planting area will reach 1998.1 million cubic meters, an increase of 23.3% over the 16.201 billion cubic meters in 2013, accounting for 32.6% of the total domestic planting area. With the continuous increase of vegetable production and the continuous improvement of residents' requirements for the quality of vegetables, residents will carry out a large number of screening when selecting vegetables. Finally, the screened vegetables are at risk of being discarded [7]. Therefore, the production of vegetable waste increases sharply, which not only causes waste but also causes a kind of pollution and even challenge to the environment. Based on the existing risk assessment methods of soil heavy metal pollution in agricultural areas, this paper puts forward a set of advanced resource potential analysis and assessment methods, which fully consider the soil and plant pollution and its accumulation trend [8]. The safe treatment and resource utilization of plant waste are the problems to be solved in China. The study area takes the alluvial plains and hilly peninsulas of the Yellow River, Huaihe River, Haihe River, and their tributaries as the research objects. It is one of the important vegetable planting areas in China, with 177 facility vegetable base counties and 68 export vegetable base counties [9]. The vegetable planting intensity is high, and there are vegetable wastes. The risk of nonpoint source pollution caused by the regional vegetable production process is high. In this paper, the source of plant waste, inventory, the advantages and disadvantages of the main treatment methods, and microbial degradation were comprehensively analyzed [10]. It was concluded that composting was the most effective way to realize the rapid utilization of resources [11].

2. Materials and Methods

2.1. Overview of the Study Area.
The Yellow River, Huaihe River, Haihe River, and their tributaries alluvial plain, as well as hills and peninsulas are the places to be studied, a total of 58 cities, drainage area: 795000 square kilometers. The soil is mainly brown soil and cinnamon soil with high yield. The

soil is rich and deep, and vegetables are planted intensively. From 2016 to 2020, the average annual horticultural output of the study area exceeded 247 million tons, accounting for 31.4% of the total national output.

According to the food and Agriculture Organization of the United Nations, the changing trend of vegetable planting area, annual output, and annual output of vegetable waste in China from 1987 to 2020 is as shown in Figure 1.

2.2. Research Methods

2.2.1. GIS and Remote Sensing.
When selecting images, the main considerations are spatial, spectral resolution, image acquisition time, image quality, image cost and availability, and the scope of the research area [12–18]. In order to meet the needs of this study, the remote sensing images used are collected and selected.

Compared with Landsat TM/ETM+, Landsat OLI data has added 2 new bands and readjusted the bands, effectively avoiding atmospheric absorption characteristics [19].

2.2.2. Risk Assessment of Vegetable Waste Pollution

(1) Estimation of Vegetable Waste Production. The horticultural output of each city in the Huanghuaihai region is from the 2010, 2015, and 2020 statistical yearbooks; the area of arable land and fertilizer consumption is taken from the 2020 provincial statistical yearbooks. In previous studies, the production waste coefficients of different types of vegetables are different. This study is based on the calculation method of agricultural nonpoint source pollution and calculates the average vegetable production waste coefficients according to the production weight of different types of vegetables. According to the national vegetable production weight and the waste generation coefficient, total nitrogen, total phosphorus, and total potassium content found in the literature, the calculation equation (1) is as follows:

$$S = \sum_{i=1}^{a=7} P_i \times S_i, \qquad (1)$$

TABLE 1: Vegetable production waste coefficient and TN, TP, and TK content.

Types of vegetables	Representative vegetables	Production waste coefficient	Moisture content	TN content	TP content	TK content
Leafy vegetables	Chinese cabbage	9.8	93.5	2.71	0.35	4.36
Melons and vegetables	Cucumber	2.6	88.3	2.35	0.94	3.42
Roots	Radish	4.3	91.3	4.05	0.45	2.65
Nightshade	Tomato	2.3	84.3	2.14	3.56	4.36
Onions and garlic	Green onions	1.8	91.5	2.32	0.36	3.12
Vegetable beans	Kidney bean	7.7	89.1	2.45	1.12	3.50
Aquatic lettuce	Lotus root	2.2	90.3	2.45	1.12	3.50

where S is the average coefficient of vegetable production waste, n represents the plant species classified by the National Bureau of Statistics of China; P_i represents the proportion of i-type vegetables, and S_i represents the i-type factory production waste coefficient. Similarly, it calculates the average moisture content, TN (total nitrogen), TP (total phosphorus), and TK (total potassium) content of vegetables, as shown in Table 1.

(2) Pollution Risk Assessment. The straw-to-wheat ratio refers to the ratio of the stalk of the crop to the yield of the crop. It is currently a generally accepted method of calculating the number of stalks in China. This study uses the plant waste generation coefficient and yearbook data to calculate the plant waste in the Huanghuaihai area Yield and its TN, TP, and TK content. The pollution intensity of agricultural nonpoint source pollution reflects the degree of agricultural intensification in certain regions and the impact of agricultural activities per unit area on water bodies. The study uses the agricultural non-point source pollution intensity method to estimate the nonpoint source pollution intensity of plant waste and uses ArcGIS to discard plants. The normalization of TN, TP, and TK pollution intensities directly reflects the spatial distribution of nonpoint source pollution of plant waste in 58 prefectures and cities in the study area (see equations (2)–(5)) [20].

$$L_V = Y \times S, \quad (2)$$

$$L_{N/P/K} = Y \times S \times C_{N/P/K}, \quad (3)$$

$$S_V = \frac{L_V}{a \times (1 - m)} \times 10000, \quad (4)$$

$$S_{N/P/K} = \frac{C_{N/P/K}}{a} \times 1000, \quad (5)$$

where L_V is the pollutant load of plant residues, S is the coefficient of production residues, $L_{N/P/K}$ is the pollutant load of TN, TP, and TK in plant residues, and $C_{N/P/K}$ is TN in plant wastes The content of TP, TK, and SV is the pollution intensity of plant waste, $S_{N/P/K}$ is the pollution intensity of TN, TP, and TK; a is the area of cultivated land, and m is the moisture content.

The risk of plant residue pollution is expressed by the pollution index. Due to the large difference in the level of index values, the dispersion of the pollution intensity values TN, TP, and TK is standardized and analyzed, and the standardized values are added with the same weight to obtain the complete pollution index. According to the risk of plant residue pollution, the pollution risk from the spread source is classified, and on this basis, the key control areas are determined. The standard deviation function is as follows [21]:

$$Q_i = \frac{X_i - X_{\min}}{X\min_{\max}}, \quad (6)$$

$$l = \frac{1}{3} \times (Q_N + Q_P + Q_K), \quad (7)$$

where Q_i is the normalized value of the evaluation factor i; X_i is the level value of the evaluation factor i; $X_{\min}$ is the minimum value of the evaluation factor; $X_{\max}$ is the maximum value of the evaluation factor; I is the global pollution index; Q_N, Q_P, and Q_K represent the normalized value of TN, TP, and TK, respectively.

2.3. Resource Utilization Potential. At present, the way to solve the problem of plant waste and pollution in China is still to use chemical fertilizer. In the process of using plant waste and fertilizer, the production of plant waste and the demand for nutrients in chemical fertilizers jointly determine the use of plant residues [22–24]. Therefore, this research uses the generation of plant waste and the demand for chemical fertilizers as the driving force to analyze the resource utilization potential of plant waste in the Huanghuaihai area. According to the statistical data of the yearbooks of the cities in the study area in 2020 [25], the prefecture-level cities are classified, and the regional percentiles of each variable are calculated, as shown in Table 2. The two-dimensional map uses ArcGIS to characterize the resource utilization potential of each city and analyze high-potential areas.

3. Results

3.1. Time Characteristics of Nonpoint Source Pollution Load of Vegetable Waste. Figure 2 shows the results of changes in the pollutant load of vegetable residues, TN, TP, and TK in the study area over time in 2010, 2015, and 2020. In 2020, the pollutant load of vegetable residues in the study

TABLE 2: Statistics of vegetable waste production and fertilizer consumption in each city in 2020.

Variable	Max	9% quantile	22% quantile	70% quantile	65% quantile	Minimum
Vegetable waste output/10^4t	88.36	53.23	38.84	21.65	12.32	1.36
Fertilizer consumption/10^4t	157.56	104.35	62.15	35.62	24.52	2.42
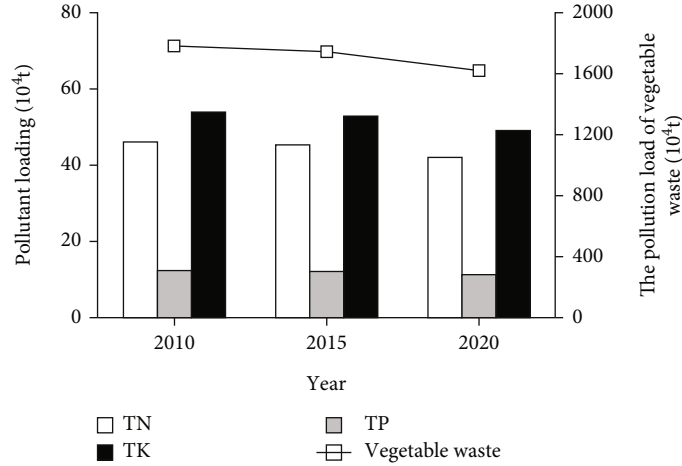
FIGURE 2: Time characteristics of vegetable waste pollution load.
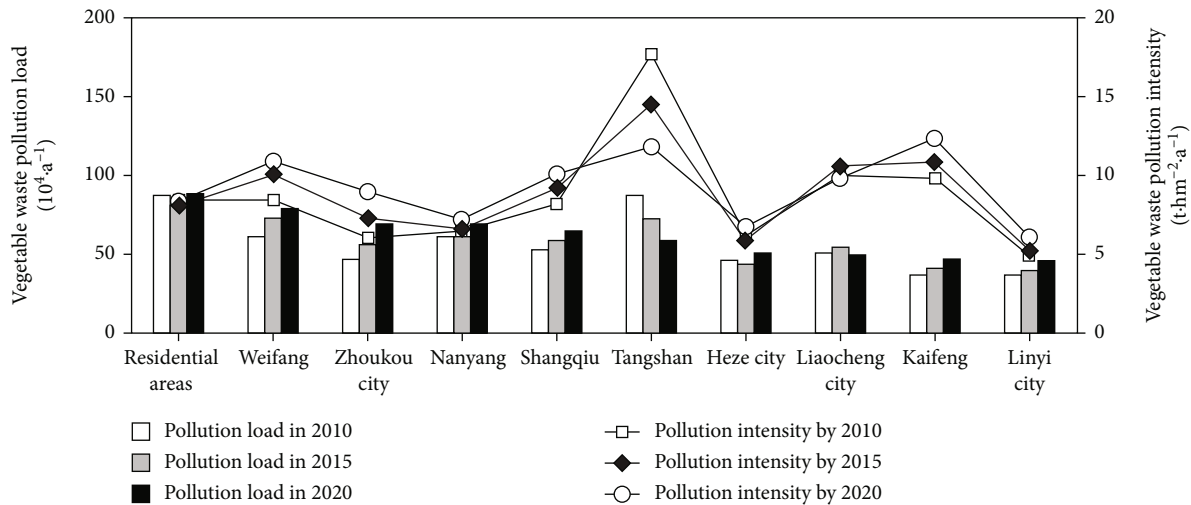
FIGURE 3: Time characteristics of pollution load and pollution intensity in the top ten cities for vegetable waste production in the study area.

area was 161,800 tons, a decrease of 8.94% compared with 2010 and a decrease of 7.08% in 2015. This may be because with the rapid development of urban-rural integration, the rural population has shown a downward trend, resulting in a decrease in vegetable output, the pollution load of plant residues decreased. In 2017, the total TN pollution load of the plant's waste was 418,800 tons, the total load of TP was 111,800 tons, and the total load of TK was 537,900 tons, which is equivalent to 7.19%, 5.10%, and 25.61 of the reduced fertilizer applications of nitrogen, phosphorus, and potassium in the district that year %.

Sort the pollutant load of plant residues in the study area from high to low, and calculate the pollutant load and pollution intensity of plant residues in 2010, 2015, and 2020. The results are shown in Figure 3. In 2020, the pollution load of

plant waste in the city was 590800 tons, which is 18.70% lower than the 726,700 tons in 2015 and 32.96% lower than the 881,200 tons in 2010. Except that the pollutant load of plant waste in 2020 is 883,800 tons, 693,400 tons, and 500,000 tons, which are not much different from 2007 and 2012, the pollutant loads of other cities have increased or decreased to varying degrees.

3.2. Spatial Characteristics of Pollution Load and Pollution Intensity. It can be seen from Table 3 that the average pollution load of plant waste in the Huanghuaihai area is 279,000 tons, with a standard deviation of 205,000 tons. The average pollution load of TN, TP, and TK is 7207.49, 1927.98, and 9274.82, and the standard deviations are 5181.26, 185.97, and 6667.40, respectively. The average pollution intensity

TABLE 3: Statistics of pollution load and pollution intensity in the study area.

Index	Number of cities	Minimum	Max	Median	Average value	Standard deviation
Pollution load of vegetable waste/(10^4t•a^{-1})	58	1.61	88.45	21.65	27.65	20.45
TN pollution load (t•a^{-1})	58	412.52	22835.42	5568.49	7207.56	5181.65
TP pollution load (t•a^{-1})	58	110.36	6108.13	1489.56	1927.65	1385.76
TK pollution load (t•a^{-1})	58	530.15	29385.46	7165.65	9274.10	6667.43
Pollution intensity of vegetable waste (t•hm^{-2}•a^{-1})	58	2.13	14.85	5.66	6.53	3.45
TN pollution intensity (kg•hm^{-2}•a^{-1})	58	4.64	26.61	32.45	23.46	18.66
TP pollution intensity (kg•hm^{-2}•a^{-1})	58	1.52	9.14	3.45	4.36	2.65
TK pollution intensity (kg•hm^{-2}•a^{-1})	58	6.36	44.65	16.36	19.36	9.55
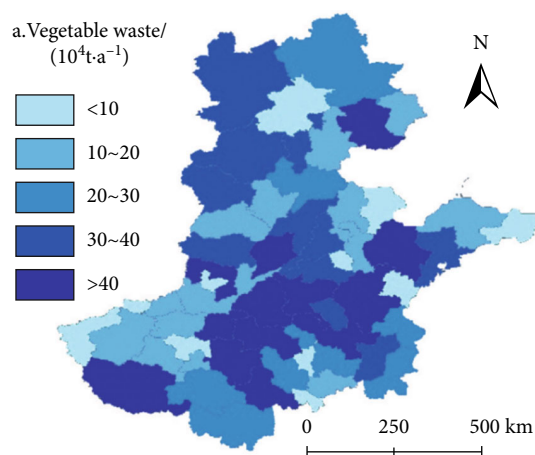
FIGURE 4: Spatial distribution of vegetable waste pollution load in the study area.
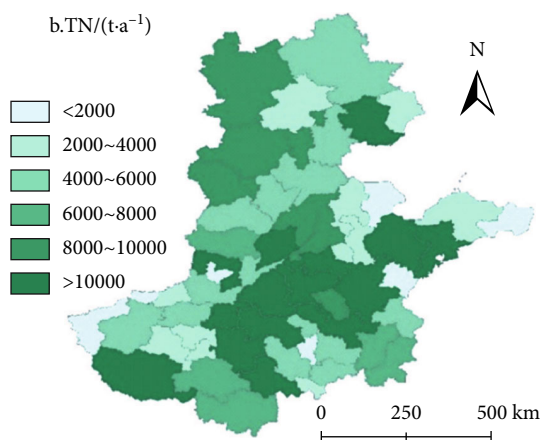
FIGURE 5: Spatial distribution of TN pollution load in the study area.

of vegetable waste in the prefecture-level cities was 6.45, with a standard deviation of 3.18; the pollution intensities of TN, TP, and TK were 15.15, 4.05, and 19.49; and the standard deviations were 7.48, 2.00, and 9.62, respectively. The pollution load and pollution intensity vary greatly in space.

The spatial distribution of plant residual pollutant load in 58 prefectures and cities in the study area is shown in Figure 4.

The spatial distribution of TN pollution load in 58 prefectures and cities in the study area is shown in Figure 5.

The spatial distribution of TP pollution load in 58 cities in the study area is shown in Figure 6.

The spatial distribution of TK pollution load in 58 prefectures and cities in the study area is shown in Figure 7.

The pollutant load of plant waste in prefecture-level cities in the study area is between 1.6 and 883,900 tons, of which 12 cities have more than 400,000 tons. These cities have large administrative areas and suitable climates. There are 10 cities where the amount of plant waste is less than 100,000 tons, most of which have less arable land and small vegetable planting area. The pollution load TN, TP, and TK of prefecture-level cities in the Huanghuaihai region are 412.45-22 835.46 t, 110.33-6 108.40 t, and 530.75-29 385.38 t, respectively, and their distribution patterns are roughly the same as those of plant residues. TN pollutant load is more than 16000 tons, TP pollutant load greater than 4000 tons, TK pollutant load greater than 19,000 tons, and
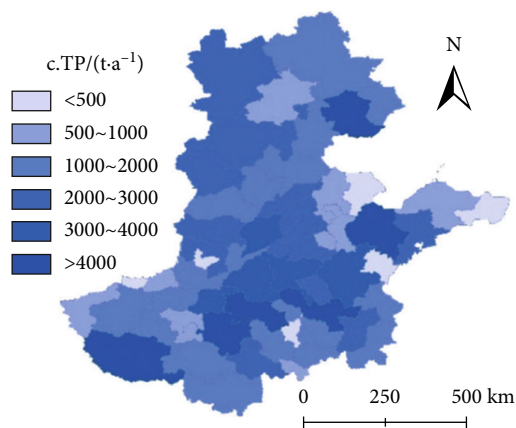
FIGURE 6: Spatial distribution of TP pollution load in the study area.

vegetable waste pollutant load, accounting for 26.44% of the total load of Huanghuaihai.

The spatial distribution characteristics of vegetable waste pollution intensity in 58 prefectures and cities in the study area are shown in Figure 8.

The spatial distribution characteristics of TN pollution intensity in 58 prefectures and cities in the study area are shown in Figure 9.
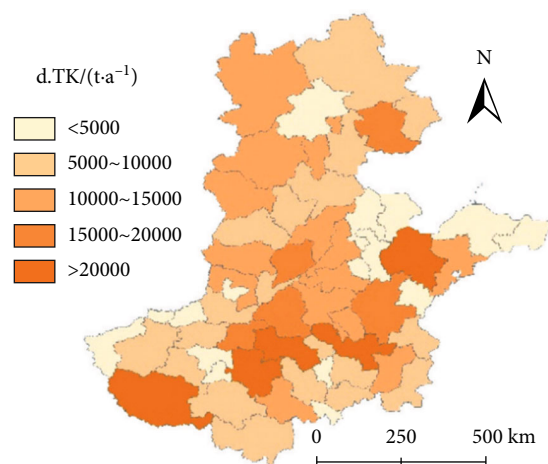
FIGURE 7: Spatial distribution of TK pollution load in the study area.

FIGURE 10: Spatial distribution of TP pollution intensity in the study area.

FIGURE 8: Spatial distribution of vegetable waste pollution intensity in the study area.
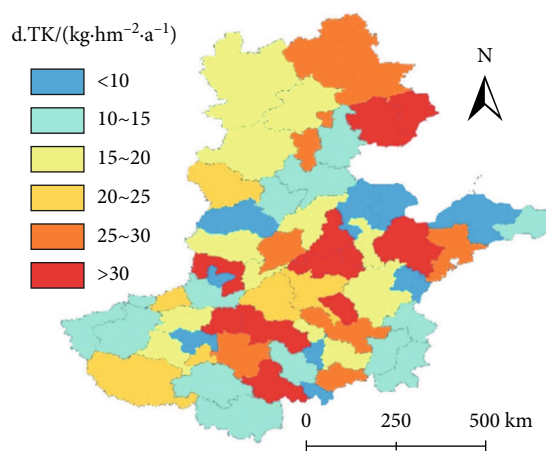
FIGURE 11: Spatial distribution of TK pollution intensity in the study area.

The spatial distribution characteristics of TK pollution intensity in 58 prefectures and cities in the study area are shown in Figure 11.

The pollution intensity of plant residues in 10 cities exceeded 10 t hm^{-2} a^{-1}, and the pollution intensity of TN, TP, and TK exceeded 23.76, 6.36, and 31.58 kg hm^{-2} a^{-1}. The average urban domestic waste in the study area the pollution intensity is 6.45 t hm^{-2} a^{-1}. In these areas, the area of arable land is relatively small, and the proportion of vegetables grown is relatively high. The pollution intensity in the south and west is relatively high. The pollution intensities of TN, TP, and TK are 4.95 -6.95, 1.32-1.86, and 7.29-8.44 kg hm^{-2} a^{-1}, respectively. It can be seen from the above results that the distribution of TN, TP, and TK pollution intensity of plant residues is relatively consistent, showing the characteristics of greater pollution in the middle and north and lower pollution in the southwest.

FIGURE 9: Spatial distribution of TN pollution intensity in the study area.

The spatial distribution characteristics of PT pollution intensity in 58 prefectures and cities in the study area are shown in Figure 10.

3.3. Spatial Analysis of Vegetable Waste Pollution Risk. The pollution risk of plant waste in the study area is more consistent with the spatial distribution of pollution intensity. There

TABLE 4: Pollution of vegetable waste in areas with high pollution risk.

| City | Pollution load | | | | Pollution intensity | | | | Comprehensive pollution index |
	Vegetable waste/ (10^4t·a^{-1})	TN/ (10^4t·a^{-1})	TP/ (10^4t·a^{-1})	TK/ (10^4t·a^{-1})	Vegetable waste/ (t·hm^{-2}·a^{-1})	TN/ (kg·hm^{-2}·a^{-1})	TP/ (10^4t·a^{-1})	TK/ (10^4t·a^{-1})	
Zaozhuang	31.65	0.54	1.30	1.65	14.96	34.95	9.36	44.49	1.01
Kaifeng city	46.35	0.12	1.52	1.45	12.45	28.46	7.45	37.27	0.91
Laiwu city	8.13	0.65	0.36	0.36	12.65	28.46	7.45	37.26	0.91
Tangshan	58.03	0.12	1.65	1.52	11.65	27.36	7.35	35.63	0.87
Tai'an city	39.03	0.45	1.34	1.65	11.35	27.16	7.26	35.70	0.87
Jinan city	37.42	0.42	1.85	1.42	11.16	27.04	7.15	34.83	0.85
Anyang	42.36	1.65	1.64	1.36	11.05	26.35	6.95	34.56	0.84
Weifang	78.12	2.46	2.62	2.46	10.59	25.46	6.64	32.62	0.79
Fuyang city	42.65	1.25	1.45	1.52	10.51	24.23	6.58	31.24	0.75
Shangqiu	65.13	1.36	2.13	2.36	10.46	23.64	6.35	30.59	0.74
Qinhuangdao city	15.42	0.34	0.56	0.75	9.26	23.59	6.12	30.09	0.72
Liaocheng	50.36	1.36	1.65	1.68	9.14	22.42	6.10	29.49	0.71
Langfang city	32.10	0.58	1.45	1.63	9.09	22.36	6.01	29.06	0.70
Chengde	21.55	0.36	0.36	0.74	9.02	21.15	5.98	27.54	0.66
Zhoukou city	69.42	1.65	2.31	2.65	8.36	20.13	5.65	26.94	0.64
Qingdao city	39.75	1.52	1.39	1.95	8.12	19.95	5.26	25.46	0.60
Xuzhou	88.35	2.36	0.45	2.48	8.69	19.45	5.21	25.36	0.60
Bengbu	19.30	0.45	2.36	0.64	8.58	19.36	5.35	25.54	0.60

are 18 cities with a comprehensive pollution index greater than 0.5. These cities have a higher risk of plant waste proliferation and pollution. The total pollutant load of plant residues is 7,846,400 tons, which is equivalent to 48.49% of the total load of the entire district, and the average pollution intensity of plant debris is 10.56 t•hm^{-2}•a^{-1}, which is 1.64 times the average pollution intensity of Huanghuaihai Lake (Table 4).

The general pollution index of urban plant waste with the highest pollution risk is 1.00, and the pollutant load of plant waste is 316,200 t•a^{-1}. The pollution loads of TN, TP, and TK are 0.82, 0.22, and 10,500 t•a^{-1}, respectively. The pollution intensity of the residue is 14.73 t•hm^{-2}•a^{-1}, and the pollution intensity of TN, TP, and TK is 14.73 t•hm^{-2}•a^{-1}. The TK is 34.57, 9.25, and 44.48 kg•hm^{-2}•a^{-1}, respectively (Figure 12).

3.4. Resource Utilization Potential of Vegetable Waste. Using plant waste as fertilizer can replace some chemical fertilizers. As can be seen from Figure 13, the plant residue output and consumption demand in the study area is up to 25%. There are 11 cities with great resource utilization potential, accounting for 19.00% of the study area. The total amount of chemical fertilizer used in these cities was 11.3771 million tons, accounting for 41.8% of the total application in the region, and the total amount of plant residues was 5,889,700 tons, accounting for 36.40% of the total application in the region. The areas with low resource utilization potential include 8 cities. The yield of plant waste and the demand for chemical fertilizers are
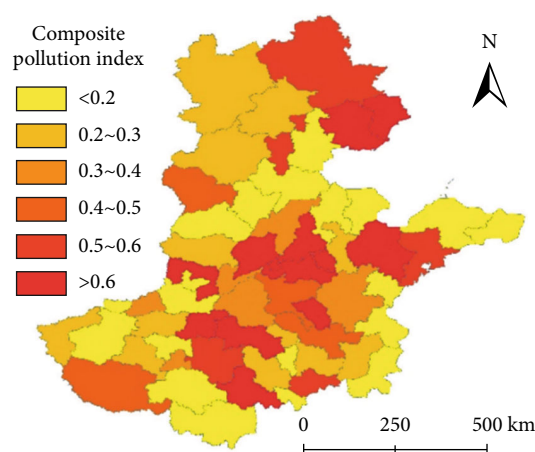
FIGURE 12: Comprehensive pollution index of vegetable waste in the study area.

at the lowest 25%. According to the 10% quantile of plant waste production and the quantile of chemical fertilizer use, the regions with high resource utilization potential are divided. It can be seen that city has the largest resource utilization potential, and plant production residues and chemical fertilizer use are ranked in the top 10%; B cities, C, D, and E are in the top 10% of fertilizer application, and crop waste production is in the top 25%. Cities F, G, and H are in the top 10% of plant waste generation, and the amount of fertilizer application is in the top 25%. The resource utilization potential is greater than that of I, J, and K cities.
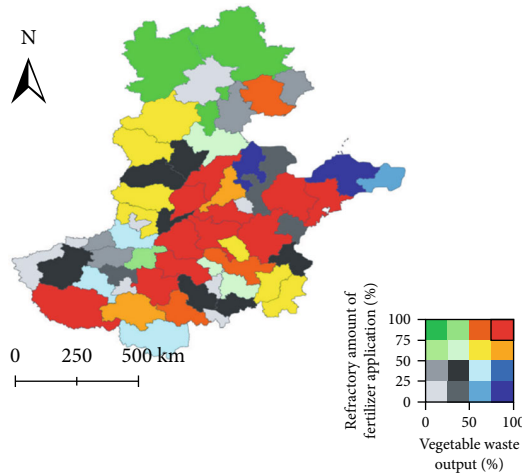
FIGURE 13: The resource utilization potential of vegetable waste in the study area.

According to the "Annual Report of China Environment Statistics" [26], the agricultural chemical oxygen demand, ammonia nitrogen, total nitrogen, and total phosphorus demand in the study basin accounted for 37.9%, 33.5%, 44.6%, and 44.2% of the top ten basins, respectively. Among them, the total nitrogen emissions they were 765,000 tons, 942,000 tons, and 350,000 tons, respectively. The total phosphorus emissions were 88,000 tons, 115,000 tons, and 39,000 tons, as shown in Table 5. The residual TN and TP pollution loads in the study area are 418,800 tons and 111,800 tons, respectively. If all the TN and TP of the plant residues enter the water body, it is equivalent to 20.3% and 20.3% of the total nitrogen and total phosphorus emissions of the marine basin's agricultural pollutants 46.2%.

4. Discussion

4.1. Risk Analysis of Vegetable Waste Pollution. As China's economic structure is an extensive agricultural economy, various agricultural wastes have become the main source of surface water pollution in rural areas. Unlike the stems of edible plants, plant remains have high moisture content, are perishable and smelly, and will pass through the sewage process. Surface runoff pollutes the surface and groundwater through scouring and leakage. The yield and waste coefficients of different types of vegetables vary greatly due to different planting and harvesting methods [27]. Compare the yield and waste coefficients of leafy vegetables, melons, and root vegetables. In the main vegetable production areas, the sown amount of various types of vegetables is relatively stable. The yield and waste coefficients are weighted by the sowing amount of different types of vegetables, which can determine the average vegetable production waste coefficient, which can overcome the difficulty in estimating the amount of vegetable waste caused by the scattered vegetable planting and uneven temporal and spatial distribution to a certain extent.

As the price of chemical fertilizers continues to rise, it is an inevitable trend for the development of modern organic agriculture to replace some chemical fertilizers with agricultural wastes. Studies have shown that the TN, TP, and TK content of plant wastes in the Huanghuaihai area can replace 908,700 tons of urea and superphosphate. Potassium sulfate 254,100 tons, potassium sulfate 1,075,800 tons. For example, after composting vegetables, they contain a lot of cellulose-decomposing bacteria, which can promote the reproduction of beneficial microorganisms in the soil, increase the content of low-molecular organic acids in the soil, and activate and effectively increase soil nutrients.

As a place to absorb organic waste, the carrying capacity of agricultural land depends not only on the nature and fertility of the soil but also on the absorption of grain and straw during harvest. The pollution intensity is the nitrogen and phosphorus nutrient pollution per unit area of the cultivated soil, which reflects pollution risk of plant waste to cultivated soil. It should be noted that the pollution level of plant waste in the 4 cities is relatively high, but the pollution intensity is relatively low. These areas have suitable climate conditions, perfect agricultural production conditions, and high vegetable yields, but the administrative area is large, the area of arable land is large, and the plant waste the pollution intensity is low. The pollution degree of plant waste in these three cities is relatively low, but the pollution intensity is relatively high, which may be related to the vegetable planting area and planting type.

The total amount of plant remains in the study area is 16.1808 million tons, which provides a good prospect for the development and application of vegetable stalks. However, the spatial distribution is wide and the yield of vegetable stalks varies greatly in different regions. Analyzed the plant waste pollution and resource utilization potential of various cities in the Huanghuaihai region. Among them, 11 cities have relatively high utilization potential. According to the natural economic conditions and agricultural development in different regions, the comprehensive utilization technology of plant residues should be promoted to the greatest extent [28]. Realize the reduction, safety, and utilization of plant residue resources.

4.2. Traditional Processing Methods of Vegetable Waste. Vegetables are generally seasonal, short in storage, difficult to transport, and perishable. The highest yield is usually in the high temperature season. In China, due to the current technical limitations, random disposal of plant residues not only causes a huge waste of resources but also it also pollutes the environment [29].

In cities, plant waste accounts for 20% to 50% of urban domestic waste. This part of plant waste is not easy to separate and dispose of separately. It is usually treated as domestic waste. In rural areas and small vegetable distribution centers, the traditional method of disposing of plant waste is mainly field accumulation [30]. Due to the high water content of plant excrement, it accumulates in large amounts in the open air and is extremely perishable and smelly, breeding mosquitoes and flies, and provides good conditions for the reproduction and transmission of pathogenic microorganisms and mineral elements in the washed and infiltrated plants. Then, the surface and groundwater pollution

TABLE 5: Agricultural pollutant discharge in the Huanghuaihai Basin (10^4t).

Watershed	Cod	Ammonia	Total nitrogen	Total phosphorus
Haihe	154.2	7.5	76.3	8.1
Huaihe	175.6	13.1	94.1	11.4
Yellow River	75.2	3.6	35.4	3.6
Total	405.3	24.5	205.9	24.5
Vegetable waste	—	—	41.30	11.19
Potential contribution rate/%	—	—	20.6	46.5

are caused by surface runoff leakage [31]. For example, in the Dianchi Lake Basin in Yunnan, farmers randomly collect or dispose of plant waste in lakes and rivers, and the non-point source pollution caused by them is far greater than that caused by industrial production. In addition, the plant debris will contain a large number of pests and diseases. The accumulated leakage will pollute the soil and affect the growth of subsequent crops. The burning of the construction site will produce a large amount of dense smoke, which not only pollutes the atmospheric environment but also seriously affects the inland waterway traffic and causes haze.

4.3. Comparative Analysis of Resource Utilization. According to statistics [32], the collection rate of plant waste in China is 0.80. Therefore, it is estimated that the amount of plant waste that can be recycled in China in 2021 will be approximately 215 million tons. It is estimated that in 2021, the plant residues nitrogen, phosphorus, and potassium nutrient reserves will be 954.7 thousand tons of nitrogen, 534,600 tons of phosphorus, and 82 million tons of potassium, accounting for 3.99% of the national nitrogen fertilizer consumption. 6.44% of the phosphorus fertilizers use 13.07% of the potassium application. In addition, it also contains 18.8883 million tons of organic matter and medium and trace elements necessary for plant growth.

4.3.1. Resource Utilization Method

(1) Return Directly to the Field. The ratio C/N value of plant residues is relatively low, which is more suitable for direct return to the field than straw cultivated in the field. After returning to the field, it undergoes a fermentation stage to improve the physical and chemical properties of the soil, which improves the quality and yield of the plant. Studies have shown that the average annual return rate of plant waste is 16%, and the generation and return rates of annual residues have a relatively high trend. Studies have shown that direct application of plant residues with microbial agents can significantly increase the yield of Chinese cabbage [33].

(2) Feed Utilization. Studies have shown that normal growing vegetable waste does not contain any other toxic and harmful substances [34]. Except for some tissues that have disease and insect pests, vegetable waste contains a lot of cellulose, which can be used as feed after proper treatment. At present, for the treatment of plant residues in feed, silage technology, ammonia treatment technology and microbial treatment conversion technology are mainly used to process

them into microbial protein products. Zhang et al. developed high-quality protein foods with the waste of Chinese cabbage as raw materials and added bran to ferment the solid mixed bacteria together [35]. WGP uses plant waste as the main raw material and bran as the auxiliary material. It uses nonsterile solid fermentation technology to produce single cells. Protein feed, then, the protein content of the product increased by 75%. Studies have shown that plant waste and fishery by-products after fermentation and heat treatment can be used as alternative feed ingredients for pigs. Today, feed production using plant residues as raw materials not only brings huge benefits to the environment but also improves feed quality and reduces feed production costs.

(3) Simple Anaerobic Refining. Studies have shown that trace elements from plant waste can be partially converted into liquid organic fertilizer after 96 days of fermentation and exist in an effective form that plants can use. In addition, the GI value in the original fertilizer solution is as high as 80%, which is less toxic and can be diluted or directly used in farmland. Research on the effects of vegetable waste retting and chemical fertilizers on the yield and quality of rape has shown that the collection of plant residues can significantly increase the yield and quality of canola, but excessive use will inhibit the yield.

(4) Biogasification and Utilization. According to China's agricultural waste resource analysis, plant waste biogasification produces 477.75×109 m^3 of biogas per year. Vegetable waste has a high water content and a total solid content of about 10%, which is usually consistent with anaerobic digestion. The ratio of chemical oxygen demand to nitrogen (COD: N) is $(100:4.:4) \sim (128:4)$. Vegetable by-products are nutritious, and anaerobic fermentation can be carried out without adding nitrogen and nutrient sources. After anaerobic fermentation, not only can produce biogas, but biogas waste and the liquid produced can be used as fertilizer for plants. The use of biogas residue as fertilizer can not only significantly improve crop resistance and inhibit the persistence of soil-borne diseases but also significantly improve the physical and chemical properties of soil and can also be used as a food additive.

However, not all plant wastes are suitable for anaerobic digestion into biogas. The cellulose content in the plant residues is low. The excessively fast hydrolysis rate during anaerobic fermentation leads to the accumulation of volatile acids and the decrease of pH, which leads to the inactivation of methanogens. Inhibiting or even destroying the methane

production process, vegetable straw is rich in lignin and cellulose, and its unique high polymerization state can resist microbial degradation and reduce the hydrolysis rate of anaerobic fermentation.

4.4. Mixed Aerobic Composting. Aerobic composting is the process of microbial degradation of organic waste under aerobic conditions to produce biological fertilizers. At present, many studies [36] have shown that aerobic digestion can produce high-quality organic fertilizers by using common composts such as plant residues and crop straws, manure, and plant residues. Compared with chemical fertilizers, compost made of plant waste has the characteristics of comprehensive nutrition and rapid yield increase, which promotes the improvement of crop growth and the quality of agricultural products. It can also increase the content and activity of soil organic matter, improve physical and chemical properties, and eliminate soil hazards. The residue of the substance and the inhibition of the growth of soil pathogens play an important role here. Studies have shown that when plant residues are applied during the cucumber growth period, the temperature of cucumber roots is higher than that of conventional fertilizer, and its maturity time, yield, and output are better than conventional compost. Other studies have shown that the application of compost to alkaline soil can significantly reduce the pH value and EC value of alkaline soil, reduce soil bulk density, increase porosity, and significantly increase soil organic matter content and alkaline soil content.

Composting plant waste in the factory's greenhouse can solve the problem of carbon dioxide deficiency. Using potato vines and other plant wastes and chicken manure to compost in the greenhouse can significantly increase the CO_2 concentration in the greenhouse, and the fermentation product can be used as a high-quality biological fertilizer, not only reaching the original position. Treating harmless plant wastes can also increase the yield and quality of vegetables by adding carbon dioxide gas to fertilizers. Vegetable waste compost is not only a high-quality organic fertilizer, it can also meet the requirements of seedling substrates in terms of compost density, total porosity, water retention holes, and vent holes. It is an environmentally friendly alternative to peat, which is renewable and does not contain on-site pollutants.

4.5. Comparison of Advantages and Disadvantages of Different Resource Utilization Methods. Plant waste has a high resource potential. The most important resource utilization options today is direct return to the field, feed utilization, simple anaerobic recycling, biogas utilization, and mixed aerobic composting. Each resource treatment method has its own advantages and disadvantages. Vegetables have serious pests and diseases. Plant waste contains pests and diseases. Plant wastes are particularly easy to rot during the high temperature period of summer and autumn, which promotes the spread of harmful pathogens. They are returned directly to the field or simply retorted to the field. The field can greatly increase the incidence of plant diseases and insect pests in the next season and even cause a large number of deaths, which affects normal production. Although the fermentation time of surface solid phase fermentation to produce food protein is short, it requires aseptic operation. The reliability requirements are high, and part of the waste has been decomposed in a large amount, which is not suitable for large-scale production and promotion. However, due to the biodegradability and structural strength characteristics of plant waste, biochemical treatment technology is more suitable for treating plant waste, but the biogasification anaerobic fermentation time is long, the cycle treatment volume is small, and the fermentation conditions are demanding. In addition, anaerobic fermentation technology has higher requirements for fermentation equipment, and the scale of the factory is severely restricted. Sewage and garbage treatment will also increase additional costs. Improper treatment will also cause secondary pollution. Aerobic high-temperature compost keeps the compost at high temperature and effectively kills. To kill pathogenic microorganisms, it can also produce high-efficiency organic fertilizers. The nutrient cycle occurs through the absorption of plants. The high-temperature aerobic composting fermentation time is short, and the requirements for processing equipment are low. It is designed according to local conditions, such as terrain and climate. Second, vegetable production in developed countries is highly concentrated, large-scale, and mechanized. Vegetable residues are easy to collect, and most of them are anaerobic fermentation. However, vegetable planting areas in China are relatively scattered, with a large number and wide distribution of plant residues, which are distributed in various concentrated areas. It is very diverse. Therefore, high-temperature aerobic composting is easier to realize the rapid utilization of China's plant waste resources.

5. Conclusion

In the last decades, the process of China's agricultural industrialization is accelerating, the degree of agricultural intensification is rapidly increasing, and agricultural nonpoint source pollution has become increasingly prominent, which has become a major factor in China's water environment security. Pollution from scattered agricultural sources is affected by many factors, such as agricultural production activities, rainfall, topography, soil, and land use, which vary greatly in space. Based on the quantitative study of the spatial distribution of point source pollution and nonpoint source potential pollution, this study established a spatial pollution assessment model and a point source pollution risk assessment spatial model. Then divide the exposure level and risk level, determine the key areas of nonpoint source pollution control, and build a regional classified monitoring technology system to provide research basis for China's agricultural nonpoint source pollution control. In this work, the TCLP method was used to determine the effective content of heavy metals in the soil, and the continuous BCR extraction method was used to determine the content of various chemical forms of heavy metals in the soil. Then, the distribution rules of heavy metals in plant soils in different regions, soil depths, and soil types were studied, and the cumulative risk, pollution risk,

ecological risk, and health risk of heavy metal pollution in plant soil were evaluated. Bioavailability of heavy metals in soil. Vegetable soil includes the ability of various vegetable varieties to absorb and accumulate different heavy metals and the correlation between the content of heavy metals in vegetables and the total amount, available state content and content of various chemical forms of heavy metals in soil. Plant waste has a risk of pollution, but it is also an important source of organic materials. It is rich in nutrients and organic matter. After safe resource development and treatment, it can be used as an important source of organic fertilizer, reducing the contribution of chemical fertilizers and the source of straw pollution, which can be effective reduce agricultural production costs. Understanding the quantity and spatial distribution of plant wastes is a prerequisite for reducing agricultural diffusion source pollution in key plant production areas and promoting the utilization of straw resources. However, the complex sources of plant waste, scattered distribution, and diverse migration paths make accurate estimation difficult. Through the comprehensive analysis of this article, thermo-aerobic composting is currently the most suitable solution for resource waste and plant waste pollution in China. However, the thermo-aerobic composting technology for plant waste in China is not yet mature. With high water content, low C/N, microorganisms, pathogens, and high nitrogen content, future research should pay more attention to the development of conditioners and process equipment suitable for composting high-humidity materials to achieve efficient, fast, and safe treatment of plant waste. Thoroughly solve the economic and environmental problems caused by China's plant waste, realize recycling, and minimize safety and factory waste.

Data Availability

The data used to support the findings of this study are available from the corresponding author upon request.

Additional Points

Conflicts of Interest

The authors declare that they have no competing interests.

References

[1] A. Anaya-Gregorio, J. S. Armstrong-Altrin, M. L. Machain-Castillo, P. C. Montiel-García, and M. A. Ramos-Vázquez, "Textural and geochemical characteristics of late Pleistocene to Holocene fine-grained deep-sea sediment cores (GM6 and GM7), recovered from southwestern Gulf of Mexico," *Journal of Palaeogeography*, vol. 7, pp. 253–271, 2018.

[2] J. S. Armstrong-Altrin, M. L. Machain-Castillo, L. Rosales-Hoz, A. Carranza-Edwards, J. A. Sanchez-Cabeza, and A. C. Ruíz-Fernández, "Provenance and depositional history of continental slope sediments in the southwestern Gulf of Mexico unraveled by geochemical analysis," *Continental Shelf Research*, vol. 95, pp. 15–26, 2015.

[3] J. Benkhelil, P. Giresse, C. Poumot, and G. Ngueutchoua, "Lithostratigraphic, geophysical and morpho-tectonic studies of the South Cameroon shelf," *Marine & Petroleum Geology*, vol. 19, no. 4, pp. 499–517, 2002.

[4] S. A. T. M. Rahman, T. Hosono, J. M. Quilty, J. Das, and A. Basak, "Multiscale groundwater level forecasting: coupling new machine learning approaches with wavelet transforms," *Advances in Water Resources*, vol. 141, article 103595, 2020.

[5] O. Rahmati, S. A. Naghibi, H. Shahabi et al., "Groundwater spring potential modelling: comprising the capability and robustness of three different modeling approaches," *Journal of Hydrology*, vol. 565, pp. 248–261, 2018.

[6] T. Rajaee, H. Ebrahimi, and V. Nourani, "A review of the artificial intelligence methods in groundwater level modeling," *Journal of Hydrology*, vol. 572, pp. 336–351, 2019.

[7] A. M. Ramos, L. F. Sarmiento, M. G. Trujillo, J. P. Macias, and A. C. Santos, "Linear discriminant analysis to describe the relationship between rainfall and landslides in Bogotá, Colombia," *Landslides*, vol. 13, pp. 671–681, 2015.

[8] N. R. Regmi, J. R. Giardino, and J. D. Vitek, "Modeling susceptibility to landslides using the weight of evidence approach: western Colorado, USA," *Geomorphology*, vol. 115, no. 1-2, pp. 172–187, 2010.

[9] J. Remondo, A. González, J. R. De Terán, A. Cendrero, A. Fabbri, and C. J. Chung, "Validation of landslide susceptibility maps; examples and applications from a case study in northern Spain," *Natural Hazards*, vol. 30, no. 3, pp. 437–449, 2003.

[10] R. Said, *The Geology of Egypt*, Elsevier Publishing Company, Amsterdam, New York, 1962.

[11] R. Said, *The Geological Evaluation of the River Nile*, Springer-Verlag, New York, 1981.

[12] L. Zhang, Y. Xu, H. Liu et al., "Effects of coexisting Na^+, Mg^{2+} and Fe^{3+} on nitrogen and phosphorus removal and sludge properties using A^2O process," *Journal of Water Process Engineering*, vol. 44, article 102368, 2021.

[13] W. Liu, J. Zheng, X. Ou et al., "Effective extraction of Cr (VI) from hazardous gypsum sludge via controlling the phase transformation and chromium species," *Environmental Science & Technology*, vol. 52, no. 22, pp. 13336–13342, 2018.

[14] K. Zhang, S. Wang, H. Bao, and X. Zhao, "Characteristics and influencing factors of rainfall-induced landslide and debris flow hazards in Shaanxi Province, China," *Natural Hazards and Earth System Sciences*, vol. 19, no. 1, pp. 93–105, 2019.

[15] J. Chen, L. Du, and Y. Guo, "Label constrained convolutional factor analysis for classification with limited training samples," *Information Sciences*, vol. 544, pp. 372–394, 2021.

[16] G. Zhou, F. Yang, and J. Xiao, "Study on pixel entanglement theory for imagery classification," *IEEE Transactions on Geoscience and Remote Sensing*, vol. 60, pp. 1–18, 2022.

[17] K. Zhang, M. H. Shalehy, G. T. Ezaz, A. Chakraborty, K. M. Mohib, and L. Liu, "An integrated flood risk assessment approach based on coupled hydrological- hydraulic modeling and bottom-up hazard vulnerability analysis," *Environmental Modelling & Software: With Environment Data News*, vol. 148, article 105279, 2022.

[18] Y. Liu, K. Zhang, Z. Li, Z. Liu, J. Wang, and P. Huang, "A hybrid runoff generation modelling framework based on spatial combination of three runoff generation schemes for semi-humid and semi-arid watersheds," *Journal of Hydrology*, vol. 590, article 125440, 2020.

[19] M. Mohajane, A. Essahlaoui, F. Oudija et al., "Land use/land cover (LULC) using landsat data series (MSS, TM, ETM+ and OLI) in Azrou Forest, in the central middle atlas of Morocco," *Environments*, vol. 5, no. 12, p. 131, 2018.

[20] M. I. Sameen, B. Pradhan, and S. Lee, "Self-learning random forests model for mapping groundwater yield in data-scarce areas," *Natural Resources Research*, vol. 28, no. 3, pp. 757–775, 2019.

[21] K. S. Sandford, "The Pliocene and Pleistocene deposits of Wadi Qena and of the Nile Valley between Luxor and Assiut (QAU)," *Quarterly Journal of the Geological Society*, vol. 85, no. 1-4, pp. 493–548, 1929.

[22] K. Zhang, A. Ali, A. Antonarakis et al., "The sensitivity of North American terrestrial carbon fluxes to spatial and temporal variation in soil moisture: an analysis using radar-derived estimates of root-zone soil moisture," *Journal of Geophysical Research. Biogeosciences*, vol. 124, no. 11, pp. 3208–3231, 2019.

[23] T. Zhao, J. Shi, D. Entekhabi et al., "Retrievals of soil moisture and vegetation optical depth using a multi-channel collaborative algorithm," *Remote Sensing of Environment*, vol. 257, article 112321, 2021.

[24] S. Wang, K. Zhang, L. Chao et al., "Exploring the utility of radar and satellite-sensed precipitation and their dynamic bias correction for integrated prediction of flood and landslide hazards," *Journal of Hydrology*, vol. 603, article 126964, 2021.

[25] K. S. Sandford, "Paleolithic man and the Nile Valley in Upper and Lower Egypt. The University of Chicago press," *Oriental Institute Publications*, vol. 3, pp. 1–131, 1934.

[26] P. Vorpahl, H. Elsenbeer, M. Märker, and B. Schröder, "How can statistical models help to determine driving factors of landslides?," *Ecological Modelling*, vol. 239, pp. 27–39, 2012.

[27] L. Duarte, J. Espinha Marques, and A. C. Teodoro, "An open source GIS-based application for the assessment of groundwater vulnerability to pollution," *Environments*, vol. 6, no. 7, p. 86, 2019.

[28] A. M. Youssef, M. Al-Kathery, and B. Pradhan, "Landslide susceptibility mapping at Al-Hasher Area, Jizan (Saudi Arabia) using GIS-based frequency ratio and index of entropy models," *Geosciences Journal*, vol. 19, pp. 113–134, 2014.

[29] A. M. Youssef, B. Pradhan, M. N. Jebur, and H. M. El-Harbi, "Landslide susceptibility mapping using ensemble bivariate and multivariate statistical models in Fayfa area, Saudi Arabia," *Environmental Earth Sciences*, vol. 73, pp. 3745–3761, 2014.

[30] M. Zabihi, F. Mirchooli, A. Motevalli et al., "Spatial modelling of gully erosion in Mazandaran Province, northern Iran," *Catena*, vol. 161, pp. 1–13, 2018.

[31] F. K. Zaidi, Y. Nazzal, I. Ahmed, M. Naeem, and M. K. Jafri, "Identification of potential artificial groundwater recharge zones in northwestern Saudi Arabia using GIS and Boolean logic," *Journal of African Earth Sciences*, vol. 111, pp. 156–169, 2015.

[32] C. Yun, C. Yan, Y. Xue, Z. Xu, T. Jin, and Q. Liu, "Effects of exogenous microbial agents on soil nutrient and microbial community composition in greenhouse-derived vegetable straw composts," *Sustainability*, vol. 13, no. 5, p. 2925, 2021.

[33] X. Liu, S. Gu, S. Yang, J. Deng, and J. Xu, "Heavy metals in soil-vegetable system around e-waste site and the health risk assessment," *Science of the Total Environment*, vol. 779, no. 25, article 146438, 2021.

[34] B. Tang, M. He, Y. Dong, J. Liu, and W. Zhang, "Effects of different forms of vegetable waste on biogas and methane production performances in a batch anaerobic digestion reactor," *Energy Sources, Part A: Recovery, Utilization, and Environmental Effects*, vol. 3, pp. 1–11, 2020.

[35] Z. Zhang, C. Luo, and Z. Zhao, "Application of probabilistic method in maximum tsunami height prediction considering stochastic seabed topography," *Natural Hazards*, vol. 104, no. 3, pp. 2511–2530, 2020.

[36] A. Sahoo, S. Sarkar, B. Lal, P. Kumawat, S. Sharma, and K. De, "Utilization of fruit and vegetable waste as an alternative feed resource for sustainable and eco-friendly sheep farming," *Waste Management*, vol. 128, pp. 232–242, 2021.

Retraction

Retracted: Index Construction and Application of School-Enterprise Collaborative Education Platform Based on AHP Fuzzy Method in Double Creation Education Practice

Journal of Sensors

This article has been retracted by Hindawi following an investigation undertaken by the publisher [1]. This investigation has uncovered evidence of one or more of the following indicators of systematic manipulation of the publication process:

(1) Discrepancies in scope

(2) Discrepancies in the description of the research reported

(3) Discrepancies between the availability of data and the research described

(4) Inappropriate citations

(5) Incoherent, meaningless and/or irrelevant content included in the article

(6) Manipulated or compromised peer review

The presence of these indicators undermines our confidence in the integrity of the article's content and we cannot, therefore, vouch for its reliability. Please note that this notice is intended solely to alert readers that the content of this article is unreliable. We have not investigated whether authors were aware of or involved in the systematic manipulation of the publication process.

Wiley and Hindawi regrets that the usual quality checks did not identify these issues before publication and have since put additional measures in place to safeguard research integrity.

We wish to credit our own Research Integrity and Research Publishing teams and anonymous and named external researchers and research integrity experts for contributing to this investigation.

The corresponding author, as the representative of all authors, has been given the opportunity to register their agreement or disagreement to this retraction. We have kept a record of any response received.

References

[1] Z. He and X. Sun, "Index Construction and Application of School-Enterprise Collaborative Education Platform Based on AHP Fuzzy Method in Double Creation Education Practice," *Journal of Sensors*, vol. 2022, Article ID 7707384, 15 pages, 2022.

Research Article

Index Construction and Application of School-Enterprise Collaborative Education Platform Based on AHP Fuzzy Method in Double Creation Education Practice

Zhenzhen He and **Xiuhong Sun**

Baoding University, Hebei, Baoding 071000, China

Correspondence should be addressed to Zhenzhen He; hezhenzhen@bdu.edu.cn

At present, China's education reform is developing rapidly, and many schools begin to study and implement school-enterprise cooperative education. There are also some conceptual deviations. In addition, the government's weak implementation of the guarantee policy for the implementation of combination of school and enterprise education, coupled with the lack of relevant laws and regulations, rarely leads to the success and enthusiasm of combination of school and enterprise education. With the development of collaborative training companies, the participation rate needs to be improved, and the influence of school-enterprise colearning is not significant enough. Therefore, we should do more theoretical research on combination of school and enterprise education, so as to further improve the present situation of combination of school and enterprise education in China and promote the in-depth development of combination of school and enterprise education. At the same time, we should constantly improve relevant practices and systems, improve relevant laws and regulations, learn from the successful experience of cooperation between schools and enterprises training at home and abroad, and design a unique path of cooperation between schools and enterprises in combination with China's reality. First of all, this paper deeply analyzes the synergy degree of combination of school and enterprise education. By defining the concepts of the combination of industry and teaching and the combination of colleges and enterprises, synergy degree, and cooperative development level, this paper makes an in-depth interpretation of the education and teaching of schools and enterprises. From the perspective of synergetic theory and interactive mechanism, school-enterprise cooperation needs to be strengthened. Secondly, the model is created through the analytic hierarchy process, in which the hierarchical model uses the 10/10-18/2 scaling method to form the classification matrix. Finally, this paper analyzes on the factors affecting the combination of school and enterprise education and puts forward some perfect countermeasures from three angles of government, school, and enterprise.

1. Introduction

We introduce a method to deal with fuzzy analytic hierarchy process, which uses degree analysis method to determine the comprehensive degree value of pairwise comparison method. Applying the comparison principle of fuzzy numbers, under certain criteria, this decision-making process is illustrated by an example [1]. We propose a degree analysis method of fuzzy analytic hierarchy process and get a clear priority vector from the triangular fuzzy matrix of the equation. Experiments show that the hierarchical analysis method cannot estimate the true weight of fuzzy reference matrix, which leads to a large num-

ber of abuses. This paper illustrates with examples that the priority vector determined by degree analysis does not represent the relative importance of decision criteria or procedures [2]. An evaluation system based on analytic hierarchy process and fuzzy comprehensive evaluation is proposed to select the best supplier for garment enterprises. This paper mainly introduces a social manufacturing framework, which can be used to perceive and influence customers and meet the needs of mass customization. Both qualitative and quantitative factors are considered in this method. Its efficiency and feasibility have been verified in Dongguan garment enterprises [3]. The fuzzy overall evaluation method of AHP, through the study of

highway widening trend, will provide a framework for the formulation of highway widening scheme and provide quantitative objective basis for subjective decision-making of highway widening [4]. Based on the performance, aesthetics and ecology of golf courses, the landscape index system is constructed as the target of the landscape evaluation of the lakeview golf course in Kunming. The method, index, and model of the landscape evaluation of the city golf course are discussed by using the semantic differential method, the analytic hierarchy process, and the fuzzy comprehensive evaluation of the landscape evaluation of the lake-view golf course in Dianchi Lake [5]. Aiming at the limitation of AHP fuzzy comprehensive evaluation method, an improved AHP fuzzy comprehensive evaluation method is proposed, which has isomorphism and test evaluation set, and will continue to be applied to the evaluation of higher education quality and comprehensive evaluation of colleges and universities. The results show that the improved method can better test and evaluate the expected consistency of each evaluation factor [6]. The combination of schools and enterprises is a form of talent training that adapts to the development of the times. Make full use of resources from all aspects to enhance practical ability. Therefore, it is of great significance to put forward improvement measures and accelerate the formation of an effective cooperation model for national education and social development [7]. It is of great practical value to form a cooperative education community between schools and enterprises for cultivating students' professional skills. By changing the traditional classroom teaching methods, the connection between professional skills and professional skills is realized, which increases students' professional knowledge and enriches students' professional skills. It provides a new way for students' emotional attitude and character [8]. This paper analyzes the necessity of implementing entrepreneurship education in cooperation between schools and enterprises from the perspective of educational institutions and entrepreneurship education in colleges and universities and puts forward that the curriculum system of entrepreneurship education in colleges and universities should be carried out by both parties. Work together to create a campus entrepreneurial culture atmosphere and improve the effectiveness of entrepreneurship education [9]. This paper analyzes the importance of cooperation between schools and enterprises, suggests setting key courses according to the skills required by specific tasks, and studies the construction methods of modular curriculum design, curriculum improvement, and grading system design [10]. College students' innovation and entrepreneurship education has been paid more and more attention by the society. This is not only the requirement of the times, but also the charm of innovation and entrepreneurship education itself. In view of the present situation of applied entrepreneurship and the difficulties in applied finance, this paper summarizes the reasons that affect students' entrepreneurial ability and discusses the ways to improve financial students' entrepreneurial ability and self-realization [11]. It is the requirement of the progress and development of market economy and the inevitable choice of innovation and entrepreneurship in China to strengthen the innovation and entrepreneurship education of college students to help them consolidate the concept of innovation

and entrepreneurship and improve their awareness of innovation and entrepreneurship. The traditional college model lacks innovation and entrepreneurship awareness and innovation and entrepreneurship theory. According to the requirements of innovation construction, colleges and universities should renew their concepts, establish a correct understanding of their abilities, and carry out fundamental reforms and innovations in the concepts, mechanisms, contents, methods, management, and innovative entrepreneurial skills of entrepreneurship education [12]. Many colleges and universities do not mention increasing innovation and entrepreneurship in their personnel training objectives. Moreover, institutional innovation and entrepreneurship education are only forms. Therefore, innovation and entrepreneurship education has not yet penetrated into the whole process of talent development. Some school-enterprise cooperation lacks deep integration into the whole education system and vocational training [13]. It is very important for the development and prosperity of the country to improve students' innovation and entrepreneurship ability and employment development competitiveness in the financial crisis. Combined with the present situation of colleges and universities in China, this paper puts forward some countermeasures to promote students' innovation and entrepreneurship from two main angles: colleges and students themselves [14]. Based on the innovation and entrepreneurship needs of students majoring in tourism management in tourism development, this paper combs the problems existing in the tourism management ability system from three angles of innovation consciousness, innovation ability, and innovation ability and puts forward targeted countermeasures and suggestions [15]. By improving the school's participation in collaborative education and deepening the degree of collaboration between schools and enterprises, it is conducive for the school to set up majors, formulate courses, compile teaching materials, build internal and external training and practice bases, and employ front-line technical skill masters of enterprises to provide practical skill guidance, so as to effectively improve the quality of talent training, ensure that students can meet the requirements of industry enterprises for technical talents through systematic learning of theoretical knowledge and practical skills, effectively shorten the time of students' post adaptation, and truly cultivate skilled talents required by industry enterprises and society.

2. The Current Situation of Students' Dual-Innovation Ability under the Mode of Cooperation between Schools and Enterprises

2.1. Failure to Fully Understand the Importance of Cultivating Innovation and Entrepreneurship. Under the background of education reform, the Ministry of Education has launched various corresponding policies. Under the effect of these policies, colleges and universities have begun to attach importance to the cultivation of entrepreneurial talents and focus on building a talent training platform to provide talents for the society. However, the research shows that some universities do not fully understand the importance of improving entrepreneurial skills, and higher vocational colleges are less invested in this

area than undergraduate colleges, and there are still obvious problems. At present, some universities pay attention to improving students' professional teaching and learning ability according to the cooperation between schools and enterprises model but do not recognize the value of innovative and entrepreneurial courses and activities. Although most VET institutions have established similar training bases in the synergy between enterprises, they often focus on skills training, which runs counter to the VET concept in the new era of schools and is not conducive to the all-round development of students.

2.2. The Existing Cooperation Mechanism Still Needs to Be Improved. Under the existence of many drawbacks, there are obvious defects in the relevant mechanism of cooperation between schools and enterprises at present, especially in cultivating students' innovative and entrepreneurial ability, which only focuses on the improvement of students' professional skills and seriously lacks practical characteristics, which makes it difficult for students to invest in innovative and entrepreneurial activities under such a mechanism and cannot improve their practical ability. Under the new situation, colleges and universities should establish a stable cooperation mechanism with modern enterprises, carry out targeted education, and provide students with an environment and platform for innovation and entrepreneurship.

2.3. Lack of Innovative Practice Platform. At present, the resources of campus bases such as innovation studios and workshops are scarce, and the utilization rate is low. Cooperation between schools and enterprises mode is still under study, and comprehensive operation modes such as negotiation, contact, docking, and monitoring have not yet been formed. It is not well combined with college students' mass entrepreneurship and innovation. Therefore, students' practice of participating in innovation and entrepreneurship is less, and their achievements have not gone out of school and gone to the society in a large scale, so they cannot be tested by the market.

3. Improvement of Analytic Hierarchy Process

By analyzing the specific implementation steps of analytic hierarchy process, the hierarchical model after construction is evaluated. After extensive analysis, an improved algorithm is proposed, and the efficiency of the algorithm is ensured by the practical application of the system. The improved algorithm of the system can effectively reduce the amount of computation, and the algorithm has wide adaptability. The algorithm is not only suitable for the case that all the estimated relative weights $a\_ij = \mu\_i/\mu\_j$ of $I, j(I, j = 1, 2, \cdots, n)$ are completely valid, but also suitable for the following cases: there is no complete confirmation.

3.1. Optimal Selection of Scale. The values of each element of the evaluation matrix reflect the subjective cognition and evaluation of decision makers. In the practical application of analytic hierarchy process, the general scaling methods are three scaling methods, 0.5-0.9 scaling methods, 9/9-9/1 scaling methods, and 10/10-18/2 scaling methods.

Three-scale method: only three values can be selected in the judgment of matrix, which are -1, 0, and 1 as shown in the formula

$$a_{ij} \begin{cases} -1, \text{Means } I \text{ is less important than } J, \\ 0, \text{It means that } I \text{ and } J \text{ are equally important}, \\ 1, \text{Indicates that } i \text{ is more important than } j. \end{cases} \quad (1)$$

a_{ij} denotes the relative weight of element I compared to element J, and $A = (a_{ij})_{mn}$ is the pairwise judgment matrix, where a_{ij} has the following properties: $a_{ij} > 0, a_{ij} = 1/a_{ji}, a_{ii} = 1$.

The pairwise comparison classification matrix formed according to this definition is shown in the formula

$$A = \begin{pmatrix} a_{11} & \cdots & a_{1n} \\ \vdots & \ddots & \vdots \\ a_{n1} & \cdots & a_{nn} \end{pmatrix}. \quad (2)$$

Then, the optimal transfer matrix B of the judgment matrix A is shown in the formula

$$B = \begin{pmatrix} b_{11} & \cdots & b_{1n} \\ \vdots & \ddots & \vdots \\ b_{n1} & \cdots & b_{nn} \end{pmatrix}, \text{where, } b_{ij} = \frac{1}{n} \sum_{k-1}^{n} (a_{ik} + a_{jk}). \quad (3)$$

The transition matrix B is further transformed into the consistency matrix C.

For matrix $A = (a_{ij})_{nn}$, it is a positive and inverse n-multiplicity matrix. If every $I, j, k = 1, 2, \cdots, n$ has $a_{ij} * a_{ji} = 1$, it is a consistent matrix, as shown in the formula

$$C = \begin{pmatrix} c_{11} & \cdots & c_{1n} \\ \vdots & \ddots & \vdots \\ c_{n1} & \cdots & c_{nn} \end{pmatrix}, \text{where, } c_{ij} = \exp (b_{ij}). \quad (4)$$

Consistency matrix C is the evaluation matrix needed by AHP.

9/9-9/1 scaling method: the specific values are investigated by Delphi method.

0.5-0.9 scaling method: if A_I is considered as important as A_J, then $a_{ij} = 0.5$; if A_I is more important than A_J, then $a_{ij} = 0.9$; in other cases, it is between 0.5 and 0.9. The even reference matrix $A = (a_{ij})_{mn}$ generated by 0.5-0.9 scaling method has the following properties: $a_{ij} > 0, a_{ij} = 1 - a_{\mu}$; $a_{11} = 0.5$, and the matrix generated by 0.5-0.9 scaling method are complementary matrices.

10/10-18/2 scaling method: in order to improve the paired estimation matrix scaling method, there is also a 10/10-18/2 scaling method. In the 1/9 scaling method, the corresponding ratio to the 9/9-9/1 scaling method is shown in Table 1.

TABLE 1: Importance of three scale methods.

1-9 scale method	9/9-9/1 scale method	10/10-18/2 scale method	The importance of the representation
1	9/9	10/10	The same important
3	9/7	12/8	A little important
5	9/5	14/6	Important
7	9/3	16/4	Strong important
9	9/1	18/2	Very important
$K1, 2, \cdots 9$	$9/(10 - K)1, 2, \cdots 9$	$(9 + k)/(11 - K)1, 2, \cdots 9$	Range of structural formula K

3.2. Improvement of Algorithm for Calculating Ranking Weight. Suppose there is a criterion C, then the relative weights of specific layers $u_1, u_2, u_3, \cdots, u_n$ of the classification matrix A are carried out, and then the consistency test is carried out. Once the weight vector of a specific layer element relative to the previous layer element is calculated under the criterion, the combined weight of each element relative to the total amount of the target layer is finally obtained.

The sequence weight vectors of the $k - 1$ elements of the $k - 1$ layer are shown in the formula

$$\omega^{(k-1)} = \left(\omega_1^{k-1}, \omega_2^{k-1}, \cdots, \omega_{k-1}^{k-1} \right). \tag{5}$$

The ordering vector of $k - 1$ elements of the k layer is shown in the formula

$$p_j^{(k)} = \left(p_{1j}^{(k)}, p_{2j}^{(k)}, p_{3j}^{(k)}, \cdots, p_{kj}^{(k)} \right). \tag{6}$$

The elements of k layer are sorted according to the elements of $k - 1$ layer as

$$p^{(k)} = \left(p_{1j}^{(k)}, p_{2j}^{(k)}, p_{3j}^{(k)}, \cdots, p_{kj}^{(k)} \right). \tag{7}$$

Elements that calculate the weight of the k layer relative to the target are shown in the formula

$$\omega^{(k)} = \left(\omega_1^{(k)}, \omega_2^{(k)}, \cdots, p_k^{(k)} \right) T = P^{(k)} * \omega^{(k-1)}. \tag{8}$$

Or use the summation method as shown in the formula

$$\omega_1^{(k)} = \sum_{j=i}^{k-1} p_{ij}^{(k)} * \omega_k^{(k-1)}, i = 1, 2, \cdots, n. \tag{9}$$

Because calculating the relative weight of each layer element is familiar with calculating the relative weight of the total object, this paper does not propose them one by one.

3.2.1. Eigenvalue Method. If the elements obtained from the hierarchical model satisfy $a_{ij} > 0$ and $a_{ij} = 1/a_{ji}, a_{11} = 1$ and $a_{ik} * a_{kj} = a_{ij}$ at the same time, $A\omega = \lambda\omega$ can be normalized to obtain the relative weight vector. The following methods are as follows:

A judgment matrix constructed under a single criterion between levels: $A = \left(a_{ij} \right)_{n*n}$, where $a_{ij} = \mu_1/\mu_2$ then has formula (10) according to linear algebraic knowledge

$$\begin{pmatrix} a_{11} & \cdots & a_{1n} \\ \vdots & \ddots & \vdots \\ a_{n1} & \cdots & a_{nn} \end{pmatrix} \begin{pmatrix} a_1 \\ \vdots \\ \mu_n \end{pmatrix} = \begin{pmatrix} \dfrac{\mu_1}{\mu_2} & \cdots & \dfrac{\mu_2}{\mu_n} \\ \vdots & \ddots & \vdots \\ \dfrac{\mu_n}{\mu_2} & \cdots & \dfrac{\mu_n}{\mu_n} \end{pmatrix} \begin{pmatrix} \mu_1 \\ \vdots \\ \mu_n \end{pmatrix} = n \begin{pmatrix} \mu_1 \\ \vdots \\ \mu_n \end{pmatrix}. \tag{10}$$

There are $A\mu = n\mu$, where

$$\mu = \begin{pmatrix} \mu_1 \\ \vdots \\ \mu_n \end{pmatrix}. \tag{11}$$

Then n is the eigenvalue of Eigen equation $A\omega = \lambda\omega$, and the corresponding eigenvector is

$$\mu = \begin{pmatrix} \mu_1 \\ \vdots \\ \mu_n \end{pmatrix}. \tag{12}$$

Then normalize, that is, $i = 1, 2, \cdots, n$, get $\omega_i = \mu_i/\sum_{j=1}^n \mu_j$, and get $\omega = (\omega_1, \omega_2, \cdots, \omega_n)^T$. The above is the ideal case where the ranking of scoring matrix A is 1; that is, the paired scoring matrix only meets the requirements of positive and negative attributes and consistency. However, if $a_{1k} * a_{kj} = a_{ij}$ is invalid, the largest right root is not equal to N. It is necessary to check and adjust the consistency of matrix in order to achieve satisfactory consistency of matrix.

3.2.2. Power Method. In the actual situation of this study, it is found that the amount of calculation is very large. Therefore, when dealing with complex situations, the calculation of square root method becomes more and more limited. Assuming that the matrix is consistent satisfactorily, in order to reduce the system constraints, the power method effectively reduces the computational complexity.

Suppose that the eigenvalue of the judgment matrix is A: $\lambda_1, \lambda_2, \cdots, \lambda_n$, and at the same time $|\lambda_1| > |\lambda_2| > |\lambda_3| > \cdots > |\lambda_n|$, the corresponding eigenvector is $\mu_1, \mu_2, \cdots, \mu_n$, and for

every nonzero $x^{(0)}$, there must be an $a_1, a_2, \cdots, a_n$ such that $a_1 = \sum_{j=1}^{n} a_j \mu_j$. Use the iterative formula $x^{(k+1)} = Ax^{(k)}$, $k = 0, 1, \cdots$ to find the point sequence and get $\{x^{(0)}, x^{(1)}, \cdots\}$. Then according to what we can get, $x^{(k+1)} = Ax^{(k)} = A^k x^{(0)} = A^k * \sum_{j=1}^{n} a_j A^k \mu_j = \sum_{j=1}^{n} a_j \lambda_j^k \mu_j = \lambda_1^k [a_1 \mu_1 + \sum_{j=2}^{n} (\lambda_1/\lambda_2)^k \mu_j]$, because $|\lambda_1| > |\lambda_2| > |\lambda_3| > \cdots > |\lambda_n|$, so if $\sum_{j=2}^{n} a_j (\lambda_1/\lambda_2)^k \mu_j$ is large enough and K is small enough, we can get

$x_i^{(k+1)}/x_i^{(k)} = (A^k x^{(0)})/(A^{k-1} x^{(0)}) \approx \lambda_1$, so $x_i^{(k+1)}/x_i^{(k)}$ is an approximate estimate of λ_1. The actual calculation ensures that if $|\lambda_1| < 1$ or $|\lambda_1| > 1$, $|\lambda_1^k|$ tends to infinity or infinity. Namely $a = \max \{x_i^{(k)} | i = 1, 2, \cdots, n\}$, and then $x^{(k+1)} = A * (1/a) x^{(k)}, k = 1, 2, \cdots$.

3.2.3. Square Root Method. The square root method is to carry out geometric average on each row vector of judgment matrix A first, and then normalize it. First, a product operation is performed on the elements of the estimated value A of each row that is shown in the formula

$$M_i = \left(\prod_{j=1}^{n} a_{ij} \right)^{1/n}, \tag{13}$$

where $i = 1, 2, \cdots, n$. Normalization is then performed, as shown in the formula

$$\omega_i = \frac{M_i}{\sum_{j=1}^{n} M_1}, i = 1, 2, \cdots, n. \tag{14}$$

Then the maximum eigenvalue of judgment matrix A is shown in the formula.

$$\lambda_{\max} = \frac{1}{n} \left(\sum_{i=1}^{n} \frac{(A\omega)_i}{w_i} \right). \tag{15}$$

In the formula, $(A\omega)_i$ is the i components of $A\omega$, and $\omega = (\omega_1, \omega_2, \cdots, \omega_n)^T$.

3.2.4. Least Square Method. The judgment matrix

$$A = \begin{pmatrix} a_{11} & \cdots & a_{1n} \\ \vdots & \ddots & \vdots \\ a_{n1} & \cdots & a_{nn} \end{pmatrix} = \begin{pmatrix} \mu_1/\mu_2 & \cdots & \mu_2/\mu_n \\ \vdots & \ddots & \vdots \\ \mu_n/\mu_2 & \cdots & \mu_n/\mu_n \end{pmatrix} \tag{16}$$

is not valid. In other words, the estimated relative weight $a_{ij} = \mu_i/\mu_j$ is not fully applicable to all $I, j(I, j = 1, 2, \cdots, n)$. In this case, the value of $a_{ij} \mu_j - \mu_1$ is not all zero, and the weight set $\{u_1, u_2, u_3, \cdots, u_n\}$ is selected to minimize the sum of squares, as shown in the formula

$$\text{Min } Z = \sum_{i=1}^{n} \sum_{j=1}^{n} (a_{ij} - \mu_1)^2,$$

$$\text{S.t.} \sum_{j=1}^{n} \mu_1 = 1. \tag{17}$$

The generated program is a typical nonlinear program. We use Lagrange coefficients to make nonlinear programming a purely quantitative programming problem and construct Lagrange functions as shown in the formula

$$L = \sum_{i=1}^{n} \sum_{j=1}^{n} (a_{ij} \mu_j - \mu_1)^2 + 2\lambda \left(\sum_{j=1}^{n} \mu_1 - 1 \right). \tag{18}$$

In analytical mechanics, the Lagrange function of a dynamic system is a function that describes the dynamic state of the whole physical system. For general classical physical systems, it is usually defined as kinetic energy minus potential energy, which is expressed by the equation, where L is the Lagrange quantity, λ is the kinetic energy, and μ is the potential energy.

In analytical mechanics, assuming that the Lagrange function of a system is known, the Lagrange quantity can be directly substituted into the Lagrange equation, and the motion equation of the system can be obtained with a little operation.

Perform the first partial derivative operation on the above formula as shown in the formula

$$\frac{\partial_L}{\partial_{\mu_1}} = 2 \sum_{i=1}^{n} (a_{i1} \mu_1 - \mu_i) a_{i1} - 2 \sum_{j=1}^{n} (a_{j1} \mu_1 - \mu_i) + 2\lambda = 0, \tag{19}$$

where $l = 1, 2, \cdots, n$. $\partial_L/\partial_\lambda = 2(\sum_{i=1}^{n} \mu_1 - 1) = 0$.

First, list the steps of the algorithm in theory:

(1) Construct judgment matrix A

(2) Using the least square method to get the maximum eigenvalue $\lambda_{\max}$ and get the corresponding eigenvector

(3) Normalized eigenvector

(4) Calculate the conformance index $CI(0)$, and get the $CR(0)$ of any conformance index RI. If $CR(0) < 0.1$, no iteration is required. The relative weight vector obtained is

$$\omega^{(0)} = \left(\omega_1^{(0)}, \omega_2^{(0)}, \cdots, \omega_n^{(0)} \right)^T. \tag{20}$$

Otherwise, you need to build a complete consistency matrix as shown in the equation

$$B^{(0)} = \begin{pmatrix} \dfrac{\omega_1^{(0)}}{\omega_1^{(0)}} & \cdots & \dfrac{\omega_1^{(0)}}{\omega_n^{(0)}} \\ \vdots & \ddots & \vdots \\ \dfrac{\omega_n^{(0)}}{\omega_1^{(0)}} & \cdots & \dfrac{\omega_n^{(0)}}{\omega_n^{(0)}} \end{pmatrix}. \qquad (21)$$

Adopting iterative equation: $A^{(1)} = tA^{(0)} + (1-t)B^{(0)}$, carrying out iterative operation.

After iteration, the maximum eigenvalue of the judgment matrix is checked for consistency. If the consistency requirement is met, only the eigenvector corresponding to the maximum eigenvalue is normalized, which is the final ranking weight. If the consistency requirement is not met, the iteration must continue until the consistency requirement is met.

Use the talent evaluation system example in this article to demonstrate the algorithm:

This paper only introduces the "comprehensive quality" evaluation system, and the demonstration methods of other evaluation systems in the system are known, so this paper will not list them separately.

First, build the hierarchical model as follows in Figure 1:

Hierarchical model uses 10/10-18/2 scaling method to create classification matrix, it is shown in Table 2.

Then, the maximum eigenvalue of the scoring matrix is obtained by using the least square method: $\lambda_{\max}^{(0)} = 6.6357$; the corresponding eigenvector and the normalized eigenvector are shown as

$$\omega^{(0)} = \left(\omega_1^{(0)}, \omega_2^{(0)}, \cdots, \omega_n^{(0)} \right)^T = (0.1377, 0.1998, 0.2348, 0.2138, 0.2138)^T, \qquad (22)$$

$$CI = \frac{\lambda_{\max} - n}{n-1} = \frac{6.6357 - 5}{5-1} = 0.4089, \qquad (23)$$

$$RI = 1.12, \qquad (24)$$

$$CR = \frac{CI}{RI} = \frac{0.4089}{1.12} = 0.3650 > 0.1. \qquad (25)$$

Obviously, the requirement of consistency is not met. Achieve consistency through iterative method.

Construct a complete consistency matrix as shown in the formula

$$B^{(0)} = \begin{pmatrix} \dfrac{\omega_1^{(0)}}{\omega_1^{(0)}} & \cdots & \dfrac{\omega_1^{(0)}}{\omega_n^{(0)}} \\ \vdots & \ddots & \vdots \\ \dfrac{\omega_n^{(0)}}{\omega_1^{(0)}} & \cdots & \dfrac{\omega_n^{(0)}}{\omega_n^{(0)}} \end{pmatrix} = \begin{pmatrix} 1 & 0.6892 & 0.5694 & 0.624 & 0.624 \\ 1.4621 & 1 & 0.8418 & 0.9541 & 0.9541 \\ 1.7265 & 1.7265 & 1 & 1.1018 & 1.1018 \\ 1.5521 & 1.0971 & 0.9823 & 1 & 1 \\ 1.6567 & 1.0989 & 0.9811 & 1 & 1 \end{pmatrix}. \qquad (26)$$

Iterative equation: $A^{(1)} = tA^{(0)} + (1-t)B^{(0)}$; take $t = 0.9$ and iterate, as shown in the formula

$$A^{(1)} = 0.9A^{(0)} + 0.1B^{(0)} = \begin{pmatrix} 1 & 1.323 & 1.3581 & 1.6224 & 1.5618 \\ 0.8934 & 1 & 3.9821 & 3.9321 & 0.8721 \\ 4.5622 & 0.3299 & 1 & 5.2217 & 3.9809 \\ 3.0098 & 2.9832 & 0.9721 & 1 & 0.3750 \\ 0.9023 & 2.3255 & 3.9227 & 3.0445 & 1 \end{pmatrix}. \qquad (27)$$

The maximum eigenvalue of $A^{(1)}$ is calculated, and the corresponding eigenvectors are shown as

$$\omega^{(0)} = \left(\omega_1^{(0)}, \omega_2^{(0)}, \cdots, \omega_n^{(0)} \right)^T = (0.3987, 0.5171, 0.7689, 0.8093, 0.5609)^T, \qquad (28)$$

$$CI = \frac{\lambda_{\max} - n}{n-1} = \frac{6.672 - 5}{5-1} = 0.418, \qquad (29)$$

$$RI = 1.12, \qquad (30)$$

$$CR = \frac{CI}{RI} = \frac{0.418}{1.12} = 0.3732 > 0.1. \qquad (31)$$

Need to continue iteration.

After 4 iterations, the maximum eigenvalues are shown as

$$\begin{aligned} \lambda_{\max}^{(1)} &= 5.579, \\ \lambda_{\max}^{(2)} &= 5.498, \\ \lambda_{\max}^{(3)} &= 5.4623, \\ \lambda_{\max}^{(4)} &= 5.41, \end{aligned} \qquad (32)$$

$$CI = \frac{\lambda_{\max} - n}{n-1} = \frac{5.41 - 5}{5-1} = 0.1025, \qquad (33)$$

$$RI = 1.12, \qquad (34)$$

$$CR = \frac{CI}{RI} = \frac{0.1025}{1.12} = 0.0915 < 0.1. \qquad (35)$$

That is to say, satisfactory consistency requirements are achieved. Then the corresponding eigenvectors are normalized to get the final weight value.

4. Experimental Research and Results

4.1. Data Acquisition and Index Weighting

4.1.1. Data Collection and Processing. This study is distributed to schools in two ways: electronic questionnaire and paper proofreading enterprise training site from 2013 to 2018. There are 341 valid questionnaires, excluding invalid questionnaires. The interest rate is 96.6%, which meets the requirements. And based on this information, explore the cooperation between schools and enterprises in educating people.

4.1.2. Weighting Method of Evaluation Index. In this paper, subjective and objective weighting methods are mainly used to determine and jointly determine the index weight. Entropy
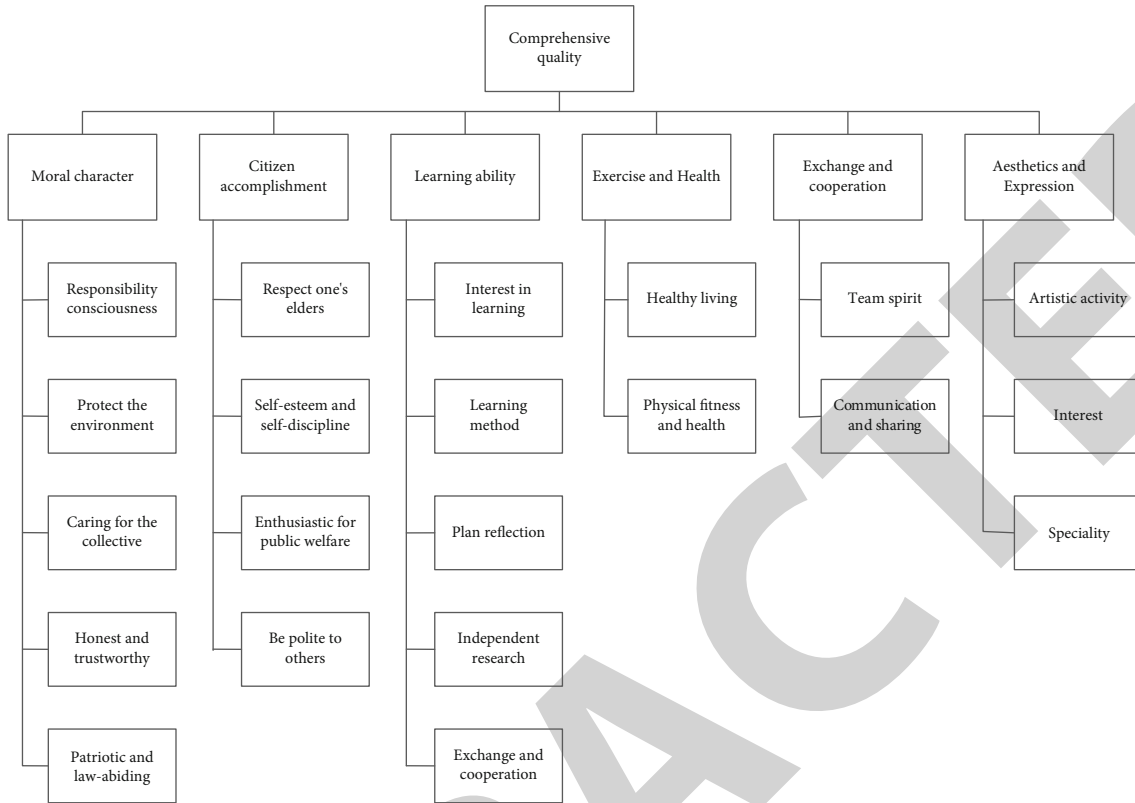
FIGURE 1: Comprehensive quality hierarchy model.

TABLE 2: Judgment matrix under scale method.

Criterion 1	B1	B2	B3	B4	B5	B6
B1	10/10	10/10	12/8	14/6	14/6	18/2
B2	10/10	10/10	14/6	16/4	18/2	18/2
B3	8/12	6/14	10/10	16/4	16/4	18/2
B4	6/14	4/16	4/16	10/10	10/10	14/6
B5	6/14	2/18	4/16	4/16	10/10	12/8
B6	2/18	2/18	2/18	6/14	8/12	10/10

method and coefficient of variation method are used to determine the index weight, and finally combined weighting method is used to determine the final weight to weigh the advantages and disadvantages of different methods. This index makes up for the deficiency of single weight model and makes the effectiveness of the index more reasonable.

4.2. Determining the Weight of the Cooperative Education System between Schools and Enterprises

4.2.1. Determine the Weight of Each Index of School-Enterprise Education System.
Entropy method. According to the calculation formula, the weight of each index is obtained. See Table 3 for specific data.

Variation coefficient method. According to the weighting formula of variation coefficient method, the characteris-

tic value of each index is substituted into the formula, and the index weight of school general education system is obtained. See Table 4 for details.

Combination weight. According to the calculation formula of combination weight, β is 0.5, and the comprehensive weight of each item in the index system of coeducational system is obtained according to Table 5.

4.2.2. Determine the Weight of Each Index of Enterprise Cooperative Training System.
Entropy method. According to the weighting principle of entropy method, the relevant indexes of cooperative training system are weighted, and the weights of each index are obtained according to Table 6.

Variation coefficient method. According to the weighting formula of variation coefficient method, the characteristic value of each index is substituted into the corresponding formula, and the index weight of business cooperation training system is obtained, as shown in Table 7.

Combination weight formula. According to the combination weight calculation formula $\beta = 0.5$, the total weight of the cooperative training system index system can be obtained, as shown in Table 8.

To sum up, the weight of the corresponding indicators of school collaborative education and enterprise collaborative education can be obtained. See Table 9 for more detailed information.

4.3. Empirical Analysis of the Synergy Degree of School-Enterprise Collaborative Education

TABLE 3: Index weight.

Metric	Entropy value	1-E	Entropy right
D1	0.8713	0.1287	0.0289
D2	0.7875	0.2125	0.0478
D3	0.8101	0.1899	0.0427
D4	0.8473	0.1527	0.0343
D5	0.8577	0.1423	0.032
D6	0.8298	0.1702	0.0383
D7	0.8454	0.1546	0.0348
D8	0.7895	0.2105	0.0473
D9	0.8196	0.1804	0.0406
D10	0.775	0.225	0.0506
D11	0.8242	0.1758	0.0395
D12	0.8535	0.1465	0.0329
D13	0.824	0.176	0.0396
D14	0.8055	0.1945	0.0437
D15	0.778	0.222	0.0499
D16	0.8039	0.1961	0.0441
D17	0.8055	0.1945	0.0437
D18	0.8583	0.1417	0.0319
D19	0.5512	0.4488	0.1009
D20	0.7968	0.2032	0.0457
D21	0.6225	0.3775	0.0849
D22	0.7968	0.2032	0.0457

TABLE 4: Index weight of school collaborative education system under coefficient of variation method.

Metric	Coefficient of variation	Weight
D1	0.0568	0.0784
D2	0.0573	0.0791
D3	0.004	0.0055
D4	0.032	0.0441
D5	0.044	0.0607
D6	0.0302	0.0417
D7	0.0582	0.0803
D8	0.0579	0.08
D9	0.0658	0.0908
D10	0.0284	0.0392
D11	0.0552	0.0762
D12	0.0281	0.0388
D13	0.0216	0.0298
D14	0.0223	0.0308
D15	0.0354	0.0489
D16	0.0522	0.072
D17	0.0129	0.0177
D18	0.0138	0.019
D19	0.0277	0.0382
D20	0.0022	0.003
D21	0.0129	0.0177
D22	0.0058	0.008

4.3.1. Analysis of Comprehensive Development Level of School-Enterprise Collaborative Education System. Multiplying the respective index weights in the index system of school-enterprise collaborative education system with the original data after entropy method, the comprehensive development level of school-enterprise collaborative education system from 2013 to 2018 can be obtained, respectively, as shown in Table 10 for details.

Analysis Table 10 knows:

(1) From the time point of view, the overall development level of combination of school and enterprise education system is on the rise. Among them, the upward trend of enterprises is clear and develops rapidly, while schools are stable and grow steadily. The overall development level of coeducation in schools has steadily increased from 0.1804 in 2013 to 0.8826 in 2018, with a steady growth rate and almost no growth in recent six years. The overall development speed is slow, showing a gradual upward trend; the overall development level of the joint venture training system increased from 0.1257 in 2013 to 0.4561 in 2016 and from 0.1257 in 2013 to 0.4561 in 2016. The development speed was rapid in 2017, and in 2013: 0.2051671. In the past two years, the overall development level has been significantly improved. To sum up, from 2013 to 2018, the overall development level of cooperation between schools and enterprises in running schools has chan-

ged, but the development speed is slightly faster than that of schools, and the overall development level is generally higher

(2) The overall development level of the cooperative school-running system is different from that of the cooperative school-running system, which leads to obvious differences between the two systems in the development process. Overall, the overall development level of coeducation in enterprises increased slightly faster than that in schools from 2013 to 2018. The gap between the overall development level of cooperative education and the overall development level of cooperative education can be divided into two stages: the first stage, the positive distribution stage after 2013. Until 2016, it was the collaborative education system of the school. The overall development level of human system is faster than that of cooperative education system. At present, the overall development level of the general education system in schools has increased from 0.1804 in 2013 to 0.5412 in 2016, while the development level of companies has increased from 0.1257 in 2013 to 0.4561 in 2016. Company leading to the overall development level of the school collaborative training system is better than the overall development level of the company collaborative training system; The second stage, the negative gap stage from 2017

TABLE 5: Comprehensive weight.

Metric	Entropy weight method	Variability coefficient method	Comprehensive weight
D1	0.0289	0.0784	0.0537
D2	0.0478	0.0791	0.0634
D3	0.0427	0.0055	0.0241
D4	0.0343	0.0441	0.0392
D5	0.032	0.0607	0.0464
D6	0.0383	0.0417	0.04
D7	0.0348	0.0803	0.0575
D8	0.0473	0.08	0.0637
D9	0.0406	0.0908	0.0657
D10	0.0506	0.0392	0.0449
D11	0.0395	0.0762	0.0579
D12	0.0329	0.0388	0.0359
D13	0.0396	0.0298	0.0347
D14	0.0437	0.0308	0.0373
D15	0.0499	0.0489	0.0494
D16	0.0441	0.072	0.0581
D17	0.0437	0.0177	0.0307
D18	0.0319	0.019	0.0254
D19	0.1009	0.0382	0.0696
D20	0.0457	0.003	0.0244
D21	0.0849	0.0177	0.0513
D22	0.0457	0.008	0.0268

TABLE 6: Weight of enterprise education system under entropy method.

Metric	Entropy value	1-E	Entropy right
D23	0.8057	0.1943	0.0387
D24	0.7804	0.2196	0.0437
D25	0.8054	0.1946	0.0388
D26	0.857	0.143	0.0285
D27	0.795	0.205	0.0408
D28	0.8018	0.1982	0.0395
D29	0.867	0.133	0.0265
D30	0.8775	0.1225	0.0244
D31	0.6854	0.3146	0.0627
D32	0.7492	0.2508	0.05
D33	0.7528	0.2472	0.0492
D34	0.8023	0.1977	0.0394
D35	0.6523	0.3477	0.0693
D36	0.8115	0.1885	0.0375
D37	0.7517	0.2483	0.0495
D38	0.8605	0.1395	0.0278
D39	0.8237	0.1763	0.0351
D40	0.7808	0.2192	0.0437
D41	0.6459	0.3541	0.0705
D42	0.7923	0.2077	0.0414
D43	0.7132	0.2868	0.0571
D44	0.8722	0.1278	0.0255
D45	0.8451	0.1549	0.0309
D46	0.852	0.148	0.0295

to 2018, means that the overall development level of the education system based on enterprise cooperation is faster than that of the school cooperative education system. After the overall development level improved steadily from 2013 to 2016, the overall development level of the joint venture training system improved rapidly in 2017, from 0.4561 in 2016 to 0.7462 in 2017 and then to 0.8485 in 2018, which is a great increase. From 2017 to 2018, the overall development level of coeducation is higher than that of coeducation in schools. The main reasons are as follows: First, from the perspective of industrial transformation and renewal, China's economy has been declining in recent years. Traditional industries are in urgent need of reform and modernization, and enterprises also urgently need to change traditional product production processes, improve product quality, and cooperate with schools to develop new products, which not only contributes to the reform and renewal of enterprise products, but also disappears China's human capital dividend from the perspective of human resource demand. At present, enterprises are in urgent need of high-quality technology and professional skills that can work at zero distance. Some universities are the main supply sources of technical capabilities, and enterprises can cooperate with them to meet their own needs. School-enterprise cooperation requires a certain degree of high-quality technology and techni-

cal ability; Finally, from the perspective of improving the competitiveness of enterprises, innovation is the motive force of enterprise development. In the past, many enterprises invested a lot of money in displaying innovative talents, developing new product patents and innovating products. In order to save the cost of innovation, more and more enterprises are setting up new product development centers in colleges and universities and implementing industrial education integration schools. Enterprises cooperate in educating people and jointly research and develop new processes, technologies, projects, and products with teachers and students, which significantly reduces the research and development costs of enterprises and improves the competitiveness of enterprises. Since 2017, the overall development level of enterprise collaborative education system has gradually exceeded the school level, and there is a negative gap in the development trend

4.3.2. Analysis on the Development Level of Collaborative Education Subsystem between Schools and Enterprises

(1) Analysis on the Development Level of Collaborative Education in Schools. From the analysis of Figure 2, it can be seen that the comprehensive development level of school

Table 7: Index weight of enterprise collaborative education system under coefficient of variation method.

Metric	Coefficient of variation	Weight
D23	0.0466	0.0591
D24	0.0434	0.055
D25	0.0093	0.0117
D26	0.0525	0.0666
D27	0.0436	0.0553
D28	0.0471	0.0597
D29	0.033	0.0419
D30	0.0347	0.044
D31	0.0234	0.0297
D32	0.0334	0.0424
D33	0.0434	0.0551
D34	0.001	0.0013
D35	0.0358	0.0454
D36	0.0424	0.0538
D37	0.0348	0.0442
D38	0.0316	0.0401
D39	0.0199	0.0253
D40	0.0382	0.0484
D41	0.0345	0.0438
D42	0.0465	0.059
D43	0.0251	0.0319
D44	0.0233	0.0295
D45	0.0205	0.026
D46	0.0244	0.031

Table 8: Comprehensive weight of enterprise education system indicators.

Metric	Entropy weight method	Variability coefficient method	Comprehensive weight
D23	0.0387	0.0591	0.0489
D24	0.0437	0.055	0.0494
D25	0.0388	0.0117	0.0252
D26	0.0285	0.0666	0.0475
D27	0.0408	0.0553	0.0481
D28	0.0395	0.0597	0.0496
D29	0.0265	0.0419	0.0342
D30	0.0244	0.044	0.0342
D31	0.0627	0.0297	0.0462
D32	0.05	0.0424	0.0462
D33	0.0492	0.0551	0.0522
D34	0.0394	0.0013	0.0203
D35	0.0693	0.0454	0.0573
D36	0.0375	0.0538	0.0457
D37	0.0495	0.0442	0.0468
D38	0.0278	0.0401	0.0339
D39	0.0351	0.0253	0.0302
D40	0.0437	0.0484	0.046
D41	0.0705	0.0438	0.0572
D42	0.0414	0.059	0.0502
D43	0.0571	0.0319	0.0445
D44	0.0255	0.0295	0.0275
D45	0.0309	0.026	0.0284
D46	0.0295	0.031	0.0302

collaborative education system has steadily improved from 2013 to 2018. From 0.1804 in 2013 to 0.8826 in 2018, the subsystems that constitute the coeducation system in schools show a mixed development trend, but the overall development level has improved. Among them, in 2015, the mechanism construction, teaching staff construction, curriculum construction, and teaching materials construction all exceeded the overall level of school collaborative education system development, and the talent curriculum construction exceeded the overall level of school development. School. In 2016, schools will jointly run schools. In 2013, the infrastructure construction also exceeded the overall development level of running schools together. This shows that compared with other subsystems, the first five subsystems contribute more to the overall development level of school collaborative education system. And the other five subsystems are education and apprenticeship system, education evaluation, work quality, social welfare and social satisfaction with schools, and the comprehensive development level of school-based education system. The contribution degree is slightly lower than the first five subsystems, and the influence of the system on the overall development level of the school can be ignored. On this basis, generally speaking, although the development level of each subsystem is different, it contributes to the overall development level of the school cooperative training system to varying degrees.

(2) Analysis on the Development Level of Enterprise Collaborative Education Subsystem. From the analysis of Figure 3, it can be seen that from 2013 to 2018, the overall development level of enterprise cooperative training system has been rapidly improved. From 0.1257 in 2013 to 0.8485 in 2018, the overall development level has been improved to varying degrees in different periods. In its subsystem, the participation of enterprises in the construction of curriculum materials and the development of personnel training projects exceeds the overall level of collaborative business training system development in 2014, while the mechanism construction does not exceed the overall development level. In 2015, the overall development level of the collaborative training system is basically at the same level, which indicates that compared with other subsystems and schools, the contribution of enterprises participating in the construction of teacher training bases to the overall development level of the joint training system is slightly lower than the share of the overall development level of the joint training system of schools. Therefore, by increasing the participation of enterprises in the construction of school teachers and training centers, the overall development level of enterprise collaborative training system can be effectively improved. The development level of the other six subsystems is as follows: participation in education and training programs,

TABLE 9: Weight table of index system of collaborative education system between schools and enterprises.

System level	Functional layer	Index layer	Index layer weight	Function layer weight
School collaborative education system	Mechanism construction	The government supervises the number of cooperative education mechanisms in schools	0.0537	0.1171
		Number of school assessment and management collaborative education system	0.0634	
	Teacher construction	The proportion of double-qualified teachers are full-time teachers	0.0241	0.1097
		The proportion of part-time teachers are full-time teachers	0.0392	
		The proportion of temporary teachers in enterprises are full-time teachers	0.0464	
	Curriculum and teaching material construction	Introduce enterprises or jointly develop the number of courses	0.04	0.1612
		Introduce enterprises or jointly develop the number of textbooks	0.0575	
		The proportion of part-time teachers teaching in the total professional class hours	0.0637	
	Talent training plan formulation	Organize the number of revisions of the talent training plan	0.0657	0.1156
		Organize the demonstration times of talent training program	0.0449	
	Construction of training base	The number of on-campus practical training bases jointly built by schools and enterprises	0.0579	0.0938
		Number of off-campus training bases jointly built by schools and enterprises	0.0359	
	Training internship arrangement	Number of cooperative enterprises per specialty	0.0347	0.072
		Arrange the number of practical training instructors	0.0373	
	Teaching evaluation	Number of courses inviting companies to participate in the evaluation	0.0494	0.1075
		The number of courses unilaterally evaluated by the entrusted enterprises	0.0581	
	Quality of employment	First-time employment ratio of graduates	0.0307	0.0561
		Corresponding employment ratio of graduates	0.0254	
	Social effect results benefit	Get the enterprise collaborative research and development project funds	0.0696	0.094
		Train the number of employees for enterprises	0.0244	
	Social satisfaction with schools	Student satisfaction with the school	0.0513	0.0781
		Enterprise satisfaction with students	0.0268	
Enterprise collaborative education system	Participate in mechanism construction	The government supervises the number of cooperative education mechanism conducted by enterprises	0.0489	0.983
		Number of enterprise assessment and management collaborative education system	0.0494	
	Participate in the construction of teachers	The proportion of employees participating in teaching employees in the enterprise	0.0252	0.0727
		The total number of teachers temporarily employed in the school	0.0475	
	Participate in the construction of courses and teaching materials	Number of participation in professional course development	0.0481	0.1319
		Number of participants in the development of professional textbooks	0.0496	
		Number of courses taught by part-time teachers	0.0342	
	Participate in the formulation of talent training plan	Participated in the formulation and revision of the talent training program for times	0.0342	0.0804
		Participate in the demonstration times of the talent training program	0.0462	
		The number of on-campus practical training bases donated	0.0462	0.0984

Table 9: Continued.

System level	Functional layer	Index layer	Index layer weight	Function layer weight
	Participate in the construction of the practical training base	Number of practical training bases for donated equipment	0.0522	
	Participate in the practical training and practice arrangement	Number of students receiving practical practice	0.0203	0.1233
		Arrange the number of practical training instructors	0.0573	
		Pay the average monthly salary of graduate interns	0.0457	
	Participate in teaching evaluation	The number of courses assessed by unilateral evaluation	0.0468	0.0807
		Number of courses participating in the assessment and evaluation	0.0339	
	Student retention rate	The percentage of students in interns	0.0302	0.0762
		Pay per capita monthly salary for first employment	0.046	
	Collaborative research and development innovation	Number of enterprise-university collaborative innovation projects	0.0572	0.1074
		The number of benefit projects generated by enterprise-school collaborative innovation	0.0502	
	Enterprise investment funds	Invest in the practical training and practice funds	0.0445	0.072
		Investment in the project research and development funds	0.0275	
	School satisfaction with the enterprise	Student satisfaction with enterprises	0.0284	0.0568
		School satisfaction with the enterprise	0.0302	

Table 10: Development level of school-enterprise collaborative education department.

A particular year	Comprehensive development level of school collaborative education (PT)	The comprehensive development level of enterprise collaborative education (PE)	PT-PE
2013	0.1804	0.1257	0.0547
2014	0.2913	0.2271	0.0642
2015	0.3667	0.3294	0.0373
2016	0.5412	0.4561	0.0851
2017	0.6033	0.7462	-0.1429
2018	0.8286	0.8485	-0.0199

participation in education evaluation, student retention, R&D innovation, enterprise financial investment, and school satisfaction with enterprises that do not exceed the overall level of school development. Training system based on business cooperation shows that the contribution of cooperative education system to the overall development level is relatively low. Companies can improve the efficiency of the common education system by increasing students' participation in education and practical arrangements and teaching evaluation and by increasing investment in coeducation in schools. The overall development level has improved the participation and synergy of enterprises in coeducation. Improve. Generally speaking, although each subsystem has different contributions to the overall development level of collaborative training system, the situation of enterprises participating in collaborative training shows an increasing trend year by year, and the synergy between them is con-

stantly enhanced. The combination of production and training will also be realized by improving synergy.

(3) Analysis of the Collaborative Development Level of Cooperation between Schools and Enterprises and Collaborative Education. According to the above evaluation model, we can calculate the overall development level of the cooperative training system between schools and enterprises from 2013 to 2018, the degree of coordination between the two systems, and the development level of cooperation, as shown in Table 11.

As shown in Figure 4, the development level of cooperation between schools and enterprises has steadily improved and has experienced an upgrading process from subversion to subversion-difficult coordination-priority coordination.

The in-depth analysis of the synergy and development level of schools and enterprises that cooperate to educate
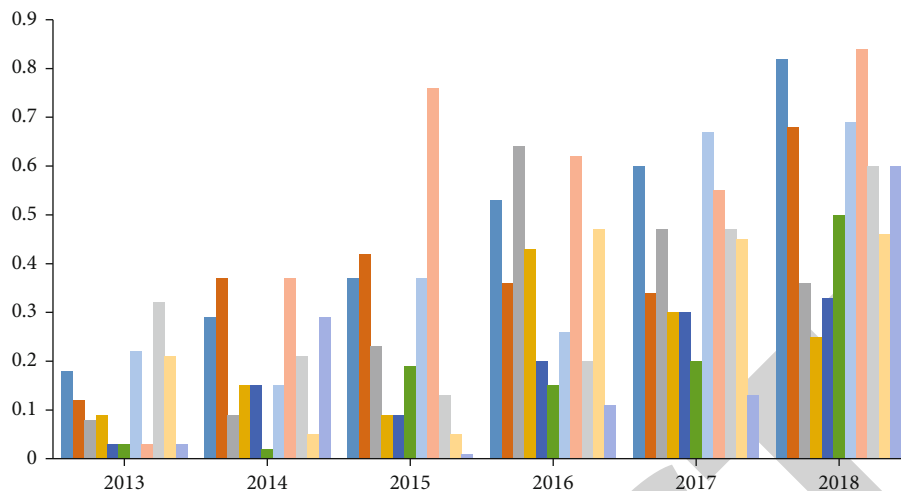
Figure 2: Development level of school collaborative education subsystem.
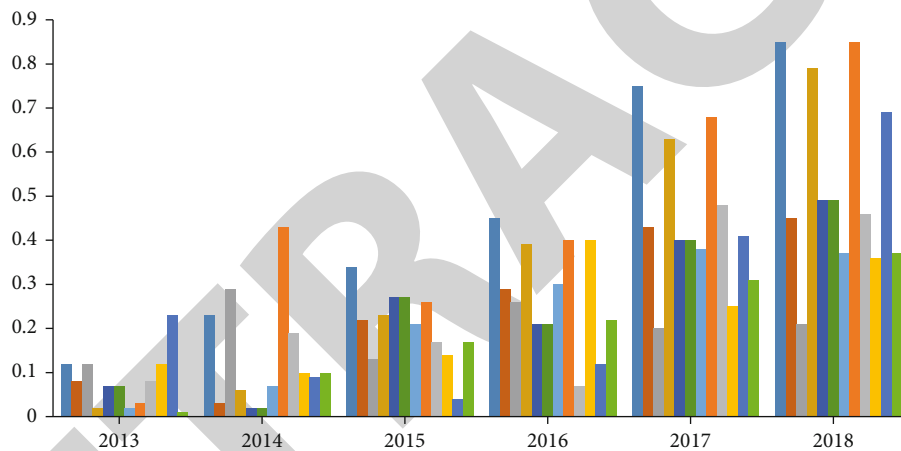
Figure 3: Development level of enterprise collaborative education subsystem.

Table 11: Collaborative development level of collaborative education between schools and enterprises from 2013 to 2018.

A particular year	Comprehensive development level of school collaborative education	Comprehensive development level of enterprise cooperative education	Collaborative degree	Coordinated development level
2013	0.1804	0.1257	0.484	0.2722
2014	0.2913	0.2271	0.4923	0.3572
2015	0.3667	0.3294	0.4986	0.4166
2016	0.5412	0.4561	0.4964	0.4975
2017	0.6033	0.7462	0.4944	0.5776
2018	0.8286	0.8485	0.4999	0.6475
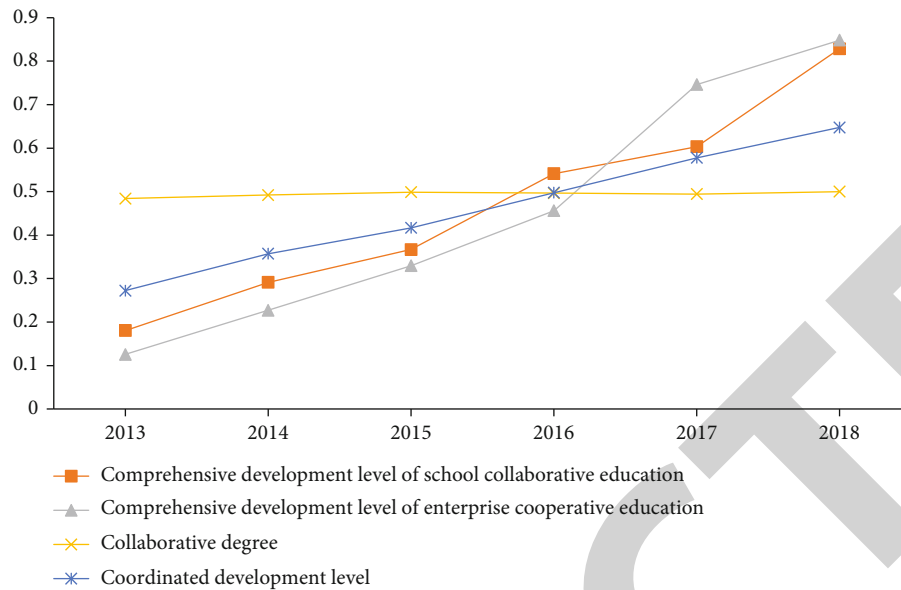
Figure 4: Collaborative development level.

students shows that the synergy of school-enterprise collaborative education fluctuates slightly, but the overall level has been improved. The level of coordinated development has been generally improved, showing a steady growth trend. The functional coordinated development of collaborative education between schools and enterprises is insufficient. The synergy between schools and enterprises in educating people is not well coordinated in time dimension. The coordinated state of collaborative education between schools and enterprises is not sustainable.

5. Concluding Remarks

As a part of the national policy of combining production with education and coconstruction between schools and enterprises, this paper investigates the degree and countermeasures of cooperation between schools and enterprises in tourism professional management. To clear the research ideas as a starting point, review the existing comprehensive evaluation of the integration of production and education and cooperation between schools and enterprises training, demonstrate the feasibility of this study, and seek the breakthrough of this research. Taking the interactive mechanism of S Tourism Vocational School as an example, this paper analyzes the current situation of cooperation between schools and enterprises training. The comprehensive evaluation index system and evaluation model of school-enterprise cooperation need to be tested in tourism secondary vocational education. Finally, this paper analyzes the factors that affect the cooperative training level between tourism colleges and tourism enterprises, puts forward effective countermeasures for the influencing factors, and finally forms a clear research idea and detailed analysis and research route.

Data Availability

The experimental data used to support the findings of this study are available from the corresponding author upon request.

Conflicts of Interest

The authors declared that they have no conflicts of interest regarding this work.

References

[1] D. Y. Chang, "Applications of the extent analysis method on fuzzy AHP," *European Journal of Operational Research*, vol. 95, no. 3, pp. 649–655, 1996.

[2] Y. M. Wang, L. Ying, and Z. Hua, "On the extent analysis method for fuzzy AHP and its applications," *European Journal of Operational Research*, vol. 186, no. 2, pp. 735–747, 2008.

[3] X. Gang, Y. Chen, and X. Shang, "AHP fuzzy comprehensive method of supplier evaluation in social manufacturing mode," in *Proceeding of the 11th World Congress on Intelligent Control and Automation*, pp. 3594–3599, Shenyang, June 2015.

[4] C. Y. Yuan and L. Q. Shi, "Study on reconstruction scheme of expressway in China and optimization within the AHP-fuzzy method," in *CICTP 2014: Safe, Smart, and Sustainable Multimodal Transportation Systems*, Shanghai, China, 2014.

[5] L. Niu, "Landscape evaluation of urban golf courses based on the AHP-fuzzy method: a case study of Dianchi Lakeview Golf Course in Kunming, Yunnan, China," *Journal of Landscape Research*, vol. 11, no. 4, 2019.

[6] K. Yuan, H. Li, and M. Jiang, "Research on AHP-fuzzy comprehensive evaluation method and application," *Journal of Physics: Conference Series*, vol. 1592, no. 1, article 012045, 2020.

Retraction

Retracted: Scene Classification Using Deep Networks Combined with Visual Attention

Journal of Sensors

This article has been retracted by Hindawi following an investigation undertaken by the publisher [1]. This investigation has uncovered evidence of one or more of the following indicators of systematic manipulation of the publication process:

(1) Discrepancies in scope

(2) Discrepancies in the description of the research reported

(3) Discrepancies between the availability of data and the research described

(4) Inappropriate citations

(5) Incoherent, meaningless and/or irrelevant content included in the article

(6) Manipulated or compromised peer review

The presence of these indicators undermines our confidence in the integrity of the article's content and we cannot, therefore, vouch for its reliability. Please note that this notice is intended solely to alert readers that the content of this article is unreliable. We have not investigated whether authors were aware of or involved in the systematic manipulation of the publication process.

Wiley and Hindawi regrets that the usual quality checks did not identify these issues before publication and have since put additional measures in place to safeguard research integrity.

We wish to credit our own Research Integrity and Research Publishing teams and anonymous and named external researchers and research integrity experts for contributing to this investigation.

The corresponding author, as the representative of all authors, has been given the opportunity to register their agreement or disagreement to this retraction. We have kept a record of any response received.

References

[1] J. Shi, H. Zhu, Y. Li, Y. Li, and S. Du, "Scene Classification Using Deep Networks Combined with Visual Attention," *Journal of Sensors*, vol. 2022, Article ID 7191537, 9 pages, 2022.

Research Article

Scene Classification Using Deep Networks Combined with Visual Attention

Jing Shi [ID],[1,2] Hong Zhu [ID],[1] Yuxing Li [ID],[1] YangHui Li,[1] and Sen Du [ID][1]

[1]*School of Automation and Information Engineering, Xi'an University of Technology, Xi'an 710048, China*
[2]*Shaanxi Key Laboratory of Complex System Control and Intelligent Information Processing, Xi'an University of Technology, Xi'an 710048, China*

Correspondence should be addressed to Jing Shi; shijing@xaut.edu.cn and Hong Zhu; zhuhong@xaut.edu.cn

In view of the scene's complexity and diversity in scene classification, this paper makes full use of the contextual semantic relationships between the objects to describe the visual attention regions of the scenes and combines with the deep convolution neural networks, so that a scene classification model using visual attention and deep networks is constructed. Firstly, the visual attention regions in the scene image are marked by using the context-based saliency detection algorithm. Then, the original image and the visual attention region detection image are superimposed to obtain a visual attention region enhancement image. Furthermore, the deep convolution features of the original image, the visual attention region detection image, and the visual attention region enhancement image are extracted by using the deep convolution neural networks pretrained on the large-scale scene image dataset Places. Finally, the deep visual attention features are constructed by using the multilayer deep convolution features of the deep convolution networks, and a classification model is constructed. In order to verify the effectiveness of the proposed model, the experiments are carried out on four standard scene datasets LabelMe, UIUC-Sports, Scene-15, and MIT67. The results show that the proposed model improves the performance of the classification well and has good adaptability.

1. Introduction

As a basic problem in the field of computer vision and image understanding, scene image classification has received extensive attention and research [1–7]. The most important problem to be solved in scene classification is to give proper expression to the content in the scene. In order to improve the accuracy of scene classification, the researchers constantly explore new ways, which has advantage of global features and local features as well as the middle to form visual word bag; the bag will represent a visual scene image word combination methods [8] and, by iteration and cross-validation, get the image block with degree of differentiation, as image middle expression method of [9]. The mean-shift algorithm is used to find the distinguishing mode in the image block distribution space, so as to create the image representation method of middle-level scene [10]. By establishing metric learning formulas and learning the best metric

parameters, online metric learning and parallel optimization of large-scale and high-dimensional data can be solved [2]. Although these methods have achieved certain classification effects, the classification performance is reduced when there are many objects or complex contents in the scene image.

In recent years, the proposal of deep convolutional networks has made it possible to obtain richer high-level semantics of images [11–13]. Donahue et al. directly use convolutional neural networks (CNNs) [14], which are pretrained on ImageNet dataset, for scene classification. Zhou et al. constructed a large-scale dataset centered on the scene and trained convolutional neural network on this basis [15], which significantly improved the performance of scene classification. Bai proposed that through CNN transfer learning, deep features were used to express special scene targets for classification [16]. Zou et al. built a fusion method based on nonnegative matrix factorization, which can preserve feature nonnegative properties and improve their representation performance.

Furthermore, an adaptive feature fusion and boosting algorithm is developed to improve the efficiency of image features. There are two versions of the proposed feature fusion method for non-negative single-feature fusion and multifeature fusion [1].

Zhang et al. proposed a spatially aware aggregation network for scene classification, which detects a set of visually semantically significant regions from each scene through a semisupervised and structurally reserved nonnegative matrix decomposition (NMF). Gaze shift path (GSP) was used to characterize the process of human perception of each scene image, and a spatial perception CNN called SA-NET was developed to describe each GSP in depth. Finally, the deep GSP function learned from the whole scene image is integrated into the image kernel, which is integrated into the kernel SVM to classify the scene [3]. Yee et al. propose a DeepScene model that leverages convolutional neural network as the base architecture, which converts grayscale scene images to RGB images. Spatial Pyramid Pooling is incorporated into the convolutional neural network [17]. These methods have greatly improved the effect of scene classification.

However, most of the current algorithms regard the scene as a combination of multiple objects [18–20] and lack description of contextual semantic relations between objects, thus restricting the accuracy of scene classification [21]. For this purpose, the significance of detection algorithm based on context [22], annotation in the scene visual focus area, and the area contains the main target in the scene and can express the context of a part of the background region and at the same time, combined with the depth of the convolutional neural network, build a kind of fusion depth scene classification characteristic of visual attention model. It overcomes the limitation of using object and structure feature to classify effectively and obtains good scene classification performance.

2. The Construction of Scene Classification Model

In order to adapt to the diversity of images, this article will image the context of the significant characteristics as visual attention characteristics, superimposed onto the original image and into the depth of the convolution network; build scene classification model; make the model of images to express deep intrinsic characteristics at the same time; andalso can express the target in the scene context between semantic features.

2.1. Detection of Areas of Visual Attention. The area that has a major influence on visual judgment is called the area of visual attention. Here, the context-based saliency detection algorithm proposed by Goferman et al. is used to extract the visual areas of interest of the image [22]. The extracted saliency areas take full account of global and local features at different scales and mark saliency targets with their adjacent areas to varying degrees. It well reflects the contextual relationship between the objects in the scene and the surrounding scenery and filters out some repetitive texture information.

The image block is taken as the comparison unit and compared in Lab color space. The closer the distance is, the greater the difference is and the more significant it is.

The difference degree of the two image blocks is expressed as

$$d\left(p_i, p_j\right) = \frac{d_c\left(p_i, p_j\right)}{1 + c \cdot d_p\left(p_i, p_j\right)}, \tag{1}$$

where p represents the image block, i is the central pixel point of p_i, and $d_c(p_i, p_j)$ and $d_p(p_i, p_j)$ represent the color distance and spatial distance between the two blocks, respectively.

For the difference degree value under a single scale, usually, only the difference degree value between the previous block and a certain block and the significance value of the pixel point under the scale need to be calculated as follows:

$$S_i^r = 1 - \exp\left\{-\frac{1}{M}\sum_{m=1}^{M} d(p_i^r, p_m^r)\right\}, \tag{2}$$

where M is the most similar front block taken, $\{p_m\}_{m=1}^{M}$, and r represents a certain scale.

In order to make the detected significance region significant in multiple scales, it is necessary to calculate multiple single-scale significance values and then take the average value, as follows:

$$\bar{S}_i = \frac{1}{K}\sum_{r \in R} S_i^r, \tag{3}$$

where K represents the number of scales and R represents the scale space.

In addition, it is necessary to combine the context of the image to make the region with different distances from the saliency target have different saliency. The significance value of pixel point is finally defined as

$$\hat{S}_i = \frac{1}{K}\sum_{r \in R} S_i^r \left(1 - d_f^r(i)\right), \tag{4}$$

where $d_f^r(i)$ represents the Euclidean distance between the pixel point i at the scale r and the nearest pixel point in the significant region. K represents the number of scales, and R represents the scale space.

Figure 1 is an example of detecting the area of visual attention. The brightness value in Figure 1(b) is the visual attention of this position. It can be seen that the attention of the background area varies with the change of closeness to the target.

2.2. Construction of Enhanced Images of Visual Areas of Concern. Although the scene information contained in the original image was comprehensive, it could not distinguish effective information from invalid information. In order to enhance the scene area containing different information to different degrees, the detection map of visual area of concern was superimposed on the original image to obtain the enhanced image of visual area of concern.

(a) Original images   (b) Visual attention area detection images

FIGURE 1: Example of visual area of attention detection.

FIGURE 2: Enhanced images of areas of visual attention.

Assume that $f(i, j)$ is the original image, $f_s(i, j)$ is the detection map of visual area of concern, and $f_e(i, j)$ is the enhancement map of visual area of concern. Before stacking, the size of the original image and the detection map of visual area of concern are normalized to 256×256, and the significance value of the detection map of visual area of concern is normalized to $[0,1]$.

$$f_e(i, j) = f_s(i, j).*f(i, j), \quad i \in M, j \in N. \tag{5}$$

Figure 2 shows the enhancement of visual attention area. It can be seen that different areas in the scene have different visual attention, and some repeated textures and less obvious regional information in the scene have been effectively suppressed, such as the passage in the airport scene and the decorative paintings in the bedroom. While preserving visual attention, the superimposed images supplement the information of some gray areas (transitional areas between the attention and unattention areas).

2.3. Deep Feature Fusion. In order to describe the content attributes of scene images effectively, AlexNet network model, which has been pretrained on large-scale scene dataset Places, is used to extract the deep convolution features of original image, visual area of concern detection image, and visual area of concern enhancement image. In addition, since different layers of the deep convolutional network have different abstract expressions of the original image data, the output of multiple fully connected layers of the deep convolutional network is used in this paper to form the deep fusion feature as the final expression of the scene image.

As shown in Figure 3, in the full connection layer of AlexNet, convolution feature is expressed in layer 6, and classification association feature is expressed in layer 7.

Therefore, in this paper, the 4096-dimensional output feature of layer 7 and layer 6 is connected in series to generate the deep fusion feature of the image, and the calculation formula is as follows:

$$F_c = [F_{fc7}, F_{fc6}], \tag{6}$$

where F_c is the depth fusion feature of FC7 and FC6, F_{fc7} is the output feature of layer FC7, and F_{fc6} is the output feature of layer FC6.

Then, the deep fusion features of the original image, the detection image of visual focus area, and the enhanced image of visual focus area of the same image are spliced to generate the deep visual focus features. The calculation formula is as follows:

$$F_{VS} = [F_c, F_{c\_s}, F_{c\_e}], \tag{7}$$

where F_{VS} are the features of deep visual attention, F_c, F_{c_s}, and F_{c_e} are the deep fusion features of the original image, the detection image of visual attention area, and the enhanced image of visual attention area, respectively.

Finally, the depth visual attention features of the training images in the target dataset are sent into the random forest to train the classifier, and the trained classifier is used for scene classification. Because the extracted features have both the contextual semantic relationship between objects in the image and the intrinsic characteristics of scene depth, the effectiveness of scene classification is greatly improved.

3. Experimental Results and Analysis

3.1. Datasets and Experimental Settings. This paper conducted tests on four common standard scene datasets, LabelMe (OT) [23], UIUC-Sports (SE) [24], Scene-15 (LS) [23, 25, 26], and MIT67 (IS) [27], respectively, partial images of each scene dataset are shown in Figure 4. In order to compare with similar algorithms, experiments were carried out according to the training and testing ratios of different datasets in the references, and the average classification accuracy of 10 experiments was taken as the final test result.

  (i) The LabelMe (OT) dataset contains 2688 color images of 8 categories, all 256×256 in size. In each category, 200 images were randomly used for training, and the rest images were used as test images
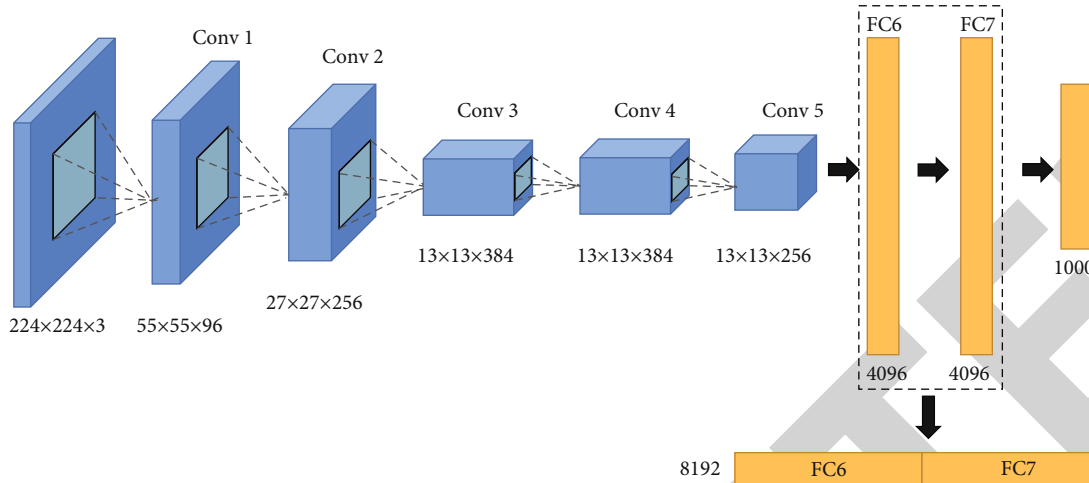
Figure 3: Schematic diagram of generating deep fusion features.

Figure 4: Partial images of each dataset.

(ii) UIUC-Sports (SE) dataset contains 1579 color sports scene images of different sizes in 8 categories. Each category was randomly assigned 70 images for training and 60 images for test

(iii) Scene-15 (LS) dataset contains a total of 4485 indoor and outdoor scene images of 15 categories, of which 8 categories are the same as the LabelMe dataset. 100 images were randomly used in each category for training, and the rest of the images were used as test images

(iv) MIT67 (IS) is a challenging indoor scene image dataset containing a total of 15,620 images in 67 categories. 80 images were randomly used in each category for training, and 20 images were used as test images

3.2. Classification Performance Evaluation. Figure 5 shows the comparison test results of classification on four datasets between deep learning features without visual attention region detection and features proposed in this paper by using the same classification method.

It can be seen that all the features proposed in this paper have certain effects on the test datasets, and the classification accuracy effect is most significantly improved in the LS dataset, mainly because the dataset contains indoor and outdoor scenes, which indicates that the algorithm is universal. In addition, the classification effect of simple outdoor scenes is also significantly improved. However, the effect of the SE and IS dataset is limited, mainly due to the fact that there are many objects in the scene, and the context relationship of prominent objects in the scene is complex. People in many scenes are not the main objects to distinguish scenes,
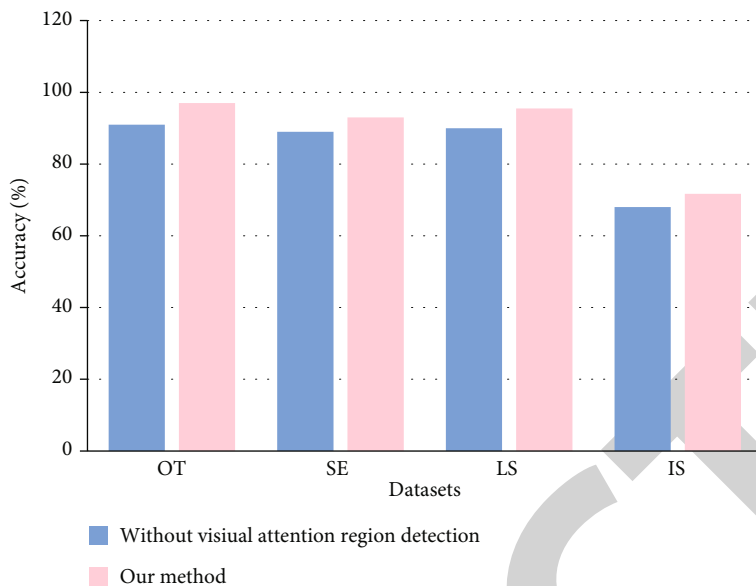
Figure 5: Comparison of experimental results using visual attention area detection.

■ Without visiual attention region detection
■ Our method

Table 1: Fusion matrix of the OT dataset.

Category	1	2	3	4	5	6	7	8	Recall (%)
MITcoast (1)	154	2	—	—	—	4	—	—	96.3
MITforest (2)	—	127	—	—	1	—	—	—	99.2
MIThighway (3)	—	—	59	—	—	1	—	—	98.3
MITinsidecity (4)	—	—	—	108	—	—	—	—	100
MITmountain (5)	—	1	—	—	171	2	—	—	98.3
MITopencountry (6)	7	5	—	—	1	197	—	—	93.8
MITstreet (7)	—	—	—	—	—	—	91	1	98.9
MITtallbuilding (8)	—	—	—	—	—	—	—	156	100
Precision (%)	95.7	94.1	100	100	98.8	96.6	100	99.4	

but sometimes, they are enhanced as prominent objects, which interferes with the discrimination of scene content. In particular, scene discrimination in the SE dataset is mainly determined by the relationship between characters' actions and scenes, while characters' actions are sometimes very similar in multiple scenes. Therefore, the classification effect of visual area of concern detection algorithm on these datasets is limited.

Precision and recall were used to evaluate and analyze the OT, SE, and LS dataset, respectively.

Table 1 shows the fusion matrix obtained by a test of the method in this paper on the OT dataset. It can be seen that this method can achieve 100% accuracy and recall rate in the "MITinsidecity" class and can also achieve good classification effect for other categories. It is easy to confuse the "MITopencountry" class with the "'MITcoast" class. Figure 6 shows partial misclassification images of the OT dataset. These two images misclassify images of "MITopencountry" into "MITcoast," because the context relationship between sky and land in "MITopencountry" is similar to that of sky and coast in "MITcoast." Lawns and deserts on the slopes have a similar texture to sea level.

Figure 6: Misclassification images in OT.

Table 2 shows the fusion matrix obtained by the proposed method in a certain test on the LS dataset. The most confusing categories are "Bedroom" and "Livingroom" and "MITtallbuilding" and "Industrial." Figure 7 shows partial segmentation images of the LS dataset. In (a), the scene images of "Industrial" are misclassified to "MITtallbuilding," because the high-rise buildings in the image are very similar in appearance to tall buildings, and the context relationship with the surrounding environment is similar to that of

Table 2: The fusion matrix of the LS dataset.

Category	1	2	3	4	5	6	7	8	9	10	11	12	13	14	15	Recall (%)
Bedroom (1)	107	—	—	—	9	—	—	—	—	—	—	—	—	—	—	92.2
CALsuburb (2)	—	141	—	—	—	—	—	—	—	—	—	—	—	—	—	100
Industrial (3)	—	—	192	1	1	—	—	—	3	—	—	1	5	—	8	91.0
Kitchen (4)	—	—	—	103	2	—	—	—	—	—	—	—	—	4	1	93.6
Livingroom (5)	4	—	—	2	179	—	—	—	1	—	—	—	—	2	1	94.7
MITcoast (6)	—	—	—	—	—	252	2	—	—	1	5	—	—	—	—	96.9
MITforest (7)	—	—	—	—	—	—	221	—	—	6	1	—	—	—	—	96.9
MIThighway (8)	—	—	1	—	—	—	—	158	—	—	1	—	—	—	—	98.8
MITinsidecity (9)	—	2	5	3	—	—	—	—	194	—	—	3	1	—	—	93.3
MITmountain (10)	—	—	—	—	—	—	—	—	—	273	1	—	—	—	—	99.6
MITopencountry (11)	—	—	—	—	—	6	1	—	—	6	297	—	—	—	—	95.8
MITstreet (12)	—	—	3	—	—	—	—	—	2	—	—	186	—	—	1	96.9
MITtallbuilding (13)	—	—	9	—	—	—	2	—	1	—	—	—	243	—	1	94.9
PARoffice (14)	1	—	—	3	1	—	—	—	1	—	—	—	—	109	—	94.8
Store (15)	—	—	1	1	1	—	—	—	—	—	—	—	1	—	211	98.1
Precision (%)	95.5	98.6	91.0	91.2	92.7	97.7	97.8	100	96.0	95.5	97.4	97.9	97.2	94.8	94.6	

(a)   (b)
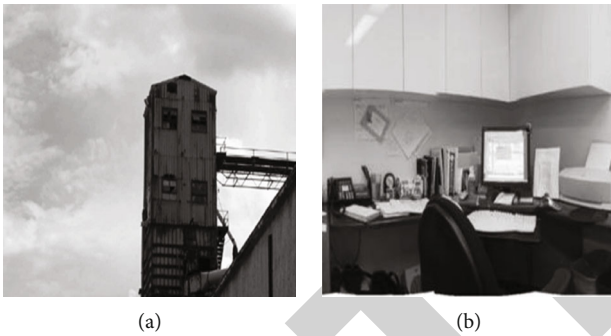
Figure 7: Misclassification images in LS.

"MITtallbuilding." On the right, the scene image of "PARoffice" is misclassified into "Kitchen." The reason is that the cabinet in the upper part of the image has the same position and appearance with the cabinet, and the context relationship with the desktop is similar to that of "Kitchen," thus causing the misclassification.

Table 3 shows the fusion matrix obtained by a certain test of the method in this paper on the SE dataset. It can be seen that the method can achieve 100% accuracy and recall rate in the "Sailing" class. However, "Bocce" has the lowest accuracy and recall rate, and it is most easily confused with "Croquet," mainly because the identification of these two scenes is mainly based on character movements and the relationship between character and scene, and the character movements of these two sports are very similar to the surrounding environment, so it is easy to misjudge.

3.3. Comparison of Experimental Results. The experimental results of the proposed method on four standard scene datasets were compared with those of the reference method.

The comparison test results on the OT dataset are shown in Table 4. It can be seen that the algorithm using deep convolutional network has obvious advantages over the traditional feature extraction algorithm. GECMCT method [28] adds the far neighborhood information to the nonparametric transformation calculation and spatial information. Gist feature and spatial correction census transform are combined to form a new image descriptor, but this method lacks the deep description of scene images. HGD algorithm [29] uses pLSA to train multichannel classifier on the topic distribution vector of each image, which is not only complex in modeling but has also limited classification effect. Compared with other algorithms using deep convolutional networks, the deep convolutional classification model constructed in this paper based on the visual area of interest of images has obviously better classification effect.

The comparative test results on the SE dataset are shown in Table 5. It can be seen that the classification performance of the model in this paper is significantly better than other classification algorithms. Among them, SKDES+Grad+color+shape method [8] embeds image and label information into block-level kernel descriptors to form supervised kernel descriptors and uses visual word bags to learn low-level block expressions. The implementation process of this method is relatively complex. And the representational ability of visual word bag is limited. LGF methods classified using global and local features of images, not the analysis on the contents of the image; using visual attention area detection algorithms on different areas of the image effectively; and combining the depth have been trained on the Places dataset convolution network and can better access the spatial structure of image information [30]. AdaNSFF-Color boost [1] proposes a novel fusion framework of adaptive nonnegative feature fusion (AdaNFF) for scene classification. The AdaNFF integrates nonnegative matrix factorization, adaptive feature fusion, and feature fusion

TABLE 3: The fusion matrix of the SE dataset.

Category	1	2	3	4	5	6	7	8	Recall (%)
Badminton (1)	57	3	—	—	—	—	—	—	95.0
Bocce (2)	3	45	9	—	2	—	—	1	75.0
Croquet (3)	—	5	54	—	—	1	—	—	90.0
Polo (4)	1	3	—	56	—	—	—	—	93.3
RockClimbing (5)	—	—	—	—	59	—	—	1	98.3
Rowing (6)	—	—	—	—	—	60	—	—	100
Sailing (7)	—	—	—	—	—	—	60	—	100
Snowboarding (8)	1	—	—	—	—	—	—	59	98.3
Precision (%)	91.9	80.4	85.7	100	96.7	98.4	100	96.7	

TABLE 4: Comparative test results on the OT dataset.

Methods	Accuracy (%)
CENTRIST [31]	76.49
CMCT [32]	79.91
GIST [23]	82.60
LPC [33]	83.40
GECMCT [28]	86.95
HGD [29]	87.80
ImageNet-CNN [14]	92.83
Places-CNN [15]	94.30
DSPMK+RVFs+BSRC [34]	95.11
Ours	97.70

TABLE 5: Comparative test results on the SE dataset.

Methods	Accuracy (%)
Object bank [19]	76.30
LRML-PCDM [2]	76.97
GECMCT [28]	77.96
GIST [23]	82.60
O2C kernels [18]	86.02
CENTRIST [31]	86.22
SC+LCSR [35]	87.23
LGF [41]	88.52
AdaNSFF-Color boost [1]	90.21
SKDES+grad+color+shape [8]	91.00
Ours	93.75

TABLE 6: Comparative test results on the LS dataset.

Methods	Accuracy (%)
Bow [25]	74.80
CMN [36]	77.20
SPMSM [37]	82.50
GECMCT [28]	82.96
EMFS [38]	85.70
DLGB (saliency) [5]	87.40
O2C kernels [18]	88.80
ISPR+IFV [39]	91.06
Hybrid-CNN [15]	91.59
DGSK [3]	92.30
MKL [30]	92.50
DDSFL+Caffe [11]	92.81
DeepScene [17]	95.60
SDO+ fc features [4]	95.88
Ours	96.01

TABLE 7: Comparative test results on the IS dataset.

Methods	Accuracy (%)
GECMCT [28]	36.57
Object bank [19]	37.60
Midlevel elements+IFV [10]	66.87
ImageNet-CNN [14]	56.79
MOP-CNN [12]	68.88
Places-CNN [15]	68.24
Hybrid-CNN [15]	70.80
DeepScene [17]	71.00
S2ICA [6]	71.20
DLGB(saliency) [5]	71.40
CNNaug+SVM [13]	71.90
RF-CNNs [40]	72.35
Ours	72.37

boosting into an end-to-end process. However, although this method fuses and enhances features, the training data lacks pertinence, which affects its generalization ability.

The comparison test results on the LS dataset are shown in Table 6. The algorithm in this paper still has a good classification effect, which is not only better than traditional classification methods but also better than many classification methods using deep learning. The features of SDO+fc algorithm of cooccurrence with all objects in the scene mode [4] and the correlation of different objects in the scene configuration to choose representative and distinguish between objects, thus, enhance the discriminability between the clas-

ses, with the emergence of identifying objects in the image block probability to represent the image descriptors and to eliminate the influence of the public target. Although the algorithm considers the correlation between objects in the

scene, it is still limited to the simple object and does not consider the surrounding background area adjacent to the object, so the classification effect is limited. DeepScene [17] integrates Spatial Pyramid Pooling into the convolutional neural network to perform multilevel pooling on the scene image and implements the weighted average ensemble of convolutional neural networks to fuse the class scores thus improving the overall performance in scene classification. However, this method still takes the scene as a whole and does not enhance the information representing of scene, so the classification effect is limited.

The comparative test results on the IS dataset are shown in Table 7. It can be seen that, similar to the results of other datasets, the effect of using convolutional neural network is significantly better than that of traditional features in general, and the classification results in this paper still have obvious advantages. Among them, the Places-CNN algorithm [15] using the Places dataset pretraining network outperforms the ImageNet-CNNS algorithm [11] using the ImageNet dataset pretraining network by nearly 12%, mainly because the network using the scene training is more effective in judging the scene category. However, hybrid-CNN algorithm uses the pretrained network of ImageNet and Places datasets to extract deep convolution features of images [15]. Therefore, the classification effect is improved compared with the first two algorithms. However, the algorithm in this paper only uses the pretrained convolutional neural network of the Places dataset and combines the context information of the visual attention area of the image to achieve a better classification effect than hybrid-CNN algorithm.

4. Conclusions

This paper proposes a scene classification model based on the depth feature of visual focus area. Based on the context of significant regional detecting scene image visual interest areas in the image, with the original image overlay, enhance image visual interest area, then, will the three images into AlexNet, respectively, extraction depth visual focus features, in the end, will it into to the random forest classifier for training and classification.

Since the feature extraction model of deep visual attention in this paper also describes the target information in the image and the contextual semantic information between the target and the surrounding scene, different visual attention is constructed and the expression ability of scene characteristics is improved. Combined with the feature of multilayer deep convolution, the deep visual expression of scene image is constructed. The test results on four standard scene image sets verify the effectiveness of the proposed method, and it is better than several methods with good characteristics.

The method for the classification of the test datasets as a whole has a good effect, but when individual scene image content itself exists, ambiguity or visual attention content area does not fully express the scene; there is still a fault phenomenon, to this, and another step in the future research work will be digging deeper visual focusing on context information, in order to obtain better classification effect.

Data Availability

The data used to support the findings of this study are available from the corresponding author upon request.

Conflicts of Interest

The authors declare that there is no conflict of interest regarding the publication of this paper.

Acknowledgments

References

[1] Z. Zou, W. Liu, and W. Xing, "AdaNFF: a new method for adaptive nonnegative multi-feature fusion to scene classification," *Pattern Recognition*, vol. 123, article 108402, 2022.

[2] G. Sun, Y. Cong, Q. Wang, and X. Xu, "Online low-rank metric learning via parallel coordinate descent method," in *2018 24th International Conference on Pattern Recognition (ICPR)*, pp. 207–212, Beijing, China, 2018.

[3] A. Trouilloud, L. Kauffmann, A. Roux-Sibilon et al., "Rapid scene categorization: From coarse peripheral vision to fine central vision," *Vision Research*, vol. 170, pp. 60–72, 2020.

[4] X. Cheng, J. Lu, J. Feng, B. Yuan, and J. Zhou, "Scene recognition with objectness," *Pattern Recognition*, vol. 74, pp. 474–487, 2018.

[5] L. Zhang, R. Liang, J. Yin, D. Zhang, and L. Shao, "Scene categorization by deeply learning gaze behavior in a semisupervised context," *IEEE Transactions on Cybernetics*, vol. 51, no. 8, pp. 4265–4276, 2021.

[6] M. Hayat, S. H. Khan, M. Bennamoun, and S. An, "A spatial layout and scale invariant feature representation for indoor scene classification," *IEEE Transactions on Image Processing*, vol. 25, no. 10, pp. 4829–4841, 2016.

[7] Y. Li, B. Geng, and S. Jiao, "Dispersion entropy-based Lempel-Ziv complexity: a new metric for signal analysis," *Chaos, Solitons & Fractals*, vol. 161, article 112400, 2022.

[8] P. Wang, J. Wang, G. Zeng, W. Xu, H. Zha, and S. Li, "Supervised kernel descriptors for visual recognition," in *Proceedings of the IEEE conference on computer vision and pattern recognition*, pp. 2858–2865, Portland, Oregon, USA, 2013.

[9] S. Singh, A. Gupta, and A. A. Efros, "Unsupervised discovery of mid-level discriminative patches," in *European Conference on Computer Vision*, A. Fitzgibbon, S. Lazebnik, P. Perona, Y. Sato, and C. Schmid, Eds., vol. 7573 of Lecture Notes in Computer Science, pp. 73–86, Springer, Berlin, Heidelberg, 2012.

[10] C. Doersch, A. Gupta, and A. A. Efros, "Mid-level visual element discovery as discriminative mode seeking," *Neural Information Processing Systems*, vol. 26, pp. 494–502, 2013.

[11] Z. Zuo, G. Wang, B. Shuai, L. Zhao, and Q. Yang, "Exemplar based deep discriminative and shareable feature learning for

Hindawi

Retraction

Retracted: Data Collection and Analysis in Sports Practice Teaching Based on Internet of Things Technology

Journal of Sensors

This article has been retracted by Hindawi following an investigation undertaken by the publisher [1]. This investigation has uncovered evidence of one or more of the following indicators of systematic manipulation of the publication process:

(1) Discrepancies in scope

(2) Discrepancies in the description of the research reported

(3) Discrepancies between the availability of data and the research described

(4) Inappropriate citations

(5) Incoherent, meaningless and/or irrelevant content included in the article

(6) Manipulated or compromised peer review

The presence of these indicators undermines our confidence in the integrity of the article's content and we cannot, therefore, vouch for its reliability. Please note that this notice is intended solely to alert readers that the content of this article is unreliable. We have not investigated whether authors were aware of or involved in the systematic manipulation of the publication process.

Wiley and Hindawi regrets that the usual quality checks did not identify these issues before publication and have since put additional measures in place to safeguard research integrity.

We wish to credit our own Research Integrity and Research Publishing teams and anonymous and named external researchers and research integrity experts for contributing to this investigation.

The corresponding author, as the representative of all authors, has been given the opportunity to register their agreement or disagreement to this retraction. We have kept a record of any response received.

References

[1] L. Yang, "Data Collection and Analysis in Sports Practice Teaching Based on Internet of Things Technology," *Journal of Sensors*, vol. 2022, Article ID 2741517, 10 pages, 2022.

Research Article

Data Collection and Analysis in Sports Practice Teaching Based on Internet of Things Technology

Li Yang [iD]

Hunan University of Information Technology, Hunan, Changsha 410151, China

Correspondence should be addressed to Li Yang; liyang@hnuit.edu.cn

Since entering the new century, people's living standards have been continuously improved, living conditions have been continuously improved, which is the embodiment of the improvement of the country's comprehensive strength, the increase in national strength has made the development of sports faster and faster, and the annual output value of sports is also increasing year by year. However, there are still many places that do not pay attention to practical content; in view of these problems, we use the Internet technology to collect and analyze the data of sports practice teaching; in this chapter paper, we use the 2SPLM observation matrix method and CS-MDGA algorithm, so that the collected sports practice teaching data is more quick and convenient to be analyzed. This paper also uses a large number of chart data to confirm the correctness and accuracy of their views, making the paper more reliable. The study shows that the teaching of physical education in China is increasing year by year, indicating that the teaching of physical practice in China is developing in a better direction. The mathematical modeling in the abstract section of the article uses computational methods such as constrained nonnegative matrix decomposition and constrained nonnegative matrix decomposition model optimization algorithm that integrates external information for research.

1. Introduction

In recent years, the Internet of Things technology has developed towards the direction of information technology in sports practice. This paper mainly introduces the rapid development of the Internet of Things (IoT) technology and its wide application in sports practice, mainly according to the actual situation of the Internet of Things technology; the control network and information network integration of the Internet of Things technology are studied, and it is proposed to combine the Internet of Things technology and sports practice teaching. At the same time, a professional information system was designed [1]. Based on the content of the Internet of Things technology, the application principle of the Internet of Things technology that can be used for sports practice teaching management is studied. The system architecture model and data processing logical structure model of the physical education visual management system are designed. Through research, the system can sense the body production environment sensors and physical condition sensors, so that it can predict, warn, and

actively control various hazards to the body. Information from human body sensors and production progress sensors can be sensed to improve the efficiency of exercise and reduce the consumption required by the body. Improve the decision-making ability of athletes and improve the effectiveness of exercise [2]. This paper focuses on the connection between the Internet of Things (IOT) technology and the teaching of physical education practice. In view of the many problems in the development process of traditional physical education practice teaching, a series of the Internet of Things technology models are proposed. Through comparative research, the advantages of the information utilization model from information to function are verified. Finally, the model proposes that based on unified information collection, the true interconnection of transportation can be realized. It can greatly save the cost of technology transfer, tap the potential value of information, and promote the emergence of sustainable information service markets and industrial upgrading [3]. In this paper, a case study is presented to illustrate how off-the-shelf IoT components can be combined into a secure and low-cost sensing system that

can be used for a variety of physical education practice teaching applications. Examples include smart sports practice operation or logistics chain monitoring. Our goal is to provide end-to-end security between deployed sensor gateways and sports users. Our solutions are aligned with the data-centric security concept in future sports practices currently under development [4]. Aiming at the shortcomings of traditional sports safety monitoring system, this paper designs a sports safety monitoring system based on the Internet of Things (IoT). The system establishes a network overheating and humidity sensor through Zigbee, a gas sensor to detect physical health parameters, and then transmits data to the ARM server, stores the received data in the database, and accesses the Internet through the network, and the client computer and smart phone access the ARM server data in various modes through the Internet [5]. This paper finds that the imperfection of the old teaching and sports system and to create a more perfect teaching system, provide effective physical education practice teaching for various colleges, and provide talents for each college [6]. This article explains the various mistakes and problems in the practice of school sports, and tries to further discuss the innovation and ideas of college sports practice in the current situation of college sports [7]. This thesis is mainly to observe the collection and interview of three physical education teachers over a period of 16 weeks, joint teaching practice, so that students can establish the core values of trust and respect, so that in the school PE class, we can be more practiced and better used in colleges and universities [8]. Under the background of quality education, physical education practice teaching faces the problem of insufficient education training methods, and this paper proposes a solution by constructing a practical teaching model. A sound system of teaching quality and evaluation of physical education practice has been established, and the steps for the realization of this model are proposed [9]. In this paper, the teaching schemes and techniques on how to improve the physical education teaching practice are discussed, and the physical education teaching practice plan is also optimized and combined, and this set of physical education teaching has been proved to be feasible in practice. It promotes the improvement of the quality of physical education practice and makes the teaching purpose more easily achievable [10]. This paper mainly demonstrates the design and methods of collecting data for decision-making and problem solving in the practice of physical education in colleges and universities. General guidelines are provided for practice, and a set of data analysis is proposed to develop estimates and solutions [11]. This paper mainly introduces that data collection and analysis is the basic condition of society; due to the dynamic behavior of various behaviors that may produce false data, we will analyze contemporary information and historical cases in order to reduce false information, so that the data becomes more accurate and reliable [12]. As mobile technology becomes more common in modern society, users are finding more and more innovative ways to take advantage of the collection and analysis of the latest data. Data collection, in particular, has changed dramatically thanks to wireless technology [13, 14]. This paper mainly introduces the equipment of data collection and analysis, compares historical data and stores it in a unit with collector collection, and converts the results of the analysis into historical graphs, so that the analysis of data becomes simpler and clearer [15]. Data collection and analysis covers quantitative and qualitative methods of data collection and analysis in social research, making data collection and analysis more simple and convenient and easy to understand [16].

2. The Importance of Teaching Professional Practice in Physical Education

In school teaching, practice is an important lesson to test students' practice results and plays an important role in developing college students' sense of innovation and improving the quality of talent training in colleges and universities and is an indispensable value. In China's 13th Five-Year Plan, it is proposed to accelerate the integration of industry and education and the cultivation of applied and skilled talents, deepen the practical teaching of college students, and comprehensively develop the innovation and entrepreneurship capabilities of college students. From this, we can conclude the important value of professional practice teaching in physical education in colleges and universities. It is the professional practice teaching of physical education that can promote the improvement of college students' education and teaching level, better adapt to the requirements of the workplace, and help the continuous improvement of the training standards of physical education professionals in colleges and universities.

2.1. Physical Education Professional Practice Teaching Objective System. Physical education professional practice teaching goal system is an important standard to lead the professional practice teaching of physical education. In the process of professional practice teaching of physical education, the development of students' cognitive ability, physical education teaching skills, educational emotional values, and other aspects of the level of physical education cognitive ability refers to the abstract theoretical knowledge mastered by college students through physical education time teaching, transformed into more emotional; scientific physical education teaching rational cognition and practice helps college students to better transform the sports skills mastered into practical teaching capabilities, so as to meet the job skill needs of college students' physical education teaching. Similarly, in the process of practical teaching, the skills training of college students also includes the organization skills of teaching plan design, sports meetings and other activities, and school sports work skills.

2.2. Optimize the Teaching of Professional Practice Courses in Physical Education. The construction of the physical education professional practice teaching content system is an important starting point for accelerating the exercise of the practical teaching ability of college physical education majors; promoting the improvement of college students' employability; comprehensively increasing the cognition, action skills, and values of physical education college

students in colleges and universities; and further attaching importance to theory in the current practical teaching curriculum system, increasing practicality, focusing on development, comprehensively optimizing the curriculum architecture, and cultivating the ability of college students. Accelerate the cultivation of application-oriented talents.

2.3. Organize Campus Sports Practice Activities to Enhance Physical Fitness. Organizing campus sports activities is a key measure to enhance physical fitness and achieve physical education goals. On the basis of not affecting the basic teaching order, we should be able to enrich physical activities as much as possible, and truly let sports enter the campus and enter life, thereby improving students' participation in sports activities and providing support for further realizing the quality education goals of physical education classrooms. Under the pressure of heavy schoolwork, students have time and opportunities to relax and achieve physical fitness.

3. Algorithm Data Design Implementation and Collection

3.1. Network Model with Problem Description. Compression perception technology is an emerging data compression theory; for signals with sparsity, compression perception can be compressed sampling at a frequency lower than Nyquist sampling; to achieve signal projection transformation from high-dimensional to low-dimensional, the use of optimal reconstruction algorithm to achieve high-precision reconstruction of compressed signals, due to its excellent compression performance, has been widely studied and applied in various fields 1 Link State Matrix. LSM records the matrix of link state information, the size of which is $M \times N$, where M is a number and N is an intermediate number of this computer, and the LSM formula is

$$L = (l(i, j))_{M \times N} = \begin{cases} 0, x_j \notin X, \\ 1, x_j \in X. \end{cases} \quad (1)$$

Definition 1 Dense random projections (DRP). DRP is a dense observation matrix, which contains O(N) nonzero elements per row, usually selecting (2) to construct a dense observation matrix:

$$\Phi_d = (\delta(x, y))_{M \times N}. \quad (2)$$

The actual link to construct a sparse observation matrix with random characteristics and its structure can be obtained by the matrix point multiplication operation between LSM and DRP as

$$\Phi_s = L\Phi_d. \quad (3)$$

The error rate for untrusted links is p, so in the SPLM matrix, the values of each element are shown as

$$\delta_s(i, j) = \begin{cases} +1, \text{with prob.} \dfrac{(1-p)}{2}, \\ -1, \text{with prob.} \dfrac{(1-p)}{2}, \\ 0, \text{with prob.} p. \end{cases} \quad (4)$$

SPLM matrix design observation matrix needs to ensure that it satisfies the RIP condition with most orthogonal radicals. Proving the RIP condition is an N-P difficult problem, pointing out that if the observation matrix is full, the data projected by the matrix will be reconstructed precisely with a probability that tends to "1." The design of the observation matrix needs to ensure that it satisfies the RIP condition with most orthogonal bases, but it is proved that the RIP condition is an N-P difficult problem, indicating that if the observation matrix is full, the matrix forwarded data is reconstructed precisely, and the probability becomes "1." Because each number in SPLM can achieve the discrete arbitrary distribution shown in the formula (4), RIP can actually be seen as depicting the similarity of a matrix to a standard orthogonal array. The L2 energy (norm square) after the change to the vector does not change more than the energy of the original vector. RIP is very effective for stability analysis. The RIP nature only needs to be $0 < \delta < 1$. Then Φ_s each row looks as a random variable ζ_n and produces a random sequence that can be used as a results. $\{\zeta(n), n = 1, 2, \cdots, N\}$ indicates that in the sensing network, if N points are randomly arranged within the layout range, the perception data collected by them is recorded. If d is in a group $\psi_{n \times n}$ under sparse, the different data is $\Phi = (\delta)_{m \times n}$, and the observation carrier is Y$M \times 1$; sink nodes optimize the problem by equations (5) and (6) to reconstruct the original data under certain accuracy constraints:

$$Y = \Phi - S = \Phi - \Psi^T \cdot d = \Theta \cdot d, \quad (5)$$

$$d = \arg \min \|d\|_p, \quad (6)$$

thereinto, $\Theta = \Phi - \psi_T$; for the transmitted value, $d\,p$ represents the lp norm of the vector d, called

$$\|d\|_p = \begin{cases} \left(\sum_{i=1}^{N} |x_i|^p \right)^{1/p}, 0 < p < +\infty. \\ \max_{i=1,2,\cdots N} |x_i|. \end{cases} \quad (7)$$

In the data collection process of the wireless sensing network, each round of data collection of the CS is divided into M independent observations, and its mathematical expression can be described as

$$\begin{bmatrix} y_1 \\ y_2 \\ \vdots \\ y_M \end{bmatrix} = \begin{bmatrix} \varphi_{11} & \varphi_{12} & \cdots & \varphi_{1N} \\ \varphi_{21} & \varphi_{22} & \cdots & \varphi_{2N} \\ \vdots & \vdots & \ddots & \vdots \\ \varphi_{M1} & \varphi_{M2} & \cdots & \varphi_{MN} \end{bmatrix} \begin{bmatrix} d_1 \\ d_2 \\ \vdots \\ d_N \end{bmatrix}. \quad (8)$$

3.2. SPLM Observation Matrix Design. For the problem that the sensory data in the decompression differs from the observation matrix sample, a sparse measurement matrix of the loss rate matrix (SPLM) is designed. By not observing the lost packet node information during each observation, the observation array converts the data loss problem collected by CS data under the tree route into an observation matrix projection problem based on sparse matching, which not only realizes a large number of observation sampling of the data in the network, but also avoids the false judgment of the data collection situation at the Sink end, and the specific implementation process is as follows: Suppose that the sensing network is set by nodes $\{s_1, s_2, s_3, \cdots, s_n\}$ and a nonimmovable sink node, where the sense node is randomly and evenly deployed $a \times a$, sink is located in the focus of photography without moving. The perception node periodically collects and uploads the perception and can adaptively and dynamically adjusts its own transmission power; sink node has strong computing performance, periodically collects and reconstructs the network-wide perception data, and can obtain the location information of the nodes in the network. Generate minimum data (MST) routes across network nodes to complete various types of data, that is, to generate a picture of the direction of the connection $G = (V, E(q))$; thereinto, $V = \{V_1, V_2, \cdots, V_N\}$ represents a collection of perception nodes, $E(q) = \{e_1(q), e_2(q), \cdots, e_N(q)\}$ represents a link collection for MST, $e_i(q)$. The connection estimate is q, and if $p = 1 - q$, then p represents the loss rate of the link. Other than that, the sensor network adopts the data collection method of compressing perception, which has the following characteristics: (1) The sparse transformation base of the perception data vector $\psi_{n \times n}$ discrete Fourier transform (DFT) is used, and dilution exchange and orthogonal sparse groups are shown in equations (9) and (10), respectively; (2) after receiving M numbers at the receiving port, the original number is reconstructed using arbitrary catch-up (OMP); (3) the CS reconstruction accuracy adopts the relative error shown in equation (11). η is the measure; the smaller its value, the higher the reconstruction accuracy; if the reconstruction error is higher than 5%, it is considered that the reconstruction does not meet the accuracy requirements, that is, the reconstruction fails.

$$X(k) = \sum_{n=0}^{N-1} x(n) e^{-j(2\pi/N)kn} = \sum_{n=0}^{N-1} x(n) W_N^{kn}, \quad (9)$$

$$\Psi_j(t) = \frac{1}{\sqrt{N}} e^{j2\pi jt/N}, \quad (10)$$

$$\eta = \frac{\left\| \widehat{x} - x \right\|_2}{\|x\|} = \frac{\sqrt{\sum_{n=0}^{N-1} \left(\widehat{x} - x \right)^2}}{\sqrt{\sum_{n=0}^{N-1} x_n^2}}. \quad (11)$$

Formula $\sum 5j = 1\delta_i, jxj$ is expressed as the sum of all data from S1 to S5; the file between S5 and the receipt of the data lose all the data corresponding to S5, that is, packets $\sum 5j = 1\delta_i, jxj$. All packets are lost. Due to the unreliability of the link between S5 and sink nodes, all the data collected by nodes S1 through S5 is lost. As shown in Figure 1, the closer you throw away the file to the receiving machine, the more node data is lost; in addition, because in the CS data collection process, the nodes send a weighted superposition packet, the sink node receives a weighted superposition data after each observation is completed, so when getting the data in the network, regardless of whether the link drops packets or not, the number of packets is lost, and the sink node is unknown to this information, and assumes that the received data weighted overlay and (that is, the data values of this observation) of the whole network node, and reconstructs the original perception data X based on this observation. Therefore, CS data collection under unreliable links has the following characteristics: (1) a packet loss in a link will cause the loss of sensing data of multiple nodes, that is, there is a "correlation effect" of packet loss in the link; (2) the sink node is unknown about the data loss of the nodes in the network and takes the observation value received in each round as the sensing data projection of the nodes in the whole network to participate in the data reconstruction process, that is, the compressive sensing data is not matched with the observation matrix sampling; (3) because that sink node cannot know whether the data of the nodes S1 to S5 are lost, the received observation data is assumed to be the credible data of the whole network, and a new round of reconstruction is carried out on the observation data on the basis of the assumption. The matrix Φs is an independent and identically distributed discrete random sequence, and the random variables constituting the sequence all obey the distribution law of formula (11), and then the matrix has a full rank tending to "1." Proof assumes that the matrix Φs satisfying the above conditions has a nonfull rank, that is, for the ith row of the matrix, there exists a set of coefficients such that:

$$\zeta_i = a_1 \zeta_1 + a_2 \zeta_2 + \cdots + a_{i+1} \zeta_{i+1} + \cdots + a_M \zeta_M, \quad (12)$$

$$EX(n) = \left[\frac{(+1)(1-p)}{2} \right] + \left[\frac{(-1)(1-p)}{2} \right] + 0 \times p = 0, \quad (13)$$

$$DX(n) = E[X(n) - EX(n)]^2 = E[X(n)]^2 = 1 - p. \quad (14)$$

Make a random process $\{Y(n), n = 0, 1, \cdots, N\}$ for $a_1 \zeta_1 + a_2 \zeta_2 + \cdots + a_i + 1\zeta_i + 1 + \cdots + a_M \zeta_M$, and then the mean number and functions are

$$EY(n) = E\left[\sum_{j \in [1,M], j \neq i} a_j \xi_j(n) \right] = \sum_{j \in [1,M], j \neq i} a_j E\xi_j(n) = 0, \quad (15)$$

$$DY(n) = E[Y(n) - EY(n)]^2 = E[Y(n)]^2$$
$$= \sum_{j \in [1,M], j \neq i} a_j D\xi_j(n) = \sum_{j \in [1,M], j \neq i} a_j^2 (1-p). \quad (16)$$

Therefore $X(n)$ and $Y(n)$ describe different stochastic processes, respectively. For a discrete stochastic process $X(n)$, the value of its random variable $X(i)$ is $\{+1, -1, 0\}$, and then the length of the state space IX is 3N; for a discrete
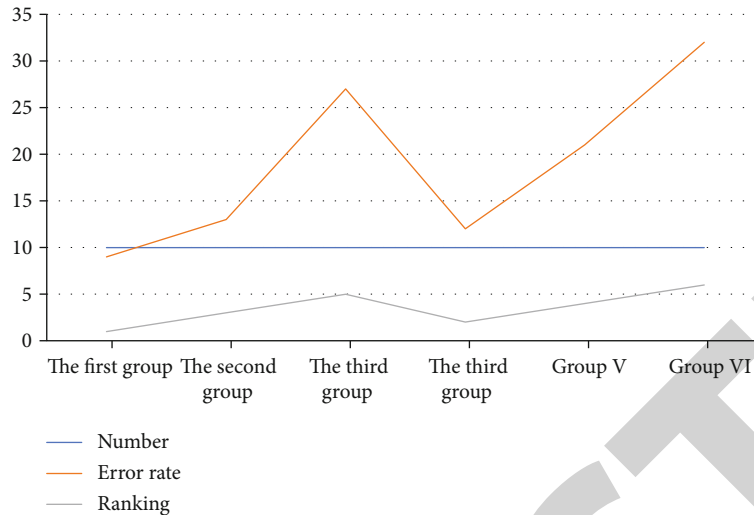
FIGURE 1: Comparison chart of assessment results.

stochastic process $Y(n)$, the value of its random variable is $-M+1 \leq Y(I) \leq M-1$, and then the length of the state space IY is 2M-1. If the event A is that formula (12) holds; event B is the coefficient $a_1, a_2, \cdots, a_M$; not all are zero. Event C is the coefficient $a_1, a_2, \cdots, a_M$. Only one in the middle is not zero; rule:

$$p(ab) < p(ac). \tag{17}$$

Solve $p(ab)$. This can be transformed is a stochastic process that solves independent homologous distributions $X_1(n)$ and $X_2(n)$. The probability of having the same state at the same time, according to the distribution law shown in equation (4), is a stochastic process $X(n)$. In the state space, different states have different probability values; for ease of analysis and without losing the generality, take the parameters in equation (4) and

$$p(ab) < p(ac) = \frac{1}{3 < 10^{-3}}. \tag{18}$$

Thus, event A holds as a minimal probability event, i.e., the null hypothesis substandard, so matrix Φ_s. The probability of approaching "1" is full of rank.

3.3. CS-MDGA Algorithm. For CS data collection in an unreliable tree topology under the link, it has both a packet loss "correlation effect" and a false positive problem of packet reception by the sink, while the SPLM false positive problem of the sink side, so it is necessary to discover relevant systems to solve the problem of losing "relevant data" search. In essence, the "correlation effect" of packet loss is caused by the weighted superposition processing of data packets in the process of CS data collection, which is also the advantage of CS data collection. Therefore, the most effective way to solve the "correlation effect" of packet loss is to ensure the reliability of link transmission and avoid the occurrence of correlation packet loss. Under premise of ensuring that data compression ratio is unchanged, the number of observations

is required by different network sizes. The process of obtaining data is different, which in turn changes the value of the type of judgment result, so different types of proportions will not only lead to all the data of computer but also affect integrity copy path construction cs between two points and the safety of transportation, which in turn affects the algorithm performance. The cost of achieving reliable transmission guarantee for the entire network of roads is huge, drastically reducing its value, and SPLM observed the ability of the matrix to observe and found a way to cross-compress the perception of the data; the entire website data is evenly distributed entry (TF) and CS, where TF is used to collect and forward numbers, it is not related to the file, the CS data is sent and obtained in the CS data acquisition data, and the lost files are consistent. For the obtained data at the center of the TF point, the use of SPLM observations can only defeat the missing values that have a relationship with cs; in addition to the use of SPLM observation, other mechanisms are designed to ensure the safety performance of CS node transportation. CSMA/CA (Carrier Sense Multiple Access with Collision Avoidance) is a random competition MAC protocol with simple algorithms and good performance. Its Chinese name is Carrier Listening For Multiple Access/Collision Avoidance.

4. Multipath Transmission Mechanism

This article found a completely new transport mechanism that makes data transfer between CS nodes safe and reliable. Generally speaking circumstances, if the data is lost on the CS road, the data transmission mode Si will change the direction of transportation so that other roads send data for sign-off. There are many ways to do this from start to finish to reduce breakage on the way; this paper adopts the construction method of the minimum energy consumption spanning tree route; native consumption of the network is rolled out (19):

$$E(d) = 2\alpha_1 + \alpha_2 d^n, \tag{19}$$

thereinto, a_1 is the expression consumed in the circuit, a_2 is the power amplification factor, d is the length of the transport, and N is breakage factor ($2 \leq n \leq 5$, in any position usually $n = 2$); the lowest consumption indicates the problem of the formula (20), where the start point to the target point d_i is the distance from the destination to the road.

$$\min \left(\sum_{i=1}^{k} 2\alpha_1 + \alpha_2 d_i^n \right) \tag{20}$$

$$s.t. \sum_{i=1}^{k} d_i = d_0$$

$$d_{\text{char}} = \left(\frac{2\alpha_1}{\alpha_2(n-1)} \right)^{1/n}. \tag{21}$$

This problem is done using Lagrange multiplication; when the content between the point and the start point is equal, the loss of content is minimal, and the value of the distance d_{char} is given (21); then the optimal hops kopt takes the quotient upper limit of d and d_{char}. This article found that completing other substitution methods, the data were obtained: (1) The sink side calculates the straight-line distance from sink node to each CS node according to the geographical full information for each target d; (2) sink side linear is the distance d of each number and the size of the image distance d_{char}, if $d \leq d_{\text{char}}$, then build a single-hop backup path, if $d > d_{\text{char}}$, first calculate the optimal number of hops kopt, according to the optimal hops kopt, on the CS node to sink straight path, based on the principle of equal distance of each hop, and calculate the theoretical ideal relay node geographical location; (3) according to the ideal relay geographical coordinates, the sink side selects the node closest to the coordinates as the relay node; (4) sink distributes the built CS node minimum energy consumption route the corresponding middle node. The CS-MDGA algorithm first constructs an MST routing tree of the whole network nodes, and the number of all child nodes of the nodes in the tree is w_i, In particular, for a sink node $w_{\sin k} = N$, for a node $w_i = 0$, located at the end of the link, $\varepsilon = M - 1$ is defined as the threshold for distinguishing node types. According to the size of w_i of each node, if $w_i > \varepsilon$, node i participates in data collection in CS mode, which is called CS node. If $w_i \leq \varepsilon$, the node participates in data collection in the traditional forwarding mode, which is called TF node. Then, during the data collection process, the number of data packets PN(i) sent by node i is:

$$PN(i) = \begin{cases} \omega_i + 1, \omega_i \leq \varepsilon, \\ M, \omega_i > \varepsilon. \end{cases} \tag{22}$$

In the process of obtaining data in the CS-MDGA method, the TF point is routed along the MST route with a normal forwarding effect to obtain the result, as shown in the effect in Figure 2, and its data does not produce a "special effect"; CS points participate in data discovery along the MST in the CS data state, thus achieving the purpose of algorithm data design. The above algorithm is based on the 2SPLM observation matrix and CS-MDGA algorithm decomposition of the algorithm data design and implementation of the whole process and can achieve the purpose of data algorithm design and implementation; after obtaining the characteristics of the data, you can carry out other work arrangements for the user.

5. Analysis of Important Indicators in the Teaching of Physical Education Practice

5.1. Practical Teaching Results Analysis. We evaluated the findings in three parts: skill assessment, skill development assessment, and athlete endurance goal assessment. Test scores from all students are collected almost weekly as a reference for talent assessment to better understand student skills and skill management. The athletic abilities demonstrated on site will serve as a source of data to evaluate the analysis of students' athletic abilities [17].

The examination process is defined as:

Step 1. Student comes for the exam in accordance with the group for the on-site sports skills display, the assessment place is the school gymnasium, and 7 physical education call the teacher to grade each student.

Step 2. The assessment takes place in classrooms where they are usually trained. Teachers assess students' development potential based on the recordings of students' regular training. On-site skill performance and growth points are calculated with a maximum of 100 points.

Step 3. The assessment location is the equipment room; the teacher opens the student's examination file in the equipment room, and analyzed by different mathematical techniques, the student's difficulty failure rate is counted.

Step 4. Compare the scores to the six groups horizontally and then in portrait orientation.

5.2. Analysis of the Results. From the data analysis in Table 1, it can be seen that the overall performance of Dan's three students remained stable, while the ratings of "very good," "good," and "poor" did not change, although the best training was not in physical education class. With specific guidance, they can achieve great results. The outcomes of the traditional learning model and its professional level are stable and maintained at a certain level. However, the comparison of the six groups shows that the first three groups are slightly higher than the latter three groups at the same level, and the average score of the first three groups is 1.9 points higher than the corresponding comparison. In practice performance, the third group scored 5.4 points higher than the sixth group average. The data shows that the intermediate group has a slight advantage over the traditional group in skill assessment, and the final score is slightly higher than the other groups.

From the data in Table 2, we can see that the 6 groups have the same number of 10 people. The average score of
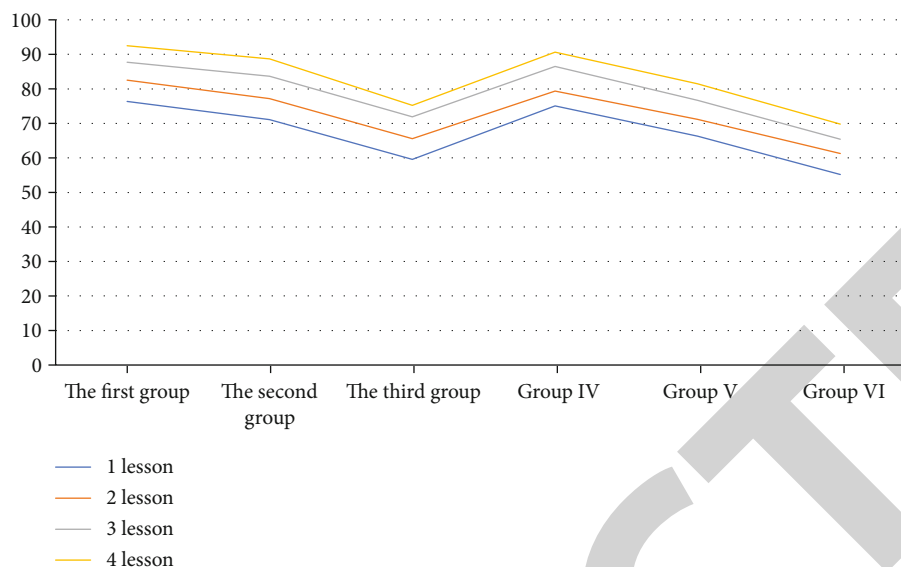
Figure 2: Performance comparison in different periods.

Table 1: Sports live display assessment statistics table.

Constituencies	Number	Average score	Ranking
Group I	10	92.5	1
Group II	10	88.7	2
Group III	10	75.2	3
Group IV	10	90.6	4
Group V	10	81.5	5
Group VI	10	69.8	6

Table 2: Sheet of physical practice ability assessment.

Constituencies	Number	Average score	Ranking
Group I	10	83.6	2
Group II	10	91.4	1
Group III	10	81.7	3
Group IV	10	80.4	4
Group V	10	79.3	5
Group VI	10	75.5	6

Table 3: Statistical table of error rates in sports practice assessment.

Constituencies	Number	Error rate	Ranking
Group I	10	9	1
Group II	10	13	3
Group III	10	27	5
Group IV	10	12	2
Group V	10	21	4
Group VI	10	32	6

the first group is 83.6, ranking second; the average score of the second group is 91.4, ranking first; the average score of the three groups is 81.7, ranking 3rd; the average score of the fourth group is 80.4, ranking 4th; the average score of the fifth group is 79.3, ranking 5th; the average score of the sixth group is 75.5, ranking 6th. The error rate in Table 3 refers to the frequency of mistakes by the number of people surveyed who have taken the difficulty of testing in sports practice performances.

The results in Table 3 are basically the same as the experimental results in Table 1, indicating that the student has a good foundation in the traditional teaching mode and has a good performance. Compared with the students, the conventional teaching mode with good qualities has a good performance. Compared with the first three groups of students, the effect of grasping the error rate is not very good. The first group had a 3% lower error rate than the fourth group; the second group had an 8% lower error rate than the fifth group; the third group had a 5% lower error rate than the sixth group. The environment of the on-site drill under the stadium and the usual practical training is quite different, and the simulated real sports practice created by the special training technology makes the students get better promotion in training, so the first three groups of students in the same environment play more stable and excellent. It can be seen that the accumulation of students' performance experience through the practical training applied by special training techniques is helpful to the grasp of the details of sports training. The data of the three scoring tables that are integrated to obtain a comparative figure of the result is shown in Figure 1.

The analysis of Figure 1 shows that students who use digital audio technology in their teaching experience significant improvements in skills, learning efficiency, and error management. Emphasize students' traditional teaching skills, emphasizing experiences of learning and
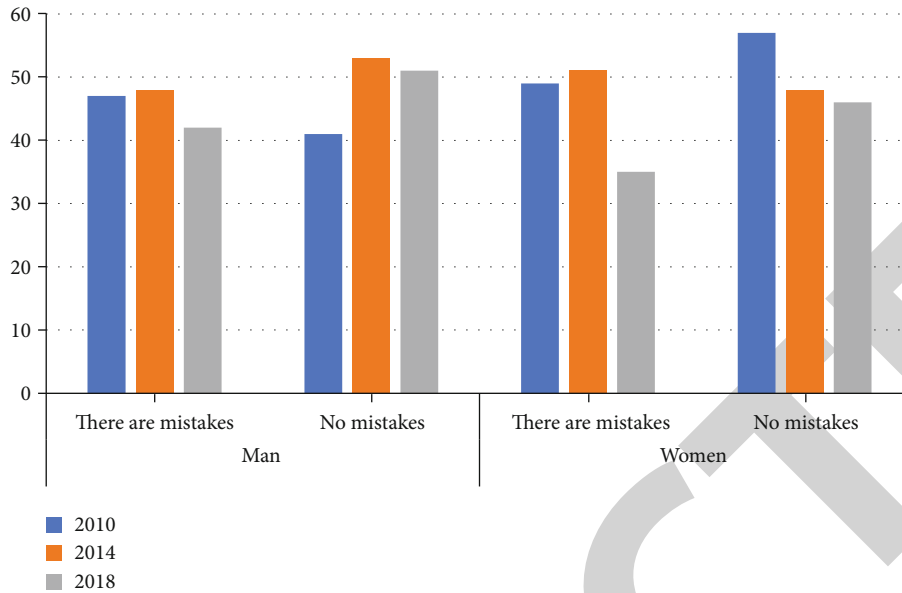
Figure 3: Comparison of male and female athletes' mistakes.
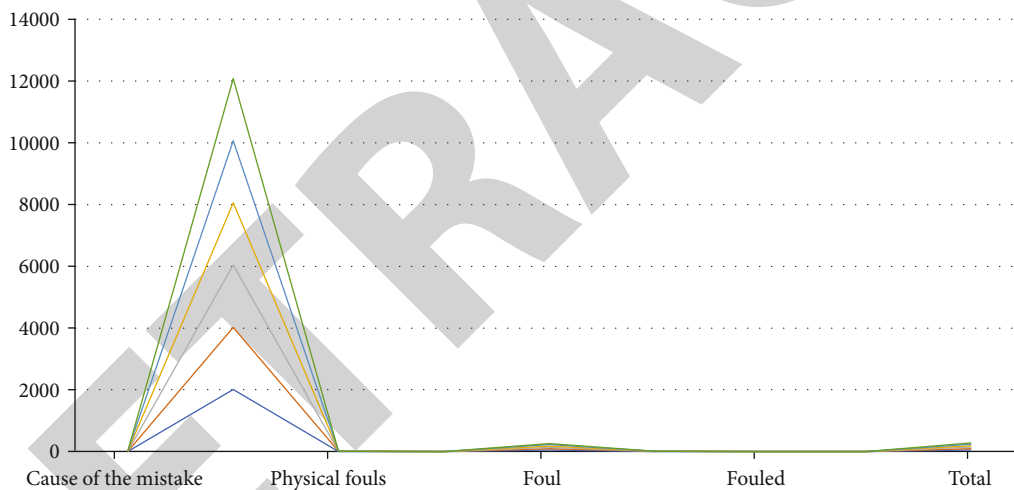
Figure 4: Causes and types of errors.

correcting mistakes, but they are slightly inferior to the number group.

To better assess the impact of learning methods on learning outcomes, teachers also assessed students' practical training on the target trajectory recorded in each lesson after each major, based on the students' skill level. In practical classes, the fourth year is chosen from the final grades. After the scores were combined, the mean was calculated, and the data was analyzed, resulting in the comparison table of ordinal scores in Figure 2.

The ordinate coordinates in Figure 2 represent the average of the students' technical skills displayed in the practical training after the unified scoring is calculated by group. Analyzing Figure 2, as the teaching progresses, the teaching time of the application of digital audio technology increases, and the results achieved by the students' skill demonstration

have increased accordingly and exceed the teaching results achieved in the general pattern. It can be seen that special training techniques have a proven role in promoting students' skills upgrading.

5.3. Analysis of Sports Practice Errors. Comparison of male and female athletes' mistakes is shown in Figure 3.

In Figure 3, we can see that in 2010, men had 47 mistakes and women had 49 mistakes; in 2014, men had 48 mistakes and women had 51 mistakes; in 2018, men had 42 mistakes. Women had 35 mistakes.

5.4. Types of Mistakes and Their Causes. The types of errors are shown in Figure 4

Figure 4 shows that the main selection types of athletes account for 60.58% of the total number of male athletes and
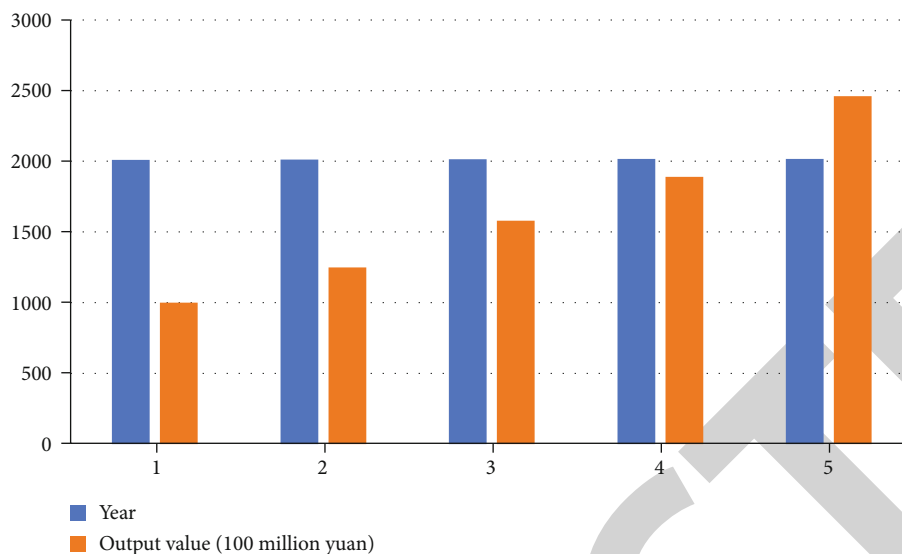
Figure 5: Annual output value of sports.
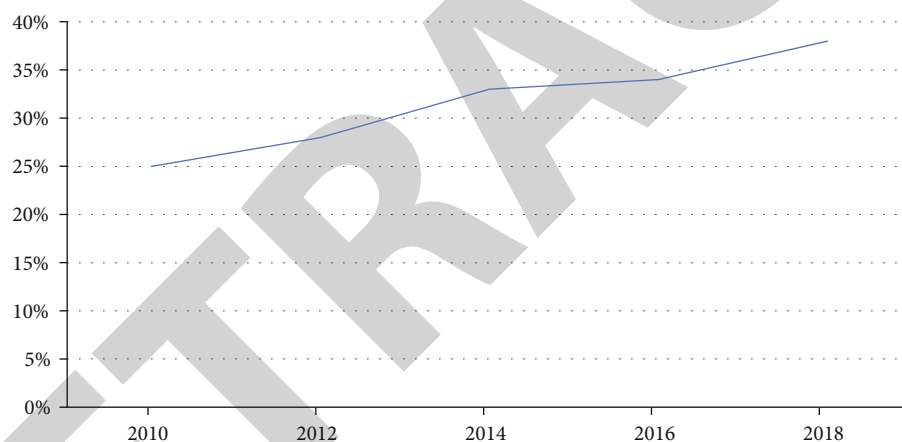
Figure 6: Annual output growth rate of sports.

65.92% of the total number of female athletes. It seems that most errors occur during playback. Both male and female athletes suffer from physical causes, but the corresponding errors will affect the athlete's state adjustment, and when the athletes cannot adjust their mentality correctly, it will affect the performance of the competitors. The abscissa of Figure 4 represents the types of mistakes made by athletes in competitions and is the cause of various errors collected from athletes in a large amount of competition data.

Annual output value and grownth rate are shown in Figures 5 and 6

In the analysis of Figures 5 and 6, the annual output value of sports in 2010 was 10 billion yuan, the annual output value of sports in 2012 was 125 billion yuan, the annual output value of sports in 2014 was 162 billion yuan, the annual output value of sports in 2016 was 194 billion yuan, and the annual output value of sports in 2018 was 240 billion yuan. The strategy of a sports power has led to an increase in the annual output value of sports and an annual output value of more and more large, and the annual output value growth rate of sports will continue to accelerate according to this trend.

6. Conclusion

Through the matrix algorithm and experimental comparison, it can be concluded that the study of sports state is an important material, because sports is a complex art form, and the physical state of the athletes is good, so communication is the starting point of the coach. If you want to be proficient in psychology, you need to strengthen psychological training, continuously accumulate practical experience, develop your psychological processing ability, and have a deeper understanding of the meaning of psychology. Only

Retraction

Retracted: Prediction and Analysis of College Sports Test Scores Based on Computational Intelligence

Journal of Sensors

This article has been retracted by Hindawi following an investigation undertaken by the publisher [1]. This investigation has uncovered evidence of one or more of the following indicators of systematic manipulation of the publication process:

(1) Discrepancies in scope

(2) Discrepancies in the description of the research reported

(3) Discrepancies between the availability of data and the research described

(4) Inappropriate citations

(5) Incoherent, meaningless and/or irrelevant content included in the article

(6) Manipulated or compromised peer review

The presence of these indicators undermines our confidence in the integrity of the article's content and we cannot, therefore, vouch for its reliability. Please note that this notice is intended solely to alert readers that the content of this article is unreliable. We have not investigated whether authors were aware of or involved in the systematic manipulation of the publication process.

In addition, our investigation has also shown that one or more of the following human-subject reporting requirements has not been met in this article: ethical approval by an Institutional Review Board (IRB) committee or equivalent, patient/participant consent to participate, and/or agreement to publish patient/participant details (where relevant).

Wiley and Hindawi regrets that the usual quality checks did not identify these issues before publication and have since put additional measures in place to safeguard research integrity.

We wish to credit our own Research Integrity and Research Publishing teams and anonymous and named external researchers and research integrity experts for contributing to this investigation.

The corresponding author, as the representative of all authors, has been given the opportunity to register their agreement or disagreement to this retraction. We have kept a record of any response received.

References

[1] P. Cui, "Prediction and Analysis of College Sports Test Scores Based on Computational Intelligence," *Journal of Sensors*, vol. 2022, Article ID 4070030, 10 pages, 2022.

Hindawi

Research Article

Prediction and Analysis of College Sports Test Scores Based on Computational Intelligence

Pengtao Cui (iD)

Shaoxing University Yuanpei College, Shaoxing, Zhejiang 312000, China

Correspondence should be addressed to Pengtao Cui; cuipt@usx.edu.cn

Nowadays, colleges and universities are paying more and more attention to the physical condition of students. Many schools set up physical education courses to exercise students and improve their physical quality. They also conduct physical examinations every semester to test students' conditions. In order to ensure more accurate sports results, this paper uses optimization of the neural group particle group model method to forecast the physical culture test scores of the investigated students. In addition, to guarantee accuracy the particle swarm optimization neural network model method, we compare the GXD method and the LM method with our method. It has the advantage of high precision, optimal prediction effect, strong versatility, higher recall rate, stronger antinoise performance, and wider application range. The article compares the neural network model method for particle swarm optimization with the GXD way and the LM way to ensure precision the neural network model method for particle swarm optimization.

1. Introduction

A raw good training technology based on a hybrid neural network has been trained and tested by the actual results of football match from the Italian A series. Finally, the results of the model are compared with other statistical prediction models. The results indicate that the new model is more accurate, so that the efficiency of all teams offers a better assessment [1]. By using the method of the document, logical analysis, and statistical data, the article analyzes and studies the 2012 ranking of tennis players who joined the 12th total game and predicts the distribution of tennis medals for the 12th total game [2]. We use video computer technology to build motion and analysis detection systems using RGB cameras and depth educational models. It can be identified from the RGB image, follow the overall assessment, and retour data in real time. RGB images are processed in two subsystems: human detection system and performance analysis system. The human detection system is used to detect a gesture with the user, and the performance analysis system is intended to return feedback from the details of the user gesture. The result of the system is satis-

factory: in a human detection system, overall accuracy can reach more than 99%, which means that nearly four activities can be accurately classified. In the case of performance analysis systems, the results and details can be returned based on small differences in levels CM. The delay of the entire system is in milliseconds, which means that the system can bet the detection and analysis of real-time. Golf driving is used as an example to illustrate how the system works. Moreover, the system can promote other sports [3] in the research to survey various physical characteristics of successful archery and provide main attributes that help the results of high archery. In this study, 32 arms from arches from different arched students participated. Perform standard physical fitness tests and note the last recording result, multivariate primary analysis techniques (PCA), layered agglomeration analysis, and discriminatory analysis (DA). VARIMAX-rotated PCA represents two variables with 12 and 2 variators (VF). Standard, backward, and forward stepwise reach classes from 14 predictors with 74.2%, 96.7%, and 93.6% accuracies, appropriately. The results of the current investigation can help in assigning arched athletes in accordance with their bodily characteristics [4].

Fast search and control over attitude changes; a method for designing a multimedia model is suggested. In the physical model and the kinematic model of the body, they quickly distinguish information about location and attitude information about the human body. Multimedia image analysis and intelligent control of the process that simulates the training of human traffic analyze the parameters of spatial traffic planning limits to achieve changes in attitude, which achieves optimal controls for sports training and sports planning. The simulation results show that the design based on the multimedia simulation of the computer is checked, and the error prediction of the traffic control parameters is low, and the ability to be the multimedia sport training model is stronger, and the effect of sports training has improved. In addition, simulation results will verify the efficiency of the internet [5]. Continuous development of computer and graphic technology, mode and image processing technology, and intelligent video tech techniques combine these related technologies and set image descriptions and supervision between images. Intelligent video analysis technology is widely used as in military and economic sectors. During the badminton training, when the trainer explains the behavior of the player, the video will be played and analyzed [6]. Machine learning (ML) is an intelligent approach to classification and prediction. This paper provides a detailed analysis of the M1 literature, focusing on the application of artificial neural networks (ANNs) in predicting traffic outcomes, as well as learning methods, data sources, appropriate model evaluation methods, and challenge-specific methods for predicting certain motion outcomes [7]. The main goal of this study is to build an intelligent mathematical model to predict the sports achievement of pole jumping in men; the method of the study consists of using five variables as the input to the neural network, which is the pathway of speed (m/sec in front distance 05 m closest and 05 m closest, maximum speed in the last 5 m total approach distance 30 m, conversion factor ratio of horizontal speed to vertical speed, conversion factor ratio of horizontal speed to vertical speed, and fist height at full pole long above); these are variables that are considered independent, while the correlated variables are the predictions that predict achievement (final height achieved by jumpers) as output. The neural network architecture is represented by three layers; the first layer is an input layer with five variables, and one layer is hidden and contains a node, while the last layer is an output layer representing the result of the prediction of athletic achievement male weight jumps [8]. The submission of recurrent neural networks (RNN) is learned in the prediction of sports outcomes of athletes in the Internet of Things (Internet of Things) environment. Specifically, the 3000 m slope enzymes and the corresponding outcomes of athletes were analyzed with RNN. Next model prediction of performance of athletes with 3000 M slope enzymes is determined by different algorithms, where IOT technology is used to predict and analyze the relationship between physical parameters and the efficiency of athletes [9]. Three algorithms of combined prediction of a gray model and neural network: GM-NN1: first, the original sports performance dataset is used to derive the error

sequence using the MG (1, 1) model, and then, to get error sequence prediction, build a neural network to train error sequence regression. This new model uses a neural network to correct the error predicted by the GM model (1, 1), GM-NN2: this model uses some datasets for original traffic performance to make a set of universal data models (1, 1) and build a nervous network. The original data define a nonlinear relationship between the adjustment values; the resulting network estimated prediction trends for a group of generic (1, 1) models on partial data and achieved better results in sports achievement prediction [10]. By analyzing the students' vital indices as measured by their weight, height, and waist, this paper uses principal component regression analysis to set up a linear model for predicting exercise outcomes at 50 and 800 meters. In this way, it assists students to improve exercise results during their daily exercise [11]. Using physical testing methods, research has shown that although slightly more than the 2011 test results, men and women experience very large differences in physical life shape, physical function, body mass, and overall assessment that should draw attention. According to the "IT Public Plan for Reform of teaching sports university," the corresponding countermeasures were implemented to improve, the Western University Sport Sports Plan Reform of the course was set up. In 2013, the "IT College Sports Club" was implemented to provide theoretical reference [12]. Contributing to be a literature by developing a regression model that offers football results, we use prediction accuracy measures and wagering simulations to evaluate model performance. The model developed may equal or exceed the results of existing statistical models with a similar structure. Taken together, these results suggest that public odds for multiple soccer matches invested are slightly less effective, but these low performance does not cause the revenue of the statistical gambling algorithm. The results also show that the results of the historic alliance are the most important components in the statistical model of football forecasts and completed the moderate accuracy of these components and other data [13]. Prediction accuracy of various methods such as prediction markets and selection evaluates the ability to systematically produce the market and subtitles to produce the profit on the game market. We have introduced empirical results of the 678-837 study of the German Premiere Association game. The forecast market and the chance of plants are also applied to predictive accuracy, but both methods are very complicated [14]. Machine leather algorithm are accustomed to build models to predict physical student performance. The particle group optimization algorithm is used to select model parameters. This model applies to modeling physical properties and forecasts of specific universities. Application results show that the machine's algorithm can eliminate the learning of the shortcomings of traditional models and improve the effect of prognosis in sports activities, and the predicted results can lead to reforms of university sports [15].

2. College Sports Test Scores

2.1. Current Situation of College Sports Test Scores. At present, the physical quality of students is declining year by year,

and the current exercise situation is not satisfactory: only 34.2% of the students exercise regularly, and most of the students do not exercise often, and their consciousness is weak. Boys perform better than girls on sports tests and, in different classes, have higher minimum scores than others. The intensity of exercise awareness, exercise time, and exercise frequency are not ideal and cannot produce good exercise effects. There are differences between male and female students and students of different grades. Because most students lack sports and choose to stay in dormitories most of the time, it can be seen from the results of college sports tests that most of the indicators are declining year by year, getting lower year by year.

The physical fitness of college students is declining year by year, and the current situation of physical exercise is also unsatisfactory. Only 34.2% of the students regularly participate in exercise, and most of the students rarely exercise, and they are not conscious of physical exercise. College students' physical exercise awareness intensity, exercise time, and exercise frequency are not ideal, and they cannot achieve good results of physical exercise. It can be seen from the results of college sports tests that most of the indicators are declining year by year, getting lower year by year.

2.2. Problems Existing in College Sports Testing. First of all, the evaluation of students' physical education performance largely relies on the evaluation of athletic ability, in order to systematically obtain sufficient information on students' personal physical fitness and learning achievements and to evaluate the degree of students' achievement of teaching goals. Physical education: there is no doubt that it is reasonable to use examinations as an important means of evaluating students' learning outcomes, but the problem is that the current examination form, content, and evaluation criteria are too monotonous and difficult to be comprehensive and accurate. Individual training subjects to measure: second, the understanding of the objectives of higher education physical education courses is not clear enough or incomplete; it only emphasizes the evaluation of explicit factors such as physical fitness, sports technology, and skills, while ignoring the coordinated development of hidden factors such as psychology and group relations, thus forming an evaluation process. Physical and mental separation, lack of awareness of the relationship between the purpose of diagnosis, and the purpose of physical education result in a certain degree of disconnection between the two. Third, theory and practice are the two most basic assessment elements to measure students' quality and performance. If only focus on practice and ignore theory in the process of talent training, only mechanical technology can be used to train robots. In quality education, special emphasis is placed on cultivating students' innovative ability. Talking about innovation without theoretical guidance can only be a slogan. Without mastering theoretical knowledge, students' development space will be limited. Participation in sports activities will inevitably lead to blindness and sometimes unnecessary physical and mental harm. Fourth, the purpose and function of the evaluation of students' academic performance are not clear, which leads to the use of summative evaluation as the main evaluation method for evaluating academic performance, which has obvious drawbacks.

2.3. The Benefits of Computational Intelligence in the Predictions of the Results of Sports Tests. So as to implement the policy of the comprehensive development of morality, intelligence, and physique in universities and universities, the Ministry of Education of the People's Republic of China has issued the "Qualification Standards for College Students' Sports" for colleges and universities across the country. Students' sports performance is mainly divided into body type indicators, physical indicators, and sports quality. Body size is directly related to athletic performance. How to use the body shape index to predict sports performance not only has certain guiding significance for the role of teachers and students in teaching and daily exercise but also allows students to choose the appropriate body shape according to their physical fitness. The current state of the art in predicting student athletic performance is analyzed, and the reasons for the low prediction accuracy of current models are identified. An intelligent support vector machine is used to establish a student's sports performance prediction model, and the intelligent model is used to apply the model to college sports performance, modeling, and predicting characters. The intelligent algorithm can overcome the shortcomings of traditional models and improve the effect of predicting sports results. And predictive outcomes may lead to college sports reform.

Current research states forecast that indicate the execution of students who indicate the causes of low accuracy of predicting the current model. Calculate the intelligent machine for the support vector to determine a model prediction of the sporting efficiency of students, using intelligent models. Finally, the model applies to college sports results, Modeling and class prediction. The intelligent algorithm can overcome the shortcomings of traditional models and improve the effects of predicting a college sport efficiency, and the results of the forecasts can carry out a reform of the university sports disciplines.

2.4. Optimization of College Sports Test Scores. First, performance assessment is a significant section of physical education systems engineering and is intently involved to the personal interests of the students. The content and standards of the test should be as objective as possible, students should be assessed academically, and the classroom test prepared by teachers should be combined with the unified test at the classroom level, one-time, and continuous. Class exams, teaching, and exam drills by exam panels of teachers (classrooms) and classroom teachers who do not take class exams. Second, after the special courses are launched, the widely collected high-quality textbooks can be combined with the national physical exercise standard test. Among many projects of the same quality, several textbooks with lower technical requirements should be selected for use. The balance of textbooks, hours, and test standards is based on mathematical statistics, the correct selection of test standards, and the average score of qualitative categories dropped by 1 point to 50 points, which is in line with the

national sports activities standard scoring method. For a small number of students with special difficulties in physical and physiological conditions, the relative performance assessment method should be used to evaluate their performance. The fourth is to strengthen the research on teaching methods and further improve the quality of education. The use of intelligent algorithms can conquer the defect of traditional models and improve the predictive effect of physical education outcomes in colleges and universities, and the prediction results can drive the reform of college sports disciplines.

3. Computational Intelligence Prediction Model for College Sports Test Scores

3.1. Neural Network Model for Particle Swarm Optimization

3.1.1. Neural Networks. The neural network is a multilayer feed-forward network, and one-way propagation generally falls on three or more layers. Here are the steps on how a neural network works:

In the first step, set a random nonzero number; its Vkl is relatively small, and set the weight coefficient of each layer to its range.

In the second step, the output sample is

$$A = (a_1, a_2 \cdots, a_m). \tag{1}$$

The corresponding expected output is

$$E = (e_1, e_2, \cdots, e_m). \tag{2}$$

The third step is to calculate the output of each layer and the kth neuron output in the hth layer as follows:

$$G_k^h = \sum V_{kl} A_k^{h-1}, \tag{3}$$

$$A_k^h = s\left(G_k^h\right). \tag{4}$$

Usually, Equations (3) and (4) will be represented by the Sigmoid function, as follows:

$$s(a) = \frac{1}{(1 - \exp(-a))}. \tag{5}$$

The fourth step is to evaluate the learning error d of each layer, in the output layer $h = n$,

$$f_k^n = A_k^n (1 - A_k^n)(A_k^n - E_k^n). \tag{6}$$

The other remaining layers exist:

$$f_k^h = A_k^h \left(1 - A_l^h\right) \sum V_k f_k^{h+1}. \tag{7}$$

The fifth step is to change the weight factor Vkl, as follows:

$$V_{kl}(p + 1) = V_{kl} - q \cdot f_k^h \cdot A_l^{h-1}. \tag{8}$$

The sixth step is to determine if the calculated weight is coefficients of each tier can meet the request. If the requirements can be met, the calculations can be ended.

(1) Set a random nonzero number whose V_{kl} is relatively small, and set the weight coefficient of each layer to its range

(2) Output samples and corresponding expectations

(3) Calculate the output of each layer, and the output of the kth neuron in the h layer

(4) Evaluate the learning error d of each layer, and output each layer

(5) Correct the weight coefficient V_{kl}

(6) Define if the calculated weighting factors for each level meet the request. If the requirements can be met, the calculations can be aborted. Else, go back to step 3

3.1.2. Particle Swarm Optimization Method. The best answer for the current particle group optimization is gbestos, and the best explanation for the present group is gbestos. The fit performance depicting the advantages and disadvantages of a single particle is structured as follows:

$$\text{fitness} = \frac{1}{2N} \sum_{i=1}^{N} \sum_{j=1}^{D} \left(y_{ij} - t_{ij}\right)^2. \tag{9}$$

The primary random explanation of the particle swarm majorization way repeatedly iterates to discovery the optimal answer, and the particle follows two extreme worth in each iteration to guarantee that the particle itself can be renewed. The two extreme worth are t_{Best} and u_{Best} separately, the best explanation found by the particle itself is t_{Best}, and the optimal solution found by the whole population is u_{Best}. The particle location and velocity are updated by these two extreme worth using Equations (10) and (11). ω represents the speed of the particle; present represents the position of the particle itself; x_1 and x_2 represent the learning factor; y_1 and y_2 represent a random number between (0, 1).

$$\omega = \omega + x_1 \times y_1 \times (t_{\text{Best}} - \text{present}) + x_2 \times y_2 \times (u_{\text{Best}} - \text{present}), \tag{10}$$

$$\text{present} = \text{present} + \omega. \tag{11}$$

The first particle on the right edge of the velocity Equation (10) has no memory capacity and is random. It will search for a new region and has a powerful global majorization ability. But, in functional claims, it is essential to perform an entire finding to enhance the rate of search astringent and then use local search to obtain a more precise solution. σ represents the inertia weight. The larger the value of σ, the stronger the global search ability of the particle swarm optimization method, and vice versa.

The larger the worth of σ, the stronger the entire find power of the particle swarm optimization method; the lower the worth of σ, the weaker the entire find power of particle swarm optimization method.

$$\omega = \sigma \times \omega + x_1 \times y_1 \times (t_{\text{Best}} - \text{present}) + x_2 \times y_2 \times (u_{\text{Best}} - \text{present}), \tag{12}$$

$$\text{present} = \text{present} + \omega. \tag{13}$$

Advantage:

(1) It can deal with some traditional methods that cannot be dealt with

Shortcoming:

(1) Not very good on some points

(2) Coding network weights and selecting genetic operators are sometimes difficult

3.1.3. Correct the Variance and Weight of the Web. When optimizing a neural network with particle swarm optimization methods, optimization is necessary in two parameters, variance σ_i ($i = 1, 2, \cdots, h$) of neural network basis function and the weight $V_0, V_1, \cdots, V_K$, and the dimensions of the two parameters are the same as the network structure. Correlation, uniformly encode the weights and variances of the neural network, and a set of the weights and variation of neural networks are depicted by the particle. Taking the root mean square error as the fitness function, it can reflect the approximation error of the particle. a is the overall count of specimens; y_1^i and y_2^i are actual produced worth and the nervous net forecast value, respectively. The healthy worth of the particle is as follows:

$$\text{RMSE}(i) = \sqrt{\frac{1}{a} \sum_{j=1}^{a} (y_1^i - y_2^i)^2}. \tag{14}$$

3.2. Prediction Model of Sports Achievements of the University. Modeling of university sports results with nervous net model for particle swarm optimization. Optimization of neural network models using a swarm of particles for modeling of sports performance in colleges and universities, assuming that the initial performance time series is as follows:

$$A^{(0)}(p) = \left\{ a^{(0)}(1), a^{(0)}(2), \cdots, a^{(0)}(m) \right\}, \tag{15}$$

$$B^{(0)}(p) = \left\{ b^{(0)}(1), b^{(0)}(2), \cdots, b^{(0)}(m) \right\}. \tag{16}$$

Taking the first-order differential operation formula (14), formula (17) is obtained as the first-order differential sequence:

$$A^{(1)}(p) = \left\{ a^{(1)}(1), a^{(1)}(2), \cdots, a^{(1)}(m) \right\}. \tag{17}$$

Table 1: Prediction results of college students' sports performance.

Iterations/time	Prediction error	Convergence time (s)
100	0.032	4.2
200	0.039	2.9
300	0.042	5.1
400	0.049	5.6
500	0.053	6
600	0.056	6.2
700	0.061	6.7
800	0.063	7.1
900	0.069	7.8
1000	0.072	8.1

In the first-order mean surgery formula (16), the first-order mean sequence is obtained as

$$B^{(1)}(p) = \left\{ b^{(1)}(1), b^{(1)}(2), \cdots, b^{(1)}(m) \right\}. \tag{18}$$

The prediction model is established by formula (6), c and parameters, such as

$$\frac{f a^{(1)}}{f p} = c a^1 = \lambda. \tag{19}$$

Solving Equation (19), the albino differential equation predicting sports results colleges and universities is obtained, such as

$$\widehat{a}^1(h + 1) = \left(a^{(0)}(1) - \frac{\lambda}{c} \right) d^{-ch} + \frac{\lambda}{c} (h = 1, 2, 3, \cdots, m). \tag{20}$$

Using the neural network description formula (20), the nervous net parameters are gained by practice in the light of the key in and produce specimen data, and the best target shining upon the formula (20) is blanket.

4. Prediction and Analysis of College Sports Test Scores Based on Computational Intelligence

Taking the 1000-meter long-distance running performance of 50 freshmen in a university as the experimental object, after many calculations and analysis, the data truly reflects the students' sports trends. The neural network used in this method has 3 input nodes, 1 output node, and 10 hidden units. The population of the particle swarm optimization method is $m = 40$, the initial inertial mass value is 1, and the inertial mass is reduced to 0.5. The number of iterations gradually increases the values of af, $x1$, and $x2$ which are all equal to 3, and [-19.19] is the link weight change interval. The iteration stops when the number of iterations reaches the maximum value.

4.1. This Paper Method. A neural network model was used to optimize the particle swarm to predict the performance of
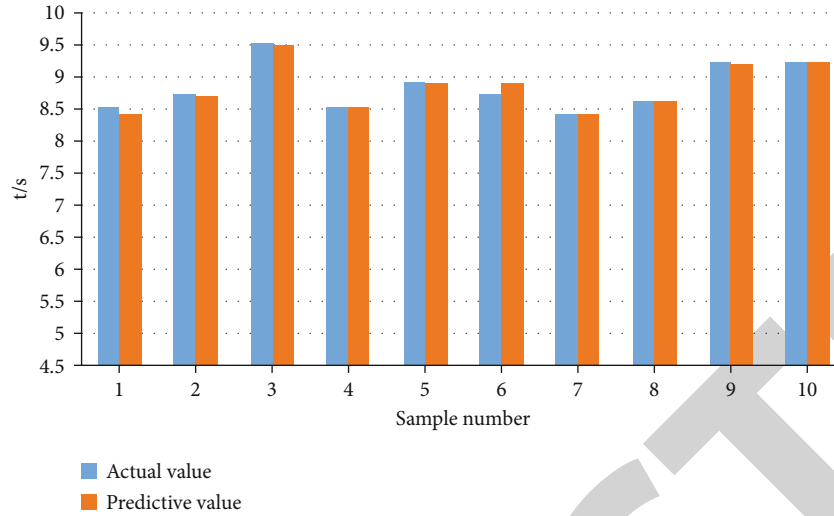
Figure 1: Comparison of predicted and actual results.

the subjects' movement. When the frequency of iterations is 100, the prediction mistake is the least, the prediction error is 0.032, and the convergence time is 4.2 s; when the frequency of iterations is 1000, the forecast error is the largest, the forecast error is 0.032, and the convergence time is 8.1 s. When the frequency of iterations is 200, the forecast error is 0.039, and the convergence time is 2.9 s; when the frequency of iterations is 300, the forecast error is 0.042, and the convergence time is 5.1 s; when the frequency of iterations is 400, the forecast error is 0.049, and the convergence time is 5.6 s; when the frequency r of iterations is 500, the forecast error is 0.053, and the convergence time is 6 s; when the iteration frequency is 600, the forecast error is 0.056, and the convergence time is 6.2 s; when the iteration frequency is 700, the forecast error is 0.061, and the convergence time is 6.7 s; when the frequency of iterations is 800, the forecast error is 0.063, and the convergence time is 7.1 s; when the frequency of iterations is 900, the forecast error is 0.069, and the convergence time is 7.8 s, as shown in Table 1.

10 students were randomly selected from the experimental subjects, and the particle swarm majorization nervous net method was formed to test comparison between the forecasted results and the actual values. There is no significant difference between the forecasted results obtained by this model and the actual values that are approximately equal. Actual value of sample 1 is 8.5 s, and the forecasted value is 8.4 s; the actual value of sample 2 is 8.7 s, and the predicted value is 8.68 s; the actual value of sample 3 is 8.5 s, and the predicted value is 8.49 s; the actual value of sample 4 is 8.49 s. The actual value of sample 5 is 8.9 s, and the predicted value is 8.88 s; the actual value of sample 6 is 8.7 s, and the predicted value is 8.89 s; the actual value of sample 7 is 8.4 s, and the predicted value is 8.89 s. The actual value of sample 8 is 8.6 s, and the predicted value is 8.6 s; the actual value of sample 9 is 9.2 s, and the predicted value is 9.19 s; the actual value of sample 10 is 9.2 s, and the predicted value is 9.2 s, as shown in Figure 1.

Table 2: Prediction results of college students' sports performance.

Iterations/time	Prediction error	Convergence time (s)
100	0.037	10.3
200	0.041	10.7
300	0.046	11.2
400	0.053	11.9
500	0.056	12.5
600	0.059	13.1
700	0.064	14.5
800	0.066	15.3
900	0.073	16.2
1000	0.078	17.6

4.2. GDX Method. Using the GDX method to predict the sports performance of the experimental subjects, when the frequency of iterations is 100, the forecast error is the smallest, the forecast error is 0.037, and the convergence time is 10.3 s; when the frequency of iterations is 1000, the forecast error is the largest, and the forecast error is 0.078, the convergence time is 17.6 s. When the frequency of iterations is 200, the forecast error is 0.041, and the convergence time is 10.7 s; when the frequency of iterations is 300, the forecast error is 0.046, and the convergence time is 11.2 s; when the frequency of iterations is 400, the forecast error is 0.053, and the convergence time is 11.9 s; when the frequency of iterations is 500, the forecast error is 0.056, and the convergence time is 12.5 s; when the frequency of iterations is 600, the forecast error is 0.059, and the convergence time is 13.1 s; when the frequency of iterations is 700 and when the frequency of iterations is 800, the forecast error is 0.066, and the convergence time is 15.3 s; when the frequency of iterations is 900, the forecast error is 0.073, and the convergence time is 16.2 s, as shown in Table 2.

10 students were randomly selected from the experimental subjects, and the GDX method was used to test the
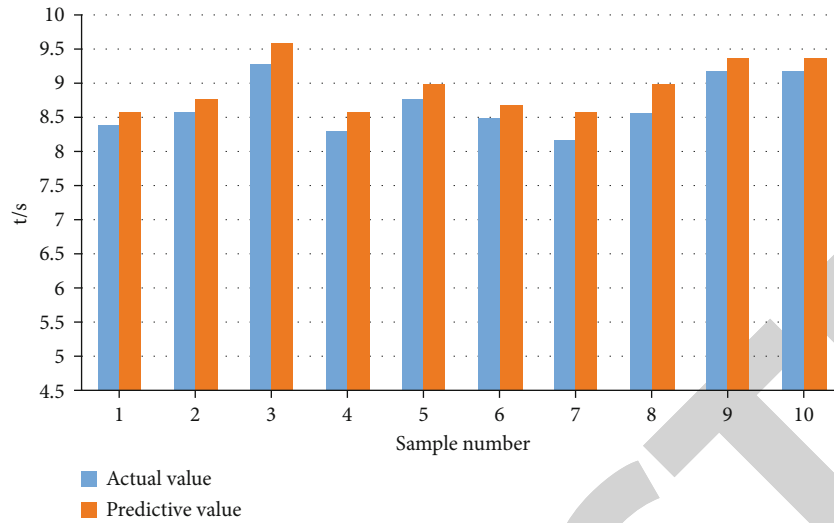
Figure 2: Comparison of predicted and actual results.

comparison between the forecasted results and the actual values. There is a significant difference between the forecasted results obtained by this model and the actual values. The actual value of sample 1 is 8.4 s, and the predicted value is 8.6 s; the actual value of sample 2 is 8.6 s, and the predicted value is 8.8 s; the actual value of sample 3 is 9.3 s, and the predicted value is 9.6 s; the actual value of sample 4 is 9.6 s. The actual value of sample 5 is 8.8 s, and the predicted value is 9.0 s; the actual value of sample 6 is 8.5 s, and the predicted value is 8.7 s; the actual value of sample 7 is 8.2 s, and the predicted value is 8.7 s. The actual value of sample 8 is 8.58 s, and the predicted value is 9.0 s; the actual value of sample 9 is 9.2 s, and the predicted value is 9.4 s; the actual value of sample 10 is 9.2 s, and the predicted value is 9.4 s, as shown in Figure 2

4.3. LM Method. The LM method is used to predict the sports performance of the experimental subjects. When the frequency of iterations is 100, the forecast error is the smallest, the forecast error is 0.043, and the convergence time is 15.3 s; when the frequency of iterations is 1000, the forecast error is the largest, and the forecast error is 0.087, and the convergence time is 24.5 s. When the frequency of iterations is 200, the forecast error is 0.047, and the convergence time is 16.5 s; when the frequency of iterations is 300, the forecast error is 0.056, and the convergence time is 17.2 s; when the frequency of iterations is 400, the forecast error is 0.059, and the convergence time is 18.9 s; when the frequency of iterations is 500, the forecast error is 0.067, and the convergence time is 19.2 s; when the frequency of iterations is 600, the forecast error is 0.071, and the convergence time is 20.2 s; when the frequency of iterations is 700 and when the frequency of iterations is 800, the forecast error is 0.079, and the convergence time is 22.2 s; when the frequency of iterations is 900, the forecast error is 0.082, and the convergence time is 23.6 s, as shown in Table 3.

10 students were randomly selected from the experimental subjects, and the LM method was used to test the comparison between the forecasted results and the actual

Table 3: Prediction results of college students' sports performance.

Iterations/time	Prediction error	Convergence time (s)
100	0.043	15.3
200	0.047	16.5
300	0.056	17.2
400	0.059	18.9
500	0.067	19.2
600	0.071	20.2
700	0.076	21.8
800	0.079	22.2
900	0.082	23.6
1000	0.087	24.5

values. There is a significant difference between the forecasted results obtained by this model and the actual values. The actual value of sample 1 is 8.5 s, and the predicted value is 8.2 s; the actual value of sample 2 is 8.6 s, and the predicted value is 8.5 s; the actual value of sample 3 is 9.4 s, and the predicted value is 9.2 s; the actual value of sample 4 is 9.2 s and 8.5 s, and the predicted value is 8.3 s; the actual value of sample 5 is 8.9 s, and the predicted value is 8.5 s; the actual value of sample 6 is 8.6 s, and the predicted value is 8.4 s; the actual value of sample 7 is 8.4 s, and the predicted value is 8.4 s. The actual value of sample 8 is 8.7 s, and the predicted value is 8.5 s; the actual value of sample 9 is 9.2 s, and the predicted value is 9.1 s; the actual value of sample 10 is 9.2 s, and the predicted value is 9.2 s, as shown in Figure 3.

4.4. Comparison of This Method with GDX Method and LM Method. After comparing the prediction effect of the method in this paper with the GDX method and the LM method, it is necessary to verify the generality of predicting students' sports performance. These three methods are used to predict the average sports performance of 200 m sprint, 400 m sprint, 800 m sprint, long jump, high jump, and shot put.
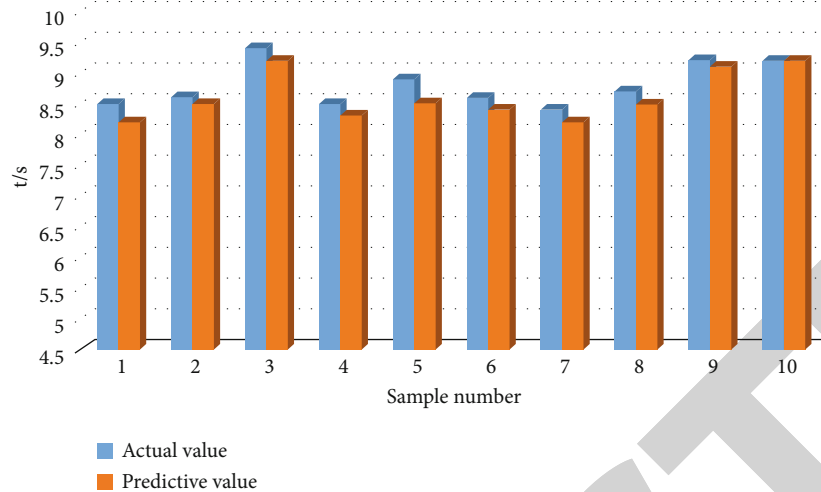
Figure 3: Comparison of predicted and actual results.
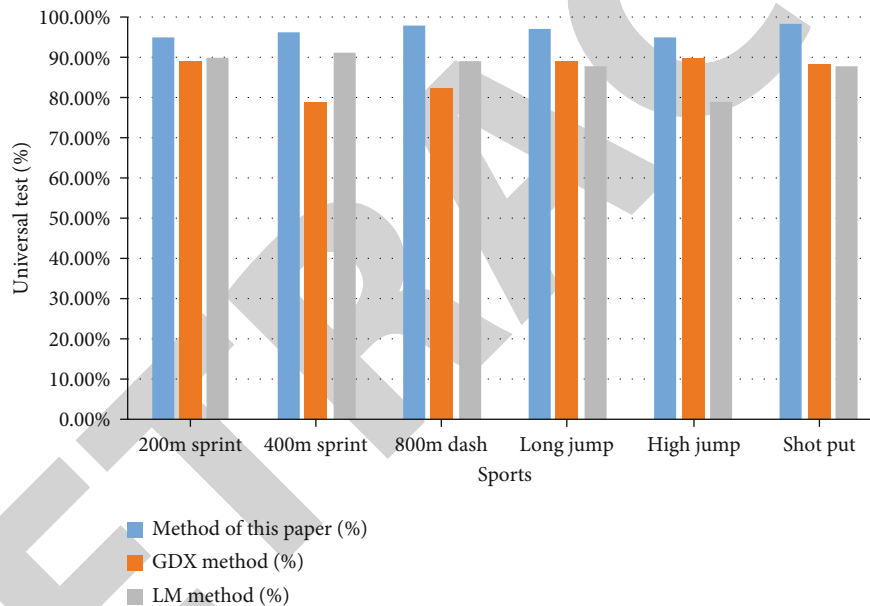
Figure 4: Universal test of college students' sports performance prediction.

Score prediction accuracy: looking at the figure below, you can see that the generality test of the method in this paper ranks first in sports, and the generality test results are above 95%. In the 200 m sprint, the generality test result of the method in this paper is 95.32%, the generality test result of the GDX method is 89.23%, and the generality test result of the LM method is 90.15%; the generality test result of GDX method is 78.99%, and the generality test result of LM method is 91.28%; in the 800 m long-distance running, the generality test result of this method is 98.36%, the generality test result of GDX method is 82.59%, and the generality test result of LM method is 98.36%. The result is 89.47%; in the long jump, the method generality test score in this document is 97.25%, and the method generality test score is 89.17%, and the generality test result of the LM method is 88.13%; in high school, the generality test result of the

method in this paper is 95.36%, the generality test result of GDX method is 90.10%, and the generality test result of LM method is 79.18%; in shot put, the generality test result of this method is 98.75%, the generality test result of GDX method is 88.28%, and the generality test result of LM method is 95.36%. The sex test result was 88.19%, as shown in Figure 4.

As can be seen from the figure below, the particle swarm optimization nervous net method used in this paper has the highest recall rate, with a recall rate of 98.50%; the LM method has the lowest recall rate, with a recall rate of 92.3%; the GDX method has the highest recall rate. The completion rate ranks second with a recall rate of 94.60%, as shown in Figure 5.

So, to verify the antinoise effectiveness of the suggested way in predicting students' athletic performance, interference
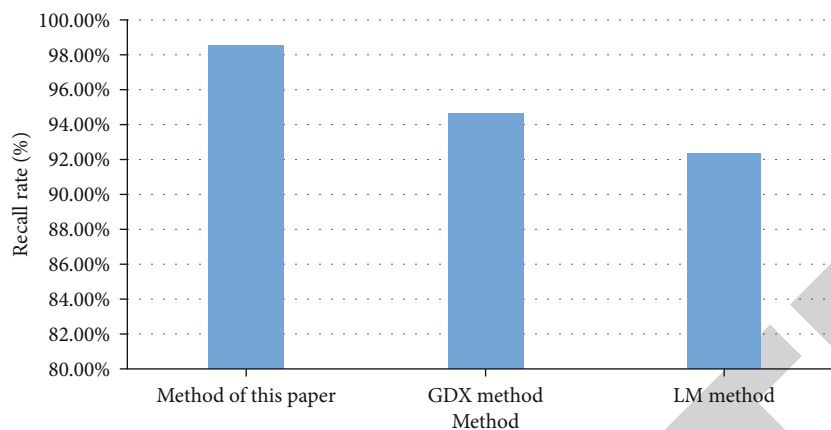
Figure 5: Comparison of the recall rate of college students' sports scores.

Table 4: SNR output results of different methods.

Method Number of iterations	This paper method/Db		GDX method/Db		LM method/dB	
	10	20	10	20	10	20
10	5.87	8.95	4.26	7.59	4.15	7.28
20	6.95	9.14	5.48	8.14	5.68	8.14
30	7.59	10.58	6.86	9.25	6.47	9.26
40	8.65	11.67	7.24	10.35	7.59	10.47
50	9.66	12.69	8.16	11.27	8.26	11.54
60	10.87	13.48	9.24	12.64	9.47	12.67
70	11.58	14.47	10.48	13.47	10.59	13.54
80	12.98	15.21	11.27	14.67	11.68	14.13
90	13.88	16.47	12.68	15.47	12.64	15.72
100	14.69	17.68	13.54	16.79	13.59	16.93
Average value	10.27	13.03	8.92	11.96	9.01	11.96

was added to the collected students' athletic show. In the 10th and 20th times of the method in this paper, the signal-to-noise ratio output of the method is higher than the other two methods; the signal-to-noise ratio output results are 10.27 dB and 13.03 dB, respectively. The 20th time SNR output results are 8.92 dB and 11.96 dB, respectively; the 10th and 20th time SNR output results of the LM method are 9.01 dB and 11.96 dB, respectively, as shown in Table 4.

The utility of the sports show forecast method is evaluated by testing the performance of the three methods. The paper is mostly better than the performance of the other two methods in all aspects. In terms of convergence speed, the convergence speed of the method in this paper is fast, the speed of GDX method is medium, and the speed of LM method is slow; in terms of model structure, the structure of this method is simple, the structure of GDX method is medium, and the structure of LM method is medium; in terms of antinoise strength, the strength of the method in this paper is strong, the strength of the GDX method is medium, and the strength of the LM method is medium; in terms of data requirements, the requirements of the method in this paper are medium, the requirements of the GDX method are strong, and the requirements of the LM

Table 5: Integrity performance comparison of different methods.

Performance	Method of this paper	GDX method	LM method
Convergence speed	Quick	Medium	Slow
Model structure	Simple	Medium	Medium
Antinoise strength	Powerful	Medium	Medium
Data request	Medium	High	High
Prediction accuracy	High	Low	Low
Scope of use	Wide	Medium	Medium
Prospects	Big	Medium	Medium

method are strong; in terms of accuracy, the method in this paper is strong, the GDX method is low, and LM method is low; in terms of scope, the method in this article is wider, the GDX method is medium, and the LM method is medium; in terms of development prospects, the method in this paper is large, and the GDX method is medium and is moderate, and the LM method is moderate, as shown in Table 5.

Hindawi

Retraction

Retracted: Effects of Different Soil Modifiers on Salt Improvement and Distribution, Crop Growth of the Gully Land Consolidation on Loess Plateau

Journal of Sensors

This article has been retracted by Hindawi following an investigation undertaken by the publisher [1]. This investigation has uncovered evidence of one or more of the following indicators of systematic manipulation of the publication process:

(1) Discrepancies in scope

(2) Discrepancies in the description of the research reported

(3) Discrepancies between the availability of data and the research described

(4) Inappropriate citations

(5) Incoherent, meaningless and/or irrelevant content included in the article

(6) Manipulated or compromised peer review

The presence of these indicators undermines our confidence in the integrity of the article's content and we cannot, therefore, vouch for its reliability. Please note that this notice is intended solely to alert readers that the content of this article is unreliable. We have not investigated whether authors were aware of or involved in the systematic manipulation of the publication process.

Wiley and Hindawi regrets that the usual quality checks did not identify these issues before publication and have since put additional measures in place to safeguard research integrity.

We wish to credit our own Research Integrity and Research Publishing teams and anonymous and named external researchers and research integrity experts for contributing to this investigation.

The corresponding author, as the representative of all authors, has been given the opportunity to register their agreement or disagreement to this retraction. We have kept a record of any response received.

References

[1] Y. Yang, B. Zhou, and L. Feng, "Effects of Different Soil Modifiers on Salt Improvement and Distribution, Crop Growth of the Gully Land Consolidation on Loess Plateau," *Journal of Sensors*, vol. 2022, Article ID 5282344, 17 pages, 2022.

Research Article

Effects of Different Soil Modifiers on Salt Improvement and Distribution, Crop Growth of the Gully Land Consolidation on Loess Plateau

Yang Yang [ID],[1] Beibei Zhou [ID],[1] and Lei Feng [ID][2]

[1]*State Key Laboratory of Eco-Hydraulics in Northwest Arid Region of China, Xi'an University of Technology, Xi'an 710048, China*
[2]*Zhongnan Engineering Corporation, Changsha 410014, China*

Correspondence should be addressed to Beibei Zhou; 1180411049@stu.xaut.edu.cn

Due to the strong evaporation and leakage loss, secondary saline-alkali was the main problem in the watershed of gully land consolidation on Loess Plateau. Through field farming experiments, five modifiers (maize stalk (MS), humus acid (HA), Yan Ke (YK), He Kang (HK), and nanobiochar (NB)) were studied to investigate the effects of these soil modifiers on soil water and salt distribution, leaf photosynthetic characteristics, and maize growth and yields, as well as economic benefits in secondary saline-alkali soils of gully land consolidation watershed on Loess Plateau in 2019 and 2020. The results showed that soil modifiers could increase the water-holding capacity of the soil, reduce the salt content of the soil profiles, and decompose the accumulation of salt. The maximum desalination rate obtained in 2019 and 2020 increased, respectively, by 71.57% and 46.02%, compared to that in the control treatment. Soil modifiers could increase the net photosynthetic rate (Pn), transpiration rate (Tr), stomatal conductance (Gs), and decreased the intercellular CO_2 concentration (Ci). The output increased by 13.63%-31.84%, and revenue increased by 6.48%-38.01%. According to analyzing the production of soil modifier application, we found that the highest net profit was achieved when HK application rate was 52.4 kg/ha. Therefore, this study suggested that 52.4 kg/ha might be recommended as an appropriate soil modifier application strategy to deal with crop growth and improve economic benefit in secondary saline-alkali soils of Northwest China.

1. Introduction

Land degradation caused by irrational human activities has seriously threatened the sustainability development of world agriculture [1–3]. According to statistics, 65% of the world's land has been degraded, and secondary saline-alkali is a major manifestation of soil degradation [4]. In the early 20th century, due to the large-scale returning farmland to forest, the area of cultivated land decreased in some areas of the Loess Plateau [5, 6]. In order to control the decrease of cultivated land area, gully land consolidation area construction was conducted in the Loess Plateau basin [7]. Though such construction measurement effectively increased local cultivated land area, some problems such as secondary saline-alkali occurred with strong evaporation, leakage loss, and high salt contents in underground water with low

groundwater level [8]. Secondary saline-alkali has become one of the serious obstacle to crop growth and yield in this area.

Hydraulic engineering was adopted initially by many researchers, but the construction cost was high. During the construction period, crop farming will be affected as well [9–11]. Biological improvement methods are beneficial for crops that are resistant to disease, salt, insect pests, and drought but improper use may bring about harm to biodiversity. Thus, there is still a long way to before we safely used those biological methods [12–14]. Physical improvement methods mainly include isolation layer salt control, straw covering, irrigation leaching, drainage leaching, irrigation, and drainage combined leaching [15, 16]. The isolation layer and straw mulch are mainly used to reduce surface temperature and cut off the contact surface between the soil surface
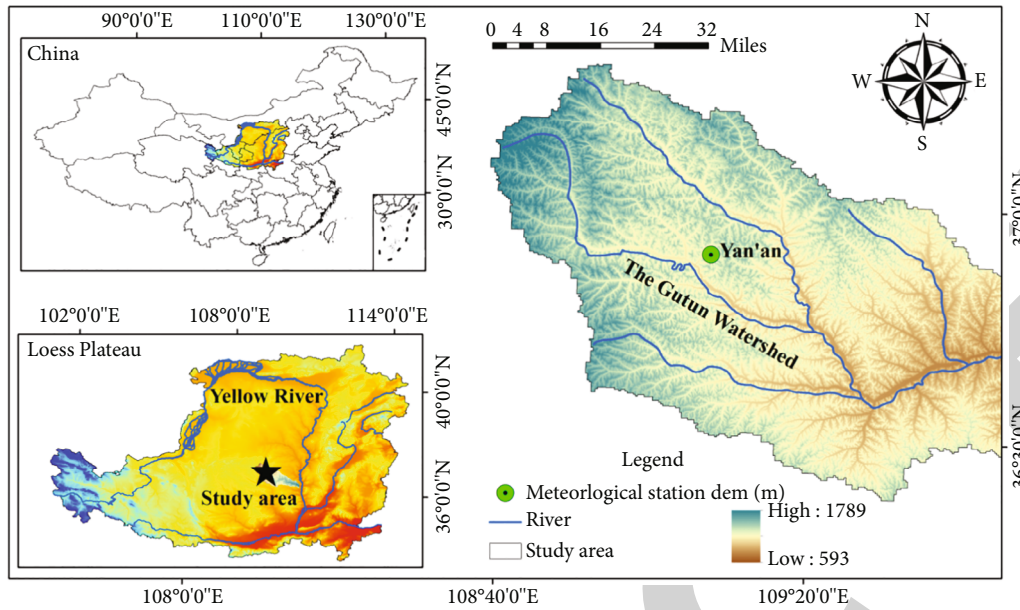
Figure 1: Location of research site.

and air, thus slowing down phreatic water evaporation, reducing the upward accumulation of salt, and inhibiting the accumulation of salt surface [17, 18].

Chemical improvement method is also an effective way in improving soil structure, promoting salt leaching, and adjusting soil pH. Nanocarbon has a good effect on improving saline-alkali soil and promoting crop growth and development [19, 20]. Humus acid (HA) can regulate soil, effectively improve soil structure, increase soil organic matter, reduce soil salinity, promote crop growth, and increase crop yield [21–23]. Yan Ke (YK) has the ability of ion exchange property, which can effectively reduce the concentration of exchangeable sodium and other salt ions in the soil, improve the physical and chemical properties of the soil, improve the nutrient absorption environment of crops, and regulate the soil pH. HK can reduce the toxicity and osmotic pressure caused by salt molecules by combining organic macromolecules with salt ions in the soil, improve the physical and chemical properties of the soil, increase water and nutrients, and improve the drought-resistant ability of crops [24–26]. These methods can improve saline-alkali soil conditions and are more effective than traditional ones. Some things to note are that the test results of these studies are only obtained through laboratory experiments and soil column simulated experiments. However, the research of soil modifiers under field conditions is still not system experiments. In consequence, we assume that adding soil modifiers into the secondary saline-alkali soils can improve the formation of soil water and salt distribution, stimulate crop growth and crop yields, and enhance economic benefit under field conditions. Therefore, in the past two years from 2019 to 2020, we conducted a consecutive field experiment in the Loess Plateau region.

This article carries out systematic research on the effectiveness of 5 currently rapidly developed soil modifiers

(MS, HA, YK, HK, and NB) in improving the fertility of secondary saline-alkali soil and promoting the growth of typical crops and thus expects to provide implications to the improvement of secondary saline-alkali soil and of the growth of crops.

2. Materials and Methods

2.1. Introduction to Research Site. Field experiments were conducted during the maize (Xianyu 1483) growing seasons in May to October in 2019 and 2020. The station (latitude $36°45'16''$–$36°50'24''$N, longitude $109°46'18''$–$109°51'05''$ E) is located in Ganguyi Town, Yan'an City, Shaanxi Province, China. The basin is located in the middle temperate semiarid region with a total length of 12.5 km and an area of about 2435 km^2 (see Figure 1). The annual average temperature was 10.3°C. The maximum and minimum temperature are -17.4°C and 30.3°C. The annual mean precipitation is 4947 mm [8]. The rainfall in 2019 and 2020 is concentrated from June to October (Figure 2), and the rainfall in 2019 and 2020 growing seasons is 4060 mm and 5146 mm, respectively. The average daily temperature in the growing season (May-October) in 2019 and 2020 was 25.2°C and 24.1°C, respectively (Figure 2). The soil types in the basin include black loess, red soil, and loessal. The soil in the experiment fields belonged to sandy soil. The basic physical and chemical properties in the initial soil profile are shown in Table 1.

2.2. Experimental Materials. The tested maize variety was Xianyu 1483 and can be cropped on sandy soil and suitable local cultivation. The tested He Kang soil modifier (HK) was a crop nutrition type (formulation-type medium) with a density of 1.1 g/cm^3-1.2 g/cm^3 and a pH of 2.0-3.0. The tested maize stalk (MS) was local straw, which was dried
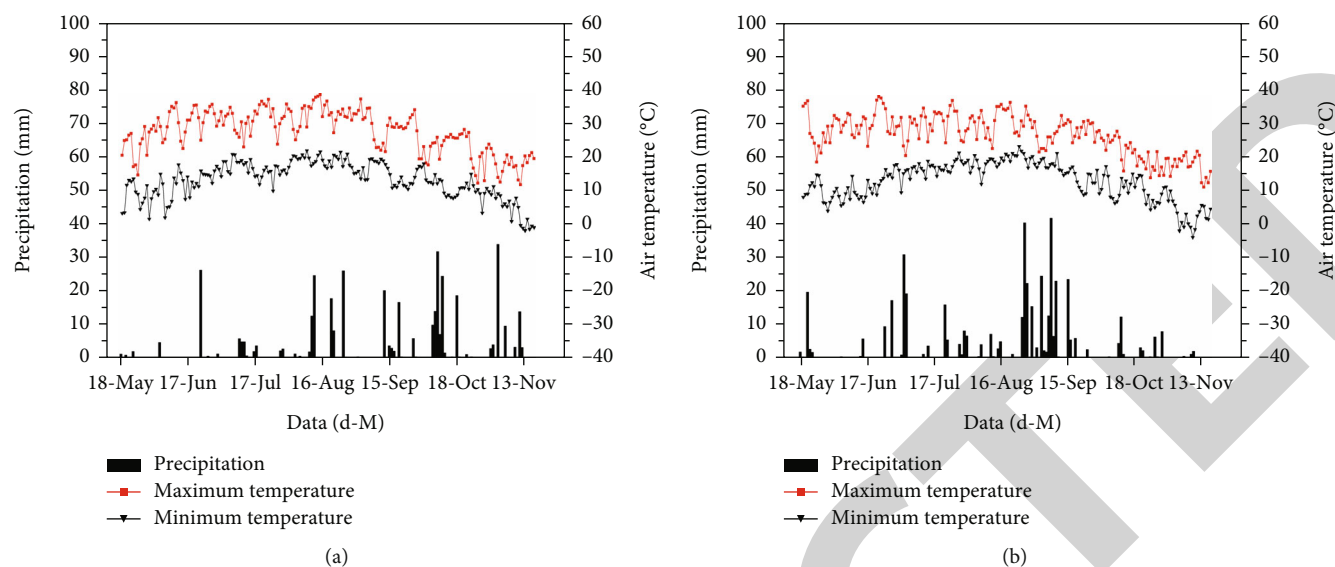
Figure 2: Distribution of precipitation and mean air temperature at the studied area during the maize growing seasons of (a) 2019 and (b) 2020.

and broken into pieces of about 2 mm. The humus acid (HA) soil modifier was from Shaanxi Meike Biotechnology Co., Ltd., $K_2O \geq 8.0$, humus acid $\geq 55\%$, and fulvic acid ≥ 37 %. Yan Ke (YK) soil modifier is from Shaanxi Meike Biotechnology Co., Ltd., and soluble organic carbon $\geq 45\%$, $(N + P_2O_5 + K_2O) \geq 40\%$. Nanobiochar (NB) is a black powder. The prepared nanobiochar has a pH of 9.6, a volume density of $0.38\,g/cm^3$, and a diameter of 40 nm. The tested compound fertilizer was "Meffro," with the total nutrient $(N + P_2O_5 + K_2O) \geq 40\%$.

2.3. Experiment Treatment. The experimental plot was the local agricultural land. The maize was sown between May 4 and 6 and then harvested on October 9 and 1, in 2019 and 2020, respectively. Maize seed density was 56700 crops/ha^{-1}, with a row spacing of 50 cm and between the crop pacing of 25 cm. In the experimental design, five different soil modifier contents (52.4 kg/ha (HK), 48.4 kg/ha (MS), 11.3 kg/ha (HA), 86.1 kg/ha (NB), and 45.0 kg/ha (YK)) were mixed well with 0-20 cm surface soil and then applied into the soil layer.

Plots without soil modifier adding were used as controls (CK). Each plot had 3 replicates and 18 experimental plots. Before sowing, 0.864 kg phosphate fertilizer (P_2O_5), 1.558 kg nitrogen fertilizer (N), and 0.854 kg potassium fertilizer (K_2O) were evenly applied in experimental plots. Irrigate the plots before maize sown.

2.4. Experimental Project and Methods

2.4.1. Determination Method of Soil Water Content, Salt Content, Available Nutrients, and Leaf Photosynthetic Characteristics. Five points of each plot in different growth stages (seedling stage, shooting stage, tasselling stage, filling stage, and maturation stage) of maize were sampled in a "S" sampling method, and soil samples of 0-2, 2-4,

4-6, 6-8, 8-10, 10-15, 15-20, 20-25, 25-30, 30-35, and 35-40 cm soil layers were collected by soil drill in layers and placed in sampling bags in layers for testing. Soil particle composition was measured by mastersizer-2000 laser particle size analyzer. Soil water content in different soil layers at different growth stages was randomly measured by Watchdog moisture sensor. The leaves, stems, and roots from maize were also randomly measured at the same growth stages (seedling stage, shooting stage, tasselling stage, filling stage, and maturation stage). At the different farmland soil profile depths, the soil moisture content was determined by the Trime-pico32 TDR soil moisture sensor. The salt content of the different farmland soil profiles was measured by DDSJ-308 conductivity instrument. At filling stage, maize plant of three in each plot was chosen and the maize leaf photosynthetic characteristics were measured on sunshine day at 10 AM. The net photosynthetic rate (Pn), transpiration rate (Tr), stomatal conductance (Gs), and intercellular CO_2 concentration (Ci) were determined by the CIRAS-3 portable photosynthetic measurement system.

2.4.2. Crop Height, Stem Diameter, Leaf Area, and Yield. At different maize growth stages (seedling stage, shooting stage, tasselling stage, filling stage, and maturation stage), three representative maize crops were randomly selected from each plot in 2019 and 2020. The crop height and stem diameter of the maize were measured by ruler and caliper, and the yield was weighed by scale with the precision of 0.01 g.

2.5. Data Processing and Analysis

2.5.1. Soil Salt Content Analysis. Given a stable salt composition, the level of soil salt content (SSC) can be reflected by soil electrical conductivity (SEC), with a linear relationship between them [27]. Based on the analysis of the soil samples, we had the calibration curve of soil salt content and electrical

TABLE 1: The physical and chemical properties of the soil of experimental plot.

| Soil | Depth (cm) | Soil bulk density (g·cm⁻³) | Particle content (%) | | | pH | Total salt (g·kg⁻¹) | Organic matter (g·kg⁻¹) | Total nitrogen (g·kg⁻¹) | Available phosphorus (g·kg⁻¹) | Available potassium (g·kg⁻¹) |
			Clay <0.002 mm	Silt 0.002-0.02 mm	Sand 0.02-2 mm						
Sandy soil	0-20	1.58	5.88	34.17	59.95	8.41	2.84	6.14	0.39	13.61	130.67
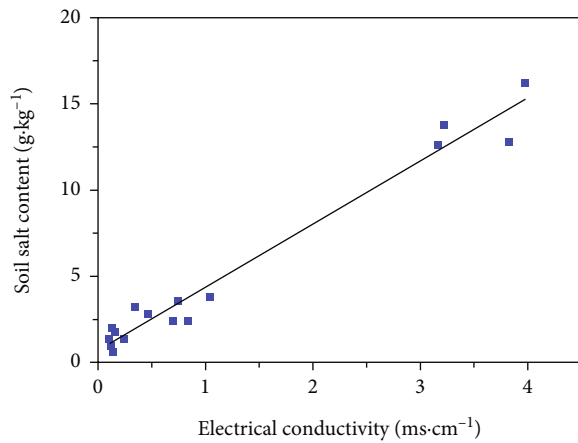
Figure 3: Relationship between soil salt content (SSC) and electrical conductivity (SEC) of soil extract.

conductivity of soil leaching solution (see Figure 3). The fitted relationship between SSC and SEC of soil leaching solution was illustrated as follows:

$$EC = 3.6485S + 0.7319,$$
$$R^2 = 0.9703,$$

(1)

where S is the soil electrical conductivity (SEC) value and EC is soil salt content (SSC) of the soil extract.

2.5.2. Cost–Benefit Analysis. In this study, net income per unit area is taken as the economic benefit evaluation index. The input of maize production mainly includes the cost of seeds, fertilizers, pesticides, and other agricultural means of production, as well as the cost of renting land, agrolabor management, and the cost of maize harvesting. Maize production income mainly comes from maize kernel sales. The difference between maize kernel sales revenue per unit area and production input is the net income per unit area, which is calculated according to the following formula (the results are shown in Table 2).

$$F = Y \times P_1 - (Y \times P_2 + L \times P_3 + S \times P_5 + Z + N + H + J),$$

(2)

where F is net income per hectare, ¥·ha^{-1}, Y is yield, kg·ha^{-1}, P_1 is the purchase price of maize rains, ¥·ha^{-1}, P_2 is the unit price of maize harvesting, ¥·ha^{-1}, L is the unit price of the modifier, ¥·ha^{-1}, P_3 is the amount of improver per unit area, ¥·ha^{-1}, S is the sowing amount per unit area, ¥·ha^{-1}, P_5 is the unit price of maize seed, ¥·ha^{-1}, Z is the rental fee per unit area, ¥·ha^{-1}, N is the farmland management fee per unit area, ¥·ha^{-1}, H is the cost of chemical fertilizers and pesticides per, ¥·ha^{-1}, and J is cropping cost, ¥·ha^{-1}.

2.5.3. Statistical Analysis. The data were the mean value of three replicates. Microsoft Excel 2010 and SPSS Statistics 17.0 software were used for statistical analysis (ANOVA) and charting of relevant parameters. The least significant difference (LSD) tests at $P < 0.05$ level were used to determine significant differences between the treatments. Origin Function software, Arcgis 10.2, and Microsoft Visio 2003 were used to draw figures.

3. Results

3.1. Effects of Different Soil Modifier Contents on the Distribution of Water and Salt in Soil Profile

3.1.1. Effects of Different Soil Modifier Contents on Moisture Content of Soil Profile. Because of the high precipitation in the experimental area during the maize growth period, the farmland was not irrigated [8]. Figure 4 describes the effects of different soil modifiers on the soil profile water content in the field of the test plot in each growth stage of maize. It can be seen that in the whole maize growth period 0-40 cm soil profile, because of the plot in maize, temperatures, and sunshine time extension, and farmland is not in the water supply moisture to the soil, the test of soil evaporation is higher, and the surface soil moisture content is low. With the increase of soil depth, the influence of evapotranspiration on the deep soil layer gradually decreases, and the soil water content gradually increases. Compared with CK, the soil moisture content of 0-10 cm surface soil under different soil modifier treatments was all higher than that of CK. The variation of soil water content was the most obvious after adding HA and showed the same trend in 2019 and 2020. The 10-20 cm soil moisture content curve also showed a trend of fluctuation due to the addition of soil modifier, but the fluctuation of the curve was smaller than that of the surface soil in general. On the whole, the soil moisture content of 20-40 cm fluctuated steadily with the growth stage. Soil water contents in HA plots were the largest in tasseling stage and filling stage, while the water content of HK treatment decreased the least from filling to maturity stage. Thus, the addition of soil modifiers can increase the water holding capacity of the soil.

3.1.2. Effects of Different Soil Modifier on the Soil Salt Content of Farmland in Different Growth Periods of Maize. The measured conductivity value was put into Equation (1) to calculate the soil profile salt content of each treatment, and it follows the relation diagram of the change of soil profile salt content in the whole growth period in the field of the test plot with different soil modifiers shown in Figure 5. It can be seen that the changing trend in 2019 and 2020 is the same, that is, during the entire growth period, the overall trend of the 0-40 cm soil profile turns out to have higher salt content in the surface layer. As the depth of the soil profile increases, the salt content of the soil gradually decreases. Compared with the impact on the salt content of maize with CK, the addition of soil modifiers has a more significant impact on the salt content of the soil profile. After the addition of soil modifiers, the salt content of the soil profile is significantly less than that of CK. Based on further analysis of Figure 5, it can be seen that in 2019 and 2020, the salt content of the soil profile at 0-20 cm changes most obviously, and the group with CK is significantly higher than the test group with the soil modifiers. In addition,

Table 2: Maize planting, harvesting, and selling prices.

Category	Selling price ($¥·kg^{-1}$)	Farm machinery ($¥·ha^{-1}$)	Maize seeds ($¥·ha^{-1}$)	MS price ($¥·kg^{-1}$)	YK price ($¥·ha^{-1}$)	HA price ($¥·ha^{-1}$)	HK price ($¥·kg^{-1}$)	NB price ($¥·ha^{-1}$)	Land rentals ($¥·ha^{-1}$)	Farmland management fee ($¥·ha^{-1}$)	Chemical fertilizers ($¥·ha^{-1}$)
Price	3	750	300	242	900	169	1048	1322	1500	1000	750

Figure 4: Continued.

(e)

(f)
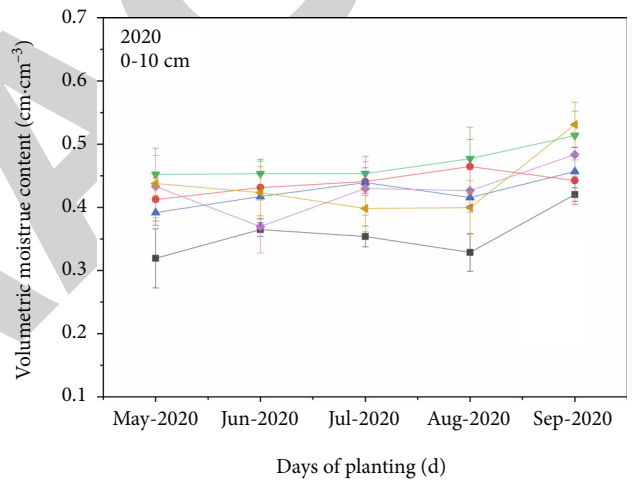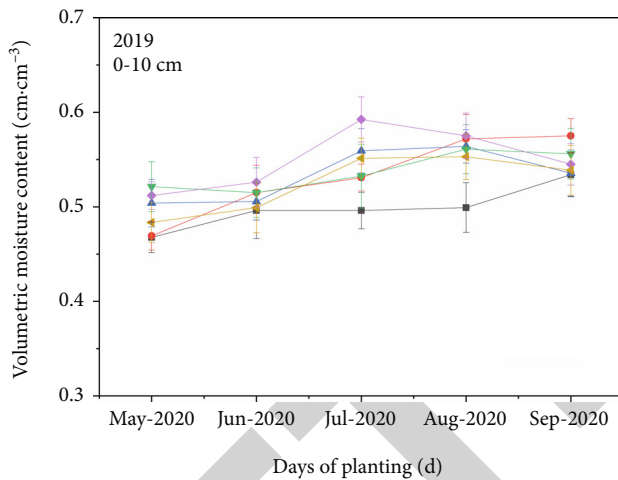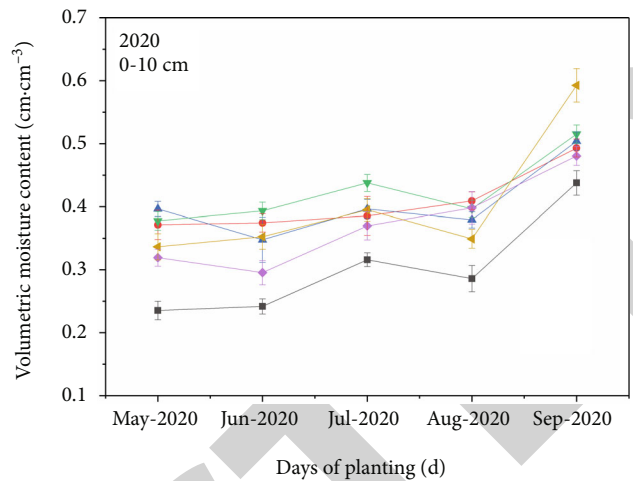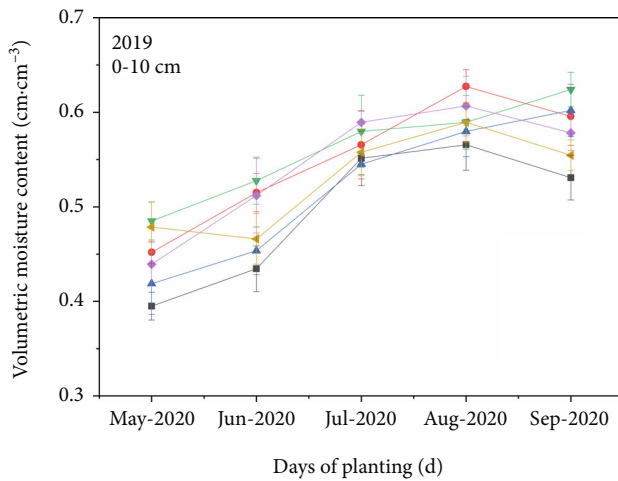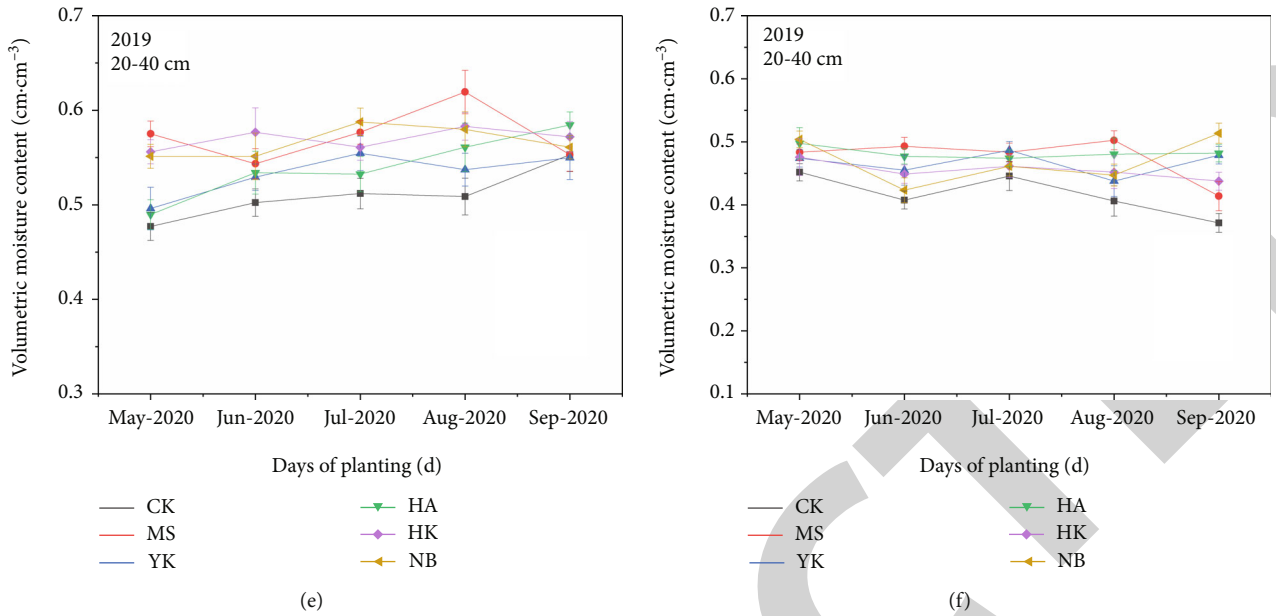
Figure 4: Distribution of the effect of different soil modifier contents on soil profile moisture content of (a) 0-10 cm, 2019, (b) 0-10 cm, 2020, (c) 10-20 cm, 2019, (d) 10-20 cm, 2020, (e) 20-40 cm, 2019, and (f) 20-40 cm, 2020, respectively.

(a)

(b)
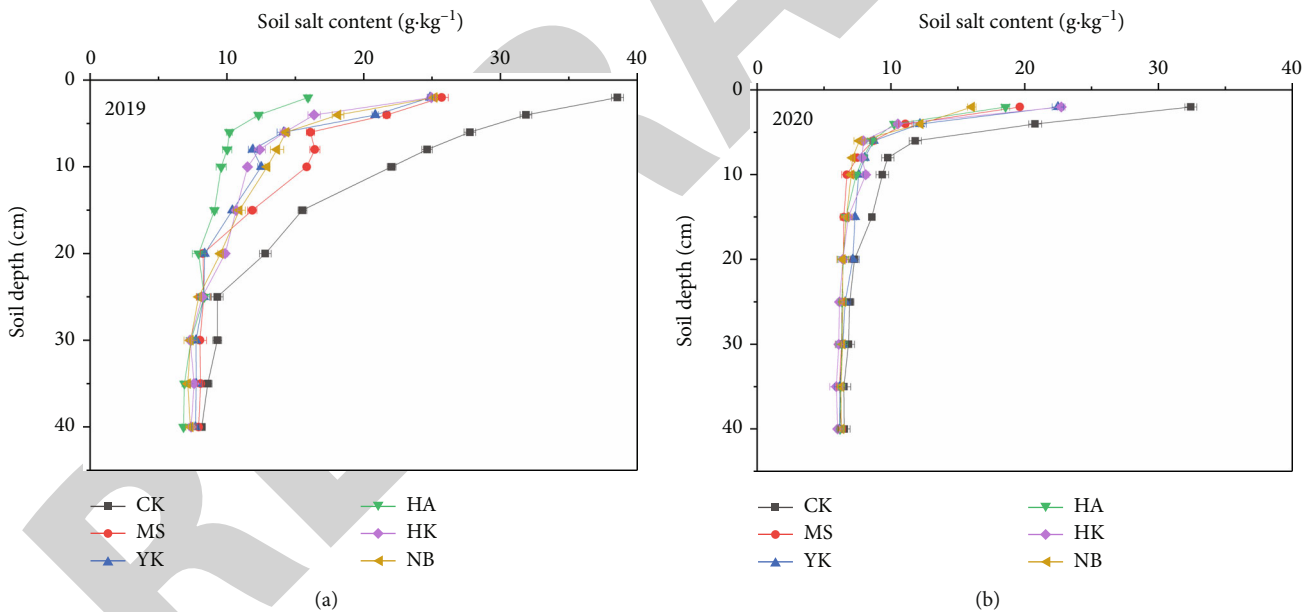
Figure 5: Distribution of the effects of different soil modifier on soil profile salt content during the whole growth period of (a) 2019 and (b) 2020.

the effect of soil modifiers on salt distribution in 2019 is more obvious. Such trend attributes to the temperature in 2019 are high, and the amount of precipitation is less than in 2020, so the improvement effect in 2019 is more obvious.

3.1.3. Effects of Different Soil Modifiers on the Salt Distribution of Farmland in Different Growth Periods of Maize. According to the measured data, Figure 6 illustrates the changes of different soil modifiers on farmland salt dis-

tribution in 0-10 cm (a), 10-20 cm (b), and 20-40 cm (c) in each maize growth period in 2019 and 2020. It can be seen 0-40 cm soil layer has higher salt content compared to that in 0-10 cm and 10-20 cm soil layer. With the increase of soil profile depth, the salt content of the 20-40 cm soil layer gradually decreases. The effect of soil modifiers on the soil salt content is more significant, which is shown as the salt content of the test plots with soil modifiers less than that of CK. With the growth of maize, the overall soil salt content
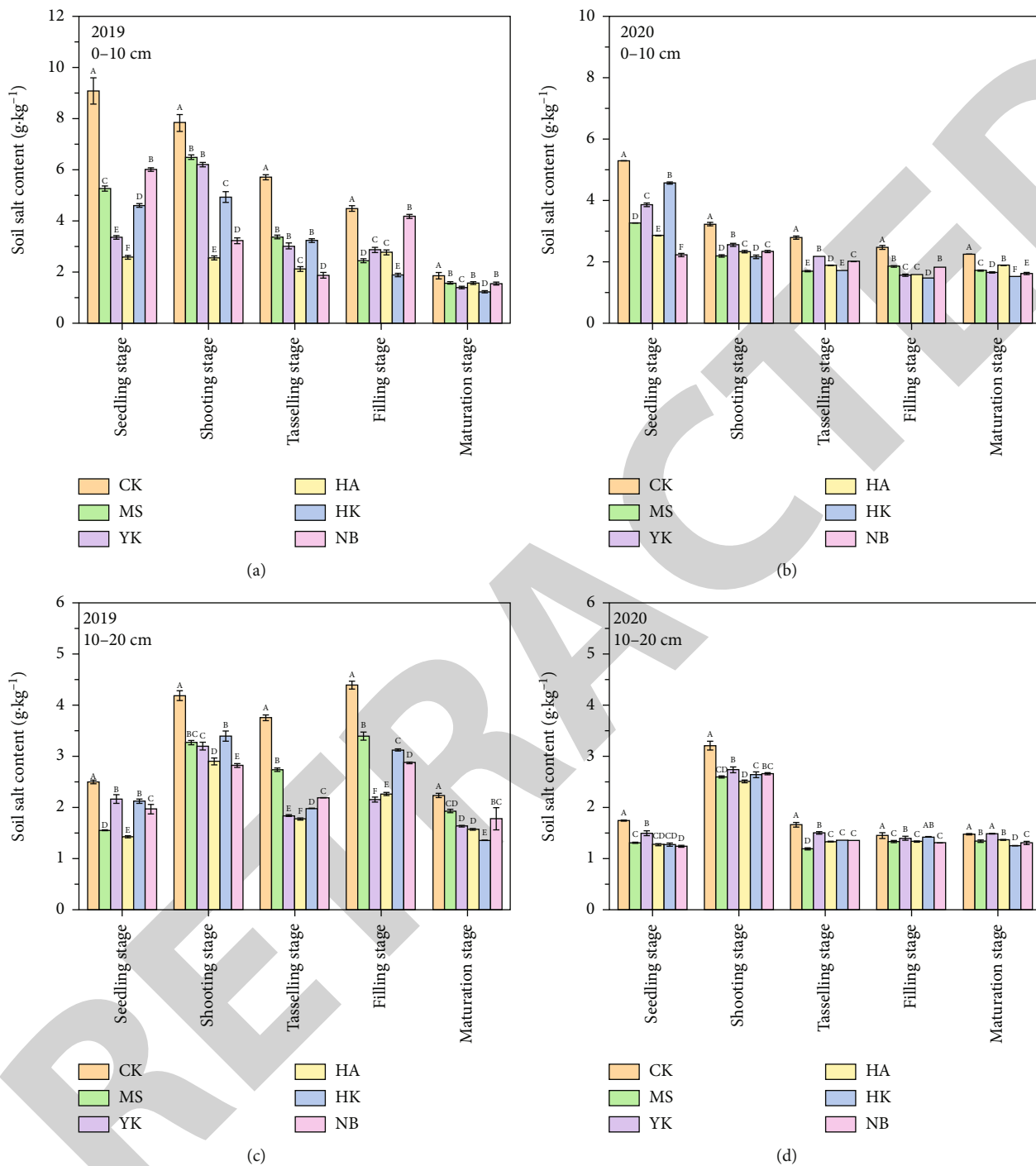
FIGURE 6: Continued.
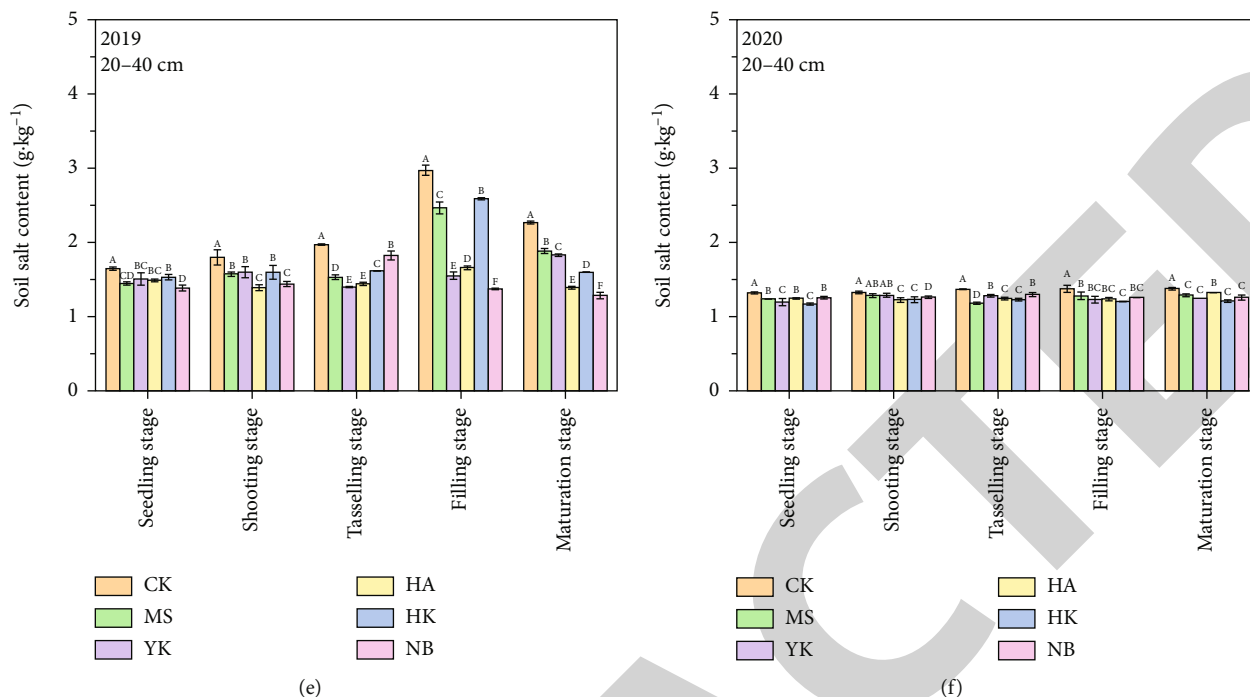
Figure 6: Distribution of the effects of different soil modifiers on the dynamic changes of soil salinity in the growing period of (a) 0-10 cm, 2019, (b) 0-10 cm, 2020, (c) 10-20 cm, 2019, (d) 10-20 cm, 2020, (e) 20-40 cm, 2019, and (f) 20-40 cm, 2020, respectively.

increased first and then decreased. It is also shown in Figure 6 that compared to CK, soil modifiers have more obvious effects on the salt distribution in the shooting stage, tasseling stage, and the filling stage. Such results mainly attributed to the high temperature, the high evaporation strength, and low rainfall. Therefore, it can be seen that applying soil modifiers can reduce evaporation while reducing the accumulation of salt.

By subtracting the salt content of different soil modifiers in each soil layer from the salt content of CK and dividing by CK, it follows the results of the influence of different soil modifiers on the desalination rate of soil layer in 2019 and 2020 (see Table 3). It can be seen from Table 3 that the desalination effect of each test plot varies greatly with the soil depth during the whole growth period of maize. In each growth period, the desalination rate of soil profile increased with different soil modifiers agents. In the 0-40 cm section, the desalination effect at seedling, shooting, and tasseling stages was better than that at filling stages and maturation stages. At the seedling stage of 0-10 cm, the trend of 2019 and 2020 was consistent, that is, the test plots with HA added had the best desalination, which was 71.57% and 46.02%, respectively. In the 10-20 cm section, the desalination rate of the HA test plot was the highest at the tasseling stage, 51.92%. In the 20-40 cm section, the desalination rate of the YK test plot at the filling stage is the highest of 47.8%.

3.2. Effects of Different Soil Modifiers on the Growth, Yield, and Economic Benefit of Maize

3.2.1. Effects of Different Soil Modifiers on Maize Growth.
The seedling growth of maize was slow, and there was no

significant difference in crop height, leaf area, and stem diameter between different soil modifiers treatments. After entering the shooting stage (60 days), a significant difference in different soil modifiers could be found in the crop height, leaf area, and stem diameter. After the tasseling stage (90 days), the growth rate of maize crop height decreased and then was stabilized, and the leaf area and stem diameter decreased gradually after reaching the maximum (Figure 7).

3.2.2. Effects of Different Soil Modifiers on Leaf Photosynthetic Characteristics of Maize.
The effect of the five soil modifiers on leaf photosynthetic characteristics of maize at the filling stage are shown in Table 4. Table 4 shows that compared with the CK, soil modifier can significantly influence the leaf photosynthetic characteristics of maize. The influence of leaf photosynthetic characteristics varies from different modifiers. In order to clarify the influence of the soil modifiers on the experimental results, one-way ANOVA was conducted on the net photosynthetic rate (Pn), transpiration rate (Tr), stomatal conductance (Gs), and intercellular CO_2 concentration (Ci) ($P < 0.05$), and the results are listed in Table 4. It can be seen that the application of soil modifier has a very significant correlation with the net photosynthetic rate (Pn), transpiration rate (Tr), stomatal conductance (Gs), and intercellular CO_2 concentration (Ci), and the P value is far less than 0.01, so the application of soil modifier has a very significant effect ($\alpha = 0.05$). It can be seen that the application of soil modifiers can increase the net photosynthetic rate (Pn), transpiration rate (Tr), and stomatal conductance (Gs) and decrease the intercellular CO_2 concentration (Ci).

Table 3: Effects of soil modifier contents on desalinization rates in different growth stages.

Soil modifier/(g·m^{-2})	Growth stages	Soil depth/(cm)					
		2019			2020		
		0-10	10-20	20-40	0-10	10-20	20-40
MS	Seedling stage	41.98%	37.96%	1.85%	38.34%	25.01%	6.13%
	Shooting stage	14.74%	21.97%	1.56%	32.06%	19.16%	3.33%
	Tasselling stage	25.69%	27.06%	16.07%	39.32%	28.48%	7.92%
	Filling stage	22.54%	22.75%	16.97%	25.06%	8.02%	6.98%
	Maturation stage	3.19%	-15.92%	16.80%	23.67%	9.25%	6.63%
YK	Seedling stage	63.03%	13.42%	4.30%	27.11%	14.22%	9.23%
	Shooting stage	17.91%	23.62%	11.08%	20.90%	14.79%	2.89%
	Tasselling stage	29.61%	51.04%	23.31%	22.23%	9.52%	-6.35%
	Filling stage	17.81%	50.96%	47.80%	36.75%	4.02%	10.54%
	Maturation stage	5.10%	15.30%	19.34%	26.35%	-0.49%	9.50%
HA	Seedling stage	71.57%	42.93%	2.87%	46.02%	26.82%	5.37%
	Shooting stage	58.08%	30.72%	13.07%	27.75%	21.80%	7.66%
	Tasselling stage	39.46%	51.92%	20.91%	32.64%	20.05%	3.18%
	Filling stage	18.92%	48.47%	44.19%	35.72%	8.32%	9.88%
	Maturation stage	3.17%	18.52%	38.64%	16.03%	7.62%	3.88%
HK	Seedling stage	49.26%	15.10%	5.94%	13.65%	27.03%	11.21%
	Shooting stage	31.86%	18.92%	-12.60%	33.00%	17.90%	7.26%
	Tasselling stage	27.26%	47.32%	11.29%	38.54%	18.25%	4.17%
	Filling stage	28.64%	28.90%	12.85%	40.84%	2.13%	12.34%
	Maturation stage	6.98%	29.85%	29.55%	32.35%	15.26%	12.25%
NB	Seedling stage	33.79%	21.34%	4.28%	38.01%	28.84%	4.71%
	Shooting stage	50.69%	32.64%	10.02%	27.69%	17.12%	4.89%
	Tasselling stage	42.23%	41.66%	18.02%	28.05%	18.53%	-1.20%
	Filling stage	3.36%	34.55%	53.86%	26.07%	9.82%	8.28%
	Maturation stage	3.44%	7.73%	43.36%	27.97%	11.59%	8.63%

3.2.3. Effects of Different Soil Modifiers on Maize Yield. Table 5 shows that compared with the CK, soil modifier can significantly increase the thousand kernel weight and yield of maize. The increase of maize yield varies from different modifiers. The average yield of maize with MS, YK, HA, HK, and NB applied in 2019 was 13.63%, 13.76%, 15.09%, 21.12%, and 23.84% higher than maize with CK, respectively, and in 2020 18.42%, 16.65%, 23.31%, 29.68%, and 31.84%, respectively. The yield increase rate of maize that applied all the five soil modifiers showed an increase in 2019 and 2020 (NB>HK>HA>YK>MS). In order to clarify the influence of the soil modifiers on the experimental results, one-way ANOVA was conducted on the 1000-grain weight and yield ($P < 0.05$), and the results are listed in Table 5. It can be seen that the application of soil modifier has a very significant correlation with the 1000-grain weight and yield, and the P value is far less than 0.01, so the application of soil modifier has a very significant effect on the yield ($\alpha = 0.05$). It can be seen that the application of soil modifiers has an important effect on maize yield.

3.2.4. Effects of Different Soil Modifiers on Economic Benefits of Maize. The economic benefit is another important indica-

tor to estimating cropping patterns. When calculating the income per hectare, this study conducted an investigation on the agricultural materials market of Yan'an city in 2018 and 2019 and obtained the relevant parameters in Equation (2) (Table 2). Through calculation and investigation statistics, the expenditure and gross income of each unit area under the application of different modifiers are obtained, as shown in Table 6. It follows that the rank of upfront expenses of maize with the five soil modifiers is NB>HK>YK>HA>MS>CK. The expenditure in the later stage is the same because of the same harvesting mode. By comparing the net income in 2019 and 2020, it can be seen that, compared with CK, the net income after applying soil modifier is higher than that of CK, and the net income of the experimental plots in HK is the highest, increasing by ¥ 3257.74 and ¥ 2168.23, respectively. The overall net income is HK>HA>YK>MS>NB>CK.

4. Discussion

4.1. Influence of Different Soil Modifiers on Water Content in Maize Field. In agriculture production, soil modifiers had great potential for water-saving [16, 20, 26, 28]. And it could
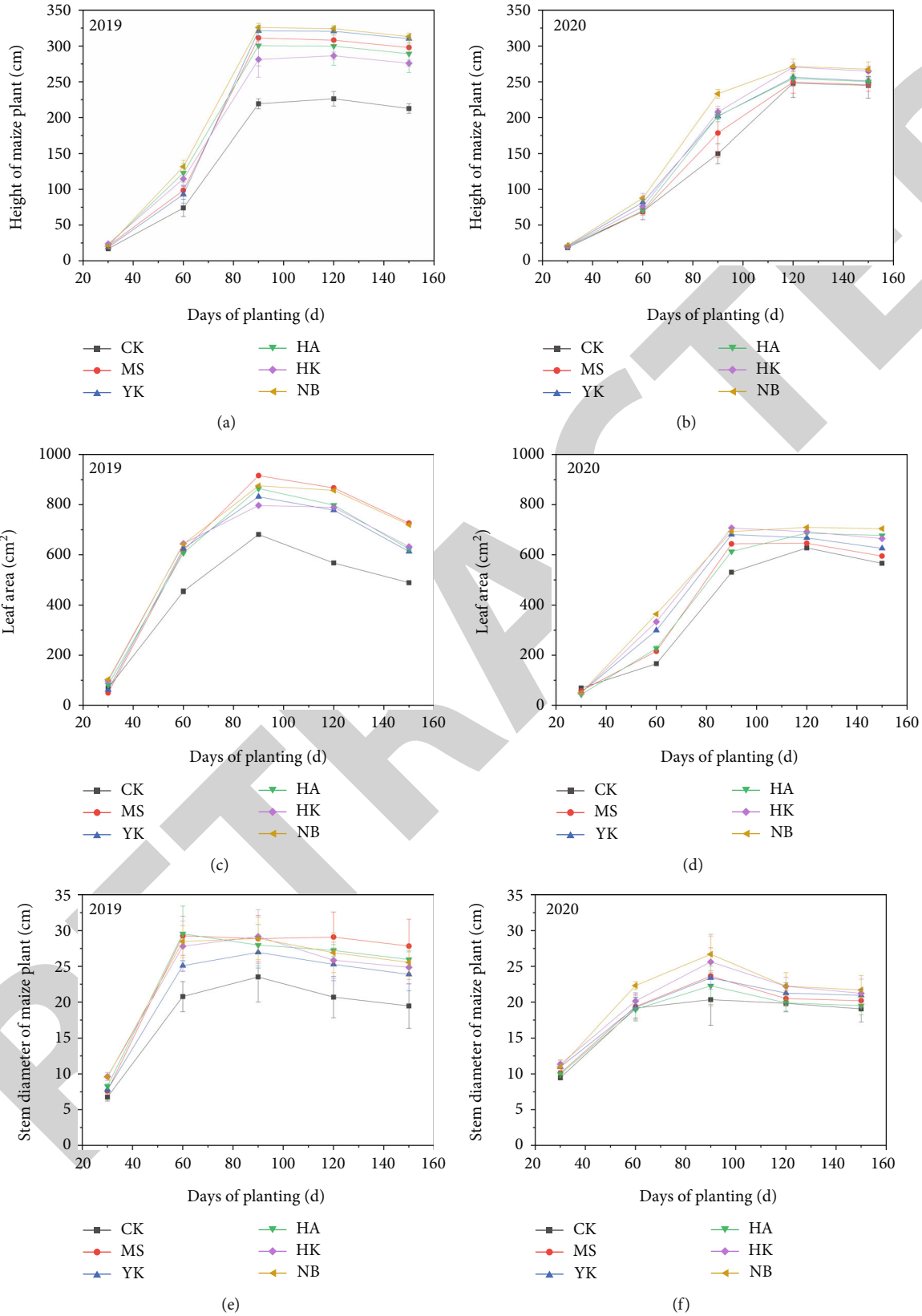
Figure 7: Distribution of the effects of different soil modifiers on maize growth of (a) height of maize plant, 2019, (b) height of maize plant, 2020, (c) leaf area, 2019, (d) leaf area, 2020, (e) stem diameter of maize plant, 2019, and (f) stem diameter of maize plant, 2020, respectively.

TABLE 4: The effects of different soil modifiers on leaf photosynthetic characteristics.

Year Plot	2019				2020			
	$Pn/(\mu mol\ CO_2/(m^2{\cdot}s))$	$Gs/(\mu mol/(m^2{\cdot}s))$	$Ci/(\mu L/L)$	$Tr/(mmol\ H_2O/(m^2{\cdot}s))$	$Pn/(\mu mol\ CO_2/(m^2{\cdot}s))$	$Gs/(\mu mol/(m^2{\cdot}s))$	$Ci/(\mu L/L)$	$Tr/(mmol\ H_2O/(m^2{\cdot}s))$
CK	23.21 ± 2.23^e	0.1 ± 0.03^c	331.69 ± 44.00^a	3.21 ± 0.70^d	20.12 ± 1.93^e	0.09 ± 0.03^c	287.57 ± 38.15^a	2.79 ± 0.60^d
MS	26.27 ± 0.76^d	0.25 ± 0.08^b	316.41 ± 60.20^a	3.99 ± 0.53^c	24.12 ± 0.70^d	0.23 ± 0.07^b	290.46 ± 55.26^a	3.66 ± 0.49^c
YK	27.2 ± 2.27^d	0.21 ± 0.04^b	288.39 ± 21.73^b	4.24 ± 0.42^b	25.39 ± 1.72^d	0.19 ± 0.03^b	258.68 ± 19.49^b	3.81 ± 0.38^c
HA	31.25 ± 2.44^c	0.23 ± 0.04^b	275.69 ± 30.14^b	4.26 ± 0.20^b	30.03 ± 2.35^c	0.22 ± 0.04^b	264.94 ± 28.97^b	4.09 ± 0.19^b
HK	33.12 ± 2.45^b	0.31 ± 0.08^a	248.48 ± 19.11^c	5.67 ± 0.87^a	34.2 ± 2.80^b	0.3 ± 0.08^a	212.84 ± 33.97^c	5.28 ± 0.85^a
NB	36.44 ± 1.04^a	0.34 ± 0.03^a	208.14 ± 34.55^d	5.21 ± 0.35^a	35.27 ± 1.00^b	0.33 ± 0.03^a	201.48 ± 33.44^d	5.05 ± 0.34^a
P	1.75×10^{-7} **	1.43×10^{-2} **	3.68×10^{-8} **	4.53×10^{-2} **	1.54×10^{-6} **	1.40×10^{-2} **	1.56×10^{-8} *	8.76×10^{-2} * *

Note: Data in the table are mean ± standard deviation. Different letters in the same column represent significant differences between different treatments at the 0.05 level (Duncan's method). ** indicates that there is a very significant correlation between experimental factors and results ($P < 0.01$).

TABLE 5: The effects of different soil modifiers on maize grain yield.

Year	2019			2020		
Plot	1000-grain weigh/(g)	Yield/(kg·ha^{-1})	Increase over control/(%)	1000-grain weigh/(g)	Yield/(kg·ha^{-1})	Increase over control/(%)
CK	290.05 ± 1.04[d]	3695.22 ± 78.11[c]	-	274.54 ± 2.46[e]	3204.58 ± 38.57[d]	-
MS	415.07 ± 0.87[b]	4278.43 ± 90.51[b]	13.63	323.88 ± 4.84[d]	3928.34 ± 186.49[c]	18.42
YK	378.64 ± 3.77[c]	4285.07 ± 244.46[b]	13.76	396.67 ± 7.44[b]	3844.96 ± 20.32[c]	16.65
HA	368.95 ± 0.95[c]	4347.55 ± 233.87[b]	15.01	361.11 ± 2.54[c]	4178.86 ± 42.95[b]	23.31
HK	416.58 ± 1.41[b]	4684.63 ± 160.61[a]	21.12	404.22 ± 2.04[a]	4557.16 ± 43.10[a]	29.68
NB	425.48 ± 1.53[a]	4852.08 ± 130.68[a]	23.84	408.22 ± 2.99[a]	4701.66 ± 79.66[a]	31.84
P	4.92×10^{-9} **	1.28×10^{-10} **	5.92×10^{-3} **	1.41×10^{-8} **	$5.72 \times 10 -9$**	$4.23 \times 10 -3$**

Note: Data in the table are mean ± standard deviation. Different letters in the same column represent significant differences between different treatments at the 0.05 level (Duncan's method). ** indicates that there is a very significant correlation between experimental factors and results ($P < 0.01$).

TABLE 6: Expenditure, gross income, and net income after applying different soil modifiers.

Year	Soil modifier	Seed	Upfront costs				Extensions	Farm machinery	¥·ha^{-1}	
			Soil modifier	Rent	Farm management	Chemical fertilizers			Gross income	Net income
2019	CK	300	0	1500	1000	750	3550	750	11085.66	6785.66
	MS	300	150	1500	1000	750	3700	750	12835.29	8285.29
	YK	300	250	1500	1000	750	3850	750	12855.21	8355.21
	HA	300	225	1500	1000	750	3775	750	13042.65	8517.65
	HK	300	1050	1500	1000	750	4600	750	14053.89	8953.89
	NB	300	3000	1500	1000	750	6550	750	14556.24	7256.24
2020	CK	300	0	1500	1000	750	3550	750	9613.74	5313.74
	MS	300	150	1500	1000	750	3700	750	11484.99	6934.99
	YK	300	300	1500	1000	750	3850	750	11534.85	7034.85
	HA	300	225	1500	1000	750	3775	750	12536.55	8011.55
	HK	300	600	1500	1000	750	4150	750	13671.48	8571.48
	NB	300	3000	1500	1000	750	6550	750	14104.95	6804.95

enhance soil water-holding capacity and effectively improve the water content. This showed consistency with our current findings. In this study, application soil modifiers significantly increased soil profile water content compared with CK (Figure 4). This is because the application of soil modifiers can increase the soil water-holding capacity. This could account for three possibilities. On the one hand, in terms of soil modifiers' molecular structure, soil modifier is a polymer with a great number of peptide bonds and hydrophilic groups. Such property enables it to facilitate its cross-link with soil moisture and absorb a large amount of water accordingly [29]. On the other hand, because of the difference sowing time. Studies have shown that sowing time has a significant effect on crop yield and nutrient absorption [30]. Moreover, the instability of continuous perennial and long-term precipitation in semiarid areas affects the stability of soil profile moisture content [28]. Soil modifiers stimulated the formation of soil aggregates and improved their stability. Soil aggregates could adjust soil moisture [29], as well as effectively store irrigation water and reduce soil water loss through evaporation [26].

4.2. Effects of Different Soil Modifiers on Salt Content and Salt Distribution of Maize Field. The application of soil modifiers to saline-alkali soils has aroused wide public concern and has been considered to be a good way to improve saline-alkali soil, in the past decades. The addition of soil modifiers to saline soil can improve its physical properties and salt content. The application of soil modifiers led to different changes in soil profile water, salt, and nutrients [16, 20, 26, 28, 30]. As an important indicator to measure the improvement effect of saline-alkali soil, soil salt content can better reflect the fertility characteristics and water permeability [31, 32]. The consequences showed the addition of five soil modifiers could decrease soil salt content, and the data in Figures 5 and 6 and Table 3 support our research. This shows consistency with the findings of previous researches that supported the significant decrease of soil salt caused by soil modifiers [29, 33–35]. The results reported by Pang et al. indicated that when the straw application amount of 3,600 kg/hm^2 was applied after MS, the comprehensive improvement effect on the structure, salinity, and other physical and chemical properties of coastal saline-alkali soil

was relatively obvious. Dietrich found that the application of HA can effectively inhibit the increase of water-soluble K^+, Ca^{2+}, Mg^{2+}, and other base ions in the soil, thus reducing the electrical conductivity of the soil [34]. The application of HK soil modifier can increase the desalination rate of soil, and appropriate deep application could effectively improve the improvement effect of saline-alkali soil [29]. NB is beneficial to soil salt leaching under brackish rotation irrigation, and the desalination rate and the desalination zone depth coefficient are increased by 9.1%-15.0% and 1.1%-7.5%, respectively [35].

4.3. Effects of Different Soil Modifiers on Maize Growth, Leaf Photosynthetic Characteristics of Maize, and Yield. The maize growth of crop and yield increased strikingly in adding soil modifiers in soils, which is similar to previous research [16, 20, 28, 36]. Yang et al. also argued significant enhancement of maize growth and yield by soil modifier [26]. Moreover, Chen et al. showed that soil modifiers could improve drought-resistant of crop seedlings by adjusting soil moisture [20]. In this study, maize growth of crop and yield were affected by soil modifiers and obvious differences with different soil modifiers. The application of soil modifiers can promote crop growth and achieve higher yields. Based on the application of traditional soil modifiers, we introduced a new soil modifier. The new soil modifier used in this study has greater potential than the traditional soil modifier in promoting crop growth, improving crop yield. The data in Figure 4 and Tables 4 and 5 support these hypotheses. For example, in 2019 and 2020, maize yield increased by 13.63%-31.84%, and yield increases by NB>HK>HA>YK>MS. Studies from other regions have shown that applying soil modifiers can further crop growth and enhance crop yield than CK. This might be because of the following mechanisms. On one hand, soil modifiers enhanced soil water-holding capacity and hence promote increasing water use efficiency, crop growth, and crop yield [37]. On the other hand, MS and NB function in terms of storing, water availability improvement for crops, and thus the enhancement of crop growth and crop yield [20, 38]. The results reported by Nakayama et al. and Körner et al. indicated that the stomatal density decreased, stomatal and conductance (Gs) and the intercellular CO_2 concentration (Ci) decreased, ultimately leading to the decrease of net photosynthetic rate (Pn) [39, 40]. The results of this study also showed that NaCl stress restricted the growth and development process of maize, which was embodied in the reduction of plant biomass and the decrease of the net photosynthetic rate (Pn) the decreased. According the experimental, the result showed the application of soil modifiers had a significant impact on the photosynthetic characteristics of maize leaves.

In the process of decomposition, straw can absorb and use mineral elements in the soil to increase the soil organic matter and thus enhance the growth and yield of the crop [33]. NB can alleviate salt stress, and a high dose of NB can reduce the lethal effect of salt on crops [41]. The application of HK can improve maize crop growth and signifi-cantly increase maize yield [26]. Finally, soil modifiers promoted the formation of soil aggregates and increased the ability of nutrient adsorption, therefore enhancing crop yield. Application of HA had positive effects on the growth and appearance of crops under salt stress [42, 43]. Application of NB could promote the growth of common bean with higher Na^+ adsorption capacity [35]. These results are consistent with the experimental results in this experiment.

4.4. Appropriate Soil Modifier Application Strategy. From the viewpoint of agriculture production, we were hopeful in improving secondary saline-alkali soils with fewer soil modifiers to produce more, that is, achieving higher economic benefits. The results in this present study showed that applying soil modifiers can provide economic benefits than CK. The income increased 6.48%-38.01%, respectively, HK>HA>YK>MS>NB. According to analyzing the production of soil modifier application, we found that the highest net profit was achieved when HK application rate was 26.2 kg/ha^{-1}. Similarly, Yang et al.'s research reported that the highest crop yield was obtained when the recommended optimal HK application rate was 35 kg/ha^{-1} [26]. When it comes to economic benefits, the farmers showed more interest in the achievement of the largest net profit. Therefore, this study recommends that 26.2 kg/ha^{-1} might be an appropriate soil modifier application rate, which is beneficial to the improvement of crop growth as well as economic benefit in secondary saline-alkali soils of Northwest China.

5. Conclusion

Based on the application of traditional saline-alkali soil improvement, this study put forward a method of applying soil conditioning agents (soil conditioning agents: MS, HA, YK, HK, and NB) to reduce the impact of soil salt accumulation on typical crops in the Loess Plateau and improve soil saline-alkali. Compared with that of CK, the application of soil modifiers can increase soil water holding capacity, reduce soil profile salt content, and reduce salt accumulation, and the trend of desalination rate in 2019 and 2020 showed consistency, of which the increase is 71.57% and 46.02%, respectively. The average yield increases of the maize applied MS, YK, HA, HK, and NB were respectively 13.63%, 13.76%, 15.09%, 21.12%, and 23.84% in 2019 and 18.42%, 16.65%, 23.31%, 29.68%, and 31.84% in 2020. The rank of the net income of maize with five soil modifiers shows as HK>HA>YK>MS>NB>CK. Therefore, applying soil modifiers as an economic and environmentally friendly soil remediation method can effectively improve the saline-alkali soil and promote the increase of yield and income.

Data Availability

The data that supports the findings of this study are available in this article.

Conflicts of Interest

The authors declare no conflict of interest.

Acknowledgments

References

[1] J. O. Adejuwon and O. Ekanade, "A comparison of soil properties under different landuse types in a part of the Nigerian cocoa belt," *Catena*, vol. 15, no. 3-4, pp. 319–331, 1988.

[2] U. Nachshon, "Soil degradation processes: it's time to take our head out of the sand," *Geosciences*, vol. 11, no. 1, 2021.

[3] S. G. K. Adiku, D. S. Maccarthy, and S. K. Kumahor, "A conceptual modelling framework for simulating the impact of soil degradation on maize yield in data-sparse regions of the tropics," *Ecological Modelling*, vol. 448, no. 448, p. 109525, 2021.

[4] U. N. Safriel, "The Assessment of Global Trends in Land Degradation," in *Climate and Land Degradation. Environmental Science and Engineering (Environmental Science)*, M. V. K. Sivakumar and N. Ndiang'ui, Eds., Springer, Berlin, Heidelberg, 2007.

[5] C. Jiang, F. Wang, H. Zhang, and X. Dong, "Quantifying changes in multiple ecosystem services during 2000-2012 on the Loess Plateau, China, as a result of climate variability and ecological restoration," *Ecological Engineering*, vol. 97, pp. 258–271, 2016.

[6] L. Li, S. U. Khan, X. Xia, H. Zhang, and C. Guo, "Screening of agricultural land productivity and returning farmland to forest area for sensitivity to rural labor outward migration in the ecologically fragile loess plateau region," *Environmental Science and Pollution Research*, vol. 27, no. 21, pp. 26442–26462, 2020.

[7] Z. Jin, L. Guo, Y. Wang et al., "Valley reshaping and damming induce water table rise and soil salinization on the Chinese Loess Plateau," *Geoderma*, vol. 339, pp. 115–125, 2019.

[8] Y. Yunlong, H. Lin, J. Zhao, C. Guangchen, and Z. Jing, "Ammonia dynamics in reservoirs in response to rainfall events in a gully-filled loess catchment in Yan'an City, Shaanxi Province," *Quaternary Sciences*, vol. 37, no. 6, pp. 1204–1221, 2015.

[9] B. Fu, Y. Liu, Y. Lü, C. He, Y. Zeng, and B. Wu, "Assessing the soil erosion control service of ecosystems change in the Loess Plateau of China," *Ecological Complexity*, vol. 8, no. 4, pp. 284–293, 2011.

[10] Y. Yue, J. Ni, P. Ciais et al., "Lateral transport of soil carbon and land-atmosphere CO_2 flux induced by water erosion in China," *Proceedings of the National Academy of Sciences of the United States of America*, vol. 113, no. 24, pp. 6617–6622, 2016.

[11] S. Wang, B. Fu, S. Piao et al., "Reduced sediment transport in the yellow river due to anthropogenic changes," *Nature Geoscience*, vol. 9, pp. 38–41, 2016.

[12] M. F. Bakry, "The improvement of hydraulic efficiency of irrigation systems with particular reference to biological control method," *Irrigation and Drainage Systems*, vol. 8, no. 2, pp. 123–133, 1994.

[13] L. Duan, "Effect of different soil amendments on quality improvement of chemically contaminated soil based on biological evaluation method," *Chemical Engineering Transactions (CET Journal)*, vol. 71, pp. 361–366, 2018.

[14] A. F. Carvalho, F. C. de Figueiredo, T. S. Campioni, G. M. Pastore, and P. de Oliva Neto, "Improvement of some chemical and biological methods for the efficient production of xylanases, xylooligosaccharides and lignocellulose from sugar cane bagasse," *Biomass and Bioenergy*, vol. 143, article 105851, 2020.

[15] Z. Chemia and H. Koyi, "The control of salt supply on entrainment of an anhydrite layer within a salt diapir," *Journal of Structural Geology*, vol. 30, no. 9, pp. 1192–1200, 2008.

[16] X. Shi, H. Wang, J. Song et al., "Impact of saline soil improvement measures on salt content in the abandonment- reclamation process," *Soil and Tillage Research*, vol. 208, article 104867, 2021.

[17] W. Xie, Q. Chen, L. Wu, H. Yang, J. Xu, and Y. Zhang, "Coastal saline soil aggregate formation and salt distribution are affected by straw and nitrogen application: a 4-year field study," *Soil and Tillage Research*, vol. 198, article 104535, 2020.

[18] Z. Hy, C. Lu, P. Hc, N. Li, Z. Xl, and L. Yy, "Straw layer burial to alleviate salt stress in silty loam soils: impacts of straw forms," *Journal of Integrative Agriculture*, vol. 19, no. 1, pp. 265–276, 2020.

[19] S. Iijima, "Helical microtubules of graphitic carbon," *Nature*, vol. 354, no. 6348, pp. 56–58, 1991.

[20] X. Chen, B. Zhou, Q. Wang, W. Tao, and H. Lin, "Nano-biochar reduced soil erosion and nitrate loss in sloping fields on the Loess Plateau of China," *Catena*, vol. 187, p. 104346, 2020.

[21] A. C. García, R. L. Berbara, L. P. Farías et al., "Humic acids of vermicompost as an ecological pathway to increase resistance of rice seedlings to water stress," *African Journal of Biotechnology*, vol. 11, no. 13, pp. 3125–3134, 2012.

[22] M. Shaaban, M. Abid, and A. S. Rai, "Amelioration of salt affected soils in rice paddy system by application of organic and inorganic amendments," *crop Soil and Environment*, vol. 59, no. 5, pp. 227–233, 2013.

[23] X. Zhang, S. Dou, B. S. Ndzelu, X. W. Guan, B. Y. Zhang, and Y. Bai, "Effects of different corn straw amendments on humus composition and structural characteristics of humic acid in black soil," *Communications in Soil Science and crop Analysis*, vol. 51, no. 1, pp. 107–117, 2020.

[24] L. Zhang, X. Sun, and L. Zhang, "Effect of Hekang soil Improver on cotton field secondary salinization," *Xinjiang Agricultural Science and Technology*, vol. 5, p. 13, 2007.

[25] G. Ru, "Application effect test of Hekang saline-alkali soil improver in cotton field," *Rural Science and Technology*, vol. 5, pp. 26-27, 2013.

[26] Y. Yang, M. Duan, B. Zhou et al., "Effect of organic acid amendment on secondary saline soil amelioration in gully land consolidation area in northern Shaanxi, China," *Arabian Journal of Geosciences*, vol. 13, no. 23, p. 1273, 2020.

[27] X. Zhao, J. Yang, and R. Yao, "Relationship between soil salt dynamics and factors of water balance in the typical coastal area of northern Jiangsu province," *Journal of Agricultural Engineering*, vol. 26, no. 3, pp. 52–57, 2010.

[28] X. Qian, H. Zang, H. Xu et al., "Relay strip intercropping of oat with maize, sunflower and mung bean in semi- arid regions of Northeast China: yield advantages and economic benefits," *Field Crops Research*, vol. 223, pp. 33–40, 2018.

Hindawi

Research Article

A Novel Portable Soil Water Sensor Based on Temperature Compensation

Hao Tian [iD],[1,2] **Chongchong Yu** [iD],[1,2] **Tao Xie** [iD],[1,2] **Tong Zheng** [iD],[1,2] **and Mei Sun**[1,2]

[1]*School of Artificial Intelligence, Beijing Technology and Business University, Beijing 100048, China*
[2]*China Light Industry Key Laboratory of Industrial Internet and Big Data, Beijing Technology and Business University, Beijing 100048, China*

Correspondence should be addressed to Chongchong Yu; chongzhy@vip.sina.com

Soil water sensors based on the standing wave rate (SWR) principle are affected by temperature in long-term operation. To address this problem, a temperature compensation model based on the binary regression analysis method is proposed. The measurement results of the temperature-compensated standing wave rate (TCSWR) sensor at different temperatures and soil volumetric water content are analyzed, and the least-squares principle is used to identify the parameters to be determined in the compensation model for temperature for the SWR soil water sensor. A portable tapered TCSWR sensor with built-in temperature compensation model was developed on this basis. The calibration results show that the standing wave measurement circuit of the TCSWR sensor can effectively respond to changes in soil water, and the coefficient of the fitted equation exceeds 0.95. A comparison of the results before and after temperature compensation proves that compensation can significantly reduce the measurement error of the TCSWR sensor and improve the measurement accuracy. The static and dynamic characteristics of the TCSWR sensor show that the measurement range of the TCSWR sensor is 7.50%-31.50%, the measurement accuracy is ±0.63%, the stability is good, the resolution is a minimum of 0.05%, and the dynamic response time is less than 1 s. The absolute error of the TCSWR sensor measurement is less than 1% in comparison with similar sensors, demonstrating that the measurement results of the TCSWR sensor are reliable.

1. Introduction

Soil water is an important parameter in the fields of soil physics, botany, and other agriculture [1]. The main methods used to measure soil water content include the weighing and drying method, electric measurement method, and radiometric method [2]. The most commonly used methods are based on electrical measurement. The electrical measurement methods can be divided into capacitive and dielectric methods, and capacitive methods include bridge and resonance methods. Anderson was the first to explore the use of audio bridges to determine the water content of soil [3]; however, the measurement accuracy of the bridge method is not high owing to the high cost and susceptibility to the interference of soil temperature and conductivity [4]. Babb first studied the use of the resonance method to measure soil water content [5]. Subsequently, Hardy and Bell

and others attempted to use a high resonant frequency to improve the measurement accuracy [6, 7]. However, simply increasing the measurement frequency does not eliminate the error, and finding ways to eliminate the interference of conductance during measurement is still necessary for the capacitance method. The dielectric method, which is used to measure soil water content through the dielectric properties of soil, is the most widely used soil water content measurement technique and is mainly divided into time domain reflection (TDR), time domain transmissometry (TDT), frequency domain reflection (FDR), and standing wave rate (SWR). Fellner-Feldegg was the first to use TDR for the study of the electrical properties of liquids [8]. Topp et al. applied it to soil water content measurement and conducted related studies [9, 10]. Thereafter, the soil water content measurement based on the TDR method has been researched in depth and has been applied increasingly. The

TDR method soil water sensor is less sensitive to soil properties and external temperature changes and is the most accurate in actual measurement, but it is expensive and not suitable for large-scale promotion [11–13]. Meanwhile, research on soil water content measurement technology based on TDT and FDR is also being conducted, and related products have been developed [14–17]. Gaskin and Miller proposed the use of the SWR to measure soil water content based on electromagnetic wave theory [11, 18]. On this basis, scholars have further studied soil water content measurement based on the SWR principle and developed related sensors [4, 19–22]. SWR sensors provide fast, accurate, automated measurements with a fast dynamic response for volumetric water content measurements in many types of soil and are widely used in long-term monitoring processes in soil water networks owing to their low cost, ease of use, and low power consumption.

Because the dielectric constant of the medium can vary at different temperatures and there is also a temperature drift in the sensor hardware, the study of temperature compensation methods for soil water sensors is important in the field of soil water measurement. Some scholars have proposed optimizing the measurement results of the instrument to improve the detection accuracy [23–26]. Western and Seyfried constructed temperature-compensated calibration curves to improve the measurement accuracy by studying the relationship between temperature, soil pore space, and soil conductivity [27]. Bogena et al. studied the influence of temperature variation and conductivity on capacitive soil water sensors and developed a compensating mathematical model based on experimental results [28]. Kapilaratne and Lu proposed an automatic calibration algorithm for the TDR soil water sensor temperature to eliminate measurement errors caused by different soil types [29]. However, the related temperature compensation research is mainly focused on TDR sensors and FDR sensors, and there have been few reports on research and compensation methods for the temperature sensitivity of SWR sensors [29–32]. Therefore, in this study, a temperature compensation method for soil water measurement based on the SWR method was established by analyzing the relationship between the temperature and SWR method measurement results. The focus of this study includes (1) the development of a portable temperature-compensated standing wave rate (TCSWR) sensor for soil water, (2) the development of a mathematical model for temperature compensation, and (3) an analysis of the performance of the TCSWR sensor.

2. Materials and Methods

2.1. Experimental Site.
The indoor location is divided into an indoor laboratory and field. The indoor laboratory has a dry box (BD-200HEGW, Haier, China, −40°C to 10°C, PT100 temperature sensors (Heraeus, Germany), measuring range of −50–250°C, accuracy of ±0.1°C), high- and low-temperature alternating test chamber (GDJ-1500B, Beijing Cheek Test Equipment Co., Ltd., China, temperature control range of −40–150°C, humidity control range of 0–100% RH, temperature control accuracy of ±1.5°C, and humidity con-

trol accuracy of ±1% RH), precision electronic scale (JE-301, HEEYII, China, accuracy of 0.01 g, measurement range of 0–2500 g), and TDR soil water sensor (TRIME-HD2, IMKO, Germany, measurement accuracy 1%, measurement range 0–100%).

The field base is located at Sanqingyuan Nursery, Haidian District, Beijing, China (116° 21″ 14″ E, 40° 0″ 54″ N, altitude 52 m). The soil in the nursery was artificially placed clay loam soil with a thickness of 80 cm.

2.2. Experimental Materials.
The experimental soil samples were sandy soil (85% sand mass fraction, 10% powder mass fraction, and 5% clay mass fraction, collected from Gongqing Forestry Field, Shunyi District, Beijing, 116.73° E, 40.11° N), clay loam soil (11% sand mass fraction, 71% powder mass fraction, and 18% clay mass fraction, collected from Sanhaoyuan Nursery, Haidian District, Beijing 116.34° E, 40.00° N), and loess soil (15% sand mass fraction, 65% powder mass fraction, and 20% clay mass fraction, collected from Zhenyuan County, Qingyang City, Gansu Province 107.03° E, 35.54° N) dried in a drying oven (105° C, 48 h) and sieved using a 40-mesh sieve to obtain experimental soil samples of 50 kg for each type of soil. The soil samples were added to each volume of water and stirred for 10 min until the water was well mixed with the soil, such that the water content of the soil after the addition of water was uniform. The sample was added to a polyvinyl chloride (PVC) calibration barrel (diameter: 40 cm, height: 25 cm) and compacted with a nylon rod (diameter: 50 mm, length: 50 cm), and then, the barrel was sealed and left for 48 h until the water transport in the barrel reached equilibrium. Finally, experimental samples with different volumes of water content were obtained.

2.3. Soil Water Measurement Principle.
The TCSWR sensor uses the standing wave principle to measure the volumetric water content of soil. When the volumetric water content of the soil is different, the dielectric constant of the soil is different, and the high-frequency electromagnetic wave forms a standing wave on the transmission line because the impedance of the measurement probe does not match that of the transmission line during transmission along the coaxial transmission line [11, 18]. This in turn causes a change in the voltage at both ends of the transmission line, and the volumetric water content of the soil can be measured by detecting the change in voltage at both ends of the transmission line. The measurement principle is shown in Figure 1, where the signal source is a 100 MHz sine wave, and the characteristic impedance of the coaxial transmission line is 50 Ω. When the standing wave at both ends of the transmission line is detected and a differential signal amplifier is used for small-signal amplification, the voltage signal can be obtained, and the transmission line theory can equate Figure 1 to the total set parameter circuit shown in Figure 2 [33].

The RC parallel circuit is shown in Figure 2 as the dielectric physical model of the soil to be measured, and the expression for the instantaneous voltage $\widehat{U}(t)$ at both ends of the transmission line is
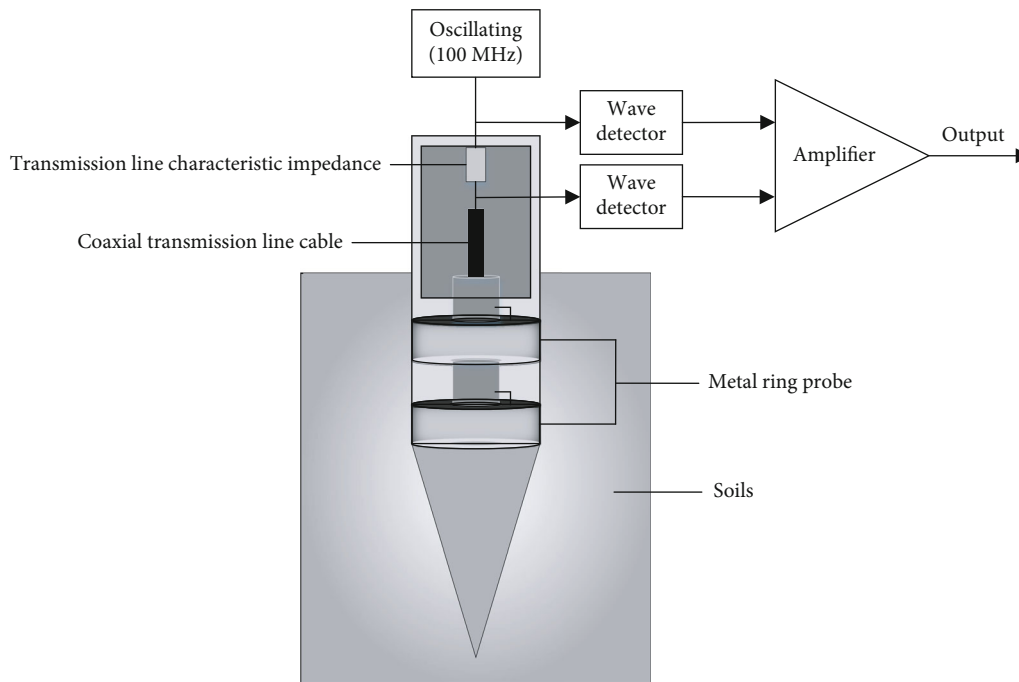
FIGURE 1: Principle diagram of soil water measurement.
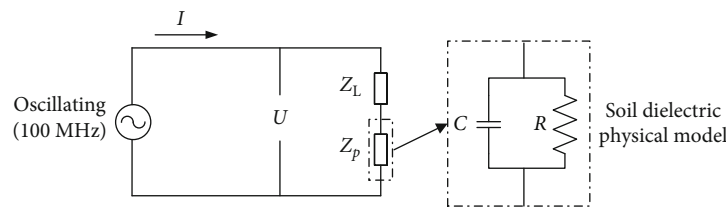
FIGURE 2: Equivalent circuit diagram, where U is the potential difference between the two ends of the transmission line, Z_P is the impedance at the measurement probe, Z_L is the characteristic impedance of the coaxial transmission line, R is the soil impedance resistance component, C is the soil impedance reactance component, and I is the current.

$$\widehat{U}(t) = A(\cos \omega t + \rho * \cos \omega(t - 2\beta)), \qquad (1)$$

where A is the voltage amplitude, ρ is the transmission line reflection coefficient, β is the phase shift constant, and ω is the angular frequency. According to Equation (1), the voltage peak of the standing wave crest $\widehat{U}_a$ and the voltage peak of the standing wave trough $\widehat{U}_b$ are

$$\begin{aligned} \widehat{U_a} &= A(1 + \rho) \\ \widehat{U_b} &= A(1 - \rho) \end{aligned} \qquad (2)$$

Therefore, the voltage difference between the two ends of transmission line U can be obtained as

$$U = \widehat{U_a} - \widehat{U_b} = 2A\rho = 2A\frac{Z_P - Z_L}{Z_P + Z_L} \qquad (3)$$

where U is the potential difference between the two ends of the transmission line, Z_P is the impedance at the measurement probe, and Z_L is the characteristic impedance of the coaxial transmission line. The voltage amplitude A and transmission line impedance Z_L are constant values, and the potential difference between the two ends of the transmission line is related only to the measurement probe impedance Z_P. The measurement probe impedance Z_P is determined by the probe size, soil dielectric constant at the measurement, and operating frequency, and the probe size and operating frequency are fixed values; i.e., different soil dielectric constants at the measurement cause the measurement probe impedance Z_P to change, which is reflected in the change in the potential difference U at the two ends of the transmission line.

2.4. TCSWR Sensor for Soil Water Measurement. The overall TCSWR sensor developed in this study consists of a water measurement cone head, connecting rod, and fixed base group length, as shown in Figure 3(a). The tapered head and connecting rod are marked with a scale to measure the insertion depth of the probe with an accuracy of 1 mm. The water measurement cone head diameter is 20 mm, and cone angle is 30°. An internal embedded PT100 temperature measurement probe is connected to the water measurement
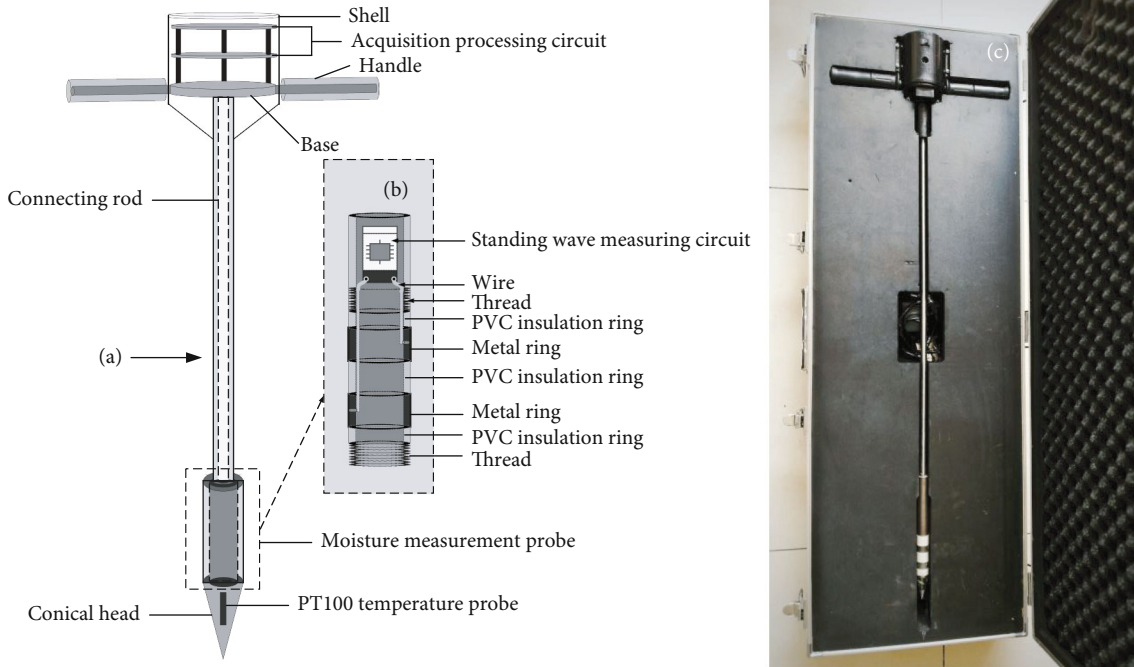
Figure 3: Assembly of a combined TCSWR probe: (a) detailed schematic diagram showing the parts of the instrument, (b) components of the double-metal-ring SWR probe, and (c) photograph of the actual physical model fabricated during the study. This figure is reproduced from Tian et al. 2019 under the Creative Commons (Attribution License).

probe using M16 thread. The water measurement cone head of the bimetallic ring SWR probe is shown in Figure 3(b). Two metal ring probes (20 mm outer diameter, 18 mm inner diameter, and 10 mm spacing) are embedded in a solid corundum column with grooves. The corundum column has M16 threads on both sides for connecting the cone head and cone rod. A water measurement probe is installed on three PVC rings (20 mm outer diameter, 18 mm inner diameter, and installation distance of 10 mm) on the metal ring probe for insulation isolation to ensure that the metal probe does not cause a short circuit between each other or with other connections. A water measurement circuit is installed in the upper part of the metal ring probe, and the circuit is waterproof, which permits the shortest coaxial transmission line and thus minimizes the impact of impedance changes around the coaxial transmission line on the measurement results. The water measurement probe has an overall length of 150 mm (60 mm long metal ring probe installation part, 90 mm long water measurement circuit installation part), a 630 mm connecting rod, and a physical sensor, as shown in Figure 3(c).

The principle block diagram of the TCSWR sensor data-processing system is shown in Figure 4, which includes the sensor acquisition motherboard, water measurement unit, temperature measurement unit, and display control unit. The corresponding printed circuit board (PCB) is shown in Figure 5. The sensor acquisition motherboard includes a data acquisition controller (STM32103RBT6, STMicroelectronics, Switzerland), analog-to-digital converter (AD623ARZ, Analog Devices Inc., USA), power control module (K7805-1000R3, DEXU Electronics, China), and clock control module (RX-8025T, Epson Toyocom, Japan). The sensor measurement motherboard includes a water measurement unit and a tem-

perature measurement unit. The water measurement unit consists of a bimetallic ring probe and standing wave measurement circuit. The temperature measurement unit consists of a PT100 measuring probe and temperature measurement circuit. The display control unit includes a display module (OLED-0.96, Telesky, China) and a keypad module (Pushbutton Switch-12 ∗ 12 ∗ 5, Telesky, China).

2.5. Calibration of TCSWR Sensor.

The TCSWR sensor was inserted into the soil sample calibration bucket, and the voltage value output by the water content measurement probe after digital-to-analog conversion was recorded as the measured voltage of the sample. Simultaneously, the samples in the calibration barrel were sampled with a ring knife (100 mL), and two ring knife drying samples were taken and dried in a drying oven (105°C) for 24 h. The volumetric water content was calculated using the drying method, and the volumetric water content of the two drying samples was averaged as the volumetric water content of the current soil sample. Experimental samples with different volumetric water contents were obtained by adding different volumes of water to the samples. Eight different volumetric water contents were configured for each soil sample, and the voltages measured by the sensors at the corresponding volumetric water contents were recorded. A linear fit was made between the voltage values and the volumetric water content, and the calibration equation was established as

$$\theta_w = k * U + b, \tag{4}$$

where θ_w is the soil volumetric water content, U is the analog voltage value output from the water measurement unit, and k and b are the calibration coefficients.
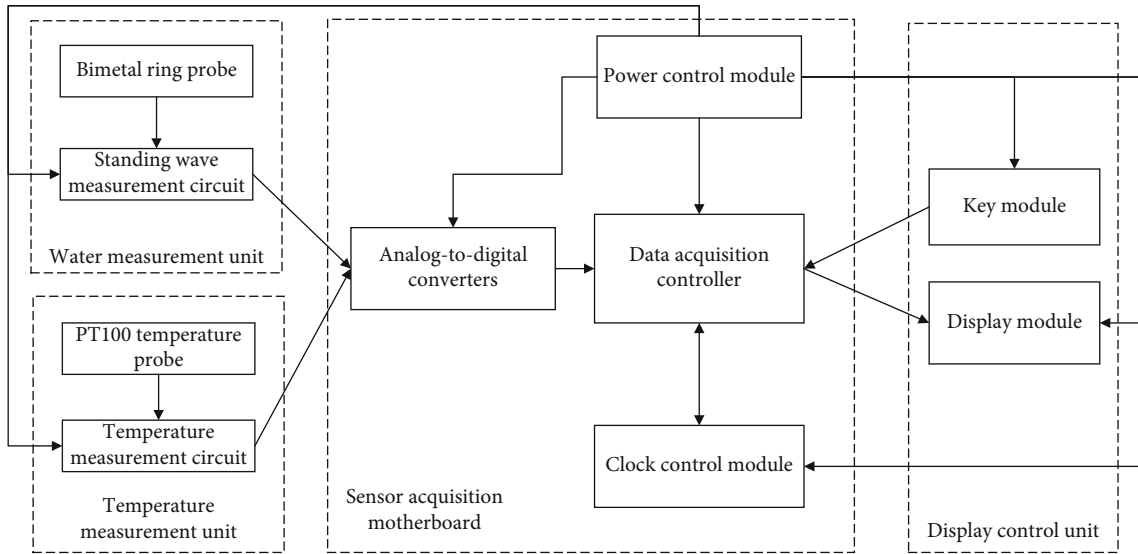
FIGURE 4: Block diagram of the TCSWR sensor system.
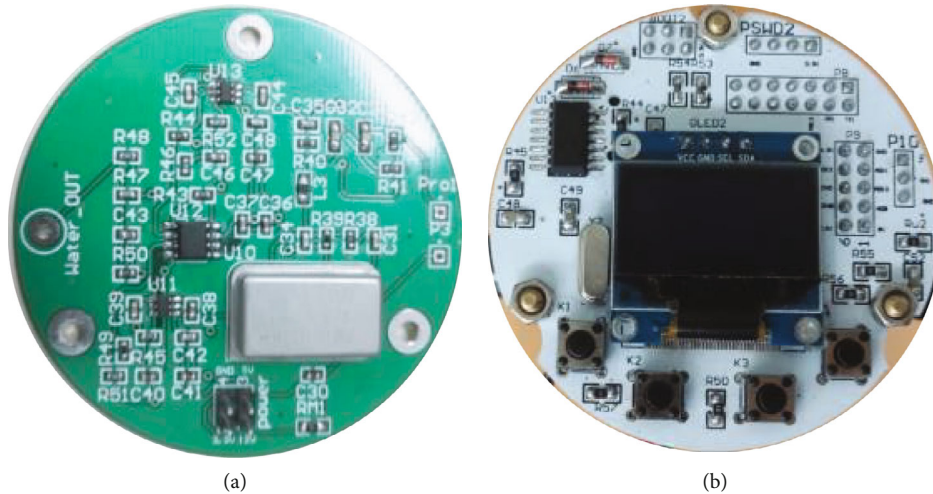
FIGURE 5: PCB of TCSWR sensor: (a) sensor measurement motherboard; (b) sensor acquisition motherboard.

2.6. Temperature Compensation Model. The TCSWR sensor was inserted into a cylindrical Plexiglas barrel and sealed with a plastic film to prevent water dissipation. The experimental sample equipped with the sensor was put into the high- and low-temperature alternating test chamber, and the initial temperature was set as 5°C, and the initial air humidity was 30%; after the soil temperature remained stable and unchanged, the temperature of the chamber was adjusted to increase by 1°C and measured continuously until the soil temperature increased to 45°C. The temperature T measured by the TCSWR sensor was recorded with the soil volumetric water content θ_w. The above experiments were repeated for samples configured with different soil volumetric water contents, as listed in Table 1; the volume of the soil sample can be known by measuring the bottom area of the Plexiglas barrel and the height of the soil sample inside the barrel, while the volumetric water content of the sample can be calculated very quickly by simply recording the volume of water added to the soil sample, and the final results

of the SWR soil water sensor measurements with soil temperature were obtained.

By analyzing the experimental data, this study established a temperature compensation model based on the least-squares curve fitting method. The soil volumetric water content parameter θ_{wt} obtained after the data fusion processing of θ_w with T can be expressed as

$$\theta_{wt} = f(\theta_w, T). \quad (5)$$

Therefore, the binary regression equation can be predetermined to calculate the volumetric water content of the soil sample as

$$\theta_{wt} = \gamma_0 + \gamma_1\theta_w + \gamma_2 T + \gamma_3\theta_w{}^2 + \gamma_4\theta_w T + \gamma_5 T^2 + \delta_0, \quad (6)$$

where γ_0, γ_1, γ_2, γ_3, γ_4, and γ_5 are constant term coefficients; δ_0 is a high-order infinitesimal; and the constant coefficients

TABLE 1: Volumetric water content of the configured soil samples.

Samples	Volumetric water content (%)							
Soil samples	7.50	12.00	18.00	21.00	23.00	26.50	28.50	31.50

are determined by least-squares approximation to fit the curve, which should minimize the error sum of squares $\|\varphi\|_2^2$, and $\|\varphi\|_2^2$ is

$$\|\varphi\|^2 = \sum_{i=1}^{m} \omega(x_i) \left[\theta_{\mathrm{wt}_i}(x_i) - \theta_{\mathrm{w}_i}\right]^2, \tag{7}$$

where i denotes different moments, m denotes the final moment, $\omega(x_i)$ is the weight function indicating that the data weights at different moment points $(x_i, \theta_{\mathrm{wt}_i}(x_i))$ are different, and θ_{w_i} is the soil volumetric water content before compensation at the corresponding moment point. Because the temperatures at different moments in the experiment are different, the measurement data at each moment are unique, and thus, $\omega(x_i) = 1$. The mean square error (MSE) is chosen as the evaluation index of the fitting effect between the calculated value of the binary regression equation and the standard value of soil volumetric water content. Then, the mean square difference between the two should be taken as the minimum, and the mean square difference is

$$I(\gamma_0, \gamma_1, \gamma_2, \gamma_3, \gamma_4, \gamma_5) = \frac{1}{m} \sum_{i=1}^{m} \sum_{j=0}^{5} \left(\gamma_j \varphi_{ij} - \theta_{\mathrm{w}_i}\right)^2, \tag{8}$$

where φ_{i0} is 1, φ_{i1} is $\theta_{\mathrm{w}i}$, φ_{i2} is T, φ_{i3} is $\theta_{\mathrm{w}i}^2$, φ_{i4} is $\theta_{\mathrm{w}i}T$, φ_{i5} is T^2, and the minimum value of Equation (7) can be converted into the problem of finding the minima of the multivariate functions. From the necessary conditions for determining the extreme value of the multivariate functions, one can obtain

$$\sum_{i=1}^{162} \left[\sum_{j=0}^{5} \gamma_j \varphi_{ij}\right] \cdot \varphi_{ij} - \sum_{i=1}^{162} \theta_i \varphi_{ij} = 0, \tag{9}$$

where 162 is the total number of experimental samples. The experimental measurement data are substituted into Equation (9), and all coefficients of the binary regression Equation (6) are obtained instantly by writing a program to solve it to obtain the temperature compensation model. Finally, we wrote the temperature compensation model into the microcontroller code of the TCSWR sensor using C language. The TCSWR sensor is able to measure the current soil temperature and soil volumetric water content (before compensation) in real time during the actual measurement, and the measurement result is substituted into the temperature compensation model in the microcontroller to calculate and output the compensated soil volumetric water content value.

2.7. Static and Dynamic Characteristic Experiments. Static characteristics indicate the input–output relationship characteristics of the sensor when the input is constant or the input changes very slowly. For the requirements of using water sensors, the static performance test of TCSWR sensors includes measurement range, measurement accuracy, stability, and resolution [34, 35]. The measurement range is obtained by calculating the range between the minimum value that the sensor can measure and the maximum value. The measurement accuracy is obtained by configuring 15 samples with different water content gradients, obtaining eight measurements for each sample, and calculating the maximum value of the measurement error. The stability is obtained by placing the sensor in a single sample, obtaining 100 consecutive measurements, and recording the sensor output. The resolution refers to the ability of the TCSWR sensor to sense the smallest change measured, and it is calculated according to the sampling accuracy of the analog-to-digital converter in the sensor.

The dynamic characteristics are the response characteristics of the sensor to the input quantity that changes with time. The process of inserting the sensor into the soil is used as the input signal, the input is a first-order step signal, and the dynamic characteristics are obtained by measuring the change in the output with the input [36, 37]. The TCSWR sensor rapidly penetrates the soil until the output is stable, the real-time measurement results are recorded, the dynamic characteristic curve is plotted, and the dynamic characteristic index of the sensor is calculated using the dynamic characteristic curve.

2.8. Soil Water Measurement Experiment. Soil water measurements were conducted in the laboratory and in the field. In the laboratory, three samples with different volumetric water contents were configured, the volumetric water contents of the configured soils were measured using TCSWR and TDR sensors, and the measurement data were recorded.

The field measurement site was at the Sanqingyuan Nursery. Seven sites were randomly selected in the nursery, and the TCSWR sensor was used to measure the volumetric water content of the soil at each site. The corresponding site was sampled and dried using a ring knife at the same time, and the corresponding volumetric water content of the soil was calculated using the drying method. The measurement performance of the sensor was verified by comparing the measurement results.

3. Results and Discussion

3.1. Calibration of TCSWR Sensor. A previously described method [33, 38] was used to obtain the linear fitting curves of the output voltage of the TCSWR sensor water measurement circuit and the volumetric water contents of the experimental soil samples, as shown in Figure 6. The coefficients of determination of the primary linear fitting curves of the sandy soil, clay loam soil, and loess soil samples were 0.95,
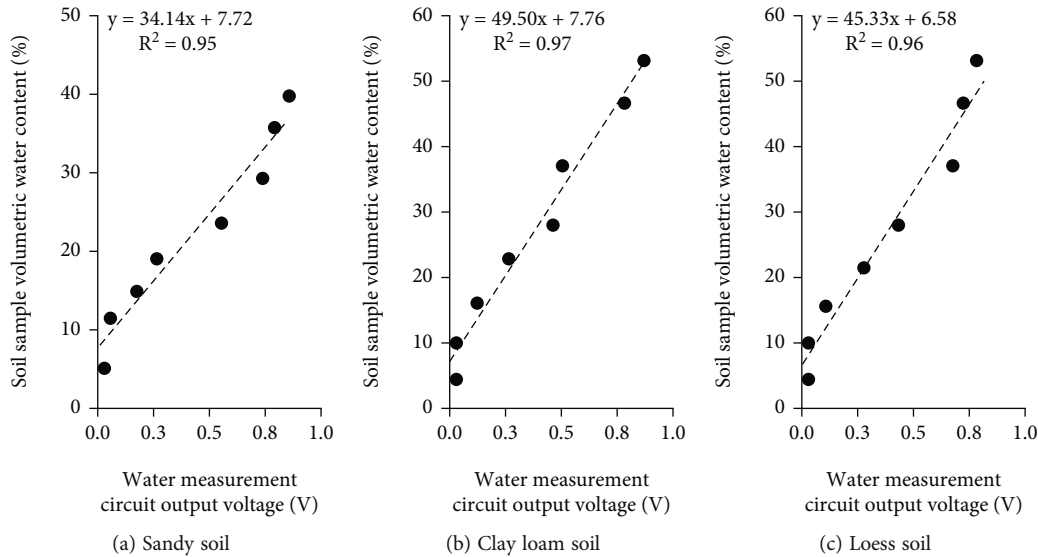
FIGURE 6: Calibration curves of the TCSWR sensor water measurement.

0.97, and 0.96, respectively, and the fitting coefficients reached more than 0.95, indicating that the volumetric water content between the voltage value and the measured sample soil had good linear relationships. Calibration coefficients for the three soils were obtained according to the fitted curve equations, where the k values were 34.14, 49.50, and 45.33, and the b values were 7.72, 7.76, and 6.58, respectively.

3.2. Effect of Temperature on Measurement Results. The variation curves of the measurement results of the TCSWR soil sensor at different temperatures are shown in Figure 7. The measurement results did not change significantly in the range of 28.50% to 31.50% of the volumetric water content of the soil. The maximum value of the variance of the measurement results was calculated to be 0.15%, and the maximum value of the mean variance was 0.39%, indicating that this TCSWR sensor can work stably and accurately at this time. While the soil volumetric water content was within 7.50% to 28.50%, the measurement results increased significantly with an increase in temperature; thus, the TCSWR sensor compensation was mainly in the range of 7.50% to 26.50% in this study. Or and Wraith suggested that water near the particle surfaces of the finer-textured soils is increasingly becoming "invisible" to the dielectric measurement because of surface forces. However, with increasing soil temperatures, these surface forces reduce in strength, thereby causing a positive relationship between water content and temperature [39]; the variation of soil volumetric water content from 7.5% to 28% in Figure 7 also supports this conclusion. Meanwhile, the dielectric constant of water decreases with increasing temperature [29, 30], and as the proportion of water contained in the soil increases, the effect of surface forces on soil particles gradually decreases, and the effect of the dielectric constant of water on the overall dielectric constant of the soil gradually increases [40]; as the temperature increases, the rate of increase in the volumetric water content of the soil shows a decrease, as evidenced by the rate of change of the curve in Figure 7; when the water in the soil is close to saturation, the effect of the dielectric constant of water on the overall dielectric constant of the soil gradually increases due to the dielectric constant which dominates the overall dielectric constant of the soil; the volumetric water content of the soil decreases slightly with increasing temperature, so the output of the sensor seems to decrease slightly with increasing temperature at 28.50% to 31.50%.

Change in temperature affects not only the dielectric constant of the soil under test but also the dielectric constant [27, 28]. They can also cause a temperature drift in the sensor hardware circuitry [41, 42]. Therefore, temperature compensation for sensor measurements must be considered from both perspectives. The output voltages of the TCSWR sensor water measurement circuit at different temperatures were recorded, and the results are shown in Figure 8. The error of the voltage value caused by the temperature change was 0.003 V. Combining the calibration coefficients k and b and substituting them in Equation (4) yield the corresponding errors of 0.10%, 0.15%, and 0.14%, which proves that the measurement error caused by the temperature drift of the TCSWR sensor hardware circuit is very small. Therefore, the temperature compensation can ignore the effect of hardware circuit temperature drift.

For the case in which the effect of hardware circuit temperature drift is ignored, the TCSWR sensor measurements at different temperatures are substituted into Equation (9), and all coefficients of the binary regression Equation (6) can be obtained by writing a MATLAB program to solve it. The temperature compensation model is obtained as in Equation (10), and the coefficient of determination R^2 of the fitted curve is 0.998, which is in good agreement. The significance level is 0.05, indicating that the temperature compensation model is reliable.

$$\theta_{wt} = 0.92153\theta_w - 0.17341T - 0.00124\theta_w{}^2 + 0.00509\theta_w T$$
$$+ 0.00007T^2 + 3.78133.$$

$$(10)$$

(a) Sandy soil   (b) Clay loam soil   (c) Loess soil
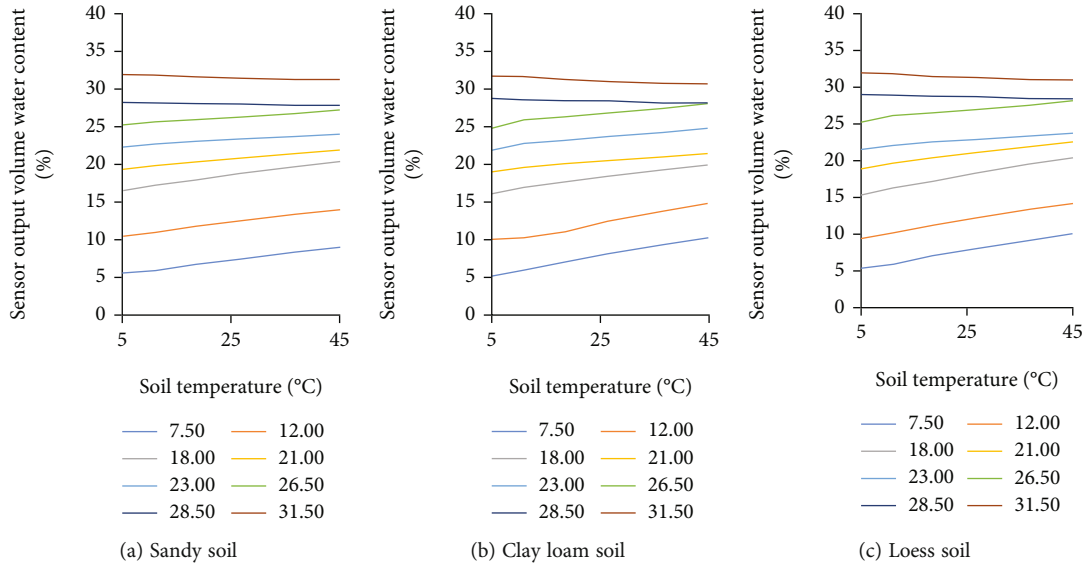
Figure 7: Variation curves of measurement results of TCSWR soil sensors at different temperatures.
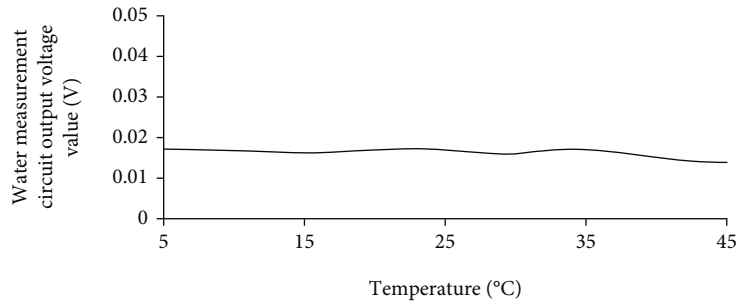
Figure 8: Temperature drift characteristic curve of TCSWR sensor hardware circuit.

At the same time, we write the temperature compensation model (Equation (10)) into the microcontroller code of the TCSWR sensor in C language, which enables the TCSWR sensor to calculate and output the compensated soil volumetric water content value in real time during the field measurement.

3.3. Soil Water Measured by TCSWR Sensor after Temperature Compensation.

The results of the soil volumetric moisture content measured by the TCSWR sensor after the temperature compensation model are shown in Figure 9; it can be seen that the volatility of the soil moisture content measured by the TCSWR sensor with temperature changes is significantly reduced after the temperature compensation. Zheng et al. proposed to use the sensitivity temperature coefficient to measure the degree of influence of the sensor measurement value by temperature [43], and it is calculated that the average sensitivity temperature coefficient of the TCSWR sensor measurement result is reduced from 4.1059×10^{-2}%/°C to 1.3933×10^{-2}%/°C before the compensation, which proves that the temperature sensitivity of the sensor is significantly reduced after the temperature compensation.

The mean absolute error (MAE) and MSE of the measurement results before and after compensation were calcu-

lated using the temperature compensation model for the TCSWR sensor measurement results. The results are shown in Table 2, which reveals that the MAE and MSE were significantly reduced after compensation, proving that compensation can greatly reduce measurement error and improve measurement accuracy [30, 32].

For the temperature compensation of SWR soil water sensor, Kapilaratne and Lu designed an automatic temperature correction algorithm to remove the rain effect from SWC data by combining statistical inference techniques with temperature correction algorithm [29]. Zhao et al. studied the temperature drift characteristics of a 4-probe-type SWR soil water sensor and established a corresponding temperature compensation [44]. However, the above temperature compensation schemes are all postcompensation on the computer software after obtaining the measurement results; TCSWR sensor can get the compensated soil water measurement results in real time in the field measurement by building the temperature compensation model into the microcontroller code, which is more convenient for field application and saves manpower [30–32].

3.4. Analysis of Static and Dynamic Characteristics of TCSWR Sensors.

The sensor measurement range is between the minimum and maximum values that the sensor can

(a) Sandy soil   (b) Clay loam soil   (c) Loess soil
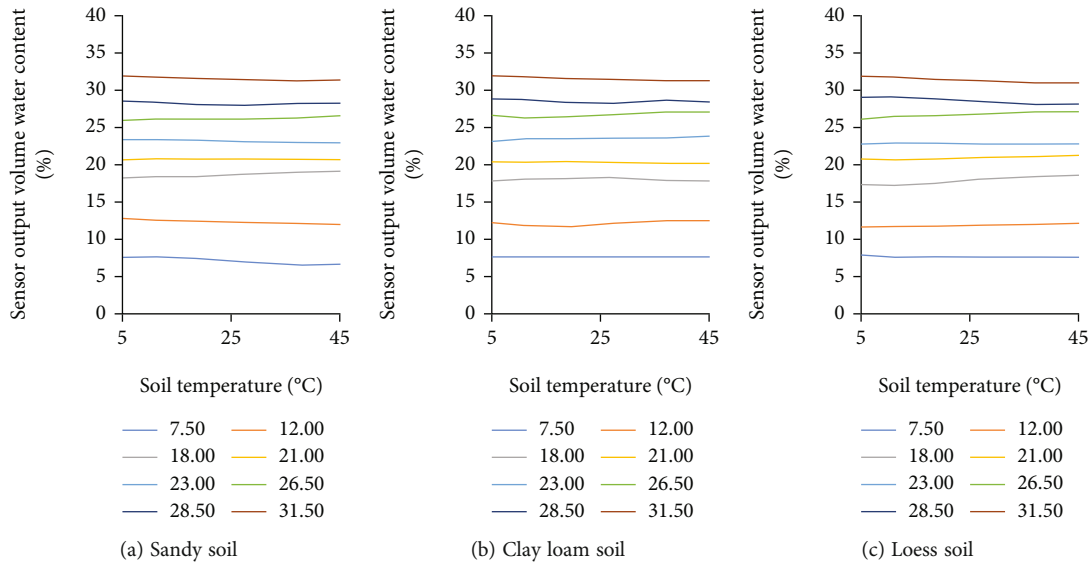
FIGURE 9: Variation curves of measurement results of TCSWR soil sensors at different temperatures after temperature compensation.

TABLE 2: Comparison of temperature compensation effects.

Temperature compensation	Soil samples	Indicators	Soil volumetric water content (%)					
			7.50	12.00	18.00	21.00	23.00	26.50
Before compensation	Sandy soil	MAE	1.03	1.04	1.17	0.74	0.47	0.53
		MSE	0.40	0.40	0.46	0.29	0.18	0.21
	Clay loam soil	MAE	1.48	1.45	0.80	0.79	0.84	0.82
		MSE	0.56	0.54	0.31	0.33	0.33	0.33
	Loess soil	MAE	1.37	1.33	1.45	0.96	0.57	0.78
		MSE	0.52	0.51	0.55	0.38	0.23	0.31
After compensation	Sandy soil	MAE	0.54	0.33	0.63	0.24	0.23	0.26
		MSE	0.22	0.13	0.23	0.08	0.10	0.09
	Clay loam soil	MAE	0.11	0.35	0.25	0.65	0.54	0.42
		MSE	0.04	0.13	0.11	0.22	0.19	0.18
	Loess soil	MAE	0.14	0.18	0.58	0.25	0.17	0.44
		MSE	0.06	0.07	0.22	0.10	0.06	0.18

measure [34, 35]. The TCSWR sensor measures the volumetric water content of the soil. The sensor output is 0% (empty load under ideal conditions) when the sensor is placed in air and 100% (full-scale range under ideal conditions) when the sensor is placed in water. The volumetric water content of the soil becomes larger with the sensor measurement value becomes linearly larger; and the soil moisture measured in the experiment in this paper is 7.5%-31.5%; thus, the measurement range of the sensor is 7.5%-31.5%. Using the samples with different water content gradients, multiple measurements were made, and the maximum value of the error was calculated to be 1.26%; thus, the sensor measurement accuracy was ±0.63%. Stability experiments for multiple measurements of the same sample were performed, and the measurement results are shown in Figure 10. In the measured data, the maximum volumetric water content was 25.68%, the minimum volumetric water content was 23.74%, and the standard deviation was 0.49%. The stability of the sensor output was good, and it could be used for repeated measurements. The TCSWR sensor is based on

the standing wave principle of the water content detection circuit. The standing wave at both ends of the transmission line is detected and then amplified through an amplifier to output an analog voltage signal. Then, the volumetric water content of the soil is obtained through the AD sampling module for voltage acquisition and processing; thus, the resolution of the sensor is determined by the sampling accuracy of the analog-to-digital converter. The sampling accuracy of the analog-to-digital converter is 0.8 mV, corresponding to a resolution of 0.05%. At the same time, the dynamic response of the sensor is determined by the sensor itself, and the transition time of the TCSWR sensor is 0.58 s as calculated by the dynamic characteristic test; this shows that the dynamic response of the sensor is fast and can meet the actual demand.

3.5. Measurement Performance Verification of TCSWR Sensor. The TDR sensor and TCSWR sensor were used to measure the soil samples with different volumes of water content configured in the laboratory, and the measurement
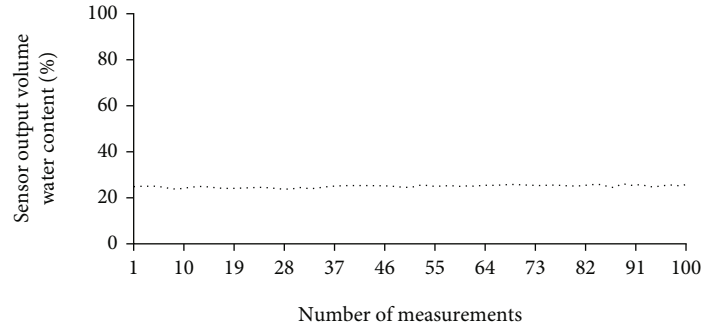
FIGURE 10: Variation curve of multiple measurements of the TCSWR sensor for a single sample.

TABLE 3: Comparison of measurement results.

Soil samples	Sensor type	Soil volumetric water content (%)						
Sandy soil	TDR	7.26	10.74	14.89	17.12	20.89	26.40	30.11
	TCSWR	7.86	11.11	14.10	16.74	20.53	25.57	30.33
	Absolute errors	0.60	0.37	0.79	0.38	0.36	0.83	0.22
Clay loam soil	TDR	6.57	9.18	16.63	22.34	25.07	28.52	32.14
	TCSWR	6.26	10.07	16.10	21.62	25.43	28.40	31.89
	Absolute errors	0.31	0.89	0.53	0.72	0.36	0.12	0.25
Loess soil	TDR	6.96	12.61	14.82	17.41	20.68	26.44	33.31
	TCSWR	7.37	11.84	13.92	16.48	21.12	27.36	33.85
	Absolute errors	0.41	0.77	0.90	0.93	0.44	0.92	0.54

SWR
Drying method
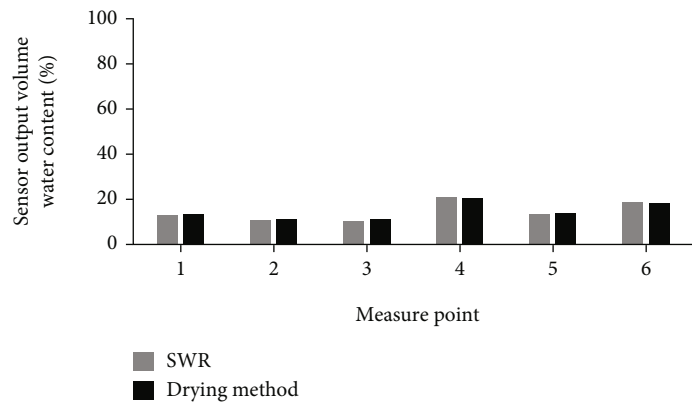
FIGURE 11: Comparison of measurement results of field experiments.

results are compared in Table 3. The absolute error between the TCSWR and TDR sensor measurement results is 0.93% at most. The absolute error is less than 1%, indicating that the accuracy of TCSWR and TDR sensor measurements is comparable and meets practical application requirements [45].

In the outdoor experiment, measurements were performed at seven randomly selected locations in the nursery. The volumetric water content of the soil measured using the TCSWR sensor and the drying method is shown in Figure 11; then, the decision error of the TCSWR sensor and drying method measurement results was calculated (Table 4); the maximum absolute error is 0.98% (measurement point 3) and is less than 1%; this meets the actual

requirements of soil water content measurement. Furthermore, the volumetric water content of the soil varied greatly from site to site. The analysis showed that the difference in volumetric water content was caused by the plants planted at the randomly selected sites and by whether the site had been irrigated recently. Based on the observation of the actual sample sites, sites 4 and 6 were recently irrigated, so the volumetric water content was obviously high. Sites 2 and 3 were sample sites without any plants, so the water content was the lowest. Site 1 was a lawn, and site 5 was an apple tree sample site, and the volumetric water content was slightly higher than that for sites 2 and 3. This proves that plants have a role in maintaining the soil water content and water conservation [46–48]. The soil volumetric water

Table 4: Absolute errors of measurement results of TCSWR sensor and drying method.

Measurement point	TCSWR (%)	Drying method (%)	Absolute errors (%)
1	12.7	13.22	0.52
2	10.2	10.94	0.74
3	9.8	10.78	0.98
4	21	20.3	0.7
5	12.9	13.26	0.36
6	18.4	17.92	0.48

content of sites 4 and 6 was about 9% higher than that of sites 2 and 3, while the soil volumetric water content of sites 1 and 5 was only about 3% higher than that of sites 2 and 3, indicating that irrigation can significantly increase the water content of the soil and providing support for the need for irrigation in agricultural production [49, 50].

3.6. Potential Limitations. In the calibration of the TCSWR sensor and establishment of a temperature compensation model, because of the limitation of the soil samples available in the laboratory, only sandy soil, clay loam, and loess were calibrated when establishing the temperature compensation model. Through the performance analysis of the TCSWR sensor and a comparison of similar sensors, the results show that the TCSWR sensor with temperature compensation is a low-cost soil water measurement sensor; however, to make the TCSWR sensor applicable to various types of soil with complex soil types, it is necessary to collect abundant soil texture samples for experiments to improve the accuracy of the temperature compensation model.

4. Conclusions

The measurement results of the TCSWR sensor were analyzed under different temperatures and soil volumetric water contents. A temperature compensation method was established for the TCSWR sensor to advance the development of SWR soil water sensors. A portable tapered TCSWR sensor with built-in temperature compensation model was developed on this basis. The calibration results showed that the standing wave measurement circuit designed in this study could effectively respond to the variation in water within the soil, and the coefficient of the fitted equation exceeded 0.95. When the possible influence of temperature was addressed, it was found that the measurement error caused by the temperature drift of the hardware circuit was small. The static and dynamic characteristics of the TCSWR sensor showed that the measurement range was 7.50%-31.50%, the measurement accuracy was ±0.63%, the stability was good, the resolution was a minimum of 0.05%, and the dynamic response time was less than 1 s, which can meet the experimental requirements. In comparison with the internationally recognized TDR water content sensor and drying method measurement results, the absolute measurement error was less than 1%, demonstrating that the measurement results of the TCSWR sensor are reliable. It is

also possible to combine TCSWR sensors with smart internet of things and artificial intelligence algorithms [51–54] to study soil water prediction problems at different time scales [55–57] and can be applied to other engineering systems in combination with environmental parameters [58–60].

Data Availability

The data used to support the findings of this study are available from the corresponding author upon request.

Conflicts of Interest

The authors declare no conflicts of interest.

Authors' Contributions

The work was designed and planned by Hao Tian. The experiments were conducted and data were acquired by Hao Tian and Tao Xie. Data were interpreted by Hao Tian, Tong Zheng, and Mei Sun. The paper was written by Hao Tian and reviewed by Chongchong Yu. All authors read and approved the final manuscript.

Acknowledgments

References

[1] H. Eller and A. Denoth, "A capacitive soil moisture sensor," *Journal of Hydrology*, vol. 185, no. 1-4, pp. 137–146, 1996.

[2] S. L. Su, D. N. Singh, and M. S. Baghini, "A critical review of soil moisture measurement," *Measurement*, vol. 54, pp. 92–105, 2014.

[3] A. B. C. Anderson, "A method of determining soil-moisture content based on the variation of the electrical capacitance of soil, at a low frequency, with moisture content," *Soil Science*, vol. 56, no. 1, pp. 29–42, 1943.

[4] D. Wobschall, "A frequency shift dielectric soil moisture sensor," *IEEE Transactions on Geoscience Electronics*, vol. 16, no. 2, pp. 112–118, 1978.

[5] A. T. S. Babb, "A radio-frequency electronic moisture meter," *Analyst*, vol. 76, no. 898, pp. 12–18, 1951.

[6] J. R. Hardy, *Survey of methods for the determination of soil moisture content by remote sensing methods*, Balkema, 1980.

[7] J. P. Bell, T. J. Dean, and M. G. Hodnett, "Soil moisture measurement by an improved capacitance technique, part II. Field techniques, evaluation and calibration," *Journal of Hydrology*, vol. 93, no. 1-2, pp. 79–90, 1987.

[8] H. Fellner-Feldegg, "Measurement of dielectrics in the time domain," *The Journal of Physical Chemistry*, vol. 73, no. 3, pp. 616–623, 1969.

[9] G. C. Topp, G. St-Amour, B. A. Compton, and J. Caron, "Measuring cone resistance and water content with a TDR-

penetrometer combination," in *Proc 3rd East Canada Soil Struct Work*, pp. 21-22, 1996.

[10] G. C. Topp, J. L. Davis, and A. P. Annan, "Electromagnetic determination of soil water content: measurements in coaxial transmission lines," *Water Resources Research*, vol. 16, no. 3, pp. 574–582, 1980.

[11] G. J. Gaskin and J. D. Miller, "Measurement of soil water content using a simplified impedance measuring technique," *Journal of Agricultural Engineering Research*, vol. 63, no. 2, pp. 153–159, 1996.

[12] P. A. Ferré, J. D. Redman, D. L. Rudolph, and R. G. Kachanoski, "The dependence of the electrical conductivity measured by time domain reflectometry on the water content of a sand," *Water Resources Research*, vol. 34, no. 5, pp. 1207–1213, 1998.

[13] S. J. Zegelin, I. White, and D. R. Jenkins, "Improved field probes for soil water content and electrical conductivity measurement using time domain reflectometry," *Water Resources Research*, vol. 25, no. 11, pp. 2367–2376, 1989.

[14] R. C. Harlow, E. J. Burke, and T. P. A. Ferré, "Measuring water content in saline sands using impulse time domain transmission techniques," *Vadose Zone Journal*, vol. 2, no. 3, pp. 433–439, 2003.

[15] R. Zheng, Z. Li, and Y. Gong, "Measurement of soil water content for different soil types by using time domain transmission technology," *Transactions of the Chinese Society of Agricultural Engineering*, vol. 25, pp. 8–13, 2009.

[16] S. Dey, P. Kalansuriya, and N. C. Karmakar, "A novel time domain reflectometry based chipless RFID soil moisture sensor," in *2015 IEEE MTT-S Int Microw Symp*, pp. 1–4, 2015.

[17] E. R. Ojo, P. R. Bullock, J. L'Heureux, J. Powers, H. McNairn, and A. Pacheco, "Calibration and evaluation of a frequency domain reflectometry sensor for real-time soil moisture monitoring," *Vadose Zone Journal*, vol. 14, no. 3, 2015.

[18] J. D. Miller, G. J. Gaskin, and H. A. Anderson, "From drought to flood: catchment responses revealed using novel soil water probes," *Hydrological Processes*, vol. 11, pp. 533–541, 1997.

[19] Z. Yandong and W. Yiming, "Study on the measurement of soil water content based on the principle of standing-wave ratio," *Transactions of the Chinese Society for Agricultural Machinery*, vol. 33, pp. 109–111, 2002.

[20] X. Yan, Y. Zhao, Q. Cheng, X. Zheng, and Y. Zhao, "Determining forest duff water content using a low-cost standing wave ratio sensor," *Sensors*, vol. 18, no. 2, p. 647, 2018.

[21] S. Manatrinon, W. Chantaweesomboon, J. Chinrungrueng, and K. Kaemarungsi, "Moisture sensor based on standing wave ratio for agriculture industry," in *2016 7th Int Conf Inf Commun Technol Embed Syst*, pp. 51–56, 2016.

[22] J. Behari, "Measurement of soil water content," *Microwave Dielectric Behavior of Wet Soils*, pp. 41–65, 2005.

[23] K. Roth, R. Schulin, H. Flühler, and W. Attinger, "Calibration of time domain reflectometry for water content measurement using a composite dielectric approach," *Water Resources Research*, vol. 26, no. 10, pp. 2267–2273, 1990.

[24] E. Kellner and L.-C. Lundin, "Calibration of time domain reflectometry for water content in peat soil," *Hydrology Research*, vol. 32, no. 4-5, pp. 315–332, 2001.

[25] C. H. Roth, M. A. Malicki, and R. Plagge, "Empirical evaluation of the relationship between soil dielectric constant and volumetric water content as the basis for calibrating soil mois-

[26] ture measurements by TDR," *Journal of Soil Science*, vol. 43, no. 1, pp. 1–13, 1992.

[26] S. Pepin, N. J. Livingston, and W. R. Hook, "Temperature-dependent measurement errors in time domain reflectometry determinations of soil water," *Soil Science Society of America Journal*, vol. 59, no. 1, pp. 38–43, 1995.

[27] A. W. Western and M. S. Seyfried, "A calibration and temperature correction procedure for the water-content reflectometer," *Hydrological Processes: An International Journal*, vol. 19, no. 18, pp. 3785–3793, 2005.

[28] H. R. Bogena, J. A. Huisman, C. Oberdörster, and H. Vereecken, "Evaluation of a low-cost soil water content sensor for wireless network applications," *Journal of Hydrology*, vol. 344, no. 1-2, pp. 32–42, 2007.

[29] R. G. C. J. Kapilaratne and M. Lu, "Automated general temperature correction method for dielectric soil moisture sensors," *Journal of Hydrology*, vol. 551, pp. 203–216, 2017.

[30] L. Yu, W. Gao, R. R. Shamshiri et al., "Review of research progress on soil moisture sensor technology," *International Journal of Agricultural and Biological Engineering*, vol. 14, no. 3, pp. 32–42, 2021.

[31] F. Kizito, C. S. Campbell, G. S. Campbell et al., "Frequency, electrical conductivity and temperature analysis of a low-cost capacitance soil moisture sensor," *Journal of Hydrology*, vol. 352, no. 3-4, pp. 367–378, 2008.

[32] M. J. Oates, A. Fernández-López, M. Ferrández-Villena, and A. Ruiz-Canales, "Temperature compensation in a low cost frequency domain (capacitance based) soil moisture sensor," *Agricultural Water Management*, vol. 183, pp. 86–93, 2017.

[33] W. Yiming and Z. Yandong, "Study on the measurement of soil water content based on the principle of standing wave ratio," in *Beijing Proceeding Int Conf Agric Eng*, 1999.

[34] R. E. Yoder, D. L. Johnson, J. B. Wilkerson, and D. C. Yoder, "Soilwater sensor performance," *Applied Engineering in Agriculture*, vol. 14, no. 2, pp. 121–133, 1998.

[35] B. G. Leib, J. D. Jabro, and G. R. Matthews, "Field evaluation and performance comparison of soil moisture sensors," *Soil Science*, vol. 168, no. 6, pp. 396–408, 2003.

[36] C. Luo, H. Wang, D. Zhang et al., "Analytical evaluation and experiment of the dynamic characteristics of double-thimble-type fiber Bragg grating temperature sensors," *Micromachines*, vol. 12, p. 16, 2021.

[37] M. Y. Doghmane, F. Lanzetta, and E. Gavignet, "Dynamic characterization of a transient surface temperature sensor," *Procedia Engineering*, vol. 120, pp. 1245–1248, 2015.

[38] J. D. González-Teruel, R. Torres-Sánchez, P. J. Blaya-Ros, A. B. Toledo-Moreo, M. Jiménez-Buendía, and F. Soto-Valles, "Design and calibration of a low-cost SDI-12 soil moisture sensor," *Sensors*, vol. 19, no. 3, p. 491, 2019.

[39] D. Or and J. M. Wraith, "Temperature effects on soil bulk dielectric permittivity measured by time domain reflectometry: a physical model," *Water Resources Research*, vol. 35, no. 2, pp. 371–383, 1999.

[40] Z. Huan, H. Wang, C. Li, and C. Wan, "The soil moisture sensor based on soil dielectric property," *Personal and Ubiquitous Computing*, vol. 21, no. 1, pp. 67–74, 2017.

[41] J. Cao, J.-W. Zhang, and L.-P. Sun, "Dynamic compensation method on temperature drift in Pt-resistance temperature online measuring system," in *2005 Int Conf Mach Learn Cybern*, pp. 1249–1255, 2005.

[42] M. R. Valero, S. Celma, B. Calvo, and N. Medrano, "CMOS voltage-to-frequency converter with temperature drift compensation," *IEEE Transactions on Instrumentation and Measurement*, vol. 60, no. 9, pp. 3232–3234, 2011.

[43] Z. H. E. N. G. B-R, W. Xue, C. Zhou, and M. Zhang, "Sensitivity temperature coefficient compensation based on pressure sensor integrated constant current," *China Mechanical Engineering*, vol. 21, p. 800, 2010.

[44] Y. Zhao, Z. Chen, Z. Gao, X. Zhang, and M. Yu, "Temperature drift characteristics and compensation of SWR soil moisture sensor," *Transations of the Chinese Society of Agricultural Machinery*, vol. 50, no. 8, pp. 257–263, 2019.

[45] O. Adeyemi, T. Norton, I. Grove, and S. Peets, "Performance evaluation of three newly developed soil moisture sensors," in *Proc CIGR-AgEng Conf Aarhus*, pp. 26–29, Denmark, 2016.

[46] F. J. Veihmeyer and A. H. Hendrickson, "Soil moisture in relation to plant growth," *Annual review of plant physiology*, vol. 1, no. 1, pp. 285–304, 1950.

[47] J. Sardans and J. Peñuelas, "Plant-soil interactions in Mediterranean forest and shrublands: impacts of climatic change," *Plant and Soil*, vol. 365, no. 1-2, pp. 1–33, 2013.

[48] J. R. R. Hernández, J. N. Pedreño, and I. G. Lucas, "Evaluation of plant waste used as mulch on soil moisture retention," *Spanish Journal of Soil Science: SJSS*, vol. 6, pp. 133–144, 2016.

[49] R. R. Manda, V. A. Addanki, and S. Srivastava, "Role of drip irrigation in plant health management, its importance and maintenance," *Plant Archives*, vol. 21, Suppliment-1, pp. 1294–1302, 2021.

[50] M. Giordano, R. Namara, and E. Bassini, *The impacts of irrigation: a review of published evidence*, The World Bank, 2019.

[51] J. Kong, C. Yang, J. Wang et al., "Deep-stacking network approach by multisource data mining for hazardous risk identification in IoT-based intelligent food management systems," *Computational Intelligence and Neuroscience*, vol. 2021, Article ID 1194565, 16 pages, 2021.

[52] Y.-Y. Zheng, J.-L. Kong, X.-B. Jin, X.-Y. Wang, T.-L. Su, and M. Zuo, "CropDeep: the crop vision dataset for deep-learning-based classification and detection in precision agriculture," *Sensors*, vol. 19, no. 5, p. 1058, 2019.

[53] X.-B. Jin, W.-Z. Zheng, J.-L. Kong et al., "Deep-learning forecasting method for electric power load via attention-based encoder-decoder with bayesian optimization," *Energies*, vol. 14, no. 6, p. 1596, 2021.

[54] X.-B. Jin, W.-Z. Zheng, J.-L. Kong et al., "Deep-learning temporal predictor via bidirectional self-attentive encoder–decoder framework for IOT-based environmental sensing in intelligent greenhouse," *Agriculture*, vol. 11, no. 8, p. 802, 2021.

[55] X.-B. Jin, W.-T. Gong, J.-L. Kong, Y.-T. Bai, and T.-L. Su, "PFVAE: a planar flow-based variational auto-encoder prediction model for time series data," *Mathematics*, vol. 10, no. 4, p. 610, 2022.

[56] X.-B. Jin, W.-T. Gong, J.-L. Kong, Y.-T. Bai, and T.-L. Su, "A variational Bayesian deep network with data self-screening layer for massive time-series data forecasting," *Entropy*, vol. 24, no. 3, p. 335, 2022.

[57] X. Jin, J. Zhang, J. Kong, T. Su, and Y. Bai, "A reversible automatic selection normalization (RASN) deep network for predicting in the smart agriculture system," *Agronomy*, vol. 12, no. 3, p. 591, 2022.

[58] J. Kong, C. Yang, Y. Xiao, S. Lin, K. Ma, and Q. Zhu, "A graph-related high-order neural network architecture via feature aggregation enhancement for identification application of diseases and pests," *Computational Intelligence and Neuroscience*, vol. 2022, Article ID 4391491, 16 pages, 2022.

[59] J. Kong, H. Wang, C. Yang, X. Jin, M. Zuo, and X. Zhang, "A spatial feature-enhanced attention neural network with high-order pooling representation for application in pest and disease recognition," *Agriculture*, vol. 12, no. 4, p. 500, 2022.

[60] J. Kong, H. Wang, X. Wang, X. Jin, X. Fang, and S. Lin, "Multistream hybrid architecture based on cross-level fusion strategy for fine-grained crop species recognition in precision agriculture," *Computers and Electronics in Agriculture*, vol. 185, article 106134, 2021.

Retraction

Retracted: Stress Analysis of Concrete Materials Based on Finite Element Analysis

Journal of Sensors

This article has been retracted by Hindawi following an investigation undertaken by the publisher [1]. This investigation has uncovered evidence of one or more of the following indicators of systematic manipulation of the publication process:

(1) Discrepancies in scope

(2) Discrepancies in the description of the research reported

(3) Discrepancies between the availability of data and the research described

(4) Inappropriate citations

(5) Incoherent, meaningless and/or irrelevant content included in the article

(6) Manipulated or compromised peer review

The presence of these indicators undermines our confidence in the integrity of the article's content and we cannot, therefore, vouch for its reliability. Please note that this notice is intended solely to alert readers that the content of this article is unreliable. We have not investigated whether authors were aware of or involved in the systematic manipulation of the publication process.

Wiley and Hindawi regrets that the usual quality checks did not identify these issues before publication and have since put additional measures in place to safeguard research integrity.

We wish to credit our own Research Integrity and Research Publishing teams and anonymous and named external researchers and research integrity experts for contributing to this investigation.

The corresponding author, as the representative of all authors, has been given the opportunity to register their agreement or disagreement to this retraction. We have kept a record of any response received.

References

[1] R. Yang and S. Yuan, "Stress Analysis of Concrete Materials Based on Finite Element Analysis," *Journal of Sensors*, vol. 2022, Article ID 1826598, 11 pages, 2022.

Research Article

Stress Analysis of Concrete Materials Based on Finite Element Analysis

Rui Yang [ID] **and Shengli Yuan**

Department of Civil Engineering and Architecture, Xinxiang University, 453000 Xinxiang, China

Correspondence should be addressed to Rui Yang; yangrui01@xxu.edu.cn

China's construction industry standard "technical code for concrete special-shaped column structure" has been implemented since 2006, and the use of special-shaped walls in the actual construction of buildings is more common. The cross-section wall can effectively reduce the protruding angle of the building, thereby expanding the effective building area of the room, reducing the proportion of the building components themselves, and making the structure layout of the building more beautiful. In order to analyze the dynamic characteristics of eccentrically compressed prestressed concrete beams, the finite element simulation of different reinforcement parameters, longitudinal reinforcement diameter, and reinforcement ratio was constructed. Through comparison, the load flexibility curve change law of concrete stress cloud and reinforcement stress cloud under various working conditions and the influence change law of test mold are studied, and the influence change law of dynamic characteristics under the above four conditions and unidirectional bias pressure is clarified.

1. Introduction

Concrete is a composite material widely used in the construction industry and other fields. For a long time, scientists and engineers have conducted a systematic research on all aspects of condensing ten materials. However, concrete is traditionally regarded as a uniform material, mainly by studying the macroscopic properties of materials. Since the middle of the last century, the micromechanics has provided a necessary theoretical basis to explore the essential characteristics of concrete materials from the fine view and from the microscopic level. Advanced experimental instruments help us to further understand the paper formation and internal structure of condensing ten materials. In the past ten years, the computer bin and the computing speed make the numerical method become an important means to analyze the characteristics of concrete materials. Therefore, it is of theoretical and practical significance to study the characteristics of concrete materials from the fine view or micro-level [1].

Columns with unconventional cross-section types usually have T-shaped, L-shaped and cross-shaped cross-section types, and the length to thickness ratio of the column limb shall not exceed four [1]. The main section types are shown in Figure 1. People can not only learn from it but also be different from each other through its use [2].

With the promulgation of China's "technical code for concrete special-shaped column structure" in 2006, the application of special-shaped beam structure in actual construction is more common. The utilization characteristics, design aesthetic rationality, and excellent bearing characteristics of the reinforced concrete special-shaped column structure are organically integrated to create a perfect indoor environment for modern consumers. It conforms to the characteristics of room design and is reasonably connected with the wall (refer to infilled wall), which is sought after by real estate developers and many consumer groups. In recent years, there is a wide application of reinforced concrete special-shaped columns in the actual building construction system [3].

(a) L-shaped column

(b) T-shaped column

(c) Cruciform column
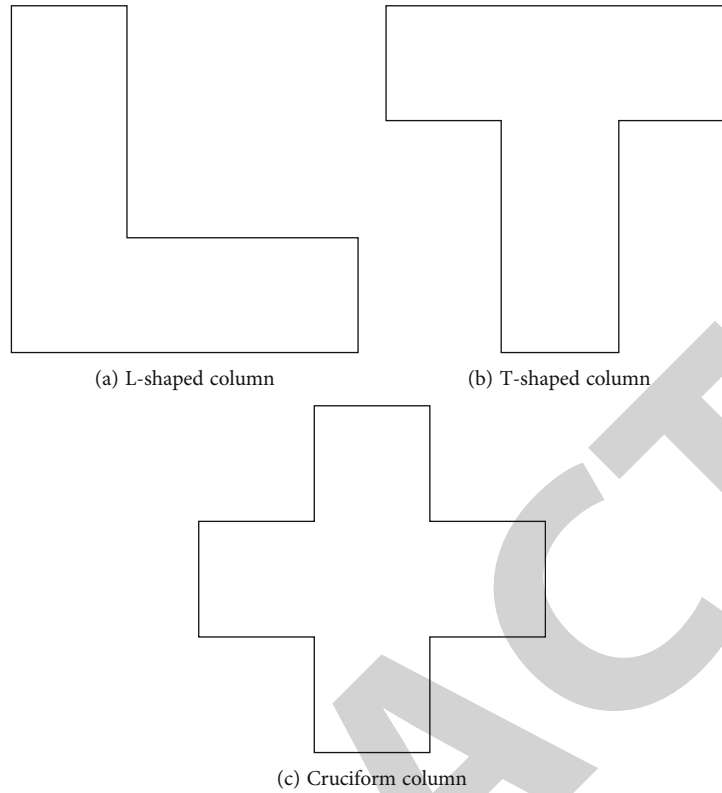
FIGURE 1: Section style of shaped column.

The special-shaped wall frame system includes the cast in situ reinforced large-diameter concrete special-shaped wall frame and special-shaped column frame shear wall system used for light infilled walls and partitions. The reinforced concrete special-shaped column structure system is a special engineering structure system produced in the process of modern building structure design and construction in China, which makes the development and research of the reinforced concrete special-shaped column structure system in China ahead of the world [4]. Since the in-depth research on the technical system of reinforced concrete special-shaped column structure, considerable progress has also been made. For example, at present, the national research and development of the reinforced concrete special-shaped column structure system focuses on the fact that experts have carried out a lot of relevant experimental research and development work on the reinforced concrete special-shaped column structure, and for the corresponding regional-reinforced concrete special-shaped columns, they also put forward suggestions and opinions for the local technical standards of reinforced concrete special-shaped columns, for example, the industrial standard of Liaoning Province Technical Specification for reinforced concrete special-shaped column structure [5].

The research on the structural system of special-shaped reinforced concrete columns in China is very different from that in China. For example, the foreign research focuses on the offset, while the domestic research focuses on the earthquake resistance. At the same time, because of the existence of multiple limbs, the special-shaped column also has the problem of geometric asymmetry, resulting in the obvious brittleness of the structure of the concrete special-shaped column, and the deformation energy of the special-shaped column is weaker than that of the general rectangular column. Although there are the above problems in the special-shaped wall section column, based on the current design specifications of China, some places with relatively low seismic stiffness and meeting the corresponding height width ratio and elevation conditions can still be used in the actual construction. In the normal application of special-shaped columns, the probability of fracture caused by seismic effect is very small, so it is very important to increase the research on the dynamic characteristics of special-shaped columns under bias pressure [6]. The specific work of this paper is shown in Table 1.

2. State of the Art

ABAQUS finite element analysis software: ABAQUS is one of the most widely used analysis software in the professional field, with high-precision numerical simulation ability and super strong calculation ability. ABAQUS can generate a large number of analysis elements by using finite element software, which can be applied in different industries [7].

ABAQUS finite element software has the following features over other software in the field of numerical simulation.

(1) Easy to use and comprehensive functions

ABAQUS finite element analysis software is one of the most powerful engineering research and design application

software, which can be used to model and study systems and fluids. These finite element analysis programs have brought effective calculation methods to relevant technical researchers, shortened the research process, and greatly improved the efficiency. In the actual project of using ABA-QUS software to analyze the model, researchers can directly display the modeling results and the structural characteristics of simulated parts in the program.

The important data analysis modules of ABAQUS/FEA software include ABAQUS/explicit and ABAQUS/standard templates, as well as ABAQUS/CAE templates, which are the basic user interfaces of graphic solutions. Each data analysis software module has different classification methods, calculation methods, and key points. The main advantage of ABAQUS/obvious template is that it can visualize the whole dynamic scoring calculation process. However, in fact, ABAQUS/obvious template is in the calculation process. The advantage of ABAQUS/standard analytical model is that it can run on a solver that simultaneously calculates multiple eigenvalues, which is also a more commonly used method in linear dynamic analytical calculation. Finally, the advantage of ABAQUS/CAE standard analytical model is that it can establish more detailed numerical simulation model more quickly.

(2) Comprehensive cell library and material model library

There are about 400 types of basic units in the unit library of thermodynamic properties of various metal materials [7]. The element library in ABAQUS finite element software can roughly contain eight basic elements [8].

ABAQUS has a variety of material model libraries to model the thermodynamic properties of various materials. At the same time, we can define different material models according to different failure criteria and inherent structural relationships. Scientific researchers can select appropriate material model library from ABAQUS according to the structural characteristics of the special model materials they are developing. Through previous application research and exploration, people found that ABAQUS FEA software can more realistically simulate the characteristics of various materials in engineering practice.

(3) Strong compatibility

ABAQUS finite element analysis software system has strong compatibility. The software has a complete system interface, which can provide a good connection for the later secondary development, thus saving a lot of manpower, material resources and investment. ABAQUS finite element software has been applied to many problems and analysis [9].

(4) High operability

In ABAQUS FEA program, the whole working process mainly includes pre-processing (modeling, analysis and calculation) and post-processing. Each of the above links can be gradually realized through various components in the graphical interface, which is practical and does not require much work.

The commonly used ABAQUS/CAE analysis model includes parts, characteristics, assembly, steps, interactions, loads, grids, jobs and dozens of modeling operation modules [10].

(5) Accurate nonlinear analysis

The calculation process of ABAQUS finite element software can not only solve the problem of studying model materials under various characteristics and test pieces under various stress environments, but also the relevant calculation tools have added the load information required by the research into the whole calculation process in the form of load steps, so as to obtain the correct nonlinear research conclusion more accurately. Similarly, in the ABAQUS FEM nonlinear calculation process, the whole calculation process can be regarded as a loading increment that changes continuously with the increase of time, and then, through iterative calculation, the final result is obtained. In the process of nonlinear calculation by ABAQUS finite element software, the software can intelligently change the rate of load increase and the convergence rate of control calculation, so that more accurate results can be obtained through the nonlinear research of ABAQUS software in practical problems [11]. The block diagram of the analysis of the concrete material using the ABAQUS software is shown in Figure 2.

ABAQUS finite element analysis software is a powerful and widely used engineering simulation application software. ABAQUS FEM software has a cell library that can simulate the characteristics of all building geometric components and a model library that uses the characteristics of various building metal materials, which can simulate the characteristics of metal materials used in all typical buildings. For example, the mechanical properties of reinforced concrete special-shaped beams under the influence of eccentric load can be analyzed using ABAQUS finite element analysis software [12].

There are many reasons to change the dynamic characteristics of reinforced concrete under eccentric load, including limb length ratio, reinforcement strength grade, concrete reinforcement ratio, and load eccentricity [12]. At the same time, during the actual test, many interference factors may cause deviation and interference to the conclusions of some tests, and other factors in the process of some tests may also cause errors to the conclusions [13]. In the specific process, the results are directly affected by other reasons, such as the repeatability of the operation, the relatively large investment required in the experiment, and the reading errors of scientific researchers. Therefore, this section will focus on ABAQUS finite element analysis software to illustrate the accuracy and effectiveness of the FEA model constructed in this paper [14].

3. Methodology

3.1. Ontogenetic Model of the Material

3.1.1. Ontogenetic Model of Concrete. In the finite element software ABAQUS, there are two main methods applicable

TABLE 1: Research content and conclusion.

1	By using the finite element analysis software ABAQUS, the finite element model of reinforced concrete shaped column is established based on the test data in the relevant literature, and the accuracy of the model establishment is analyzed by verifying the load-displacement curve and ultimate bearing capacity obtained after the test
2	On the basis of verifying the correctness of the analytical finite element model, the cross-sectional form of reinforced concrete shaped column is designed, the relevant specimen parameters are set, and the specimen parameters required to be studied under each working condition are determined, and then, the finite element models are established separately to obtain the concrete stress cloud, reinforcement stress cloud, and load-displacement curve under the structural form of eccentricity, loading angle, concrete, strength and reinforcement ratio
3	Compare and analyze the changes of concrete stress cloud, steel stress cloud, and load-deflection curve of the shaped column under different working conditions and the damage pattern of the specimen, respectively, and determine the influence law of the mechanical properties of the shaped column under the above four working conditions and one-way bias pressure

to the simulation of cement as a building material, one is damage plastic simulation, and the other is diffusion crack simulation. It refers to dividing the reinforcement into plain cement and reinforced concrete according to the reinforcement requirements of building components. The modeling and analysis methods and research principles often used by these two forms of concrete are very different. Among them, the diffusion fracture mode is mainly applied to the theory of isotropic plasticity and directional failure strength to describe the nonlinear panel behavior of concrete and is mainly applied to analyze some types of monotonic loading on the vertical deformation of concrete. The research principle of damage plastic mode mainly adopts Kachanov's classical damage mode. The basic operation principle of damage plastic mode is to equivalent the damage degree of concrete material to the form of the most effective area variable. The specific parameters of damage deformation equation can be expressed as follows:

$$D = \frac{(A - \bar{A})}{A}. \tag{1}$$

In the formula, A is the effective cross-sectional area of the material before damage. $\bar{A}$ is the effective cross-sectional area of the material after damage.

According to Lemaitre's hypothesis "strain equivalence assumption," the specific damage variables can be expressed as follows.

$$D = 1 - \frac{E'}{E}, \tag{2}$$

where E is the modulus of elasticity of the material before damage and E' is the modulus of elasticity of the material after damage.

Based on Equations (1) and (2), the specific expressions for the damage variables were regrouped by Yu, as shown below.

$$D = 1 - \frac{K}{K_0}. \tag{3}$$

The main structural simulation of buildings in this paper is the failure and plastic simulation of concrete structures in ABAQUS finite element software system. When ABAQUS finite element software is used to simulate the numerical simulation calculation process, it is assumed that the damage plastic model is used for simulation calculation, and the curve of the inherent structure model of cement is shown in Figure 3. The specific calculation method of cement damage and deformation has been explained, and the specific calculation process will not be explained. The corresponding inherent structure relationship of cement is deduced according to the above calculation formula [15].

3.1.2. Principal Structure Model of Reinforcement. The main dimension parameters of reinforcement can be obtained by measuring and determining the corresponding thermodynamic parameters. According to the main structure relationship of steel bar and iron obtained from the experimental results, the simulation curve is shown. As we can see, the main design performance curve of steel includes the following five sections, which can be divided into strength (OA), elastoplasticity (AB), yield (BC), strengthening (CD), and necking (DE) [16].

As shown in Figure 4, if the longitudinal axis f_p is a proportional limit, when the internal stress value of the test mold is insufficient or exceeds f_p, the inherent relationship of the steel at this stage also satisfies Hooke's law. When the internal stress can be removed from the test mold, the internal stress of the measured sample can also return to its original state, which indicates that the steel at this stage belongs to the most ideal elastic deformation stage. When the tensile stress on the specimen is between f_p and f_y, it means that the steel is in the elastic-plastic stage. The longitudinal axes f_y and f_u in the figure represent the yield point and tensile resistance of steel. When the stress of the sample exceeds the f_y value, the sample will also yield. When the pressure of the sample reaches the f_u value, the steel sample will also reach the necked state and then quickly break and lose strength [17].

The stress-strain relationship curve of the reinforcement can be more intuitive to see the intrinsic structure of the reinforcement, although the intrinsic structure of the reinforcement obtained from such a test can be more intuitive and realistic to describe the situation of the concrete at different stages of stress, but because such an intrinsic structure model is more complicated when calculated by ABAQUS
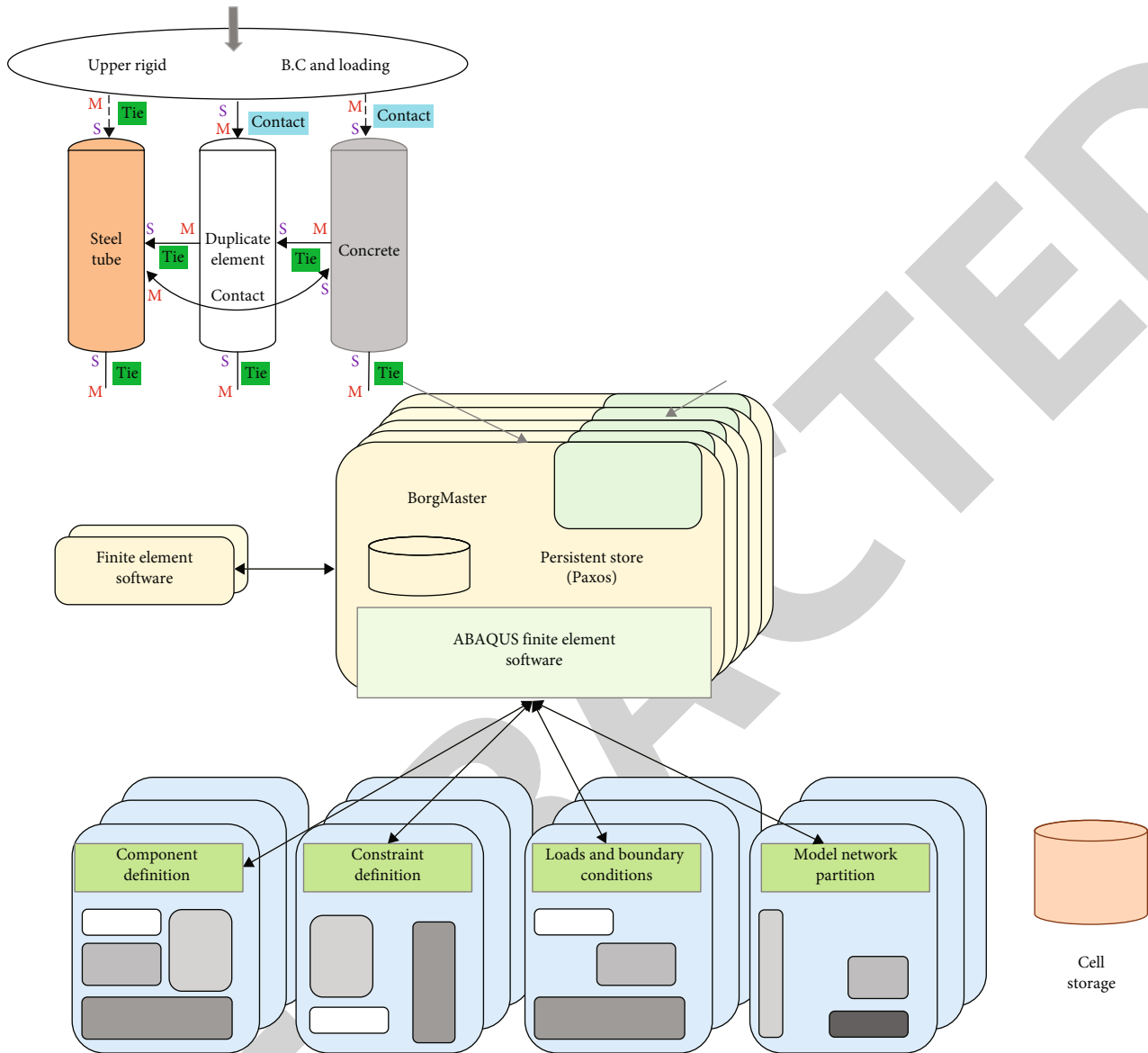
FIGURE 2: Stress analysis of concrete materials based on finite element analysis.

finite element software, it will lead to a complicated and tedious process of solution, so it is not widely used in the actual analysis [18]. The bilinear model main structure model found by people mainly includes two types [19]. The first type is the most ideal double elastic-plastic main structure model, as shown in Figure 5. (the first type is an ideal elastic-plastic transient model, as shown in (b), which is a transient model obtained without considering the reinforcement effect; The other is the bilinear through reinforcement model. As shown in Figure 5(a), the Mises yield criterion is that under certain deformation conditions, when an equivalent force point exceeds a certain value, it will enter the plastic state from that point [20].

3.2. L-Shaped Anisotropic Section Column Shape Center Formula. Since this paper focuses on the mechanical properties of the prestressed reinforced special-shaped column under eccentric load, the central part of the formwork of

the special-shaped column must be determined before the discussion and research. And the displacement and volume of the normal regular section at the center of the shape can be easily expressed. Therefore, people can find and derive the method of describing the static moment, that is, the static moment algebra of each moment component of the heterogeneous section to one axis is equivalent to the static moment of the heterogeneous section to the same axis, and then deduce that the static moment of a heterogeneous section can be described as:

$$S_x = \sum_{i=1}^{n} A_i \bar{y}_i, \tag{4}$$

$$S_y = \sum_{i=1}^{n} A_i \bar{x}_i. \tag{5}$$

(a)

(b)
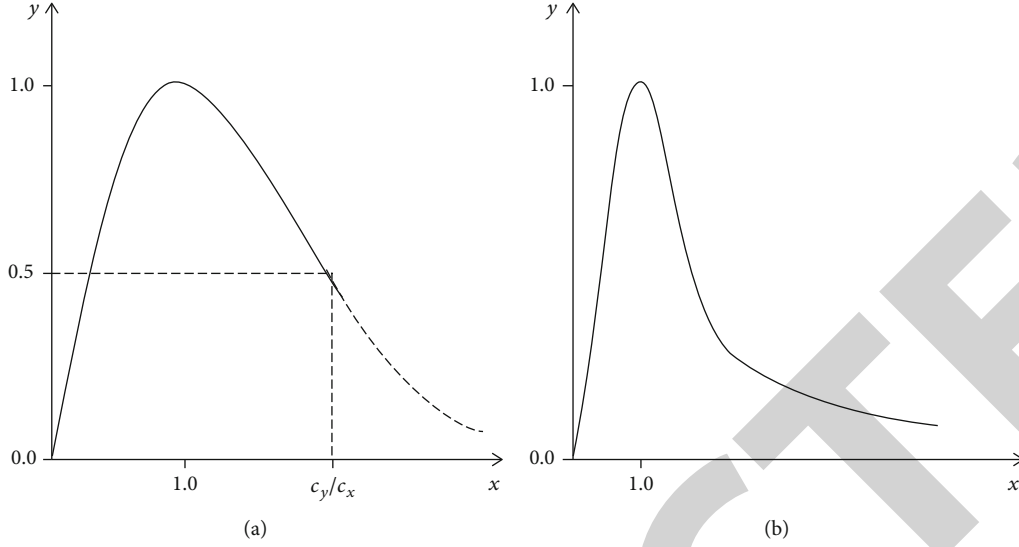
Figure 3: The principal structure relationship curve of concrete.

In Equations (4) and (5), the symbols A_i and $\bar{x}_i$, n, and $\bar{y}_i$ denote the area of a certain rectangular cross-section composing a heterogeneous section and the coordinate position of the shape center of this section, respectively, and n denotes the number of rectangular sections composing a heterogeneous section. Therefore, according to the knowledge of theoretical mechanics, it is known that the specific coordinate equation of the form center of a heterogeneous section in the right-angle coordinate system is shown as follows.

$$\bar{x} = \frac{S_y}{\sum_{i=1}^{n} A_i},$$
$$\bar{y} = \frac{S_x}{\sum_{i=1}^{n} A_i}. \tag{6}$$

The cross-sectional form of the shaped column analyzed in this study is L-shaped, and the specific form is as follows. Based on the above calculation method of the formula for the form center of a column with a shaped section, we can derive the specific coordinates of the form center of a column with an L-shaped section as $\bar{x}$ and $\bar{y}$, as shown in the following equation.

$$\bar{x} = \frac{b^2 h + h_f' \left(b_f' - b \right) \left(b_f' + b \right)}{2bh + 2h_f' \left(b_f' - b \right)},$$
$$\bar{y} = \frac{bh^2 + h_f' 2 \left(b_f' - b \right)}{2bh + 2h_f' \left(b_f' - b \right)}. \tag{7}$$

The limb thickness of the column limb along the x-axis in Figure 6 is h_f', and the limb height is b_f' and the limb height along the y-axis is h and the limb thickness is b
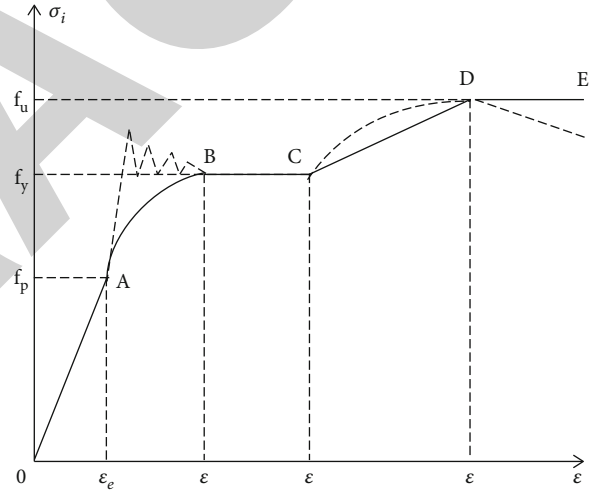
Figure 4: Stress-strain relationship curve for reinforcing steel.

3.3. Citation of Reference Test Data. The parameters of the finite element simulation of the reinforced concrete section column of the L-shaped frame are consistent with the standard data studied in the references, and a measurement sample in the references is selected to simulate and test and analyze the rationality of the internal problems of the simulation test. The longitudinal reinforced concrete structure size is also the same, that is, eight frame cement sizes of HRB 335 with a length of 12 mm are used, and the reinforced concrete ratio is C30, The compressive strength of frame cement is 34.57 MPa.

3.4. Simplification of L-Shaped Column Model. According to the computational mechanical model tested in Ref., we need to simplify the mechanical model of reinforced concrete L-shaped section column under eccentric load.

3.5. Establishment of Finite Element Model. This paper focuses on the dynamic characteristics of eccentrically
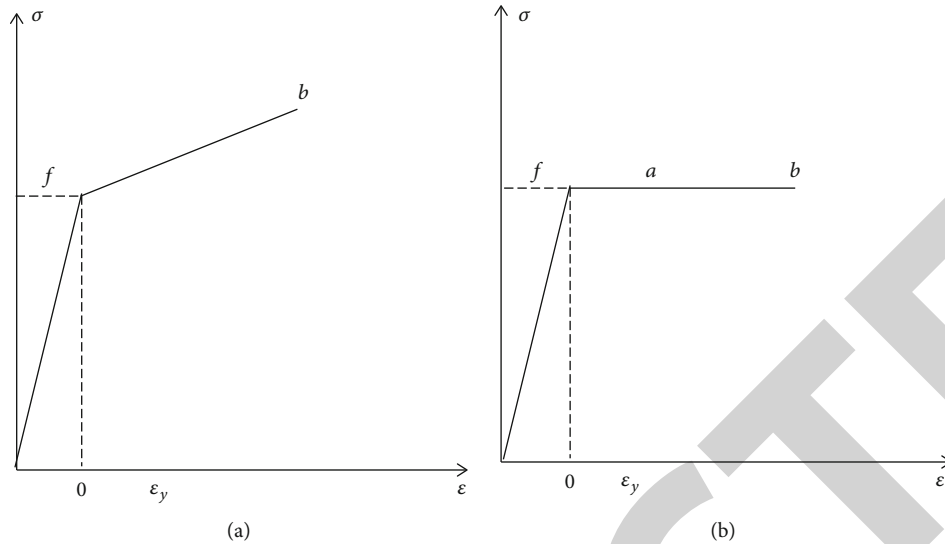
Figure 5: Simplified stress-strain principal structure relationship curve for steel reinforcement.

loaded steel-concrete L-shaped beam. In order to apply load to the L-shaped column, a rigid pad is placed at the top of the L-shaped column, and the load is applied here for control during the simulation of finite element specimens. The purpose is to prevent the stress concentration phenomenon in the subsequent loading process and thus affect the results of the simulation test and also to provide researchers with a more intuitive understanding of the specific shape of the specimen under eccentric loading.

When we build the FEA model (that is, the finite element analysis model) of reinforced concrete L-shaped column for operational analysis, it is assumed in advance that the bonding occlusion between the steel and concrete is good and can work together, and the existence of relative slip between the steel and concrete is also not considered.

3.5.1. Creating Parts and Defining Properties. The concrete L-shaped column, longitudinal reinforcement, hoop, steel plate spacer, and other base components of the reinforced concrete L-shaped column are created separately by using the "Component" module in the finite element analysis software ABAQUS, and then, the "Property" module in the finite element software is used to define the material properties of each part of the specimen (reinforcement, concrete, end, spacer, etc.), which contains the mechanical properties such as density, intrinsic structure relationship, and Poisson's ratio, as shown in Table 2. The relevant data are shown for the plastic loss model of concrete. Finally, after setting, the section properties of each component are assigned to all drawn components, respectively, so that the drawing and section properties of each component are completed.

3.5.2. Definition of Assemblies and Constraints. Assemblies refer to in the "Assembly" module, the L-shaped concrete column, longitudinal reinforcement, hoop, and end components are defined as independent states, and then the components with section properties are placed at the appropriate spatial locations using the "Move," "Rotate,"
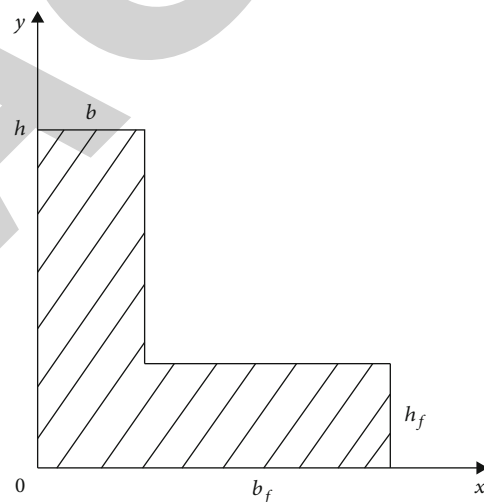
Figure 6: Schematic diagram of L-section coordinates.

and "Array" commands. Then, use the "Move," "Rotate," and "Array" commands to place the parts with section properties in the appropriate space of the reinforced concrete L-shaped column, and then, use the "Merge" command to combine the longitudinal reinforcing bars and hoops to form the reinforcing cage skeleton. The cage skeleton is also set to the independent state.

After assembling each component with properties, the contact and constraint relationships between the components are defined. First, the reinforcing cage skeleton is placed in the concrete L-shaped column as a "built-in area," in which the reinforcing cage skeleton is the "embedded" part, and the whole reinforced concrete L-shaped column model is selected as the main area, thus completing the constraint relationship between the reinforcing cage skeleton and the concrete. This completes the constraint relationship between the reinforcing cage skeleton and the concrete components. Then, the reference point RP-1 is created by using

Table 2: Table of plastic damage model parameters of concrete.

Expansion angle	Eccentricity	K	f_{b0}/f_{c0}	Viscous parameters
30°	0.1	0.667	1.16	0.0005

Table 3: Comparison of bearing capacity of specimens and deflection in columns.

	Experimental value (kN)	Analog value (kN)	Percentage of error (%)
Load carrying capacity	190	191	0.53
Deflection in the column	6.9	9.1	31

the toolbar "Reference Point," and the displacement load in the reference document is applied to the created reference point RP-1, and the eccentricity of the reference point location is consistent with the eccentricity of the selected verification analysis specimen. Finally, set the constraint relationship between the reference point RP-1 and the rigid end pad as "coupling," select the reference point as the "subordinate area" of the coupling constraint, and select the upper surface of the rigid end pad as the "main area" of the coupling constraint. This completes the definition of the constraint between the rigid end pad and the reference point RP-1.

Constraints refer to the concrete and rigid end pads which are then set as "binding" constraints, the specific meaning of the binding constraint is to assume that the rigid end pads and the top surface of the L-shaped column are well adhered to each other throughout the process of applying the load, and no peeling will occur between the two, where the top surface of the reinforced concrete L-shaped column is selected as the main surface and the rigid end pads are selected as the slave surface. The upper surface of the reinforced concrete L-shaped column is selected as the main surface and the rigid end spacer is selected as the follower surface.

3.5.3. Setting up Analysis Steps and Output Variables. Set the analysis step in the "Analysis Step" module, create the initial analysis step "Initial" and the analysis step "Step-1," and then select the Newtonian solution technique method. As the solution technique for model research and analysis, set the initial incremental step, the minimum incremental step, and the maximum incremental step to 0.02, 1×10^{-7}, and 0.5, respectively, in the "Analysis Step," where the maximum number of incremental steps is set to 20,000 and the total time length of calculation is set to 1. In the analysis step, enter the displacement load to be applied in "Step-1," and then select "General, Static" type in order.

Finally, variable schemes such as displacement and reaction external force can be selected from "field input and output". In the simulation analysis process, as long as the input and output variables are reduced, the time limit of the finite element software simulation operation samples can be effectively shortened, and the required calculation result information can be more conveniently obtained in the postprocessing process. At the same time, because it is conducive

to observing and obtaining the real displacement of the later calculation results, is set to "Set" (Set-1).

3.5.4. Defining Loads and Boundary Conditions. In order to simulate and analyze the full bearing capacity curve of the concrete L-shaped section width beam under eccentric load, the load method of the simulation test adopts the moving load method, and the pressure deflection relationship curve of the concrete L-shaped column is obtained by using the finite element software simulation analysis method. The boundary condition of the bottom surface of reinforced concrete L-shaped column is first defined in the "pressure" model. Finally, it is constrained on the six degrees of freedom of the bottom surface of the concrete special-shaped column to ensure that the concrete special-shaped column is completely stable and the FEA model can operate correctly.

3.5.5. Model Meshing. In the "grid" model, the reinforced concrete L-shaped column formwork is divided into grids, and the overall unit size of the whole model is set to zero zero zero two. However, since the rigid end pad on the upper part of the special-shaped column is not the key object of the simulation analysis, the end pad is set to facilitate loading. The global setting unit size is 1. In order to produce good convergence of the calculation results, the unit form is designed as a regular hexahedron element. Then, the reinforcement cage skeleton is divided into grids, and then, the element form of the reinforcement cage is determined by this method; that is, the reinforcement cage skeleton is determined as the truss element of T3D23D. The unit form of the rigid end pad and the reinforcement is selected as the C3D8R unit form, that is, the solid three-dimensional eight-node linear hexahedron unit form.

3.5.6. Job Submission Analysis and Postprocessing. After the completion of the meshing operation, enter the "Job" module, subsequent analysis each time you need to create a new job and then submit, and finally wait for the computer to complete the analysis job. In the process of submitting the simulation analysis job, you can also see the whole calculation process of the shaped column more intuitively through the "monitoring" function and can also be prompted at any time during the calculation of errors and warning information.

TABLE 4: Main reasons for the deviation of the test simulation.

1	When the FEA model was established with ABAQUS software, it was assumed that the bond between the reinforcement and concrete was good, and there was no slippage between the reinforcement and concrete before the specimen reached the ultimate bearing capacity, so there was a certain difference between the actual test force and the FEA simulation value and the test value of the reference literature.
2	We use ABAQUS software to simulate the FEA model, and the material's intrinsic structure relationship is applied to the FEA by reviewing other data and doing a lot of experiments with instrumental data, so the intrinsic structure relationship of the FEA simulation may be inaccurate with the experimental intrinsic structure data of the reference literature.
3	The determination of the cube compressive strength of concrete in the test is obtained under more ideal conditions, while in the actual test, there is a certain degree of error in the production of concrete cube specimens, and there may also be a certain degree of human error in the collection and collation of test data, which leads to a certain difference between the data obtained from the ABAQUS finite element simulation and the data from the reference literature.

TABLE 5: Analysis of results.

Eccentricity	With the increase of eccentricity, the height of the concrete flange compressed area decreases, the distribution of large compressive stress in the corresponding area gradually shifts from the middle of the column to the two ends of the column, and the shape of the large pressure distribution is also concentrated from the high through the column to the two ends of the column, respectively; the eccentricity has little effect on the stress of the reinforcement; the bearing capacity gradually decreases with the increase of the eccentricity, and the ductility has a small increase with the increase of the eccentricity.
Load angle	As the loading angle changes, the neutral axis of the L-shaped column rotates and the pressurized area changes from 0°, 45°, 80°, 100°, and 135° first gradually increases and then gradually decreases; in 80° and 100°, the number of hoops reaching yield is the highest, and the bearing capacity tends to rise first with the loading angle and then gradually decreases at 80° and 100°, reaches the peak, and then gradually decreases.
Concrete strength	With the increase of concrete strength, concrete stress, reinforcement stress, and concrete bearing capacity also increase gently, and the deflection corresponding to the ultimate bearing capacity decreases accordingly.
Longitudinal reinforcement rate	As the diameter of longitudinal reinforcement increases, the reinforcement ratio of longitudinal reinforcement increases, and the load is mostly borne by the reinforcement in the web part of the L-shaped column, and the compressive stress in the flange part decreases accordingly; the ultimate bearing capacity increases, but the corresponding deflection increases instead.

Finally, select the "visualization" template first, and then enter the postprocessing phase. In the postprocessing process, the strain range and stress of any part of the prestressed concrete L-shaped column can be obtained from the results calculated by the finite element software, and the numerical value can be obtained, and then, the load deflection curve of the vertical deformation can be drawn to extract the ultimate bearing capacity of the simulated vertical deformation, and the stress evolution process of the vertical deformation and the stress state of each part can be observed through the stress cloud of the simulated specimen, i.e., position distribution of reinforced concrete L-shaped section column sample. By observing the stress cloud in the simulated specimen, the corresponding pressure distribution of the concrete L-shaped section column specimen can also be observed.

3.5.7. FEA Convergence Criterion. If the result does not exceed the required error range, the iterative operation can still be continued. On the contrary, once the expected error level is exceeded, it can be considered that the FEA iteration result has converged or met the requirements, and the current analysis iteration of the calculation can be terminated, and the FEA result is finally obtained. Assuming the nonequilibrium force after the termination of the i-th iteration,

the calculation equation is as follows:

$$\{\psi(\delta_i)\} = \{F(\delta_i)\} \bullet \{R\}. \tag{8}$$

The convergence requirement of the nonequilibrium force criterion can be expressed as

$$\|\{\psi(\delta_i)\}\|_2 \le \alpha_F \|\{R\}\|, \tag{9}$$

where $\{R\}$ is the horizontal vector of the external load, $\{F(\delta_i)\}$ is the nodal force vector obtained by integrating the cell after the i-th iteration, α_F is the tolerance for the convergence of nonequilibrium forces, which usually takes the value range from 0.1% to 5%, and the default value of the finite element software ABAQUS is 0.5%, and $\|\{\psi(\delta_i)\}\|_2$ is the Euclidean parametric number.

4. Section Results and Analysis

The following results analysis and model validation are carried out, mainly using the finite element software ABAQUS simulation analysis of the test piece as the main object of study, based on the parameters obtained from the finite element analysis software operations and the test results data

measured in the test in the reference literature to verify whether the model of the simulation analysis is correct.

4.1. Load-Deflection Relationship Curve Comparison and Ultimate Bearing Capacity Comparison. The load-deflection relationship curve of the specimen simulated with ABAQUS finite element software is similar to the load-deflection curve in the reference literature, and the change pattern and distribution of the curve match well, so the intrinsic structure relationship model used in the simulated analysis specimen can be used to reflect the mechanical properties of the test specimen and the trend of internal mechanical changes, but the load-deflection relationship curve is not completely consistent with the test results. In order to ensure the correctness of the simulated specimen, it is necessary to further extract the ultimate bearing capacity of the specimen from the simulated specimen according to the need and then carry out a control analysis, and the proposed specific bearing capacity data are as follows. Table 3 shows the specific bearing capacity data.

It can be seen from Table 3 that the maximum deviation proportion between the bearing capacity of the simulation sample and the reference sample is 0.53% and the maximum deflection deviation proportion in the column is not 31%. Therefore, it can be seen that the error between the finite element simulation results of the two test L-shaped columns and the maximum ultimate strength in the experimental results in the literature is only 10%. This further demonstrates the consistency between the finite element analysis model established by the finite element software and the reference specimen, with good accuracy and precision, which can be used for subsequent analysis.

4.2. Error Analysis. It can be seen from the previous section that the load displacement curve calculated by referring to the load deflection relationship curve in this paper and the model established by the finite element software ABAQUS is only approximate to the ultimate bearing capacity of two reinforced concrete L-shaped columns, but not quite the same. Through analysis of the main factors of test simulation error, the following aspects are shown in Table 4.

4.3. Analysis of Results. In this chapter, the middle limb L-shaped prestressed concrete column in the literature is taken as the basic structure, and the validity of its construction mode is verified through the simulation of the test structure by the large-scale commercial general nonlinear finite element software ABAQUS. On the basis of correctly studying the concrete stress-strain curve and the reinforcement stress-stress curve, the four influence factors of eccentricity and loading angle are also studied. Based on the research results of the four influencing factors of concrete tensile strength and longitudinal reinforcement ratio and longitudinal reinforcement ratio, there are three aspects: concrete stress, reinforcement stress, and load-deflection curve. The following results were obtained, shown in Table 5.

5. Conclusion

In this paper, a finite analysis model is constructed according to the characteristics of sludge concrete. Analyze the stress situation of the structure under the least favorable load to obtain the strength index that the interlayer bonding layer material and the asphalt mixture should achieve. Comprehensive calculation results show that the shear breakage between layers is the main form of breaking; in the case of horizontal load and overload, the horizontal shear stress and longitudinal shear stress between the layers should be considered, and the angle of the shear stress force is between the longitudinal bias of 15-30 degrees. The stress cloud and load-displacement curve of steel reinforcement under the structural forms of concrete stress cloud, eccentricity, load angle, concrete strength, and reinforcement ratio are obtained, and the influence law of the mechanical properties of the special-shaped column under these four working conditions and unidirectional bias pressure is determined.

Data Availability

The labeled datasets used to support the findings of this study are available from the corresponding author upon request.

Conflicts of Interest

The authors declare that there are no conflicts of interest.

References

[1] X. Bi, Y. Yang, and Z. Zhang, "The mechanical analysis of cement concrete surface layer with load - transfer bar for joints based on computer," *Journal of Physics: Conference Series*, vol. 1744, no. 2, p. 022084, 2021.

[2] S. Samarakoon and B. Hodne, "Parametric study of different unbonded tendon layouts in pre-stressed concrete flat plates," *International Journal of Concrete Structures and Materials*, vol. 14, no. 1, pp. 12–33, 2020.

[3] Z. Si, Y. Li, L. Wen, and X. du, "Simulation and analysis of the temperature field and the thermal stress of an inverted-siphon concrete structure based on the contact friction element," *KSCE Journal of Civil Engineering*, vol. 24, no. 8, pp. 2449–2457, 2020.

[4] Z. Z. Wang, W. M. Gong, G. L. Dai, and L. F. Liu, "Analysis of bond behavior of FRP-confined concrete piles based on push-out test," *Advances in Materials Science and Engineering*, vol. 2020, 17 pages, 2020.

[5] M. Da and Z. Su, "Stress and deformation analysis of concrete-facing sand–gravel dam based on inversion parameters," *Geotechnical and Geological Engineering*, vol. 39, no. 2, pp. 1399–1408, 2021.

[6] A. Ghasemipanah and R. Z. Moayed, "Analysis of concrete piles under horizontal and vertical simultaneous loading with P-Y method and finite element analysis," *Geotechnical and Geological Engineering*, vol. 39, no. 8, pp. 5857–5877, 2021.

[7] D. S. Wang, K. J. Yang, H. Yang, and P. P. Zhang, "Computational analysis of laser cladding of preset MCrAlY coating based on ANSYS ii-stress field," *Materials Science Forum*, vol. 1020, no. 4, pp. 148–156, 2021.

Research Article

Research on the Bionic Flexible End-Effector Based on Tomato Harvesting

Tiezheng Guo ⓘ,[1] **Yifeng Zheng** ⓘ,[1,2] **Weixi Bo** ⓘ,[1] **Jun Liu,**[2] **Jie Pi,**[2] **Wei Chen,**[1] **and Junzhuo Deng** ⓘ[1]

[1]*Industrial Center, Nanjing Institute of Technology, Nanjing 211167, China*
[2]*Institute of Agricultural Facilities and Equipment, Jiangsu Academy of Agricultural Sciences, Key Laboratory of Protected Agriculture Engineering in the Middle and Lower Reaches of Yangtze River, Ministry of Agriculture, Nanjing 210014, China*

Correspondence should be addressed to Tiezheng Guo; guotiezheng@njit.edu.cn

Aiming at the problems that tomatoes are fragile and the traditional end-effector design is not suitable for tomato picking, a combination of the bionic principle of FRE structure and finger design was proposed. Based on the physical properties of tomatoes, a flexible underactuated end-effector for tomato picking and sorting was designed. The optimal structural parameters of fingers were determined by finite element analysis, and the tomato grasping experiment was carried out. The results show that the flexible end can grasp and transport tomatoes with diameters ranging from 65 to 95 mm without damage, which can withstand 7 N tensile force, the load is more than 2 times of its own weight, the tomato coverage rate is greater than 23.6%, and the effective grab rate is 100% and has the advantages of the strong stability, universality, and protection. The research provides a novel solution for the design and application of the tomato picking and sorting robot end-effector.

1. Introduction

Tomato is an important vegetable crop, with a total annual output of 177 million tons and a planting area of about 5 million hectares [1]. China has the huge amount of cultivation and consumption of tomatoes, with an area of 1.109 million hectares and an annual yield of 64.832 million tons [2]. In the entire tomato production chain, the picking and sorting period are the most time-consuming and laborious part. Its labor demand accounts for more than 50% of the entire planting and production process. Until now, it has been mostly done manually, and has met the problems such as expensive labor, low efficiency, and large workload [3]. In recent years, tomato harvesting robots have become the new trend with the visual recognition and intelligent control technology development and progress [4]. The end-effector, as the terminal component of the picking and sorting robot interacting with tomato, has a significant impact on the robot's work efficiency, fruit damage rate, and other operational performance. It has become one of the key technolo-

gies in the research and development of tomato harvesting robots.

The picking and sorting end-effectors have developed so far can be divided into two categories: rigid end-effectors and flexible end-effectors. Rigid end-effector, as the most commonly used agricultural harvesting end-effector, started early in research and had achieved many results. It is widely used in the harvesting of apples, citrus, sweet peppers, and other fruits and vegetables [5–7] and has the advantages of high precision requirements, fast response speed, and large grasping force. Naoshi Kondo's team at Kyoto University has developed a rigid end-effector for picking tomato clusters [8]. Its large size makes it difficult to carry out actual picking operations, and the picking success rate is only around 50%. Kochi University in Japan has developed a tomato thermal cutting actuator [9], which used resistance wire to cut the stalk. However, the cutting method has the certain security risks. Hiroaki Yaguchi's team at the University of Tokyo designed a three-finger rigid gripper. Due to the too large opening of the jaw design, multiple tomatoes

were caught or blocked by tomato vines, resulting in a successful picking rate of only 62.2% [10].

In contrast to traditional rigid end-effectors, the finger portion of the flexible end-effector is made of stretchable material. The material itself has good adaptability. It obtains infinite degrees of freedom by continuously deforming as it interacts with the object, replacing rigid joints and links. It has obvious advantages when grasping soft, fragile, or irregular objects. Structural deformation of flexible materials can be achieved in various ways, such as vacuuming the filling bag using the particle blocking principle [11, 12], changing the temperature to induce deformation of the shape memory material [13, 14], and inflating and deflating the elastic chamber [15, 16]. However, these flexible ends are limited to certain scenarios. Due to the small grasping force, if it is applied to fruit and vegetable picking and sorting, further research is required.

To sum up, most end-effectors are prone to damage the fruit during the working process or are not suitable for fruit picking and sorting in realistic scenarios. It will seriously affect the quality and storage time of the fruit and ultimately reduce the market price and economic benefits. The main reason is that the factors considered in the design of the end-effector are not comprehensive, resulting in unreasonable design. Therefore, in view of the crispness and particularity of tomato, a flexible underactuated end-effector suitable for tomato picking and sorting was designed based on the bionic principle of FRE (Fin Ray Effect) structure in this paper. Based on the experiment of tomato physical properties, the flexible finger structure was designed and optimized, and the finite element simulation analysis of finger force was completed. In order to provide the novel solution for the design and application of tomato picking and sorting robot end-effector, an experimental platform was built to conduct clamping experiments on the flexible end-effector, and the economy, reliability, and repeatability of the end-effectors were verified.

2. Physical Properties of Tomatoes

In order to make the designed flexible end-effector more suitable for tomatoes picking and sorting, research on the physical properties of tomatoes was carried out. The experiments included tomato geometry, mass, compression, and damage characteristics. The experimental subjects are Provence tomato varieties.

2.1. Research Methods

2.1.1. Tomato Geometry and Quality Tests. The flexible finger structure design is influenced by the size and weight of the tomato. Experimental site is greenhouse tomato planting base of Jiangsu Academy of Agricultural Sciences and experiment time May 6, 2022. A total of 5 rows of Provencal tomatoes were grown in the greenhouse. There were 10 plants in each row, and each plant had about 2 to 3 tomato clusters. 2 ripe tomatoes were randomly picked from each tomato plant, for a total number of 100. 57 tomatoes were randomly selected from 100 tomatoes, numbered 1 to 57.

A vernier caliper was used to measure the lateral diameter L_1, longitudinal diameter L_2 and height L_3 of the lateral diameter of the tomato. The specific measurement positions are shown in Figure 1. The mass m of tomato was measured with an electronic balance JA5001.

2.1.2. Compression Mechanical Properties Test. When the tomato is grasped by flexible fingers, the pulp of the tomato is squeezed, and the middle part of the tomato is the least compressive [17]. In order to study the compressive resistance of the middle position of the tomato, the compressive mechanical properties test was carried out on the tomatoes. The 57 tomatoes were divided into 19 groups, of which 18 were the experimental group and 1 group was the control group. The experiments were carried out using a TMS-TOUCH texture analyzer (FTC, USA). The test platform is shown in Figure 2(a). In the loading test, the test mode of the texture analyzer was selected as "Measure Force in Compression" mode. The running program was selected as "Return to Start" mode [18]. The test parameters are set as follows: the probe type of the instrument is a flat probe with a diameter of 50 mm. The probe and stage is covered with a layer of spacer made of TPU material, and the thickness of the material spacer is 1 mm. The probe loading speed is 30 mm/min, which belongs to the quasi-static range [19]. The speed before and after the test set to 60 mm/min. The initial distance between the probe and the stage is 110 mm, which is guaranteed to exceed the maximum transverse diameter of the tomato. Put the tomato longitudinally on the stage, and the probe is loaded with the maximum transverse diameter of the tomato, as shown in Figure 2(b). The loading displacement of the tomatoes was set to 1~18 mm, and they were divided into 18 groups, and each group was tested with 3 tomatoes.

2.1.3. Damage Characteristic Tests. Nondestructive gripping of tomato is an important research factor in the end-effector design process. Mechanical damage to tomatoes takes two forms. In the first, the tomato peel is not broken, but the cell structure is destroyed. The compressed part of the tomato undergoes an enzymatic reaction and darkens the color. The respiration of tomato cells is accelerated, and the compressed position loses a lot of water and contracts. Another type of damage is the rupture of the tomato peel, the exposure of the internal tissue, and the appearance of mildew on the surface of the tomato [20]. After passing the compression characteristic test, the tomatoes were damaged to varying degrees. Placed tomatoes on a lab bench labeled 0~18 mm and stored at room temperature in the lab. Wrinkling or molding of tomatoes with different loadings was recorded over 15 days.

2.2. Analysis of Physical Properties of Tomatoes

2.2.1. Size and Quality of Tomatoes. The measurement results of 57 tomatoes showed that the lateral diameter L_1 of the tomatoes ranged from 66.4 to 92.7 mm, the longitudinal diameter L_2 ranged from 52.6 to 81.3 mm, the lateral diameter and height L_3 ranged from 35.1 to 62.7 mm, and the tomato mass ranged from 152.7 to 378.2 g. The test
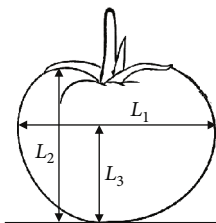
Figure 1: Schematic diagram of tomato size measurement.

(a)   (b)
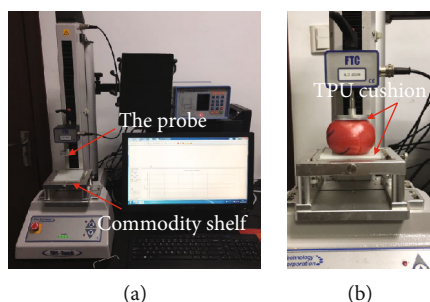
Figure 2: Compression mechanical properties experiment: (a) the composition of the texture analyzer; (b) loading experiment of tomato.

Table 1: Classification results of tomato geometry and quality.

Size/ (mm)	Proportion (%)	Maximum mass/(g)	Maximum transverse diameter height/ (mm)
65~70	3.5%	179.3	38.8
70~75	8.8%	210.6	42.7
75~80	43.9%	290.4	45.8
80~85	36.8%	305.2	50.5
85~90	5.2%	370.7	58.4
90~95	1.8%	400.4	62.7

results by size are shown in Table 1. In an ideal gripping state, the fingertips of the flexible fingers need to exceed the height of the maximum transverse diameter of the tomato, and the opening diameter of the finger end should be larger than the maximum transverse diameter of the tomato. Therefore, the length of the finger structure should be greater than 65 mm, and the maximum opening diameter of the finger should be greater than 95 mm.

2.2.2. Compression Mechanical Properties of Tomatoes. In the compressive mechanical properties test, the experimental results of the loading displacement of 18 mm are shown in Figure 3. The tomato compression process is divided into three stages: elastic compression stage, damage stage, and rupture stage. The loading force curve of tomato initially show an S-shaped curve. When the pressure exceeds the maximum elastic compression threshold of the tomato, the curve oscillates, and the pressure drops rapidly. Then it enters the stage of tomato damage, and the pressure gradually increases. After reaching the maximum, the tomato enters the burst stage, and the pressure drops again. The elastic compression stage is the range where the loading displacement is less than 10.5 mm in the figure. The damage stage is in the range of loading displacement of $10.5 < d < 16.5$ mm, and the tomato is obviously deformed at this stage. When the rupture stage is reached, the tomato cracks, and the maximum value of the pressure in the curve is the rupture force of the tomato.

After 18 groups of experiments, it was found that most of the tomatoes had obvious cracks in the experimental groups with a loading displacement of more than 11 mm. In the experimental group with a loading displacement of more than 5 mm, most of the tomatoes showed obvious

indentation. Therefore, the clamping force of the flexible fingers should be less than 30 N to ensure that the tomato will not be obviously damaged in appearance.

2.2.3. Damage Characteristics of Tomatoes. The 18 groups of tomatoes after the compression mechanical property test were used as experimental samples, and the uncompressed tomatoes were used as control samples, which were stored at room temperature for 15 days to observe the storage conditions of tomatoes. For tomatoes under pressure of about 30 N, no damage to the tomatoes can be observed, and there is no obvious indentation. But over time, the stressed skin of the tomatoes wrinkled and lost water. The storage results are shown in Table 2. With the increase of compressive force and compressive displacement, the storage time of tomatoes gradually shortened. When the compressive displacement is less than 2 mm, and the compressive force is less than 8 N, the storage time of tomatoes is more than 14 days. When the tomato compression displacement exceeds 5 mm, the storage time has decreased significantly. When the compression displacement is greater than 10 mm, the tomato has no storage conditions. Therefore, in order to achieve nondestructive picking of tomatoes, the clamping force of flexible fingers should be at least less than 8 N to ensure the longest storage time of tomatoes.

3. Structure Design and Optimization of Flexible End-Effector

3.1. Principles of Bionics. The FRE structure is inspired by the biological phenomenon of fish fins. When one side of the fin is pushed by the hand, the fin does not bend in the direction of the force but in the opposite direction [21]. Compared with the most widely used pneumatic fingers, the finger structure based on the fin ray effect principle does not require complicated air source control. The FRE structure allows compliant wrapping of objects by passively deforming upon contact with the target object without any external actuation. Following the FRE principle, the geometry of the finger is determined as a triangle consisting of two inclined fins fixed at one end and ribs evenly distributed in the middle. As shown in Figure 4, the fingers are broken down into three main modules: the base module, the middle module, and the fingertip module. The base module is mounted on a rigid fixed assembly that provides support for the closed chain structure as well as the entire finger

element. The middle module consists of a rib-like structure that provides mechanical properties for the fingers, and the number can be extended to n. The fingertip module consists of a triangular structure.

In the existing research, some end-effectors equipped with such fingers have realized the adaptive grasping function for fruits of various shapes [22, 23]. However, after putting it into the tomatoes harvesting experiment, there are two problems to be solved. On the one hand, the finger design is overall longer to accommodate the most fruit sizes. When used to grasp the tomato, the finger does not completely wrap the tomatoes. On the other hand, the fins and rib structures of the fingers are designed to be thicker, resulting in a smaller amount of deformation of the fingers when they come into contact with the tomatoes. The load applied to the tomatoes was not buffered and was an indirect trigger for impaired tomato gripping. The advantage of the layer blocking effect of this type of finger structure is not exploited. Aiming at the above two problems, the key parameters such as the number and inclination of ribs of this type of fingers are deeply studied.

3.2. Mathematical Modeling of Single Finger. To better understand the kinematics of fingers, a closed-chain structural mathematical model is established. Fingers for mathematical modeling consist of a base module, two intermediate modules, and a fingertip module. Based on the closed-chain finger structure shown in Figure 5(a), the state vector of the system is as follows:

$$\boldsymbol{\gamma} = [a, k_1, k_2, k_3, k_4, k_5, k_6, k_7, k_8, \alpha_1, \alpha_2, \alpha_3]^T, \tag{1}$$

where $k_i(i \in \{1, \cdots, 8\})$ are the curvature of the flexible link, a is the stroke of the fixed joint, and $\alpha_j(j \in \{1, 2, 3\})$ are the angle of the rotating joint:

$$\begin{aligned} \theta_1 &= \frac{\pi}{2} + L_1 k_1 + \alpha_1, \\ \theta_2 &= \frac{\pi}{2} + L_1 k_1 + L_2 k_2 + \alpha_2, \\ \theta_3 &= \frac{\pi}{2} + L_1 k_1 + L_2 k_2 + L_3 k_3 + \alpha_3, \end{aligned} \tag{2}$$

where L_m $(m \in \{1,2,3\})$ is the curved length of the flexible link. θ_n $(n \in \{1,2,3\})$ is the angle between the flexible link and the rib.

3.2.1. Forward Kinematics. To establish a closed-chain positive kinematics model, it is necessary to determine the constraint equations between joint variables and motion variables. The finger structure has 12 joint variables and 8 constraints, which are defined as follows:

$$\overline{AB} + \overline{BC} + \overline{CI} + \overline{IJ} + \overline{JA} = \lambda_1(a, k_1, \alpha_1, k_8) = 0, \tag{3}$$

$$\overline{CD} + \overline{DH} + \overline{HI} + \overline{IC} = \lambda_2(\alpha_1, k_2, \alpha_2, k_7) = 0, \tag{4}$$

$$\overline{DE} + \overline{EG} + \overline{GH} + \overline{HD} = \lambda_3(\alpha_2, k_3, \alpha_3, k_6) = 0, \tag{5}$$

$$\overline{EF} + \overline{FG} + \overline{GE} = \lambda_4(\alpha_3, k_4, k_5) = 0. \tag{6}$$

Determining the four joint variables in equation (1) as closed-chain system inputs, equations (3)–(6) can be used to solve for the remaining joint variables.

The analysis of a single flexible link is shown in Figure 5(b). When the fixed link is vertical (initial angle $\alpha = 0$), the position of point A in the Cartesian plane (x, y) is

$$\begin{aligned} A_x(\beta = 0) &= R - R \cos\left(\frac{L}{R}\right) = \frac{1 - \cos (Lk)}{k}, \\ A_y(\beta = 0) &= R \sin\left(\frac{L}{R}\right) = \frac{\sin (Lk)}{k}, \end{aligned} \tag{7}$$

where R is the radius of curvature $(R = 1/k)$ and L is the arc length of the flexible link. If β increases, the position of the connecting rod tip is

$$\begin{aligned} \begin{bmatrix} A_x \\ A_y \\ 0 \end{bmatrix} &= \mathbf{R}_z(\beta) \begin{bmatrix} \dfrac{1 - \cos (Lk)}{k} \\ \dfrac{\sin (Lk)}{k} \\ 0 \end{bmatrix} \\ &= \begin{bmatrix} \cos (\beta) \dfrac{1 - \cos (LK)}{K} - \sin (\beta) \dfrac{\sin (LK)}{K} \\ \sin (\beta) \dfrac{\sin (LK)}{K} + \cos (\beta) \dfrac{1 - \cos (LK)}{K} \\ 0 \end{bmatrix}. \end{aligned} \tag{8}$$

Equation (8) and the standard kinematics are defined above, and the function λ_1, λ_2, λ_3, and λ_4 in equations (3)–(6) can be calculated.

3.2.2. Inverse Kinematics. In addition to constraint equations (3)–(6), the inverse kinematics of the closed chain employs additional constraints $(\overline{AF}$ and $\theta)$ given by the position and orientation of the fingertip points, expressed by equations (9) and (10). Choose an input variable from equation (1) to solve equations (3)–(6), (9) and (10).

$$\overline{AB} + \overline{BC} + \overline{CD} + \overline{DE} + \overline{EF} - \overline{AF} = \lambda_5(a, k_1, k_2, k_3, k_4) = 0, \tag{9}$$

$$\beta + L_1 k_1 + L_2 k_2 + L_3 k_3 + L_4 k_4 = \theta. \tag{10}$$

3.3. Design of Flexible Finger Structure. The finger structure was improved according to the experimental results of tomato physical properties to minimize the initial contact force when the finger interacted with the tomato (before the layer interference) and generate a relatively large clamping force after grasping the tomato (after the layer interference) while maintaining the dexterity needed for the fingers to passively adapt to the tomato shape.
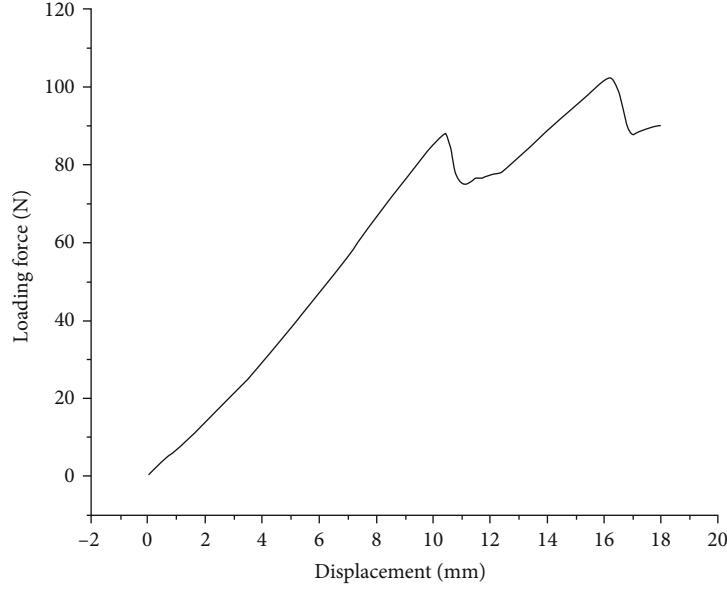
FIGURE 3: Pressure-displacement curve of tomato.

TABLE 2: Experimental results of damage characteristics.

Compression displacement/(mm)	Maximum compression force/(N)	Average storage days/(day)
0	0	15
1	5.56	14
2	8.03	14
3	13.42	12
4	15.28	10
5	27.15	8
6	35.78	7
7	43.56	5
8	40.03	6
9	57.09	4
10	68.57	3
11	80.89	2
12	82.71	1
13	87.36	0
14	90.12	1
15	90.69	1
16	101.23	0
17	112.33	0
18	110.79	0

FIGURE 4: Finger structure diagram: (a) no load state; (b) load state.

As shown in Figure 6, the finger is made of TPU material, and the basic structure remains unchanged. Set the fin length h to 70 mm to ensure that the fingertip position exceeds the maximum transverse diameter height when the finger is grasping the tomato, which solves the problem of excessive opening at the end. The base width is set to 36 mm to fit the finger fixing base. The thickness m of the fins in contact with the tomato is reduced to 1.5 mm, which ensures that the fingers are easily deformed when interacting with the tomato, and the initial contact force is minimized. At the same time, in view of the problem that the root position of the noncontact fin is prone to structural damage, the thickness n of the noncontact fin is set to 3 mm. Aiming at the problem of smooth surface of tomato, the contact fin surface is designed with different characteristic structures to increase the friction force and reduce the sliding during grasping. By changing the number of ribs, rib thickness t, inter-rib width e, and rib inclination angle θ, the relationship between the rib distribution law based on the layer blocking principle and the finger grip strength is further weighed.

First, determine the optimal number of ribs inside the finger, which is helpful for subsequent tests of rib thickness and angle changes. Secondly, the influence of fin structure changes on finger deformation is studied. By changing the rib thickness t, the effect of the rib thickness on the displacement of the fingertip was evaluated, and the most suitable rib size was selected. By changing the initial rib angle θ, the intercostal layer blocking effect during finger deformation is improved. Make the contact force between the finger and the tomato to the best state (when the θ changes, the rib width e will be adjusted appropriately).

(a)

(b)
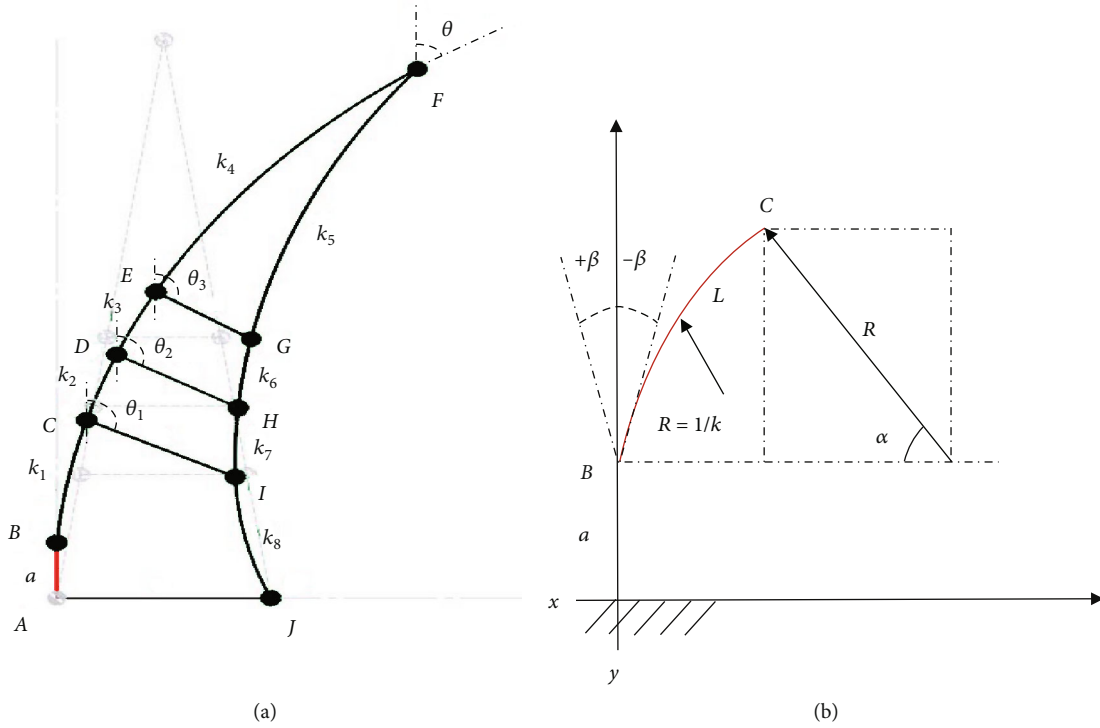
FIGURE 5: Mathematical model: (a) the composition of the single-finger structure; (b) single constant curvature section.
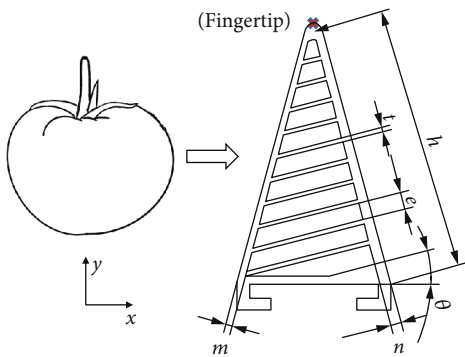
FIGURE 6: Key design parameters of new flexible finger.
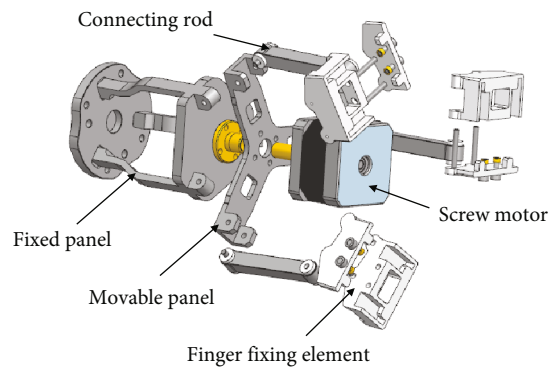
FIGURE 7: Design of fixed components.

3.4. Design of Fixed Components. Some progress has been made in the design method of the end-effector fixed components, but the rationality of the design still needs to be improved. For example, in the end structure design of reference [24], the screw motor passes through the fixed plate vertically upward and drives the slider to move up and down along the *z*-axis direction. However, the protruding lead screw takes up some of the space for the end-effector to grab the fruit. If the distance to the tomato is not properly controlled during the picking task, the rigid screw will come into contact with the crispy tomato on the surface, causing damage to the skin.

Therefore, based on the previous research experience, the structure of the end-effector is redesigned. The optimized fixing assembly consists of the finger fixing element,

the support base, and the screw motor. Its structural exploded diagram is shown in Figure 7. The finger fixing element is fixed in cooperation with the flexible finger bottom structure. The support base is composed of a fixed panel, a movable panel and three connecting rods. The fixed panel is used to assemble the screw motor and support the rotation of the finger fixing element. In order to realize the rotational movement of the finger fixing element, the movable panel moves in coordination with the screw motor through the coupling. The two ends of the connecting rods are, respectively, connected in rotation with the movable panel part and the finger fixing element to drive the fingers to open and close. The support base can be connected with the robotic arm through accessories such as flanges.

(a)   (b)
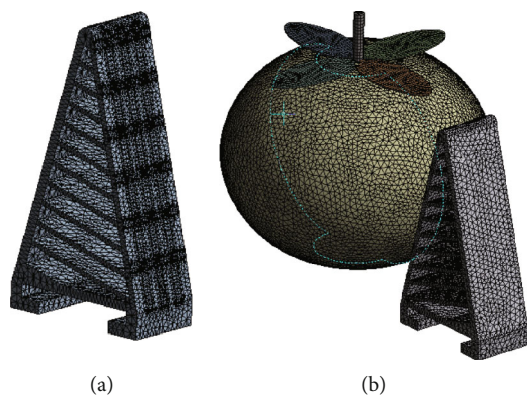
FIGURE 8: Network model of tomato and fingers: (a) single-finger network diagram; (b) network diagram of tomato and finger assembly.

4. Finite Element Simulation

TPU material has the advantages of high tension and tensile force, but its deformation is difficult to predict due to the nonlinear factors of geometry and materials. Therefore, the finite element analysis software ANSYS (ANSYS 2020 R2) is used to simulate the static structure of fingers and tomato to analyze the bending performance. The key parameters of the TPU material are set as follows: Shore hardness = 85 A, density = 1200 kg/m³, Young's modulus = 11.7 MPa, and Poisson's ratio = 0.45 [25]. Create a Static Structural module in ANSYS Workbench, add TPU material properties, and enter the parameters to get the model. Take one of the fingers as an example, determine the mesh accuracy of the finger, and use tetrahedral elements to divide the model, as shown in Figure 8. Set the element size to 1 mm, and the fingers are divided into 74942 nodes and 41455 elements.

4.1. Analysis of Single-Finger Force

4.1.1. Change in the Number of Ribs.
The number of ribs inside the finger was set to 6, 8, and 10; the rib angle θ was uniformly set to 0°; and loads of 5, 10, and 15 N were applied to the finger surface, respectively. When a tomato is in contact with a finger, the initial contact area is about 60 square centimeters. The stress area is selected in the middle of the finger, 20 unit surfaces are selected horizontally, and 3 unit surfaces are selected vertically, which are consistent with the actual contact area to the greatest extent. The simulation results are shown in Table 3. When a finger with 6 ribs is subjected to a load of 5 N, the total deformation of the finger is about 8.896 mm, which shows better extensibility than other fingers. But broken phenomenon appeared when subjected to 10 and 15 N loads. Fingers with 8 ribs can withstand loads of 5 and 10 N but break down when subjected to a load of 15 N. It is proved that the rigidity of these two finger structures is insufficient. The fingers with 10 ribs have a certain degree of stretchability while ensuring the load

TABLE 3: Simulation results of fingers with different numbers of ribs.

Number of fins	Total deformation (mm)		
	5 N	10 N	15 N
6	8.896	Fracture	Fracture
8	7.223	12.748	Fracture
10	6.795	10.831	14.346

conditions. Therefore, it is more appropriate to set 10 ribs inside the finger.

4.1.2. Rib Thickness Variation.
The influence of the thickness of the rib on the overall stiffness of the finger is analyzed. Set the fin thickness t to 0.6, 1.2, 1.8 mm, which is an integer multiple of the nozzle diameter of the 3D printer to ensure smooth printing. The rib angle θ is uniformly set to 0° to control the variable. A load force of 10 N was applied to the finger surface to obtain the tip displacements in the x and y directions of the finger for different rib thicknesses. As shown in Figure 9(a), when a load of 10 N is applied, the fingertip with a 1.8 mm rib thickness is displaced 11.2 mm along the x-axis, while the finger with a 0.6 mm rib thickness has only a displacement of 4.5 mm. The less tip travel on the x-axis indicates that the fingertip displacement is absorbed by the internal structure of the finger and the more passively adaptive the finger is. As shown in Figure 9(b), the fingertip with 1.8 mm rib thickness is displaced 5.3 mm along the y-axis direction, while the 0.6 mm rib tip is displaced by 8.7 mm. It is proved that the thinner the rib, the greater the deformation of the middle of the finger structure along the x-axis and the greater the travel of the fingertip along the y-axis. To sum up, the finger structure with 0.6 mm rib thickness is more in line with the design principles and requirements.

4.1.3. Rib Inclination Variation.
Increasing the rib inclination can reduce the initial contact force of the fingers. The maximum contact force was increased by the layer blocking effect. Set the rib thickness to 0.6 mm, the number of ribs to 10, and the rib inclination angle θ to be 0~60° in increments of 10°. A 10 N load was applied to the finger surface, and the layer blocking effect and the maximum displacement of the finger structure with different rib inclination angles were analyzed. The simulation effect is shown in Figure 10. When the rib inclination angle is 10° and 20°, the ribs do not appear to fit each other, and the difference in the maximum displacement of the finger deformation is small. When the inclination angle of the rib reaches 30°, the finger exhibits a layer blocking effect, and the maximum displacement decreases significantly.

As shown in Figure 11, as the inclination angle of the rib increases, the maximum displacement of the finger deformation fluctuates up and down. When the rib inclination angle is 30°, the layer blocking effect is obvious, and the displacement reaches the minimum. When the inclination angle continues to increase, the maximum displacement shows

(a)

(b)
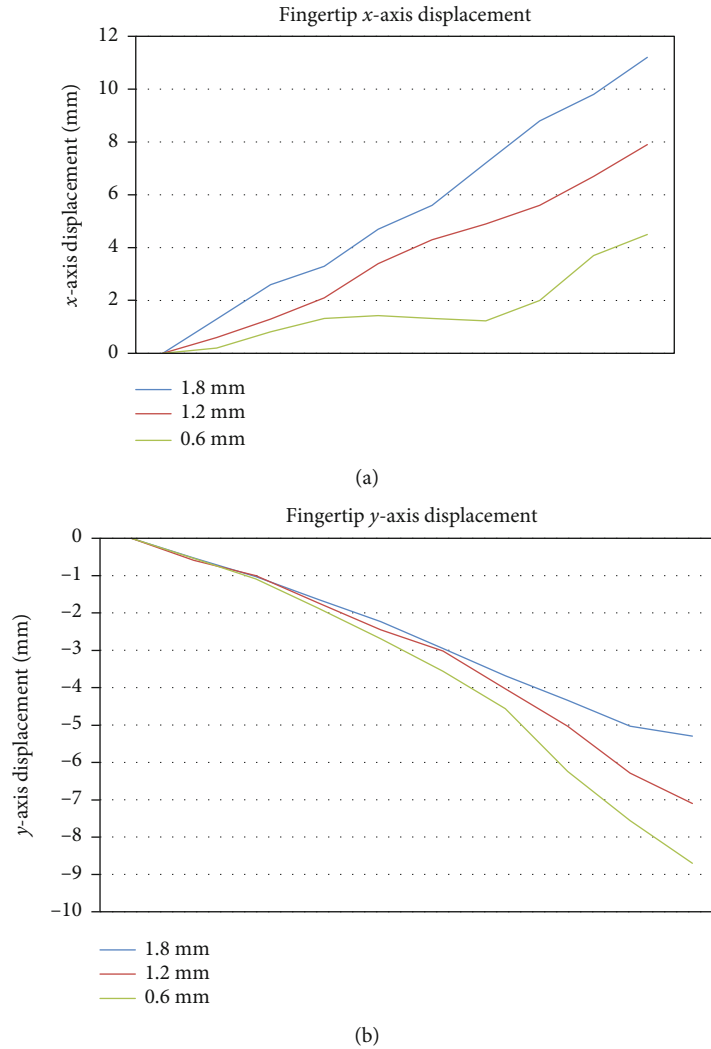
FIGURE 9: Simulation of fingertip displacement: (a) x-axis displacement; (b) y-axis displacement.

an upward trend again. It shows that the excessive dip angle has an adverse effect on the layer blocking effect. Therefore, the finger structure produces the best layer blocking effect at a rib inclination angle of 30°.

4.2. Simulation of Single-Finger Interaction with Tomato. The tomato is set as a fixed support, and the contact area between the finger and the tomato is set as frictionless contact. The interaction force is set to 10 N, the large deflection setting in the solver is turned on, and the total deformation is solved. The simulation results are shown in Figure 12. After comparing the total deformation of the finger and the displacement of the fingertip in the x and y directions with the single-finger analysis above, it is found that the data error is within ±0.2 mm, which verifies the accuracy of the data and conclusions.

In summary, through the analysis of the simulation results, the optimized finger structure parameters are obtained: the number of ribs is 10, the rib thickness is 0.6 mm, and the rib inclination angle is 30°.

5. Experimental Verification

5.1. Fabrication of the End-Effector. The finger structure of TPU material and the finger holder of resin material were printed with the standard FDM printer X-max. The rest of the panels are made of aluminum alloys. The total mass of the end-effector is 464.7 g. As shown in Figure 13, an Arduino Mega 2560 microcontroller is used as the control core, and a two-phase four-wire stepper motor is used to power the end-effector. The thin film pressure sensor is fixed on the surface of the finger to detect and record the force of each grasping tomato.

5.2. Single-Finger Experiment

5.2.1. Experiments on Finger Surface Features. The surface of the tomato is smooth. In order to avoid sliding during grasping, three structures with different surface features were designed on the contact surface of the flexible fingers to increase the friction force, numbered 1 to 3, as shown in Figure 14(a). An experimental platform was built to test

(a)

(b)

(c)
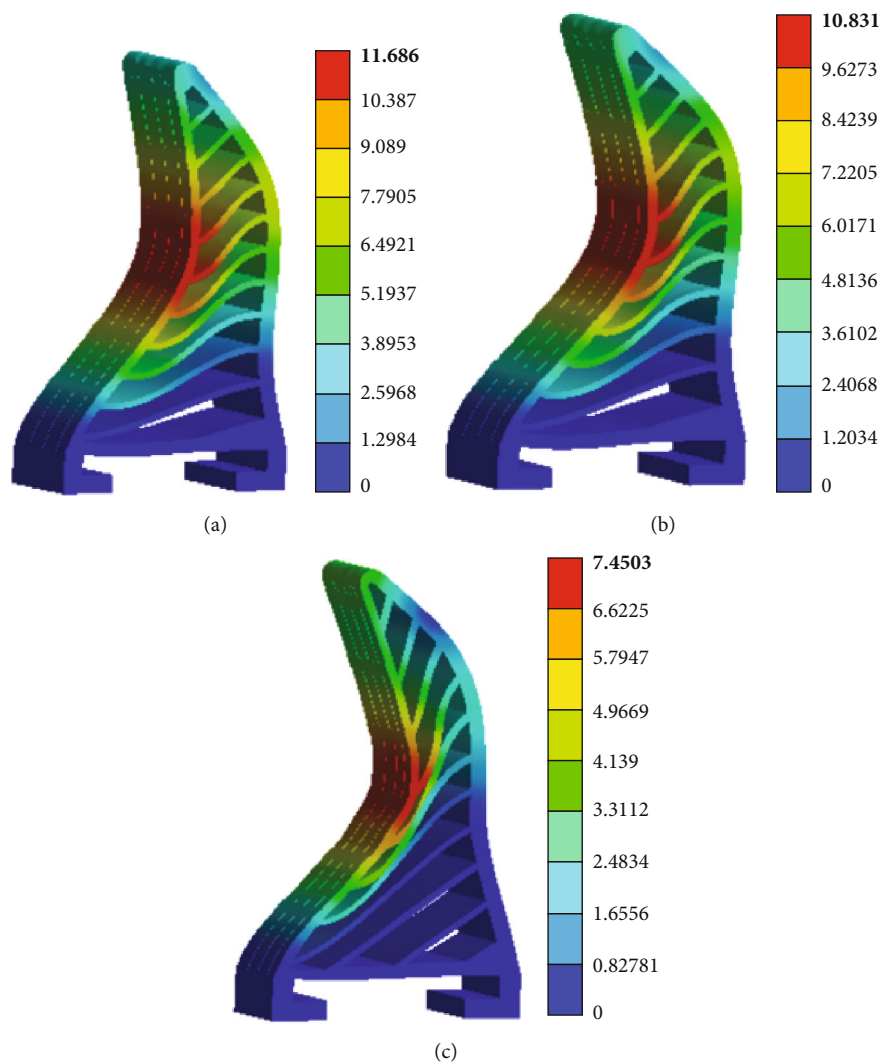
FIGURE 10: Layer blocking effect simulation of fingers: (a) 10° inclination; (b) 20° inclination; (c) 30° inclination.
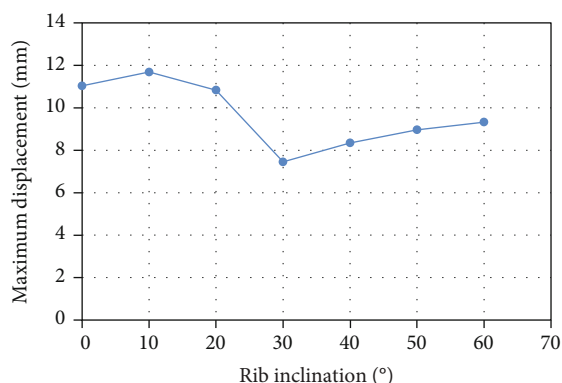
FIGURE 11: Relationship between maximum displacement and rib inclination.
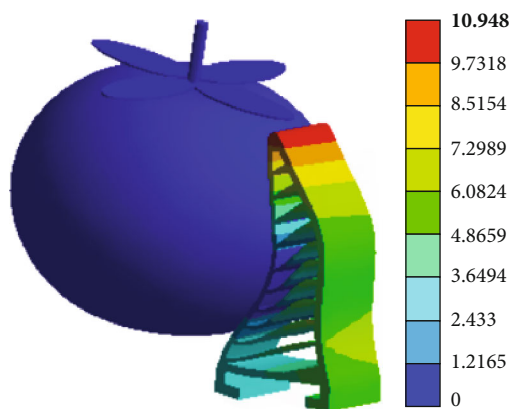
FIGURE 12: Simulation of tomato and finger interaction.

the frictional force generated when different surface features interact with tomatoes. As shown in Figure 14(b), the three surface feature structures were made into thin surfaces with an area of 10×15 cm and fixed on the test bench. Place the tomato on a thin surface and connect the dynamometer to the tomato through a string, so that it is on the same level as the tomato. The tension meter moves at a uniform speed
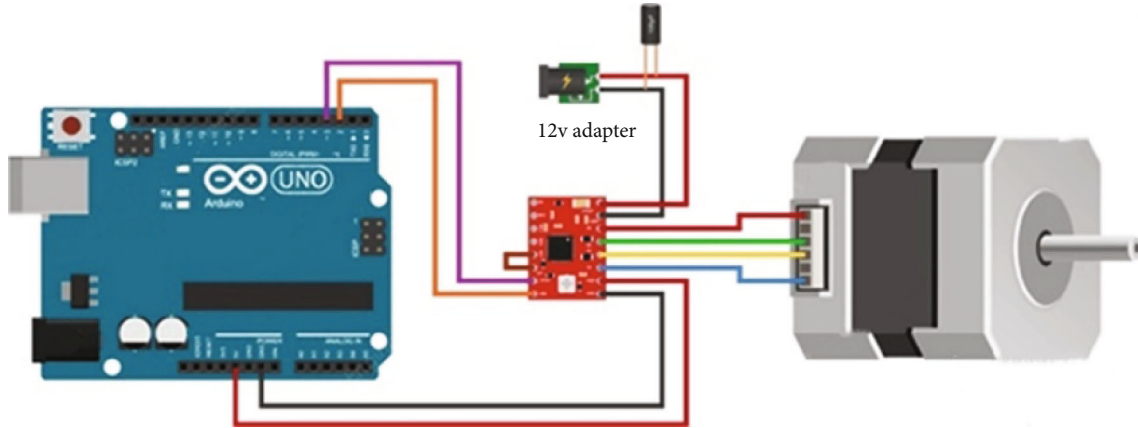
FIGURE 13: Control system of end-effector.

1.51N	1.45N	1.67N	1.39N
1	2	3	4

(a)   (b)
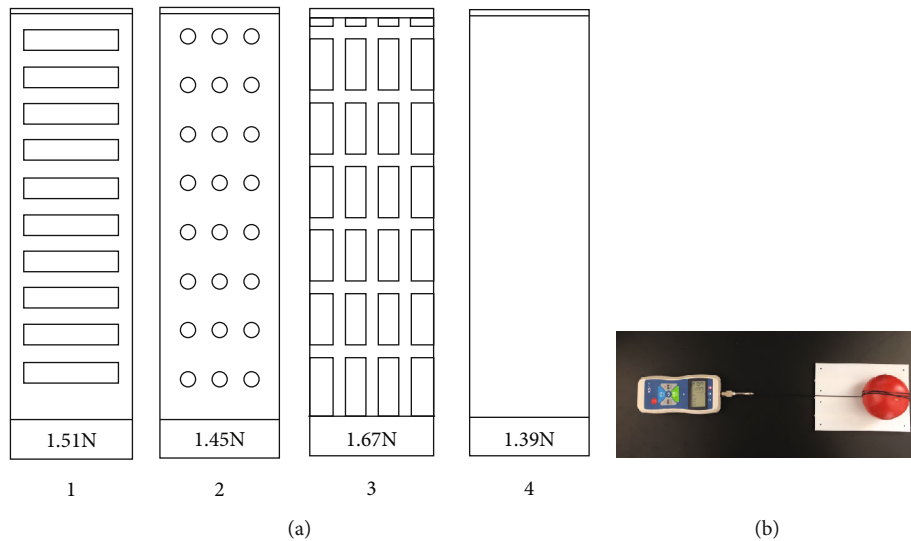
FIGURE 14: Friction test: (a) structure of different surface features; (b) experimental device.

along a straight line, pulling the tomato to displace until the tomato moves away from the thin surface. Record the maximum pulling force during this process. The experiment was repeated 10 times for each structure and averaged. Compared to the smooth surface structure (No. 4), the surface with the characteristic structure produces better friction effect. Comparing different surface feature structures, the No. 3 grid is selected as the finger surface feature structure.

5.2.2. Experiment on Finger Deformation. The finger load experiment was carried out to analyze the deformation of four typical finger structures under 10 N pressure. The bottom of the finger is fixed in a vise, and a load of 10 N is applied to the middle of the surface of the finger fin using a tension gauge. The position before and after the force is recorded at the position, and the displacement is calculated. As shown in Figure 15, the six-rib finger structure suffered structural damage under 10 N pressure. The 10-rib finger structure can withstand 10 N loads. When the rib inclination angle is 0°, the maximum displacement generated by the

finger is about 11.1 mm, and there is no layer blocking phenomenon. When the rib inclination angle is 30°, the maximum displacement of the finger reaches the lowest 7.8 mm due to the obvious layer blocking effect. The error with the simulation result is no more than ±0.2 mm, which verifies the correctness of the above simulation.

5.3. Clamping Experiment

5.3.1. Static Clamping Experiment. The end-effector grabs the tomato, and the tension gauge is connected to the tomato. Simulate the working state of the robot pulling tomatoes when picking, and test whether the gripping force of the end-effector meets the requirements. During the test, the average reading of the tension gauge was around 7 N, as shown in Figure 16(a). It is verified that the flexible end-effector can withstand a tensile force of 7 N, the load is more than 2 times its own weight, and the performance is excellent, which meets the needs of picking operations.

The tomato was divided into three intervals of 65~75 mm, 75~85 mm, and 85~95 mm for the clamping

(a)   (b)

FIGURE 15: Fingers bear 10 N load: (a) six-rib finger structure; (b) ten-rib finger structure.

(a)   (b)

FIGURE 16: Static clamping experiment: (a) force test; (b) stability test.

TABLE 4: Experimental results.

Tomato size (mm)	Maximum clamping force (N)	Average coverage (%)	Effective grab rate (%)
65~75	5.61	32.5	100
75~85	6.84	26.9	100
85~95	7.86	23.6	100

5.3.2. Dynamic Clamping Experiment. Typically, after the end-effector holds the tomato, a dynamic transport process takes place. Therefore, 20 tomatoes were randomly selected to simulate the working environment of the sorting robot for testing. The test steps are shown in Figure 17. The end-effector moves to the designated position to hold the tomato, moves up 10 cm vertically, moves 30 cm horizontally, and finally moves down 10 cm vertically and places it on the workbench. Tomatoes did not fall off, and the surface was not damaged during this process, which was counted as an effective sorting. The experimental results showed that the tomato did not fall off, and the tomato did not suffer from damage to the clamping. It is proved that the flexible end-effector has superior performance and is fully suitable for tomato picking and sorting.

According to the real picking scene, the tomato picking experiment was carried out on the end-effector. A comparative experiment is carried out on the two most common three-finger end-effectors. As shown in the picking experiment in Figure 18(a), the fingers of the pneumatic soft end-effector are made of silicone. In the inflated state, the inner finger air bag expands, and the finger size increases. If there is a slight angle deviation, the soft fingertips will easily touch the tomato. The fingers will bend inward, causing the grasp to fail. In the tensile test, the tensile force meter reading is only 4.83 N. The clamping force is small, which causes the tomatoes to slip easily, and the picking success rate is low. The rigid end-effector shown in Figure 18(b) has a larger clamping force. However, due to the immature research on the control strategy of the current end-effector, there is no closed-loop control between the motor drive and the sensor feedback, which often leads to the occurrence

experiment. 10 tomatoes were selected in each interval to verify the versatility of the end-effector for tomato grasping. The end-effector held the tomato for 30 seconds, and the peel was not damaged after release, which was counted as a valid grab. Record each thin film piezoelectric sensor reading as shown in Figure 16(b). Calculate the approximate surface area S_1 ($S_1 = \pi R^2$) of the tomato with the lateral diameter R, and record the gripping range of the fingers during the gripping process. Calculate the surface utilization area S_2 of the finger fins. Finally, calculate the average coverage ρ ($\rho = S_2/S_1$) of the fingers on tomatoes of different sizes.

The experimental results are shown in Table 4. For tomatoes with larger diameter sizes, the coverage is over 20%. For tomatoes with smaller diameters, the coverage is over 30%. The average clamping force is less than 8 N, and the effective grasping rate is 100%. Therefore, the flexible end-effector can achieve stable and nondestructive grasping of tomatoes with diameters ranging from 65 to 95 mm, which proves the rationality of the improved finger design.

FIGURE 17: Dynamic clamping experiment.

| (a) | (b) | (c) |

FIGURE 18: Actual picking experiment: (a) flexible pneumatic end-effector; (b) rigid end-effector; (c) the end-effector designed in this paper.

of tomato damage by clamping. Comparing with the existing products, it is found that the end-effector fixing component designed in this paper and the finger structure and size design optimized by simulation and experiment are more reasonable. As shown in Figure 18(c), while ensuring nondestructive grasping, the grasping force is large. It has strong adaptability for complex tomato picking scenes.

6. Conclusion

(1) A flexible underactuated end-effector suitable for tomato picking and sorting was designed according to the brittleness and particularity of tomato, combined with the principle of bionics. Mainly for the harvest of tomato with a diameter of 65~95 mm and a mass of not more than 500 g.

(2) Based on the experiment of tomato physical properties, it was obtained that the lateral diameter of the

tomato ranged from 66.4 to 92.7 mm, the height of the lateral diameter ranged from 35.1 to 62.7 mm, and the maximum nondestructive clamping force was 8 N. Combined with the bionics principle of the FRE structure, the flexible finger structure was designed, and the finite element analysis of the finger was carried out. The optimal structural parameters of the finger are obtained: the number of ribs is 10, the thickness of the ribs is 0.6 mm, and the inclination angle of the ribs is 30°.

(3) The single-finger experiment was performed on the end-effector, and the grid-like structure was obtained as the most suitable surface feature structure of the finger. The finger force deformation experiment verifies the correctness of the simulation results and the rationality of the finger design. The static clamping experiment of the end-effector verifies that the flexible end can withstand a tensile force of 7 N, and the

load exceeds 2 times its own weight. The coverage rate of tomato is 23.6~32.5%, and the effective clamping rate is 100%. It has strong versatility and meets the requirements of picking operations. The results of dynamic clamping experiments proved that the end-effector can hold and transport tomatoes of different sizes stably and nondestructively. It has strong protection and meets the requirements of sorting operations. Compared with the existing two common end-effectors, that is found that the end-effector designed in this paper has a large grasping force while ensuring nondestructive grasping. It has strong adaptability for complex tomato picking scenarios and provides solutions for the design and application of tomato picking and sorting robot end-effectors.

(4) In the future research, we will focus on the research of tomato visual recognition and localization and picking strategies. Solve the problems that still exist in tomato picking, such as the tomato recognition rate is not up to standard, the picking strategy is not perfect, and the picking sequence and pose are unreasonable. The designed flexible manipulator was put into a large-scale tomatoes picking scene for application research.

Data Availability

The data used to support the findings of this study are available from the corresponding author upon request.

Conflicts of Interest

The authors declare no conflict of interest.

Acknowledgments

References

[1] R. Gupta, S. Y. Kwon, and S. T. Kim, "An insight into the tomato spotted wilt virus (TSWV), tomato and thrips interaction," *Plant Biotechnology Reports*, vol. 12, no. 3, pp. 157–163, 2018.

[2] Z. Xin, Y. Cui, X. Yang, L. Kong, and Q. Lin, "Research progress on the status quo of the global vegetable industry and the development path of vegetable breeding in China," *Molecular Plant Breeding*, vol. 20, no. 9, pp. 3122–3132, 2022.

[3] A. Bechar, S. Yosef, S. Netanyahu, and Y. Edan, "Improvement of work methods in tomato greenhouses using simulation," *Transactions of the ASABE (American Society of Agricultural and Biological Engineers)*, vol. 50, no. 2, pp. 331–338, 2007.

[4] N. Ni, X. Wang, S. Wang, S. Wang, Z. Yao, and Y. Ma, "Structure Design and Image Recognition Research of a Picking Device on the Apple Picking Robot," *6th IFAC Conference on Bio-Robotics*, vol. 51, pp. 489–494, 2018.

[5] A. I. Setiawan, T. Furukawa, and A. Preston, *A low-cost gripper for an apple picking robot, Robotics and Automation*, Proceedings. ICRA '04.2004 IEEE International Conference on. IEEE, 2004.

[6] B. Wei, J. He, Y. Shi, G. Jiang, X. Zhang, and Y. Ma, "Design and experiment of underactuated citrus end-effector," *Transactions of the Chinese Society for Agricultural Machinery*, vol. 52, no. 10, pp. 120–128, 2021.

[7] L. van Herck, P. Kurtser, L. Wittemans, and Y. Edan, "Crop design for improved robotic harvesting: a case study of sweet pepper harvesting," *Biosystems Engineering*, vol. 192, pp. 294–308, 2020.

[8] T. Fujinaga, S. Yasukawa, and K. Ishii, *Development and Evaluation of a Tomato Fruit Suction Cutting Device*, 2021 IEEE/SICE International Symposium on System Integration (SII), 2021.

[9] Zhipeng Li, *Design and Research of Navel Orange Picking Robot, [Ph.D. thesis]*, Nanchang University, 2020.

[10] H. Yaguchi, K. Nagahama, T. Hasegawa, and M. Inaba, *Development of an Autonomous Tomato Harvesting Robot with Rotational Plucking Gripper*, 2016 IEEE/RSJ International Conference on Intelligent Robots and Systems (IROS), 2016.

[11] J. Lee, W. Han, E. Kim, I. Choi, and S. Yang, *A Stiffness-Controlled Robotic Palm Based on a Granular Jamming Mechanism*, 2020 17th International Conference on Ubiquitous Robots (UR), 2020.

[12] A. Alsakarneh, S. Alnaqbi, M. Alkaabi et al., "Experimental analysis of the holding-force of the jamming grippers," *Advances in Science and Engineering Technology International Conferences (ASET)*, vol. 2018, pp. 1–3, 2018.

[13] Q. Ge, A. H. Sakhaei, H. Lee, C. K. Dunn, N. X. Fang, and M. L. Dunn, "Multimaterial 4D printing with tailorable shape memory polymers," *Scientific Reports*, vol. 6, no. 1, p. 31110, 2016.

[14] Y. Miyahara and R. Kato, *Development of Thin Vibration Sheets Using a Shape Memory Alloy Actuator for the Tactile Feedback of Myoelectric Prosthetic Hands*, 2021 43rd Annual International Conference of the IEEE Engineering in Medicine & Biology Society (EMBC), 2021.

[15] M. Zhu, Y. Mori, T. Wakayama, A. Wada, and S. Kawamura, "A fully multi-material three-dimensional printed soft gripper with variable stiffness for robust grasping," *Soft Robotics*, vol. 6, no. 4, pp. 507–519, 2019.

[16] Z. Wang and S. Hirai, "Chamber dimension optimization of a bellow-type soft actuator for food material handling," *IEEE International Conference on Soft Robotics (Robo Soft)*, vol. 2018, pp. 382–387, 2018.

[17] K. Zhou, L. Xia, J. Liu, M. Qian, and J. Pi, "Design of a flexible end-effector based on characteristics of tomatoes," *International Journal of Agricultural and Biological Engineering*, vol. 15, no. 2, pp. 13–24, 2022.

[18] C. Jaren, S. Arazuri, I. Arana, N. Arias, P. Riga, and B. Epalza, "Detection of mealiness in tomato by textural analysis," *Acta Horticulturae*, vol. 934, pp. 1135–1140, 2012.

[19] S. K. Min, L. M. Duizer, and A. Grygorczyk, "Application of a texture analyzer friction rig to evaluate complex texture attributes in apples," *Postharvest Biology and Technology*, vol. 186, article 111820, 2022.

[20] Z. Li, J. Liu, and P. Li, "Relationship between mechanical properties and mechanical damage of tomato in robot picking,"

Agricultural Industry Journal of Engineering, vol. 26, no. 5, pp. 112–116, 2010.

[21] M. H. Ali, A. Zhanabayev, S. Khamzhin, and K. Mussin, *Biologically Inspired Gripper Based on the Fin Ray Effect*, 2019 5th International Conference on Control, Automation and Robotics (ICCAR), 2019.

[22] J. H. Shin, J. G. Park, D. I. Kim, and H. S. Yoon, "A universal soft gripper with the optimized fin ray finger," *International Journal of Precision Engineering and Manufacturing-Green Technology*, vol. 8, no. 3, pp. 889–899, 2021.

[23] W. Crooks, S. Rozen-Levy, B. Trimmer, C. Rogers, and W. Messner, "Passive gripper inspired by Manduca sexta and the Fin Ray® Effect," *International Journal of Advanced Robotic Systems*, vol. 14, no. 4, p. 172988141772115, 2017.

[24] Y. A. Lei, *Flexible Mechanical Claw*, CN214136081U, Guangdong Province, 2021.

[25] C. Emminger, U. D. Çakmak, R. Preuer, I. Graz, and Z. Major, "Hyperelastic material parameter determination and numerical study of TPU and PDMS dampers," *Materials*, vol. 14, no. 24, p. 7639, 2021.

Research Article

Spatial and Temporal Variations in the Ecological Vulnerability of Northern China

Chunwei Song and Huishi Du [iD]

College of Tourism and Geographical Science, Jilin Normal University, Siping 136000, China

Correspondence should be addressed to Huishi Du; duhs@jlnu.edu.cn

Ecological vulnerability is the focus of research on global environmental impact, regional sustainable development, ecological civilization, and green development. There are eight deserts and four sandy lands in northern China. The ecological environment is sensitive to climate change and human activities. It is of great significance to carry out long-term sequential ecological vulnerability assessments. Therefore, taking northern China as the research area, this paper selects 13 data indicators such as climate, topography, and soil based on the ecological sensitivity-ecological recovery-ecological pressure model (SPR) and uses the spatial principal component analysis method (SPCA) to quantitatively evaluate the spatial and temporal differentiation characteristics and driving forces of ecological vulnerability in this area from 1980 to 2020. The results showed that areas with extreme, severe, and moderate vulnerability dominated northern China, accounting for 74.58% of the total area. The analysis revealed a decrease in ecological vulnerability from west to east and north to south. Meanwhile, from the perspective of timing, the overall level of ecological vulnerability showed an upward trend before 2000, and the overall level of ecological vulnerability continued to decline after 2000, and the quality of the ecological environment improved. During the study period, areas in northern China with severe vulnerability and slight vulnerability showed a change of 15.53% and -14.01%, respectively. The main reason for the change in ecological vulnerability is the frequent transformation between forest land, grassland, water, and cultivated land. In addition, the study found a spatial autocorrelation of ecological vulnerability of northern China and a significantly positive correlation. After 2000, the spatial aggregation of vulnerability was high-high cluster, which was mainly distributed in northwest China. The study's findings will provide a robust scientific basis for ecosystem management and sustainable development.

1. Introduction

Ecological vulnerability theory originated from the ecological transition zone theory proposed in the early 20th century, which refers to the sensitivity of ecosystems to external interference [1]. Due to global environmental change and the intensification of human-land relation research, ecological vulnerability assessment, restoration and reconstruction, and sustainable development management have become research hotspots globally [2, 3]. Ecological vulnerability can reflect the causes of ecosystem changes in specific regions to a certain extent. It is of great practical significance for regional eco-environmental protection, rational utilization of resources, ecological sustainable development, and ecological protection. At the same time, it provides reference and decision-making support for ecological restoration projects [4].

The current evaluation methods include the comprehensive index method and analytic hierarchy process [5, 6]. Boori et al. built a drive-pressure-state-impact-response (DPSIR) model based on remote sensing (RS), geographic information system (GIS), and AHP and selected 23 indicators to analyze the spatiotemporal changes in ecological vulnerability of the Russian Republic of Tatarstan [7]. Li et al. used the entropy weight analysis to comprehensively evaluate the ecological vulnerability of the Karst mountainous areas of southwest China [8]. Ma et al. used the "pressure-state-response" evaluation model and selected 18 indicators

to comprehensively evaluate the ecological vulnerability of the Three Gorges Reservoir Area from 2001 to 2010 [9]. Researchers have improved their understanding of ecological vulnerability using different models, but with few limitations. Although these models can be used to analyze the driving force objectively, they are not suitable for exploring the spatial changes and comprehensively evaluating ecological vulnerability specifically for a region. At the same time, when these methods assign weights to each factor, human subjective factors considerably influence the results. Therefore, it is urgent to adopt more objective quantitative research methods to reduce the subjectivity of artificial effect, improve the objectivity and accuracy of ecological vulnerability assessment, and comprehensively assess the ecological vulnerability situation in the region by analyzing spatial heterogeneity characteristics and overall change trends.

Recently, China has developed "The Belt and Road Initiative" to enhance economic development; it has improved the strategic position of northern China. As a part of this initiative, it is important to discuss the sustainable development of northern China from the perspective of ecological vulnerability. In the past, scholars paid more attention to the ecological vulnerability of a small region, which did not reflect the overall characteristics. Ecological vulnerability is actually the result of a series of comprehensive factors dominated by the regional environment itself. Therefore, it is necessary to monitor and evaluate the spatial characteristics and evolution patterns of the research area from a global perspective and macrosystem thinking. The present study based on the SRP model, the slope, temperature, precipitation, and other data from 1980 to 2020 which are selected as vulnerability evaluation indicators in northern China. Using the SPCA method, the spatial and temporal distribution of ecological vulnerability in northern China is explored, the spatial pattern and evolution process of ecological vulnerability are clarified, and the ecological vulnerability is scientifically monitored and evaluated in northern China. The study's findings will reveal the protection and sustainable development of ecological functions of northern China and provide a reference for further research on ecological vulnerability in this area.

2. Data Sources and Research Methods

2.1. Study Area. Northern China (28°–55°N, 67°–125°E) has a total area of $5.64 \times 10^6 \, \mathrm{km}^2$, accounting for about 58.6% of the total land area of China. The administrative division has 15 provinces (cities and autonomous regions), including Beijing, Tianjin, Heilongjiang, Jilin, Liaoning, Hebei, Henan, Shandong, Shanxi, Inner Mongolia, Shaanxi, Ningxia, Gansu, Qinghai, and Xinjiang. The area mainly has temperate monsoon, continental, and plateau mountain climates. The landforms in northern China are complex and diverse, and the terrain is variable. The topography is mainly plateaus, mountains, basins, and plains, including the Altai Mountains, the Aljin Mountains, the Tianshan Mountains, the Kunlun Mountains, the Qilian Mountains, the Tarim Basin, the Junggar Basin, the Turpan Basin, and the Songnen Plain (Figure 1). This region has temperate mixed forests,

cold temperate coniferous forests, temperate grasslands, deciduous broad-leaved forests, subtropical evergreen broad-leaved forests, temperate deserts, and cold vegetation from the east to the west. The soil types are complex and diverse; regions from east to west have mainly black soil, cold brown soil, black calcium soil, brown soil, yellow-brown soil, gray calcium soil, gray desert soil, and brown desert soil. The annual precipitation in this area gradually decreases from the southeast (1000 mm) to the northwest (100 mm), with a temperature ranging from -5°C to 20°C.

2.2. Data Sources and Preprocessing. Digital elevation data were obtained from the geospatial data cloud platform (http://www.gsclound.cn), with elevation, slope, topographic fluctuation, and river network density details based on the digital elevation model (DEM). The meteorological data were obtained from the China Meteorological Data Network (http://data.cma.cn), which uses the Kriging interpolation method to interpolate the annual average precipitation data and the annual average temperature data. Vegetation coverage data were derived from the NASA website (http://search.earthdata.nasa.gov) to calculate the normalized vegetation index using the pixel dichotomy model and the raster calculator. Land use data and soil erosion intensity data were obtained from the Resource and Environmental Science Data Center of the Chinese Academy of Sciences (http://www.resdc.cn), and the bioabundance index of northern China was calculated. Data on population density, per capita GDP density, and primary productivity were derived from the *China Statistical Yearbook*; these data were obtained by dividing the statistics in the Yearbook by the area of the administrative region.

2.3. Construction of an Ecological Vulnerability Index System

2.3.1. Metric Selection. The SRP model (the concept model of "ecological sensitivity-ecological resilience-ecological pressure") is a comprehensive evaluation model that reflects the quality of the ecological environment based on the habitat quality index [10]. Ecological sensitivity demonstrates the ability of an ecological environment to resist interference. Elevation, slope, topographic fluctuation, and river network density were selected to reflect the topographic characteristics. The average temperature and average precipitation were used to reflect the changes in meteorological factors. The land use types were used to reflect the changes in surface factor. The soil erosion intensity was used to reflect the changes in soil factor. Meanwhile, ecological resilience refers to the ability of an ecosystem to recover after being damaged by an external disturbance. Vegetation coverage, bioabundance index, and net primary productivity were selected to reflect ecological resilience. Ecological pressure refers to the degree of interference caused by human social activities to the ecosystem. Population density and GDP per capita were used to reflect the environmental impact of human activities and economic development [11].

2.3.2. Standardization of Indicators. The nature and attributes of each indicator used to assess the ecological vulnerability are different; therefore, ecological vulnerability can be
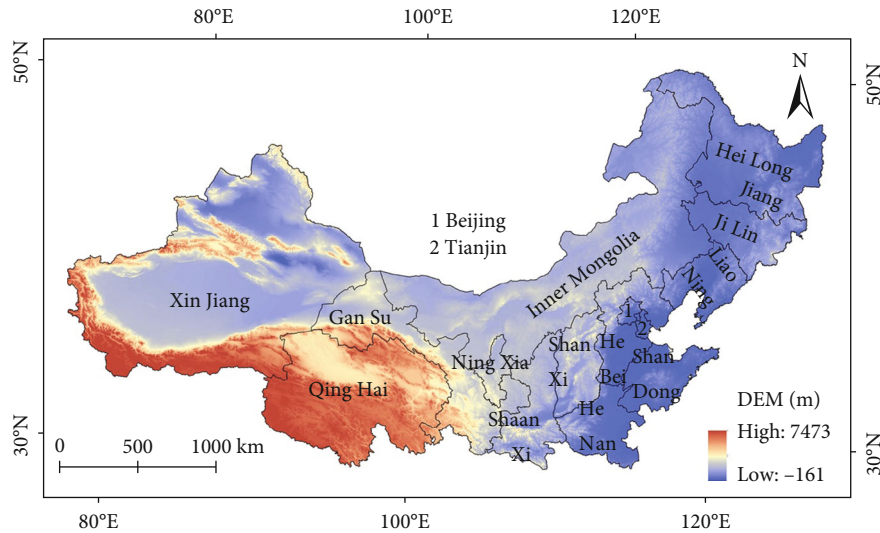
FIGURE 1: Elevation of the research area.

assessed directly. According to the ecological vulnerability impact of each index, this study divided the evaluation index into positive and negative indicators (Table 1). The index standardization adopted the extreme difference standardization method, using the formula as follows [12]:

$$R_T = \frac{X - X_{\min}}{X_{\max} - X_{\min}},$$
$$R_G = \frac{X_{\max} - X}{X_{\max} - X_{\min}}, \quad (1)$$

where R_T is the standardized value of the forward indicator, R_G is the standardized value of the negative indicator, and $X_{\max}$ and $X_{\min}$ indicate the maximum and minimum values of indicator X.

2.3.3. Ecological Vulnerability Index. Spatial principal component analysis (SPCA) is based on the principle of mathematical statistics. By rotating the spectral-spatial coordinate axis of the feature, multiple spatial index data are converted into a few comprehensive layers. When calculating the weights of ecological sensitivity, ecological resilience, and ecological pressure indicators by SPCA, the artificial weight of the index is reduced. At the same time, the main components of the ecological vulnerability of northern China in 1980, 1990, 2000, 2010, and 2020 were analyzed. Finally, north China's ecological vulnerability index (EVI) was calculated based on the top five main components, including a major component greater than 85%. EVI was calculated as follows [13]:

$$\text{EVI}_n = R_1 \text{PC}_{1n} + R_2 \text{PC}_{2n} + \cdots + R_n \text{PC}_{kn}, \quad (2)$$

where EVI_n is the ecological vulnerability index, $R_1, R_2 \cdots R_n$ indicate the corresponding indicator weights, $\text{PC}_{1n}, \text{PC}_{2n} \cdots \text{PC}_{kn}$ indicate the main components with a cumulative contribution rate greater than 85%, and n is the year. The

larger the ecological vulnerability index, the more fragile the ecological environment in the region, conversely, the better the ecological environment in the region.

Further, to compare the ecological vulnerability across various periods, the results of ecological vulnerability in 1980, 1990, 2000, 2010, and 2020 were standardized as follows [14]:

$$\text{SEVI} = \frac{\text{EVI} - \text{EVI}_{\min}}{\text{EVI}_{\max} - \text{EVI}_{\min}} \times 10, \quad (3)$$

where SEVI is the standardized value of the ecological vulnerability index, which ranges from 0 to 10; EVI is the ecological vulnerability index of the research area; $\text{EVI}_{\max}$ is the maximum value of the ecological vulnerability index within the research area; and $\text{EVI}_{\min}$ is the minimum value of the ecological vulnerability index within the research area.

Referring to the environmental characteristics and the histogram distribution and standard deviation of the ecological vulnerability in northern China and comprehensively considering north China's unique ecological and environmental attributes, the EVI of northern China was classified according to the natural breakpoint method. The ecological vulnerability of northern China was divided into five levels: slight vulnerability [0–1.5], light vulnerability (1.5–3.0), moderate vulnerability (3.0–5.1), severe vulnerability (5.1–7.1], and extreme vulnerability (7.1–10].

2.3.4. Spatial Autocorrelation Analysis. Spatial autocorrelation analysis is an important method of monitoring the relevance of spatial properties and their changes using a collection of spatial data analysis methods and technologies [15]. At present, spatial autocorrelation for a single element can be described by two indicators: global Moran'I and local Moran'I. The global Moran'I index characterizes the correlation degree of ecological vulnerability of the adjacent space units and reveals the impact of spatial structural elements on ecological vulnerability. Meanwhile, the local Moran'I index

TABLE 1: Ecological vulnerability evaluation index system in northern China based on SRP model.

Target layer	Criterion layer	Basic index layer
Ecological sensitivity	Topographic factors	Elevation (+), slope (+), topographic fluctuation (+), river network density (-)
	Surface factor	Land use types (+)
	Soil factor	Soil erosion intensity (+)
Ecological resilience	Meteorological factors	Average temperature (-), average precipitation (-)
	Vegetation factors	Vegetation coverage (-), bioabundance index (-), net primary productivity (-)
Ecological pressure	Social factors	Population density (+), GDP per capita (+)

Note: +/- indicates forward indicators and negative indicators, respectively.

expresses the spatial distribution structure and distribution characteristics of ecological vulnerability and shows the overall law of spatial variation. The spatially related local indicator cluster diagram (LISA) was used to evaluate the spatial clustering by calculating the local Moran'I index. It mainly includes five aggregation modes: high-high cluster, high-low outlier, low-high outlier, low-low cluster, and not significant.

The global Moran'I index was calculated as follows:

$$I = \frac{\sum_{i=1}^{n}\sum_{j=1}^{n} W_{ij}(X_i - \bar{X})(X_j - \bar{X})}{\sum_{i=1}^{n}\sum_{j=1}^{n} W_{ij}\sum_{i=1}^{n}(X_i - \bar{X})^2}. \quad (4)$$

Meanwhile, the local Moran'I index was calculated as follows:

$$I = \frac{(X_i - \bar{X})}{S^2}\sum_j W_{ij}(X_j - \bar{X}). \quad (5)$$

I is the Moran'I index; X_i, X_j indicate the mean of the vulnerability index in the i and j evaluation units; $\bar{X}$ is the mean vulnerability of all evaluation units; W_{ij} is the spatial weight matrix; and S is the sum of the elements of the spatial weight matrix.

3. Results and Analysis

3.1. Temporal Variations in Ecological Vulnerability in Northern China.
Between 1980 and 2020, the areas with severe vulnerability and extreme vulnerability in northern China showed a 15.53% and 6.38% increase, respectively; the areas showed a 14.01%, 11.83%, and 2.17% decrease, respectively (Figure 2). Meanwhile, the areas with slight vulnerability, light vulnerability, and moderate vulnerability in northern China showed a 26.84%, 17.80%, and 21.96% decrease, respectively, from 1980 to 2000. However, the areas with severe and extreme vulnerability showed a 60.26% and 8.14% increase. Among them, Gansu, Shandong, and Henan Provinces mainly had areas that transformed from slight vulnerability to moderate and severe vulnerability, while Heilongjiang, Jilin, Liaoning, Inner Mongolia, and Shaanxi Provinces had areas that transformed from moderate to severe and extreme vulnerability. This change occurred due to the rapid socioeconomic development during the 1980–2000 period, especially in the agricultural field,

which led to a continuous decline in the ecological conditions and the ability to change the ecological environment, subsequently increasing ecological vulnerability. From 2000 to 2020, the areas with extreme and severe vulnerability decreased by 1.63% and 27.91%, respectively, while the areas with moderate, light, and slight vulnerability increased by 25.39%, 7.26%, and 14.92%, respectively. Among them, Heilongjiang Province, Jilin Province, Inner Mongolia Autonomous Region, Shandong Province, Hebei Province, Beijing City, and Tianjin City mainly transformed from severe vulnerability to moderate vulnerability, probably due to the large-scale conversion of farmlands to forests, grasslands, and lakes in response to regional ecological problems and the establishment of nature reserves and other nature conservation activities, subsequently reducing the ecological vulnerability.

3.2. Spatial Variations in Ecological Vulnerability in Northern China.
From 1980 to 2020, the ecological vulnerability of northern China was mainly concentrated at three levels: extreme vulnerability, severe vulnerability, and moderate vulnerability (Figure 3). In 2000, northern China's extreme vulnerability and severe vulnerability reached the maximum, accounting for 54.57% of the area, while moderate vulnerability reached the minimum, accounting for 22.32% of the area. In 1980, the areas with different ecological and environmental vulnerability levels in northern China were in the following order: moderate vulnerability > extreme vulnerability > light vulnerability > severe vulnerability > slight vulnerability (28.60% > 25.55% > 20.62% > 16.81% > 8.42%). By 2020, the areas under the different ecological vulnerability levels were in the following order: moderate vulnerability > extreme vulnerability > severe vulnerability > light vulnerability > slight vulnerability (27.98% > 27.18% > 19.42% > 18.18% > 7.24%).

Further analysis showed that the ecological vulnerability of northern China decreased from west to east and from north to south. The western part, including Xinjiang, Gansu, north-central Ningxia, northwest Qinghai, north Shaanxi, and western Inner Mongolia, had mainly areas with extreme vulnerability and severe vulnerability, probably because these areas had less precipitation and large evaporation, poor vegetation cover, and shallow soil layer. Meanwhile, areas with light vulnerability and slight vulnerability were mainly distributed on the south side of Xinjiang and Qinghai, located in the protected zone and at a high altitude. The eastern part, including Heilongjiang, Jilin, Liaoning, and eastern Inner Mongolia, had areas with severe vulnerability and
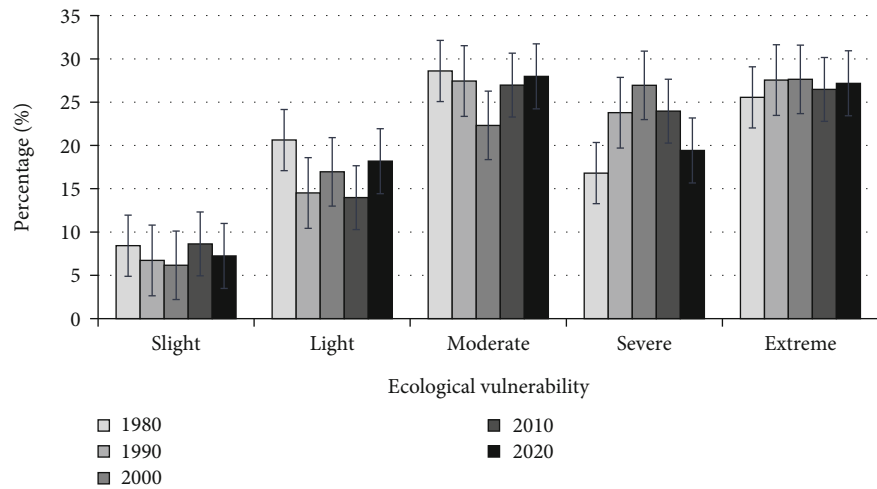
Figure 2: Characteristics of different levels of ecological vulnerability in northern China.

(a)

(b)

(c)

(d)

(e)
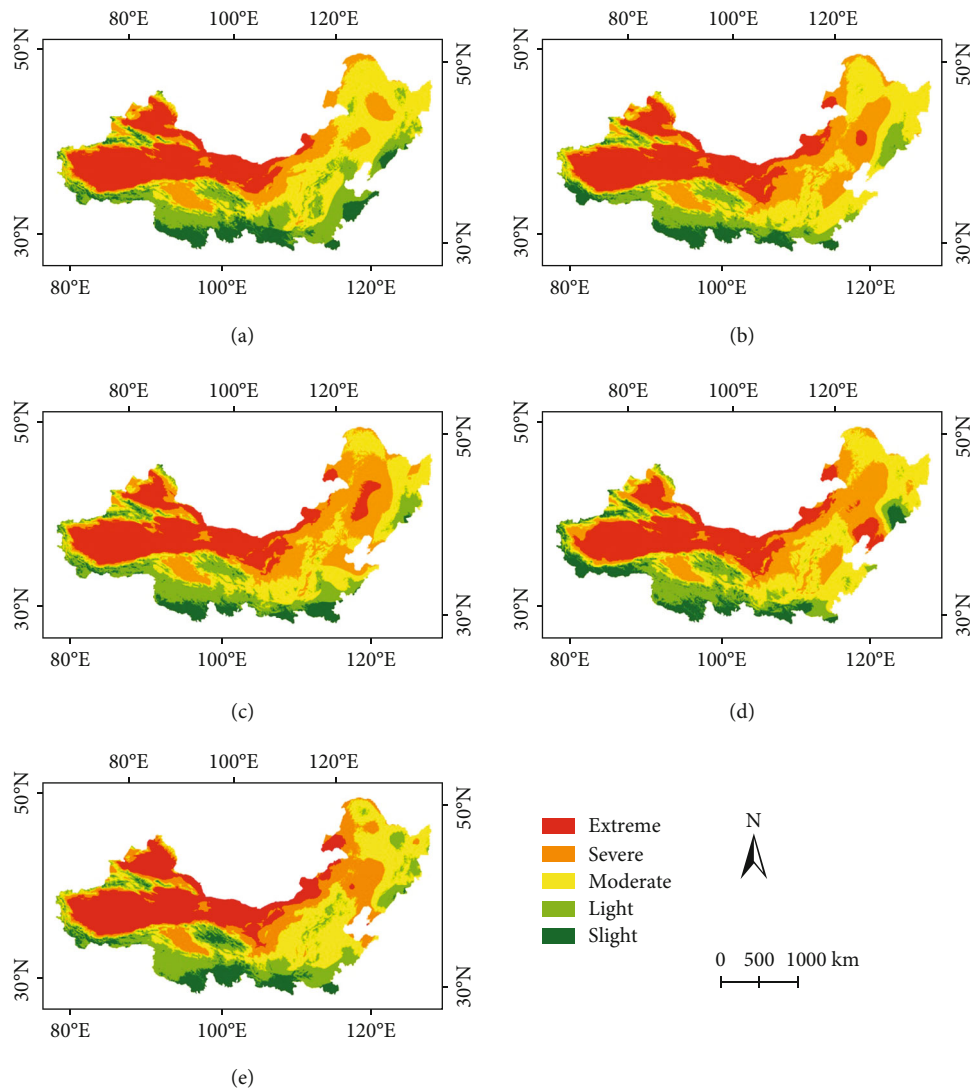
Figure 3: Spatial distribution of ecological vulnerability in northern China: (a) 1980; (b) 1990; (c) 2000; (d) 2010; (e) 2020.

moderate vulnerability because the average annual temperature was relatively different, the winter was long and cold, the summer was short and warm, and the soil was frozen for a long time. Meanwhile, areas with light vulnerability and slight vulnerability were mainly distributed in the southern part of Jilin and Liaoning, with mountains located in nature reserves. The central part of the research area, including Beijing, Tianjin, Shandong, Shanxi, Hebei, and Henan, belonged to a semiarid region. The ecological vulnerability of areas from north to south gradually reduced from severe to slight vulnerability, with increasing average annual temperature. At the same time, Qinghai, Shaanxi, Henan, and Shandong had a relatively humid climate due to Qinghai Lake and the Yellow River. Therefore, the vulnerability of these ecological habitats was relatively low.

3.3. Spatiotemporal Variations in Ecological Vulnerability among the Different Land Use Types in Northern China. Various evaluation indicators were graded and assigned according to the graded assignment method. According to the water resource capacity of different land uses, the land uses were arranged from low to high in the following order: forest land and water < grassland < cultivated land < urban land < unused land. Overall, the area of forest land, grassland, and water body area in northern China initially decreased and then increased from 1980 to 2020 (Figure 4), reaching the lowest value in 2000. Forest land, grassland, and water area accounted for 5.11%, 35.47%, and 2.28% of the total area in 2000. The cultivated land area first increased and then decreased, reaching a maximum of $575,280 \, \text{km}^2$ in 2000, which accounted for 10.20% of the total area. From 1980 to 2020, the area under construction increased by 31.20%. Thus, the research area showed changes in ecological vulnerability mainly due to the conversion of forest land, grassland, water, and cultivated land. The forest land, grassland, and water areas decreased by 17.64%, 4.78%, and 8.80%, respectively, from 1980 to 2000, while the cultivated land increased by 27.50%. From 2000 to 2020, the cultivated land area decreased by 30.88%, while the forest land, grassland, and water areas increased by 35.42%, 10.18%, and 22.37%, respectively, mainly due to the continuous reclamation by humans, resulting in forest land, grassland, water bodies, and converted cultivated land.

The areas with slight and light vulnerability in the western ecoregion of the study area were mainly distributed in forest land, grassland, and water. Areas with moderate vulnerability and severe vulnerability were primarily distributed in the cultivated land and the urban and rural construction land, while the extremely vulnerable regions in the northwest were almost entirely concentrated in the unused land. Meanwhile, areas with slight vulnerability were widely distributed in grassland because of the better ecological background of forest land, grassland, and water areas and the larger grassland in the northwest region. The areas with slight vulnerability and light vulnerability in the eastern ecological area were mainly distributed in Changbai Mountain and other areas. The area mainly had forest land and was a nature reserve. Meanwhile, areas with moderate and severe vulnerability were mainly distributed in the cultivated land,

grassland, water, urban land, and unused land. The areas with slight vulnerability and light vulnerability of the central ecoregion were mainly distributed in forest land, grassland, and water. In contrast, moderately vulnerable and severely vulnerable areas were primarily distributed in the cultivated land and urban land in other areas, with less unused land.

3.4. Spatial Aggregation Characteristics of Ecological Vulnerability in Northern China. From 1980 to 2020, the ecological vulnerability of northern China showed significant spatial aggregation, with an almost similar overall trend (Figure 5). The high-high cluster was mainly distributed in Xinjiang, western Inner Mongolia, northwestern Qinghai, northern Gansu, and north Ningxia; most of these regions were extremely vulnerable. The low-low cluster was mainly distributed in the eastern and central regions and slightly in north Xinjiang; most regions were dominated by slightly vulnerable, lightly vulnerable, and moderately vulnerable areas. The remaining aggregation evaluation units were not significant. Besides, aggregation expansion and migration were detected over the years. In 2000, the low-low cluster in northern China reached maximum due to the frequent conversions of the forest land, grassland, cultivated land, and urban land, resulting in a strong ecological vulnerability. Since 2000, the expansion of high-high clusters in the northwest mainly occurred in the Taklimakan Desert in Xinjiang, as China has been transforming via a semigovernance and semiutilization method, maintaining the green planting of the Taklimakan Desert while continuously exploiting minerals and resources in the desert and maximizing the use of resources in the desert.

4. Discussion

4.1. Driving Force of Ecological Vulnerability. Northern China is affected by the comprehensive factors of natural conditions and humanistic factors, and the land use has changed dramatically [16]. Environmental factors are one of the causes of regional ecological vulnerability [17]. This study found that the spatial variations in ecological vulnerability are mainly related to topographic, meteorological, and soil factors, which is consistent with the previous. For example, Guo et al. analyzed the driving mechanisms of ecological vulnerability in the northern semiarid desert grassland ecological area and found that the intensity of natural factors, such as topography, temperature, and precipitation, was significantly related to the changes in vulnerability [18]. Similarly, the present study found that the changes in temperature and precipitation greatly changed the hydrothermal balance of northern China, which had a significant impact on the environment, changing the ecosystem process. This conclusion confirms the conclusion of predecessors regarding ecologically fragile areas in parts of northern China; for example, Zhang et al. found that vegetation coverage and precipitation were the main driving factors controlling the spatial and temporal changes in ecological vulnerability in the Loess Plateau. The group also detected that vulnerability varied greatly across regions and land use types [19]. Therefore, the research results of the natural factors of this study on ecological vulnerability are convincing [20].
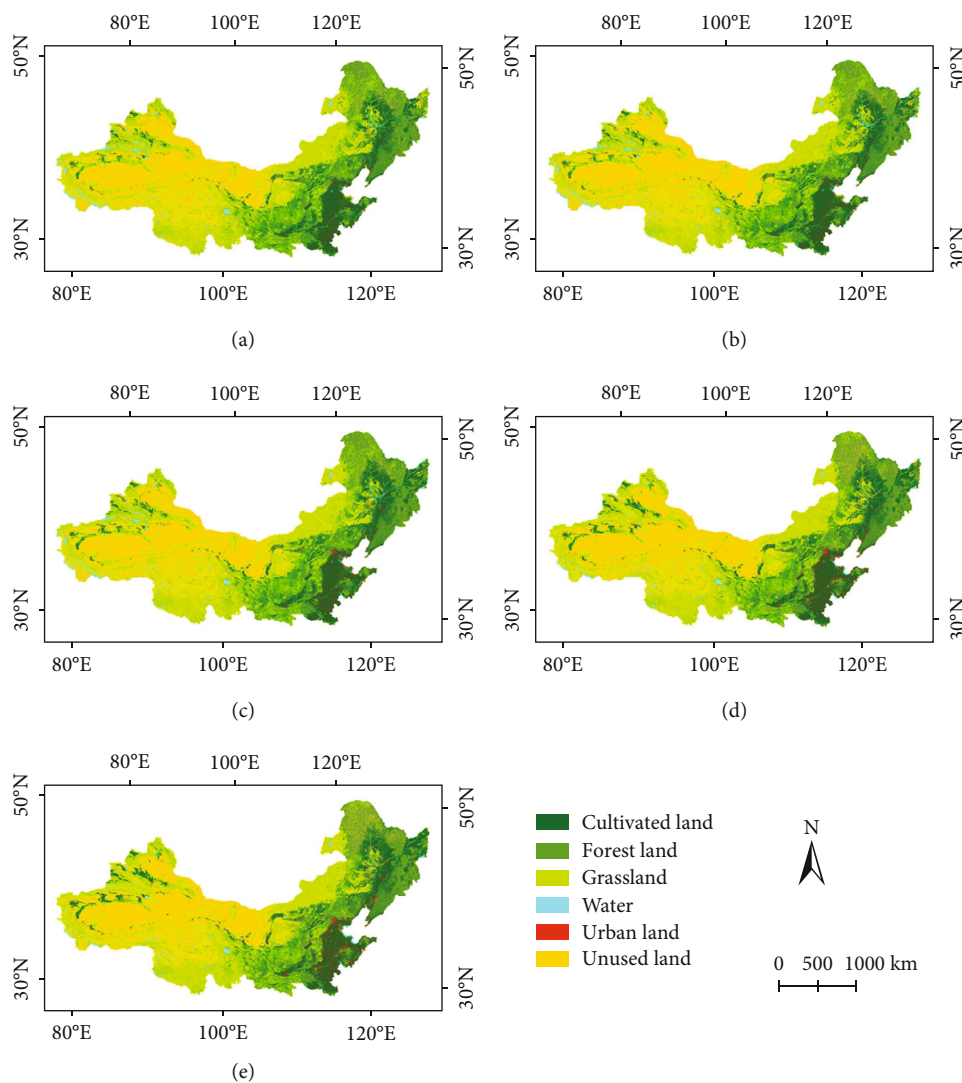
Figure 4: Monitoring the dynamics of land use in northern China: (a) 1980; (b) 1990; (c) 2000; (d) 2010; (e) 2020.

Anthropogenic activity is another factor affecting the ecological vulnerability of the region [21]. The changes in land use type reflect the human influence on nature and are one of the key factors affecting ecological vulnerability, which is consistent with the previous research results [22]. For example, Tian et al. used RS-based and GIS-based technologies to evaluate the ecological vulnerability under land use changes around Hangzhou Bay [23]. The construction land increased significantly in this area, reflecting urbanization. Research has also proven that the changes in ecological vulnerability in northern China may be related to the continuous expansion of cultivated land. Due to the intensification of human activities, the areas under cultivation and construction have significantly changed. Due to the geographical location of northern China and population increase, large areas of forest land, grassland, and water have been converted into cultivated land and construction land, which shows the continuous socioeconomic and urban-rural development and urbanization and the increasing impact of human activities. The research results are consistent with those of Zhou et al. [24]. They proved the significant impact of land use change on ecological vulnerability in Huinan County of

China. Forestlands of Huinan County have been transformed into cultivated lands, leading to changes in ecological vulnerability. In recent years, China has systematically restored "mountains, fields, forests, lakes, and grasses," coordinated the balance between agricultural production and ecological brittleness in northern China, and took appropriate measures to curb the increase in ecological vulnerability. This is in line with the support of national policies for ecological construction and environmental protection [25].

From the research results, the spatial distribution status and spatial pattern of ecological vulnerability are relatively reasonable, which shows that the selection of indicators, evaluation criteria, and evaluation methods of ecological vulnerability assessment are feasible. There are many methods for evaluating ecological vulnerability. Which method is more scientific and reasonable to evaluate ecological vulnerability and how to build a more scientific evaluation index system need to be studied in depth. The evaluation criteria for the ecological vulnerability of indicator factors proposed in this study are based on existing standards, so they need to be further studied.

(a)

(b)

(c)

(d)

(e)
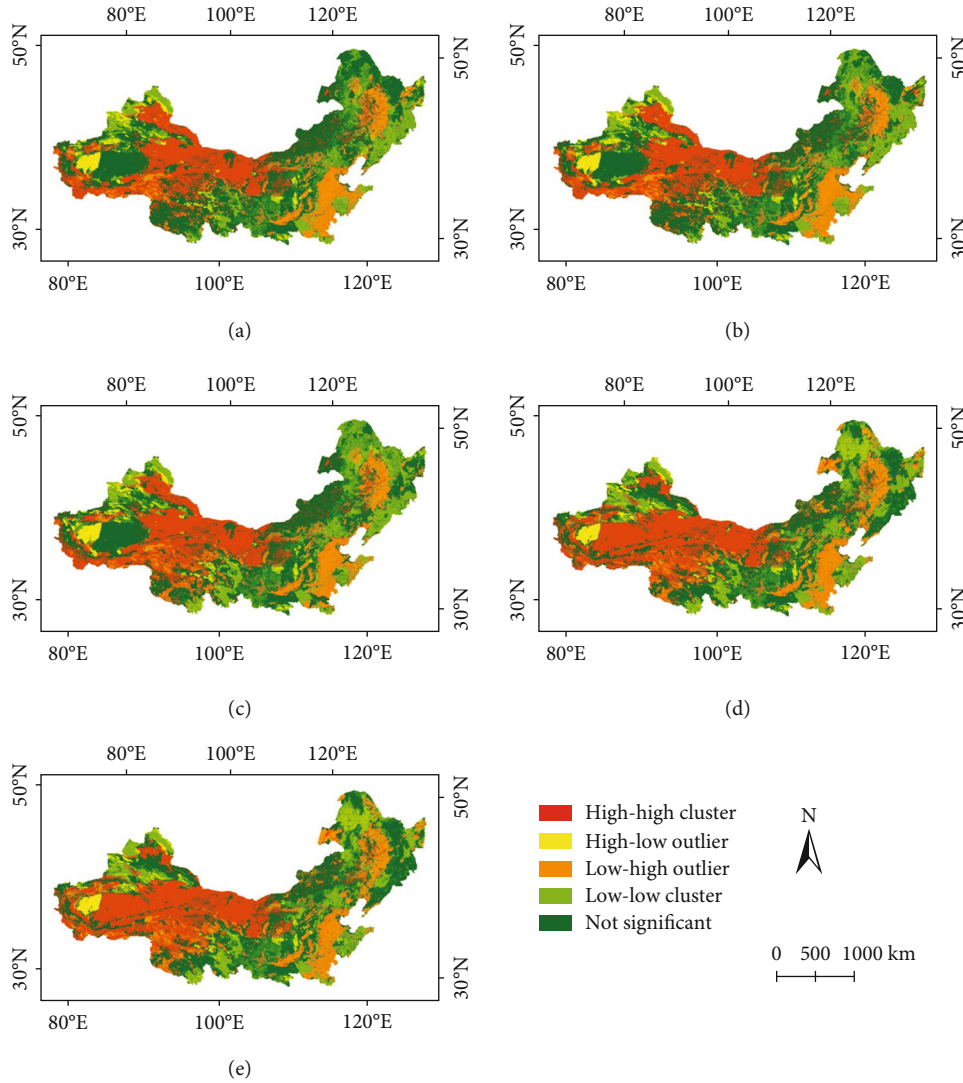
Figure 5: Local spatial autocorrelation LISA cluster map in northern China: (a) 1980; (b) 1990; (c) 2000; (d) 2010; (e) 2020.

4.2. Ecological Management and Optimization Strategy for Northern China. Northern China has unique geographical features, including climate, vegetation, soil, and hydrology, as well as distinct social, economic, and cultural characteristics [26]. To help decision-makers plan strategies to improve the ecological environment, northern China is divided into six ecological optimization areas: ecological protection areas, ecological monitoring areas, ecological concern areas, ecological restoration areas, ecological control areas, and ecological optimization areas.

Ecological protection areas are composed of slightly vulnerable and lightly vulnerable areas throughout the year. Ecological reserves are mostly nature reserves and should maintain ecological protection policies and protect the ecological environment quality [27]. In addition, to support the "green water and green mountains are golden mountains and silver mountains" concept, we should strengthen publicity and education, enhance the people's awareness, and create an atmosphere to protect the treasured plants [28]. Ecological monitoring areas are composed of extremely vulnerable areas throughout the year. This is because the area

has less precipitation and evaporates vigorously; therefore, the impact of human activities should be reduced, and buffer zones should be established on the edge. We should also aim to control the degradation of land, soil, and vegetation caused by misuse of land, overgrazing, and overirrigation and curb further desertification [29]. Ecological concern areas are composed of moderately vulnerable and severely vulnerable areas throughout the year. Moreover, human activities are frequent in this area. Therefore, human activity is mainly farming, the soil quality should be protected, and ecological stability should be maintained. We should comprehensively plan for land use and regional ecological governance, adapt local conditions, promote strengths and avoid weaknesses, strengthen soil and water conservation and desertification control measures, and encourage comprehensive regional development [30].

Ecological restoration areas have low ecological vulnerability. The region has changed from high to low vulnerability. Due to improved protection, the ecological policies in the region are constantly decreasing; therefore, we should aim to maintain the original environmental policies [31].

We should continue to implement ecological forest-bearing areas; grasp the agricultural, forestry, and animal husbandry structure; and establish green barriers. Ecological control areas are those with increasing ecological vulnerability. The region has transformed from low to high vulnerability mainly due to economic development. Moreover, the primary industry accounts for a relatively high proportion in this region, but the ecological management lags behind. Therefore, we should strengthen people's awareness of protecting the environment and formulate new environmental policies [32]. We should also completely utilize solar energy, geothermal energy, wind energy, and other natural resources. Ecological optimization areas demonstrate fluctuating ecological vulnerability. The irrational social activities of human being led to the continuous degradation of the ecological environment. Therefore, the government has been implementing ecological projects, such as converting farmland to forests and grassland to lakes, to maintain ecological stability [33].

5. Conclusion

The study found that northern China has areas (>70.96%) with extreme vulnerability, severe vulnerability, and moderate vulnerability. From 1980 to 2020, the overall ecological vulnerability in northern China increased first and then decreased. Here, the ecological vulnerability increased until 2000, beyond which it increased. Thus, from 2000 to 2020, the quality of the ecological environment and the stability of the ecosystem have improved.

The ecological vulnerability in northern China gradually weakened from west to east and from north to south. During the study period, the areas with severe vulnerability increased (15.53%), while those with slight vulnerability decreased (-14.01%). The vulnerability of the ecological environment has a significant spatial autocorrelation and a significant positive correlation. It is a significant high-high cluster in the western part of the research area, and the aggregation characteristics have migrated and expanded spatially.

Spatiotemporal variation of ecological vulnerability in northern China is mainly affected by natural factors and human activities in the region. Further, our study found that natural factors, such as temperature and precipitation, and human activities resulted in spatiotemporal variations in ecological vulnerability in northern China. At the same time, the socioeconomic factors contribute to ecological vulnerability, and their impact tends to gradually increase.

Data Availability

The data used to support the findings of this study are available from the corresponding author upon request.

Conflicts of Interest

The authors declare that they have no conflicts of interest.

References

[1] X. R. Zhang, Z. B. Wang, and J. Lin, "GIS based measurement and regulatory zoning of urban ecological vulnerability," *Sustainability*, vol. 7, no. 8, pp. 9924–9942, 2015.

[2] Y. Q. Sun, X. Yang, and L. N. Hao, "Spatial and temporal differentiation and driving mechanism of ecological vulnerability along Sichun-Tiber railway during 2000-2020 based on SRP model," *Bulletin of Soil and Water Conservation*, vol. 41, no. 6, pp. 201–208, 2021.

[3] Q. F. Wei, Y. Shao, and X. C. Wang, "Preliminary evaluation of Gaofen-3 quad-polarized SAR imagery for Longbao protected plateau wetland reserve," *Journal of Sensors*, vol. 2019, Article ID 8789473, 7 pages, 2019.

[4] D. Liu and L. N. Li, "Spatiotemporal change and driving factors of land use in the northern border transect of China, 1995-2015," *Resources Science*, vol. 43, no. 6, pp. 1208–1221, 2021.

[5] R. Turvey, "Vulnerability assessment of developing countries: the case of small-island developing states," *Development and Policy Review*, vol. 25, no. 2, pp. 243–264, 2007.

[6] M. Mahapatra, R. Ramakrishnan, and A. S. Rajawat, "Coastal vulnerability assessment using analytical hierarchical process for South Gujarat coast, India," *Natural Hazards*, vol. 76, no. 1, pp. 139–159, 2015.

[7] M. S. Boori, K. Choudhary, R. Paringer, and A. Kupreyanov, "Using RS/GIS for spatiotemporal ecological vulnerability analysis based on DPSIR framework in the Republic of Tatarstan, Russia," *Ecological Informatics*, vol. 67, p. 101490, 2022.

[8] H. G. Li, X. Zhou, Y. Xiao, X. Luo, R. G. Liang, and D. F. Yang, "Temporal and spatial changes of ecological vulnerability in southwestern karst mountains based on SRP model," *Ecological Science*, vol. 40, no. 3, pp. 238–246, 2021.

[9] J. Ma, C. X. Li, H. Wei et al., "Dynamic evaluation of ecological vulnerability in the Three Gorges Reservoir Region in Chongqing Municipality, China," *Acta Ecologica Sinica*, vol. 35, no. 21, pp. 7117–7129, 2015.

[10] Y. H. Li, Q. Fan, X. Wang, J. C. Xi, S. Y. Wang, and J. Yang, "Spatial and temporal differentiation of ecological vulnerability under the frequency of natural hazard based on SRP model: a case study in Chaoyang County," *Acta Ecologica Sinica*, vol. 35, no. 11, pp. 1452–1459, 2015.

[11] G. L. Sun, H. Y. Lu, J. X. Zheng, Y. Y. Liu, and Y. J. Ran, "Spatio-temporal variation of ecological vulnerability in Xinjiang and driving force analysis," *Arid Zone Research*, vol. 39, no. 1, pp. 258–269, 2022.

[12] C. X. Xu, C. X. Lu, and S. L. Huang, "Study on ecological vulnerability and its influencing factors in Zhangjiakou area," *Journal of Natural Resources*, vol. 35, no. 6, pp. 1288–1300, 2020.

[13] Q. Zhu, Y. N. Wang, W. M. Zhou, L. Zhou, D. P. Yu, and L. Qi, "Spatiotemporal changes and driving factors of ecological vulnerability in Northeast China forest belt," *Chinese Journal of Ecology*, vol. 40, no. 11, pp. 3474–3482, 2021.

[14] Z. C. Guo, W. Wei, S. F. Pang, Z. Y. Li, J. J. Zhou, and B. B. Xie, "Spatio-temporal evolution evolution and motivation analysis of ecological vulnerability in arid inland river basin based on SPCA and remote sensing index: a case study on the Shiyang

River Basin," *Acta Ecologica Sinica*, vol. 39, no. 7, pp. 2558–2572, 2019.

[15] J. H. Lin, G. J. Hu, X. H. Qi et al., "Ecological environmental vulnerability and its driving forces in urban agglomeration in the Fujian Delta region," *Acta Ecologica Sinica*, vol. 38, no. 12, pp. 4155–4166, 2018.

[16] T. A. Okey, S. Agbayani, and H. M. Alidina, "Mapping ecological vulnerability to recent climate change in Canada's Pacific marine ecosystems," *Ocean and Coastal Management*, vol. 106, pp. 35–48, 2015.

[17] C. X. Luo, A. D. Pan, and H. S. Qian, "The assessment of ecosystem vulnerability to climate change of Xinjiang," *Arid Environment Monitoring*, vol. 20, no. 1, pp. 39–43, 2006.

[18] B. Guo, W. H. Kong, F. Han, J. J. Wang, L. Jiang, and Y. F. Lu, "Dynamic monitoring of ecological vulnerability in the semiarid desert and steppe ecological zone of northern China based on RS and its driving mechanism analysis," *Journal of Tropical and Subtropical Botany*, vol. 26, no. 1, pp. 1–12, 2018.

[19] L. X. Zhang, J. W. Fan, H. Y. Zhang, and D. C. Zhou, "Spatial-temporal variations and their driving forces of the ecological vulnerability in the Loess Plateau," *Environmental Sciences*, vol. 46, pp. 1–12, 2022.

[20] Q. Zhang, R. Y. Yuan, V. P. Singh et al., "Dynamic vulnerability of ecological systems to climate changes across the Qinghai-Tibet Plateau, China," *Ecological Indicators*, vol. 134, p. 108483, 2022.

[21] J. Li, "A study on the vulnerability of social-ecosystem based on tourism: a case study of Sanjiangyuan," *Ground Water*, vol. 34, no. 2, pp. 210-211, 2012.

[22] P. Wang, W. Zhao, and X. L. Ke, "Evaluation and spatiotemporal evolution of ecological vulnerability of Qinjiang based on SRP model," *Research of Soil and Water Conservation*, vol. 28, no. 5, pp. 347–354, 2021.

[23] S. Tian, F. Gui, L. Z. Wang, S. Zhao, and Z. Shao, "Land use change and ecological vulnerability evaluation around Hangzhou Bay," *Territory & Natural Resources Study*, vol. 6, pp. 17–23, 2021.

[24] Y. Zhou, Y. H. Zhang, and Y. J. Zhai, "Analysis of ecological vulnerability based on land-use changes in mountain plain transition zones," *Terri Natural Resource Study*, vol. 6, pp. 29–32, 2013.

[25] S. Q. Wang, Z. F. Tao, P. L. Sun, S. J. Chen, H. Y. Sun, and N. Li, "Spatiotemporal variation of forest land and its driving factors in the agropastoral ecotone of northern China," *Journal of Arid Land*, vol. 14, no. 1, pp. 1–13, 2022.

[26] X. Y. Zhang, W. Wei, L. Zhou et al., "Analysis on spatiotemporal evolution of ecological vulnerability in arid areas of Northwest China," *Acta Ecologica Sinica*, vol. 41, no. 12, pp. 4707–4719, 2021.

[27] X. Y. Zhang, K. Liu, S. D. Wang et al., "Spatiotemporal evolution of ecological vulnerability in the Yellow River Basin under ecological restoration initiatives," *Ecological Indicators*, vol. 135, p. 108586, 2022.

[28] S. S. Cao, Y. H. Wang, F. Z. Duan, W. J. Zhao, Z. H. Wang, and N. Fang, "Coupling between ecological vulnerability and economic poverty in contiguous destitute areas, China: empirical analysis of 714 poverty-stricken counties," *Chinese Journal of Applied Ecology*, vol. 27, no. 8, pp. 2614–2622, 2016.

[29] Z. C. Guo, W. Wei, P. J. Shi et al., "Spatiotemporal changes of land desertification sensitivity in the arid region of northwest China," *Acta Geographica Sinica*, vol. 75, no. 9, pp. 1948–1965, 2020.

[30] E. Y. Yu, L. Qi, L. M. Dai et al., "Correlation analysis of elements in the mountains-rivers-forests-farmlands-lakes-grasslands life community: using Changbai mountains as an example," *Acta Ecologica Sinica*, vol. 39, no. 23, pp. 8837–8845, 2019.

[31] B. Li, Z. T. Zhang, S. H. Tan, J. H. Wang, X. Y. Zhang, and N. Zhang, "Improving the policy and mechanism of grassland ecological protection promoting the integration and development of forest and grass system and mechanism," *Forestry Economics*, vol. 41, no. 4, pp. 3–9, 2019.

[32] L. J. Duan, Y. S. Zhuang, and D. G. Sun, "Preliminary evaluation on the status of Changbai Mountain biodiversity conservation priority area (Jilin region)," *Environmental Protection*, vol. 47, no. 13, pp. 57–60, 2019.

[33] Y. Huang, J. Cheng, and P. Wang, "Spatiotemporal evolution pattern and driving factors of ecological vulnerability in agro-pastoral region in northern China: a case of Yanchi County in Ningxia," *Arid Land Geography*, vol. 44, no. 4, pp. 1175–1185, 2021.

Hindawi

Retraction

Retracted: Research on Home Product Design and Intelligent Algorithm Recommendation considering Ergonomics

Journal of Sensors

This article has been retracted by Hindawi following an investigation undertaken by the publisher [1]. This investigation has uncovered evidence of one or more of the following indicators of systematic manipulation of the publication process:

(1) Discrepancies in scope

(2) Discrepancies in the description of the research reported

(3) Discrepancies between the availability of data and the research described

(4) Inappropriate citations

(5) Incoherent, meaningless and/or irrelevant content included in the article

(6) Manipulated or compromised peer review

The presence of these indicators undermines our confidence in the integrity of the article's content and we cannot, therefore, vouch for its reliability. Please note that this notice is intended solely to alert readers that the content of this article is unreliable. We have not investigated whether authors were aware of or involved in the systematic manipulation of the publication process.

Wiley and Hindawi regrets that the usual quality checks did not identify these issues before publication and have since put additional measures in place to safeguard research integrity.

We wish to credit our own Research Integrity and Research Publishing teams and anonymous and named external researchers and research integrity experts for contributing to this investigation.

The corresponding author, as the representative of all authors, has been given the opportunity to register their agreement or disagreement to this retraction. We have kept a record of any response received.

References

[1] X. Wang, "Research on Home Product Design and Intelligent Algorithm Recommendation considering Ergonomics," *Journal of Sensors*, vol. 2022, Article ID 1791269, 10 pages, 2022.

Research Article

Research on Home Product Design and Intelligent Algorithm Recommendation considering Ergonomics

Xianya Wang [1,2]

[1]*Suqian University, Suqian 223800, China*
[2]*Catholic University of Korea, Gyeonggi-do, 14662, Republic of Korea*

Correspondence should be addressed to Xianya Wang; 18064@squ.edu.cn

Under the modern design concept, consider ergonomics to design home products. With the progress of civilization and technology, the improvement of life quality in the process of urbanization, and the increasing abundance of home life and home products, people's requirements for living environment and environmental products are continuously improving. In order to further meet the necessities of life and solve the reasons such as limited living space at home, people are no longer satisfied with purchasing household products in large quantities but are more suitable for household needs. According to the user's requirements for ergonomic home product design, a criterion layer is established, and the weight of the criterion layer is calculated to obtain its corresponding weight value. It can be obtained that consumers think that safety is the most important, followed by ease of use, functionality, and aesthetics. In the second criterion level, the order of importance is stable operation, safe use of materials, invisible circuit, strong practicability, massage function, safety guardrail, convenient installation, easy cleaning, intelligent operation, home style, structural strength, easy to move, natural materials, air purification, easy disassembly, suitable size, simple shape, convenient function, timely after-sales, soft color tone, noise reduction, simple decoration, single color matching, and comfortable function. The addition of the nearest neighbors improves the accuracy of the CFCNN-CL algorithm and the REPREDICT PCC algorithm in terms of smart algorithm recommendations for home products considering ergonomics. But compared between the two, the CFCNN-CL algorithm has better performance and better accuracy than the REPREDICT PCC algorithm. In terms of the influence of data sparseness, UCF-Jaccard has a smaller MAE value than other methods in general and is less susceptible to the influence of sparse data, and the MAE value does not change much. Among the group filtering methods, the RRP-UICL method has better prediction accuracy than the commonly used group filtering methods.

1. Introduction

In the context of a design item, the article depicts ergonomic studies and analyses that can be performed on concurrent engineering design models at any phase of the design procedure. During the design procedure, ergonomic experts were asked to suggest designers on end-user feature and assist in evaluating the impact of design choices made under the perfect future activity methodology. Therefore, ergonomics is defined as a factor of innovation and safety [1], because an ergonomic way enhances quality of life and activities of daily living. Gerontology decreases the results of age-related constraints through technological equipment and special

designs for the family environment. Physical fall makes daily activities at home more difficult as you age. The article focuses on "common sense" and specific design recommendations for entrances and kitchens to improve independence in older adults, while geriatric technology can play a special role in improving comfort and safety for older adults [2]. Globalization, technological intricacy, the development of more ripe markets that require diverse or high-quality products, and competitive pressures to decrease development time and costs have led to the wider use of methods and technologies that deal with human factors in different ways. Consequently, a number of approaches and techniques have been developed, each offering different and complementary

approaches to better understand human-relevant design requirements. An overview of current trends in consumer product design involves ergonomics and human factors to understand the strengths, weaknesses, and challenges facing researchers and practitioners; methodologies and techniques throughout the product life cycle (PLC), including design and the innovation process, are important [3]. Consider that ergonomic product quality is an essential part of successful product development. Product designers involved in basic product development activities must support an approach that considers ergonomic and other product requirements. The first part examines how people working in product development organizations communicate with their product users, the second part analyzes the factors that influence ergonomic integration in product design, and the third part evaluates and discusses. This paper introduces computer-aided ergonomics as a means of integrating ergonomics with product design; the purpose of part IV is to explore how human simulation tools can help designers consider the diversity of the human body. This work evaluates different approaches to generate specific virtual series that can be used as test suites for matched trials in virtual designs. Research has shown a greater understanding of design approaches that support the integration of ergonomics into the product design process, with a focus on anthropometric diversity in vehicle design [4]. Introduce ergonomic design thinking into all aspects of product design for research, analyze the inverse results of the use and operation of ergonomics from two aspects of physiological and psychological factors, and put forward the rational application of ergonomic design thinking in product design importance in [5]. How to follow ergonomics in product design, take the humanization, personalization, and emotional humanization factors of products as inspiration, examine the metric and coordination relationship between human factors and human-machine in traditional products, and connect some modern product cases for discussion and express the relationship between modern product design factors and human body size coordination is the field of interest. Under certain circumstances, the conclusion of ergonomics is the basic requirement of product design. Only when the most basic ergonomic standards are met can the product meet the basic requirements of the product for human use [6]. Kinesiology is a science focused on studying human health and reducing fatigue and discomfort through product design. This science is widely used to design all kinds of furniture in homes and offices, keeping in mind that furniture is designed for the user. The study focused on the issues faced by students at Shah Jalal University of Technology, Sylhet, Bangladesh, when using tabloid chairs in their everyday classrooms. The purpose is to identify ergonomic perspectives through the use of tabloid chairs and related limitations or issues in the classroom. To understand the limitations of using the tabloid chair, an updated tabloid chair was designed and developed based on anthropometric data obtained from these 160 students. The tabloid chair was produced taking into account the proposed ergonomic design [7]. Using the DFA method in the case of ergonomic intervention in the product redesign process of a home appliance enterprise is

helpful to obtain the technical solution used by the product. The assembly method is aimed at reducing various assembly procedures, reducing the number of parts, and facilitating the assembly process. QFD, Kano, and Pugh analyses are some other examples of methods and techniques used in the industry to combine a participatory approach to ergonomics with a design and DFA perspective. However, in addition to simplifying the design structure and reducing assembly costs, the use of the DFA method can also be used in product redesign situations to improve workplace ergonomics [8]. The generation and development of ergonomic skills in product design and development can be understood as a dynamic innovation process created by internal and external forces within an organization. Using a comparative case study approach, it focuses on six organizations (three pairs) operating at their New Zealand manufacturing base. Data was collected through in-depth interviews, documents, archival sources, and observations. Provide a framework for understanding the emergence and evolution of ergonomic features in product design and development. While ergonomics is the core concept of this model, four other key elements were also identified. These are personnel procedures, top management orientation, organizational configuration, and external environment [9]. On the basis of understanding and comparing various mainstream recommendation algorithms, the collaborative filtering algorithm is mainly tested, and an improved user model filtering recommendation algorithm is proposed. The algorithm builds an offline user model, which enables the algorithm to achieve better recommendation performance. Two series of experiments were designed based on mean absolute error (MAE). A series of experiments tested the parameters of the algorithm, and another series of experiments compared the proposed algorithm with other algorithms. Experimental results show that the proposed method performs well in both recommendation accuracy and recommendation effectiveness [10]. The new algorithm is a data-driven Intelligent Train Operation (ITO) algorithm that derives monitors from driver experience and uses input and output data to optimize online through downhill grades. The proposed algorithm is tested in a MATLAB/Simulink simulation model using real data from the Beijing Yizhuang subway line. Compared with the Proportional Integral Derivative (PID) algorithm, the algorithm has the advantages of low energy consumption, high comfort, and high parking accuracy and can meet the dynamic travel time control. Furthermore, the results of the ITO algorithm are comparable to those of the driver, both for runway transitions and working modes [11]. Simple response times cannot be directly used to estimate the response speed of different signal patterns in a multisensory console. In this choice-response task, a better visual intensity effect was observed, which was more pronounced in the SR-mapped mating conflict condition. Based on studies showing that spatial SR compatibility and signal modality are two important interface design factors for improving operator response performance in multisensory consoles, ergonomic recommendations have been developed to improve interface design in multisensory consoles based on these findings [12]. Key challenges and advances in smart workplaces and

personalized ergonomics, gathering the most relevant results from various international research projects, are divided into three main parts: personalized ergonomic examination to prevent musculoskeletal disorders and improve the workplace, the need for practical and reliable risk assessment methods, and ubiquitous technology in the smart workplace, identifying opportunities and challenges for technology-based interventions and security and privacy issues in the smart workplace. Transforming work environments into healthy and smart spaces can not only support ergonomic experts, workers, and employers but also provide solutions for the sustainability of our current social safety net [13]. A method, system, and computer program for promoting the ergonomic health of computer workplace users are presented; the method includes the step of detecting problems with computer workplace ergonomic users, wherein the ergonomic issues are relevant to current reality time. A user health algorithm is implemented to generate ergonomic recommendations, using the user's work parameters as input data to present ergonomic recommendations to correct ergonomic issues for the user [14]. Intuitive tools combine virtual reality with physics-based avatars for ergonomic research. In a real-time physics simulation, the user can manipulate the avatar to explore different poses, and the user can cause the avatar to apply forces to its environment while controlling shared torque. The virtual human uses a programming-based square controller to control the torque, ensuring a dynamically consistent position and torque of the joints. The tool features hand push experiments with different morphologies and target positions. The quantitative results obtained in the experiments are consistent with the expected effects of morphology and target position on joint torque, making the method promising in ergonomic conditions during workplace prototyping [15].

2. Ergonomic Home Product Design

2.1. Problems Existing in Home Product Design. At this stage, almost all household items in our country are very similar. This phenomenon has seriously restricted the development of household product design in our country. China's household products have always been low-end, and although they occupy the international market at low prices, there is no end to the problem. Among the Chinese household goods, there is only the "Chinese style" in the Ming and Qing dynasties. The articles are used all the time and gradually run out of new ideas. On the contrary, in the process of exploring Chinese culture and interpreting Chinese elements from a Western perspective, Western design always emphasizes new concepts and design styles. The home furnishing market has no unique features. Following Western fashion and blindly copying, "no design" has become the status quo of the current home furnishing market. When analyzing the current situation of home furnishing products in our country and synthesizing the market conditions of home furnishing products, the human-machine coordination, human-machine environment coordination, cultural identity, and emotional attraction of products should be considered in home furnishing design. Furniture products and
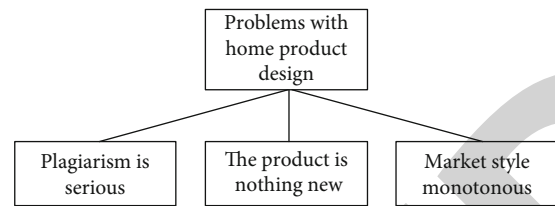
Figure 1: Problems existing in home product design.

other aspects are the research content of product design and human design methods. To understand the classification of home products and product analysis of classic home brands, we will start with ergonomic theory and analyze the relationship between product design and ergonomics, as shown in Figure 1.

Almost all household products in our country look alike, which greatly restricts the development of the design of household products in our country.

The Chinese elements contained in domestic household products are only "Chinese style" during the Ming and Qing dynasties. These elements have been used all the time and have no new ideas.

The domestic home furnishing product market does not have its own unique characteristics. It has always followed the fashion trend of the West and blindly copied it.

2.2. The Embodiment of Ergonomics in Home Product Design. When it comes to solving the "human" problem of a system, the primary approach to ergonomics is to create machines and environments suitable for human use and to design machines that are more suitable for the environment. In the process of ergonomic development, changing the way of thinking and adjusting the ideological foundation, accepting the people-oriented optimization consideration, reflecting the interests of people to a large extent, and putting forward the concept of "interaction," it is more intuitive and in line with the development trend of ergonomics. It emphasizes people and extensively considers the "human factor," which refers to various parameters of human growth scale and space in the family environment, strengthens personal psychological factors, and analyzes and designs human-machine interfaces that meet the needs of users. Taking into account the ergonomic design of the environmental space, the personalized design of the space needs to reasonably arrange the model according to the family structure, lifestyle, and regional living habits and adapt to the different needs of the space, and the supervision relationship is relatively independent. Ergonomic design emphasizes the concept of humanization. Because of the difference in family structure and life concept, the concept of humanization is emphasized. It must not only be in line with the overall design thinking of the space but also conform to the people-oriented principle, as shown in Figure 2.

2.3. The Advantages of Ergonomic Home Product Design. Correct use of ergonomics in home products allows for optimal design of home products to meet the needs and wants of people for different groups, different spaces, and different requirements. One is to better define the overall scale of

FIGURE 2: Four levels of ergonomics.

FIGURE 3: The development direction of ergonomics in interior and furniture design.

household products. Through the use of ergonomics, various household products can be designed to be optimal for human use. By measuring human data, we can calculate the human activity, required activity space, and biomechanics caused by the use of household products and apply the data structure to the design of household products, so that household product users can work in the best way. The design can also reduce unnecessary costs, and by adapting to specific groups of people, it can improve the efficiency of mass production and reduce production costs. Second, in order to give better play to the design effect of home products combined with ergonomics, home products designed on the basis of measurement and calculation can not only give full play to the advantages of interior design but also provide enough space for home products. The ergonomic measurement of home products can compare indoor space data with human body data, integrate reference space and human body data into the design, ensure that product design and interior design are integrated, and realize the integration of interior design, product design, and human body as much as possible. Harmony and unity improve interior space layout and overall furniture coordination through overall design. The overall size of household products can be better determined. By using ergonomics, different household products can be designed into the most suitable state for people to use. The effect of home product design can be better played. Combined with ergonomics, home products designed through measurement and calculation can not only play the advantages of interior design but also ensure that home products have enough space for use and indoor comfort match.

2.4. The Development Direction of Ergonomics in Home Product Design. At this stage, most household items tend to be mass-produced to keep costs down. While this meets people's needs in most cases, it may not meet everyone's needs due to individual differences. Therefore, home product design needs to develop personal design. Therefore, people's specific needs can be met according to personalized design, and the shortcomings of mass production can be compensated for through personalized design. Of course, human-based personalization will significantly increase the cost of design and implementation, but the comfort of designing the same home product will increase accordingly.
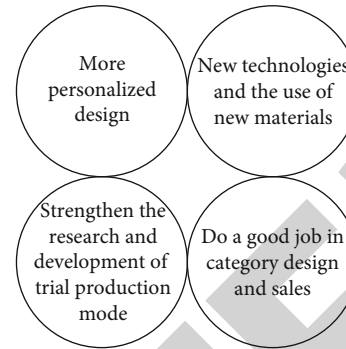
In order to avoid design problems, furniture designs must be presented and manipulated as intuitively as possible, with flaws found in detail from actual objects. Due to technical reasons and the application of ergonomics in the design of household appliances and household products in my country, the development time is relatively short, as well as the collection of human data and the research and development of pilot production systems; it is necessary to carry out the research and development of pilot production models. Not only can the design quality of home products be improved but also it can give you good feedback after the products are put on the market. In product design, the use of new materials can improve the desired design effect. The use of new technologies and new materials can best meet the design requirements, and the use of new technologies and new materials in production can often provide geometric development space for the practicability and comfort of products. It can also inspire designers to overcome existing limitations by updating technologies and materials to create products that are more comfortable and more responsive to people's psychological and physical needs. Different ethnic groups, different regions, and different age groups in my country have different characteristics, and many situations need to be considered when designing products. Data collection for relevant groups should be done well, and design and sales should be targeted, as shown in Figure 3.

The development directions of ergonomics in home product design in this article are defined:

(1) More personalized design

(2) The use of new technologies and new materials

(3) Strengthen the research and development of trial production mode

(4) Do a good job in classification design and sales

3. Intelligent Algorithm Recommendation

3.1. Coordinated Filtering Recommendation Algorithm. In the neighborhood filtering recommendation algorithm, finding similar users is an important step, and the main goal of similar users is to obtain the most relevant recommended items for the target users. The user-based algorithm is

mainly divided into three steps: one is similarity calculation, the other is to select the "nearest neighbor" according to the similarity, and the third is to calculate the point value for prediction and recommendation. The similarity measure looks for users who are "nearest neighbors" and is mainly calculated based on the items being rated. Suppose I_u is the set of items rated by user u, $I_u \cap I_v$ is the set of items rated by users u and v, $r_{u,i}$ is the rating of item i by user u, and $\bar{r}_u$ is the average of the ratings. The following are the most common ways to calculate similarity.

Corrected cosine matching (ACos) was performed, using formula (1) to calculate the matching of user u and user v.

$$\text{sim}(u, v) = \frac{\sum_{i \in I_u \cap I_v} (r_{u,i} - \bar{r}_u)(r_{v,i} - \bar{r}_v)}{\sqrt{\sum_{i \in I_u} (r_{u,i} - \bar{r}_u)^2 (r_{v,i} - \bar{r}_v)^2}}. \tag{1}$$

Pearson correlation (PC) was performed, using formula (2) to calculate the similarity between user u and user v.

$$\text{sim}(u, v) = \frac{\sum_{i \in I_u \cap I_v} (r_{u,i} - \bar{r}_u)(r_{v,i} - \bar{r}_v)}{\sqrt{\sum_{i \in I_u \cap I_v} (r_{u,i} - \bar{r}_u)^2} \sqrt{\sum_{i \in I_u \cap I_v} (r_{v,i} - \bar{r}_v)^2}}. \tag{2}$$

Pearson constrained correlation (constrained PC, CPC) was performed, using formula (3) to calculate the similarity between user u and user v. r_{med} is the median of the rating scale.

$$\text{sim}(u, v) = \frac{\sum_{i \in I_u \cap I_v} (r_{u,i} - r_{\text{med}})(r_{v,i} - r_{\text{med}})}{\sqrt{\sum_{i \in I_u \cap I_v} (r_{u,i} - r_{\text{med}})^2} \sqrt{\sum_{i \in I_u \cap I_v} (r_{v,i} - r_{\text{med}})^2}}. \tag{3}$$

Jaccard computes the Jaccard match between user u and user v using equation (4). $|I_u \cap I_v|$ is the number of items jointly rated by user u and user v.

$$\text{sim}(u, v) = \frac{|I_u \cap I_v|}{|I_u \cup I_v|}. \tag{4}$$

After determining the similarity between the target user's "nearest neighbor" and him, you can calculate the target user's rating for the recommended item and then recommend the position with the highest rating in the recommended item set to the target user. Use equation (5) to predict the target user's score for item i, where $\text{sim}(u, v)$ is the similarity between user u and user vi, and N_u is the set of "nearest neighbors" of user u.

$$R_{u,i} = \bar{r}_u + \frac{\sum_{v \in N_u} \text{sim}(u, v)(r_{v,i} - \bar{r}_v)}{\sum_{v \in N_u} \text{sim}(u, v)}. \tag{5}$$

The calculation principle of the item-based algorithm is the same as that of the user-based algorithm, but the calculation object is different, and the user must be replaced by the item.

The recommendation algorithm based on collaborative filtering does not require detailed content. When the details of the content are not accessible or it is difficult to collect or analyze the details, the collaborative filtering method is very effective, and the method can find the item that the target user wants among the massive items. However, it also faces the problem of scoring sparsity, as well as the cold start of new users and new projects.

3.2. Model-Based Collaborative Filtering.
In the SVD model, the original rating matrix R is decomposed into three matrices:

$$R = USV^T, \tag{6}$$

where U and V are two orthogonal matrices, S is a diagonal matrix of size $r \times r$, and r is the rank of R, which consists of some values of the fractional matrix. This matrix can be reduced by omitting the minimum value, resulting in a matrix, where $k < r$ and S_k is the decomposed form of the reconstructed matrix:

$$R = U_K S_K V_K^T. \tag{7}$$

The scoring prediction formula is

$$R_{u,i} = \bar{r}_u + U_K \sqrt{S_K^T}(u) \sqrt{S_K} V_K^T(i). \tag{8}$$

3.3. Content-Based Recommendation Algorithm.
Currently, the most widely used computational method for information retrieval is the TF-IDF method, which is used to develop vector space models in content-based recommendation algorithms. This method regards the content of item as document d, then extracts keyword t from it, and then calculates the formula for the TF value of keyword t in document d as shown in

$$\text{TF}_{t,d} = \frac{N_{t,d}}{\sum_k N_{k,d}}. \tag{9}$$

Among them, $N_{t,d}$ represents the number of times the keyword t appears in the document d and the calculation of the IDF value corresponding to the keyword t. The formula is shown in

$$\text{IDF}_t = \log \frac{|D|}{1 + |d \in D : t \in d|}, \tag{10}$$

where D represents the collection of documents and $1 + |d \in D : t \in d|$ represents the number of keywords t contained in document d.

3.4. CFCNN-CL Algorithm.
Calculate similarity between users based on possible "nearest neighbors." There are many ways to calculate similarity, most of which are mainly based on rating positions shared among users in user-provided rating data, which leads to data dilution issues and reduced accuracy.

$$\text{sim}(u, v) = \frac{\max\left(1, |I_u \cap I_v|\right)\sum_{i \in I_u}\sum_{j \in I_v} r_{u,i}/r_{v,j}}{|I_u||I_v||I_u \cup I_v|}. \quad (11)$$

Among them, I_u represents the set of user rating items u, I_v represents the set of user rating items v, $|I_u|$ and $|I_v|$ represent the number of rating items, and $r(u, i)$ represents the rating of item i by user u.

Once the similarity between the target user's "nearest neighbor" you and him is determined, the target user's rating for the item can be calculated. This paper uses formula (12) to calculate the target user's rating value for item i.

$$r_{u,i} = \bar{r}_u + \frac{\sum_{v \in N_u} \text{sim}(u, v)(r_{u,i} - \bar{r}_v)}{\sum_{v \in N_u} \text{sim}(u, v)}. \quad (12)$$

The common rating items among users in the rating data provided by users will suffer from data sparseness, resulting in reduced accuracy.

3.5. RRP-UICL Algorithm. Rating value prediction is the last important step of the recommendation algorithm. Rating value is predicted by calculating the matching degree of the user's direct "nearest neighbor" with the target user. This paper uses the weighted average method to predict the rating value of a feature item. To recommend an item, a weight must be calculated based on the target user's direct "nearest neighbor" score and the target user's indirect "nearest neighbor" score, and a weight must be used to calculate the score for each item. With the final prediction result, the steps of the prediction method are as follows:

First, the average rating of featured articles needs to be calculated. For recommended items, the average score is calculated according to

$$\bar{r}_i = \frac{\sum_{v \in N_u^d \cup N_u^{id}} r_{v,i}}{\left| N_u^d \cup N_u^{id} \right|}. \quad (13)$$

N_u^d is the direct "nearest neighbor" of user u and N_u^{id} is the indirect "nearest neighbor" of user u. It can be seen from equation (13) that the direct "nearest neighbor" and the intermediate "nearest neighbor" of the target user need to be obtained, and the information is extracted to determine the average score of each feature item.

To predict the ranking of a recommended location, use formula (14) to predict the location score $R_{u,i}$ of the target user u, $r_{v,i}$ represents the location score i of the "nearest neighbor" user v, a is the highest ranking set, and $|r_{v,i} - \bar{r}_i|$ represents the user's "nearest neighbor" v's The average score of position judgment deviation i, $a - |r_{v,i} - \bar{r}_i|^2 - 1$, is the final weight of item i.

$|r_{v,i} - \bar{r}_i|$ denotes the "nearest neighbor" user v's rating deviation from the average rating for item i, and $a -$

Table 1: Index system of home product design considering ergonomics.

Criterion level one	Criterion level two
Ease of use	Easy to install
	Practical
	Easy to move
	Easy to clean
	Easy to disassemble
	Timely after sale
	Run smoothly
Safety	Structural strength
	Safety fence
	Circuit stealth
	Safe use of materials
	Appropriate size
	Simple shape
Aesthetic	Single color
	Pastel tones
	Home style
	Natural material
	Simple decoration
	Comfort function
	Massage function
Feature	Smart operation
	Purifying air
	Reduce noise
	Convenience function

Table 2: Comparison of the importance of elements in the first level of the criterion.

	Ease of use	Safety	Aesthetic	Feature
Ease of use	1	1/3	5	3
Safety	3	1	7	5
Aesthetic	1/5	1/7	1	3
Feature	1/3	1/5	1/3	1

Table 3: Criterion layer one indicator weight.

	Ease of use	Safety	Aesthetic	Feature	w_i
Ease of use	0.21	0.24	0.30	0.31	0.28
Safety	0.67	0.48	0.48	0.46	0.47
Aesthetic	0.07	0.12	0.12	0.08	0.10
Feature	0.10	0.16	0.16	0.15	0.16

$|r_{v,i} - \bar{r}_i|^2 - 1$ denotes the final weight of item i.

$$R_{u,i} = \frac{\sum_{v \in N_u^d} r_{v,i}\left(a - |r_{v,i} - \bar{r}_i|^2 - 1\right) + \sum_{v \in N_u^{id}} r_{v,i}\text{sim}(u, v)\left(a - |r_{v,i} - \bar{r}_i|^2 - 1\right)}{\sum_{v \in N_u^d}\left(a - |r_{v,i} - \bar{r}_i|^2 - 1\right) + \sum_{v \in N_u^{id}}\text{sim}(u, v)\left(a - |r_{v,i} - \bar{r}_i|^2 - 1\right)}. \quad (14)$$

TABLE 4: Stochastic consistency indicators.

Order	3	4	5	6	7	8	9	10	11	12	13
R.I.	0.583	0.892	1.118	1.243	1.319	1.411	1.446	1.492	1.522	1.539	1.555

3.6. Semantic Differences: AHP. The application of AHP should follow the following two basic definitions:

Set $A = (a_{ij})$. If $a_{ij} > 0$, then formula (15) is obtained, which is applicable to any set of i, j. Then, A is called the positive reciprocal inverse matrix. The set of inverse matrices of order n is $M_{p^{n+}}$.

$$a_{ij} = \frac{1}{a_{ij}}. \tag{15}$$

If $A = (a_{ij})$ belongs to $M_{p^{n+}}$, formula (16) is applicable to any $i, j,$ and k. Then, A is called the consistency matrix. The set of n-order consistency matrices is denoted M_{c_n}.

$$a_{ij} = a_{ik} a_{jk}. \tag{16}$$

Use the sum-product method to solve the weights of the indicators of the first criterion layer. The steps are as follows:

Let the judgment matrix be $M = (a_{ij})_{4 \times 4}$, and normalize the elements in the matrix by column:

$$\bar{a}_{ij} = \frac{a_{ij}}{\sum_{k=1}^n a_{kj}} \quad (i, j = 1, 2, \cdots, n). \tag{17}$$

Row summation of the normalized matrix is

$$\bar{w} = \sum_{i=j}^n \bar{a}_{ij} \quad (i, j = 1, 2, \cdots, n). \tag{18}$$

Find the largest eigenvalue and perform a consistency check. After the element weight data is obtained, it does not mean that the calculation is over. It is necessary to pass the consistency check to prove the validity of the calculation result. The largest eigenroot is

$$\lambda_{\max} = \frac{1}{n} \sum_{i=1}^n \frac{(Mw)_i}{w_i}. \tag{19}$$

The consistency index C.I. of the judgment matrix M is

$$\text{C.I.} = \frac{\lambda_{\max} - n}{n - 1}. \tag{20}$$

The consistency evaluation index is introduced by Satty, and R.I. is a random consistency index, namely,

$$\text{C.R.} = \frac{\text{C.I.}}{\text{R.I.}}. \tag{21}$$

The basic steps of semantic difference-analytic hierarchy process in intelligent algorithm recommendation are defined as follows:

TABLE 5: Index weights and ranking of criterion layer 2.

Criterion level two	Weights	Sort
Easy to install	0.063	7
Practical	0.105	4
Easy to move	0.028	12
Easy to clean	0.054	8
Easy to disassemble	0.018	15
Timely after-sales	0.011	19
Run smoothly	0.181	1
Structural strength	0.030	11
Safety fence	0.069	6
Circuit stealth	0.128	3
Safe use of materials	0.173	2
Appropriate size	0.017	16
Simple shape	0.017	16
Single color	0.005	23
Pastel tones	0.010	20
Home style	0.033	10
Natural material	0.025	13
Simple decoration	0.006	22
Comfort function	0.005	23
Massage function	0.071	5
Smart operation	0.036	9
Purifying air	0.023	14
Reduce noise	0.010	20
Convenience function	0.015	18

Step 1. Treat the problem to be analyzed or the solution to be decided as a system.

Step 2. Sort or reorganize the different elements or indicators relevant to the issue or decision.

Step 3. Use the problem to be solved as the target layer and the index or the element as the criterion layer and the scheme layer to construct the hierarchical model.

Step 4. Construct a matrix according to the ratio of two elements at each level.

Step 5. Through the matrix solution and matrix consistency test, the weight of each index is obtained.

Step 6. Make decisions based on weights.

4. Experiment Analysis of Home Product Design and Intelligent Algorithm Recommendation considering Ergonomics

4.1. Ergonomic Home Furnishing Product Design Based on Semantic Difference: AHP. According to the user's needs for ergonomic home product design, the criterion layer is established, and a total of two layers are established. The first
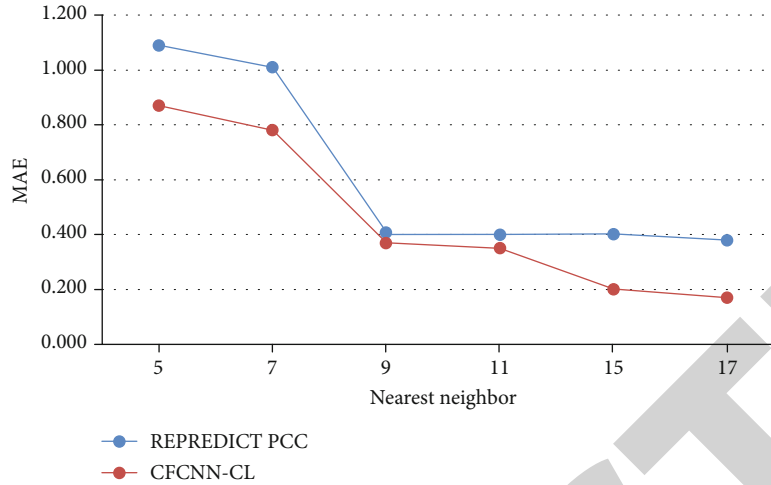
Figure 4: MAE comparison of different nearest neighbors.

level of the criterion is functionality, safety, aesthetics, and ease of use; the second level of the criterion is being easy to install, practical, easy to move, easy to clean, and easy to disassemble, after-sales service, stability in operation, structural strength, safety guardrail, invisible circuit, safe use of materials, suitable size, simple shape, single color matching, soft tones, home style, natural materials, simple decoration, comfortable function, massage function, intelligent operation, air purification, noise reduction, and convenient function, as shown in Table 1.

By comparing the importance of the elements of criterion 1, we get that ease of use is slightly less important than safety, ease of use is more important than aesthetics, ease of use is slightly more important than functionality, safety is more important than aesthetics, and safety is more important than aesthetics. Functionality is more important, and aesthetics are slightly more important than functionality, as shown in Table 2.

According to the weight calculation of the indicators of the criterion layer one, the weight of safety is the largest, the weight is 0.47, the weight of aesthetics is the smallest, the weight is 0.1, the weight of usability is 0.28, and the weight of function is 0.16; that is, the safety is in the criterion layer one, which is the most important, followed by ease of use, functionality, and aesthetics, as shown in Table 3.

According to the arbitrary coherence index and formula (21), the matrix coherence judgment index MC.R. = 0.012, C.R.<0.1 can be obtained, so the matrix M satisfies the consistency requirement. Through semantic difference analysis, the layered process of pairwise comparison of four indicators in the first layer shows that safety has the largest proportion in the design of home products considering ergonomics, accounting for 47%, followed by ease of use, accounting for 28%. Again, functionality accounts for 16%, and finally, aesthetics accounts for 10%, that is, safety > ease of use > function > aesthetics, as shown in Table 4.

The importance of the second level of the criterion is stable operation, with a weight of 0.181, followed by safe material use, invisible circuit, strong practicability, massage function, safety guardrail, convenient installation, easy

cleaning, intelligent operation, home style, structural strength, being easy to move, natural material, air purification, easy disassembly, suitable size, simple shape, convenient function, timely after-sales, soft color tone, noise reduction, simple decoration, single color matching, and comfortable function, as shown in Table 5.

4.2. Intelligent Algorithm Recommendation for Home Products considering Ergonomics. It can be seen from the figure that the trend lines of MAE and RMSE values of REPREDICT PCC are always above those of CFCNN-CL. The trend lines of CFCNN-CL and REPREDICT PCC both decrease with the increase in adjacent neighbors, so the increase in the nearest neighbors increases the two methods of the accuracy. The CFCNN-CL algorithm has better performance and better accuracy than the REPREDICT PCC algorithm, as shown in Figures 4 and 5.

In the comparison of MAE values of different methods in the dataset, it can be seen that when $N = 5$, the MAE value of UCF-CPC is the largest, and the MAE value of UCF-Jaccard is the smallest; when $N = 10$, the MAE value of UCF-CPC is the largest, followed by RRP-UICL, UCF-ACos, UCF-PC, and UCF-Jaccard; when $N = 15$, the MAE value of RRP-UICL is the largest, followed by UCF-CPC, UCF-ACos, UCF-PC, and UCF-Jaccard; when $N = 20$, the MAE values of UCF-CPC and UCF-PC were the largest, followed by UCF-PC, RRP-UICL, and UCF-Jaccard. In general, the MAE value of UCF-Jaccard is smaller than that of other methods, indicating that this method is less affected by data sparseness, and the change of MAE value is not very obvious, as shown in Figure 6.

In the comparison of MAE values of different methods in the dataset, it can be seen that when $N = 5$ and 10, the MAE value of UCF-CPC is the largest; when $N = 15$, the MAE value of RRP-UICL is the largest; when $N = 20$, the MAE values of CPC and UCF-PC are the largest; the MAE values of UCF-Jaccard are generally smaller than those of other methods, indicating that this method is less affected by data sparseness, and the changes in MAE values are not very obvious.
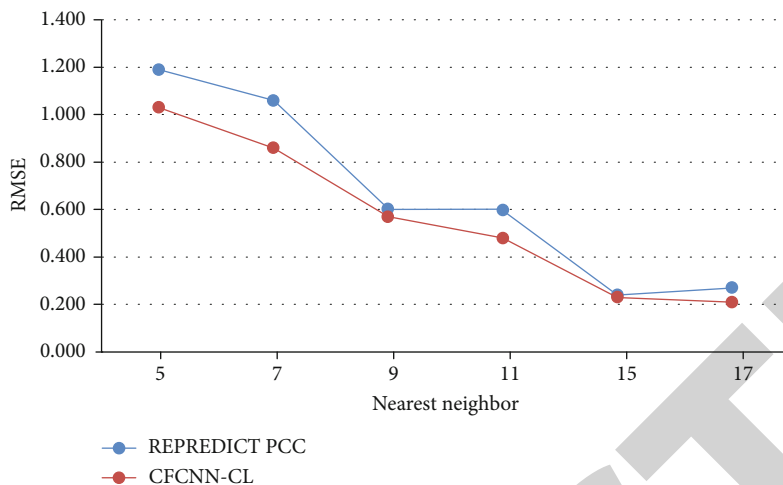
Figure 5: RMSE comparison of different nearest neighbors.
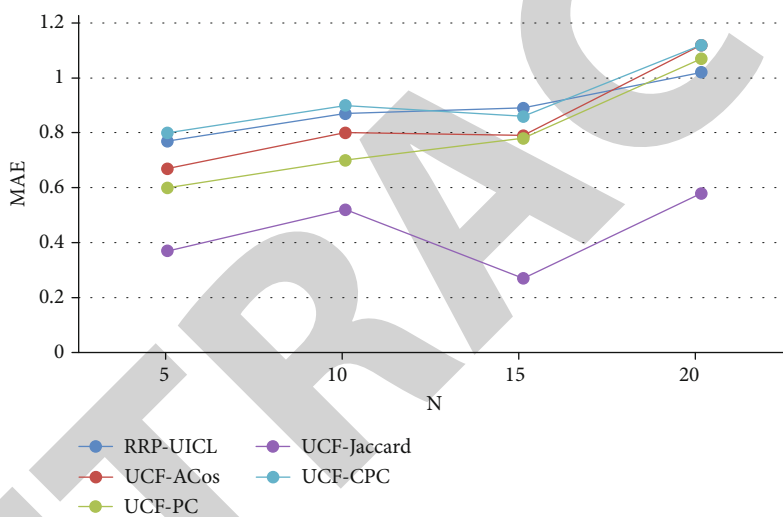
Figure 6: Comparison of MAE values for different methods in the dataset.
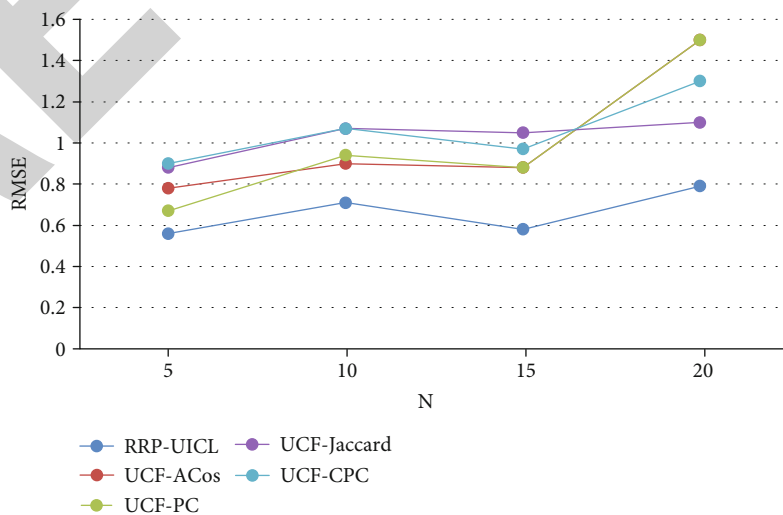
Figure 7: Comparison of RMSE values of different methods on the dataset.

Retraction

Retracted: Efficient Management and Application of Human Resources Based on Genetic Ant Colony Algorithm

Journal of Sensors

This article has been retracted by Hindawi following an investigation undertaken by the publisher [1]. This investigation has uncovered evidence of one or more of the following indicators of systematic manipulation of the publication process:

(1) Discrepancies in scope

(2) Discrepancies in the description of the research reported

(3) Discrepancies between the availability of data and the research described

(4) Inappropriate citations

(5) Incoherent, meaningless and/or irrelevant content included in the article

(6) Manipulated or compromised peer review

The presence of these indicators undermines our confidence in the integrity of the article's content and we cannot, therefore, vouch for its reliability. Please note that this notice is intended solely to alert readers that the content of this article is unreliable. We have not investigated whether authors were aware of or involved in the systematic manipulation of the publication process.

Wiley and Hindawi regrets that the usual quality checks did not identify these issues before publication and have since put additional measures in place to safeguard research integrity.

We wish to credit our own Research Integrity and Research Publishing teams and anonymous and named external researchers and research integrity experts for contributing to this investigation.

The corresponding author, as the representative of all authors, has been given the opportunity to register their agreement or disagreement to this retraction. We have kept a record of any response received.

References

[1] C. Cheng, Y. Xu, and G. Daniels, "Efficient Management and Application of Human Resources Based on Genetic Ant Colony Algorithm," *Journal of Sensors*, vol. 2022, Article ID 9903319, 13 pages, 2022.

Hindawi

Research Article

Efficient Management and Application of Human Resources Based on Genetic Ant Colony Algorithm

Cheng Cheng,[1] Yuguang Xu [iD],[2] and Graciela Daniels[3]

[1]*Nanchang Institute of Technology, Nanchang Jiangxi 330044, China*
[2]*Binzhou Medical University, Binzhou Shandong 256699, China*
[3]*Central Arizona College, Coolidge, 85128 AZ, USA*

Correspondence should be addressed to Yuguang Xu; xuyuggmw@bzmc.edu.cn

With the increasing demand of human resources, the cost of staffing and management is increasing, and it is difficult to dynamically allocate and adjust personnel among different parts. It is the key of intelligent management technology to realize efficient application and mining in human resource management. In the aspect of human resource allocation and management, this paper puts forward the efficient management and application of human resource based on the genetic ant colony algorithm. Firstly, this paper describes the process management and parameter application of the genetic algorithm and ant colony algorithm and manages the resource allocation and management process under the two algorithms. Secondly, several current test functions are applied to the genetic algorithm and ant colony algorithm to test the efficiency of the algorithm, which has obvious advantages in convergence efficiency. Finally, the paper uses the efficient management configuration of human resources for comprehensive application and management and applies the system uploading and downloading services on human resumes, respectively. The genetic ant colony algorithm has obvious advantages in efficiency. In human resource data matching, the genetic algorithm is slightly better than the ant colony algorithm in the case of relatively few data in the early stage, and the accuracy of the ant colony algorithm is slightly better than the genetic algorithm in the later stage. The ACO-GA algorithm is more consistent with the actual value, which not only ensures the stability but also ensures the accuracy of prediction, which is more in line with the actual needs.

1. Introduction

The country and even the whole world are full of confidence in the future development of intelligent computing and vigorously recommend the integration of intelligent computing into people's lives. At the same time, they hope that intelligent computing can solve the problem of uneven distribution and mismatch of resources. The allocation of human resources is also included. When the allocation of human resources is not handled properly, it will lead to a series of problems such as cost increase and brain drain. Therefore, it is necessary to make the process of human resources allocation more digital and technical. Human resources need to have high-efficiency performance at the same time of low cost, which is the premise of rationalization of allocation. This can show respect for talents. Intelli-

gent computing can be said to be its savior in this respect, and they complement each other, which not only solves problems but also makes intelligent computing involved more widely.

Traditional intelligent computing has not been broken through in the past. In today's important fields [1], such as big data computing, traditional intelligent computing needs high manpower and material costs to study. For the emerging intelligent computing, it can make up for the defects of the traditional one. According to the investigation, in the aspect of quantum heuristics, the inclusion of intelligent computing brings advantages to this technology but also brings disadvantages and challenges to the future. It is necessary for researchers to study it further [2]. Because of its high efficiency in solving nonlinear problems, computational intelligence is proposed to solve such
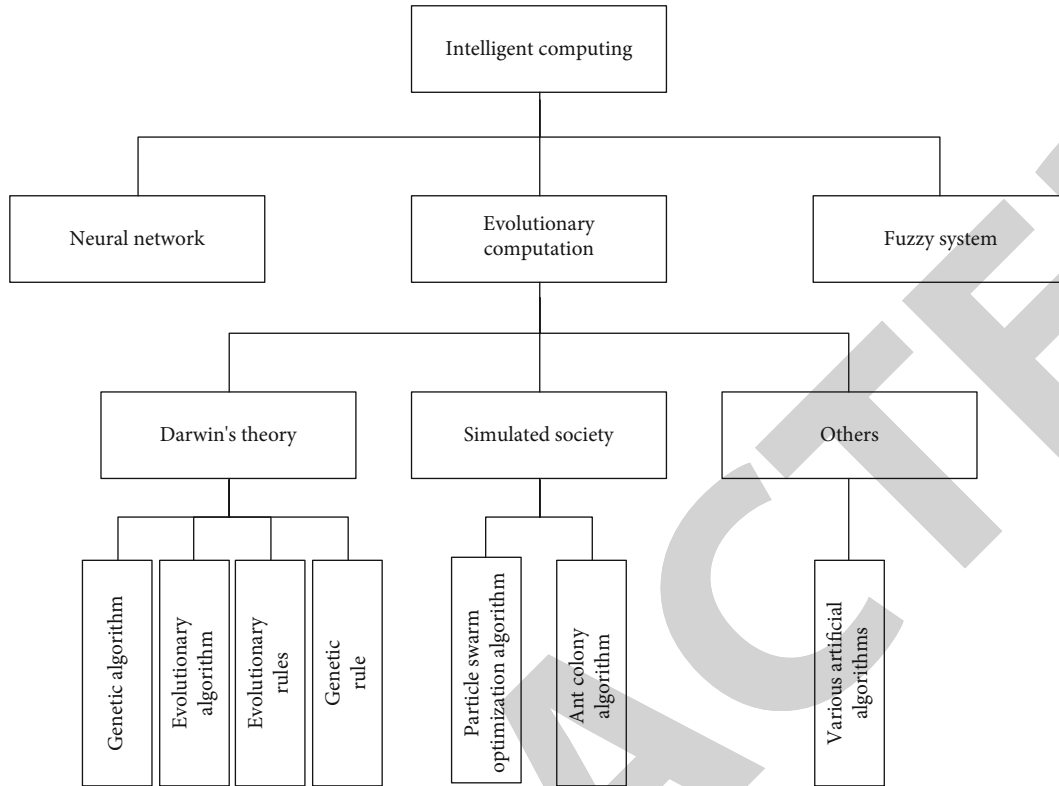
Figure 1: Classification diagram of intelligent computing.

problems as power outages, so that power can be quickly resupplied and redundant parts can be unloaded [3]. It contains most algorithms. In order to make these methods more efficient, it is necessary to further study these methods. Different from traditional technologies, intelligent computing has more advantages, but it also has its own limitations, which will lead to limited use. Intelligent computing [4] is also used in power load specialty, and because of its importance, it has attracted the attention of most relevant personnel. Some researchers put forward a method of using model-free technology to test power load based on NN and FL. Through a series of case studies, the advantages and special performance of this method are demonstrated to the public under geographical environment and other conditions. One part of intelligent computing, artificial neural networks, is good at solving the problem of air pollution modeling. It will simulate the ozone layer with pollution parameters. After putting this model into real life, experiments show that this model is very powerful in dealing with such problems [5]. Intelligent computing can also be applied to electrical islanding detection technology [6]. Because the electrical islanding detection technology is not very efficient in solving problems in nonlinear systems, intelligent computing is introduced to improve the accuracy of solving problems, which can provide accurate data and solutions for relevant researchers. Intelligent computing is also used in computer Go [7]. In the world-class computer Go competition held in Taiwan, many Go masters want to

compete with intelligent computing MoGo. MoGo, blessed by RAVE and UCT, has four high-performance attributes. From the outcome of the battle, we can see that intelligent computing can be used in computer Go to achieve a high level of Go battle, and its future development is immeasurable. Literature [8] at the same time, intelligent computing is getting higher and higher in solving problems related to biology, chemistry, and medicine, and its influence is getting bigger and bigger. Combining it with statistical methods, a new model is obtained. In the study of human resource allocation in large companies [9], it is found that human factors have the greatest impact. Generally speaking, in order to reduce the mismatch of resource allocation, personnel performance is generally controlled. Human resource allocation is the top priority in any project. In order to improve the allocation of human resources [10], a series of operations such as shortening project time and reducing costs have been taken. However, if the fundamental factors are not solved, these operations will be lost. The influence of human resource allocation on enterprises should not be underestimated [11]. However, although many schemes have been put forward, the problems still exist. Most of them are caused by not paying attention to the team. Therefore, some researchers have studied from various aspects and put forward a predictive model based on multilayer perceptron. Researchers put this model into practical experiments and finally get the conclusion that this model can improve the efficiency of human resource
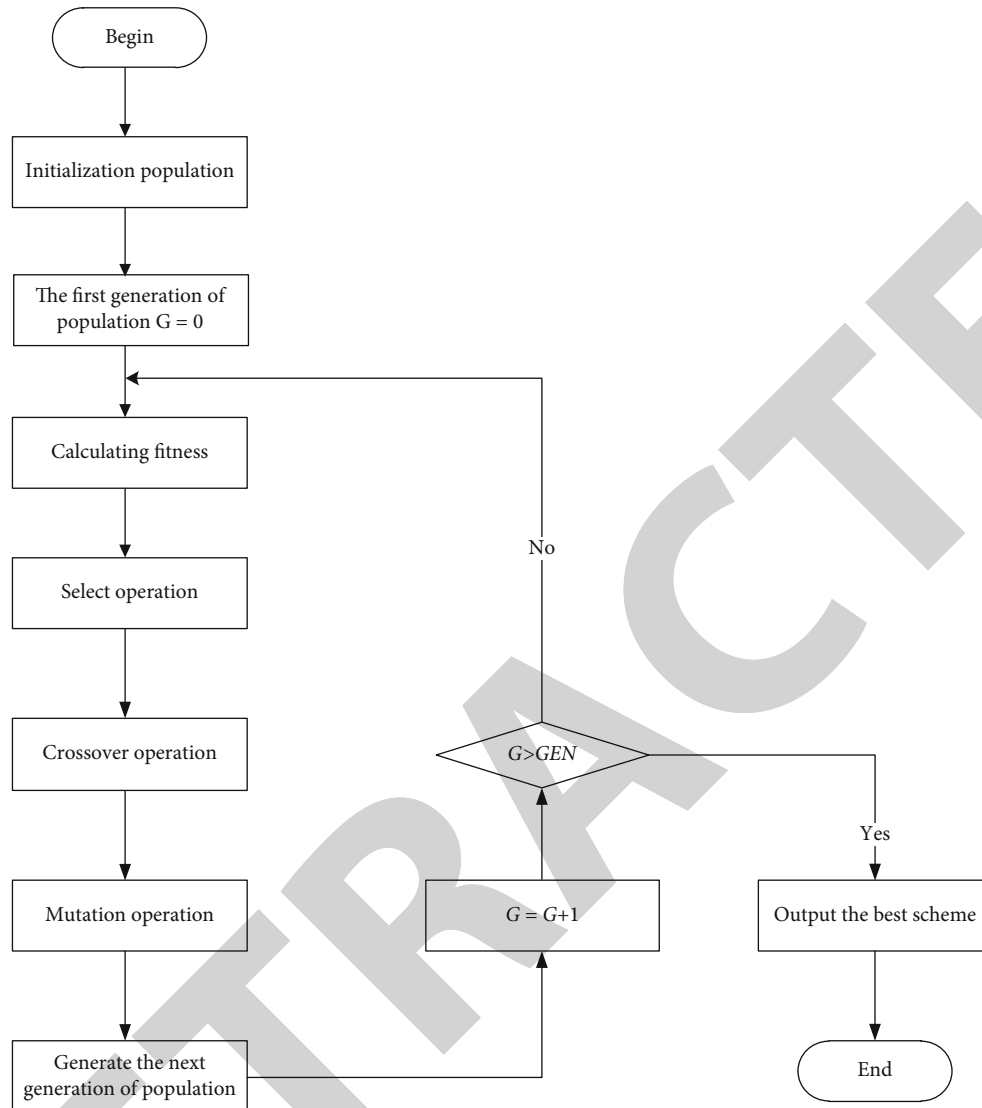
Figure 2: Flow chart of the genetic algorithm.

allocation. In the allocation of human resources, the most important criterion for the classification of personnel is personality, but the personality should be objective and complete [12]; otherwise, it is useless. Therefore, researchers propose to use high-performance algorithms to get more realistic data, which can minimize the error. In order to improve the utilization rate of scarce resources, researchers introduce decentralization factors and resource allocation with the help of software evaluation and portfolio planning and propose new allocation methods to solve the problem of improving the resource allocation of nonsmall R&D organizations [13]. In order to develop the human resource management of shelters, researchers propose to match the theory with people to get a model [14]. In this way, more influencing factors can be considered more comprehensively. The model is put into the experiment and finally found that there is a certain relationship between the working hours and the vacation time; so, in the shelter,

the human resources and vacation need to be set reasonably. The allocation of human resources has also brought troubles to the country. Therefore, the state also attaches great importance to optimizing its allocation and improving its utilization rate [15]. The intelligent method is quoted in human resources. Most researchers aim at the low utilization rate and unreasonable resource allocation in the process of human resources. In the process of algorithm implementation, there is slow convergence. Therefore, the paper proposed the ACO-GA algorithm to solve the above problems.

2. Intelligent Computing Analysis

2.1. Basic Concepts. Intelligent computing is a success for people to transform data into logic. At the same time, it can enable human beings to cultivate their ability to think independently. Most algorithms are its members, but it
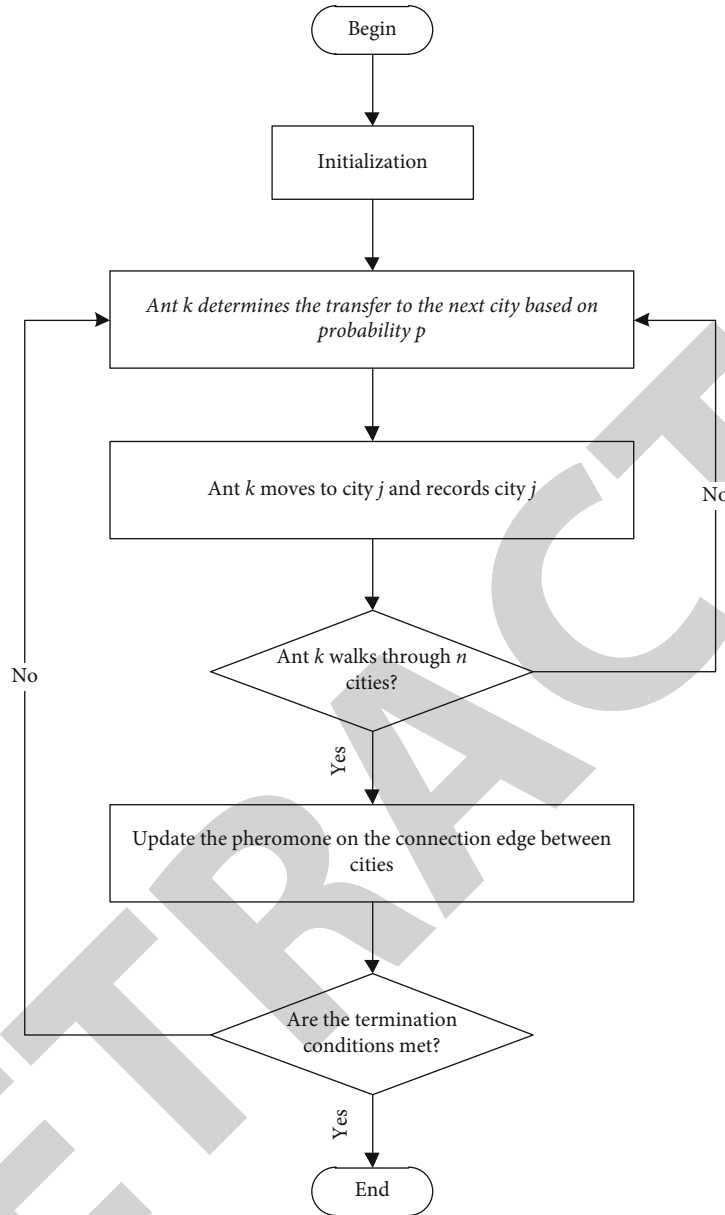
FIGURE 3: Flow chart of the ant colony algorithm.

does not go its own way but is based on calculation and continuously improved. The classification is shown in Figure 1.

2.2. Genetic Algorithm

2.2.1. Basic Concepts. Natural selection heredity is the foundation of this algorithm; that is, chromosomes are abstracted into body objects and then encoded. Only in this way can we search randomly and efficiently in this space. Among them, genetic operation is divided into selection, crossover, and variation.

After the formation of the first generation population, according to the law of the survival of the strong in the theory of biological evolution, a series of more and more excellent approximate solutions are produced through iteration. Moderate function is a strict judge, and excellent individuals can pass its selection. Then, these excellent people will choose, cross, and mutate. They have become completely different from before, and they are a brand-new population. The genetic algorithm flow is shown in Figure 2.

The genetic algorithm is divided into pattern H. The formula of general mathematical expression is as follows:

$$M[H(t + 1)] \geq M[H(t)]\frac{f(H(t))}{f(t)}\left[1 - \frac{P_c \times \delta(H)}{L - 1}\right](1 - P_m)^{O(H)},$$

$$(1)$$
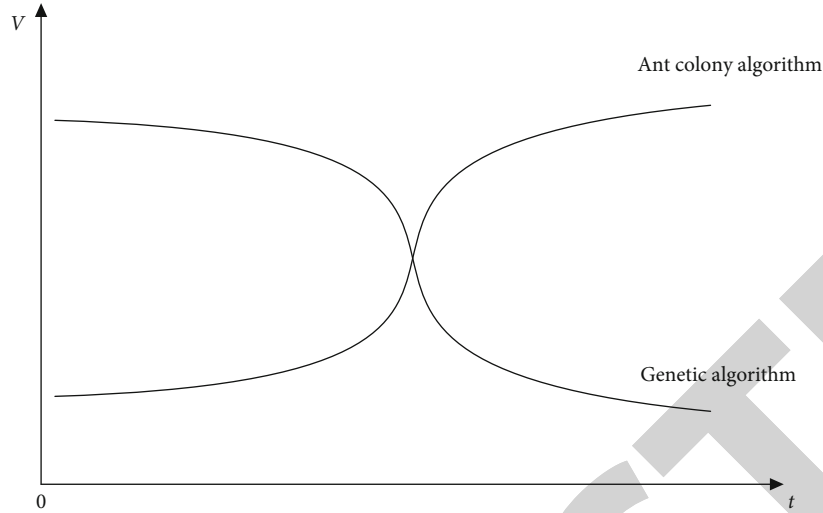
Figure 4: Time situation diagram of overall evolution rate.

$$f(H(t)) = \frac{\sum_{i \in H} f_i}{M[H(t)]}. \tag{2}$$

$M(H(t+1))$ is the expected number of pattern H in population after $t + 1$ iteration, P_c is the crossing probability, P_m is the mutation probability, $f(t)$ is the average fitness value, $f(H(t))$ is the average fitness value of population model H, f_i is the i-th individual fitness value, and $\delta(H)$ is the pattern definition distance, that is, the distance between the initial and last determined positions in pattern H.

2.2.2. Related Issues. In the aspect of human resource allocation, the algorithm is not perfect. If the two are combined, the matching resources needed by the enterprise organization at first can have idealized results. The reason is that the convergence speed of the optimal solution is fast in the early stage of the algorithm. With the continuous operation, in the later stage of the algorithm, the efficiency of human resource allocation plummeted due to the increase of allocation times and the decrease of convergence speed. The two are not suitable and need to be improved.

2.3. Ant Colony Algorithm

2.3.1. Basic Concepts. When the number of ants is $k(k = 1, 2, \cdots, m)$ and the number of cities is $(i, j = 1, 2, \cdots, n)$, i and j, the distance between them is d. And set the initialization pheromone concentration $\tau_{ij}(0) = \tau_0$. The flow chart of the ant colony algorithm is shown in Figure 3.

After t iterations, the probability $P_{ij}^k(t)$ formula for the k-th ant to successfully move from city i to j is as follows:

$$P_{ij}^k(t) = \begin{cases} \dfrac{[\tau_{ij}(t)]^\alpha \cdot [\eta_{ij}(t)]^\beta}{\sum_{s \in J_k(i)} [\tau_{is}(t)]^\alpha \cdot [\eta_{is}(t)]^\beta} & j \in J_k(i), \\ 0 & j \notin J_k(i). \end{cases} \tag{3}$$

α is the relative importance of pheromone, β is the relative importance of heuristic factors, $\tau_{ij}(t)$ is the pheromone concentration of city i and j paths after t iterations, $\eta_{ij}(t)$ is the heuristic function, the heuristic degree that ants can smoothly from city i to j in the t iteration, and $J_k(i)$ is a collection of cities that ants can visit next.

The heuristic factor is calculated by the following formula:

$$\eta_{ij} = \frac{1}{d_{ij}}. \tag{4}$$

The update formula of pheromone concentration in intercity path is as follows:

$$\tau_{ij}(t + 1) = (1 - \rho)\tau_{ij}(t) + \Delta\tau_{ij}, \tag{5}$$

$$\Delta\tau_{ij} = \sum_{k=1}^{n} \Delta\tau_{ij}^k. \tag{6}$$

ρ is the volatilization coefficient of pheromone, and the value range is (0, 1), $\Delta\tau_{ij}$ is the pheromone increment of edges i and j in this iteration, and $\Delta\tau_{ij}^k$: in this iteration, the amount of pheromones left on edges i and j is related to the k-th ant.

For $\Delta\tau_{ij}$, there are three calculation models:

The formula for the ant cycle system is as follows:

$$\Delta\tau_{ij}^k = \frac{Q}{L_k}. \tag{7}$$

L_k is the length of the path taken by ant k.
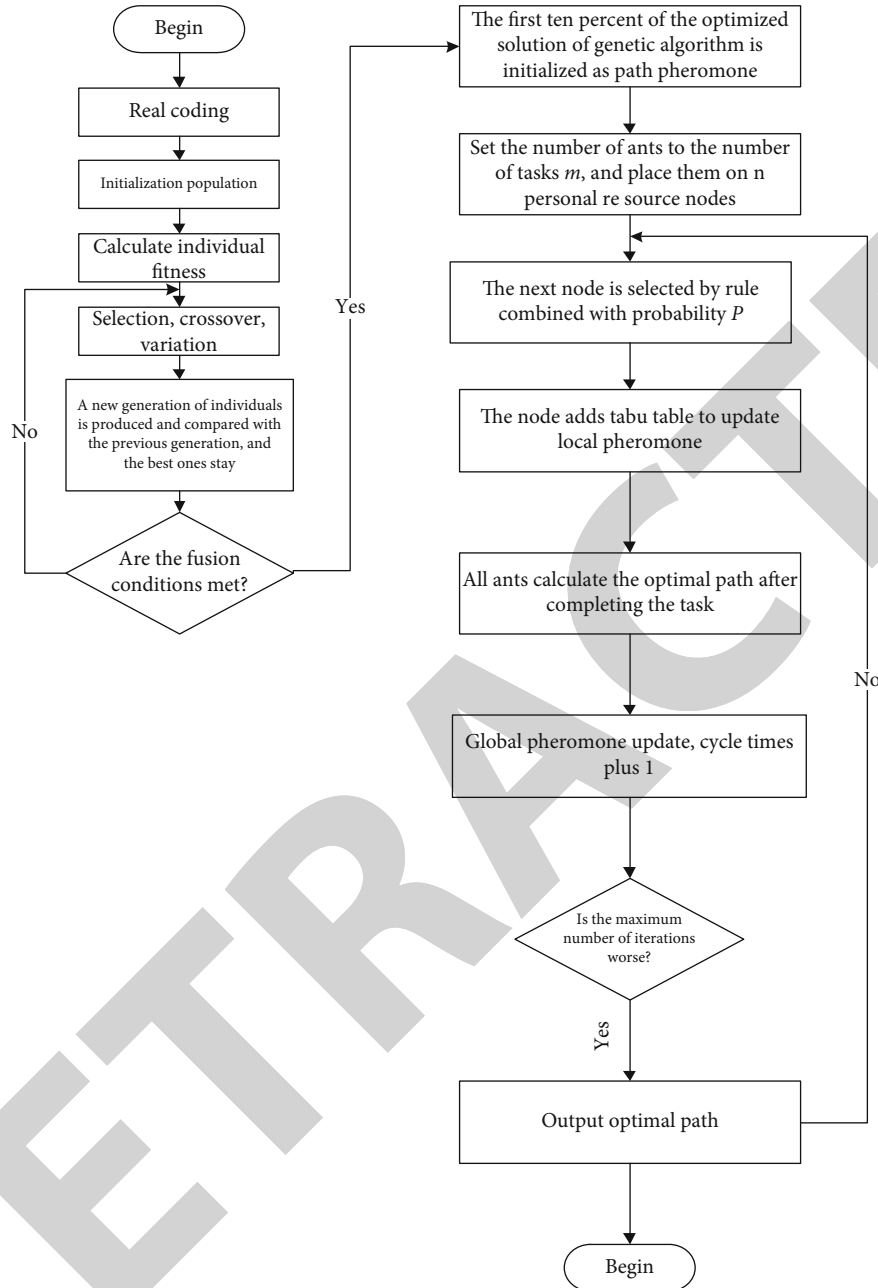
FIGURE 5: Flow chart of the genetic ant colony algorithm.

The formula for the ant quantity system is as follows:

$$\Delta\tau_{ij}^k = \frac{Q}{d_{ij}}. \tag{8}$$

The formula for the ant density system is as follows:

$$\Delta\tau_{ij}^k = Q. \tag{9}$$

Q is a normal number, which represents the total number of pheromones produced by ants after this iteration.

2.3.2. Related Issues. The influence of the ant colony algorithm on human resource allocation is just opposite to the new genetic algorithm. In the early stage of the algorithm, due to pheromone initialization, the ant's optimization ability is reduced. This means that in the allocation of human resources, in the early stage of allocation, human resource information cannot be rationalized, which will lead to reduced efficiency, increased costs, and brain drain. With many iterations, the pheromone concentration increases, which greatly increases the ant's optimization ability. This will greatly increase the matching efficiency in human resource allocation.

TABLE 1: Comparison of execution time and execution cost data.

Number of tasks	Type	Genetic algorithm	Ant colony algorithm	Genetic ant colony algorithm
30	Execution time	30	30	30
	Execution cost	45	45	25
60	Execution time	50	45	40
	Execution cost	76	75	52
90	Execution time	63	55	50
	Execution cost	100	101	88
120	Execution time	81	64	60
	Execution cost	162	161	109
150	Execution time	118	77	70
	Execution cost	177	177	146
180	Execution time	146	91	85
	Execution cost	220	221	175
210	Execution time	162	95	90
	Execution cost	250	248	208
240	Execution time	184	117	107
	Execution cost	288	290	247
270	Execution time	216	128	124
	Execution cost	321	323	268
300	Execution time	239	130	128
	Execution cost	361	360	300
330	Execution time	250	130	130
	Execution cost	426	425	339

3. Optimization Algorithm

The time trend of the overall evolution rate of the two algorithms is shown in Figure 4.

As can be seen from the figure, the disadvantages of the two are just the opposite. Therefore, this paper proposes to improve the two first and then combines them to complement each other. In this way, a new algorithm, namely, genetic ant colony algorithm, can be obtained. The algorithm can absorb the advantages of the former two, and ensure that the convergence speed does not decrease with iteration, and is more stable. The purpose of this algorithm for human resource allocation is to keep the efficiency of human resource allocation efficient and stable.

3.1. Improved Genetic Algorithm. For resource scheduling, assuming population size = popsize, subtasks = n, and schedulable resources = m, then the total length of parameters = n, then the range of each individual is $[1, m]$. The formula in the form of individual X is as follows:

$$X = (x_1, x_2, \cdots, x_n) \quad x_t \in R, i = 1, 2, \cdots n. \quad (10)$$

In order to compare the length of time required for information tasks in human resource allocation, the formula is as follows:

$$\text{totaltime}(I) = \max_{j=1}^{m} \sum_{i=1}^{n} T_{ij}, \quad (11)$$

$$T_{ij} = \frac{T_t(\text{length})}{\text{vm}_j(\text{mips})} + \frac{T_t(\text{inputfilesize})}{\text{vm}_j(\text{bw})} + \frac{T_t(\text{outputfilesize})}{\text{vm}_j(\text{bw})} + T_t(\text{wait\_time}), \quad (12)$$

$$\text{vm}_j(\text{mips}) = \text{pe\_num}_j \times \text{pe\_mips}. \quad (13)$$

$\text{vm}_j(\text{mips})$ is the CPU computing power, pe_num_j is the number of virtual machine processors, pe_mips is the virtual machine vm_j processor speed, $\text{vm}_j(\text{bw})$ is the wideband processing capability of virtual machine vm_j, and $T_t(\text{wait\_time})$ is the waiting time of subtask i.

In human resources, in order to get suitable resource information individuals, the formula of their fitness function is as follows:

$$f_1(j) = \frac{1}{\text{totaltime}(I)} \times u_{\text{LB}}, \quad (14)$$

$$u_{\text{LB}} = \frac{\sum_{j=1}^{m} \sum_{i=1}^{n} T_{ij}}{m \times \text{totaltime}(I)}. \quad (15)$$

u_{LB} is the balance the load factor, which is proportional to the utilization of resources.

$$f_2(j) = \frac{1}{\sqrt{\sum_{j=1}^{m}(\text{task}(i, j) - n/m)^2/m}} 1 < i < \text{popsize}, \quad (16)$$

$$f(j) = \omega f_1(j) + (1 - \omega)f_2(j) 0 < \omega < 1, \quad (17)$$
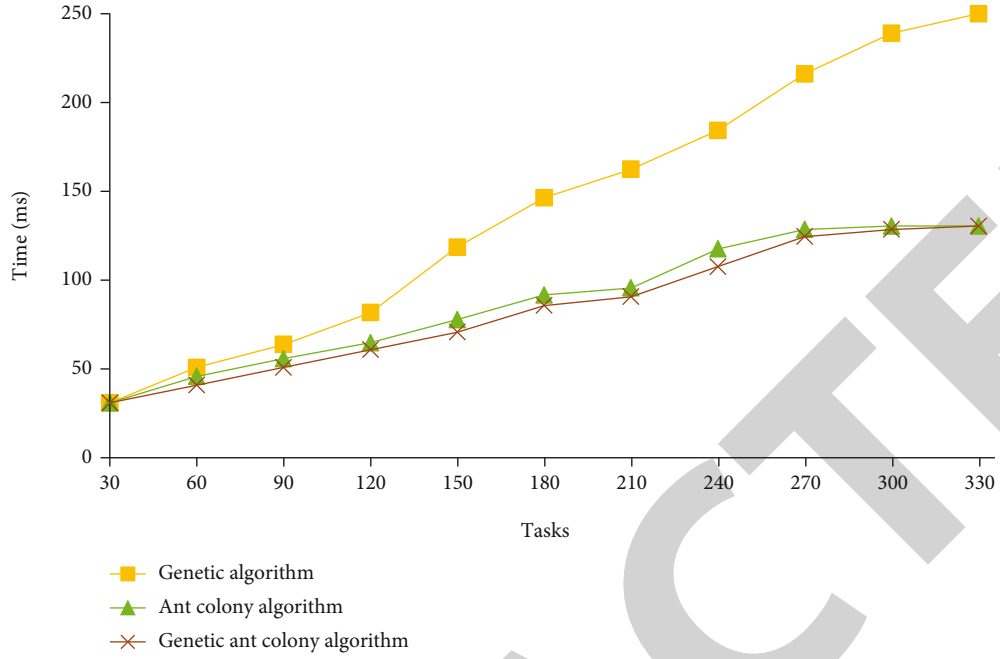
FIGURE 6: Comparison of the execution time length of the three algorithms.
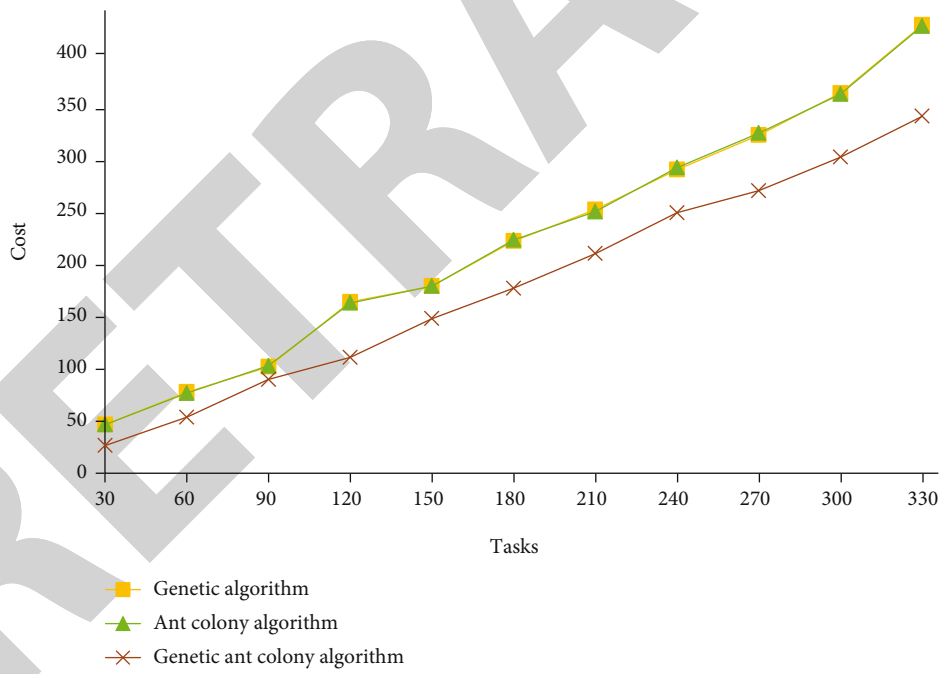
FIGURE 7: Comparison of the execution costs of the three algorithms.

in this which $\text{task}(i, j)$ is the task to which the virtual machine j of the individual i is assigned.

The formula of selection probability is as follows:

$$P_i = \frac{f(i)}{\sum_{j=1}^{m} f(j)}. \tag{18}$$

The formula of crossover probability is as follows:

$$P_c = \begin{cases} P_{c1} - \dfrac{(P_{c1} - P_{c2})\left(f' - f_{\text{ave}}\right)}{f_{\text{max}} - f_{\text{ave}}} & f' \geq f_{\text{ave}}, \\ P_{c1} & f' < f_{\text{ave}}, \end{cases} \tag{19}$$

$$P_{c1} = 0.9, P_{c2} = 0.6.$$

TABLE 2: Resume data size.

Number	Size
1	25 KB
2	30 KB
3	35 KB
4	40 KB
5	45 KB
6	50 KB
7	55 KB
8	60 KB
9	65 KB
10	70 KB

f_{max} is the maximum fitness value in the current population, f_{ave} is the average value of fitness in the current population, and f', compared with two cross individuals, is the maximum fitness value.

The mutation probability formula is as follows:

$$P_m = \begin{cases} P_{m1} - \dfrac{(P_{m1} - P_{m2})(f' - f_{ave})}{f_{max} - f_{ave}} & f' \geq f_{ave}, \\ P_{m1} & f' < f_{ave}, \end{cases} \quad (20)$$

$$P_{m1} = 0.1, P_{m2} = 0.001.$$

3.2. Improved Ant Colony Algorithm. In conventional algorithms, the randomness of ants is not high when they move, which will lead to problems when ants search for similar optimal resource information. In order to solve this problem, new rules have been formulated. The formula is as follows:

$$j = \begin{cases} \arg \max \left\{ \left[\tau_{ij}(t) \right]^\alpha \cdot \left[\eta_{ij}(t) \right]^\beta \right\} & \rho \leq \rho_0, \\ P & \rho > \rho_0. \end{cases} \quad (21)$$

ρ is the uniformly distributed random values with a value range of [0, 1], and ρ_0 is the constant value.

The formula of HR multiservice quality requirement function related to pheromone update rule is as follows:

$$F(I) = \varphi_1 \frac{\text{totaltime}_{ij} - \text{totaltime}_{min}}{\text{totaltime}_{max} - \text{totaltime}_{min}} + \varphi_2 \frac{\cos t_{ij} - \cos t_{min}}{\cos t_{max} - \cos t_{min}}. \quad (22)$$

totaltime_{ij} is the expected task execution time, totaltime_{max} is the maximum expected task execution time, totaltime_{min} is the minimum expected task execution time, $\cos t_{ij}$ is the expected task execution cost, $\cos t_{max}$ is the Maximum cost of expected task execution, $\cos t_{min}$ is the minimum cost of expected task execution, and φ_1, φ_2 are the time weight coefficient and cost weight coefficient.

TABLE 3: Data on upload speed and operating cost.

Number	Type	Genetic algorithm	Ant colony algorithm	Genetic ant colony algorithm
1	Upload speed	90.3	85.3	98.7
	Operating cost	0.003	0.004	0.0008
2	Upload speed	64.2	83.2	95.2
	Operating cost	0.007	0.004	0.001
3	Upload speed	84.9	83.0	90.8
	Operating cost	0.005	0.005	0.003
4	Upload speed	69.1	74.8	88.4
	Operating cost	0.009	0.006	0.004
5	Upload speed	55.6	68.2	83.9
	Operating cost	0.012	0.008	0.005
6	Upload speed	67.1	51.3	80.7
	Operating cost	0.009	0.011	0.006
7	Upload speed	66.3	60.4	75.3
	Operating cost	0.010	0.013	0.006
8	Upload speed	55.6	56.9	72.6
	Operating cost	0.014	0.014	0.008
9	Upload speed	49.4	50.1	70.7
	Operating cost	0.017	0.016	0.008
10	Upload speed	45.8	47.9	70.2
	Operating cost	0.020	0.018	0.008

Time weight coefficient φ_1 and cost weight coefficient φ_2 are in [0, 1], and $\varphi_1 + \varphi_2 = 1$.

When calculating the local pheromone increment, the ant updates the resource every time it completes the resource allocation. The formula is as follows:

$$\Delta \tau_{ij}(t) = \frac{\text{const}_1}{F(I)}. \quad (23)$$
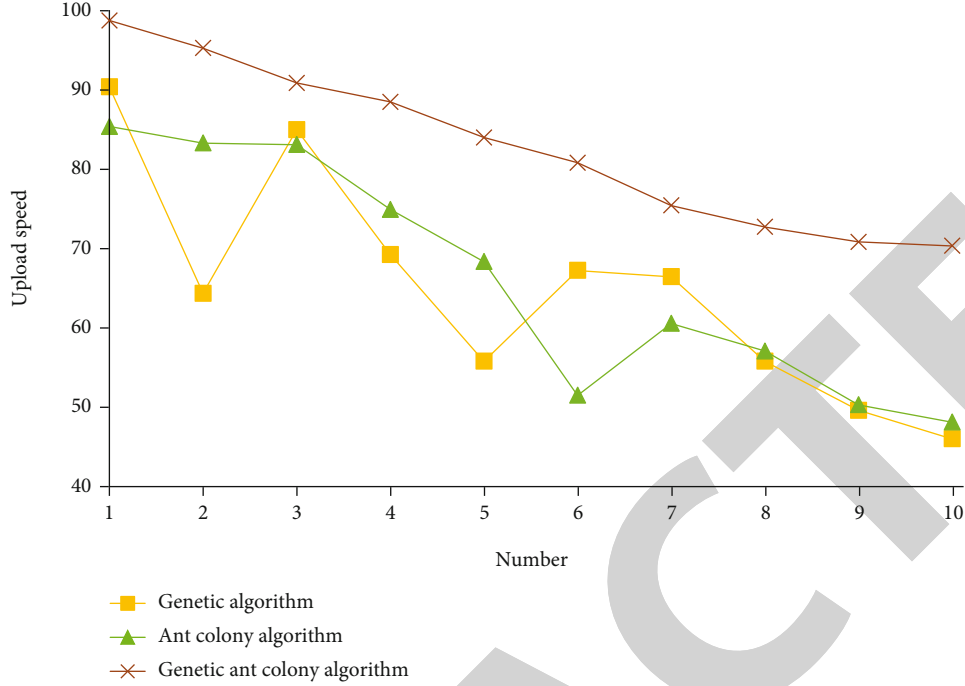
Figure 8: Comparison of data upload speed.

When calculating the global pheromone increment, each ant completes the resource allocation once before updating. The formula is as follows:

$$\Delta\tau_{ij}(t) = \frac{\text{const}_2}{F(I)_{\text{best}}}. \qquad (24)$$

And $\tau_{\min} \leq \tau_{ij}(t) \leq \tau_{\max}$ is specified, so as to avoid the stagnation of the algorithm caused by the disparity of path pheromones.

In the ant colony algorithm, the distance between two cities is the same as heuristic information. However, this cannot guarantee the optimal solution; so, we need to refer to the load model to improve the expression of heuristic information. The heuristic factor function is expressed as follows:

$$\eta_{ij} = \frac{1}{\sum_{i=1}^{\text{task}} T_i(\text{length}) + T_i(\text{length})/\text{vm}_j(\text{mips})}. \qquad (25)$$

$T_i(\text{length})$ is the length of task i, and task is the number of tasks that have been run on virtual machine j.

3.3. Genetic Ant Colony Algorithm.
When $g_{\text{now}} < g_{\text{max}}$, compare $g_{\text{ratio}}, g_{\text{pop}}$, and when the comparison result is $g_{\text{pop}} < g_{\text{radio}}$ and occurs many times, the algorithm begins to transform.

g_{now} is the current number of iterations, g_{max} is the maximum number of iterations g_{min} is the minimum number of iterations, g_{ratio} is the minimum evolution rate, and g_{pop} is the progeny evolution rate.

When the optimal solution of ant colony algorithm is = τ_G, the pheromone value of the ant colony algorithm is $\tau_S = \tau_{\min} + \tau_G$ at the initial stage. The algorithm flow is shown in Figure 5.

4. Simulation Experiment

4.1. Algorithm Testing.
Set popsize = 100, $g_{\max}$ = 150, $g_{\max}$ = 50, g_{radio} = 0.5%, the maximum number of iterations is 120, and $\rho = 0.3, \alpha = \beta = 1$. The overall parameter sets the task length $\in [1000, 10000]$ and the total number of tasks $\in [30, 330]$ and $200 \leq \text{mips} \leq 1000$, bw = 1000Mb.

The data pairs obtained through experiments are shown in Table 1.

Execution cost index human resource allocation in the system uses the cost needed to reflect the human resource system allocation of scientific and optimal degree. The lower the execution cost, the higher the optimization degree of human resources allocation, and the relatively reasonable cost.

An alignment of execution times is shown in Figure 6.

The pair of execution costs is shown in Figure 7.

It can be seen from this that the GAACO algorithm is superior to the other two algorithms in terms of execution time and execution cost. It can be clearly seen that with the increase of the number of tasks, the execution time and cost of the ACO-GA algorithm are lower and lower than those of the other two algorithms, which shows that when the number of tasks increases gradually, the running speed of ACO-GA is better and better than those of the other two algorithms, that is, the ACO-GA algorithm has the characteristics of high efficiency, stability, and low cost.
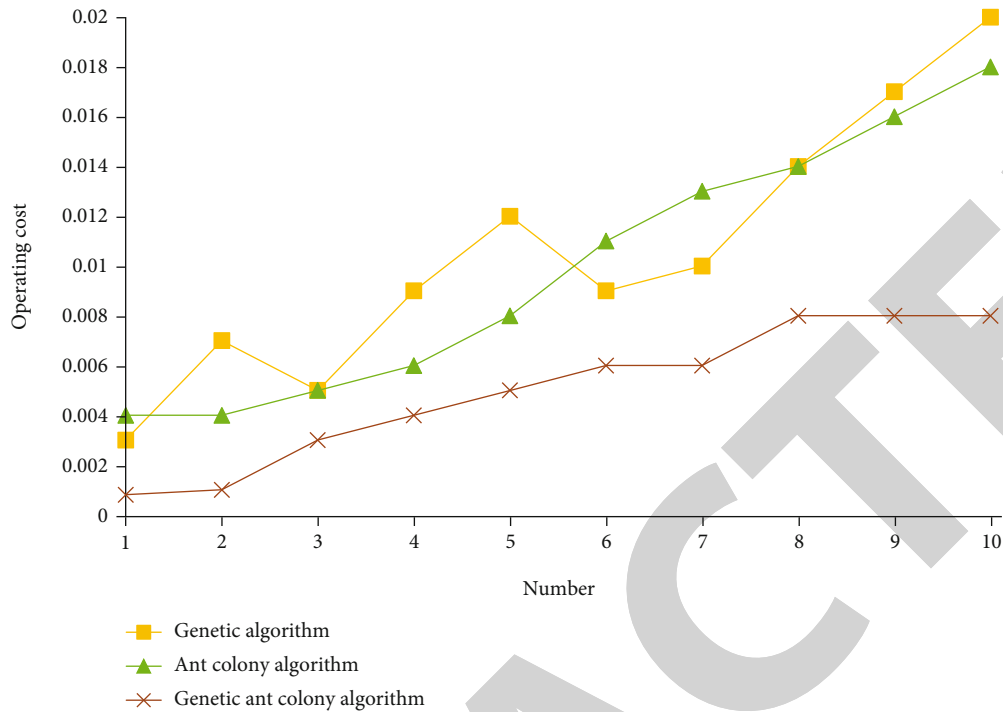
Figure 9: Comparison chart of data operation cost.

4.2. Experiments and Results

4.2.1. Establishing the Objective Function.
Establish the database of human resource allocation and digitize the resumes of relevant personnel, that is, change the characteristic attributes of personnel into vector features, such as transforming resumes A and B into $A = (a_1, a_2, a_3)$, $B = (b_1, b_2, b_3)$. The distance between the vectors they transform is the similarity between the two resumes, and the formula is as follows:

$$S = \sqrt{\sum_{i=1}^{n} (a_1 - b_1)^2}. \qquad (26)$$

The formula for judging employee grades is as follows:

$$S(A, B, C) = \sum_{i=1}^{n} f(A, B) \times C_i. \qquad (27)$$

$f(A, B)$ is the functional relationship between files A and B, that is, similarity, and C_i is the similarity distribution weight.

At the end, the formula for matching the similarity of data is as follows:

$$D = \left\{ \sum_{i=1}^{n} (S_{mn} - S_{11}) \times C_i \right\}^{1/2}. \qquad (28)$$

S_{mn} is the maximum value of weight characteristic, and S_{11} is the minimum value of weight attribute,

Table 4: Comparison of similarity between predicted value and actual value of algorithm.

Number	Actual value	Genetic	Ant colony	Genetic ant colony
1	80%	70%	68%	75%
2	78%	67%	65%	75%
3	85%	71%	70%	83%
4	75%	68%	70%	77%
5	83%	75%	77%	81%
6	80%	65%	70%	83%
7	86%	70%	71%	85%
8	76%	65%	65%	77%
9	79%	64%	66%	80%
10	75%	60%	62%	77%

4.2.2. Simulation Experiment and Result Analysis.
Suppose a total of 10 resumes have been uploaded to the database, the data are uploaded and run in the order from small to small. Record the uploading speed and running cost of these 10 data under the three algorithms and compare them. The data sizes are shown in Table 2.

The data of upload speed and running cost obtained by experiments of the three algorithms are shown in Table 3.

The data upload speed pair is shown in Figure 8.

The data running cost pair is shown in Figure 9.

After testing and comparing the running speed and cost of the algorithms, this paper proposes to test the predicted values of the three algorithms and compare them with the
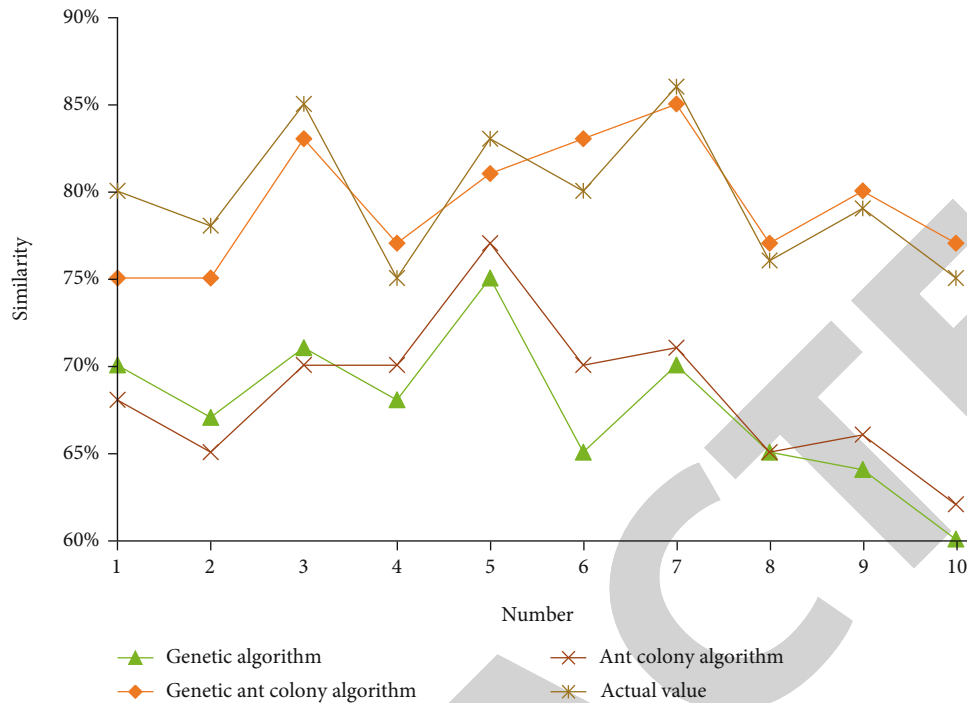
FIGURE 10: Similarity comparison data graph.

actual values according to the objective function of human resource allocation similarity set above. Set up each post standard information vector characterization, compare the above 10 human resources data with post standard data, calculate similar values, and compare them. Comparative data are shown in Table 4.

The similarity comparison data diagram is shown in Figure 10.

It can be seen that in human resource data matching, the accuracy of the first two is not ideal. When the data is relatively small in the early stage, it can be seen that the genetic algorithm is slightly better than the ant colony algorithm, and the accuracy of the ant colony algorithm is slightly better than the genetic algorithm in the later stage. On the other hand, the ACO-GA algorithm is more consistent with the actual value, which not only ensures the stability but also ensures the accuracy of prediction, which is more in line with the actual demand. The next research work needs to analyze the execution efficiency of the intelligent optimization algorithm in different stages, aiming at the problems of local convergence and insufficient execution in different stages. Further expand the human resource optimization program, from the implementation system and online analysis programs to analyze the problems in human resources.

5. Conclusion

The ACO-GA algorithm is improved and fused by the basic algorithm. At the beginning of the design, it was designed to make it take the strengths of the two and promote the weaknesses of the two. Through experiments, it is found that this method can really keep the convergence speed at a high level in the early and late stages and keep a high stability. Therefore, in the human resource allocation module, the ACO-GA algorithm is a successful example of improvement.

Data Availability

The experimental data used to support the findings of this study are available from the corresponding author upon request.

Conflicts of Interest

The authors declared that they have no conflicts of interest regarding this work.

References

[1] G. B. Huang, E. Cambria, K. A. Toh, B. Widrow, and Z. Xu, "New trends of learning in computational intelligence [guest editorial]," *IEEE Computational Intelligence Magazine*, vol. 10, no. 2, pp. 16-17, 2015.

[2] A. Manju and M. J. Nigam, "Applications of quantum inspired computational intelligence: a survey," *Artificial Intelligence Review*, vol. 42, no. 1, pp. 79–156, 2014.

[3] J. A. Laghari, H. Mokhlis, A. Bakar, and H. Mohamad, "Application of computational intelligence techniques for load shedding in power systems: a review," *Energy Conversion and Management*, vol. 75, pp. 130–140, 2013.

[4] S. Tzafestas and E. Tzafestas, "Computational intelligence techniques for short-term electric load forecasting," *Journal of Intelligent & Robotic Systems*, vol. 31, pp. 7–68, 2001.

Hindawi

Retraction

Retracted: Analysis and Application of the Ideological and Political Evaluation System of College Students Based on Text Mining

Journal of Sensors

This article has been retracted by Hindawi following an investigation undertaken by the publisher [1]. This investigation has uncovered evidence of one or more of the following indicators of systematic manipulation of the publication process:

(1) Discrepancies in scope

(2) Discrepancies in the description of the research reported

(3) Discrepancies between the availability of data and the research described

(4) Inappropriate citations

(5) Incoherent, meaningless and/or irrelevant content included in the article

(6) Peer-review manipulation

The presence of these indicators undermines our confidence in the integrity of the article's content and we cannot, therefore, vouch for its reliability. Please note that this notice is intended solely to alert readers that the content of this article is unreliable. We have not investigated whether authors were aware of or involved in the systematic manipulation of the publication process.

Wiley and Hindawi regrets that the usual quality checks did not identify these issues before publication and have since put additional measures in place to safeguard research integrity.

We wish to credit our own Research Integrity and Research Publishing teams and anonymous and named external researchers and research integrity experts for contributing to this investigation.

The corresponding author, as the representative of all authors, has been given the opportunity to register their agreement or disagreement to this retraction. We have kept a record of any response received.

References

[1] J. Geng, T. Wang, and S. Zhang, "Analysis and Application of the Ideological and Political Evaluation System of College Students Based on Text Mining," *Journal of Sensors*, vol. 2022, Article ID 4263974, 14 pages, 2022.

Research Article

Analysis and Application of the Ideological and Political Evaluation System of College Students Based on Text Mining

Jing Geng,[1] **Ting Wang,**[2] **and Shunyou Zhang** [3]

[1]*Baoding Vocational and Technical College, Baoding, Hebei 071000, China*
[2]*School of Art, Hebei College of Science and Technology, Baoding, Hebei 071000, China*
[3]*Hebei Institute of Communications, Shijiazhuang, Hebei 051430, China*

Correspondence should be addressed to Shunyou Zhang; zhangsy@hebic.edu.cn

Under the background of the new era, the ideological and political theory courses in universities are the key courses to cultivate people by virtue. It is very important for college students in their own ideological and political construction and consciousness. At the present stage, there is little research on the ideological and political current situation of college students, most of them improve the teaching program from the teacher level, and there is no research on the ideological and political evaluation system of college students. In order to understand the current situation of the ideological and political evaluation of college students, we will study it from the two aspects of the school and the society. This paper excavates and analyzes the ideological and political aspects of college students and those in the society: first of all, the ideological and political evaluation of teachers on large social platforms such as Zhihu and Weibo and the moral quality and political consciousness of college students in the society. It was then processed and analyzed using the Python language. Draw the word frequency and word cloud map of the keywords in the evaluation for analysis. Then, use the text data preprocessing method based on the word frequency statistics law (Data Preprocessing Based on Term Frequency Statistics Rules (DPTFSR)). Processing the text data and finally conducting the relevant emotional analysis show the university ideological and political system to understand the ideological and political situation of college students in the new era and to improve the ideological and political education program according to its performance.

1. Introduction

In some contemporary research on contemporary ideological and political education, it shows that it needs to explore [1] from the perspective of systematic integration in the process of promoting the high-quality ideological and political development of college students. The moral, intellectual, physical, aesthetic, and labor qualities of college students in daily life are a manifestation of the ideological and political consciousness of college students, and the ideological and political evaluation of college students is influenced by multiple factors. For example, the attraction of university ideological and political theory courses to college students is related to the effectiveness of ideological and political education to a certain extent [2]. In the era of smart education, ideological and political education should be tailored to things, progressive and new according to the situation [3–5]. Its difficulty is due to current affairs about the ideological and political changes of college students, and the clear perception of this change is teachers. And the comments on social media platforms are [6] for the quality of ideological and political courses. This is related to the status of ideological and political construction.

In fact, in the thousands of evaluations, teachers and society show the ideological and politics of college students from different perspectives, and extracting useful information from a large number of comments is helpful to the objective evaluation of the ideological and politics of college students. Therefore, this paper uses the text mining technology [7–9] to mine and analyze the evaluation of college students and gives reasonable suggestions for ideological and political education according to the results of the analysis system. This helps to reflect the recognition of college students' ideological and political courses, college students'

recognition of teaching programs and content, and the influence of teachers' acceptance of ideological and political courses. First, the text positioned the data objects to be collected and analyzed, and it was found that the question and answer method of the Zhihu website [10] is very helpful for exploring the ideological and political evaluation of college students. Therefore, the data source of this article is the Zhihu website. Firstly, the crawler technology of python is used to collect the data of questions and answers related to the Zhihu website, and then, the data is preprocessed, because only the most basic word segmentation methods and stop words can be completed in the current preprocessing stage of literature mining. The utilization of huge data is also low. Therefore, in this paper, the text data preprocessing method based on the statistical law of word frequency is first carried out [11]. Then, after the low-frequency words are removed in the preprocessing stage, the word segmentation method and the stop words of the basic data are completed. The basic data after pretreatment are obtained. Finally, Python [12] is used again to draw the word frequency map and word cloud map of the preprocessed data for keyword analysis, and emotional analysis technology [13, 14] is used to obtain the social evaluation of contemporary college students' ideology and politics. It is found that the evaluation mainly comes from several aspects, including the sense of honor of the whole country and society, personal values, and moral values.

2. Data Collection

Search for questions about topics related to "college students' ideological and political evaluation" on the homepage of Zhihu. There are about 300 questions, and the number of answers below each question is more than a few hundred and less than three or four, and there is a personal evaluation of this answer below each answer. The number of texts is very complex and huge, so this paper will choose three extended topics, such as "contemporary college students' outlook on life and values," "contemporary college students' ideological and political status," and "current college students' personal moral quality evaluation." Because these questions are the direct display of college students' ideological and political consciousness facing the society, they have a direct and valuable reference for understanding college students' ideological and political consciousness. As Zhihu, Weibo, massive open online course, and other website platforms are the main routes for online comment exchange in China, this writing platform can freely discuss and publish its own opinions. Compared with the usual text information, the text of the website has its unique characteristics, and the process of its integration and analysis is more complex. Therefore, it is important to carry out useful means to obtain and sort out useful information from complex website data. Zhihu is a question-and-answer website, on which users can post questions and invite other users to answer. The answers are not standardized. The class will give comments according to their own feelings and thoughts, and other people can also comment and praise under the reply content of the respondent to express different or the same views with

the respondent. This model is more friendly and concentrated, which reflects the social collective's reflection on a certain problem. Weibo is where one person publishes content and others evaluate his views. And there is a need for text collection of data as much and detailed as possible; the model of this platform is very good in line with this demand. Therefore, this paper will collect and analyze the evaluation of related topics of "ideological and political evaluation of college students" in Zhihu.

Due to the wide variety of text mining technologies on the market, in order to find the text mining technologies with high efficiency and high accuracy, the three common mining algorithm technologies first compare the relevant content classification effect of the ideological and political evaluation of college students, and the most suitable and the most relevant one is selected. These three methods are the simple Bayesian method, K-nearest adjacency reference classification algorithm, and first-order rule learning. More mainstream text mining techniques are shown in Figure 1.

To understand how these methods compare different types of web classification efficiency, the tables in three databases are used. Since the data information of some companies and schools is externally visible, this data can be used first to compare the efficiency of several algorithms. First, the database information of several companies and schools was tested comprehensively, namely, Hoovers28, Hoovers255, and Univ6. For a single web page, associated words, and marker language, the results are shown in Table 1.

Then, compare the runtime with similar recall and precision weight again, shown in Table 2.

The appeal data are plotted as a line of Figures 2 and 3.

These performances are related to the kinds of problems to be dealt with. For school-related web pages, these three methods are not very good for classifying single pages, while for the other two data, the naive Bayes method and K-nearest neighbor reference classification algorithm are significantly less efficient for handling related words and html titles. Finally, we found that these methods are not applicable to the classification query of Zhihu webpage information, so we will implement another method next.

After determining the web page to be collected, we will collect the data in the web page as a web crawler. In general, there are two ways: one is dedicated crawler software, and the other is to write a code script in the programming language to collect data. In addition, there are many programming languages that can realize the crawler, such as Python, C++, and Java, while this paper uses simple and flexible Python to realize the data collection, and the specific structure framework is shown in Figure 4.

First of all, log into Zhihu to determine the URL of the three questions: "outlook on life, values," "ideological and political status of contemporary college students," and "evaluation of personal moral quality of current college students", and check the answers under each question. The data in the network is basically based on the HTTP protocol, and the data is generally stored in the HTNML web page tags. The flow chart of crawler capture on the Zhihu website based on the ideological and political evaluation of college students is shown in Figure 5.
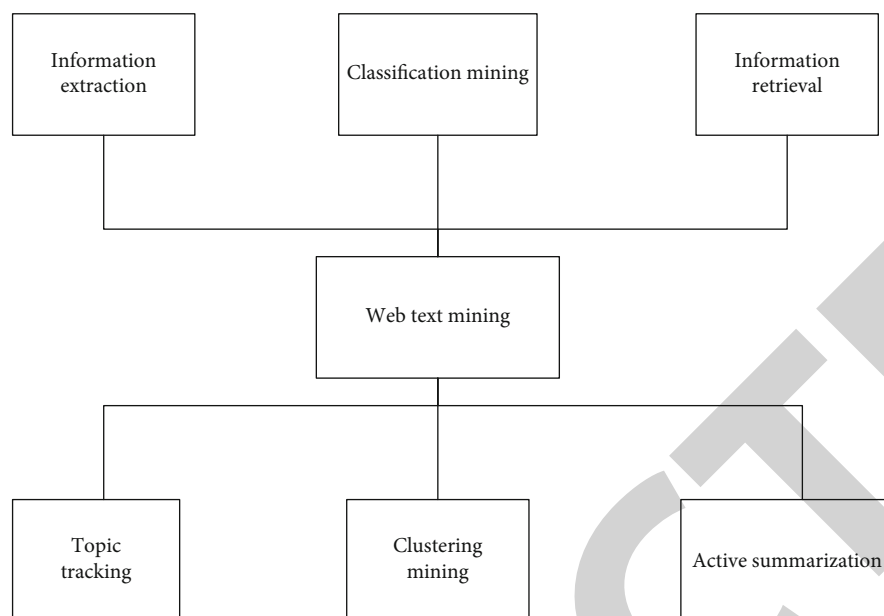
Figure 1: Web text mining techniques.

Table 1: Test results for the different algorithms under the three databases.

| Attribute | Hoovers28 | | | Hoovers255 | | | Univ6 | | |
	NB	KNN	FOIL	NB	KNN	FOIL	NB	KNN	FOIL
Single page	55.1	58.1	31.5	32.5	32	11.6	69.6	83	82.7
Related words	40.1	38.6		18.9	20.4		74.1	86.2	
Tagged words	49.2	49	31.8	24	26.9	12.1	76.3	88	86
HTML title	40.8	43.3	28.7	17.9	22.6	11.5	78.6	81.5	86.3

Table 2: Average runtime of the CPU under the three algorithms.

| Attribute | Single page | | | Related words | | | Tagged words | | |
	NB	KNN	FOIL	NB	KNN	FOIL	NB	KNN	FOIL
Hoovers28	1.5	5	288.4	2	23		2.3	12	304.3
Hoovers255	3	2.5	315.6	3.5	3.1		3.5	3.9	274.5
Univ6	0.07	0.97	2.8	0.1	2.8		0.27	1.3	10.25

To crawl data, you need to send a Get request to HTTP in advance, and the server will return a Responde object after receiving the request. There are many libraries of functions of methods implementing this request in Python such as re, urllib, and requests [15]. This article uses the request library with the GET method in Python. request. get() obtains the main information of the web page and makes the GET request for HTTP for obtaining the data through the specified URL. The full parameters of the Get method are as Requests.get (url, params = None, ∗∗kwargs).

The url is the url connection of the CNKI question page, params is another data in the connection, and ∗∗ kwargs is the 12 empty visit parameters. Create a request object that requests content from the server, and return a request object to represent the server's response, as shown in Table 3.

Finally, we saved the data collected by the crawler as an xlsx format d file for later data preprocessing.

3. Data Preprocessing

In the digital age, the inherent characteristic of text mining is the scarcity of valuable data. The conflict between a large number of words and a small number of key features results in the lack of effectiveness when a large number of useful information is mentioned and also limits the effect of literature mining, so it is very important to do a good job of efficient data preprocessing before effective analysis of literature information. In order to improve the high performance of the analysis results, the text preprocessing method in this paper is the text data preprocessing method (Data Preprocessing Based on Term Frequency Statistics Rules
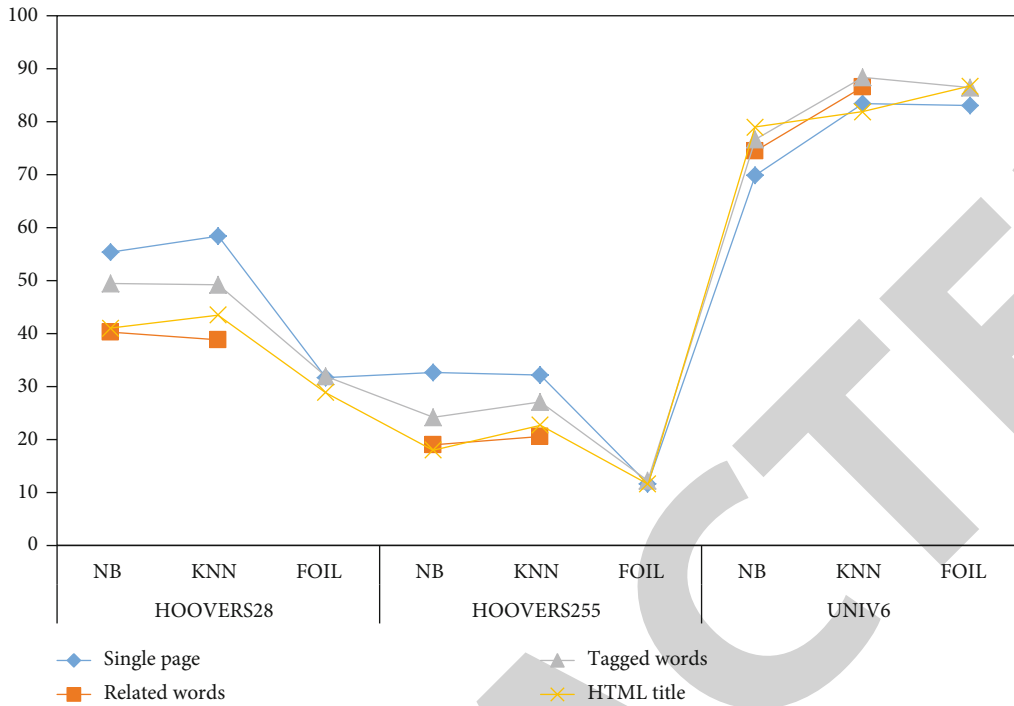
FIGURE 2: Test results of the different algorithms under the three databases.
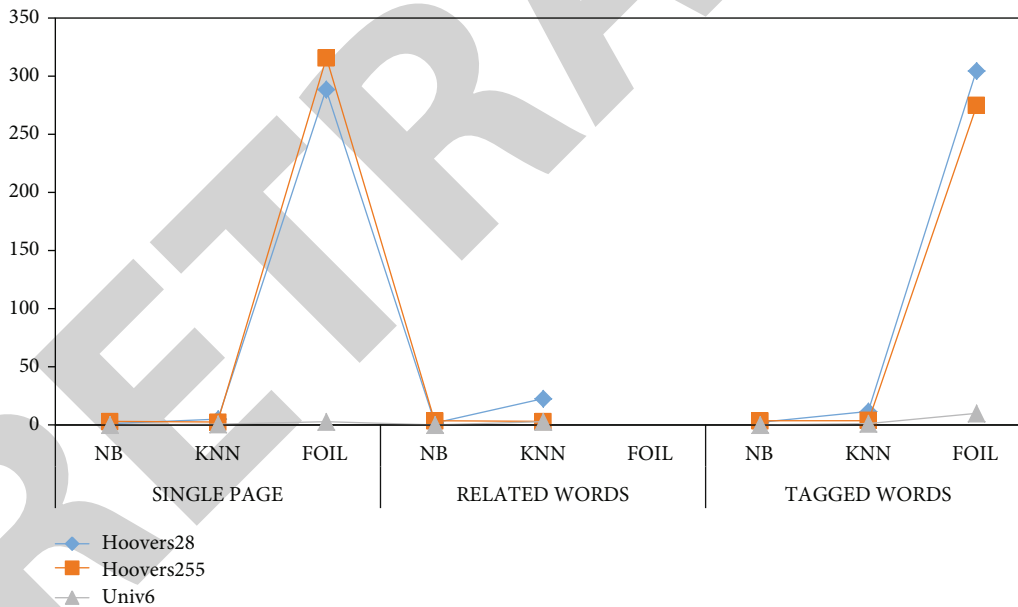
FIGURE 3: Average runtime of the CPU under the three algorithms.

(DPTFSR)) based on the word frequency statistical law, and then, the collected text data is preprocessed by deleting, segmenting, and removing stop words. The basic step is to first initialize the dictionary dict1, dict2, and dict3 and the corresponding storage word frequency of $TF_n = 1$, $TF_n = 2$, and $TF_n > 2$ counters count1, count2, and count3, define the word list TermList and the counter word_count, and then perform the word separation operation and record the word frequency of each word. Then, classify them according to

different word frequencies, and record the number of words in each frequency. Then, the data is preprocessed based on the word frequency statistics; finally, the different word frequency word sets, corresponding total number of words, and preprocessing list are returned. The following shows the number of appearances of the same word represents the number of appearances of the word i in the text document TFn, n is how much of the word appears, while TF_k (ti) represents the word frequency of the word ti which is k
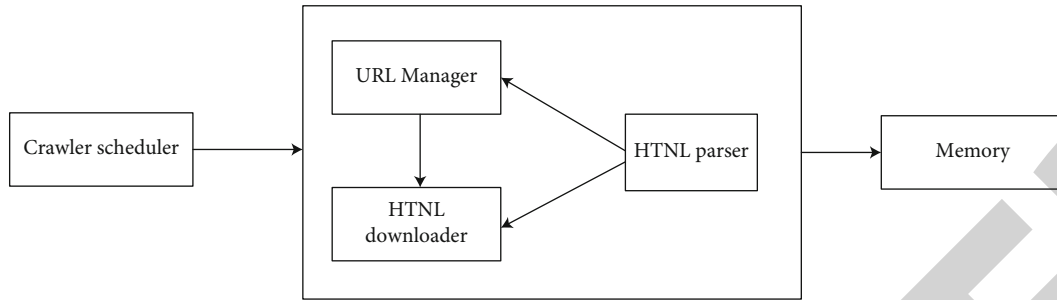
FIGURE 4: The Python crawler frame.
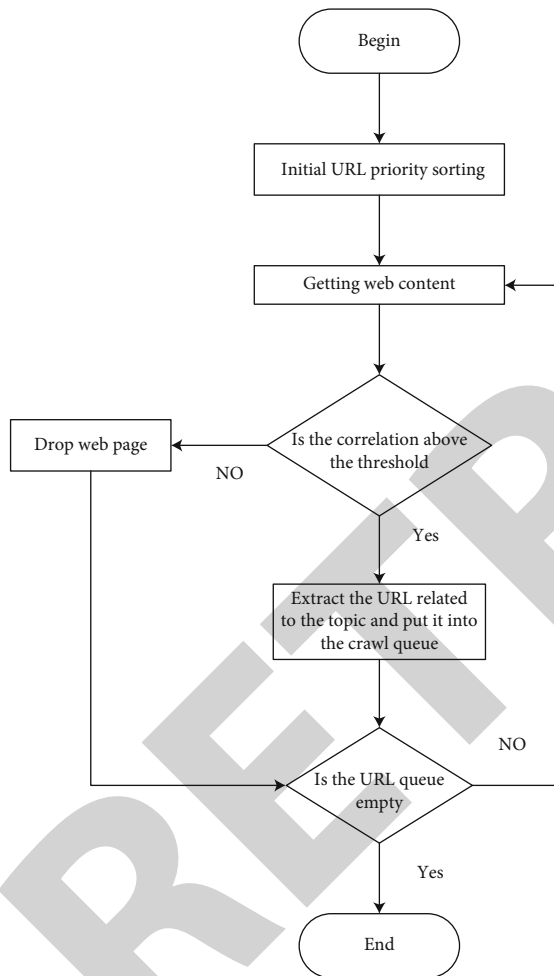
FIGURE 5: Network crawler grasping process.

. The number of words at the same frequency is recorded as NTIF_n. Using a set of words {ti} in the document, you can meet the expression $\text{TF}_k(\text{t1}) = \text{TF}_k(\text{t2}) == \text{TF}_k(\text{tq}) = \text{T F} k = \text{T F} k = k$, so ti is a set of the same word frequency k; the total number is q. Frequency refers to the frequency produced in the article and the ratio between the frequency and the length of the article, expressed as $f_n = \text{TF}_n/L$. The word rank is expressed as a TR_n. When $\text{TF}_k = \text{TF}_n$, $\text{TR}_k = 1$; when $\text{TF}_k = $ a moment, $\text{TR}_k = \text{TR}_n$. You can also use Zipf's law [16, 17] to push the expression of the same frequency word number, which is one of the three widely used laws of computation in the field of text mining techniques [18].

$$f_n \cdot \text{TR}_n = K(K \text{ is a constant}), \tag{1}$$

$$\text{TF}_n \leq f_n \cdot \text{L} < \text{TF}_{n+1}, \tag{2}$$

where K in formula (1) is a nondeterministic value, $K = 1/(\ln N_{\text{diff}} +)$, changing [19] around a central fluctuation. The following expression for NTIF_n can be derived from

$$\text{NTIF}_n = \frac{K \cdot L}{\text{TF}_n \cdot \text{TF}_{n+1}}. \tag{3}$$

Put formula (1) into formula (3) to get

$$\text{TF}_n \leq \frac{K \cdot L}{\text{TR}_n} < \text{TF}_{n+1}. \tag{4}$$

Formula (5) is obtained:

$$\begin{cases} \text{TR}_{n_{\max}} = \dfrac{K \cdot L}{\text{TF}_n}, \\ \text{TR}_{n_{\min}} = \dfrac{K \cdot L}{\text{TF}_{n+1}}. \end{cases} \tag{5}$$

The number of common frequency words NTIF_n of the word frequency TF_n satisfies

$$\text{NTIF}_n = \text{TR}_{n_{\max}} - \text{TR}_{n_{\min}}. \tag{6}$$

Finally, the above expression can derive the expression of the required number of the same frequency words:

$$\text{NTIF}_n = \frac{K \cdot L(\text{TF}_{n+1} - \text{TF}_n)}{\text{TF}_n \cdot \text{TF}_{n+1}}. \tag{7}$$

Table 3: Common properties of the response object.

Attribute	Describe
r.status_code	Return status of the HTTP request, 200 means a connection is successful, 404 means a connection failure
r.context	Binary form of the HTTP response content
r.encoding	Guess the response encoding mode from the HTTP headers
r.apparent_encoding	Response content encoding method derived from the content analysis
r.text	The string form of the HTTP response content, the url corresponds to the page content

The maximum method is used to refine expressions for the number of words of the same frequency, because NTIF_n does not fully apply to the case where the word frequency TF_n takes any value, because it is based on Zipf's law, but Zipf's law does not well reflect the distribution of words with very low word frequency. Next, the maximum value method is used to perfect the expression of $\mathrm{TF}_n = 1, 2$ (formula (8)) same frequency words, where TR_n and word frequency TF_n are the corresponding reverse order relationship; the maximum value is sent to determine TR_n; the words rank the same with the same, and select the largest word rank; then, the difference between the two adjacent words is

$$\mathrm{NTIF}_n = \mathrm{TR}_n - \mathrm{TR}_{n+1}. \tag{8}$$

And the expression of the number of words with the same word frequency when the word frequency is $\mathrm{TF}_n = 1$ and 2, which are obtained according to the maximum value method, is

$$\mathrm{NTIF}_n = \frac{N_{\mathrm{diff}}}{\mathrm{TF}_n \cdot \mathrm{TF}_{n+1}}, \quad n = 1, 2. \tag{9}$$

N_{diff} is the total number of different words that appear in the text document. Then, expression (1) yields

$$\mathrm{TR}_{n_n} = \frac{K}{f_n} = \frac{K \cdot L}{\mathrm{TF}_n}, \tag{10}$$

$$\mathrm{TR}_n = \frac{K}{f_{n+1}} = \frac{K \cdot L}{\mathrm{TF}_{n+1}}. \tag{11}$$

You can find that the expressions of (10), (11), and (8) can derive expression (3). Statistical observation of the whole data shows the results of word frequency and word rank multiplication approach N_{diff} when the word frequency equals 2.

$$\mathrm{TR}_n \cdot \mathrm{TF}_n = N_{\mathrm{diff}}, \quad n = 1, 2. \tag{12}$$

Combine N_{diff}'s expressions with (8) for

$$\mathrm{NTIF}_n = \frac{N_{\mathrm{diff}}(\mathrm{TF}_{n+1} - \mathrm{TF}_n)}{\mathrm{TF}_n \cdot \mathrm{TF}_{n+1}} = \frac{N_{\mathrm{diff}}}{\mathrm{TF}_n \cdot \mathrm{TF}_{n+1}}, \quad n = 1, 2. \tag{13}$$

Then, the full expression of NTIF_n obtained from the joint same-frequency words (3) and (9) is as follows:

$$\mathrm{TIF}_n = \begin{cases} \dfrac{K \cdot L}{\mathrm{TF}_n \cdot \mathrm{TF}_{n+1}}, & n > 2, \\[2mm] \dfrac{N_{\mathrm{diff}}}{\mathrm{TF}_n \cdot \mathrm{TF}_{n+1}}, & n = 1, 2. \end{cases} \tag{14}$$

According to the obtained processing method of text data, the word set of different word frequency and the corresponding total number of word frequency were counted. Then, we preprocessed the collected word data and finally obtained the preprocessed data list. Figure 6 presents a text mining flow chart based on the word frequency statistical law.

4. Mining and Analysis Process of Ideological and Political Evaluation of College Students

For the data of the ideological and political evaluation text of college students that has been handled well, the value information in the mining and analysis is mainly the analysis of ideological and political keywords and the analysis of college students' emotional tendency. Since the ideological and political performance of college students can be shown from several aspects, according to the top 10 ideological and political evaluation of college students online, we can see the social concern for the ideological and political performance of universities and also reflect the importance of the society to the ideological and political performance of college students from the side. Then, for the positive and negative evaluation of college students' ideological and politics, we summarize what aspects of the ideological and political contemporary universities are missing and what aspects meet the requirements. Through the comparison of the map, we can intuitively see the comparison of the two-level ratings.

4.1. Keyword Analysis. The analysis of key words is conducted with word cloud map and word frequency map. For the preprocessed evaluation data, the Jieba package can be called out directly after using the word frequency command to complete the word frequency statistics. Then, the relatively high words frequently appear in the whole evaluation library, and then, the statistical results of the word cloud library are used and visualized to draw the relevant word cloud map and word frequency map, as shown in Figure 7.

As can be seen from Figure 7, in the text data collected, among the words "mission, sense of gain, positive,"
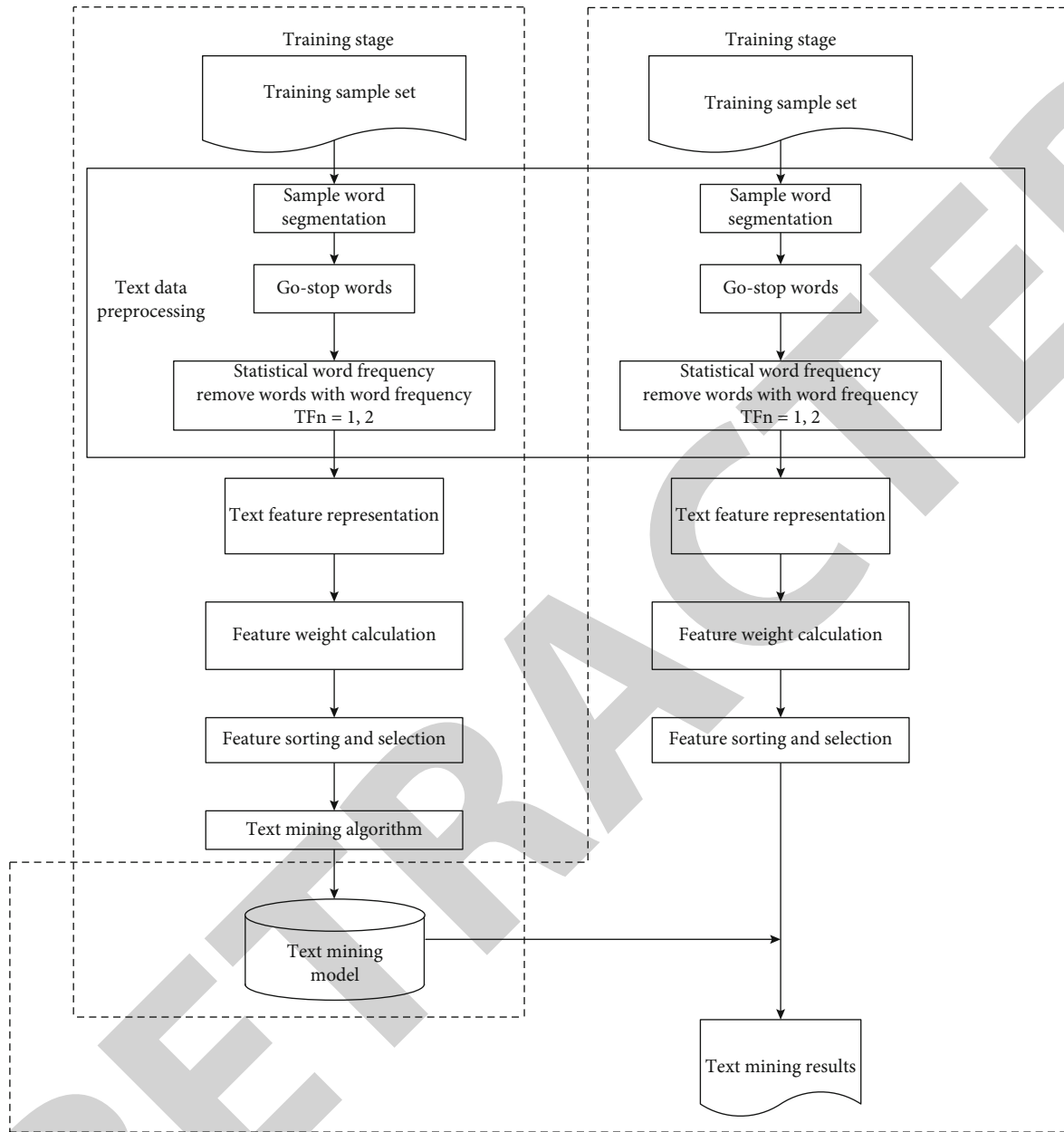
FIGURE 6: Statistical flow chart of word frequency based on text mining.

the most frequently appeared is "positive," appearing more than 300 times. It can be seen that the evaluation of ideological and political college students in the society attaches more importance to whether college students have the ideological and moral qualities that can fulfill the mission of completing the great rejuvenation of the country. This is also one of the keys to the effectiveness of ideological and political education in colleges and universities. Secondly, the most common ones are the "sense of gain" and the students' recognition of ideological and political education in practice and the recognition of ideological and political courses. It shows that the students' sense of gain for ideological and political courses directly affects

the college students' acceptance of ideological and political courses and thus forms their value system, as shown in Figure 8.

As can be seen from Figure 8, the words "mission, feelings, pressure," and so on occupy a relatively large area, so the number of occurrence in the social ideological and political evaluation of universities is relatively high. It can be seen that the identity of college students who attach more importance to the whole country is the key. First of all, we must have the overall situation before we can see their own times.

4.2. Sentiment Analysis. Classified according to text processing, it can be divided into emotion analysis based on product
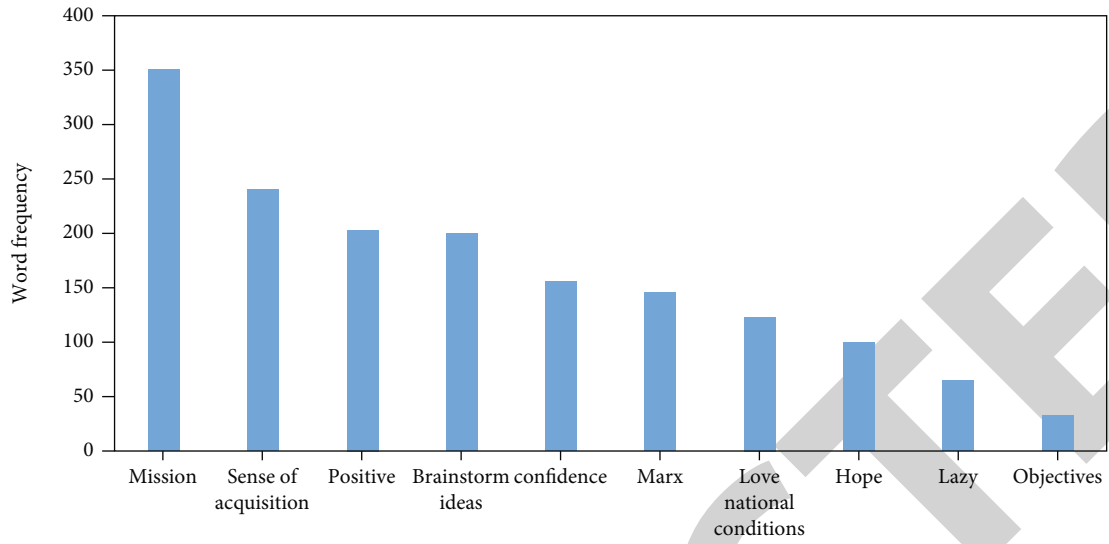
FIGURE 7: Keyword frequency distribution diagram.
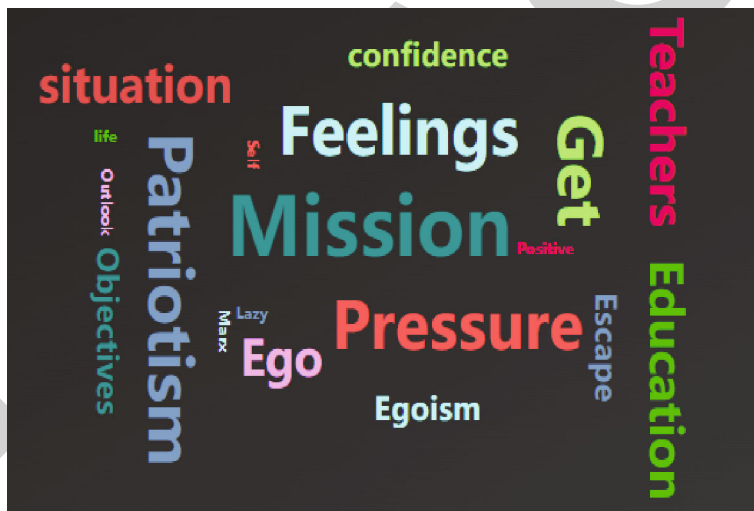
FIGURE 8: Keyword word cloud map.
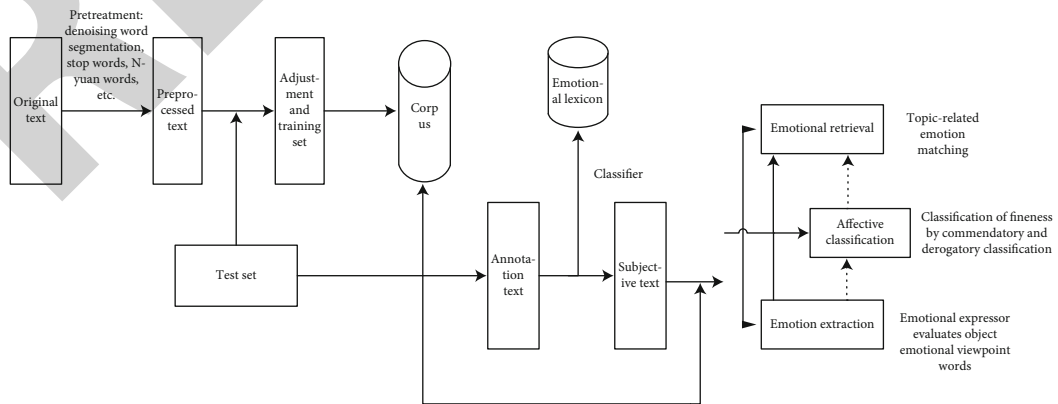
FIGURE 9: Basic flow chart of text emotion analysis
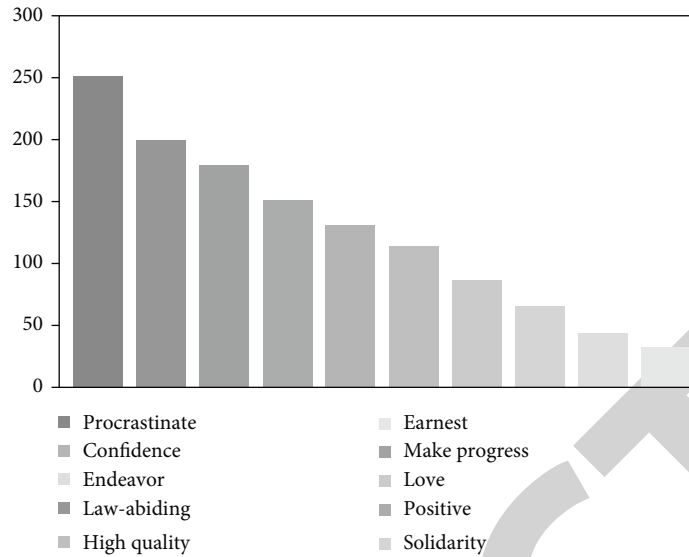
Figure 10: Distribution diagram of the positive evaluation word frequency.

evaluation and emotion analysis based on news evaluation. According to the classification of the task, [20] can also include text emotional analysis, emotional retrieval, and emotional acquisition. The basic process of text emotion analysis is shown in Figure 9, including the whole process of crawling of the original text.

(a) Dictionary construction

The establishment of emotion dictionary is the basic premise and cornerstone of modern emotion classification. At present, it can be divided into four kinds in real use: general emotional noun, degree adverb, negative word, and domain noun. At present, most of the formation of emotional dictionaries in China uses the expansion of existing electronic dictionaries to make emotional dictionaries. On the other hand, English [21], on the basis of artificially establishing seed adjectives, is used to determine the emotional tendency of words, thus evaluating the true views of opinions. Zhu et al. [22] used the repetition of language meaning to obtain the meaning similarity between the word and the basic emotional related word set and deduced the emotional expression of the word.

(b) Construction of the tendency calculation algorithm

Based on the meaning of emotional dictionary feature calculation, it is different from the required practice machine learning method, mainly using the collection of emotional words and grammar library analysis of the special structure and emotional tendency words, using weighted calculation method instead of the traditional human discrimination or only using simple statistical method of emotional classification. Emotional words with different emotional intensity are given different weights and then accumulated according to different weights. Document [23] uses a weighted averag-

ing method (15) calculation, which can help improve the efficiency and accuracy of emotion classification in special fields, such as

$$E = \frac{\sum_{i=1}^{N_p} wp_i + \sum_{j=1}^{N_n} wp_j}{N_p + N_n}. \tag{15}$$

Among these, p and n represent the number of words for both positive and negative emotions. The wp_i is the weight of the number of words indicating the positive emotions, and the wp_j represents the weight of the number of negative emotion words, mainly based on the different emotional intensity given to the words.

(c) Determine the threshold to determine the text orientation

If correct, the weighted calculation is negative, while the zero result has no tendency to be positive or negative. The result evaluation uses the value of accuracy F to summarize the final results in natural language. As for the combination of emotion words and compared with the traditional computer learning classification mode, although it is full of biased classification mode, it is easier to run with the emotion word set after good practice, and the text in the usual field can quickly classify emotion words.

According to the emotional emotion tendency in the emotion analysis model, the ideological and political evaluation of college students is divided into positive evaluation and negative evaluation, and the word frequency statistical map and word cloud map of positive evaluation and negative evaluation are drawn. See results (Figures 10 and 11).

As can be seen from the positive word frequency distribution map, for the ideological and political evaluation, "patriotism, law-abiding" appeared the most times, with
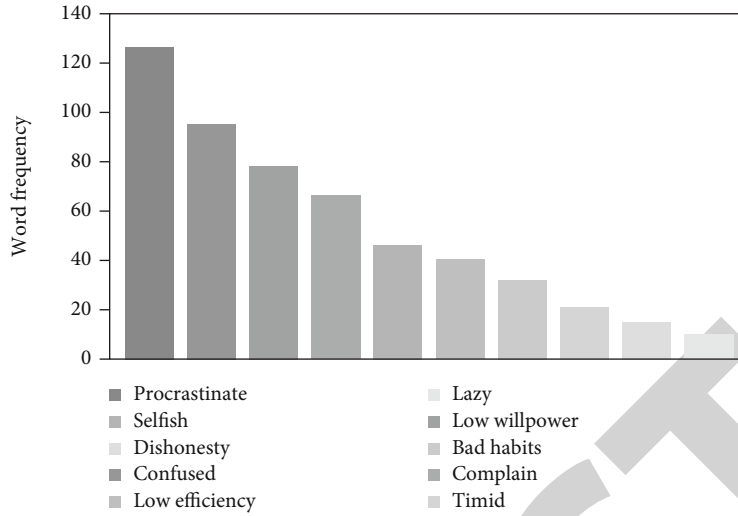
FIGURE 11: Distribution diagram of the negative evaluation word frequency.

TABLE 4: The performance comparison of the SVM classifier before and after the data preprocessing in the ideological and political evaluation topic of the data set.

Special topic of ideological and political evaluation	Traditional SVM model					The SVM model is based on the word frequency statistics rule				
	Accuracy (%)	Precision (%)	Recall (%)	F1 (%)	Time (s)	Accuracy (%)	Recall (%)	Precision (%)	F1 (%)	Time (s)
Acq	87.89	76.36	70.99	73.58	2279	88.63	78.03	72.53	75.18	611
Crude	94.28	50.61	47.98	49.25	2037	94.55	53.09	49.71	51.34	574
Earn	84.65	84.63	75.02	79.54	2285	86.29	86.99	77.04	81.71	637
Grain	92.94	70.49	61.70	65.80	2196	93.38	72.98	63.22	67.75	605
Interest	94.55	42.75	41.26	41.99	1986	94.28	45.59	43.36	44.45	632
Money	93.92	58.12	54.88	56.45	1959	94.15	59.80	56.74	58.23	553
Ship	96.59	39.74	36.05	37.81	1891	96.72	42.68	40.70	41.67	548
Trade	94.68	45.04	40.41	42.60	2025	94.92	47.73	43.15	45.32	571
Macro average	92.44	58.47	53.66	55.96	2082	92.93	60.86	55.81	58.23	591

more than 200. It can be seen that general people believe that the basic moral quality of college students is passed. It can be seen from the negative frequency distribution of negative words that college students have many bad habits in entering and leaving the society, which shows that the process of college students only accepts the ideological course, which is not implemented into the actual life, which is very unfavorable for personal development. Whether it is positive or negative evaluation is based on the evaluation of college students "knowledge, affection, meaning, action" dimension evaluation, from a comprehensive understanding of the ideological and political performance of college students from these four aspects.

4.3. Text Mining Comment Analysis. In order to extract more efficient information about the ideological and political evaluation of college students, two different methods will compare the accuracy, precision rate, recall, and F1 mea-

sures. A large number of articles were selected to verify the efficiency of the two methods.

(a) Data set

This article selects the special topics on ideological and political evaluation and the ideological and political report. Among them, there are 21,578 documents in 135 categories. Documents in eight categories were Acq (1659), crude (405), earn (2775), grain (773, corn and wheat under grain), interest (335), money (502), ship (200), and trade (340). The ideological and political report is divided into four categories: Comp (1162), Rec (1190), Sci (1183), and Talk (975); the experiment is binary in one-to-one categories. The ratio of both the training set to the test set was 7 : 3, as shown in Tables 4 and 5.

In order to compare more clearly, the accuracy, accuracy, recall, and F1 metric of the two models of ideological and political evaluation thematic data set were drawn, respectively, as shown in Figures 12–15.

TABLE 5: The sexual comparison of the classifier before and after the data preprocessing based on the word frequency statistics law on the data ideological and political report.

Ideological and political report	Traditional SVM model					The SVM model is based on the word frequency statistics rule				
	Accuracy (%)	Precision (%)	Recall (%)	F1 (%)	Time (s)	Accuracy (%)	Recall (%)	Precision (%)	F1 (%)	Time (s)
Comp vs. Rec	87.50	89.12	85.44	87.24	3647	88.78	90.88	88.89	88.89	953
Comp vs. Sci	75.31	76.09	73.15	74.59	3418	77.87	78.28	77.43	77.43	892
Comp vs. Talk	96.02	96.79	95.899	96.33	4065	96.49	96.73	96.77	96.77	1067
Rec vs Sci	73.58	76.09	69.99	92.91	3734	76.99	74.12	75.88	75.88	981
Rec vs. Talk	83.27	86.25	82.78	84.48	3849	86.00	85.04	86.78	86.78	1078
Sci vs. Talk	76.14	80.04	75.23	77.56	4276	79.19	77.94	80.42	80.42	1113
Macro average	81.97	84.06	80.41	82.19	3830	84.22	82.90	84.48	84.48	1014
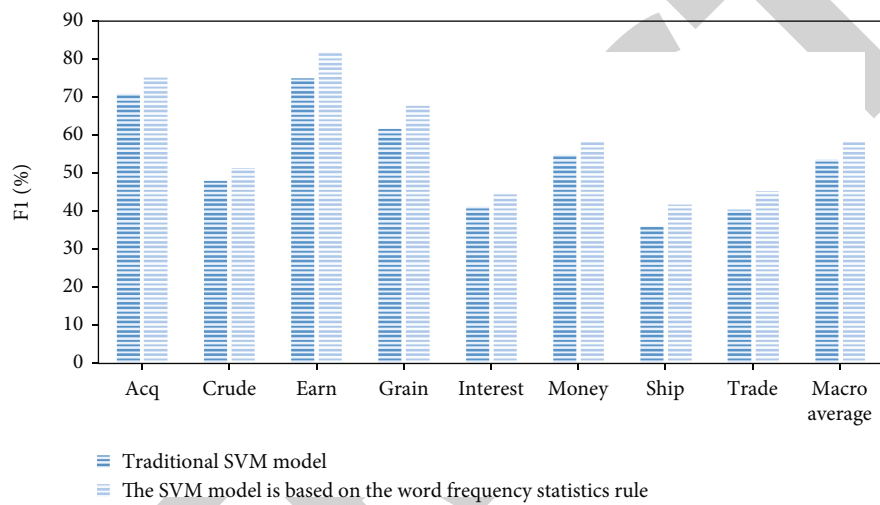
FIGURE 12: Comparison diagram of F1 measures of the traditional SVM and SVM based on word frequency statistics in the ideological and political evaluation topic.
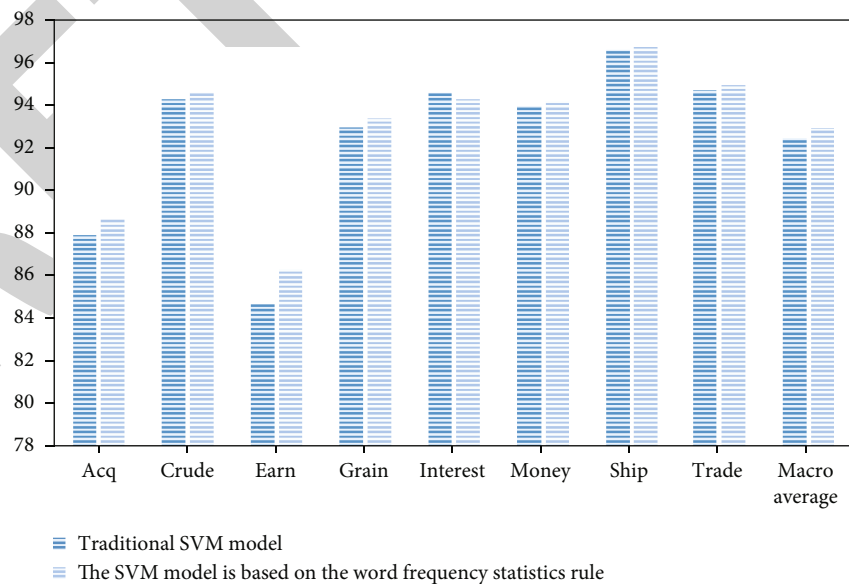
FIGURE 13: Comparison of the traditional SVM and SVM based on word frequency statistics in the ideological and political evaluation topic.
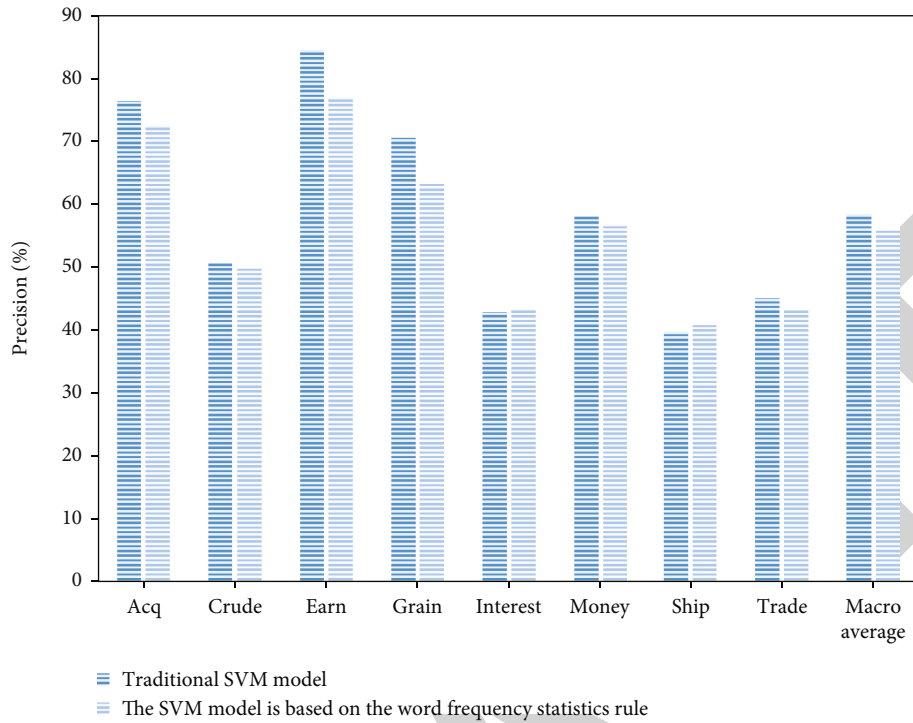
Figure 14: Comparison figure of the traditional SVM and SVM based on word frequency statistics in the ideological and political evaluation topic.
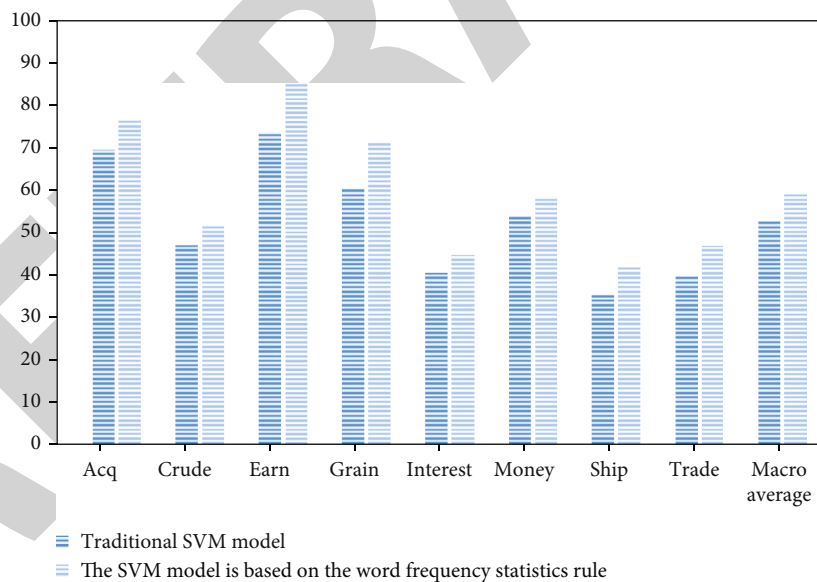
Figure 15: Comparison of the traditional SVM and SVM based on word frequency statistics in the ideological and political evaluation topic.

Through experimental comparison, the traditional preprocessing method cannot solve the problems of the data, so this paper finally adopts an improved text preprocessing method based on word frequency rule statistics and then overcome this problem. It can be seen from the figure that the text data preprocessing method based on the text mining law is higher than the traditional performance, and the running time is shorter. Therefore, the preprocess-

ing method based on text mining will be adopted in the ideological and political evaluation of college students based on word frequency statistics. And because the SVM model based on word frequency statistics denoises low-frequency words during preprocessing, it can greatly reduce the feature dimension under the premise of ensuring the accuracy of text mining, significantly reduce the complexity of space-time, reduce the average running time

by more than 70%, and effectively improve the performance of text mining.

5. Conclusion

According to the results of the online evaluation and analysis on the ideological and political evaluation of college students on Zhihu, the society has both positive and negative ideological and political evaluation of college students, and most of them are rather positive. The positive view gives affirmation to the moral quality of college students, and contemporary college students have a good performance in terms of public moral quality. It shows that students have a high level of their own knowledge-based cognitive value cognition. The overall ideological and political evaluation of college students is divided into four dimensions, namely, knowledge, emotion, meaning, and practice. College students finally face the society, so they should improve the effectiveness of the quality of ideological and political education from the four dimensions of knowledge, affection, meaning, and action. Ideological and political education can not be simply preprocessed, improve the quality of ideological and political education of college students in the new era [24], optimize the ideological and political education team, and accelerate the construction of the education system. In terms of knowledge dimension, it is believed that college students have formed their own unique values in the process of school education, and most people think that it is positively in line with the characteristics of the times, and the way of thinking to deal with problems is still more dogmatic. In the evaluation of the emotional dimension, the contemporary college students are more qualified in the emotional identity, mind emotion, and self-emotion management and adjustment. It is generally believed that 70 percent of college students have a strong sense of family and social responsibility, and a small number of college students have a weak awareness in this respect. Then, there is the evaluation of the meaning dimension. The results show that contemporary college students have a strong legal concept and abide by the discipline. And daily life can make good use of the legal thinking ability to safeguard the rights and interests that are not infringed. Finally, in the above evaluation, college students lack self-regulation and self-development. Although the general moral quality of college students is good, in the face of personal cognition, development is relatively confused. The evaluation shows that 80% of college students' self-regulation ability is not very good, they have not made their own life planning, they are in a confused state after graduation, their behavior habits, behavior ability, and behavior are in the primary stage, their thinking is generally not very mature, and the law of life is also very irregular, which is closely related to the daily development of students in school.

Data Availability

The experimental data used to support the findings of this study are available from the corresponding author upon request.

Conflicts of Interest

The authors declared that they have no conflicts of interest regarding this work.

References

[1] Onjani, "Evaluation "research on the quality evaluation of ideological and political education in colleges and universities in the new era"," *Journal of Tropical Crop*, vol. 42, no. 11, p. 3430, 2021.

[2] H. Tan, "Research on the promotion path of ideological and political theory course in universities in the new era," *Educational Theory and Practice*, vol. 41, no. 33, pp. 36–39, 2021.

[3] X. Lin, P. Wei, and L. Xu, "Research on the precision of the quality evaluation of ideological and political education in colleges and universities under the background of big data," *Journal of Higher Education*, vol. 29, pp. 170–173, 2020.

[4] Z. Lei and J. Bing, "Research on the rational connotation and implementation path of college curriculum ideological and political construction," *Journal of Jilin Provincial Institute of Education*, vol. 37, no. 12, pp. 59–62, 2021.

[5] I. Yu, "Qingfeng. Study on the realization path of ideological and political courses and courses," *Journal of Social Sciences, Jiamusi University*, vol. 39, no. 6, pp. 85–88, 2021.

[6] X. Guanghui, "Research on ideological and political practice path of college wushu education course," in *2021 National Wushu Education and Health Conference and National Traditional Sports into Campus Seminar Summary Compilation (2)*, p. 299, 2021.

[7] M. Xin and X. Guifen, "Review of text-mining techniques," *Journal of Jiangsu University (Natural Science Edition)*, vol. 5, pp. 72–76, 2003.

[8] W. Yan, D. Bin, X. Deng, and J. He, "Electric text mining and classification based on natural language processing technology," *Automation Technology and Application*, vol. 40, no. 10, pp. 60–63, 2021.

[9] Yin, "Experimental design and implementation of text mining," *Information Technology and informatization*, vol. 9, pp. 94–96, 2021.

[10] F. Wang, Z. Rui, and G. Haili, "Design and implementation of a distributed crawler based on the Scrapy framework," *Information Technology*, vol. 3, pp. 96–101, 2019.

[11] Yunxian, Z. Shuliang, L. Yan, G. Lin, Z. Junpeng, and L. Chao, "Text data preprocessing method based on the word frequency statistics law," *Computer Science*, vol. 44, no. 10, pp. 276–282, 2017.

[12] F. Yanru, "Design and implementation of the network crawler system based on Python," *Computer and Information Technology*, vol. 29, no. 6, pp. 47–50, 2021.

[13] C. Wang, Z. Hui, M. Xioliang, and W. Yang, "Review of Weibo sentiment analysis," *Computer Engineering and Science*, vol. 44, no. 1, pp. 165–175, 2022.

[14] R. W. Picard, E. Vyzas, and J. Healey, "Toward machine emotional intelligence: analysis of affective physiological state," *IEEE Trans on Pattern Analysis & Machine Intelligence*, vol. 23, no. 10, pp. 1175–1191, 2001.

[15] C. Yusen, "Based on Python," *Information and Computer (Theory Edition)*, vol. 33, no. 21, pp. 41–44, 2021.

[16] G. K. Zipf, G. Zipf, and G. Zipf, "Book reviews: human behavior and the principle of least effort: an introduction to human

Hindawi

Retraction

Retracted: Analysis of Key Factors of College Students' Ideological and Political Education Based on Complex Network

Journal of Sensors

This article has been retracted by Hindawi following an investigation undertaken by the publisher [1]. This investigation has uncovered evidence of one or more of the following indicators of systematic manipulation of the publication process:

(1) Discrepancies in scope
(2) Discrepancies in the description of the research reported
(3) Discrepancies between the availability of data and the research described
(4) Inappropriate citations
(5) Incoherent, meaningless and/or irrelevant content included in the article
(6) Peer-review manipulation

The presence of these indicators undermines our confidence in the integrity of the article's content and we cannot, therefore, vouch for its reliability. Please note that this notice is intended solely to alert readers that the content of this article is unreliable. We have not investigated whether authors were aware of or involved in the systematic manipulation of the publication process.

Wiley and Hindawi regrets that the usual quality checks did not identify these issues before publication and have since put additional measures in place to safeguard research integrity.

We wish to credit our own Research Integrity and Research Publishing teams and anonymous and named external researchers and research integrity experts for contributing to this investigation.

The corresponding author, as the representative of all authors, has been given the opportunity to register their agreement or disagreement to this retraction. We have kept a record of any response received.

References

[1] W. Lu, D. Huo, and S. Jia, "Analysis of Key Factors of College Students' Ideological and Political Education Based on Complex Network," *Journal of Sensors*, vol. 2022, Article ID 6577878, 10 pages, 2022.

Research Article

Analysis of Key Factors of College Students' Ideological and Political Education Based on Complex Network

WeiPing Lu,[1] DeCai Huo,[2] and Sibo Jia [ID][3]

[1]*Human Resources Department, Yanching Institute of Technology, Langfang, 065201 Hebei Province, China*
[2]*Center of Employment Guidance and School Enterprise Cooperation, Yanching Institute of Technology, Langfang, 065201 Hebei Province, China*
[3]*In the International Business School of Yanching Institute of Technology, Langfang, 065201 Hebei Province, China*

Correspondence should be addressed to Sibo Jia; jsb@yit.edu.cn

Rapid updating and complex network means bringing more development opportunities for the education industry. As for ideological classes and political science at colleges and universities, how to use sophisticated online technology to educate and educate ideological and political classes and improve the formation of ideological and political classes has been a complex theory in the education industry in recent years. Complex network is an abstract representation of complex systems in the real world, with broad research value and application prospects, and has many advantages in complex network research, with interpretability, expression ability, generalization ability, flexibility, etc., and has been used in various network analysis tasks, such as community discovery, link prediction, network representation, and political learning. The second part of this article focuses on (1) the concept of ideological education, (2) the advantages of ideological education, (3) the contradiction of the mode of ideological education, and (4) how to innovate ideological education. The third part proposes the basic characteristics and models of complex networks and proposes the emergence of fractal structures. The fourth part analyzes complex network models in detail and compares the number of points and sides of the real network with the respective irregular networks, indicating that the real world is not fully defined or completely irregular, and that the real network has the nature of a small world and a high-quality cluster. The key factors of complex networks applied propose theoretical and political education and ultimately influence theoretical and political teachers and students in the complex networks examined through empirical questionnaires. He proposes that large universities should be able to use a network environment to promote ideological and political education.

1. Introduction

In this paper, the synchronization characteristics of relative oscillators present an understanding of the effective methods of modules in complex networks. The performance of the algorithm has been tested on known computer-generated and real networks, especially when the module elements are very mixed and other methods are difficult to detect [1]. The purpose of this paper is to apply the theoretical knowledge and empirical development of complex network literature to the background of adaptive systems, to promote the development of supply chain theory; the author hopes to reflect the complex net-

work characteristics of the real supply chain, in order to develop a suitable supply chain network theory; the author hopes to reflect the characteristics of the complex network model with the real supply chain. Design/Methods/Methodologies - the author reviews the complex web literature of multiple disciplines extracted from top scientific journals [2]. As can be seen from the undirected network diagram, these seismic networks are small-function networks without scale, distribution of electrical rule links, high increase factors, and a small average length route. It shows that the network's current methods show the complexity of sewed activity in new ways [3]. According to the document, in complex networks, "rich club pregnancy" means

that high knots are more closely related to shallow knots. The presence of this behavior may reflect interesting and advanced networking features, such as hub failure resiliency. In complex networks, "rich club events" mean that high joints are more closely related than fewer joints [4]. In large, complex networks, the scale-free feature evolves through the process of self-organization, more precisely is the priority dependency. New network nodes will connect to other already well-connected nodes. Movement in the network is efficient because traffic is mainly directed at angles that are too tightly connected and concentrated, so the diameter of the network is small [5]. This article introduces a complex network that describes how organizations in the system interact. The structure of these networks is believed to influence processing. Clustering Factor C, a network structure measure, measures how close nodes are. It has also been suggested that the network structure affects a wide range of memory-related information processes, such as word memory, long-term memory, and short-term memory [6]. This article is essentially done through activities aimed at human development. It is a humanities discipline characterized by typical humanities and is essentially carried out through activities aimed at human development. It is a humanities discipline characterized by typical humanities [7]. The article suggests that environmental civilization openly presents the entire process and aspects of students' theoretical and political education as an important place for the creation of knowledge and talents. To improve the environmental education of students and to promote environmental knowledge, some effective measures need to be taken, fighting for the current situation of environmental education in professional schools [8]. This information tells us that by continuing to improve technology, internet communications have entered the lives of college students. Cyber and political studies of college and university commentary create political and political knowledge on the Internet by illustrating the difficulties the Internet will face. This article discusses different political views and online learning. Therefore, the full use of the program is now a public, socialized, and political orientation, as well as improved academic and political education [9]. The paper concludes that "opposing classrooms" are new concepts and models that can be used to enhance the attractiveness and participation of political education in political and ideological learning. Classrooms centered on "teaching" have become classrooms centered on "learning," the interaction between form and content, and the reform of assessment methods has changed, and the teaching activities of political ideology education have changed; students can turn passive recipients into active researchers, and teaching activities are more interactive [10]. This paper proposes that in a rapidly changing society, the purpose of ideological and political education shows a dynamic development, and the reversal conflict between the "educated" and the "educated" gradually intensifies. Putting aside the thinking of social one-way influence, social interconfiguration theory places individuals and groups, socialized subjects, and objects at the level of

equality and mutual structure, and transforms reversible conflicts into positive and harmonious changes, which has far-reaching significance for the innovation of ideological and political education subjects [11]. The author points out that while interpreting educational values, there is a trend of applying rationalist and functionalist theories at the same time, and the research model of moral education is developing in the direction of positivism. The author believes that in a multicultural environment, emphasizing the cultivation of moral cognitive ability belongs to the "third way" in Western moral education theory. So the study of significance and progress became very important [12]. This paper is not optimistic about the network environment in colleges and universities. To improve it, we will adhere to the principles of integrity, positivity, positivity, and participation, change the old concept of ideological and political education. In colleges and universities, students are encouraged to make independent choices and decisions, create ideological and political educational websites and networks, create teaching models with Internet federations, develop relevant programs, manage the network environment, ideological, and political educational groups, and improve the overall quality of college students [13]. This article emphasizes that under new circumstances, ideological and political teachers should fully understand and fully utilize the positive opportunities created by the new media, abandon their ideas and find new ways and ways to do ideological and political work in the sector of new media, and increase the efficiency of ideological and political education [14]. The article suggests that the introduction of populist thought into the theoretical and political education of leading colleges and universities is crucial for promoting and improving theoretical and political education in secondary schools and universities and for the growth and development of students. The document addresses the main ideas of ideological and political education to the public in colleges and universities and recognizes that people's objective sense of ideological and political education in schools and universities should include caring for people, developing people, and serving the people [15].

2. Content on Intellectual and Political Education

2.1. The Concept of Intellectual and Political Education.
The concept of self-esteem for students accepts the concept of ideology as an important part of education, explores the right perspective on global life and values, and explains your mission to make modernization a reality. Teachers should create good conditions in using all factors to create a healthy development environment for college students student height. Education of ideological and political standards in a rich and diverse spiritual and cultural life, promote awareness and social responsibility, adhere to the norms of fair expression in society, and properly demonstrate and apply the correct concept of China's great national spirit in teaching about collective and socialist love.

2.2. Advantages of Ideological and Political Education. In the Internet era, information content presents diversified transmission characteristics, and along with various types of information resources, foreign culture and local culture will also form a certain collision; this would make it difficult to teach traditional and political ideas. After students are exposed to the network environment, they are surrounded by all kinds of complex and comprehensive information, and the negative impact of some content, if it penetrates into the depths of students' ideological consciousness, will inevitably affect their learning confidence and values. For example, foreign hedonism, and egoism, the impact of cultural origin will make students have a wrong perception of the ideological level. This requires in the development of intelligence, politics, environmental education, student reading, education development laws, etc., creating a comprehensive and effective curriculum that ensures all forms of pregnancy education based on the impact of expected education and politics.

2.3. Correctly Understand Ideological and Political Education. First, for the traditional concept of education, teachers should learn from a position of strength in them, build an ideological and political education system, and focus on developing unique talents, transforming and political education. Education in talent training plan. Second, colleges and universities need to allocate independent class hours and credits to ensure their effectiveness, help college students form excellent moral character, make them a talent who abides by professional ethics, and lay a solid foundation for the improvement of their comprehensive ability. Third, in the process of educating people, people should ensure the close connection, and after studying Marx's practical teaching, strengthen students' political consciousness and enable them to shoulder the glorious mission of building the country. Teachers should lead practical activities with socialist core values and devote themselves to cultivating college students with advanced ideas and firm political stances. In accordance with China's basic national conditions and international political situation, we should scientifically innovate the teaching mode of ideological and political practice. It accurately locates the value and goal of talent training and optimizes the practice link along the right direction and path. The education classroom should become an important place for students to absorb advanced concepts and to conduct in-depth discussions and practices on relevant cultures and theories. Teachers should handle the relationship between various teaching elements, and the subject and object should participate in practical teaching activities with correct role positioning, emphasis on progressive nature and focus on modernizing the ideological and political classes. Truly nurture talent with the spirit and ideas of today's pioneers.

2.4. Contradictions in the Ideological and Political Education Model. At the present time in developing teaching objectives, using teaching methods and methods, college students pass exams, and a current curriculum is more developed by colleges and universities in terms of student evaluation. In addition, teachers give assessment standards to students, which have nothing to do with teaching and practice; students themselves have learning goals, ignoring the importance of conceptual curriculum, the effect of open thinking. Political education is also down sharply. In real education, it is not enough for everyone to know ideology and moral education, lack of learning objectives, and empty teaching makes students' ideological and political knowledge excellent and instructive. Conflict in the current curriculum.

2.5. Innovative Ideological and Political Education Methods. Traditional academic explains students' thoughts and behaviors through data analysis, and in the world of big data, grades are provided by data. Research and research are carried out to ensure the accuracy and effectiveness of student analysis. Universities are necessary to find out what kind of ideological need more according to big data and adopt educational methods that are more in line with students' favorites, such as pictures, videos, or other websites, and push them to students. In addition, universities can also use big data to predict education, track students' thoughts and behaviors in real time through data analysis results, and predict their future trends, for example, teachers can analyze students' thought changes through high-click rate hot news on the WeChat platform, and integrate them into the teaching content, more targeted adjustment of lesson preparation content, change the way of education, when chatting with students, it is found that students have great interest in the current Syrian war, but also have a lot of doubts. Therefore, teachers can develop a teaching courseware based on the Syrian war, through which students understand that the strength of the country can directly determine the future of the country and the damage of the war to the country and the family. Through big data to collect the latest trends in the war and the views of people from all walks of life on the Syrian war, and combined with the classroom content to tell the teachers' personal views, students can more deeply feel the happiness of living in China, a peaceful country, and the sense of responsibility of a strong teenager and a strong China. It is improved by using great information to reform ideological systems and by moving away from traditional educational models through self-awareness. The rapid development of the Chinese economy has raised the standard of living and increased the importance of society for education. And the era of the big data has entered the global economy. The gradual growth of science and technology has led to innovation. In recent years, the approach to talent development in colleges and universities has provided opportunities for theoretical and political education for universities and colleges, as well as facing many challenges.

3. Fractal Characteristics of Complex Networks

3.1. Fundamental Properties of Complex Networks. To study complex network G, (1) Complex structure: The core feature of a complex network is that the structure is complex, and any network component is randomly intercepted, and the

number of nodes is huge. (2) Network evolution: It is a study of professional data that actually have evolutionary functions. (3) Node diversity: In the complex structure of a complex network, each node can represent any kind of thing. Complex topological network features, such as the humble medium cluster multiplier and network diameter, can act as feature surveyors. The mapping relationship between the exhaustion vector and the network is bidirectional complex and inverse, and if the complex network G is transformed T, a new function vector can be obtained $\vec{\mu}_T$. You can do this by studying the degree of change in the function vector $\Delta\vec{\mu} = \vec{\mu} - \overrightarrow{\mu_T}$ to dive into complex networks. In a directed network, the number of distances directly associated with the group is defined in a balanced instrument, in the middle group provided for the sum of all things in the network, which is clearly expressed as (k).

$$k_i = \sum_{j=1}^{n} a_{ij},$$
$$<K> = \frac{1}{N}\sum_{i=1}^{N} k_i = \frac{1}{N}\sum_{i,j=1}^{N} a_{ij}. \quad (1)$$

If the difference between class I and level J is the shortest form of two sets of connections, and the same communication length is described as two hundred lengths, plus the road is the same as two hundred different areas, which can be sued the average length of the v.

$$L = \frac{1}{1/2N(N-1)}\sum_{i \geq j} d_{ij}. \quad (2)$$

The network diameter is the maximum distance between each network node between two network nodes, or ·

$$D = \max_{i,j} d_{ij}. \quad (3)$$

A degree k for the definition of clustering coefficient C of node i

$$C_i = \frac{2E_i}{k_i(k_i\text{-}1)}. \quad (4)$$

There into $E_i = 1/2\sum_{j,k} a_{ij}a_{jk}a_{ki}$. Connect to k_i nodes in existing lands or neighbor pairs.

Degree distribution of unconventional networks Pk, defined as a very randomly selected probability of a degree of network of Pk. The most common and important probability distribution is the normal distribution, and the common hypergeometric distribution, binomial distribution, and Poisson distribution can be regarded as discrete forms of the normal distribution under certain conditions. These distributions are usually symmetrical by methods, such as the length of a person. The distribution of personal wealth has a long tail, and this distribution is called a long-tail distribution. Unlike the normal distribution, the long-tailed distribution does not have a certain degree of characteristics,

so it is called a rowless distribution. In a mathematical sense, the curtain rate distribution is the only long-tail distribution without scale features, i.e.,

$$P(k) \sim k^{-\gamma}. \quad (5)$$

There into $\gamma>0$ is the curtain index, usually taken between 2 and 3. To handle noise in phase distributions, plotting a cumulative scale distribution is a common smoothing method, i.e.,

$$p_k = \sum_{k'=k}^{\infty} P\left(k'\right). \quad (6)$$

If the network level is the distribution of the screen rate, the cumulative distribution of the western digital level roughly corresponds to the distribution of the screen rate of the screen indicator.

3.2. Basic Model of Complex Networks

3.2.1. Random Graph.
The ER random graph model is a W option P connection between n isolated nodes. At the time, the random graph has the following appearance or phase transition attribute: whether almost every irregular graph has any attribute (such as a connection) for every common probability, or almost every irregular graph has this attribute.

The average degree of the ER random plot is $<k> = p(N\text{-}1)$. The average path length is sufficient $L_{ER}\alpha \propto (\ln N)/\ln <K>$. It has a smaller global feature, but grouping is a coefficient. This means that the random ER chart has no clustering attribute. The approximate random distribution of the ER planning phase is approximately the Poisson distribution:

$$P(k) = (n,k)p^k(1-p)^{N-K} \approx \frac{<k>^k e^{-<k>}}{k!}. \quad (7)$$

3.2.2. Network Model.
Complex networks provide a small, global WS model that establishes the probability that E randomization will reconnect to each edge of the nearest neighbor network. Obviously, depending on a fully regulated network, it can be done by adjusting the c value from fully accepted small-world model WS is

$$C_i = \frac{2E_i}{k_{i(k_i-1)}}. \quad (8)$$

The WS is a unified or exponential network; the small-world model was first demonstrated experimentally by Stancy Milgram in the 1960s as a sociological problem, and, i.e., it is possible to pass messages from one person to another in society through the transmission of an average of 6 people and to explain the structure of the display rate distribution mechanism, the scaleless BA model takes into account two important network constraints: network range and preferred communication. Ba's mismatch model

structure algorithm is: whenever a new node enters the M node network, it is linked to an M node and connected to a connected probability node category, after step T. The edge of the MT BA node is generated by the scaleless BA model, its average path length. The average path length L is another important parameter of the network. For most real-world networks, regardless of size, the average path length is generally small.

$$L \propto \frac{\log N}{\log \log N}. \tag{9}$$

Illustrate that the network model is also small world. Its clustering coefficient is

$$C = \frac{m^2(m+1)^2}{4(m\text{-}1)} \left[\ln \left(\frac{m+1}{m} \right) - \frac{1}{m+1} \right] \frac{[\ln(t)]^2}{t}. \tag{10}$$

The average aggregation coefficient in this article is the same as that of the BA network model, so the number of network nodes m can be used as the abscissa and the network scale can be used as the ordnance.

The degree distribution of the BA network model can be obtained by the principal equation method. The BA network model is the BA network evolution model first proposed by Barabasi and Albert.

$$P(\text{k}) \frac{2m(m+1)}{k(k+1)(k+2)} \propto 2m^2 k^{-3}. \tag{11}$$

3.3. Fractal Structure of Complex Networks. In fact, complex systems have many freckled structures and complex network learning, where complex systems also have worrying abstract features? At first, people were skeptical of the problem, because the most common symptom of fragmented objects is self-probability at the magnitude of change, and this metaphor requires the realization of an energy-rights relationship. However, complex networks often have a small global dimension, i.e., network quickly connects to the diameter of work, rather than the expected power-law relationship. Why is the power-law relation so important in the same problem of separate shapes? Academician Zhang, a famous Chinese scientist, elaborated on this: "The growth process and emergence of its own uniform structure can be concentrated in the simple embodiment of the power law, which is an important state of self-development, under its domination, the system can maintain a smooth evolution and development, the level of its own structure is uniform, and the fractal dimension or relative index is the evaluation criterion of the system function."Until 2005, Song et al. extended the rearranging group analysis method and the box coverage method in fractal theory to the study of complex networks, and found that a large number of real networks have self-similar structures on all long indicators, indicating fractal characteristics, thus eliminating doubts about this theory. The purpose of the reconstructed group analysis method is to change the observation scale and obtain quantitative changes in an individual. For example, suppose that the purpose of the reconstructive swarm analysis method is to change the observation scale to obtain a value of p, expand the observation scale to twice the original, and once again measure the value of the physical quantity to h, using the appropriate scale change2 f such that p and h have the following conversion relationship:

$$p' = f(h). \tag{12}$$

f subscript 2 indicates a tripling of the scale of observations, and if the proportion of observations is doubled again, the relationship is as follows:

$$p'' = f\left(p'\right) = f_2 \cdot f_2(h) = f_4(h). \tag{13}$$

As can be seen in the definition of the analytical method of the recombinant group above, this is closely related to the decentralized image. Fractals have the characteristics of "no change after scale changes," and it can be said that shapes that can still retain their original state after group reorganization are fractals. Song et al. generalized the method of box superposition in fractal geometry into complex networks, which included the process of reformulating the network. The specific implementation step is: the total length of the given box is denoted as L_B. calling it all sets of boxes in this group. The distance between any two nodes in this series collection is less than L_B. Each box is then treated as a new node (if there is at least one end between nodes in different boxes, there is a connection edge between the new nodes), creating a new network that reuses the box length on this new network L_B. The box covers the network, repeating the above process until it becomes a single network node. After in-depth derivation and empirical analysis of some current complex networks, Song came to four important conclusions: the minimum required N_B With box size L_B Power-law relationship:

$$N_B \approx L_B^{-d_B}. \tag{14}$$

The power of the network degree distribution means that during the reorganization process, the allocation capacity of the network class will remain unchanged. Remember the degree of the node, that is, k is the degree of the network node after rearranging, and there are:

$$p(k) \approx k^{-\gamma} \longrightarrow p\left(k'\right) \approx \left(k'\right)^{\gamma}. \tag{15}$$

The degree k of the box (new node) after reordering can be met with the maximum contained in the box without reordering.

$$k' \sim S(L_B)k. \tag{16}$$

There into $S(L_B)$ with the size of the box L_B satisfies the meditative relationship.

$$S(L_B) \approx L_B{}^{-d_k}. \tag{17}$$

There into d_k called the box index.

Box index , power exponent, and kernel dimension of the network degree distribution d_k satisfy

$$\gamma = 1 + \frac{d_B}{d_k}. \tag{18}$$

These conclusions indicate that complex networks have self-similar structures and fractal features. Exposing the fractal features of complex networks once again gives people insight into the beauty of complex network searches, while also giving people a new perspective to better understand and understand the topological characteristics of networks. In fractal geometry, fractals are generally considered to be indistinguishable from autographic similarity. In fractal geometry, fractals are generally considered to be no different from automatic similarity. However, fractal and autosimilar in complex networks are two different concepts, where autosimilarity refers to the scale invariance of the reconstructed network, and fractal characteristics mean that the size of the box is power law in the smallest number of boxes required to cover the entire network. Gallos et al. studied the autosimilarity of complex networks and found that even complex networks without fractal features may exhibit self-similarity properties after reformulation.

3.4. Emergent Research on Fractal Structures of Complex Networks. Since there are many truly complex networks, the self has similarities and fractals. So how did fractal structures come about? What is the relationship between fractal structures and small-world phenomena, such as small-world events and scaleless properties? Scientists are interested in these questions. First of all, the strong isolation of network nodes led to the emergence of fractal structures. According to the proposal of the Dynamic Growth Model (DGM), the dynamic growth process of DGM can be seen as a reversal of restructuring. The model k creates fractal and nonfractal networks, the original node of the query node with the degree of & at the size scale of i-time, and the new node of mib (black node) added at $t + 1$ moment and connected to the initial node. It can be calculated that the mathematical framework of DGM is as follows:

$$N(t) = nN(t - 1), \tag{19}$$

$$\tilde{k}(t) = s\tilde{k}(t - 1), \tag{20}$$

$$L(t) + L_0 = a(L(t - 1) + L_0), \tag{21}$$

there into $N(t)$ of nodes in the network representing t-time, $k(\mathrm{t})$ represents of a node at t-time, and Z represents the diameter of the i-time network, which can be recorded as

the initial network diameter. The value of n has nothing to do with e, and $n = 2m + 1$ is reasonably deduced from the iterative process.

4. Complex Networks Are Key Factors in the Application of Ideological and Political Education

4.1. Classification and Model of Complex Networks

4.1.1. Small-World Network Model. Experimentally demonstrated most of the real networks on the world have the shortest path of the small-world network, and the focus coefficient is relatively large, as shown in Table 1. However, when the rule network has focus, the average path is relatively large. So the small-world network has the nature of a small world, and the aggregation coefficient is very small. In this paper, a preferential small-world network model is studied, based on which the relationship between the synchronization ability of the network and the various geometric features in it (such as the cluster coefficient, the degree distribution, and the median number) is studied in detail.

The subscripts calculated in the network model are arbitrary, and the number of points and edges of the actual network can be compared to this random network to see real work has high cluster coefficient properties. Visible and stochastic networks do not accurately characterize the actual network and show that the.in the years of important breakthroughs in complex network research, proposed a network model that is both small world and high aggregation, randomly configuring network shortcut networks between conventional networks and random networks, and connecting each edge of the rule network to new nodes large cluster coefficients, both the rule network and the random network. In each particular case, a rule network and a random network are special cases of networking.

4.1.2. Scaleless Network. While small-world models may represent small world and high aggregation in the real world, theoretical analysis suggests that a degree of nodes is still exponential. Empirical results show that the degree distribution described by power-rate distribution for most large real-world networks can be relatively accurate. This is shown in Table 2.

The subtext and the ratio of external distribution power (in) degrees show that most networks have capital in the distribution of rank. It represents the average path length calculated from subscripts and real networks, stochastic network models, and network models, respectively. The power-rate distribution does not have the peak of the exponential distribution, most nodes have only a few connections, there is no feature scale in the random network, and it can be said that this degree of distribution for the network has the power rate of the network characteristics. Explaining the network mechanism, Magic and got the network model, claiming the first are constantly connected, and the second means that new nodes enter, and it is best to choose nodes of degrees in the connect. In addition to determining the sample algorithm and the

TABLE 1: Actual network small-word phenomenon.

Network	Size	<k>	L	L_{rand}	C	C_{rand}
https://www.sitelevel/	153,127	35.21	3.1	3.35	0.1087	0.00023
Internet, domain level	3,015-6,209	3.52-4.11	3.7-3.76	6.18-6.3	0.18-0.3	0.001
Movieactors	225,226	61	3.65	2.99	0.79	0.00027
MEDLINE, co-authorship	1,520,251	18.1	4.6	4.91	0.066	0.00005
Math.co-authorship	70,975	3.9	9.5	8.2	0.59	0.000054
E. coli, reaction graph	315	28.3	2.62	1.98	0.59	0.09
SilWoodParkfoodweb	154	4.75	3.4	3.23	0.15	0.03
Workds, synonyms	22,311	13.48	4.5	3.84	0.7	0.0006
Powergrid	4,941	2.67	18.7	12.4	0.08	0.005
C. elegans	282	14	2.65	2.25	0.28	0.05

TABLE 2: Scale-free of the actual network.

Network	Size	<k>	γ_{out}	γ_{in}	L_{real}	L_{rand}	L_{pow}
WWW, site	325,729	5	2.45	2.1	11.2	8.32	4.77
Internet, router	150,000	3	2.4	2.4	11	12.8	7.47
Movieactors	212,250	29	2.3	2.3	4.54	3.65	4.01
SPIRES, co-authors	56,627	173	1.2	1.2	4	2.12	1.95
Math.co-authors	70,975	120	2.5	2.5	9.5	8.2	6.53
E. coli, metabolic	778	7	2.2	3.4	3.2	5.1	1.5
S. cerev, protein	1870	2.39	2.4	2.4	1.2	3.2	2.89
Citation	783,339	9	3.5	6	2.3	1.7	4.4
Phone call	111	3	1.2	2.1	2.1	5.2	2.1
Word, co-occurrence	460,902	70	2.7	2.7	3.0	2.1	5.3

simulation analysis, they obtained the analytical solution using the mean field strength method in statistical physics, for which the results showed that after a sufficiently long evolutionary period, the volume distribution of the network no longer changed over time. The degree distribution is stable to an exponential power-law distribution.

4.2. Students Hope that Network Resources Will Be Used in the Teaching of Ideology and Politics.
From Figures 1 and 2, it can be seen that students have high expectations for the use of network resources in political classroom teaching, and even indicate that the use of network resources to teach will increase their preference for the course. Therefore, teachers of science point of interest of students and introduce the Internet into the classroom to cultivate the core literacy of ideological and political science.

4.2.1. Ideological and Political Teachers Have a High Degree of Attention to the Internet.
Teachers in science and thought classes pay more attention to opinion than students, so they focus on the political elements of public events the most. What this shows is that teachers in science and political classes are generally somewhat sensitive to political consciousness.

4.2.2. Ideological and Political Teachers and Students Recognize the Value and Impact of Networking.
According to Table 3, science generally believes that online public opinion will greatly affect students' ideological concepts, because it has become an important task to educate students on public opinion in the teaching of political science. According to the figure, 60% of teachers believe that the teachers of the high school political science class before the network public opinion have realized that the use of network public opinion resources in classroom teaching is not only important but also of great value.

4.2.3. Ideological and Political Educator Are Less Willing to Resort to Complex Networks.
Educators in school not only undertake of inheriting the fine moral character of the Chinese nation and the moral quality of the new era. At present, the network + technology of school widely used, many ideological political workers in colleges and universities are affected by their own quality level and are unwilling to deeply use the Internet relevant education and teaching work, which also affects the overall work. Through the investigation of the understanding and application of Internet technology by science class, as shown in Table 4.

The results of Table 4 show 28% of those who "know, often use," 60% of those who "understand, but do not often use," 10% of those who "do not understand," and 2% who do not understand at all. Although many teachers have solid professional knowledge of master Internet-related operation technology, they are reluctant teaching complex networks. In the face of emerging problems, colleges and universities will also actively introduce relevant talents to make up for the vacancies work and will also actively organize politicians who are already on the job to receive training activities on Internet knowledge.

4.2.4. The Entertainment and Fragmentation of Complex Networks Have a Great Impact on the Ideological and Political Education of Colleges and Universities.
The content of ideological and political education in colleges and universities itself is a complete knowledge framework, there is an inevitable. Carried out based on the Internet shows the characteristics of fragmentation, which will split the complete
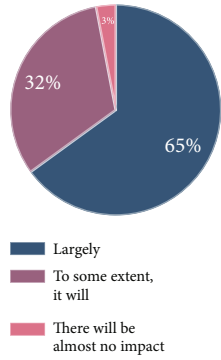
Figure 1: Whether network resources affect students' liking for ideological and political education.
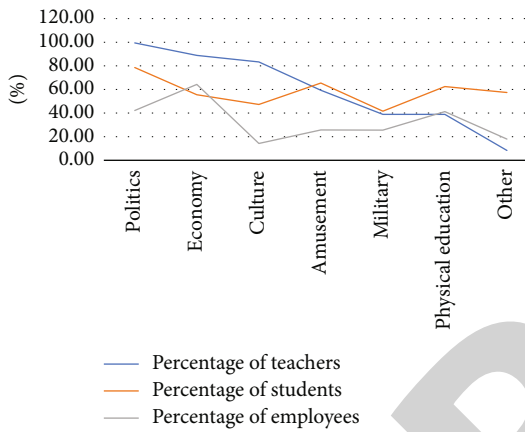

Figure 2: People's attention to ideological and political education.

Table 3: Teachers and students feel the influence of network politics.

The influence of the Internet on ideological politics	The impact is very large	The impact is generally large	Almost no impact
Number of students	50	45	5
Percentage	50%	45%	5%
Number of teachers	60	25	15
Percentage	60%	25%	15%

Table 4: Survey of teachers' understanding and application of network technology.

Whether to borrow the network	Number	Proportion
Understand, use often	70	28%
Learned, but not used often	150	60%
Do not understand, rarely use	25	10%
Do not understand, do not use	5	2%

knowledge system, or let students re-learn some key knowledge, which will also have some adverse effects on the development of students. Table 5 is a survey of the impact of that on content, and the survey 78.2% of people believe that has

Table 5: Degree of influence of network technology on ideological and political education.

The degree of influence of network technology on ideological and political education	Number	Proportion
Cripple	860	78.20%
Intensifier	140	12.70%
I do not know	100	9.10%

weakened the impact of ideological and political education, and 12.7% of people believe that Internet + technology has enhanced ideological and political education and has a great impact.

4.2.5. The Degree of Influence of Online Ideological and Political Education. Because of limited time available to complete the survey online, we compiled a total of 33 questions. Of these, 27 were about choice, respondents' ideological values, and ideal attitudes. There are 6 selection questions, mainly related to students' work in networking and political ideology education and outcome evaluation; The setting question is closely related to the topic of the article, which provides an appropriate basis for the content of this chapter. As shown in Table 6, of the 1145 students, 52.22% were male and 47.78% were female, and the male and female samples were relatively moderate in terms of gender; in terms of grade distribution, 21% in freshman year. This figure is also relatively average. Students rely heavily on the Internet during their daily internet access, and the survey surveyed 1,145 students with varying degrees of Internet access. For the time spent on the Internet every day, the proportion of people who spend 0-2 hours is 1.59%, the proportion of people who spend 2-4 hours is 12.47%, the proportion of people who spend 4-8 hours is 29.88%, and the proportion of people who spend more than 8 hours is actually 52.47% of the total population. It can be seen in Table 6 that the current Internet world has a huge attraction to students, and there is also a huge temptation on the Internet, and the inability to control their behavior and the lack of ability to resist temptation are also important factors that cause students have time on the Internet every day, which shows that it is of great significance to use effective online.

4.3. Data Analysis on Students' Ideological and Political Education Teaching Objectives. In the first part, students know little about the purpose of the lesson before class. As Figure 3 shows, during your learning process, the system asks you, "Do you have a clear understanding of the learning objectives of this lesson before each lesson begins?" At the time, 155 of the 565 respondents said they regularly understood the academic goals of each lesson, 27.43% said they sometimes understood the teaching goals of each lesson clearly, and 50.97% said they never knew the educational goals of each lesson. "Can you clearly understand the attention and difficulties of any political education?" Of the 565 people who often clearly identified teaching problems, 104

TABLE 6: Degree of influence of network ideology and politics on students.

Variable content	Category	Number	Percentage
Gender	Man	598	52.22%
	Woman	547	47.78%
Age	Freshman	247	21.60%
	Sophomore	235	20.49%
	Junior	238	20.74%
	Senior	195	17.04%
	Graduate student	230	20.12%
The length of time spent online each day	0-2 hours	59	5.19%
	2-4 hours	143	12.47%
	4-8 hours	342	29.88%
	More than 8 hours	601	52.47%
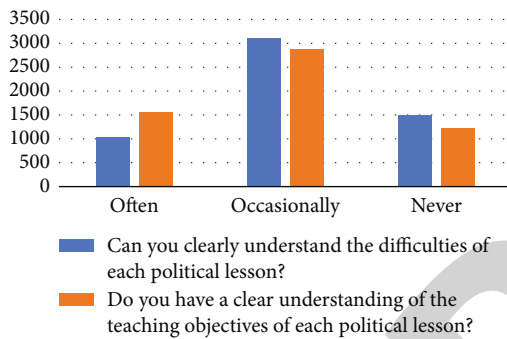
FIGURE 3: Whether students are clear about the teaching objectives and difficulties of this lesson before class.
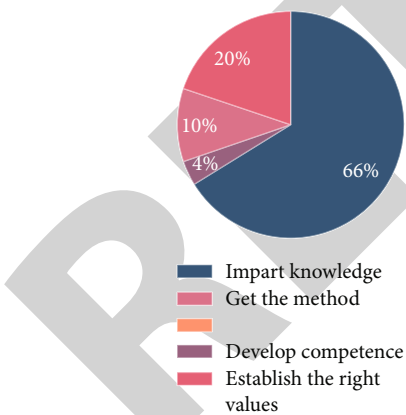
FIGURE 4: Students' views on the purpose of teaching by teachers.

asked. 18.41%, 311% said that people can clearly identify problems in teaching from time to time, which is 55.04%. 150 people never knew the teaching difficulties, accounting for 26.55%.

This experiment is a questionnaire survey of the teaching what goals do you pay more attention to in the three-dimensional goal? At the time of the survey, 36 of the 44 teachers surveyed said that it was more important to achiev-

ing their knowledge goals, accounting for 81.82%. As shown in Figure 4, the question in this survey is: Why are your political teachers more important in their goals? Of the 565 people surveyed, 374 said that teachers paid more attention to classroom knowledge transfer, accounting for 66.19%, 20 said teachers paid more attention to training ability, accounting for 3.54%, and 59 said that teachers paid more attention to teaching teachers, accounting for 10.44%. Teachers are more likely to help create the right values in teaching, accounting for 19.82%. For most teachers in political science training courses, the data show that bachelor's degrees place great emphasis on imparting knowledge to students in teaching, and a small number of teachers move away from educational philosophies and begin to focus on fitness goals, targeted abilities of procedures and methods, and an understanding of the value of effective behavior.

As shown in Figures 4 and 5, the survey question is "Can we better understand the basic principles of Marxism, the course of Marxism, the course of Marxism, and the theoretical achievements of political science?" At that time, 230 of the 565 respondents said that they had an in-depth understanding of related knowledge accounted for 40.71%, 318 respondents said that they had a basic understanding of related knowledge accounted for 56.28%, 15 people said that they did not know much about knowledge accounted for 2.65%, and there was almost no understanding of related knowledge. So from the data, most students have an understanding of politics.

5. Conclusion

In network technology, the number of people using complex network technology is expanding, of which young students occupy the main position, and young students are the objects of that technology + era. However, there is a contradiction between the high demand for college students to seek self-worth recognition and growth and development in complex networks and the insufficient supply of students. The construction of online carriers lacks the tracking and application of new technologies, the integration between different platforms is not enough, and the interactivity and user

Hindawi

Retraction

Retracted: The Influence of Multisensor Fusion Machine Learning on the Controllable Fabrication of MOF (UIO-66)/ZrAl Ceramic Composite Membranes

Journal of Sensors

This article has been retracted by Hindawi following an investigation undertaken by the publisher [1]. This investigation has uncovered evidence of one or more of the following indicators of systematic manipulation of the publication process:

(1) Discrepancies in scope

(2) Discrepancies in the description of the research reported

(3) Discrepancies between the availability of data and the research described

(4) Inappropriate citations

(5) Incoherent, meaningless and/or irrelevant content included in the article

(6) Manipulated or compromised peer review

The presence of these indicators undermines our confidence in the integrity of the article's content and we cannot, therefore, vouch for its reliability. Please note that this notice is intended solely to alert readers that the content of this article is unreliable. We have not investigated whether authors were aware of or involved in the systematic manipulation of the publication process.

Wiley and Hindawi regrets that the usual quality checks did not identify these issues before publication and have since put additional measures in place to safeguard research integrity.

We wish to credit our own Research Integrity and Research Publishing teams and anonymous and named external researchers and research integrity experts for contributing to this investigation.

The corresponding author, as the representative of all authors, has been given the opportunity to register their agreement or disagreement to this retraction. We have kept a record of any response received.

References

[1] X. Xu, X. Yang, S. Shao, C. Zhu, and X. Xu, "The Influence of Multisensor Fusion Machine Learning on the Controllable Fabrication of MOF (UIO-66)/ZrAl Ceramic Composite Membranes," *Journal of Sensors*, vol. 2022, Article ID 3039064, 9 pages, 2022.

Research Article

The Influence of Multisensor Fusion Machine Learning on the Controllable Fabrication of MOF (UIO-66)/ZrAl Ceramic Composite Membranes

Xiaobing Xu [1,2] **Xu Yang,**[1] **Shiyuan Shao,**[1] **Chunling Zhu,**[1] **and Xiaoyong Xu** [1,2]

[1]*College of Material Science and Engineering, Chaohu University, Hefei 238000, China*
[2]*Key Laboratory of Functional Material Processing and Application, Chaohu University, Hefei 238000, China*

Correspondence should be addressed to Xiaoyong Xu; 053063@chu.edu.cn

This study is aimed at improving the utilization efficiency of resources and enhancing the experiments' effect of various composite membrane research. Firstly, the meaning and preparation process of Metal-Organic Frameworks (MOFs) are discussed. Then, the theoretical knowledge of fusing machine learning and multisensor technology is outlined. Finally, based on the controllable fabrication concept of MOF [UIO- (Universitetet I Oslo-) 66]/ZrAl ceramic composite membranes, a multisensor model incorporating machine learning is designed. The results show that the designed radial sensor backpropagation (RS-BP) fusion multisensor model has the highest error rate of about 0.87. When the number of training is about 100 times, the model's error rate tends to be stable, and the minimum error rate is about 0.01. Secondly, the maximum adsorption capacity of the composite membrane under the controllable preparation of the model is 800 cm^3/g Spanning Tree Protocol (STP). Additionally, the adsorption capacity decreases slowly, and the overall adsorption energy is higher than that of the traditional preparation method. Finally, the catalytic efficiency of membranes prepared by fusing multiple sensors is 90%-97%. The research achieves innovation in technology and improves the feasibility of rational application of MOF (UIO-66)/ZrAl ceramic composite membranes. This study not only provides technical support for the development of machine learning fusion multisensing technology but also contributes to the comprehensive improvement of the resource utilization effect.

1. Introduction

With the development of science and technology, a variety of sensor technologies are widely used in human society, providing a lot of technical support for the development of human society. Additionally, it has developed tremendously on its own and merged with a variety of other technologies to create more technical approaches. As a relatively advanced and widely used science and technology, machine learning and sensor fusion play an important role in the innovation and expansion of the two [1]. MOF (UIO-66) [Metal-Organic Frameworks (Universitetet I Oslo-66)]/ZrAl ceramic composite membrane provides great technical support in human research experiments and social and environmental governance. It is necessary to optimize it by scientific

and technological means to improve its comprehensive performance [2].

Zhang et al. pointed out that Metal-Organic Framework (MOF) compounds known as coordination polymers were developed about 20 years ago. MOF compounds have infinite lattices, which are mainly composed of two main components (metal ions or clusters), inorganic lattice, and organic network structure. The two main components are linked to each other by coordination bonds and also react with other indirect molecules to form an infinite topology with pore structures occupied by solvent molecules. In recent years, MOFs have attracted extensive attention as a relatively new porous material in the literature reports in the field of MOFs. In recent decades, the development of multifunctional applications of MOFs has attracted more

scientists' interest than more excellent new structures and explorations in earlier decades. Since the structure of MOFs is closely related to their potential properties, the design of their structure and the exploration of their properties have become very important topics. Most of the structural properties of MOFs are occupied by their pores. Therefore, the construction of MOFs with suitable pore size, shape, and environment is very attractive and more helpful for their functional applications [3]. Li et al. pointed out that traditional energy consumption has accelerated, and the problem of climate change has become increasingly prominent. Therefore, nuclear energy has become an important choice for energy development in various countries and regions. However, nuclear safety and environmental issues are the bottlenecks restricting the development of nuclear power, especially the removal and enrichment of uranium from radioactive wastewater and the extraction of uranium from seawater which are closely related. Therefore, searching for efficient, fast, and selective uranium separation nanoporous materials is of great significance. MOFs are a new member of the nanoporous material family, which have attracted more and more attention and research due to their porosity, large specific surface area, and structural diversity [4]. Shepelev et al. pointed out that the neural network can self-organize and self-learn and adaptively discover the inherent characteristics and regularities contained in the sample data during the learning process. This self-learning capability is different from the methods employed in traditional pattern recognition. The latter often relies on the programmer's prior knowledge of the recognition rules. Additionally, the neural network does not need to make any assumptions about the distribution state of the object to be processed in the sample space but directly learns the relationship between samples from the data. Thus, they can also solve recognition problems that cannot be solved because the sample distribution is unknown [5]. At present, metal frameworks have been widely used in social industries, but the research on their preparation technology is not perfect. In the process of its application, the influence of uncontrollable factors is very large, and more research is needed to provide technical support for its controllable preparation and improve the rational application of metal frameworks.

In summary, firstly, the properties and preparation process of MOF (UIO-66)/ZrAl ceramic composite membranes are comprehensively discussed. Then, the theoretical knowledge of multisensor technology fused with machine learning is outlined. Finally, a multisensor model incorporating machine learning is designed based on the controllable fabrication concept of MOF (UIO-66)/ZrAl ceramic composite membranes. The innovation lies in breaking through the traditional preparation method of the MOF (UIO-66)/ZrAl ceramic composite membrane and creating a novel controllable preparation technology. The research not only provides technical support for the development of multisensor technology incorporating machine learning but also contributes to the controllable preparation of composite membranes.

2. Methods

2.1. The Basic Idea of Metal-Organic Frameworks. MOFs and supramolecular coordination complexes (SCCs) are collectively referred to as metal-organic materials (MOMs). MOFs refer to metal ions or metal clusters and organic ligands matching each other through their own bonds to form a one-dimensional or multidimensional infinite network structure. This material has a new type of crystalline complex with three-dimensional pores and has the characteristics of strong ligand-metal interaction, crystallinity, and porosity [6]. MOFs were proposed in 1995 and had many advantages. The more prominent ones are large porosity and surface area, and their powerful functions also have the advantages of size controllability and so on. Therefore, when using MOF materials, their structures can be designed and modified according to the requirements to realize the modification and regulation of their functions, and a new generation of membrane materials can be obtained. However, the preparation of MOF films with better compactness and functional regulation and modification is still less. Due to the size difference between the MOF film and gas molecules and the molecular weight difference between gas molecules, in most cases, it is very difficult to separate gas molecules with similar molecular weight and size well. Therefore, it has become a new method to utilize the interaction between gas molecules and functional groups on the surface of MOF membrane pores to achieve efficient gas separation. This method has also been favored by many researchers [7].

In applying metal framework films, the storage and classification of small molecules is a widely used purpose, such as the storage of H_2, CO_2, and CH_4. In 2003, the phenomenon that metal framework compounds were used to store H_2 was reported, and about 200 kinds of metal framework compounds can store H_2. In terms of natural gas storage, the separation of H_2 from CH_4 is an important process. In the separation process, the impact of CO_2 should be reduced. It includes the blockage of CO_2 on natural gas pipelines and the impact on the natural environment. Therefore, the use of metal framework materials for CO_2 separation has become a current research hotspot [8].

At present, many groups have successfully fabricated metal framework films and have also proposed many fabrication methods to point out the application value of metal framework films. The preparation of the metal skeleton film mainly depends on the secondary growth process of the metal skeleton powder. The film can be directly prepared from the metal skeleton powder, and the film preparation requirements can be met through its growth. However, the degree of controllability is too low, and the preparation results are not ideal. The current relatively advanced preparation method uses functional group-modified metal as a carrier to prepare membranes. A typical example is the preparation process for MOF-5. The main principle is to make the crystal and the carrier tightly combined to form an ideal membrane structure. The main principle of its utilization is the secondary growth method of metal skeleton powder. However, this method improves the controllability of the membrane, and its practicality is relatively high [9]. The basic structure of MOF is shown in Figure 1.
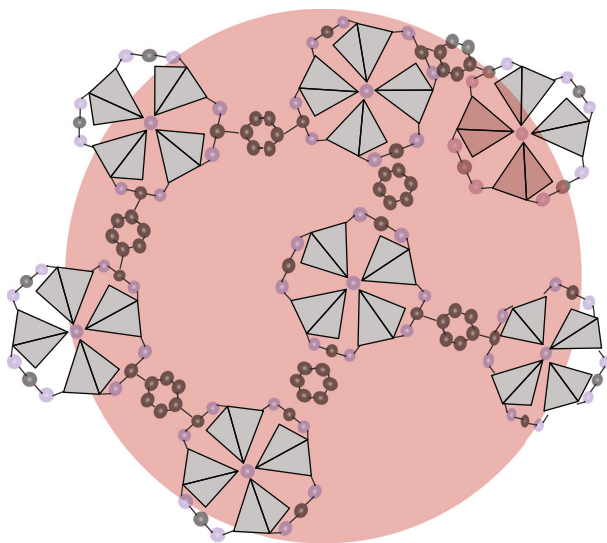
Figure 1: Basic structure of MOF.

Figure 2: Schematic representation of the complex structure of UIO-66 and the building block $Zr_6O_4(OH)_4$ stimulation unit and their synthesis.

In Figure 1, the preparation process of MOF films is not only stable but also highly efficient. On metal supports, different concepts are derived from growing metal frameworks to prepare films. First, it is directly grown or deposited in the mother liquor, that is, prepared by deposition in the liquid made of MOF powder. Next, the crystals are individually synthesized and then assembled into films. Then, the MOFs are grown on the support layer by layer to form a film, or the MOFs are electrochemically deposited on the metal support to form a film, that is, a method of growing another MOF film on the MOF film. Finally, the sandwich method deposited MOF films [10].

2.2. UIO-66 Series. UIO-66 is a three-dimensional porous framework formed by the metal ion structural unit $Zr_6O_4(OH)_4$ connected with 12 organic ligands, respectively. UIO-66 has super stability. This feature mainly relies on the matching Zr-O bond between terephthalic acid (H_2BDC) and the structural unit $Zr_6O_4(OH)_4$, which also explains its wide application in sewage treatment and heterogeneous catalysis [11]. The schematic diagram of the complex structure of UIO-66 and the structural unit $Zr_6O_4(OH)_4$ stimulation unit and their synthesis is shown in Figure 2.

In Figure 2, $Zr_6O_4(OH)_4$ is an octahedral structure unit. There are six Zr^{4+} ions in its octahedral structure unit and four oxygen atoms or hydroxyl groups at each small interface center point of its eight interfaces [12]. These metal nodes are individually coordinated to twelve H_2BDC ligands, thereby coordinating Zr atoms to eight oxygen atoms in H_2BDC. Finally, the theoretical pore volume and theoretical surface area of UIO-66 are $0.45\,cm^3/g$ and $1018\,m^2/g$, respectively. The actual surface area of UIO-66 is usually between 800 and $1200\,m^2/g$, depending on its preparation method [13]. The main structures of UIO-66 and its secondary components are shown in Figure 3.

Figure 3 shows the spatial structures of Al_2O_3 and UIO-66 at different scales and the structure of their fusion product Al_2O_3-ZrO_2. Different structures of UIO-66 have differ-

ent functions. Therefore, controllable preparation of UIO-66 according to its different functions and properties of different spatial structures is a method to utilize UIO-66 complexes [14] effectively. UIO-66 is generally prepared by accurately weighing $0.053\,g$ of $ZrCl_4$ ($0.227\,mmol$) into $24.9\,g$ of DMF ($340\,mmol$) solvent and sonicated to dissolve completely. Then, $0.034\,g$ of $C_8H_6O_4$ ($0.227\,mmol$) is added to the solvent, dissolved by ultrasonic vibration, and uniformly mixed. Then, the mixed solution is transferred into a $50\,ml$ autoclave. The reaction kettle is placed in an oven and reacted at $120°C$ for $24\,h$. After the reaction, it is naturally cooled to room temperature, and the reaction kettle is taken out and filtered with suction. Then, chloroform and methanol are alternately washed for one day. Finally, the reagent is filtered and vacuum dried, and the white product UiO-66 is obtained [15]. The structure of the UiO-66 complex is relatively subtle, and it is difficult to control it during the preparation process. Therefore, this problem has become the main research project for the preparation of UiO-66 at present.
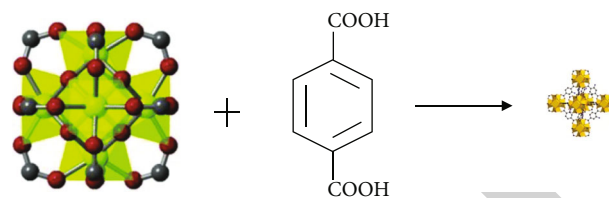
2.3. Multisensor Controllable Technology Incorporating Machine Learning. Today, with the development of science and technology, sensors have developed rapidly, providing a lot of convenience for the development of human beings. With the expansion of its application range, more and more types of performance have also been greatly improved. Therefore, this greatly promotes the generation of multisensor systems for different application backgrounds. In complex multisensor systems, the diversity of data types, huge data capacity, and the relationship between complex data and information will lead to the traditional data fusion methods that can no longer meet the requirements of complex systems [16] for high-precision and high-speed data fusion. Therefore, how to accurately and quickly fuse multidimensional data from different information systems and multiple sensors, quickly carry out more accurate, efficient, and reasonable fusion, and make an accurate estimation has become an urgent problem to be solved. This multisensor system needs to use new methods to process many multidimensional data. In this application background, a new data processing method, that is, the multisensor data fusion technology method, came into being [17].

As a new science and technology type, machine learning has become a current innovative technology by integrating with sensors. Machine learning is a multidomain interdisciplinary subject involving probability theory, statistics, approximation theory, convex analysis, algorithm complexity theory,

(a)

(b)
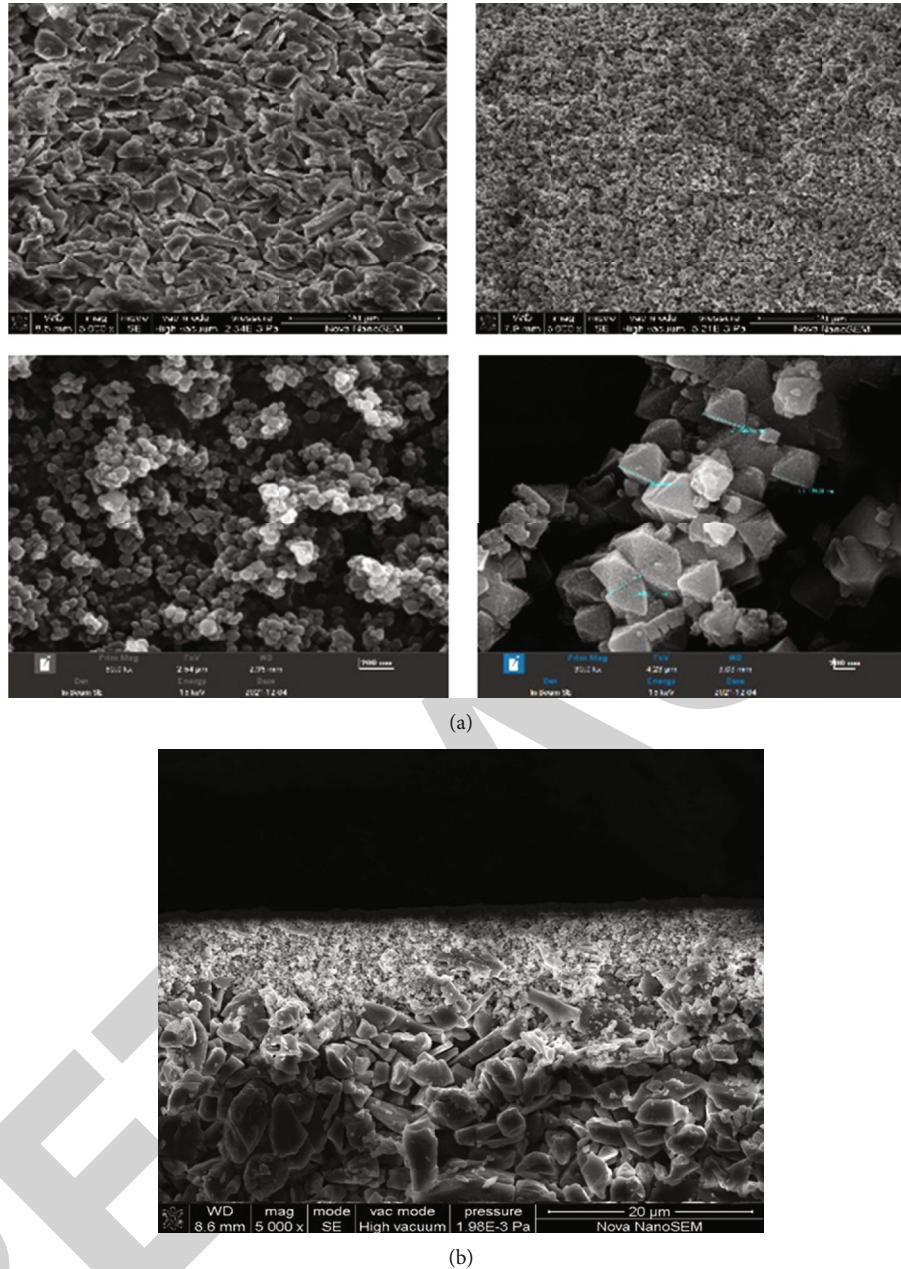
FIGURE 3: The main structures of UIO-66 and its secondary components are (a) the two structures of Al_2O_3 and UIO-66 and (b) the structure of Al_2O_3-ZrO_2.

and other disciplines. It specializes in how computers simulate or realize human learning behaviors to acquire new knowledge or skills and reorganize existing knowledge structures to improve their performance continuously. It is the core of artificial intelligence and the fundamental way to make computers intelligent [18]. Machine learning encompasses a variety of techniques. Among them, Backpropagation Neural Network (BPNN) technology, as an advanced machine learning technology, can provide important technical support for the fusion of various sensors. When BPNN is applied to multisensor data fusion, it is necessary to select an appropriate neural network model. The selection criteria are the requirements of the fusion system and the characteristics of the sensors, including net-

work topology, neuron characteristics, and learning rules [19]. Additionally, the connection between input and sensor information, output, and system decision-making is established. Then, the distribution of weights is determined according to the acquired sensor information and the corresponding system decision-making information to complete the training of the network [20]. BPNN has arbitrarily complex pattern classification ability and excellent multidimensional function mapping ability and solves some problems that simple perceptrons cannot solve. Structurally, BPNN has an input layer, a hidden layer, and an output layer. In essence, BPNN takes the square of the network error as the objective function and uses the gradient descent method to calculate the minimum

value of the objective function. The basic BPNN includes two processes signal forward propagation and error backpropagation [21]. Error outputs are calculated in the input-to-output direction, and weights and thresholds are adjusted in the output-to-input direction. During forward propagation, the input signal acts on the output node through the hidden layer, and after nonlinear transformation, the output signal is generated. If the actual output does not match the expected output, it turns to the backpropagation process of the error [22]. Error backpropagation is to backpropagate the output error layer by layer to the input layer through the hidden layer, distribute the error to all units in each layer, and use the error signal obtained from each layer as the basis for adjusting the weights of each unit. By adjusting the connection strength between the input node and the hidden layer node, the connection strength between the hidden layer node and the output node, and the threshold, the error decreases along the gradient direction. After repeated learning and training, the network parameters (weights and thresholds) corresponding to the minimum error are determined. At this time, the trained neural network can automatically process the nonlinearly transformed information with the smallest output error for the input information of similar samples [23]. The principle of neural network technology fusion multisensor technology is shown in Figure 4.

In Figure 4, BPNN technology provides important support for the development of sensor technology. Radial basis function (RBF) neural network models optimize multisensor fusion techniques. Therefore, the designed model is RS-BP (radial sensor backpropagation) multisensor data fusion technology [24]. Among them, RBF neural network technology is the main technology of this model. Its activation function is shown in

$$R(\|\text{dist}\|) = e^{-\|\text{dist}\|^2}. \tag{1}$$

$\|\text{dist}\|$ represents the distance between the input vector and the weight. There are four radial basis functions of the RBF neural network model, which are thin-plate spline function, multiquadratic function, inverse multiquadratic function, and Gaussian function, as shown in

$$\phi(x) = x^2 \lg(x), \tag{2}$$

$$\phi(x) = \left(x^2 + c\right)^{1/2}, \quad c > 0, \tag{3}$$

$$y_k = \sum_{j=1}^{j} w_{jk} h_j(x), \quad k = 1, 2, \cdots K, \tag{4}$$

$$\phi(x) = \exp\left(-\frac{x - c_j}{2\sigma_j^2}\right). \tag{5}$$

x represents the input vector, c and k represent the fixed parameters, w represents the weight, j represents the input vector sequence, and σ represents the variance of the Gaussian function [25]. The RBF neural network has input, output, and hidden layers. Among them, the node calculation
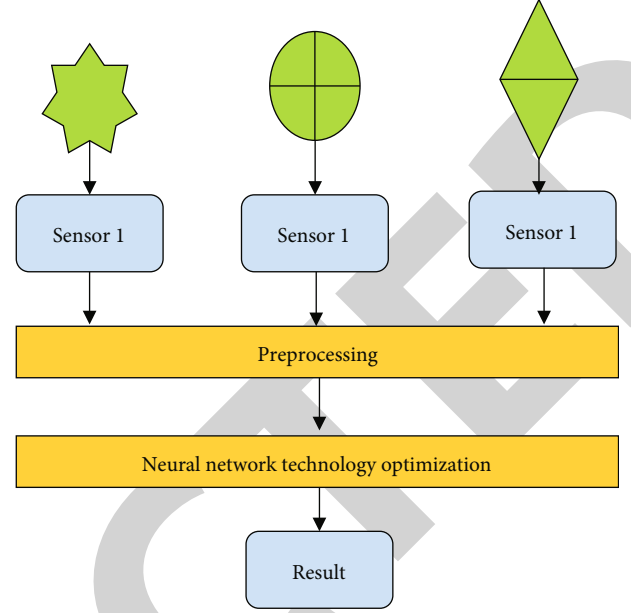
FIGURE 4: The principle of neural network technology fusion multisensor technology.

of the hidden layer is shown in

$$n = \sqrt{m + p} + d. \tag{6}$$

n represents the number of nodes in the hidden layer, m represents the number of nodes in the input layer, p represents the number of nodes in the output layer, and d is a fixed constant. The calculation of the output layer result is shown in

$$h_j(x) = \phi\left(-\frac{X - c_j}{\sigma_j}\right), \quad j = 1, 2, \cdots J. \tag{7}$$

j represents the position of the calculation element in the output layer, σ_j represents the center of the Gaussian function, c_j represents the variance of the Gaussian function, and the remaining parameters are the same as the above equations [26]. However, the model still needs to be trained. Therefore, the training results are calculated as

$$E = \frac{1}{2} e^2, \tag{8}$$

$$\Delta c_j = \eta \frac{w_j}{\delta_j^2} e \sum_{i=1}^{M} G(X_i - c_j)(X_i - c_j), \tag{9}$$

$$\Delta \delta_j = \eta \frac{w_j}{\delta_j^3} e \sum_{i=1}^{M} G(X_i - c_j)(X_i - c_j)^2, \tag{10}$$

$$\Delta w_j = \eta e \sum_{i=1}^{M} G(X_i - c_j). \tag{11}$$

G is a Gaussian function, and c_j, δ_j, and w_j, respectively, represent the weights between the three levels of the RBF

(a)

(b)

FIGURE 5: The training results of (a) the RBF neural network model and (b) the RS-BP multifusion sensor model.

neural network [27]. The activation function of the RBF neural network is shown in

$$R(x_p - c_i) = \exp\left(-\frac{1}{2\sigma^2} x_p - c_i{}^2\right). \tag{12}$$

$x_p - c_i$ represents the Euclidean norm and c_j represents the center of the Gaussian function [28]. The output of the network structure is shown in

$$y_j = \sum_{i=1}^{h} w_{ij} \exp\left(-\frac{1}{2\sigma^2} x_p - c_i{}^2\right). \tag{13}$$

The variance calculation of the Gaussian function is shown in

$$\sigma = \frac{1}{P} \sum_{j}^{m} d_j - y_j c_i{}^2. \tag{14}$$

d represents the network sample data [29]. Firstly, the designed RS-BP model is trained, and the model's performance is evaluated. The datasets selected for training are Canadian Institute for Advanced Research-10 (CIFAR-10) and CIFAR-100 datasets, respectively. Among them, the CIFAR-10 dataset contains a total of 60,000 colors (RGB) images with a size of $32 * 32$. Among the 60,000 images, 50,000 are used as training sets and 10,000 are used for testing. There are 100 categories in the CIFAR-100 dataset, and each category has 600 images. The CIFAR-100 dataset contains many samples, which provides a sufficient basis for model evaluation. Among them, the sample conforms to the design connotation of the model. Therefore, it is very reasonable that the CIFAR-100 dataset is chosen as the training dataset. Then, MOF (UIO-66) ZrAl ceramic composite films are prepared by using a model and sensor, and corresponding tests evaluate the products.

3. Results

3.1. Evaluation of Multisensor Technologies Incorporating Machine Learning.
The fusion machine learning multisensor technology can not only fuse the performance of multiple sensors but also optimize the performance of the fusion sensor through RBF neural network technology so as to design a fusion sensor device that can comprehensively identify and provide accurate data. This can provide technical support for the controllable preparation of MOF (UIO-66) ZrAl ceramic composite films. The training results of the RBF neural network model and the RS-BP fusion multisensor model are shown in Figure 5.

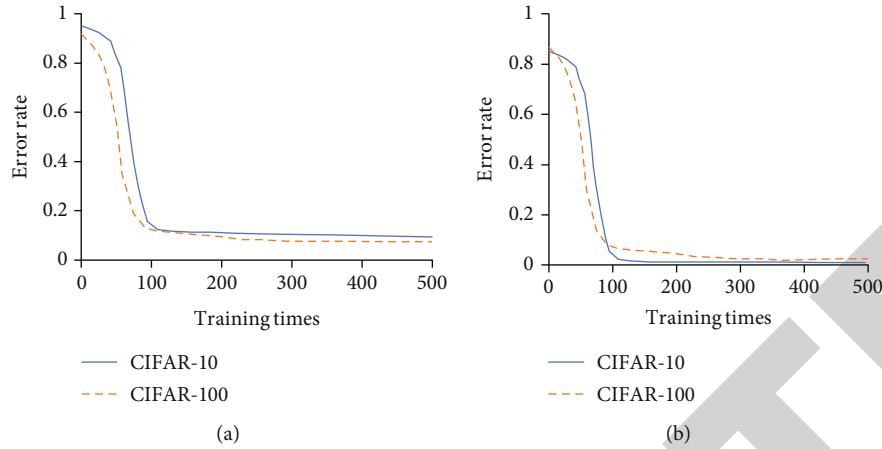In Figure 5, in the training results of the RBF neural network model, the highest error rate of the model is around 0.90, and the overall error rate of the training results in the two datasets decreases rapidly. When the number of training times reaches 100, the model's error rate is basically stable, and the minimum error rate is about 0.09. In the training results of the RS-BP multifusion sensor model, the error rate of the training results of the two datasets is the highest at about 0.87. When the training is about 100 times at this time, the model's error rate tends to be stable, and the error rate is the lowest at about 0.01.

3.2. Controllable Preparation of MOF (UIO-66) ZrAl Ceramic Composite Membranes.
The preparation process of the MOF (UIO-66) ZrAl ceramic composite membrane is complicated, and its structure is difficult to control artificially. Therefore, contemporary science and technology is innovative research on its controllable preparation. The preparation of MOF (UIO-66) ZrAl ceramic composite membranes is studied by the multisensor model technology fused with machine learning. Figure 6 shows the comparison of the performance of the films made by traditional preparation and fusion multisensor preparation methods.

In Figure 6, under the traditional preparation method, a relatively fixed composite membrane preparation method is formulated through the support of theoretical knowledge. This study has a relatively weak ability to control the preparation process, and the membrane performance is relatively
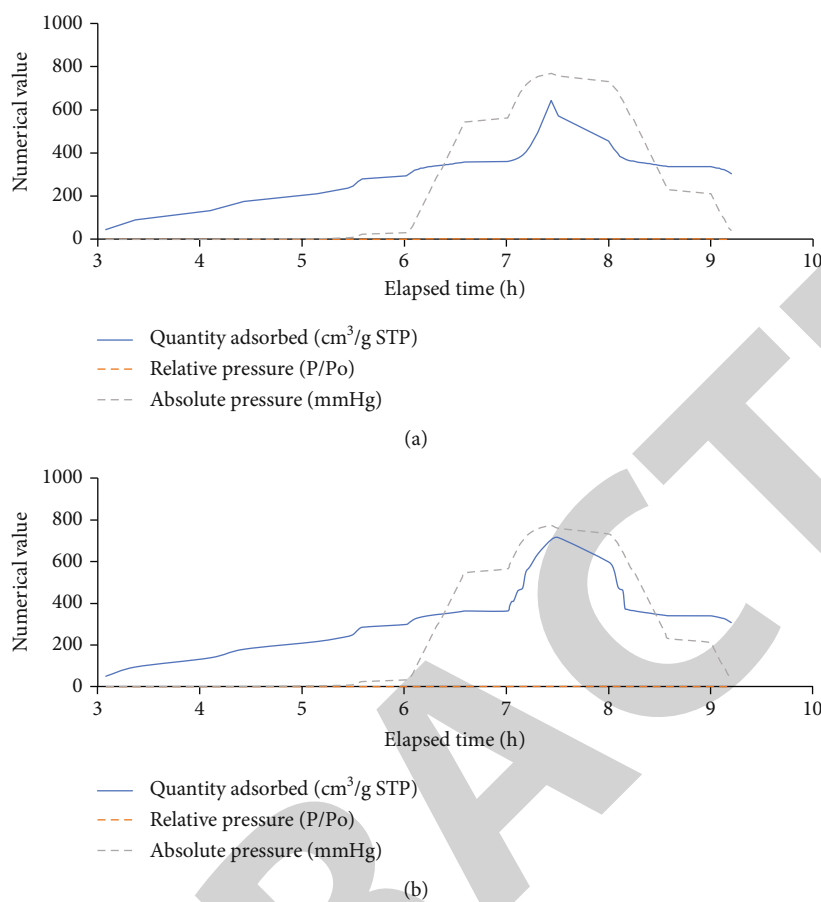
Figure 6: Comparison of the performance of films made by (a) traditional preparation and (b) fusion multisensor preparation.
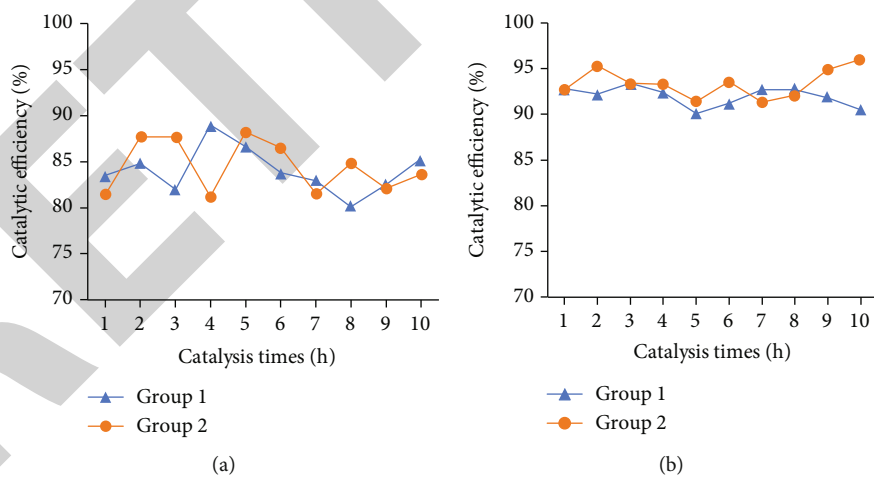
Figure 7: Evaluation of the catalytic performance of UIO-66 composite membrane: (a) the traditional preparation method and (b) the preparation method of fusion of multiple sensors.

weak. The gas adsorption capacity of the traditional film preparation method increased significantly at about 7 hours, and the maximum is 700 cm^3/g STP, and it decreased rapidly after reaching the highest adsorption capacity. Therefore, the overall adsorption capacity is relatively low. The preparation method of the fusion multisensor can control the properties of the membrane according to the properties of the prepara-

tion components and the comprehensive changes in the reactor during the preparation process and improve the adsorption capacity of the membrane. Therefore, the adsorption capacity of the fusion multisensor preparation method increased significantly in about 7 hours, and the maximum adsorption capacity is around 800 cm^3/g STP. Additionally, the adsorption capacity decreased slowly, and

the overall adsorption energy is higher than that of the traditional preparation method. In order to reflect the advantages of the designed model, the designed model is compared with the traditional preparation method through two groups of studies, which improves the value of the comprehensive performance evaluation of the model. Figure 7 shows the photocatalytic performance evaluation of UIO-66 composite films under different preparation methods.

In Figure 7, under the traditional preparation method, the catalytic efficiency of the membrane is about 80%-88%. The vegetation method that fuses multiple sensors can control the microstructure of the membrane to prepare a membrane with strong comprehensive performance. Therefore, the catalytic efficiency of membranes prepared by fusing multiple sensors is around 90%-97%.

4. Conclusion

This study is aimed at improving the comprehensive properties of MOF (UIO-66)/ZrAl ceramic composite membranes and improving the utilization efficiency of various resources. Firstly, the preparation process and properties of MOF (UIO-66)/ZrAl ceramic composite membranes are discussed. Then, the technical concept of machine learning fusion of multisensors is outlined. Finally, the controllable preparation technology of the MOF (UIO-66)/ZrAl ceramic composite membrane is designed by fusing neural network technology and multisensor. The results show that the error rate of the designed RS-BP fusion multisensor model training results is about 0.87. When the number of training is about 100 times, the model's error rate tends to be stable, and the minimum error rate is about 0.01. Secondly, the maximum adsorption capacity of the composite membrane under the controllable preparation of the model is about $800\,cm^3/g$ STP, and the adsorption capacity decreases slowly. Therefore, the overall adsorption energy is higher than that of the traditional preparation method. Finally, the catalytic efficiency of the membrane prepared by fusing multiple sensors is 90%-97%, which significantly improves the comprehensive performance of the composite membrane. Although this study has designed a relatively complete RS-BP multifusion sensor model, the research on its comprehensive application in practice is not perfect. Therefore, in the future, the research in this field and the development and comprehensive application of sensor fusion machine learning technology will be further strengthened.

Data Availability

The data used to support the findings of this study are included within the article.

Conflicts of Interest

The authors declare that they have no conflicts of interest.

References

[1] J. Fonseca, T. Gong, L. Jiao, and H. L. Jiang, "Metal–organic frameworks (MOFs) beyond crystallinity: amorphous MOFs, MOF liquids and MOF glasses," *Journal of Materials Chemistry A*, vol. 9, no. 17, pp. 10562–10611, 2021.

[2] N. Shaukat, A. Ali, M. Javed Iqbal, M. Moinuddin, and P. Otero, "Multi-sensor fusion for underwater vehicle localization by augmentation of RBF neural network and error-state Kalman filter," *Sensors*, vol. 21, no. 4, p. 1149, 2021.

[3] N. Shaukat, A. Ali, M. Javed Iqbal, M. Moinuddin, and P. Otero, "Metal–organic frameworks (MOFs) based electrochemical biosensors for early cancer diagnosis in vitro," *Coordination Chemistry Reviews*, vol. 439, no. 3, article 213948, 2021.

[4] S. Li, Y. Gao, N. Li, L. Ge, X. Bu, and P. Feng, "Transition metal-based bimetallic MOFs and MOF-derived catalysts for electrochemical oxygen evolution reaction," *Energy & Environmental Science*, vol. 14, no. 4, pp. 1897–1927, 2021.

[5] V. Shepelev, S. Aliukov, K. Nikolskaya, A. Das, and I. Slobodin, "The use of multi-sensor video surveillance system to assess the capacity of the road network," *Transport and Telecommunication*, vol. 21, no. 1, pp. 15–31, 2020.

[6] K. Wang, Q. Li, Z. Ren et al., "2D metal-organic frameworks (MOFs) for high-performance BatCap hybrid devices," *Small*, vol. 16, no. 30, article 2001987, 2020.

[7] Y. Yan, C. Li, Y. Wu, J. Gao, and Q. Zhang, "From isolated Ti-oxo clusters to infinite Ti-oxo chains and sheets: recent advances in photoactive Ti-based MOFs," *Journal of Materials Chemistry A*, vol. 8, no. 31, pp. 15245–15270, 2020.

[8] J. B. Pan, B. H. Wang, J. B. Wang et al., "Activity and stability boosting of an oxygen-vacancy-rich $BiVO_4$ photoanode by NiFe-MOFs thin layer for water oxidation," *Angewandte Chemie International Edition*, vol. 60, no. 3, pp. 1433–1440, 2021.

[9] M. Wang, R. Dong, and X. Feng, "Two-dimensional conjugated metal–organic frameworks (2Dc-MOFs): chemistry and function for MOFtronics," *Chemical Society Reviews*, vol. 50, no. 4, pp. 2764–2793, 2021.

[10] M. Lv, W. Zhou, H. Tavakoli et al., "Aptamer-functionalized metal-organic frameworks (MOFs) for biosensing," *Biosensors and Bioelectronics*, vol. 176, no. 8, article 112947, 2021.

[11] X. Liu, "Metal-organic framework UiO-66 membranes," *Frontiers of Chemical Science and Engineering*, vol. 14, no. 2, pp. 216–232, 2020.

[12] N. Rabiee, M. Bagherzadeh, M. Heidarian Haris et al., "Polymer-coated NH2-UiO-66 for the codelivery of DOX/pCRISPR," *ACS Applied Materials & Interfaces*, vol. 13, no. 9, pp. 10796–10811, 2021.

[13] G. Wang, C. T. He, R. Huang, J. Mao, D. Wang, and Y. Li, "Photoinduction of Cu single atoms decorated on UiO-66-NH_2 for enhanced photocatalytic reduction of CO_2 to liquid fuels," *Journal of the American Chemical Society*, vol. 142, no. 45, pp. 19339–19345, 2020.

Hindawi

Retraction

Retracted: Design of Active Display Stand Combing the Pressure Sensor and Kinematics Algorithm

Journal of Sensors

This article has been retracted by Hindawi following an investigation undertaken by the publisher [1]. This investigation has uncovered evidence of one or more of the following indicators of systematic manipulation of the publication process:

(1) Discrepancies in scope

(2) Discrepancies in the description of the research reported

(3) Discrepancies between the availability of data and the research described

(4) Inappropriate citations

(5) Incoherent, meaningless and/or irrelevant content included in the article

(6) Manipulated or compromised peer review

The presence of these indicators undermines our confidence in the integrity of the article's content and we cannot, therefore, vouch for its reliability. Please note that this notice is intended solely to alert readers that the content of this article is unreliable. We have not investigated whether authors were aware of or involved in the systematic manipulation of the publication process.

Wiley and Hindawi regrets that the usual quality checks did not identify these issues before publication and have since put additional measures in place to safeguard research integrity.

We wish to credit our own Research Integrity and Research Publishing teams and anonymous and named external researchers and research integrity experts for contributing to this investigation.

The corresponding author, as the representative of all authors, has been given the opportunity to register their agreement or disagreement to this retraction. We have kept a record of any response received.

References

[1] M. Ma and L. Yong, "Design of Active Display Stand Combing the Pressure Sensor and Kinematics Algorithm," *Journal of Sensors*, vol. 2022, Article ID 9275062, 8 pages, 2022.

Hindawi

Research Article

Design of Active Display Stand Combing the Pressure Sensor and Kinematics Algorithm

Minhai Ma [ID] and Lei Yong

College of Mechanical and Electrical Engineering, Ningbo Polytechnic, Ningbo, 315800 Zhejiang, China

Correspondence should be addressed to Minhai Ma; 1001719@nbpt.edu.cn

To solve the trouble of cervical vertebra disease caused by long working hours, this work is aimed at designing an active monitor stand to achieve the best dynamic trajectory planning. The stand operation system consists of image input, face positioning, and robotic arm. According to the user's face positioning, the inverse kinematics method is used to calculate the steering angle in each direction, and the height and angle are adjusted to make the corresponding selection for the user's display position on the screen. The C++ is used to program the algorithm, and its core is to control the rotation speed of the motor to ensure that the display screen will not cause any interference to the normal work of the user when the bracket moves. In the inverse operation, the Piper method is used to solve the inverse kinematics issues. After testing, the sliding wedge stroke of the developed active display stand is 0.6 mm, and the height position difference at the reference zero point after the display stand is measured with a digital altimeter is 7.12 mm, which indicates that the stand shows a large deformation after being mounted. This work is of important reference value for realizing the movement of active display stand.

1. Introduction

In today's development of the information society, computers and the Internet have become a major part of people, especially young and middle-aged people, in their work and life [1–3]. However, "computer disease" caused by improper operation also appears, especially cervical spondylosis. Common symptoms include neck pain, numbness in fingers, and dizziness. If it is due to improper computer use, it can lead to muscle tension and fatigue in the neck, resulting in degeneration of the discs and facet joints in the neck. As a result, the monitor stand came into being [4–6]. Most of modern office and study need to face the computer for a long time. The height and low angle of the monitor are adjusted through the monitor stand. The appropriate monitor position helps to improve the sitting posture of the human body.

At present, most of the display screens on the market are manually adjusted or use a physical method to maintain the height of the screen, and it is impossible to adjust the user's

state at any time [7–9]. The lifting frame of the adjustable liquid crystal display (LCD) screen can flexibly adjust the height of the LCD screen and obtain a comfortable experience of using the computer. In the display system of the computer, the trajectory planning, navigation, and obstacle avoidance functions of the robotic arm of the monitor stand play key functions [10, 11]. Kumar et al. [12] performed a kinematic analysis of the motion degrees of freedom of the stent, thereby addressing the total inverse, rotational inverse, and forward kinematics.

This work is mainly aimed at the computer users who have been sitting for a long time, using the principle of pressure sensing and motion, to design a bracket that can control the stepper motor so that the monitor can move slowly and autonomously without affecting people's office, so as to prevent the occurrence of cervical spondylosis. The system consists of image input, face positioning, and robot arm. According to the current face and the center of the camera, the inverse kinematics method is used to calculate the steer-

ing angle in each direction and adjust the height and angle to provide the user with a suitable display position. The use of active display brackets ensures that the display fixed calipers of the rack can realize multiangle rotation adjustment of screen rotation of 360°, lateral rotation of ±180°, and upper arm lateral rotation of 360°, allowing users to have a larger adjustment range and multiple adjustment viewing angles. The stepper motor controlled by the 51 single-chip microcomputer proposed and designed in this work can make the monitor move slowly and autonomously without affecting the office work, so that the office worker can prevent cervical spondylosis unconsciously. In addition, the design cost is low, and the space occupied is relatively small.

2. Materials and Methods

2.1. How the Active Display Stand Works. The main part of the display stand is the boom, "cantilever" as it literally means it can spread freely like an arm. In addition, it is made of aluminum or carbon steel, fixed diagonally, protected on all four sides, and can be rotated without opening the clip. The monitor stand mainly includes the upper support arm, the lower support arm, the monitor connector, and the platen fixing device. The most important core part is located on the upper support arm, which uses the elastic deformation of the upper arm to support the monitor [13–15]. Compared with the original base, the advantages of the active display stand are obvious. It can be retracted and hovered at any height, the screen can be rotated at 360°, and it can maintain a certain field of view. In addition, it does not occupy the desktop space, easy to manage the desktop, and realize the combination of multiple screens at the same time. There are two main types of monitor mounts on the market today: air spring and mechanical. The pneumatic spring type monitor stand has good handling and good handling performance, but its usage time is lower than that of the mechanical type. Due to the long-term action of the air spring, the sealing performance will decrease, resulting in a decrease in the service life. The types of common robotic arm monitor brackets are shown in Table 1.

Figure 1 shows the track on which the display moves. The designed bracket rail is square; and 1, 2, 3, and 4 are the four end points of the rail. The length of the bracket diagonal rail is represented by L1 and L2, and the angle between the diagonal and each side is 45°. The display screen is connected to the guide rail, and the pulley is adopted to move slowly along the track according to the set program. The set program allows the display screen to move only at an angle of 45 degrees [16, 17]. To achieve smooth motion and no noise when the display is moved to the end, the trajectory of the corresponding tips of 1, 2, 3, 4, and diagonal intersection 5 is designed to be smooth, resulting in a 45 degree rotation at the end, and when cornering, torque is minimized. This maintains stability for the maintenance of the motor and even the entire mobile support system. According to the above description, after a cycle of trajectory movement, the good effect of 360° activity of the cervical spine can be achieved without affecting the work of the office worker.

2.2. Single-Chip Pressure Measurement and Control System. Most computer monitor pedestals have no adjustment function during operation. Most of the current display brackets are based on weight and realize multiangle adjustment, but the manufacturing cost is high due to their many structures [18–20]. Due to the inappropriate cooperation between people and devices, there are often many redundant connecting rods, and automatic adjustment of the connecting rods cannot be realized during operation. The C++ is used to program the algorithm, and the core is to control the rotation speed of the motor to ensure that the display screen will not cause any interference to the normal work of the workers during movement. C++ has rich library functions, fast operation speed, high compilation efficiency, and good portability and can directly control the system hardware. By designing a cyclic function, the display is made to perform periodic line movements. The steering of the motor is controlled by the program to achieve the purpose of turning the display at a 45° angle. Then, the speed of the stepper motor is controlled by the delay() function, thereby controlling the movement speed of the display.

The pressure measurement control device mainly monitors the pressure of the support. Each device is equipped with four sensors, which can connect the hydraulic cavity of the support column, balance jack, and probe jack [21–23]. After the receipt of the instruction of the communication measurement and control system, the pressure of the four channels was measured, and then, the four sound pressure signals were transmitted to the measurement and control center through the communication measurement and control system and then transmitted to the ground through the communication measurement and control center. The pressure measurement control system is equipped with a button; when pressed, the pressure value of the four channels can be displayed in the LCD window cyclically. In the pressure measurement control system, 80C51 expands 8K EPROM (27C64) and 8 K SRAM (6264) as external program memory and data memory. The lower 6 MHz is selected as the operating frequency of the 80C51 single-chip microcomputer, which can meet the data acquisition requirements and reduce the power consumption of the single-chip microcomputer. The basic hardware composition controlled by the single-chip microcomputer is shown in Figure 2.

In the display stand control system developed in this work, its communication and each measurement and control system belong to the master-slave communication network. To adapt to this long-distance, multipoint, and large-interference communication condition, the RS-485 interface is selected. The interface using MAX483 is a small transceiver for RS-485 produced by MAXIM, including a driving device and a receiving device. The device is characterized in that the transmission speed of the driving device can be reduced to the maximum, the interference of electromagnetic waves can be reduced to the maximum, and the influence caused by incorrect cable termination can be reduced.

2.3. Robotic Arm Control Based on Pressure Sensor. As the tactile unit of the robotic arm skin, the pressure sensor needs

Table 1: Common robotic arm monitor stand.

Type of robotic arm	Functions and characteristics	Craft and design	Application scenarios
Wall-mounted rocker	Installed and fixed on the wall, the display can be adjusted at large angles, front and rear, left and right	Aluminum alloy casting or carbon fiber composite material, relying on bolt locking device to achieve rotation angle	Libraries, exchanges, and training institutions,
Stand-up rocker arm	Installed and fixed on the desktop, the monitor can be adjusted front and rear, left and right angles	Aluminum alloy casting or carbon fiber composite material, relying on bolt locking device to achieve rotation angle	Office, studio, and meeting room
Taili multiscreen	Multiple monitors can be moved left and right at the same time, and the tilt angle can be adjusted	Aluminum alloy casting or carbon fiber composite material, relying on bolt locking device to achieve rotation angle	Studio, exchange monitoring center, and home intelligent monitoring system
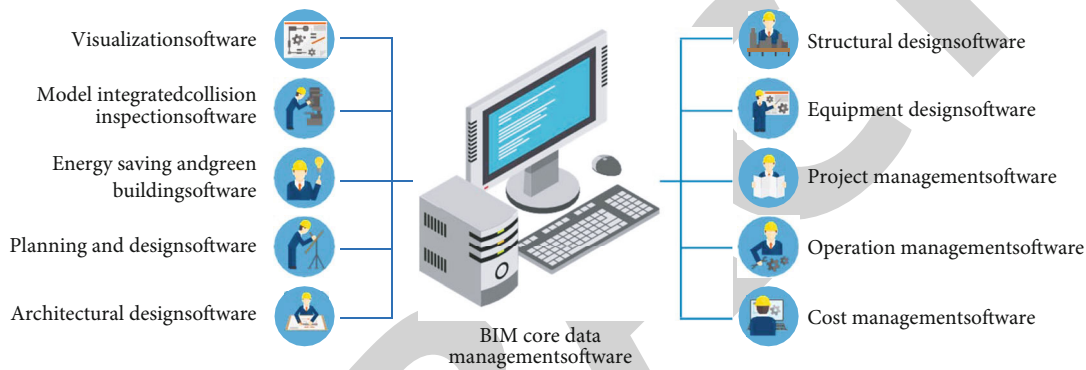
Figure 1: Movement track of the display.

to have two characteristics. Firstly, the overall physical properties of the sensor, such as sensitivity and detection range, meet the design standards; secondly, the sensor must be flexible enough to be attached to the cylindrical surface of the robotic arm [24–26]. The robot's forelimb is equipped with 6 groups of pressure sensors, with a total of 388 detection points, which can conduct a comprehensive detection of the robot's body surface. The two arrays are arranged as a set and are connected to a piece of sensing circuit. When a pressure is applied to the sensor, the circuit converts the voltage value into a pressure value, such as analog multiplexer, signal amplification, and ADC sampling. Among them, the acquisition card of the pressure sensor mainly uses the D/A conversion circuit for analog output [27, 28]. The detectors are arranged horizontally on the testing machine, and then, the detection objects are placed in the corresponding places. Through the detection of the target, the target is detected by the sensor array and processed through the acquisition loop to obtain the corresponding specific value, and then, the table is programmed through the MATLAB program to obtain the stereo image of the detected object. On this basis, a method for detection is presented, as shown in Figure 3.

The pressure-sensitive element MPU6050 developed in this work is based on micro mechanics. The sensor system includes a three-axis accelerometer, a three-axis gyrometer, and an adaptive thermometer. The system can be used for
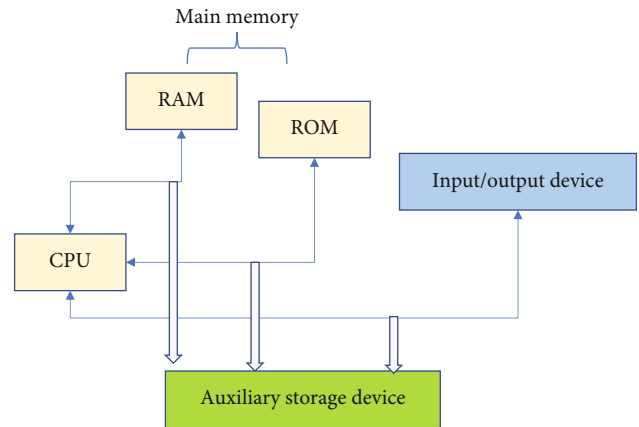
Figure 2: The basic hardware composition of single-chip microcomputer control.

the measurement of various parameters, such as acceleration, velocity, orientation, and displacement. Firstly, the various wires are connected on the robotic arm of the monitor stand to the computer terminal, and then, it is squeezed hard with both hands to measure the working state of the pressure sensor in the human body. The system has high flexibility and elasticity, which not only ensures the safety of the inner

sensor but also ensures the safety in human-machine interaction. The pressure distribution test device developed in this paper has good elasticity and uses a 0.1 mm thick mesh tactile pressure sensor, which enables pressure detection on a variety of contact surfaces.

Tekscan's pressure sensors are two thin polyacetate membranes that are arranged in the shape of a wellhead and arranged in a fence. The outer surfaces of these wires are coated with a special varistor. The pressure between the two contacting surfaces is tested with a flexible membrane sensor. In addition, with dedicated acquisition software and software, the pressure between the gaps can be better understood to optimize product design, quality, and production. Compared with the conventional method, this method not only is cost-effective but also obtains the effect of the test in an intuitive and real-time manner. In this work, the local averaging method is used to predict the measurement results. In the pressure value area, it should select a point as a section, average the pressures of all pressure measuring points in this section, and use this value to replace the pressure of this pressure measuring point:

$$h(i, j) = \frac{1}{M} \sum_{(k,l) \in N} f(k, l) \times \omega_{k,l},$$
$$\sum_{(k,l)} \omega_{k,l} = M. \tag{1}$$

In the above two equations, $f(k, l)$ refers to the pressure value at position (k, l) within the field N, M is the sum of the pressure measurement points within the field, and $\omega_{k,l}$ is the weighting factor.

The data of each collection point of the body pressure distribution sensor is undertaken as a variable, and the pressure value of the collection point in each distribution map as a sample; the pressure distribution histogram can be obtained. $(X_1, X_2 \cdots X_n)$ is set as the pressure value sequence of each collection point; then, the calculation formula of the statistic can be expressed as

$$S^2 = \frac{1}{n-1} \sum_{i=1}^{n} \left(X_i - \bar{X}\right)^2,$$
$$\bar{X} = \frac{1}{n} \sum_{i=1}^{n} X_i. \tag{2}$$

In the above two equations, S^2 represents the variance of the collected pressure value samples.

2.4. Robotic Arm Kinematics Algorithm for the Display Stand. Since the length of the connecting rod of the robotic arm is known, the final position and direction of the endeffector can be determined as long as the rotation angle of each joint are determined, which is called forward kinematics. If the final position and orientation of the end-effector are known, the angle of each joint can also be derived, which is called inverse kinematics. There are two types of inverse kinematics algorithm solutions: one is an analytical solution,
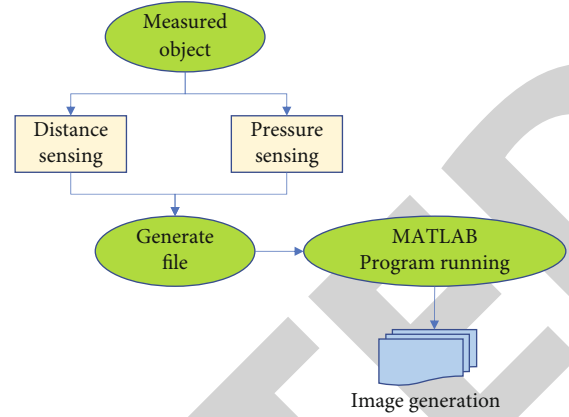
Figure 3: Test flow of sensor acquisition system.

and the other is a numerical solution. MATLAB uses a numerical solution method, which can be understood as iterative optimization, or approximate solution. The positive kinematics solution of the tandem robot is relatively simple, which is just a transformation of position and attitude. This time, the standard D-H algorithm (rotate around the z-axis first) is used to push it to the positive kinematics solution. It can specify a reference coordinate system for each joint axis, determine the relationship between any two adjacent coordinate systems, and obtain the total transformation matrix from the robotic arm end effector to the base coordinate system.

$$T = A_1 A_2 A_3 A_4 A_5 A_6. \tag{3}$$

In equation (3), T is the transformation matrix of the robot end position, and A_i is the transformation matrix of the i-th axis.

In the inverse kinematics algorithm, since the axes of the three axes of the robot end intersect at one point, which satisfies the piper algorithm, the piper algorithm is used to derive the inverse solution. The robotic arm structure in Figure 4 shows that the axes of the three axes at the end of the robotic arm intersect at the position where axis 5 is located, that is, the wrist point position. From the perspective of the reference coordinate system, if the angles of the first three axes are determined, the position of the wrist point will also be fixed, and the angles of the last three axes only affect the posture of the wrist point, not the position of the wrist point.

In the case of different joint angles of the actuator, the attitude and position expression of the end effector relative to the coordinate system that acts as a reference are different, which is a problem solved by the forward kinematics of the robot. The plane geometry method is adopted to inversely solve the three middle joints, all of which rotate in the vertical plane. The projection of the robotic arm on the xy plane in Figure 5 illustrated that the coordinate (x, y) of the end point P consists of three parts, $(x_1 + x_2 + x_3, x_1 + x_2 + x_3)$. Among it, θ_1, θ_2, and θ_3 are the angles of the steering gear to be solved, and α is the angle between the joint carrying the display and the horizontal plane.
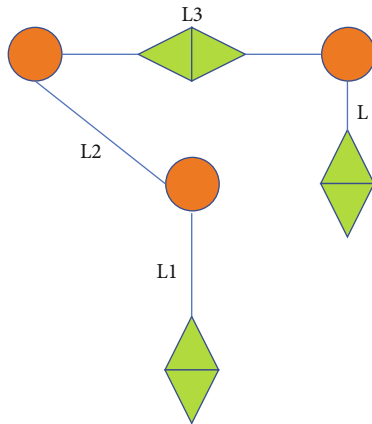
Figure 4: The structure of robotic arm.
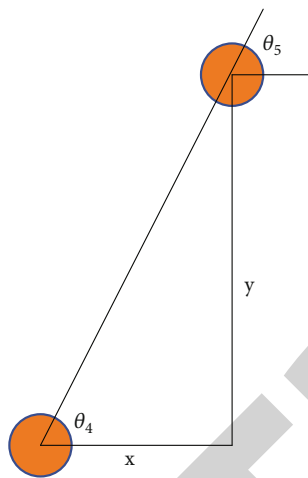
Figure 5: Projection of robotic arm on xy plane.

It should calculate from the base coordinate system the lengths of the connecting rods which are L_1 and L_2, respectively. It should choose a fixed coordinate system $\{0\}$ with the origin coincident with the base joint and assume that the actuator $\{3\}$ is fixed on the second link. The orientation of the actuator coordinate system Cartesian coordinate (x, y) is undertaken as a function of joint angle (θ_1, θ_2); the equation is as follows:

$$
\begin{aligned}
x &= L_1 \cos \theta_1 + L_2 \cos (\theta_1 + \theta_2) + L_2 \cos (\theta_1 + \theta_2 + \theta_3), \\
y &= L_1 \sin \theta_1 + L_2 \sin (\theta_1 + \theta_2) + L_2 \sin (\theta_1 + \theta_2 + \theta_3), \\
\phi &= \theta_1 + \theta_2 + \theta_3.
\end{aligned}
\tag{4}
$$

The wedge mechanism is an important mechanism to realize power transmission and movement direction conversion, and its mechanism is mainly composed of an active wedge and a driven sliding wedge. Commonly used wedge mechanisms are horizontal motion wedge mechanism and inclined motion wedge mechanism. In the mechanism, under the action of vertical external force, the wedge moves

vertically downward, while the sliding wedge moves horizontally to the left or right. On the premise of ignoring the friction of the inclined plane, set the vertical pressure from the wedge to be, and the horizontal resistance of the sliding wedge to be; then the horizontal sliding wedge resistance is as follows:

$$
F = \frac{P}{\tan \theta}.
\tag{5}
$$

The wedge angle is set as θ, and the wedge stroke as L; then the sliding wedge stroke can be expressed as follows:

$$
S = L \times \tan \theta.
\tag{6}
$$

When the three-section wedge mechanism is designed, it is first required that the upper and lower wedges will not fall off horizontally in the wedge groove and ensure that the wedge and sliding wedge have sufficient horizontal sliding wedge stroke and vertical wedge stroke when sliding. This ensures the effective use of the three-section wedge locking structure.

3. Results and Discussion

3.1. Active Safety Control of Display Stand Robotic Arm. Based on the robot kinematics, the desired trajectory of the robotic arm is tracked and controlled by taking the position, velocity, and acceleration of the robotic arm end or each degree of freedom as expectations. When the robotic arm is in contact with the object during the movement, it is the control of restricted motion. This kind of control not only requires the robotic arm to move along a certain trajectory but also controls the contact force between it and the environment. In the robotic arm safety control research experimental platform, a flexible skin with a pressure sensing array can be wrapped on the robotic small arm. By observing the indicator light of the pressure signal acquisition circuit board, the working status of the sensor can be monitored in real time to ensure the stable operation of the sensor. The safe detour experiment consists of two parts: the upper detour and the lower detour. The corresponding joint angle changes are shown in Figures 6 and 7.

When the robotic arm senses that there is an obstacle ahead, it will follow up slowly. When it reaches a certain close distance, the robotic arm suspends its movement and judges the size of the obstacle gap. If it is confirmed that the gap cannot be passed and the new passable area is detected above the robotic arm, the robotic arm performs a small pullback motion and moves upward. When the robotic arm perceives an obstacle ahead, it will follow up slowly. When it reaches a certain close distance, the robotic arm suspends its movement and judges the size of the obstacle gap. If it is confirmed that the gap cannot be passed and the new passable area is detected under the robotic arm, the robotic arm performs a small pullback motion and moves downward.
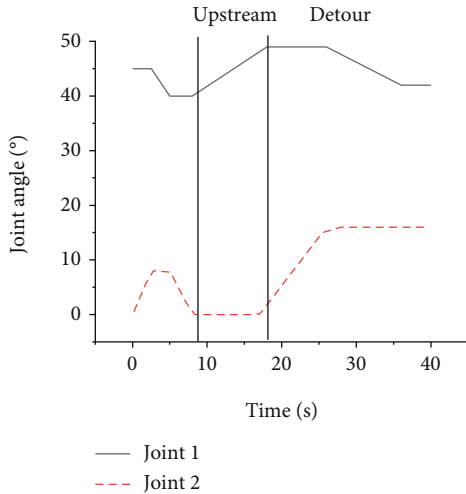
Figure 6: Joint angle change during upper detour.
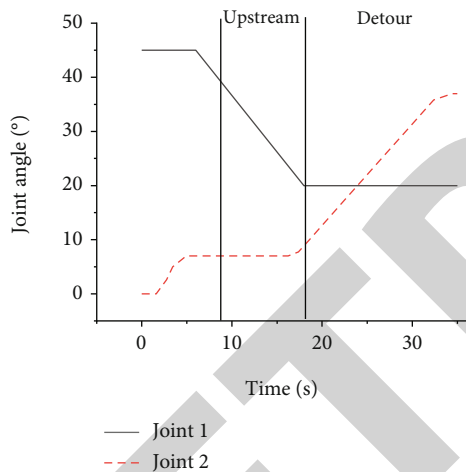
Figure 7: Joint angle change during lower detour.

3.2. Functional Testing of the Display Stand. The rotating arm assembly is installed on the pole assembly, and the height of the arm assembly from the desktop is required to be 230 mm. The active control method is mainly that the robotic arm can foresee the occurrence of danger and adopt safe strategies to avoid danger. A digital altimeter is adopted to measure the height dimension of the bracket before it is mounted, and its height is set as the reference zero point, and the sliding wedge stroke of the bracket is 0.6 mm. Figure 8 is a schematic diagram of the reference zero point of the display stand. A digital altimeter is adopted to measure the height position difference at the reference zero point after the monitor bracket is mounted; it is 7.12 mm, which indicates that there is a large deformation phenomenon after the bracket is mounted. Compared with the maximum displacement deformation of 10.55 mm obtained by the finite element analysis of the arm assembly, the two are approxi-

Figure 8: Schematic diagram of the reference zero point of the monitor stand.

mately equal, indicating that the overall stiffness and strength of the monitor stand meet the technical requirements of the original design.

4. Conclusion

At present, LCD has been widely used, and various new display support structures have appeared. In this work, the static display is moved according to the set trajectory. The designed bracket is mainly assembled by the supporting main rod, the positioning and erecting plate, the monitor holder, and the host holding arm and other parts. According to the pressure sensing and the kinematic algorithm of the robotic arm, the three-stage oblique wedge-shaped locking device can be used to easily complete the disassembly and locking of the display stand. The pressure sensor is the tactile element of the robotic arm. It has the comprehensive physical characteristics of the sensor and can touch the human body efficiently and quickly. Secondly, the sensor is elastic and can be attached to the cylindrical surface of the robotic arm. With 51 single-chip microprocessor as the core, the core control system development of active display stand is realized. It is implemented by a loop function to achieve a periodic linear movement. Using the inverse kinematics method, the movement direction of each joystick is calculated, and the precise positioning of the joystick is achieved through the angle and height of the robotic arm. The sliding wedge stroke of the active monitor stand developed in this work is 0.6 mm. The height position difference at the reference zero point is 7.12 mm after the monitor stand is measured with a digital altimeter, indicating that the stand has a large deformation after being mounted.

Due to the complexity of the ROS system, the full-parameter kinematics algorithm of the manipulator cannot

be integrated in ROS, and the follow-up work can consider the forward kinematics of the manipulator. In the following research, since the practical promotion of the active display stand designed in this study should still be a difficult process, it is necessary to continuously update the algorithm iteratively and improve the user experience of the system.

Data Availability

The data used to support the findings of this study are included within the article.

Conflicts of Interest

The authors declare no conflicts of interest regarding the publication of this paper.

Acknowledgments

References

[1] M. Rana and V. Mittal, "Wearable sensors for real-time kinematics analysis in sports: a review," *IEEE Sensors Journal*, vol. 21, no. 2, pp. 1187–1207, 2020.

[2] W. Pitt, S. H. Chen, and L. S. Chou, "Using IMU-based kinematic markers to monitor dual-task gait balance control recovery in acutely concussed individuals," *Clinical biomechanics*, vol. 80, article 105145, 2020.

[3] J. S. Tan, S. Tippaya, T. Binnie et al., "Predicting knee joint kinematics from wearable sensor data in people with knee osteoarthritis and clinical considerations for future machine learning models," *Sensors*, vol. 22, no. 2, p. 446, 2022.

[4] P. Lisiński, A. Wareńczak, K. Hejdysz et al., "Mobile applications in evaluations of knee joint kinematics: a pilot study," *Sensors*, vol. 19, no. 17, p. 3675, 2019.

[5] L. Pacher, C. Chatellier, R. Vauzelle, and L. Fradet, "Sensor-to-segment calibration methodologies for lower-body kinematic analysis with inertial sensors: a systematic review," *Sensors*, vol. 20, no. 11, p. 3322, 2020.

[6] A. Triantafyllou, G. Papagiannis, S. Stasi et al., "Application of wearable sensors technology for lumbar spine kinematic measurements during daily activities following microdiscectomy due to severe sciatica," *Biology*, vol. 11, no. 3, p. 398, 2022.

[7] H. Chander, E. Stewart, D. Saucier et al., "Closing the wearable gap—part III: use of stretch sensors in detecting ankle joint kinematics during unexpected and expected slip and trip perturbations," *Electronics*, vol. 8, no. 10, p. 1083, 2019.

[8] G. Di Raimondo, B. Vanwanseele, A. van der Have et al., "Inertial sensor-to-segment calibration for accurate 3d joint angle calculation for use in OpenSim," *Sensors*, vol. 22, no. 9, p. 3259, 2022.

[9] J. L. Escalona, P. Urda, and S. Muñoz, "A track geometry measuring system based on multibody kinematics, inertial sensors and computer vision," *Sensors*, vol. 21, no. 3, p. 683, 2021.

[10] Z. A. Abro, Z. Yi-Fan, C. Nan-Liang, H. Cheng-Yu, R. A. Lakho, and H. Halepoto, "A novel flex sensor-based flexible smart garment for monitoring body postures," *Journal of Industrial Textiles*, vol. 49, no. 2, pp. 262–274, 2019.

[11] N. Haralabidis, D. J. Saxby, C. Pizzolato, L. Needham, D. Cazzola, and C. Minahan, "Fusing accelerometry with videography to monitor the effect of fatigue on punching performance in elite boxers," *Sensors*, vol. 20, no. 20, p. 5749, 2020.

[12] S. Kumar, B. Bongardt, M. Simnofske, and F. Kirchner, "Design and kinematic analysis of the novel almost spherical parallel mechanism active ankle," *Journal of Intelligent & Robotic Systems*, vol. 94, no. 2, pp. 303–325, 2019.

[13] H. Keshavarzi, C. Lee, M. Johnson, D. Abbott, W. Ni, and D. L. M. Campbell, "Validation of real-time kinematic (RTK) devices on sheep to detect grazing movement leaders and social networks in merino ewes," *Sensors*, vol. 21, no. 3, p. 924, 2021.

[14] V. Shia, T. Y. Moore, P. Holmes, R. Bajcsy, and R. Vasudevan, "Stability basin estimates fall risk from observed kinematics, demonstrated on the Sit-to-Stand task," *Journal of Biomechanics*, vol. 72, pp. 37–45, 2018.

[15] S. Y. Shin, R. K. Lee, P. Spicer, and J. Sulzer, "Quantifying dosage of physical therapy using lower body kinematics: a longitudinal pilot study on early post-stroke individuals," *Journal of Neuroengineering and Rehabilitation*, vol. 17, no. 1, pp. 1–9, 2020.

[16] B. Oubre, J. F. Daneault, K. Boyer et al., "A simple low-cost wearable sensor for long-term ambulatory monitoring of knee joint kinematics," *IEEE Transactions on Biomedical Engineering*, vol. 67, no. 12, pp. 3483–3490, 2020.

[17] A. Szafarczyk, "Kinematics of mass phenomena on the example of an active landslide monitored using GPS and GBInSAR technology," *Journal of Applied Engineering Science*, vol. 17, no. 2, pp. 107–115, 2019.

[18] R. L. Greene, M. L. Lu, M. S. Barim et al., "Estimating trunk angle kinematics during lifting using a computationally efficient computer vision method," *Human Factors*, vol. 64, no. 3, pp. 482–498, 2022.

[19] S. A. Evans, K. Ballhause, D. A. James, D. Rowlands, and J. B. Lee, "The development and validation of an inertial sensor for measuring cycling kinematics: a preliminary study," *Journal of Science and Cycling*, vol. 10, no. 3, pp. 34–44, 2021.

[20] C. Young, M. L. Oliver, and K. D. Gordon, "Design and validation of a novel 3D-printed wearable device for monitoring knee joint kinematics," *Medical Engineering & Physics*, vol. 94, pp. 1–7, 2021.

[21] B. J. C. Bastiaansen, E. Wilmes, M. S. Brink et al., "An inertial measurement unit based method to estimate hip and knee joint kinematics in team sport athletes on the field," *JoVE (Journal of Visualized Experiments)*, vol. 4, no. 159, article e60857, 2020.

[22] C. Talens-Estarelles, J. J. Esteve-Taboada, V. Sanchis-Jurado, Á. M. Pons, and S. García-Lázaro, "Blinking kinematics characterization during digital displays use," *Graefe's Archive for Clinical and Experimental Ophthalmology*, vol. 260, no. 4, pp. 1183–1193, 2022.

[23] P. Pujayanto, R. Budiharti, E. Adhitama, N. R. A. Nuraini, and H. V. Putri, "The development of a web-based assessment system to identify students' misconception automatically on linear kinematics with a four-tier instrument test," *Physics Education*, vol. 53, no. 4, article 045022, 2018.

Retraction

Retracted: Evaluation and Analysis of Assisted Instruction and Ability Improvement Based on Artificial Intelligence

Journal of Sensors

This article has been retracted by Hindawi following an investigation undertaken by the publisher [1]. This investigation has uncovered evidence of one or more of the following indicators of systematic manipulation of the publication process:

(1) Discrepancies in scope

(2) Discrepancies in the description of the research reported

(3) Discrepancies between the availability of data and the research described

(4) Inappropriate citations

(5) Incoherent, meaningless and/or irrelevant content included in the article

(6) Manipulated or compromised peer review

The presence of these indicators undermines our confidence in the integrity of the article's content and we cannot, therefore, vouch for its reliability. Please note that this notice is intended solely to alert readers that the content of this article is unreliable. We have not investigated whether authors were aware of or involved in the systematic manipulation of the publication process.

In addition, our investigation has also shown that one or more of the following human-subject reporting requirements has not been met in this article: ethical approval by an Institutional Review Board (IRB) committee or equivalent, patient/participant consent to participate, and/or agreement to publish patient/participant details (where relevant).

Wiley and Hindawi regrets that the usual quality checks did not identify these issues before publication and have since put additional measures in place to safeguard research integrity.

We wish to credit our own Research Integrity and Research Publishing teams and anonymous and named external researchers and research integrity experts for contributing to this investigation.

The corresponding author, as the representative of all authors, has been given the opportunity to register their agreement or disagreement to this retraction. We have kept a record of any response received.

References

[1] Z. Li, Z. Guang, and W. Sun, "Evaluation and Analysis of Assisted Instruction and Ability Improvement Based on Artificial Intelligence," *Journal of Sensors*, vol. 2022, Article ID 9979275, 13 pages, 2022.

Research Article

Evaluation and Analysis of Assisted Instruction and Ability Improvement Based on Artificial Intelligence

Zhi Li [ID],[1] **Zhao Guang,**[2] **and Wen Sun** [ID][3]

[1]*Academy of Tourism and Media, Xi'an Siyuan University, Xi'an, Shaanxi 710038, China*
[2]*Academy of Business, Xi'an Siyuan University, Xi'an, Shaanxi 710038, China*
[3]*Air Force Engineering University, Xi'an, Shaanxi 710043, China*

Correspondence should be addressed to Wen Sun; jessiesun2000@163.com

Teachers are a very important part of university education. They have the responsibility of teaching and educating people, and it is also their unshakable responsibility to train all-round talents for the country. If we want to improve students' quality, we must improve teachers' teaching quality and pay attention to the research of teachers' teaching ability. This paper analyzes the connotation of artificial intelligence-assisted instruction. Then, Bayesian active learning modeling is used. This paper mainly adopts the way of questionnaire and empirical research methods and launches a basic investigation on the teaching ability of university teachers. Through investigation, the following problems are summarized: (1) insufficient self-knowledge reserve and weak teaching theoretical foundation and (2) inaccurate orientation of teaching objectives and single teaching methods. Schools need to enrich training methods, establish multiple effective mechanisms for evaluation, meet the basic requirements of each teacher, and play the role of inspiring teachers. As for teachers, they need to have a good attitude, be full of interest in teaching and educating people, have a strong sense of responsibility, and constantly improve themselves and improve themselves.

1. Introduction

This paper emphasizes the importance of task environment as the decisive factor of agent proper design. The work of artificial intelligence is explained by the definition of intelligent agent and its functions in production system, reactive agent, real-time conditional planner, neural network, and rich decision system [1]. How teachers' ability will directly affect the cultivation of students. Therefore, in order to cultivate innovative talents, teachers should improve their teaching level and teaching ability [2]. Constrained programming is a powerful paradigm for solving combinatorial search problems, which absorbs a wide range of technologies from artificial intelligence, computer science, databases, programming languages, and operational research. Based on constrained programming, the manual provides a fairly comprehensive coverage of work in all these areas, enabling readers to have a fairly accurate concept of the whole field and its potential [3]. This paper is mainly aimed at advanced undergraduates who want to engage in Bayesian network

technology and computer science. The first is what I call practitioners. Practitioners are interested in learning sufficient material on the subject to be able to assist domain experts in building Bayesian network systems [4]. Information teaching has new requirements for teachers. This paper analyzes the practical guidance, teaching reflection, and other aspects and gives which aspects to train teachers from [5]. This book shows that most of the ideas behind intelligent systems are simple and clear, and the methods used in the book have been widely tested through several courses provided by the author. The book introduces the field of computer intelligence. In university settings, this book can be used as an introductory course for computer science, information systems, or engineering departments [6]. This paper explains how matrix theory appears and effectively participates in a process and has a feasible application in game theory. Matrix technology shows itself to be essential, and their introduction can provide us with a simple and accurate method to find solutions [7]. This book emphasizes the importance of task environment as the decisive factor of

agent proper design, interprets agent learning as expanding programmer's scope in unknown environment, and shows how this role limits its design, which is beneficial to the representation of knowledge and explanatory reasoning [8]. In this paper, we review the extensive research on time representation and reasoning without focusing on any specific applications. We outline the basic problems, methods, and results in these two fields and summarize the latest developments in related fields [9]. This paper introduces the application of finite element analysis software ANSYS buckling analysis in the teaching of material mechanics. The advanced CAE method makes the column stable and makes full use of computer simulation means to make up for the lack of practice and improve students' knowledge level [10]. This paper uses neural network technology to build a teaching quality evaluation model. On the basis of introducing the neural network model and teaching quality evaluation, the paper also verifies its effect, and the results are almost the same as expected. Finally, the information processing in teaching evaluation is discussed [11]. With the development of the times, it is more and more common to add computer technology in the teaching process. This paper presents an online intelligent diagnosis and evaluation scheme based on J2EE. As an auxiliary teaching algorithm, the system has many functions such as teaching, diagnosis, testing, and feedback through automatic modification of subjective and objective questions and personalized design of diagnosis results [12]. In the past decade, many computer-based interactive physics programs have emerged at the university level. This paper considers one such project, the Cognitive and Emotional Results Studio Physics Program, which integrates the initial implementation of the unified physics learning environment [13]. This article, through the teacher's trial lesson for video, let all the participants to evaluate and then put forward the teaching methods need to improve the place. The results show that their teaching ability has been improved and they have learned new teaching methods [14]. The application of electronic card in student escort is to design and build a system based on Arduino Uno microcontroller and RFID module. The system is expected to facilitate lecturers to check attendance, reduce students' habit of checking attendance, and increase the use intensity of student identification cards [15].

2. Connotation of Artificial Intelligence-Assisted Instruction

2.1. Help the Common Improvement of Machine Intelligence and Human Intelligence. In the era of artificial intelligence, machine teaching is more flexible and humanized in technology, which can effectively improve the learning ability of teachers and students. Under the future educational situation, the symbiotic evolution of man and machine will become the inevitable trend of the combination of artificial intelligence and education, and the intelligent evolution of teaching machines will certainly contribute to human understanding of nature and people. With the in-depth development of knowledge transfer, interaction, and knowledge sharing among teachers, teachers and students, and students,

massive knowledge, behavioral data, teaching tasks, and cases are spreading into the infinite wisdom sharing system, becoming the original floating force for continuous intelligent learning. At the same time, the highly intelligent teaching machine is constantly updating the comprehensive accumulation of human wisdom, using comprehensive wisdom and big data to break the blind spot of human thinking, generating a large number of new information that is difficult to extract by traditional methods, and providing it to teachers and students. Learning machines also use data storage capacity to enhance the depth and breadth of memory, improve the science and technology-art interaction between teachers and students through man-machine dialogue, support decision-making, improve the efficiency and effect of teacher education management, and expand widely the wisdom and skills of teachers and students.

2.2. Break the Dualism of Subject and Object of Education. In the era of artificial intelligence, the traditional connotation of machines has changed. First of all, machine-assisted training supported by teaching machines has become an important part of teaching and education, which almost penetrates into all directions of the training process. Intelligent machines have more and more human abilities through experiential learning and teacher feedback. Teachers and machines become each other's topics and objects in the process of education, and they coexist and develop harmoniously. Second, in the era of artificial intelligence, machine-assisted training retains the characteristics of resource carrier and computer-assisted, but with the improvement of intelligence level, machines have become teachers, and the characteristics of resources have weakened and the subjective components have increased. Machines do most of the work for human teachers, so it is difficult for students to feel the difference between real teachers and machine teachers. Third, technological innovation accelerates man-machine integration. The communication between people and machines has become smoother. Machines can provide people with arithmetic and memory support and give people the ability to think and act that they could not do before.

2.3. Promote the Cooperation and Integration of Teachers, Machines, and Students. Machine-assisted instruction in the era of artificial intelligence is dedicated to building a paradigm connecting teachers, machines, and students, emphasizing the cooperation and evolution among teachers, machines, and students, and promoting man-machine integration and teaching. In contrast, human teachers are more experienced in teaching and problem-solving. At the same time, people's advanced characteristics such as abstract thinking, logical reasoning, and learning have strong adaptability and adaptability to educational scenes, which is conducive to teaching interaction and enhances learning effect. Massive data storage, calculation, retrieval, and other functions of intelligent machines can help teachers quickly process and analyze data and perform many complex tasks on their behalf. Students who use intelligent teaching machines can get accurate personalized services, and students' feedback data can also support the improvement of machine-

assisted functions. In the era of artificial intelligence, machine-assisted education combines the interests of teachers and machine students. Human intelligence and intelligent machines capable of dichotomy, mutual adaptation, and spiral coevolution realize social cooperation. Training methods can also undergo qualitative changes.

3. Active Learning Modeling of Bayesian Extreme Learning Machine

3.1. Bayesian Extreme Learning Machine Modeling Method

3.1.1. Extreme Learning Machine. ELM is a neural network model. Its network structure is shown in Figure 1. Given N training samples $\{X \in \mathbb{R}^{N \times m}, t \in \mathbb{R}^N\}$, the regression model can be expressed as

$$\widehat{t}_i = \sum_{k=1}^M h(a_i, b_i, x_i)\beta_k, \tag{1}$$

where β_k is the output weight from the k-th hidden layer node to the output layer, a_i and b_i are the weight and offset of the i-th hidden layer node, respectively, $\widehat{t}_i$ is the predicted output of x_i, $h(\cdot)$ is the activation function, and the activation function in this paper is sigmoid function, which makes ELM have nonlinear fitting ability.

Simplify the above formula to obtain

$$\widehat{t} = H\beta, \tag{2}$$

where $\beta = [\beta_1, \beta_2, \cdots, \beta_M]^T$, $\widehat{t} = [\widehat{t}_1, \widehat{t}_2, \cdots, \widehat{t}_M]^T$, and H are hidden layer mapping matrices of ELM.

Then, the objective function of ELM is shown in

$$\min\left(\|\widehat{t} - t\|^2\right) = \min\left(\|H\beta - t\|^2\right). \tag{3}$$

The output weight calculation formula is shown in

$$\beta = H^+ t, \tag{4}$$

where H^+ is the generalized inverse of H.

3.1.2. Bayesian Extreme Learning Machine. BELM is an ELM algorithm based on Bayesian framework. Similar to ELM, the regression model of BELM can be expressed as

$$t = h\beta + \varepsilon. \tag{5}$$

The conditional probability distribution of t is shown in

$$p(t|h, \beta, \sigma^2) = N(h \cdot \beta, \sigma^2). \tag{6}$$

The probability distribution of β is shown in

$$p(\beta|\alpha) = N(0, \alpha^{-1} \cdot I), \tag{7}$$

where I is the identity matrix and α is the hyperparameter. Assuming that the prior function and likelihood function
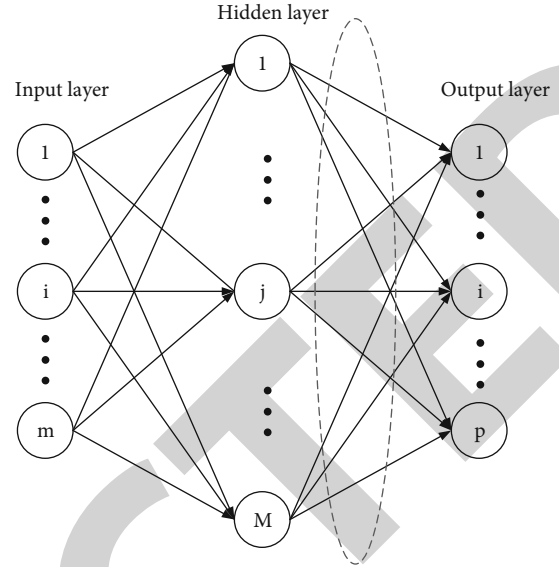
Figure 1: ELM network structure diagram.

of β obey Gaussian distribution, the maximum likelihood estimation is shown in

$$\widehat{\beta} = \sigma^{-2}SH^T t, \tag{8}$$

$$S = \left(\alpha I + \sigma^{-2}H^T H\right)^{-1}. \tag{9}$$

The parameters in the above formula need to be solved by iteration, and the specific derivation process is shown in

$$\gamma = M - \alpha \cdot tr(S), \tag{10}$$

$$\alpha = \frac{\gamma}{\widehat{\beta}^T \widehat{\beta}}, \tag{11}$$

$$\sigma^2 = \frac{\sum_{i=1}^N \left(t_i - h_i\widehat{\beta}\right)^2}{N - \gamma}. \tag{12}$$

For a given input sample x_q, the corresponding mean and variance are shown in

$$y_q = h_q\widehat{\beta}, \tag{13}$$

$$\sigma_q^2 = \sigma^2 + h_q \cdot S \cdot h_q^T. \tag{14}$$

3.2. Active Learning Methods

3.2.1. Definition of Global Variance Change. Sample sets are divided into labeled and unlabeled. n_l and n_u are the number of labeled samples and unlabeled samples, respectively, and m is the number of auxiliary variables. x_i^u is an unlabeled sample in X^U, x' is a sample to be tested, and the prediction variance change of sample to be tested x' after adding sample x_i^u in BELM model is defined as $\Delta\sigma^2(x', x_i^u)$, as shown in

Formula (15). Because the change of super parameter is not considered, this index does not depend on the actual label value of x_i^u.

$$\Delta\sigma^2\left(x', x_i^u\right) = \sigma^2\left(x'|x^L\right) - \sigma^2\left(x'\Big|\begin{bmatrix} X^L \\ x_i^u \end{bmatrix}\right). \tag{15}$$

The overall variance change of the model is defined as

$$\eta = \sum_{x' \in X} \Delta\sigma^2\left(x', x_i^u\right). \tag{16}$$

3.2.2. Sample Selection Strategy of Bayesian Extreme Learning Machine. In order to improve the efficiency of the algorithm, we propose

$$\Delta\sigma^2\left(x', x_i^u\right) = h\left(x'\right)(S_n - S_{n+1})h\left(x'\right)^T, \tag{17}$$

where $h(x')$ is the hidden layer mapping vector corresponding to x', S_n is the posterior variance of β without adding unlabeled samples, and S_{n+1} is the posterior variance of β after adding x_i^u.

Combined with formula (9), the posterior variance can be expressed as

$$S_n = \left(aI + \sigma^{-2}\left(H^L\right)^T H^L\right)^{-1}, \tag{18}$$

$$S_{n+1} = \left(aI + \sigma^{-2}\begin{bmatrix} H^L \\ h_i^u \end{bmatrix}^T \begin{bmatrix} H^L \\ h_i^u \end{bmatrix}\right)^{-1}$$
$$= \left(aI + \sigma^{-2}\left(H^L\right)^T H^L + \sigma^{-2}(h_i^u)^T h_i^u\right)^{-1}, \tag{19}$$

where h_i^u is the hidden layer mapping vector corresponding to x_i^u, the Sherman-Morrison-Woodbury criterion is used to expand formula (19), and formula (20) is obtained.

$$S_{n+1} = \left(aI + \sigma^{-2}\left(H^L\right)^T H^L\right)^{-1} - \frac{S_n\sigma^{-2}(h_i^u)^T h_i^u S_n}{1 + h_i^u S_n \sigma^{-2}(h_i^u)^T}$$
$$= S_n - \frac{S_n\sigma^{-2}(h_i^u)^T h_i^u S_n}{1 + h_i^u S_n \sigma^{-2}(h_i^u)^T}. \tag{20}$$

Formula (20) is substituted into formula (17) for simplification, and the predicted variance change amount of the sample x' to be measured after the sample x_i^u is added is shown in

$$\Delta\sigma^2\left(x', x_i^u\right) = h\left(x'\right)\frac{S_n\sigma^{-2}(h_i^u)^T h_i^u S_n}{1 + h_i^u S_n \sigma^{-2}(h_i^u)^T}h\left(x'\right)^T. \tag{21}$$
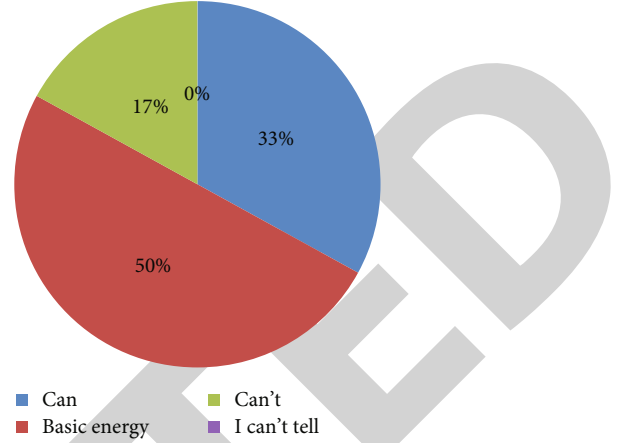
Figure 2: Degree of hardware facilities meeting teachers' teaching needs.
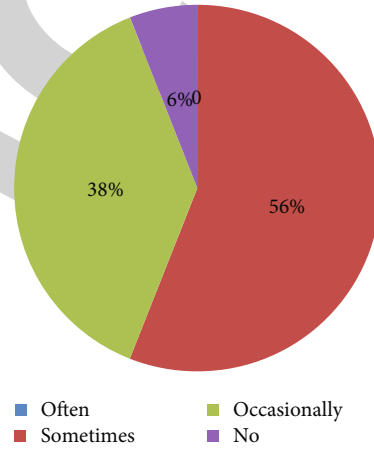
Figure 3: Failure frequency of multimedia equipment in college during class.
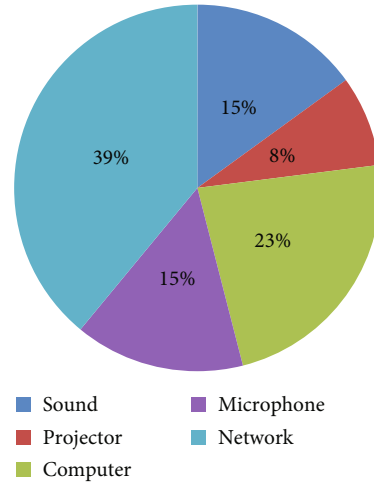
Figure 4: Hardware equipment that teachers think needs to be improved.
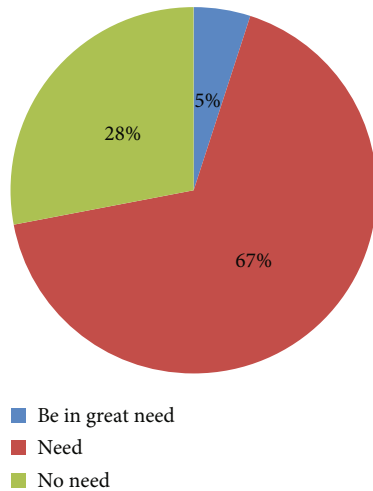
Figure 5: Teachers' training needs for multimedia technology.
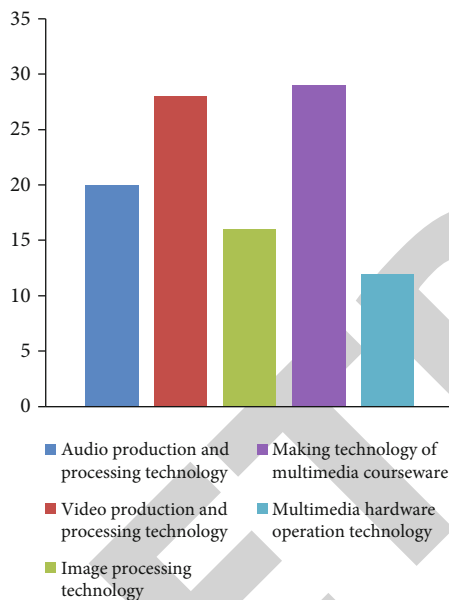
Figure 6: Teachers' demand for multimedia technology types.

By substituting formula (21) into formula (16) to further simplify η, the overall variance change η of the BELM model can be expressed as

$$\eta = \sum_{x' \in X} \Delta\sigma^2\left(x', x_i^u\right) = tr\left(h(X) \frac{S_n \sigma^{-2}(h_i^u)^T h_i^u S_n}{1 + h_i^u S_n \sigma^{-2}(h_i^u)^T} h(X)^T\right). \tag{22}$$

The BELM strategy is shown in

$$x^* = \arg\max_{h_i^u \in X^U} \eta. \tag{23}$$

The generalization performance of the model is maximized by using formula (23).
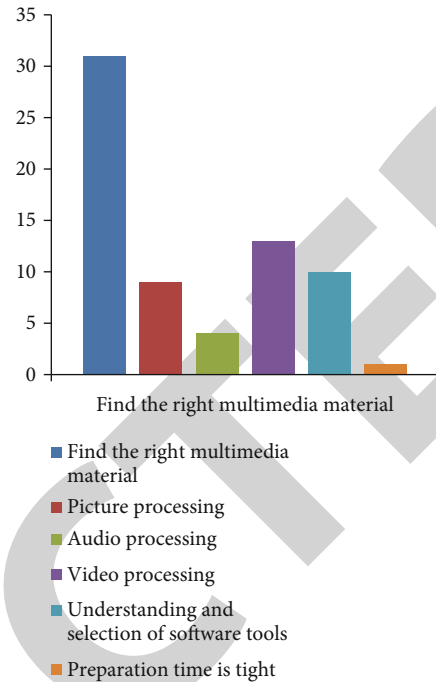
Figure 7: Difficulties encountered in the process of making courseware.
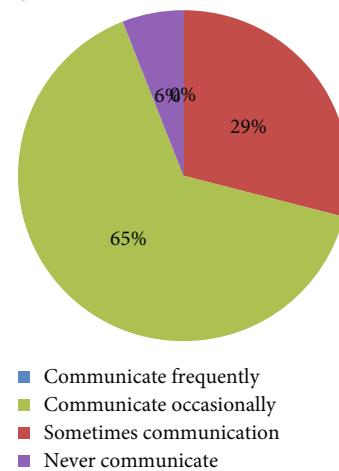
Figure 8: Teachers' communication on multimedia courseware making.

3.2.3. Modeling Process. In order to avoid the increase of operation cost, this chapter designs a batch sample selection and labeling method without considering the change of BELM model parameters. Assuming that the number of batch labeled samples in the iterative process is n_s, the BELM sample selection strategy is updated to

$$\begin{cases} X^L := \begin{bmatrix} X^L \\ x_i^u \end{bmatrix}, \\ X^U := \{x_i^u\}_{i=1,\cdots,i-1,i+1,\cdots n_u}. \end{cases} \tag{24}$$
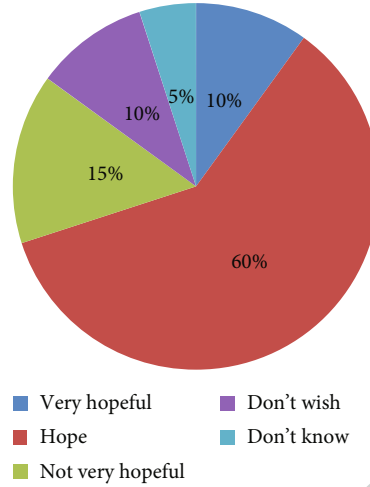
FIGURE 9: Teachers' attitude towards sharing multimedia teaching resources.

TABLE 1: KMO and Bartlett tests.

Kaiser-Meyer-Olkin metric with sufficient sampling		0.854
Bartlett's sphericity test	Approximate chi-square	4222.902
	Df	946
	Sig.	0

TABLE 2: Reliability statistics.

Scale name	Number of projects	Cronbach coefficient
Teaching cognitive ability	7	0.818
Instructional design ability	14	0.806
Teaching implementation ability	9	0.783
Teaching reflection ability	7	0.72
Teaching research ability	7	0.842
Total amount table	44	0.912

TABLE 3: Sample sources of questionnaires.

School name	Survey sample	Questionnaire recovery number	Recovery rate
Heilongjiang University	40	35	88%
Harbin Normal University	43	43	100%
Jiamusi University	50	48	96%
Harbin Engineering University	46	41	89%
Harbin University of Commerce	40	38	95%
Qiqihar University	41	41	100%
Overall	260	246	95%

After updating the training set, as shown in

$$S_n := S_n - \frac{S_n \sigma^{-2} (h_i^u)^T h_i^u S_n}{1 + h_i^u S_n \sigma^{-2} (h_i^u)^T}. \tag{25}$$

According to the updated X^L, X^U, and S_n after iteration, sample evaluation is carried out again by using formula (23), and new unlabeled samples are selected. When the number of selected unlabeled samples reaches a preset n_s, n_s unlabeled samples selected in the iteration process are labeled in batches, and BELM model parameters are reoptimized, and a new soft sensing model is established at the same time.

4. Experimental Analysis

4.1. Teachers' Needs in the Application Environment of Multimedia Technology

TABLE 4: Test of total amount table and subscale.

	KMO value	Bartlett's sphericity test
Subscale 1: teaching cognitive ability	0.799	0
Subscale 2: instructional design ability	0.88	0
Subscale 3: teaching implementation ability	0.821	0
Subscale 4: teaching reflection ability	0.825	0
Subscale 5: teaching research ability	0.84	0
Total amount table	0.895	0

TABLE 5: Summary of factor analysis results of measured questionnaire.

Subscale name	Cumulative interpretation rate	Factor name	Behavior realization	Factor load
Subscale 1: teaching cognitive ability	67.15%	Self-cognition	B1	0.832
			B2	0.8
			B3	0.793
			B4	0.771
		Student cognition	B5	0.895
			B6	0.732
			B7	0.725
			B8	0.613
		Teaching objectives	B9	0.881
Subscale 2: instructional design ability	60.73%		B11	0.661
			B12	0.677
			B13	0.751
		Teaching structure	B14	0.753
			B15	0.784
			B16	0.753
			B17	0.571
		Teaching method	B19	0.797
			B20	0.733
			B21	0.699
		Transmit teaching information	B22	0.721
			B23	0.789
			B24	0.587
Subscale 3: teaching implementation ability	65.12%	Stimulate interest in learning	B25	0.621
			B26	0.785
			B30	0.621
		Classroom regulation	B27	0.789
			B28	0.799
			B29	0.621
Subscale 4: teaching reflection ability	67.59%	Self-reflection	B31	0.543
			B32	0.912
			B33	0.558
		Reflection on teaching activities	B34	0.863
			B35	0.755
		Teaching theory research	B39	0.867
			B40	0.856
Subscale 5: teaching research ability	74.59%		B41	0.799
			B42	0.658
		Teaching practice research	B43	0.845
			B44	0.809

Table 6: Statistical table of reliability analysis of measured questionnaire.

Scale name	Number of projects	Cronbach coefficient
Subscale 1: teaching cognition	7	0.819
Self-cognition	4	0.837
Student cognition	3	0.734
Subscale 2: instructional design	12	0.875
Teaching objectives	3	0.714
Teaching structure	6	0.852
Teaching method	3	0.723
Subscale 3: teaching implementation	9	0.809
Transmit teaching information	3	0.618
Stimulate interest in learning	3	0.7
Classroom regulation	3	0.745
Subscale 4: teaching reflection	5	0.758
Self-reflection	2	0.602
Reflection on teaching activities	3	0.699
Subscale 5: teaching research	6	0.886
Teaching theory research	3	0.865
Teaching practice research	3	0.765
Total amount table	39	0.935

Table 7: Test demographic data.

Background disguise		Frequency (person)	Percentage (%)
Gender	Male	85	34.6
	Woman	161	65.4
Graduate of Fan College	Yes	101	41.1
	No	145	58.9
Age	Under 30 years old	74	30.1
	31-35 years old	95	38.6
	36-40 years old	77	31.3
Teaching experience	Less than one year	50	20.3
	2-3 years	69	28
	4-5 years	22	8.9
	Over 5 years	105	42.7
Educational background	College and below	0	0
	Undergraduate	14	5.7
	Master graduate student	125	50.8
	Doctoral students	107	43.5
Professional title	Teaching assistants	31	12.6
	Lecturer	143	58.1
	Associate professor	44	17.9
	Teachers	28	11.4
Type of institution	Double first-class universities and colleges	86	34.9
	Double first-class colleges and universities	83	33.7
	Nondual institutions	91	31.4

TABLE 8: Statistical table of work stress of respondents.

		Frequency	Percentage	Effective percentage
	Very large	50	20.3	20.3
	Larger	99	40.2	40.2
Effective	General	85	34.6	34.6
	Less	4	1.6	1.6
	No	8	3.3	3.3
	Total	246	100	100

TABLE 9: Statistical table of respondents' reasons for choosing jobs.

		Frequency	Percentage	Effective percentage
	Personal interest	62	25.2	25.2
	The wishes of parents and others	53	21.5	21.5
Effective	Professional restriction	28	11.4	11.4
	The occupation is relatively stable	103	41.9	41.9
	Total	246	100	100
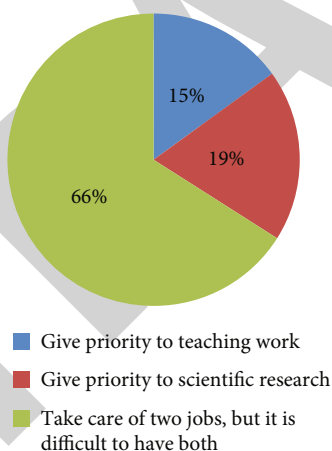
FIGURE 10: Emphasis of respondents on scientific research and work.

4.1.1. Survey of Demand for Multimedia Facilities. Looking at Figures 2–4, we can draw that 94% of teachers said that they would encounter multimedia equipment failure in the teaching process. In the investigation of whether the equipment can meet the teaching needs, almost all teachers think that it can meet their teaching needs. Multimedia equipment is the basic material of artificial intelligence-assisted teaching. Schools should provide teachers with a good teaching environment to ensure the normal teaching.

In the investigation of what aspects of multimedia equipment need to be improved, teachers put forward that the network environment, computer configuration, projector, microphone, and audio need to be optimized.

4.1.2. Investigation on Teachers' Demand for Multimedia Technology. Through the data in Figures 5–7, we can know

that most teachers are not confident in their multimedia technology and need to receive training.

4.1.3. Investigation on Teachers' Sharing of Resources. Observing the results in Figures 8 and 9, we can know that most teachers have little communication on courseware making, which is very unfavorable to the sharing of excellent teaching resources, and will lead to the reduction of teachers' teaching efficiency. In the same courseware making process, if teachers communicate more, they will save a lot and effectively improve courseware making.

In the investigation of resource sharing, most teachers still hope to share resources, because sharing resources is related to the protection of teachers' labor achievements, which can be solved by establishing courseware material resource library. Teachers can voluntarily upload the
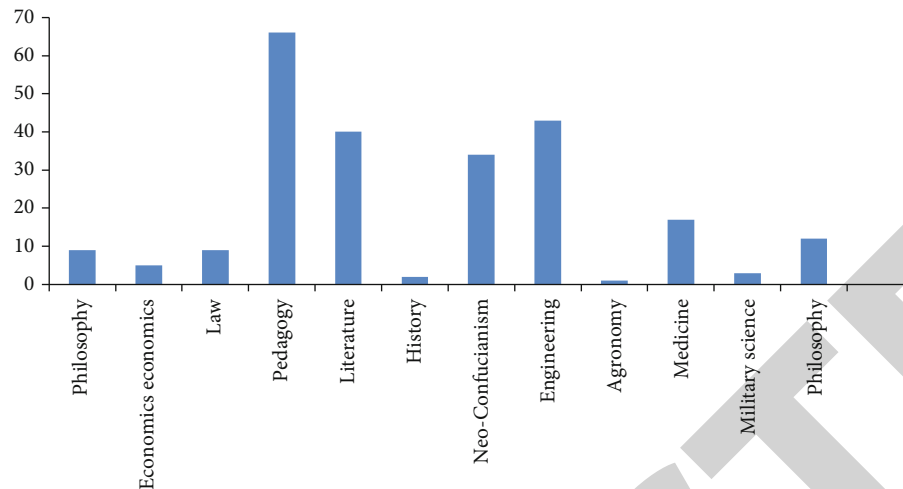
FIGURE 11: Distribution of teaching fields of respondents.

TABLE 10: Descriptive statistical analysis.

	Sample size	Maximum value	Minimum value	Average	Standard deviation
Subscale 1: teaching cognition ability	246	1	3	2.4123	0.36967
Self-cognition	246	1	3	2.3325	0.43911
Student cognition	246	1	3	2.5786	0.42901
Subscale 2: instructional design ability	246	1	3	2.5843	0.35199
Teaching objectives	246	1	3	2.4702	0.44033
Teaching structure	246	1	3	2.6463	0.38632
Teaching method	246	1	3	2.4255	0.42336
Subscale 3: teaching implementation ability	246	1	3	2.3785	0.38577
Transmit teaching information	246	1	3	2.5542	0.42217
Stimulate interest in learning	246	1	3	2.1667	0.52748
Classroom regulation	246	1	3	2.0146	0.49366
Subscale 4: teaching reflection ability	246	1	3	2.4236	0.42147
Self-reflection	246	1	3	2.4472	0.51035
Reflection on teaching activities	246	1	3	2.3058	0.44635
Subscale 5: teaching research ability	246	1	3	2.0935	0.55661
Teaching theory research	246	1	3	1.9702	0.66121
Teaching practice research	246	1	3	2.2168	0.5714
Total amount table	246	1	3	2.4128	0.31983

courseware they are willing to share to the resource library, which not only improves the efficiency of making courseware but also protects the success of teachers.

4.2. Subjects and Contents of the Survey

4.2.1. Validity Analysis of Pretest Questionnaire. Usually, we judge whether a data is suitable for factor analysis according to KMO value and Bartlett spherical test.

Using this analysis method, the results are shown in Table 1.

From the data obtained in Table 1, it can be found that the prequestionnaire structure is very good, which is especially suitable for factor analysis.

4.2.2. Reliability Analysis of Pretest Questionnaire. Whether the research results are stable or not is usually tested by reliability. According to this principle, the results in Table 2 are obtained:

Looking at Table 2, we can conclude that the questionnaire is very trustworthy and has very high internal consistency, which can be carried out as a formal questionnaire.

4.2.3. Investigation and Analysis of Measured Questionnaires. After we preinvestigated the questionnaire in the previous section, we can start the formal questionnaire survey. This time, the method of sampling survey was selected, as shown in Table 3.

TABLE 11: Summary of teaching ability results of teachers of different genders.

		F	Sig.	T value	Degree of freedom	Significance (bilateral)	Mean difference
Subscale 1: teaching cognition ability	Assuming methods are equal	1.067	0.303	1.162	244	0.247	0.4027
	Assuming methods are not equal			1.155	168.303	0.25	0.4027
Subscale 2: instructional design ability	Assuming methods are equal	0.776	0.379	-0.603	244	0.547	-0.3422
	Assuming methods are not equal			-0.594	163.404	0.554	-0.3422
Method design	Assuming methods are equal	7.795	0.006	-1.856	244	0.065	-0.3145
	Assuming methods are not equal			-1.688	132.324	0.094	-0.3145
Subscale 3: teaching implementation ability	Assuming methods are equal	2.37	0.125	-1.22	244	0.224	-0.56719
	Assuming methods are not equal			-1.172	153.196	0.243	-0.56719
Classroom regulation	Assuming methods are equal	5.171	0.024	-1.979	244	0.049	-0.39065
	Assuming methods are not equal			-1.847	141.576	0.067	-0.39065
Subscale 4: teaching reflection ability	Assuming methods are equal	8.481	0.004	-3.036	244	0.003	-0.8437
	Assuming methods are not equal			-2.818	139.519	0.006	-0.8437
Self-reflection	Assuming methods are equal	9.944	0.002	-2.389	244	0.018	-0.32386
	Assuming methods are not equal			-2.231	141.83	0.027	-0.32386
Reflection on teaching activities	Assuming methods are equal	7.223	0.008	-2.94	244	0.004	-0.51984
	Assuming methods are not equal			-2.779	146.355	0.006	-0.51984
Subscale 5: teaching research ability	Assuming methods are equal	2.485	0.116	-1.072	244	0.285	-0.47965
	Assuming methods are not equal			-1.026	151.827	0.306	-0.47965
Theoretical research	Assuming methods are equal	5.532	0.019	-0.567	244	0.571	-0.15097
	Assuming methods are not equal			-0.544	152.724	0.587	-0.15097
Total amount table	Assuming methods are equal	2.184	0.141	-1.095	244	0.275	-1.83003
	Assuming methods are not equal			-1.063	157.428	0.29	-1.83003

In order to verify whether the presupposition theory is reasonable, we carried out factor analysis in Table 4.

The results in Table 3 show that the questionnaires all meet the criteria of factor analysis.

Factor analysis is performed on each data, and the results are shown in Table 5.

Then, the reliability analysis of the questionnaire is carried out, and the results are shown in Table 6:

Looking at Table 6, we can conclude that the reliability of the data is very good, and we can continue the next research.

4.3. Analysis of Survey Results

4.3.1. Analysis of Demographic Variables. Looking at Tables 7 and 8, we conclude that most teachers are stressed, and only a small part are not stressed.

From Table 9, we can conclude that most people choose the profession of teachers because it is more stable than other industries, and only a few people are forced to choose the profession of teachers because of professional problems.

Looking at Figures 10 and 11, we can find that most teachers still choose both scientific research and teaching, so we can know that weighing the direct weight of the two is a big problem for teachers.

4.3.2. Analysis of the Overall Situation of Teachers' Teaching Ability. Through descriptive analysis of teachers' teaching ability, we get Table 10.

From the overall situation, it shows that teachers' teaching ability is still very high. Only the low score of teaching theory shows that teachers' cognition in this aspect is not enough and needs to be improved.

4.3.3. Difference Analysis under Different Variables. Differences between genders are as follows.

Table 11 shows that the gender differences make teachers have obvious scores in teaching ability. Among them, the differences in instructional design are mainly reflected in the design and selection of teaching methods. The differences in teaching implementation are mainly reflected in the adjustment and control of classroom, the differences in teaching reflection are mainly reflected in teachers' self-reflection and reflection on teaching activities, and the differences in teaching research are mainly reflected in teachers' theoretical research.

4.3.4. Differences between Different Educational Backgrounds. Observing Table 12 shows that teachers with different educational backgrounds are different in all aspects, and the main difference is reflected in cognition.

According to the above research, we can conclude that there are significant differences in gender, graduation from normal colleges, professional titles, teaching years, and work pressure, which shows that these factors have certain influence on the improvement of teachers' teaching ability. Therefore, schools should consider the above factors in the

TABLE 12: Summary of teaching ability results under different educational backgrounds.

		F	Sig.	T value	Degree of freedom	Significance (bilateral)	Mean difference
Subscale 1: teaching cognition ability	Assuming methods are equal	16.079	0	3.837	244	0	1.25224
	Assuming methods are not equal			4.008	240.781	0	1.25224
Self-cognition	Assuming methods are equal	7.43	0.007	3.939	244	0	0.87115
	Assuming methods are not equal			4.028	230.799	0	0.87115
Student cognition	Assuming methods are equal	13.454	0	2.305	244	0.022	0.38109
	Assuming methods are not equal			2.389	237.764	0.018	0.38109
Subscale 2: instructional design ability	Assuming methods are equal	10.159	0.002	4.382	244	0	2.31417
	Assuming methods are not equal			4.603	242.414	0	2.31417
Goal design	Assuming methods are equal	4.575	0.033	3.046	244	0.003	0.51287
	Assuming methods are not equal			3.144	235.879	0.002	0.51287
Process design	Assuming methods are equal	6.344	0.012	3.688	244	0	1.08037
	Assuming methods are not equal			3.841	239.831	0	1.08037
Method design	Assuming methods are equal	4.027	0.046	2.483	244	0.014	0.40451
	Assuming methods are not equal			2.587	239.835	0.01	0.40451
Subscale 3: teaching implementation ability	Assuming methods are equal	0.451	0.503	5.178	244	0	2.21632
	Assuming methods are not equal			5.293	230.474	0	2.21632
Teaching information rack transmission	Assuming methods are equal	15.271	0	3.791	244	0	0.60601
	Assuming methods are not equal			3.945	239.387	0	0.60601
Subscale 4: teaching reflection ability	Assuming methods are equal	2.834	0.094	5.484	244	0	1.41605
	Assuming methods are not equal			5.678	237.322	0	1.41605
Reflection on teaching activities	Assuming methods are equal	8.389	0.004	5.262	244	0	0.86719
	Assuming methods are not equal			5.482	239.889	0	0.86719
Subscale 5: teaching research ability	Assuming methods are equal	1.775	0.184	4.662	244	0	1.93745
	Assuming methods are not equal			4.62	208.361	0	1.93745
Theoretical research	Assuming methods are equal	0.034	0.853	4.626	244	0	1.14278
	Assuming methods are not equal			4.636	216.78	0	1.14278
Total amount table	Assuming methods are equal	1.672	0.197	6.048	244	0	9.13622
	Assuming methods are not equal			6.243	235.856	0	9.13622

selection and training of teachers, including the cultivation and promotion of teaching ability.

5. Concluding Remarks

The educational level of school teachers will directly affect the educational quality of school staff and will also affect the employment and future development of students. It is a very important subject to improve the teaching ability of college teachers at present. This study mainly focuses on improving teachers' teaching ability. Based on the actual situation of teachers in colleges and universities, through questionnaire survey, personal interview, and data collection, we can understand the first-hand information of teachers' training and summarize the present situation. Based on the relevant literature, this paper analyzes the factors affecting the improvement of young college teachers' teaching ability from the aspects of education administration, schools, and teachers and puts forward corresponding development strategies. The purpose of this paper is to find an effective way to improve the teaching ability of college teachers and then improve the quality of personnel training and help the progress of education.

Data Availability

The experimental data used to support the findings of this study are available from the corresponding author upon request.

Conflicts of Interest

The authors declared that they have no conflicts of interest regarding this work.

References

[1] P. Norvig and S. Russell, "Artificial intelligence: a modern approach (all inclusive), 3/E," *Applied Mechanics & Materials*, vol. 263, no. 5, pp. 2829–2833, 1995.

Hindawi

Retraction

Retracted: Variation Factors and Dynamic Modeling Analysis of Tennis Players' Competitive Ability Based on Big Data Mining Algorithm

Journal of Sensors

This article has been retracted by Hindawi following an investigation undertaken by the publisher [1]. This investigation has uncovered evidence of one or more of the following indicators of systematic manipulation of the publication process:

(1) Discrepancies in scope

(2) Discrepancies in the description of the research reported

(3) Discrepancies between the availability of data and the research described

(4) Inappropriate citations

(5) Incoherent, meaningless and/or irrelevant content included in the article

(6) Manipulated or compromised peer review

The presence of these indicators undermines our confidence in the integrity of the article's content and we cannot, therefore, vouch for its reliability. Please note that this notice is intended solely to alert readers that the content of this article is unreliable. We have not investigated whether authors were aware of or involved in the systematic manipulation of the publication process.

Wiley and Hindawi regrets that the usual quality checks did not identify these issues before publication and have since put additional measures in place to safeguard research integrity.

We wish to credit our own Research Integrity and Research Publishing teams and anonymous and named external researchers and research integrity experts for contributing to this investigation.

The corresponding author, as the representative of all authors, has been given the opportunity to register their agreement or disagreement to this retraction. We have kept a record of any response received.

References

[1] Y. Xie, B. Bai, and Y. Zhao, "Variation Factors and Dynamic Modeling Analysis of Tennis Players' Competitive Ability Based on Big Data Mining Algorithm," *Journal of Sensors*, vol. 2022, Article ID 3880527, 8 pages, 2022.

Hindawi

Research Article

Variation Factors and Dynamic Modeling Analysis of Tennis Players' Competitive Ability Based on Big Data Mining Algorithm

Yanan Xie,[1] **Bing Bai,**[2] **and Yunpeng Zhao** [2]

[1]*School of Physical Education and Health, Hainan Tropical Ocean University, Sanya, Hainan 572000, China*
[2]*Department of Physical Education, Hainan Medical College, Haikou 570100, China*

Correspondence should be addressed to Yunpeng Zhao; 140237@stu.ahu.edu.cn

In order to fully tap the potential of tennis players, speed, strength, and endurance are further improved in physical factors. Improve the overall competitiveness of tennis to a higher level and further improve the scientific level of tennis training. This paper truly reflects the adaptability of athletes' functional state to training load. At the same time, the data mining algorithm is used to analyze the correlation between athletes and athletes in the application of techniques and tactics. The results show that timely adjustment of training plan and training load can provide a scientific and objective basis for improving the guidance of combat readiness training. At the same time, adjusting the training plan and training load provides a scientific and objective basis for further improving the guidance of combat readiness training. This paper improves the metacognitive level of athletes' participation, accurately and timely adjusts the athletes' personal goals and realistic positioning, and timely feeds back the relevant information of the competition. Only by being good at creating a competition environment can athletes give full play to their advantages and actively seek and pursue improvement in the stage of competitive ability.

1. Introduction

The characteristics of tennis determine that tennis players should have comprehensive competitive ability. The main factors affecting the competitive ability of tennis players are tactics, physical fitness, and psychology [1]. The training process of tennis players has the characteristics of long-term, systematic, and complex. This process is not only divided into different stages in time, such as sports material selection, basic training, special training, and high-level training [2]. The law of tennis competition is the concentrated embodiment of skills and tactics and their own competitive ability; the relationship between training and competition is the core to promote the positive variation of competitive ability; the variation factors of tennis players' competitive ability can be divided into self-control factors and non-self-control factors [3]. It refers to the synthesis of various physical abilities necessary for athletes to improve their sports technical and tactical level and create excellent sports

results, including athletes' body shape, physical function, physical health, and sports quality [4]. In other words, the transformation from closed scene to open scene has changed the performance and performance of athletes. This result is positive and negative [5]. The changes of tennis players' competitive ability are mainly caused by self-control factors. The best way to test athletes' sports ability level or obtain social recognition is sports competition, as well as the differences in time and space conditions between sports competition and sports training [6].

In competitive competitions, there are changes in "rhythm" and "athletes' competitive ability," that is, the change law of athletes' competitive ability in the time structure during the competition [7]. Tennis technology is an open technology. In tennis competitions with high requirements for technology and accuracy, tennis players must respond according to the situation of their opponents and move quickly and accurately to ensure the continuity of the competition [8]. The smooth realization of athletes'

competitive ability from realistic state to target state "has experienced a qualitative change from relative disorder to highly ordered structure in time and space" [9]. In terms of functional regulation, we need to examine the potential of storing and transferring substances, as well as the ability to adapt to comprehensive changes in the environment. Use some method to measure and identify the patterns found by data mining, and evaluate their effectiveness and applicability [10]. Improve the proportion of young athletes, shorten the training time, and prolong the athletes' sports career; at the microlevel, strengthen the monitoring of the scientific training process to make the training content more targeted and effective [11]. Among them, physical fitness, as an important basis for competitive ability of competitive athletes, is the basis for supporting other competitive ability elements and normal play of super level competition [12]. It is these characteristics that make footwork and physical strength play an important role in the competition, and physical strength is an important guarantee to win. The relative stability of sports technology and the uniformity of real-time strain make sports technology have a stable sports structure, which changes continuously with the site, environmental conditions, and situation of opponents [13].

According to the physical, technical, intellectual, and psychological advantages of athletes, focus on cultivating athletes' special abilities and interests in sports training. The unbalanced potential difference promotes the orderly development of competitiveness [14]. Data mining integrates the knowledge and achievements of many disciplines in the development process, so its research has produced various types of data mining methods [15]. For professional tennis players, competition training has run through the whole year, and competition has become a part of training. Form a competitive ability structure with differences, nonunity, and particularity. If the competitive ability describes the subjective situation of athletes from the content of athletes participating in training and competition, then the competitive strength is obtained from athletes through training to meet the athletes' response to the competition. This fierce competition and continuous competition is a great challenge to the physical quality and recovery ability of athletes and integrated into the process of special sports [16]. Therefore, athletes need to have high anaerobic endurance, and tennis players should have a high level of anaerobic glycolysis. This paper aims to study the changing factors of tennis players' competitive ability and data mining algorithm [17], achieve satisfactory results in the game, and even get the description of the subjective and objective conditions of game victory [18]. For long-time multishot and multiround shooting, athletes need high aerobic capacity. Aerobic endurance is the basis for athletes to quickly recover strength in the long-term competition and high-frequency events [19]. At the same time, people also judge the competitive level of athletes by observing their competitive ability in the competition and finally make a comprehensive evaluation of sports performance according to the situation of athletes' competitive ability.

This paper presents a data mining algorithm to analyze the changing factors of tennis players' competitive ability.

In short, the contributions of this paper are as follows: (1) The algorithm is a new data mining algorithm to analyze the changing factors of tennis players' competitive ability. (2) The algorithm has a wide applicability in data mining environment and has a high applicability to the analysis of tennis players' competitive ability. (3) The algorithm has a high operation efficiency, good recognition effect, and good visualization effect.

2. Related Work

McGawley et al. believed that healthy physical quality is necessary to promote health, prevent diseases, and improve daily life efficiency, including cardiopulmonary endurance, muscle endurance, muscle endurance, flexibility, and appropriate percentage of body fat. Physical quality can be divided into competitive physical quality and healthy physical quality. Competitive physical fitness refers to the body elements required by athletes to achieve excellent results in competitive competitions [20]. Hoffmann Jr. and others found that training to improve strength quality has a direct impact on the performance of tennis players. In strength training, we should increase the training of multiple muscle groups. The front of the body of excellent athletes is very strong, including chest and deltoid muscles. The posterior rotator muscle is an important muscle group, which can improve joint stability and protect joints [21].

Vescovi proposed the "comprehensive theoretical model" in their research in 2014. Due to the different degree of automation of athletes' skills, there are obvious differences in competition experience and self-consciousness, their psychological function process is destroyed, and the sports process is declining. Therefore, they stressed that the characteristics and technical level of exercise should be considered when analyzing the mechanism of "asphyxia." It is also considered that precompetition emotion is an intermediary variable in the relationship between athletes' training level and competition level [22]. Torres-Luque et al. pointed out in 2015 that there is a "stage inspection" mechanism in sports competitions, especially when the strength of athletes is comparable; the probability of this "stage inspection" phenomenon is higher [23]. da Silva and others considered the causes, phenomena, and results of a series of events in sports competitions, namely "small probability events." The competition environment, the timing of the use of sports technology, and the super level are all related to the emergence of "small probability events" in the stadium. The emergence of "small probability events" is an inevitable and irreversible phenomenon in the law of sports behavior [24].

3. Materials and Methods

Suitable load refers to the training principle of giving corresponding measured load in training according to the actual possibility of athletes, the training adaptation law of human function, and the demand of improving athletes' competitive ability, so as to achieve ideal training effect. Athletes' body will inevitably produce corresponding training effect after experiencing a certain sports load, and the body will adapt

to the load. At this time, if the sports load cannot change with the improvement of athletes' competitive level, there will be a bottleneck period. The change of space-time conditions leads to the change of the structural elements of competitive ability obtained by athletes before the competition and then leads to the change of competitive ability function. The relationship between competitiveness elements is shown in Table 1 and Figure 1. The diversity of competitive ability performance is reflected in the different achievements of the same athlete under different competition conditions, and different athletes also have different achievements under the same competition conditions. Generally speaking, physical fitness and technical tactics are the main contents of training, and there are few links of psychological training and ideological education. When athletes have similar sports ability or strength, physical quality is the key to achieve excellent sports results. Tennis players are a technology-oriented and body-based network confrontation project. Only when tennis players have comprehensive skills and strong special physical fitness can they adapt to the changeable competition situation and the needs of different venues. Tennis technology mainly includes bottom line technology, front net technology, high-pressure ball and hanging ball technology, small ball technology, and service and receiving technology. With the trend of athletes mastering fine and comprehensive technology and tactical flexibility, technology and tactics have become a balance point, and physical quality is the key to break this balance. Basically, the overall training of athletes shall be comprehensively arranged. The results of various indicators of fitness test will feed back the effectiveness of the plan. Its project characteristics determine that the unbalanced compensation of tennis players' competitive ability structure mainly focuses on the compensation of physical and tactical ability. It can be said that without good physical strength as the basis, techniques, and tactics will not play a role.

Tennis players should have comprehensive, solid, and skilled basic skills, master special skills, and practice killer mace on the basis of comprehensive technology. The tactical ability mainly focuses on their own specific playing methods and makes rational use of various tactics. Therefore, speed and quality are still the key to obtain "space-time advantage." Competing for jet lag and space advantage, whether we can catch the coming ball in advance needs speed to support. Without fast movement and reaction speed, even if the prediction is correct, it is also a passive shot, because physical quality is the basis to ensure that athletes can give full play to their technical and tactical abilities in the competition. The accuracy and subtlety of sports observation and the clarity and richness of sports imagination are the intellectual functions that tennis players need to pay attention to. Tactical literacy, brain shackles, changes in technology and tactics, and changes in hitting points are all good examples of sports intelligence. In other words, athletes' physical quality will affect their competitive level to a great extent and then affect the achievement of sports results. In normal training, in order to adapt to the fast moving speed in the competition and win valuable time for athletes, it is necessary to strengthen the training of reaction ability and

Table 1: The relation of competitive ability elements.

	Balance	Level
Skill	10.50	8.05
Physical fitness	9.72	7.18
Mind	9.02	8.19
Intelligence	8.91	8.22

increase the experience of dealing with various competition situations. Otherwise, it is either normal or unstable, and its final effect will not reach the ideal expectation. Therefore, in sports competitions, especially some special events, the requirements for athletes are normal and can give stable play to their competitive ability.

The specific motion quality parameters are shown in Table 2 and Figure 2. Tennis players are in a special stage of progress. According to sports training theory, the main task of basic training stage is to develop general sports ability. The main task is to improve their special competitiveness. The training content includes specific techniques and tactics. The increase of athletes' muscle volume is only the primary stage of strength training with additional conditions in some sports. The further improvement of power level mainly depends on the control and coordination of nervous system. Explosive power training is regarded as the training of coordination ability to a great extent. The main contents of training include basic sports ability; some basic technologies and parameters are shown in Table 3 and Figure 3.

ATP-CP is a multi-intermittent and fierce confrontation project. Its energy supply is characterized by providing 8-10 seconds of exercise time and fast and explosive energy under anaerobic conditions. From the characteristics of tennis energy supply, it is mainly provided by ATP-CP and anaerobic digestion in the short term, and the overall physical quality of individuals is also unbalanced. Only by adopting the training suitable for athletes' internal biological adaptation can we play a beneficial biological role and improve athletes' competitive ability. Individual competitive ability is the basis of training and competition, whether in individual or collective sports. It is unrealistic to change the adaptability of athletes' physical function in a short time. If you can't give full play to your technical advantages in the game, it will have a negative impact on the whole game process, resulting in the failure of the game. In sports with two or more people, the tactical combination and arrangement of coaches, based on individual competitive ability, constitute the competitive ability of the group under certain conditions. Combining theory with tennis, the basic quality of the body is not only the basis for mastering various techniques, but also the premise for using and perfecting techniques in the competition. Therefore, the good protection and play of each part of competitive ability is an important factor affecting the change of athletes' competitive ability. The change factors of competitiveness participation are shown in Table 4 and Figure 4. Although the collective project emphasizes the integration of the overall competitiveness level, it is also based on the combination and arrangement change of individual competitiveness.
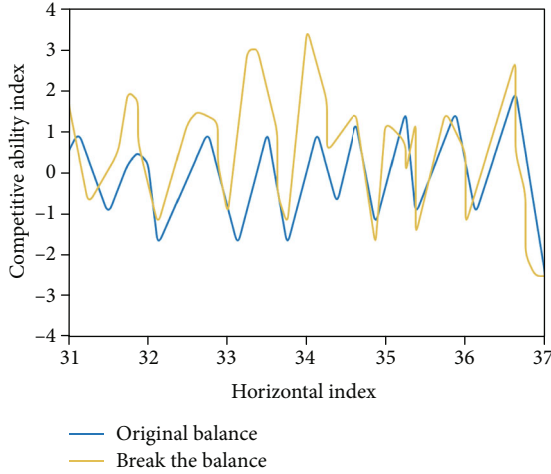
Figure 1: The relation of competitive ability elements.

Table 2: Training tasks in the special improvement phase.

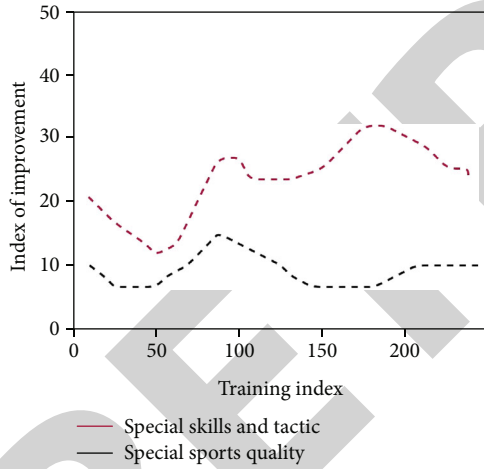|	Train	Increase
Special skills and tactics	10.08	8.06
Special sports quality	9.62	7.95

Figure 2: Training tasks in the special improvement phase.

Table 3: Training tasks in basic training stage.

	Train	Increase
Basic sports ability	15.05	13.12
Several basic technologies	10.25	9.18

4. Result Analysis and Discussion

In data mining, all data objects are first put into a group, and then a group is divided into smaller groups in each iteration until each data is recorded in a separate group or meets a condition. Through the game data collected by the data acquisition module in the tennis technical and
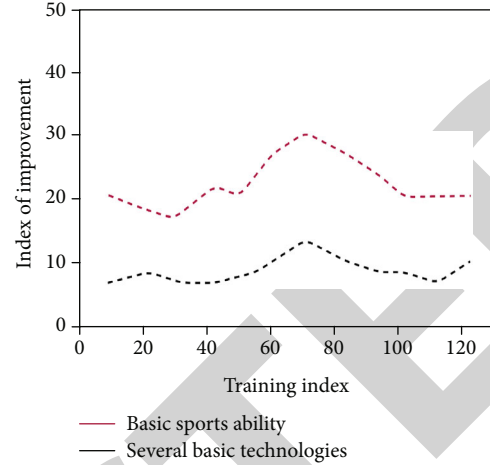
Figure 3: Training tasks in basic training stage.

tactical analysis system, the developed class library is introduced into the comprehensive analysis module to analyze the selected game. In many cases, the body is in an unbalanced state. Through core training, it can strengthen the balance and stability of the body, help prevent injury, and integrate the whole body strength to hit the ball. At the same time, it is also the main link of comprehensive strength. It plays a key role in the coordination of upper and lower limbs. If there is any unforced error, emotional disorder, psychological tension, etc. at the critical moment of the game, that is, the score, count, and game score, it is easy to lead to the failure of the game. The numerical distribution under iteration is shown in Table 5, and the data mining analysis process is shown in Figure 5. Tennis is a sport based on anaerobic metabolism. At the same time, it is also the main link of the whole army. It plays a key role in the coordination of upper and lower limbs. In many cases of hitting the ball, the body is in an unbalanced state. The function of each component of athletes' competitive ability will directly affect the result of competition, which is a direct factor affecting athletes' competitive ability. Monitoring this index will help to improve the physical exercise content of aerobic metabolism and anaerobic metabolism in time, helps prevent injuries, and integrates full body strength to hit the ball. During exercise, the proportion and quantity of lactic acid produced are large. Through core training monitoring, the balance and stability of the body can be strengthened.

In the process of evaluating the variation of tennis players' competitive ability in competition, the technical indexes can be directly substituted into the formula to calculate the positive value:

$$
\begin{aligned}
y_i &= f\left(\sum_j w_{ij} x_j - \theta_i\right), \\
O_t &= f\left(\sum_i T_{li} - \theta_l\right).
\end{aligned}
\tag{1}
$$

Table 4: Variation factors of competitive ability in competition.

	Influence	Judge
Personal factors	23.05	5.06
Psychological factor	19.13	3.27
Environmental factor	19.05	3.05
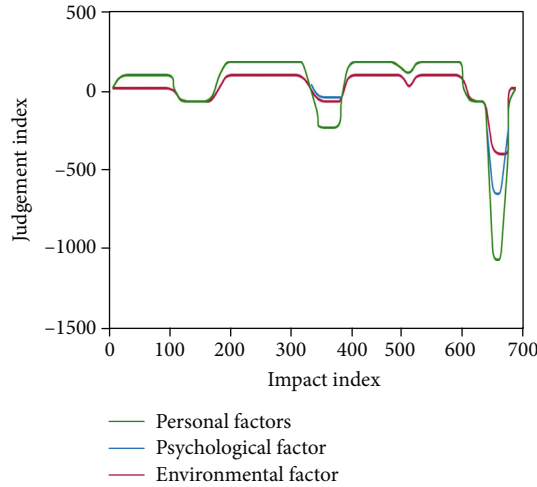
Figure 4: Variation factors of competitive ability in competition.

Table 5: Weight assignment.

	Extract	Weight
Data preparation	17.16	9.56
Association rule mining	16.52	9.13

Through various references, it is concluded that the judgment of competition variation is based on the precompetition training (or competition) results of an athlete:

$$w_{ij}(k+1) = w_{ij}(k) + \eta\delta_i x_j,$$
$$F_P = (P_A - P_B)A_P. \tag{2}$$

The variance shown by the difference in performance derived from the formula must be combined with the qualitative evaluation of coaches and athletes. Only the difference in performance is incomplete:

$$I_\omega \ddot{\delta} = F_r d - K_\omega \dot{\delta} - C_\omega \delta - K_1 e\delta. \tag{3}$$

The difference of the main body and the change of the main body's self-control factors are the direct factors leading to the variation of the competition:

$$Q_i = C_q A_i \sqrt{\frac{2\Delta P_i}{\rho}}. \tag{4}$$

Changes in the object of the game are indirect factors that contribute to the variation of the competition:

$$P_S - P_A = \frac{\rho}{2C_q^2 A_1^2} Q_1^2. \tag{5}$$

In this step of data mining, the corresponding algorithm must be selected according to the characteristics of the data itself and the functions expected to be implemented, so that the implicit mode is extracted from the data by continuously updating the weights:

$$a = f(wp + b). \tag{6}$$

To calculate the error between the nodes in the hidden layer, you need to weight the error connected to the node in the next layer:

$$n = \sum_{i-1}^{R} P_l W_{l,j} + b,$$
$$n = W * P + b. \tag{7}$$

The error of propagation is reflected by updating the weight and offset. The formula for weight update is as follows:

$$f(x) = \frac{1}{1 + e^{-x}}. \tag{8}$$

The offset is updated by the following formula. Change amount formula:

$$E_p = \frac{\sum (t_{pi} - o_{pi})^2}{2}. \tag{9}$$

The basic purpose of tennis training is competition, and competition is the most direct way and ultimate goal. Therefore, sports competition is the way to show and develop competitive ability. In order to achieve the ideal training effect, only by grasping the leading factors closely related to the specific characteristics and carrying out key training in a hierarchical and orderly manner, the structure and development of individual competitive ability can better meet the competitive needs of a certain stage. Physical fitness has become a key factor affecting the success of the competition. Therefore, we should treat the relationship between physical fitness and tactics differently and realize that physical fitness and tactics are independent in the elements of competitive ability and unified in the competition. The length of competition time also plays a role in the change process of competition. The competition process is short. If there is competition variation, the process is also short. Once it is formed, the athletes' self-regulation mechanism is difficult to play a role, especially in the case of negative variation, because time does not allow athletes to make rapid and effective judgment and adjustment. According to the characteristics of tennis, observing and analyzing the changes of athletes' body shape not only has the significance of material
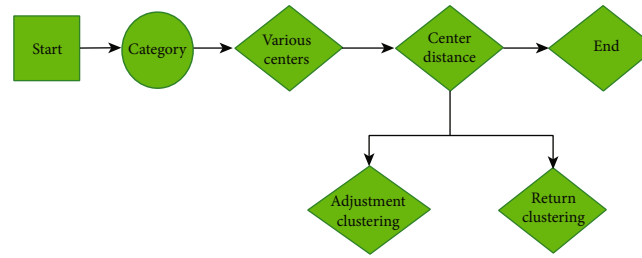
Figure 5: Data mining analysis flow chart.

selection, but also feeds back the training effect and effect from one side. At the same time, it is a platform for athletes to transform the subjective conditions of participating in competitive sports activities into objective reality, which is carried by athletes' performance and social evaluation. The significance of group variation is that it is based on individual variation and is closely related to the characteristics of different sports. Therefore, it determines the change of competitive variation among different individuals and ultimately affects the competitive process and results. In the game, save each resolved action. Through the analysis of game data, some rules can be found. The data can be saved in the string array by intercepting the data, so as to analyze the game data. The relationship between different types of changes is shown in Figure 6.

In the competition, athletes need to change the application of technology, size control, rhythm control, and emotional expression according to the changes of the field. The change of athletes' emotion plays an important role in the achievement of excellent sports results. Athletes' good emotional state in the competition is the psychological feature of competition success. It helps athletes to better tap the potential of the body, give better play to their technical level, and win the competition. The application of tennis technology requires the body to play a better role in balance, and coordination quality also plays an important role in maintaining body balance. Each training stage has its specific main training tasks. In order to accurately reflect the real situation of these systems, it is necessary to measure and evaluate specific indicators in order to achieve these indicators.

The change process of tennis players' competitive ability participation is shown in Figure 7. After the athletes have the basic competitive ability, for the athletes in the indirect confrontation group, the competition is mainly caused by objective conditions. Therefore, the phased characteristics of the development and construction of competitive ability structure determine the phased nature of the sports training process. The complete process of the development and construction of athletes' competitive ability structure is composed of multiple interrelated different training stages. Through various tennis competitions, according to the sports performance of the competition and the level of personal tennis competition, receive tennis professional training, obtain the unique sports ability of tennis, and reach a certain tennis training level. For the team athletes in direct confrontation, the subject is also due to the role of the object. The change of activity mode includes the change of time and
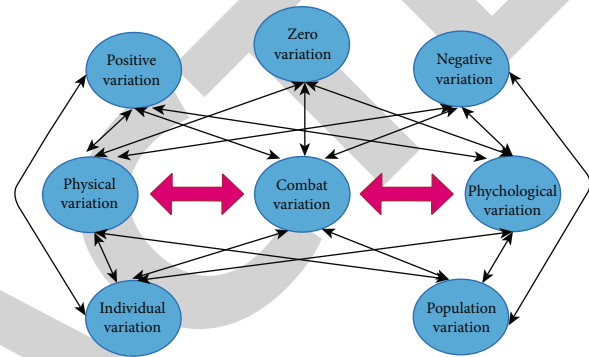
Figure 6: Interrelation among variations of different species.
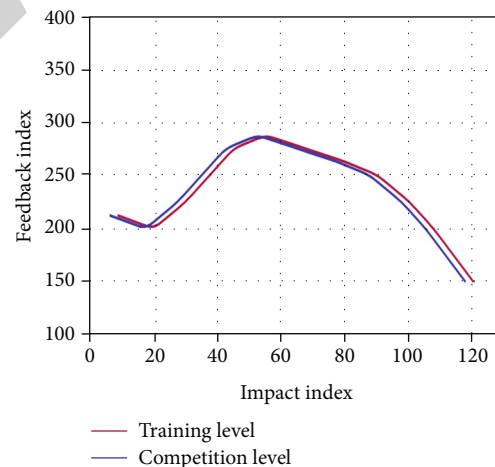
Figure 7: Variation of tennis athletes' competitive ability in competition.

space of technical action and the change of tactical adjustment. Judge the level of athletic ability of tennis players.

5. Conclusion

In tennis matches, some techniques and tactics are often used to train and improve athletes' memory, imagination, and thinking ability and help athletes make rational use of professional theoretical knowledge and correctly understand coaches' training intention, so as to greatly shorten the

process of learning and mastering sports skills. Based on data mining algorithm, this paper analyzes the changing factors of tennis players' competitive ability. Combined with the idea of data mining, this paper looks for the action combination often used by athletes in the process of competition. Technical warfare can make the project group have the characteristics of group integration and symbiosis, core technology and tactical guidance, attack and defense transition control, and bureaucratic point outbreak. The skill advantage group has the characteristics of target fear polarization and variability of variation process. People are the main body of tennis. Tennis training and competition are the research objects. In training and competition, the difference between subject and subject control factors is the direct factor leading to the competition. The strength, speed, and endurance of athletes develop with the arrangement of training contents. The improvement of flexibility is partly due to the original physical condition of athletes, and athletes have sports injuries, so there is little improvement or change. However, there is no in-depth analysis of the lack of self-control ability and countermeasures in this paper. Self-control is the stimulating factor that causes athletes' psychological response in the competition. Therefore, a series of measures should be taken in the future research.

Data Availability

The experimental data used to support the findings of this study are available from the corresponding author upon request.

Conflicts of Interest

The author declared that they have no conflicts of interest regarding this work.

References

[1] K. Goddard, C.-M. Roberts, J. Byron-Daniel, and L. Woodford, "Psychological factors involved in adherence to sport injury rehabilitation: a systematic review," *International Review of Sport and Exercise Psychology*, vol. 14, no. 1, pp. 51–73, 2021.

[2] Y. C. Liu, M. Y. Wang, and C. Y. Hsu, "Competition field perceptions of table-tennis athletes and their performance," *Journal of Human Kinetics*, vol. 61, no. 1, pp. 241–247, 2018.

[3] D. Forsdyke, A. Smith, M. Jones, and A. Gledhill, "Infographic: psychosocial factors associated with outcomes of sports injury rehabilitation in competitive athletes," *British Journal of Sports Medicine*, vol. 51, no. 7, pp. 561–561, 2017.

[4] J. A. Cotter, S. T. Jamison, S. A. Schloemer, and M. W. Chaudhari Ajit, "Do neuromuscular dentistry–designed mouthguards enhance dynamic movement ability in competitive athletes?," *Journal of Strength and Conditioning Research*, vol. 31, no. 6, pp. 1627–1635, 2017.

[5] S. P. Walker, "Self-compassion mediates the relationship between dispositional mindfulness and athlete burnout among adolescent squash players in South Africa," *South African Journal of Sports Medicine*, vol. 33, no. 1, pp. 1–6, 2021.

[6] J. Han, G. Waddington, J. Anson, and R. Adams, "Level of competitive success achieved by elite athletes and multi-joint proprioceptive ability," *Journal of Science and Medicine in Sport*, vol. 18, no. 1, pp. 77–81, 2015.

[7] L. C. Páez and I. C. Martínez-Díaz, "Training vs. competition in sport: state anxiety and response of stress hormones in young swimmers," *Journal of Human Kinetics*, vol. 80, no. 1, pp. 103–112, 2021.

[8] T. Timpka, J.-M. Alonso, J. Jacobsson et al., "Injury and illness definitions and data collection procedures for use in epidemiological studies in athletics (track and field): consensus statement," *British Journal of Sports Medicine*, vol. 48, no. 7, pp. 483–490, 2014.

[9] L. P. Adriano, V. Freitas, F. M. Arruda, M. A. Saldanha, I. Loturco, and F. N. Yuzo, "The activity profile of young tennis athletes playing on clay and hard courts: preliminary data," *Journal of Human Kinetics*, vol. 50, no. 1, pp. 211–218, 2016.

[10] T. Perri, R. Duffield, A. Murphy, T. Mabon, and M. Reid, "Competition scheduling patterns of emerging elite players in professional men's tennis," *Journal of Sports Sciences*, vol. 39, no. 18, pp. 2087–2094, 2021.

[11] J. D'Hondt, L. Chapelle, L. Van Droogenbroeck, D. Aerenhouts, P. Clarys, and E. D'Hondt, "Bioelectrical impedance analysis as a means of quantifying upper and lower limb asymmetry in youth elite tennis players: an explorative study," *European Journal of Sport Science*, vol. 2021, pp. 1–12, 2021.

[12] A. C. Cudlip, J. M. Maciukiewicz, B. L. Pinto, and C. R. Dickerson, "Upper extremity muscle activity and joint loading changes between the standard and powerlifting bench press techniques," *Journal of Sports Sciences*, vol. 40, no. 9, pp. 1055–1063, 2022.

[13] I. Jeong and S. Park, "Participation motivation and competition anxiety among Korean and non-Korean wheelchair tennis players," *Journal of Exercise Rehabilitation*, vol. 9, no. 6, pp. 520–525, 2013.

[14] C. Hausswirth, J. Louis, A. Aubry, G. Bonnet, R. Duffield, and Y. Le Meur, "Evidence of disturbed sleep and increased illness in overreached endurance athletes," *Medicine & Science in Sports & Exercise*, vol. 46, no. 5, pp. 1036–1045, 2014.

[15] C. S. Patterson, R. I. Dudley, E. Sorenson, and J. Brumitt, "Preseason functional tests discriminate injury risk in female collegiate volleyball players," *Physical Therapy in Sport*, vol. 51, pp. 79–84, 2021.

[16] L. Irineu, R. A. D'Angelo, F. Victor et al., "Relationship between sprint ability and loaded/unloaded jump tests in elite sprinters," *Journal of Strength and Conditioning Research*, vol. 29, no. 3, pp. 758–764, 2015.

[17] S. Russell, D. G. Jenkins, S. L. Halson, L. E. Juliff, and V. G. Kelly, "How do elite female team sport athletes experience mental fatigue? Comparison between international competition, training and preparation camps," *European Journal of Sport Science*, vol. 22, no. 6, pp. 877–887, 2022.

[18] R. Ramírez-Campillo, C. Henríquez-Olguín, C. Burgos et al., "Effect of progressive volume-based overload during plyometric training on explosive and endurance performance in young soccer players," *Journal of Strength and Conditioning Research*, vol. 29, no. 7, pp. 1884–1893, 2015.

[19] R. M. Malcata and W. G. Hopkins, "Variability of competitive performance of elite athletes: a systematic review," *Sports Medicine*, vol. 44, no. 12, pp. 1763–1774, 2014.

Retraction

Retracted: Correlation Analysis between Sports and Antiaging Based on Medical Big Data

Journal of Sensors

This article has been retracted by Hindawi following an investigation undertaken by the publisher [1]. This investigation has uncovered evidence of one or more of the following indicators of systematic manipulation of the publication process:

(1) Discrepancies in scope

(2) Discrepancies in the description of the research reported

(3) Discrepancies between the availability of data and the research described

(4) Inappropriate citations

(5) Incoherent, meaningless and/or irrelevant content included in the article

(6) Manipulated or compromised peer review

The presence of these indicators undermines our confidence in the integrity of the article's content and we cannot, therefore, vouch for its reliability. Please note that this notice is intended solely to alert readers that the content of this article is unreliable. We have not investigated whether authors were aware of or involved in the systematic manipulation of the publication process.

In addition, our investigation has also shown that one or more of the following human-subject reporting requirements has not been met in this article: ethical approval by an Institutional Review Board (IRB) committee or equivalent, patient/participant consent to participate, and/or agreement to publish patient/participant details (where relevant).

Wiley and Hindawi regrets that the usual quality checks did not identify these issues before publication and have since put additional measures in place to safeguard research integrity.

We wish to credit our own Research Integrity and Research Publishing teams and anonymous and named external researchers and research integrity experts for contributing to this investigation.

The corresponding author, as the representative of all authors, has been given the opportunity to register their agreement or disagreement to this retraction. We have kept a record of any response received.

References

[1] Y. Yang, "Correlation Analysis between Sports and Antiaging Based on Medical Big Data," *Journal of Sensors*, vol. 2022, Article ID 3810676, 9 pages, 2022.

Research Article

Correlation Analysis between Sports and Antiaging Based on Medical Big Data

Ying Yang ⃝iD

Wuchang University of Technology, Wuhan 430223, China

Correspondence should be addressed to Ying Yang; 120100762@wut.edu.cn

With the aging of the population in China and even in the world becoming more and more serious, China has become the country with the largest proportion of the elderly population, and a series of social problems such as health and medical care brought about by aging are being actively responded by policies. Aging has also become a natural law that human beings cannot break free from. Although exercise cannot reverse the aging process, it can weaken the adverse effects caused by aging. Having good physical quality, keeping a happy mood, comfortable living environment, and friendly social relations are the secret recipe for prolonging life and resisting cell aging. On the contrary, if physical and mental exhaustion, various chronic diseases, negative life events, bad living environment, and social relations will seriously affect human life and quality of life. Sports promote the metabolism of the whole body. Exercise can stabilize blood sugar, avoid cardiovascular diseases, and even get a good mood. At the cellular level, exercise facilitates the transmission and absorption of nutrients, thus making tissues healthier to cope with the stress of daily life. According to the statistics of loving sports and not loving sports through medical big data, the physical fitness and cell health of the elderly who love exercise every day are better than those who do not love sports. Sports are controlled by the central nervous system, and there is a correlation between changes in motor ability and cognitive impairment. Aging is accompanied by the deterioration of skeletal muscle quality and strength, which is mainly due to the rapid degradation and slow synthesis of protein in skeletal muscle. Therefore, exercise is one of the most effective ways to delay the aging of muscles and bones. According to the great potential value of medical big data, this paper analyzes and explains the correlation between sports and antiaging.

1. Introduction

At present, the sharing level of medical big data in China has not reached a higher level, which provides reference and basis for the correlation analysis between sports and antiaging, hoping to promote the transformation of medical care, medical insurance, medicine, medical research, and medical policy decision-making and help the development of related medical industries. Literature [1] tells the health problems of the elderly, and the community should set up corresponding fitness service facilities. Literature [2] tells us that sitting for a long time will accelerate the aging speed, and only exercise can maintain a healthy and youthful form. Literature [3] expounds the research and analysis of taking traditional Chinese medicine to delay aging. Literature [4] expounds the application scenarios of intelligent decision-making service

of medical information in different fields. Literature [5] states that intelligent neurosurgery has gradually entered the stage of orbital, systematic, and large-scale development. Many R&D sections, such as big data mining, machine learning/deep learning/neural network, clinical decision support system/expert system, surgical navigation, and robot, have initially matured. Related applications have covered clinical diagnosis, treatment decision-making, surgical assistance, prognosis evaluation, simulated teaching, and other scenarios of various diseases in neurosurgery, but the whole is still in its infancy. Literature [6] studies the analysis and sharing of big data in precision medicine to provide a stable data base for medical development. Literature [7] analyzes that medical big data and artificial intelligence (AI) have great potential in improving the utilization rate of medical resources and service quality, but they also bring

challenges in privacy protection and technical risks. Literature [8] studies and analyzes the accurate application of big data in cancer diagnosis and treatment, clinical medication guidance, chronic disease prevention and control, and other fields. Literature [9] shows the construction and development of medical science in the era of big data. Literature [10] expounds that artificial intelligence technology integrates big data and cloud computing in the medical industry to effectively promote the intelligent development of medical diagnosis and treatment. Literature [11] expounds the data management of hospital clinical by big data and the construction of medical engineering in literature [12]. Literature [13] expresses the application exploration of medical diagnosis under the background of big data. Literature [14] looks forward to the help of big data to the development of world medicine. Literature [15] says that intelligent medicine will eventually change the future of medicine. Literature [16] puts forward thoughts on the problems of artificial intelligence, literature [17] points out the application research of medical big data in tumors, literature [18–20] talks about the future development of artificial intelligence in the medical field, literature [21, 22] expounds the application value of medicine under the background of big data, and literature [23] applies big data to evaluate health.

2. Sports Situation of the Elderly at Home and Abroad

2.1. Sports Situation of the Elderly Abroad. After big data [24], Australia is rich in fitness activities for the elderly, among which the middle-aged and elderly sports meeting is one of the large-scale sports activities active in the middle-aged and elderly people in Australia. The development of community sports activities in the United States is mainly funded by government sponsorship or collection of membership fees. Most of the residents of the United States carry out very rich sports and physical fitness activities, which cover a wide range of exercise projects, and the quality of their activities is quite high. Japan is already the country with the highest proportion of the elderly population in the world. The elderly in Japan have relatively more leisure time, pay more attention to their physical and mental health, and tend to be able to carry out various sports and health care activities independently. In the choice of sports, they hope that the sports rules are easy to understand, the technology has certain technical content, and it is easy to learn to experience the fun of sports.

2.2. Sports Situation of the Elderly in China. With the development of the times, there are various forms of sports, but according to statistics [25], the sports choices of the elderly in China are relatively single, among which walking is the most favored by the elderly. Secondly, running, square dancing, cycling, and other activities have a wide audience. These events do not need too many skills or special sports equipment. They are the cheapest and simplest events with relatively small difficulty coefficient. Some common sports equipment in the home, such as table tennis, badminton, swimming, skipping rope, kicking shuttlecock, and other activities, are also within the scope of activities of the elderly, and a small number of elderly people with strong physical fitness will participate in some professional activities, such as mountaineering, basketball, diabolo shaking, softball, folk dance, martial arts, and health qigong (See Table 1 for details).

3. Sports Statistical Algorithm Model

3.1. Logistic Regression Model

3.1.1. General Linear Regression Model. In statistical analysis with less fluctuation, the lever value of general linear model is defined as shown in the formula:

$$h_{ii} = X(X^T X)^{-1} X_i, \tag{1}$$

where h_{ii} is the i-th diagonal element of the matrix $H = X(X^T X)^{-1} X_i$.

The target value is estimated by the least squares of the general linear model, and the predicted value $\hat{y}_i$ can be written as follows:

$$\hat{y}_i = \sum_{j=1}^{n} h_{ij} y_j = h_{ii} y_i + \sum_{j \neq i}^{n} h_{ij} y_j. \tag{2}$$

$\hat{y}$ takes the partial derivative of y_i, as follows:

$$\frac{\partial \hat{y}_i}{\partial y_i} = h_{ii}, i = 1, 2, \cdots, n. \tag{3}$$

The subsampling algorithm of general linear model is an important subsampling strategy based on normalized empirical statistical lever score of input matrix X. The calculation of sampling probability distribution is as follows:

$$\pi_I^{\text{leverage}} = \frac{h_{ii}}{\sum_{i=1}^{n} h_{ii}}, i = 1, 2, ..n. \tag{4}$$

3.1.2. Sensitivity to Misclassification. The formula for the logistic regression model is defined as follows:

$$P(y_i = 1 \mid x_i) = p_i(\beta) = \frac{\exp(x_i^T \beta)}{1 + \exp(x_i^T \beta)}. \tag{5}$$

When a certain i is selected, it is assumed that the tested event y_i is misclassified symmetrically with the probability q_i and that all other observations are correctly classified, that is, the probability of misclassification of these observations is $q_i = 0$, $j \neq i$. If the sensitivity to error classification is calculated in the presence of error classification, the probability distribution of response variables is recorded as the following formula:

$$P(y_i = 1 \mid u_i = 0) = P(y_i = 0 \mid u_i = 1) = q_i. \tag{6}$$

Table 1: Statistical table of sports project names for the elderly in community.

Sports events	Number of people	Percentage (%)
Walk	540	29.7
Running	320	17.6
Square dance	334	18.4
Table tennis	210	11.5
Skipping rope	184	10.1
Martial arts	145	7.9
Mountaineering	82	4.5

The marginal probability of observed event $y_i = 1$ is obtained as follows:

$$P(y_i = 1) = P(y_i = 1 \mid u_i = 0) + P(y_i = 1 \mid u_i = 1)$$
$$= \frac{\left(1 - q_j\right) \exp\left(x_j^T \beta\right) + q_j}{1 + \exp\left(x_j^T \beta\right)}. \tag{7}$$

When $q_i = 0$, there is a special case and there is no wrong classification. When $q_i = 1$, the opposite is true.

Since y_i is a misclassified observation, the probability of y_i being symmetrically correctly classified is as follows:

$$P(y_i = 0 \mid u_i = 0) = P(y_i = 1 \mid u_i = 1) = 1 - q_i. \tag{8}$$

The likelihood function of logistic regression is as follows:

$$L(\beta) = \Pi_{j=1}^n \Pr\left(y_j \mid x_j\right) = \Pi_{j=1}^n \left[p\left(x_j, \beta, q_j\right)^{y_j}\right]\left[1 - p\left(x_j, \beta, q_j\right)^{1-y_j}\right]$$
$$= \Pi_{j=1}^n \left[\frac{\left(1 - q_j\right) \exp\left(x_j^T \beta\right) + q_j}{1 + \exp\left(x_j^T \beta\right)}\right]^{y_j} \left[\frac{\left(1 - q_j\right) + q_j \exp\left(x_j^T \beta\right)}{1 + \exp\left(x_j^T \beta\right)}\right]^{1-y_j}. \tag{9}$$

Take the logarithm and the formula is as follows:

$$l(\beta) = \sum_{j=1}^n \left[y_j \ln \frac{\left(1 - q_j\right) \exp\left(x_j^T \beta\right) + q_j}{1 + \exp\left(x_j^T \beta + q_j\right)} + \left(1 - y_j\right) \ln \frac{\left(1 - q_j\right) \exp\left(x_j^T \beta\right)}{1 + \exp\left(x_j^T \beta + q_j\right)}\right]. \tag{10}$$

Formula (10) derives β and makes the derivative equal to zero, resulting in the scoring equation as follows:

$$\sum_{j=1}^n \left[\frac{y_j\left(1 - q_j\right) \exp\left(x_j^T \beta\right)}{\left(1 - q_j\right) \exp\left(x_j^T \beta\right) + q_j}\right.$$
$$\left. + \frac{\left(1 - y_j\right) q_j \exp\left(x_j^T \beta\right)}{q_j \exp\left(x_j^T \beta\right) + \left(1 - q_j\right)} - \frac{\exp\left(x_j^T \beta\right)}{1 + \exp\left(x_j^T \beta\right)}\right] x_j = 0. \tag{11}$$

The value of the differential of β to q_j at $q_j = 0$ is as follows:

$$\left.\frac{\partial \widehat{\beta}_i}{\partial q_i}\right|_{q_i} = (1 - 2y_i) \exp\left[(1 - 2y_i) x_i^T \widehat{\beta}\right] H^{-1} x_i. \tag{12}$$

In the above formula, the expression for H is

$$H = \sum_{j=1}^n \frac{\exp\left(x_j^T \beta\right)}{\left[1 + \exp\left(x_j^T \beta\right)\right]^2} x_j x_j^T. \tag{13}$$

3.1.3. Prediction Probability Sensitivity. Logistic regression model mainly predicts whether it is misclassified by the size of $p_i(\beta)$. Therefore, after estimating the coefficient, the prediction ability of the model can be verified according to the prediction probability $p_i(\beta)$, and the formula is as follows:

$$\widehat{p} = \frac{\exp\left(x_j^T \beta\right)}{1 + \exp\left(x_j^T \beta\right)}. \tag{14}$$

The sensitivity of wrong classification is analyzed, and the derivative of prediction probability p with respect to classification probability $\widehat{p}$ at $q_i = 0$ is taken as prediction probability, and the formula is as follows:

$$\left.\frac{\partial \widehat{p}_i}{\partial q_i}\right|_{q_{i=0}} = \left(\left.\frac{\partial \widehat{p}_i}{\partial \widehat{\beta}}\right|_{q_{i=0}}\right)' \left(\left.\frac{\partial \widehat{\beta}_i}{\partial q_i}\right|_{q_{i=0}}\right)$$
$$= (1 - 2y_i) \frac{\exp\left[2\left(1 - y_j\left(x_j^T \beta\right)\right)\right]}{\left[1 + \exp\left(x_j^T \beta\right)\right]^2}. \tag{15}$$

3.2. Subsampling Algorithm. Based on the gradient expression of loss function estimated by least squares, a self-adaptive gradient subsampling algorithm is proposed. The main steps of the algorithm are as follows.

Find the loss function of the logistic regression model of the set $\{(x_i, y_i)\}_{i=1}^n$, and the formula is as follows:

$$\vartheta(\beta, x_i) = \frac{1}{n} \sum_{i=1}^n \left[y_i \log_{p_\beta}(x_i) + \log\left\{1 - p_\beta(x_i)\right\}\right]. \tag{16}$$

The loss function is derived from β:

$$\frac{\partial \vartheta(\beta, x_i)}{\partial \beta} = \frac{1}{n} \sum_{i=1}^n \left[y_i - p_\beta(xi)\right] x_i. \tag{17}$$

The gradient formula of loss function of the i test sample is as follows:

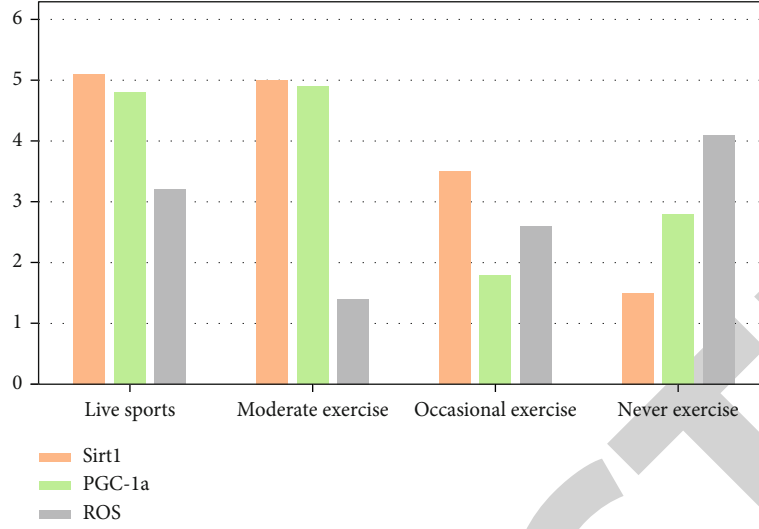$$\delta_i = \left[y_i - p_\beta(xi)\right] x_i. \tag{18}$$

Figure 1: Protein activity bar chart.

The definition of subsampling probability of the i test sample for loss function gradient is as follows:

$$\pi_i^{\delta} = \frac{|\delta i|}{\sum_{i=1}^{n} |\delta i|}. \tag{19}$$

3.2.1. Optimized Subsampling Algorithm. The asymptotic properties of weighted gradient subsampling maximum likelihood estimators for logistic regression models are studied. Given the total sample $\{(x_i, y_i)\}_{i=1}^{n}$, when the response variable satisfies certain conditions, r is the subsample size, and when $n \to \infty$, $r \to \infty$, the formula is as follows:

$$V^{-1/2}\left(\tilde{\beta} - \widehat{\beta}_{MLB}\right) \longrightarrow N(0, 1). \tag{20}$$

In the above formula, the expressions for V and V_c are as follows:

$$V = M_X^{-1} V_c M_X^{-1}, $$
$$V_c = \frac{1}{rn^2} \sum_{i=1}^{n} \frac{\left\{ y_i - \widehat{\beta}_{MLB} \right\}^2 x_i x_i^T}{\pi_i}. \tag{21}$$

The asymptotic mean square error of $\tilde{\beta}$ is equivalent to the trace of matrix V, that is,

$$\text{AMSE}\left(\tilde{\beta}\right) = tr(V). \tag{22}$$

Optimize according to the thinking mode of "A-optimality":

$$\min \ \text{AMSE}\left(\tilde{\beta}\right) = \min \ tr(V) \tag{23}$$

$tr(V)$ takes the minimum value, and the sampling probability is as follows:

$$\pi_i^{mMSE} = \frac{\left| y_i - \widehat{\beta}_{MLB} \right| \left| M_X^{-1} x_i \right|}{\sum_{i=1}^{n} \left| y_i - \widehat{\beta}_{MLB} \right| \left| M_X^{-1} x_i \right|}. \tag{24}$$

Optimize the problem and get

$$\pi_i^{MVE} = \frac{\left| y_i - \widehat{\beta}_{MLB} \right| \left| M_X^{-1} x_i \right|}{\sum_{i=1}^{n} \left| y_i - \widehat{\beta}_{MLB} \right| \left| M_X^{-1} x_i \right|}. \tag{25}$$

4. Experiment

4.1. Sample Population Selection. In the logistic regression model, samples are the most important step in the experimental study. Samples are selected from three groups: excessive sports, moderate sports, occasional sports, and never sports. The differences in sample selection also affect the final analysis results. The sample used in this study is the middle-aged and elderly people of similar age in the community. According to their sports situation, the correlation between sports and aging is analyzed.

4.2. Experimental Testing. We know that exercise can improve the activity of protein mitochondria and exercise can improve the activity expression of Sirt1 and the ability of antioxidant system. Below, we use logistic regression model to test and count the aging of the sample population by sports, as shown in Figure 1.

From Figure 1, we can know that the longevity factor Sirt1 has the highest activity in moderate exercise and can achieve antiaging effect more than other degrees of exercise. Based on logistic regression model, we count

TABLE 2: Manifestations of various parts of central nervous system.

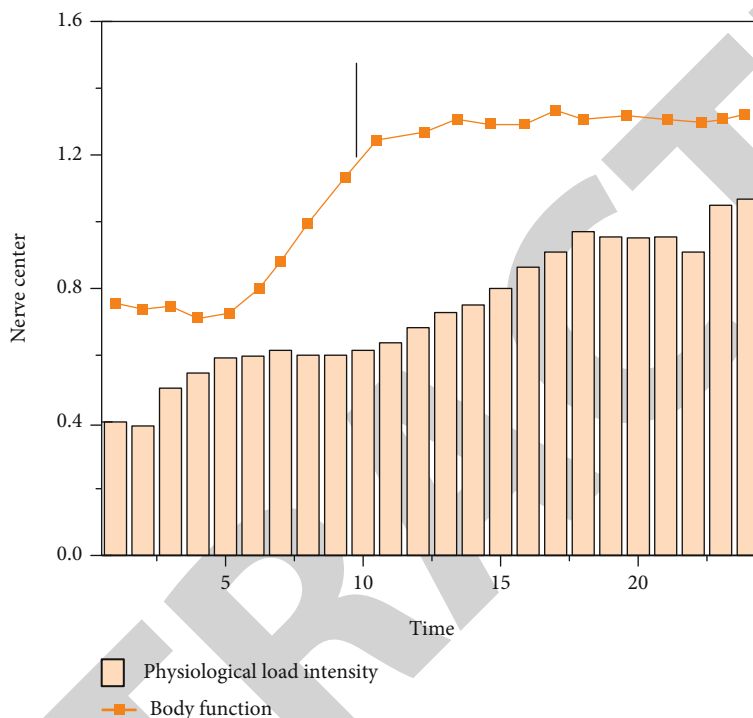| Sample population	Cerebellum	Cerebellum	Brainstem	Spinal cord
Live sports	Excellent	Good	General	General
Moderate exercise	Excellent	Excellent	Excellent	Excellent
Occasional exercise	Excellent	Good	Good	Good
Never exercise	Excellent	General	General	General

FIGURE 2: Central nervous system.

TABLE 3: Cardiopulmonary function.

Sample population	Load peak/w	VO$_2$/ml/min	Cardiopulmonary index HRR/times/points	Pulse accounts for the predicted value
Live sports	130.2 ± 38.1	1360.21 ± 340.02	37.1 ± 17.23	92.1 ± 20.01
Moderate exercise	117.3 ± 36.1	1190.21 ± 335.02	27.3 ± 15.21	82.1 ± 11.01
Occasional exercise	122.2 ± 37.2	1290.41 ± 338.09	32.1 ± 17.11	87.1 ± 20.61
Never exercise	131.2 ± 41.1	1490.21 ± 345.01	38.1 ± 19.21	92.3 ± 23.01

the central nervous system, cardiopulmonary system, and digestive system of the sample population based on medical big data as follows:

The performance of each part of the central nervous system of the sample population is shown in Table 2.

For the elderly with Alzheimer's disease, the statistical central nervous system situation after one month of appropriate exercise is shown in Figure 2.

After a month of proper exercise, the central nervous system has obviously improved, and the physical function has gradually improved.

Based on the cardiopulmonary function of the sample population with medical big data, the statistical data are shown in Table 3.

For the elderly with poor cardiopulmonary function, the statistical changes of cardiopulmonary indexes after one month's appropriate exercise are shown in Figure 3.

Figure 3 shows that proper exercise is also of great help to the elderly with poor cardiopulmonary function, and various indicators are also developing in this good direction.

Statistics of digestive system indicators of sample population based on medical big data is shown in Table 4.
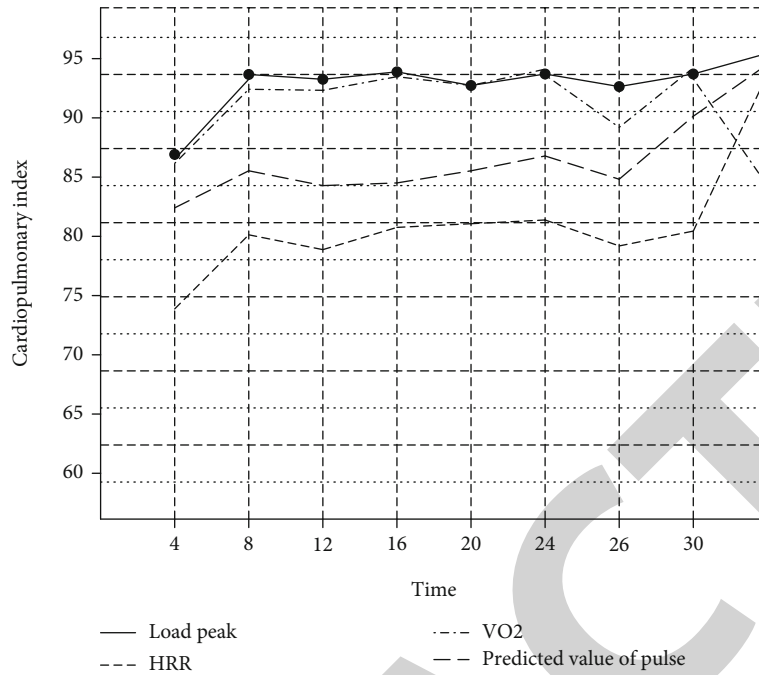
FIGURE 3: Cardiopulmonary function diagram.

TABLE 4: Digestive system.

Sample population	Digestive system index			
	Carcinoembryonic antigen	Alpha-fetoprotein	Carbohydrate antigen	Carbohydrate antigen242
Live sports	5.1	10.1	27.1	17
Moderate exercise	4.4	8.2	25.2	15.1
Occasional exercise	5.0	9.8	27.3	17.1
Never exercise	5.5	12	28.2	17.5

Based on medical big data, the sports situation of the elderly suffering from digestive diseases in the community is counted, as shown in Figure 4.

4.3. Model Comparison. We compare and analyze the logistic regression model with the subsampling model algorithm and the large sample model algorithm and analyze the correlation analysis of sports against aging through the algorithm as shown in Figure 5.

4.4. Experimental Analysis. Based on the specific research and analysis of sports and antiaging, in order to highlight the great role of sports in human aging, we selected some aging monkeys as samples, and we compared four schemes:

Scheme 1: The aging monkeys were overtrained every day, and the experimental training lasted for 3 months

Scheme 2: Training aging monkeys occasionally for 3 months

Scheme 3: The aging monkeys should exercise properly every day for 3 months

Scheme 4: The aging monkeys only watch TV every day without any training. After 3 months, we will count the heart and lung conditions of aging monkeys as shown in Figure 6

Percentage of disease (%)
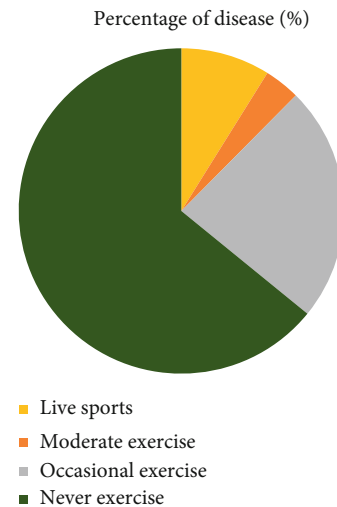
FIGURE 4: Pie chart of digestive tract diseases.

After the experimental comparison of the four schemes, only the third scheme has the smoothest and most stable cardiopulmonary indexes.
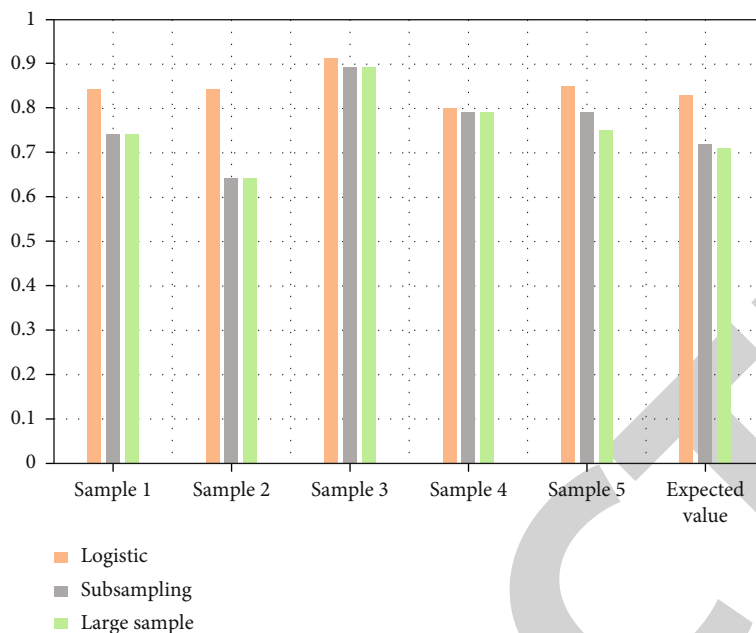
FIGURE 5: Model comparison diagram.
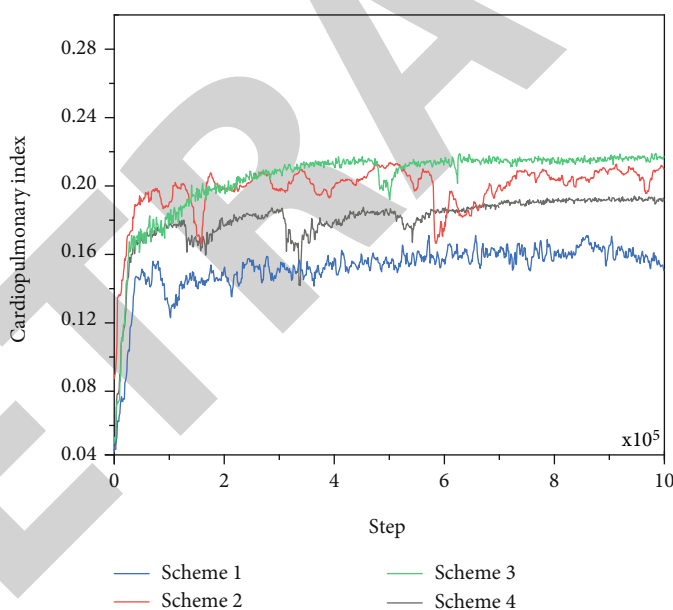
FIGURE 6: Schematic diagram of cardiopulmonary indexes.

The experimental data obtained after several months of training are shown in Figure 7.

According to the experimental comparison of five indexes of aging monkeys, the five indexes of monkeys with suitable training are indeed superior to those of monkeys with other exercise degrees, which fully confirms our experimental goals.

4.5. Contrast Test. According to the logistic regression model in the paper, we classify and compare the intensity of sports. The sports with the greatest intensity are set as rock climb-

ing, followed by basketball, tai chi, and TV. The relationship between aging and aging is analyzed, as shown in Table 5.

Table 5 lists the analysis data of aging caused by liking four different intensity sports based on logistic regression model. It can be clearly seen that not loving strenuous exercise is the most effective in antiaging, but doing some suitable physical exercise can delay the aging of the body. Of course, watching TV every day without exercise will not delay the aging of the body.

For the influence on cognitive function of the elderly with different exercise intensity, the experiment was carried out for 6 months (schematic Figure 8).
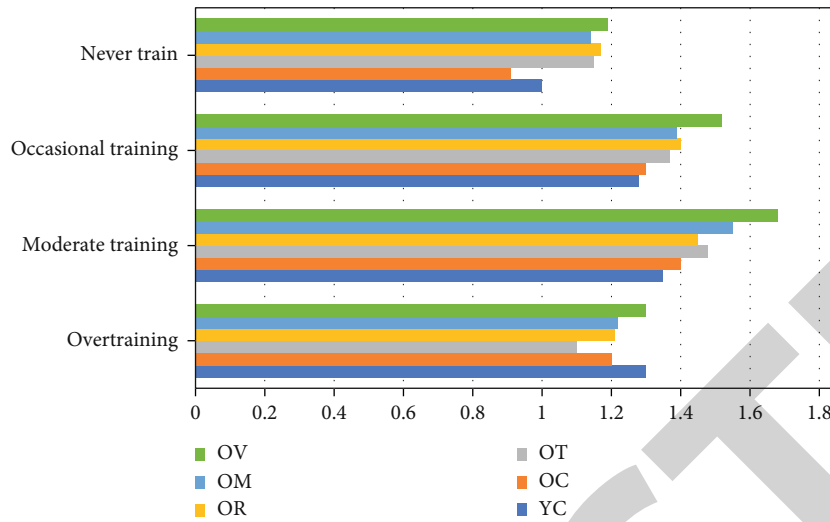
Figure 7: Comparison diagram of experimental rats.

Table 5: Comparative experiment.

| Sample population | Logistic regression model | | | |
	Number of illnesses	Health coefficient	Cell senescence	Sirt1 activity
Rock climbing	3	1.0	0.9	Stronger
Play basketball	1	0.8	0.7	Stronger
Play tai chi	0	0.6	0.8	Strong
Watch TV	3	1.2	1.5	Weak
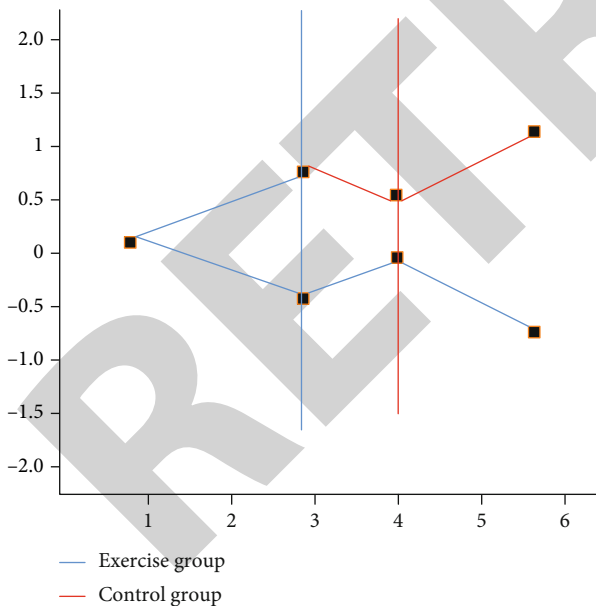
Figure 8: Influence of exercise on cognitive function of the elderly.

5. Conclusion

The increasing aging population leads to the gradual aggravation of the aging problem. Nowadays, our country has become a country of "getting old before getting rich," and aging has brought a series of social problems that need us to solve. For personal health, how to keep a healthy body and delay one's own aging is the most important thing. Through logistic regression model, this paper studies and analyzes sports and aging:

(1) We compare logistic regression model with subsample algorithm and large sample algorithm and obviously draw the conclusion that logistic regression model has more statistical significance

(2) Based on the use of medical big data, we can know that patients with poor cardiopulmonary function, digestive function, and nerve center function have improved through proper exercise

(3) For people who do not exercise, they suffer from digestive tract diseases as high as 70%, and proper exercise can improve the cognitive function of the elderly

Data Availability

The experimental data used to support the findings of this study are available from the corresponding author upon request.

Conflicts of Interest

The author declared that there are no conflicts of interest regarding this work.

Retraction

Retracted: Research on the Communication Path of Public Opinion in University Ideological and Political Network for Big Data Analysis

Journal of Sensors

This article has been retracted by Hindawi following an investigation undertaken by the publisher [1]. This investigation has uncovered evidence of one or more of the following indicators of systematic manipulation of the publication process:

(1) Discrepancies in scope

(2) Discrepancies in the description of the research reported

(3) Discrepancies between the availability of data and the research described

(4) Inappropriate citations

(5) Incoherent, meaningless and/or irrelevant content included in the article

(6) Peer-review manipulation

The presence of these indicators undermines our confidence in the integrity of the article's content and we cannot, therefore, vouch for its reliability. Please note that this notice is intended solely to alert readers that the content of this article is unreliable. We have not investigated whether authors were aware of or involved in the systematic manipulation of the publication process.

Wiley and Hindawi regrets that the usual quality checks did not identify these issues before publication and have since put additional measures in place to safeguard research integrity.

We wish to credit our own Research Integrity and Research Publishing teams and anonymous and named external researchers and research integrity experts for contributing to this investigation.

The corresponding author, as the representative of all authors, has been given the opportunity to register their agreement or disagreement to this retraction. We have kept a record of any response received.

References

[1] S. Xu, J. Liu, K. Chen, and Y. Yang, "Research on the Communication Path of Public Opinion in University Ideological and Political Network for Big Data Analysis," *Journal of Sensors*, vol. 2022, Article ID 8354909, 9 pages, 2022.

Research Article

Research on the Communication Path of Public Opinion in University Ideological and Political Network for Big Data Analysis

Shengyu Xu,[1] Jiayu Liu [1], Kan Chen,[2] and Yuling Yang[3]

[1]*School of Marxism, Sichuan University of Media and Communications, Chengdu 611745, China*
[2]*Sinoseal Holding Co., Ltd., Chengdu 610031, China*
[3]*Sichuan Institute of Administration, Chengdu 610072, China*

Correspondence should be addressed to Jiayu Liu; yura@scmc.edu.cn

In recent years, with the rapid development of information technology, the Internet has gradually become an interactive platform for people to exchange ideas, collide emotions, spread information, and release emotions. The openness, anonymity, and inclusiveness of the Internet have reduced the obstacles of information dissemination and triggered the conflict of public opinion on the Internet. In addition, students actively express their opinions, attitudes, and feelings on important topics in life and study on the Internet, forming a certain scale of online opinions reflecting students' unique political attitudes, moral concepts, and values. Because college students are immature physically and mentally and the network environment is full of phenomena, it is easy to arouse their emotional resonance. Therefore, the free and diverse network environment presents new challenges and higher requirements of the times for the stable operation of college network public opinion guidance. Therefore, how to form systematic education in universities combined with ideological and political network public opinions under big data has become an important problem to be solved. Based on this paper presents the communication pattern of network public opinion and model it, namely, the random network public opinion transmission model. By comparing the scope and influence of the two transmission paths of network public opinion, the paper draws the conclusion and strengthens the teaching practice of ideological and political courses. Finally, it is pointed out that the research of the ideological and political network public opinion communication path is a complex digital communication system project, which requires the government, the media, and the schools together to give suggestions in the guidance of the network public opinion.

1. Introduction

There are many independent sources of datasets involving big data. This paper provides an overview of HACE theory and major data processing models, including models and security concepts for private data storage, and analyzes challenging problems [1].It attempts to provide a broader definition of big data to capture its other unique and defining features. Through the definition of scholars, we propose the unification of big data, emphasizes the necessity of designing new tools for the prediction and analysis of structured big data, and designs a statistical method to infer the actual situation from sample data [2]. Advances in technology have led to the rapid development of big data in various fields, as well as the development of informal systems. This

paper provides the platform to provide readers with a picture, formulates their own plans, defines and analyze big data, introduces the Hadoop framework, and outlines the evaluation benchmarks and potential research directions for big data systems [3]. In universities, student financial aid can effectively promote student progress and improve ideological and political awareness. It serves students and can solve life problems faced by students [4].The full text analyzes the multifaceted development of students and believes that school ideological and political education is an important component of adolescent growth, the basis for mutual trust between teachers and students, and an important prerequisite for students' personality development [5].The full text expounds how the school in the new era strengthens and improves the ideological and political

education of students and clarifies the importance of cultural education in the ideological and political education of colleges and universities [6].Combined with the needs of online public opinion research, here forward the automatic detection method of hot information in the hot information list by deleting stopped words and combining multiple keywords by using Chinese word segmentation and word frequency statistics [7].The number of sudden network public opinion events has surged, leading to the extremely serious security monitoring and early warning situation of network public opinion. This paper studies the formation and influencing factors, establishes the differential equation model, and makes the corresponding measures to provide a reference for the government [8]. Public opinion is gradually forming, the traditional media also plays an important role in the network public opinion, and the public opinion and the traditional media complement each other. This paper analyzes the formation of the current traditional media public opinion [9]. Through the study of various aspects of the current emergency network public opinion, it is found that there are many problems and found the specific manifestations of the problems. The main manifestations are as follows: theory and practice need to be combined, insufficient quantitative analysis of the system and framework, lack of deep microanalysis, lack of social network structure and group behavior research, lack of visual presentation, and tracking technology application prospects are broad [10]. It uses the network data and the public opinion under the mobile environment, analyzes the communication path and the law that the news and the public opinion play an important role, analyzes the communication characteristics of the network public opinion on the network, and ensures the effectiveness of the communication [11].It present a practical and robust method for estimating time delays between process measurements using crosscorrelation functions and to make a model of the causal propagation path is proposed [12].This paper presents a new method to establish a spatial model using EKF to trace propagation paths. The DMC model describes distributed scattering in the channel, and as part of the underlying noise process, a new dynamic dimension estimator is proposed and supported by MIMO [13]This paper presents a new model of microcellular communication in urban scenarios to form a rectangular grid of buildings and streets, and the authors use relevant concepts of the image to determine the location of the diffraction points [14]. Through the analysis and research of the value of public opinion, this paper lays a foundation for further exploring the research of various public opinions under the network data mode [15].

2. Research on Public Opinion and Sentiment Communication

2.1. Communication Characteristics of Online Public Opinion in the Era of Big Data.
With the rapid development of Internet technology, computers, watches, mobile phones, and other smart terminals have been integrated together, and people have entered the field of big data technology. The new media based on the Internet has become a new social media method and an important window for the public to participate and express public opinion. The Internet is integrated into the basic elements of public opinion, such as rich information, many carriers, instant visibility, and instant distribution, and integrates the pan-media trend, display, and advanced inspection brought by the use of Internet technology, and the dissemination of network views is becoming more and more important. Because of the complexity, this goal of the network increases the difficulty of guiding public opinion. In general, the improvement of social network information in the era of big data reflects the following four characteristics. First, the network public opinion information processing is more independent. Second, the public vision of the public network end is more diversified. Third, the online public opinion dissemination is more accurate. Fourth, the network public opinion organization operates more effectively.

2.2. Characteristics of Online Public Opinion in Colleges and Universities.
(1) Special subject is as follows: the main body of college network public opinion mainly includes two parts: one is the other which is college teachers and college students. With certain education, they have certain progress in knowledge reserve and way of thinking, and their knowledge, insight, and experience have certain frontier, which makes the college teachers have over the public opinion influence in each network platform. College students have a certain knowledge reserve, sense of responsibility, curiosity, and sense of participation, but lack of social practice, thought and psychology are immature, vulnerable to bad network thoughts and behavior, so as to become the makers and disseminator of bad ideas; (2) diversified content is as follows: college teachers and students are influenced by different family, majors, interests, study, work, and other backgrounds. They focus on different contents and fields, involving all aspects of life, which are more diverse. The content of public opinions created is also diversified. (3) The transfer speed is faster. With the development of the Internet, network platforms are also constantly innovating, which has the characteristics of fast update speed, large number of users, wide user age group, and low registration threshold. As a medium, its content is highly efficient. On the one hand, the network platform has many users and shares information among various platforms; on the other hand, the continuous development of Internet technology makes information storage more portable and spread faster.

2.3. Research on Online Public Opinion Communication Mode in Universities.
The second mode of communication proposed by Lazarsfield (see Figure 1) emphasizes the role of ideological leaders in disseminating information. Similarly, it is the job of network leaders or network promoters to guide and broadcast public opinion on social media, and they play a key role in guiding the spiritual direction of public opinion.

Among these, A and B are communicators and recipients, and X is part of the social environment. This mode of communication regards the transmission process of information as a system. These three elements work together to
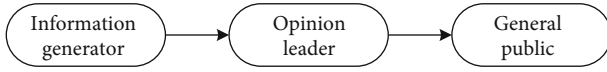
FIGURE 1: Secondary propagation pattern diagram.

emphasize the role of the social environment. In the context of online public opinion dissemination, it is not difficult to understand the relationship between topics and social objects. The role of social network analysis and social network perception is closely related to changes in social reality, and the dissemination of public opinion in network society must be analyzed on the basis of a changing process, as shown in Figure 2.

It is shown in Figure 3. In the Wesley-McLean model, A is the sender, B is the receiver, C is the "gatekeeper," and F is the data feedback process. As can be seen, data reporting and gatekeepers are important in this model. Similarly, report opinions and portal methods are very fast in the network public opinion dissemination; from the initial stage of network public opinion to the binding and final elimination of public opinion, the interactive dissemination of network information and the guidance of the gatekeeper have played a role not to be underestimated. This model emphasizes the role of gatekeepers and feedback in the communication process. Before passing to the receiver, all types of information must be filtered by the gatekeeper. The feedback from the receiver is multifaceted and can be fed back to the gatekeeper, and the gatekeeper can then feed it back to passersby, that is, the sender, or it can be directly fed back to sender.

2.4. The Relationship between Ideological and Political Affairs and Network Public Opinion. Campus emergencies form a real worldview, ideas, and values. Ideological and political education refers to the process in which teachers and scholars internalize some ideas, values, and moral norms into their own ideological and moral norms through theoretical knowledge propaganda and practical research. Both indoctrination and nurturing the mind essentially involve spiritual guidance, and the two complement each other.

3. Research on the Path Algorithm of Network Public Opinion Communication

3.1. Hypothesis of Network Public Opinion Communication Model. Assuming that in the case of a public opinion event, the total number of college students is 1, the proportion of public opinion information is $x(t)$, the proportion of public opinion information at the same time is $y(t)$, the transmission rate of people who receive public opinion information to those who do not know public opinion information is u, and the degradation rate of participating in public opinion communication is v. To build a mathematical model, in which u and v are fixed values, they are all constant values when there is a relationship with t. The proportion of the number of people increasing within t time after the information is $ux(t)y(t)$, and the proportion of people withdrawing from public opinion is $vx(t)$. It can be concluded that the total number of public opinion information dissemination
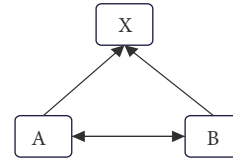
FIGURE 2: The Newcomb pattern diagram.
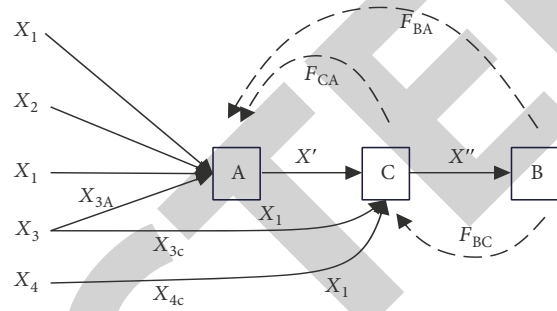
FIGURE 3: Wesley-McLean pattern diagram.

is $x(0) + ux(t)y(t) - vx(t)$; so, the increase rate of public opinion communication is the formula (1):

$$ux(t)y(t) - vx(t). \tag{1}$$

It can be concluded that the increase rate for the public opinion participants is the formula (2):

$$px(t) = (ux(t)y(t) - vx(t)). \tag{2}$$

3.2. Model Definition. When $t = 0$, set $t = 0$ at initial $x(0) = x_0$, since formulae (3)–(4) are as follows:

$$p(x(t)) = \frac{d_x}{d_t} = ux(1-x) - vx, \tag{3}$$

$$\begin{cases} \dfrac{d_x}{d_t} = ux(1-x) - vx, \\ x(0) = x_0. \end{cases} \tag{4}$$

Solve the above equation: $x(t) = $ ans, because there is $(u - v)$ in the denominator, you need to discuss whether $(u - v)$ is equal or not. When $u \neq v$ has a formula (5),

$$x(t) = \left[\frac{u}{u-v} + \left(\frac{1}{x_0} - \frac{u}{u-v} \right) e^{-(u-v)^t} \right]^{-1}. \tag{5}$$

When z has the formula (6),

$$x(t) = \frac{1}{x_0} + ut. \tag{6}$$

Organize available formula (7)

$$x(t) = \begin{cases} \dfrac{u}{u-v} e^{u-1}, u \neq v \\ \left[\dfrac{1}{x_0} + ut \right]^{-1} \end{cases}. \tag{7}$$

From this formula, it will discuss the random network public opinion transmission model. Its defined as follows: each node in the N nodes of the network can have three states: unknown state (I), gradual state (S), and idle state (R). A node that has not received the information in any network and is ready to receive it is in an unknown state. The node that has received the information and is ready to propagate it is in a progressive state. The information is received, but the nodes that are no longer interested in forwarding the message for other reasons (e. g., full storage and low power) are idle. Their densities are expressed as follows: $i(t)$, $s(t)$, and $r(t)$, respectively. It is defined as shown in formulas (8)–(10):

$$i(t) = \frac{N_i(t)}{N}, \tag{8}$$

$$s(t) = \frac{N_s(t)}{N}, \tag{9}$$

$$r(t) = \frac{N_r(t)}{N}, \tag{10}$$

where$N_i(t)$, $N_s(t)$, and $N_r(t)$ are the number of nodes in unknown time y, gradual, and idle, respectively. Furthermore, the state of each node is one of I, S, and R.Thus, one of the normalization conditions of the equation is shown in formula (11):

$$i(t) + s(t) + r(t) = 1. \tag{11}$$

All three density changes satisfy formulas (12)–(14):

$$\frac{d_i}{d_t} = -\alpha k t_i s_t, \tag{12}$$

$$\frac{d_s(t)}{d_t} = \alpha k(t)i - \beta k i s_t(s + r), \tag{13}$$

$$\frac{d_r}{d_t} = \beta k i s(s + r). \tag{14}$$

Now, assume a node moves at speed r within radius p and can detect other nodes in that range with total a nodes at N, so it can represent how many nodes a node can exchange during the move. Existing formulas (15)–(17) are as follows:

$$\rho = \frac{N}{A}, \tag{15}$$

$$S = 2r \cdot vt + \pi r^2, \tag{16}$$

$$k = S \cdot \rho, \tag{17}$$

where ρ represents the density of nodes within a region, S represents the area covered by the node moving from a to b at speed v in time, and $S \cdot \rho$ represents the number of communicable nodes k in time t. At different times, $k'(0k' \leq k)$ has different values, and hence the formula (18) is as follows:

$$k' = K(t) = [k \times P(t)], \tag{18}$$

where $P(t)$ is a probability density function, the value of $P(t)$, and the time correlation, and $[k \times P(t)]$ represents the integer part of m. In mathematics, the probability density function of a continuous random variable is the output value that describes this variable, and if there is a relationship between the two, the cumulative distribution function is the integral value of this probability density function. Replacing $K(t)$ differential equations with expressions (15)–(18) into formulas (19)–(21),

$$\frac{d_i(t)}{d_t} = -\alpha \left[\left[2r \cdot vt + \pi r^2 \right] \times P(t) \right] i(t)s(t), \tag{19}$$

$$\frac{d_s(t)}{d_t} = (\alpha - \beta) \left[2r \cdot vt + \pi r^2 \cdot \frac{N}{A} \right] \times P(t), \tag{20}$$

$$\frac{d_r(t)}{d_t} = \beta \left[\left[2r \cdot vt + \pi r^2 \cdot \frac{N}{A} \right] \times P_t \right] (s + r), \tag{21}$$

where α is the propagation is rate, and β is the ratio of the propagating state nodes.

3.3. The Algorithm Expression and Model Construction of the Propagation Path Model.

We regard the process of public opinion dissemination in the network as a dynamic process of a complex network; so, every entity involved in the dissemination of public opinion in the network is its node. In this respect, assuming that n different data coexist in the network, nodes in the network can be easily classified into ($n + 1$) classes, a set of strongly connected nodes (S) and n set of master nodes i contaminated with u data. All the public opinion information of the network can reach the highly connected nodes and other main nodes, and this o-kind of information spreads to other nodes at the propagation rate of $a_1, a_2, a_3 \cdots a_n$. When the master node accepts and accepts the new information, it becomes a new information dissemination channel. Based on the interaction between the subjects, the following mathematical equations can be generated for the subject interaction model spreading public opinion in the network, as shown in formula (22).

$$\begin{cases} \dfrac{ds(t)}{dt} = -[a_1 I_1(t) + a_2 I_2 + \cdots + a_n I_n], \\ \dfrac{dI_1(t)}{dt} = a_1 I_1 S - a_2 I_1 + a_1 I_1. \end{cases} \tag{22}$$

The algorithm rule stipulates the propagation rate a_1, $a_2, a_3 \cdots a_n \in [0, 1]$. We regard the sum of the data in the network public opinion field as "1," so that the opinions of the

public opinion subject meet the normalization conditions; as can be seen from the system of equations, the larger l, the more complex the solution of the equation. Here, simplify the model, let n to analyze the transmission of information from the established network interaction model to the dissemination of public opinion and get the formula (23)

$$\begin{cases} \dfrac{ds(t)}{dt} = -[a_1 I_1(t) + a_2 I_2 + \cdots + a_n I_n], \\[2mm] \dfrac{dI_1}{dt} = a_1 I_1 S(t) - a_2 I_2(t) I_1(t) + a_1 I_1, \\[2mm] \dfrac{dI_3(t)}{dt} = a_3 I_3(t) S(t) - a_1 I_1(t) I_3(t) + a_3 I_3(t) I_2(t). \end{cases} \tag{23}$$

Meet the algorithm rules: $S(t) = 1 - I_1(t) - I_2(t) - I_3(t)$, and then the solution equation can introduce the formula (24):

$$\begin{cases} \dfrac{dI_1(t)}{dt} = a_1 I_1 - a_2 I_2, \\[2mm] \dfrac{dI_2(t)}{dt} = a_3 I_3 - a_1 I_2. \end{cases} \tag{24}$$

Once the information in the network public opinion field is fully disseminated and interactive, we believe that the network public opinion communication system is stable, and the strong connection node group is zero. Meet the formula (26)

$$-a_2 I_2(t) I_1(t) + a_1 = a_3 I_3(t) + a_2 I_2(t) I_1(t), \tag{25}$$

$$a_3 + a_2 = -a_1 I_1(t) I_3(t) + a_3 I_3(t) I_2(t). \tag{26}$$

There is a formula (27).

$$\frac{a_1}{I_2(t)} = \frac{a_3}{I_1(t)} = \frac{a_2}{I_3(t)}. \tag{27}$$

From this, the stable solutions $I_1(t)$, $I_2(t)$, and $I_3(t)$ can be shown in formula (28)

$$\begin{cases} I_1(t) = \dfrac{a_3}{a_1 + a_2 + a_3}, \\[3mm] I_2(t) = \dfrac{a_1}{a_1 + a_2 + a_3}, \\[3mm] I_3(t) = \dfrac{a_2}{a_1 + a_2 + a_3}. \end{cases} \tag{28}$$

It can be concluded that when the diffusion rate of the three data is the same, each object receives equal data value, the distribution of network public opinion is stable, and the fluctuation range of public opinion is essentially the same; when the diffusion rate of the three different data is different, each subject has its own role.

4. Empirical Research on the Transmission Path of Online Public Opinion in Universities

4.1. Research on Online Public Opinion Data in Universities

4.1.1. Data Selection Problem. On the data selection of higher education online public opinion survey, the following questions need to be clarified: first, higher education online public opinion survey and its path is an important topic. According to statistics, a few years ago, there were more than 3,000 institutions of higher learning in China, with about 38 million students. Therefore, in order to accurately understand the context of public opinion in the ideological and political network of colleges and universities, and to formulate possible signals, it is impossible to carry out hundreds of thousands or even tens of thousands of investigations or field visits to different schools. Second, now that individuals and enterprises have the ability to collect and analyze data on a large scale, the research method of "sample = population" is no longer out of reach. Based on this, in order to make the research in this paper more global, it is decided to directly select the national data needed for this research from the database for analysis, comparison, and summary, so as to better understand the current ideological and political public opinion network in universities, and then promote the transfer of relevant exploration paths.

4.1.2. Quantitative Analysis of the Data. In 2017, Chinese Internet users spent 28 hours online a week, up 0.6 hours from 2016. According to the Tracking up Survey on Employment, Life, and Values of Chinese College Students and Graduates, the average Internet time of college students was more than five hours a day in 2016, far exceeding the average Internet time of Chinese Internet users. Students also often participate in online activities, such as China 2018 (see Table 1).

According to the table above, nearly half of people often use the Internet for information, and more than half use it for social activities. This is basically consistent with the penetration rate of Internet applications among college students as shown in the 2015 Youth Internet Behavior Research Report (see Table 2).

Table 2 shows that the Internet has become the most important source of information for students today, and students have also become important publishers of Internet information. According to the China Application Behavior Research Report of the China Internet Network Information Center, TikTok, live streaming, and Sina Weibo have become Internet applications for users to search and exchange information (Figure 4). Although most students remain sane and cautious about WeChat, many students are not aware of the complexity of the network environment and the inaccuracy of the network information.

Social contradictions are the root cause of public opinion events. How students view social contradictions determines the sensitivity, seriousness, scope, and speed of ideological and political network public opinion in colleges and universities. Students are too sensitive to social conflicts in China.

TABLE 1: Frequency of online activity among college students.

Types of activities	Never	Once in a while	Sometimes	Often
When browsing the news, understand the social developments and get the information	4.7	26.5	23.9	44.9
Keep in touch with your friends or meet new friends through the Internet	4.7	18.8	21.3	55.3
Publish your opinions and comments on some events through the Internet	21.7	39.9	23.8	14.6
Take the network as a diary, record their own mood	31.3	39.3	19.2	10.3
Play through the Internet	4.4	23.2	31.8	40.6
Learn professional or business knowledge through the Internet	4.1	25.7	40.4	29.8
Through the network to facilitate daily life, such as online shopping and online ticket booking	7.8	24.7	32.9	34.6

TABLE 2: The penetration rate of various Internet applications among college students.

Apply	Proportion
Netnews	21%
Microblog	30%
Network music	17%
Shopping online	28%
Internet finance	2%
E-mail	2%

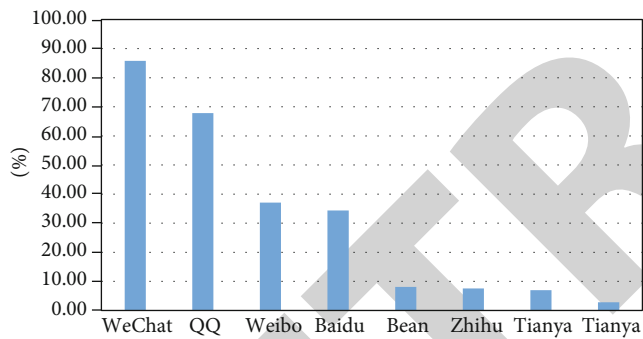FIGURE 5: College students' perception of social contradictions.

FIGURE 4: Utilization rate of major Internet applications in 2016.

More than half of the students think that the contradiction between rich and poor in China is "very serious." In fact, the contradiction of rich and poor is relatively low. Public opinion pressure is ranked in the 6 types of contradictory gathering points as shown in Figure 5.

The ordinate in Figure 5 represents the proportion of the public opinion pressure understood by college students among the six types of conflict aggregation points in China. The level of the ordinate can indicate the degree of college students' perception of social conflicts. Based on the above information, the following conclusions are preliminarily drawn: first, young college students play an important role in the dominant position of the network in China, and students live in universities; so, the two are closely related. Second, the Internet has become the main way of communication for young college students. In colleges and universities, young students publish information on the Internet to express their wishes and feelings, and young students have become the recipients and publishers of Internet information. Therefore, guiding the network public opinion

in colleges and universities helps young college students to remain focused and alert to the complex network and not be misled by intentional groups. Third, the traditional network community has become the center of the network public opinion, and the leading public opinion research in universities must examine the law of network information communication, network cluster, and network communication in the new era. Fourth, due to the relative lack of ideological and political education, young college students tend to trust the network and network information, and the identification ability is weak. It is necessary to change the traditional ideological and political ideas, modes, and methods of the characteristics of young students. Fifth, social conflict is the cause of network public opinion events, and network new media has become the main cause of public opinion events. It is of great significance to study the relationship between social conflict and online public opinion; poor young students have high risk of social conflict and low loyalty to government image. Therefore, it is necessary for the university network to clarify the direction and follow the principles.

4.2. Comparison of Public Opinion Communication Modes. When public disputes cannot be solved or controlled, it will directly lead to the outbreak of public opinion, and when public opinion breaks out, there are generally two modes of communication, specifically as follows:

First, the communication mode of network media: in today's economic and social environment, network media is the best way of communication, and the personality characteristics of modern young students give us the unique gender characteristics of network public opinion in universities.

When network public opinion or university network public opinion is formed, there are two trends: one direction is that network public opinion or university network public opinion affects the network community or the whole online community of college students. Publishers express their attitudes, opinions, comments, and feelings on the influence of public opinion on network media, further expand online public opinion, respond to public opinion events affecting public opinion, solve, promote, or amplify social conflicts; another development is that the outbreak of public opinion directly causes relevant ministries or education systems and universities to guide them, and its influence also determines the resolution, mitigation, improvement, and outbreak of contradictions. In this process, there are two more points that need to be solved. First, the emergence of new online media like Douyin and live broadcasting will gradually replace most traditional online communities. Another is college students, which can affect the whole network community, which also means that the public opinion of colleges and universities can affect the public opinion of the whole network. Second, the traditional media communication mode: the information of public opinion events is transmitted through secondary communication channels such as newspapers, television, and radio and directly causes public opinion by means of conflict resolution, mitigation, intensification, and outbreak. Public opinion information about the incident is spread to secondary media such as newspapers, television, and radio, which will directly trigger public opinion. However, compared with network public opinion, public opinion lacks channels and ways to spread to the media, which is difficult to express accurately, and the scale is obviously insufficient.

The Internet has become the main position for the outbreak of public opinion events. Taking public opinion on educational public opinion as an example, in the first exposure media of hot educational public opinion events in 2014-2016, new media and traditional media account as shown in Figure 6. It can be seen from the table that the proportion of new media is more than twice that of traditional media, which makes it necessary for universities to carry out online public opinion guidance. The dissemination method of online media has become the fastest way of disseminating online public opinion in today's economic and social environment. From 2014 to 2016, new online media has gradually replaced traditional media in the dissemination of public opinion, but traditional media is also essential less.

4.3. *Public Opinion Case Data Analysis.* According to the Annual Report on Chinese Education Public Opinion in 2016 (Figures 7 and 8), there were 381 educational public opinion events in 2014-2016, with a relatively low proportion in 2014. In 2015, it accounted for 29.7% annually, with a high growth rate and a growth rate of 18.5%. From 2015 to 2016, the education public opinion was basically stable, but the number of cases remained high at 35.2%. Among them, the share of public opinion in higher education was 38.1%, 50.0%, and 45.1%, respectively, ranking first in each education stage. Therefore, the necessity to control the path
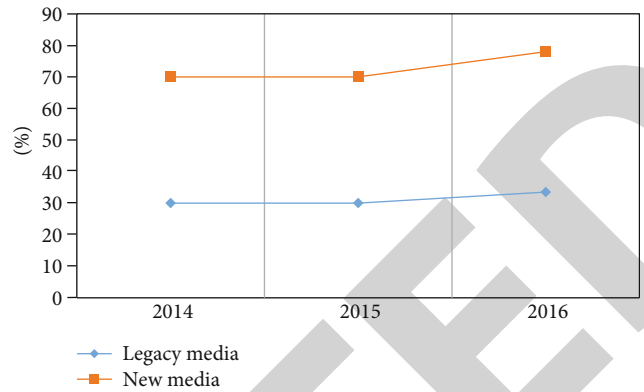
Figure 6: Comparison of the first exposure media types in the hot events of education public opinion in 2014-2016.
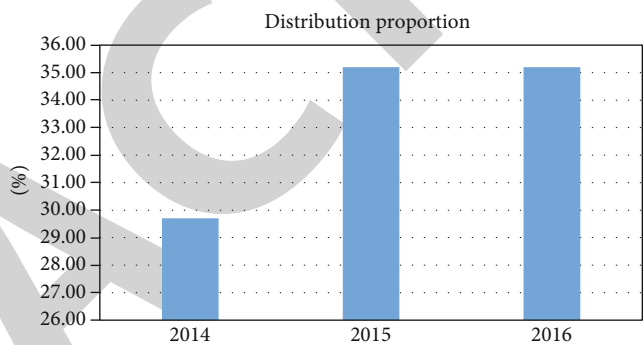
Figure 7: Annual distribution of hot events of education public opinion in 2014-2016.
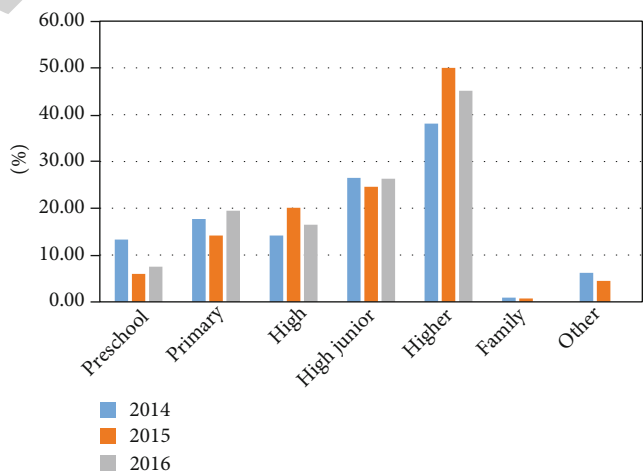
Figure 8: Annual distribution of hot public opinion events in different education stages from 2014 to 2016.

of propaganda and ideological and political public opinion in universities is obvious.

Through in-depth study of the hot topics of educational public opinion in 2014-2016, as shown in Figures 9 and 10, the annual average proportion of cases involving students, teachers, and schools in 29.4%, 22.0%, 21.4%, and 23.1, respectively, the proportion of public opinion published

Figure 9: Distribution of subjects involved in hot events of educational public opinion from 2014 to 2016.

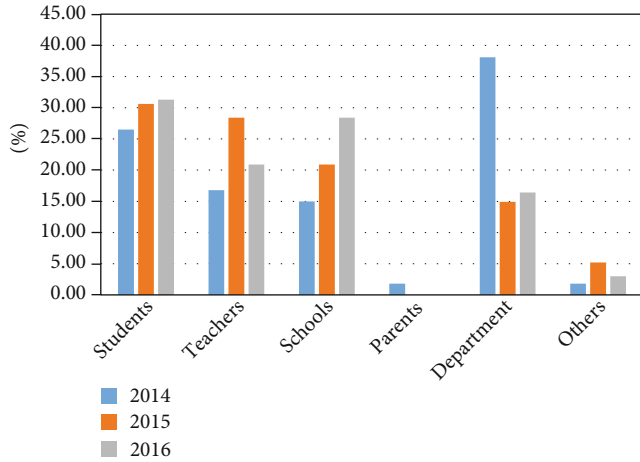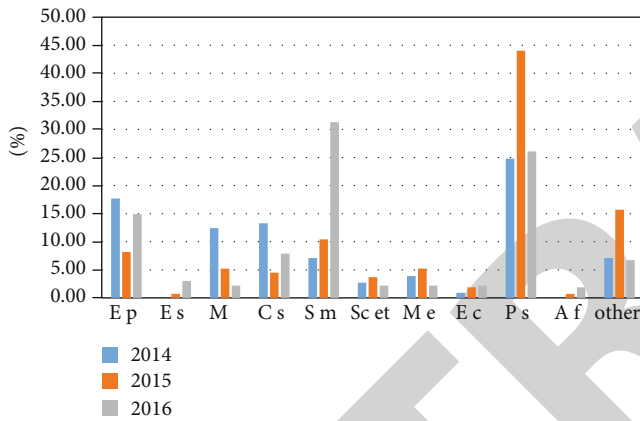Figure 10: Content distribution of hot events in education public opinion from 2014 to 2016.

Table 3: Distribution of public opinion tendency in the proportion of events from occurrence to exposure time from 2014 to 2016.

Event occurrence to the exposure time difference	Public opinion tendency		
	Front	Neutral	Downside
Exposure occurred earlier than	24.2	17.4	1.5
Occurrence and exposure	41.2	34.3	26
Within half a day	14.9	22.4	27
Half a day-1 day	9.3	12.8	12.9
2-3 days	2.6	3.7	9.9
4-6 days	2	2.2	5.1
7-15 days	2	4.4	3
15-30 days	1.1	1.2	2.7
January-March	1.1	0.9	3.2
March-June	0.7	0.3	1.9
More than half a year	0.7	0.3	6.7
Amount to	100	100	100

through words and deeds is 31.9%, 54.4%, and 57.4%, among which the proportion of students and schools has increased steadily in the past three years. Thus, it can be seen that the higher education management and ideological and moral education are relatively insufficient, the online public opinion consultation and management of such education and moral education is not enough, and the effect is not obvious.

Conduct actual statistics on the relationship between public opinion tendency and time of public opinion events and get the investigation data (see Table 3).

In Table 3, the exposure time of the case is earlier than when it happened, and the public opinion tends to be more positive. It can also be found that the negative public opinion within half a day after the incident is the peak period, and 12 hours later is the best time for the network public opinion guidance. After that, various public opinion trends gradually weaken with the passage of time. The tendency of public opinion refers to the position, point of view, interest, etc. of the public opinion disseminator towards objective facts, which are reflected either explicitly or implicitly in the media that shows completely different tendencies. Tendency also refers to the reporting opinions and basic opinions

formed by newspapers and other news media in a period of time. In Table 3, according to the size of the survey data, it can be judged whether the public opinion tendency is positive or negative or moderate sex.

4.4. Experimental Results. In the current era of big data, the main channel of public opinion communication on the ideological and political network in colleges and universities is network new media, which has a wide range and great influence. The dissemination of public opinion event information to the whole network community produces public opinion, and the dissemination to colleges and universities leads to network public opinion in colleges and universities. When there is network public opinion or network public opinion formation, network public opinion expands the university ideological teaching space, enriches the ideological teaching content, strengthens the ideological course public opinion teaching practice, and promotes positive mainstream theme and mainstream values but also have false, deception, violence, pornography, and even anti-Marx and anti-socialist speech, which lead to students' values and values confusion and distortion. Therefore, ideological and political course teachers should enrich the content of traditional political courses, conform to The Times, improve the concept of time and educational resources, strengthen online mental health education and media learning, provide ideological solutions, and improve the teaching materials of ideological and political learning.

5. Conclusion

College students are an important part of netizens. For students, the Internet is not only a source of information services but also a platform for information exchange. Through network public opinion research, especially college students' public opinion research, we can better understand students' ideological dynamics and internal needs, To provide students with targeted education, services, and guidance, to

Retraction

Retracted: Construction and Index Analysis of Whole Chain Linkage Talent Training System Based on Fuzzy AHP Model

Journal of Sensors

This article has been retracted by Hindawi following an investigation undertaken by the publisher [1]. This investigation has uncovered evidence of one or more of the following indicators of systematic manipulation of the publication process:

(1) Discrepancies in scope

(2) Discrepancies in the description of the research reported

(3) Discrepancies between the availability of data and the research described

(4) Inappropriate citations

(5) Incoherent, meaningless and/or irrelevant content included in the article

(6) Manipulated or compromised peer review

The presence of these indicators undermines our confidence in the integrity of the article's content and we cannot, therefore, vouch for its reliability. Please note that this notice is intended solely to alert readers that the content of this article is unreliable. We have not investigated whether authors were aware of or involved in the systematic manipulation of the publication process.

In addition, our investigation has also shown that one or more of the following human-subject reporting requirements has not been met in this article: ethical approval by an Institutional Review Board (IRB) committee or equivalent, patient/participant consent to participate, and/or agreement to publish patient/participant details (where relevant).

Wiley and Hindawi regrets that the usual quality checks did not identify these issues before publication and have since put additional measures in place to safeguard research integrity.

We wish to credit our own Research Integrity and Research Publishing teams and anonymous and named external researchers and research integrity experts for contributing to this investigation.

The corresponding author, as the representative of all authors, has been given the opportunity to register their agreement or disagreement to this retraction. We have kept a record of any response received.

References

[1] L. Yi and S. Yan, "Construction and Index Analysis of Whole Chain Linkage Talent Training System Based on Fuzzy AHP Model," *Journal of Sensors*, vol. 2022, Article ID 7106274, 12 pages, 2022.

Research Article

Construction and Index Analysis of Whole Chain Linkage Talent Training System Based on Fuzzy AHP Model

Liu Yi [1] **and Sun Yan** [2]

[1] *School of Management, Hunan University of Information Technology, Changsha 410151, China*
[2] *Office of Human Resources, Hunan University of Information Technology, Changsha 410151, China*

Correspondence should be addressed to Liu Yi; liuyi0706@hnuit.edu.cn

The construction and analysis of the entire chain linkage talent training system can measure the level of education and at the same time improve talents and drive development for the society. This paper uses the AHP model and CPII model to analyze the construction and index analysis of the entire chain linkage talent training system. The research shows that the weight value of personality literacy is the largest, followed by innovation literacy, emotional intelligence literacy, leadership and management ability literacy, and scientific literacy; in the analysis of the importance of the first-level indicators, it is found that most people think that personality literacy is the most important; in the consistency test of the first-level indicators, it shows that the results have good consistency; in the comment set of the second-level indicators, the highest comment value is expertise, independence and practicality, and diligence. Through the evaluation of the talent training system and its operation quality, it can provide reform ideas for education and management departments and can fully play the role of talents, create a good working atmosphere, and create suitable ways to improve capabilities. Through AHP's research on the construction of the entire chain linkage talent training system and indicators, it is found that the personality literacy has the largest weight value among the five first-level indicators. The cultivation of leadership, management ability, scientific literacy, etc. can better reflect the characteristics of talents.

1. Introduction

According to the needs of enterprises, the article forms a quality evaluation system of ability training from three aspects: basic ability, work ability, and expansion ability, which consists of 15 sub-indicators. The evaluation results are analyzed by data envelopment analysis (DEA), fuzzy comprehensive evaluation (Fuzzy), and analytic hierarchy process (AHP), which helps to optimize the talent training program [1]. In the process of determining the classification system of key stakeholders based on the enterprise stakeholder theory, this paper uses the analytic hierarchy process to determine the weights of the relevant attributes of different stakeholders when using the stakeholder theory to determine the classification system of key stakeholders. Are synthesized and ordered using the Analytical Hierarchy Process. At the same time, the article uses the expert selection

decision support package to conduct an overall evaluation of the company's stakeholder classification system and combines case studies and innovative thinking to study the research methods of stakeholder theory in theoretical research and practice. [2]. Establishing an evaluation system of scientific talent training mode that meets the needs of professional talents is of great significance for promoting the development of tourism English in colleges and universities and the social needs of cultivating high-skilled talents. Using AHP, firstly, establish a hierarchical analysis indicator system structure model and describe each index; then, establish a mathematical model, including two steps of judgment matrix and hierarchical single ranking; finally, calculate the weight of the indicator system according to the solution steps. When developing the training model, the training of key indicators and other nonmain indicators should be strengthened [3]. This paper proposes Analytical Hierarchy

Process (AHP) as a potential safety management assessment method. Few safety performance assessment models can reflect the dynamic performance of construction project sites, so take the problem of building dynamic models as an example. According to the input content, the construction projects are arranged in descending order, so that the weak links of the safety performance of the construction projects can also be judged, and it is hoped that the application of safety management professionals can be encouraged to evaluate the AHP [4]. This paper analyzes the new requirements for sports media practitioners in the new media era from the aspects of personal quality, professional quality, and professional skills. This paper discusses the basic idea of talent education system evaluation through the process of analyzing levels and vague general evaluation methods [5]. In this paper, the construction of the evaluation set of the index system, the determination of the index weight, the solution of the fuzzy evaluation matrix, the calculation of the comprehensive evaluation vector, and the establishment of the evaluation model. Through the evaluation of the talent training system and its operation quality, it provides reform ideas for teaching [6]. The AHP fuzzy evaluation method is to design quantitative indicators for qualitative decision-making problems and establish a quality evaluation model based on the evaluation criteria and the setting of factor weights. This article discusses the feasibility and effectiveness of the indicators of the talent training quality evaluation system by establishing an AHP model and improves the work efficiency of talents [7]. With the advent of the information age, the demand for computer professionals such as network maintenance engineers, security engineers, and development and operation and maintenance engineers has gradually increased, and computer software has become one of the most popular industries at present and in the future. This paper uses the Analytic Hierarchy Process (AHP) to analyze the established evaluation index system of software technology majors in higher vocational colleges and explores effective strategies to strengthen the application of high-efficiency personnel training mode for software technology majors in higher vocational colleges [8]. In view of the society's demand for talents, this paper adopts the analysis level process to conduct qualitative and quantitative analysis and decision-making and draws the conclusion that the proportion of comprehensive personnel training under the overall goal of G is 41.867%, and the proportion of research-oriented personnel training under the overall goal of G is 42.1456% %, and the proportion of skilled personnel training is 15.9874% G's overall goal [9]. This paper discusses the basic idea of talent education system evaluation through the process of analyzing levels and vague general evaluation methods and establishes an index system. This paper studies the application of the Analytic Hierarchy Process (AHP) model in the evaluation of college students' educational quality, promotes the basic principles of the quality evaluation of students' talent training, and designs an evaluation index system. And pointed out that in order to improve the quality of college students, we must focus on training programs, training measures, and quality evaluation in the order of importance [10]. Establishing an

evaluation system of scientific talent training mode that meets the needs of professional talents is of great significance for promoting the development of tourism English in colleges and universities and the social needs of cultivating high-skilled talents. The result of using AHP analysis is that colleges and universities should strengthen the training of key indicators and other nonmain indicators when formulating training models [11]. Through the exploration frontline talent training project, the evaluation index system of the geological exploration front-line talent training project was creatively established from the three dimensions of input index, process index, and output index, and the weight of each index in the system was determined by the analytic hierarchy process; research and establishment of geological exploration Comprehensive analysis model of front-line talent training, evaluation methods and evaluation standards [12]. This paper clarifies the object of international economic and trade professional personnel training, uses the analytic hierarchy process to build a talent quality system, and puts forward suggestions for the optimization of the international economic and trade professional personnel training system [13]. This paper discusses how to construct a regional scientific and technological innovation evaluation system based on AHP and calculates the index weight of the evaluation system, aiming to provide a reference for the decision-making and formulation of relevant policies. By constructing such an evaluation system, it will play a role in the technological innovation in Jiuquan area [14]. Guided by talent theory, system theory, and education quality theory, this paper analyzes the current situation of domestic credit management talent training based on talent quality theory and literature analysis, and uses brainstorming and Delphi methods to build an innovative and high-quality structural framework, and employs a hierarchical process of analysis to determine the weighting of quality elements to provide benchmarks for decision-making to improve creative excellence [15].

2. Construction of the Whole Chain Linkage Personnel Training System

2.1. The Connotation of the Whole Chain Linkage Personnel Training System. Due to the lack of the highest-level education system design, China's current talent education system is basically a fragmented point-like structure, but in reality it is superficial, estranged, and at different speeds. In this way, the core points of each link in the talent training system can form a complementary and progressive "chain", making the "whole chain" a reality. Linked personnel training system construction has formed an institutional environment and a good atmosphere that encourages the healthy growth and development of professional and skilled personnel training and ensures the sustainable and healthy development of professional and skilled personnel training.

2.2. The Value of the Whole Chain Linkage Personnel Training System. With the gradual development of this concept, the concept of the chain connecting the entire human education has gradually extended to all aspects of society.

The process of its integration into talent education is to link school education, talent development, and social monitoring. Entrepreneurship service aims to ensure the controllable inheritance of human resources in the stage of social development, which is consistent with the purpose of building a domestic higher education talent training system and strengthening social practice research throughout my country's talent training goals. At the same time, there are problems such as unbalanced resource allocation and weak market awareness in the current process of domestic scientific and technological innovation and entrepreneurial talent training. The above two aspects are the theoretical induction and analysis of the construction of the entire talent training chain system.

2.3. Build a "Whole Chain" Linkage Talent Training System.
First, the talent incubation system, the focus of "whole chain" talent training is to provide long-term high-quality human resources for the society, so the talent training system can establish a special talent training institution, which is mainly responsible for the formulation of human resources planning and talent training planning, the implementation of the annual talent training plan, the evaluation of the training effect and other related matters, or cooperation with colleges and universities to specially train the required technical talents, so that the talent training can be integrated into the whole process, and give full play to the role of teaching, production, and scientific research in improving students' practical skills and professional skills. The function of collaborative development; it can also play the role of industry organizations in talent training. Second, the talent allocation system, after completing the talent training, it is necessary to establish a talent allocation system to allocate talents scientifically and reasonably. Such an approach can maximize the benefits of talent investment and is necessary to promote development. Under such a background, different career development plans should be established for different talents according to their situation, so that talents can work and study according to the corresponding plans. Promote talents to continuously improve their comprehensive ability, so as to realize the comprehensive development of society. Third, the peripheral support system for talents, which is also a very critical part of the talent training process. In the peripheral support system, the most important position is financial support. Due to the long period of talent training, it is necessary to have sufficient funds as backup support in the process of talent training, and special funds can be set up as reserve funds for talent training.

2.4. The Importance of the Whole Chain Linked Person Training System.
The establishment of a whole chain talent education system is conducive to building an excellent team that can adapt to the design and development strategy, and build a group of outstanding talents with leadership, pioneering and innovative, institutional innovation, technological innovation, and sharp vitality for my country's economic development. Strengthening of social quality and talent education level. Fully understand the importance of talents, cultivate talents, establish a healthy talent guarantee mechanism, improve the talent incentive system, effectively guarantee the flow of talents, give full play to the maximum role of talents, create a good working environment, and create a suitable environment for talents to cultivate talents.

3. Fuzzy AHP Model

3.1. Establishment of Hierarchical Hierarchy

3.1.1. Hierarchical Structure and Composition.
The AHP process begins by layering the decision problem. The so-called hierarchical structure divides the problem into different components according to the nature of the problem and the goal to be achieved and groups them in a nonuniform layer according to the degree and degree of correlation between the factors. AHP first divides the level into different levels. The top layer is called the paint layer; this layer has only one element, that is, the problem must achieve the goal or desired result, the middle layer is the standard layer, and the element of this layer is the dimension. Approved policies, guidelines, etc. to achieve goals. The standard layer can have multiple layers, which can be divided into standard layers and substandard layers according to the size and complexity of the problem, and the lowest layer is the model layer, with options to achieve the goal. In a hierarchy, each level consists of several factors. When a hierarchy contains many factors, the hierarchy can be further subdivided into several sublevels. Generally speaking, the number of elements controlled by each factor at each level should generally not exceed 9, because too many control elements will cause pairwise comparisons to be difficult, as shown in Figure 1.

Generally, no more than 9 objects are compared under one criterion, because psychologists believe that making pairwise comparisons is too much beyond human judgment. At most, it is roughly between 5 and 9. If it is limited to 9, it is appropriate to use a 1-9 scale to express the difference between them.

3.2. Constructing the Comparison Judgment Matrix.
Once the hierarchy is established, the connections between the top and bottom elements are determined. Assuming that the element C of the previous layer is a criterion, and the proportion of the next dominant layer is $u1, u2, \cdots, un$, our purpose is to give the corresponding weights $u1, u2, \cdots, un$ according to their effect on C. The relative importance of is given corresponding weights. Some questions can be directly weighted, such as student test scores and project investment amounts but in most socioeconomic activities, especially in more complex questions, the weights of elements cannot be directly obtained, which requires appropriate methods to derive their weights. The method used by AHP to deduce the weight is the pairwise comparison method, which compares the characteristics of the judgment matrix:

(1) $a_{ij} > 0$

(2) $a_{ij} = 1/a_{ji}$

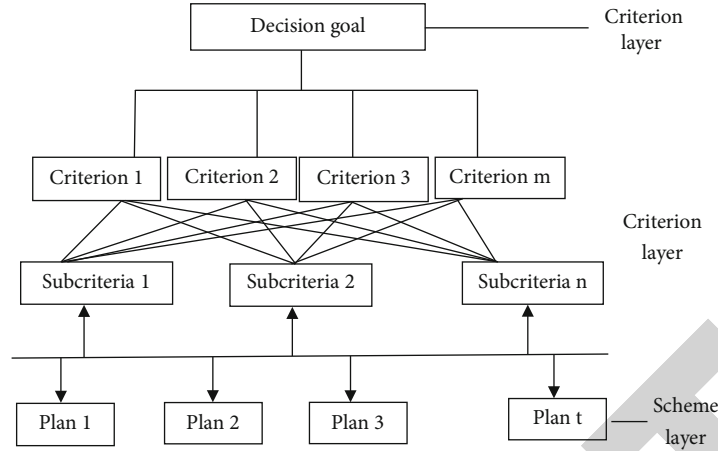(3) $a_{ii} = 1 (i, j = 1, 2, 3, \cdots n)$

Figure 1: Typical hierarchical hierarchy.

The judgment matrix A is

$$A = \begin{pmatrix} 1 & a_{12} & \cdots & a_{1n} \\ 1/a_{12} & 1 & \cdots & a_{2n} \\ \cdots & \cdots & \cdots & \cdots \\ 1/a_{1n} & 1/a_{2n} & \cdots & 1 \end{pmatrix}. \tag{1}$$

A matrix of order n with the above three characteristics is called a positive and negative matrix.

All elements a_{ij} must be transitive, i.e., a_{ij} the equation needs to be satisfied:

$$a_{ij}a_{jk} = a_{ik}(i,j,k = 1,2,\cdots,n). \tag{2}$$

If the n-order matrix A is a positive and inverse matrix, it has for all i, j, and $ka_{ij}a_{jk} = a_{ik}(i,j,k = 1,2,\cdots,n)$, then A is called a consistent matrix.

According to the reference estimation matrix A, when comparing n factors, only $n(n-1)/2$ pairwise comparisons are required. But the consistency A of the outer matrix of order $n(n-1)/2$ must be satisfied. Comparing all the same is too strict, so in practice, we do not require the equation matrix A to be consistent.

When comparing n factors with a certain factor, some people think that it only needs to do $n-1$ times. The disadvantage of this approach is that any error in judgment may lead to unreasonable sorting. For systems that are difficult to quantify, errors in judgment should be avoided as much as possible. Doing $n(n-1)/2$ pairwise comparisons can provide more information and compare them from different angles to get a reasonable ordering.

3.3. Sorting and Consistency Test under Single Criterion

3.3.1. Sorting under a Single Criterion. The AHP database is a comparative assessment matrix. Because each criterion controls multiple factors at the next level, a comparative evaluation matrix of each criterion and the factors it controls can be obtained. Therefore, the process of calculating the relative order weights of each factor $u_1, u_2, \cdots, u_n$ according to the reference matrix is called sorting according to a criterion. There are many calculation methods for the weights $w_1, w_2, \cdots, w_n$, among which the signature root method is a relatively mature and widely used method in the AHP, which is of great significance to the theoretical and practical development of the AHP.

3.3.2. Method for Finding Positive and Negative Matrix Sorting Vector. For positive matrices, there is a simple algorithm (power method) to find the eigenvectors. The following theorem provides the theoretical basis for the power method. Let n be a matrix where V is the eigenvector corresponding to the largest eigenvalue of A and c is a constant. If $x = e$ (e is a unit vector), then W is the normalized eigenvector corresponding to the largest eigenvalue of A, hereinafter referred to as the weight vector or the sorting vector.

In the first step, normalize the column items of the judgment matrix:

$$\tilde{A}_{ij} = \left(\frac{a_{ij}}{\sum_{i=1}^{n} a_{ij}} \right). \tag{3}$$

In the second step, the $\tilde{A}_{ij}$ by line:

$$\tilde{w} = \left(\sum_{j=1}^{n} \frac{a_{1j}}{\sum_{i=1}^{n} a_{ij}}, \sum_{j=1}^{n} \frac{a_{2j}}{\sum_{i=1}^{n} a_{ij}}, \cdots \sum_{j=1}^{n} \frac{a_{nj}}{\sum_{i=1}^{n} a_{ij}}, \right)^{T}. \tag{4}$$

In the third step, the $\tilde{w}$ after normalization:

$$W = (\omega_1, \omega_2, \cdots \omega_n)^{T}. \tag{5}$$

In the fourth step, λ is the largest eigenvalue of A:

$$\lambda = \frac{1}{n} \sum_{i=1}^{n} \frac{(AW)_i}{\omega_i}. \tag{6}$$

In the first step, normalize the column vector of the judgment matrix.

In the second step, the $A_{ij}{}^{\sim}$ by row:

$$\bar{W} = \left(\left(\prod_{j=1}^{n} \frac{a_{1j}}{\sum_{i=1}^{n} a_{ij}} \right)^{1/n}, \left(\prod_{j=1}^{n} \frac{a_{2j}}{\sum_{i=1}^{n} a_{ij}} \right)^{1/n}, \cdots, \left(\prod_{j=1}^{n} \frac{a_{nj}}{\sum_{i=1}^{n} a_{ij}} \right)^{1/n} \right)^{T}.$$
(7)

In the third step, the $w^{\sim}$ after normalization:

$$W = (\omega_1, \omega_2, \cdots \omega_n)^T.$$
(8)

In the fourth step, λ is the largest eigenvalue of A:

$$\lambda = \frac{1}{n} \sum_{i=1}^{n} \frac{(AW)_i}{\omega_i}.$$
(9)

3.3.3. Consistency Check. The complexity of objective things makes our judgments subjective and one-sided, so that every comparison and judgment cannot require exactly the same standard of thinking. Therefore, we do not require all $n(n+1)/2$ equations to be consistent when constructing the base matrix. However, it may also be that A and B are more important, B is more important than C, and C is more important than A, and this comparison is very inconsistent. When we compare rating matrices, we do not need to require ratings to be consistent. But a confusing and untenable comparative evaluation matrix can lead to wrong decisions, so we want the evaluations to be generally consistent. The above method for calculating weights is questionable when the estimated matrix deviates too much from the consistency. Therefore, when sorting each level by one criterion, it is necessary to check for consistency. Let A be a positive and inverse matrix of order n, we know from the theorem.

$$AW = \lambda_{\max} W, \text{ and } \lambda_{\max} \geq n.$$
(10)

Like $\lambda_{\max}$ is much larger than n, then the degree of inconsistency of A is such that

$$CI = \frac{\lambda_{\max} - n}{n - 1}.$$
(11)

In $\lambda_{\max}$, the largest eigenvalue is A, and CI can be used as a quantitative standard to measure the degree of inconsistency, which is called the consistency index. When $CR < 0.1$, the consistency of the reference matrix is considered acceptable; otherwise, the evaluation matrix must be checked accordingly.

The CR value is less than 0.1, which meets the judgment requirements, indicating that the results have good consistency, and vice versa.

3.4. Hierarchical Total Sorting. Computing the relative importance scale (also known as the ranking weight vector) of all elements of the same level to the highest level (overall target) is called the overall ranking of the level.

3.4.1. Steps of Hierarchical Total Sorting

(1) Calculate the relative weight from the weight vector of all factors in the same layer to the highest layer; this process is carried out layer by layer from top to bottom

Suppose that by calculating the k-th layer, there are $k-1$ layers with n_{k-1} a vector of sorting weights obtained by elements of elements relative to the total objects

$$\omega^{k-1} = \left(\omega_1{}^{(k-1)}, \omega_2{}^{(k-1)}, \cdots, \omega_{n_{k-1}}{}^{(k-1)} \right)^T$$
(12)

Layer Kn_k elements, they depend on some factors from the previous layer ($k-1$ layer) u_i the full vector for single criterion sort is:

$$p_i{}^k = \left(\omega_{1i}{}^k, \omega_{2i}{}^k, \cdots, \omega_{n_k i}{}^k \right)^T.$$
(13)

For the correspondence with no dominance relation to the i-th element of the $k-1$ layer, u_{ij} value is 0.

(2) The k-th layer n_k the sorting weight vector of elements relative to the total target is:

$$\left(\omega_1{}^{(k)}, \omega_2{}^{(k)}, \cdots, \omega_{n_k}{}^{(k)} \right)^T = \left(p_1{}^{(k)}, p_2{}^{(k)}, \cdots, p_{k-1}{}^{(k)} \right) \omega^{(k-1)}$$
(14)

3.4.2. Total Ranking Consistency Check. When one compares the elements of each level, even if each level uses essentially the same benchmark, there may still be differences between the levels accumulated in the overall ranking of the levels calculated step-by-step, and it is necessary to test whether the accumulation of this difference scale has any effect on the overall model. Significantly, the testing process is called Hierarchical Universal Classification Conformance Testing.

Assuming that the j-th factor of the ($k-1$-th layer is the reference standard, the first-level and first-level consistency indicators for the pairwise comparison of each factor in the k-th layer are:

$$\left(\omega^{(k-1)} \text{represents the total ranking vector of} \right.$$

$$\text{the total target of the } k-1 \text{ layer} \Big)$$

$$RI^k = RI^{k-1} \cdot \omega^{(k-1)},$$

$$CR^k = CR^{k-1} + \frac{CI^k}{RI^k} (3 \leq k \leq n).$$
(15)

If $CR^k < 0.1$, it can be considered that the evaluation model has achieved local satisfaction at the k-layer level.

3.5. Adjustment of Judgment Matrix. When a comparative judgment matrix deviates too much from consistency, its

reliability is questionable, and the judgment matrix must be adjusted at this time. In practical applications, the judgment matrix needs to be adjusted many times before it can pass the consistency test. At present, there are many ways to modify the judgment matrix, which can be roughly divided into three categories:

(i) Experience adjustment method: Let experts readjust some elements of the judgment matrix. This kind of method has a certain degree of subjective arbitrariness and lacks theoretical scientific basis

(ii) Construct a completely consistent judgment matrix with a certain method and extract the information of the original judgment matrix and the completely consistent matrix through the formaldehyde method, so as to achieve the purpose of adjustment. Such methods have certain blindness

(iii) Using the relationship between changes in matrix elements and consistency, identify key elements that affect consistency and make adjustments. Such methods change less elements of the original judgment matrix and retain more original information

The following is the third type of evaluation matrix adjustment method, which is called the forward-looking algorithm of adjusting the AHP to evaluate the consistency of the matrix. The specific algorithm is as follows:

Construct the matrix: Determine the elements of matrix A, a_{ij} used is replaced by $a_{ik}a_{kj}$, and a_{ik} use $1/a_{ik}a_{kj}$, the matrix obtained after substitution, namely, $A_{ij}^{(k)} = (a_{ij}^{(k)})$.

$$a_{st}^{(k)} = \begin{cases} a_{sk}a_{kt} & s = i, t = j \\ 1/a_{sk}a_{kt} & s = j, t = i \ . \\ a_{st} & \text{other} \end{cases} \quad (16)$$

Because $a_{sk}a_{kt}$ may be greater than 9, $1/a_{sk}a_{kt}$ may be less than 1/9. This is inconsistent with the definition of judging oranges and may need to be fine-tuned, as follows:

$$a_{st}^{(k)} = \begin{cases} F(a_{sk}a_{kt}) & s = i, t = j \\ 1/F(a_{sk}a_{kt}) & s = j, t = i \ . \\ a_{st} & \text{other} \end{cases} \quad (17)$$

In,

$$F[x] = \begin{cases} 9 & x \geq 9 \\ [x] & 1 \leq x < 9 \\ \dfrac{1}{[1/x]} & 1/9 \leq x < 1 \\ 1/9 & 0 < x < 1/9 \end{cases} \ . \quad (18)$$

Calculation $\Delta_{ij}^{(k)}$ and Δ_{ij}:

$$\Delta_{ij}^{(k)} = C.R(A) - C.R\left(A_{ij}^{(k)}\right), k \neq i, j; k \in N. \quad (19)$$

There are $n - 2$ improvement degrees, such as $\Delta_{ij}^{(k)} = C.R(A) - C.R(A_{ij}^{(k)}) \leq 0$. It shows that the k-th adjustment does not help or even hinders the consistency of the judgment matrix, so it is set to 0 in the algorithm display.

Δ_{ij} is the element in the judgment matrix $A a_{ij}$ the n-2 maximum possible improvements. Like $\Delta_{ij}=0$, all adjustment directions of a_{ij} do not help to improve the consistency of the judgment matrix.

$$\Delta_{ij} = \max_{\substack{k \in N \\ k \neq i, j}} \left[C.R(A) - C.R\left(A_{ij}^{(k)}\right) \right]. \quad (20)$$

Calculation T_{ij}

T_{ij} is the adjustment strategy number corresponding to the maximum possible improvement and D_{ij} degree of a_{ij} to moment consistency. If $D_{ij} = 0$, it means that all the adjustment directions of a_{ij} do not help to improve the consistency of the matrix.

$$T_{ij} = \arg\max_{\substack{k \in N \\ k \neq i, j}} \left[C.R(A) - C.R\left(A_{ij}^{(k)}\right) \right]. \quad (21)$$

(1) Adjust the empirical method. Let experts readjust some elements of the judgment matrix, but this method does have a theoretical basis. (2) Construct a consistent judgment matrix by the method, and extract the information of the original and consistent matrix by the formaldehyde method, and achieve the purpose of adjustment all the time. (3) Using the relationship between matrix element changes and consistency, determine and adjust the elements that affect consistency.

3.6. Calculation of Evaluation Set. Establishing an index set according to the evaluation index system $X = (x_1, x_2 \cdots x_m)^T$ and weight set $w = (w_1, w_2, \cdots w_m)$, the relationship between the evaluation index set Y, the factor set, and the weight set is:

$$Y = \left(W_n^1\right)^T X = \sum_{i=1}^m w_i x_i, \quad (22)$$

where Y is the final evaluation value of talent training.

(1) Establish a hierarchical structure of the system. (2) Construct a pairwise comparison judgment matrix. (3) Calculate the sorting weight vector of the next level to a certain criterion of the previous level. (4) Total sorting is to calculate the sorting weight vector of each scheme to the total system target.

TABLE 1: The whole chain linkage talent training index system.

| Primary element	Secondary elements
Personality	Independence
	Career
	Be realistic and diligent
Innovation literacy	Innovative mind
	Creative thinking
	Innovative spirit
Emotional intelligence literacy	Emotional perception
	Emotional expression ability
	Emotion regulation ability
Leadership and management literacy	Communication and resilience
	Teamwork
	Organization and coordination capacity
Scientific ethics	Basic knowledge
	Professional knowledge
	General knowledge
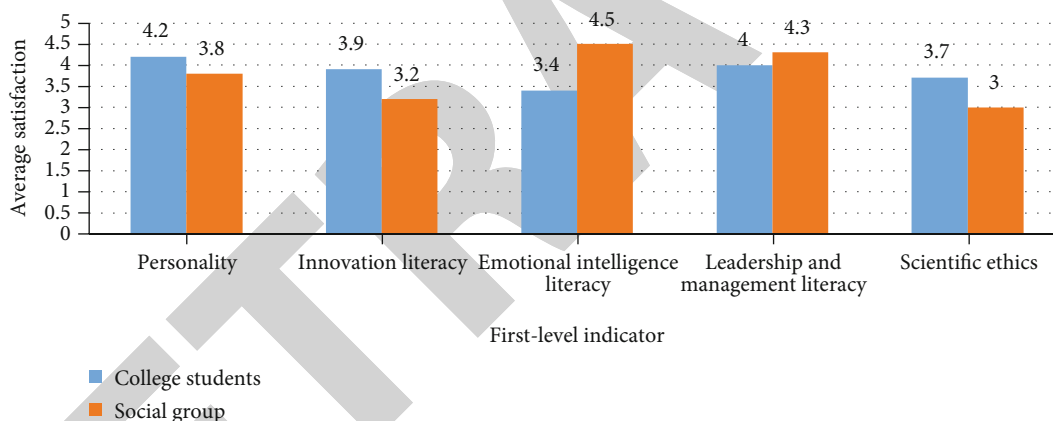
FIGURE 2: Average satisfaction level 1 indicator.

4. The Whole Chain Linkage of AHP Model and CIPP Model Talent Training Analysis Index Analysis

Aiming at the analysis of the indicators of talent training in the whole chain linkage, the questionnaires were distributed through the network platform. A total of 900 questionnaires were distributed in this study, and a total of 856 questionnaires were recovered, which were distributed to college students and social groups, respectively. The number of questionnaires was 467, and the effective recovery rate was 93.4%. 400 questionnaires were distributed to the public, and 389 questionnaires were effectively recovered, with an effective recovery rate of 97.25%.

4.1. Construct the Whole Chain Linkage Talent Training Index System. To build the whole chain linkage talent training index system, first divide the whole chain linkage talent

training index into two elements. The first-level indicators include five aspects: personality literacy, innovation literacy, emotional intelligence literacy, leadership and management literacy, and scientific literacy; two first-level indicators are, respectively, refined for the first-level indicators, and there are a total of 18 small indicators. The 18 impact factors are assigned and calculated to form a quantitative evaluation index, as shown in Table 1.

4.2. Satisfaction with Primary Indicators. Through the survey on the satisfaction of college students and social groups with their own first-level indicators, the satisfaction score is 5 out of 5 points, and the obtained data is analyzed. It can be seen from Figure 2 that in terms of personality literacy, college students' satisfaction with themselves is higher than the social population, the average satisfaction of college students is 4.2, and the average satisfaction of the social population is 3.8; in terms of innovation literacy, the satisfaction of college
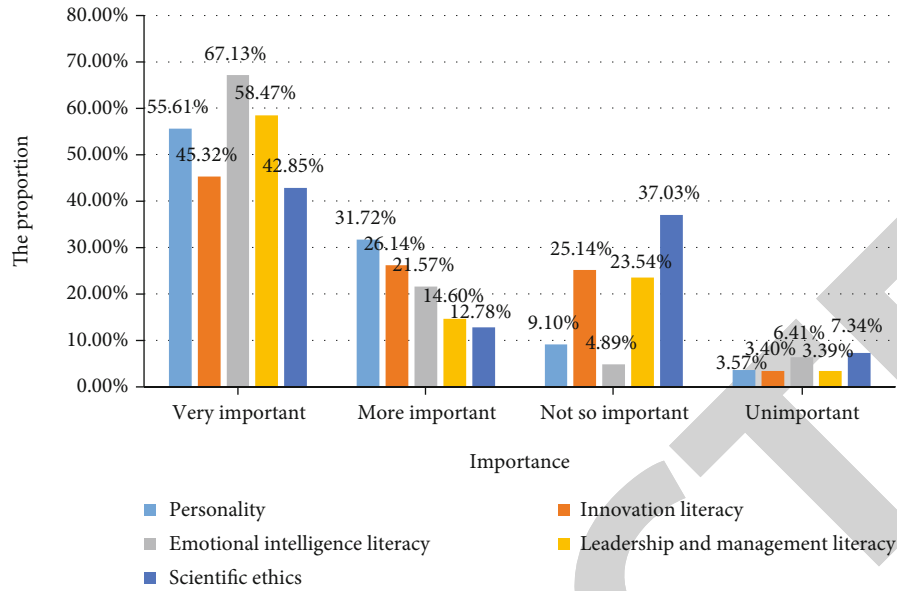
Figure 3: Importance of primary indicators.

Table 2: Consistency test of first-level indicators.

Serial number	Personality	Innovation literacy	Emotional intelligence	Leadership and management	Scientific ethics		CR
1	0.524	0.141	0.218	0.055	0.062	5.387	0.086
2	0.221	0.427	0.093	0.06	0.199	5.36	0.082
3	0.129	0.101	0.344	0.115	0.311	5.282	0.063
4	0.169	0.294	0.147	0.222	0.169	5.077	0.017

students is higher than that of the social population; the average satisfaction of college students is 3.9, and the social population is 3.2; in terms of emotional intelligence literacy, social groups are significantly higher than college students, with an average satisfaction rate of 3.4 for college students and 4.5 for social groups; in terms of leadership and management literacy, social groups are higher than college students, with an average satisfaction rate of 4, the social group is 4.3, and the difference between the two is not significant; in terms of scientific literacy, college students are higher than the social group; the average satisfaction of college students is 3.7, and the social group is 3.7.

4.3. Importance of Primary Indicators.

Through the choice of the respondents, statistics of the data and drawing into a bar chart can more intuitively see which respondents generally think are more important. As can be seen from Figure 3, most people think that emotional intelligence literacy is very important, ranking first in "very important", accounting for 67.13%; ranking second is leadership and management literacy, accounting for 58.47%; the proportion of innovation literacy and scientific literacy is not significantly different, and the importance of college students and social groups is similar. Among the "more important," most people think that personality literacy is more important, accounting for 31.72%; among the "more important" is "scientific literacy";

Table 3: Ranking of the weights of the first-level indicators.

Indicator name	Weights
Personality	0.25
Innovation literacy	0.23
Emotional intelligence literacy	0.2
Leadership and management literacy	0.18
Scientific ethics	0.15

most people think that scientific literacy is not very important, accounting for 37.03; there is little difference between innovation literacy and leadership and management literacy; among the unimportant, the number of people who choose "scientific literacy" is the largest, accounting for 7.34%.

According to Figure 3, it can be seen that most people think that emotional intelligence literacy is very important, ranking first in "very important"; in "more important," most people think that personality literacy is more important; in "less important," most people rated scientific literacy as less important; among "not important," the highest number chose "scientific literacy."

4.4. Analysis of Indicators Based on AHP

4.4.1. Index Consistency Test Results. It can be seen from Table 2 that the CR value of No. 1 is 0.086 and less than
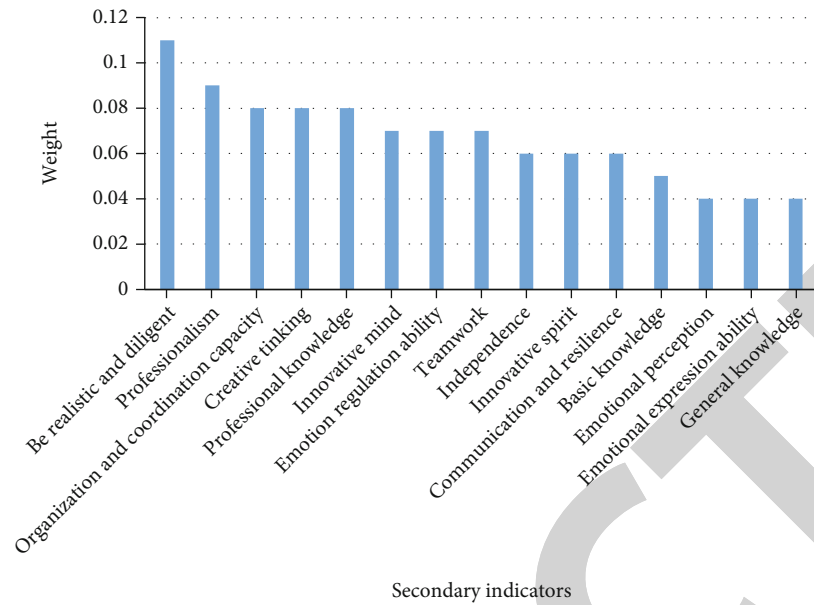
Secondary indicators

FIGURE 4: Weights of secondary indicators.

TABLE 4: Secondary index comment set.

Primary element	Secondary elements	Very good	Good	Better	Poor
Personality	Be realistic and diligent	0.4	0.3	0.2	0.1
	Professionalism	0.32	0.35	0.18	0.15
	Organization and coordination capacity	0.3	0.4	0.15	0.15
Innovation literacy	Creative thinking	0.33	0.35	0.2	0.12
	Professional knowledge	0.2	0.24	0.36	0.2
	Innovative mind	0.15	0.3	0.25	0.3
Emotional intelligence literacy	Emotion regulation ability	0.3	0.25	0.3	0.15
	Teamwork	0.25	0.43	0.22	0.1
	Independence	0.32	0.28	0.25	0.15
Leadership and management literacy	Innovative spirit	0.37	0.2	0.25	0.18
	Communication and resilience	0.25	0.37	0.23	0.15
	Basic knowledge	0.25	0.37	0.2	0.18
Scientific ethics	Emotional perception	0.3	0.28	0.22	0.2
	Emotional expression ability	0.4	0.3	0.15	0.15
	General knowledge	0.3	0.2	0.38	0.12

0.1, which meets the judgment requirements; the CR value of No. 2 is 0.082 and less than 0.1, which meets the judgment requirements; the CR value of No. The CR value of 0.017 is less than 0.1, which meets the judgment requirements, indicating that the results have good consistency and all meet the judgment requirements.

4.4.2. Weights of Primary Indicators. According to the method, the weight of the first-level indicators is calculated, and the importance is sorted. As can be seen from Table 3, among the five indicators, personal quality has the largest weight, with a weight of 0.25; the second is innovation literacy, with a weight of 0.23; the third is emotional intelligence,

with a weight of 0.2; the fourth is leadership and management ability literacy, with a weight of 0.18; the fourth is scientific literacy, with a weight of 0.15.

4.4.3. Ranking of Weight Values of Secondary Indicators. As shown in Figure 4, the second-level weights are arranged from large to small as being realistic and diligent > career > organizational coordination ability = innovative thinking = professional knowledge > innovative awareness = emotional regulation ability = team awareness > independence = innovative spirit = communication and resilience > basic knowledge of emotions > emotional perception skills = emotional expression skills = general knowledge.

TABLE 5: Hierarchical single order and total order table.

| Primary element	Weights	Secondary elements	Hierarchical single sorting weights	Hierarchical total ranking weight
Personality	0.3021	Be realistic and diligent	0.2242	0.065
		Professionalism	0.4504	0.0998
		Organization and coordination capacity	0.3254	0.0651
Innovation literacy	0.2317	Creative thinking	0.2431	0.085
		Professional knowledge	0.4271	0.0937
		Innovative mind	0.3298	0.072
Emotional intelligence literacy	0.1124	Emotion regulation ability	0.2546	0.0518
		Teamwork	0.2462	0.0651
		Independence	0.4992	0.0511
Leadership and management literacy	0.1814	Innovative spirit	0.3874	0.0473
		Communication and resilience	0.4732	0.0456
		Basic knowledge	0.1394	0.0341
Scientific ethics	0.1724	Emotional perception	0.3346	0.0768
		Emotional expression ability	0.4517	0.0926
		General knowledge	0.2137	0.055
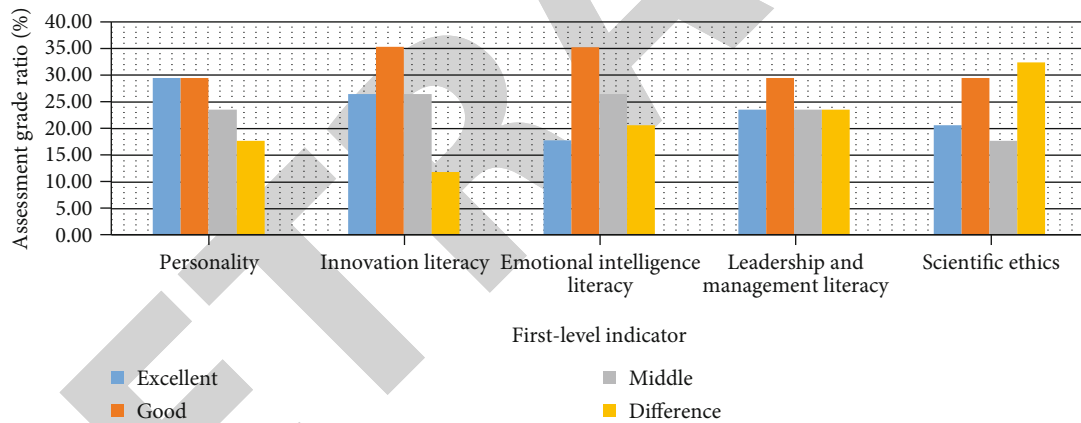
FIGURE 5: Levels of first-level indicator evaluation.

4.4.4. Comment Set for Each Secondary Indicator. Among personality qualities, the highest value of "very good" is independence, with a value of 0.2; the highest value of "good" is truth-seeking and diligence, and the value of "good" is 0.4; independence, the evaluation value is 0.2, and the "poor" evaluation value is the highest for professionalism, truth-seeking, and diligence, and the evaluation value is 0.15; in the innovation literacy, the "very good" evaluation value is the highest for innovation consciousness, and the evaluation value is 0.33; the highest value of "good" is innovation consciousness, and the value of "good" is 0.3, the highest value of "good" is innovative thinking, the value of "poor" is 0.36, and the value of "poor" is the spirit of innovation, and the evaluation value is 3; in the EQ literacy, the "very good" evaluation value is the highest emotional regulation ability, and the evaluation value is 0.32; the "good" evaluation value is the largest emotional expression ability, and

the evaluation value is 0.43; the "good" highest evaluation value is emotional perception ability, and the evaluation value is 0.3; and the "poor" evaluation value is emotional perception ability and emotional regulation ability, and the evaluation value is 0.15; in leadership and management literacy, the "very good" highest comment value is communication ability and adaptability, and the comment value is 0.37; and the "good" comment value is the team awareness and organization and coordination ability, and the evaluation value is 0.37; the "better" evaluation value is the communication ability and adaptability, and the evaluation value is 0.25; the "poor" evaluation value is the communication ability and adaptability, organization and coordination ability. The evaluation value is 0.18; in the scientific literacy, the "very good" evaluation value is the largest for professional knowledge, and the evaluation value is 0.4; the "good" evaluation value is the largest professional knowledge, and the evaluation

value is 0.3; the "good" evaluation value is the largest. The highest value is general knowledge, with a review value of 0.38, and the highest value of "poor" is basic knowledge, with a review value of 0.2, as shown in Table 4.

4.5. Analysis of Indicators Based on CIPP

4.5.1. Hierarchical Single Sorting and Total Sorting Table. As can be seen from Table 5, among the first-level indicators, the most weighted is personality literacy, with a weight of 0.3021; the second is innovation literacy, with a weight of 0.2317; the third is leadership and management literacy, with a weight of 0.1814; the first is scientific literacy, with a weight of 0.1724; the fourth is emotional intelligence literacy, with a weight of 0.1124. In the second-level indicators, the ranking weight is hierarchical. In personality literacy, the single ranking weight of career aspiration is the largest, with a weight of 0.4504; in innovation literacy, the single ranking weight of innovative thinking is the largest, with a weight of 0.4271; in emotional intelligence literacy, the single-ranked weight of emotional control ability is the largest, with a weight of 0.4992; in scientific literacy, the single-ranked weight of team awareness is the largest, with a weight of 0.4732; in leadership and management literacy, the single-ranked weight of professional knowledge is the largest, with a weight of 0.4517. In the total ranking weight of the hierarchy, the greatest is career, followed by innovative thinking, professional knowledge, basic knowledge, and innovative spirit.

4.5.2. First-Level Indicator Evaluation Level. As can be seen from Figure 5, the highest evaluation level is personal literacy, accounting for 29.41%; the highest evaluation level is innovation literacy, accounting for 35.29%; the highest evaluation level is innovation literacy and emotional intelligence literacy. The ratio is 26.47%; the highest evaluation level is scientific literacy, with a ratio of 32.36%.

5. Conclusion

Under the current development trend, it is very necessary to carry out the evaluation of the entire chain linkage talent training system with the fuzzy AHP model, which has a great effect on the quality of talents. By using the fuzzy AHP model and the CPII model, and comparing the results of the two models, the weights of each indicator in talent training are obtained. The analysis shows that in the construction of the entire chain linkage talent training, it is necessary to strengthen personal quality, innovation quality, emotional intelligence quality, and emotional intelligence. The cultivation of leadership and management ability literacy, scientific literacy, etc. can better reflect the characteristics of talents; however, the AHP model can more comprehensively analyze the evaluation of the entire chain linkage talent training system. It is very simple and convenient to use AHP as an evaluation for analyzing the entire chain linkage talent training system, and the results are also credible, which can provide a reference for the society to build talent training indicators, and can also serve as a basis for decision-making by the education department. Realize the construction of a "whole chain" linkage talent training system, so as to build an institutional environment and a good atmosphere that are conducive to the growth and functioning of skilled talents.

Data Availability

The experimental data used to support the findings of this study are available from the corresponding author upon request.

Conflicts of Interest

The authors declared that they have no conflicts of interest regarding this work.

References

[1] S. H. Dai Ying and L. Haiyan, "Evaluation of talent training quality in general university based on fuzzy AHP analysis," *Journal of Chongqing University of Technology (Social Science)*, vol. 28, pp. 127–130, 2014.

[2] Q. L. Zhang and SCUFN, Wuhan, "The construction of the categorized system of the stakeholders based on AHP," *Journal of South-Central University for Nationalities (Natural Science Edition)*, vol. 27, no. 3, p. 762-276, 2006.

[3] L. Wang, "Construction of index system of talent training mode of computer for tourism English Majors," *Electronic Test*, vol. 17, no. 8, pp. 189–241, 2001.

[4] Y. Q. Bai and S. S. Cheng, "Application of AHP in construction engineering project safety assessment model," in *International Conference on Construction & Real Estate Management*, Orlando, FL, USA, 2009.

[5] Z. Wang and J. K. Zhang, "Research on talent training quality evaluation system for private colleges based on AHP model," *Value Engineering*, vol. 12, no. 10, pp. 278–935, 2018.

[6] Z. Wang, Y. Zhang, and X. Zhao, "Evaluation model of sports media talent training system in the new media era," in *Advances in Artificial Systems for Medicine and Education IV. AIMEE 2020. Advances in Intelligent Systems and Computing, vol 1315*, Z. Hu, S. Petoukhov, and M. He, Eds., Springer, Cham, 2021.

[7] J. Cao, "Higher vocational talents training quality evaluation research of AHP fuzzy evaluation system," *The Journal of Shandong Agriculture and Engineering University*, vol. 82, no. 11, pp. 255–261, 2018.

[8] L. Feng, "Research on the application of computer technology in software technology talents training system in higher vocational colleges," *Journal of Physics Conference Series*, vol. 1915, no. 3, article 032035, 2021.

[9] J. B. Ma and Z. X. Li, "Notice of retraction: study of colleges and universities talent training program based on AHP," in *2010 International Conference on Computer and Communication Technologies in Agriculture Engineering*, pp. 119–261, Chengdu, China, June 2010.

[10] Y. Xue, "The application of AHP model in college students education quality assessment," in *Proceedings of the 2016 2nd International Conference on Education Technology, Management and Humanities Science*, pp. 524–527, Atlantis Press, January 2016.

Retraction

Retracted: Evaluation Method of English Talent Training Quality Based on Deep Learning Model

Journal of Sensors

This article has been retracted by Hindawi following an investigation undertaken by the publisher [1]. This investigation has uncovered evidence of one or more of the following indicators of systematic manipulation of the publication process:

(1) Discrepancies in scope

(2) Discrepancies in the description of the research reported

(3) Discrepancies between the availability of data and the research described

(4) Inappropriate citations

(5) Incoherent, meaningless and/or irrelevant content included in the article

(6) Manipulated or compromised peer review

The presence of these indicators undermines our confidence in the integrity of the article's content and we cannot, therefore, vouch for its reliability. Please note that this notice is intended solely to alert readers that the content of this article is unreliable. We have not investigated whether authors were aware of or involved in the systematic manipulation of the publication process.

Wiley and Hindawi regrets that the usual quality checks did not identify these issues before publication and have since put additional measures in place to safeguard research integrity.

We wish to credit our own Research Integrity and Research Publishing teams and anonymous and named external researchers and research integrity experts for contributing to this investigation.

The corresponding author, as the representative of all authors, has been given the opportunity to register their agreement or disagreement to this retraction. We have kept a record of any response received.

References

[1] Q. Fu, "Evaluation Method of English Talent Training Quality Based on Deep Learning Model," *Journal of Sensors*, vol. 2022, Article ID 6726931, 9 pages, 2022.

Hindawi

Research Article

Evaluation Method of English Talent Training Quality Based on Deep Learning Model

Qijun Fu [ID]

School of General Education, Hunan University of Information Technology, Hunan Changsha, 410151, China

Correspondence should be addressed to Qijun Fu; fuqijun2022@hnuit.edu.cn

This paper studies and analyzes three aspects: DL model, English talent training, and quality evaluation analysis, so as to get more rigorous and accurate quality evaluation results, and make relevant plans for future research directions. This paper focuses on model and method analysis to carry out experiments and analysis on three aspects: DL, personnel training, and quality evaluation. The experiment and inquiry of deep learning are divided into correct rate and loss. In 0-70 epoch, the highest training correct rate is 0.975, and with the increase of training times, the training correct rate is also increasing. According to the statistical investigation, 42.91% of English teachers are satisfied with their academic level, 38.48% with their oral English level, 38.89% with their teaching quality, 41.02% with their teaching methods, 40.29% with their teaching spirit, and 39.88% with their knowledge structure. At the same time, according to the statistics of students, graduates and teachers' problems in English talent training, the largest proportion is the poor level of teaching resources, so we should improve the efficiency from the level of teaching resources. In order to improve the efficiency of quality evaluation method, this paper combines AF algorithm and BQ algorithm under deep learning. The error rate of algebraic algorithm is compared. Through six groups of sample data, it can be seen that the highest error rate of AF algorithm is 5.86% and the lowest is 0.92%, the highest error rate of BQ algorithm is 10.70% and the lowest is 1.10%, and the highest error rate of algebraic algorithm is 10.70% and the lowest error rate is 5%. In contrast, the error rate of AF algorithm is lower and more stable. Next, this paper compares and analyzes the performance of the AF algorithm, BQ algorithm, and algebraic algorithm. According to the experimental results, it can be seen that the AF algorithm is more accurate than the BQ algorithm and algebraic algorithm in accuracy, recall rate, $F1$, accuracy rate, etc. Therefore, it is more intuitive and accurate to evaluate the quality of English talents training through AF algorithm under deep learning.

1. Introduction

This paper mainly explores the quality evaluation methods of related personnel training under the deep learning model. In view of training loss and effective loss, with the increase of training times, the loss does not decrease much. Next, this paper analyzes English talents; first analyzes English teachers' studies, oral English, quality, method, spirit and structure; then analyzes the existing problems; and finally evaluates and analyzes the overall quality of teachers, graduates, and students. Finally, the evaluation methods are analyzed, and the relevant experiments show that the error of AF algorithm is smaller than that of BQ algorithm and algebraic algorithm. In terms of performance, the AF algorithm is also superior to

the BQ and algebraic algorithms in precision, recall rate, $F1$, and accuracy, so the AF algorithm under deep learning has more advantages for quality evaluation.

In this paper, CNN, LN, GLM, and other models are used to analyze multilayer neural circuits. One of the core challenges of sensory neuroscience is understanding the neural computational and electrical mechanisms that underpin the coding of behaviorally relevant natural stimuli [1]. In this paper, multiple groups of pictures are used for recognition and analysis. Through deep learning method, simple leaf images of healthy and diseased plants are used for plant disease detection and diagnosis [2]. In this study, it is suggested to use depth neural network to locate sound source in reverberation environment by using microphone array

[3]. In this paper, the fundamental solution to this problem, therefore, the best option to counteract the effects of algal blooms, is to improve early warning [4]. In this paper, the background of deep learning is studied, and the development is planned. It will go back to the original belief of connectionism in brain modeling and return to its early realization: neural network [5]. We comprehensively diagnosed the training and evaluation process of the deep learning model to estimate the age on the two largest data sets [6]. This paper analyzes the relevant social needs of graduates. Information management specialty is a comprehensive and practical characteristic discipline [7]. In order to focus on training English scholars, the school popularizes related activities for teachers and student service personnel. The objectives and structure of these teacher development activities and their outcomes, as well as the impact of such training, are discussed [8]. Reflective teaching practice has almost become the central theme of preservice teachers' educational level and professional growth [9]. This study examines the second language English ability of pupils with and without music training [10]. This paper argues that English training in schools relies too much on spoken and written languages. The article calls on educators, linguists, teacher trainers, and practitioners to cooperate to carry out further research in order to formulate policies and practices suitable for a more inclusive future [11]. To determine and understand the effectiveness of projects, qualitative methods should be an important part of large-scale project evaluation [12]. This paper briefly discusses the objective and subjective methods of video quality evaluation [13]. In this paper, the components of the design are analyzed in depth. Scoring function is one of the most important components of structure-based drug design [14]. This paper evaluates the education and learning of e-learning. The basic nature of e-learning as a teaching medium is quite different from face-to-face teaching, so a new hybrid method is needed to evaluate its impact [15].

2. Deep Learning and Training of English Talents

2.1. Neural Network Structure. The neural structure consists of multiple neurons, which are composed of the output layer, hidden layer, and input layer [16]. In the modified neural network structure, different nodes are connected with each other [17]. The signal is transmitted from the input layer to the hidden layer and finally to the output layer [18], as shown in Figure 1.

As far as neural network is concerned, the hidden layer can be a single-layer structure or single-layer structure. When the hidden layer is a multilayer structure, it is called a multilayer neural network structure. Neural networks are composed of multiple neurons, and the nodes are connected with each other even in different layers of nodes.

2.2. Cultivation of English Talents. The cultivation of English talents includes the cultivation of language ability, cultural awareness, thinking quality, and learning ability [19]. The cultivation of language ability includes the cultivation of lan-
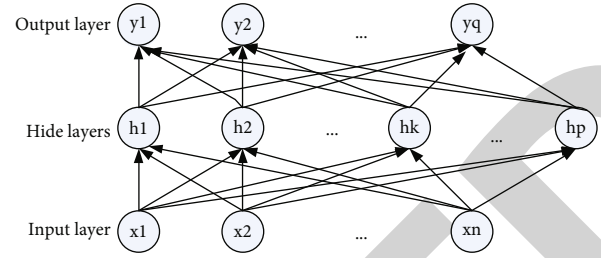

Figure 1: Neural network structure diagram.

guage knowledge, language cognition, and language application [20]. The cultivation of thinking quality includes the cultivation of understanding, inference, and creativity [21]. Cultivating English talents from various aspects can make the training efficiency more [22], as shown in Figure 2.

The cultivation of cultural awareness of English talents includes cultural identity, cultural identification ability, and cultural communication ability; learning ability includes active learning ability, cooperative learning ability, and deep learning ability. Through the cultivation of language ability, cultural awareness ability, thinking quality, and learning ability, we can promote the cultivation of English talents and improve the efficiency of English talents cultivation.

3. Correlation Formula

3.1. Deep Learning

3.1.1. Single Neuron. Sigmoid activation function:

$$f(z) = \frac{1}{1 + \exp(-z)}. \tag{1}$$

Neuron activation function:

$$f(z) = \tanh(z) = \frac{e^z - e^{-z}}{e^z + e^{-z}} \tanh. \tag{2}$$

3.1.2. Neural Network Calculation Steps. N_1 denotes the number of neural network layers, L_{nl} is the output layer, and $a_i^{(l)}$ denotes the output value of the i node of the one layer [23].

$$a_1^{(2)} = f\left(W_{11}^{(1)}x_1 + W_{12}^{(1)}x_2 + W_{13}^1 x_3 + b_1^{(1)}\right),$$

$$a_2^{(2)} = f\left(W_{21}^{(1)}x_1 + W_{22}^{(1)}x_2 + W_{23}^1 x_3 + b_2^{(1)}\right),$$

$$a_3^{(2)} = f\left(W_{31}^{(1)}x_1 + W_{32}^{(1)}x_2 + W_{33}^1 x_3 + b_3^{(1)}\right),$$

$$h_{W,b}(X) = a_1^{(3)} + f\left(W_{11}^{(2)}a_1^{(2)} + W_{12}^{(2)}a_2^{(2)} + W_{13}^{(2)}a_3^{(2)} + b_1^{(2)}\right). \tag{3}$$

Simplified as follows:

$z_i^{(l)}$ is used to represent the activation value of the i node in the l layer.

$$z^{(2)} = W^{(1)}x + b^{(1)},$$
$$a^{(2)} = f\left(z^{(2)}\right),$$
$$z^{(3)} = W^{(2)}a^{(2)} + b^{(2)},$$
$$h_{W,b}(x) = a^{(3)} = f\left(z^{(3)}\right). \tag{4}$$

After activating the function, you can get

$$z^{l+1} = W^{(1)}a^{(1)} + b^{(l)},$$
$$a^{(l+1)} = f\left(z^{(l+1)}\right). \tag{5}$$

3.1.3. Reverse Conduction Algorithm. Batch gradient descent method is used to solve the neural network.

M sample set $\{(x^{(1)}, y^{(1)}), \cdots, (x^{(m)}, y^{(m)})\}$ and single sample (x, y).

$$J(W, b\,; x, y) = \frac{1}{2}\left\|h_{W,b}(x) - y\right\|^2. \tag{6}$$

Variance cost function.

$$J(W, b) = \left[\frac{1}{m}\sum_{i=1}^{m} J\left(W, b\,; x^{(i)}, y^{(i)}\right)\right] + \frac{\lambda}{2}\sum_{l=1}^{n_{l-1}}\sum_{i=1}^{s_i}\sum_{j=1}^{s_i+1}\left(W_{ji}^{(1)}\right)^2$$
$$= \left[\frac{1}{m}\sum_{i=1}^{m}\frac{1}{2}\left\|h_{W,b}\left(x^{(i)}\right), y^{(i)}\right\|^2\right] + \frac{\lambda}{2}\sum_{l=1}^{n_{l-1}}\sum_{i=1}^{s_i}\sum_{j=1}^{s_i+1}\left(W_{ji}^{(1)}\right)^2. \tag{7}$$

The parameters W and b are fine-tuned by gradient descent method.

$$W_{ij}^{(1)} = W_{ij}^{(1)} - \alpha\frac{\partial}{\partial W_{ij}^{(1)}}J(W, b),$$
$$b_i^{(1)} = b_i^1 - \alpha\frac{\partial}{\partial b_i^{(1)}}J(W, b). \tag{8}$$

Calculation method of partial derivative.

$$\frac{\partial}{\partial W_{ij}^1}J(W, b) = \left[\frac{1}{m}\sum_{i=1}^{m}\frac{\partial}{\partial W_{ij}^{(1)}}J\left(W, b\,; x^{(i)}, y^{(i)}\right)\right] + \lambda W_{ij}^{(1)},$$
$$\frac{\partial}{\partial b_i^{(1)}}J(W, b) = \frac{1}{m}\sum_{i=1}^{m}\frac{\partial}{\partial b_i^{(1)}}J\left(W, b\,; x^{(i)}, y^{(i)}\right). \tag{9}$$

3.2. Quality Evaluation Method. Where TC is the total and $A_d(C_i)/M_d(C_i)$ is the number of attributes in class C_i.

$$\text{AHF} = \sum_{i=1}^{\text{TC}}\sum_{m=1}^{A_d(C_i)}\frac{(1 - V(A_{mi}))}{\sum_{i=1}^{\text{TC}}A_d(C_i)},$$
$$V(A_{mi}) = \sum_{j=1}^{\text{TC}}\frac{\text{is\_visible}\left(A_{mi}, C_j\right)}{(TC - 1)},$$
$$\text{is\_visible}\left(A_{mi}, C_j\right) = \begin{cases} 1, & \text{iff}\begin{cases} j \neq i, \\ C_j \text{ may reference } A_{mi}, \end{cases} \\ 0, \text{ otherwise}, \end{cases}$$
$$\text{MHF} = \sum_{i=1}^{\text{TC}}\sum_{m=1}^{M_d(C_i)}\frac{(1 - V(M_{mi}))}{\sum_{i=1}^{\text{TC}}M_d(C_i)},$$
$$V(M_{mi}) = \sum_{j=1}^{\text{TC}}\frac{\text{is\_visible}\left(M_{mi}, C_j\right)}{(TC - 1)},$$
$$\text{is\_visible}\left(M_{mi}, C_j\right) = \begin{cases} 1, & \text{iff}\begin{cases} j \neq i, \\ C_j \text{ may call } M_{mi}, \end{cases} \\ 0, \text{ otherwise}, \end{cases}$$
$$\text{AIF} = \frac{\sum_{i=1}^{\text{TC}}A_i(C_i)}{\sum_{i=1}^{\text{TC}}A_a(C_i)},$$
$$A_a(C_i) = A_d(C_i) + A_i(C_i). \tag{10}$$

4. Model and Method Analysis

4.1. Deep Learning Analysis

4.1.1. Accuracy Analysis of Deep Learning Model Evaluation Method. The training accuracy rate and effective accuracy rate of the deep learning model are compared and analyzed in different periods. The training accuracy rate changes gently from 0 to 70 epoch, with the lowest being 0.93 and the highest being 0.975, and the value difference is not big. At 10 epoch, the training acc is the same as the effective acc value, which is 0.95. In 0-70 epoch, the lowest value is 0.78 in 30 epoch, and the highest value is 0.97 in 70 epoch. In 0-70 epoch, when the difference between training accuracy and effective accuracy is about 30 epoch, the training accuracy is 0.96 and the effective accuracy is 0.78. The trend of training accuracy and effective accuracy is the same in other periods, as shown in Figure 3.

It can be seen from the images that the trend of training acc is the same as that of effective acc, which shows that the deep learning model is more accurate for the accuracy analysis of evaluation methods after many trainings, so DL can promote the related quality evaluation methods. Through its numerical values, it can be seen that DL model is more accurate for correlation analysis after many trainings.
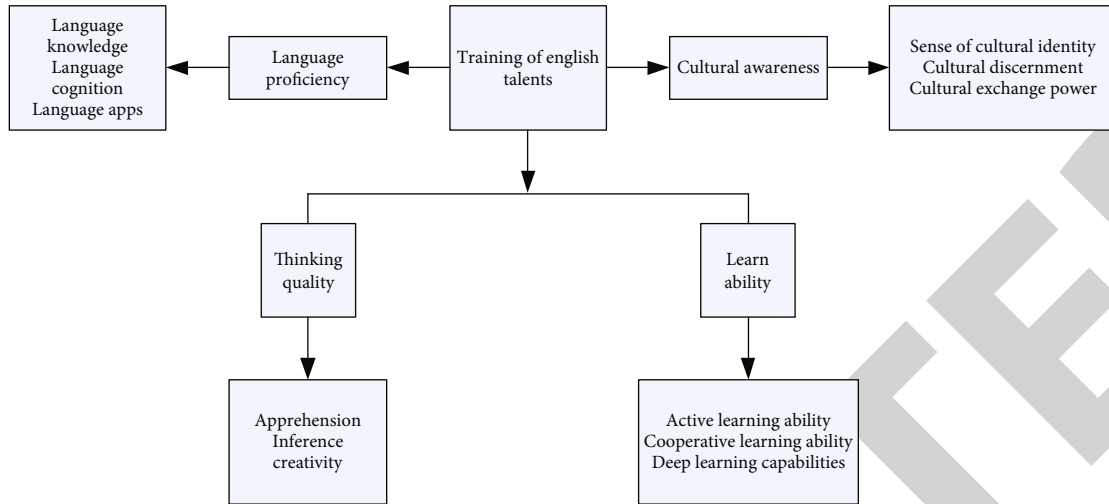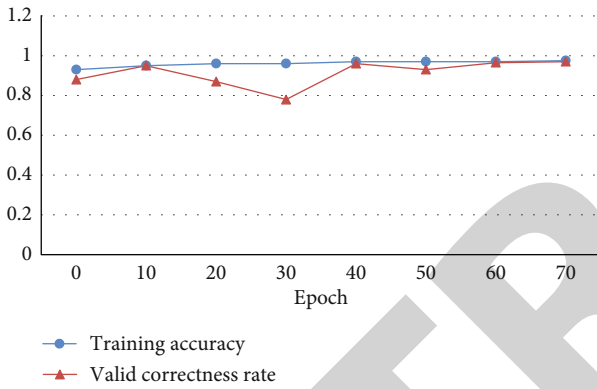
Figure 2: Flow chart of English talent training.

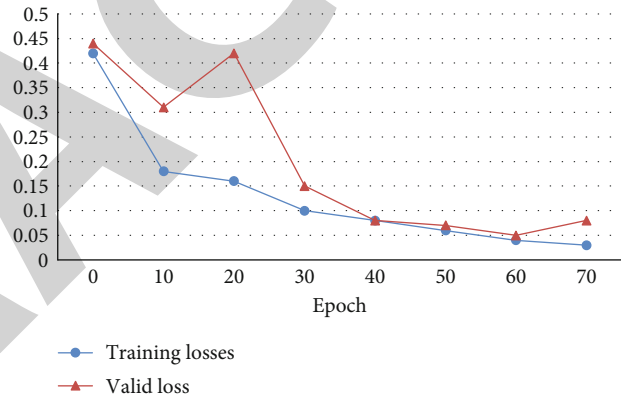
Figure 3: Training and analysis of effective accuracy.

Figure 4: Training and effective loss analysis.

4.1.2. Analysis of Loss Change of Deep Learning Model Evaluation Method. In this experiment, by comparing and analyzing the training loss with the effective loss, in 0-70 epoch, the values range from 0.42 to 0.18 to 0.16 to 0.1 to 0.08 to 0.06 to 0.04. At 70 epoch, the value dropped to 0.03, the training loss value shown in the image shows a gradual downward trend, from the highest 0.42 to 0.03 at 70 epoch. It can be seen that with the increasing of training times and epoch numbers, the training loss gradually decreases, the numerical loss gradually decreases, and the related loss also decreases, indicating that with the increase of training times, the loss value of DL model decreases and the numerical accuracy increases. By analyzing the effective loss curve, we can see that the general trend is the same as that of training loss. In 0-70 epoch, the value changes from 0.44 to 0.31 to 0.42 to 0.15 to 0.08 to 0.07 to 0.05 to 0.08, and in 20poch, the value increases to 0.42. From the curve trend, we can see that the effective loss basically shows a downward trend with the change of training times, except for 20 and 70 epoch. Through the trend analysis of two curves, the loss rate gradually decreases with the increase of training times, which shows that in order to get more

accurate change analysis, the training should make the value more accurate, and the DL model can promote the quality evaluation method, as shown in Figure 4.

4.2. Cultivation of English Talents

4.2.1. Evaluation of English Teachers. In order to improve and promote the cultivation of English talents, we should make an in-depth analysis of the evaluation of English teachers and improve English teaching through the analysis results, so as to fundamentally promote the cultivation of English talents. Through the study of English teachers, oral English, quality, methods, spirit, structure of many aspects of teachers for a total score of 100% satisfaction assessment. As far as academics are concerned, the highest evaluation value is satisfaction, with 42.91% satisfaction, among which very satisfactory, satisfactory and general evaluation satisfaction is higher, and the poor and very poor evaluation percentages are 3.7% and 3.03%, respectively, indicating that the relevant voters are satisfied with the academic level of English teachers. For oral English level, the highest evaluation rate of satisfaction level is 38.48%, and the lowest

Table 1: Analysis of English teacher evaluation.

Project	Evaluation of English teachers					Overall
	Very satisfied	Satisfied	General	Poor	Very poor	
Academic level	14.22%	42.91%	36.14%	3.7%	3.03%	100%
Oral proficiency	16.88%	38.48%	33.79%	8.13%	2.72%	100%
Teaching quality	15.24%	38.89%	33.76%	8.08%	4.03%	100%
Teaching method	33.58%	41.02%	19.12%	4.93%	1.35%	100%
Teaching spirit	12.75%	34.71%	40.29%	9.21%	3.13%	100%
Knowledge structure	13.69%	39.88%	36.12%	8.81%	1.5%	100%

evaluation rate of poor level is 2.72%. As far as teaching quality is concerned, the highest rate of satisfactory grade evaluation is 38.89%, and the lowest rate of poor grade evaluation is 4.03%. The highest rate of satisfactory grade evaluation of teaching methods is 41.02%, and the rate of poor grade evaluation is 1.34%. As far as teaching spirit is concerned, the highest evaluation rate of general grade is 40.29%, and the lowest evaluation rate of very poor grade is 3.13%. As far as knowledge structure is concerned, the highest rating rate of satisfaction is 39.88%, and the lowest rating rate of poor rating is 1.5%. Through the evaluation of relevant data, it can be seen that the evaluation of English teachers is generally satisfactory [24], as shown in Table 1.

From the trend of related images, it can be seen that the evaluation of teachers is generally satisfactory in terms of academic performance, oral English, quality, method, spirit, and structure, with the lowest proportion of poor and very poor. It can be seen from the relevant evaluation rate that voters are satisfied with teachers' evaluation. In order to cultivate English talents, we should focus on improving teachers' satisfaction in six aspects: academic performance, oral English, quality, method, spirit, and structure and improve the evaluation rate of very satisfactory grade to cultivate more and better English-related talents, as shown in Figure 5.

4.2.2. Problem Analysis.
In order to better train English talents, this paper evaluates and analyzes the problems existing in the training of English talents from three aspects: students, graduates, and teachers. This paper makes statistics on the problems in seven aspects of English talents training, including practice, form, teaching and content, time, effect, content, and level. For students, most of them think that the poor level of teaching capital is the biggest problem, with an evaluation rate of about 24.4%, and that the evaluation rate is the lowest for short teaching time. Secondly, students think that the current teaching content should be updated. As far as graduates are concerned, most of them think that the biggest problem in English talent training is the poor level of teaching resources, followed by outdated teaching content and lack of English communication practice. As far as teachers are concerned, they think that lack of practice, single form, and poor effect are the major problems in the training of English talents. As can be seen from the image, for students and graduates, teachers analyze the problems existing in the training of English talents and draw the
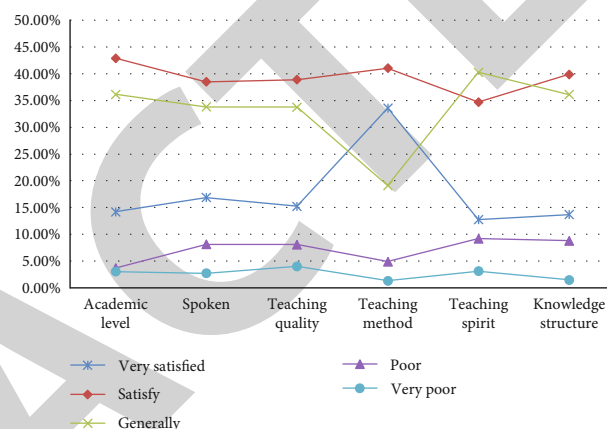

Figure 5: English teacher evaluation chart.

following conclusions. Among graduates, students, and teachers, they think that the poor level of teaching capital, single teaching form, and poor effect are the main problems, followed by a small number of graduates, students, and teachers think that there are more or less related problems in practice, teaching, content, and time. As shown in Figure 6.

4.2.3. Overall Quality Evaluation.
Through the evaluation and analysis of the overall quality of English talents training from three aspects: teachers, graduates, and students, it can be seen from the images that most teachers, graduates and students evaluate the overall quality as good or average, followed by poor, and finally very good or very poor. In order to improve the evaluation of the overall quality, we should improve the overall quality according to the analysis of related problems and the evaluation of teachers, improve the very good evaluation rate, and reduce the poor and very poor evaluation rate, so as to improve the overall quality evaluation, improve the satisfaction of teachers, graduates, and students, and improve the efficiency and quality of English talent training, as shown in Figure 7.

4.3. Evaluation Method of Personnel Training Quality

4.3.1. Evaluation Content.
In order to evaluate and analyze the quality of personnel training, the goal of personnel training is divided into quality goal and ability goal; the first-level index of quality goal is divided into psychological quality, ideological morality, and knowledge culture; the second-level index of psychological quality is will, personality, and
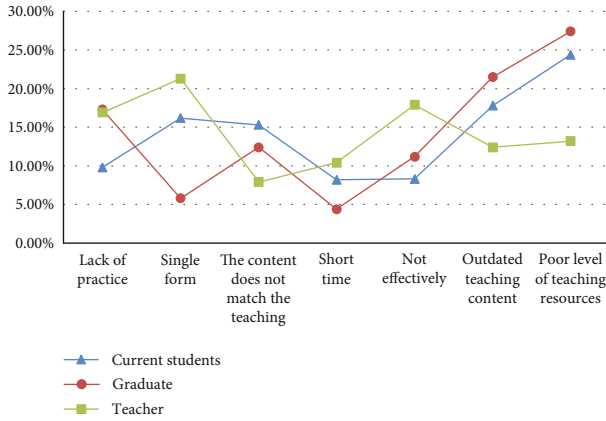
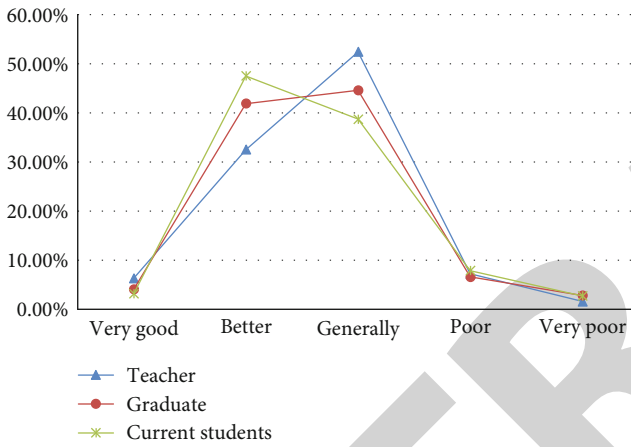Figure 6: Analysis diagram of existing problems.

Figure 7: Overall quality evaluation chart.

self-awareness; the second-level goal of ideological morality is divided into thought and morality; and the second-level goal of knowledge culture accomplishment is divided into professional and extracurricular knowledge. The first-level index of ability goal is divided into learning, communication, and practical ability; learning ability is divided into learning interest and skills, and practical ability is divided into innovation and practical ability. Through the detailed division of the first-level goal and the second-level goal in many aspects, we can make a more in-depth evaluation of the evaluation content in many aspects, so as to obtain a more in-depth and accurate evaluation of the quality of personnel training, as shown in Table 2.

4.3.2. Algorithm Comparison. Through the comparison of the AF algorithm, BQ algorithm, and algebraic algorithm, the quality evaluation method with the best performance is obtained. Through 1-6 sample numbers, the prediction values of the AF algorithm, BQ algorithm, and algebraic algorithm are compared with the expected values, so as to obtain the relevant error rates. Sample 1 shows that the predicted value of AF algorithm is 6.65, the predicted value of BQ algorithm is 6.43, the predicted value of algebraic algo-

rithm is 7.12, and the expected value is 6.5. Through calculation, the error of AF algorithm is 0.92%, the error of the BQ algorithm is 1.1%, and the error of the algebraic algorithm is 9.5%. In sample 2, the error of the AF algorithm is 1%, the error of the BQ algorithm is 6.2%, and the error of the algebraic algorithm is 8%. The sample 3AF error is 2.85%, the BQ algorithm error is 2.14%, and the algebraic algorithm error is 5.71%. The sample 4AF algorithm error is 1.66%, BQ algorithm error is 2.16%, and algebraic algorithm error is 5%. The sample 6AF algorithm error is 2.5%, BQ algorithm error is 4.29%, and algebraic algorithm error is 10.7%, as shown in Table 3.

It can be seen from sample number 5 that the expected value is 7, the predicted value of AF algorithm is 7.41, and the error is 5.86%. The predicted value of BQ algorithm is 7.75, and the error is 10.7%. The prediction value of algebraic algorithm is 6.5, and its error is 7.14%. Compared with the expected value of 7, the error of AF algorithm is the smallest.

It can be seen from the curve trend that the error rate of the AF algorithm is lower than that of the BQ algorithm and algebraic algorithm, and the result is more accurate. Therefore, in order to obtain a better evaluation method of English talent training quality, the AF algorithm under the DL model should be used to improve the accuracy, as shown in Figure 8.

For performance comparison, by analyzing the accuracy, recall rate, $F1$, accuracy, and other performances of the AF model, BQ model, and algebraic algorithm [25]. Through image trend analysis, we can see that the accuracy, recall, $F1$, and accuracy of the AF algorithm is higher than the BQ algorithm and algebraic algorithm, followed by the BQ algorithm, while the algebraic algorithm has lower performance, as shown in Figure 9.

Accuracy:

$$\text{Accuracy} = \frac{\text{TP} + \text{FN}}{\text{TP} + \text{TN} + \text{FP} + \text{FN}}. \quad (11)$$

It is an index used to evaluate the classification model, and the model predicts the proportion of the correct quantity to the total.

Precision:

$$\text{Precision} = \frac{\text{TP}}{\text{TP} + \text{FP}}. \quad (12)$$

Accuracy is the difference between the average value of each independent measurement and the known true value of the data (the degree of agreement with the theoretical value).

Recall:

$$\text{Recall} = \frac{\text{TP}}{\text{TP} + \text{FN}}. \quad (13)$$

The recall rate is for our original sample, which indicates how many positive cases in the sample are predicted correctly.

TABLE 2: Table of evaluation contents.

Talent training goal	First-class index	Secondary index
		Will
	Psychological quality	Personality
		Self-consciousness
Quality goal	Ideological and moral quality	Ideological morality
		Moral quality
	Knowledge and cultural accomplishment	Professional knowledge cultivation
		Extracurricular knowledge cultivation
	Learning ability	Interest in learning
		Learning skills
Ability goal	Communication skills	Communication skills
	Practical ability	Innovation ability
		Practical hands-on ability

TABLE 3: Algorithm comparison table.

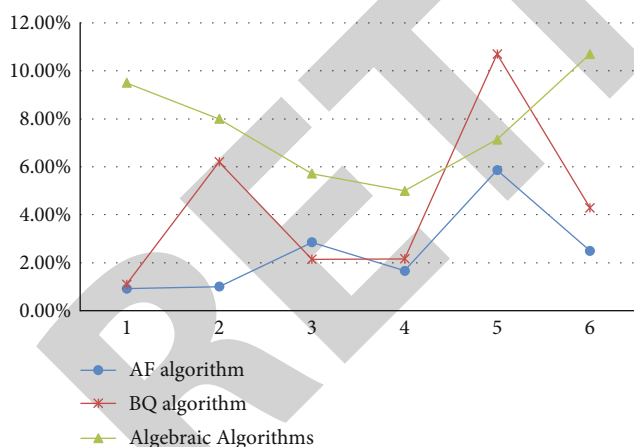| Sample label	AF algorithm Predicted value	Error	BQ algorithm Predicted value	Error	Algebraic algorithm Predicted value	Error	Expected value
1	6.56	0.92%	6.43	1.1%	7.12	9.5%	6.5
2	4.95	1%	5.31	6.2%	5.4	8%	5
3	7.2	2.85%	6.85	2.14%	7.4	5.71%	7
4	6.1	1.66%	5.87	2.16%	6.3	5%	6
5	7.41	5.86%	7.75	10.7%	6.5	7.14%	7
6	6.8	2.5%	7.3	4.29%	7.75	10.7%	7

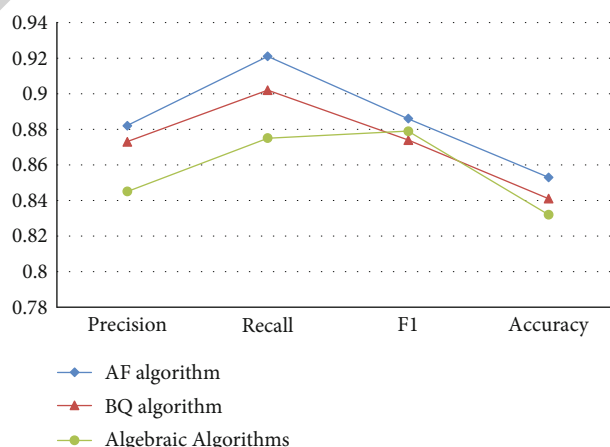FIGURE 8: Algorithm error comparison diagram.

FIGURE 9: Algorithm performance comparison diagram.

F1:

$$F\text{-measure} = \frac{2 * \text{Precision} * \text{Recall}}{\text{Precision} + \text{Recall}}. \tag{14}$$

It is an index used to measure the accuracy of binary classification model in statistics. It takes into account both the accuracy and recall of the classification model.

5. Conclusion

In order to analyze the quality of English talents training under the deep learning model, this paper makes statistics on the training and effective accuracy of deep learning for many times within 0-70 epoch. Experiments show that the curve trend of training acc and effective acc is the same, which shows that the accuracy of deep learning is more accurate after many times of training. In the same way, the

training and effective loss experiments show that with the increase of the number of experiments, the training loss and effective loss are also effectively reduced. At the same time, it evaluates English teachers and analyzes the existing problems. Finally, it makes a statistical analysis of the overall evaluation results to improve the quality of English talents training.

In order to improve the quality evaluation method to obtain more accurate evaluation, the error and performance of the AF algorithm, BQ algorithm, and algebraic algorithm are compared. Through numerical analysis, it can be seen that the error of the AF algorithm is lower than that of the BQ algorithm and algebraic algorithm, and the performance of the AF algorithm is better than that of the BQ algorithm and algebraic algorithm in numerical accuracy, recall rate, $F1$, and accuracy rate. Therefore, the AF algorithm under the DL model is more beneficial for evaluation and analysis.

Data Availability

The experimental data used to support the findings of this study are available from the corresponding author upon request.

Conflicts of Interest

The authors declared that they have no conflicts of interest regarding this work.

Acknowledgments

References

[1] L. T. Mcintosh, N. Maheswaranathan, and A. Nayebi, "Deep learning models of the retinal response to natural scenes," *Advances in neural information processing systems*, vol. 29, pp. 1369–1377, 2017.

[2] K. P. Ferentinos, "Deep learning models for plant disease detection and diagnosis," *Computers and Electronics in Agriculture*, vol. 145, pp. 311–318, 2018.

[3] N. Yalta, K. Nakadai, T. Ogata, Intermedia Art and Science Department, Waseda University, and Honda Research Institute Japan Co., Ltd., "Sound source localization using deep learning models," *Journal of Robotics and Mechatronics*, vol. 29, no. 1, pp. 37–48, 2017.

[4] L. Sangmok and L. Donghyun, "Improved prediction of harmful algal blooms in four major South Korea's rivers using deep learning models," *International Journal of Environmental Research & Public Health*, vol. 15, no. 7, p. 1322, 2018.

[5] H. Wang and B. Raj, "A survey: time travel in deep learning space: an introduction to deep learning models and how deep learning models evolved from the initial ideas," *Computer science*, vol. 226, no. 1-4, pp. 23–34, 2015.

[6] J. Xing, K. Li, W. Hu, C. Yuan, and H. Ling, "Diagnosing deep learning models for high accuracy age estimation from a single image," *Pattern Recognition*, vol. 66, pp. 106–116, 2017.

[7] H. Y. Wu, "Training practice talents of information management professional," *Advanced Materials Research*, vol. 143-144, pp. 571–575, 2010.

[8] C. Meskill, "Infusing English language learner issues throughout professional educator curricula: the training all teachers project," *Teachers College Record*, vol. 107, no. 4, pp. 739–756, 2005.

[9] A. Al-Issa and A. Al-Bulushi, "Training English language student teachers to become reflective teachers," *Australian Journal of Teacher Education*, vol. 35, no. 4, pp. 41–64, 2010.

[10] S. Swathi, "Music training and second-language English comprehension and vocabulary skills in Indian children," *Psychological Studies*, vol. 58, no. 2, pp. 164–170, 2013.

[11] G. Wamae and R. W. Kang'ethe-Kamau, "The concept of inclusive education: teacher training and Acquisition of English language in the hearing impaired," *British Journal of Special Education*, vol. 31, no. 1, pp. 33–40, 2004.

[12] F. Elortondo, M. Ojeda, M. Albisu, J. Salmerón, I. Etayo, and M. Molina, "Food quality certification: an approach for the development of accredited sensory evaluation methods," *Food Quality & Preference*, vol. 18, no. 2, pp. 425–439, 2007.

[13] J. Slayton and L. Llosa, "The use of qualitative methods in large-scale evaluation: improving the quality of the evaluation and the meaningfulness of the findings," *Teachers College Record*, vol. 107, no. 12, pp. 2543–2565, 2005.

[14] P. Corriveau and A. Webster, "VQEG evaluation of objective methods of video quality assessment," *SMPTE Journal*, vol. 108, no. 9, pp. 645–648, 1999.

[15] E. B. Mandinach, "The development of effective evaluation methods for E-learning: a concept paper and action plan," *Teachers College Record*, vol. 107, no. 8, pp. 1814–1835, 2005.

[16] D. J. Treffinger and S. G. Isaksen, "Creative problem solving: the history, development, and implications for gifted education and talent development," *Gifted Child Quarterly*, vol. 49, no. 4, pp. 342–353, 2005.

[17] F. GagneTen, "Ten commandments for academic talent development," *Gifted Child Quarterly*, vol. 51, no. 2, pp. 93–118, 2007.

[18] S. Ollis, A. Macpherson, and D. Collins, "Expertise and talent development in rugby refereeing: an ethnographic enquiry," *Journal of Sports Sciences*, vol. 24, no. 3, pp. 309–322, 2006.

[19] C. Cushion, P. R. Ford, and A. M. Williams, "Coach behaviours and practice structures in youth soccer: implications for talent development," *Journal of Sports Sciences*, vol. 30, no. 15, pp. 1631–1641, 2012.

[20] L. Barlow, "Talent development: the new imperative," *Development & Learning in Organizations*, vol. 20, no. 3, pp. 6–9, 2006.

[21] L. Sun and E. Ifeachor, "New methods for voice quality evaluation for IP networks," *Teletraffic Science and Engineering*, vol. 5, pp. 1201–1210, 2003.

[22] Y. Bengio, "Deep learning of representations: looking forward," in *International Conference on Statistical Language and Speech Processing*, vol. 18, no. 2pp. 2–29, Springer Berlin Heidelberg, 2013.

Research Article

Construction and Analysis of Public Management System Indicators Based on AHP (Analytic Hierarchy Process)

Pengcheng Zhao[1] and Peiling He [2]

[1]*Safety and Security Department, Guizhou Polytechnic of Construction, Guiyang, Guizhou Province 550000, China*
[2]*Bank of Guiyang Co., Ltd., Guiyang, Guizhou Province 550000, China*

Correspondence should be addressed to Peiling He; hepeiling@bankgy.com.cn

In the era of intelligent network, my country's public management services are in a transition period, and many problems have gradually occurred, which have a certain impact on public management. In the previous management mode, the latest management requirements could not be met, and there were many problems in the actual management process. With the rapid development of social economy, public management is the key to promote social development. Only by constructing a reasonable index system of public management can public management play its due role in the era of rapid development. Therefore, this paper uses Bohr formula, Shannon formula, and entropy weight method to construct the public management system index based on AHP. The research results of this paper are in the stage of model checking, and the accuracy of this method is the highest in different data sets. The accuracy of big data analysis method and the original method decreases with the increase of data sets, which reflects the obvious advantages of this method. The response time of big data analysis methods increases gradually due to the increase of data sets, but the method in this paper grows slowly. All indicators show that the constructed public management index system has high reliability and validity.

1. Introduction

The rapid economic development has put forward higher and higher requirements for public management. With the gradual improvement of the level of social modernization, public management measures also need to be improved accordingly. In order to continuously optimize my country's public management system, this paper uses Bohr's formula, Shannon's formula, and entropy weight method to construct a public management system index system based on AHP and analyzes it in detail. This paper has received a lot of support on the basis of previous research results. AHP is an organic combination of qualitative and quantitative methods [1]. AHP pays more attention to qualitative analysis and judgment than general quantitative methods [2]. AHP does not require more quantitative data information [3]. AHP is a simple and general decision-making method

[4]. AHP is to decompose the decision problem into different levels in order [5]. AHP is a system analysis method [6]. It is both practical and effective when dealing with complex decision problems [7]. Public management emphasizes the "publicity" of management objectives [8]. On the other hand, it emphasizes the scientific method of using public power [9]. Public management is a management concept and management model that is produced in response to the defects of government management [10]. Public management emphasizes the supervision, restriction, and regulation of public power [11]. The subject of public administration is diverse [12]. The regulation of public management functions [13]. An indicator system refers to an organism composed of several interrelated statistical indicators [14]. The establishment of the index system is the premise and foundation of prediction or evaluation research [15].

2. AHP (Analytic Hierarchy Process)

Analytical hierarchy process [16] is a method of quantitatively evaluating qualitative conclusions by combining a series of theories with time. By grading complex problems, simplifying complexity, and taking weights as ideas, it provides a basis for choosing the best solution.

2.1. Features of AHP.

The characteristics of AHP: (1) the thinking of decision makers has become more logical and hierarchical, and the overall decision-making process has become clearer, forming a logical chain. (2) Be clearer about the factors involved in the decision-making process and their relationships [17]. (3) The introduction of quantitative analysis in the judgment process can improve the scientificity and logic of decision makers' thinking and make the decision-making process more scientific.

The advantages and disadvantages of AHP are shown in Table 1 below.

2.2. Building a Hierarchical Model

2.2.1. Steps to Build a Hierarchical Model.

Building a practical and efficient hierarchical model requires the following steps:

Step 1. Collect and organize relevant information and data.

Step 2. Identify the characteristics of information and classify it.

Step 3. Build the overall structure of the target, and establish the basic hierarchical structure of the target and the target network structure.

Step 4. Extract attributes from the target structure.

Step 5. Filter out unnecessary influencing factors and common features, and select key distinguishing features.

Step 6. Use decision-making methods to assess influencing factors.

Step 7. Discuss the selection results and make a final decision.

2.2.2. Hierarchical Model.

Hierarchical model is shown in Figure 1.

The AHP structure model divides the relationship among objectives, standards, and schemes into the highest level, the middle level, and the lowest level. Among them, the highest level represents the purpose of decision-making, and the problem to be solved is the overall goal. The middle tier represents factors and criteria that need to be considered. The bottom layer represents the alternatives considered when solving the problem when making a decision.

2.3. Weight Calculation of AHP

2.3.1. Subjective Weight Calculation.

The steps of using AHP to determine the index weight are as follows [18]. Establish a progressive hierarchy model is defined as follows:

Step 1. Constructing the judgment matrix

Assuming that evaluation object R is affected by n factors $\{a_1, a_2, \cdots, a_n\}$ of an index layer, according to the scaling method, the relative importance of a_i and a_j to evaluation object R is expressed in numbers, marked as a_{ij} and a_{ji}, respectively. According to the construction of the judgment matrix, a_{ij} and a_{ji} should satisfy the following:

$$a_{ij} > 0, a_{ji} > 0, a_{ij} = \frac{1}{a_{ji}}, a_{ii} = 1, (i \neq j). \tag{1}$$

From this, the judgment matrix composed of relative attributes can be obtained:

$$A = \left(a_{ij}\right)_{n \times n}. \tag{2}$$

Step 2. Calculate the weight of each factor

The weight coefficient of each factor is the eigenvector W of the judgment matrix [19]. It can be obtained by the following formula:

$$AW = \lambda_{\max} W. \tag{3}$$

Generally speaking, the calculation of eigenvectors generally adopts the square root method, the power method, the arithmetic mean method, the geometric mean method, etc. In this article, the square root method is used to calculate the weight coefficient of the index. The specific steps are as follows:

Multiplying the values of each row of the judgment matrix $A = \left(a_{ij}\right)_{n \times n}$, you can get the following:

$$M_i = \prod_{j=1}^{n} a_{ij} (i = 1, 2, \cdots, n). \tag{4}$$

Taking the n-rd root of M_i, we get the following:

$$W_i = \sqrt[n]{M_i} (i = 1, 2, \cdots, n). \tag{5}$$

Normalize the vector $W = (W_1, W_2, \cdots, W_n)^T$ to get the following:

$$W_i = \frac{W_i}{\sum_{i=1}^{n} W} (i = 1, 2, \cdots, n). \tag{6}$$

The obtained matrix $W = (W_1, W_2, \cdots, W_n)^T$ is the weight coefficient of each index.

Calculate the maximum eigenvalue $\lambda_{\max}$ of the judgment matrix.

$$\lambda_{\max} = \sum_{i=1}^{n} \frac{(AW)_i}{nW_i}, \tag{7}$$

$$\lambda_{\max} = \frac{1}{n} \sum_{i=1}^{n} \frac{(BW)_i}{W_i}, \tag{8}$$

$$\lambda_{\max} = \frac{1}{n} \sum_{i=1}^{n} \frac{\sum_{j=1}^{n} a_{ij} W_j}{W_i}, \tag{9}$$

where $(AW)_i$ is the i component of AW.

TABLE 1: Advantages and disadvantages of AHP.

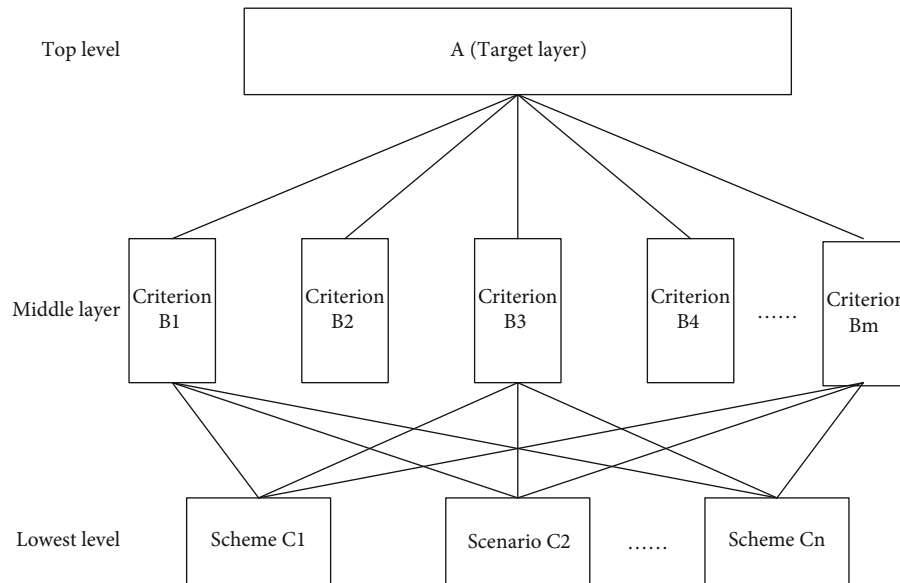| Advantage	Shortcoming
Systematic approach to analysis	Inability to provide new options for decision-making
Simple and practical decision-making method	Less quantitative data, more qualitative components, less convincing
Less quantitative data information required	The exact method of eigenvalues and eigenvectors is more complicated

FIGURE 1: AHP structure model.

Step 3. The consistency test of the judgment matrix

Because the comparison of the importance of indicators is subjective, a consistency test of the judgment matrix is required [20]. The inspection steps are as follows:

Calculate the consistency index (CI).

$$CI = \frac{\lambda_{\max} - n}{n - 1}. \tag{10}$$

Calculate the consistency ratio (CR).

$$CR = \frac{CI}{RI}. \tag{11}$$

Among them, RI is the average random matching index. The smaller the CR, the better the consistency of the judgment matrix. When $CR < 0.1$, the difference of the judgment matrix is considered to be within the allowable range and has consistency.

Step 4. Get the combined weight vector

By weighted fusion of subjective weights W_1 and W_2, a combined weight vector W_2 is obtained [21]. The formula is as follows:

$$W = \frac{W_1 + W_2}{2}. \tag{12}$$

2.3.2. Objective Weight Calculation. The calculation of the target weight can use the entropy weight method. When the difference between the evaluation index values is larger, the entropy value is smaller, and the amount of information carried by the index is larger, and a larger weight can be given to it. In contrast, indexes carry less information.

The steps to determine the index using the entropy weight method are as follows:

Standardize the data.

Let matrix $X = (X_{ij})_{n \times m}, (i = 1, 2, \cdots, n; j = 1, 2, \cdots, m)$ be the original data matrix composed of n evaluated objects and m average indicators. Normalize various types of data:

$$y_{ij} = \frac{X_{ij} - \min X_{ij}}{\max X_{ij} - \min X_{ij}}, \tag{13}$$

$$y_{ij} = \frac{\max X_{ij} - X_{ij}}{\max X_{ij} - \min X_{ij}}. \tag{14}$$

To get the matrix,

$$Y = (y_{ij})_{n \times m}. \tag{15}$$

Among them, y_{ij} is the j evaluation index [22]. Normalize the value on the i-rd evaluation subject, and $y_{ij} \in [0, 1]$.

Normalize the judgment matrix.

$$R' = (y'_{ij})_{n \times m}, \tag{16}$$

$$R' = \frac{y_{ij}}{\sum_{i=1}^{m} y_{ij}(i = 1, 2, \cdots, n; j = 1, 2, \cdots, m)}. \quad (17)$$

Calculate the entropy value of an evaluation index.

$$H_j = -\frac{1}{\ln m} \sum_{i=1}^{m} y'_{ij} \ln \left(y'_{ij}\right)(i = 1, 2, \cdots, n; j = 1, 2, \cdots, m). \quad (18)$$

When $y'_{ij} = 0$, the objective weight coefficient of the indicator is as follows:

$$W_i = \frac{1 - H_j}{m - \sum_{j=1}^{m} H_j}. \quad (19)$$

2.3.3. Combination Weight Calculation of AHP-Entropy Weight Method. The combined weight model is optimized using the least squares method [23]. Get weight W^*:

$$\min F(W^*) = \sum_{i=1}^{n} \sum_{j=1}^{m} \left\{ \left[(W^* - W)b_{ij}\right]^2 + \left[(W^* - W_i)b_{ij}\right]^2 \right\}. \quad (20)$$

Restrictions are as follows:

$$\sum_{j=1}^{m} W^* = 1, W^* \geq 0 (j = 1, 2, \cdots, m). \quad (21)$$

3. Construction of Public Management System Indicators

3.1. Public Administration. Public administration is generally defined as the management activities of public organizations, especially government agencies, and the study of the law. Public administration is the activity of a public authority for the provision of public property and public services. It is more about obtaining results and their responsibility [24].

3.1.1. Essence. The essential meaning of public management is "public." The theoretical system of public management consists of public meaning and classification system [25], as shown in Table 2.

Therefore, the essence of the significance of public management lies in strengthening and improving the responsibility mechanism of the public sector itself, establishing and developing a social public responsibility mechanism, and fulfilling its obligations through the public sector, so that the citizens can fully implement it. Uphold and fulfill their obligations and public good. Ultimately realize the interests of political domination, thereby strengthening and maintaining the existing basic social order and strengthening the social mobilization capacity and public solidarity of public agencies such as government public departments and nongovernmental agencies.

3.1.2. Main Features. There are four main characteristics of public management: public management is the activities that take place in public organizations; the basis of public management is public power; the main task is to provide public goods and public services to all members of society; public organizations achieve goals and achieve good results; the key is coordination, as shown in Table 3.

3.2. Mathematical Model of Public Administration. This paper derives the mathematical model of public management according to Bohr formula and Shannon formula.

3.2.1. Model Assumptions. The public management system is a relatively closed and isolated system with less information, energy, and material exchanges with the environment.

There are energy disparities within the public management system and are in a state of imbalance.

3.2.2. Mathematical Model Representation Method.

$$S_1 = \sum_{i=1}^{n} K_i S_i, \quad (22)$$

where i is the factor affecting the relatively closed public management system, K_i is the weight of various influencing factors at a specific stage, and S_i is the value generated between various influencing factors.

$$S_i = -K_B \sum_{i=1}^{n} P_{ij} \ln P_{ij}, \quad (23)$$

where K_B is the public management coefficient, j is the subfactors included in each public management influencing factor, and P_j is the probability that each subfactor affects the public management change. P_j is defined as follows:

$$\sum P_j = 1. \quad (24)$$

Because public management systems can lead to public management inefficiencies, the formula for organizational inefficiency can also be used to represent the internal processes of public management systems.

$$Y = \text{Re}^{-X}, \quad (25)$$

$$X = f(a_1 X_1, a_2 X_2, \cdots, a_n X_n) = \sum_{i=1}^{n} a_i X_i. \quad (26)$$

Among them, Y is the efficiency of public management, R is the structural constant of public management, X_i is the function of the influencing factors of public management efficiency, and a_i is the weight of each influencing factor.

3.3. Building a Public Management System. This paper builds a public management system model based on AHP, the target layer is public management, the middle layer is 2 first-level indicators and 8 second-level indicators, and

TABLE 2: The essence of public management.

Essential connotation	Content
Main body of public administration	In other words, it is not private enterprises and private institutions, but public institutions such as the public sector, nonprofit sector, and third sector, as well as authoritative institutions with government administrative agencies as the core.
The nature of public administration	All public management of human society has the nature of implementing the will of the state and its subordinate government departments, maintaining the political order of the state, and displaying functions, procedures, elements, and processes in the form of actions. The nature of specific activities of public administration manifests itself differently in historical eras and under various developing political and economic systems.
Social responsibility and obligation of public management	Provide public services according to public needs. In addition, through a public responsibility mechanism with strict performance goals and performance management, it is ensured that the public management body is responsible to the general public in the competition, and the service quality and customer satisfaction are improved.

TABLE 3: Main features of public administration.

Main features	Content
Public management is an activity that takes place in public organizations, and public management takes the realization of social public interests as its overall goal	This goal can be divided into several subgoals. Subgoals tend to be contradictory and contradictory, and these decisions and choices often affect the directionality of values that require balance and compromise.
The foundation of public management is public power, which is the guarantee for coordinating social and social resources.	Public power comes from the recognition and coercion of people by law. Therefore, public management should emphasize public responsibility and be overseen by society as a whole.
The main task of public management is to provide public goods and public services to all members of society.	Both tangible and intangible goods are included in public goods. Public services mainly include the provision of public safety and order, as well as the resolution and handling of safety issues.
The key to achieving goals and achieving good results in public organizations is adjustment.	Adjustment includes not only adjustment activities, but also adjustment activities between organizations and between organizations and societies. Since people are the center of various elements that make up people, various complex relationships in public institutions still exist among people, and adjustment activities are mainly carried out for people. People have both material and spiritual needs and are also affected by various social factors, so the means and methods of adjustment must be diversified.

the program layer is 25 third-level indicators, as shown in Figure 2.

Figure 2 describes the overall indicator system, showing the classification and indicator names of different indicator systems. This allocation scheme has good scientific significance and can better evaluate the public management system.

3.4. Public Management System Indicators. According to the meaning and characteristics of public management, using the AHP, the public management system indicators are constructed from multiple levels, as shown in Table 4.

4. Experimental Analysis

4.1. Model Testing. This paper builds a public management system index model based on AHP (analytic hierarchy process). In order to test the effect of the model, a comparative experiment is used to compare the effect of this method with the big data analysis method and the original analysis method.

The experimental samples in the model test are set to 5 different data sets of different sizes, and other factors are excluded. The experimental samples are tested by the big data analysis method, the original method, and the method in this paper, and the accuracy and success rate of the three methods are compared, as well as response time. The results are shown in Table 5.

According to the data in Figure 3, it can be concluded that the method in this paper has the highest accuracy in the 7 data sets tested, the highest accuracy rate is 99.7%, the highest accuracy rate of the big data analysis method is 95.4%, and the highest accuracy rate of the original method was 87.2%. It shows that the method in this paper has the highest accuracy and the best accuracy.

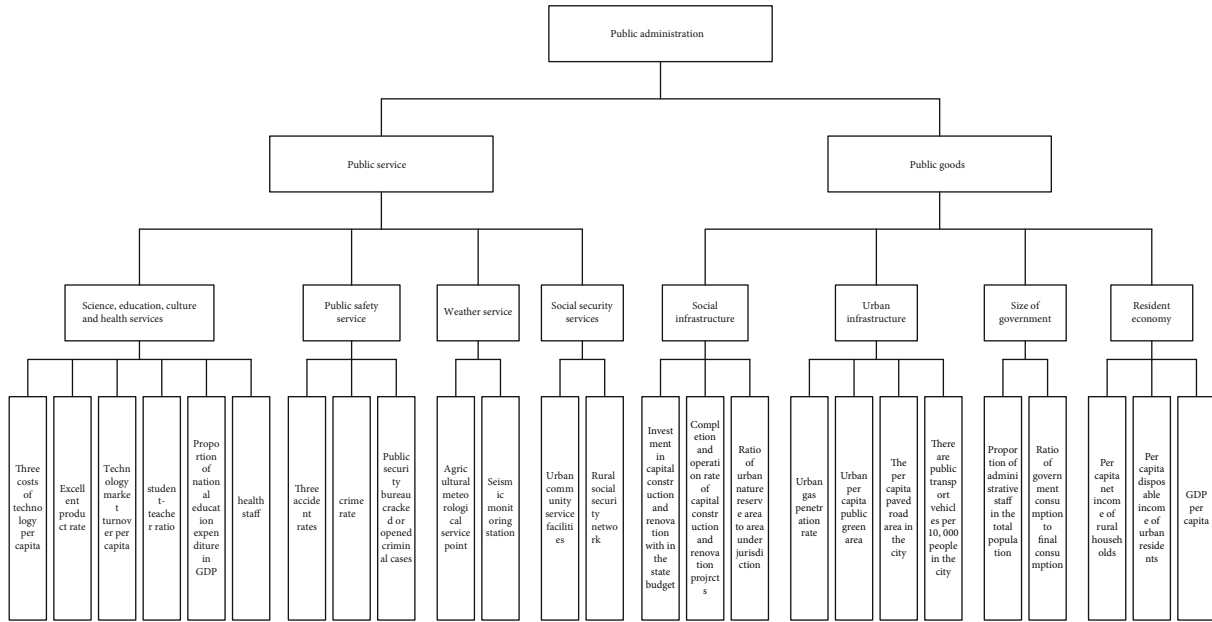As can be seen from Figure 4, the correct rate of the method in this paper is 100%, while correct rate of

FIGURE 2: Public management system model.

TABLE 4: Public management system indicators.

Main target	First-level indicator	Secondary indicators	Three-level indicator
Public administration	Public service	(A) Education, science, culture, health services	A1: per capita science and technology three expenses
			A2: product excellent rate
			A3: technology market turnover per capita
			A4: student-teacher ratio
			A5: national education expenditure as a percentage of GDP
			A6: health staff
		(B) Public safety services	B1: three accident rates
			B2: criminal case rate
			B3: Public Security Bureau cracked or opened a criminal case
		(C) Weather services	C1: agricultural meteorological service point
			C2: seismic monitoring station
		(D) Social security services	D1: urban community service facilities
			D2: rural social security network
	Public goods	(E) Social infrastructure	E1: state budget capital construction and improvement investments
			E2: capital construction and renovation project completion and commissioning rate
			E3: ratio of urban nature reserve area to jurisdiction area
		(F) City infrastructure	F1: city gas penetration rate
			F2: city per capita public green area
			F3: cities have paved road area per capita
			F4: cities have public transport vehicles per 10,000 people
		(G) government size	G1: administrative staff as a percentage of the total population
			G2: ratio of government consumption to final consumption
		(H) Resident economy	H1: per capita net income of rural households
			H2: per capita disposable income of urban residents
			H3: GDP per capita

TABLE 5: Model test data.

| Model	Data set	200	500	1000	1500	3000	5000	10000
	Accuracy (%)	99.7	99.7	99.7	99.6	99.1	98.7	98.3
The method of this paper	Success rate (%)	100	100	100	100	100	100	100
	Response time (ms)	22	36	59	78	112	138	152
	Accuracy (%)	95.4	93.1	92.4	90.1	88.6	85.3	82.1
Big data analysis methods	Success rate (%)	100	99.5	99.4	98.6	98.3	97.8	97.3
	Response time (ms)	49	68	87	114	148	189	231
	Accuracy (%)	87.2	84.7	83.2	78.6	75.4	74.3	70.1
Original method	Success rate (%)	100	99.3	99.1	98.2	97.5	97.1	96.8
	Response time (ms)	53	79	127	156	179	276	301
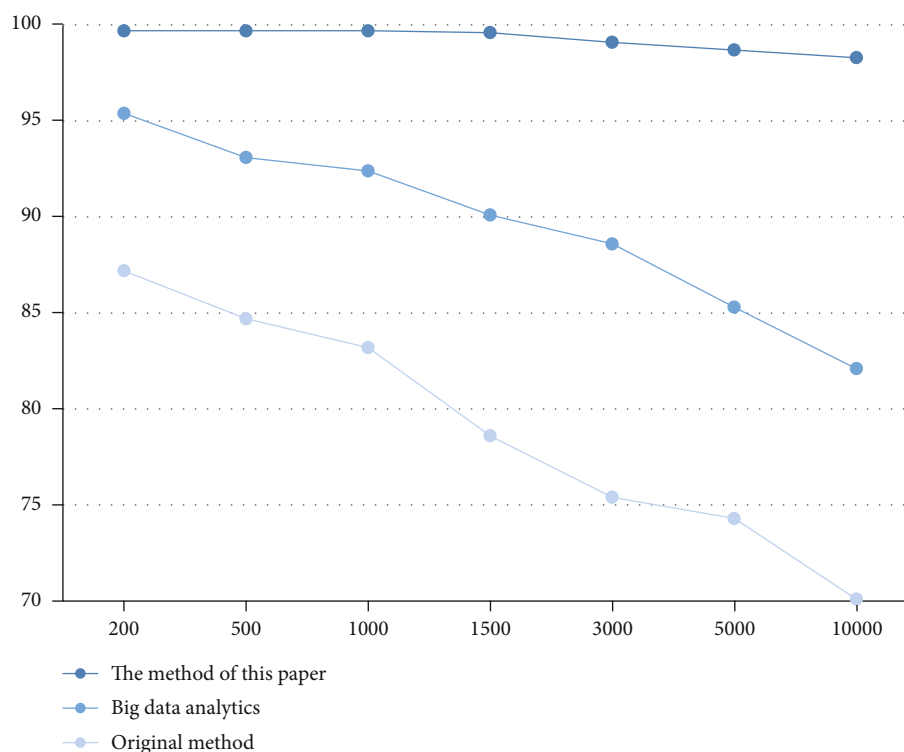
FIGURE 3: Accuracy in different method.

the big data analysis method and the original method is decreasing with the increase of the data set. It shows that with the increase of the data set, the accuracy of the big data analysis method and the original method cannot be guaranteed, and the accuracy will gradually decrease, which reflects the obvious advantages of the method in this paper.

Figure 5 intuitively reflects the obvious advantages of the method in this paper. The minimum response time of the method in this paper is 22 ms, the minimum response time of the big data analysis method is 49 ms, and the minimum response time of the original method is 53 ms. Although the response time gradually increases with the increase of the data set, the method in this paper increases relatively slowly. There is a way.

4.2. Indicator Weights. The research scope of public management takes government departments as the main body, and the experimental analysis of index weights takes the government departments of a city as the research scope and the government staff as the research objects. 100 government workers were randomly selected as the research objects, the data was collected through questionnaires, and the final index weight of the public management system was obtained according to the analytic hierarchy process.

After calculating the collected questionnaire data through a series of steps of AHP, the weights of each indicator are obtained: the weights of public services and public goods in the first-level indicators are 0.56 and 0.44, respectively.
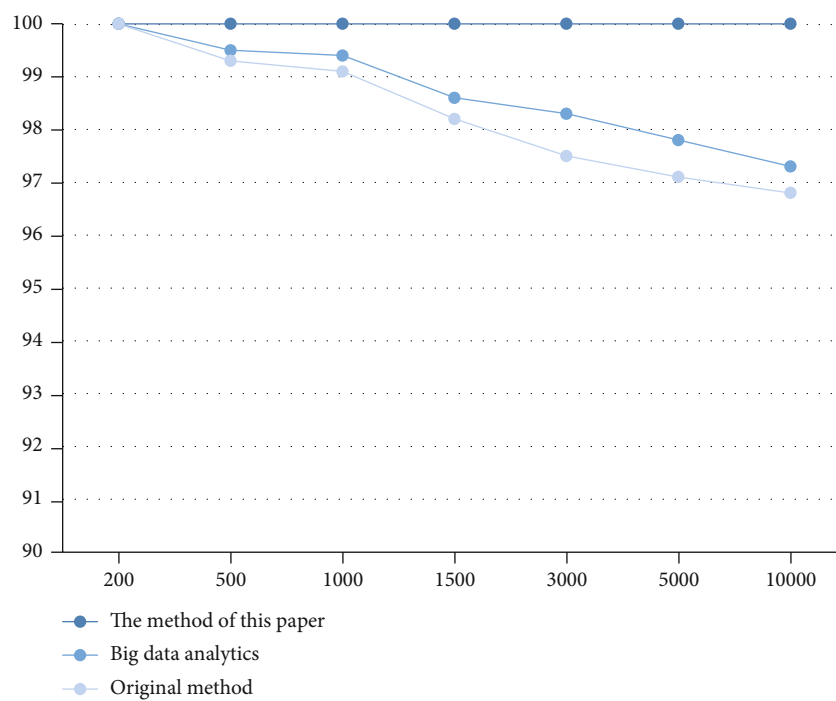
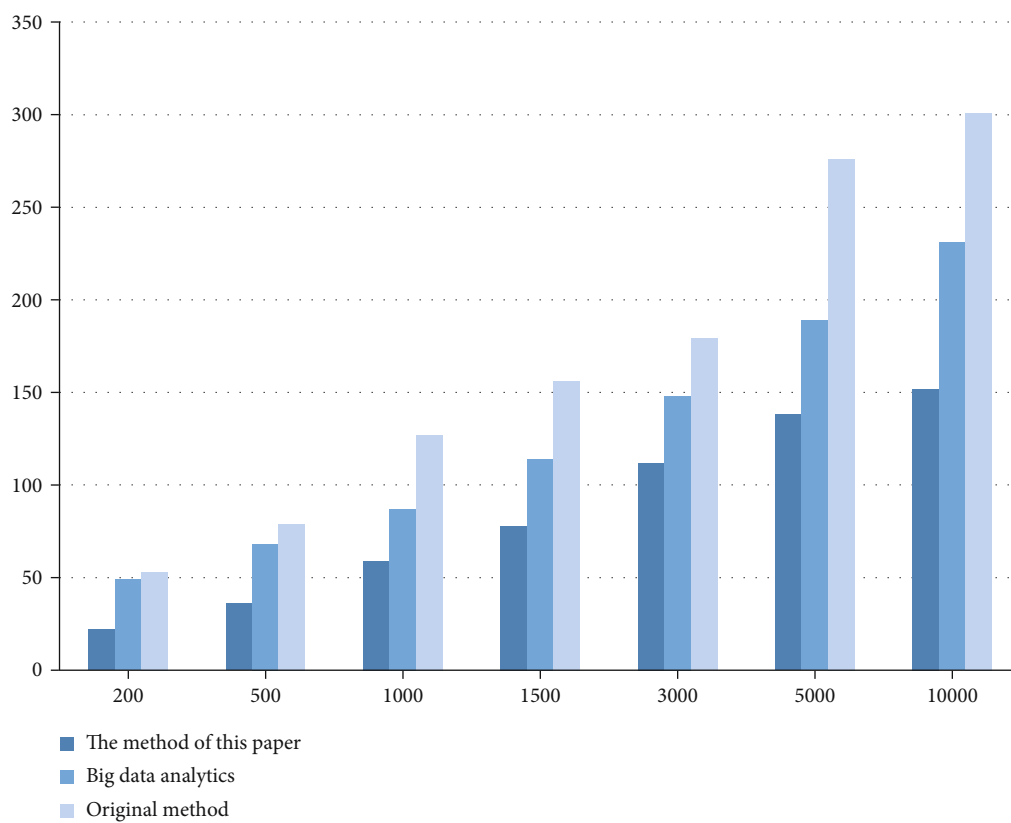FIGURE 4: Correct rate in different method.
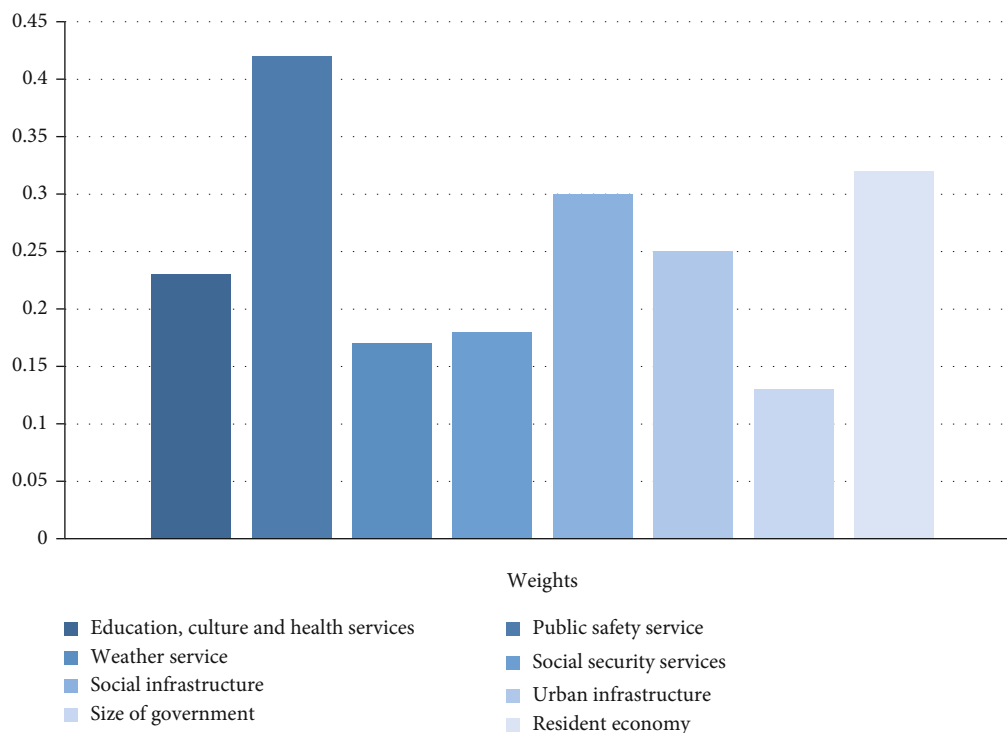

FIGURE 5: Response time.

FIGURE 6: Secondary indicators.

4.2.1. Secondary Indicators. The second-level indicators are obtained based on the first-level indicators. The weights of the indicators at each level in the second-level indicators are as follows: education, science, culture, health service 0.23, public safety service 0.42, meteorological service 0.17, social security service 0.18, social infrastructure 0.3, 0.25 for urban infrastructure, 0.13 for government size, and 0.32 for resident economy, as shown in Figure 6.

The weight of each secondary indicator is above 0.1, and most of them are between 0.15 and 0.25. The weight of public safety service is the highest, and the weight of government scale is the lowest. The index weights of public security services, social infrastructure, and residents' economy are all greater than or equal to 0.3. The weight of each indicator is different, indicating that the focus of public management is different. From the weight of each indicator, it can be seen that safety is the most concerned issue, and the weight of public safety services accounts for 0.42. The safety of a city is its most important guarantee.

4.2.2. Three-Level Indicators. It can be seen from Figure 7 that the weight of each indicator is different, indicating that the importance of each indicator is different, and the focus of government management is also different. The weights of all three-level indicators are above 0.1, and the weights of C2, D1, and G2 are all above 0.5. The highest indicator weight is 0.672 for urban community service facilities. Most of the three-level indicators are concentrated between 0.2 and 0.4.

4.3. Reasonability Test. In order to determine whether the public management index system constructed in this article

is reasonable, 10 experts were invited to evaluate the indicators established in this article, and the alpha coefficient of the test reliability and the S-value of the test validity were calculated according to the feedback from the expert CVI.

If the experimental results show that the α coefficients are all above 0.8, and the S-CVI values are all greater than or equal to 0.9, it indicates that the reliability and validity of the index system are good, and the index meets the standard and can be used. The data results are shown in Figure 8.

The data results show that the alpha coefficients of 25 tertiary indicators are all above 0.8, and the alpha coefficient of 9 tertiary indicators is above 0.9, which is the best level, indicating that the constructed public management indicator system has high reliability.

The average S-CVI of the third-level indicators is above 0.9, and the highest S-CVI is 0.983. Among them, the S-CVI of two indicators is below 0.9 but both are above 0.8, 0.832, and 0.897, respectively. It shows that the validity of the constructed public management index system is good.

Combining the results of α coefficient and S-CVI, it can be concluded that the public management index system constructed in this paper has good reliability and validity and has certain scientific rationality.

5. Conclusion

The public management system based on AHP refers to a major improvement of the public management index system and has great advantages compared with other methods in terms of accuracy, correctness, and response time. The Bohr formula, Shannon formula, and entropy weight method
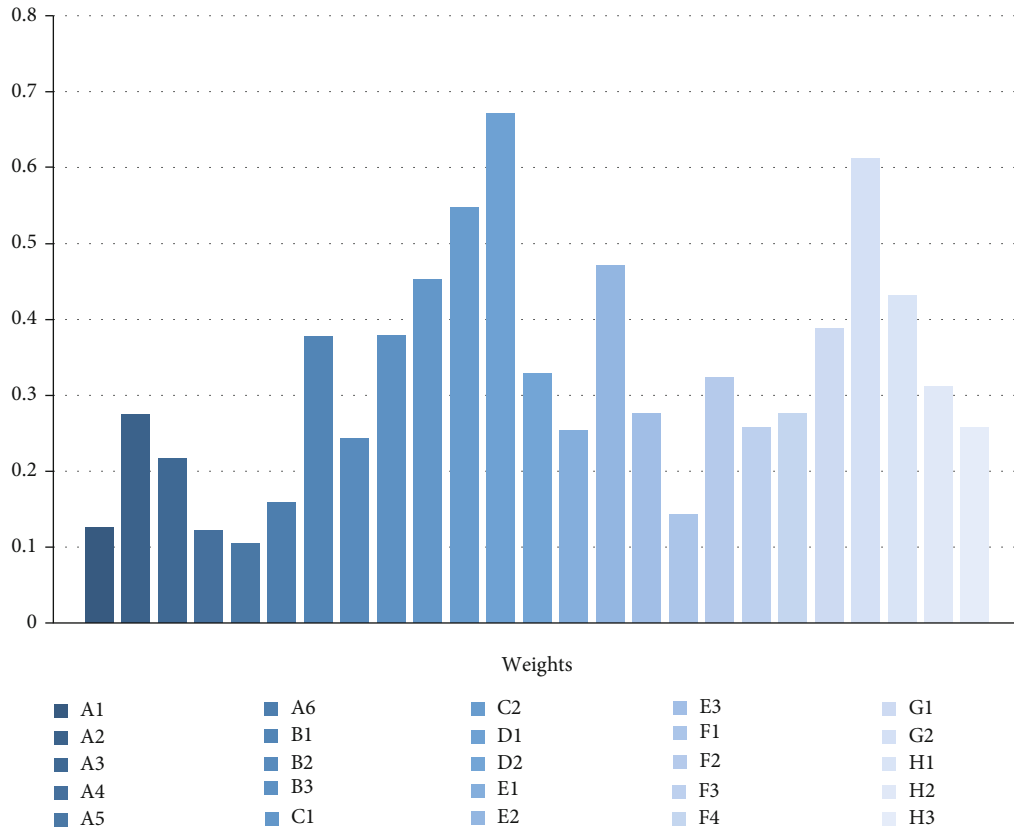
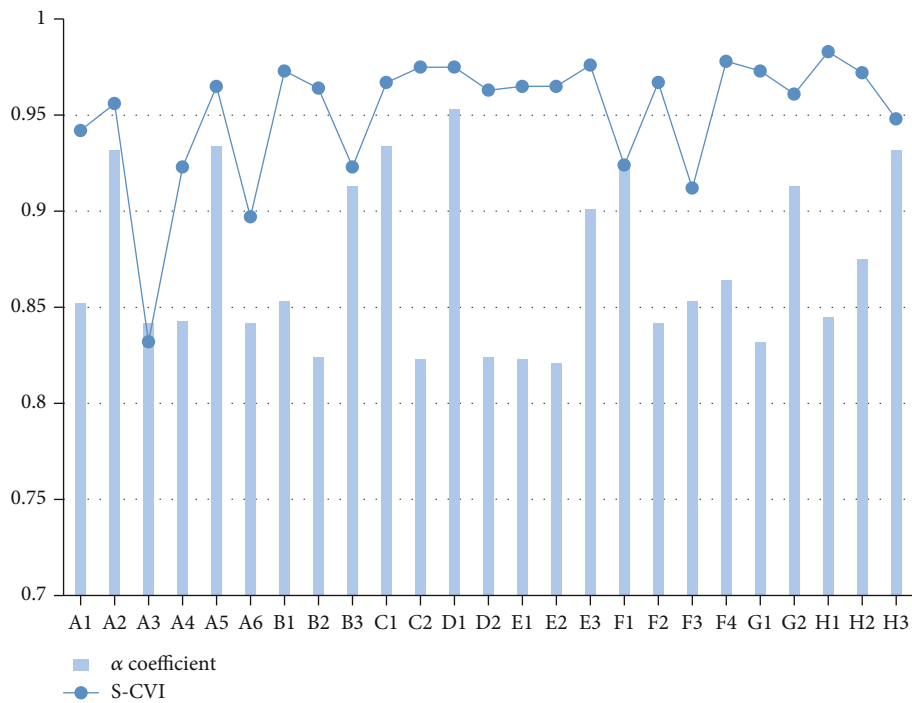Figure 7: Three-level indicators.

Figure 8: Rationality test.

adopted in this paper have provided great help to the construction of the system on a certain basis. In the era of rapid economic development in my country, the indicators of public management system constructed in this article have brought new experience to the public management model.

The findings of the article show that

(1) In the model testing stage, the accuracy rate of the method in this paper is the highest in different datasets, with the highest accuracy rate of 99.7%. It shows that the method in this paper has the highest accuracy and the best accuracy

(2) The correct rate of the method in this paper is 100%, while the correct rate of the big data analysis method and the original method both decrease with the increase of the data set, which reflects the obvious advantages of the method in this paper

(3) The minimum response time of the method in this paper is 22 ms, the minimum response time of the big data analysis method is 49 ms, and the minimum response time of the original method is 53 ms. Although the response time increases gradually with the increase of the dataset, the method in this paper increases slowly

(4) In the second-level indicators, the weights of indicators at all levels are above 0.1, mainly between 0.1 and 0.3, and the highest weight is 0.42 for public safety services

(5) The weights of all three-level indicators are above 0.1, and the weights of C2, D1, and G2 are all above 0.5. The highest indicator weight is 0.672 for urban community service facilities, and most of the three-level indicators are concentrated between 0.2 and 0.4

(6) The alpha coefficients of 25 third-level indicators are all above 0.8, of which 9 third-level indicators have alpha coefficients above 0.9, which are the best level. The average S-CVI of the third-level indicators is above 0.9, and the highest S-CVI is 0.983, and there are two indicators whose S-CVI is below 0.9 but above 0.8, 0.832, and 0.897, respectively. It shows that the constructed public management index system has high reliability and validity

It can be seen from the experimental results that public management attaches great importance to safety. The following focuses on improving the public management system reform plan, improving the public management awareness of employees, establishing a comprehensive social public management system, and paying attention to improving management and supervision. Ensure that people's living standards and happiness are improved. Although the AHP-based public management system indicators have obvious advantages in all aspects, they still have certain limitations. This model is suitable for public management research. It is hoped that in the following research, in-depth research can be carried out on the scope of application to improve the scope of use of the model and increase the generality of the model.

Data Availability

The experimental data used to support the findings of this study are available from the corresponding author upon request.

Conflicts of Interest

The authors declared that they have no conflicts of interest regarding this work.

References

[1] C. K. Kwong and H. Bai, "A fuzzy AHP approach to the determination of importance weights of customer requirements in quality function deployment," *Journal of Intelligent Manufacturing*, vol. 13, no. 5, pp. 367–377, 2002.

[2] Z. Sinuany-Stern, A. Mehrez, and Y. Hadad, "An AHP/DEA methodology for ranking decision making units," *International Transactions in Operational Research*, vol. 7, no. 2, pp. 109–124, 2000.

[3] F. Chan and N. Kumar, "Global supplier development considering risk factors using fuzzy extended AHP-based approach," *Omega*, vol. 35, no. 4, pp. 417–431, 2007.

[4] A. S. Al-Harbi, "Application of the AHP in project management," *International Journal of Project Management*, vol. 19, no. 1, pp. 19–27, 2001.

[5] M. Tam and V. Tummala, "An application of the AHP in vendor selection of a telecommunications system," *Omega*, vol. 29, no. 2, pp. 171–182, 2001.

[6] M. Kurttila, M. Pesonen, J. Kangas, and M. Kajanus, "Utilizing the analytic hierarchy process (AHP) in SWOT analysis — a hybrid method and its application to a forest-certification case," *Forest Policy and Economics*, vol. 1, no. 1, pp. 41–52, 2000.

[7] C. Macharis, J. Springael, K. De Brucker, and A. Verbeke, "PROMETHEE and AHP: the design of operational synergies in multicriteria analysis. Strengthening PROMETHEE with ideas of AHP," *European Journal of Operational Research*, vol. 153, no. 2, pp. 307–317, 2007.

[8] P. Dunleavy and C. Hood, "From old public administration to new public management," *Public Money & Management*, vol. 14, no. 3, pp. 9–16, 1994.

[9] E. Vigoda, "From responsiveness to collaboration: governance, citizens, and the next generation of public administration," *Public Administration Review*, vol. 62, no. 5, pp. 527–540, 2002.

[10] R. Kramer, "Government is us: public administration in an anti-government era," *Journal of Organizational Change Management*, vol. 77, no. 6, pp. 685-686, 1998.

[11] R. C. Box, "Running government like a business: implications for public administration theory and practice," *The American Review of Public Administration*, vol. 29, no. 1, pp. 19–43, 1999.

[12] R. Long, "The intellectual crisis in American public administration.by Vincent Ostrom," *Journal of Politics*, vol. 36, no. 3, pp. 803–805, 1974.

[13] S. Bhuiyan, "Modernizing Bangladesh public administration through e-governance: benefits and challenges," *Government Information Quarterly*, vol. 28, 2011.

[14] Z. Y. Zhao, X. J. Zhao, K. Davidson, and J. Zuo, "A corporate social responsibility indicator system for construction enterprises," *Journal of cleaner production*, vol. 29, no. 1, pp. 54–65, 2012.

[15] G. Yong, F. Jia, and J. Sarkis, "Towards a national circular economy indicator system in China: an evaluation and critical analysis," *Journal of Cleaner Production*, vol. 23, no. 1, pp. 216–224, 2012.

[16] T. Kaya and C. Kahraman, "Multicriteria renewable energy planning using an integrated fuzzy VIKOR & AHP methodology: the case of Istanbul," *Energy*, vol. 35, no. 6, pp. 2517–2527, 2010.

[17] V. S. Lai, K. W. Bo, and W. Cheung, "Group decision making in a multiple criteria environment: a case using the AHP in software selection," *European Journal of Operational Research*, vol. 137, no. 1, pp. 134–144, 2002.

[18] E. U. Ceb, "Fuzzy AHP-based decision support system for selecting ERP systems in textile industry by using balanced scorecard," *Expert Systems with Applications*, vol. 36, no. 5, pp. 8900–8909, 2009.

[19] C. C. Sun, "A performance evaluation model by integrating fuzzy AHP and fuzzy TOPSIS methods," *Expert Systems with Applications*, vol. 37, no. 12, pp. 7745–7754, 2010.

[20] M. N. Kritikos, "A full ranking methodology in data envelopment analysis based on a set of dummy decision making units," *Expert Systems with Application*, vol. 77, pp. 211–225, 2017.

[21] F. A. Lootsma, "Scale sensitivity in the multiplicative AHP and SMART," *Journal of Multi-Criteria Decision Analysis*, vol. 2, no. 2, pp. 87–110, 1993.

[22] S. Lipovetsky and W. M. Conklin, "Robust estimation of priorities in the AHP," *European Journal of Operational Research*, vol. 137, no. 1, pp. 110–122, 2002.

[23] Z. Aya and R. G. Zdemir, "A fuzzy AHP approach to evaluating machine tool alternatives," *Journal of Intelligent Manufacturing*, vol. 17, no. 2, pp. 179–190, 2006.

[24] J. Wong and H. Li, "Application of the analytic hierarchy process (AHP) in multi-criteria analysis of the selection of intelligent building systems," *Building & Environment*, vol. 43, no. 1, pp. 108–125, 2008.

[25] X. Ying, G. M. Zeng, G. Q. Chen, L. Tang, K. L. Wang, and D. Y. Huang, "Combining AHP with GIS in synthetic evaluation of eco-environment quality—a case study of Hunan Province, China," *Ecological Modelling*, vol. 209, no. 2-4, pp. 97–109, 2007.

Research Article

Application of GIS Sensor Technology in Digital Management of Urban Gardens under the Background of Big Data

Jiang Chang ⓘ **and Yingying Tan** ⓘ

School of Modern Agriculture and Biotechnology, Ankang University, Ankang, Shaanxi 725000, China

Correspondence should be addressed to Jiang Chang; changjiang_009@aku.edu.cn

Since the reform and opening up, China's urbanization level has been continuously improved, and the national demand for urban greening is also increasing. However, at present, there are many problems in domestic urban gardens, such as low management quality and high management cost, which have a certain negative impact on urban development and residents' life. In this study, a digital management system of urban garden plant growth state based on sensor client/server structure, GIS (geographic information system) sensor technology and big data technology are designed, and its practicability is tested. The test results show that 52.90% and 40.70% of the people have positive comments on the satisfaction of the system client and the sensor comprehensive application value of the system based on WebGIS sensor technology, respectively. The former is 12.2 percentage points higher than the latter, and the server response speed and CPU (central processing unit) resource consumption of the former are also better. In addition, the robustness of the former is not significantly different from that of the latter. The data show that the digital sensor management system for the growth state of urban garden plants designed in this paper has complete and normal functions and good user experience.

1. Introduction

With the development of China's economy and society, the national urbanization rate shows a steady upward trend. More and more residents choose to live in cities, which brings greater demand for urban landscaping. Therefore, in order to better meet the needs of residents, garden big data, smart planting management, and other technologies are constantly applied to urban garden management. On the other hand, the application premise of these technologies is to have a certain amount of relevant garden plant data. However, at present, the garden management in most cities in China is still mainly realized manually, and there is a lack of garden plant growth status data. On the one hand, this phenomenon leads to an increase in the labor cost of relevant government departments in garden management. On the other hand, managers cannot accurately grasp the growth state of the garden they are responsible for. In view of this, the research integrates big data and GIS sensor technology to build a digital management system for the growth

state of urban garden plants, in order to reduce the cost of urban garden management and promote the digitization of urban garden management process.

In the research process, GIS sensor technology is used to collect the image data of garden plants to be tested. GIS is a technical system for geographic data acquisition, storage, calculation, analysis, and display of the earth's surface space including the atmosphere with the support of computer hardware and software system [1]. It is a computer-based technical tool. Technicians often integrate GIS sensor technology with database functions to facilitate users to query and upload relevant information. Because the objects of landscape vegetation management in large- and medium-sized cities are often distributed in a wide range of regions, and there are many vegetation objects to collect data, urban landscape plants with these characteristics are more suitable for data collection and management using GIS sensor technology.

The innovation of this research is to use GIS and big data technology to deal with the management of urban garden plant growth state. So that the scattered, diverse, and large-

scale garden plant data in the city can be efficiently and accurately collected and managed. The urban garden plant growth state system developed based on big data and GIS sensor technology can analyze the plant growth state according to the collected plant image data, so as to automatically provide the fertilization. Management suggestions such as pest control and planting are helpful to improve the management efficiency and quality of urban garden plants.

The paper consists of three parts. The first part is used to discuss the research results and research methods of domestic and foreign researchers in GIS sensor technology and urban garden digital management. The second part focuses on the construction of urban garden plant growth state management system based on GIS and big data technology, including the selection of plant image data acquisition mode, the overall architecture and function plate design of the system, the specific structure and workflow design of each plate function, and the development of system trial version. The third part is to test the practicability of the system designed by the Research Institute, including the operation efficiency test of the server and the function test of the client, and summarize the advantages, disadvantages, and application prospects of the system according to the test results.

2. Related Works

Many research results show that computer technology, including GIS and big data technology, is more and more applied to urban garden management, which helps to improve the efficiency and quality of urban garden management. Yu et al. believe that the focus of plant protection and management is to protect the soil microbial environment, so they designed a garden management system based on GIS sensor technology. The test shows that the system can meet the needs of plant protection in most garden management [2]. Chen et al. applied GIS sensor technology and Oracle database to design an urban intelligent planning management information system. In the system, the query statement formulated by Oracle command is used, and the geometric code of data dictionary is used to represent the combined integrated data. The test results show that the impact of the system on the environment is small and controllable, which meets the expected standard [3]. Tresch et al. selected 81007 soil animal samples from 120 species, analyzed the role of soil animal activities and development on plant litter decomposition, and found that soil animal species richness plays an important role in garden plant growth [4]. Korpilo et al. collected tourist data of a park using the web-based public participation geographic information system and analyzed the impact of tourist trampling behavior on the growth status of different species of plants [5]. Hiscock et al.'s research team used the high-precision GIS images obtained by overpass technology to create a multifunctional classification system of urban land cover. Through case study, it was found that the overall classification accuracy reached 89.3%, which is conducive to improving the working method of urban water management [6]. Deng et al. applied GIS sensor technology to collect and analyze the data of community buildings in Changsha, China. The

results show that the overall accuracy is 86%. The data show that GIS system is helpful to efficiently determine the year of building construction [7]. In order to explore the impact of different types of gardeners on garden management, Home et al. selected several gardeners with different types of work from 18 gardens in Zurich, Switzerland, for garden management test. The test results show that the garden species richness of conservative gardeners who spend the most management energy is the highest. It shows that a certain degree of garden management and detection is helpful to improve the species richness of gardens [8]. Schneider et al. developed an application based on GIS sensor technology and web technology to solve the problem of poor coordination between private gardens and municipal planning and insufficient utilization of the potential as a wildlife corridor and habitat. Users can provide relevant information about their own gardens through this application. The trial results of the application show that this application can have a positive impact on urban sustainable planning and development [9]. Mirshafiei et al. developed an underground water network management system based on WebGIS sensor technology to solve the water leakage problem of urban underground pipe network. The trial effect of the system is evaluated by the water distribution network of Tehran District 5. The test results show that the system improves the safety of urban water network and has certain popularization operability [10]. Dereli built an urban land planning and prediction system based on remote sensing data and GIS system to solve the problems of unreasonable residential settlements and traffic planning in rapidly developing cities. The test results show that the system can effectively predict the situation of land construction. It is conducive to assisting urban land planning [11].

According to the above analysis, GIS sensor technology has been widely used in agriculture, urban planning, and other fields, and some application results have been achieved. However, there are few studies on the application of it and big data technology to urban landscape management. Therefore, this study attempts to apply them to urban garden plant management, in order to provide some convenience and constructive suggestions for relevant managers.

3. Design of Urban Garden Digital Management System Integrating Big Data and GIS Sensor Technology

3.1. Data Processing and Evaluation Index Design of Urban Garden Plant Growth State. In this section, according to the garden plant image data collected by the sensor, the indexes such as leaf area and coverage are extracted. At the same time, the image is denoised, segmented, and feature calculated for subsequent input to the urban garden growth state management system built based on big data storage, processing technology, and GIS sensor technology, so as to judge the growth state of garden plants and assist professionals to manage fertilization and construction. The image processing process and methods are described in detail below [12].

NDVI, fully known as normalized difference vegetation index, is the necessary data for calculating the key growth state indicators of vegetation. In this study, portable spectral sensors are used to collect relevant optical signals, and then, the reflectance R_{810} and R_{650} of vegetation in 810 nm and 650 nm bands are calculated through the definition of reflectance, so as to calculate NDVI through

$$\text{NDVI} = \frac{R_{810} - R_{650}}{R_{810} + R_{650}}. \qquad (1)$$

In order to further improve the signal acquisition accuracy, empirical formula (2) is used to correct the original NDVI.

$$N\_\text{NDVI} = 1.3559 O\_\text{NDVI} - 0.0474, \qquad (2)$$

where O_NDVI and N_NDVI are NDVI before and after correction, respectively. Then, take N_NDVI as the variable to calculate the leaf area index, coverage, and other indicators of vegetation. These indicators are calculated by querying the corresponding books, which will not be repeated here. Then, design the image processing flow of vegetation. First, denoise the image, and design the image denoising flow as shown in Figure 1.

The method to detect whether there is noise in Figure 1 is to create an $n \times n$ window and use candy edge detection algorithm to detect the window edge. If pixels with gray value greater than 128 are found, the window is considered invalid. The noise power P_w calculation method of the effective window is shown in

$$P_W = \frac{\sum_{p \in w} (P(x, y) - \bar{P})^2}{n \times n}, \qquad (3)$$

where $P(x, y)$ is the gray level of the pixel p in the window and $\bar{P}$ is the average gray level of all pixels in the window. Then, the noise type is determined by calculating the image kurtosis coefficient K, and the calculation formula is as follows:

$$K = \frac{C_4}{P_W^2}. \qquad (4)$$

In equation (4), C_4 represents the fourth-order central moment of the gray value of the pixel. When K is not less than 5, the noise is considered as salt and pepper type, when K is not more than 3, the noise is considered as Gaussian type, and when K is in the range of (3,5), both kinds of noise are considered to exist. Finally, the number of noisy windows is set as the threshold to judge whether there is noise in the image [13].

Due to the influence of shooting ambient light, image denoising also needs to be enhanced; otherwise, it will seriously affect the computer's recognition of image features [14]. In this paper, a Gaussian wave algorithm is used to better achieve Gaussian denoising. The idea of the algorithm is to use Gaussian template to calculate the weighted sum of
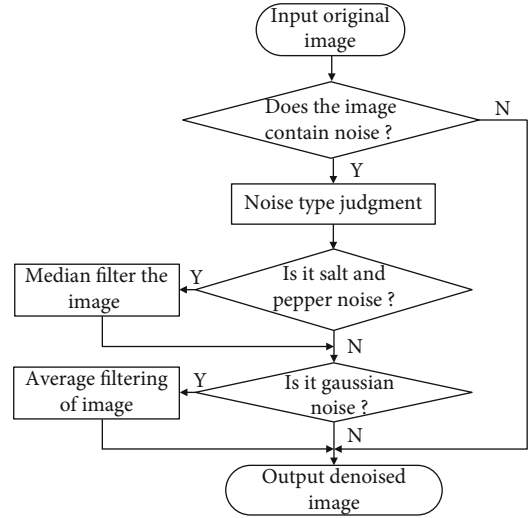

FIGURE 1: Denoising process of garden vegetation image.

the gray values of all pixels in the neighborhood of the pixel to be processed. The weighted result replaces the gray value of the pixel to be processed to achieve the denoising effect. This linear smoothing method can better preserve the edge and detail information of the image. The algorithm is simple and easy to implement and has better visual effect and higher accuracy. Considering that the portable hardware device with weak performance is used to process data in this study, the histogram equalization algorithm with the least amount of calculation is selected to enhance the image [15].

After the image collection and preprocessing, the image needs to be segmented in order to calculate the plant growth index. In this study, the algorithm based on visible light color index is used to convert the image color, and then, Otsu (i.e., maximum interclass variance) threshold algorithm is used to classify the converted image. The calculation process is as follows. Suppose there are n_i pixels with the original gray level of M and the gray level of i; first, normalize the gray histogram according to

$$P_i = \frac{n_i}{M}. \qquad (5)$$

In equation (5), P_i is the normalized gray value. The occurrence probability of pixels of types C_0 and C_1 is shown in

$$\begin{cases} W_0 = \sum_{i=0}^{t} P_i, \\ W_1 = \sum_{i=t+1}^{M-1} P_i = 1 - W_0. \end{cases} \qquad (6)$$

In equation (6), t is the set gray value threshold for classifying images. Then, the average gray value of various

types can be calculated according to formula (7).

$$\begin{cases} \mu_0 = \dfrac{\sum_{i=0}^{t} iP_i}{W_0}, \\ \mu_1 = \dfrac{\sum_{i=0}^{M-1} iP_i - \sum_{i=0}^{t} iP_i}{1 - W_0}. \end{cases} \quad (7)$$

$\mu(t)$ and μ_T in equation (7), respectively, represent the cumulative gray value of the gray level range $0 \sim M$ when the gray level is t. See equations (8) and (9) for the calculation method.

$$\mu(t) = \sum_{i=0}^{t} iP_i, \quad (8)$$

$$\mu_T = \sum_{i=0}^{M-1} iP_i. \quad (9)$$

Since there is a relationship between $W_0\mu_0 + W_1\mu_1 = \mu_T$ and $W_0 + W_1 = 1$ among the above variables, the variance within each pair of pixels can be described by

$$\begin{cases} \sigma_0^2 = \dfrac{\sum_{i=0}^{t} (i - \mu_0)^2 P_i}{W_0}, \\ \sigma_1^2 = \dfrac{\sum_{i=i+1}^{M-1} (i - \mu_0)^2 P_i}{W_1}. \end{cases} \quad (10)$$

In order to quantify the interclass variance of pixels at gray level, the following definitions are made:

$$\begin{cases} \sigma_W^2 = W_0\sigma_0^2 + W_1\sigma_1^2, \\ \sigma_B^2 = W_0 W_1 (\mu_1 - \mu_0)^2, \\ \sigma_T^2 = \sum_{i=0}^{M} (i - \mu_T)^2 P_i, \\ \lambda = \dfrac{\sigma_B^2}{\sigma_W^2}, \\ \eta = \dfrac{\sigma_B^2}{\sigma_T^2}. \end{cases} \quad (11)$$

It can be seen from equation (11) that there is also a relationship of $\sigma_W^2 + \sigma_B^2 = \sigma_T^2$. So far, the image classification problem is transformed into finding an optimal t_m so that when $t = t_m$, λ and η values are the largest. Therefore, η is selected as the objective function to obtain

$$\sigma_B^2 = \dfrac{\left(\sum_{i=0}^{t} P_i \sum_{i=0}^{M-1} iP_i - \sum_{i=0}^{t} iP_i\right)^2}{\sum_{i=0}^{t} P_i \left(1 - \sum_{i=0}^{t} P_i\right)}. \quad (12)$$

When the Otsu segmentation algorithm runs, it will traverse the gray level within the range of [0, M-1], calculate the gray level that makes equation (12) obtain the maximum value, and take it as the optimal segmentation threshold of the algorithm. After the image is classified by the segmentation algorithm, the leaf area index of the plant is estimated based on the data to deduce other growth parameters. In this study, the commonly used method in the industry is used to calculate the leaf area index LA, as shown in

$$LA = -2 \ln P_0(\theta). \quad (13)$$

In formula (13), $P_0(\theta)$ is the canopy porosity of garden plants, and its calculation method is shown in

$$P_0(\theta) = \dfrac{N_{bg}}{N_{count}}. \quad (14)$$

In equation (14), N_{bg} is the number of pixels in the background in the plant canopy image, and N_{count} is the total number of pixels in the image.

3.2. Construction of Urban Garden Growth State Management System Based on Big Data and GIS Sensor Technology. At present, the commonly used method for trace component analysis is to use a spectrophotometer. Its principle is to measure the absorbance by using the light absorption characteristics of the substance, estimate the composition of the substance by the position of the absorption peak, and estimate the content of the component by using the height of the peak. The traditional spectrophotometer is mainly used in the analysis and detection of substances, and its function is relatively single. With the development of chip integration technology and the progress of grating technology, the spectrophotometer has undergone revolutionary changes in function, volume, and detection speed. For example, the use of spectrophotometer to form a field soil monitoring network can detect the material content of soil in real time, so that agricultural producers can effectively improve the soil in a certain area to improve the productivity. In order to obtain garden vegetation image data, a specially assigned person needs to carry a smartphone equipped with mobile GIS application to sample the area to be detected, which requires optimization and calculation of the trajectory of mobile sampling [16]. The research improves the traditional fixed frequency point taking recording method. Its principle is to appropriately increase the frequency of position recording and judge whether the recorder is moving or stationary according to the distance between two adjacent positions, so as to determine whether to record the position of the point. The calculation method of the distance D_{ab} between two points (X_a, Y_a) and (X_b, Y_b) (coordinate values are expressed by longitude and latitude, X_a and X_b are longitude, Y_a and Y_b are latitude) is

$$\begin{cases} C = \sin(X_a)\sin(X_b)\cos(X_a - X_b) + \cos(Y_a)\cos(Y_b), \\ D_{ab} = \dfrac{R \times \arccos(C)\pi}{180}. \end{cases} \quad (15)$$
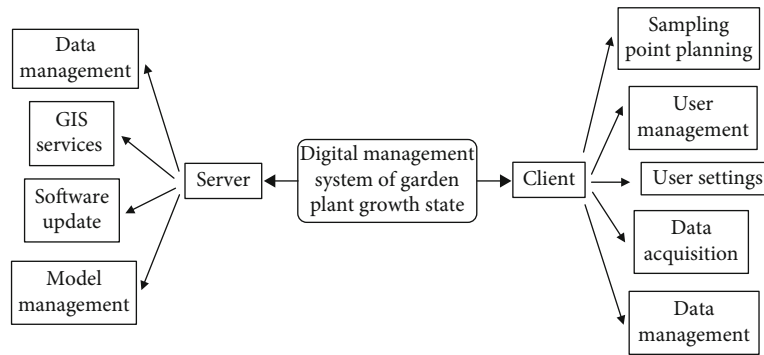
FIGURE 2: Functions of garden plant growth state management system.

In equation (15), C is the intermediate substitution variable and D_{ab} is the radius of the earth, taking 6371 km. Set a threshold K. If the distance between the current acquisition point and adjacent track points is less than K, it will be classified into one nearest neighbor point set. Otherwise, another nearest neighbor point set will be created to include it. After all acquisition points are divided, the k-means algorithm is used to find the center point of each nearest neighbor point set, delete other points in the set, and take the sequential connection of each center point as the sampling track [17].

The urban garden growth state management system of this research is developed based on Android platform and ArcGIS Server. The system uses client/server structure, the client development tool is Android studio, and the server uses eclipse as the development tool. According to the function, the whole system is divided into three layers: data storage, network service, and client application [18]. The data storage layer mainly stores spatial data and attribute data. The storage and management of the former is carried out through the ArcGIS spatial data engine and the spatial data model of SQL server. The latter includes plant canopy parameters and sampling point parameter data, which are stored on SQL server. ArcGIS Server in the network service layer provides map services and some GP (i.e., geoprocessing tool). The client is an application developed based on Android platform. Its main functions are garden plant information management, image acquisition, sampling point positioning, etc. Combined with the above design ideas, the functional planning of the system is obtained, as shown in Figure 2.

Next, the system functions in Figure 2 are designed in turn. The user management module is used to manage the basic information of the user, including creating and modifying the user's account and name. It can also bind accounts to common image sensors [19]. The setting module is used for users to modify image annotation, application language, software update, and set image acquisition sensing mode (manual or automatic acquisition). The function of the data acquisition module is to collect the spectral signal data collected by the sensor and calculate the NDVI, leaf area, and other parameters of vegetation. The sampling point planning module is used to plan the sampling point scheme

according to the user's setting preference and plant growth law. The data management module is used to manage the collected data, such as uploading the data to the server in the form of JSON, sharing the data to the designated user, and deleting and modifying the data [20]. The function of GIS service module is realized through ArcGIS Server, which mainly provides GIS function support and base map data for the system. The sensor model management part is used to store the parameter calculation program of the power plant and send the latest calculation program to the mobile terminal. In order to meet the processing and storage requirements of the system for urban garden big data, the database adopts the SQLite type of Android. The sensor database shall contain six data tables: user information table, activity track table, track information node information table, sampling scheme table, sampling schedule, and sampling point location table. The database allows a single user to create multiple sampling schemes. Each sampling scheme can correspond to multiple sampling activities, and each sampling corresponds to a unique acquisition track. Each acquisition track is composed of multiple two-dimensional coordinate point information.

4. Practicability Test of Urban Garden Growth State Management System

4.1. Running Efficiency Test of Urban Garden Growth State Management System. The hardware equipment used in this paper includes portable plant phenotype imaging spectrometer, mobile GIS application MAPGIS explorer, Xiaomi 8 smart phone, and HP war 99 workstation (as a server). The system is designed according to the research scheme, which verifies the practicability of the system designed in this study. At the same time, in order to compare with the system, the corresponding urban garden growth state management system is built by using traditional sensor and web technology and WebGIS sensor technology commonly used in the industry. Firstly, the response efficiency of each system is analyzed, and the Apache JMeter test tool is used to simulate the process that the client initiates a service request to the server. The number of simulation request applications starts at 1 and then increases to 50, 100,... 500 every 2 seconds. In order to reduce the test error, it is
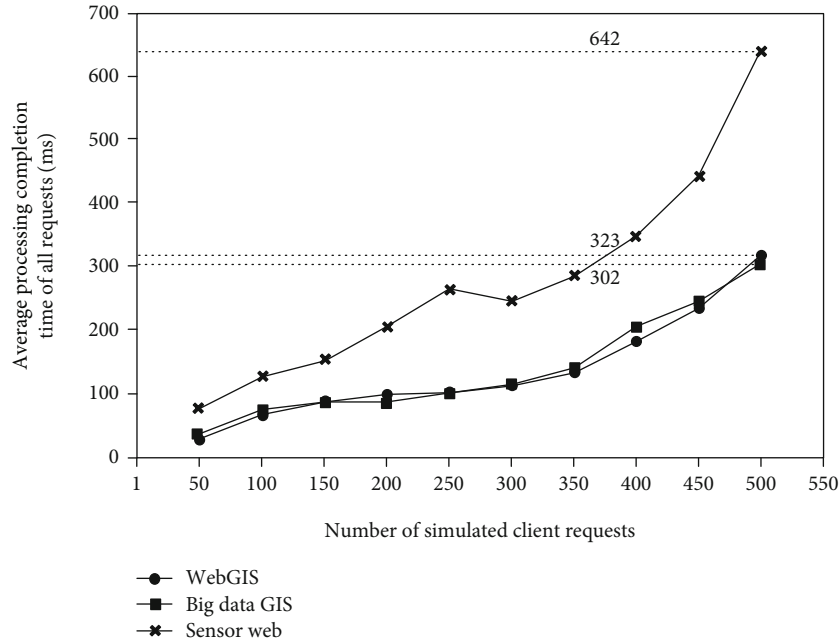
FIGURE 3: Relationship between request processing time of each system and the number of analog applications.
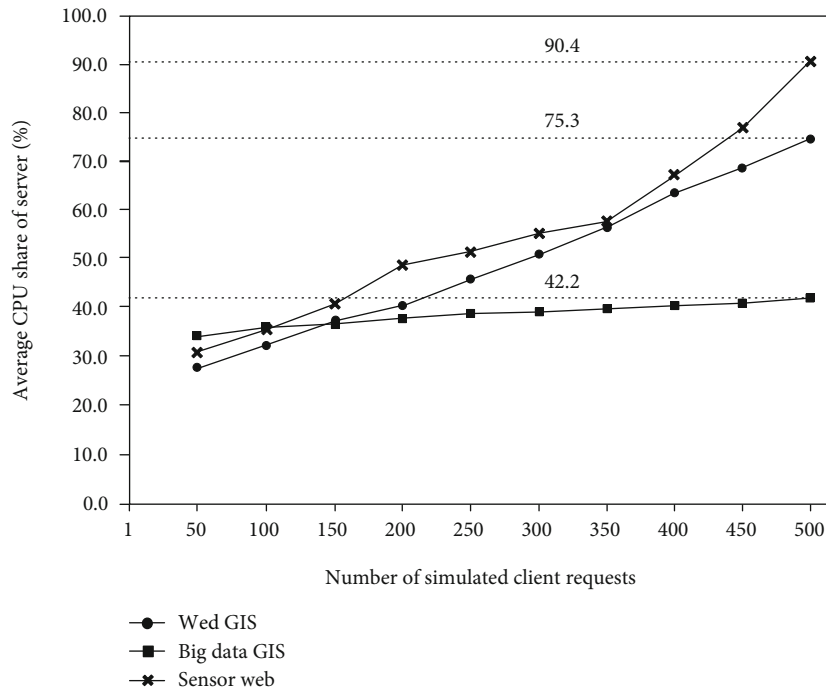

FIGURE 4: Relationship between CPU occupancy of each system server and number of analog applications.

necessary to repeat the test for 5 times under each condition and take the average value of the data to be tested. The statistical results are shown in Figure 3.

"Big data GIS" in Figure 3 is the system designed in this study. According to Figure 3, the corresponding time of the system designed in this study based on big data and GIS sensor technology and WebGIS sensor technology is significantly lower than that based on sensor and web technology calculation. When the number of simulation applications is

500, the average response time of the three is 302, 323, and 642 ms, respectively. Then, count the server CPU share of each system in the test, as shown in Figure 4.

It can be seen from Figure 4 that after the number of simulated applications is greater than 200, the average CPU share of the system server using SQLite database in this study is significantly lower than the other two. When the number of simulation applications reaches 500, the average CPU share of the system server built based on big data and
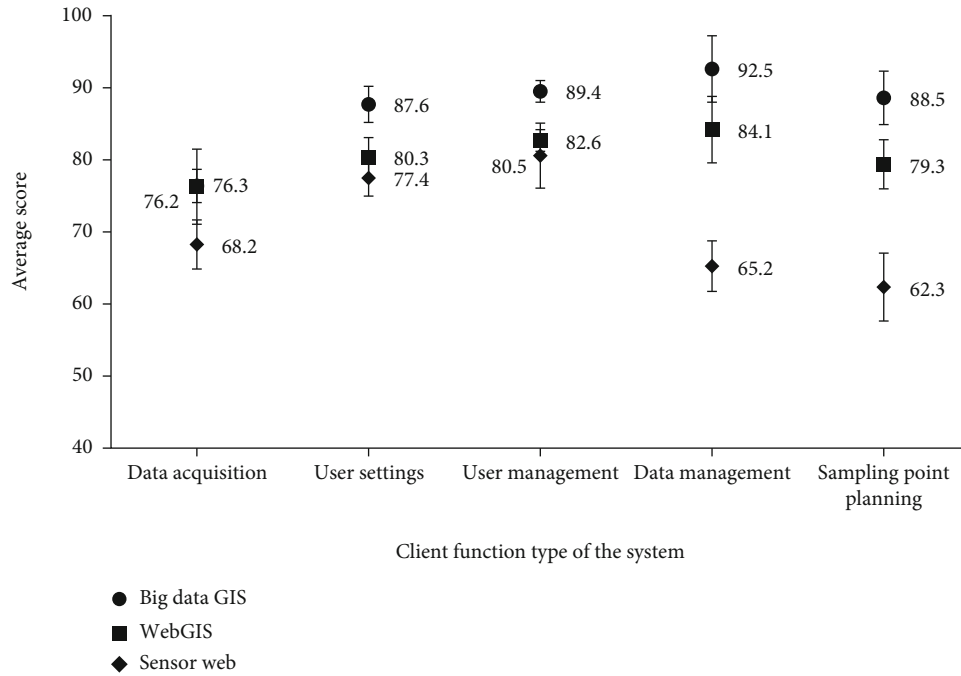
FIGURE 5: Statistics of expert satisfaction score of each system client.
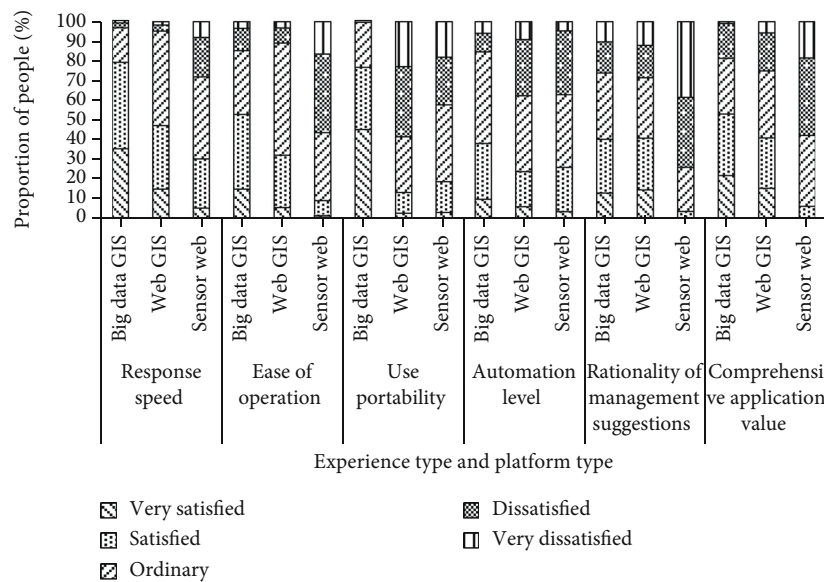

FIGURE 6: Evaluation statistics of client trial satisfaction of each system.

GIS sensor technology, WebGIS sensor technology, and sensor and web technology is 42.2%, 75.3%, and 90.4%, respectively.

4.2. Functional Evaluation of Urban Garden Growth Management System. 36 garden management experts were selected from China, invited to try out the client functions of the three systems, and scored the satisfaction of various client functions of the system according to the trial process. The statistical scoring results are shown in Figure 5.

It can be seen from Figure 5 that there is no significant difference in the average satisfaction scores of the

two systems based on big data, GIS sensor technology, and WebGIS sensor technology in the data acquisition section, but in the user setting, user management, data management, and sampling point planning sections, the average satisfaction scores of the former are 87.6, 89.4, 92.5, and 88.5, which are 9.09%, 8.23%, 9.98%, and 11.60% higher than the latter, respectively. Then, 248 relevant practitioners willing to participate in the study were randomly selected from China to use the clients of the three systems, and the satisfaction of the main module functions of the clients was evaluated. The statistical results are shown in Figure 6.
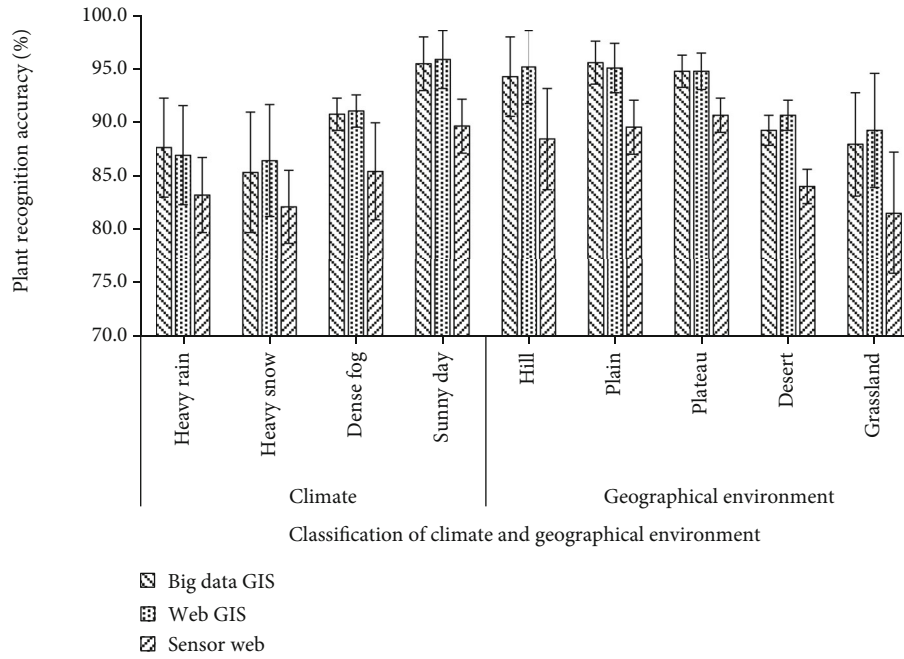
FIGURE 7: Statistics of plant image recognition accuracy of each system in different environments.

It can be seen from Figure 6 that the system built based on sensor and web technology has a negative evaluation on other client function modules except response speed. Specifically, the positive satisfaction of the research and design system and the system based on WebGIS sensor technology in response speed, ease of operation, ease of use, automation level, rationality of management suggestions, and comprehensive application value modules (i.e., evaluated as "very satisfied" and "satisfied") is 79.30%, 52.70%, 76.70%, 37.90%, 40.00%, 52.90%, and 47.00%, respectively, 31.90%, 12.90%, 23.50%, 40.60%, and 40.70%. The former is +32.30, +20.80, +63.80, +14.40, -0.60, and +12.20 percentage points higher than the latter, respectively. Finally, the robustness of the system is tested. Each system client is tested in different climate and geographical environment, and the image recognition accuracy is counted, as shown in Figure 7.

As shown in Figure 7, the image recognition accuracy of the system based on sensor and web technology is significantly lower than the other two in various environments because it has not undergone image denoising and enhancement processing. The difference absolute values of the image recognition accuracy of the system built based on big data, web technology, and WebGIS sensor technology in heavy rain, heavy snow, heavy fog, and sunny climate and hilly, plain, plateau, desert, and grassland environment are 0.70%, 1.10%, 0.30%, 0.40%, 0.90%, 0.50%, 0.00%, 1.40%, and 1.30%, respectively. The basic idea of particle system is to use many small particles with simple shape as basic elements to represent irregular fuzzy objects. These particles have their own life cycles, and they all go through three stages in the system: generation, movement, growth, and extinction. Particle system is a system with "life." Therefore, unlike traditional methods, it can only generate instanta-

neous and static object pictures. Instead, it can generate a series of moving and evolving pictures, which makes it possible to simulate dynamic natural scenery. It can be seen that the system designed in this study has good robustness.

5. Conclusion

Aiming at the problems of high cost and untimely management of urban garden monitoring and management, this study combines big data and GIS sensor technology to build a digital management system for the growth state of urban garden plants and tests the practicability of the system. The test results show that the server response speed and CPU share of the system using big data and GIS sensor technology are significantly better than other comparison systems. In terms of client functions, the average satisfaction scores of the system built based on big data and GIS sensor technology in user setting, user management, data management, and sampling point planning are 9.09%, 8.23%, 9.98%, and 11.60% higher than those of the system built based on WebGIS sensor technology, respectively. At the same time, the former in response speed, operation difficulty, convenience, automation level, rationality of management suggestions. The change values of the proportion of positive satisfaction evaluation in the comprehensive application value module compared with the latter are 32.30%, 20.80%, 63.80%, 14.40%, -0.60%, and 12.20%, respectively. In addition, the image recognition accuracy of the system designed in this study in heavy rain, heavy snow, heavy fog, and sunny climate and hilly, plain, plateau, desert, and grassland environment is not significantly different from that of the system based on WebGIS sensor technology. The above data prove that the client function of the system is also better. There are some limitations in this paper, and

the research has not discussed the sensor simulation results in different environments. This may make the generalization ability of research results low. This needs further discussion in future research.

Data Availability

The data used to support the findings of this study are available from the corresponding author upon request.

Conflicts of Interest

The authors declare that they have no conflicts of interest.

Acknowledgments

References

[1] C. Chen and C. Lin, "Evaluation of seismic evacuation behavior in complex urban environments based on GIS: a case study of Xi'an, China," *International Journal of Disaster Risk Reduction*, vol. 43, no. 5, article 101366, 2019.

[2] L. Yu, X. Xie, and L. Wei, "Green urban garden landscape design and soil microbial environmental protection based on virtual visualization system," *Arabian Journal of Geosciences*, vol. 14, no. 12, pp. 1–16, 2021.

[3] Z. Chen, R. Chen, and S. Chen, "Intelligent management information system of urban planning based on GIS," *Journal of Intelligent and Fuzzy Systems*, vol. 40, no. 1-2, pp. 1–10, 2020.

[4] S. Tresch, D. Frey, R. C. Le Bayon et al., "Litter decomposition driven by soil fauna, plant diversity and soil management in urban gardens," *Science of the Total Environment*, vol. 658, pp. 1614–1629, 2019.

[5] S. Korpilo, T. Virtanen, T. Saukkonen, and S. Lehvävirta, "More than A to B: understanding and managing visitor spatial behaviour in urban forests using public participation GIS," *Journal of Environmental Management*, vol. 207, pp. 124–133, 2018.

[6] O. H. Hiscock, Y. Back, M. Kleidorfer, and C. Urich, "A GIS-based land cover classification approach suitable for fine-scale urban water management," *Water Resources Management*, vol. 35, no. 4, pp. 1339–1352, 2021.

[7] Z. Deng, Y. Chen, X. Pan, Z. Peng, and J. Yang, "Integrating GIS-based point of interest and community boundary datasets for urban building energy modeling," *Energies*, vol. 14, no. 4, p. 1049, 2021.

[8] R. Home, O. Lewis, N. Bauer et al., "Effects of garden management practices, by different types of gardeners, on human well-being and ecological and soil sustainability in Swiss cities," *Urban Ecosystem*, vol. 22, no. 1, pp. 189–199, 2019.

[9] A. K. Schneider, M. W. Strohbach, M. App, and B. Schröder, "The 'GartenApp': assessing and communicating the ecological potential of private gardens," *Sustainability*, vol. 12, no. 1, p. 95, 2020.

[10] P. Mirshafiei, A. Sadeghi-Niaraki, M. Shakeri, and S. M. Choi, "Geospatial information system-based modeling approach for leakage management in urban water distribution networks," *Water*, vol. 11, no. 8, p. 1736, 2019.

[11] M. A. Dereli, "Monitoring and prediction of urban expansion using multilayer perceptron neural network by remote sensing and GIS technologies: a case study from Istanbul Metropolitan City," *Fresenius Environmental Bulletin*, vol. 27, no. 12A, pp. 9337–9344, 2018.

[12] W. Huang, J. Ren, T. Yang, and Y. Huang, "Research on urban modern architectural art based on artificial intelligence and GIS image recognition system," *Arabian Journal of Geosciences*, vol. 14, no. 10, pp. 1–13, 2021.

[13] X. Wang and H. Xie, "A review on applications of remote sensing and geographic information systems (GIS) in water resources and flood risk management," *Water*, vol. 10, no. 5, p. 608, 2018.

[14] M. E. Feyissa, J. Cao, and H. Tolera, "Integrated remote sensing–GIS analysis of urban wetland potential for crop farming: a case study of Nekemte district, western Ethiopia," *Environmental Earth Sciences*, vol. 78, no. 5, 2019.

[15] C. Yu, "Climate environment of coastline and urban visual communication art design from the perspective of GIS," *Arabian Journal of Geosciences*, vol. 14, no. 4, p. 310, 2021.

[16] R. Wenzel and N. Van Quaquebeke, "The double-edged sword of big data in organizational and management research," *Organizational Research Methods*, vol. 21, no. 3, pp. 548–591, 2018.

[17] K. Liu, Y. Murayama, and T. Ichinose, "A multi-view of the daily urban rhythms of human mobility in the Tokyo metropolitan area," *Journal of Transport Geography*, vol. 91, article 102985, no. 91, 2021.

[18] L. Manny, M. Duygan, M. Fischer, and J. Rieckermann, "Barriers to the digital transformation of infrastructure sectors," *Policy Sciences*, vol. 54, no. 4, pp. 943–983, 2021.

[19] M. Locurcio, P. Morano, F. Tajani, and F. di Liddo, "An innovative GIS-based territorial information tool for the evaluation of corporate properties: an application to the Italian context," *Sustainability*, vol. 12, no. 14, p. 5836, 2020.

[20] J. Wang, "Massive information management system of digital library based on deep learning algorithm in the background of big data," *Behaviour and Information Technology*, vol. 40, no. 9, pp. LXVII–LLXXV, 2021.

Retraction

Retracted: The Theoretical Topology and Implementation of Enterprise Social Security in the Digital Age Based on Big Data and Artificial Intelligence

Journal of Sensors

This article has been retracted by Hindawi following an investigation undertaken by the publisher [1]. This investigation has uncovered evidence of one or more of the following indicators of systematic manipulation of the publication process:

(1) Discrepancies in scope

(2) Discrepancies in the description of the research reported

(3) Discrepancies between the availability of data and the research described

(4) Inappropriate citations

(5) Incoherent, meaningless and/or irrelevant content included in the article

(6) Peer-review manipulation

The presence of these indicators undermines our confidence in the integrity of the article's content and we cannot, therefore, vouch for its reliability. Please note that this notice is intended solely to alert readers that the content of this article is unreliable. We have not investigated whether authors were aware of or involved in the systematic manipulation of the publication process.

Wiley and Hindawi regrets that the usual quality checks did not identify these issues before publication and have since put additional measures in place to safeguard research integrity.

We wish to credit our own Research Integrity and Research Publishing teams and anonymous and named external researchers and research integrity experts for contributing to this investigation.

The corresponding author, as the representative of all authors, has been given the opportunity to register their agreement or disagreement to this retraction. We have kept a record of any response received.

References

[1] D. Wang, T. Lin, and H. Xu, "The Theoretical Topology and Implementation of Enterprise Social Security in the Digital Age Based on Big Data and Artificial Intelligence," *Journal of Sensors*, vol. 2022, Article ID 7814886, 11 pages, 2022.

Research Article

The Theoretical Topology and Implementation of Enterprise Social Security in the Digital Age Based on Big Data and Artificial Intelligence

Dandan Wang , Ting Lin , and Hongmei Xu

The Department of Business Administration Yantai, Yantai Nanshan University, Shandong 265706, China

Correspondence should be addressed to Ting Lin; 161849057@masu.edu.cn

At present, there are some problems in the social security of employees in enterprises, such as incomplete security and low reliability. According to this background, this paper studies a topological method for enterprise social security data analysis based on data adaptive analysis strategy and strong learning data stream coprocessing. According to this background, this paper studies a topology method of enterprise social security data analysis based on data adaptive analysis strategy and strong learning data flow and designed a convolutional neural network method based on mutual interference deepening strategy and advanced learning classification mode convolution neural network based on mutual interference deepening strategy and intensive learning classification pattern. According to the coverage error strategy of different types of data, the high-precision matching analysis of enterprise employee social security data is realized, and the Cartesian formula is used to correct the error and topology analysis of the analysis results. According to the experimental data and results, the topology method of enterprise social security data analysis is based on the experimental data and results. We can know that the topological method of enterprise social security data analysis is based on convolutional neural network. Enterprise social security theory can effectively improve the scope and speed of social security. This theory effectively completes the high-precision matching of different types of data and indirectly improves employees' cognition of enterprise values.

1. Introduction

At present, the whole economy is facing great adjustments and changes, and the economic risks and uncertainties faced by people are greatly increased. This uncertainty has a profound impact on people's attitudes and consumption patterns, causing social and macroeconomic turmoil and sharp decline. As a macrostabilizer of reform, state-owned enterprises have provided social security in most reform periods, creating basic conditions for stable and rapid economic development. Social security is an inherent goal in the operation of state-owned enterprises. Therefore, it is not only a part of the economic benefits of state-owned enterprises but consumes also the resources of state-owned enterprises (in other words, it brings a burden to the production of other products of state-owned enterprises). Therefore, when evaluating the economic benefits of state-owned

enterprises, it is incomplete to include specific tangible products into the output and ignore the "certainty" provided by state-owned enterprises to the society. State-owned enterprises have long provided unemployment insurance for society.

At present, the social security methods adopted by enterprises mostly focus on the traditional recursive management and security strategy and rarely carry out multidimensional correlation management in combination with the needs and matching degree of enterprise employees [1]. Since entering the 21st century, a variety of intelligent technologies have also developed vigorously, especially the wide application of big data analysis and artificial intelligence technology, which has been applied on a large scale in many industries and has been able to solve some practical problems [2]. Therefore, how to combine big data and artificial intelligence technology to realize the iterative upgrading of enterprise

social security methods has become the mainstream research direction [3]. At present, although the existing enterprise social security system has many high relevance application rules, there are still many deficiencies, such as inability to ensure the comprehensiveness of enterprise employee social security and low processing efficiency of enterprise employee social security [4]. According to the above research background, this research proposes a topological method for enterprise social security data analysis based on data adaptive analysis strategy and coprocessing of strong learning data flow.

Aiming at the problems of poor migration application and low quality in the current enterprise social security theoretical analysis model, this paper studies the topology model of enterprise social security theory based on data adaptive analysis strategy and strong learning data flow intelligent matching algorithm; the content of this research is divided into four chapters. The first chapter introduces the analysis and application background of enterprise social security data and the innovative solutions proposed by this study. Based on data adaptive analysis strategy and strong learning data flow intelligent matching algorithm, the content of this research is divided into four chapters. Section 1 introduces the analysis and application background of enterprise social security data and the innovative solutions proposed in this study; Section 2 summarizes and analyzes the research status of big data application, enterprise social security theory, and application methods at home and abroad. Section 3 is the data self-adaptive analysis strategy and strong learning data flow intelligent matching algorithm and constructs the topological analysis model of digital enterprise social security theory. Section 3 constructs a digital topology analysis model of enterprise social security theory based on data adaptive analysis strategy and strong learning data flow intelligent matching algorithm. Combined with the multi-interconnect Einstein constant analysis strategy, it constructs the enterprise social security data analysis system and evaluation index system based on artificial intelligence analysis. Section 4 analyzes and verifies the feasibility and data matching degree of the topology analysis model of enterprise social security theory constructed in this paper and draws a conclusion.

Different from the traditional data stream matching type and conditional judgment-based social security analysis mode, the innovation of this paper lies in relying on the convolutional neural network algorithm, combining the data adaptive analysis strategy and the strong learning data stream intelligent matching idea, to realize the enterprise social security data. High-efficiency analysis is used to improve the utilization of social security data. On this basis, it can quickly and accurately extract high-quality and effective data information from massive dynamic social security data, realize the efficient combination of enterprise social security topology data, and use multitransformed Einstein factors to conduct quantitative analysis and high-accuracy fitting of different types of enterprise social security data types, so as to realize high-precision matching and fitting of different types of data.

2. Related Work

At present, the research on enterprise social security mainly focuses on theoretical research, specific case analysis, and

application of migration model, while there are few research on combined innovation with artificial intelligence and big data analysis technology [5]. According to the difference of consumption record information of enterprise employees' social security, Wei et al. proposed an adaptive matching analysis model based on difference data analysis to realize high-accuracy analysis and adaptation of different types of social security data [6]. Through experiments, Masterson et al. found that the relevance behind different types of social security data groups is significantly different and presents different change rules. Therefore, a high matching equipment data analysis model based on difference feature analysis is proposed, which can effectively improve the relevance of different types of data groups [7]. Greatbatch and Lee fused the social security data of multiple enterprises. Through specific visits to enterprise employees, they found that the employee happiness of different enterprises is closely related to the enterprise social security data and cited the high-precision analysis model based on the equipment type data analysis module. The model can effectively improve the high-accuracy matching analysis of different types of social security data [8]. Mayro proposed a method to establish an enterprise social security privacy database based on multidimensional correlation data matching and tracking analysis, which makes use of the differences of employee rank in different enterprises to realize the redistribution of packet data at all levels and realizes the high-precision analysis and mining of social security data in terms of utilization efficiency [9]. According to the idea of data combination in the traditional establishment mode of social security data collection system in a general sense, Lang et al. effectively combine the social security data types of enterprises with the high-precision matching analysis strategy of employees to achieve a high degree of unity at the data level and put forward a data matching tracking analysis model based on the edge effect development strategy [10]. By highly summarizing and unifying different types of enterprise social security data mining models, Egevad et al. try to realize the standardization, unified management, and intelligent analysis of different enterprise social security data from the perspective of intelligent distribution of the model [11]. Based on the research and analysis of social security theory in the literature, scholars such as Safarnejad L chose a strength free matching analysis model of standardized social security analysis model, which can carry out high-strength matching analysis according to the social security data types of different countries. This model can effectively classify the data ideas of different strategy types and realize the optimal utilization of different social security policies and strategies [12]. Verganti et al. manage the loyalty and happiness of enterprise employees from the types, classification, and data storage of enterprise social security storage data and realize the high-quality analysis of enterprise social security data through adaptive and integrated tracking and analysis of dynamic employee social security data changes [13]. The research results of Kai et al. show that the enterprise social security information interaction method based on the two in one coupling model of data acquisition and data analysis has higher efficiency in enterprise data

processing and can improve the accuracy of at least 10% compared with the traditional social security data management method [14]. In order to improve the stability and authenticity of enterprise employee social security data, Liu et al. have carried out various high-dimensional calculations on different enterprise employee social security data to achieve high-precision acquisition and discrete processing of different types of data, which can effectively improve the matching rate of different types of data groups, but there are high requirements for the scope of application [15]. Goodarzian et al. have proved through experiments that the social security data groups of different enterprises in different regions have obvious characteristics of simplification and difference and can efficiently carry out high-precision analysis on different types of enterprise data guarantee groups [16].

To sum up, it can be seen that there are some problems in the theoretical research of enterprise social security, such as lagging simplification method (uneven matching of valid data) [17–19]. Although current scholars have achieved preliminary innovative applications in the data application of social security and the application of multidimensional change pattern matching, there are few research results in practical application and artificial intelligence technology iterative analysis, and there are no demonstrative achievements in the normalization and innovative application of corporate social security data, similar to two-dimensional spatial decomposition strategy [20, 21].

3. Methodology

With the iterative updating of different artificial intelligence technologies in recent years, it is possible to apply big data analysis technology in different industries [22]. In the field of big data analysis technology, different analysis strategies have different advantages. As a typical intelligent analysis method, neural network algorithm plays an important role in the development needs of enterprises [23]. However, the traditional neural network algorithm is not suitable for solving the application problems of all industries. Some scholars have improved the algorithm for different types of data applications. Therefore, intelligent collaborative algorithms based on data adaptive analysis strategies and strong learning data stream collaborative processing came into being. The convolution neural network algorithm not only has the advantages of fuzzy class analysis of neural network algorithm; the accuracy and efficiency of data analysis have also been greatly improved [24]. The theory of enterprise social security has also been constantly updated with the real needs of society, so there is also a large room for improvement. How to apply the fast-growing big data and artificial intelligence technology in recent years to the theory of enterprise social security and realize the intelligent analysis of social security data is the current research hotspot [25]. The principle of intelligent collaborative algorithm based on data adaptive analysis strategy and strong learning data stream collaborative processing is shown in Figure 1.

In the process of coupling analysis of enterprise social security data, convolutional neural network will evolve into various types of business support data groups through coupling management of different types of social security data groups. When different data groups are identified with high accuracy by compiler, their internal relevance also shows a high change law. Therefore, it is necessary to carry out iterative update processing. After different degrees of data iterative processing, its internal relevance data groups will show different types of high-accuracy translation efficiency, so its internal interconnection influence will be characterized, and different types of data groups will realize relevance analysis according to different digital features. Therefore, after perfecting the social security theory database of many enterprises, its internal relevance presents different expression characteristics. Then, according to its internal local efficiency data group, it realizes the high-accuracy information extraction of different types of data groups and realizes the local optimization and feature extraction of data.

3.1. Establishment Process of Multiple Grey Convolution Neural Network Model Based on Big Data. For the correlation analysis of various data groups, the selection standard to eliminate unnecessary data in the data group is the result of correlation analysis. In the process of analyzing enterprise social security data, we can eliminate unnecessary data in the data group through the correlation analysis of various data groups. Then, according to the characteristics of different types of differentiation, realize the high-intensity analysis of its internal data. After the analysis, according to its different correlation types, realize the high-intensity disturbance analysis of different data groups, then match the correlation degree of these effective information data groups, and finally, form the correlation data matching with differentiation characteristics. Figure 2 shows the data flow operation process of the social security topology analysis model based on the data adaptive analysis strategy and the strong learning data flow cooperative processing intelligent collaborative algorithm.

The process of data processing is divided into several stages. The first stage is to classify n enterprise social security data groups. These data groups are original data groups and have obvious characteristics—each data group has m correlation data nodes with different dimensions. After high-intensity matching of these data nodes, the sequence can be obtained as follows:

$$Y_1 = 1 + \sqrt{\frac{(x_1(1), x_1(2), \cdots, x_1(n))}{x_1(1) + x_1(2) + \cdots + x_1(n)}},$$

$$Y_2 = Y_1 + \sqrt{1 + \sqrt{\frac{(x_2(1), x_2(2), \cdots, x_2(n))}{x_2(1) + x_2(2) + \cdots + x_2(n)}}},$$

$$Y_3 = Y_2 + \sqrt{1 + \sqrt{\frac{(x_3(1), x_3(2), \cdots, x_3(n))}{x_3(1) + x_3(2) + \cdots + x_3(n)}}},$$

$$Y_M = Y_n + \cdots + \sqrt{1 + \sqrt{\frac{(x_3(1), x_3(2), \cdots, x_m(n))}{x_3(1) + x_3(2) + \cdots + x_m(n)}}}.$$
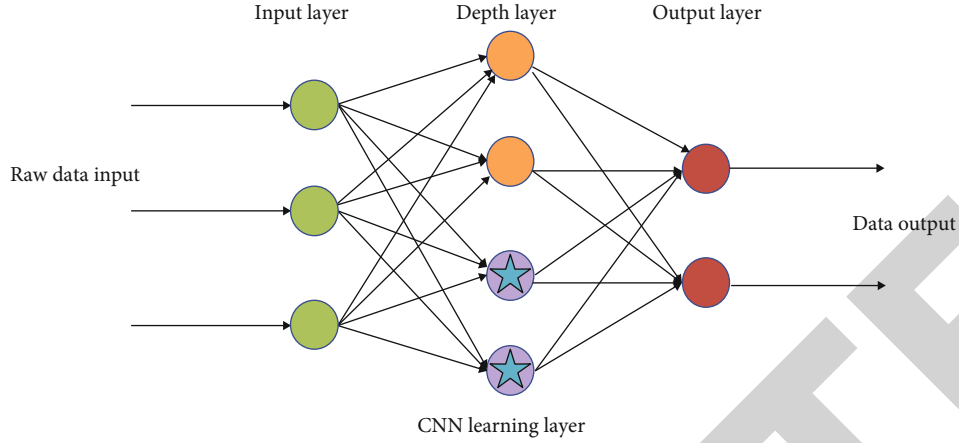
(1)

FIGURE 1: Operation principle of intelligent collaborative algorithm based on data adaptive analysis strategy and strong learning data stream collaborative processing.
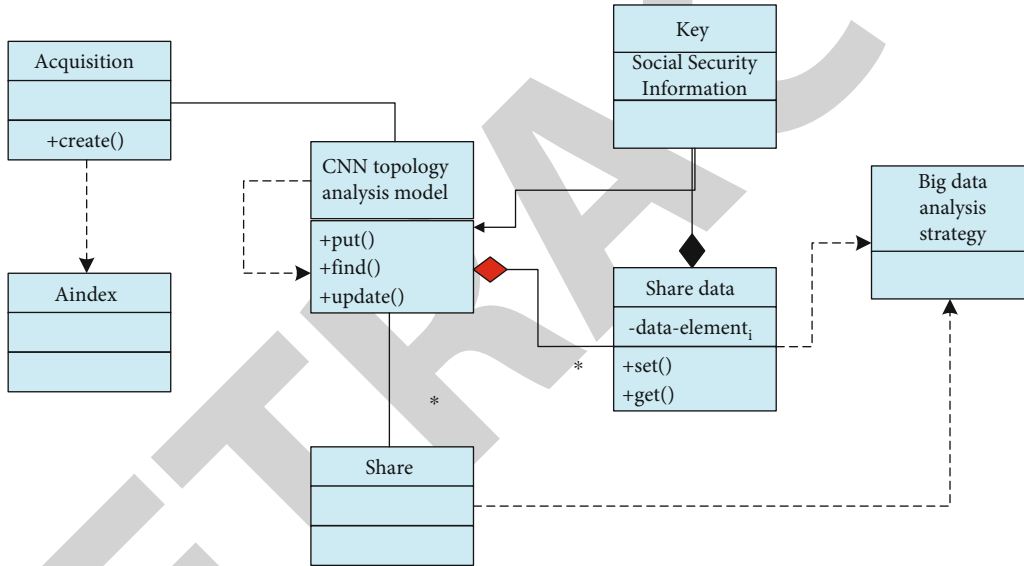

FIGURE 2: Data flow operation process of social security topology analysis model based on data adaptive analysis strategy and strong learning data flow cooperative processing intelligent collaborative algorithm.

Therefore, when topological analysis is required for different types of data, only the internal weight coefficient $\aleph$ of Y_i and Y_j needs to be calculated, and the calculation formula is

$$\aleph = \frac{\sqrt{1 + \sqrt{(Y_m + Y_{m+1})/(Y_m + Y_{m-1})}}}{Y_m - Y_{m-1}}. \quad (2)$$

Then, according to the weight coefficient index, the coupling degree of different types of social security data groups is solved, and the coupling degree function is

$$U(x) = \sqrt{\frac{\aleph x^2 + (\aleph + 1)x^4 + 1}{\aleph x^2 + (\aleph - 1)x^3 + (\aleph - 2)x^4 + 2}} \aleph_{ii}, \quad (3)$$

where $\aleph_{ii} = 1$; $i = 1, 2, \cdots, m$. After completing the above analysis, it is also necessary to analyze the high-value matching degree according to the correlation degree of different enterprise types and evolve it into a low-latitude social security data group index. The simulation results are shown in Figure 3.

The simulation results of level 1 artificial intelligence matching analysis for different types of enterprise social security data types are shown in Figure 4.

The simulation results of two-dimensional and three-level artificial intelligence matching analysis for different types of enterprise social security data types are shown in Figure 5.

The simulation results of three-dimensional 4-level artificial intelligence matching analysis for different types of enterprise social security data types are shown in Figure 6.

It can be seen from the four groups of data results in Figures 3–6 that after analyzing different types of enterprise social security data groups according to different types of
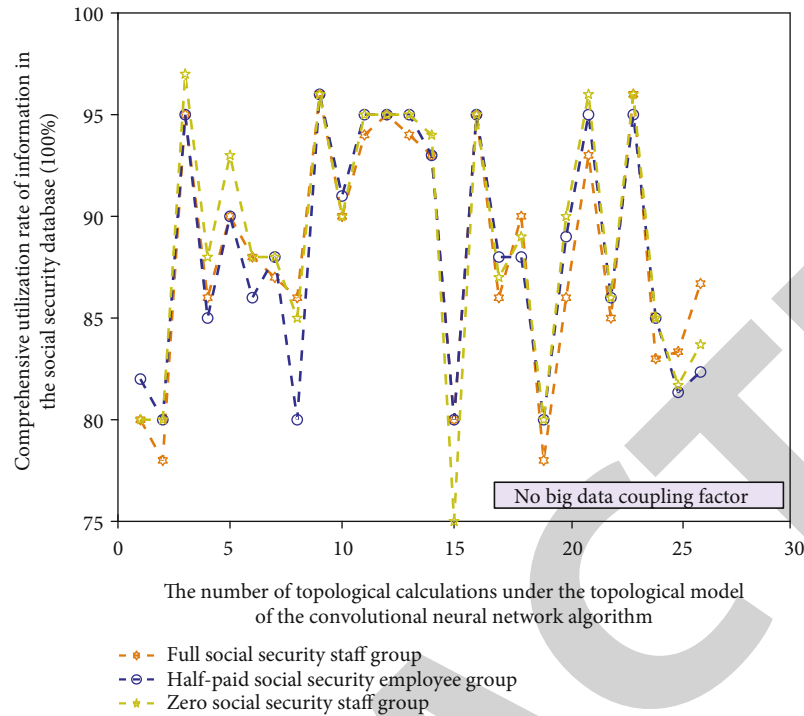
Figure 3: The corresponding simulation analysis results under the low-latitude social security data set indicators.
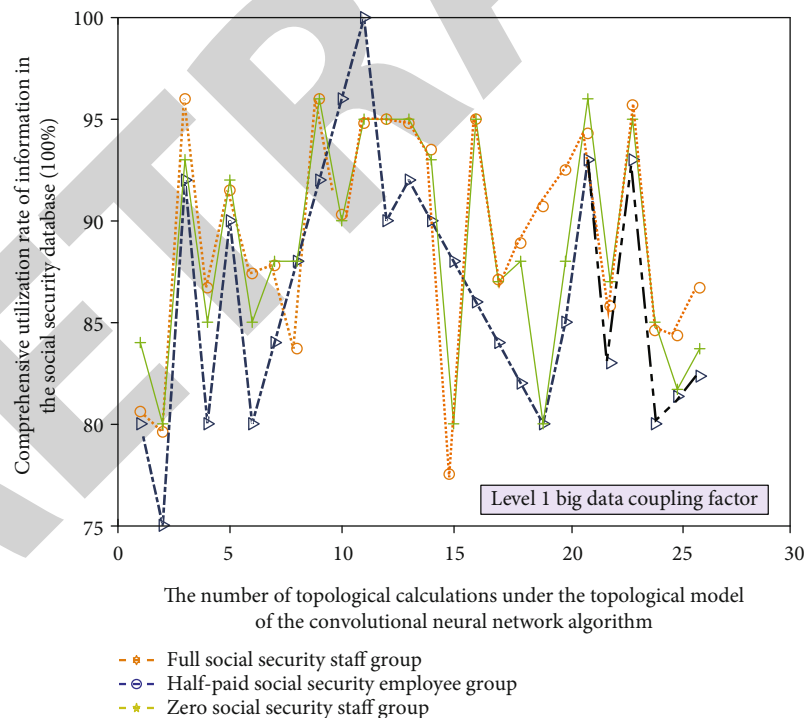

Figure 4: The corresponding simulation analysis results under the social security data group index under the first-level line change.

high-value matching, combined with convolution neural network algorithm, when using big data and artificial intelligence topology analysis strategy for high-value matching analysis, it is also necessary to perform association calculation and processing for different types of data groups (0/1/2/3 level AI high matching factor). Due to the need to combine high intensity and high factor in the matching analysis of social security data, the data model of these
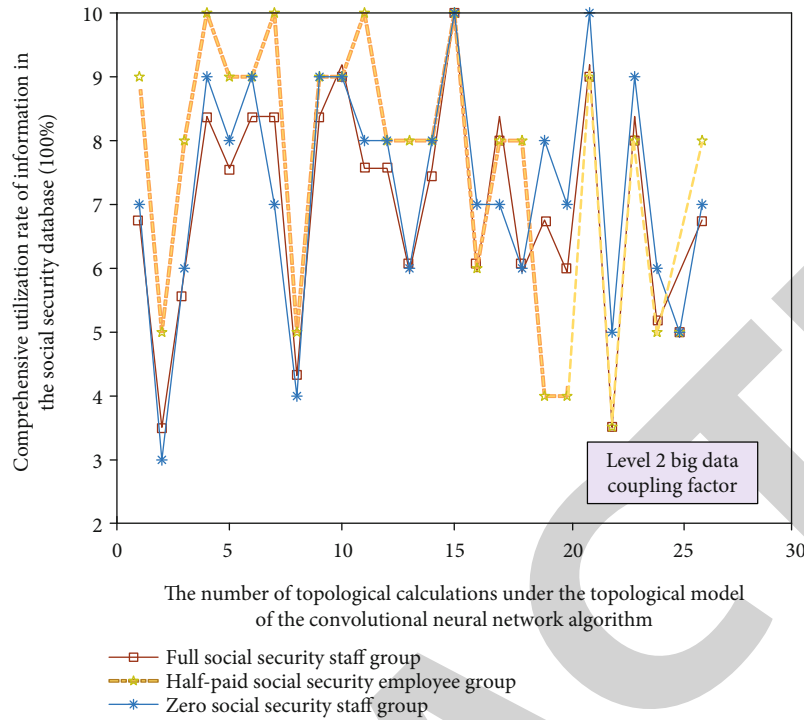
Figure 5: The corresponding simulation analysis results under the social security data group index under the second-level discrete behavior change.
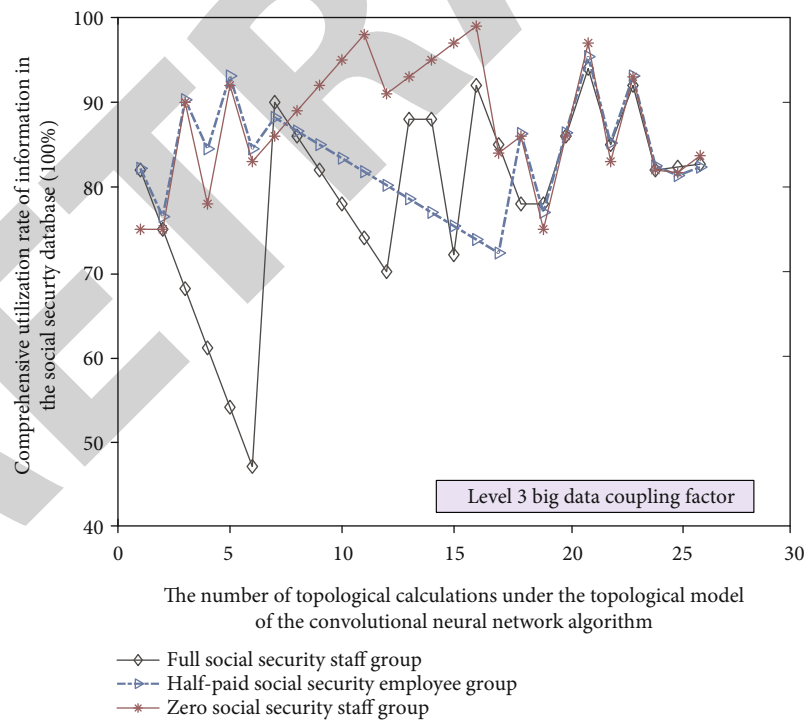

Figure 6: The corresponding simulation analysis results under the social security data group index under the three-level aggregated behavior change.

factors will have strong internal correlation, matching degree, and disturbance of value function. Therefore, with the change of topology analysis times, the redundant infor-

mation in the internal authentication database will be dynamically updated with the incompleteness of topology. The corresponding convolution network marking function

in this process is recorded as $I_j^k(x)$:

$$I_j^k(x) = \frac{\sqrt{\left(x - x_j^k(1)\right)/\left(x_j^k(3) + x_j^k(2)\right)} + \sqrt{\left(x + x_j^k(1)\right)/\left(x_j^k(2) + x_j^k(1)\right)}}{x_j^k(2) + x_j^k(1) + x_j^k(3)}. \tag{4}$$

$x_j^k(*)$ is the topology node of social security theory. After the calculation, it is also necessary to carry out high-precision topology analysis for different types of social security data types. In this stage, the precision extreme value measurement function $P(x)$ is required, and its expression is

$$P(x) = \sqrt{\frac{\aleph x_j^k(4) - x}{x_j^k(4) - x_j^k(3)} + \frac{\aleph x_j^k(4) - x}{x_j^k(4) - x_j^k(3)}}. \tag{5}$$

In addition, after analyzing the topological structure of different types of enterprise social security theory, it is also necessary to measure and score different types of high-value topological data. The expression of continuous measurement function is formula (6), and the expression of discrete measurement function is formula (7).

$$L(x) = \frac{P(x) + \left(\left(x_j^k(4) - x\right)/\left(x_j^k(4) - x_j^k(2)\right)\right)}{P(x) + P(x - 1)}, \tag{6}$$

$$K(x) = \sqrt{\frac{I_j^k(x) + P(x)}{I_j^k(x) + P^2(x-1)} + \frac{x - x_j^k(1)}{x_j^k(2) - x_j^k(1)}}. \tag{7}$$

$x_j^k(*)$ is the topology node of social security theory.

3.2. Data Processing Process of Topological Sparse Model of Enterprise Social Security Theory Based on Convolutional Neural Network. In this model, in order to carry out variable weight analysis on different types of enterprise social security data, different types of enterprise social security databases need to be updated and maintained regularly. The iterative calculation and update of the weight coefficients are realized by determining the data adaptive analysis strategy and the strong learning data flow high-strength coincidence variables. The high-intensity analysis and iterative calculation of different types of data groups can be realized from the two-dimensional level. The high-dimensional variable weight coefficient $\mathfrak{I}$ required in this process can be expressed as

$$\mathfrak{I} = \frac{\sqrt{\sum_{j-1}^{m} I_j^k(x_{ij}-1) + \aleph_j^k + \sum_{j=1}^{m} I_j^k(x_{ij}) \cdot \aleph_j^k}}{I_j^k(x_{ij}) + \aleph_j^k}. \tag{8}$$

Specifically, there are

$$\mathfrak{R}_i^2 = \left(\sum_{j=1}^{m} I_j^1(x_{ij} - 1) \cdot \aleph_j^1, \sum_{j=1}^{m} I_j^2(x_{ij} - 2) \cdot \aleph_j^2, \cdots, \sum_{j=1}^{m} I_j^s(x_{ij} - s) \cdot \aleph_j^s\right). \tag{9}$$

The above formula is the high-dimensional variable weight coefficient in the topology analysis structure, and its corresponding high-intensity expression function is

$$\mathbb{R} = \sqrt{\frac{\aleph_j^k + \mathfrak{R}_j^k}{I_j^k(x_{ij}) + \aleph_j^k}}. \tag{10}$$

After completing the above links, in order to further carry out Gaussian mixture analysis on different types of enterprise social security data and realize the analysis of high accuracy and low error rate based on Einstein factor, Figure 7 shows the analysis and simulation results and changing trends of the social security weight coefficient groups that change in different modes.

It can be seen from Figure 7 that in the process of analyzing enterprise social security data, with the increase of the number of topological structures, the coupling functions corresponding to different types of influencing factors also show different change laws, because different types of social security theory databases have significant differences in characteristics. The data analysis data of different dimensions will show high-intensity extreme value changes of different values, and the corresponding extreme value change function can be expressed as $A(x)$.

$$A(x) = \frac{\sqrt{\sum_{j=1}^{m} Y_j^1(x_j) + \sum_{j=1}^{m} I_j^1(x_j)}}{\mathfrak{R}_j^1 + \aleph_j^1}. \tag{11}$$

The result under the analysis strategy after multidimensional discretization can be expressed as $A'(x)$ and

$$A'(x) = \frac{\sum_{j=1}^{m} Y_j^1(x_j) + \sum_{j=1}^{m} I_j^1(x_j)}{\mathfrak{R}_j^1 A(x)}. \tag{12}$$

After completing this link, it is also necessary to evaluate the extreme value of different types of high-accuracy social security value, and its internal correlation also needs to be calibrated. Therefore, in the process of fuzzy search and screening of unknown corporate social security data targets (newly collected corporate employee social security information), the corresponding discrete discriminant function is $D(x)$ and the expression is

$$D(x) = \sqrt{\frac{\beta_j^1 + \bar{\mathfrak{R}} \sum_{j=1}^{m} (x_j - \bar{x})}{\sum_{j=1}^{m} (\mathfrak{R}_j - \bar{\mathfrak{R}}) + \aleph_j^1 \bar{x}}}, \tag{13}$$

where β_j^1 is the topological reinforcement coefficient of social security.

4. Result Analysis and Discussion

4.1. Experimental Design and Data. In order to analyze the coupling and real effect of the corporate social security data analysis topology method based on data adaptive analysis
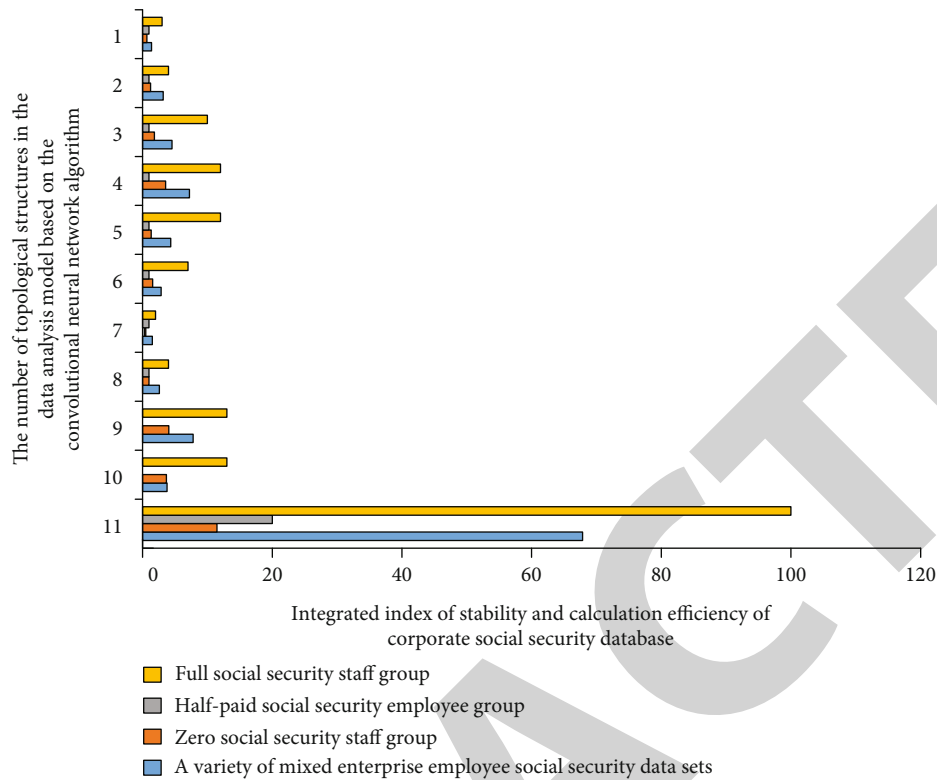
FIGURE 7: Correspondence analysis of social security weight coefficient groups that change in different modes and simulation results of changing trends.

strategy and strong learning data stream coprocessing in the actual process of social security data processing, it is necessary to combine different types of high-intensity enterprise social security data groups for coupling management analysis, so the corresponding confirmatory experiment is designed. In the experiment process, the completely public data is used, and the discrete random change rule is adopted, and it is input into the original database enterprise employee social security information data. In the process of coupling analysis of different types of enterprise social security data groups, its targeted evaluation indicators also need to be set. Therefore, this study is screened according to the existing international standards. Finally, 25 indicators are selected to evaluate the randomness and accuracy of the topology of corporate social security theory. During the experiment, the database information of the enterprise is related to different types of high-strength continuity characterization functions, and industries are selected as the experimental verification data group for topology analysis and verification. The experimental analysis results are shown in Figure 8.

It can be seen from Figure 8 that during the experiment, different groups have different accuracies under different types of data processing, their corresponding high-intensity function values have strong stability and gradual change, and their internal correlation also shows different change laws. This is because their corresponding data analysis rules will also change under large data and artificial intelligence analysis technology. Therefore, its internal relevance can be displayed through the artificial intelligence data analysis system, and so can the internal data relevance.

4.2. Experiment Result Analysis of Enterprise Social Security Data Analysis Topology Method Based on Data Adaptive Analysis Strategy and Strong Learning Data Flow Coprocessing. From the experimental results in Figure 8 and the accuracy analysis results of social security data in Figure 9, it can be seen that there is little difference in volatility after analyzing the social security data of different enterprises used in the experimental process. In addition, different types of data groups also have great differences in the correlation degree and matching degree. In addition, among multiple evaluation quantifications for perturbation analysis on different data sets, there will be obvious differences in the internal pertinence change and correlation matching degree, which will lead to obvious fluctuations in the correlation data between data groups.

Therefore, it can be seen from the above analysis and experimental results that in the process of processing experimental data, this study combines data adaptive analysis strategy and adopts strong learning data flow collaborative processing method based on iterative data high-dimensional analysis based on data adaptive analysis strategy intelligent algorithm, which can schedule, match, and track the enterprise social security data information of different industries from any angle, and through the coupling and error of different data and the stability differences within the enterprise, the internal relevance platform of data groups can be guaranteed to realize the high-intensity analysis and data representation of different data groups. Then, according to the vector difference, length difference, and other dimensional information of data groups in different columns in the enterprise social security database, the
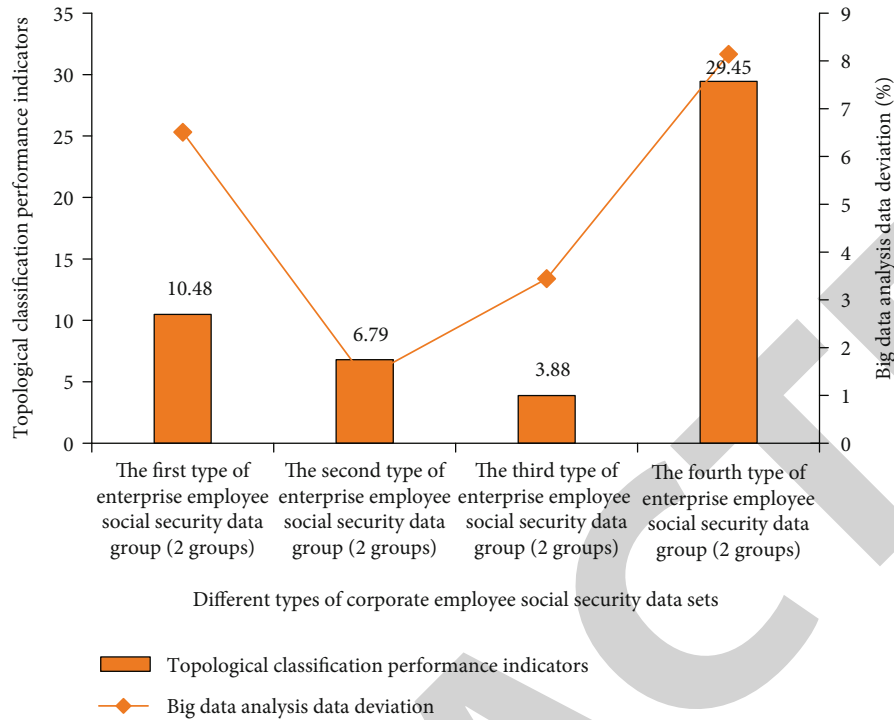
Figure 8: Topological analysis to verify the experimental results of employee social insurance data of 4 types (8 groups, 2 groups for each type) of enterprises.
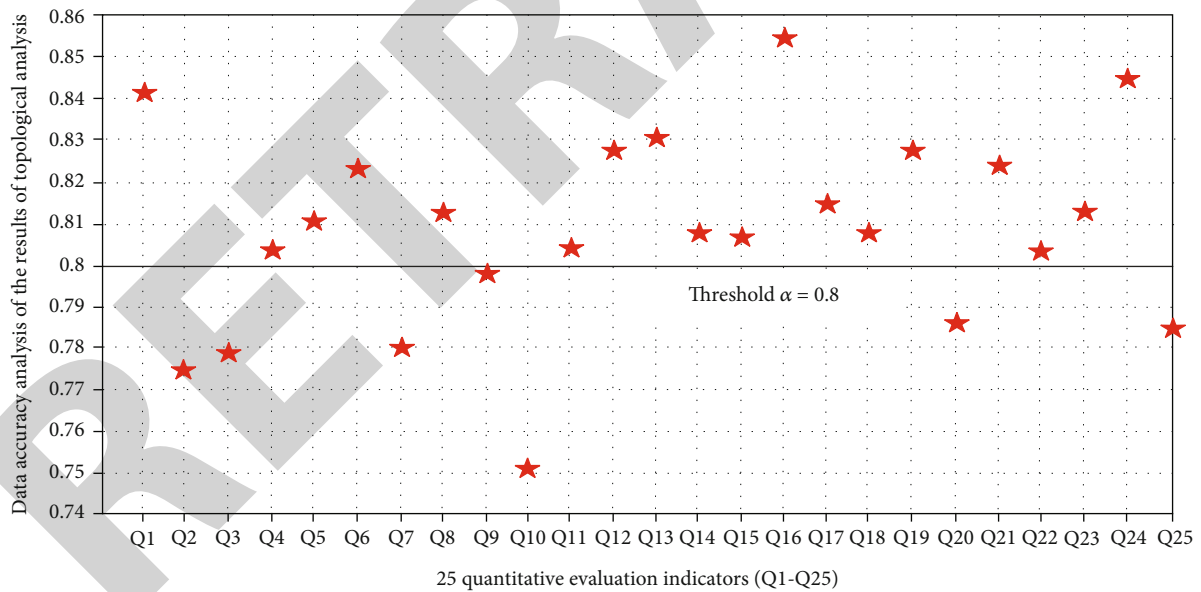

Figure 9: Data analysis of experimental results.

iterative hierarchical division and high-intensity planning of different social security data are realized. Finally, through the neural network algorithm and artificial intelligence analysis technology, the high-accuracy analysis process of social security data information in different dimensions is realized. Finally, combined with the differences of different types of data groups, the iterative classification is carried out to realize the intelligent adaptive law of social security data in dif-

ferent enterprises, combined with the sophisticated analysis of social security enterprise data groups, analyze the probability distribution and error coupling degree of the internal social security data, realize the topological change analysis and prediction of the enterprise social security data type, and then complete the internal representation of the information contained in the enterprise social security data and the rapid analysis of the correlation degree.

5. Conclusion

At present, there are some problems in the social security of employees in enterprises, such as incomplete security and low reliability. Based on this, this paper studies a new model of topology optimization of enterprise social security theory based on big data and artificial intelligence data analysis strategy and designs an intelligent extraction model of enterprise employee social security data based on the coprocessing method based on data adaptive analysis strategy and strong learning data stream of different types of data, the high-precision matching analysis of enterprise employee social security data is realized, and the Cartesian formula is used to correct the error and topology analysis of the analysis results. The results show that the topology optimization model with continuous digital matching pursuit and perceptual analysis strategy enterprise social security theory based on convolutional neural network can effectively improve the scope and speed of social security, effectively complete the high-accuracy matching of different types of data, and indirectly improve employees' recognition of enterprise values. Compared with the normalized and discrete traditional social security, treatments have limitations, and the innovation of this paper is to combine the big data analysis strategy with the artificial intelligence analysis strategy and use the convolution neural network algorithm to intelligently analyze the enterprise social security data information. On this basis, combined with different types of enterprise social security data, intelligent matching is carried out according to its internal relevance and coupling, and the factors affecting the topology accuracy of social security data are customized. However, the enterprise social security data analysis model proposed in this study can only conduct high-intensity value analysis on the internal relevance of data types and does not take other potential influencing factors in the social security database into account. Therefore, further research can be carried out in terms of redundancy and robustness.

Data Availability

The data used to support the findings of this study are included within the article.

Conflicts of Interest

The authors declare that they have no conflicts of interest.

References

[1] M. Marino, P. Ni, L. Kazis, D. Brandt, and A. Jette, "Demographic and functional differences among social security disability claimants," *Quality of Life Research*, vol. 30, no. 6, pp. 1757–1768, 2021.

[2] K. Ivaturi and A. Bhagwatwar, "Mapping sentiments to themes of customer reactions on social media during a security hack: a justice theory perspective," *Information & Management*, vol. 57, no. 4, p. 103218, 2020.

[3] B. Wang, Y. Sun, T. Q. Duong, L. D. Nguyen, and N. Zhao, "Popular matching for security-enhanced resource allocation in Social Internet of Flying Things," *IEEE Transactions on Communications*, vol. 68, no. 8, pp. 5087–5101, 2020.

[4] M. M. Haglund, A. B. Cutler, S. Alexander, R. Dharmapurikar, S. P. Lad, and K. E. McDaniel, "The surgical autonomy program," *Neurosurgery*, vol. 88, no. 4, pp. E345–E350, 2021.

[5] Y. P. Chang, H. H. Hu, and C. M. Lin, "Consistency or hypocrisy? The impact of internal corporate social responsibility on employee behavior: a moderated mediation model," *Sustainability*, vol. 13, no. 17, p. 9494, 2021.

[6] X. Wei, P. Bossuyt, S. Vermeire, and R. Bisschops, "Assessing disease activity in ulcerative colitis using artificial intelligence: can "equally good" be seen as "better"?," *Gastroenterology*, vol. 159, no. 4, pp. 1625-1626, 2020.

[7] V. A. Masterson, P. S. Lamoureux, T. S. Choksi, V. Streibel, and F. Abild-Pedersen, "Combining artificial intelligence and physics-based modeling to directly assess atomic site stabilities: from sub-nanometer clusters to extended surfaces," *Physical Chemistry Chemical Physics*, vol. 23, no. 38, pp. 22022–22034, 2021.

[8] N. Fawzi, N. Steindl, M. Obermaier et al., "Concepts, causes and consequences of trust in news media–a literature review and framework," *Annals of the International Communication Association*, vol. 45, no. 2, pp. 154–174, 2021.

[9] E. L. Mayro, "Letter to the Editor: Comment on "The application of artificial intelligence for the diagnosis and treatment of liver diseases"," *Hepatology*, vol. 74, no. 3, p. 1710, 2021.

[10] Q. Lang, T. E. Tan, H. W. Chan et al., "Artificial intelligence for diagnosis of inherited retinal disease: an exciting opportunity and one step forward," *British Journal of Ophthalmology*, vol. 105, no. 9, pp. 1187–1189, 2021.

[11] L. Egevad, J. P. Janet, C. Duan, A. Nandy, F. Liu, and H. J. Kulik, "Navigating transition-metal chemical space: artificial intelligence for first-principles design," *Accounts of Chemical Research*, vol. 54, no. 3, pp. 532–545, 2021.

[12] J. Shen, C. Yang, T. Li, X. Wang, Y. Song, and M. Guizani, "Interactive artificial intelligence meets game theory in next-generation communication networks," *IEEE Wireless Communications*, vol. 28, no. 2, pp. 128–135, 2021.

[13] R. Verganti, V. L. Mango, M. Sun, R. T. Wynn, and R. Ha, "Should we ignore, follow, or biopsy? Impact of artificial intelligence decision support on breast ultrasound lesion assessment," *American Journal of Roentgenology*, vol. 214, no. 6, pp. 1–8, 2020.

[14] F. Kai, O. Méndez-Lucio, B. Baillif, D. A. Clevert, D. Rouquié, and J. Wichard, "De novo generation of hit-like molecules from gene expression signatures using artificial intelligence," *Communications*, vol. 11, no. 1, 2020.

[15] C. Liu, J. Arribas, G. Antonelli et al., "Standalone performance of artificial intelligence for upper GI neoplasia: a meta-analysis," *Gut*, vol. 70, no. 8, pp. 1458–1468, 2021.

[16] F. Goodarzian, J. L. Merrill, and U. M. Schmidt-Erfurth, "Clinical practice settings vs clinical trialsis artificial intelligence the answer?," *JAMA Ophthalmology*, vol. 138, no. 1, pp. 1-2, 2020.

[17] H. Takeshima, S. Gonem, W. Janssens, N. Das, and M. Topalovic, "Applications of artificial intelligence and machine learning in respiratory medicine," *Thorax*, vol. 75, no. 8, pp. 695–701, 2020.

[18] Z. Liu, L. Tan, D. Tivey et al., "Part 1: artificial intelligence technology in surgery," *ANZ Journal of Surgery*, vol. 90, no. 12, pp. 2409–2414, 2020.

Retraction

Retracted: Correlation Analysis between Tourism and Economic Growth Based on Computable General Equilibrium Model (CGE)

Journal of Sensors

This article has been retracted by Hindawi following an investigation undertaken by the publisher [1]. This investigation has uncovered evidence of one or more of the following indicators of systematic manipulation of the publication process:

(1) Discrepancies in scope

(2) Discrepancies in the description of the research reported

(3) Discrepancies between the availability of data and the research described

(4) Inappropriate citations

(5) Incoherent, meaningless and/or irrelevant content included in the article

(6) Manipulated or compromised peer review

The presence of these indicators undermines our confidence in the integrity of the article's content and we cannot, therefore, vouch for its reliability. Please note that this notice is intended solely to alert readers that the content of this article is unreliable. We have not investigated whether authors were aware of or involved in the systematic manipulation of the publication process.

Wiley and Hindawi regrets that the usual quality checks did not identify these issues before publication and have since put additional measures in place to safeguard research integrity.

We wish to credit our own Research Integrity and Research Publishing teams and anonymous and named external researchers and research integrity experts for contributing to this investigation.

The corresponding author, as the representative of all authors, has been given the opportunity to register their agreement or disagreement to this retraction. We have kept a record of any response received.

References

[1] S. Wang, "Correlation Analysis between Tourism and Economic Growth Based on Computable General Equilibrium Model (CGE)," *Journal of Sensors*, vol. 2022, Article ID 6497125, 8 pages, 2022.

Research Article

Correlation Analysis between Tourism and Economic Growth Based on Computable General Equilibrium Model (CGE)

Shiyu Wang [ID]

Tourism College, Huangshan University, Anhui 245041, China

Correspondence should be addressed to Shiyu Wang; wangshiyu@hsu.edu.cn

The current tourism industry has the problems of low service efficiency, poor coordinated development, and slow economic growth in terms of service volume and economic growth. This paper is based on computable general equilibrium (CGE) model. Firstly, a CGE data analysis model based on bee colony intensive breakthrough algorithm is established to store and analyze the data in the whole chain of tourism. Then, combined with the comparative analysis of tourism economic data over the years, it is fed back to the CGE model for error analysis. Finally, relevant experiments are designed to analyze the relationship between tourism and economic growth. The correlation degree of local economic growth is analyzed. The results show that, compared with the traditional research method of tourism economic growth based on module data analysis, this CGE model can realize the correlation analysis of the data involved in the process of tourism economic growth and analyze the factors affecting the speed of economic growth, which has the advantages of good reliability and strong pertinence.

1. Introduction

With the advent of the industrial 4.0 era and the rapid development of Internet data technology, tourism also presents great changes in service mode and business processing [1]. In recent years, with the rapid development of blockchain technology and the emergence and application of big data economic analysis model and CGE model, tourism is also facing an important transformation of digital development [2]. Therefore, data diversification and intelligence have become the necessary conditions for the future development potential of tourism [3]. On the other hand, although there are many tourism economic growth analysis models, there are still many problems [4]. For example, in the analysis of the development potential of tourism, the current analysis model generally does not have large-scale applicability, and its suggestions and conclusions are quite different from those in the actual implementation process [5]. Based on this background, this paper studies the correlation analysis system between tourism and economic growth and puts forward a computable general equilibrium model, which can quantitatively analyze and characterize the internal correlation between tourism and economic growth.

Aiming at the problems of poor coordinated development, slow economic growth, and low service efficiency in the process of market-oriented economic operation of the existing tourism industry, this paper studies the application of CGE model based on bee colony intensive breakthrough algorithm in tourism economic growth, which is mainly divided into four parts. Chapter 1 introduces the background, overall framework, and innovation of this study. Chapter 2 introduces the evaluation methods of tourism economic growth in different regions at home and abroad and the research status of data mining methods in tourism. Chapter 3 constructs the CGE model based on the bee colony intensive breakthrough algorithm and constructs the evaluation system of the correlation between tourism and economic growth by using the Laplace hyperbolic equation method. Chapter 4 tests the relevance evaluation system between tourism and economic growth, analyzes the results, and draws a conclusion.

The current mainstream analysis model of tourism economic growth (mainly based on the quantitative correlation analysis model based on neural network strategy algorithm or particle swarm optimization iterative optimization strategy algorithm) there is a disadvantage that it is necessary to set

known parameters and gradient interval. The innovation of this paper is to construct the correlation analysis method between tourism and economic growth through the bee colony intensive breakthrough algorithm, combined with the CGE model in the field of artificial intelligence and image recognition technology. On this basis, the model can not only record and store the data between tourism and economic growth in multiple regions but also make full use of the differential information of economic growth between each tourism area to analyze its correlation through CGE model. On the other hand, using Laplace factor quantitative index to complete the correlation analysis between tourism and economic growth can reduce the evaluation error.

2. Related Work

The existing tourism industry has the problems of poor coordinated development, slow economic growth, and low service efficiency in the process of market-oriented economic operation. Most scholars have analyzed the correlation between tourism and economic growth and tried to solve the above problems [6]. In order to solve the problem of transition analysis in the development of tourism, Rockicki other scholars put forward a comprehensive evaluation model of tourism growth and economic analysis based on the characteristics of regional development, so as to strengthen the analysis and weaken the management of the internal relevance of tourism [7]. According to the differential characteristics of different tourism industries in development, Zhao et al. put forward a development analysis strategy evaluation method based on CNN network. Experiments show that tourism can play a key role in economic growth [8]. Aiming at the problem of high cost in the process of user growth in tourism, Lin and other scholars used the convolution neural network algorithm of second-order least square method to analyze the correlation degree of factors affecting economic development and found that there is a strong correlation between cost and user growth strategy [9]. Aiming at the problem of low data utilization in the development of tourism, Cao and other scholars put forward an economic growth model combined with local economic development through experimental verification [10]. According to the traditional model theory and practical experience of tourism development, Peng and other scholars found that there are large differences in cross regional tourists' habits in the current local tourism areas in the process of economic growth. Therefore, they proposed an adaptive comprehensive evaluation method based on machine vision algorithm [11]. Hoffmann put forward a new scenic spot economic growth method based on Tourism Group trajectory analysis, which uses the deformed footprint map sequence to characterize the economic development of the tourism area on a large scale and realizes the determination of the optimal scheme in the process of tourism economic evaluation [12]. Through quantitative analysis of different scenic spots, Siddig and other scholars have made the regional tourism resources reach a state of near infinite saturation in the process of development. Experiments show that this strategy analysis and evaluation method have the advantages of fast comprehensive evaluation speed and obvious effect, but it is necessary to set the known

data gradient interval [13]. In order to further study the influencing factors in the process of tourism economic development, scholars such as Gilliland et al. proposed a variable step economic data analysis method combined with the idea of computable general equilibrium model. This method can effectively improve the income of tourism, but it is necessary to set known parameters and data gradient interval [14]. Rui and other scholars put forward a new tourism economic growth analysis method based on K-means image recognition strategy according to the macroeconomic theory in economy and established a multifactor coupling analysis model. The model also needs to set known parameters and gradient interval [15]. Aiming at many unreasonable problems in the process of tourism economic development, Paroussos and other scholars put forward a feature recognition and analysis strategy based on neural network. After practical verification, the results show that the economic evaluation method based on image recognition and analysis strategy has good evaluation effect and is suitable for the comprehensive evaluation of the development of characteristic scenic spots in tourism [16]. Feuerbacher and other scholars have made a comprehensive evaluation from the aspects of the selection of evaluation forms for the economic development of tourism, the classification of evaluation scenic spots, and the management ability of regions. Experimental experiments are carried out in different regions. The results show that it can improve the profitability of scenic spots [17].

Based on the above research results, we can know that in the current research on tourism and economic growth, in the mainstream analysis models of tourism economic growth (mainly based on neural network algorithm or particle swarm optimization algorithm), most of them need to set the known data gradient interval as a priori information [18–20]. On the other hand, in the quantitative evaluation of tourism economic development, most economic development analysis models need to summarize the industrial data of different ranges first and then conduct unified analysis and processing, which leads to the overall analysis efficiency becoming very low [21, 22]. Therefore, it is of great significance to study the correlation analysis method between tourism and economic growth based on computable general equilibrium model.

3. Methodology

3.1. Application of Computable General Equilibrium Model Based on Bee Colony Dense Breakthrough Algorithm in Economic Growth Analysis. Bee colony dense breakthrough algorithm is one of the commonly used algorithms in data mining. This method solves the calculation problems with high dimension and large amount of data by simulating the idea of cooperative movement of bee colony in the process of group survival and realizes the sampling solution of complex problems. The computable general equilibrium model (CGE) includes three salient features. The first is "general." That is, it makes an external setting for the behavior of economic subjects. In this model, one of the representative features is the pursuit of utility maximization. Manufacturers follow the decision-making principle of cost minimization and also include economic subjects such as government, trade organizations, importers, and exporters, which respond to

price changes [23]. Secondly, it is "equilibrium," which means that it includes two aspects of demand and supply. Many prices in the model are determined by both supply and demand, and price changes finally make the market realize equilibrium [24]. Finally, it is "computable." This is because the model reflects actual data and actual economic problems, which is closer to reality, involving industrial policy, income distribution, environmental policy, employment, etc. [25]. Therefore, the CGE model combined with bee colony intensive breakthrough algorithm can well solve the problem of correlation analysis between tourism and economic growth. The data correlation analysis process of tourism and economic growth based on CGE model is shown in Figure 1.

3.2. Data Analysis Process of CGE Model in Tourism Economic Growth. The tourism policy means concerned by the tourism CGE model are also divided into two categories: the first category is various tourism related laws, regulations, standards, and orders formulated by administrative means. The other is market-based and various economic means represented by tax, including direct tourism tax and indirect taxes such as hotel tax, gambling tax, and sales tax. In view of the above two types of policies, CGE model mainly discusses the impact of tourism industry policies on production (mainly including cost and productivity) and consumption (focusing on macro income and tourist welfare) in economic activities.

In order to better study the correlation between tourism and economic growth and conduct quantitative evaluation, after establishing the CGE model, it is necessary to quantitatively discuss the data analysis process of CGE model in tourism economic growth. According to the necessary conditions of macroeconomic model, it is necessary to design the operation threshold, termination condition, and evaluation standard of CGE model. Therefore, the economic growth operation threshold function $Q(x)$, the termination condition function $W(x)$, and the preliminary quantitative evaluation function $E(x)$ are set as follows:

$$Q(x) = \frac{\sqrt{\sum_{k=1}^{p} x_k^2 / x_{k+1}^2 / k\bar{x}_p}}{\sum_{p=1}^{k} k\bar{x}_p}, \tag{1}$$

$$W(x) = \frac{p!}{1 + \bar{x}_p} \sqrt{\frac{x_1 + x_k + x_p}{\bar{x}_{p+k-1}}}, \tag{2}$$

$$E(x) = \frac{\sqrt{\sum_{k=1}^{p} (x_k - \bar{x}_p)^2 + \sum_{k=1}^{p} (x_k + \bar{x}_p)^2}}{(k+1)\bar{x}_p}. \tag{3}$$

x_k is the daily operation data of tourism, p is the total number of users of tourism, k is the service type of tourism, and $\bar{x}_p$ is the average data of quarterly economic growth.

After normalizing the above three functions, the corresponding expression is as follows:

$$Q'(x) = 1 + \sqrt{\frac{\sum_{k=1}^{p} x_k^2 / x_{k+1}^2}{k\sum_{k=1}^{p} (x + \bar{x}_p / 1 + \bar{x}_p)^2}}, \tag{4}$$

$$W'(x) = \frac{(p+1)!}{p + \bar{x}} \sqrt{\frac{x_1 + x_k + x_p}{\bar{x}_{p+k-1}}}, \tag{5}$$

$$E'(x) = \frac{\sqrt{2 + \sum_{k=1}^{p} (x_k + \bar{x}_p)^2}}{1 + k\sum_{k=1}^{p} (x + \bar{x}_p / 1 + \bar{x}_p)^2}. \tag{6}$$

Through the statistics of tourism economic growth data in different regions, it is divided into regions according to the growth rate, and different types of economic growth data are distinguished in high dimensions to form multiple data envelopment analysis centers, and their data center groups are input into this CGE model. The simulation analysis results of these data groups on the correlation degree of tourism economic development are shown in Figure 2.

It can be seen from Figure 2 that the change trends of the three groups of databases are similar and are within a relatively stable change range, and the association analysis accuracy of the second group of databases is the highest. This is because after setting the operation threshold, and it is also necessary to quantitatively sort the relevant data affecting economic growth according to the utilization rate and carry out variable weight analysis. The module length analysis function $A(x)$, the economic growth solution function $S(x)$, and the nondisturbing error function $D(x)$ used in the vector comparison process in the above simulation analysis stage are as follows:

$$A(x) = \frac{\sqrt{|x|^2 + m|x| + \sqrt{|x|}}}{\sqrt{k|x| + m|x|^2} + \sqrt{k}}, \tag{7}$$

$$S(x) = \frac{\sqrt{\sum_{k=1}^{m} \sqrt{m|x|^2 + m|x| + \sqrt{|x|}} / m|x| + k|x|^2 + mk}}{3mk + \sqrt{m + kx}}, \tag{8}$$

$$D(x) = \frac{kS^2(x) + mA(x)}{kS(x) + mx} \sqrt{\left(1 + \frac{A(x)}{km}\right)}. \tag{9}$$

$|x|$ is the module length of tourism economic data vector, and m and k are the quantitative value and change type in the process of tourism economic growth, respectively. After fuzzifying the above three functions, the corresponding expression is as follows:

$$A'(x) = \frac{\sum_{k=1}^{m} \sqrt{|x|^2 + m|x| + \sqrt{|x|}} / k|x| + m|x|^2 + k}{m + k}, \tag{10}$$

$$S'(x) = k \frac{\sqrt{\sum_{k=1}^{m} \sqrt{m|x|^2 + m|x| + \sqrt{|x|}} / m|x| + k|x|^2 + mk}}{\sqrt{m|x| + k|x|^2} + mk}, \tag{11}$$

$$D'(x) = \sum_{k=1}^{m} \frac{D'(x)}{mA(kx) + kS(kx)}. \tag{12}$$
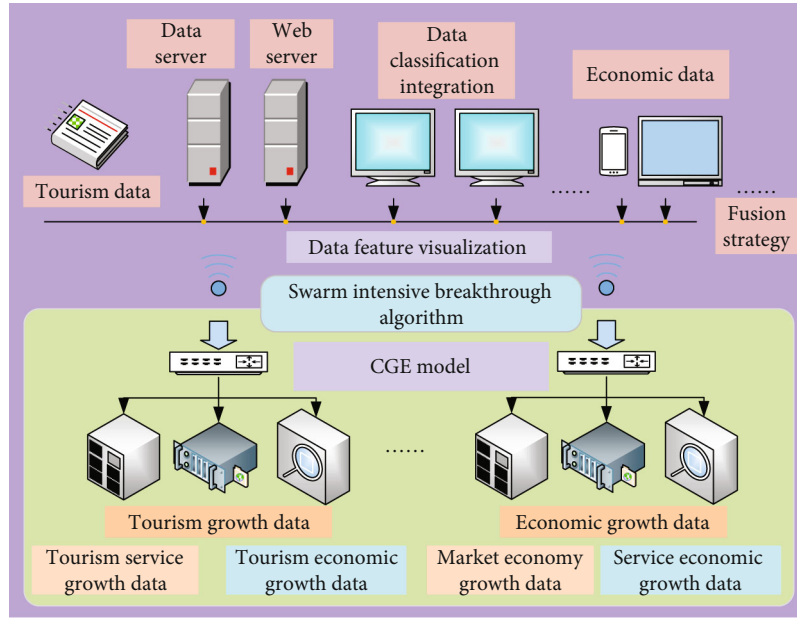
Figure 1: The analysis process of data association degree between tourism industry and economic growth based on CGE model.
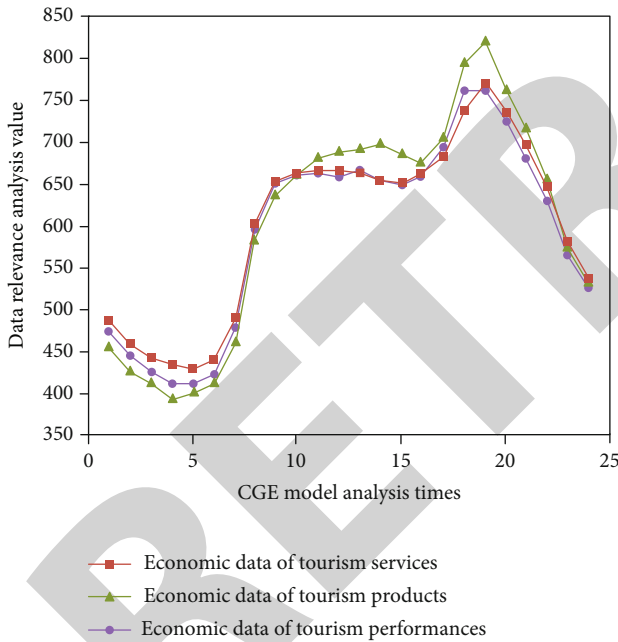

Figure 2: Simulation analysis result of tourism data set to economic development relevance.

$|x|$ is the module length of industrial economic data vector, and m and k are the number and type of tourism industry, respectively. In this stage, the economic growth simulation analysis results of CGE model on two types of random tourism economic data are shown in Figure 3.

It can be seen from Figure 3 that under the CGE model based on the bee colony dense breakthrough algorithm, with the increase of the number of simulation analysis, the correlation index of economic growth data in the two types of

data shows different trends, and there are four intersections, because in general, due to the problem of computer programming, at present, the economic growth data analysis method in the tourism information data management system cannot reach the level of artificial intelligence. There is inconsistency in the information analysis and data feature extraction between the economic data content of tourism in different regions and the economic information value of tourism stored in the cloud.

3.3. Simulation Verification Process of Quantitative Analysis of Economic Growth Combined with CGE Model. Based on the above analysis results, in order to further improve the accuracy of the analysis process of the correlation between tourism and economic growth, this part makes an accurate comparative analysis of a number of economic data within the tourism industry. The analysis process is shown in Figure 4.

For the known tourism economic development data, the corresponding identification error rate and correlation evaluation results are different, because for the calculation and identification of similarity, it can be corrected, compensated, and classified through the computable general equilibrium model according to the difference and similarity of data information in the tourism economic process. The simulation analysis results after correction are shown in Figure 5.

It can be seen from Figure 5 that the repair amount of tourism data under the CGE model is different, and the difference is obvious. This is because although the disturbance amount of the CGE model analysis method is very small, the data itself will have some differences, so there will be less data information reflected in the final analysis process. Finally, in the process of analysis, the high self-adaptive evaluation function $Z(x)$ and similarity function $X(x)$ based on bee colony dense breakthrough algorithm are introduced, and their mathematical expressions are as follows:
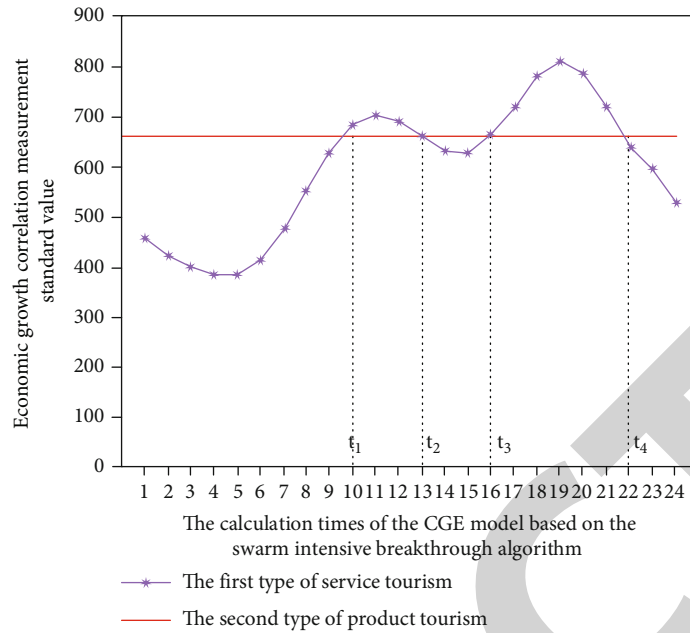
Figure 3: Economic growth simulation analysis results of two types of stochastic tourism industry operating data based on CGE model.
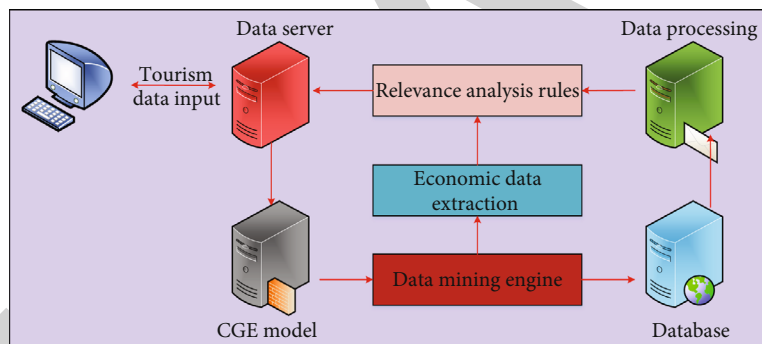

Figure 4: Accurately compare and analyze multiple economic data within the tourism industry.

$$Z(x) = 1 + \frac{\sqrt{\sum_{j=1}^{p}\left(jx_j^2 + \bar{x}^3\right)}}{\sqrt{1 + \sum_{k=1}^{p}\left(kx_k^2 - \bar{x}^2\right)^2}}, \tag{13}$$

$$W(x) = x - \frac{\sqrt{1 + \sum_{k=1}^{p}\left(kx_k^2 - \bar{x}^2\right)^2}}{1 + p\bar{x}}, \tag{14}$$

where x represents different economic growth data processing samples, k and j represent different numbers, and p represents the maximum number. In the process of error reduction of CGE model and result correction of overall operation function, it is necessary to normalize the sample data. The function set determined by the central data used in this process is as follows:

$$P(x) = \frac{l + rx}{lx + r}\sqrt{\frac{(l+r)(\sum_{i=1}^{m}x - 1 + \sum_{i=1}^{r}x)}{x}}, \tag{15}$$

where it represents the tourism economic growth function with certain rules, x represents different processing samples, and l and r represent different economic growth analysis rules.

4. Result Analysis and Discussion

4.1. Confirmatory Test of Correlation Analysis between Tourism and Economic Growth Based on CGE Model. After constructing the tourism and economic growth evaluation system based on CGE model, it is necessary to verify and analyze its practicability and scientificity. Therefore, this study combines the tourism economic data of Beijing in recent 5 years as the experimental data to verify. The preliminary analysis results of three groups of experimental data during the experiment are shown in Figure 6, in which the horizontal axis represents the number of experiments and the vertical axis represents the standardized correlation evaluation value based on CGE model.

As can be seen from Figure 6, under the bee colony dense breakthrough algorithm, with the increase of the number of
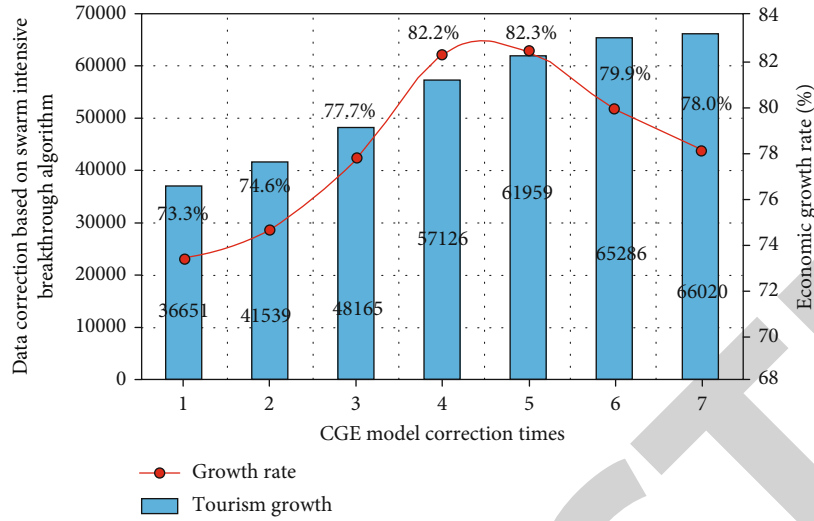
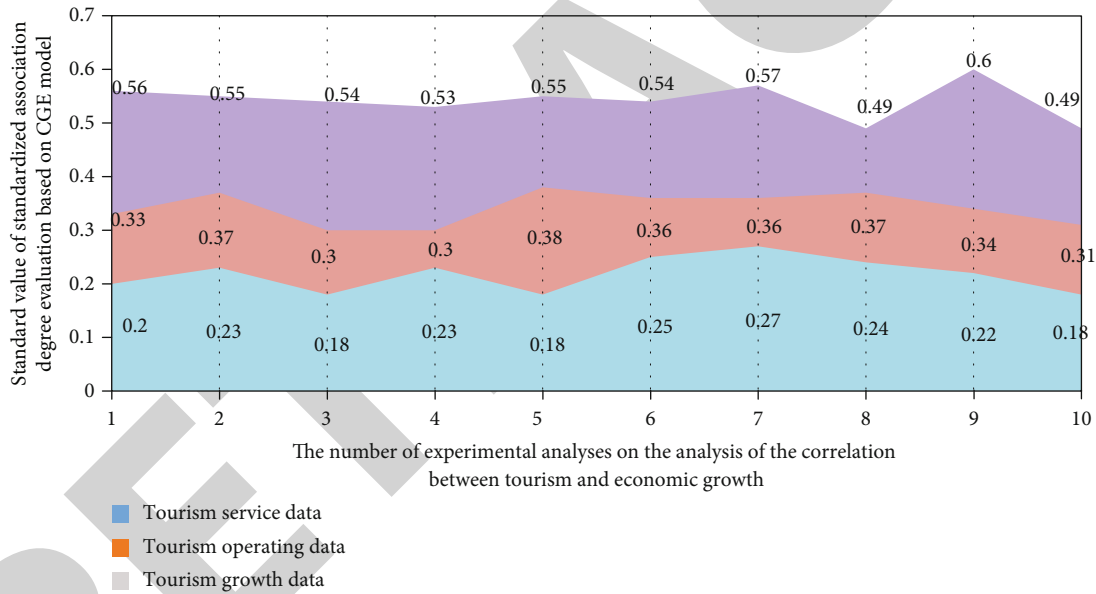Figure 5: Simulation analysis result after correction based on CGE model.

Figure 6: Preliminary experimental analysis results of 3 sets of experimental data.

experiments, the number of consistent data shows a trend of decreasing first and then stable. Compared with the data group without correction factor, the tourism data group with correction factor has more standardized correlation and economic growth data. This is because the operation method adopted this time is the improved tourism economic correlation analysis model combined with the CGE model of bee colony intensive breakthrough algorithm, and the threshold parameters of three data envelopment sets are set to characterize the correlation between tourism and economic growth. In addition, the CGE model will be based on the tourism user group data of Beijing, China, in recent 5 years. Through the comparative analysis of different parameters, it ensures the equal weight of each data in the process of correlation analysis, so as to reduce the data

analysis error in the experimental process and improve the objective accuracy and persuasion of the experimental process.

4.2. Experimental Results and Analysis. In the process of analyzing the experimental results, this study is based on the revenue and expenditure data disclosed by all scenic spots in Beijing in recent 5 years. The experimental group adopts CGE model, and the control group adopts the analysis model of conventional method (modular data analysis). The analysis results are shown in Figure 7.

Through the analysis of the results in Figure 7, it can be found that under the CGE model, the error of data correlation analysis is getting lower and lower, and the evaluation accuracy of the control group in the process of analyzing
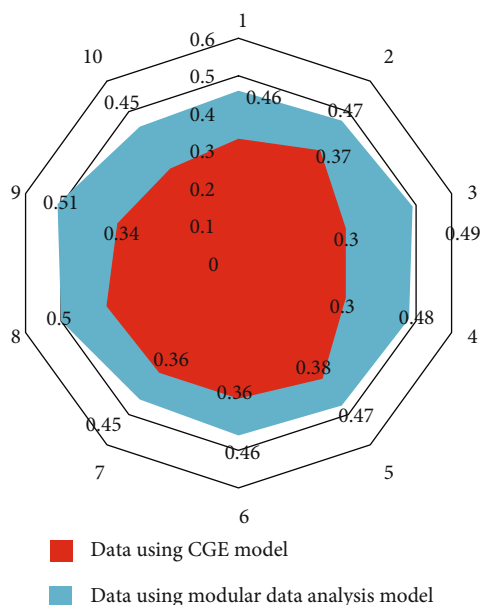
Figure 7: Analysis of the correlation error degree of the experimental results.

the economic cycle of tourism is lower and lower. Therefore, in the process of actual tourism revenue creation, it is necessary to set different types of threshold management in combination with the economic characteristics of tourism in different regions, so as to realize the efficient coordination of the relationship between tourism and regional economic growth.

5. Conclusion

At present, the tourism industry has the problems of low service efficiency, poor coordinated development, and slow economic growth in terms of service volume and economic growth. Compared with the disadvantages of setting known data gradient interval in the current mainstream tourism economic growth analysis model (mainly based on genetic control strategy algorithm or particle swarm optimization iterative optimization strategy algorithm), this paper studies the analysis model based on computable general equilibrium (CGE) model. Firstly, a CGE data analysis model based on bee colony intensive breakthrough algorithm is established to store and analyze the data in the whole tourism chain. Then, combined with the comparative analysis of tourism economic data in previous years, it is fed back to the CGE model for error analysis. Finally, relevant experiments are designed to analyze the relationship between tourism and economic growth. The correlation degree of local economic growth is analyzed. The results show that, compared with the traditional research method of tourism economic growth based on module data analysis, this CGE model can realize the correlation analysis of the data involved in the process of tourism economic growth and analyze the factors affecting the speed of economic growth, which has the advantages of good reliability and strong pertinence. This paper still has some limitations: the error analysis content of data correlation analysis is too short. It is necessary to discuss the economic characteristics of tourism in different regions. Not detailed

enough in terms of protecting multiple security of data, therefore, this paper makes an in-depth study on the enhancement of tourism security and regional economic growth in different regions.

Data Availability

The data used to support the findings of this study are available from the corresponding author upon request.

Conflicts of Interest

The authors declare no conflicts of interest.

References

[1] Y. Weng, S. Chang, W. Cai, and C. Wang, "Exploring the impacts of biofuel expansion on land use change and food security based on a land explicit CGE model: a case study of China," *Applied Energy*, vol. 236, pp. 514–525, 2019.

[2] R. Langarita, R. Duarte, G. Hewings, and J. Sánchez-Chóliz, "Testing European goals for the Spanish electricity system using a disaggregated CGE model," *Energy*, vol. 179, pp. 1288–1301, 2019.

[3] X. Li, X. Yao, Z. Guo, and J. Li, "Employing the CGE model to analyze the impact of carbon tax revenue recycling schemes on employment in coal resource-based areas: evidence from Shanxi," *The Science of the Total Environment*, vol. 720, article 137192, 2020.

[4] Y. Fu, G. Huang, L. Liu, and M. Zhai, "A factorial CGE model for analyzing the impacts of stepped carbon tax on Chinese economy and carbon emission," *Science of the Total Environment*, vol. 759, article 143512, 2021.

[5] T. Zhang, Y. Ma, and A. Li, "Scenario analysis and assessment of China's nuclear power policy based on the Paris Agreement: a dynamic CGE model," *Energy*, vol. 228, article 120541, 2021.

[6] G. Li, R. Zhang, and T. Masui, "CGE modeling with disaggregated pollution treatment sectors for assessing China's environmental tax policies," *Science of the Total Environment*, vol. 761, article 143264, 2021.

[7] B. Rokicki, E. A. Haddad, J. M. Horridge, and M. Stępniak, "Accessibility in the regional CGE framework: the effects of major transport infrastructure investments in Poland," *Transportation*, vol. 48, no. 2, pp. 747–772, 2021.

[8] J. Zhao, D. Greenwood, N. Thurairajah, H. J. Liu, and R. Haigh, "Value for money in transport infrastructure investment: an enhanced model for better procurement decisions," *Transport Policy*, vol. 118, pp. 68–78, 2022.

[9] B. Lin and Z. Jia, "Economic, energy and environmental impact of coal-to-electricity policy in China: a dynamic recursive CGE study," *Science of the Total Environment*, vol. 698, article 134241, 2020.

[10] Z. Cao, G. Liu, S. Zhong, H. Dai, and S. Pauliuk, "Integrating dynamic material flow analysis and computable general equilibrium models for both mass and monetary balances in prospective modeling: a case for the Chinese building sector," *Environmental Science & Technology*, vol. 53, no. 1, pp. 224–233, 2019.

[11] D. Peng, Q. Yang, H.-J. Yang, H. Liu, Y. Zhu, and M. Yongtong, "Analysis on the relationship between fisheries economic growth and marine environmental pollution in

Retraction

Retracted: Research on Teaching Quality Evaluation of Ideological Politics Teachers in Colleges and Universities Based on a Structural Equation Model

Journal of Sensors

This article has been retracted by Hindawi following an investigation undertaken by the publisher [1]. This investigation has uncovered evidence of one or more of the following indicators of systematic manipulation of the publication process:

(1) Discrepancies in scope

(2) Discrepancies in the description of the research reported

(3) Discrepancies between the availability of data and the research described

(4) Inappropriate citations

(5) Incoherent, meaningless and/or irrelevant content included in the article

(6) Peer-review manipulation

The presence of these indicators undermines our confidence in the integrity of the article's content and we cannot, therefore, vouch for its reliability. Please note that this notice is intended solely to alert readers that the content of this article is unreliable. We have not investigated whether authors were aware of or involved in the systematic manipulation of the publication process.

Wiley and Hindawi regrets that the usual quality checks did not identify these issues before publication and have since put additional measures in place to safeguard research integrity.

We wish to credit our own Research Integrity and Research Publishing teams and anonymous and named external researchers and research integrity experts for contributing to this investigation.

The corresponding author, as the representative of all authors, has been given the opportunity to register their agreement or disagreement to this retraction. We have kept a record of any response received.

References

[1] X. Fu and W. Chen, "Research on Teaching Quality Evaluation of Ideological Politics Teachers in Colleges and Universities Based on a Structural Equation Model," *Journal of Sensors*, vol. 2022, Article ID 3047700, 12 pages, 2022.

Hindawi

Research Article

Research on Teaching Quality Evaluation of Ideological Politics Teachers in Colleges and Universities Based on a Structural Equation Model

Xinggan Fu [1,2] **and Wenyan Chen** [3]

^{1}*Hainan College of Vocation and Technique, Haikou Hainan 570216, China*
^{2}*College of Management and Economics, Tianjin University, 300072, China*
^{3}*Department of Ideological and Political Education, Hainan College of Vocation and Technique, Haikou, Hainan 570216, China*

Correspondence should be addressed to Xinggan Fu; xinggan.fu@tju.edu.cn and Wenyan Chen; 2823163271@qq.com

With the dawn of a new era, ideological politics education plays an increasingly high role in college education, so the responsibilities given to ideological politics teachers in universities are increasing. The traditional teaching quality estimate model lags behind in accuracy, precision, and recall rate. Therefore, aiming at this phenomenon, this paper puts forward a teaching quality evaluation model for ideological politics teachers in universities based on the structural equation model. The purpose is to improve the estimated test time and improve the evaluation accuracy and accuracy. The research results of the article show the following: (1) The comparison results of the four models show that the estimate results of the model constructed in this paper have the highest accuracy, accuracy, and recall, with an average accuracy of 98.49%, an average accuracy of 98.31%, and an average recall rate of 98.28%. (2) After testing, the structural equation model takes the least time, with an average test time of 9.4 ms, which is far lower than the test time of the other three models. (3) According to the statistics of the weight of each index, among the first-class indexes, the weight of teachers' self-evaluation is the lowest, and the weight of students' evaluation is the highest, accounting for 0.625. The weights of the middle class, teaching implementation, and teaching and educating people in the secondary indicators are all above 0.5, and most of the rest are between 0.2 and 0.4. (4) For the formal estimate of teachers' teaching quality, the results show that the scores of the test subjects are above 90 points, the highest score is 99, and the average score is 94.5, which meets the test standard. (5) Finally, the model is evaluated, and it is concluded that each score is above 4.5, the highest score is 4.9, and the average score is 4.7, indicating that the model meets the standards and is highly recognized in people's hearts.

1. Introduction

Ideological politics education is in the stage of rapid development, so it is necessary to establish a scientific and reasonable estimate system of teaching quality. Ideological politics education is a particularly important subject in the current social development. The responsibility of ideological and political teachers is self-evident. Therefore, we should pay attention to improving the teaching quality of ideological and political teachers. Structural equation modeling is a reliable and flexible statistical method [1] and has a high value,

especially for evaluation research. Now, it has become a popular method [2], used to estimate complex models with potential variables and their relationships. Evaluation researchers are increasingly interested in structural equation model technology [3]. The structural equation model is of great significance in evaluation research [4]. The advantage of this method is that the analysis can be replicated according to the matrix and information specific to the model [5]. This model describes one of the most prominent research methods across multiple disciplines [6]. The structural equation model is a comprehensive statistical method [7]. It is

TABLE 1: Estimate principles of teachers' teaching quality.

Principle	Content
Objectivity principle	The teaching quality estimate is aimed at measuring, analyzing, and evaluating the effectiveness of teachers' teaching work. Its evaluation standards, evaluation methods, and attitudes of evaluation subjects must be objective to ensure the authenticity of evaluation results.
Systemic principle	Teachers' teaching quality is influenced by many factors such as teaching attitude, teaching methods, and teaching means. For the sake of reflecting the real teaching effect, teachers' teaching quality evaluation must comprehensively consider various influencing factors and adopt qualitative and quantitative methods to comprehensively evaluate.
Testability principle	Evaluation indicators must be measurable, so that the evaluation subject can quickly and accurately make judgments according to the evaluation indicators.
Guiding principle	The evaluation results should be inspiring and guiding and should point out the future direction for the evaluators.

TABLE 2: Modeling steps of structural equation model.

Step	Content
Model building	To establish the model, we must first fully understand the development of research content and establish the model on the basis of the correct theory. It should be fully aware of the various relationships between emerging variables and identify potential variables and observed variables and their relationships.
Model identification	Model identification is to judge whether the structural equation model can run and fit successfully after introducing data. There are three types of recognition: unrecognized, just recognized, and overrecognized.
Model fit	Model fitting is to import the collected data into the Amos software for parameter estimation. Firstly, the measurement model is estimated and tested by confirmatory factor molecules, and then the structural model is estimated and tested by path analysis.
Model evaluation	Model evaluation refers to judging whether the index value of the output results meets the preset fitness standard of the model after the establishment of the structural equation model, including the absolute adaptation criteria and relative adaptation criteria of the model.
Model correction	After model fitting, if the fitting index reflects that the model fitting is not good, it needs to be adjusted by model modification. Model revision should be cautious. It is necessary to add or delete variables according to the fitting index and adjust the path or parameters to achieve the best fitting degree.

mainly used to test hypotheses about the relationship between observed variables and potential variables. Structural equation modeling now uses the maximum likelihood method to deal with missing data [8]. This is a technology widely used in instrument verification and model testing [9]. We use this method to evaluate the teaching quality of teachers [10]. On the basis of teaching quality management in colleges and universities, the evaluation model of teaching quality is constructed by using the analytic hierarchy process [11]. The evaluation of education quality needs to go through the stages of task determination, standard proposal, development, and exploration [12]. To construct the quality evaluation system of ideological politics education in colleges and universities, we must adhere to the leadership of the Party, seek quality orientation in moral education, and pay attention to the internal and external coordination of ideological and political education quality. For the sake of improving teachers' teaching quality, we can implement the evaluation method of teachers' teaching quality [13]. The model takes student evaluation as the main body [14]. It is helpful to master teachers' teaching situations and improve teaching quality. The evaluation of teachers' teaching quality is the judgment of teachers' values [15].

2. Theoretical Basis

2.1. Structural Equation Model

2.1.1. Introduction to Structural Equation Modeling. The structural equation model (SEM) is also called a causality model [16]. In the 1870s, Swiss scholars put forward this method by combining the measurement characteristics of factor analysis with the regression modeling characteristics of path analysis.

2.1.2. Structural Equation Model Expression. Structural equation modeling includes a measurement model and structural model. Formula (1) is the structural model, and formulas (2) and (3) are the measurement equations. The mathematical expression is as follows:

$$\eta = B\eta + \Gamma\xi + \zeta, \tag{1}$$

$$y = \Lambda_y \eta + \varepsilon, \tag{2}$$

$$x = \Lambda_x \xi + \delta, \tag{3}$$

where η represents endogenous latent variables, ξ represents exogenous latent variables, and ζ represents random term
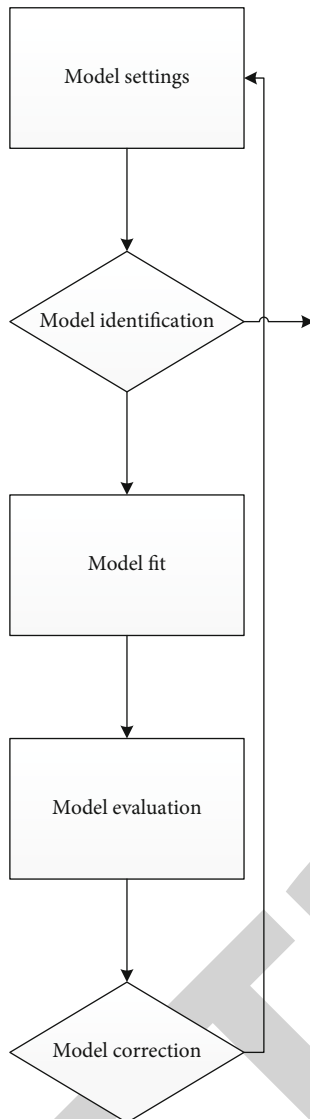
Figure 1: Structural equation model evaluation steps.

vectors. y and x are both observable variables, and ε and δ are random vectors.

2.2. Maximum Likelihood Estimation Method.

Maximum likelihood estimation (MLE) is the most commonly used means in structural equation modeling [17].

2.2.1. Discrete Type.

If the population X is discrete, its probability distribution is listed as

$$P\{X = x\} = p(x\,;\theta), \tag{4}$$

where θ is an unknown parameter. The joint assignment law of $(X_1, X_2, \cdots, X_n)$ is $\prod_{i=1}^{n} p(x_i\,;\theta)$ [18]. The probability of the observed value is

$$L(\theta) = L(x_1, x_2, \cdots, x_n\,;\theta) = \prod_{i=1}^{n} p(x_i\,;\theta). \tag{5}$$

Then $L(\theta)$ is the likelihood function of the sample.

2.2.2. Continuous Type.

If the population X is continuous, its probability density function is

$$f(x\,;\theta), \tag{6}$$

where θ is the unknown parameter. Assuming that a group of observations of $(X_1, X_2, \cdots, X_n)$ is $(x_1, x_2, \cdots, x_n)$ [19], the function is

$$L\left(x_1, x_2, \cdots, x_n\,;\widehat{\theta}\right) = \max L(x_1, x_2, \cdots, x_n\,;\theta). \tag{7}$$

$\widehat{\theta}(X_1, X_2, \cdots, X_n)$ is called the maximum likelihood estimator of θ.

2.3. Covariance Matrix.

A structural equation model is a statistical method to analyze the relationship between variables based on the covariance matrix of variables [20].

2.3.1. Concept.

Let $X = (X_1, X_2, \cdots, X_N)^T$ be an n-dimensional causal variable, the matrix.

$$C = \left(c_{ij}\right)_{n \times n} = \begin{pmatrix} c_{11} & \cdots & c_{1n} \\ \vdots & \ddots & \vdots \\ c_{n1} & \cdots & c_{nn} \end{pmatrix}, \tag{8}$$

where C is the covariance matrix of an n-dimensional random variable X, which is denoted as $D(X)$.

$$c_{ij} = Cov\left(X_i, X_j\right), i, j = 1, 2, \cdots, n. \tag{9}$$

2.3.2. Properties.

There are three properties of the covariance matrix:

$$\begin{aligned} \text{cov}\,(X, Y) &= \text{cov}\,(Y, X)^T, \\ \text{cov}\,(AX + b, Y) &= A\,\text{cov}\,(X, Y), \\ \text{cov}\,(X + Y, Z) &= \text{cov}\,(X, Z) + \text{cov}\,(Y, Z). \end{aligned} \tag{10}$$

2.3.3. Application.

Because

$$\begin{aligned} f(x_1, x_2) &= \frac{1}{2\pi\sigma_1\sigma_2\sqrt{1-\rho^2}} \exp\left\{\frac{-1}{2(1-\rho^2)}\left[\frac{(x_1-\mu_1)^2}{\sigma_1^2}\right.\right. \\ &\left.\left. -2\rho\frac{(x_1-\mu_1)(x_2-\mu_2)}{\sigma_1\sigma_2} + \frac{(x_2-\mu_2)^2}{\sigma_2^2}\right]\right\}, \end{aligned} \tag{11}$$

TABLE 3: Teachers' teaching quality appraisal system.

| System	Appraisal content and method
Teacher self-assessment	Teachers evaluate teaching from three respects: before, during, and after class.
Student evaluation	Students can evaluate teachers' teaching quality from three aspects: classroom performance, classroom teaching, and curriculum effectiveness.
Peer review	Peer teachers evaluate teachers' teaching quality from three aspects: teaching design, teaching implementation, and teaching reform by checking the teaching plan, listening to lectures, and participating in teaching and research activities.
Supervisory evaluation	Teaching supervision evaluates teachers' teaching quality from four aspects: teaching approach, teaching substance, teaching means and methods, and teaching effect by means of patrolling and listening to classes.
Leadership evaluation	Leaders evaluate teachers' teaching quality from three aspects: teaching preparation, teaching process, and teaching and educating people through teaching plan inspection and lectures.
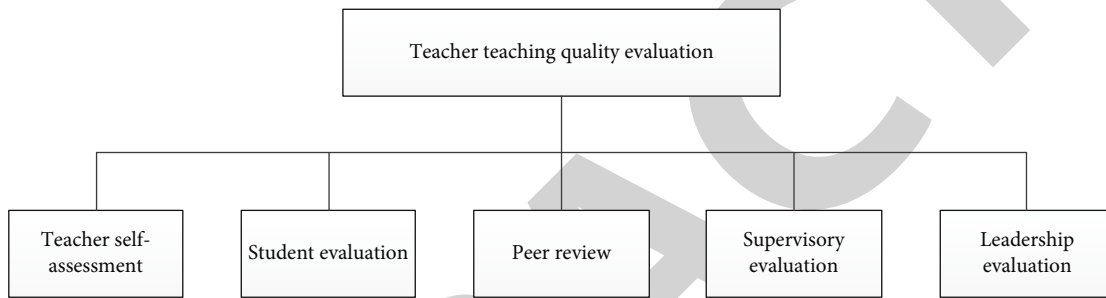
FIGURE 2: Assessment system of teachers' teaching quality.

The introduction matrix is

$$
X = \begin{pmatrix} x_1 \\ x_2 \end{pmatrix},
$$
$$
\mu = \begin{pmatrix} \mu_1 \\ \mu_2 \end{pmatrix},
\tag{12}
$$

and the covariance matrix of (X_1, X_2) is

$$
C = \begin{pmatrix} c_{11} & c_{12} \\ c_{21} & c_{22} \end{pmatrix} = \begin{pmatrix} \sigma_1^2 & \rho\sigma_1\sigma_2 \\ \rho\sigma_1\sigma_2 & \sigma_2^2 \end{pmatrix},
\tag{13}
$$

then

$$
\begin{aligned}
C^{-1} &= \frac{1}{\det C} \begin{pmatrix} \sigma_2^2 & -\rho\sigma_1\sigma_2 \\ -\rho\sigma_1\sigma_2 & \sigma_1^2 \end{pmatrix} \\
&= \frac{1}{\sigma_1^2\sigma_2^2(1-\rho^2)} \begin{pmatrix} \sigma_2^2 & -\rho\sigma_1\sigma_2 \\ -\rho\sigma_1\sigma_2 & \sigma_1^2 \end{pmatrix}.
\end{aligned}
\tag{14}
$$

Because

$$
\begin{aligned}
(X-\mu)^T C^{-1}(X-\mu) &= \frac{1}{\det C}(x_1-\mu_1, x_2-\mu_2) \\
&\begin{pmatrix} \sigma_2^2 & -\rho\sigma_1\sigma_2 \\ -\rho\sigma_1\sigma_2 & \sigma_1^2 \end{pmatrix} \begin{pmatrix} x_1-\mu_1 \\ x_2-\mu_2 \end{pmatrix},
\end{aligned}
\tag{15}
$$

then the probability density of (X_1, X_2) is

$$
f(x_1, x_2) = \frac{1}{(2\pi)^{2/2}(\det C)^{1/2}} \exp\left\{-\frac{1}{2}(X-\mu)^T C^{-1}(X-\mu)\right\}.
\tag{16}
$$

2.4. Evaluation of Teachers' Teaching Quality

2.4.1. The Purpose of Teacher Teaching Quality Evaluation. The purpose of the teachers' teaching quality estimate is to test the results of teachers' "teaching" and students' "learning" [21].

2.4.2. Principles of Teacher Teaching Quality Evaluation. The principles of teachers' teaching quality estimate include objectivity, systematicness, measurability, and orientation [22], as shown in Table 1.

2.4.3. Evaluation Methods of Teaching Quality. The evaluation methods of teaching quality mainly include qualitative

TABLE 4: Teaching quality appraisal indicators.

Main target	Primary index	Secondary index	Tertiary index
Teacher's teaching quality	Teacher self-assessment	Before class	Dedicated, hardworking, and passionate about teaching
			Well prepared before class
			The teaching content is rich and informative
			Introduce cases and link theory with practice
		In class	Explain the regulations clearly, highlighting the important and difficult points
			Integrate the ideological politics elements of the course
			Can effectively adjust the classroom atmosphere
			Students acquire knowledge and skills
		After class	Carefully correct homework, patiently guide, and answer questions
			Diagnose and improve classroom teaching actively
	Student evaluation	Classroom performance	Serious attitude and good manners
			Full of energy, strong affinity
			The language is vivid and stimulates students' curiosity
		Classroom teaching	Rich teaching resources
			Advanced teaching methods and flexible methods
			Linking theory with practice, appropriate cases
			Respect for students, harmonious relationship between teachers and students
			Be able to answer questions for students carefully and patiently
		Classroom effectiveness	Mastered the basic knowledge and basic skills
			Broadened horizons
	Peer review	Instructional design	Teaching goals are clearly defined
			Accurately grasp the key points and difficulties of teaching
			Appropriate use of teaching methods and means
			Attach importance to the cultivation of students' innovative practical ability
		Teaching implementation	Rigorous and serious academic attitude
			Lectures are refined, vivid, and accurate
			Emphasis on teacher-student communication, active atmosphere
			Students acquire knowledge and skills
		Teaching reform	Actively carry out research on teaching reform
			Continuously improve teaching and improve quality
	Supervisory evaluation	Teaching attitude	Prepare carefully and prepare well
			Full of energy and passion
		Teaching content	Proficient in content and a large amount of information
			Difficulties are highlighted, and the structure is clear
			The explanation is refined and vivid
		Teaching methods and means	The organic integration of "ideological politics education" and teaching
			Advanced methods and flexible teaching methods
			The relationship between teachers and students is harmonious, and the atmosphere is active
		Teaching effect	A high degree of achievement of teaching objectives
			Arouse students' curiosity
	Leadership evaluation	Teaching preparation	Careful preparation of lessons, full of content
			Rich teaching resources such as videos and courseware
		Teaching process	Rigorous attitude, dignified appearance
			Full of energy, strong affinity
			Accurate lectures, highlighting important and difficult points

TABLE 4: Continued.

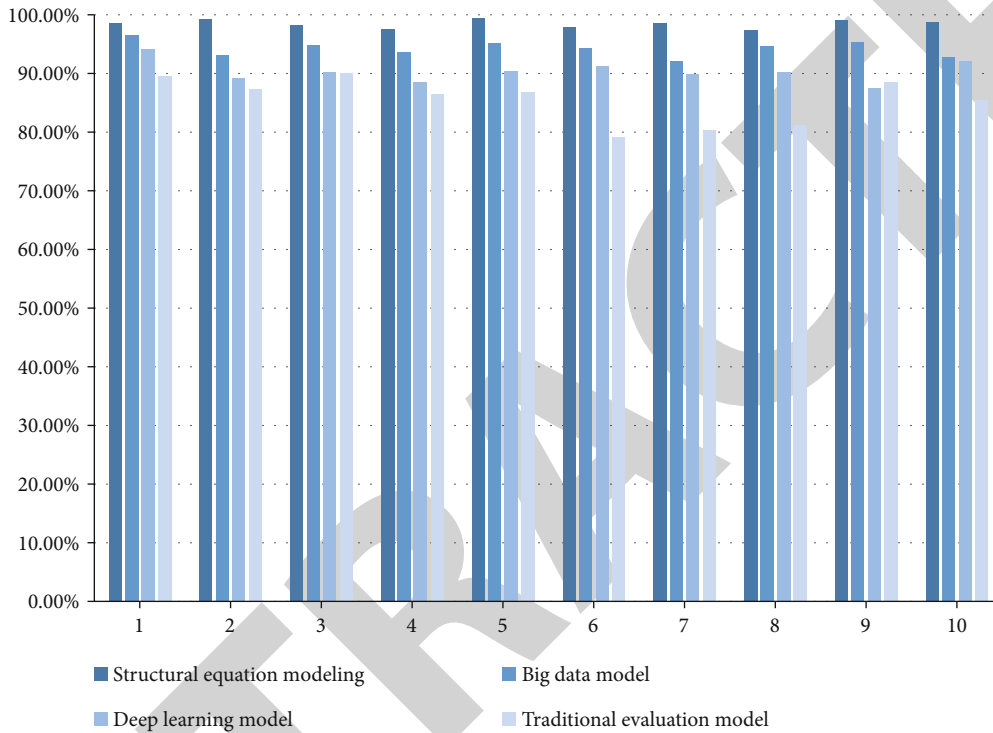| Main target	Primary index	Secondary index	Tertiary index
		Teaching and educating people	Regulation cleaning, explain in simple language
			Flexible teaching methods and advanced methods
			Students acquire basic knowledge and skills
			Reflect "Lide Shuren"
			Students' interest is nurtured and stimulated

FIGURE 3: Comparison of accuracy rates.

evaluation and quantitative evaluation: qualitative evaluation refers to the value judgment of the evaluated person, which is to draw a qualitative conclusion according to the specific performance of the evaluation subject to the evaluated person in all aspects. Quantitative evaluation means that the value judgment of the evaluator is the use of mathematical methods to evaluate the specific performance of the evaluator in various aspects to draw a conclusion.

2.5. Ideological and Political Education. Ideological politics education is mainly to integrate ideological politics education into the classroom and explain its basic theory, ideological values, and spiritual pursuit that contemporary youth should have. As the successors of the Party and the country, we should have correct political thoughts and walk on the correct ideological politics road.

In a sense, ideological politics education is to improve our ideological pursuit, enrich our spiritual thoughts, let us have correct life values, and make powerful contributions to the party and the country.

3. Model Building

3.1. The Modeling Procedure of Structural Equation Model. The modeling steps of the structural equation model are divided into modeling, model recognition, fitting, evaluation, and modification [23], as shown in Table 2.

Among them, the number of parameters to be solved in model identification t should satisfy

$$t \leq \frac{(p+q)(p+q+1)}{2}. \tag{17}$$

$p + q$ is the number of observed variables.

The evaluation procedure of the structural equation model is shown in Figure 1.

3.2. Construction of Teacher Teaching Quality Evaluation System. The appraisal system of teachers' teaching quality mainly consists of teachers' self-appraisal, students' appraisal, peer appraisal, supervision appraisal, and leadership appraisal [24], as shown in Table 3.
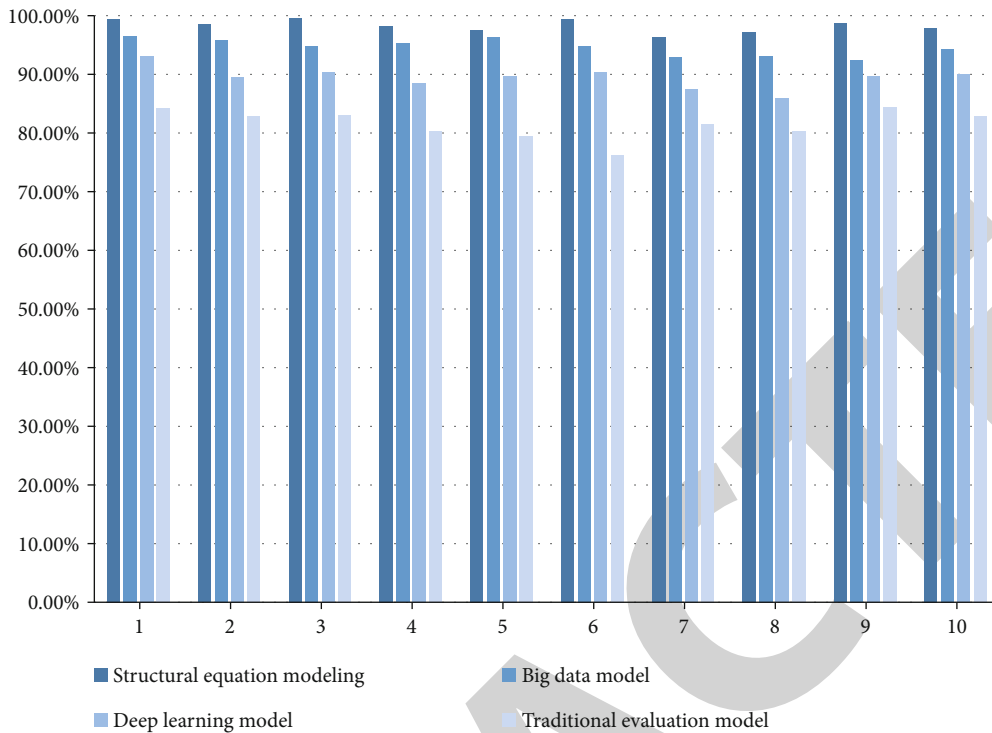
Figure 4: Comparison of accuracy rates.

The evaluation system of teachers' teaching quality is shown in Figure 2.

3.3. Evaluation Index of Teaching Quality.

According to the analytic hierarchy process, a five-dimensional analysis model of the teaching quality of ideological politics teachers in universities is constructed, and the Tertiary Index is established. The Primary Index includes teacher self-appraisal, student appraisal, peer appraisal, supervisory appraisal, and leadership appraisal; the Secondary Index includes 16 before, during, and after class; the Tertiary Index includes 50 such as "seriously correcting homework, patiently tutoring, and answering questions" and "conscientious attitude and decent behavior."

By comparing the importance of the Secondary Index to the Primary Index and the importance of the Tertiary Index to the indicators, the weights of the Secondary Index and the Tertiary Index can be obtained. The index system is shown in Table 4.

3.4. AHP.

AHP is a qualitative evaluation means [25]. The procedure of the AHP is divided into the construction of the evaluation index model, the construction of the judgment matrix, the determination of index weight, and the consistency test.

The calculation process of AHP is as follows:

$$N_{ij} = \frac{A_{ij}}{\sum_{j=1}^{n} A_{ij}} (i, j = 1, 2, 3 \cdots, n). \tag{18}$$

The sum of each row vector of a matrix is

$$T_{ij} = \sum_{i=1}^{n} T_{ij} (i, j = 1, 2, 3 \cdots, n). \tag{19}$$

The normalized matrix is

$$W_{ij} = \frac{T_i}{\sum_{i=1}^{n} T_i} (i, j = 1, 2, 3 \cdots, n). \tag{20}$$

In the consistency check, the largest eigenroot $\lambda_{\max}$ is computed as follows:

$$\lambda_{\max} = \sum_{i=1}^{n} \frac{(AW)_i}{nW_j}, \tag{21}$$

where $(AW)_i$ represents the first i element of vector AW.

The one-time indicator CI is calculated as follows:

$$CI = \frac{\lambda_{\max} - n}{n - 1}. \tag{22}$$

The consistency ratio CR is

$$CR = \frac{CI}{RI}. \tag{23}$$

4. Experimental Analysis

4.1. Model Checking.

In order to see the test results of this model more intuitively, this experiment will select
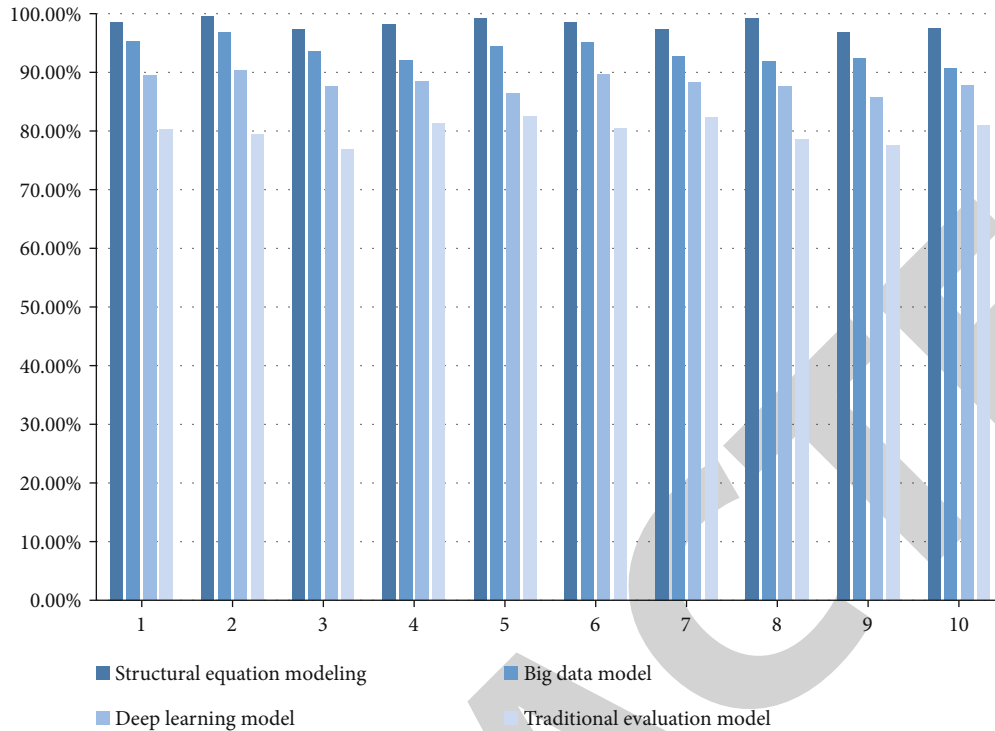
Figure 5: Comparison of recall rates.

traditional evaluation models, deep learning models, and big data models for comparative analysis. We will randomly select 100 ideological and political students from a university, 10 people will form a group, and a total of 10 groups will be tested. The test sample is students' evaluation of the teaching quality of ideological politics teachers.

4.1.1. Accuracy Comparison. First of all, the accuracy of the model will be tested so as to test the correctness of the model when evaluating the teaching quality of ideological politics teachers in the university. It is shown in Figure 3.

From Figure 3, we can see that the model constructed in the text has the highest evaluation precision, with an average evaluation precision of 98.49%. Compared to the other three models, this model is 4.25% higher than the big data model, 8.12% higher than the deep learning model, and 12.97% higher than the traditional evaluation model. Therefore, this model has higher accuracy and superiority.

4.1.2. Accuracy Comparison. Accuracy means that the error of the test result is within the specified range. By comparing the accuracy of the four models, we can know the superiority of the model. It is shown in Figure 4.

It can be seen from Figure 4 that the structural equation model has the highest accuracy, with an average accuracy rate of 98.31%. Compared with the other three models, it is 3.64% higher than the big data model, 8.8% higher than the deep learning model, and 16.73% higher than the traditional evaluation model.

4.1.3. Comparison of Recall Rates. Recall refers to the rate of correct predictions in a sample. The recall comparing results of the four models are shown in Figure 5.

It can be seen from Figure 5 that the recall rate of the structural equation model is the highest, the highest value is 99.6%, and the average recall rate is 98.28%. Compared with the other three models, it is 4.73% higher than the big data model, 10.12% higher than the deep learning model, and 18.22% higher than the traditional evaluation model, so this model is better.

4.1.4. Test Time Comparison. The four models were tested 10 times, and the time spent on their tests was recorded. The results showed that the structural equation model took the least time, with an average test time of 9.4 ms, which was much lower than the test time of the other three models. It is shown in Figure 6.

According to the results, we conclude that the structural equation model test takes the least time, which can greatly reduce the research time of teaching quality estimate and improve the work efficiency.

4.2. Indicator Weights. For the evaluation research of political science teachers' teaching quality in universities, it is necessary to determine the weight coefficient of each index, so as to be more accurate in the evaluation of teaching quality.

4.2.1. Primary Indicators. For the general goal of teaching quality ideological politics teachers in universities, we need to construct a comparison matrix C by comparing five
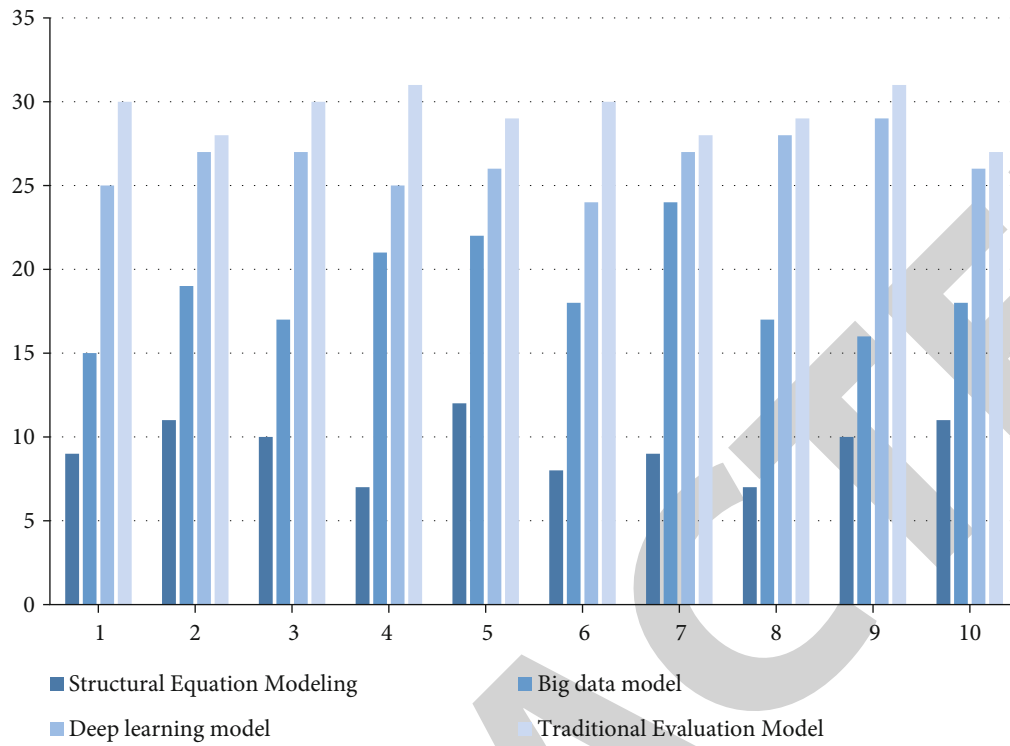
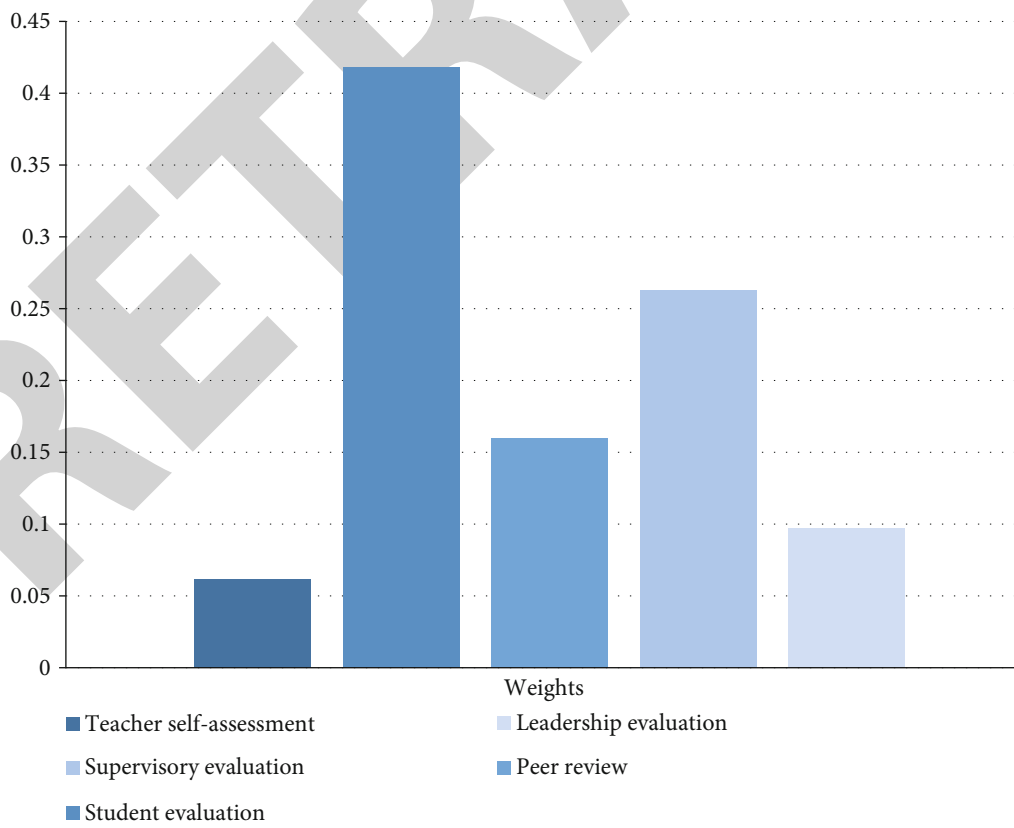Figure 6: Test time comparison.
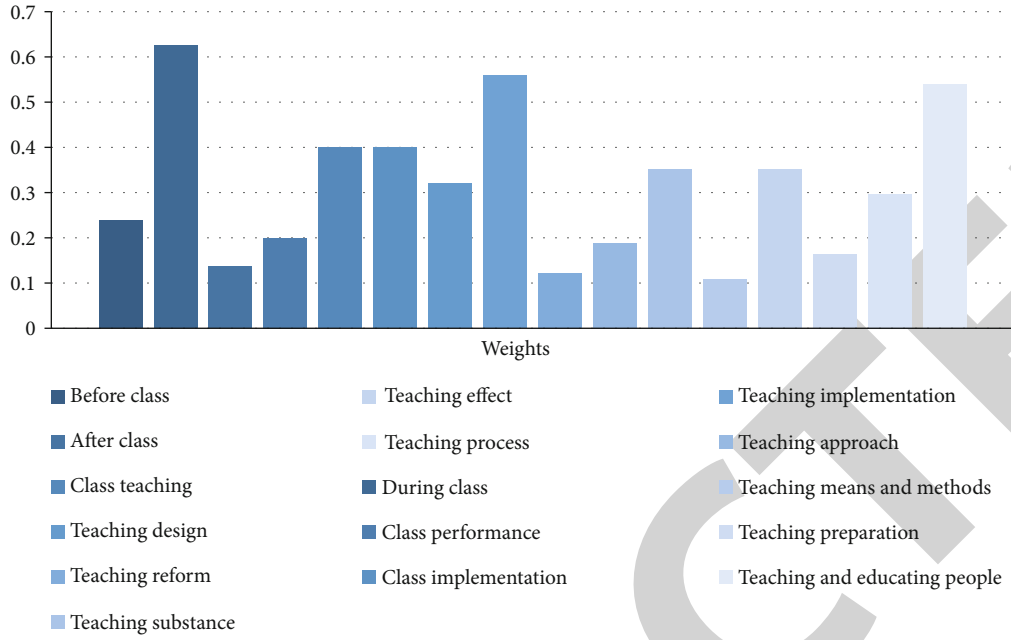

Figure 7: Primary indicators.
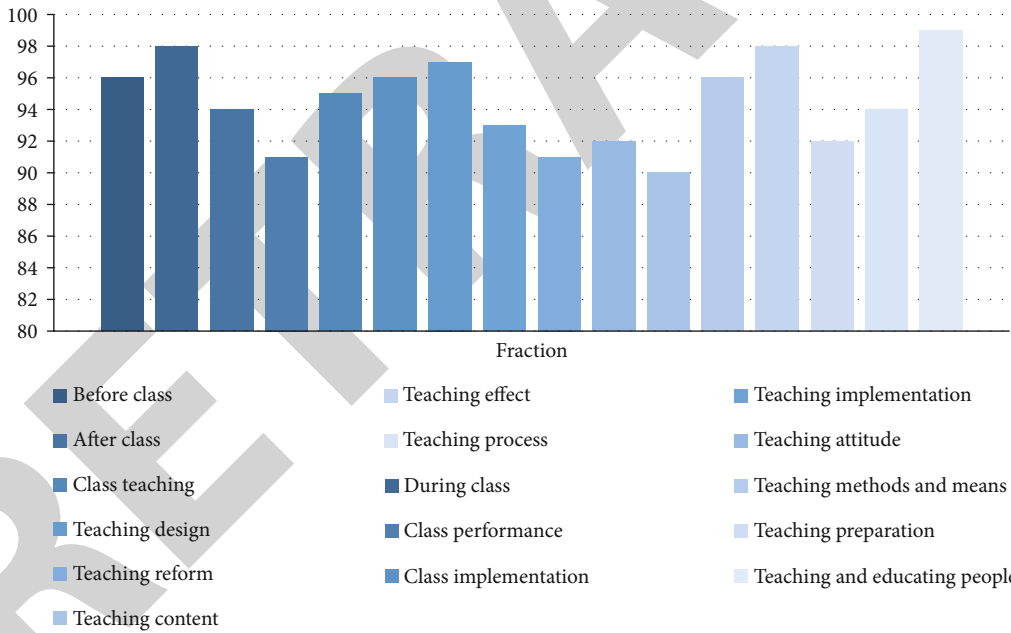
FIGURE 8: Secondary indicators.

FIGURE 9: Teaching quality evaluation.

first-level indicators:

$$C = \begin{bmatrix} 1 & 1/5 & 1/3 & 1/4 & 1/2 \\ 5 & 1 & 3 & 2 & 4 \\ 3 & 1/3 & 1 & 1/2 & 2 \\ 4 & 1/2 & 2 & 1 & 3 \\ 2 & 1/4 & 1/2 & 1/3 & 1 \end{bmatrix}. \quad (24)$$

The weight coefficients of five first-level indicators can be obtained by calculation.

The specific weights of the first-level indicators are shown in Figure 7.

4.2.2. Secondary Indicators. The specific weights of the secondary indicators are shown in Figure 8.

From Figure 7, we can see that the weight of teacher self-evaluation is the lowest, and the weight of student evaluation
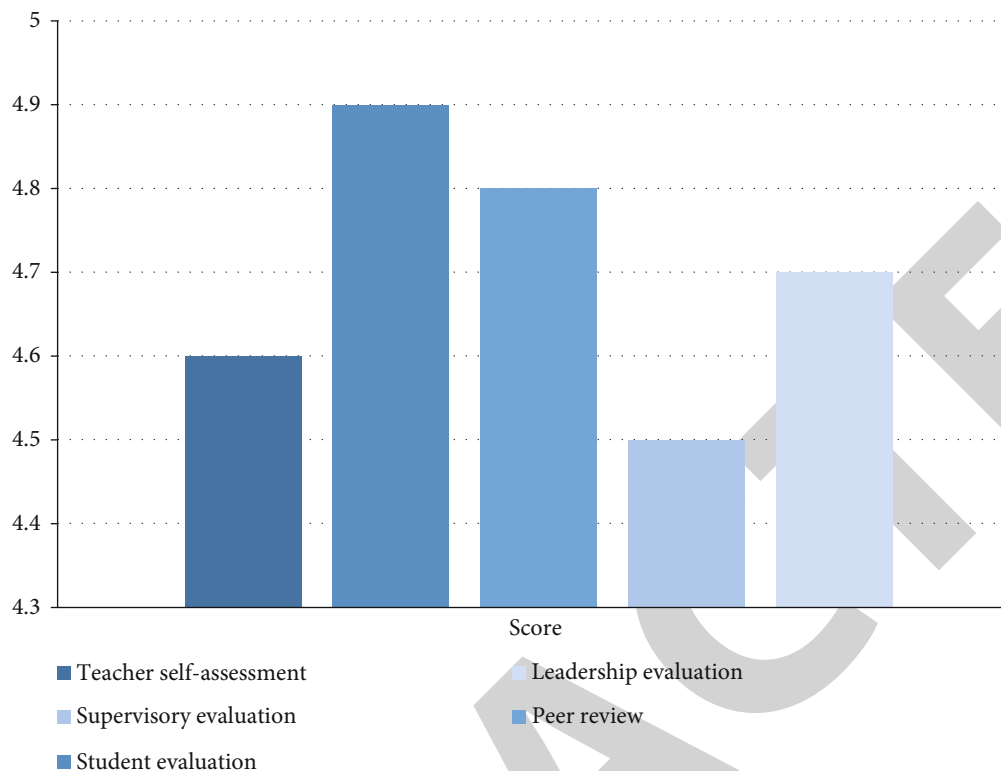
FIGURE 10: Model appraise.

is the highest, accounting for 0.625. The weight of each indicator is different, which means that each indicator has different standards and focuses on the evaluation of ideological politics and teachers' teaching quality. Some indicators are important, and some indicators are relatively unimportant and are only used as a reference. According to Figure 8, we can know that the weights of class, teaching implementation, and teaching and educating people are all above 0.5, and the rest are between 0.2 and 0.4.

4.3. Evaluation of Teaching Quality. This experiment will evaluate an ideological politics teacher in a university. The experiment will use the model designed in this article to estimate the teaching quality of ideological politics teachers in universities according to the indicators mentioned above. Taking the secondary index as the evaluation standard, the results are shown in Figure 9.

According to the results in Figure 9, the scores of each evaluation index are above 90, the highest score is 99, and the average score is 94.5. This model test can effectively reflect teachers' teaching problems, and teachers can find out their own teaching deficiencies in time and then make corrections.

4.4. Model Evaluation. For the sake of proving the practicability of the model, we asked the reviewers mentioned in the first-level index to score the model, with a total score of 5 points, and the average score above 4.5 indicates that the model has a high recognition among teaching system personnel. The scoring situation is shown in Figure 10.

As can be seen from Figure 10, the scores of each reviewer are above 4.5, the highest score is 4.9, and the average score is 4.7, indicating that the model meets the standard.

5. Conclusion

The new era gives us college students more responsibilities, and ideological politics education is one of the ways to perfect our ideological height. The traditional evaluation model has a certain lag, so this paper designs a new model to improve this problem. The evaluation model of teaching quality of ideological politics teachers in high school based on the structural equation model designed in this paper improves the correctness, precision, and recall on the basis of the traditional evaluation model and shortens the test time. It helps reviewers improve their work efficiency and is of great significance in the research of evaluating teaching quality.

The findings of the article show that

(1) The comparison results of the four models show that the evaluation results of the model constructed in this paper have the highest accuracy, accuracy, and recall rate, with an average accuracy of 98.49%, an average accuracy of 98.31%, and an average recall rate of 98.28%

(2) After testing, the structural equation model takes the least time, with an average test time of 9.4 ms, which is far lower than the test time of the other three models

(3) In the first-level indicators, the weight of teachers' self-evaluation is the lowest, and the weight of students' evaluation is the highest, accounting for 0.625. The weights of the middle class, teaching implementation, and teaching

Hindawi

Retraction

Retracted: Application of Correlation Filter Tracking Algorithm Based on Multiple Color Features in Basketball Motion Capture System

Journal of Sensors

This article has been retracted by Hindawi following an investigation undertaken by the publisher [1]. This investigation has uncovered evidence of one or more of the following indicators of systematic manipulation of the publication process:

(1) Discrepancies in scope

(2) Discrepancies in the description of the research reported

(3) Discrepancies between the availability of data and the research described

(4) Inappropriate citations

(5) Incoherent, meaningless and/or irrelevant content included in the article

(6) Manipulated or compromised peer review

The presence of these indicators undermines our confidence in the integrity of the article's content and we cannot, therefore, vouch for its reliability. Please note that this notice is intended solely to alert readers that the content of this article is unreliable. We have not investigated whether authors were aware of or involved in the systematic manipulation of the publication process.

Wiley and Hindawi regrets that the usual quality checks did not identify these issues before publication and have since put additional measures in place to safeguard research integrity.

We wish to credit our own Research Integrity and Research Publishing teams and anonymous and named external researchers and research integrity experts for contributing to this investigation.

The corresponding author, as the representative of all authors, has been given the opportunity to register their agreement or disagreement to this retraction. We have kept a record of any response received.

References

[1] B. Li and H. Quan, "Application of Correlation Filter Tracking Algorithm Based on Multiple Color Features in Basketball Motion Capture System," *Journal of Sensors*, vol. 2022, Article ID 3190206, 10 pages, 2022.

Research Article

Application of Correlation Filter Tracking Algorithm Based on Multiple Color Features in Basketball Motion Capture System

Bingyang Li and Haiying Quan

Liaoning Normal University, Dalian, Liaoning 116029, China

Correspondence should be addressed to Haiying Quan; 216082@stu.ahu.edu.cn

The application of motion capture system in basketball game can intercept the highlights of the game and improve the viewing effect. In order to improve the tracking performance of target tracking algorithm and the efficiency of traditional basketball tracking system, a correlation filtering algorithm combining multiple color features is adopted in this study. A dhcf as algorithm based on multicolor feature is established. The adaptability of traditional KCF algorithm in scene attributes such as rapid target change and illumination change is mainly studied. The success rate of multicolor tracking algorithm can reach 78.2%. At the same time, based on the traditional kernel correlation filter, the algorithm combines the discriminant color descriptor and the direction gradient histogram. The results show that the success rate and accuracy of the algorithm in otb50 are 84.2% and 82.5%, respectively. In addition, excellent tracking performance is reflected in various scene attributes. Therefore, the algorithm can improve the target tracking performance of the traditional kernel correlation filter, especially solving the adaptability of the traditional algorithm in the scene of light change, fast target movement, and so on.

1. Introduction

With the development of information technology, multimedia technology is constantly updated and upgraded and has been applied to many fields. The application of motion capture system in basketball can intercept the highlights of the game and improve the viewing effect. In addition, in basketball training, frame-by-frame analysis of elite athletes' actions through motion capture technology can improve the teaching quality [1]. The motion capture system needs to capture the movements of the target athletes accurately and quickly. In the process of basketball game, the athletes' speed is very fast, which is a great challenge to the performance of the system. The traditional tracking algorithm will carry out a large number of sample training in the sampling process, its operation process is more, and the real-time performance of the algorithm is poor. Kernel correlation filter (KCF) tracking algorithm has attracted extensive attention because of its efficient computing power. Based on the KCF algorithm with multicolor features, an adaptive multi-

feature kernel correlation filter tracking algorithm is proposed, which has more advantages in algorithm efficiency than the traditional correlation filter.

The tracking algorithm can be divided into two types: discriminant and generative. The correlation filter belongs to discriminant algorithm in the tracking algorithm. Compared with generative algorithms, discriminant algorithms such as correlation filtering have better real-time performance and operation speed, so it has become the main research method in the field of target tracking [2]. The KCF algorithm combined with multiple color features can reduce the impact caused by the change of target action. It can select multiple groups of color features and select the color descriptor with better tracking effect. Therefore, it has better target tracking ability.

The innovation of this study is that the adaptive sample set is used in the original kernel correlation filter. When the target moves too fast or is blocked, it is easy to form a large amount of invalid and redundant information, which will affect the target tracking efficiency of the algorithm. The

adaptive sample set can filter these interference information, so as to improve the target tracking accuracy and real-time performance of the motion capture system.

This research is divided into four parts. The first part comprehensively describes the current target tracking research of correlation filter algorithm, and the second part discusses and optimizes the multifeature KCF algorithm. The third part is the test and application effect analysis of the KCF algorithm of adaptive sample set used in this study. The fourth part summarizes the results of this study, reflects on the shortcomings of the experiment, and points out the direction for the follow-up research.

2. Related Work

Gong et al. proposed a KCF algorithm based on multichannel memory model. They use multichannel memory to establish a classifier update model. The model includes a control channel and two execution channels, which are used to store the target template and store the parameters and features of the classifier, respectively. Experiments show that the algorithm can still have the accuracy and robustness of target tracking in the case of target deformation and occlusion [3]. On the basis of multifeature fusion and superpixel, Zhang et al. proposed a correlation filter tracking algorithm, which reconstructs the appearance of the target through overlap analysis and deletes redundant information. Compared with the classical KCF algorithm, this algorithm has greatly improved the tracking success rate and accuracy and still has stability in complex environment [4]. Zhu et al. proposed a correlation filter based on learning spatio-temporal consistency, which makes the correlation filter have good adaptability when tracking target changes [5]. Masood et al. proposed a cohesion method to detect the target through the maximum average correlation height filtering algorithm. Compared with recent similar algorithms, this algorithm has smaller tracking error [6]. Sun et al. combine color and depth features and propose an average peak correlation energy tracking algorithm. Experiments show that the algorithm can effectively describe the appearance of the target and update the model through the confidence level, so as to improve the performance of the algorithm [7].

Xie et al. select and maintain the correlation filter through in-depth learning and then use a large number of videos to train the target appearance decision network. Experiments show that the target tracking accuracy of this method is more than 80%, which greatly improves the performance of correlation filter [8]. Wang et al. used the hybrid correlation filter for target tracking and used the combination of global filter and local filter to locate the target. The results show that the algorithm can well adapt to the complex situation that the target is occluded or changes rapidly [9]. The target tracking algorithm adopted by Yang et al. includes tracker, learning mechanism, and detector and introduces adaptive correlation filter. Experiments show that the algorithm can cope with the changes of illumination and target attitude [10]. Wang et al. proposed a target tracking algorithm based on correlation filter, which adopts the way of adaptive correction weight to deal with the problem of

inaccurate target tracking. Experiments show that this method has greatly improved the tracking accuracy compared with the traditional target tracking algorithm [11]. Fang et al. have adopted a target tracking algorithm based on deep regression network. Compared with the current mainstream tracking algorithms, this algorithm has advantages in overlap ratio [12]. Bf and Hc proposed the long-term tracking method and combined the context features in the correlation filter. Experiments show that the algorithm can achieve good tracking effect when the appearance of the target changes greatly [13]. Yuan et al. combine the multifeature fusion model with the scale change detection method, so that the algorithm can deal with the scale change of the target, so as to improve the tracking performance. The results show that the algorithm shows good tracking performance in experiments [14].

The current research results show that the traditional KCF algorithm has good target tracking efficiency. However, if the target is deformed or blocked, the tracking accuracy and real-time performance of KCF algorithm will be seriously affected. A large number of scholars have improved the KCF algorithm for this problem and achieved some research results. In this study, for several scene attributes that affect the algorithm, KCF algorithm combining multiple color features is used. The samples are compressed by adaptive sample set, so as to improve the target tracking effect of the algorithm in complex scenes.

3. Kernel Correlation Filter Tracking Algorithm Combining Multiple Color Features

3.1. Kernel Correlation Filter Tracking Algorithm with Multiple Color Features. Histogram of oriented gradient (HOG) feature is a feature descriptor used for object detection in computer vision and image processing. Hog feature is formed by calculating and counting the gradient direction histogram of the local area of the image. Based on the traditional correlation filter algorithm, KCF algorithm introduces the kernel method and the feature of histogram of oriented gradient (HOG), which improves the shortcomings of the traditional algorithm in gray value and single channel feature. Therefore, KCF algorithm has higher target tracking accuracy, especially in the case of light change and image deformation. However, if the target size and direction change, the target tracking effect of KCF will be weakened [15]. In high-intensity basketball games, the tracked target players are easy to be blocked by other personnel or equipment in the field. In order to improve the application effect of KCF algorithm in motion capture system, this study combines KCF tracking algorithm with a variety of color features to make up for the deficiency of hog feature in adapting to target changes. The operation structure of the target tracking algorithm is shown in Figure 1.

In the process of selecting color features, a discriminant color descriptor (DD) is used to obtain stronger model tracking performance. After fusing hog and DD features, a discriminant color feature hog correlation filter (dhcf) is proposed [16]. DD can freely select the required dimensions. First, divide the initial color space into x color words,
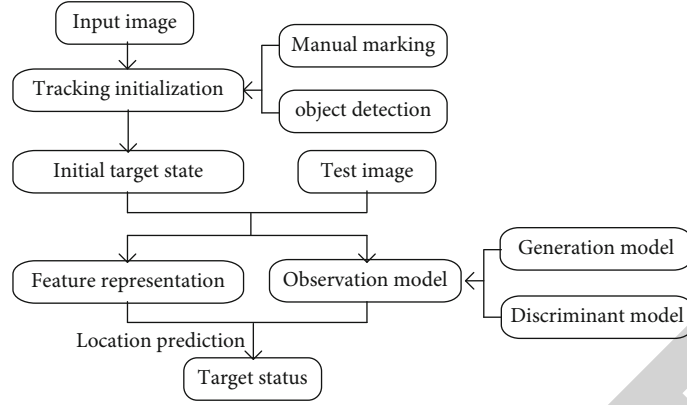
Figure 1: Structure of target tracking algorithm.

expressed as $W = \{w_1, w_2, \cdots, w_x\}$. Then, set a group of dataset classes as $C = \{c_1, c_2, \cdots, c_i\}$, and the mutual information calculation of the discriminant power of color words on dataset classes is shown in

$$I(C, W) = \sum_i \sum_t p(c_i, w_t) \log \frac{p(c_i, w_t)}{p(c_i)p(w_t)}. \qquad (1)$$

In formula (1), the joint distribution function $p(c_i, w_t)$ and the prior distribution functions $p(c_i)$ and $p(w_t)$ can be obtained by measuring the actual dataset. Set a cluster with y clusters as $W^c = \{W_1, W_2, \cdots, W_k\}$, one cluster represents a group of color words, and the total decline of all words in the cluster is shown in

$$\Delta I = \sum_j \sum_{w_t \in W_j} \pi_t KL\left(p(C|w_t), p\left(C|W_j\right)\right). \qquad (2)$$

The objective function of formula (2) is optimized to ensure that all clusters are connected with the lab space. The optimized algorithm operates alternately in the following two steps. The first step is to calculate the clustering mean, as shown in

$$p\left(C|W_j\right) = \sum_{w_t \in W} \frac{\pi_t}{\sum_{w_t \in W} \pi_t} p(C|w_t). \qquad (3)$$

The second step is to assign each color word to the nearest cluster, as shown in

$$E(m) = \sum_t \left(\psi_t^I(m_t) + \psi_t^C(m_t)\right) + \sum_{(s,t) \in \varepsilon} \psi(m_s, m_t). \qquad (4)$$

In formula (4), m_t represents the number of clusters assigned to the color word w_t. The penalty term of color block not belonging to the main component is expressed as $\psi_t^C(m_t) = \alpha_C(1 - f^t(m_t))$. Then, in order to enhance the smoothness of color representation, $\psi(m_s, m_t) =$

$\begin{cases} 0 \text{ if } & m_s = m_t \\ \alpha_D & \text{otherwise} \end{cases}$ operation is carried out. The algorithm performs cyclic operation and stops execution after ΔI is stable at a certain threshold. ΔI color descriptors can be divided into three common forms: dd-11, dd-25, and dd-50 according to different expected dimensions. At present, the most widely used feature is color names (CN). Then, color labeling is carried out according to different algorithm eigenvalues. Under different color discrimination, the accuracy of the calculation results in this paper can be greatly improved. According to the research of Li et al., the tracking performance of dd-11 feature is lower than that of CN, while the tracking performance of dd-25 and dd-50 is higher than that of CN feature. At the same time, dd-50 and dd-25 have similar tracking success rate, but dd-50 has more advantages in tracking accuracy [17]. Therefore, this study uses dd-50 as the color descriptor of the algorithm. In kernel correlation calculation, the Gaussian kernel of KCF algorithm is expressed

$$k\left(x, x'\right) = \exp\left(-\frac{1}{\sigma^2} \|x - x'\|^2\right). \qquad (5)$$

In formula (5), σ represents the functional bandwidth of Gaussian kernel. In the cyclic shift, the generating vector of the kernel correlation matrix is shown in

$$k^{xx'} = \exp\left(-\frac{1}{\sigma^2}\left(\|x\|^2 + \|x'\|^2 - 2F^{-1}\left(\hat{x}^* \odot \hat{x}'\right)\right)\right). \qquad (6)$$

In order to improve the accuracy and efficiency of the recommendation system at the same time, a new triangular distance recommendation algorithm based on multichannel feature vector is proposed. In equation (6), F represents the discrete Fourier transform function and $x = x_1, x_2, \cdots, x_c$

represents the multichannel feature vector of an image. In the Gaussian kernel function, the expression of multichannel is

$$k^{xx'} = \exp\left(-\frac{1}{\sigma^2}\left(\|x\|^2 + \|x'\|^2 - 2F^{-1}\left(\sum_c \hat{x}^* \odot \hat{x}'_c\right)\right)\right). \tag{7}$$

The target tracking performance of KCF algorithm is greatly affected by color features [18]. In order to improve the tracking performance of color features and optimize the performance of the algorithm, this study combines DD and hog through feature cascade and proposes dhcf algorithm based on KCF algorithm. Hog features have adaptive advantages in image deformation and light changes, and DD features have advantages in image size and direction changes. After the fusion of the two features, dd-hog, a feature vector with strong tracking ability, is formed. The expression of dd-hog eigenvector is shown in

$$x = [d_1, \cdots, d_m, h_1, \cdots, h_n]. \tag{8}$$

In equation (8), $d = d_1, d_2, \cdots, d_m$ represents the DD color vector extracted in the image, and $h = h_1, h_2, \cdots, h_n$ represents the hog feature vector. The extraction of hog feature is consistent with that of KCF. The extraction of DD feature is by mapping the value of RGB to its color clustering probability, and the table does not contain the value of RGB. The calculation of the descriptor is shown in

$$\text{index} = \text{floor}(R/8) + 32 * \text{floor}(G) + 32 * 32 * \text{floor}(B/8). \tag{9}$$

In formula (9), R, G, and B refer to the vector representation of each dimension on the image, and index refers to the mapping index of RGB on dd50. The flow of dh-kcf algorithm is shown in Figure 2.

3.2. Application of Multifeature Correlation Filter Algorithm in Basketball Motion Capture/Algorithm Optimization. In order to reduce the influence of invalid information and redundant information on the target tracking efficiency of the algorithm, an adaptive sample set is adopted based on dhcf algorithm. The training sample set is expressed as $\{(x_j, y_j)\}_{j=1}^n$, and n represents the number of sample sets. The search for the target appearance model parameter θ is shown in

$$J(\theta) = \sum_{k=1}^n L(\theta; x_i, y_i) + \lambda R(\theta). \tag{10}$$

In formula (10), X represents the sample space and $x_j \in X$ represents one of the eigenvectors of the sample space. Y represents the label set and $y_j \in Y$ represents the corresponding label. x_i, y_i represents a training sample, $L(\theta; x_i, y_i)$ represents the loss function of the training sample, and
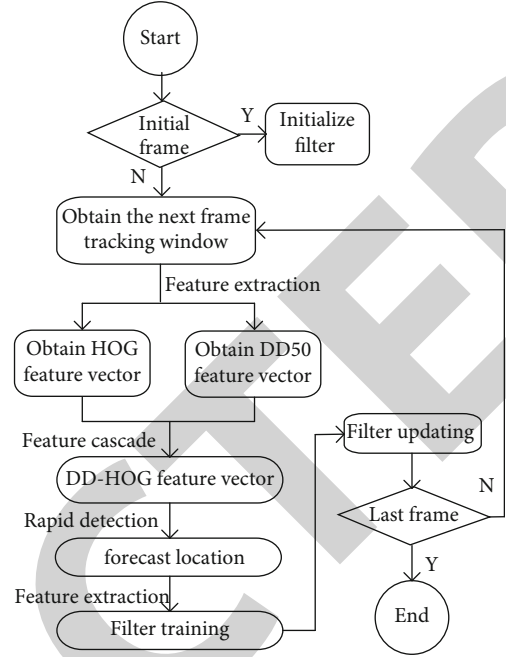

Figure 2: Target tracking flow chart of DHCF algorithm.

the loss function corresponding to the training sample is expressed as $L : \Omega * X * Y \longrightarrow R$. λ is a constant coefficient, and $R : \Omega \longrightarrow R$ represents a regular function. When training the filter, if only the first frame is used as the model feature, the filter will not be able to adapt in time when the target changes [19]. Therefore, after the training set is updated, the filter needs to learn the target model features in the first frame of the new training set. The general expression of training sample weight is shown in

$$J(\theta) = \sum_{k=1}^t \alpha_k \sum_{j=1}^{n_k} L(\theta; x_{ik}, y_{ik}) + \lambda R(\theta). \tag{11}$$

In equation (11), k represents the number of frames and j represents the number of training samples. The j training sample in the k frame is expressed as (x_{jk}, y_{jk}). n_k represents the number of samples contained in the training set. The number of frames k is in the interval of $[1, \cdots, t]$, and t represents the sequence number of the current frame. α_k is a constant term. The higher the value of α_k, the stronger the influence of sample $\{(x_{jk}, y_{jk})\}_{j=1}^{n_k}$ will be. The update of the model is realized by controlling the weight. The update strategy of KCF algorithm is as shown in

$$\begin{cases} x_t = (1 - \gamma)x_{t-1} + \gamma x, \\ \hat{\alpha} = (1 - \gamma)\hat{\alpha}_{t-1} + \gamma \hat{\alpha}. \end{cases} \tag{12}$$

In formula (12), γ is the model update rate, t represents the sequence number of the frame, x is the target feature, and $\hat{\alpha}$ represents the filter. In the KCF algorithm, the updates of the model and filter are synchronous, and the
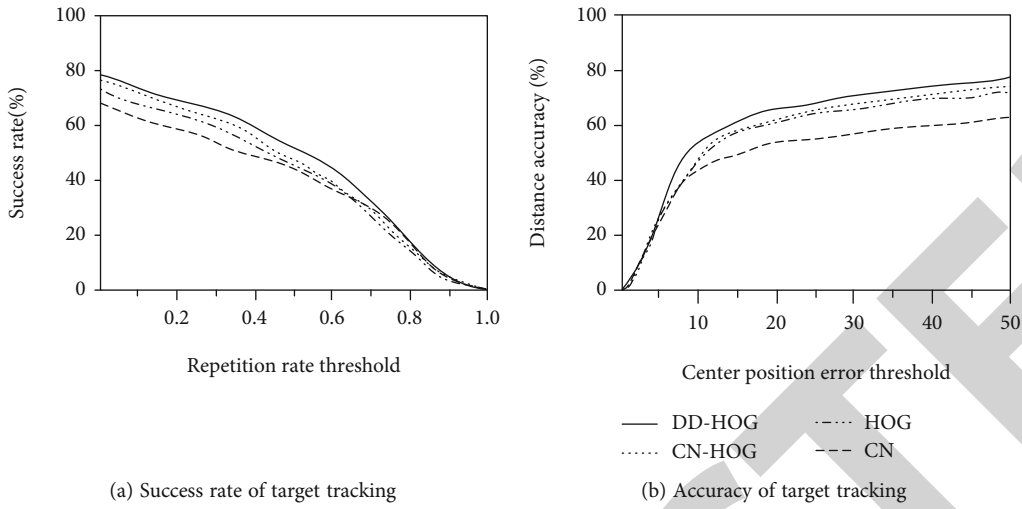
(a) Success rate of target tracking

(b) Accuracy of target tracking

FIGURE 3: Comparison of tracking success rate and tracking accuracy of four features.

(a) Background clutter

(b) Fast movement

(c) In-plane rotation

(d) Out of plane rotation
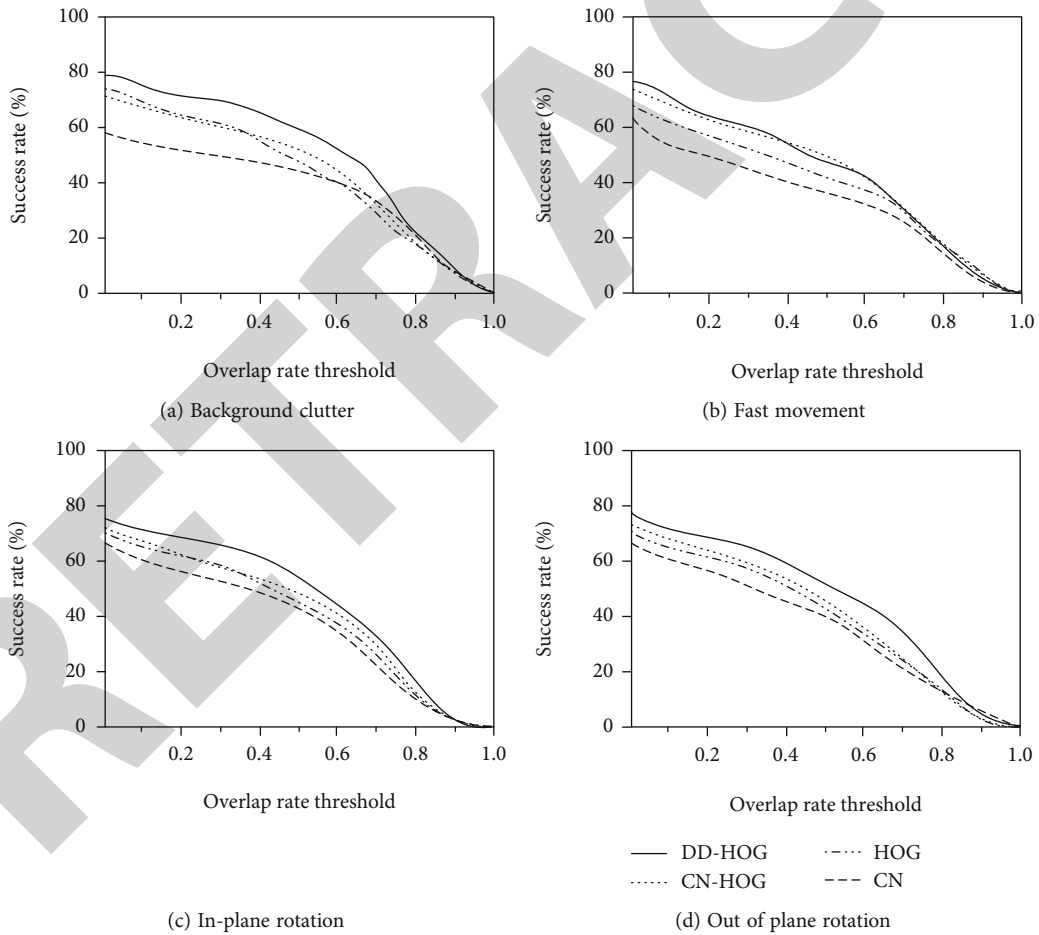
FIGURE 4: Comparison of tracking success rates of four features in BC, FM, IPR, and OPR scene attributes.

(a) Deformation

(b) Occlusion

(c) Scale variation
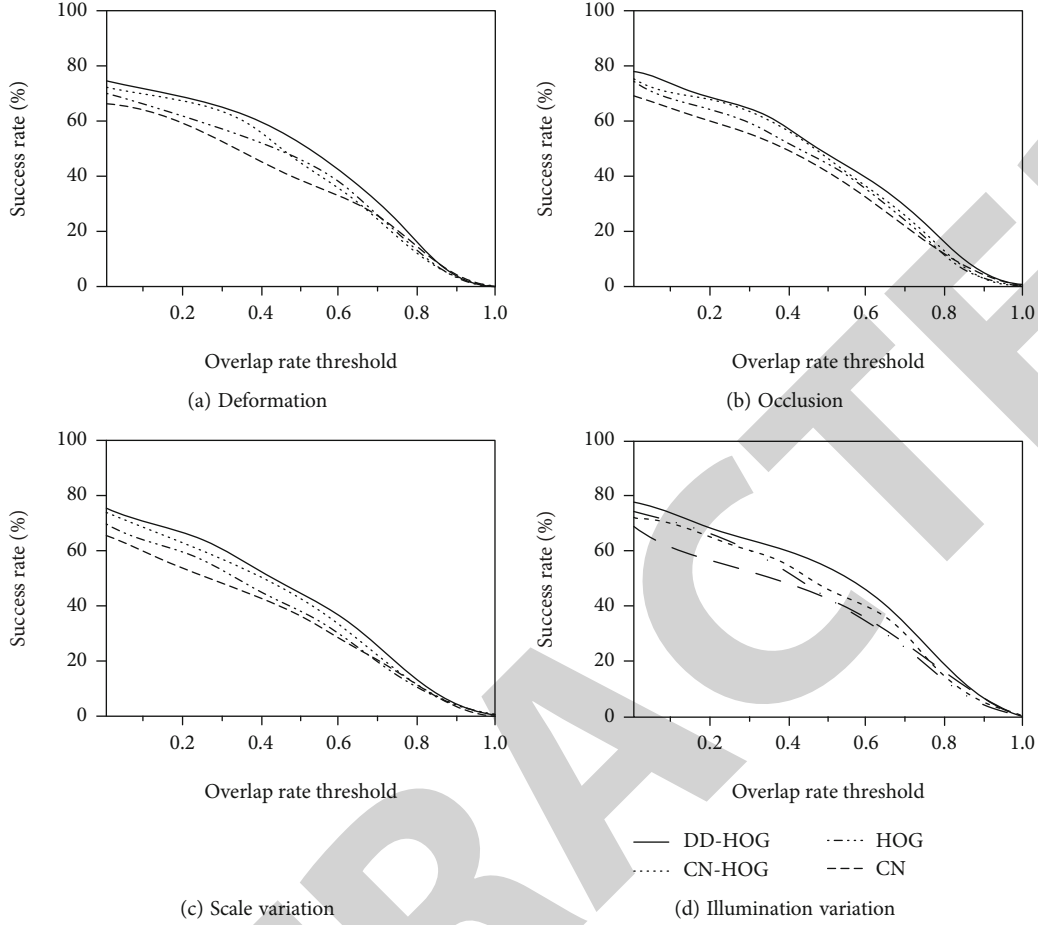
(d) Illumination variation

FIGURE 5: Comparison of tracking success rate of four features in DEF, OCC, SV, and IV attributes.

weight of the previous frame will gradually decay, while the weight of the latest frame will gradually increase. In order to improve the weight of recent samples while maintaining the update rate, the research adopts the way of compressing samples. Set the training sample set to $s = s_1, s_2, \cdots s_N$ and $s_i \in k, k \in (1, \cdots, t)$. Set the sample weight to $W = w_1, w_3, \cdots w_N$, and the loss function is

$$J(\theta) = \sum_{k=1}^{N} w_k \sum_{j=1}^{n_k} L(\theta; x_{ik}, y_{ik}) + \lambda R(\theta). \quad (13)$$

In formula (13), N represents the size of the sample set, and $N < t$. $\sum_{k=1}^{N} w_k \sum_{j=1}^{n_k} L(\theta; x_{ik}, y_{ik})$ represents the weight value of the k sample. $\sum_{k=1}^{N} w_k = 1$ and $w_k \geq 0$. The sample set is constructed by replacing the sample with the minimum weight. Since the sum of weights is fixed, when the sample set is reduced, the weight of the recent sample is increased accordingly. The KCF algorithm learns from the training sample image, and the two-dimensional Gaussian distribu-

tion centered on the target of the training sample is the output of the training, as shown in

$$g_i = \sum e^{-(x-x_j)^2 + (y-y_j)^2 / \sigma^2}. \quad (14)$$

In formula (14), f_i represents the sample image, g_i represents the training output, and σ represents the spatial bandwidth of the Gaussian function. In order to make the algorithm track the target accurately when the target is deformed or occluded, the peak to sidelobe ratio (PSR) is used as the index of confidence in this study. However, under the definition of traditional PSR, the filter is difficult to adapt to the drastic changes of the model [20]. Therefore, this study introduces adaptive sample weight based on PSR and redefines the sample weight after each update, so that the filter can reduce the learning of invalid information in the process of rapid model change. κ represents the threshold of PSR and γ represents the update rate. When $PSR > \kappa_1$, the tracking is in a normal state, which is the standard update rate γ_1. When $\kappa < PSR < \kappa$, the model changes rapidly, and the update rate is γ_2. When $PSR < \kappa_2$, the model changes rapidly and is in a distorted state, and the update rate is γ_2. After improving the KCF algorithm through

(a) Success rate of target tracking in OTB50

(b) Accuracy of target tracking in OTB50

(c) Success rate of target tracking in OTB100

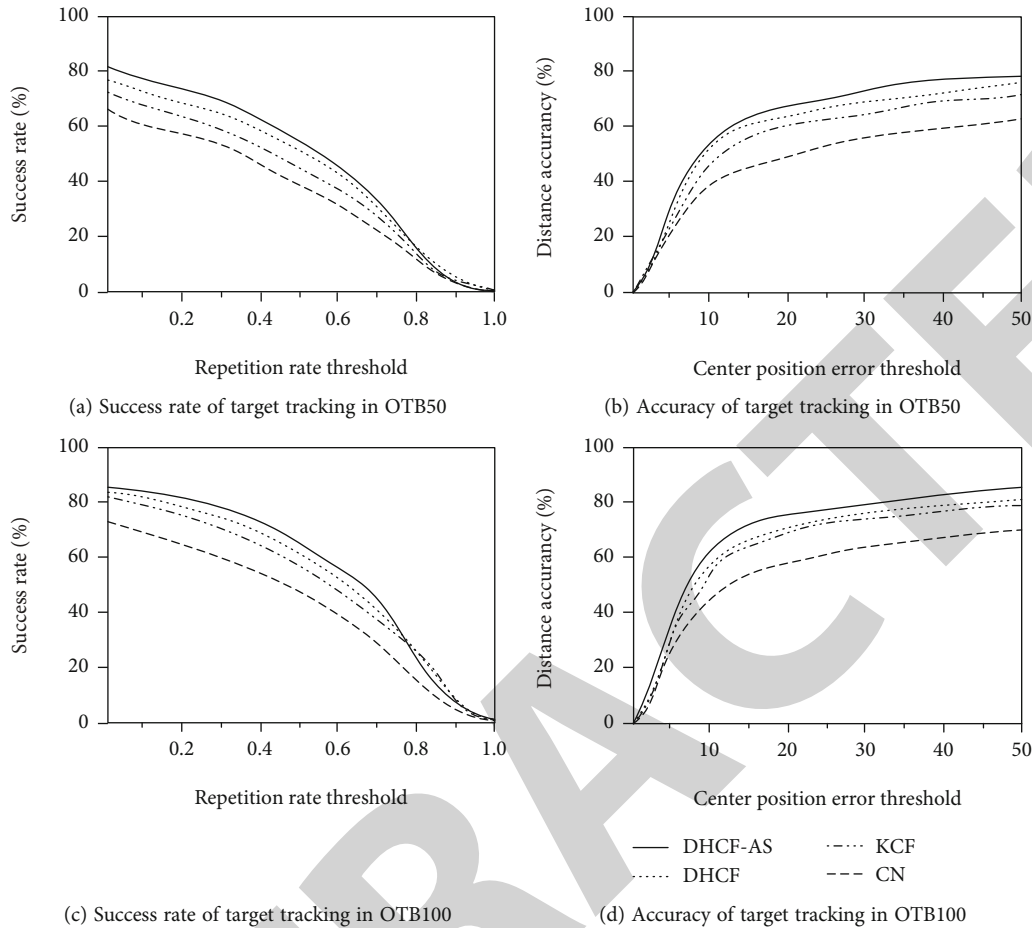(d) Accuracy of target tracking in OTB100

FIGURE 6: Comparison of tracking success rate and tracking accuracy of four algorithms in OTB50 and OTB100.

adaptive sample set, DHCF-adaptive sample and DHCF-AS algorithm are obtained. The original update strategy is as shown in

$$
\begin{cases}
\widehat{a}_t = \sum_{K=1}^{N-1} W(k)A(k) + \gamma \widehat{a}, \\
x_t = \sum_{K=1}^{N-1} W(k)X(k) + \gamma x.
\end{cases}
\tag{15}
$$

In formula (15), W represents the sample weight set, γ represents the adaptive sample weight value obtained according to PSR, A represents the historical filter set, and X represents the historical target feature set. Dhcf-as algorithm uses the initial image position to train the filter in the first frame, and then, each frame uses the target position of the previous frame for detection and updates the target position through the maximum response value.

4. Test Results of Kernel Correlation Filtering Algorithm Based on Multiple Color Features

4.1. Performance Test of Improved dhcf Algorithm Based on KCF Algorithm. In the algorithm performance test experi-

ment, the KCF algorithm uses dd-hog feature and three general features such as hog, cn-hog, and CN for target tracking test, so as to compare the target tracking performance of the four features (the KCF algorithm using dd-hog feature is the dhcf algorithm proposed in this study). In this experiment, otb50 and otb100 are used as test datasets. Otb50 represents 50 groups of video frame sequences, and otb100 represents 100 groups of video frame sequences. The comparison of the four features in target tracking accuracy and target tracking success rate is shown in Figure 3.

As can be seen from Figure 3(a), in the comparison of tracking success rate, the tracking success rate of dd-hog feature can reach 78.2%, followed by cn-hog feature, which is 76.3%. Hog feature and CN feature have lower tracking success rates, which are 73.4% and 68.2%, respectively. As can be seen from Figure 3(b), the tracking accuracy of dd-hog is still the highest among the four features, which is 75.1%. The tracking accuracy of cn-hog and hog features is similar, 70.2% and 69.7%, respectively. The tracking accuracy of CN feature is the weakest, only 60.2%. Therefore, compared with the traditional KCF algorithm using only hog feature, the dhcf algorithm using dd-hog feature improves the target tracking success rate by 4.8% and the tracking accuracy by 5.4%. Dhcf algorithm which combines hog feature and color feature has better performance than traditional algorithm. In
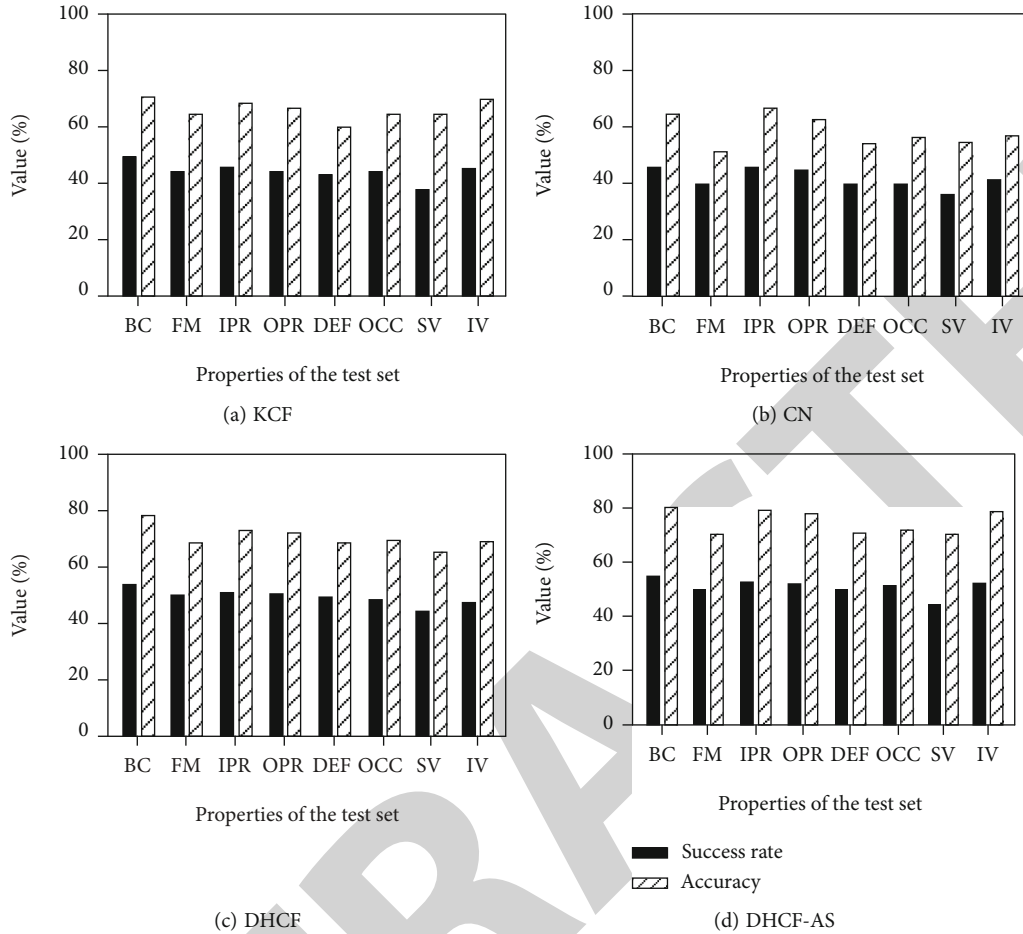
(a) KCF

(b) CN

(c) DHCF

(d) DHCF-AS

Figure 7: Target tracking comparison of each scene attribute of four algorithms in OTB100.

order to test the target tracking performance of dhcf algorithm in complex scenes, this study will test the tracking success rate of dhcf algorithm in several scene attributes. Several conventional scenes are background clutter (BC), fast motion (FM), in-plane rotation (IPR), and out of plane rotation (OPR). The experimental results are shown in Figure 4.

Figure 4 shows that the dd-hog feature has obvious advantages in the scene attributes of background clutter, in-plane rotation, and out of plane rotation. Its tracking success rates are 78.6%, 77.2%, and 72.8%, respectively, which is 2.3% higher than that of the slightly lower level feature. Dd-hog has no obvious advantage only in fast-moving scene attributes, and the tracking success rate is 1.2% higher than that of cn-hog. The KCF algorithm with four different features will be compared in four scene attributes: target deformation (DEF), target occlusion (OCC), scale variation (SV), and illumination variation (IV). The results are shown in Figure 5.

Figure 5 shows that dd-hog algorithm still has the best tracking success rate compared with the other three features in the scene attributes of DEF, OCC, SV, and IV, which are 76.3%, 77.6%, 73.5%, and 79.1%, respectively. Therefore, dhcf algorithm using dd-hog as color feature can use different scene attributes and show excellent target tracking effect. Dhcf algorithm solves the tracking ambiguity problem

caused by scene changes in traditional algorithms to a certain extent, so as to improve the efficiency and robustness of the algorithm.

4.2. Effect Test of Improved dhcf-as Algorithm in Target Tracking. This study uses MATLAB software to run dhcf and dhcf-as algorithms. In order to verify the application effect of dhcf-as algorithm in target tracking, CN, KCF, dhcf, and dhcf-as algorithms are compared in otb50 and otb100 test sets. Among the algorithm parameters, the Gaussian kernel bandwidth is 0.5, the regularization term is 10-4, and the update rate is determined according to the PSR value. The size of hog cell is 9 bins, and the size of hog block is 4 cells. The comparison results are shown in Figure 6.

As can be seen from Figure 6, in the otb50 test set, the tracking success rate of dhcf-as algorithm can reach 80.9%, and the tracking success rate in otb100 can reach 84.2%. The tracking accuracy of dhcf-as algorithm in otb50 and otb100 is 79.2% and 82.5%, respectively. In the two test sets, the performance of dhcf-as and dhcf algorithms is higher than that of KCF and CN, and dhcf-as has more advantages than dhcf. In otb50, the tracking success rate of dhcf-as algorithm is 4.2% higher than that of dhcf algorithm, and the tracking accuracy is 1.7% higher than that of dhcf algorithm. In order to test the performance of dhcf-as algorithm in

different scene attributes, the tracking results of four algorithms in different scene attributes are compared. The comparison results of tracking success rate and accuracy values of the four algorithms are shown in Figure 7.

As can be seen from Figure 7, dhcf-as has the highest tracking success rate of 56.5% in BC scene attributes and the lowest success rate of 44.7% in SV scene attributes. In the SV scenario, dhcf algorithm has the highest success rate, with a value of 47.3%, which is 2.6% higher than dhcf-as algorithm. The tracking success rate of dhcf-as algorithm in SV scene is lower than that of dhcf algorithm, but it is still higher than that of KCF and CN algorithms. In addition, dhcf-as algorithm has the best tracking success rate and tracking accuracy among several scene attributes. Therefore, compared with the traditional algorithm and the improved algorithm, the improved dhcf-as algorithm has more advantages in tracking performance. However, dhcf-as algorithm needs further improvement. The algorithm can be applied in other scenes. Compared with CN hog, hog, and CN, dhcf algorithm can show the highest tracking performance in various scenarios. Among various scene attributes, dhcf as algorithm has the best tracking performance. Only in the scene of scale change, its tracking performance is lower than that of dhcf algorithm. Therefore, in the future experiments, we should enhance its adaptability under the scale change scenario. It is necessary to improve its adaptability to scale changes and its tracking performance.

5. Conclusion

In order to improve the performance of basketball motion capture system, based on kernel correlation filtering algorithm, this paper proposes a dhcf as algorithm based on multicolor features, which mainly studies the adaptability of traditional KCF algorithm in scene attributes such as rapid target change and illumination change. The experimental results show that the tracking success rate of dhcf algorithm combined with multiple color features can reach 78.2% and the tracking accuracy can reach 75.1%. Compared with CN hog, hog, and CN [21], DD hog can show the highest tracking performance in various scenarios. The tracking success rate and accuracy of the improved dhcf as algorithm in otb50 test set are 80.9% and 79.2%, respectively, and in otb100 test set are 84.2% and 82.5%, respectively. Among various scene attributes, dhcf as algorithm has the best tracking performance. Only in the scene with scale change, its tracking performance is lower than dhcf algorithm. Therefore, in future experiments, dhcf as algorithm will be further improved to enhance its adaptability in scale change scenarios.

In this paper, the adaptive sample set is applied to the original kernel correlation filter. When the target moves too fast or is blocked, it is easy to form a large amount of invalid and redundant information, which affects the target tracking efficiency of the algorithm. The adaptive sample set can filter these interference information, so as to improve the target tracking accuracy and real-time performance of the motion capture system. The research has some limitations; for example, the paper does not simulate the filtering

algorithm and so on. Therefore, further modifications are needed in future research.

Data Availability

The experimental data used to support the findings of this study are available from the corresponding author upon request.

Conflicts of Interest

The author declared that they have no conflicts of interest regarding this work.

References

[1] J. P. Sun, E. J. Ding, B. Sun, Z. Y. Liu, and K. L. Zhang, "Adaptive kernel correlation filter tracking algorithm in complex scenes," *IEEE Access*, vol. 8, pp. 208179–208194, 2020.

[2] J. Shin, H. Kim, D. Kim, and J. Paik, "Fast and robust object tracking using tracking failure detection in kernelized correlation filter," *Applied Sciences*, vol. 10, no. 2, pp. 713–725, 2020.

[3] L. Gong, Z. Mo, S. Zhao, and Y. Song, "An improved kernelized correlation filter tracking algorithm based on multichannel memory model[J]," *Signal Processing: Image Communication*, vol. 78, pp. 200–205, 2019.

[4] H. Y. Zhang, H. S. Wang, and P. Y. He, "Correlation filter tracking based on superpixel and multifeature fusion," *Optoelectronics Letters*, vol. 17, no. 1, pp. 47–52, 2021.

[5] J. Zhu, D. Wang, and L. U. Huchuan, "Learning temporal-spatial consistency correlation filter for visual tracking," *Scientia Sinica Informationis*, vol. 50, no. 1, pp. 128–150, 2020.

[6] H. Masood, S. Rehman, A. Khan, F. Riaz, A. Hassan, and M. Abbas, "Approximate proximal gradient-based correlation filter for target tracking in videos: a unified approach," *Arabian Journal for Science and Engineering*, vol. 44, no. 11, pp. 9363–9380, 2019.

[7] X. Sun, K. Zhang, Y. Ji, S. Wang, S. Yan, and W. Sunyong, "Correlation filter tracking algorithm based on multiple features and average peak correlation energy," *Multimedia Tools and Applications*, vol. 79, no. 21-22, pp. 14671–14688, 2020.

[8] Y. Xie, J. Xiao, K. Huang, J. Thiyagalingam, and Y. Zhao, "Correlation filter selection for visual tracking using reinforcement learning," *IEEE Transactions on Circuits and Systems for Video Technology*, vol. 30, no. 1, pp. 192–204, 2020.

[9] Y. Wang, L. Xinbin Luo, J. W. Ding, and F. Shan, "Robust visual tracking via a hybrid correlation filter," *Multimedia Tools and Applications*, vol. 78, no. 22, pp. 31633–31648, 2019.

[10] X. Yang, S. Zhu, S. Xia, and D. Zhou, "A new TLD target tracking method based on improved correlation filter and adaptive scale," *The Visual Computer*, vol. 36, no. 9, pp. 1783–1795, 2020.

[11] W. Wang, K. Zhang, and M. Lv, "Robust visual tracking based on adaptive extraction and enhancement of correlation filter," *IEEE Access*, vol. 7, pp. 3534–3546, 2019.

[12] C. Fang, J. Huang, K. Cuan, X. Zhuang, and T. Zhang, "Comparative study on poultry target tracking algorithms based on a deep regression network," *Biosystems Engineering*, vol. 190, pp. 176–183, 2020.

Retraction

Retracted: Intelligent Financial Data Analysis and Decision Management Based on Edge Computing

Journal of Sensors

This article has been retracted by Hindawi following an investigation undertaken by the publisher [1]. This investigation has uncovered evidence of one or more of the following indicators of systematic manipulation of the publication process:

(1) Discrepancies in scope

(2) Discrepancies in the description of the research reported

(3) Discrepancies between the availability of data and the research described

(4) Inappropriate citations

(5) Incoherent, meaningless and/or irrelevant content included in the article

(6) Manipulated or compromised peer review

The presence of these indicators undermines our confidence in the integrity of the article's content and we cannot, therefore, vouch for its reliability. Please note that this notice is intended solely to alert readers that the content of this article is unreliable. We have not investigated whether authors were aware of or involved in the systematic manipulation of the publication process.

Wiley and Hindawi regrets that the usual quality checks did not identify these issues before publication and have since put additional measures in place to safeguard research integrity.

We wish to credit our own Research Integrity and Research Publishing teams and anonymous and named external researchers and research integrity experts for contributing to this investigation.

The corresponding author, as the representative of all authors, has been given the opportunity to register their agreement or disagreement to this retraction. We have kept a record of any response received.

References

[1] G. Cheng, "Intelligent Financial Data Analysis and Decision Management Based on Edge Computing," *Journal of Sensors*, vol. 2022, Article ID 1133275, 12 pages, 2022.

Research Article

Intelligent Financial Data Analysis and Decision Management Based on Edge Computing

Guansong Cheng [ID]

International College, Krirk University, Bangkok 10220, Thailand

Correspondence should be addressed to Guansong Cheng; 6313-3021@student.krirk.ac.th

In this era of data explosion, in order to make better use of data, people need to collect information to analyze and judge future decisions. For enterprises, the management of time, capital, and decision-making can directly affect the acquisition of enterprise profits. The sooner we analyze financial data, the earlier we use an intelligent system to assist management and promote operators to make reasonable business decisions. Traditional enterprise data management is very backward and has few functions. In order to achieve the purpose of optimal allocation of enterprise resources, information-based financial management. According to the financial status and functional requirements of enterprises, the specific functions of the system are designed. The method based on edge computing has a high reference value. This paper puts forward a financial management system of intelligent analysis. It can provide rich solutions to financial problems. Data mining and analysis of financial situation provide support for decision-making management of enterprises. The research results show that (1) after 10 times of inspection and adjustment, the system grade is all D grade, and there is no defect. (2) There is no abnormality in system response time; the average response time of F1, F2, F3, and F4 functions is in line with expectations. The fluctuation of time range is no more than 3 s; the overall average response time is 1 s. (3) After CPU detection, the CPU of the system is less than 70% of the expected utilization rate. The system is qualified. (4) The whale algorithm is used to combine new and old tasks. After comparison, it has an excellent performance in computing resources and delays energy consumption. Some follow-up improvement work needs to be optimized.

1. Introduction

With the continuous innovation of information technology and the advent of the era of big data, the world has quietly undergone unimaginable changes. With the change of computer technology, it must be the innovation and development of all walks of life. For many enterprises in China, the continuous improvement of the economic system puts forward more and stricter requirements for enterprises. This promotes the optimization of enterprise business practice in disguise. According to the existing scientific and technological support, establish a scientific financial system to reduce management pressure. So far, there are many works and researches on intelligent finance in the market, which provide a reference for the design ideas of this system.

Adopt a business intelligence method to support data analysis of a company system [1]. Artificial intelligence, information system risk management, and enterprise entre-

preneurship contribute to the influence of decision management [2]. Based on the FCM clustering algorithm, a fuzzy decision model is established to intelligently evaluate and analyze the financial performance of enterprises [3]. Building models based on artificial intelligence and machine learning involves financial analysis and decision-making policies [4]. For the application of distress prediction and evaluation cases in financial decision-making, a multistandard decision-making assistant model is proposed, and random forest and bagging CART perform well [5]. Based on edge computing, a new data processing system is proposed for analysis [6]. Design a financial intelligent decision support system for company statistics and information research [7]. In order to achieve the purpose of scientific decision-making and management, the existing distributed data-sharing platform is used to build a financial decision-making analysis system in colleges and universities [8]. Internet plus builds an intelligent financial decision support

information system in the era of big data to promote the digital transformation of finance [9]. Discuss the architecture and application trend of the intelligent financial system for enterprises [10]. In view of the abnormal financial data of enterprises, the convolution neural network is used to classify, evaluate, and analyze the constructed time series financial data [11]. According to the deep learning model, edge computing and artificial intelligence are integrated to develop edge intelligence [12]. The multiagent to design financial risk early warning information assistant decision-making system to reduce the incidence of corporate financial risk was introduced [13]. This paper analyzes the application of the intelligent financial system in scientific research institutions and provides a reference for application cases [14]. Artificial intelligence is widely used to accurately predict financial problems of enterprises [15].

The above literature describes the research direction and the architecture design of the system. Use a variety of technical guidelines to explore, and explain the problem from many aspects and angles. On the basis of a distributed system, the B/S mode is selected, and various data sources are merged into a database to improve data utilization efficiency. Finally, the performance and indexes of the system are tested to verify the influence of edge computing on the minimum cost and delay energy consumption of the system.
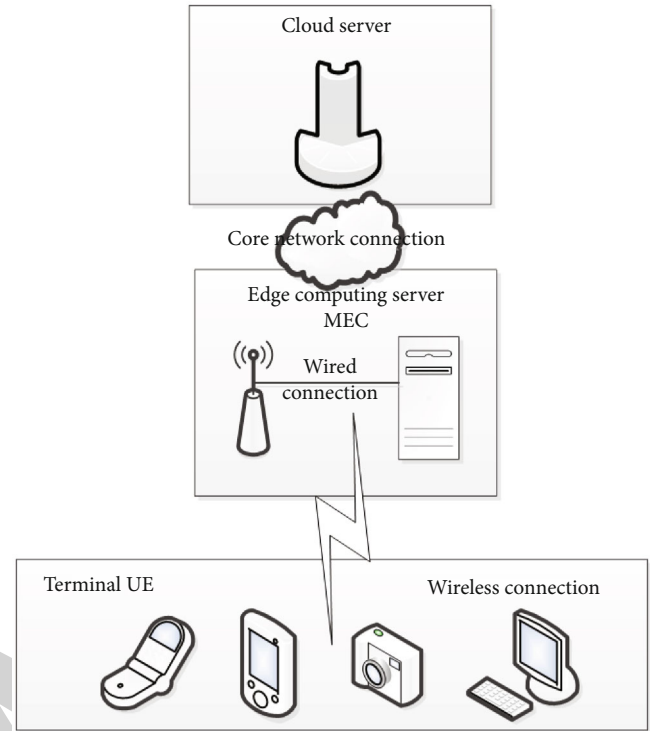
2. Theoretical Basis

2.1. Edge Computation. MEC [16]. Edge computing is an important part of 5G. Traditional network mobile services no longer meet the requirements. The proposal of edge computing can effectively solve the problem of cloud computing's own shortcomings and provide better services from the fundamental principle. NFV [17] and SDN [18]: they are the main technologies involved in MEC. It can provide computing services nearby and sink the resources of the server to the users. Because the nodes of edge computing are distributed on the access network side, the core network can better protect users' privacy and reduce the security risk of virus attack than cloud computing without bearing the pressure of data uploaded by users. In addition, edge computing adopts a distributed method to design cloud servers. Even if a single point has a small probability of downtime, the whole network service will not collapse. All kinds of computing services concentrated on the server can reduce the energy consumption of the terminal. ECC Alliance has designed the specific architecture of edge computing to promote cloud edge collaboration. The top level is the central cloud, which is the most important and powerful data processing platform. This architecture connects the cloud server and the edge computing server part well with the core network. At the bottom is the user of the terminal. It includes mobile phones, cameras, sensors, and other terminals. The middle part belongs to the core layer, which can not only receive the tasks uploaded by the terminal but also cooperate with data and control in the central cloud, as shown in Figure 1.

The cost in edge computing is analyzed. This kind of cost is not needed in the general traditional sense, and it is not

FIGURE 1: MEC architecture diagram.

the material and resource expenditure. The cost here belongs to abstract cost, which shows the user's experience in the form of cost. The better the user experience, the lower the cost of edge computing.

(1) Delay cost [19]

$$C = \alpha L, \tag{1}$$

where C represents the calculation amount of the task; α represents a variable coefficient, which is taken according to the actual situation; and L represents the size of the file.

(2) Energy consumption cost

Because the server of edge computing is not sensitive to energy consumption, when analyzing the cost of energy consumption, only the energy consumption on the terminal is analyzed. Due to the characteristics of the 5G network, the energy consumption of edge computing is far less than the processor energy in computing tasks, which can improve the experience of user terminals.

(3) Comprehensive cost

Mainly based on weight, the delay cost and energy consumption cost are transformed into superimposed problems. Consider the cost comprehensively.

2.2. Data Mining. In the past, the information accepted by people was relatively simple, but with the continuous
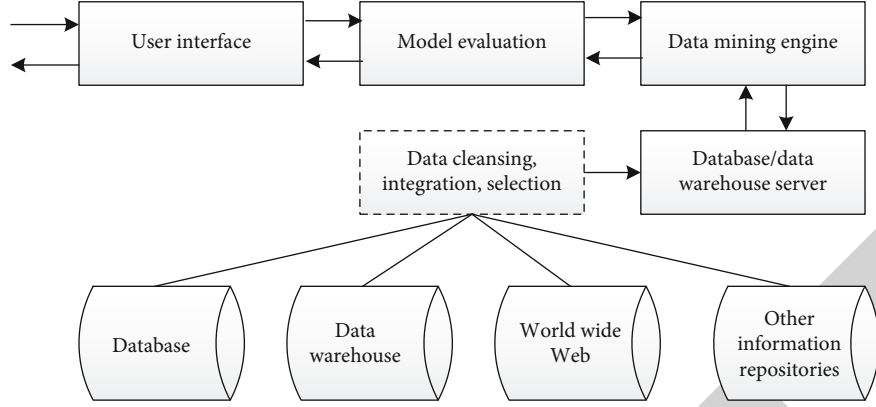
Figure 2: Data mining structure.

development and change of science and technology, it was widely used. In the era of big data, these massive redundant data come, which brings a lot of burden to people. With too much information, it is easy for people to ignore the really valuable information, resulting in the failure of information distance. If people want to select the data they need from these data and use algorithms to search for useful information, they need to do data mining. According to these data, we can predict the future trend and make decisions and judgments. This is the value of this technology, as shown in Figure 2.

2.3. OLAP Technology. OLAP [20]. It is a practical and efficient tool. Using this tool, we can help query and process historical data, provide an intuitive interface for inquirers, and help operators to obtain massive valuable things. As a result, the workload of users and those who do not use the tool is obviously compared. Users become more flexible and efficient and can make correct and accurate judgments quickly. Finally, the results can be given quickly. Many operations of the whole process are very transparent, as shown in Table 1.

2.4. System Model

(1) Communication submodel

$$r = B \log_2(1 + \text{SNR}). \tag{2}$$

Communication rate takes Shannon capacity; B is the bandwidth occupied by the wireless channel; SNR is the signal-to-noise ratio after passing through the channel.

Considering superimposed noise and electromagnetic wave channel loss:

$$\text{SNR} = \frac{hP}{\sigma^2}. \tag{3}$$

Wired connection between base station and edge computing server. The allocation scheme of communication bandwidth is determined by the search algorithm. Adjust and allocate communication resources in an iterative way.

Finally, the purpose of optimizing the system cost is achieved.

(2) System cost modeling

Consider the case where the server of edge computing has remaining resources. If you choose to uninstall to edge server computation:

Time overhead situation:

$$T_j^c = T_t + T_c. \tag{4}$$

Energy consumption of terminal:

$$E_j^c = T_t p_j. \tag{5}$$

In addition, there are

$$T_t = \frac{l_j}{r_j},$$
$$T_c = \frac{c_j}{f_j}. \tag{6}$$

When the transmission rate reaches the ideal state, there is

$$r_j = B_j \log_2\left(1 + \frac{p_j h_j}{\sigma_j^2}\right). \tag{7}$$

Select local calculation, and the corresponding ones are as follows:

$$T_j^l = \frac{c_j}{f_j^l},$$
$$E_j^l = \kappa\left(f_j^l\right)^2 c_j. \tag{8}$$

Consider the comprehensive cost of the system:

$$P_j = a_j\left(a_j T_j^c + \beta_j E_j^c\right) + \left(1 - a_j\right)\left(a_j T_j^l + \beta_j E_j^l\right). \tag{9}$$

Table 1: Main features of OLAP.

Characteristic	Description
Online [21]	The needs of customers are a problem that needs careful consideration. In order to reflect the true information of users, it is necessary to transform data. Customers can observe and infer their own needs by analyzing the future results. For customer requests, the system needs to respond quickly to the requests in terms of response time. If you do not get the response of the system for a period of time, it may affect the correctness of the analysis results. The client is likely to lose certain data information.
Analytical	Analyze the logic of relevant data and analyze the specific data situation. There are two points in total: internal data analysis of analysis tools; on the OLAP platform, the statistical results of customers are further analyzed.
Informational [22]	The system can save valuable information anytime and anywhere. These are all survived by the history it needs to obtain. The storage space of this information needs to combine the performance and efficiency of a data warehouse. Rethink and position them.
Multidimensional	It is different from a relational database. Relational databases belong to flat relationships [23]. OLAP data warehouse is from a variety of dimensions and a variety of angles to analyze and introduce the law of data. In a data warehouse, the latitude of data is the most basic and important, also known as the latitude table [24]. The fact table can be extracted separately.

Total cost [25]:

$$P = \sum_{j=1}^{J} P_j. \tag{10}$$

To sum up, the objectives and tasks of optimization are

$$\min P = \min \sum_{j=1}^{J} P_j$$
$$\text{s.t.} \sum_{j=1}^{J} a_j B_j \le B,$$
$$\sum_{j=1}^{J} f_j \le F,$$
$$a_j \in \{0, 1\}. \tag{11}$$

Redistribute the task set with the following optimization goals:

$$\min P = \min \left(\sum_{k=1}^{K} P_k + \sum_{i=1}^{I} P_i \right)$$
$$\text{s.t.} \sum_{j=1}^{J} a_k B_k \le B,$$
$$\sum_{k=1}^{J} f_k \le F + \sum_{i=1}^{I} b_i f_i^c,$$
$$\sum_{k=1}^{K} a_k c_k - \sum_{j=1}^{J} a_j c_j \le \sum_{i=1}^{I} b_i c_i^{\text{free}},$$
$$a_k \in \{0, 1\},$$
$$b_i \in \{0, 1\}. \tag{12}$$

2.5. Search Optimization Algorithm. In this paper, the system cost is modeled under the scenario of edge computing mode.

Taking the whale-based algorithm as an example, the whale algorithm is improved. In this way, the edge calculation of the system at the cost minimization is discussed.

Define the fitness function as

$$\text{fitness1}(X) = C + \text{penalty\_function1} + \text{penalty\_function2}. \tag{13}$$

The newly defined fitness function is

$$\text{fitness2}(X) = C + \text{penalty\_function1} + \text{penalty\_function2} + \text{penalty\_function3}. \tag{14}$$

WOA is optimized and improved to prevent the optimization result from being affected by the optimal whale falling into the local optimal solution. The specific algorithm flow is shown in Figure 3.

(1) Surrounding predation

$$C = 2 \, \text{rand},$$
$$D = \left| CX(t)_{\text{rand}} - X(t) \right|,$$
$$a = W_{\max} - \frac{(W_{\max} - W_{\min})t}{T_{\max}}, \tag{15}$$
$$A = 2a \, \text{rand} - a,$$
$$X(t + 1) = X(t)_{\text{better}} - AD,$$

where rand is a matrix of random numbers with values between 0 and 1, C is the swimming factor, D stands for the distance between the individual and the leading whale, t represents the current number of iterations, T represents the maximum number of iterations, a represents the convergence factor, and A is the convergence coefficient.
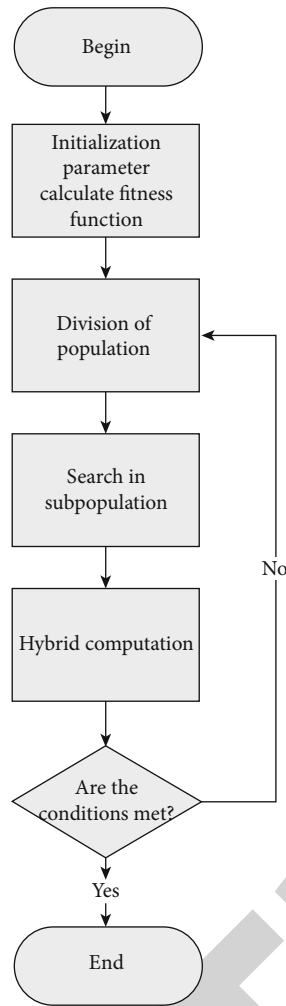
(2) Bubble netting

Figure 3: Flow chart of whale algorithm.

$$X(t+1) = De^{bl} \cos(2\pi l) + X(t)_{better}. \quad (16)$$

(3) Random search

$$D = \left| CX(t)_{rand} - X(t) \right|, \\ X(t+1) = X(t)_{rand} - AD. \quad (17)$$

3. Design of Intelligent Financial Analysis and Decision System

3.1. Present Situation and Demand Analysis

(a) Present situation analysis

Up to now, the financial management system of small and medium-sized enterprises is simple, the functional structure is not complex, and the business application that can be realized is very few. At present, enterprises have the following problems: with the continuous production and operation of this process, more and more information and data, loose enterprise management, will accumulate a large number of useful or useless business data. The task of financial analysis is huge, and the manpower and material resources are not fully utilized, resulting in certain unnecessary losses. Group enterprises cannot monitor and view key financial indicators in time and cannot effectively compare with historical data. In addition, the financial system itself lacks a secure login path, which is at risk of being leaked and maliciously attacked. And the connection between subsystems is not close, and multiple sets of superimposed systems cause trouble in use. As a result, enterprises urgently need to adapt to the development of the times and actively coordinate the work of finance and various departments.

(b) Requirement analysis

(1) Strong creativity: it should conform to the characteristics of the enterprise itself, and its style should be distinct and unique

(2) Strong maintainability: the background maintenance program interface of the system

(3) Efficiency: the design of the system page is simple and beautiful. Browse as quickly as possible and highlight the main information

(4) Reasonable structure: the system setting should be reasonable and conform to people's browsing habits

(5) Safety and stability: while fully considering the site access performance, we should pay special attention to the safety and stability of the site

(6) Strong concurrency: the system is required to support multi-input operation, establish cache mechanism, and provide users with access speed

(7) Portability and continuity: it is convenient for future upgrading and transplantation. strive to reduce the secondary development cost of enterprises

(8) Platform-independent: changing the operating platform or database only needs to be changed through simple settings

(9) Interactivity: the system requires interaction, and the feedback mechanism of the front and back office systems is established. Realize automatic response mechanism and high interaction

3.2. Database Design.
According to the actual situation of the enterprise itself and the basic principles of design, the exclusive database mode belonging to the enterprise is designed.

(1) Data granularity

Because of the complex operation of enterprises every day, a large amount of data and information will be generated. This system adopts the strategy of dual data
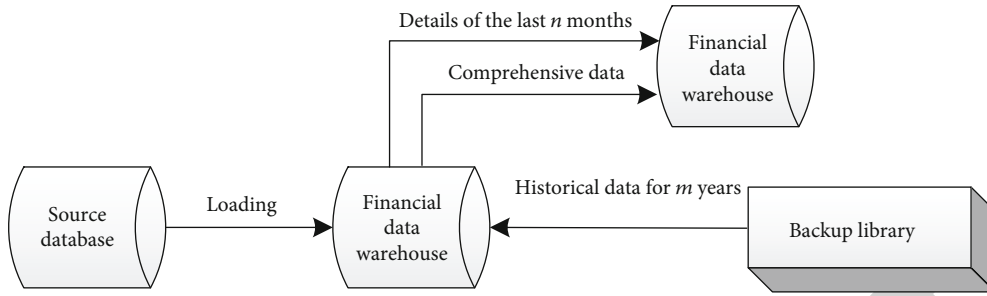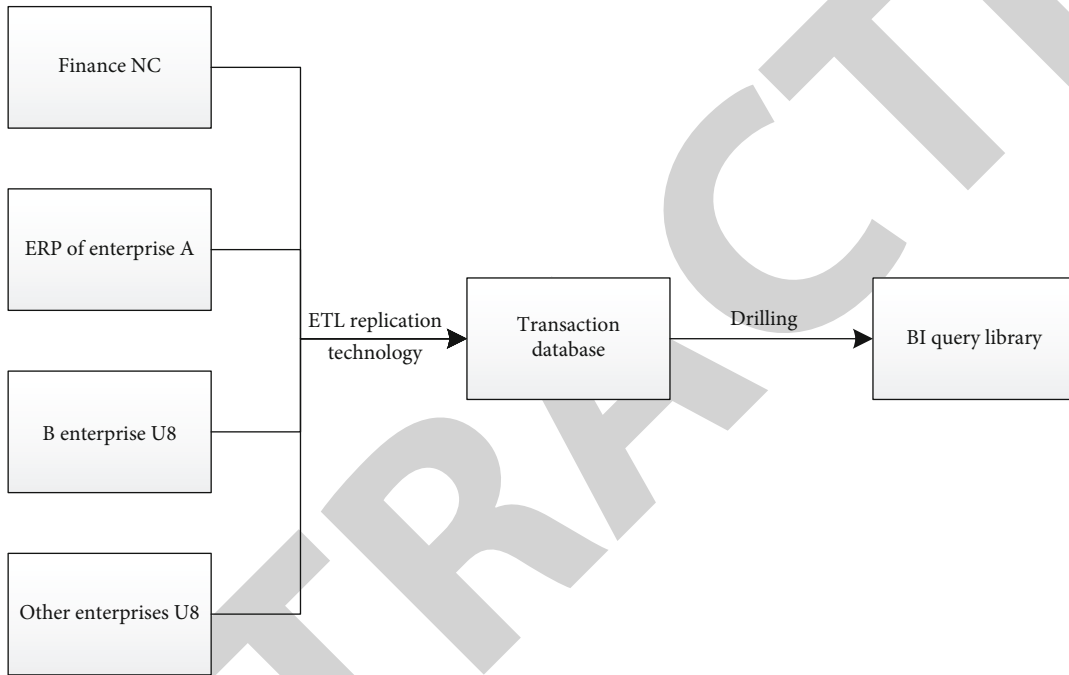
Figure 4: Dual data granularity.
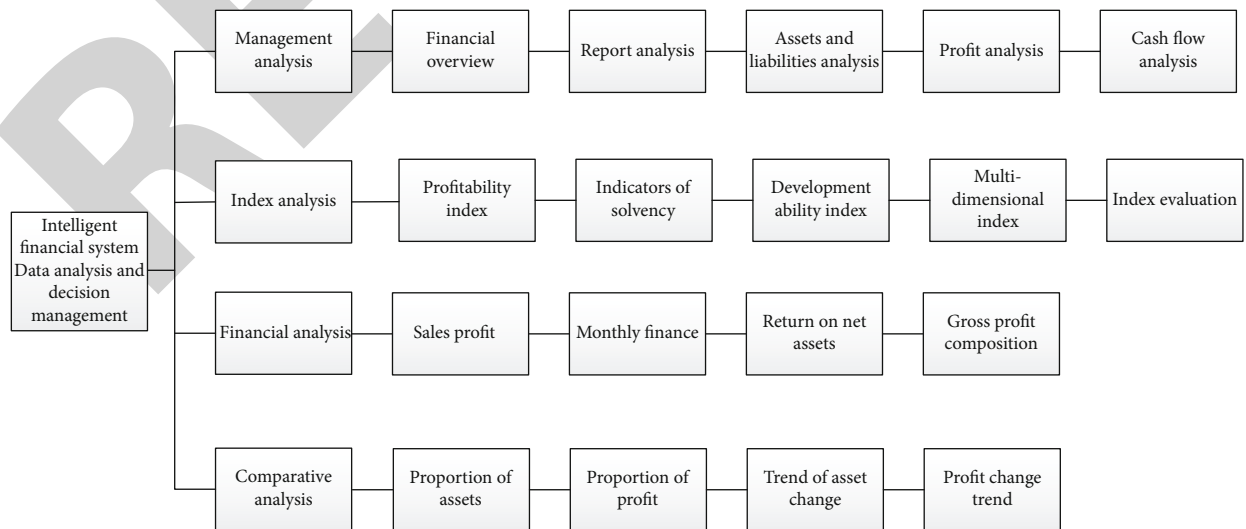

Figure 5: Data flow.

Figure 6: Functional design.
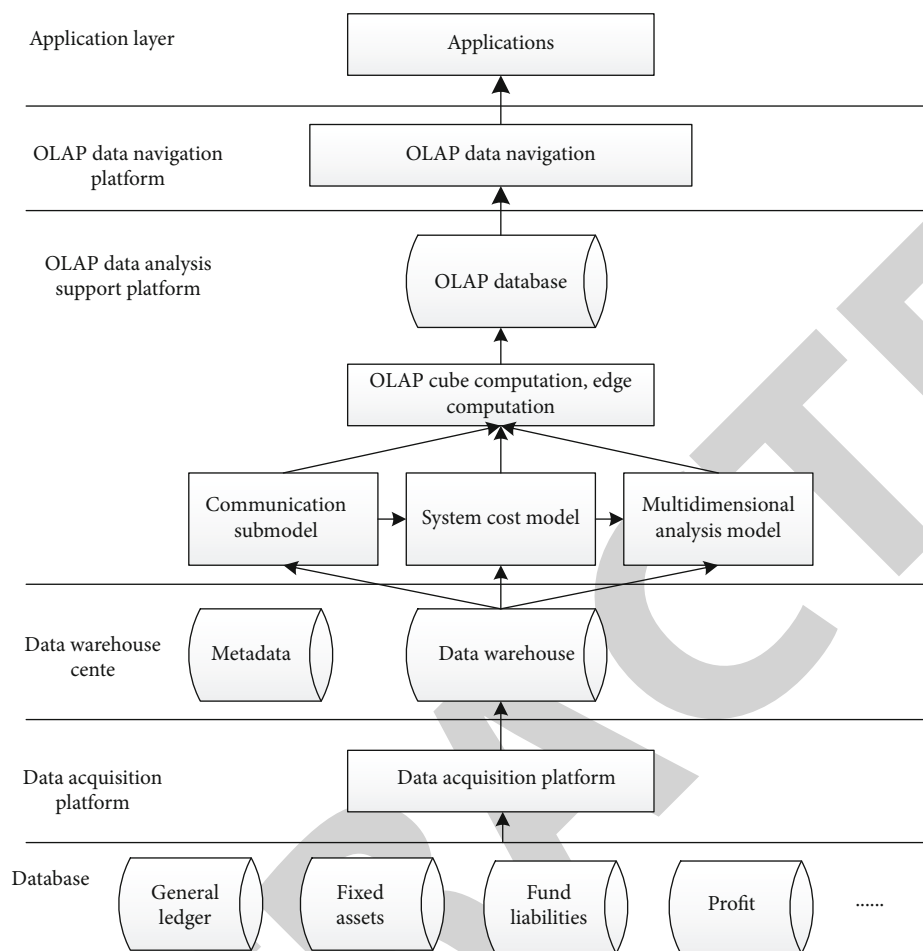
Figure 7: Architecture of the system.

Table 2: Test environment.

Project	Content
Web server	tomcat 6
Database server	MySQL 5.7
Development platform	Eclipse Indigo
Development language	JDK 1.6
Development framework	Struts2 + Spring 3.0 + Hibernate 4.1.6
Acceptance PC	Windows 7, Windows 10
Acceptance database service	Windows 10

Table 3: Evaluation criteria.

Hierarchy	Hierarchical description of system problems
A	Seriously affect the operation of the system or the use of users
B	Functional defects, which affect system operation or user use
C	It can be modified as appropriate without affecting the operation of the system
D	Defect-free

granularity. To store data, the database is a very important part of the system, which mainly stores and operates various data. We can clearly see the transformation and change of historical data. Whether it is the detailed data of recent months or the historical data of a certain year, it can be found through the database, as shown in Figure 4.
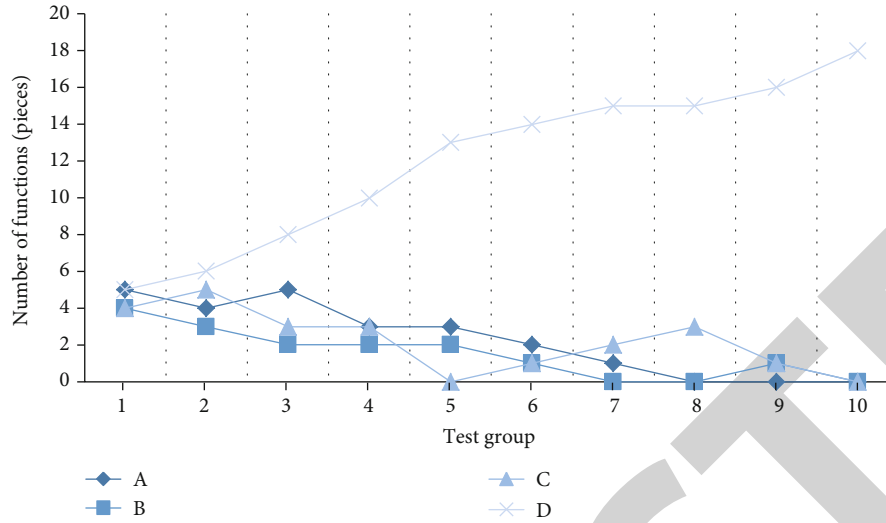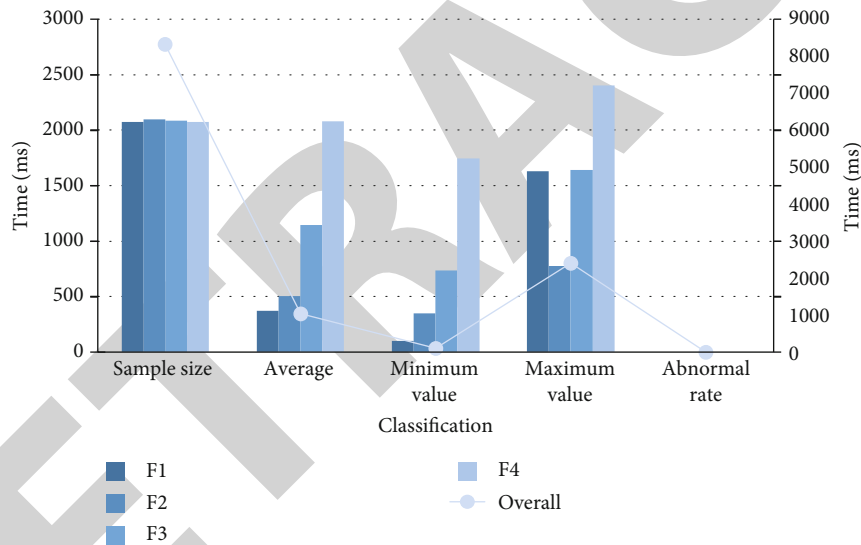
Figure 8: System evaluation.

Figure 9: Response time test.

(2) Data flow

Through ETL technology, the data scattered in each subsystem is copied and concentrated in the transaction database for integration and processing. The data of the system comes from merging different data sources. In this way, various financial data indicators can be comprehensively analyzed. The flow direction of the data set of the system, leveraging the SQL Server data platform, is shown in Figure 5.

3.3. Function Module Design. This system mainly realizes four analysis functions, including management, index, finance, and comparison. Use F1, F2, F3, and F4 to represent these four functions. There are 4 to 5 subfunctions under each function, as shown in Figure 6.

3.4. System Architecture Design. We mainly show the data architecture of the system. Collect different database data into the data collection platform; then, through the data warehouse, the processed data through several models, OLAP data calculation, and analysis; finally, through the data navigation of OLAP, the data is transmitted to the application program for the final system decision-making, as shown in Figure 7.

4. Experimental Analysis

4.1. Development Environment. The test environment of the system is mainly configured by the current mainstream software and hardware. In this test environment, our system can run normally and perform well. In this performance test, we use the JMeter tool based on JAVA to test, as shown in Table 2.
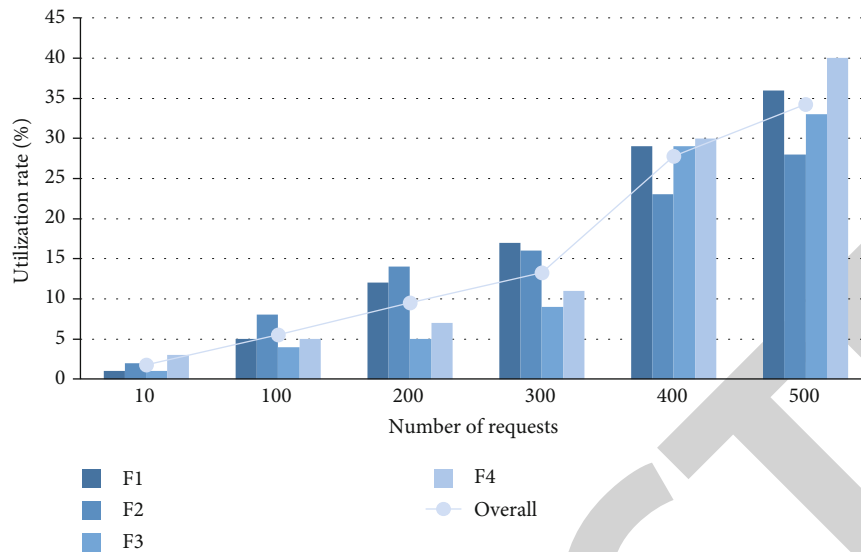
Figure 10: CPU utilization.

Table 4: Parameters.

Parameter name	The value of the parameter
Number of iterations	500
Number of terminals	25
Terminal data transmission power	0.5 W
Delay specific gravity	$\sim U(0,1)$
Terminal computing capability	500 MHz
Scale setting	60
Population number	4
Spiral characteristic constant	1

In order to better analyze and evaluate the system, we set up some evaluation criteria to determine the current status of the system. In the design of the system, if the problem reaches the A, B grade, it must be modified to solve the problem before the next system design can be carried out, as shown in Table 3.

4.2. System Test

4.2.1. Systematic Review. According to the function module designed in the third chapter of this paper, it is divided into four major functions, with a total of 18 subfunctions. This system review mainly evaluates the classification of these 18 subfunctions. A total of 10 adjustments and modifications have been made to the test group. Every time the test group tests, it is committed to reducing the number of A, B, and C grades and increasing the number of defect-free functions. Until the final system functions are all D grades, the number of A, B, and C grades is 0. There are no defects, so as to complete the state evaluation of the system, as shown in Figure 8.

4.2.2. Response Time. The test scheme we plan is to measure the page response time of the four functions of the system. The set conditions are as follows: a test scenario with a max-

imum concurrent user of 100; set the assembly point to 70; gradually increase ten users per second. We can find that no anomalies occurred during the whole test. Therefore, the abnormal rate of system response is 0%. The average response time fluctuation of the four functions (F1, F2, F3, and F4) is less than 3 s. Their overall average response time is about 1 s. The results of all functional tests meet the expected requirements, as shown in Figure 9.

4.2.3. CPU Utilization. Our experiment sets the expected goal as follows: the CPU utilization rate of the system should not exceed 70%; once exceeded, it is regarded as an unqualified index, which needs to be adjusted and modified until the utilization rate is reduced to below 70%. The system testing tends to be stable, and we check the CPU utilization of different functions according to the number of requests per second. We can find that with the increase of the number of requests, the CPU utilization trend of all functions is steadily increasing. The maximum CPU utilization rate of the system is 34%; the minimum utilization rate is 2%. In terms of functions alone, CPU utilization is up to 40% of F4 functions. To sum up, the system passed the CPU test, which was less than 70% of the expected utilization rate, and the system was qualified, as shown in Figure 10.

4.3. Edge Computing Task Optimization. The iteration times of edge calculation have a great influence on the algorithm. Therefore, we must fix the parameters of related simulation experiments well. Due to space constraints, we only show some values, as shown in Table 4.

(a) Constant parameter scheme

The whale algorithm is used to combine the old and new tasks for experiments. It is compared with the new task method, random unload method, all local method, and all upload method. We can find from the figure that it is obvious that the method in this paper is more dominant.
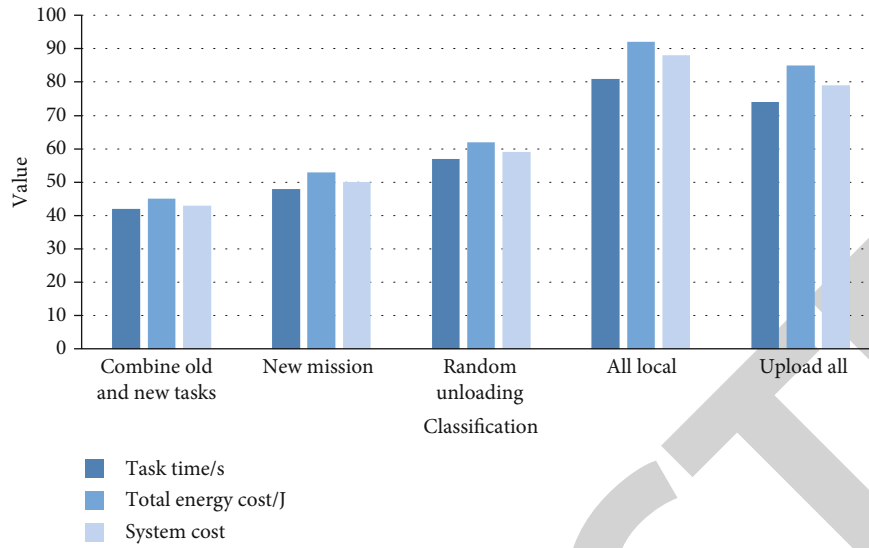
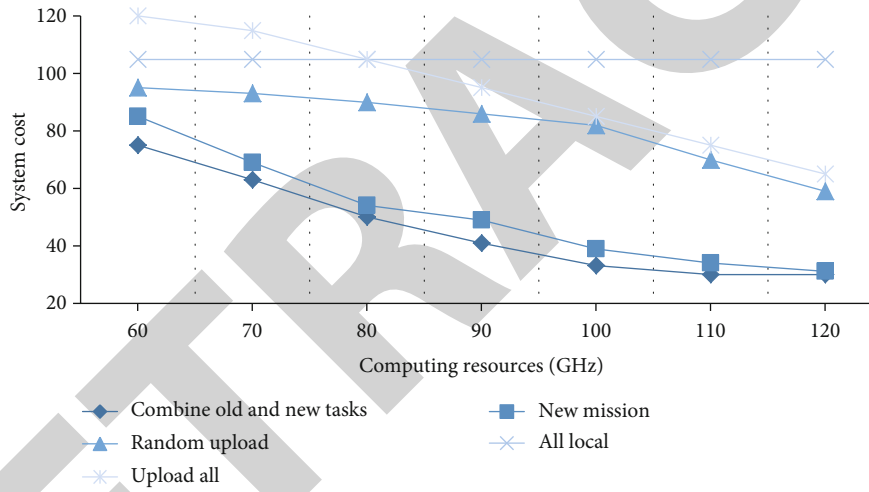Figure 11: System cost-constant parameters.

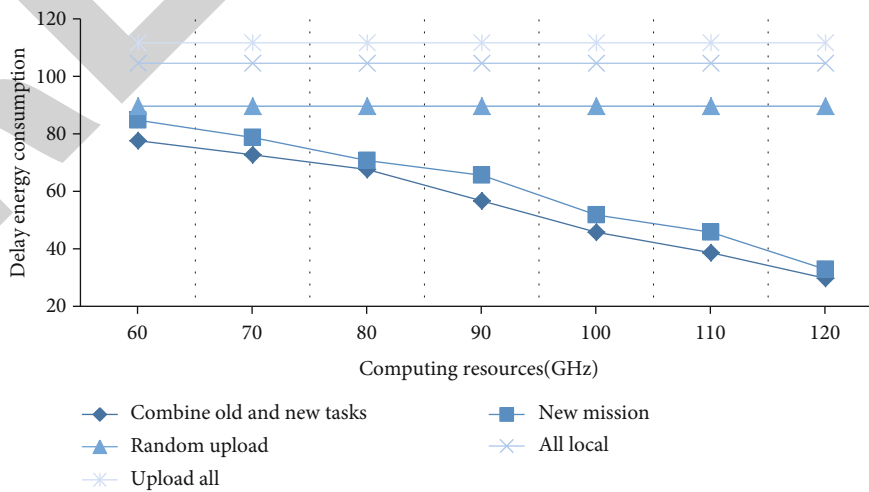Figure 12: System cost-computing resources.

Figure 13: System cost-latency energy consumption.

Whether it is the total cost of task time or energy or the system cost, this method consumes the least resources and improves the system performance more, as shown in Figure 11.

(b) Computing resources

Using the control variable method, the factor of calculation resources is changed, and other parameters remain unchanged. Here, computing resources refer to the total route processing capacity in the edge server. Total cost, which is the worst way, completely abandons the profit effect brought by edge calculation. The benefits brought by this method are the most obvious. However, we should note that the method of the new task is only slightly worse than the method in this paper. After reaching a certain bottleneck of computing resources, the gap between the two methods is equal and the system cost is similar, as shown in Figure 12.

(c) Delay energy consumption

When determining the offload decision, we can find that the delay energy consumptions of random upload, all local, and all upload are all fixed values. They are no longer affected by computing resources and will not change with the increase of resources. However, the method in this paper and the method of new tasks still decrease with the increase of computing resources. Among them, the strategy effect of this method is the best, as shown in Figure 13.

5. Conclusion

According to the various financial requirements of the development of enterprises in compliance with the times, a multisource database is established, and the architecture and functions of the intelligent system are analyzed and designed by using the edge computing platform. After analysis and verification, the research results of this paper show the following:

(1) In order to evaluate the performance of 18 functions of the system, grade evaluation of functions is carried out. After 10 adjustments, all functions are D-level, that is, the state without defects. (2) The abnormal rate of system response time is 0%. The average response time of F1, F2, F3, and F4 functions is in line with expectations. Their time range fluctuation is less than 3 s. The overall average response time of the system is about 1 s. (3) After testing, the whole system runs, and the maximum CPU utilization rate is 34%; at the smallest, it was only 2%. The system has passed CPU detection. Test less than 70% of the expected utilization rate, and the system is qualified. (4) This paper chooses the whale algorithm to combine the old and new tasks. It has an excellent performance in computing resources and delays energy consumption.

For enterprise managers, the system designed in this paper is a good auxiliary tool for decision analysis; it can intuitively view data from various sources and conveniently observe the final financial situation. Our system basically meets the performance requirements of intelligent finance.

However, it still needs further improvement and perfection. For example, improve the details of the system and expand the application scope of the financial system; perfect each functional module of the system to make the decision closer to reality and more accurate; better integration, design, and operation of databases; optimize the computing resources of edge computing. Based on the above, this paper can consider more factors in more practical scenarios, which is a long-term optimization work.

Data Availability

The experimental data used to support the findings of this study are available from the corresponding author upon request.

Conflicts of Interest

The author declared no conflicts of interest regarding this work.

References

[1] F. L. Gaol, H. L. Abdilla, and T. Matsuo, "Adoption of business intelligence to support cost accounting based financial systems — case study of XYZ company," *Open Engineering*, vol. 11, no. 1, pp. 14–28, 2021.

[2] H. Lee, "Role of artificial intelligence and enterprise risk management to promote corporate entrepreneurship and business performance: evidence from korean banking sector," *Journal of Intelligent and Fuzzy Systems*, vol. 39, no. 4, pp. 5369–5386, 2020.

[3] Z. Chen, "Research on accounting intelligence system modeling of financial performance evaluation," *Security and Communication Networks*, vol. 2021, Article ID 5550382, 9 pages, 2021.

[4] S. Patalay and M. R. Bandlamudi, "Decision support system for stock portfolio selection using artificial intelligence and machine learning," *Ingénierie des Systèmes D Information*, vol. 26, no. 1, pp. 87–93, 2021.

[5] M. M. Mousavi and J. Lin, "The application of PROMETHEE multi-criteria decision aid in financial decision making: case of distress prediction models evaluation," *Expert Systems with Applications*, vol. 159, p. 113438, 2020.

[6] Y. Chao, H. Wang, C. Yusheng, M. Yongmei, L. Xin, and M. Yongmei, "Analysis of new data processing system based on edge computing," *Light Industry Science and Technology*, vol. 10, pp. 63-64, 2021.

[7] R. Guo, "Calculation and application of financial intelligent decision support system," *Bonding*, vol. 47, no. 8, p. 5, 2021.

[8] T. Jiaqi, Y. Xindi, and D. Haoran, "Construction of university financial decision analysis platform based on distributed data sharing mechanism," *China Education Informatization*, vol. 7, pp. 85–88, 2020.

[9] J. Wu and L. Yangguang, "Innovation and practice of financial management in internet plus's big data era-intelligent financial decision support information," *System*, vol. 5, pp. 342-343, 2020.

[10] L. Qin and Y. Yang, "Discussion on the architecture, implementation path and application trend of intelligent finance," *Management Accounting Research*, vol. 1, no. 1, 2018.

Retraction

Retracted: Credibility Analysis of Accounting Cloud Service Based on Complex Network

Journal of Sensors

This article has been retracted by Hindawi following an investigation undertaken by the publisher [1]. This investigation has uncovered evidence of one or more of the following indicators of systematic manipulation of the publication process:

(1) Discrepancies in scope

(2) Discrepancies in the description of the research reported

(3) Discrepancies between the availability of data and the research described

(4) Inappropriate citations

(5) Incoherent, meaningless and/or irrelevant content included in the article

(6) Manipulated or compromised peer review

The presence of these indicators undermines our confidence in the integrity of the article's content and we cannot, therefore, vouch for its reliability. Please note that this notice is intended solely to alert readers that the content of this article is unreliable. We have not investigated whether authors were aware of or involved in the systematic manipulation of the publication process.

Wiley and Hindawi regrets that the usual quality checks did not identify these issues before publication and have since put additional measures in place to safeguard research integrity.

We wish to credit our own Research Integrity and Research Publishing teams and anonymous and named external researchers and research integrity experts for contributing to this investigation.

The corresponding author, as the representative of all authors, has been given the opportunity to register their agreement or disagreement to this retraction. We have kept a record of any response received.

References

[1] X. Chen, C. Guang, and D. Hua, "Credibility Analysis of Accounting Cloud Service Based on Complex Network," *Journal of Sensors*, vol. 2022, Article ID 5420772, 11 pages, 2022.

Research Article

Credibility Analysis of Accounting Cloud Service Based on Complex Network

Xinyou Chen [ID],[1] Cheng Guang,[2] and Du Hua[1]

[1]*Henan Province Hospital of TCM & The Second Affiliated Hospital of Henan University of TCM, Zhengzhou 450002, China*
[2]*Henan University of Engineering, Zhengzhou 450002, China*

Correspondence should be addressed to Xinyou Chen; chxyou@hactcm.edu.cn

Compared with the previous accounting information system (hereinafter referred to as AIS), the dynamic and changing environment of accounting cloud service, cloud storage away from enterprise entities, service modules selected for purchase, and seamless dynamic configuration. With the emergence of new situations such as the reconstruction of accounting information processing process, the emergence of new features increases the information risk of enterprises. Therefore, taking reasonable and effective measures can enable enterprises to intuitively understand whether AIS is credible in the accounting cloud service environment. Referring to the existing research system in the field of reliability evaluation, this paper analyzes the current situation of accounting cloud service and its characteristics compared with the previous AIS and divides it into four parts: normative inspection, index calculation, and reliability calculation to illustrate the method system for measuring the reliability of accounting cloud service. This paper analyzes the reliability requirements and reliability attributes of accounting cloud services and constructs a reliability evaluation grade model combined with fuzzy comprehensive evaluation to guide the selection of users and the quality management of cloud accounting suppliers. Considering the complexity and dynamics of AIS reliability evaluation in accounting cloud service environment, the reliability of AIS is also affected by the complex call relationship between modules; combined with the complex network theory, a reliability analysis and evaluation method of accounting cloud service based on complex network are proposed.

1. Introduction

The concept of "Internet plus" has always been well known by all walks of life. Today, enterprises are increasingly aware that with the advent of the era of big data, advanced data processing and information management mode will bring unlimited pioneers and practical benefits to enterprises [1]. Cloud accounting applies cloud computing, a big data solution, to the field of accounting informationization. While reducing the cost of accounting informatization construction and maintenance of enterprises, it will provide high-quality services such as seamless connection with external information systems of enterprises and auxiliary scheme analysis of big data processing with efficient and convenient financial business processing

and optimized service resources updated by cloud computing in real time [2]. Compared with the previous accounting information systems, the dynamic environment of cloud accounting is full of changes, far away from the service modules selected by enterprise entities for cloud storage and purchase, seamlessly connected and dynamically configured, and the emergence of new conditions and new features such as the reconstruction of accounting information processing flow increases the informationization risk of enterprises [3]. Therefore, reasonable and effective measures should be taken to let enterprises know whether AIS can be trusted in the cloud accounting environment that they want to purchase intuitively or have already used. Its informatization risk is very important in the popularization and development of accounting cloud services.

2. Complex Network Theory

2.1. Related Indicators of Complex Networks. There are various indexes to highlight the characteristics of complex networks [4]. Combined with the key points of this paper, the following indexes are selected and introduced.

2.1.1. The Diagram of the Network. In theory, a graph allows for multiple lines. However, if a graph is simple, it means that the graph has no multiple edges. In addition, there is no ring in the simple pattern, and the simple pattern contains rings [5]. When each arc has a corresponding line value, it is a weighted network; otherwise, it becomes a powerless network. For example, Figure 1 is a complex network diagram of metal trade and a visual description of system structure. Visualization technology is one of the most important technical tools when using complex network theory to study [6]. So without explanation, readers can read this picture.

In Figure 1, the connections between different network nodes are represented, and the connections between different enterprises illustrate the correlation and economic business connection of enterprises. By calculating the entry, exit, and related indicators of complex networks, we can evaluate those core enterprises.

2.1.2. Network Density. This indicates the tightness between the vertices of the network. In complex networks, network density is usually used to describe the overall density and development trend [7]. In a complex network with N vertices, the network density can be expressed by

$$d(G) = \frac{2M}{N(N-1)}. \tag{1}$$

The acquisition range of network density is always within the interval [0, 1]. In the actual network, it is found that the maximum value of network density is 0.5.

Centrality and center potential can be near centrality and near center potential and intermediate centrality and intermediate center potential.

2.1.3. Spot Degree and Spot Degree Distribution. This is the number of rows owned by vertex i degree k vertex i. In directivity network, point degree is divided into input degree and output degree. The input of a vertex is the number of arcs entering the vertex, and the outgoing degree of the corresponding vertex is the number of arcs outgoing from the vertex. They are the same only in the case of simple graphs. In addition, we can refer to the concept of point distribution, which refers to the distribution of each vertex point degree and is used to explain the overall distribution of network point degree.

2.1.4. Average Shortest Path. Path refers to the distance between vertex i and vertex j, which is denoted as d_{ij}. At the same time, the network diameter refers to the longest path between any two vertices, which is denoted as D, that is,
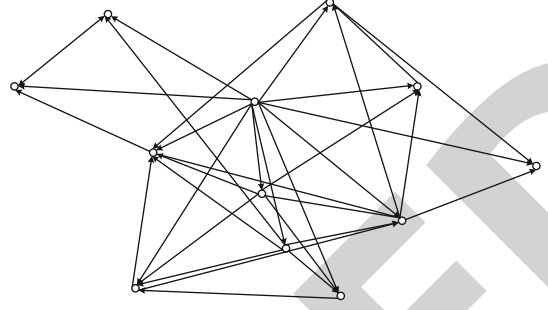
$$D = \max d_{ij}. \tag{2}$$

FIGURE 1: Complex network diagram of metal trade in a certain place.

In addition, the so-called average path refers to the average value obtained from the distance between any two vertices, which is denoted as L, that is,

$$L = \frac{1}{(1/2)N(N+1)} \sum_{i \geq j} d_{ij}, \tag{3}$$

where N is the number of network nodes.

K kernel defines a relatively dense subnet, which is helpful to find a vertex set with closer relationship, and can describe several characteristics that cannot be expressed in degree distribution.

2.2. Basic Model of Complex Network. K-shell algorithm measures the node influence of projects in the network, and PageRank algorithm integrates the node influence of projects and the diffusion relationship between projects to realize project portfolio selection [8], where the importance of nodes is measured based on the location attributes of nodes in the network.

$$Cs(i) = \left[K(i)^{\gamma} \times \left(\sum_{j=1}^{N} w_{ij} \right)^{\mu} \right]^{1/\gamma+\mu}, \tag{4}$$

where $K(i)$ denotes the degree value of the i-th node, w_{ij} denotes the weight value of the connection between node i and its adjacent node j, and γ and μ are adjustable parameters.

The classical PageRank ranking algorithm for web pages mainly pays attention to the transfer relationship between nodes in the network, and the priority ranking matrix constructed is as follows:

$$PR(p_i) = \frac{1-d}{N} + d \sum_{p_j \in M(p_i)} \frac{PR(p_j)}{L(p_j)}, \tag{5}$$

where $P_1, P_2, \cdots, P_N$ denotes web pages, $M(p_i)$ denotes the set of web pages linked to web pages p, $L(p_j)$ denotes the number of web pages linked to web pages p_j, N is the total number of web pages, and d is the damping coefficient, which is usually 0.85.

The maximum eigenvalue of the priority ranking matrix PR is entered into the corresponding eigenvector R, which can lead to the priority ranking of each node in the network, as shown in

$$MR^* = \lambda^* R^*. \tag{6}$$

2.2.1. Regular Network Model

(1) Global Coupled Network Model. Globally coupled network is the most typical regular network model. As shown in Figure 2(a), it refers to the arc connected between any two vertices in the network. The results show that if the network size is the same, the globally coupled network has significant characteristics, such as the shortest average path and the largest cluster coefficient, compared with other types of network models. This network model can reflect the cluster characteristics or small-world characteristics of the actual network to a certain extent, but because most living networks cannot be described in this model, the study of the actual network of global coupled networks has considerable defects.

(2) Nearest Neighbor Coupled Network Model. The nearest adjacent coupling network is a network model with low aggregation degree, but it is also a model studied by theory and practice. As shown in Figure 2(b), each vertex is connected to a nearby $K/2$ vertex arc (K is even). This model belongs to a highly clustered network. Therefore, the average path when K is large is as follows.

$$L \approx \frac{N}{2K} \longrightarrow \infty, \tag{7}$$

where K is even and $N \longrightarrow \infty$.

And the clustering coefficient of the nearest neighbor coupling network is

$$C = \frac{3(K-2)}{4(K-1)} \approx \frac{3}{4}. \tag{8}$$

As a result, it is difficult for this model to realize the process that requires overall coordination.

(3) Star Coupled Network (Star Coupled Network). Star coupled network is also a typical complex network model. Its structural feature is that the center is a vertex, and all vertices other than that are only connected to the middle vertex, but there is no interconnected relationship between them as shown in Figure 2(c). The average path of the model is approximate to 2, and the class coefficient is approximate to 1.

2.2.2. Scale-Free Network Model.
The research on complex network patterns in the past usually ignores two very important characteristics. One is growth; that is to say, the overall scale of the network expands with the increase of time and information. Second, it is priority connectivity, which means that the newly generated vertices of the network are easily connected with vertices with high point value.

Based on the above-mentioned two-point characteristics, the formation mechanism of BA scale-free network model is to add new vertices in turn to the existing network and connect n original vertices. In addition, the probability that the newly added vertex and the cause vertex are connected with each other is set to p.

$$P = \frac{k_i}{\sum k_j}(i \neq j), \tag{9}$$

where k represents the point degree value of vertices. Therefore, the average path length of BA scale-free network is

$$L \propto \frac{\log N}{\log \log N}. \tag{10}$$

After t-step priority connection, the clustering coefficient is

$$C = \frac{\mathrm{n}^2(n+1)^2}{4(n-1)} \left[\ln\left(\frac{m+1}{m}\right) - \frac{1}{m+1} \right] \frac{[\ln(t)]^2}{t}. \tag{11}$$

At present, there are three methods to describe the point degree distribution of BA dimensionless network, including continuous field theory, rate equation method, and master equation method. The asymptotic results obtained are identical, in which the point distribution function of BA dimensionless network derived using the master equation method is shown.

$$P(k) = \frac{2n(n+1)}{k(k+1)(k+2)} \propto 2n^2 k^{-3}. \tag{12}$$

It is found that the point degree distribution of BA dimensionless network model can be expressed by power law function approximation.

As mentioned above, the characteristics of the complex network model are summarized as shown in Table 1.

3. Construction of Accounting Cloud Service Credibility Analysis Method System

In this chapter, in the accounting cloud service, 10 modules that enterprises often customize are taken as research objects, and the reliability measurement method system is constructed. In addition, it is assumed that all enterprises have the conditions to obtain the same accounting services, and all suppliers can provide similar services. This chapter selects and constructs a complex network model from reliability indicators and divides it into four parts: normative inspection, index calculation, and reliability calculation to explain the method system of measuring the reliability of accounting cloud services (Figure 3).

3.1. Credibility Index Selection Based on Complex Network

3.1.1. Principle of Selecting Credible Indicators. In this paper, complex network is used as a tool to measure the reliability of accounting cloud services, but there are many indicators in complex network theory. In order to choose the indicators

(a)

(b)

(c)
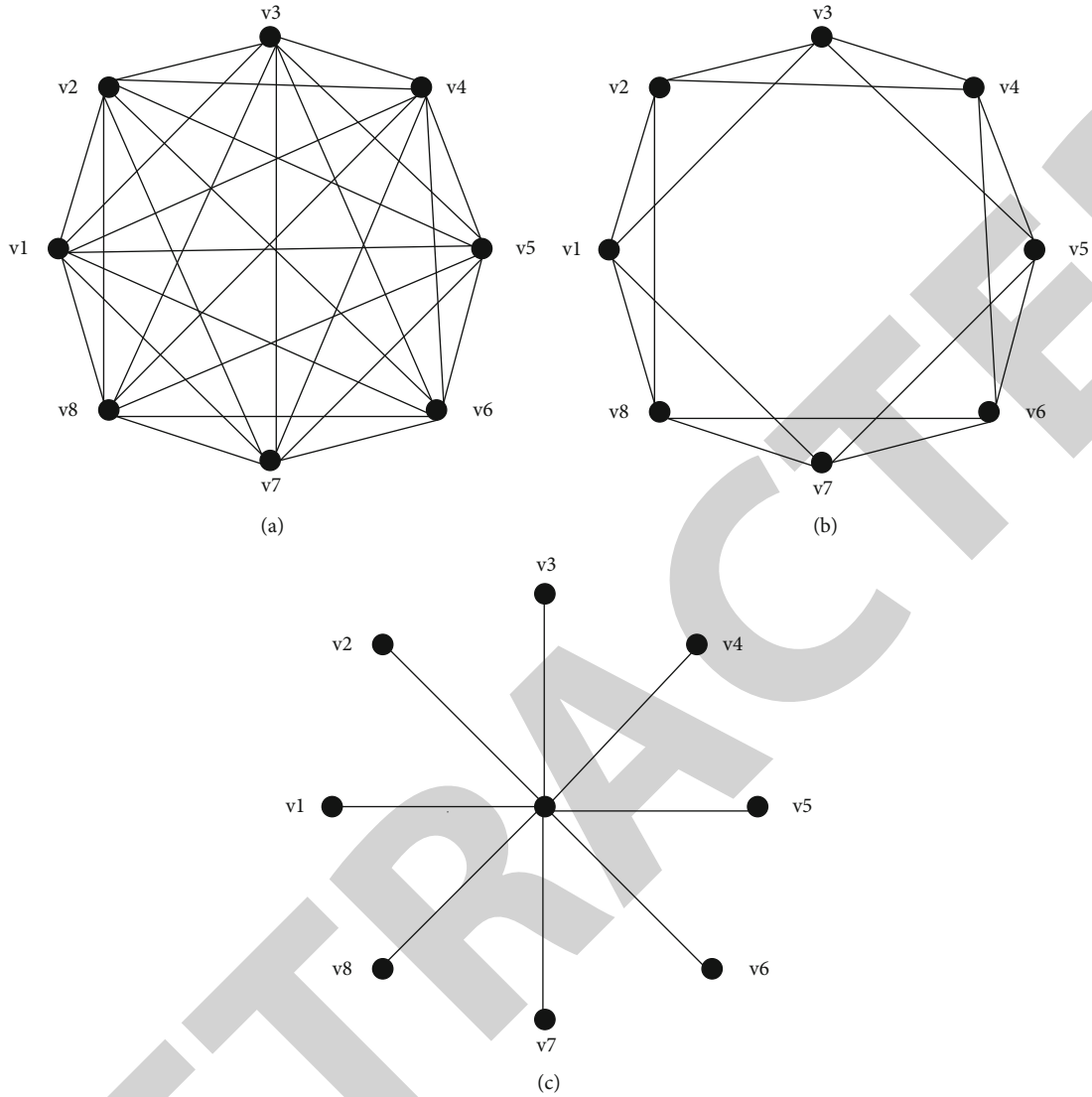
Figure 2: Regular network model.

Table 1: Characteristics of complex network model.

| Model name | Average path length L | | Clustering coefficient ($0 \leq C \leq 1$) | | Distribution law |
	Qualitative	Quantitative	Qualitative	Quantitative	
Globally coupled network	Larger	L = 1	Larger	C = 1	Function distribution
Nearest neighbor coupling network	Larger	$L \longrightarrow \infty$	Larger	$C \approx 3/4$	Function distribution
Star coupling network	Larger	$L \longrightarrow 2$	Larger	$C \longrightarrow 1$	Function distribution
Small-world network	Larger	$L(p) < <L(0)$	Smaller	$C(p) \propto C(0)$	Poisson distribution
BA scale-free network	Smaller	$L \propto \log N/\log \log N$	Smaller	$C = \left(n^2(n+1)^2/4(n-1)\right)\left[\ln(m+1/m) - 1/m + 1\right]\left([\ln(t)]^2/t\right)$	Power law distribution

FIGURE 3: Schematic diagram of accounting cloud service credibility measurement system.

FIGURE 4: Complex network of contracted accounting cloud services.

that play a practical role in this paper, the following principles should be followed [9].

(1) Principle of relevance

(2) The principle of comprehensiveness

(3) Principle of comparability

(4) Principle of quantification

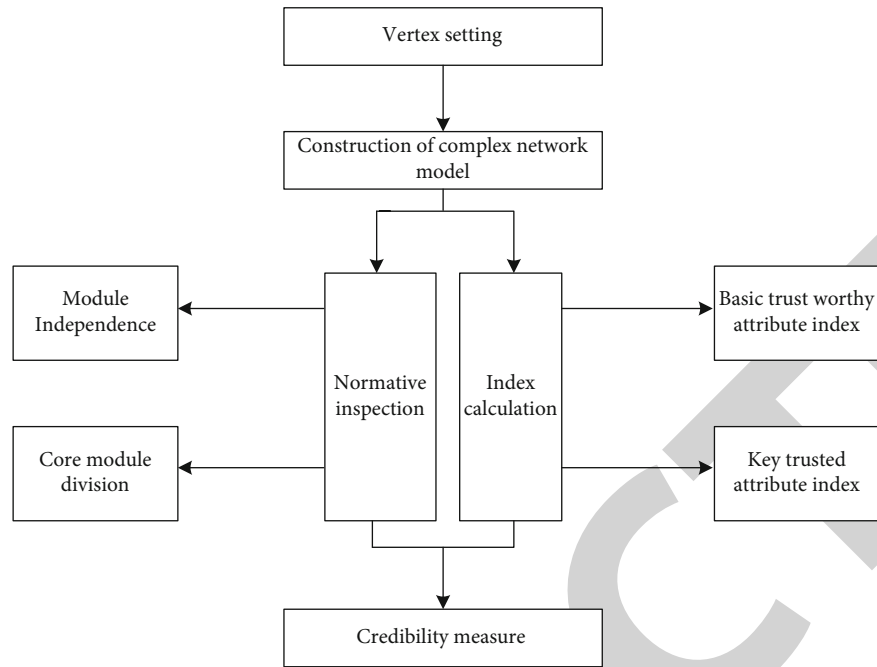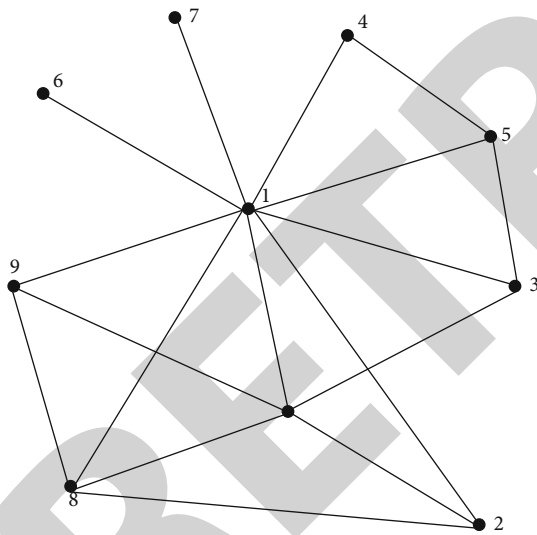*3.1.2. Selection of Specific Credible Indicators.* This paper chooses the reliability index of accounting cloud service based on complex network theory. At the same time, because third-party organizations such as accounting and auditing have no influence on the reliability of accounting cloud services, the selection of indicators does not consider strengthening the content related to reliability attributes and discusses them from two aspects: basic reliability attributes and key reliability attributes [10].

(1) Basic Reliable Attribute Measurement Index. The basic reliability attributes must meet the reliability level of all accounting cloud service systems. It means that the information exchange between cloud accounting modules is correct and timely. Based on this requirement, this paper chooses network density, centrality, and centrality in complex network theory and measures the integration of accounting cloud services.

(2) Key Trustworthy Attribute Measurement Indicators. Key reliability attributes can be divided into different levels. Based on complex network theory, this paper mainly focuses on the measurement of maturity, stability, and hierarchy and chooses the following reliability indicators.

(1) Spot degree and spot degree distribution

(2) Average shortest path

(3) *k*-nucleus

3.2. Normative Inspection and Calculation of Credible Indicators

3.2.1. Conformity of Normative Inspection. To analyze the reliability of accounting cloud services, we must first confirm whether they are normative.

TABLE 2: Vertex approach centrality.

Serial number	Approximate centrality	Vertex number	Serial number	Approximate centrality	Vertex number
1	0.342808438	6	11	0.2631854	116
2	0.2983375	179	12	0.26092996	163
3	0.29429692	166	13	0.26092896	165
4	0.291159	46	14	0.259863947	7
5	0.28896613	146	15	0.25951097	164
6	0.28212703	100	16	0.25880769	122
7	0.27965861	183	17	0.25810821	128
8	0.27482514	65	18	0.257759794	4
9	0.267527	52	19	0.25706596	99
10	0.26491085	145	20	0.25637582	120

TABLE 3: Vertex intermediary center degree.

Serial number	In the intermediary center	Vertex number	Serial number	In the intermediary center	Vertex number
1	0.63674192	6	1	0.12056193	146
2	0.34341395	179	2	0.07357198	52
3	0.27608892	166	3	0.07208597	91
4	0.24249014	46	4	0.07098372	17
5	0.21576191	146	5	0.06354360	116
6	0.16063104	100	6	0.06144943	129
7	0.15761182	183	7	0.05794528	12
8	0.15404517	65	8	0.05259543	147
9	0.14969503	52	9	0.05174976	56
10	0.126338751	145	10	0.0486913	61

(1) Module Independence. Cloud accounting system is customized by enterprises in terms of modules, and each module should be relatively independent. According to the process of accounting business, accounting treatment belonging to each module should also be able to be carried out independently. Therefore, if the complex network of cloud accounting is reduced to the network with secondary modules as its vertex, it meets the basic requirements of accounting business and can be said to be normative.

Figure 4 is a diagram using complex network analysis software. In addition, the old connectors of each vertex before shrinking will be replaced by new connectors attached to the new vertex. For example, all information transfer relationships between the purchase module and the general ledger module are replaced by connectors connecting the purchase module and the general ledger module. Therefore, cloud accounting has the independence of modules, and each module works independently, which is normative and can meet the requirements of basic reliability attributes.

(2) Core Module Partition. Using complex network theory, the modules in cloud accounting are divided into "core module," "semiedge module," and "edge module," and the three core modules will participate in accounting business more than edge module.

TABLE 4: Degree frequency distribution table.

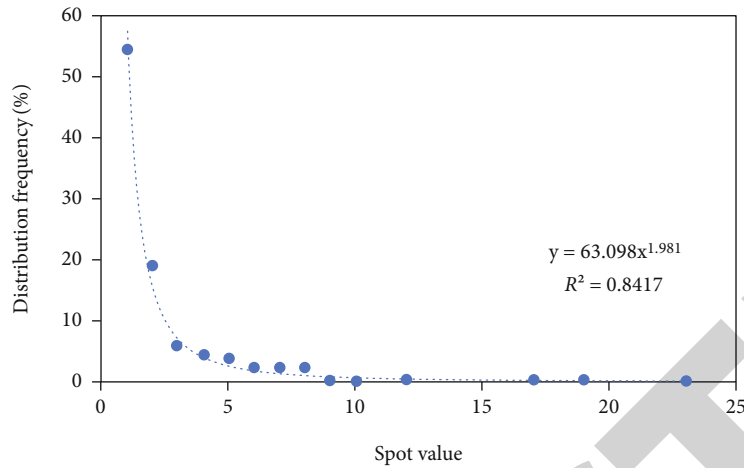| Cluster	Freq	Freq%	CumFreq	CumFreq%	Representative
1	105	54.6874	142	54.6875	vl
2	37	19.2709	105	73.9584	v8
3	12	6.2500	154	80.2082	v7
4	9	4.6874	163	84.8958	V4
5	8	4.1668	171	89.0623	v12
6	5	2.6042	176	91.6667	v46
7	5	2.6042	181	94.2706	v57
8	5	2.6042	186	96.8750	6s
9	1	0.5208	187	97.3954	v145
10	1	0.5208	188	97.9167	v183
12	1	0.5208	189	98.4373	v77
17	1	0.5208	190	98.9583	v166
19	1	0.5208	191	99.4792	v15
23	1	0.5208	192	100.0000	v6
Sum	192	100.0000	—	—	—

FIGURE 5: Distribution of accounting cloud service degree.

TABLE 5: Distribution table of entry frequency.

Cluster	Freq	Freq%	CumFreq	CumFreq%	Representative
0	51	26.5624	51	26.5622	v1
1	108	56.2501	159	82.8127	v5
2	13	6.7708	172	89.5833	v8
3	5	2.6042	177	92.1875	v4
4	5	2.6042	182	94.7917	v52
5	3	1.5625	185	96.3541	v91
6	4	2.0832	189	98.4373	v57
7	2	1.0418	191	99.4792	v77
22	1	0.5208	192	100.0000	v6
Sum	192	100.0000	—	—	—

TABLE 6: Output frequency distribution table.

Cluster	Freq	Freq%	CumFreq	CumFreq%	Representative
0	67	34.8958	67	34.8958	v5
1	85	44.2708	152	79.1667	vl
2	18	9.3750	170	88.5417	v6
3	3	1.5625	173	90.1042	v12
4	9	4.6875	182	94.7917	v71
5	3	1.5625	185	96.3542	v77
6	3	1.5625	188	97.9167	v100
7	1	0.5208	189	98.4275	v65
9	1	0.5208	190	98.9583	v183
12	1	0.5208	191	99.4792	v166
17	1	0.5208	192	100.0000	vl5
Sum	192	100.0000	—	—	—

TABLE 7: Distance between two random vertices.

Distance	1	2	3	4	5	6
Even number of points	484	2110	4560	7780	8324	6642
Distance	7	8	9	10	11	—
Even number of points	4064	1808	660	176	36	—

3.2.2. Calculation of Trustworthy Indicators

(1) Calculation of Basic Trustworthy Attribute Index. (1)1. Network Density. Calculated by complex network software, the network density of accounting cloud services selected in this chapter is 0.01325252, which indicates that only 1.35252% of all possible arcs actually appear on the network. In real networks of similar scale, it is not uncommon for the density value to be so low. The network density index is meaningful when comparing, so when selecting cloud accounting products, we can apply each index to measure the integration of optional products, judge the reliability, and give priority to purchase. At the same time, the aggregation degree between the total calculation module and other modules in the accounting cloud service system is high, and the association between some relatively independent asset modules and other modules is relatively loose.

Network density can be used to describe the density of interconnected edges between nodes in a network. Online social networks are often used to measure the intensity and evolution trend of social relationships.

Accounting cooperation between different enterprises in accounting service enterprises can be described by complex network, through which different enterprises' economic business and services can be analyzed.

(1)2. Proximity to Centrality and Proximity to Centrality Potential. The acquisition range of the proximity of each module is obtained by calculation, and Table 2 is summarized. Due to the limited space, this chapter lists the top 20 vertices close to centrality. As can be seen from Table 2, the proximity centrality of Module 6 is the largest, with a value of 0.3249. Therefore, the general ledger module is located in the middle of the network but is not the highest value that might appear in a network of the same size. At the same time, the difference of all vertices close to centrality of the network is not big; for example, the values of 163 and 165 are 0.2609, and the variation of vertex proximity of the network is small, the degree of centralization is low, and
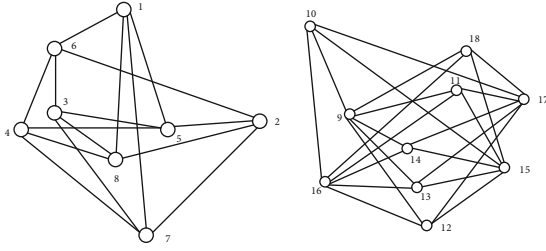
FIGURE 6: Accounting cloud service 4-core network.

TABLE 8: Cloud accounting credibility index value.

Indicator symbol	Indicator name	Index value
x_1	Network density	0.0132
x_2	Near-center potential	0.2729
x_3	Intermediary center potential	0.6187
x_4	Average point value	2.5314
x_5	Average shortest path	4.9643
x_6	K-nucleus	4

TABLE 9: Credibility index scoring table.

	x_1	x_2	x_3	x_4	x_5	x_6
x_1	0.5	1	0	0	0	1
x_2	0	0.5	0	0	0	1
x_3	1	1	0.5	0	0	1
x_4	1	1	1	0.5	1	1
x_5	1	1	1	0	0.5	1
x_6	0	0	0	0	0	0.5

TABLE 10: Reliability index score.

u_1	u_2	u_3	u_4	u_5	u_6
2.5	1.5	3.5	5.5	4.5	0.5

TABLE 11: Normalized weight of credibility index.

a_1	a_2	a_3	a_4	a_5	a_6
13.88%	8.34%	19.46%	30.56%	25.00%	2.76%

the integration is not high, so it can be seen that the performance of reliability close to centrality is better.

This distance is described by approaching the central potential from the perspective of the whole network. By calculation, the near center potential value of accounting cloud service is 0.27278020, which plays an important role in quantifying reliability and comparing with other networks.

(1)3. Intermediary Centrality and Intermediary Centrality Potential. The calculated mediation centrality is arranged in descending order, and the first 20 nodes are shown in Table 3. It can be seen from the table that the mediation degree of the accounting cloud service ranges from 0.00 to 0.6367, with a large degree of variation, so the reliability of the mediation center degree performs well. In addition, the intermediary center potential of this accounting cloud service is 0.6188, which is higher than the close center degree. It is shown in Table 3.

(2) Calculation of Key Trustworthy Attribute Index. (2)1. Degree and Degree Distribution. This paper uses point and point distribution to evaluate the maturity of cloud accounting. Accounting cloud services are network-oriented, but there are no heavy edges and rings, and the sum of degrees and degrees, so the arcs are symmetrical first. That is to say, it is discussed to change arcs in one direction or both directions into directionless edges.

From Table 4, we can know that the three nodes with the highest point value are voucher processing module, final settlement module, and inventory outbound module. This means that it is in the most active state in cloud accounting. The calculation shows that the average point value of symmetric network is 2.525. Cloud accounting shows better maturity and high reliability in point value.

The relationship between accounting cloud service distribution and distribution frequency can be fitted as

$$y = ax^b. \tag{13}$$

According to Table 4, the degree distribution diagram of the complex network of cloud accounting is shown in Figure 5.

In fact, the complex network of accounting cloud services is a simple directional graph, that is, an arc connected to the vertices of the network. Therefore, as described in Tables 5 and 6, it is necessary to calculate the in-value and out-value, respectively. The highest value is the voucher processing module, and the highest value is the sales invoice module, which meets the actual accounting requirements and has high consistency.

(2)2. Average Shortest Path. As can be seen from Table 7, the number of points with distances of 4 and 5 is the most even, and the distance between the two modules in cloud accounting is about 4 to 5. Therefore, the accounting cloud service system has relatively tight structure, high stability, low probability of errors, and high reliability.

(2)3. k-Nuclei. Because k-cores are nested, the hierarchy of accounting cloud services is represented by deleting k-cores in order lower than the highest value. By calculation, in the case of four cores ($k = 4$), the network crashes into a relatively dense system, and the visual image is shown in Figure 6.
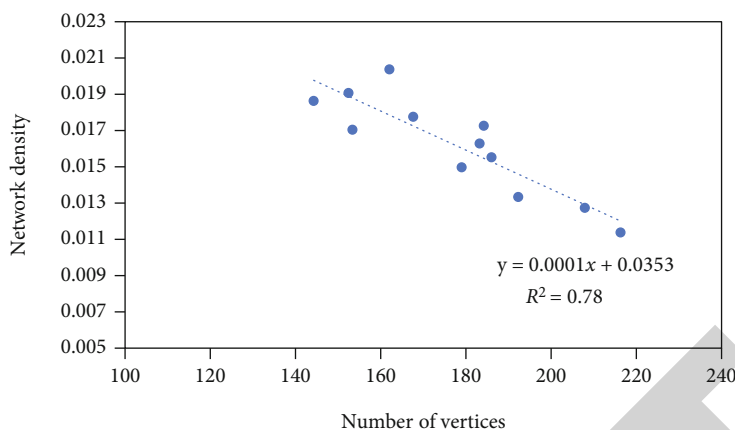
Figure 7: Relationship between network size and network density.

Table 12: Comparison of cloud accounting credibility.

Product name	1	2	3	4
Reliability (R)	2.2705	2.2463	2.3231	2.2312
Product name	5	6	7	8
Reliability (R)	2.2396	2.2391	2.2814	2.1998
Product name	9	10	11	12
Reliability (R)	2.1961	2.2502	2.1887	2.2082

This shows that accounting cloud services have a better level, and different accounting information users can obtain necessary information at different levels. Therefore, there is better reliability.

4. Experiment

4.1. Trustworthiness Measures. In order to improve the reliability of accounting cloud services more intuitively, this paper uses fuzzy comprehensive evaluation method to analyze the complex network reliability of accounting cloud services, measure its reliability correctly, and provide the basis for comparison and optimization.

In this paper, six indexes about the reliability of the whole complex network are selected. Set $X = \{x_1, x_2, x_3, x_4, x_5, x_6\}$ is used as the index value of cloud accounting, and its index value can be summarized as shown in Table 8.

4.2. Determining Weights. Because each index has different influence degree on reliability, it is necessary to evaluate the influence degree of each index. In this paper, the pecking order diagram method is used to determine the weights of the above six reliability indexes, respectively.

4.2.1. Importance Evaluation. Based on the influence of structural indexes on reliability in complex network theory, this paper evaluates the above indexes as shown in Table 9.

The reliability index scores are $U = \{u_1, u_2 \cdots u_6\}$, and the reliability index is added with the scores, and the scores of each index are shown in Table 10.

4.2.2. Weight Calculation. $A = \{a_1, a_2, a_3, a_4, a_5, a_6\}$ is the weight of reliability indicators. According to the above reliability index scores, formula (14) is used for unification, and the weight values of each index are calculated as shown in Table 11.

$$a_i = \frac{u_i}{\sum u_k}. \tag{14}$$

Set the final credibility of accounting cloud services to R. Formula (15) is used here to measure the reliability of accounting cloud service products.

$$R = \sum a_i x_i. \tag{15}$$

When the data is brought in, $R = 2.2706$; that is, the credibility of the accounting cloud service is 2.2706.

To sum up, the credibility evaluation method of accounting cloud services based on complex network proposed in this paper is highly practical.

4.3. Comparative Study on Credibility of Accounting Cloud Service Products. In this chapter, according to the 12 selected accounting cloud service products, complex network models are constructed, respectively. According to the reliability analysis method of accounting cloud service proposed above, the reliability index of each product is calculated and comparable reliability index data is obtained, and a detailed analysis is carried out.
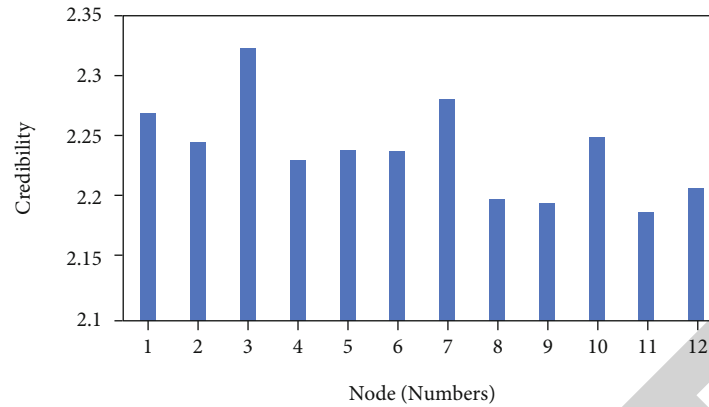
Figure 8: Comparison of credibility of accounting cloud services.

As shown in Figure 7, the relationship between network size and network density is represented by a visualization diagram and a fitting function.

As shown in Figure 7, there is a negative relationship between network density and network size. That is to say, with the increase of network scale, the network density will become smaller and smaller. In addition, the linear function fitting is $y = -0.0001x + 0.0349$, and R^2 is 0.78. Therefore, for enterprises, if many cloud accounting modules are selected, the network scale will expand rapidly and the network density will decrease, which will affect the integration of cloud accounting.

Use Equation (15) to calculate the reliability of the sample cloud accounting products, and the results are shown in Table 12.

As shown in Figure 8, a bar chart of the availability of accounting cloud services can be drawn according to Table 12.

It can be clearly seen from the figure that the reliability of No. 3 product is the highest. 11 products have the lowest reliability. Therefore, the reliability evaluation method of accounting cloud services based on complex network can clearly evaluate and compare the reliability of accounting cloud services and can provide the basis for product selection and optimization.

5. Conclusion

From the research results of this paper, the current mainstream accounting cloud service network density is very low. In many practical complex networks, such low network density is not uncommon, but the low network density has a great impact on the integration of accounting cloud services. At the same time, this paper also finds that the core potential of accounting cloud services is quite different, and their comprehensiveness is different. Integration is also the basic reliability attribute of accounting cloud services, and the overall reliability is very important. Therefore, this paper suggests that accounting cloud service providers develop more integrated new accounting cloud services. Moreover, on the premise of ensuring its basic and important reliability attributes, the reliability is improved. Moreover, for the existing accounting cloud services, providers should make every effort to optimize the network density,

make it have greater density and shorter path length, and improve integration and reliability. Only when suppliers continuously optimize the reliability of accounting cloud services can they export more and better accounting cloud services to the market.

Data Availability

The experimental data used to support the findings of this study are available from the corresponding author upon request.

Conflicts of Interest

The authors declared that they have no conflicts of interest regarding this work.

References

[1] S. Liu, "Human resource management of internet enterprises based on big data mobile information system," *Mobile Information Systems*, vol. 2021, no. 5, p. 9, 2021.

[2] H. Yue and X. Zheng, "WITHDRAWN: research on encrypting accounting data using des algorithm under the background of microprocessor system," *Microprocessors and Microsystems*, vol. 25, no. 1, 2021.

[3] S. Song, Y. Zhang, and B. Yu, "Interventions to support consumer evaluation of online health information credibility: a scoping review," *International Journal of Medical Informatics*, vol. 145, p. 104321, 2021.

[4] J. Wang, X. Yu, and L. Qiang, "Research on key technologies of intelligent transportation based on image recognition and anti-fatigue driving," *EURASIP Journal on Image and Video Processing*, vol. 2019, no. 1, p. 210, 2019.

[5] L. M. Frescura, B. Menezes, and R. Duarte, "Application of multivariate analysis on naphthalene adsorption in aqueous solutions," *Environmental Science and Pollution Research*, vol. 27, no. 3, pp. 3329–3337, 2020.

[6] M. He, J. Li, Y. Zhang, and W. Li, "Research on crack visualization method for dynamic detection of eddy current thermography," *NDT & E International*, vol. 116, p. 102361, 2020.

[7] H. Jiang, Z. Liu, C. Liu, Y. Su, and X. Zhang, "Community detection in complex networks with an ambiguous structure

Research Article

Research on Intelligent Recognition and Management of Smart City Based on Machine Vision

Rulin Liu [1] **and Longfeng Liu** [2]

[1]*College of Electronic and Information Engineering, Chongqing Technology and Business Institute, 402160 Chong Qing, China*
[2]*College of Accounting and Finance, Chongqing Technology and Business Institute, 402160 Chong Qing, China*

Correspondence should be addressed to Rulin Liu; einstlin@cqtbi.edu.cn

In recent years, with the rapid development of science and technology, people's demand for the quality of daily production and life has gradually increased, and all localities are gradually urbanized. The convenient use of water conservancy, transportation, environment, medical treatment, power grid and other aspects of cities in any country affects people's healthy life. Therefore, it is urgent to build a smart city. For smart city, intelligent identification and management is a very large and complex problem. As one of the high and new technologies, the intelligent recognition of machine vision derived from artificial intelligence has always been a hot spot of great concern. It just provides convenience for the development of smart city and becomes the development direction of smart city construction in the future. Based on this, the role of machine vision is to connect with the computer through wireless sensors such as cameras to simulate an eye that can represent human visual function. This simulated eye can be recognized intelligently in real time. It transmits the recognized information to the computer, and the computer will analyze and process the obtained information for judgment and recognition. This paper will mainly use the optimal threshold segmentation algorithm based on Machine Vision video processing to solve the problem of urban intelligent recognition, and use a specific algorithm to solve some difficulties and obstacles in intelligent recognition. The traditional optimal threshold segmentation algorithm, the optimal threshold segmentation algorithm and the improved optimal threshold segmentation algorithm are experimentally compared. After experimental comparison, it is found that the optimal threshold segmentation algorithm, the improved optimal threshold segmentation algorithm and the traditional optimal threshold segmentation algorithm can intelligently identify the types of buildings and urban traffic signs in the city, Compared with the improved optimal threshold segmentation algorithm, the improved optimal threshold segmentation algorithm improves the response speed, real-time performance, stability and accuracy of the algorithm. Therefore, the optimal threshold segmentation algorithm after the well meets the needs of building the system, and can be useful in the process of intelligent recognition. This improvement is also necessary, which is conducive to the subsequent system construction.

1. Introduction

With the gradual improvement of people's production and living standards, the convenience of life [1] has become the basic requirement of people's multi city life, and cities cover all aspects, including urban environmental problems [2], urban traffic problems [3], urban population flow problems [4], urban medical problems [5], etc, Intelligent identification [6] and management of all aspects of the city can effectively improve the happy life index [7] of the city Bureau and

provide many conveniences to urban residents. If you want the city to become intelligent [8], you mainly rely on getting information and data from all aspects of the city [9]. People mainly rely on their eyes to obtain the main information [10], but it must be within the visible range of the naked eye, so the information obtained is very little, and the information obtained by human eyes can be said to be insignificant in such a huge range of cities. The development of machine vision technology [11] provides a new idea for building a smart city. Machine vision just solves the problem

of regional limitations [12]. In all parts of the city, the information obtained by human eyes is simulated by camera [13] and other wireless sensor devices [14] and transmitted to computer [15] for processing and analysis. It can realize the functions of guidance, positioning, measurement, detection and recognition. People's eyes obtain information not only through their eyes, but also through their eyes to obtain surface information and transmit it to the brain. The brain operates at high speed to quickly analyze and process the obtained information into deeper information that is easier to understand. Machine vision is based on the principle that human eyes see everything in the world [16]. Wireless sensor devices such as cameras are equivalent to human eyes, build a bridge and send it to the brain behind the computer for rapid analysis and processing, so as to obtain deeper information data behind it. Due to the changeable and complex urban environment, the traditional detection method [17] has a single feature, and machine vision divides the urban area [18]. For the method based on single frame image, the single frame image algorithm [19] is used for detection and recognition, with fast processing speed; Based on the method of stereoscopic reference [20], images from different angles are captured from multiple cameras with different vision. Machine vision has obvious advantages over traditional vision. Compared with traditional manual detection, human eye judgment is subjective and sometimes makes mistakes. Machine vision can eliminate the interference of human subjective factors and avoid the detection results that vary from person to person. Not only that, it can also quantitatively analyze and describe the indexes of the tested objects [21], which reduces the detection and classification error and improves the efficiency and accuracy. Build a smart city to achieve healthy, reasonable and sustainable economy, harmonious, safe and more comfortable life, and intelligent information technology in management.

Nowadays, with the rapid development of science and technology, all aspects of people are gradually becoming intelligent, so the construction of smart city is urgent.

2. Machine Vision Endows Smart City

2.1. Smart City.
Smart cities integrate information technology or innovative technology into urban construction, open and integrate urban systems and services, improve resource utilization efficiency, optimize urban governance service system and improve citizens' quality of life. Smart city construction includes intelligent technology, intelligent industry and intelligent application. It is mainly reflected in transportation, power grid, medical treatment, environmental protection and many other aspects. The basic architecture of smart city is shown in Figure 1 below:

There are four aspects to build a smart city. One is the decision support system, including data mining and scenario analysis; Second, the operation and management system, including smart government affairs, smart commerce, etc; The third is shared service facilities, through service-oriented architecture such as cloud computing, and the fourth is data infrastructure, including basic database and thematic database; The last is the network infrastructure, including wireless communication network, optical fiber communication network and so on.

The former can comprehensively and deeply perceive. Through sensor technology, various sensor devices and intelligent systems are used for intelligent identification and three-dimensional perception, timely and actively analyze and process information such as urban environmental changes, so as to realize real-time perception of urban environment, improve urban environmental perception ability, and ensure the normal and efficient operation of various systems. The second is ubiquitous broadband connection. As a neural network in the smart city, it can be carried out randomly on demand to enhance the ability of urban intelligent service; The third is intelligent integration application, which integrates people's wisdom through a new generation of perception technology, creates a smart city brain, promotes the combination of cloud and end, and promotes the intelligent integration of various application facilities; Fourth, people-oriented continuous innovation. Smart city construction is people-oriented and citizens participate. Gather the strength of the masses, proceed from the needs of the masses, cooperate and innovate, and jointly build an emerging city to achieve sustainable economic, social and environmental development. The machine vision algorithm generally has the method based on single frame image. The single frame image algorithm is used for detection and recognition, and the processing speed is fast; based on the stereo method, images from different angles are captured from multiple cameras with different vision.

2.2. Machine Vision Technology.
The main principle of machine vision is to analyze and process the image information obtained by wireless sensor devices such as cameras and transmit it to the computer for in-depth analysis. The neural network is constructed by the method of deep learning, and the massive image data are learned to realize the accurate analysis of the object to be measured, and finally can be used for actual detection, measurement and control. Generally speaking, it is to simulate an eye that can represent human visual function by computer. It can realize the functions of guidance, positioning, measurement, detection and recognition. Machine vision technology has the advantages of high speed, large amount of information and many functions. It can basically complete high-intensity and complex computing work in any scene. A typical machine vision system is shown in Figure 2 below:

As shown in Figure 2, the machine vision system can enable the optical image system and image capture system to identify, analyze and process in the intelligent execution module through image acquisition and digitization and intelligent workstation. Machine vision technology can quickly and accurately capture a large number of signals, which is convenient for automatic processing and processing control information concentration. Compared with traditional manual measurement, it can eliminate the negative impact of various factors of individual subjects, avoid measurement varying from person to person, and make quantitative analysis and description of the indicators of measured objects, so as to reduce the classification error of
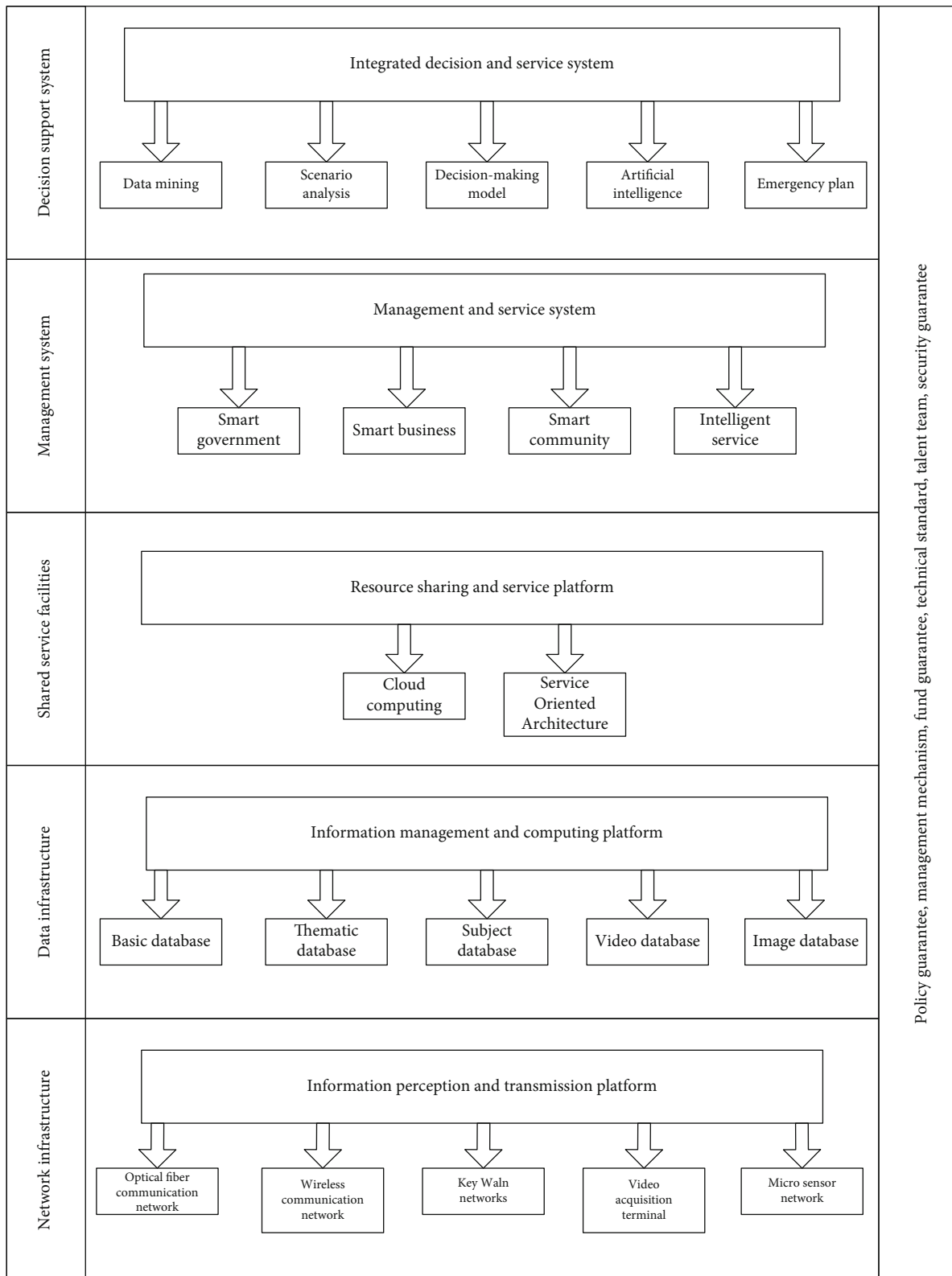
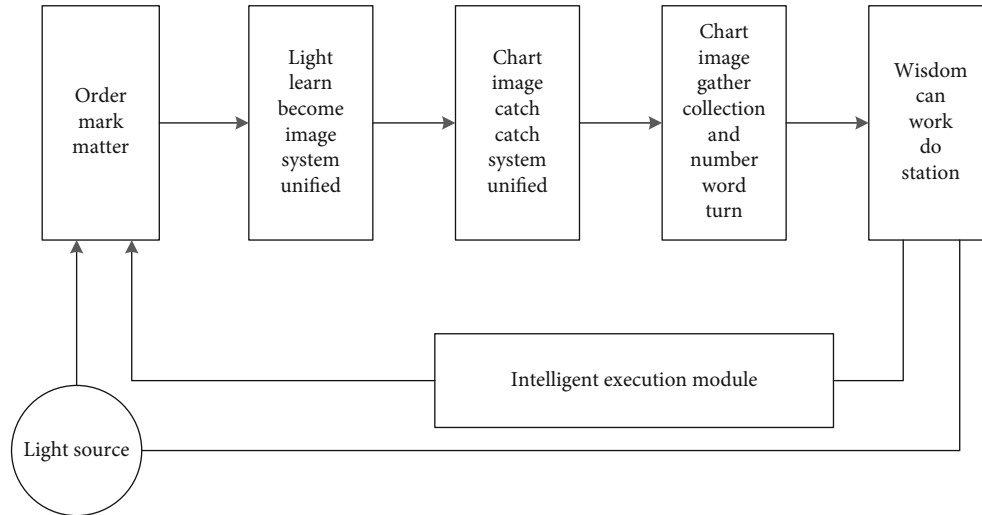FIGURE 1: Basic architecture of smart city.

```
┌──────────┐     ┌──────────┐     ┌──────────┐     ┌──────────┐     ┌──────────┐
│          │     │  Light   │     │  Chart   │     │  Chart   │     │          │
│          │     │  learn   │     │  image   │     │  image   │     │ Wisdom   │
│  Order   │     │  become  │     │  catch   │     │ gather   │     │   can    │
│  mark    │ ──► │  image   │ ──► │  catch   │ ──► │collection│ ──► │  work    │
│  matter  │     │  system  │     │  system  │     │   and    │     │   do     │
│          │     │  unified │     │  unified │     │  number  │     │ station  │
│          │     │          │     │          │     │   word   │     │          │
│          │     │          │     │          │     │   turn   │     │          │
└──────────┘     └──────────┘     └──────────┘     └──────────┘     └──────────┘
```

Figure 2: Typical machine vision system.

measurement and improve efficiency and accuracy. Building an intelligent city will realize healthy, reasonable and sustainable enterprise operation, harmonious, safe and more comfortable people's life, scientific, intelligent and information-based management.

2.3. Urban road Intelligent Recognition Technology. For the construction of a smart city, the intellectualization of urban roads is an important branch, especially important. It is a basic project, which has an important impact on people's production and life. Therefore, due to the high automation of pavement, people can more friendly solve the practical social problems such as urban traffic congestion, events, air pollution and so on. The main function of machine recognition technology is road identification and tracking. First, identify the road marking line in front, the curvature in the horizontal direction of the road and the road surface with correct marking for the driving of motor vehicle lane; Identify the pavement boundary, the curvature of the horizontal pavement and the location and orientation of the motor vehicle lane boundary on the road surface without indication; Identify the use of lane change in the front or adjacent sections; Using pavement boundary characteristics to provide real-time processing, monocular vision to identify and track large objects in the front section, and to evaluate the movement of vehicles in front through monitoring and tracking; The pitch angle of visual inspection is used to enhance the accuracy of pavement boundary characteristics evaluation; By monitoring and tracking the movement of other vehicles in adjacent sections, high-speed manual driving is used; By detecting the intersection, we can know its length and locate the center position, which can be used to control the road turning behavior; Using color image to identify road markings can improve the poor real-time performance; Real time performance can be achieved by distinguishing the relative motion of mobile Walker and automatic vehicle; Determine whether there are motor vehicles and the safe lane change by detecting the front and rear motor lanes; Finally, by analyzing the decline of image con-

trast, the field of view can be estimated in foggy days. That is, Figure 3 shows the key technologies of urban road detection, and Figure 4 shows the system flow chart:

According to the system flow chart, this intelligent recognition technology first loads the image of the detected Road, then carries out image preprocessing and processing, generates road information according to the processing results, and finally stores the information.

2.3.1. Filtering of road Image. An original image that has not been processed has some problems such as noise interference to some extent, because these noise interference affect the quality of the image, resulting in the image becoming blurred and unclear, and the key feature points of the image to be detected become difficult to find. In this case, it becomes very difficult to analyze and process the image. The purpose of image smoothing is to eliminate the interference factors on the image. This method is also called low-pass filtering. The main purpose of this algorithm is to carry out spatial filtering algorithm. Generally, spatial filtering algorithm superimposes several signals within a certain spatial range and occupies the same frequency band.

Kalman filtering algorithm uses the linear state equation to optimally estimate the influence of noise interference in the obtained data. It is conducive to computer programming and is the most widely used filtering method. The algorithm estimates the real-time data and the corresponding state of the previous moment, and recurses through the system state transition equation. For any dynamic system, Kalman filtering model can be divided into state and observation equations:

$$X_k = F_{k/k-1}X_{k-1} + G_{k-1}W_{k-1} \tag{1}$$

$$L_k = H_k X_k + V_k \tag{2}$$

Where X_k represents the n-1 order state vector at time k, L_k represents the m-1 order state vector at time k, G_{k-1} represents the system time $n \times m$ Dynamic noise matrix of
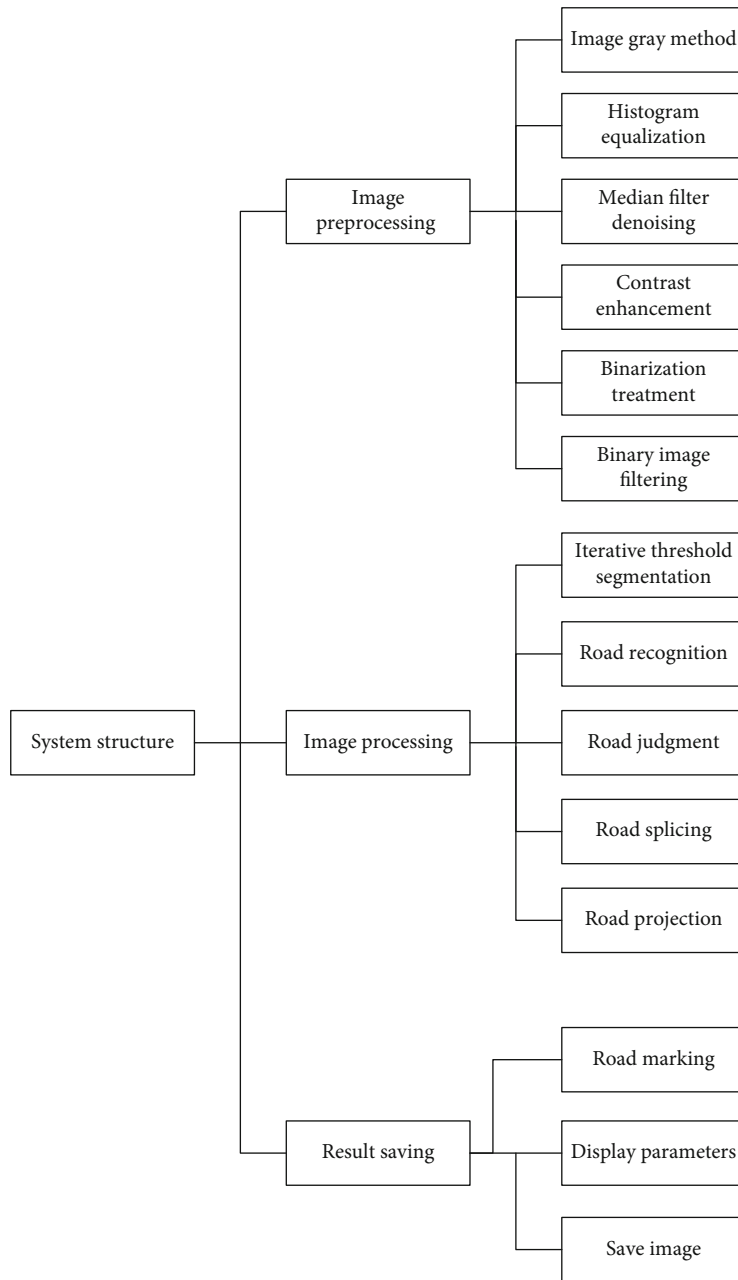
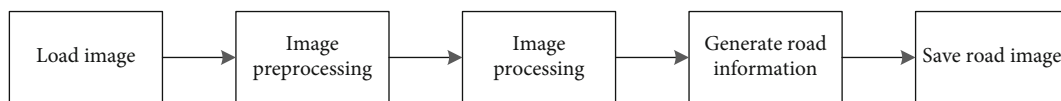FIGURE 3: Key technologies of urban road detection.

FIGURE 4: System flow chart.

order r, $F_{k/k-1}$ indicates that the system changes from time k-1 to time k n×n order state transition matrix, V_k represents the observation noise of order m-1 at time k of the system, H_k represents the system K time m×n order observation matrix. Set W_k is dynamic noise, V_k is the observation nois.

BP network can also be called back propagation neural network. Its structure can be simply divided into three layers: feedforward, multi-layer and perceptron network. This algorithm repeatedly trains the collected sample data, and constantly modifies the network weight and threshold to minimize the error and achieve the desired goal for the output data. BP generally includes input layer, middle layer (hidden layer) and output layer. Each layer consists of several neuron groups and is completely connected with the previous layer by switching weights. In the input layer, when

TABLE 1: Steps of fast median filtering.

Step	Implementation method
First step	Establish a $(2n+2) \times (2n+1)$ filter window and move 2 steps along the image line sequence
Step 2	After each move, first sort all elements in the window to get the $(2n+2) \times (2n+1)$ element sequence
Step 3	Using $(2n+1)$ elements other than $((2n+1) \times (2n+1))$, respectively, move the median pointer by the method described above to obtain the last median pointer;
Step 4	Go to the first window element and carry out one, two or three steps for the whole image in order until the end.
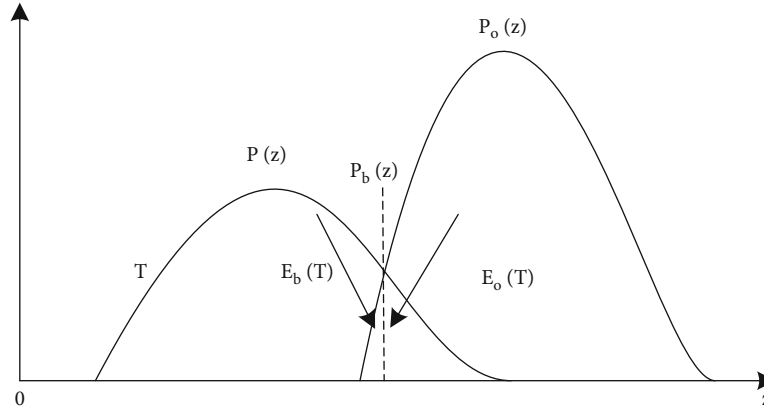
FIGURE 5: Schematic diagram of optimal threshold selection.

TABLE 2: δ interval and number of samples.

δ interval of	Number of samples	δ interval of	Number of samples
[5, +)	0	[-0.75, -0.25)	988
[4,5)	0	[-1.25, -0.75)	128
[3,4)	8	[-2, -1.25)	32
[2,3)	14	[-3, -2)	18
[1.25,2)	27	[-4, -3)	6
[0.75,1.25)	124	[-5, -4)	0
[0.25,0.75)	891	[-4, -)	0
[-0.25,0.25)	2764		

an input neuron receives a signal, it is transmitted to each neuron in the middle layer (hidden layer). In the middle layer (hidden layer), each neuron calculates the sum, and then the nonlinear activation function is used to generate the output signal and transmit it to the output layer. The processing of the last message transmitted to the output stage, that is, the subsequent upward increase, is considered to have been completed, and the starting layer is responsible for displaying the results to the outside world. If an actual loss occurs and the output does not match the expected output, an error return multiplication process needs to be performed. Output error starts from the output, adjusts and updates the weight and threshold of each layer, and gradually converts the transmission to the middle layer and input

layer. The process of repeated information forward expansion and error recovery is to adjust the weight of each layer of the whole neural network.

In the calculation process, only when the set training times or the calculated global network error is less than the general value, if the global error accuracy error is very small, the whole learning process of the algorithm ends. If you are not satisfied with the results, you must update the training mode. A round of learning process runs again until the final conditions are met, and the BP three-layer network model can meet the requirements of high precision.

Kalman algorithm and BP algorithm have their own advantages. They are widely used in many fields such as machine vision technology and have very high practical value. However, there are still some deficiencies in the application of these two algorithms to the construction of smart city. For example, Kalman algorithm must be based on the existing accurate model and existing data for calculation. For large and complex systems, the establishment of accurate model and data acquisition are not so easy, and the measurement accuracy can not be realized. BP algorithm can meet the needs of high precision, but it has some problems, such as small part, slow speed and weak ability to external interference. In order to avoid these problems, the gray value of the image must be processed first:

$$f(x, y) = \frac{1}{M} \sum_{(x,y) \in S} f(x, y) \tag{3}$$

In formula (1), the processing of image details is also weakened. Therefore, the combination of average method

TABLE 3: Specific implementation method of improved optimal threshold segmentation algorithm.

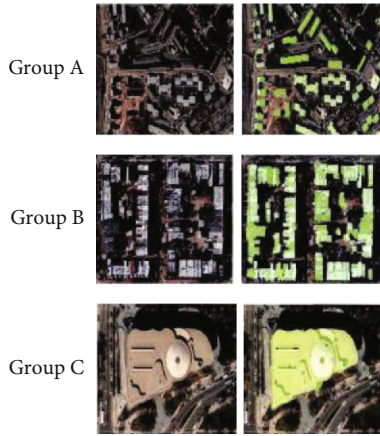| Step	Implementation method
First step	The system is initialized and the initial image is segmented row by row and column by column using the traditional optimal threshold segmentation algorithm
Step 2	Use T_i^0 segment the next frame image to get T
Step 2	To T_i^0 is assigned T, and the second step is repeated

Group A

Group B

Group C

FIGURE 6: Intercepted images.

and weighted average method can improve the problem of image detail blur. The expression is:

$$g(m, n) = \sum_{i=-M}^{M} \sum_{j=-N}^{N} W(i, j) f(m - i, n - j) \quad (4)$$

In publicity (2), w (i,j) represents the value to be weighted for the corresponding pixel, which can be changed appropriately as needed. Generally speaking, in order to keep the average gray value of the processed image unchanged, the sum of each coefficient in the template is 1.

Median filtering, this algorithm can simultaneously remove the noise of the image and protect the image target boundary from being blurred. The nonlinear processing technology is adopted, and its expression is:

$$f(x, y) = \text{median}\left\{S_{f(x,y)}\right\} \quad (5)$$

Where s is the field of point (x, y).

The steps of fast median filtering can be divided into 5 steps, as shown in Table 1 below:

Compared with the traditional median filter, the fast median filter algorithm can find the median of two windows in one arrangement, and the processing speed is also significantly improved. However, in the process of use, it should be noted that the window size should be appropriate, and too large window will also lead to the loss of effective signal, which will increase significantly.

This involves four concepts: shape sum, shape difference, shape opening and shape closing. Shape opening is expan-

sion state and shape difference is corrosion state

$$F, G \subseteq E^2, f(x, y) \quad (6)$$

I.e. form and (expansion):

$$f \oplus g(x, y) = \max (i, j)[f(x - i, y - j) + g(i, j)] \quad (7)$$

Poor morphology (corrosion):

$$f \ominus g(x, y) = \min (i, j)[f(x - i, y - j) + g(i, j)] \quad (8)$$

Form on:

$$f \circledcirc g(x, y) = f \oplus g[f \ominus g(x, y)] \quad (9)$$

Morphological closure:

$$f \odot g(x, y) = f \ominus g[f \oplus g(x, y)] \quad (10)$$

For the shape, because the shape on and shape off have the corresponding smoothing function, the singular points in the shape can be detected. Shape opening can remove all edge burrs and isolated patches in the image,

2.3.2. Image Edge Extraction. The identification of image boundary information is a key attribute to obtain image features in image recognition. It exists in the target, target, background and region. It is very key in image analysis and human vision. Generally, the boundary of the image is divided into two characteristics: orientation and amplitude. The image changing along the boundary orientation is uniform, while the image perpendicular to the boundary orientation changes sharply. The boundary detection operator checks the neighborhood between pixel points and measures the gray change rate. It also includes the definition of orientation and the way of convolution using directional derivative or mask. Robert boundary detection operator is also an operator that uses local difference operator to find pixel boundary. Its expression is:

$$G[[f(x, y)] = \sqrt{[f(x, y) - f(x - 1, y - 1)]^2 + [f(x - 1, y) - f(x, y - 1)]^2} \quad (11)$$

Where f (x, y) is an input image with integer pixel coordinates.

2.4. Optimal Threshold Segmentation Algorithm. When processing the image, we will pay attention to the conspicuous part of the image, and ignore other details. However, the
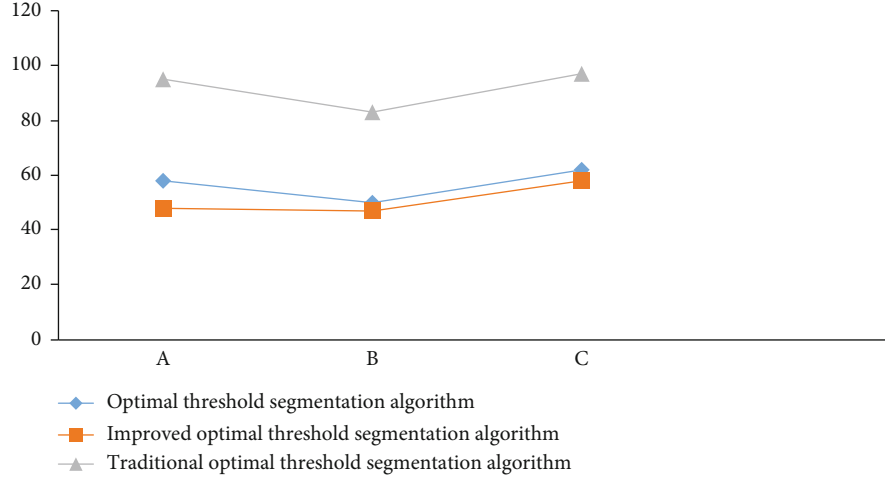
FIGURE 7: Running time.

neglected parts may also have corresponding characteristic meanings. For the overall graph, they can be called the foreground or target of the graph, while other parts of the graph that are not interested are called the background of the overall graph, which is the graph segmentation task. To segment the picture, the first step is to divide the picture into several special regions in advance. These regions should have special properties, and then extract the key targets. This method is threshold segmentation. The first key of the threshold segmentation algorithm is to set the threshold points first, and compare the threshold with the gray value on the pixel points one by one, while the image cutting expands each image in parallel, and the cutting results can directly obtain the image area. In the process of segmentation, we hope to reduce false segmentation as much as possible, so the optimal threshold method can just avoid this problem. Shown in Figure 5 below:

$$p(z) = P_b p_b(z) + P_o p_o(z)$$

$$p(z) = \frac{P_b}{\sqrt{2\pi}\sigma_b} \exp\left[-\frac{(z-\mu_b)^2}{2\sigma_b^2}\right] + \frac{P_o}{\sqrt{2\pi}\sigma_o} \exp\left[-\frac{(z-\mu_o)^2}{2\sigma_o^2}\right]$$
$$(12)$$

If $\mu_b < \mu_o$,

$$E_b(T) = \int_{-\infty}^{T} p_o(z)dz$$
$$E_o(T) = \int_{T}^{\infty} p_b(z)dz$$
$$(13)$$

Then the total error probability is:

$$E(T) = P_o E_b(T) + P_b E_o(T) \qquad (14)$$

In order to minimize the threshold of the error, e (T) can be derived from t so that the derivative is zero, and the noise

of the whole image comes from the same noise source, then:

$$\sigma_b = \sigma_o \qquad (15)$$

Then you can get:

$$T = \frac{\mu_b + \mu_o}{2} + \frac{\sigma^2}{\mu_b - \mu_o} \ln\left(\frac{P_o}{P_b}\right) \qquad (16)$$

Verification probability $P_b = P_o$ Or the noise variance is 0, then:

$$T = \frac{\mu_b + \mu_o}{2} \qquad (17)$$

3. Improved Algorithm of Optimal Threshold Segmentation

In the optimal threshold segmentation algorithm, in order to solve this problem, each row and column of the image are regarded as an image unit, respectively, and the impact of the change of contrast will be greatly reduced. However, when a row or a column of pixels is used as a pixel unit, it will take a lot of time to complete the parameter comparison of the mixed probability density function between the target and the background, which will greatly increase the pressure of the system, and the corresponding real-time performance will become worse. Then the algorithm for improving the optimal prediction threshold will clarify the definition of the optimal prediction threshold, But at the same time, it also increases the real-time performance of calculation. First, the initial value of the threshold value shall be initially divided, and its expression is:
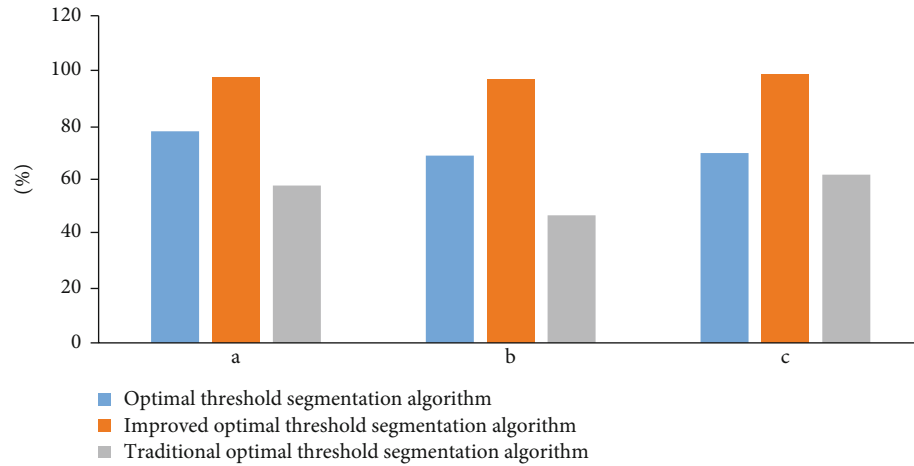
$$T = \frac{T_{\min} + T_{\max}}{2} \qquad (18)$$

FIGURE 8: Recognition accuracy.

TABLE 4: Identification and detection results of three algorithms.

Serial number	Optimal threshold segmentation algorithm		Improved optimal threshold segmentation algorithm		Traditional optimal threshold segmentation algorithm	
	Recognition accuracy	Running time (MS)	Recognition accuracy	Running time (MS)	Recognition accuracy	Running time (MS)
A	78%	58	98%	48	58%	95
B	69%	50	97%	47	47%	83
C	70%	62	99%	58	62%	97

Then iterate:

$$T = \frac{u_1 + u_2}{2} \tag{19}$$

3.1. Concept of Optimal Threshold in Segmentation. In general, the pixel gray distribution of the image follows the normal distribution $X \sim N(\mu, \sigma^2)$ Where x is the gray sample population. Then the confidence is:

$$1 - \alpha = 0.995 \tag{20}$$

The confidence interval of gray value obtained can be identified as the interval of gray value:

$$\left[\text{Int}^- \left(\bar{X} - u_{\alpha/2} \sqrt{\frac{S^2}{n}} \right), \text{Int}^+ \left(\bar{X} + u_{\alpha/2} \sqrt{\frac{S^2}{n}} \right) \right] \tag{21}$$

Overall mean:

$$\bar{X} = \frac{1}{n} \sum_{i=0}^{n} x_i \tag{22}$$

Where x_i is the sample, n is the number of samples, as μ Estimate of. be σ^2 The estimated value of 2 is:

$$S^2 = \frac{1}{n-1} \sum_{i=0}^{n} (x_i - \bar{X})^2 \tag{23}$$

Group A

Group B

Group C

FIGURE 9: Image data.

last:

$$T = \text{Int}^+ \left(\bar{X} + u_{\alpha/2} \sqrt{\frac{S^2}{n}} \right) + 1 \tag{24}$$

TABLE 5: Identification and detection results of three algorithms.

Serial number	Optimal threshold segmentation algorithm		Improved optimal threshold segmentation algorithm		Traditional optimal threshold segmentation algorithm	
	Recognition accuracy	Running time (MS)	Recognition accuracy	Running time (MS)	Recognition accuracy	Running time (MS)
A	85%	69	99%	58	61%	95
B	78%	77	97.9%	56	53%	83
C	79%	93	99.5%	63	64%	97
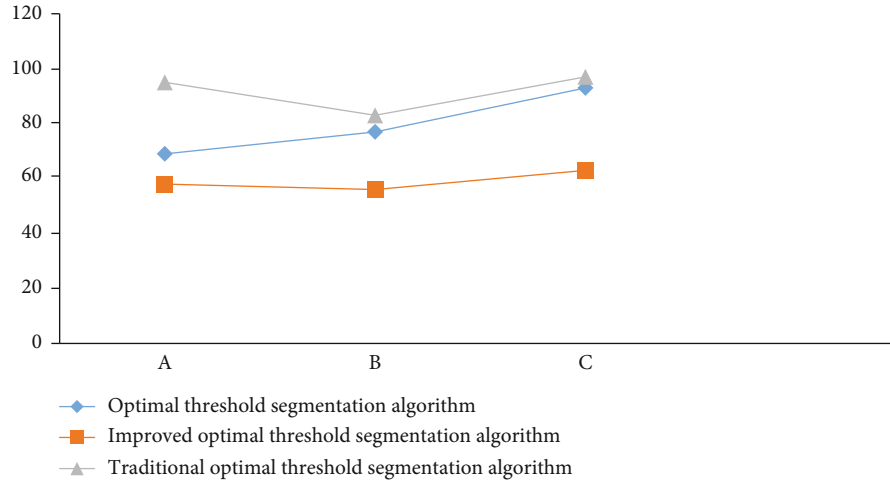
FIGURE 10: Running time.
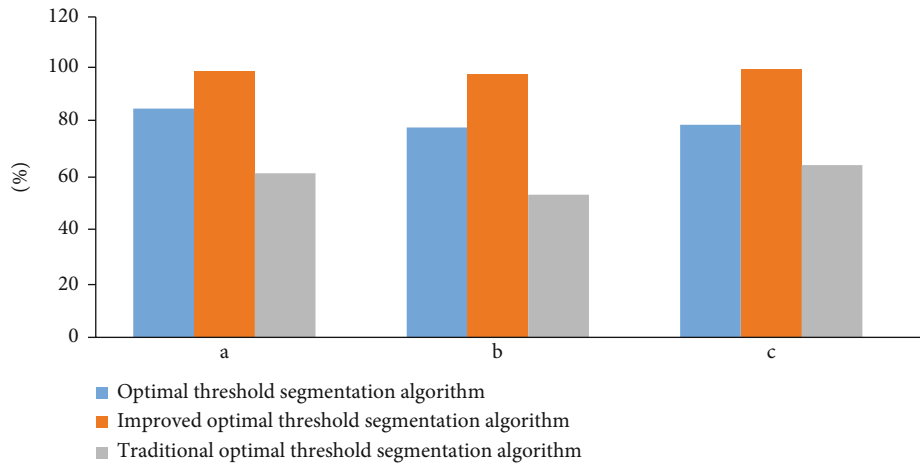
FIGURE 11: Recognition accuracy.

3.2. Improved Optimal Threshold Segmentation Algorithm for Sequential Images. At this time, the light of two light sources is fixed, and the light of two images is fixed, then make:

$$T_i (i = 90, \wedge, 239)$$
$$T_i^* ((i = 90, \wedge, 239) \tag{25}$$

Where T_i and T_i^* The relative error of is:

$$\delta = \frac{T_i - T_i^*}{T_i} \times 100\% \tag{26}$$

For this algorithm, extract δ 5000 independent samples of δ It is divided into 15 sections, as shown in Table 2 below: As shown in Table 3 below:
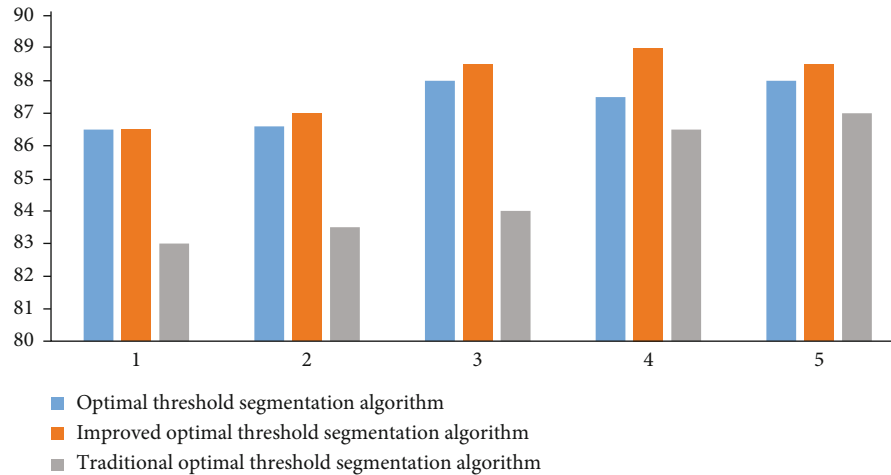
FIGURE 12: Experimental data results.

TABLE 6: Accuracy results of three algorithms.

Algorithm	Accuracy
Optimal threshold segmentation algorithm	98.61%
Improved optimal threshold segmentation algorithm	99.95%
Traditional optimal threshold segmentation algorithm	94.25%

4. Experimental Simulation

In order to test the accuracy and operation speed of the algorithm of the development system, the optimal threshold segmentation algorithm, the improved optimal threshold segmentation algorithm and the traditional optimal threshold segmentation algorithm are used to intelligently identify the types of urban buildings and urban traffic signs. Urban buildings can generally be divided into civil buildings, industrial buildings and agricultural buildings, Civil buildings can be subdivided into residential buildings and public buildings; Urban traffic signs can generally be divided into seven categories: warning signs, prohibition signs, indication signs, direction signs, tourist area signs, road construction safety signs and auxiliary signs.

4.1. Intelligent Recognition of Urban Building Types. This experiment will be divided into three groups for recognition. The above three algorithms will recognize and analyze the images intercepted in the aerial view of urban buildings. The intercepted images are shown in Figures 6–8:

From the Table 4, comparing the three algorithms, the slowest running speed of the improved optimal threshold segmentation algorithm is 58 MS/frame, the fastest is 47 MS/frame, and the average running speed is 50 ms/frame; The slowest running speed of the optimal threshold segmentation algorithm is 62 MS/frame, the fastest is 50 ms/frame, and the average running speed is 56 ms/frame; The slowest running speed of traditional threshold segmentation algorithm is 97 ms/frame, the fastest is 83 ms/frame, and the average running speed is 92 ms/frame. In the recognition accuracy, the improved optimal threshold segmentation algorithm also has the highest accuracy. Therefore, the optimal threshold segmentation algorithm is the best regardless of the real-time and accuracy of detection.

4.2. Intelligent Identification of Urban road Sign Types. They will be divided into three groups for identification, and the urban road sign images will be intercepted for identification and analysis. The intercepted road sign images are shown in Figure 9 below:

The detection results of the three algorithms are shown in Table 5, Figures 10 and 11.

From the experimental data, the recognition results and running speed of the improved optimal threshold segmentation algorithm are more accurate and faster than the other two algorithms. The slowest running speed of the optimal threshold segmentation algorithm is 93 ms/frame, the fastest is 69 ms/frame, and the average running speed is 73 ms/frame; The average running speed of the improved optimal threshold segmentation algorithm is 59 MS/frame; The average running speed of the traditional threshold segmentation algorithm is 91 MS/frame. In the recognition accuracy, the improved optimal threshold segmentation algorithm also has the highest accuracy. Therefore, the optimal threshold segmentation algorithm is the best regardless of the real-time and accuracy of detection.

4.3. Compare the Response Speed of the Three Algorithms. In order to verify the real-time and accuracy of the improved optimal threshold segmentation algorithm, the improved optimal threshold segmentation algorithm will be compared with the improved optimal threshold segmentation algorithm and the traditional optimal threshold segmentation algorithm. The experimental environment will be in CPU: PIV 1.7 g; Memory: 512 M; The image size is 320×240.

When building the system, the algorithm is the foundation and foundation of a system. The response speed of the algorithm determines the quality of the system. Therefore, it is also very important to compare the response speed of the algorithm. Five groups of experiments will be conducted, with no unit of milliseconds. The experimental data results are shown in Figure 12 below:
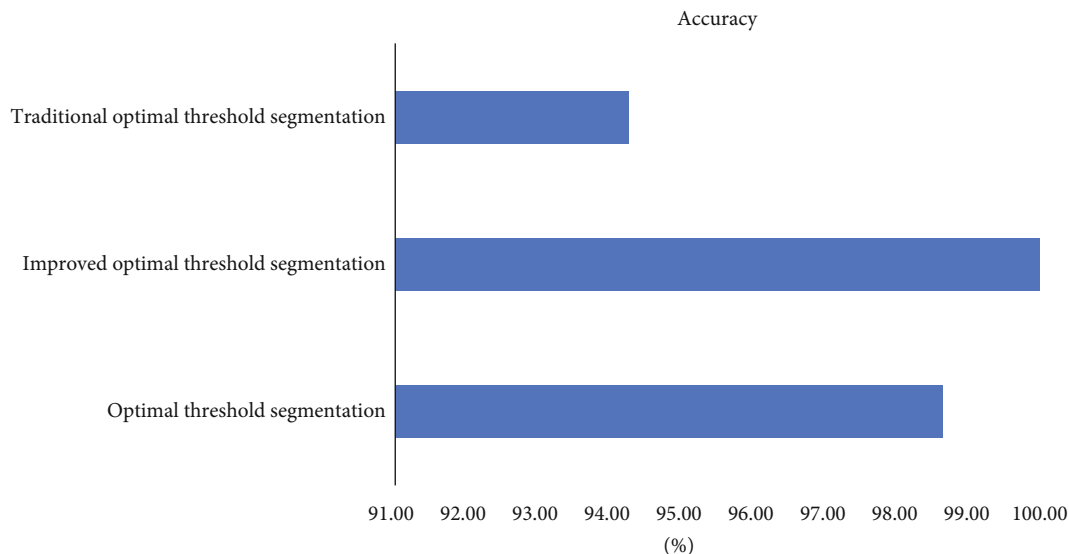
FIGURE 13: Accuracy rate of frame number of processed image.

The improved optimal threshold segmentation algorithm also has the lowest response time.

The accuracy results of the three algorithms are shown in Table 6 and Figure 13:

In terms of the accuracy of the number of processed image frames, the improved optimal threshold segmentation algorithm has higher accuracy than other traditional optimal threshold segmentation algorithms and the improved optimal threshold segmentation algorithm, and the processing accuracy is also increasing according to the increase of the number of processed frames. The accuracy of the improved optimal threshold segmentation algorithm is higher than other traditional optimal threshold segmentation algorithms and the improved optimal threshold segmentation algorithm, and the processing accuracy is also increasing according to the increase of the number of processing frames.

4.4. Evaluation Results. In this experiment, the algorithm intelligent recognition experiment is carried out under the rainy and sunny conditions, as well as the congestion and unblocked conditions of road conditions in the urban environment. Rainy days, low visual conditions, sunny days, high visibility; Road congestion has a certain impact on the response time and accuracy of intelligent identification algorithm, but the improved optimal threshold segmentation algorithm in this paper is better than the other two algorithms, so the improved algorithm is very necessary for building the system.

For different scenarios, the accuracy of the improved optimal threshold segmentation algorithm is greatly improved. Compared with the unmodified optimal threshold segmentation algorithm, it is improved in terms of algorithm response speed, real-time performance, algorithm stability and accuracy. Therefore, the optimal threshold segmentation algorithm after the well meets the needs of building the system, and can be useful in the process of intelligent recognition. This improvement is also necessary, which is conducive to laying the foundation for the subsequent system construction.

5. Conclusion

After the analysis of the above four stages, first of all, the intelligent identification and management construction of smart city will be of great help to people's production and living. It is very convenient for people and can effectively improve the quality of life. For smart city intelligent identification management, this is indeed a very large and complex project. It can not be completed only by relying on people's hands in many aspects such as urban environment, roads, transportation and so on. Machine vision is the crystallization of human wisdom. As a branch of artificial intelligence, it collects and analyzes all kinds of information in the city by means of wireless sensor devices, and solves a great problem. As one of the emerging technologies, machine vision will also become a hot research object in the future. It can be applied not only to the construction of smart cities, but also to many large manufacturing industries such as industrial manufacturing, which can provide great help in economic development and construction.

Nevertheless, today, with the development of science and technology, the existence of artificial intelligence can be felt only in the first and second tier cities. For cities with slightly backward development, artificial intelligence is not so common. Therefore, in the future, scientific and technological innovation still needs continuous efforts and learning, so as to stand first in the world and truly improve people's quality of life, Therefore, the development of machine vision still has a long way to go.

Data Availability

The experimental data used to support the findings of this study are available from the corresponding author upon request.

Conflicts of Interest

The authors declared that they have no conflicts of interest regarding this work.

Acknowledgments

References

[1] C. S. Fischer, "The public and private worlds of city life," *American Sociological Review*, vol. 46, no. 3, pp. 306–316, 1981.

[2] J. E. Hardoy, D. Mitlin, and D. Satterthwaite, *Environmental Problems in an Urbanizing World*, Earthscan, London, UK, 2001.

[3] S. Salcedo-Sanz, L. Cuadra, E. Alexandre-Cortizo, S. Jiménez-Fernández, A. Portilla-Figueras, and E. Alexandre-Cortizo, "Soft-Computing: An innovative technological solution for urban traffic-related problems in modern cities," *Technological Forecasting and Social Change*, vol. 89, pp. 236–244, 2014.

[4] A. M. Sobolev and S. Deguchi, "Pump cycles and population flow networks in astrophysical masers: an application to class II methanol masers with different saturation degrees," *The Astrophysical Journal*, vol. 433, no. 2, pp. 719–724, 1994.

[5] A. Al-Motarreb, M. Al-Habori, and K. J. Broadley, "Khat chewing, cardiovascular diseases and other internal medical problems: The current situation and directions for future research," *Journal of Ethnopharmacology*, vol. 132, no. 3, pp. 540–548, 2010.

[6] M. Jo and H. Y. Youn, "Intelligent recognition of RFID tag position," *Electronics Letters*, vol. 44, no. 4, pp. 308-309, 2008.

[7] A. P. Mller, "Successful city dwellers: a comparative study of the ecological characteristics of urban birds in the Western Palearctic," *Oecologia*, vol. 159, no. 4, pp. 849–858, 2009.

[8] J. Pearl, "Probabilistic reasoning in intelligent systems: networks of plausible inference (Judea pearl)," *Artificial Intelligence*, vol. 48, no. 8, pp. 117–124, 1990.

[9] B. Yu, H. Liu, J. Wu, Y. Hu, and L. Zhang, "Automated derivation of urban building density information using airborne LiDAR data and object-based method," *Landscape & Urban Planning*, vol. 98, no. 3-4, pp. 210–219, 2010.

[10] R. J. Bootsma, S. Ledouit, R. Casanova, and F. T. J. M. Zaal, "Fractional-order information in the visual control of lateral locomotor interception," *Journal of Experimental Psychology: Human Perception and Performance*, vol. 42, no. 4, pp. 517–529, 2016.

[11] V. Satti, A. Satya, and S. Sharma, "An automatic LEAF recognition system for plant identification using machine vision technology," *International Journal of Engineering Science & Technology*, vol. 5, no. 4, pp. 874–879, 2013.

[12] Z. Zhang, "A flexible new technique for camera calibration," *IEEE Transactions on Pattern Analysis and Machine Intelligence*, vol. 22, no. 11, pp. 1330–1334, 2000.

[13] T. Overly, G. Park, K. M. Farinholt, and C. R. Farrar, "Development of an extremely compact impedance-based wireless sensing device," *Smart Materials and Structures*, vol. 17, no. 6, 2008.

[14] R. I. Hartley and A. Zisserman, "Multi-view geometry in computer vision," *Kybernetes*, vol. 30, no. 9/10, pp. 1865–1872, 2019.

[15] D. Sanai, "You should see it on a Friday night what kind of people would you expect to see on a typical street corner of Britain such as this one? Shoppers, schoolchildren and pensioners by day, certainly. But after Darkthe pubs empty and then the fighting starts," *Journal of the Society of Materials Science Japan*, vol. 27, pp. 1158–1164, 1978.

[16] H. Luo, L. Chen, Z. Li, Z. Ding, and X. Xu, "Frontal immunoaffinity Chromatography with Mass Spectrometric Detection: A method for finding active compounds from Traditional Chinese Herbs," *Analytical Chemistry*, vol. 75, no. 16, pp. 3994–3998, 2003.

[17] C. S. Fuh, S. W. Cho, and K. Essig, "Hierarchical color image region segmentation for content-based image retrieval system," *IEEE Transactions on Image Processing*, vol. 9, no. 1, pp. 156–162, 2000.

[18] Y. Yitzhaky, "Restoration of an image degraded by vibrations using only a single frame," *Optical Engineering*, vol. 39, no. 8, pp. 2083–2091, 2000.

[19] C. Zhou and J. Zhou, "Single-Frame Remote Sensing Image Super-Resolution Reconstruction Algorithm Based on Two-Dimensional Wavelet," in *2018 IEEE 3rd International Conference on Image, Vision and Computing (ICIVC)*, pp. 360–363, Chongqing, China, 2018.

[20] N. Inaba, K. Ueda, and S. Yamauchi, "Magnified stereoscopic radiography of the skull (II. Radiographic Technology for Stereoscopic Magnification)," *Japanese Journal of Radiological Technology*, vol. 39, no. 3, pp. 333–336, 1983.

[21] J. Taube, R. Muller, and J. Ranck, "Head-direction cells recorded from the postsubiculum in freely moving rats. I. Description and quantitative analysis," *Journal of Neuroscience*, vol. 10, no. 2, pp. 420–435, 1990.

Retraction

Retracted: Model Analysis of Applying Computer Monitoring to College Students' Mental Health

Journal of Sensors

This article has been retracted by Hindawi following an investigation undertaken by the publisher [1]. This investigation has uncovered evidence of one or more of the following indicators of systematic manipulation of the publication process:

(1) Discrepancies in scope
(2) Discrepancies in the description of the research reported
(3) Discrepancies between the availability of data and the research described
(4) Inappropriate citations
(5) Incoherent, meaningless and/or irrelevant content included in the article
(6) Peer-review manipulation

The presence of these indicators undermines our confidence in the integrity of the article's content and we cannot, therefore, vouch for its reliability. Please note that this notice is intended solely to alert readers that the content of this article is unreliable. We have not investigated whether authors were aware of or involved in the systematic manipulation of the publication process.

Wiley and Hindawi regrets that the usual quality checks did not identify these issues before publication and have since put additional measures in place to safeguard research integrity.

We wish to credit our own Research Integrity and Research Publishing teams and anonymous and named external researchers and research integrity experts for contributing to this investigation.

The corresponding author, as the representative of all authors, has been given the opportunity to register their agreement or disagreement to this retraction. We have kept a record of any response received.

References

[1] S. Mao and S. Liu, "Model Analysis of Applying Computer Monitoring to College Students' Mental Health," *Journal of Sensors*, vol. 2022, Article ID 4960465, 9 pages, 2022.

Research Article

Model Analysis of Applying Computer Monitoring to College Students' Mental Health

Shufang Mao [1] and Shengmin Liu [2]

[1]*Mental Health Education and Guidance Center, Zhejiang Financial College, Hangzhou 310018, China*
[2]*Department of Psychology, School of Teacher Education, Huzhou University, Huzhou 313000, China*

Correspondence should be addressed to Shufang Mao; 161847246@masu.edu.cn

In the past 20 years, although there are many achievements in the model analysis and research, there are still problems of low data utilization and low accuracy. This paper analyzes the mental health level of college students based on chaotic algorithm. At the same time, the application of computer monitoring algorithm to students' real life psychology is discussed. According to different types of mental health analysis models, the high-precision matching analysis of different students is realized. At the same time, according to the personality characteristics and psychological changes of different students, the model is established and analyzed. Finally, an experiment is designed to carry out practical application and data analysis of the mental health analysis model. The results show that the intelligent analysis model based on computer chaos algorithm has better classification effect. In addition, the algorithm can also make different evaluation strategies according to the different personality of students and can carry out multidimensional classification for college students of different majors. It has effectively increased the proportion of college students' mental health groups. Compared with the current mainstream algorithms, the algorithm used in this study can adaptively classify college students of different majors. The accuracy of the experimental results is improved by at least 37% compared with the traditional method, and the error is low.

1. Introduction

The emergence and development of mental health education in colleges and universities in China have experienced a tortuous process. It is influenced not only by national politics, economy, and culture but also by the international mental health movement. With the unremitting efforts of the majority of psychological workers, mental health education in colleges and universities in China has begun to take shape and becomes an indispensable educational content for cultivating high-quality talents for socialist construction. Psychological education is an indispensable quality education course in higher education [1]. At present, college students are prone to various psychological problems because of their great psychological pressure [2]. Although there are many researches on college students' mental health at home and abroad, there are still no good research results that can be directly applied, and many methods still need to be analyzed

in combination with specific psychological problems [3]. This paper combines computer monitoring technology and data to better study, discusses the internal psychological expression of students, and realizes the expression analysis of high-quality characteristics of psychological education [4].

Based on this background, this paper studies the application of computer chaos algorithm in intelligent analysis, which is mainly divided into four chapters. The first chapter briefly introduces the application background and computer monitoring technology and the chapter arrangement of this study. Chapter 2 briefly introduces the research status of college students' mental health model at home and abroad and summarizes the shortcomings of the current research. The third chapter constructs the analysis model of college students' mental health based on computer chaotic algorithm. Through the disturbed intelligent analysis of different types of college students' psychological data, it realizes the high-

intensity representation of its internal correlation and carries out centralized control according to its internal error to improve the accuracy of the model. In Chapter 4, the practical application effect of the intelligent analysis model constructed is tested. By analyzing its high-intensity analysis of different data and interactive data coupling processing, the accuracy verification and analysis of the model are realized. The experimental results show that compared with the common mental health analysis matching model dominated by human interference, this paper makes a chaotic analysis of students' mental health. The results show that the modified method has high accuracy and low error rate.

The innovation of this paper is to use chaotic algorithm to analyze students' psychology. According to the psychological performance characteristics of students of different majors, the district distinguishes students of various majors. It creatively realizes psychological iterative analysis. The results show that chaos algorithm and coupling analysis can improve the accuracy of group psychoanalysis algorithm.

2. State of the Art

In recent years, scholars have made great achievements in the research of college students' mental health, but there are still many areas to be improved in different types of mental health analysis models and corresponding computer monitoring applications, such as high accuracy matching and differential feature construction of mental health analysis models [5]. In the process of studying, researchers Son et al. found that different types of health problems need different methods to solve. Therefore, they proposed a high-intensity and multitype synergetic mental health analysis system, which can effectively improve the efficiency of different types of psychotherapy [6]. Wang et al. found that different types of data groups have different differentiation characteristics, so they provided a traceable mental health network [7]. According to the characteristics of computer monitoring system, Barik et al. intelligently analyze different types of mental health models, classify different data, and use "meta learning" algorithm for in-depth analysis [8]. Zou et al. proposed a psychological analysis model of facial emotion recognition. According to the age characteristics of different students, different correlation schemes of psychological problems are put forward [9]. Kaveh et al. have adopted an intelligent adaptive allocation strategy for college students according to different types of college students' psychological thinking. The experimental results show that this strategy can carry out feature recognition and intelligent analysis according to its internal differences, which is more suitable for the psychological health treatment [10]. According to the differences in thinking of college students in different majors, Li et al. adopted neural network analysis strategy and adopted different types of mental health therapy [11]. Fu et al. rely on different types of high-end databases of mental health to carry out mental health communication and treatment for college students of different majors and put forward an adaptive mental health analysis model [12]. Georgieva et al. carry out intelligent matching and tracking of different types of databases according to different strategies of mental health therapy, and their internal relevance has good analysis and boundaries. Therefore, they can better complete the diagnosis and analysis of different mental health, but many parameters need to be determined in advance [13].

To sum up, it can be seen that the currently constructed intelligent analysis models of college students' mental health cannot efficiently complete the targeted treatment analysis of college students, and different model data need to be classified. Therefore, there are improvements in convenience and universality [14–16]. On the other hand, there are few research results combined with computer monitoring technology [17–19]. Therefore, it is very necessary to apply computer monitoring model to students' psychological analysis.

3. Methodology

3.1. Application of Monitoring Method Based on Computer Chaotic Algorithm in Intelligent Analysis of College Students' Mental Health. Chaos theory is an active frontier field developed in recent decades. It is an important branch of nonlinear science. It is known as three important scientific discoveries in the 20th century together with quantum physics and relativity [20]. Chaos is a disorder determined by order, which is similar to a random phenomenon. Chaos is a common phenomenon in nature and human social systems, but it is not easy to study. It is only due to the development of nonlinear science and the improvement of computer that chaos research becomes possible, forms a preliminary theory, and then begins to explore its practical application value [21]. In terms of solving the mental health problems of college students, computer chaos algorithm needs to conduct coupling analysis on different types of data groups first and then discrete processing. Therefore, this kind of algorithm is more marked and targeted than other artificial intelligence algorithms, and its basic thinking principle is shown in Figure 1 [22]. On the other hand, with the development of intelligent technology, different types of computer monitoring algorithms have different characteristics in analyzing different types of data groups, and their internal relevance will be different [23]. In the process of splitting mental data information, its internal relevance will also show the characteristics of high-intensity discrete difference analysis [24]. By using computer chaotic algorithm and image processing technology, its internal relevance and pertinence will also be different to varying degrees, and decentralized jurisdiction will be realized according to its internal unique characteristics, which is easier to realize the early analysis of mental health problems [25]. This analysis method shows the advantages of more convenience and speed.

3.2. Establishment Process of Psychological Intelligence Analysis Model Based on Computer Chaotic Algorithm. After the data groups of different types of mental health problems are divided, the differentiation characteristics of the internal correlation data groups show different types of decentralized characteristics, and different types of data groups appear,
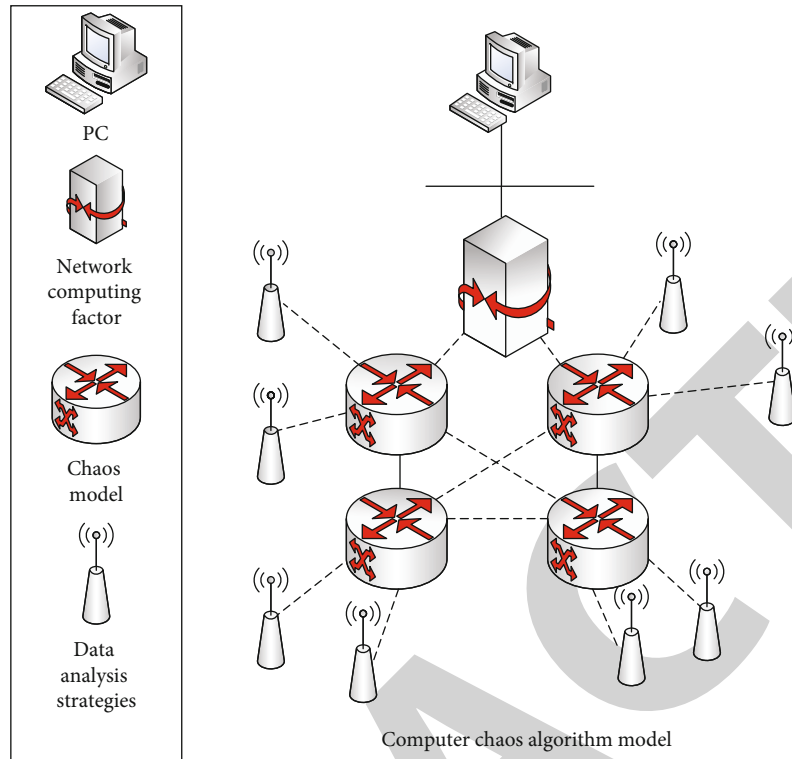
Figure 1: Computational thought of computer chaos algorithm.

which can realize the early specific behavior analysis of different mental health data groups. Therefore, it is simulated and analyzed in combination with the computer monitoring network. The data simulation and analysis process is shown in Figure 2.

It can be seen from the simulation analysis results in Figure 2 that although the trends of mental health training data sets of different ages and majors are similar, their corresponding common problem types and pyramid level proportion are different, and the difference is obvious. This is because after the combination of different types of computer monitoring networks and chaotic algorithms, its internal ultra-high-intensity matching analysis data group will carry out feature classification, and its internal model features will combine the advantages of Chaotic Hybrid Algorithm to realize pyramid hierarchical intelligent management and data difference and then show the change characteristics with similar trend. The difference of college students' mental health is mainly reflected in the corresponding color difference after the mental health problems are converted into data. It can be represented by color histogram, in which the color histogram P can be expressed as

$$P = \frac{\sum_{i=1}^{n} b_i^2!}{1 + \sum_{i=1}^{n} b_i^2!}, \tag{1}$$

where b is the strength of computer chaotic nodes. After the analysis of different types of data groups, their internal relevance and true intensity have obvious differential classi-

fication features. It is very important to extract quantitative features from images and analyze them. Figure 3 shows the quantitative model analysis results.

According to the results of Figure 3, after the computer chaotic algorithm and monitoring network are used to classify the mental health data, its internal relevance and differentiation can be quickly divided and reflected through the pyramid hierarchical structure. This is because different types of computer monitoring networks and computer chaotic algorithms can complete better data classification and data retrieval according to different types of data groups, so as to deal with college students' mental health problems in advance.

$$HSV = \frac{\sqrt{P} + \sqrt{\sum_{i=1}^{n} b_i^2!/r!(g-r)!}}{\sqrt{rW}}. \tag{2}$$

The bundle histogram of chaotic space is used to reflect the vector characteristics of chaotic space, and multiple vectors in monitoring space are standardized and quantified. The component corresponding to the vector algorithm of each monitoring space is synthesized into a normalized eigenvector, and its expression is

$$L = \frac{\lim_{s \to \infty} \sqrt{rW^2 + bP^2}}{\lim_{s \to \infty} \sqrt{bW^2 + rP^2}}, \tag{3}$$
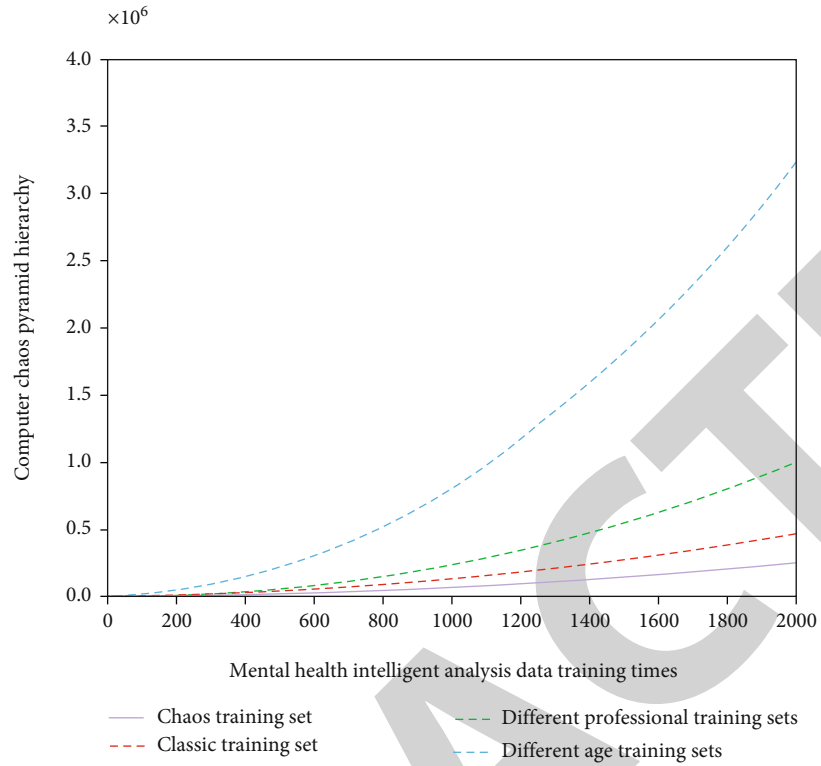
Figure 2: Data training process based on computer chaos algorithm.
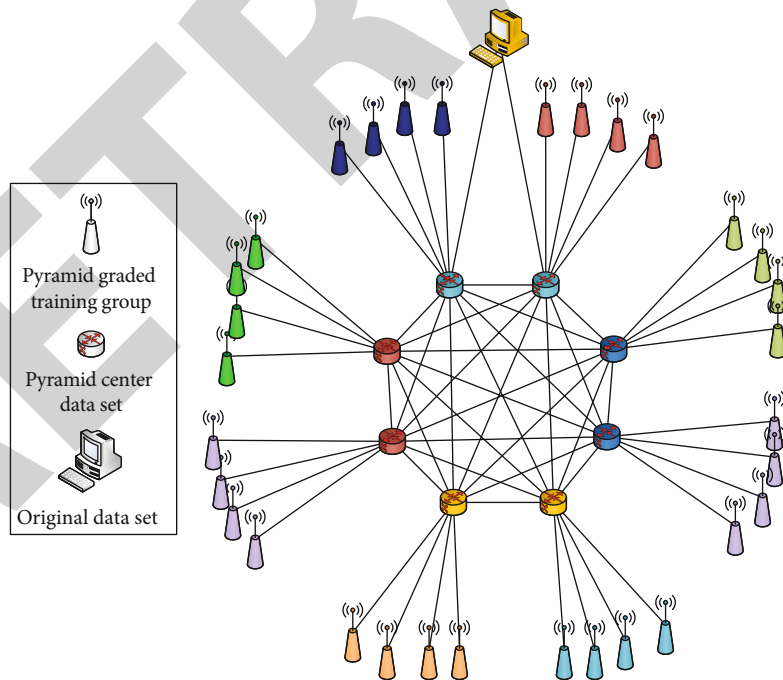

Figure 3: Pyramid-level classification results of computer network monitoring simulation analysis.

where L is the quantitative response value of the chaotic vector and the monitoring vector, and its size reflects the mutual interference degree and the discrete frequency between the chaotic vector and the monitoring vector. Different types of mental health data sets have L-dimensional vectors. The chaotic square function is a hypercentric discrete function, and the formula is expressed as

$$R(S_k) = \frac{\lim_{k \longrightarrow \infty} n_k}{L}, \tag{4}$$

where S_k represents the standard degree of discretization and n_k represents the width limit of the square function. After completing the standardized analysis, it is very important to analyze and sift out mental health data. The formula is

$$R(S_{k+1}) = \sqrt{R(S_k)^2 + n^2}, \tag{5}$$

where n is analyzed according to the standard degree and error deviation degree of chaotic vector and $R(S_{k+1})$ reflects the accurate frequency of the matching degree between chaotic square function and college students' mental health analysis. After scoring the mental health data of college students, the saturation function U_{L-1} is extracted with the help of chaotic analysis structure:

$$U_{L-1} = \sqrt{\frac{\sum P(S_L)}{W\left(\sqrt{2}S_1\right)}}. \tag{6}$$

Assuming that U_{L-1} can be normalized by combining the modulus and direction of chaotic vector, its internal relevance and mental health matching degree will also show different changes. Therefore, extract and analyze the maximum value of the corresponding chaotic vector from U_{L-1} and set it as the upper limit of the standard reference interval, then the basic reference value of $R(S_L)$ value in chaotic space can be set to 0.1, and the simulation analysis results are shown in Figure 4.

As can be seen from the figure, in different students' psychological data, the corresponding monitoring results and chaotic analysis frequencies are different, and the reference standard value will also show different change trends, because different types of data groups analyze different types of coupling data. It is necessary to carry out high-intensity fitting with the help of chaotic space matching analysis network. Therefore, after completing the high-intensity analysis of mental health, it is also necessary to carry out accuracy analysis combined with chaotic space vector. The mental health standard vector of college students specified in chaotic space belongs to $h(x)$, and x is used to represent the label of different types of mental

health data groups. Then, the corresponding standardized chaotic discriminant function can be expressed as

$$h(x) = \frac{w\sqrt{x} + bx}{w + b}. \tag{7}$$

Under the high-intensity mental health analysis model, in order to ensure the accuracy of its analysis, the following conditions need to be met:

$$\frac{y_i[h(x) + n]}{b\sqrt[3]{w} + w\sqrt[3]{b}} \geq 0. \tag{8}$$

Under the computer monitoring system and chaos analysis algorithm, the corresponding analysis matching truth function $T(x)$ is

$$T(x) = \text{sgn}\left\{ \sqrt{\sum_{i=1}^{n} a_i y_i(x_i \times x) + b*} \right\}. \tag{9}$$

In order to further improve the accuracy of college students' mental health analysis, it is necessary to add significance classification conditions under different monitoring models:

$$\frac{y_i[h(x) + n] - 1}{b\sqrt{\zeta_i}} > 0. \tag{10}$$

Under the limitation of significance, the formula corresponding to the collimation function $\phi(w, \zeta)$ is

$$\phi(w, \zeta) = \frac{\sqrt{\|w^2\|^3 + (2/3)M(\sum_{i=1}^{n} \zeta_i)}}{b + w}, \tag{11}$$

where M represents the chaos degree determination function.

It is necessary to add a standardized coupling factor expression system. At this time, the corresponding standardized judgment function in the corresponding computer monitoring network system will be transformed into

$$T'(x) = \text{sgn}\left\{ \sqrt{\left|\sum_{i=1}^{n} a_i y_i(x_i \times x) + b*\right|} \right\}, \tag{12}$$

$$T''(x) = \text{sgn}\left\{ \sqrt[3]{\left|\sum_{i=1}^{n} a_i y_i(x_i \times x) + b*\right|} \right\}, \tag{13}$$

$$T'''(x) = \text{sgn}\left\{ \frac{\sqrt[4]{\left|\sum_{i=1}^{n} a_i y_i(x_i \times x) + b*\right|}}{b^3} \right\}. \tag{14}$$

After analyzing the mental health data groups of different types of college students, combined with their significant characteristics, it is necessary to conduct value scale analysis
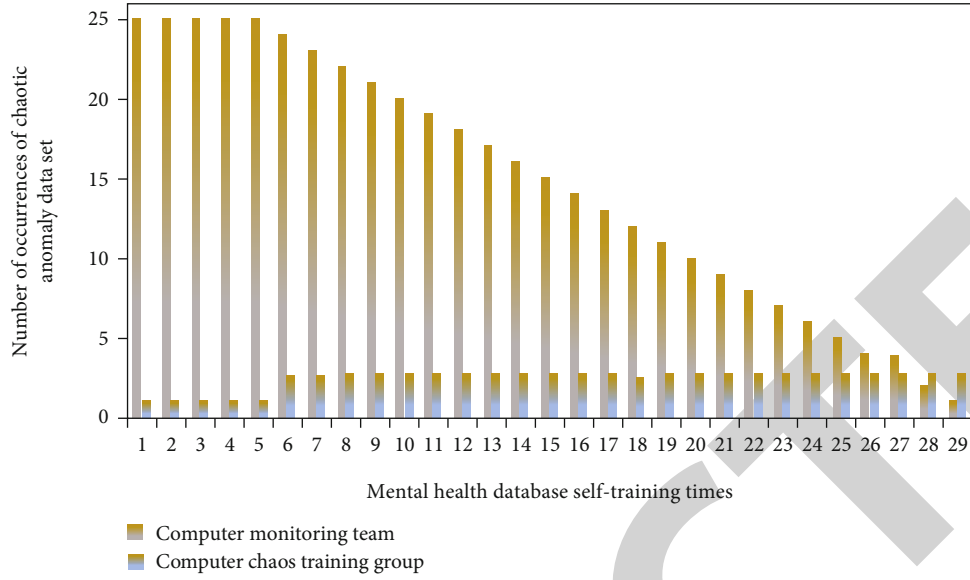
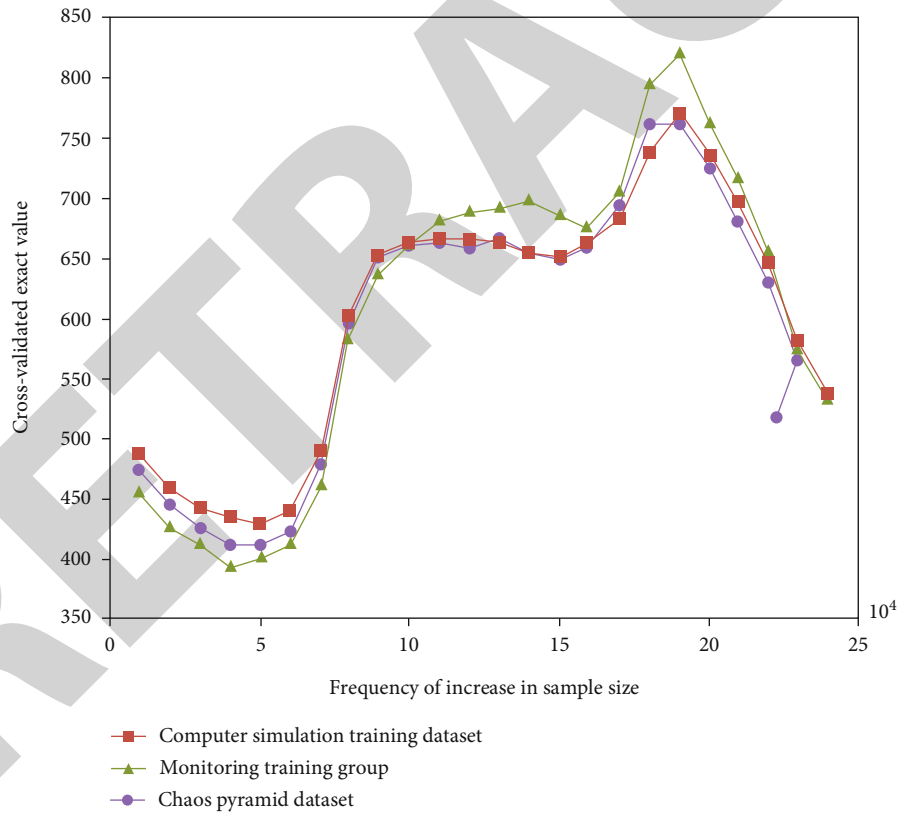FIGURE 4: Psychological analysis of children's models in different degrees.

FIGURE 5: The simulation analysis results corresponding to the cross-validation method.

in different types of mental health models. At this time, the corresponding value scale function is

$$Z\left(x_j, x_i\right) = \frac{\lim_{\delta x \longrightarrow 0}\left\{\left((\delta + 1)\sqrt{|x_i - x_j|}\right)/\delta^2\right\}}{|x_i - x_j|}. \quad (15)$$

After calculating the value scale, it is necessary to conduct high-intensity characterization analysis on different mental health model data groups, and the simulation analysis results of computer monitoring under different differentiated conditions are shown in Figure 5.
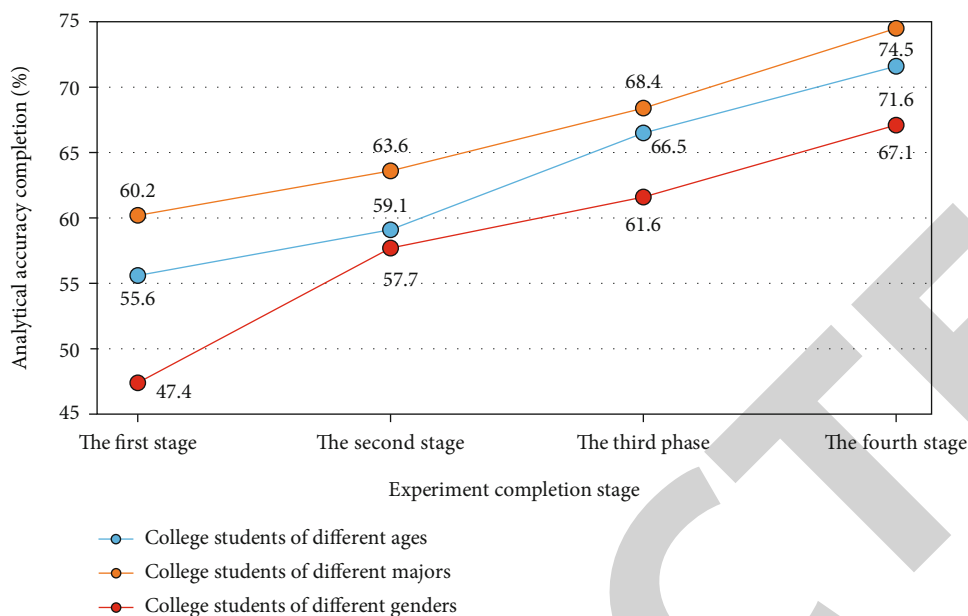
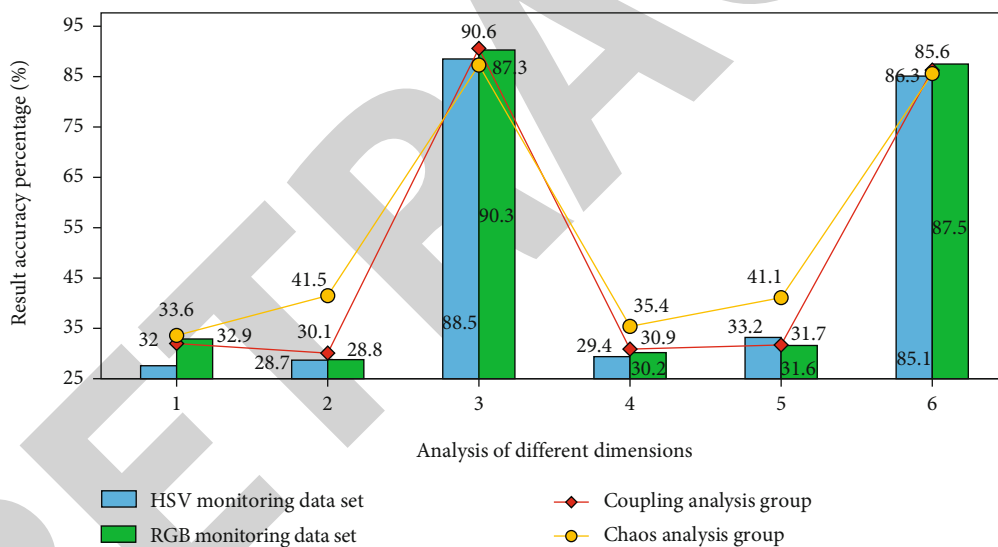FIGURE 6: Preliminary experiment results of computer chaos algorithm analysis model.

FIGURE 7: Final experimental analysis results in computer monitoring mode.

As can be seen from Figure 5, when the number of samples of college students' mental health data increases, the threshold of its corresponding incremental function changes significantly, but the curve change law corresponding to the three groups of simulation results is consistent, because different types of data groups have obvious differences in their internal relevance under the analysis of computer chaotic neural network. However, there is little difference in the correlation between groups, so it presents the characteristics of "overall similarity and local difference."

4. Results

4.1. Analysis of Psychological Model under Chaotic Algorithm.
Accurate matching analysis of the psychological characteristics of different student groups in chaotic algorithm is a limited problem to be solved. It is necessary to carry out differential analysis and processing of their internal relevance. The processing strategy used in this experiment is the hybrid strategy of computer monitoring network and computer chaotic analysis network. The matching degree

of this strategy ensures that when different types of college students' mental health problems are analyzed, their internal relevance and differences are more clearly analyzed and quantified in the form of numbers. Figure 6 is the preliminary experimental results of the computer chaotic algorithm analysis model.

In the three groups of data in Figure 6, the branch accuracy indexes of the results corresponding to the computer chaos method in the process of processing and analyzing the data of three different groups are also different, but when different types of data groups realize the expression of "spacing," their internal relevance also shows great differences, and such results also meet the experimental expectations. In addition, in the computer monitoring system, combined with the actual analysis of college students' psychological problems, both compact design and multifunctional design can be adopted to minimize the instability of the computer chaotic pyramid. Therefore, the computer chaotic algorithm can effectively combine the characteristics of deep learning to realize its differential analysis and error control.

4.2. Results and Analysis. On the basis of students' psychoanalytic health model computer monitoring application proposed in this study, the evaluation index is used as a reference. In the process of iteration and evaluation, if the frequency of the output of the network and the chaos distance of a memory vector is 0 (or close to 0), it can be considered that this mental health problem is successfully identified by the chaotic vector. If the output of the network and the chaos distance of multiple memory vectors are more than 1, it is considered that the probability of successful recognition of mental health problems is low. Therefore, data monitoring and chaos analysis strategies play an important role in classification, which will directly affect the analysis accuracy. The experimental analysis results are shown in Figure 7 (RGB and HSV evaluation strategies).

As can be seen from Figure 7, when analyzing different types of data groups, the experimental group using computer chaos strategy has the lowest error degree of corresponding data results, and its jumping and disturbance are also the lowest. This is because after using computer monitoring network and chaos analysis strategy, when the corresponding value of the Q parameter in the tracking analysis is the preset random value, the corresponding value of the Q parameter in the tracking analysis will appear δ. When it is 1, the accuracy is 82.5%; Q value is 20, random parameter δ. When it is 10, the accuracy is 77.5%; Q value is 50, random parameter δ. When it is 50, the accuracy is 67.5%; Q value is 70, random parameter δ. When it is 5, the accuracy is 90%.

5. Conclusion

In the past 20 years, although there are many achievements in the model analysis, there are still problems of low data utilization and low accuracy. The study makes an applied analysis on the psychology of students through computer model monitoring. Firstly, an intelligent analysis model of mental health based on computer chaotic algorithm is established.

Combined with the different psychology of students in different majors, different types of analysis strategies are used to establish different visual network models. Secondly, combined with different computer monitoring and analysis models, different types of college students' mental health problems are classified and analyzed. Finally, combined with different analysis strategies, the normalization analysis and error matching characterization of different types of mental health data groups are carried out. The results show that the algorithm used in this study can carry out adaptive classification for college students of different majors, and the accuracy of the experimental results is improved by at least 37% compared with the traditional methods, and the error is lower. However, this paper does not discuss the automatic classification of renderings for college students' psychological design, which needs to be analyzed and discussed from the application scope of different algorithms and the regional differences of students.

Data Availability

The data used to support the findings of this study are included within the article.

Conflicts of Interest

The authors declare that they have no conflicts of interest.

References

[1] X. Wang, C. Liu, and D. Jiang, "A novel triple-image encryption and hiding algorithm based on chaos, compressive sensing and 3D DCT," *Information Sciences*, vol. 574, pp. 505–527, 2021.

[2] A. Arab, M. J. Rostami, and B. Ghavami, "An image encryption method based on chaos system and AES algorithm," *Journal of Supercomputing*, vol. 75, no. 10, pp. 6663–6682, 2019.

[3] B. Christophers, E. Nieblas-Bedolla, J. S. Gordon-Elliott, Y. Kang, K. Holcomb, and M. K. Frey, "Mental health of US medical students during the COVID-19 pandemic," *Journal of General Internal Medicine*, vol. 36, no. 10, pp. 3295–3297, 2021.

[4] C. M. Kumar, R. Vidhya, and M. Brindha, "An efficient chaos based image encryption algorithm using enhanced thorp shuffle and chaotic convolution function," *Applied Intelligence*, vol. 52, no. 3, pp. 2556–2585, 2022.

[5] G. Gruosso, R. S. Netto, L. Daniel, and P. Maffezzoni, "Joined probabilistic load flow and sensitivity analysis of distribution networks based on polynomial chaos method," *IEEE Transactions on Power Systems*, vol. 35, no. 1, pp. 618–627, 2020.

[6] J. Son and Y. Du, "Comparison of intrusive and nonintrusive polynomial chaos expansion-based approaches for high dimensional parametric uncertainty quantification and propagation," *Computers & Chemical Engineering*, vol. 134, article ???, 2020.

[7] X. Wang and X. Chen, "An image encryption algorithm based on dynamic row scrambling and zigzag transformation," *Chaos, Solitons & Fractals*, vol. 147, article 110962, 2021.

Research Article

Optimal Arrangement of Structural Sensors in Landfill Based on Stress Wave Detection Technology

Xiankun Xie ⓘ,[1] Xiong Xia ⓘ,[1] and Zhaoguo Gao[2]

[1]*School of Environmental and Safety Engineering, Changzhou University, Changzhou 213164, China*
[2]*Jiangsu Baituo Construction Co., Ltd., Changzhou 213164, China*

Correspondence should be addressed to Xiong Xia; xiaxiong@cczu.edu.cn

Sensor arrangement is the primary link of landfill structure health monitoring, and the number of measuring points and the quality of data directly affect the effect of modal identification. Therefore, how to ensure the service safety of landfill structure has become an important research content in the field of landfill structure health monitoring. In this paper, the stress wave propagation principle and stress wave detection theory are analyzed, and an optimal sensor arrangement method based on AGSA (adaptive gravity search algorithm) algorithm is proposed. Use CS (Cuckoo search) algorithm to optimize the objective function value. The corresponding response value is calculated by the finite element model, and the initial proxy model is constructed. By comparing and analyzing the results of model correction, it is found that the error of parameters before and after correction is less than 2.5%. It is further verified that AGSA algorithm can be used to solve the optimal sensor placement problem. In this paper, the use of structural health monitoring technology for health diagnosis and performance evaluation is an important means to ensure structural safety, prolong service life, and reduce maintenance cost. As the primary link of structural health monitoring, sensor system directly determines the accuracy of structural safety diagnosis.

1. Introduction

With the rapid development of industry, hazardous waste disposal has become a major environmental problem faced by countries all over the world. At present, the disposal of solid hazardous waste in China is mainly landfill [1]. An extremely important problem to be considered in landfill treatment is the impact on the surrounding environment. To prevent the water pollution caused by the solution leaching of waste and rainwater runoff, the anti-seepage lining system of landfill is an essential facility. The investigation shows that the impervious layer will be damaged due to mechanical or artificial nonstandard operation during construction, and the impervious layer will leak due to uneven settlement of foundation, shrinkage deformation, and chemical corrosion during operation. Landfill leachate produced by rain dripping and fermentation contains a large number of toxic and harmful components. When there is leakage in landfill, these toxic and harmful components seep into the ground along with landfill leachate, polluting the sur-

rounding soil and groundwater, and the groundwater pollution caused by this seriously threatens people's life, health, safety, and quality of life [2].

China's landfill waste accounts for such a large proportion of the total waste disposal. How to improve the level of landfill and make it a real "sanitary" landfill instead of a general "landfill" is the most urgent problem to be solved in China's waste disposal and also an urgent problem to be solved by Chinese environmental protection workers. Jiang et al. [3] point out that some landfills have poor seepage control effect and obvious groundwater pollution due to poor environmental geological and hydrogeological conditions or poor construction quality. Zhijun et al. [4] have developed the steel wire grid detection technology, which is to lay two layers of steel wires under the impermeable membrane, each layer of steel wires is arranged in parallel, clay is used as the medium, and the vertical distribution of the two layers of steel wires is grid-shaped, and the existence and location of leakage points can be judged by detecting whether the upper and lower layers of steel wires have short circuits. This

detection method is low in operation cost and easy to install, and is suitable for long-term leakage detection of landfill. Sun and Ge [5] studied the double-electrode method, dipole method, and electrode grid method, and successfully developed a leakage detection system based on high-voltage DC method, which solved the problems of large amount of collected data and long transmission distance caused by large detection area of landfill. Zheng et al. [6] combine effective independence method with modal kinetic energy method, and put forward a fast calculation method of effective independence method coefficient, which avoids the problem of matrix inversion. Dai et al. [7] introduce the constraint equation into the expression of kinetic energy or strain energy of the system to reduce the mass or stiffness matrix. The principal coordinates that play a major role in modal response are reserved as measuring points. Yulianti et al. [8] combine information redundancy function with TMAC (Three-dimensional Modal Assurance Criteria), establish a sensor TMAC, and propose a hierarchical wolf pack algorithm to optimize the layout of 3D sensors. Huang et al. [9] solve the problem that it is difficult to accurately identify and select the high-order vibration modes in the weak axis direction of the structure due to the coupling vibration of nodes, aiming at the optimized sensor arrangement method based on simplified model. Yu et al. [10] By combining the condition number index of information entropy sensitivity matrix with Fisher information matrix criterion by weight, a multi-target sensor optimal arrangement method is proposed, which can be robust and accurate in parameter identification, and the effectiveness of the method is verified by a certain launch pad as an example.

The working principle of stress wave detection technology is similar to that of earthquake detection system. The initial purpose of stress wave detection technology is to detect the geological changes in mines. At present, although some achievements have been made in the research of stress wave detection technology in China, most of the stress wave detection systems that have been built at present still rely on the introduction from abroad [11]. In this paper, an optimal arrangement method of landfill structural sensors based on stress wave detection technology is proposed. Through the determination of the sensor optimal arrangement scheme of the improved optimization algorithm, the foundation is laid for the information acquisition of structural modal parameter identification. The improved intelligent optimization algorithm is introduced into the agent model to modify the structure model, which improves the precision of the structure's mathematical model.

In this paper, the principle of stress wave propagation and the theory of stress wave detection are analyzed, and a sensor optimal layout method based on adaptive gravity search algorithm (AGSA) is proposed. Research and innovation contributions include the following: (1) Vibration detection cannot be used for the detection of high vibration and noise equipment, but the effective signal frequency band of stress wave monitoring is high. This paper can solve this problem well and is suitable for the detection of high vibration and noise equipment. (2) Through the sensitivity analysis of the main parameters in the algorithm, the optimal

parameters of AGSA algorithm for solving the optimal sensor placement problem are determined. (3) Solve the parameter correction value through CS. After introducing CS, it is found that the parameter error before and after correction is less than 2.5%. It can be seen that the introduction of CS usually improves the effect of model correction. Selecting a limited number of locations from large-scale nodes to be tested in order to achieve the optimal layout effect is the core problem of this paper.

This paper is divided into five parts. The first part expounds some achievements in the research of stress wave detection technology in China. The second part describes the research methods and analyzes the overall design of the sensor optimization layout toolbox. At the same time, the stress wave signal processing is discussed. The third part analyzes the optimal layout of landfill structure sensors. The fourth part analyzes the results. Vibration detection cannot be used for the detection of high vibration and noise equipment, but the effective signal frequency band of stress wave monitoring is high, which can solve this problem well and is suitable for the detection of high vibration and noise equipment.

2. Research Method

2.1. Overall Design of Sensor Optimization Layout Toolbox. Optimal sensor placement is a problem integrating structural dynamics, finite element theory, advanced mathematics, and computer programming language, which involves complex basic theories of many disciplines and disciplines. With the continuous research of scholars at home and abroad, the theory and method of optimal sensor placement are constantly being innovated and developed. In the existing sensor arrangement methods, the modeling error and the prediction error caused by measurement noise are usually assumed to be a vector that obeys Gaussian distribution [12, 13]. This assumption does not give the specific physical meaning of modeling error, and cannot consider the influence of modeling error on the uncertainty of modal identification and sensor arrangement. In the sensor arrangement, it is meaningful to separate the measurement noise and modeling error from the prediction error, give the concrete manifestation of modeling error, and further discuss the influence of modeling error on the uncertainty of modal identification.

In structural dynamics, the modal vectors of structures are mutually orthogonal. However, in the actual test, due to the limitation of measuring instrument accuracy and environmental influence such as noise, the modal vector of the tested structure cannot be completely orthogonal. When the optimal arrangement of sensors is unreasonable, some important modal information will be lost. According to the structural dynamics, the modal vectors of each order on the structural nodes are orthogonal to each other. However, because the degree of freedom of testing with sensors is far less than the measurable degree of freedom of the structural model, and affected by the measurement error, it is difficult to ensure the orthogonality of the measured modal vectors. If the sensors are not properly configured, the spatial

intersection angle between modal vectors will be too small, and important structural information will be lost [14].

In order to solve the orthogonality problem caused by measurement error, the modal guarantee criterion is used in this paper. MAC (Modal Assurance Criteria) can effectively evaluate the orthogonality of modal vectors, choose a larger spatial intersection angle, and keep the characteristics of the original model as much as possible. The orthogonality of modes and the integrity of modal information are ensured. Therefore, in this paper, MAC is used as the fitness function of optimal sensor placement to evaluate the independence of each test mode. The expression for MAC is:

$$\text{MAC}_{i,j} = \frac{\left(\varphi_i^T \cdot \varphi_j\right)^2}{\left(\varphi_i^T \cdot \varphi_i\right)\left(\varphi_i^T \cdot \varphi_j\right)}, \tag{1}$$

where i, j is the modal vector of order i and order j, respectively.

The quantitative index to evaluate the sensor configuration effect in MAC criterion is the maximum value of off-diagonal elements of MAC matrix. The goal of sensor configuration optimization algorithm is to minimize the maximum off-diagonal elements of MAC matrix. In the optimization method, this is a minimization problem, and the objective function is described as:

$$f(\varphi_{slc}) = \min \ \max_{i \neq j}(\text{mac}_{ij}). \tag{2}$$

$0 \leq f(\varphi_{\text{slc}}) \leq 1 \quad i, j = 1, 2, \cdots, s$. The idea of solving the optimization problem is to constantly select the degree of freedom of measuring points from φ, update the content of φ_{slc}, and minimize the value of objective function f, that is, to achieve the goal of continuously optimizing the sensor configuration scheme.

The sensor optimization layout toolbox can complete the sensor optimization layout of the test structure by itself without the operator having in-depth theoretical foundation, professional scientific research personnel, and any programming operation, which improves the timeliness and initiative of engineers in monitoring the actual project, and has very important practical engineering significance.

The post-processing module of toolbox (result display and report output) should include the test structure model, calculation parameters, evaluation criteria, and the selection of candidate measuring points, and the final layout scheme can be visually output by visual layout renderings. No matter researchers or engineers, they can study the optimal arrangement of sensors in any kind of engineering structure through the toolbox. The development concept of the functional module of the sensor optimization layout toolbox is shown in Figure 1:

2.2. Stress Wave Signal Processing. The stress wave signals collected in the working equipment all contain the damage properties of the equipment, but at the same time they are also mixed with a lot of noise, such as environmental noise, equipment vibration, and voltage fluctuation. The only way to get the stress wave signal is to use the stress wave sensor to get the original stress wave signal [15, 16], and then process it by hardware or software to get effective signal data. The original stress wave data processing methods can be divided into two types: parameter analysis and waveform analysis.

Wavelet transform overcomes the shortcomings that the window size does not change with frequency, and can provide a "time-frequency" window that changes with frequency. It is an ideal tool for signal time-frequency analysis and processing. Its main feature is that it can fully highlight the characteristics of some aspects of the problem through transformation, and can analyze the localization of time (space) frequency. In this paper, wavelet denoising is realized by hardware, and the collected stress wave signal is processed by hardware. The biggest advantage of wavelet transform is that it solves the problems that Fourier transform and windowed Fourier transform cannot solve while ensuring the accuracy of time domain and frequency domain. With the in-depth study of wavelet transform, wavelet transform has been applied to a wide range of fields and plays a very important role in modern data processing.

The research of wavelet transform has become a new and flourishing field. The mathematical meaning of wavelet transform is the inner product of given function $x(t)$ and wavelet basis function, which is defined as follows:

$$\psi_{j,k}(t) = \frac{1}{\sqrt{|j|}} \psi\left(\frac{t-k}{j}\right); a, b \in R, a \neq 0. \tag{3}$$

Among them, the parameter j is a scaling factor or a scaling factor, which reflects the amplitude change and width of the wavelet function. The parameter k is a translation factor or a time shift factor, which reflects the advance or lag of the wavelet function on the time axis. The family of wavelet functions $\psi_{j,k}(t)$ is obtained by translation and expansion of wavelet function $\psi(t)$, and $\psi(t)$ is also called mother wavelet.

The mathematical expression of wavelet transform is:

$$X(j, k) = \int x(t)\psi_{j,k}(t)dt. \tag{4}$$

Because wavelet transform adopts multi-resolution method, it can well describe the non-stationary characteristics of signals, such as spikes, edges, and breakpoints. It can denoise according to the characteristics of signal and noise distribution at different resolutions, and wavelet transform can flexibly choose the basis.

The continuous wavelet transform of a signal $f(t) \in L^2(R)$ is defined as:

$$W(a, b) = \frac{1}{\sqrt{|a|}} \int_R f(t)\phi\left(\frac{t-b}{a}\right)dt \ b \in R, a \in R - \{0\}. \tag{5}$$
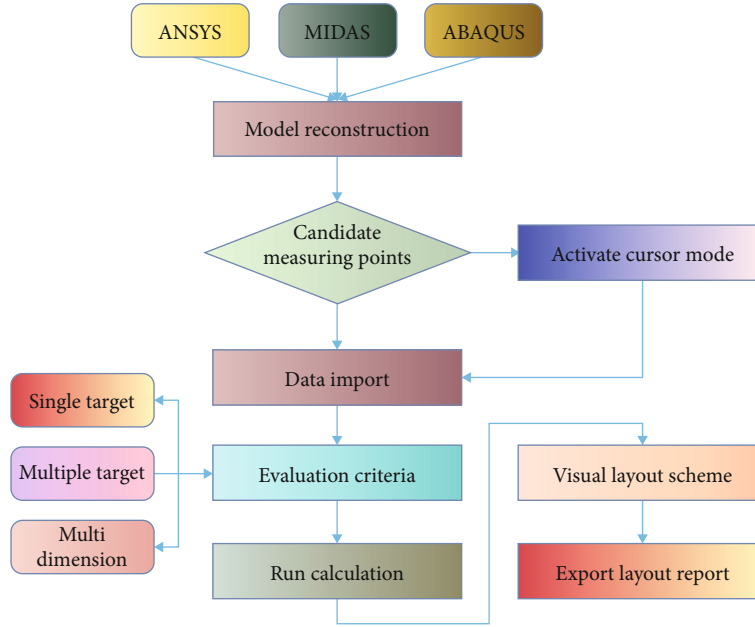
FIGURE 1: Optimization of sensor layout toolbox operation process.

If $f(t)$ is continuous at t, $f(t)$ can be reconstructed as:

$$f(t) = \frac{1}{C_\phi} \iint_2 W_f(a, b) \phi_{a,b}(t) \frac{da}{a^2} db. \tag{6}$$

From the point of view of signal processing, wavelet function is a high-pass filter. It has a window function with variable window shape. For high-frequency signals, the time window becomes narrower and the frequency window becomes wider, which is beneficial to the description of signal details. For low-frequency signals, the time window becomes wider and the frequency window becomes narrower, which is very suitable for detecting transient abnormal signals entrained in normal signals and displaying their components [17].

The principle of landfill leakage detection system based on stress wave detection technology is similar to that of earthquake monitoring system. The hardware design mainly includes the selection of stress wave sensor, the design of front-end conditioning modules such as amplification circuit and analog-to-digital conversion circuit, and the design of back-end digital processing modules such as data storage module, communication module, and human-computer interaction module. The hardware schematic diagram of stress wave detection system is shown in Figure 2.

The stress wave detection system mainly consists of three parts: data processing terminal, data collector, and stress wave sensor. The signal collected by the stress wave sensor is preliminarily screened by the filter circuit, then the filtered analog signal is analog-to-digital converted by the analog-to-digital conversion circuit, then the signal is amplified by the programmable amplifier, then the signal is sent to the main control chip for storage and preliminary

analysis, and finally the data is transmitted to the data processing terminal by Ethernet communication.

2.3. Optimal Arrangement of Landfill Structure Sensors. In practical situations, strain sensors are often placed at large deformation positions of structures to obtain local deformation information of structures as much as possible. Therefore, in the proposed multi-type sensor arrangement method, firstly, the large deformation position of the structure is taken as the initial arrangement position of the strain sensor, such as the mid-span position of each span of the multi-span landfill structure [18]. Then, the displacement modal shapes of structural joints are estimated by using the strain modal shapes at the strain positions, hoping that the positions of strain sensors can contain as much information as possible about the displacement modal shapes of joints.

After determining the specific position of the strain sensor, it is necessary to add sensors such as acceleration to the existing sensor arrangement. Here, the displacement modal shapes are obtained by using MAC criterion parity, and the arrangement of acceleration sensors is guided. When the value of the maximum non-diagonal element of MAC is less than 0.2, the distinguishability between the obtained vibration mode vectors is acceptable. Therefore, it is hoped that the maximum off-diagonal element value of MAC corresponding to the modal shapes comprehensively obtained by strain sensors and acceleration sensors will be as small as possible.

Or similar symmetrical sensor positions contain approximate modal information, so it is necessary to avoid the occurrence of such redundant modal information as much as possible. Here, a redundancy coefficient is used to measure the similarity of displacement modal shapes corresponding to different positions, that is, the redundancy of the displacement modal information contained:
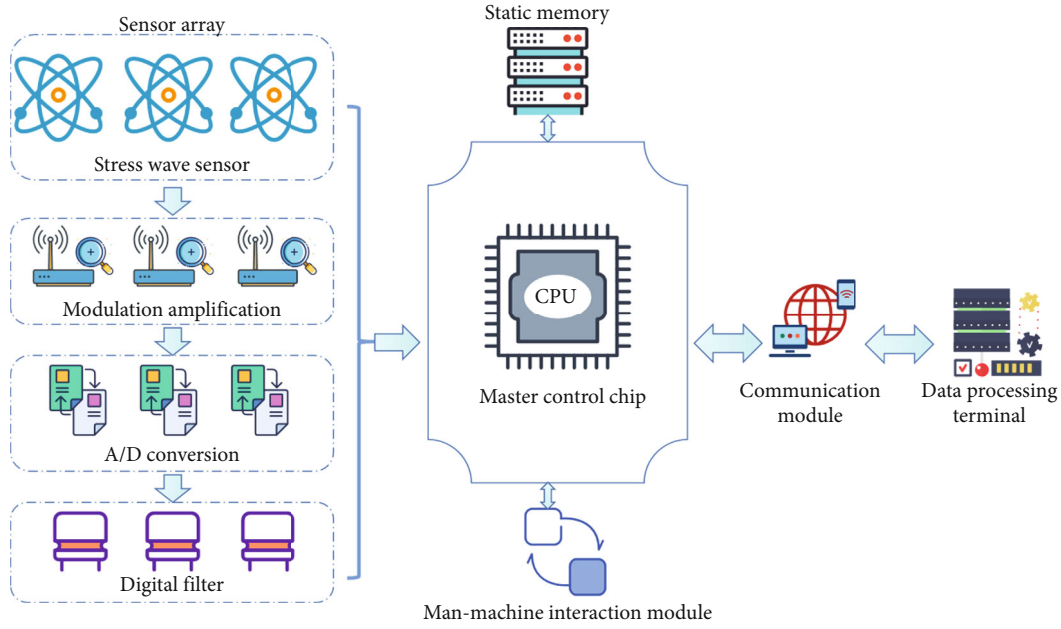
FIGURE 2: Hardware system of stress wave detection system.

$$R_{ij} = 1 - \frac{\left\| \Phi_i - \Phi_j \right\|}{\left\| \Phi_i \right\|_F + \left\| \Phi_j \right\|_F}, \tag{7}$$

where R_{ij} is the redundancy coefficient of displacement mode shape between the i and j degrees of freedom; Φ_i, Φ_j represents the displacement modal shape line vector corresponding to the i and j degrees of freedom, respectively; $\left\| \cdot \right\|_F$ represents the Frobenius norm. If the value of R_{ij} is close to 1, it means that these two positions contain nearly the same information of displacement modes, and only one of these two positions can be reserved.

We apply AGSA (adaptive gravity search algorithm) algorithm to the solution of low-dimensional test function, and the optimal placement of sensors is a discrete problem of 0-1 programming, so it is necessary to adjust the encoding mode of the adaptive gravity search algorithm to ensure that AGSA algorithm can solve the optimal placement of sensors.

The points to be arranged for the optimal arrangement of sensors are all nodes of the landfill structure, so in the coding process, 0 is used to indicate that no sensors are arranged at this node, and 1 is used to indicate that sensors are arranged at this node. The way of double coding is shown in Tables 1 and 2:

The ordered pair (x_i, s_i) composed of additional code x_i and variable code s_i is used to represent the sensor arrangement results corresponding to individual i in the population [19]. This double coding method enables AGSA algorithm to solve the problem of optimal sensor placement.

Firstly, the finite element model of the landfill structure is established, and the modal matrix of all nodes of the model is obtained by modal analysis. The obtained modal matrix is used as the input value, and the degrees of freedom corresponding to all nodes are used as the candidate points for sensor arrangement.

Secondly, assuming that the number of points to be selected is n, and the number of sensor layout points is set to m, the n candidate positions are numbered integer from $1 - n$ in turn.

The binary values calculated by different position components x_{ij} are different, so it is necessary to set a threshold δ to satisfy the following formula:

$$s_{ij} = \begin{cases} 1 & \text{if } s_{ij} > \delta \\ 0 & \text{else} \end{cases}. \tag{8}$$

In order to speed up the particle convergence, mutation operator is introduced into the particle velocity formula to increase the guiding effect of the global optimal solution on particles. The expression of mutation operator is shown in formula (9).

$$\eta = \text{rand}\left(p_g^d(t) - x_i^d(t)\right). \tag{9}$$

In the process of updating the position, the calculated acceleration and velocity components will be non-integer. Therefore, the location update in this paper is shown in the following formula:

$$v_i^d(t) = \text{ran d}_2 \times v_i^d(t) + a_i^d(t),$$
$$x_i^d(t+1) = \text{rand}\left(x_i^d(t) + v_i^d(t+1)\right), \tag{10}$$

where rand is an integer function, which ensures that the updated particle position component is in integer form.

The position component of the particle is an integer randomly generated from [-5,5]. During the position update of the particle, the value range may be exceeded. Therefore, this

TABLE 1: Dual coding mode.

Extracode	Variable code
$x(1)$	$s_x(1)$
$x(2)$	$s_x(2)$
$\vdots$	$\vdots$
$x(i)$	$s_x(i)$
$\vdots$	$\vdots$
$x(f)$	$s_x(f)$

TABLE 2: Double coding result.

Extracode	Variable code
4	0
2	1
1	0
6	0
7	1
2	0
8	1

paper stipulates that when the position component is greater than 5, take 5; when the position component is less than -5, take -5.

Figure 3 is a flow chart of optimal sensor arrangement based on AGSA algorithm.

Influenced by various uncertain factors, there are inevitably errors between the established finite element model and the test model. Therefore, it is necessary to use dynamic correction method to correct the established finite element model. The basic idea of model updating is to make the modal analysis results consistent with the experimental results by constantly changing the parameters of the finite element model [20].

CS (Cuckoo search) algorithm solves the optimization problem by simulating the parasitic brooding of cuckoo in nature. The research shows that Cuckoo search has good search accuracy and efficiency. The formula for updating the path and location of cuckoo nesting is:

$$x_i^{t+1} = x_i^t + \alpha \oplus \text{Levy}(\lambda), i = 1, 2, \cdots, n,$$
$$\alpha = \alpha_0 \left\| x_t^i - x_{\text{best}}^t \right\|, \tag{11}$$

where x_i^t represents the nest position of the ith nest in the t generation; $\oplus$ represents point-to-point multiplication; α is the step size, and the adaptive $\text{Levy}(\lambda)$ of the step size realized by formula is Lévy flight random search path; x_{best}^t represents the best individual in the t generation.

CS algorithm has attracted the attention of many scholars because of its advantages such as few parameters, simple operation, and easy realization. Therefore, CS is used to solve the optimization problem in the model updating in this paper.

3. Result Analysis

In the health monitoring of landfill structure, strain sensors are usually placed at the large deformation position of the structure to obtain the local deformation information of the structure. On the benchmark model of landfill structure, considering the monitoring of large deformation information, the positions of strain sensors are initially located on four mid-span sections. The strain mode shapes need to contain as much information of displacement mode shapes as possible to avoid invalid estimation. Therefore, the position of the strain sensor must meet both the conditions of being in the large deformation section of the structure and containing enough information of displacement modes.

Because the mid-span section where the strain sensor is located is located at the node position of the element, the strain modal shapes at each section are related to the node displacement modal shapes of two adjacent beam elements. Table 3 gives the numerical values of the error quantification indexes at eight estimated node positions.

It can be seen from Table 3 that the estimation errors of displacement modal shapes at these eight estimation nodes are similar. Because the division of beam elements in the finite element model is basically uniform, and the transformation matrices of each element are almost identical, the relative estimation errors of displacement modal shapes of the eight estimated nodes are similar.

Figure 4 shows the trend diagram of the off-diagonal element value of the maximum MAC matrix of the displacement modal shape matrix with the number of acceleration sensors under four different redundancy thresholds (1, 0.6, 0.4, and 0.2).

It can be seen from Figure 4 that when the number of acceleration sensors increased is less than 3, the maximum MAC off-diagonal element values under different redundancy thresholds are the same. This shows that after adding the first several acceleration sensor positions, the redundancy coefficient between the existing sensor arrangement positions is less than 0.2, so the same position can be selected under different redundancy thresholds.

When the redundancy threshold is 0.6 or 1, the number of positions of acceleration sensors that can be increased exceeds 15. With the decrease of the redundancy threshold, the performance of sensor arrangement on MAC criterion is getting worse, and the number of acceleration sensors that can be increased is also getting smaller. If the number of available measuring points is less, the performance of MAC criterion will naturally deteriorate.

When calculating the optimal arrangement of sensors, each working condition is calculated continuously for 5 times, and the optimal value is taken as the final value of the objective function. After calculation, the objective function values under four working conditions are shown in Table 4.

It can be seen from Table 4 that the objective function value of TMAC (Three-dimensional MAC) criterion when 35 sensors are arranged is less than that of 25 sensors, but there is little difference between them. The arrangement schemes obtained under working conditions (1) and (2)
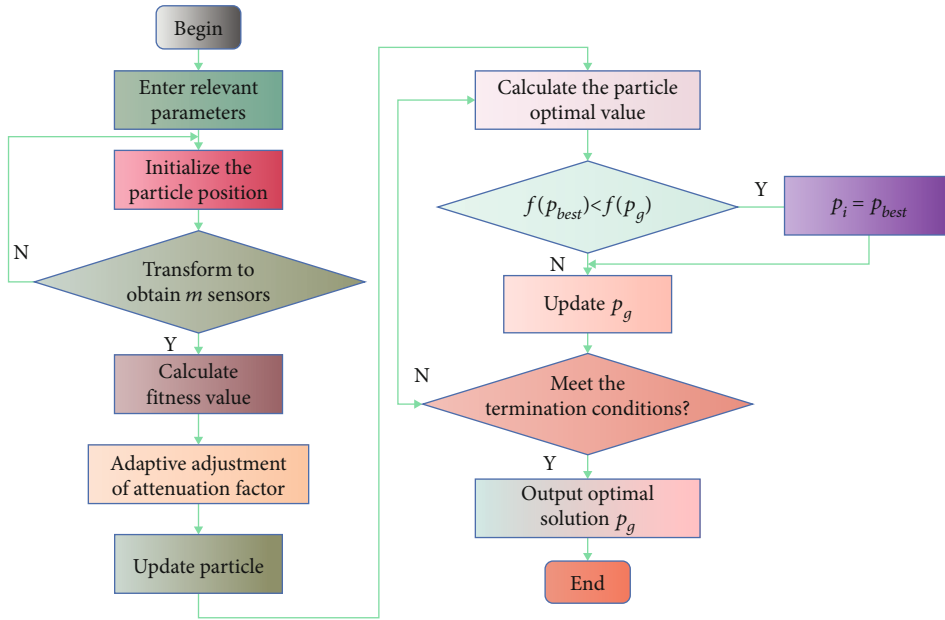
FIGURE 3: Optimal sensor layout process.

TABLE 3: Error quantification index values of 8 estimated node positions.

Node number	Index value (10^{-2})
1	1.67
2	1.71
3	1.82
4	1.71
5	1.66
6	1.73
7	1.81
8	1.82

TABLE 4: Objective function values of sensor optimal layout under four working conditions.

Working condition	Evaluation criteria	Number of sensors	Objective function value
1	TMAC	24	0.5238
2	TMAC	36	0.5122
3	TSVD	24	6.6247
4	TSVD	36	6.2239
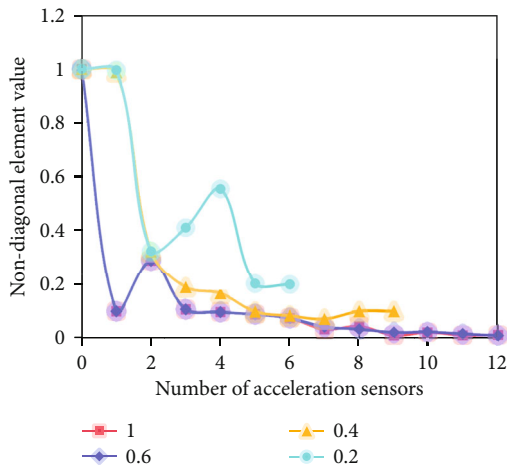
FIGURE 4: Maximum number of off-diagonal elements in MAC matrix.

are mainly distributed on the second ring, the third ring, and the outer ring support structurally. It shows that the increase of the number of sensors makes the modal identification effect better and improves the discrimination between vibration modes. The layout scheme obtained by TSVD (three-dimensional singular value ratio criterion), that is, working condition (3) and working condition (4), has better structural distribution than that obtained by TMAC criterion.

Figure 5 shows the graph of the maximum off-diagonal elements in each column vector of TMAC matrix. It can be clearly seen that the maximum value of 8 column vectors is 0.0378 and the minimum value is 0.0103. It can be seen that the optimal sensor placement results obtained by AGSA algorithm can meet the needs of practical engineering, and it also proves that AGSA algorithm is feasible for solving the optimal sensor placement problem.

With the introduction of CS, the performance of the proxy model of landfill structure, which is constructed by Kriging model, RBF (radial basis function), SVM (support vector machine), and RSM (Response Surface Methodology), is evaluated, respectively.

Assuming that the test parameter values are within the range of finite element parameter values, CS is used for iterative optimization. The number of nests is 25, and the
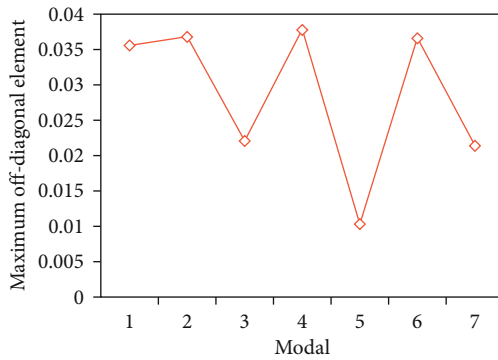
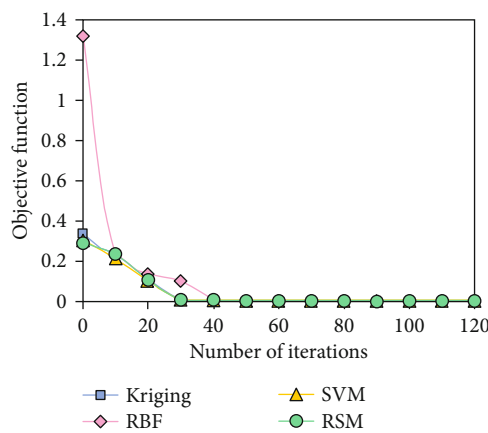Figure 5: Maximum off-diagonal element of each column vector of TMAC matrix.

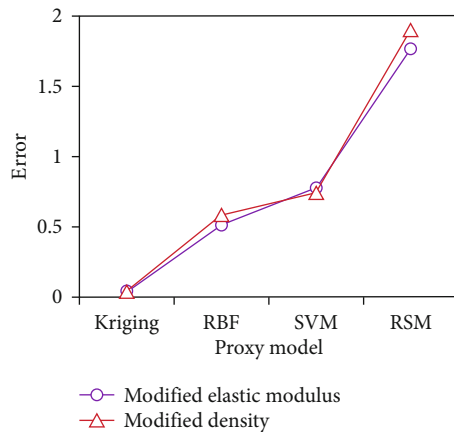Figure 6: Evolution curve of agent model based on CS.

Figure 7: Correction results of four kinds of proxy models.

maximum number of iterations is 120. The iterative convergence curves of the evolution process of the four proxy models are shown in Figure 6.

From the figure, it can be seen that the objective function can converge to 0 when the number of iterations is before 20 times, which indicates that the CS's optimization

ability is stable and the four proxy models meet the accuracy requirements.

Through the model modification of the same truss structure, the modification results of four proxy models are shown in Figure 7.

It can be seen from the comprehensive analysis that after the model modification of the same landfill structure, after the introduction of CS, the four proxy models have good fitting accuracy for the modification of the finite element model, and the error of the parameters before and after the modification is less than 2.5%. Considering the accuracy and operation efficiency at the same time, compared with other agent models, Kriging model has higher accuracy, shorter average operation time, and better comprehensive performance.

4. Conclusion

Sensor layout is the primary link of landfill structural health monitoring. The number and location of sensors directly affect the quantity and quality of monitoring data, and then affect the uncertainty of modal identification. How to select a limited number of locations from large-scale nodes to be tested in order to achieve the optimal layout effect is the core problem of this paper. Vibration detection cannot be used for the detection of high vibration and noise equipment, but the effective signal frequency band of stress wave monitoring is high, which can solve this problem well and is suitable for the detection of high vibration and noise equipment. Using the double coding method to initialize the population, the above problems are solved, and the AGSA algorithm successfully solves the problem of optimal sensor placement. Through the sensitivity analysis of the main parameters in the algorithm, the optimal parameters of AGSA algorithm for solving the optimal sensor placement problem are determined. The frequency response function is solved by minimizing the target parameter, and the frequency difference is corrected. After introducing CS, it is found that the parameter error before and after correction is less than 2.5%. It can be seen that the introduction of CS usually improves the effect of model correction. This paper has some innovation, but different types of sensors are not discussed separately, so further analysis is needed in future research.

Data Availability

The data used to support the findings of this study are available from the corresponding author upon request.

Conflicts of Interest

The authors declare no conflicts of interest.

Acknowledgments

References

[1] X. Sun, Z. Bai, K. Lin, P. Jiao, and H. P. Lu, "Optimization model of traffic sensor layout considering traffic big data," *Journal of Advanced Transportation*, vol. 2020, no. 19, Article ID 8845832, 11 pages, 2020.

[2] M. B. Hossain, M. A. Kabir, M. S. Hossain et al., "Numerical modeling of MoS2-graphene bilayer-based high-performance surface plasmon resonance sensor: structure optimization for DNA hybridization," *Optical Engineering*, vol. 59, no. 10, article 105105, 2020.

[3] F. Jiang, X. Zhang, X. Chen, and Y. Fang, "Distributed optimization of visual sensor networks for coverage of a large-scale 3-d scene," *IEEE/ASME Transactions on Mechatronics*, vol. 25, no. 6, pp. 2777–2788, 2020.

[4] W. Zhijun, L. Lu, C. Bingyan, H. Jing, and L. Zhanxian, "Optimal design and experiment research of an orthogonal-parallel six-axis force/torque sensor," *High Technology Letters*, vol. 27, no. 2, pp. 184–192, 2021.

[5] Q. Sun and Z. Ge, "Probabilistic sequential network for deep learning of complex process data and soft sensor application," *IEEE Transactions on Industrial Informatics*, vol. 15, no. 5, pp. 2700–2709, 2019.

[6] Z. Jian, Z. Ke, L. Zhifeng, and W. Zhigang, "Hand-eye calibration of welding robot based on the constraint of spatial line," *Hanjie Xuebao/Transactions of the China Welding Institution*, vol. 39, no. 8, pp. 108–113, 2018.

[7] R. Dai, H. Zhang, H. Lu, and X. Bai, "Research on structure optimization of thermoelectric MEMS microwave power sensor," *Yi Qi Yi Biao Xue Bao/Chinese Journal of Scientific Instrument*, vol. 39, no. 10, pp. 202–210, 2018.

[8] I. Yulianti, M. D. P. Ngurah, Y. Lestiyanti, and O. Kurdi, "Optimization of *ridge waveguide* structure for temperature sensor application using finite difference method," *MATEC Web of Conferences*, vol. 159, 2018.

[9] Y. Huang, Q. Xu, Q. Tan, and N. Xie, "Optimization of electric field distributions in OVS with hybrid algorithm," *IEEE Sensors Journal*, vol. 19, no. 21, pp. 9748–9754, 2019.

[10] Y. Junzhi, T. Wang, W. Zhengxing, and M. Tan, "Design of a miniature underwater angle-of-attack sensor and its application to a self-propelled robotic fish," *IEEE Journal of Oceanic Engineering*, vol. 45, no. 4, pp. 1295–1307, 2019.

[11] L. Osberger and V. Frick, "Analysis, design, and optimization of the CHOPFET magnetic field transducer," *IEEE Transactions on Electron Devices*, vol. 65, no. 8, pp. 3454–3459, 2018.

[12] F. Franco, M. Silva, S. Cardoso, and P. P. Freitas, "Optimization of asymmetric reference structures through non-evenly layered synthetic antiferromagnet for full bridge magnetic sensors based on CoFeB/MgO/CoFeB," *Applied Physics Letters*, vol. 118, no. 7, article 072401, 2021.

[13] Z. Jing, T. Zheng, J. Li, and K. Feng, "Optimized design of an anti-rotation and anti-overload structure based on missile-borne semi-strap-down inertial navigation system," *IEEE Access*, vol. 7, pp. 179646–179657, 2019.

[14] H. Chen, B. Xu, Y. Mo, and T. Zhou, "Multi-scale stress wave simulation for aggregates segregation detection of concrete core in circular CFST coupled with PZT patches," *Materials*, vol. 11, no. 7, 2018.

[15] X. Li, S. Gong, L. Dou, and Y. Chai, "Detection of stress redistribution in a complex isolated coal pillar with active SVT technology," *Arabian Journal of Geosciences*, vol. 13, no. 18, 2020.

[16] N. Z. Gurel, H. Jung, S. Hersek, and O. T. Inan, "Fusing near-infrared spectroscopy with wearable hemodynamic measurements improves classification of mental stress," *IEEE Sensors Journal*, vol. 19, no. 19, pp. 8522–8531, 2019.

[17] Y. N. Wang, R. Xu, Y. Kai, H. Wang, and B. H. Gong, "Evaluating the physicochemical properties of refuse with a short-term landfill age and odorous pollutants emission during landfill mining: a case study," *Waste Management*, vol. 121, pp. 77–86, 2021.

[18] D. P. Nascimento, V. L. Menezes, M. Carvalho, and R. Chacartegui, "Energy analysis of products and processes in a sanitary landfill," *IET Renewable Power Generation*, vol. 13, no. 7, pp. 1063–1075, 2019.

[19] Y. Xu, Y. Fu, W. Xia, D. Zhang, D. An, and G. Qian, "Municipal solid waste incineration (MSWI) fly ash washing pretreatment by biochemical effluent of landfill leachate: a potential substitute for water," *Environmental Technology*, vol. 39, no. 15, pp. 1949–1954, 2018.

[20] Y. N. Wang, R. Xu, H. Wang, H. Shi, and M. Zhan, "Insights into the stabilization of landfill by assessing the diversity and dynamic succession of bacterial community and its associated bio-metabolic process," *Science of the Total Environment*, vol. 768, article 145466, 2021.

Hindawi

Retraction

Retracted: Development and Performance Evaluation of Digital Technology and Radio and Television Integration Based on Big Data Model

Journal of Sensors

This article has been retracted by Hindawi following an investigation undertaken by the publisher [1]. This investigation has uncovered evidence of one or more of the following indicators of systematic manipulation of the publication process:

(1) Discrepancies in scope

(2) Discrepancies in the description of the research reported

(3) Discrepancies between the availability of data and the research described

(4) Inappropriate citations

(5) Incoherent, meaningless and/or irrelevant content included in the article

(6) Manipulated or compromised peer review

The presence of these indicators undermines our confidence in the integrity of the article's content and we cannot, therefore, vouch for its reliability. Please note that this notice is intended solely to alert readers that the content of this article is unreliable. We have not investigated whether authors were aware of or involved in the systematic manipulation of the publication process.

Wiley and Hindawi regrets that the usual quality checks did not identify these issues before publication and have since put additional measures in place to safeguard research integrity.

We wish to credit our own Research Integrity and Research Publishing teams and anonymous and named external researchers and research integrity experts for contributing to this investigation.

The corresponding author, as the representative of all authors, has been given the opportunity to register their agreement or disagreement to this retraction. We have kept a record of any response received.

References

[1] J. Lv and Y. Tao, "Development and Performance Evaluation of Digital Technology and Radio and Television Integration Based on Big Data Model," *Journal of Sensors*, vol. 2022, Article ID 1843753, 11 pages, 2022.

Hindawi

Research Article

Development and Performance Evaluation of Digital Technology and Radio and Television Integration Based on Big Data Model

Jing Lv [1] **and Yanrui Tao** [1,2]

[1]*Pingdingshan University, Pingdingshan Henan 467000, China*
[2]*Azman Hashim International Business School, Universiti Teknologi Malaysia, Kuala Lumpur 54100, Malaysia*

Correspondence should be addressed to Jing Lv; lvjing@pdsu.edu.cn

In today's big data era, China's radio and television broadcast volume has reached an unprecedented height, and it is diversified in quality and content richness. The realization of big data model accelerates the transformation of radio and television and constantly reaches new movie-watching heights. In the era when TV dramas, movies, animation, radio stations, and We Media are prevalent, big data is being experimentally analyzed through professional digital technology and effective methods of media integration of radio and television. In order to make China's radio and television industry present a strong industrialization development trend, it is necessary to have a suitable network system to form a pillar, so as to play a substantial role in the development of this industry. Choosing the appropriate evaluation system to evaluate the broadcast volume, ratings, box office volume, and profit income of the mass media is also a breakthrough stage of today's technical ability. The experimental results of this paper show that (1) from the ratings of only 15% in 2010 to 75% today, the successful investment of radio and television in the market has been realized, and the efficient development of modern technology has benefited the people. (2) Department executives are mainly in charge of the economic lifeline of enterprises, and 70% of economic indicators is the embodiment of small workload and high voice of key tasks, which are the main roles in performance evaluation. (3) The accuracy of the old index is only 75 while the new index is 90, so selecting excellent performance indicators is also responsible for performance appraisal. (4) The development of radio and television from urban to rural areas, from 0% of the market to 12.23% of the rural areas, is a manifestation that the development of modern science and technology benefits the whole people. Only when performance evaluation is fed back to the market can it adapt to the next stage of reform and improve the enthusiasm of employees.

1. Introduction

With the advent of the information age, the emergence of mobile Internet makes radio and television have new development concepts and goals. In the era of Internet and new media, all TV stations have a strong market competition, and they are carrying out deepening reforms in order to achieve good economic benefits. The development of each TV station has a set of powerful color theory system, but the change can maximize the benefits and gain a foothold

in the market. Nowadays, most city TV stations tend to develop private enterprises, and few enterprises have studied the development trend of state-owned enterprises, so that radio and television cannot develop comprehensively and efficiently. Therefore, the performance evaluation of radio and television media industry is the current reform road. This paper analyzes the demand of media industry for all-media talents under the background of media convergence and points out the problems existing in the construction of all-media talents [1]. Adopting principal component method

and clustering method in multivariate statistical analysis, this paper makes a preliminary study on the performance evaluation method of radio and television stations [2]. This paper analyzes and compares the company's operating performance and financial situation, puts forward the methods to optimize the film and television industry chain [3], constructs the financial competitiveness evaluation model of the company, and strengthens the content management and brand benefit measures to improve the current management mode of the company [4]. This paper analyzes how to evaluate the value of TV drama projects and puts forward how to establish a standard evaluation model [5]. This paper constructs the evaluation index system of TV drama project value and discusses the political standards of TV drama project [6]. This paper analyzes the advantages and disadvantages of developing 5G in radio and television and expounds the development goals and paths of 5G in radio and television [7]. The "signal-based method" is adopted to control the behavior of synchronous propagation of signals [8]. This paper describes the synchronous communication behavior implemented by the network, puts forward the legitimate interests of broadcasting organizations, and realizes the technology in legislation [9]. This paper analyzes the narrative method of documentary film and television and its value and probes into the related expression methods [10]. This paper discusses that technological innovation is driving TV media to accelerate the transformation to converged media, and three periods are follows: media convergence, converged media, and intelligent media [11]. This paper probes into the characteristics, motivation, and path of media convergence and provides reference for relevant practitioners to study and practice [12]. This paper introduces the importance of journalism professionals to the new development of media integration and analyzes the strategies for cultivating high-quality journalism professionals [13]. This paper deeply explores the path of integration and transformation of prefecture-level TV media and new media in China and provides some reference opinions for the sustainable development of prefecture-level TV media [14]. This paper studies the environment of media convergence and expounds the training methods of radio and television news professionals [15].

2. Management Method Based on Performance Evaluation

2.1. Performance Evaluation Method.
Performance evaluation is based on the assessor corresponding to the corresponding assessment standards, and the implementation process needs the assistance and cooperation of the assessor. After the results are summarized and approved, the assessment report is formed, and finally, the performance evaluation is implemented. The process is shown in Figure 1.

2.1.1. Performance Evaluation Method of Printing Machinery Association

(1) DEA Method. DEA method [16] analyzes the market development situation according to the input resources to

expand it and produce huge products. The relevant interest rate is calculated from the input and result data. DEA models are usually CCR and BCC models. The compressed input ratio is defined as DMU [17]. That is, as shown in

$$DMU = \frac{1/\text{Max}}{\text{Min}}. \tag{1}$$

Its Max and Min distributions represent output expansion ratio and input compression ratio.

(2) CCR Model. CCR model [18] is based on the static DEA method to carry out the actual efficiency value and compare it with efficiency 1. The model is shown in

$$\text{Max} \frac{\sum_{r=1}^{s} u_r y_{ro}}{\sum_{i=1}^{m} v_i x_{io}} \leq 1 \tag{2}$$

$$s.t \frac{\sum_{r=1}^{s} u_r y_{rj}}{\sum_{i=1}^{m} v_i x_{ij}} \leq 1, \quad j = 1, \cdots, n \tag{3}$$

$$u_r, v_i > 0, \quad r = 1, \cdots, s, i = 1, \cdots, m \tag{4}$$

Among them, the input index number is m, the output index number is s, x_{ij}, and y_{ij}, and the weight coefficient is v_i and u_r.

(3) Linear model. Linear model [19] is the transformation of CCR model. The formula expression is

$$\text{Max} \sum_{r=1}^{s} u_r y_{ro} \leq 0$$

$$s.t. \sum_{r=1}^{s} u_r y_{rj} - \sum_{i=1}^{m} v_i x_{ij} \leq 0, \quad j = 1, \cdots, n$$

$$\sum_{i=1}^{m} v_i x_{io} = 1 \tag{5}$$

$$u_r, v_i > 0, \quad r = 1, \cdots, s, i = 1, \cdots m$$

(4) Dual Model. In dual model [20], the formula is as follows:

$$F = \text{Min} \theta_o$$

$$s.t. \sum_{j=1}^{n} \lambda_j x_{rj} \leq \theta_o x_{io}, \quad i = 1, \cdots, m$$

$$\sum_{j=i}^{n} \lambda_j y_{ij} \geq y_{ro}, \quad r = 1, \cdots, s \tag{6}$$

$$\lambda_j \geq 0, \quad j = 1, \cdots, n$$

where θ_O represents the production efficiency of DMU. X_{ij} and Y_{ij} are input vectors and output vectors, respectively. J represents the contribution rate.
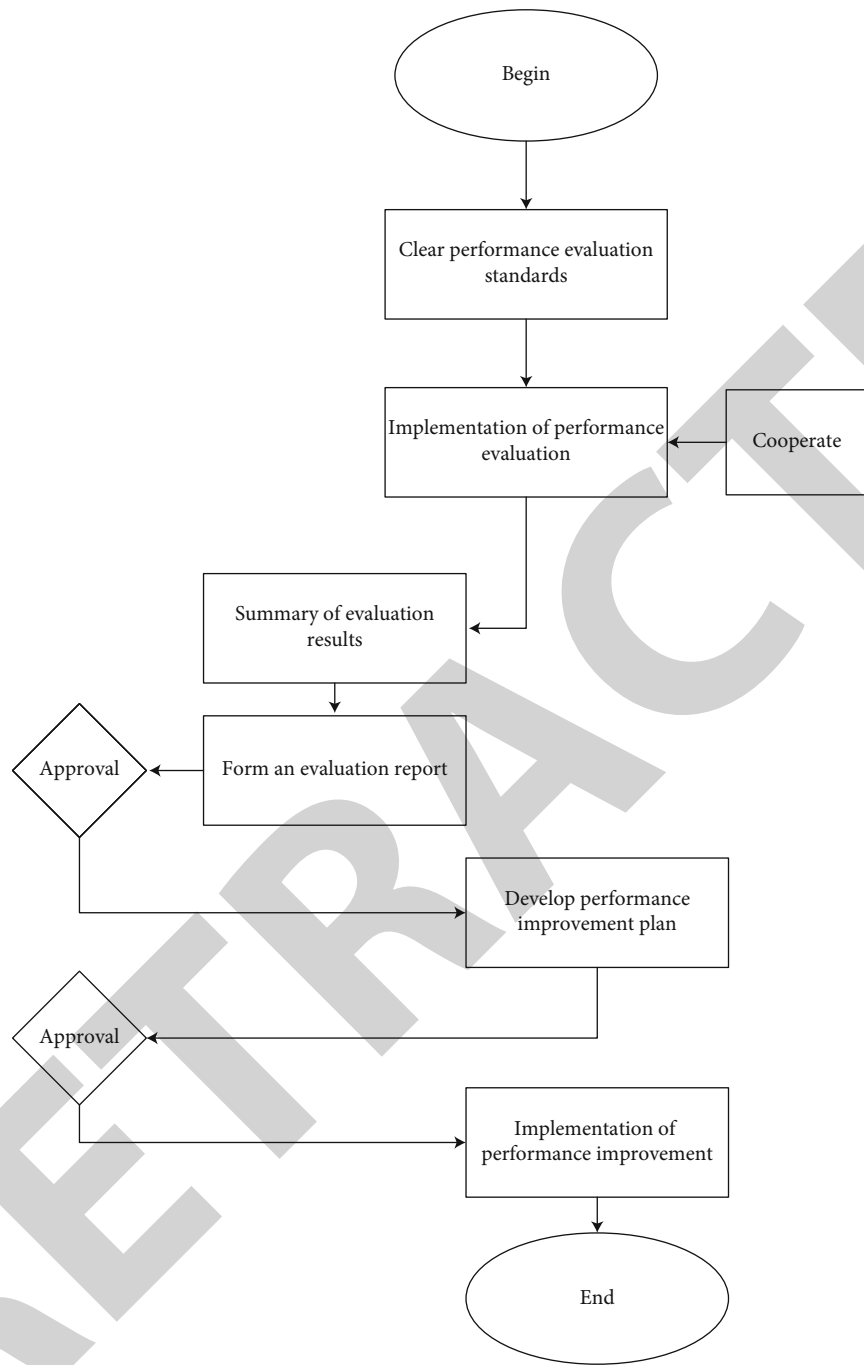
Figure 1: Performance evaluation flow chart.

(5) Guided CCR Model. In guided CCR model [21], the calculation formula is as follows:

$$F = \text{Max}\varphi_o$$

$$s.t. \sum_{j=1}^{n} \lambda_j x_{ij} \leq x_{io}, \quad i = 1, \cdots, m$$

$$\sum_{j=1}^{n} \lambda_j y_{rj} \geq \varphi_o y_{ro}, \quad r = 1, \cdots, s \tag{7}$$

$$\lambda_j \geq 0, \quad j = 1, \cdots, n$$

When $\theta_O = 1$, the DEA calculation is valid.

(6) BBC Model. BBC model is based on the assumption of DEA calculation method, which is divided into two parts: input model and output model of oriented BBC.

(6)1. Input-oriented BBC Model. In input-oriented BBC model [22], the formula is as follows:

$$F = \textbf{Min}\theta_o$$

$$s.t. \sum_{j=1}^{n} \lambda_j x_{ij} \leq \theta_o x_{io}, \quad i = 1, \cdots, m$$

$$\sum_{j=1}^{n} \lambda_j y_{rj} \geq y_{ro}, \quad r = 1, \cdots, s \tag{8}$$

$$\sum_{j=1}^{n} \lambda_j = 1$$

$$\lambda_j \geq 0, \quad j = 1, \cdots, n$$

(6)2. Output-Oriented. In output-oriented [23], the formula is as follows:

$$F = \textbf{Max}\varphi_o$$

$$s.t. \sum_{j=1}^{n} \lambda_j x_{ij} \leq x_{io}, \quad i = 1, \cdots, m$$

$$\sum_{j=1}^{n} \lambda_j y_{rj} \geq \varphi_o y_{ro}, \quad r = 1, \cdots, s \tag{9}$$

$$\sum_{j=1}^{n} \lambda_j = 1$$

$$\lambda_j \geq 0, \quad j = 1, \cdots, n$$

BBC model adds convexity hypothesis and realizes the efficiency calculation of reward. There are three kinds of efficiency evaluation: comprehensive efficiency, pure technical efficiency, and scale efficiency.

2.1.2. Tobit Regression Method. Tobit regression method [24] represents a large efficiency value between 0 and 1.
The regression model is as follows:

$$Y_i = \beta_o + \beta_t X_i + \mu_i, \tag{10}$$

where I denotes DMU, Y_i denotes the efficiency value of the ith DMU, X_i denotes the explanatory variable, β_t denotes the coefficient to be estimated, and μ_t denotes the error, obtained by Tobit model consistent estimator [25].

3. Performance Evaluation and Analysis of Radio and Television Development

3.1. Nature of Performance Evaluation Indicators

3.1.1. Systematic. In the road of developing radio and television, due to the influence of environmental and human factors, there are obvious differences in project progress. Therefore, enterprises should consider the engineering practicability of the whole system and remove unnecessary location factors when carrying out year-end performance evaluation. In the selection of evaluation indicators, the key indicators are conducive to analyzing the malpractice effects of evaluation indicators. Integrating the performance of multiple departments cannot be evaluated separately, which is not conducive to the fairness and justice of the assessment. Choosing the mode of seeking common ground and different existence at the same time of broadcasting assessment reflects the system characteristics of broadcasting system.

3.1.2. Comprehensiveness and Orientation. The object and subject of evaluation is the expenditure of diversified performance evaluation, and it is also the key point of development in the era of big data. Different evaluation objects choose different evaluation criteria, stand at different angles, and have different degrees of control over key points of performance. From the perspective of fiscal revenue, the assessment content of the ratio of expenditure to income is considered.; If it is an analysis angle on the technical level, it should be the assessment content of the technical level and the speed of completion progress; from the manager's point of view, the efficiency of work progress and economic income efficiency of the whole enterprise should be the assessment standard. Therefore, it is the qualitative and quantitative standard to analyze the assessment points from different angles. At the same time of assessment, there should be a degree of relaxation. Not all indicators are particularly important. It is necessary to judge whether the indicators meet the assessment requirements from the perspective of comprehensive consideration.

3.1.3. Operability. In the face of sufficient data to employees and the entire enterprise, performance appraisal is the right to determine the evaluation. The results of performance evaluation are the embodiment of achievements, rankings, and grades, and no matter what the results are, they are the evaluation of your labor results in a year. Reasonable operation while carrying out different evaluation types is

the correct choice, which is to follow the principle of operability. Visual analysis and convenience of a large amount of data are the basic principles of fairness and justice in the actual situation of examiners. Each enterprise has its own number of indicators, and invalid indicators are abandoned, effective indicators are evaluated, and the overall index system is convenient for efficient operation.

3.1.4. Validity.
The validity of the index needs to find the corresponding evaluation index according to the evaluation object and structure organization, so as to give full play to the validity of the data. In order to truly reflect the development trend of radio and television enterprises, we should follow the effective principle in order to clarify the development potential of television enterprises. The content of the index system followed by the effectiveness and the function of the evaluation subject are interrelated, so as to effectively analyze the evaluation results. Undertaking corresponding functions and work contents is an effective embodiment of the evaluator's ability, and the corresponding work scope indicators are the effective performance of functions.

3.2. Principles of Constructing Performance Evaluation Indicators

3.2.1. Principle of Integrity.
Analyzing the results of performance appraisal of TV enterprises, the selected evaluation index should be constructed according to individual labor achievements and market living environment: considering the development status of radio and television, taking into account the people's feelings and national conditions, and comprehensively considering the evaluation criteria, in order to fully reflect the activity characteristics, finance, and characteristics of radio and television.

3.2.2. Principle of Flexibility.
The performance appraisal of radio and television should be adjusted flexibly according to the change of environment. Different cities and regions have obvious characteristics, and seeking local characteristics is an effective measure for development. From the results of performance evaluation, we can know the development of each region, so as to make corresponding reform measures. Flexible evaluation indicators for local representatives in different regions can ensure high-quality performance evaluation results.

3.2.3. Operability Principle.
The subject and object of evaluation must be based on the index embodiment of radio and television, so as to realize the most basic operation. The setting of indicators is not only easy to use but also useful. Only by satisfying the most basic evaluation significance can the operability and significance of indicators be guaranteed. Only when the index is expressed effectively and the collected data is clear and standardized as far as possible can the index play its role.

3.2.4. Minimization Principle.
According to the criterion of assessment experience, half of the total input and output indicators can be selected to maximize the success of evaluation. Too many evaluation indexes will only cause the difficulty of work and reduce the effectiveness of evaluation. Therefore, on the premise of ensuring integrity and effectiveness, the selected indicators should try their best to minimize the number.

3.3. Weight Distribution of Performance Evaluation Indicators.
The weight distribution of performance evaluation is related to the selection of future indicators of the whole enterprise. The higher the weight index, the higher the importance in the index system. Therefore, the weight distribution given to the overall benefit index of the project should occupy an important position in the whole performance evaluation index system. The relevant weights of indicator classification are shown in Figure 2.

In the index system, the weight distribution of indicators should select the assessment angle of evaluation. Radio and television have its own personality indicators, which are direct indicators covered according to the characteristics of TV programs, and have more assessment significance than substantive indicators. In the performance appraisal, we should evaluate objectively and seek common ground and difference. The assessment involves various contents and situations, and the indicators are diversified and difficult to predict, with strong comprehensiveness. When we select indicators, we should make it clear that quantitative indicators, ordinary indicators, personality indicators, and result indicators will be given a large weight ratio.

3.4. Optimization Analysis of Performance Indicators.
Reasonable optimization of indicators has great advantages for enterprises and development, which improves the broadcasting rate of radio and television, and effectively improves the ratings. Facing the optimized index, the technical level of enterprises will be improved and the economic benefits will be maximized. The optimization feedback is shown in Figure 3.

From the beginning of collecting evaluation data of individuals or topics, employee performance appraisal forms can be formed according to the data, and performance evaluation can be carried out. The evaluation results are convenient to correct the problems of employees or enterprises in time, take the results for effective feedback of performance, and then apply them to the results analysis for in-depth analysis. After reaching the final adjustment, it can be analyzed and used cyclically.

3.5. Performance Evaluation Report.
Every performance appraisal reflects the results of personal efforts and the financial income of enterprises, which is a summary of the year. In radio and television, it is an important indicator of reform in the coming year, realizing the development pattern of improving ratings and expanding broadcasting range. The practicality of evaluation implementation is shown in Figure 4.

In the radio and television evaluation system, in order to meet the ultimate goal of enterprise operation and high income, there will be value orientation, control objectives, and feedback correction measures. Among them, the
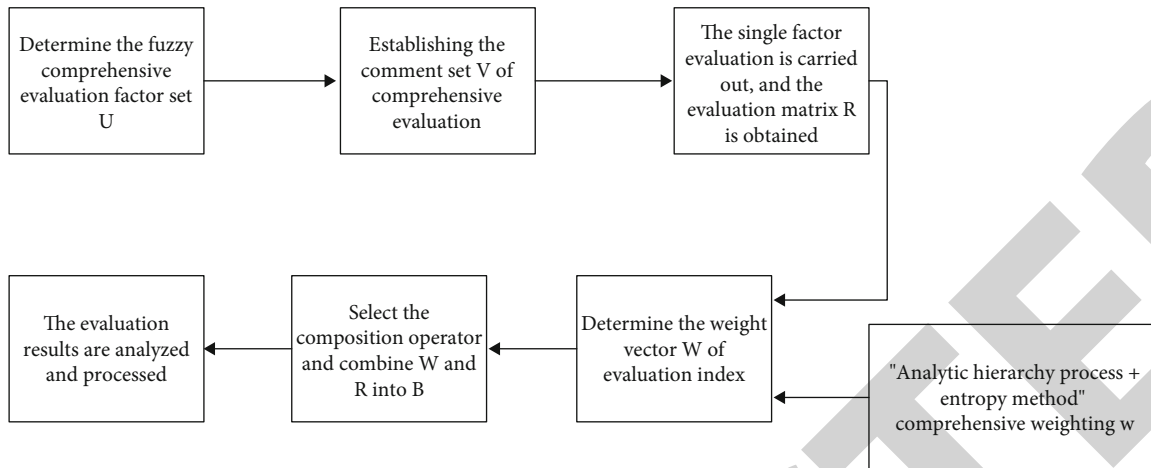
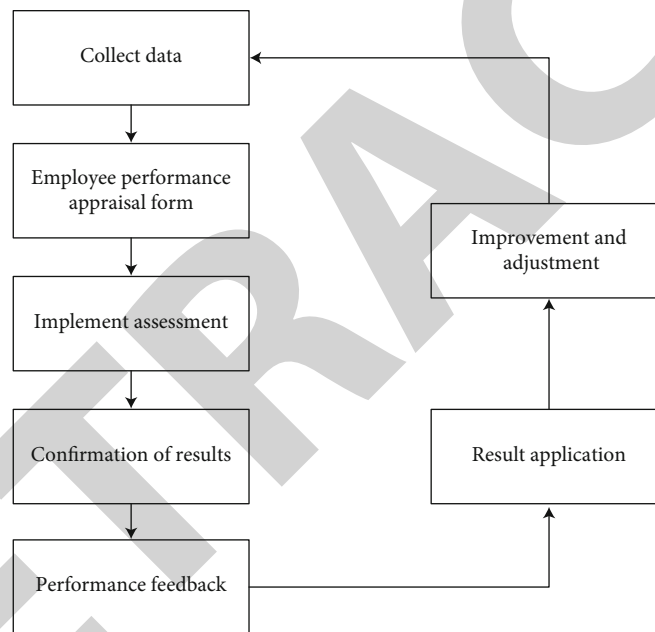FIGURE 2: Index weight distribution diagram.

FIGURE 3: Performance indicator optimization process chart.

evaluation value orientation has the characteristics of practicality, dynamics, and relevance. In the control objective, it is influenced by input factors, output factors, and efficiency factors.

4. Experimental Analysis of Radio and Television Performance Evaluation

4.1. Analysis of Input-Output Ratio. According to the quantitative analysis of enterprise ratings, input index, and output index in recent years, the development and future situation of radio and television in recent years will be observed. As shown in Figure 5.

According to the data in Figure 5, the lack of popularity of the Internet in 2012-2015 led to less than 40% of the audience rating, and most people still could not enjoy TV and film. Correspondingly, with the opening of the market and

the rise of Internet TV, it immediately caused the investment of merchants and made corresponding gains. This is also the embodiment of economic growth and efficient development of data visualization, which leads to the efficient development of radio and television.

4.2. Weight Analysis of Characteristic Indicators in Performance Evaluation. The rise of the era of big data confirms the efficient development of radio and television culture level and also actively promotes the realization of broadcasting reform system. On the premise of keeping objective performance evaluation, we use the weight ratio of multiple indicators to analyze the shortcomings of radio and television to provide reference objects. The performance evaluation weights are shown in Figure 6.

It can be seen from the chart that different positions have different proportions in job performance evaluation.
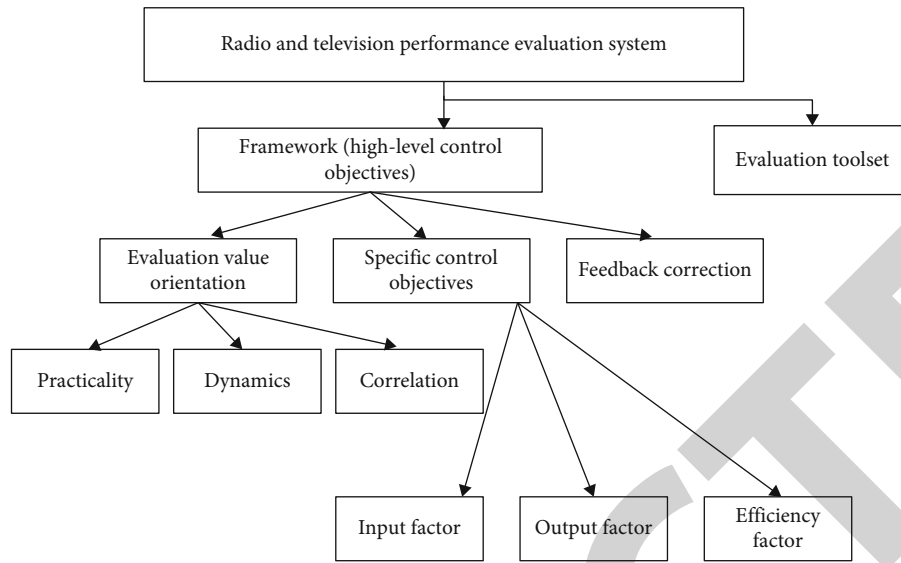
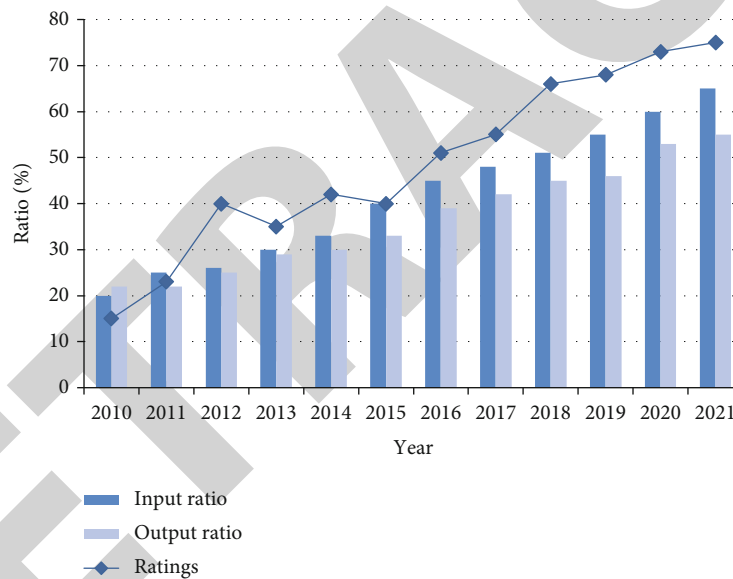FIGURE 4: Performance evaluation system diagram.

FIGURE 5: Analysis chart of TV broadcasting market in recent years.

Economic indicators account for the highest weight ratio, which also shows that economic promotion is the first development purpose of enterprises. With the corresponding increase in the tasks of basic employees, there is also an improvement in basic functional indicators. It can also be known from the figure that in the index embodiment, the sum of the performance evaluation weight ratios of relevant personnel is equal to 1.

4.3. Comparative Analysis of Index Optimization.

The indicators selected for radio and television performance evaluation directly affect the trend of assessment results. According to the characteristics of different varieties, different trading periods, and different profit models, the high effi-

ciency indicators are specially selected. The comparative analysis of optimized data is shown in Figure 7.

Obviously, it can be seen that the success of the new index in different assessment items is obviously improved, which makes the assessment results more accurate. However, the combination and fitness need to be improved, so as to make the assessment more smooth and successful. No matter what position there are suitable assessment indicators to match, which not only improves convenience but also makes it smoother.

4.4. Analysis of Asset Operation Efficiency.

Combined with the assets invested by GAC media before and after and some liabilities, it is known that the investment and success of radio and television assets have been significantly improved.
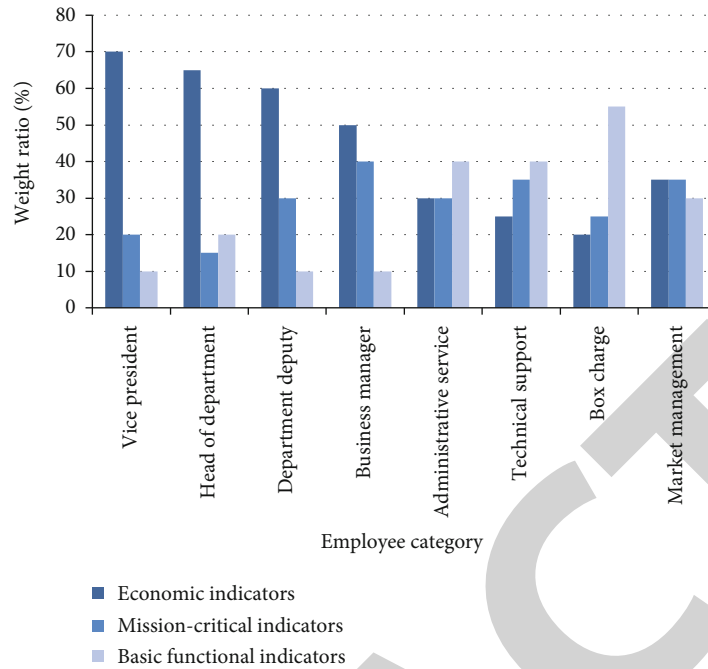
Figure 6: Weight ratio chart of employee performance evaluation index.
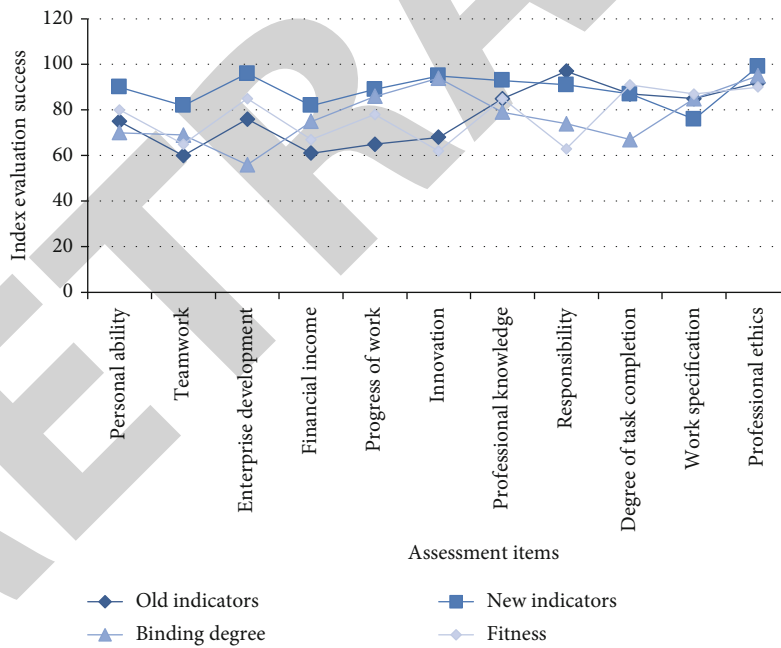

Figure 7: Comparison chart of evaluation completion of old and new indicators.

From the financing structure of short-term loans, notes payable, and long-term loans, we can know that the overall debt ratio of enterprises has been greatly reduced and the income has increased significantly. The analysis of fiscal revenue combined with operational capability is shown in Figure 8.

Account receivable turnover rate is equal to the ratio of operating income to account receivable, which indicates the number of account receivable turnover in one year. From the experimental data of radio and television, it can be seen

that compared with the annual turnover times, there is an obvious increase, but there will also be a downward trend in the economic period. For example, 12.65 times in 2014 decreased by 2.9 times compared with 15.55 times in 2013, which depends on the economic environment.

Inventory turnover is the ratio of operating costs to inventory, representing the number of inventory turnover during the year. The number of inventories is not the more the better, but according to the turnover needs of
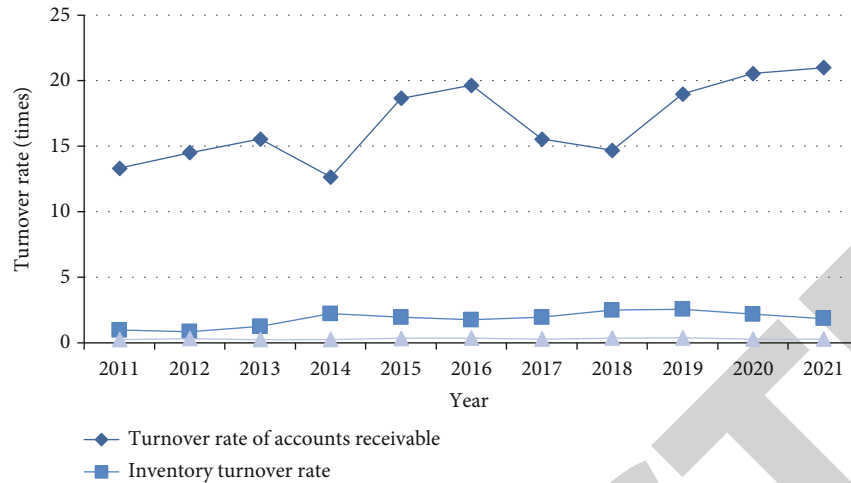
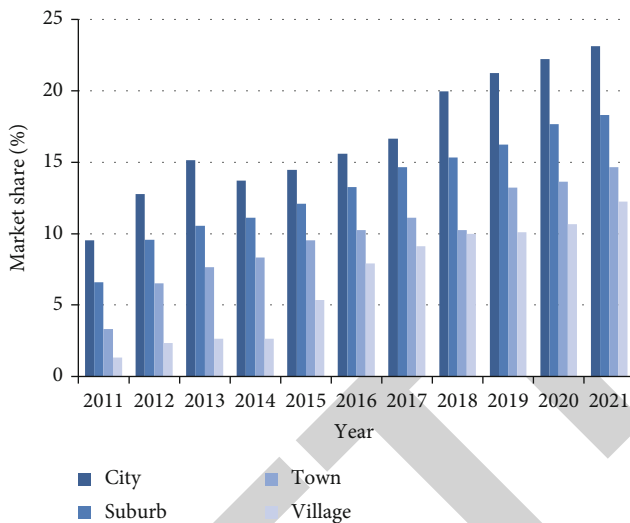Figure 8: Operational capability indicators of radio and television assets.

Figure 9: National market share.

Figure 10: Customer satisfaction measurement system.

enterprises, too much waste and too little turnover cannot be opened. Since 2011, the inventory quantity has obviously increased, but it has always maintained a relatively high level, which proves the improvement of inventory capacity and management level. From 0.97 in 2011 to 2.56 in 2019, the quantity has increased, that is, a historical high level has been produced.

Total asset turnover rate is the ratio of operating income to total assets, which indicates the number of total asset turnover in the middle of the year and reflects the average time required for enterprises to convert total assets into cash. Under the average level of 0.33 turnover times of total assets, there are still ups and downs in different years. It is higher than the average value, and it also expresses the increase of asset scale and sales revenue.

4.5. Market Share of Radio and Television. City, suburbs, towns, and rural areas in the process of realizing network integration are obviously uneven progress, which also shows
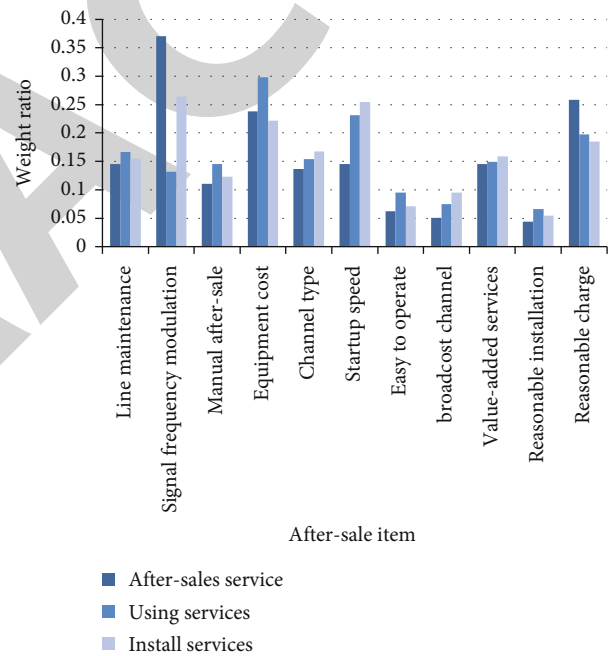
that the growth of market share in different regions is obviously different. Realizing the integration of urban and rural network is an important strategy for future development. Only by continuously improving the layout of wired network can we achieve market share, combined with market area analysis, as shown in Figure 9.

Facing the economic development of different regions, the economy of big cities is obviously higher than that of other regions, that is, the number of people with modern facilities will be higher than that of other regions, and there is a primary market. With the improvement of economic level, people's willingness to enjoy life is enhanced, and the universality of television is increasing. From 0 market in rural areas to 12% market today, it shows the success of Internet and the efficient development in the era of big data.

4.6. Research on Measurement System Based on Customer Satisfaction. Customer satisfaction is an effective evaluation of enterprise development, which reflects the reputation image of enterprise development in the crowd. The index analysis of radio and television on customer satisfaction measurement system is shown in Figure 10.

Enterprises get feedback problems according to the feedback analysis of users' satisfaction and then adopt the corresponding after-sales service to solve the problems. Being a user is the core of the first service gradient, which requires not only user satisfaction but also user perception as the ultimate service goal. This is the key practice to gain a foothold in the market and have good market praise. Let consumers feel at ease and be willing to buy many times in order to maximize the benefits and expand the market.

5. Conclusion

During the decades of Internet revolution, radio and television are developing rapidly. In these decades, radio and television are more specialized and have more people-friendly channels, which have been deeply loved by people. Through the effective analysis of digital technology of big data model, the market development of radio and television is known, which is beneficial for enterprises to realize comprehensive and in-depth reform. Using the effective analysis of data, we can know the market demand and the services that should be provided in the future in time. According to the future demand and industry development, it is an effective plan for the construction of radio and television, and it is also a challenge for the industry in the future. With the limited combination of "triple play," China's media industry will make unprecedented progress and achieve a high-quality leap. In order to better provide broadcasting products to the public, a good platform and channel support will be needed to achieve good services.

According to the analysis of the research results of this paper, the following points are summarized: (1) the development of radio and television is a practical change based on the analysis and assessment of modern data, which makes a profound analysis of adapting to the changes of the times and the development of modern enterprises. (2) Reasonable evaluation of performance is not only the responsibility of managers, but also the performance results are a powerful embodiment of the development of the enterprise in one year. Effective assessment reflects the advantages and disadvantages of the assessor, thus guiding the next stage of work of employees. (3) The development of radio and television is to determine the actual sales situation of the market through the feedback of customer satisfaction. Service is the first, which plays a vital role in the construction of media industry. (4) Economic investment is the performance of paying attention to enterprises, and high capital must be invested in order to obtain high returns. Radio and television is a necessary road for the development of service industry and mass market.

This research content and lack of items: (1) There is no consideration of human factors in the performance evaluation, which leads to the fairness of some assessors, and should be strictly standardized. (2) With the diversity of big data products, that is, the data is generalized and false, so the evaluation is strictly based on the experimental data. (3) There is a single index that cannot evaluate the performance of the assessors, and all-round indicators will be used to effectively evaluate the evaluation index of the enterprise collective. (4) From the perspective of the managers of performance evaluation, the quantification of evaluation will approach equality, and ignoring the understanding of the purpose of evaluation will be an invalid evaluation.

Data Availability

The experimental data used to support the findings of this study are available from the corresponding author upon request.

Conflicts of Interest

The authors declared that they have no conflicts of interest regarding this work.

References

[1] L. Xiaoming, "Analysis on the construction of all-media talent team under the background of media convergence," *News Research Guide*, vol. 10, no. 6, pp. 251-252, 2019.

[2] W. He, "A brief analysis of the impact of online media on TV media," *New Media Research*, vol. 1, no. 19, pp. 45-46, 2015.

[3] Z. Xiaoyan and Z. Huiqun, "Performance analysis of listed companies in film and television entertainment industry," *Journal of Beijing Institute of Printing*, vol. 25, no. 8, 2017.

[4] W. Yanni, L. Lingfei, and Z. Hong, "Research on the evaluation of financial competitiveness of listed film and television companies in China," *Journal of Shandong University of Science and Technology (Social Science Edition)*, vol. 21, no. 3, 2019.

[5] J. Tian, "Discussion on the value evaluation of TV drama projects," *Communication Research*, vol. 3, no. 25, p. 79, 2019.

[6] Z. Dan and S. Peiyi, "Research on the value evaluation of TV drama projects from the perspective of investment and financing," *Modern Communication (Journal of Communication University of China)*, vol. 41, no. 3, pp. 125–132, 2019.

[7] L. Shi, L. Zhongxiang, and G. Feng, "Analysis and thinking on the construction and development of provincial 5G platform of radio and television," *Radio and Television Technology*, vol. 47, no. 9, pp. 122–125, 2020.

[8] W. Qian, "The object of broadcasting organization right-also an analysis of "signal-based method"," *Legal Research*, vol. 39, no. 1, pp. 100–122, 2017.

[9] W. Qian, "On the expansion of broadcasting rights of broadcasting organizations. Also on article 42 of the revised draft of copyright law (draft for review)," *Legal Business Research*, vol. 33, no. 1, pp. 177–182, 2016.

[10] C. Xia, "Interpretation of storytelling, film and television narrative techniques of documentaries," *Research on communication power.*, vol. 2, no. 23, p. 58 +60, 2018.

[11] L. Xiangzhong, "From media convergence to converged media: TV people's choice and approach," *Modern Communication (Journal of Communication University of China)*, vol. 42, no. 1, pp. 1–7, 2020.

Hindawi

Retraction

Retracted: Research and Analysis of Combination Forecasting Model in Sports Competition

Journal of Sensors

This article has been retracted by Hindawi following an investigation undertaken by the publisher [1]. This investigation has uncovered evidence of one or more of the following indicators of systematic manipulation of the publication process:

(1) Discrepancies in scope

(2) Discrepancies in the description of the research reported

(3) Discrepancies between the availability of data and the research described

(4) Inappropriate citations

(5) Incoherent, meaningless and/or irrelevant content included in the article

(6) Manipulated or compromised peer review

The presence of these indicators undermines our confidence in the integrity of the article's content and we cannot, therefore, vouch for its reliability. Please note that this notice is intended solely to alert readers that the content of this article is unreliable. We have not investigated whether authors were aware of or involved in the systematic manipulation of the publication process.

In addition, our investigation has also shown that one or more of the following human-subject reporting requirements has not been met in this article: ethical approval by an Institutional Review Board (IRB) committee or equivalent, patient/participant consent to participate, and/or agreement to publish patient/participant details (where relevant).

Wiley and Hindawi regrets that the usual quality checks did not identify these issues before publication and have since put additional measures in place to safeguard research integrity.

We wish to credit our own Research Integrity and Research Publishing teams and anonymous and named external researchers and research integrity experts for contributing to this investigation.

The corresponding author, as the representative of all authors, has been given the opportunity to register their agreement or disagreement to this retraction. We have kept a record of any response received.

References

[1] Z. Miao and Y. Hu, "Research and Analysis of Combination Forecasting Model in Sports Competition," *Journal of Sensors*, vol. 2022, Article ID 5945599, 10 pages, 2022.

Hindawi

Research Article

Research and Analysis of Combination Forecasting Model in Sports Competition

Zhongli Miao and **Youhong Hu**

Department of Physical Education, Gansu Agricultural University, Lanzhou 730070, China

Correspondence should be addressed to Zhongli Miao; miaozl@gsau.edu.cn

With the increase of sports industry and various sports events, forecasting methods play an irreplaceable role in the competition system. At the same time of prediction, the selected calculation method, implementation scheme, model establishment, and other key implementation aspects have high technical requirements. In the whole prediction model, how to solve the problem of competition development is predicted and analyzed, and the best solution is selected for screening and evaluation, so as to significantly improve the prediction accuracy of the whole model. Understand the cause of the problem and solve it. Second, in the process of solving the problem, use the relevant forecasting technology theory to determine the weighted weight coefficient method of the combination forecasting model. In this paper, before the competition, select the best combination of forecasting model to sports-related personnel simulation cases and form a comparative analysis. Finally, through the combination of prediction experimental methods for the effective results of the problem, and in the later development process to get a new prediction model. In the actual process of forecasting, facing the complex combination of forecasting systems, the selected evaluation theme and the uncertainty of objects will produce great forecasting errors. Through excellent improvement, the defects of the combined forecasting model have been overcome, and the forecasting accuracy has been improved, which will greatly enhance the good development of physical education. The coordination mechanism, guarantee mechanism, and competition organization mechanism of sports competition alliance should be analyzed through prediction model. Spread Chinese sports culture, improve the level of sports competition, and carry out research and analysis on the prediction model of sports competition. The experimental results in this paper show that (1) the prediction process is generally tested in extremely unstable environment, so it will have a certain impact on the prediction accuracy, that is, there are data with the highest measurement accuracy of 0.99 and the lowest measurement accuracy of 0.92. (2) Different calculation methods will be selected for different prediction models of competitions. For example, the error coefficients of SSE are 1.6859, 1.8338, and 1.6161, respectively, which proves that different models have different contents in prediction. (3) The comprehensive promotion of sports competition will need more prediction models to select and promote. In the progress of the times, the prediction value shows an increasing trend, from 2.4 billion cubic meters to 3.3 billion cubic meters, which is the perfect realization of the prediction model. (4) In the structure of the forecasting model, the weighted geometric combination forecasting model is obtained by the statistical investigation and analysis of relevant personnel, which is the best combination forecasting model of sports competition with the optimal weight coefficient of 1.9, the forecasting value of 33.95, and the forecasting accuracy of 0.9996.

1. Introduction

With the advent of the new era and the rapid progress of human concepts, sports competition has become the achievement of the times in the era of science and technology. In today's sports competitions, it endows Li with exten-

sive knowledge and rich interest. On the one hand, it analyzes the physical talent of athletes in sports; on the other hand, it inherits personal moral norms and national glorious beliefs in sports competitions. Under the strict competition rules, the physical collision and the game of ways and strategies greatly improve the enjoyment of the competition and

show the manpower, material resources, and financial resources paid by a country to train sports talents. Under the common restriction of referees and rules, sports competitions carry out competitive contests between events and athletes in an orderly manner, which is a competition form that we try our best to own for glory. The successful development of sports competition reflects the country's high attention to the cultivation of athletes, and it is also an effective way to show the national sports achievements to the world. By using the methods of literature review, Delphi method, questionnaire survey, and statistical analysis, this paper puts forward the implementation strategy of sports league [1]. This paper probes into the internal conditions for maintaining the overall benefits and development of sports professional league and further analyzes the external factors such as politics, economy, legal system, and culture needed for the development of the league [2]. It is analyzed that strengthening the construction and development of campus sports competition is an important work of campus culture construction [3]. This paper analyzes the influence of college sports competition on campus culture, and sports competition is an indispensable and important part of campus culture [4]. High-level sports events rely on a strong university alliance system, which innovates the competition management system and business operation mode [5]. By using the methods of literature review and interview, this paper studies the main application and future development of information technology in competitive sports [6]. Sort out the related aspects of sports event management literature and research and comprehensive description of the data [7]. This paper analyzes the resource conditions of sports events and determines the index system of the resource conditions of sports events [8]. This paper analyzes the structure and characteristics of American middle school sports competition system and concludes that American middle school sports competition mainly adopts hierarchical competition, hierarchical competition, and season competition system [9]. This paper analyzes the current situation of student orientation competition organization in China and puts forward some suggestions on further standardizing and perfecting the competition organization of student orientation competition in China [10]. This paper probes into the environmental mechanism of the formation of sports competition organization and the comprehensive cognitive logic of creating the formation mechanism of sports competition organization [11]. By exploring the concept and goal, organizational structure, competition system, development effect and evaluation of American middle school sports competition, a complete competition system has been formed [12]. Twelve task modules of competition organization and management, such as the establishment of competition organization and the closing of competition work, are compiled, and the conclusion that competition is the core of large-scale sports events [13] is drawn. This paper analyzes the management and operation mechanism of sports organization, excavates the advantages of local sports resources, and offers characteristic physical education courses [14]. It reveals the inherent laws of the organization and management elements of ball games and produces a series of specialized operation skills [15].

2. Theory of Combined Prediction Model of Sports Competition

2.1. Basic Idea of Combination Forecasting Model.
From the prediction information of individual items, the effective combination of sports competition models is known, and the corresponding weight coefficients are weighted.

Standard combination forecasting model [16], as shown in the following formula:

$$y = \sum_{i=1}^{k} w_i y_i. \tag{1}$$

Wi expresses the weight of y_i in k prediction models.

2.2. Classification of Combination Forecasting Models.
Classify according to different competition events and different combination forms.

Linear combination forecasting [17].

$$f = l_1 f_1 + l_2 f_2 + \cdots + l_m f_m, \tag{2}$$

where L is the weighting coefficient of the prediction method.

Nonlinear combination forecasting [18].

$$f = g(f_1, f_2, \cdots, f_m). \tag{3}$$

Optimal and nonoptimal combination forecasting [19].

$$\max (\min) \phi = \phi(l_1, l_2, \cdots, l_m), \tag{4}$$

$$\text{s.t.} \left\{ \begin{array}{c} \sum_{i=1}^{m} l_i = 1 \\ l_i \geq 0, i = 1, 2, \cdots m \end{array} \right\}. \tag{5}$$

When solving the optimal combination forecasting model, the nonoptimal combination forecasting model is carried out when negative numbers appear.

Find the weight of positive weight combination forecasting model for nonoptimal solution.

Arithmetic average method [20].

$$w_j = \frac{1}{J}, j = 1, 2, \cdots J. \tag{6}$$

Arithmetic average method is also called equal weight average method. The advantages are simple calculation and equal weights, the disadvantages are no primary or secondary, and the prediction effect is poor.

Reciprocal variance method [21].

$$\omega_j = \frac{D_j^{-1}}{\sum_{j=1}^{j} D_j^{-1}}, j = 1, 2, \cdots, J, \tag{7}$$

where D_j represents the sum of squares of errors. The calculation method is shown in the following formula:

$$D_j = \sum_{i=1}^{N} (x_i - \hat{x}_i)^2. \tag{8}$$

Mean square reciprocal method [22].

$$\omega_j = \frac{D_j^{-1/2}}{\sum_{j=1}^{J} D_j^{-1/2}}, j = 1, 2, \cdots, J. \tag{9}$$

Standard deviation method [23].

$$\omega_j = \frac{1}{J-1} \left(1 - \frac{S_j}{\sum_{i=1}^{J} S_j}\right), j = 1, 2, \cdots, J. \tag{10}$$

S_j is the standard deviation of the model [24]. Its calculation formula is

$$S_j = \left(\frac{1}{N-1} \sum_{j=1}^{J} (x_i - \hat{x}_i)\right)^{1/2}. \tag{11}$$

2.3. Weighted Geometric Average Combination Forecasting Model. Predict the single prediction model and calculate the fitting value of the single prediction model at T time. The calculation formula is shown in the following formula:

$$\hat{Q}_t = \prod_{i=1}^{m} Q_{it}^{l_i}. \tag{12}$$

l_i satisfies

$$l_1 + l_2 + \cdots + l_m = 1, (l_i > 0, i = 1, 2, \cdots, m). \tag{13}$$

Calculate logarithmic values [25].

$$\ln \hat{Q}_t = \sum_{i=1}^{m} l_i \ln Q_{it}, \tag{14}$$

$$f = \sum_{t=1}^{N} |e_t| = \sum_{t=1}^{N} \left|\sum_{i=1}^{m} l_i e_{it}\right|. \tag{15}$$

The e_{it} calculation formula is

$$e_{it} = \ln Q_t - \ln Q_{it}. \tag{16}$$

Calculate the minimum error and carry out weighted geometric average combination forecasting model for the objective function.

$$\min f(L) = \sum_{t=1}^{N} \left|\sum_{i=1}^{m} l_i e_{it}\right|, \tag{17}$$

$$\sum_{i=1}^{m} l_i = 1, l_i \geq 0, i = 1, 2, \cdots, m. \tag{18}$$

2.4. Combination Forecasting Model with Optimal Weighted Coefficients. The combination forecasting model with variable weighting coefficient is used to calculate, which improves the accuracy and stability of the model and facilitates the simulation and analysis of weights. The calculation formula of the weighted combination forecasting model is

$$\hat{Q}_t = \sum_{i=1}^{m} l_{it} Q_{it}. \tag{19}$$

The weighting coefficient at time t.

$$\sum_{i=1}^{m} l_{it} = 1, t = 1, 2, \cdots N,$$
$$l_{it} \geq 0, 1 = 1, 2, \cdots, m, t = 1, 2, \cdots, N. \tag{20}$$

Calculate the prediction error when the combined prediction value of et is t. The formula is shown in the following formula:

$$e_t = Q_t - \hat{Q}_t = Q_t - \sum_{i=1}^{m} l_{it} Q_{it} = \sum_{i=1}^{m} l_{it} (Q_t - Q_{it}). \tag{21}$$

Let f be the sum of squares of the combined forecasting errors of the optimal nonnegative variable weighting coefficients, then, the variable weighting model of the minimum objective function is

$$\min f = \sum_{t=1}^{N} \sum_{i=1}^{m} \sum_{j=1}^{m} l_{it} l_{jt} e_{it} e_{jt}, \tag{22}$$

$$\text{s.t.} \begin{cases} \sum_{i=1}^{m} l_{it} = 1, t = 1, 2, \cdots, N, \\ l_{it} \geq 0, i = 1, 2, \cdots, N. \end{cases} \tag{23}$$

l_{jt} is the T-time weighting coefficient of the J-th prediction model, and e_{jt} represents the prediction error at T-time.

One

$$L_t = (l_{1t}, l_{2t}, \cdots l_{mt})^T,$$
$$E_t = (e_{1t}, , e_{2t}, \cdots e_{mt})^T. \tag{24}$$

Then

$$e_t = L_t^T E_t, e_t^2 = L_t^T E_t E_t^T L_t, \tag{25}$$

where L_t represents the weighting coefficient column vector; E_t represents the prediction error column vector; E Tt represents the covariance matrix.

Second

$$L = \left(L_1^T, L_2^T, \cdots, L_N^T\right)^T. \tag{26}$$

L is a dimensional column vector, which can show non-negative weighted coefficient column vector.

That is, the sum of squares of prediction errors f of combined prediction is expressed as

$$f = L^T E L. \tag{27}$$

The prediction model matrix of the minimum sum of squares of errors criterion is

$$\text{s.t.} \begin{cases} \min f = L^T E T, \\ R_t L = 1, t = 1, 2, \cdots, N, \\ L \geq 0. \end{cases} \tag{28}$$

The effective development of variable weight combination forecasting model is to adapt and change with the passage of time, find the corresponding weights, and align the corresponding forecasting stages.

3. Experimental Analysis of Combined Prediction Model of Sports Competition

3.1. Basic Steps of Competition Combination Prediction. In order to achieve accurate, reasonable, and efficient prediction, we must have a special person to arrange the work and carry out the work in a planned way, so as to achieve the maximum realization of the prediction effect. Realize the advantages of sports competition combination projects and analyze them quickly. The basic steps are as follows.

(1) Determine the purpose of the forecast

Before forecasting, we should know the problems to be solved this time and what purpose and significance should be achieved. After finding the prediction purpose and starting the prediction work, first collect materials and data. In the prediction work, it is inevitable that there will be deviations and misjudgments. Each competitor who is the object of prediction has his own characteristics, so the work is complicated. Forecasters will adopt different methods and collect different data, that is, when carrying out forecasting, they should make careful and targeted forecasting according to the actual situation.

(2) Investigate, collect, collate, and review data

Prediction work will need to be prepared in advance to identify, but the data collected to ensure high accuracy and comprehensive, otherwise, will have a huge impact on the prediction results. Before predicting, make sure to predict the personal situation of the participants, corresponding technical characteristics, competition situation, competition events, historical awards, and recent status, etc. Checking and processing the collected data to obtain the optimized data will greatly improve the prediction accuracy. The purpose of this is to have data for reference when choosing the prediction model, which greatly saves the prediction time.

(3) Selecting relevant prediction algorithms and constructing prediction models

After the effective collation, audit, and adjustment of the previous data, the appropriate prediction method is selected according to the data analysis results to establish a prediction model and start calculation and analysis. The rationalization of data and the high efficiency of prediction methods greatly improve the level accuracy of the model. With quantitative and qualitative prediction methods, athletes will know the next preparation and training intensity in advance.

(4) Analyze the prediction error

Errors in prediction are inevitable, but they are controllable. In the prediction work, the prediction error needs to be minimized and controlled at the same time, and then the causes are analyzed and the improvement methods are put forward. Analyze the prediction results obtained by different prediction algorithms, and seek the opinions of relevant experts to analyze and identify when analyzing and judging errors. Make further investigation on the prediction results, make deeper inspection and discrimination, and strive to minimize errors.

(5) Prediction conclusion and experimental analysis report are obtained

The conclusion will be written into an experimental analysis report and report to the corresponding prediction object, the first realization of the experimental conclusion will be the greatest significance of the experiment. Conclusion of the report will greatly improve the confidence of competitors and professional training and lay a solid foundation for improving competition results.

3.2. Combination Prediction Model of Sports Competition. In the process of abstract competition, the number of competitions is calculated and executed automatically, which can simulate the final results obtained by different players in the number of competitions. Every athlete has his own competition level. Some athletes can give full play to their advantages in some competitions, but there are also competitions that they are not good at. Through the measurable, evaluable, and usable results of sports competition, combined with the number of competitions, we can analyze and predict the achievements of the athlete in this sports meeting. Its prediction model is shown in Figure 1.

The data acquisition of competition times becomes the preprepapration stage, which is transmitted to the feature engineering, and the parameters are adjusted by machine learning algorithm. To achieve modeling training, in which feature engineering and model training are coordinated with each other. After completing the training stage, the integration of models is realized, and the performance prediction model is obtained. Through the abovementioned results and analysis and improvement, the athletes can achieve the key training specialty competition.
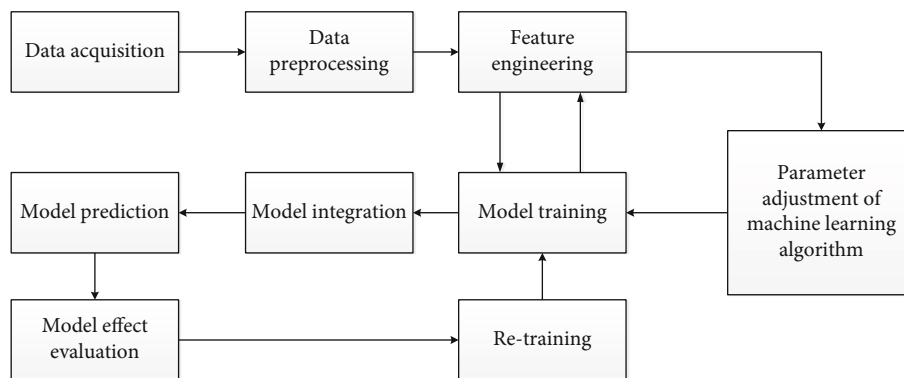
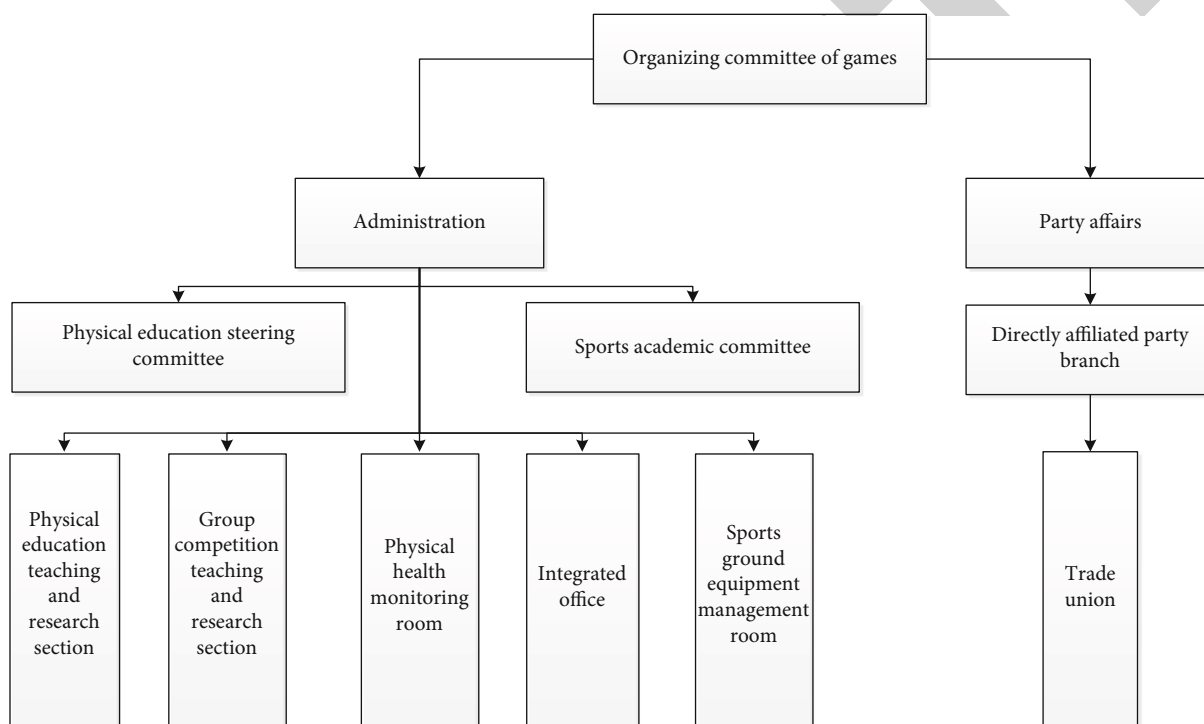Figure 1: Sports competition prediction model diagram.

Figure 2: Flow chart of competition organization structure of sports meeting.

3.3. *Based on the Analysis of Sports Competition Organization Structure.* The development of modern competition system is the product of continuous optimization and the result of organizational prediction. As the management and punctual development of sports competitions, the preparatory work before is extremely important and the guarantee of the successful development of competitions. Constructing relevant departments with clear division of labor, simplifying competition organization system, improving work efficiency, establishing distinctive modern sports events, and carrying forward the fighting spirit of athletes are all the achievements of competition organization system construction. The following is an analysis of the organizational structure of sports competitions.

It can be seen from Figure 2 that in the management organization structure of the Sports Committee, administration and party affairs are mainly responsible, and other relevant personnel cooperate in their work. In view of the development of

sports events and the cultivation of athletes, the development of physical education is conducive to the cultivation of excellent athletes. The hierarchical management of each management level and teaching and research office puts forward the operation mechanism with high quality and high requirements and forms a professional information and data processing center.

3.4. *Analysis of Prediction Model of Sports Competition Operation.* Sports events change dynamically with scale, goal, and environment, which belong to dynamic model. This requires the establishment of a complex information management system to maintain and operate. Therefore, on the basis of establishing the model, the model can be realized and operated by effective and reasonable calculation and design methods. The purpose of this is to standardize the model according to the factors of dynamic environment, diversification goal, and scale increase.
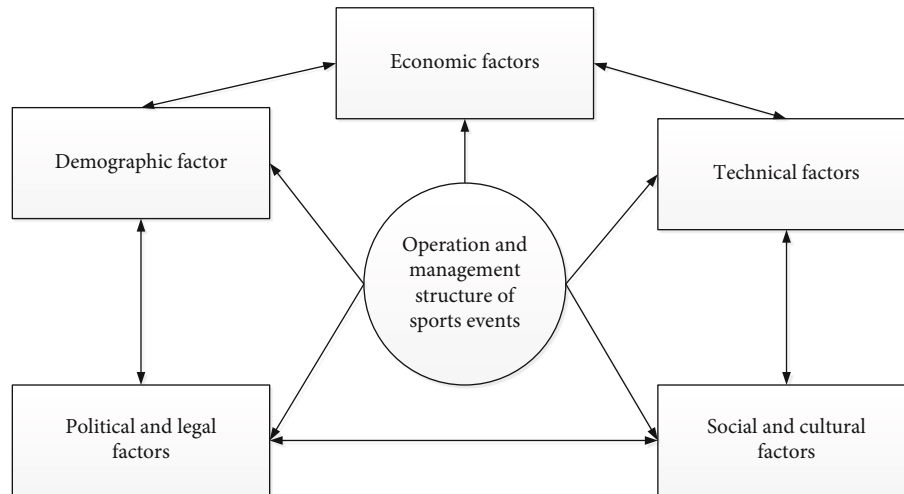
FIGURE 3: Influencing factors of internal and external environment of sports event operation institutions.

According to the essential characteristics of sports competition and management operation, the sports operation model should analyze and study each competition node and summarize the essential goal of the activity. Summarize the analysis contents involved in the establishment of sports event model as follows:

(1) Analysis of the operating environment of sports competition

The operation model of sports competition is a kind of behavior standard made according to the change of competition environment, and the analysis of operation environment is the first condition. A thorough analysis of the dynamic environment will help managers to effectively make temporary changes to the event and greatly improve the overall running progress of the event. The development of sports events will promote the politics, economy, and culture of all parts of the country rapidly, so it is necessary to consider these factors and make relevant analysis. Sports competition and internal and external environmental factors are an interactive relationship, which is a situation of mutual influence and mutual promotion. The relationship is shown in Figure 3.

(2) Operation of sports event management elements

Event management refers to the use of relevant functions and techniques in the process of competition, in accordance with the rules of the overall system of the overall analysis and control of the competition. Plan, organize, coordinate, control, and manage all stages of the competition to achieve efficient competition operation conditions. It is purposeful, organized, and innovative. It manages all aspects of event planning, on-site management and facilities and equipment, and shapes a good competition environment.

(3) Construction of sports event operation model

In view of the abovementioned competition working environment and the function analysis of managers, financial resources, material resources, and manpower, the detailed and systematic construction will be made, and the operation model of sports events will be constructed, which is expressed as follows in Figure 4.

4. Feedback Analysis of Competitive Sports Prediction Model

4.1. Analysis on the Problems Existing in the Structure of Competition Combination Forecasting Model.
In the competition organization and management structure, we should not only consider the factors of national policies but also consider the influence of human factors. Athletes and coaches have certain views on the competition organization structure, and they all deal with problems according to the structural criteria. Under the condition of ensuring the smooth development of the competition, we should do our own basic principles and take basic responsibility in the face of mistakes, so as to be in line with the spirit of sports struggle. By investigating the feedback of athletes and coaches on the organizational structure, the following Figure 5 shows.

Both coaches and athletes have a certain understanding of organizational structure, and both think that organizational structure is an indispensable part of the whole competition. As can be seen from the figure, most coaches and athletes think that the competition organization structure is incomplete, among which there are 24 people in total. Athletes are more willing to express their views than coaches, while coaches are clearer in distinguishing things. Compared with the unclear division of labor among departments, there are 15 athletes, which is much more than 4 coaches. A competition team should communicate with each other while analyzing problems.

4.2. Overall Correlation Evaluation of Combined Forecasting Model.
Obtaining excellent results from competition results for many times is conducive to enhancing athletes' training confidence. Data analysis of the current situation of the evaluation methods of competition excellence in the National Games can effectively reflect the performance of the
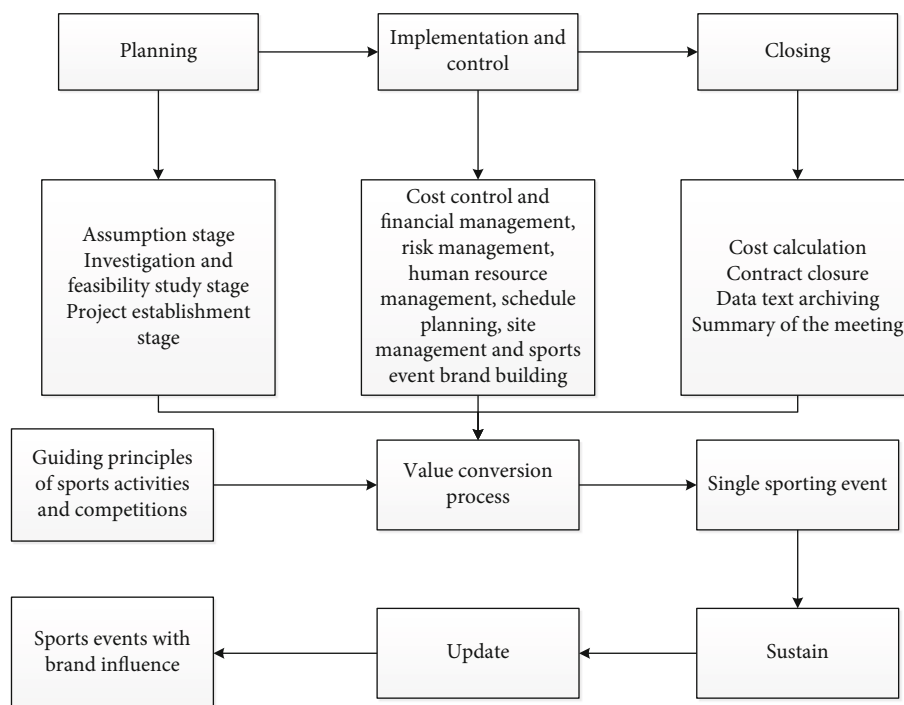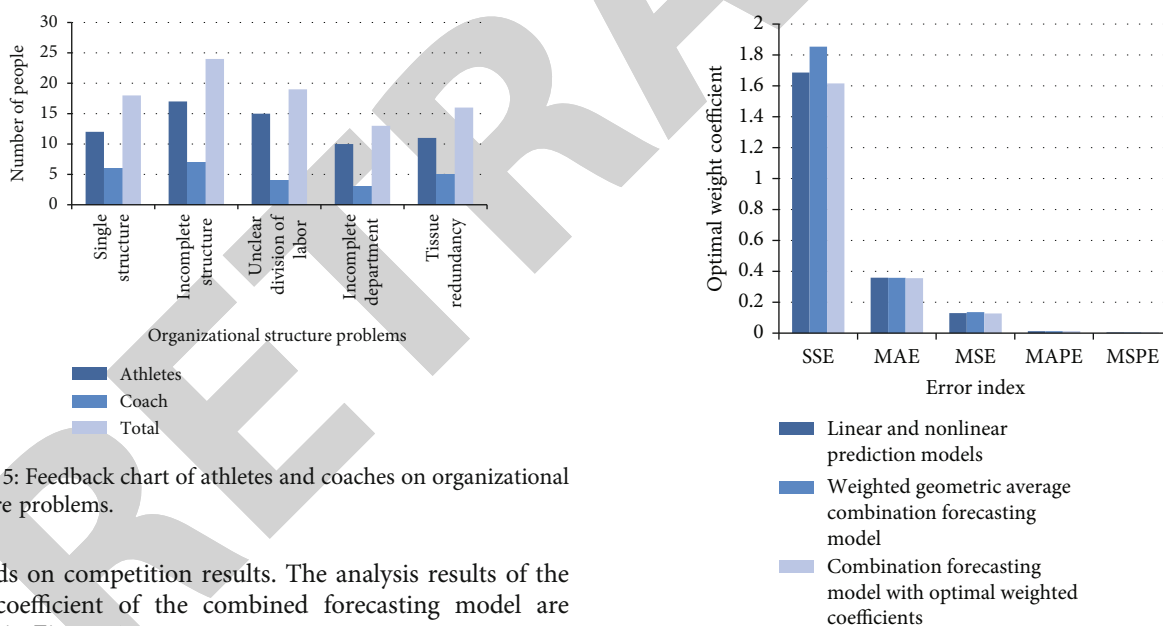
Figure 4: Expression of sports event model.

Figure 5: Feedback chart of athletes and coaches on organizational structure problems.

Figure 6: Evaluation results of combined forecasting model.

methods on competition results. The analysis results of the error coefficient of the combined forecasting model are shown in Figure 6.

It can be seen from the figure that the error coefficients of linear and nonlinear forecasting models, weighted geometric average combination forecasting model, and optimal weighted coefficient combination forecasting model are (1.6859, 0.3585, 0.1298, 0.0123, and 0.0044), respectively; (1.8538, 0.3578, 0.136, 0.0122, and 0.0045); (1.6161, 0.3555, 0.1271, 0.0122, and 0.0045). For the three forecasting models, in terms of overall effect and performance, the weighted geometric average combination forecasting model is more accurate and standard in calculating errors. The selection of sports competition model is also practical and efficient.

4.3. Analysis of Forecast Value of Various Combination Forecast Models.

In order to promote the development of sports competitions and implement the strategic development of national fitness, it is proposed to add mass events in the development strategy to enrich the competition forms and promote the coordinated development of competitive sports and mass fitness. The result of prediction is to analyze the relevant evaluation of the model through the prediction accuracy of the prediction model, and whether it can guide
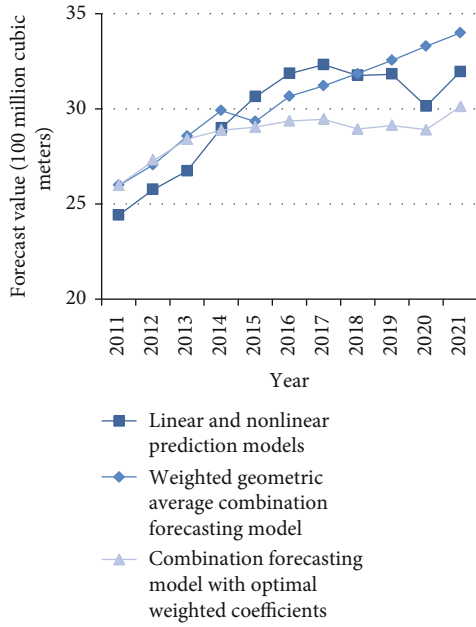
Figure 7: Predicted value data diagram of various prediction models.
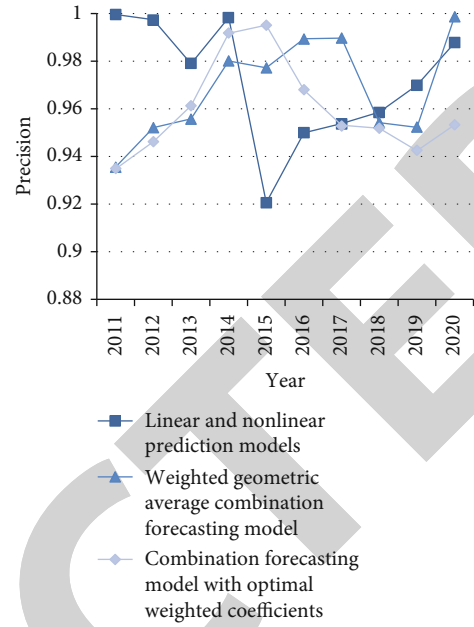

Figure 8: Accuracy data table of single prediction model.

the evaluation standard of sports competition level. Selecting the prediction results of sports competition results from 2011 to 2021, the prediction accuracy and prediction value data of three prediction models for sports event evaluation are as follows in Figure 7.

By arranging the measured competition prediction values, it is obvious that the height measurement and prediction values of the prediction model show an increasing trend in recent years. Among them, the weighted prediction model is close to the satisfactory prediction value of 3.5 billion cubic meters with the prediction value of 3.3 billion cubic meters. Efficient measurement and almost optimal prediction will effectively play the role of prediction model.

4.4. Prediction Accuracy of Single Prediction Model.

When forecasting, it is inevitable that due to the influence of environment and other factors, the prediction will have certain deviation, which will lead to the fluctuation of prediction accuracy. Every year, the level of athletes' performance will be different, and some even decline because of their age. According to the competition prediction accuracy of different combination prediction models in recent years, the effectiveness of the models is analyzed. The relevant data are shown in the following Figure 8.

In the experimental measurement, a new effective combination forecasting model will be calculated based on the order of measurement. In 2011, the accuracy of linear and nonlinear prediction models was 0.99, while the other two prediction models were only 0.93, which could not reach the prediction value. The accuracy is not high enough to meet the effective establishment of the model, and the high accuracy of the prediction model will be realized with the birth of the improved model.
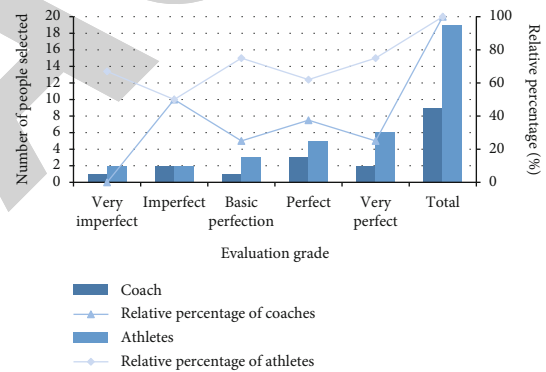

Figure 9: Validity test chart of evaluation design.

4.5. Evaluation Results of Organization Prediction Model Operation.

In order to ensure the normalization and rationalization of sports competition organization and operation, the results of organization and operation will be evaluated. Among them, the evaluation level is effectively analyzed, which will explain whether the competition is a complete success. If there are dissatisfaction, make corresponding improvements through the result analysis.

4.5.1. Test of Related Contents of Competition Prediction Model Evaluation.

From the coaches and athletes to the situation of this competition questionnaire analysis, get the situation of this activity. Make a reasonable analysis of the evaluation of this competition, look at the competition rationally, and keep the concept of "friendship first, competition second." The organizational evaluation results are shown in Figures 9–11.

From the design validity, content validity, and structure validity of competition evaluation, the evaluation analysis is carried out, and the number of people is selected for
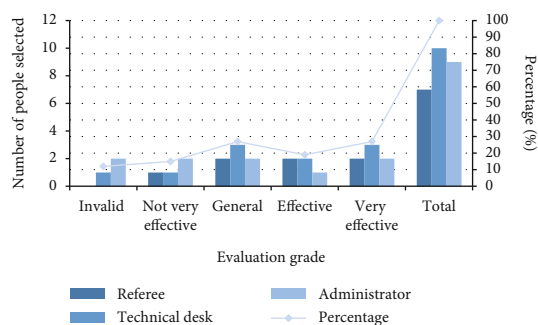
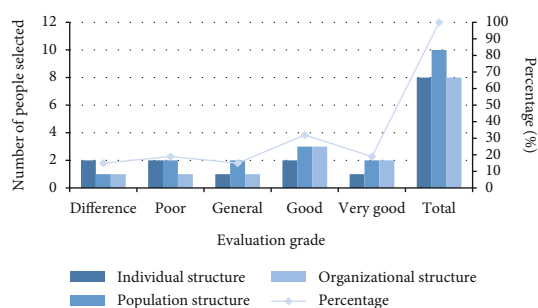Figure 10: Validity test chart of evaluation content.

Figure 11: Validity test diagram of evaluation structure.

statistical investigation. There are some problems in the whole evaluation system. Among them, 50% of athletes and coaches think that the evaluation design is imperfect. In the evaluation content, 28% of people think that the content is general, which is not enough to evaluate and cannot meet the evaluation requirements; 32% of structural personnel think that the evaluation grade is good and can be used to sort the results in sports competitions, but it lacks a certain degree of completeness. According to the analysis of organizational evaluation, the shortcomings of the whole organization will be found, and better experiences and lessons will be extracted in the next development.

5. Conclusion

Competition is the main achievement of sports training, and the main purpose of sports competition is to win by striving for excellence and defeat other players. According to the rules of the competition, the competition shows the athletes' physical strength, skills, and psychological endurance, as well as the coach's tactical system. With the expansion of the scale of sports events, competition will be carried out and competed more widely all over the world. It reflects the professionalism and skill of sports industry in various countries, which is the display process in the arena. "A few minutes on stage, ten years off stage" describes the hardship of athletes in training, and it is also the great spirit of striving for the honor of the country and itself. The development of sports competitions will promote the popularization and promotion of sports, and the established competition system will be continuously improved, from grass-roots attention to high-level embodiment. According to the experimental con-

tents of this paper, the summary is put forward: (1) predicting and analyzing the future in sports competition will greatly increase the effect of athletes getting high results in the competition, and facilitate coaches to arrange guiding tactics. (2) Competitive culture is often spread and cultivated through the window of sports competition, which is not only limited to keeping fit but also promotes the development of human society. (3) With the increase of modern sports, the value and significance will be more extensive, which is a long-term realization from promoting economic level to enriching national culture. (4) At the same time of sports competition, the evaluation and analysis of the results after the competition are beneficial to the technical reinforcement of many athletes, the results are obviously improved, and the championship is one step closer.

This paper studies the lack of content and analysis: (1) lack of subjective judgment awareness of athletes, more training according to the requirements of coaches, resulting in individual cannot play out the characteristics and advantages of performance. (2) In the statistical analysis of the number of people selected, the evaluation only based on the selection of internal personnel and did not conduct a sample survey on outsiders, resulting in the lack of data. (3) The combination model is the calculation and prediction of the highest level of sports competition, but now it is limited to the implementation of development and popularization. (4) The competition organization structure is not complete, but it does not complete the organization. The next research content will be to put forward the corresponding solutions through the integrity of the competition organization and carry out in-depth experimental analysis.

Data Availability

The experimental data used to support the findings of this study are available from the corresponding author upon request.

Conflicts of Interest

The authors declared that they have no conflicts of interest regarding this work.

References

[1] L. Yongfeng, "Restrictive factors and countermeasures for the establishment of China's men's professional basketball league," *Journal of Chengdu Institute of Physical Education*, vol. 45, no. 1, pp. 113–120, 2019.

[2] W. Rong, "Factor analysis of benefit maintenance and development of professional sports leagues," *Journal of Xi'an Institute of Physical Education*, vol. 35, no. 6, pp. 704–707, 2018.

[3] O. Yuhua and L. Qing, "A preliminary study on Chinese college students' sports competition and campus culture construction," *Journal of Chuxiong Normal University*, vol. 32, no. 3, pp. 133–137, 2017.

[4] Z. Xiaonian, "Research on the influence of college sports competition on campus culture," *Contemporary Sports Science and Technology*, vol. 8, no. 33, pp. 139-140, 2018.

Hindawi

Retraction

Retracted: Research on Sustainable Development of Olympic Games Based on Ecological Carrying Capacity Analysis

Journal of Sensors

This article has been retracted by Hindawi following an investigation undertaken by the publisher [1]. This investigation has uncovered evidence of one or more of the following indicators of systematic manipulation of the publication process:

(1) Discrepancies in scope

(2) Discrepancies in the description of the research reported

(3) Discrepancies between the availability of data and the research described

(4) Inappropriate citations

(5) Incoherent, meaningless and/or irrelevant content included in the article

(6) Manipulated or compromised peer review

The presence of these indicators undermines our confidence in the integrity of the article's content and we cannot, therefore, vouch for its reliability. Please note that this notice is intended solely to alert readers that the content of this article is unreliable. We have not investigated whether authors were aware of or involved in the systematic manipulation of the publication process.

Wiley and Hindawi regrets that the usual quality checks did not identify these issues before publication and have since put additional measures in place to safeguard research integrity.

We wish to credit our own Research Integrity and Research Publishing teams and anonymous and named external researchers and research integrity experts for contributing to this investigation.

The corresponding author, as the representative of all authors, has been given the opportunity to register their agreement or disagreement to this retraction. We have kept a record of any response received.

References

[1] B. Zhang and Y. Liu, "Research on Sustainable Development of Olympic Games Based on Ecological Carrying Capacity Analysis," *Journal of Sensors*, vol. 2022, Article ID 4907366, 13 pages, 2022.

Research Article

Research on Sustainable Development of Olympic Games Based on Ecological Carrying Capacity Analysis

Bin Zhang[1] **and YuFeng Liu** [iD][2]

[1]*Zhejiang College of Construction, Hangzhou 310000, China*
[2]*Zhejiang International Studies University, Hangzhou 310000, China*

Correspondence should be addressed to YuFeng Liu; liuyufeng@zisu.edu.cn

The Olympic Games is a comprehensive social and cultural activity with the most complicated system and the largest scale. With the development of the Olympic Games, the ecological problems brought by the Olympic Games have attracted increasing attention, and the sustainable development of the Olympic Games has been put on the agenda. Based on the comprehensive index of Ecological Carrying Capacity (ECC), Environmental Kuznets Curve, and carbon footprint analysis of the Olympic Games host city competition cycle, this study analyzes three modes of ECC of the host city: light urban ecological burden mode, heavy urban ecological burden mode, and overload urban ecological burden mode. Based on the temperature sensor and GPS positioning, the land surface temperature change map of Tokyo, Japan, from 1990 to 2015 is obtained, and the heat island effect of Tokyo is obtained. This paper analyzes the case of using sensors for intelligent event management such as venue detection in the sustainable development plan of the 2020 Tokyo Olympics; the idea and practice of thrifty hosting of 2022 Beijing Winter Olympics and 2022 Hangzhou Asian Games holds that in most cases, the ECC of the host city of the Olympic Games is under great pressure, so it is necessary to pay attention to the ECC of the host city. The sustainable development of the Olympic Games is an important issue in the development of the Olympics, but the sustainable development plan of the Olympics is still being explored. It is suggested that the sustainable development of the Olympic Games needs to evaluate the ECC of the host city in the whole cycle, establish the principle of ecological priority to avoid the overload mode of ecological burden, strive to achieve carbon neutrality in the competition, and practice the idea of scientific frugality in running the competition.

1. Introduction

The Olympic Games is a comprehensive social and cultural activity with complex system and large scale. From the bid to the hosting of the Olympic Games, huge costs need to be invested. When Albert, France, hosted the Winter Olympics in 1992, more than 30 hectares of forests were destroyed, and tens of thousands of animals and plants lost their living environment, resulting in the rapid disappearance of many local biological species. During the two weeks of the 2004 Athens Olympic Games, a total of 50 tons of CO_2 was emitted, and after the whole event, the CO_2 emission was about 500,000 tons, which brought a serious impact on the national ecological environment [1]. Therefore, in the

process of hosting the Olympic Games, it is inevitable to consider: while maximizing the economic and social benefits brought by the competition, how to reduce the negative impact of the competition on the urban ecological environment, effectively avoid the risks of the urban ecological environment and promote the sustainable development of the ecological environment of the host city. These are the important issues for the sustainable development of the Olympic Games. Although the Olympic Agenda 2020 adopted at the end of 2014 takes reducing the cost of bidding and hosting the Olympic Games and sustainable development as important issues, it is regarded as an effective reform plan to promote the sustainable development of the Olympics. However, the high budget cost of the Olympic Games has

put the thrifty Olympic Games plan pushed by the International Olympic Committee (IOC) to the test. Ultimately, the irreversible and unsustainable environmental problems such as waste of resources and ecological destruction caused by hosting the Olympic Games are the stumbling blocks to the development of the Olympic Games. Therefore, hosting the Olympic Games is not only an "economic account" but also an "environmental account."

2. The Sustainable Development of the Olympic Games

The world sports governance system represented by the United Nations and the IOC formally brings "sustainability" into the global sports policy framework. In 2012, the United Nations designed Sustainable Development Goals (SDGs) based on sustainable theory as the strategic framework of global development from 2015 to 2030. And in article 37 of "Transforming Our World: 2030 Agenda for Sustainable Development" [2], it is pointed out that "sports are also an important factor to promote sustainable development." In response to the United Nations concept of sustainable development, in December 2014, the IOC put forward in Olympic Agenda 2020 that "sustainability should be incorporated into all aspects of the Olympic Games and the daily operation of the Olympics." As the most outstanding Olympic Games in the world, the Olympic Games adopted the sustainable development standards of the United Nations in resource management and took them into real actions. In 2015, as a "permanent observer," the IOC released "The Contribution of Sports to the United Nations Post-2015 Development Agenda and Sustainable Development Goals: Position of the IOC" [3], which concluded that sports can support the sustainable development of human society. In December 2016, the IOC issued the Sustainable Development Strategy (IOC Sustainable Strategy), which promoted sustainability as the "working principle" of the Olympics and supported and implemented the sustainable development agenda of the United Nations [4]. With the implementation of sustainable development by the IOC in an all-round way, other international sports organizations also regard it as the core concept of running the Games. Table 1 shows the development of the Olympics towards sustainability.

3. Ecological Carrying Capacity Model of Olympic Games

3.1. Comprehensive Index of ECC. The comprehensive index of ECC refers to the combination of various carrying capacity indexes in a certain way, and the ECC is calculated by using parameters such as ecosystem carrying capacity index, ecosystem pressure index, and ecosystem carrying pressure degree. Different indexes have different advantages, and integrating the advantages of each index may form a more accurate comprehensive index of ECC. The general equation

is as follows:

$$ECC = f(\alpha, \beta, \gamma \cdots \cdots). \tag{1}$$

In the equation, $\alpha, \beta, \gamma \ldots \ldots$ are respective carrying capacity indexes. The comprehensive application of various carrying capacity indexes can reduce the influence of human subjectivity on the results, among which fuzzy analytic hierarchy process, grey relational comprehensive analysis method, and multifactor relational analysis method [5] are also introduced into the comprehensive carrying capacity evaluation system.

3.2. Environmental Kuznets Curve (EKC). Based on a large number of data analysis and empirical tests, American environmental economists Grossman and Krueger found that the environment deteriorated first and then improved with the increase of per capita income between environmental quality and economic growth and thus extended EKC to describe the changing trend of the relative relationship between environmental quality and economic development in a country or region [6]. As shown in Figure 1, the most representative of EKC model is quadratic polynomial function relation, which is a simplified measurement model commonly used in the world at present:

$$y = a + b_1 x + b_2 x^2 + \varepsilon. \tag{2}$$

In this equation, y is the environmental pressure index; x is the economic development index; a is a constant term, usually representing the characteristic parameters of a country or region; b_1 and b_2 represent the coefficients of the first and second terms of x; and ε is a random error term.

3.3. Analysis of Carbon Footprint during the Event in Host Cities of Olympic Games. The IOC is the first international sports organization to propose sustainable development and introduce carbon footprint to measure the environmental impact of events. At the Olympic Conference held in Paris in 1994, the IOC specially discussed sports and environment, and in 1996, the environmental and sustainable development clauses were included in the Olympic Charter [7]. The concern of the IOC for sustainable development has directly promoted the attention of the Olympic Games Organizing Committee (OGOC) of the bid countries and host countries to environmental issues. In 2004, when London applied for the 2012 Summer Olympics, it emphasized that environmental quality and sustainable development were the key contents of London's bid. In the 2008 Beijing Olympic Games, the IOC introduced the environmental impact assessment of carbon footprint on the Olympic Games. Subsequently, the host cities of all previous Summer Olympic Games and Winter Olympic Games attached great importance to sustainable development and adopted various measures in venues, energy use, material selection, garbage disposal, transportation, and other aspects to reduce the environmental burden of the Olympic Games. According to the requirements of the IOC, from 2030 onwards, the OGOC will be required to reduce and compensate the

TABLE 1: Development of the Olympics towards sustainability.

Years	Related key Olympic Games	Events related to the Olympics	World trends regarding sustainability
1992	Albertville (winter)	Albertville 1992: criticism of destruction of the natural environment	Rio Earth Summit United Nations Framework Convention on Climate Change (UNFCCC) initiated
1994	Lillehammer (winter)	Lillehammer 1994: first "greening" initiative for the Olympic Games The Centennial Olympic Congress: the environment becomes the third pillar of Olympism (alongside sport and culture)	
1996		Modification of the Olympic charter: incorporates "environment" and "sustainability" in the basic principles	
1999		Olympics' Agenda 21: sets out the basic concepts and practical activities of environmental conservation in the sports world	
2000	Sydney (summer)	Sydney 2000: "Green Olympic Games" is a key theme	
2010	Vancouver (winter)	Vancouver 2010: advanced approach to sustainability for the games	Aichi Biodiversity Targets of the United Nations Convention on Biological Diversity
2012	London (summer)	London 2012: the first sustainable Olympic and Paralympic Games	United Nations Conference on Sustainable Development (Rio+20) ISO 20121 launched
2013		Tokyo is selected to host the 2020 games	
2014		Olympic Agenda 2020: sustainability is included in all aspects of the Olympic Games and within the Olympics daily operations	
2016	Rio de Janeiro (summer)	IOC sustainability strategy: sustainability is included as a working principle of the Olympics	G7 Toyama Framework on Material Cycles
2020	Tokyo (summer)	Tokyo 2020: aims to showcase a model of a sustainable society which humankind pursues and work integrally on sustainability challenges	Target year set in the Aichi Biodiversity Targets Paris agreement begins
2022	Beijing (winter)	Beijing 2022 releases low-carbon management pregames report showcasing carbon-neutral games Sustainability for the future Beijing 2022 releases pregames sustainability report Beijing 2022 has compiled and published the sustainable sourcing guide, sustainable sourcing code, and sustainable sourcing technical criteria	
2022	Hangzhou (Asian games)	IDEA: green, smart, thrifty, and civilized	

carbon emissions directly related to its operation, so as to ensure that the positive impact of the Olympic Games on climate is greater than the negative impact [8]. Using carbon footprint to assess the impact of the Olympic Games on the ecological environment of the host city makes it possible to analyze the environmental impact of the Olympic Games and reduce carbon emissions through corresponding measures. According to the relevant documents of Tokyo Olympic Organizing Committee, the carbon emissions of Olympic Games can be divided into three stages: pre-Games, in-Games, and after-game. In pre-Games stage, the carbon emissions mainly come from the construction of supporting facilities for the competition. During the game, the carbon emissions mainly derive from the activities related to the competition; after the game, the operation and maintenance of venues emit most of the carbon [9]. Figure 2 shows the proportion of carbon footprint in different stages of the Olympic Games.

3.4. ECC Model in the Host Cities of Olympic Games. According to the threshold theory of ECC and EKC theories, this paper analyzes the relationship between the host city and the quality of ecological environment and draws the following conclusions: (1) When the impact of the Olympic Games on the ecological environment is below the warning line of ECC, then with the economic development, measures can be taken to restore the ecology. (2) When the impact of the Olympic Games on the ecological environment exceeds the warning line of ECC, but it has not yet exceeded the limit of ECC, with the development of economy, taking corresponding measures can make the ecology recover slowly. (3) When the impact of the ecological environment of the Olympic Games exceeds the ecological carrying limit, it will cause irreversible damage to the ecology. Even with the economic development, it is extremely difficult and slow to repair the ecological environment. According to the actual situation of the host cities of previous Olympic Games, the
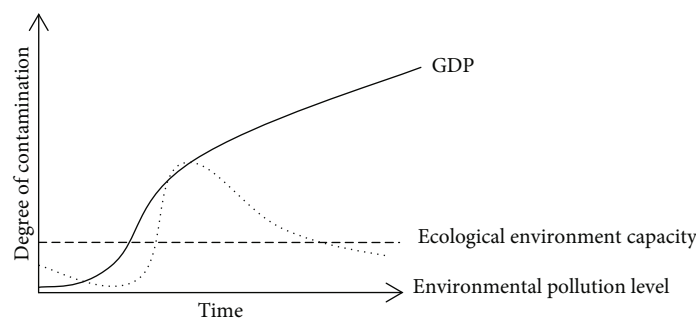
Figure 1: Environmental Kuznets Curve.

ECC of the host cities of Olympic Games is catalogued into the following three modes.

3.4.1. Light Urban Ecological Burden Mode. The first is the ideal development model. The EKC implies that the ecological threshold as an important prerequisite is large enough or the ECC is large, which assumes that no matter how serious the pollution is, it is reversible and recoverable for the ecological environment, indicating that the critical point or inflection point of the EKC always exists. As shown in Figure 3, when the carrying capacity of population, resources, transportation, and land in the development of the city hosting the Olympic Games reaches the inflection point, the degradation of environmental quality has not yet reached the threshold of ECC and is controlled within the warning line of ECC. However, after the inflection point, due to reasons such as the enhancement of environmental protection awareness of the organizers of the host city and the increase of environmental protection investment, the coercive force of the development of large-scale events on the ecological environment gradually decreases, which can realize the synchronous and benign development of large-scale events and urban ecosystem. This model depicts a bright future for the development of the urban Olympic Games; that is, the competition is well developed, and the quality of urban ecological environment is also restored.

3.4.2. Heavy Urban Ecological Burden Mode. The second is the mode of heavy urban ecological burden. As shown in Figure 4, when the overweight carrying capacity of population increases, resource consumption, environmental pollution, traffic jam, and other factors in the Olympic Games break through the warning line of ECC and reach the inflection point in conjunction with the urban ecosystem; its coercive force is within the threshold of ECC, and the trend of ecological environment degradation can still be contained in time to promote the coordinated development of the event and the city; otherwise, it will face the irreversible upward inflection point of environmental aggravation and deterioration.

3.4.3. Overload Model of Urban Ecological Burden. The third is the overload model of urban ecological burden. The EKC depicts the relationship between economy and environment, in which the environment deteriorates first and then

improves. However, people often witness that the environment in the development of sports events has not improved after deterioration, and the degree of degradation continues to rise, which ultimately affects the development of sports events. As shown in Figure 5, the initial stage of the competition is not obviously affected by the competition level and scale restrictions; that is, when the warning line of ECC is broken through, no attention is paid to it; then, when the scale of the competition expands beyond the critical point of reversibility, it crosses the threshold of ECC to automatically adjust and restore the elastic range, resulting in a series of urban ecological crises such as population explosion, resource depletion, environmental deterioration, and ecological imbalance, showing a serious overload state, which is embodied in the overload of urban traffic carrying capacity caused by population explosion, overload of urban land carrying capacity caused by excessive consumption of resources, and environmental pollution. When the development of the competition reaches the critical point, it is not only difficult to curb the serious degradation of the ecological environment quality but also makes the technical difficulty of controlling environmental pollution and ecological degradation increase, and its economic and social costs will exceed the range that the city can bear, making the economic, social, and environmental benefits unable to achieve the expected purpose.

4. Practice and Feedback of Sustainable Development of 2020 Tokyo Olympic Games

4.1. Analysis of the ECC of Tokyo City. Heat island effect is an important index to evaluate the impact of human activities on the ecological environment of megacities. The Olympic Games is the most complex and largest comprehensive social and cultural activity in the world, and the host cities of the Olympic Games are almost all megacities in the world. Tokyo is a superlarge city in the world, and its impervious surfaces such as buildings and roads are distributed on a large scale and densely. In addition, a large number of human activities have produced a large amount of urban metabolism such as water and heat. This kind of "superlarge" has a strong external interference on the urban ecosystem, and its urban heat island problem is far greater than that of other small and medium-sized cities and rural areas. As shown in Figure 6, through the temperature sensor and
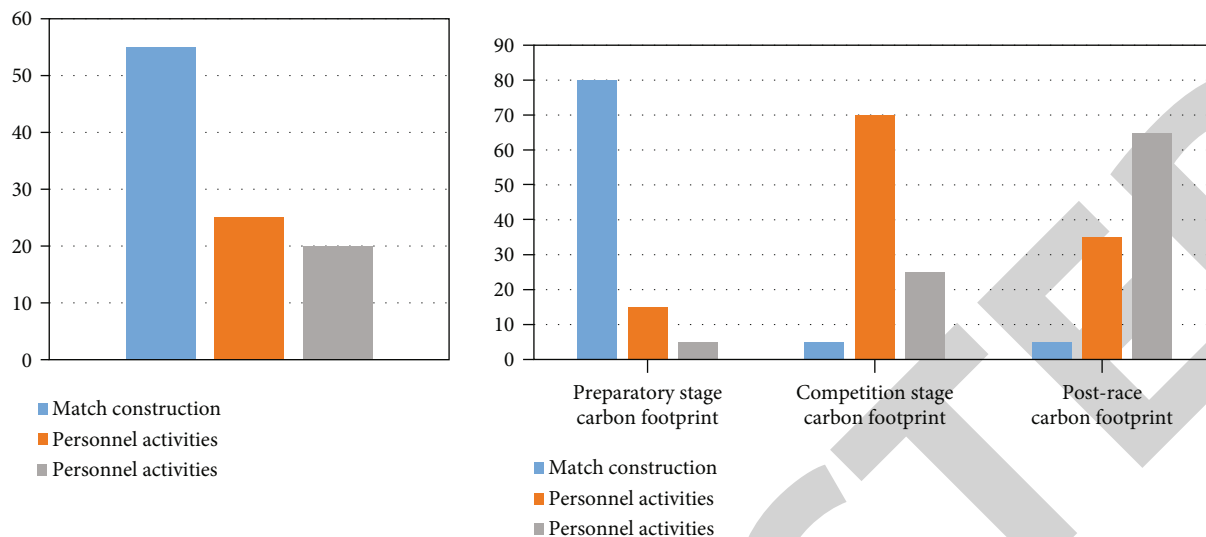
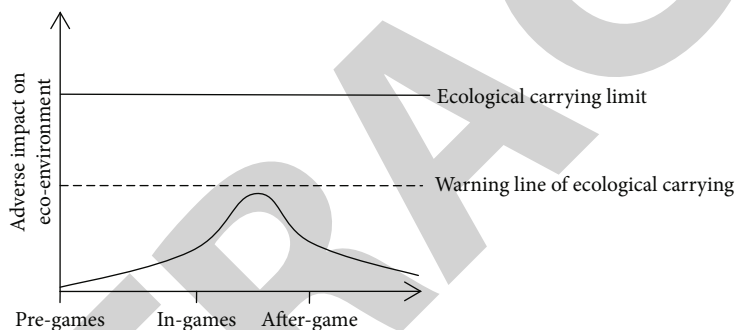Figure 2: Estimated carbon footprint of the Olympic Games.

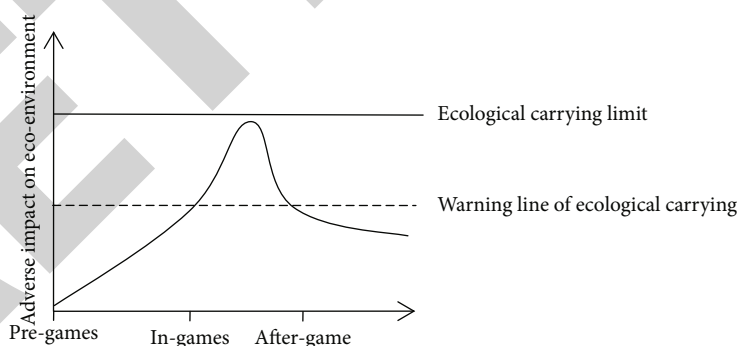Figure 3: Light urban ecological burden mode.

Figure 4: Heavy urban ecological burden mode.

GPS positioning detection, the land surface temperature change chart of Tokyo, Japan, from 1990 to 2015 was obtained, and the heat island effect of Tokyo, Japan, was obtained. This paper uses the heat island effect to analyze the ECC of Tokyo from 1990 to 2015.

As shown in Table 2, during the period of 1990-2015, the proportion of Tokyo's temperature rising area (35.35%) is higher than that of its temperature decreasing area (14.12%) (Table 2), which shows that Tokyo's cities are also

in a warming trend in general during the research period. During the research period, Tokyo's cities expanded greatly, occupying a large amount of ecological land. In addition, the proposed layout model of "multi-center and multi-group" was not well implemented, and a good green separation zone could not be formed among groups, resulting in a substantial increase in the surface temperature level. It can be found that at the beginning of hosting the 2020 Tokyo Olympic Games, the urban ecology of Tokyo was overloaded. If the
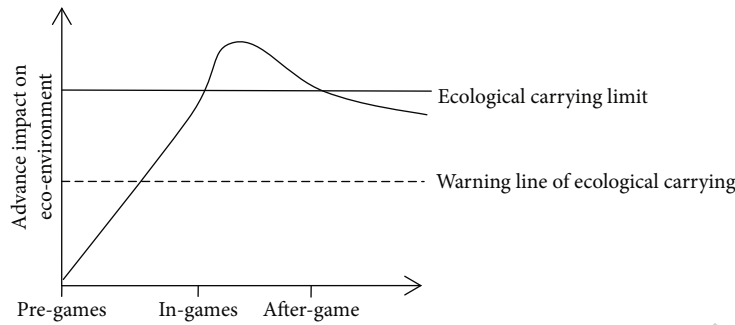
Figure 5: Overload model of urban ecological burden.

1990   2000   2015
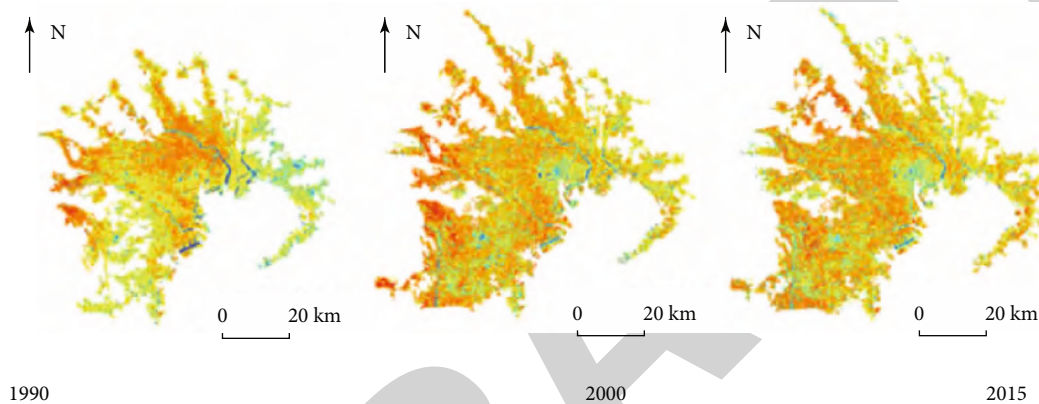
Figure 6: Surface temperature changes of Tokyo from 1990 to 2015 [10].

Table 2: Statistics of surface temperature changes of Tokyo from 1990 to 2015 [10].

Changes	Ranks	Area/km^2	Proportion/%	Total proportion/%
	-4	2.65	0.05	
	-3	15.79	0.26	
Down	-2	231.44	3.86	14.12
	-1	596.23	9.95	
Level	0	3027.8	50.53	50.53
	1	1398.82	23.34	
	2	553.93	9.24	
	3	139.32	2.33	
Up	4	22.49	0.38	35.35
	5	3.54	0.06	
	6	0.01	0.00	
Total	—	5992.02	100.00	100.00

investment in the Olympic Games is blindly increased, it is very likely that the Tokyo Olympic Games will be overloaded, causing irreparable damage to the ecological environment.

4.2. Practice and Feedback of Sustainable Development Plan for 2020 Tokyo Olympic Games. From their own needs, the Japanese government and the Tokyo Metropolitan Government responded to the reform call of the IOC and made sus-

tainability one of the most important tasks of the Tokyo Olympic Organizing Committee. The medium- and long-term goal of the Tokyo Metropolitan Government is to build it into a model of harmonious coexistence between highly developed society and environment in large cities around the world, and this long-term development vision coincides with the goal of the IOC to promote the sustainable development of the Olympic host city. As shown in Figure 7, in order to realize the sustainability vision and objectives of the Tokyo Olympic Games, the Tokyo Olympic Organizing Committee has formulated a detailed sustainability strategy and work list, which defines the key areas and specific work objectives of the sustainability work in preparation, hosting, and post-Games.

4.2.1. Active Response to Climate Change. Climate change is a major global challenge in the 21st century. It has become an international consensus and the general trend to actively respond to climate change and promote low-carbon development. The IOC clearly stated that the direct and indirect greenhouse gas emissions caused by the Olympics should be managed, and the impact of climate change should be adapted according to the actual situation of the activities [12]. In order to cope with climate change, the Tokyo Olympic Games set the goal of "zero carbon" and promised to contribute to the temperature control goal set by the Paris Agreement of the United Nations Framework Convention on Climate Change concluded in 2015. Through the use of renewable energy and energy-saving measures, it laid the

Timeline for "Developing the Tokyo 2020 Olympic and Paralympic games sustainability plan"
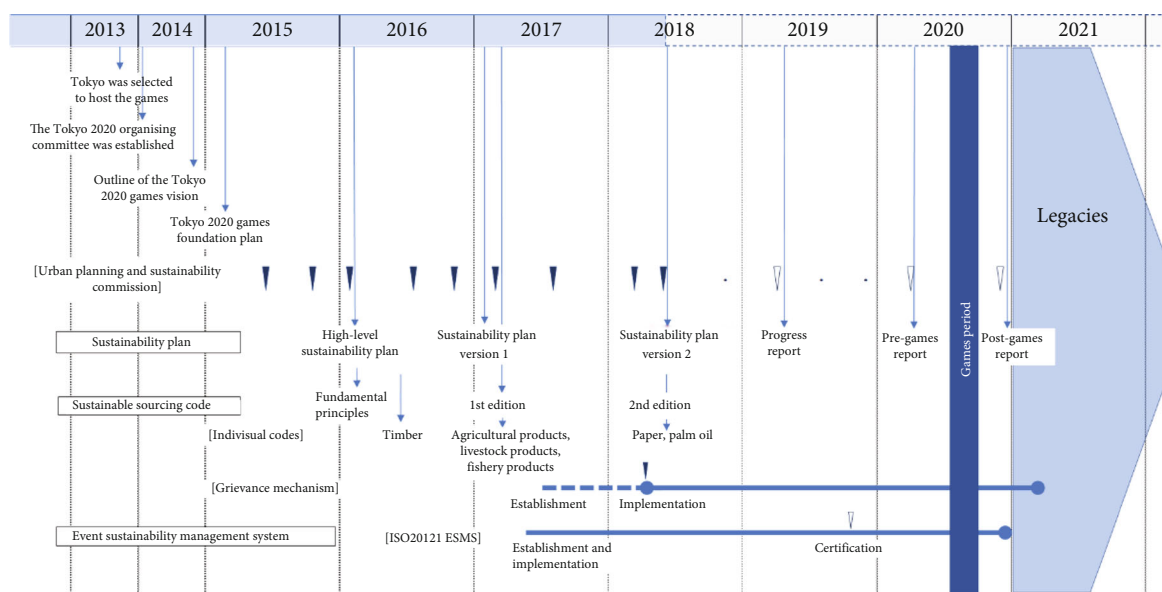

Figure 7: Timeline of the Tokyo Olympics Sustainable Development Plan [11].

foundation for Japan to build a carbon-free society and become a model for global response to climate change. As shown in Figure 8, in the field of tackling climate change, the main work included carbon accounting of benchmark emission level, determination of specific content of measures to tackle climate change and carbon management. Measures to deal with climate change were also classified into three categories: measures to avoid carbon emissions, measures to reduce carbon emissions through energy saving and renewable energy utilization, and carbon compensation measures. Through the Olympic carbon accounting work, the Tokyo Olympic Organizing Committee determined that the emission benchmark level for the whole life cycle of the Olympic Games was 3.01 million tons of carbon dioxide. In order to avoid carbon emissions, about 60% of the Olympic Games used existing facilities, which had been expected to reduce the emission level to 2.93 million tons. In addition, carbon emissions from various activities were further reduced through other energy-saving measures and renewable energy utilization measures: for example, Tokyo actively used low-pollution and energy-efficient transportation means such as fuel cell vehicles and plug-in hybrid vehicles; clean and energy-saving vehicles were used 100% during the Olympic Games to ensure that the average carbon dioxide emission intensity (G-CO2/km) generated by vehicles used in the Olympic Games was at a low level; seven permanent venues in Tokyo were equipped with renewable energy systems including about 513 kW solar photovoltaic, 462 kW solar photothermal, and about 1523 MJ geothermal. 100% of the electricity used during the Olympic Games came from renewable energy. Tokyo also made full use of the advantages of domestic hydrogen energy technology to fully use pure hydrogen energy in the planned Olympic village and its community. As shown in Figure 9, the Tokyo Olympic Organizing Committee promoted some management plans

for climate issues, such as the 2020 tourism demand management plan and procurement-related management plans, so as to promote all sectors to participate in activities to mitigate and adapt to climate change and encourage people to choose a more sustainable lifestyle. The Games carbon footprint (the amount of CO_2 and other emissions) was expected to be about 3,010,000 t-CO_2 without any measures. However, this was reduced by about 280,000 t-CO_2 as a result of implementing avoidance and reduction measures such as the use of rentals or leases, use of existing venues, renewable energy use, and adoption of energy saving facilities.

4.2.2. Effective Resource Management: The Idea of "Frugality" in Running the Competition. In order to carry out sports activities and hold sports events, it is necessary to consume a lot of resources to build sports venues, produce sports equipment, and provide energy, water, and food, as well as some technical services, such as sensor technology, are also needed as the basis for the event. Therefore, when preparing and hosting the Olympic Games, it is very important to adopt effective resource management methods to achieve the goal of sustainable development. The new main arena, the new national arena, is designed with a "Traditional and stylized"roof made of wood and steel, using wood from 47 Japanese prefectures almost everywhere inside the main arena, advocate and the surrounding environment into one of the "Forest Stadium"; the spectator did not install air-conditioning, the use of natural wind to achieve the cooling effect. In the construction of other closed sports arenas, a distributed multipoint monitoring system is installed according to the Indoor Stadium Environment, combined with temperature and humidity sensor technology, TVOC air quality sensor technology, automatic monitoring technology, and wireless technology, to achieve indoor stadium air quality, temperature and humidity, formaldehyde
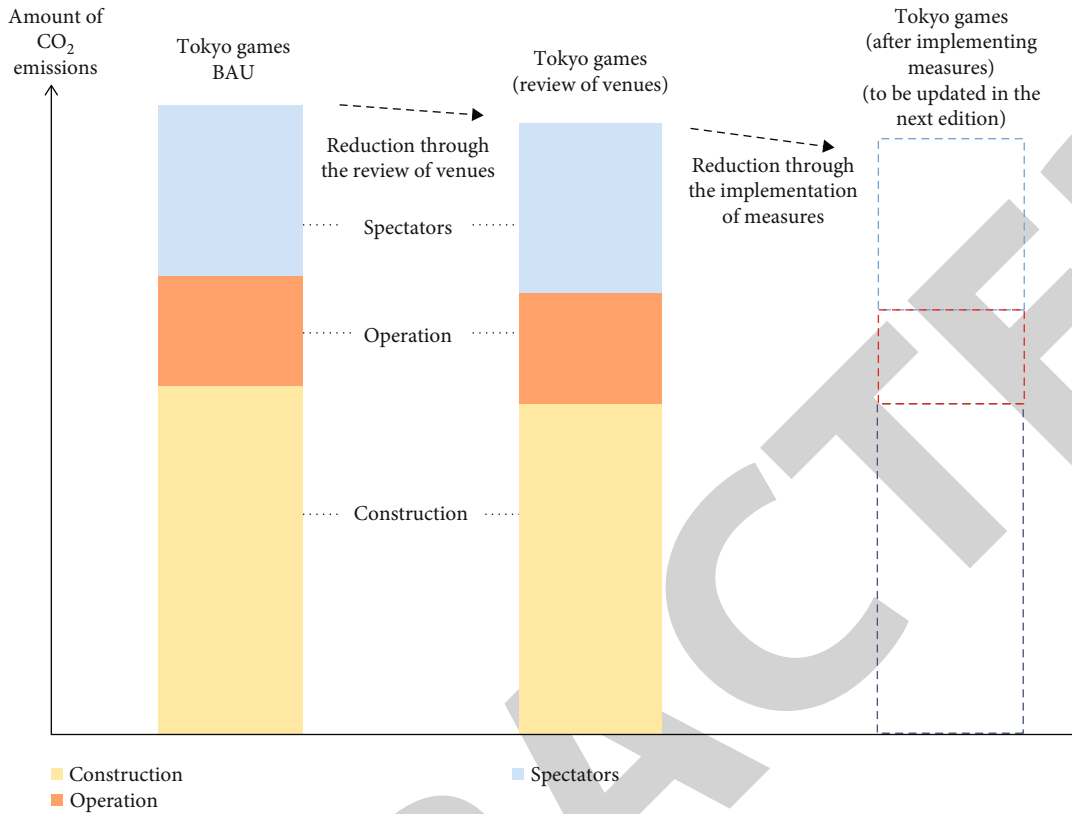
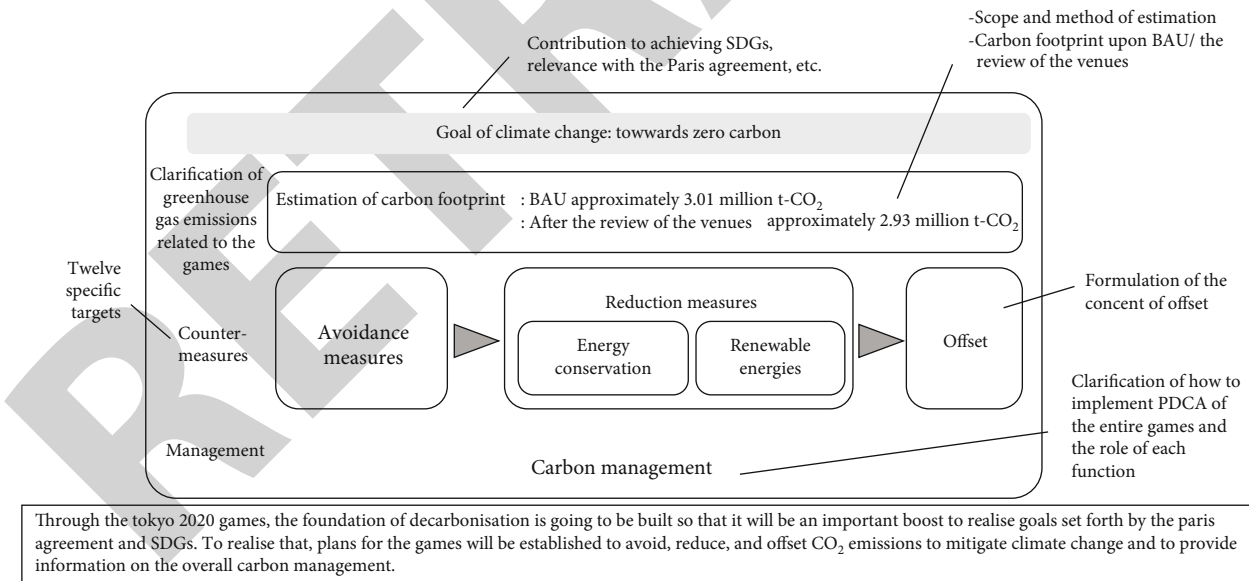FIGURE 8: Carbon footprint of the Tokyo Olympics [12].

FIGURE 9: Tokyo 2020 "Zero Carbon Plan" [12].

content, and CO2 parameters monitoring; by controlling humidifier and fan, the environmental parameters can be adjusted and controlled, in order to create the best indoor stadium environment and to ensure the normal performance of athletes and audience comfort. The resource management of Tokyo Olympic Games mainly focused on the reuse and management of waste and put forward the goal

of "zero waste" for the Olympic Games. Tokyo Olympic Organizing Committee implemented targeted resource management measures in the whole supply chain process of Olympic Games preparation and hosting, with the goal of stopping deforestation and land destruction caused by resource utilization, and minimizing the negative impact of waste and the consumption of economic circulation system
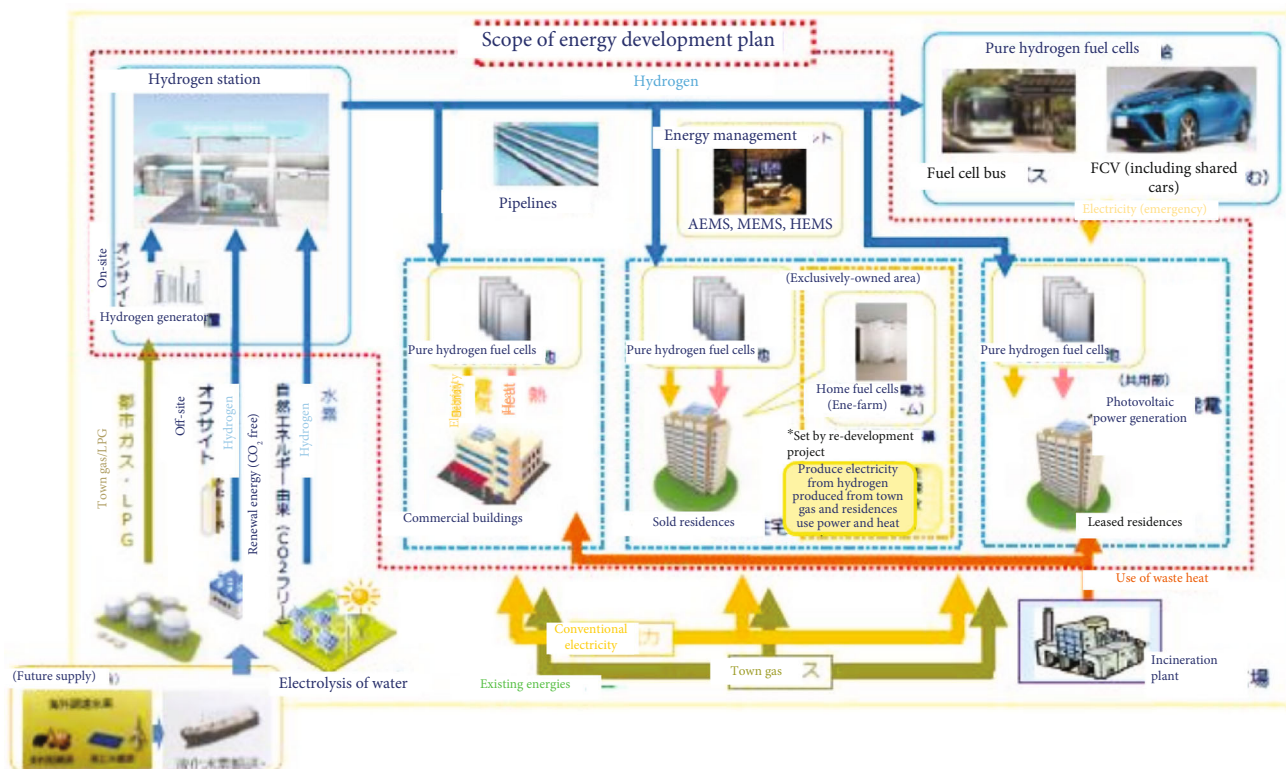
Figure 10: The entire picture of energy development (source: Olympic/Paralympic Village area energy development plan) [11].

and environment. Tokyo Olympic Organizing Committee mainly achieved the quantitative goal of efficient use of resources and waste reduction through strict procurement management; specifically, 99% of the items and commodities purchased in the Olympic Games were reused or recycled. During the operation of the Olympic Games, 65% of the wastes were reused and recycled. In Tokyo, relevant laws and management plans were formulated for waste disposal, and a lot of successful experiences were accumulated. In order to reduce the overuse of packaging materials, especially to prevent the impact of plastic packaging and disposable products on the ecosystem through marine pollution, the Tokyo Olympic Organizing Committee followed the national strategy of recycling plastic resources formulated by the Ministry of the Environment of Japan and the relevant regulations of the Tokyo Metropolitan Government and formulated procurement rules, which restricted the procurement of items and commodities that were easy to recycle and simply packaged. The Tokyo Olympic Organizing Committee formulated a recycling and recycling policy to manage procurement projects in a comprehensive way. In addition, it also tried to introduce some new management modes to help manage resources effectively: it introduced asset tracking system into asset management; it encouraged material leasing and recycling; indoor air conditioners for the Tokyo Olympic Games, for example, were basically leased, which were returned for other purposes after the competition; it provided more easy-to-understand garbage classification and identification maps to the public; it launched a horizontal recycling plan, which only allowed the use of recyclable and reusable plastic beverage bottles

during the Olympic Games. In order to promote the concept of resource conservation, the Japanese government began to recycle old household appliances and mobile phones in 2017. In three years, it collected about 79,000 tons of small household appliances, and 6.21 million used mobile phones, from which 32 kilograms of gold, 3,500 kilograms of silver, and 2,200 kilograms of copper were extracted for making Olympic medals.

4.2.3. Protection of Natural Environment and Biodiversity. Sports activities are closely related to the natural environment. Natural resources such as clean air and water, undeveloped land, and healthy ecosystems such as green urban areas, mountains, forests, rivers, lakes, and oceans are important foundations for some sports activities. Tokyo also expected to take advantage of the opportunity of hosting the Olympic Games to further improve the urban ecological environment, protect biodiversity, form a rich ecological network, enhance the comfort and attraction of the city, and transform Tokyo into a city that is more harmonious with nature. The Tokyo Olympic Organizing Committee built more green spaces around the stadium to protect and upgrade the existing green areas. The infrastructure construction of the competition avoided cutting down trees. According to *Ramsar Convention*, Kasai Jiming Marine Park was designated as a wetland reserve. In the construction of the competition venue, measures such as transplanting local trees were taken to protect biodiversity. The main roads in Tokyo, where Olympic marathon and walking race pass, as well as the roads near the competition venues, were made to be green belts that could shade athletes and spectators.

In Tokyo, sidewalks blocking the solar heat were paved along roads over 130 km in some competition areas. This can also reduce the adverse effects of urban heat island effect on competitors, spectators, and staff. Another important task for environmental protection is water resource protection. Tokyo Olympic Organizing Committee, with the hope of improving the original water circulation environment of the city, conducted substantial water resource protection and sewage treatment measures, such as water quality and temperature research in Odaiba Marine Park and real-time monitoring through underwater screens; improving the water quality of moat around the palace garden; building sewage treatment facilities to reduce the pollution load discharged into rivers, oceans, and other waters during heavy rainfall; and sewage treatment by installing advanced water circulation facilities. In the procurement process, the committee also added explicit provisions to the procurement regulations formulated to ensure that all products and services were obtained in compliance with relevant environmental laws and regulations, so as to protect biodiversity and prevent environmental pollution in procurement.

As shown in Figure 10, the figure describes the carbon footprint of the Tokyo 2020 Games. The Tokyo 2020 Games had lower carbon footprint than previous Olympic Games, because no new infrastructure was constructed specifically for the purpose of the Tokyo 2020 Games, and currently, available venues and facilities were fully utilized for effective uses after Tokyo was selected as the host city. The total amount of carbon footprint based on the BAU case is 3.01 million $t\text{-}CO_2$ which is lower than the carbon footprints of the London 2012 Games (about 3.45 million $t\text{-}CO_2$ based on BAU case) and the Rio 2016 Games (about 3.56 million $t\text{-}CO_2$ based on BAU case). In addition, the carbon footprint of the case with the review of venues is 2.93 million $t\text{-}CO_2$, indicating that greenhouse gas emissions are reduced by using existing venues.

4.2.4. ECC Overload of 2020 Tokyo Olympic Games. Although the Tokyo Olympic Games issued a series of plans for sustainable development of events, the overload of ECC and adverse effects of ecological environment in the process of running the games were not uncommon. Bloomberg reported on July 14th, 2021, that residents near the competition venue complained that "Tokyo Bay stinks", but in the subsequent broadcast of the competition, the water quality did look rather muddy. Before the official start of the competition, some athletes abandoned the competition because of the water quality of swimming pool, and some athletes vomited after landing from the swimming pool. The Tokyo Olympic Organizing Committee set unrealistic procurement standards for sustainable development, which further damaged the ecological environment. The American-based environmental organization Rainforest Action Network (RAN) found that some of the wood used in the construction of the venues of the 2020 Tokyo Olympic and Paralympic Games were cut down from the tropical forest containing the habitat of the endangered species orangutans. According to the report, the environmental protection organization confirmed that plywood manufactured by Indonesian enterprises was used in the construction site of Ariake Arena in 2018, and a number of related enterprises as supply sources were found in the nonpublic information. The environmental protection organization analyzed the situation of tropical forests in Kalimantan island managed by these enterprises, finding that in 2016 and 2017, when it was possible to supply timber to the venues, the forest area decreased by about 7,000 hectares in total.

4.2.5. Controversial Measures of Sustainable Development Plan of 2020 Tokyo Olympic Games. Many initiatives of thrifty competition in the sustainable development plan of Tokyo Olympic Games have been accused of being flashy. At the beginning of the preparation, the Tokyo Olympic Organizing Committee announced that the 3R concept of "Reduce," "Reuse," and "Recycle" should be regarded as one of the leading concepts of the Olympic Games. Among those comments, the 18,000 sets of cardboard beds in the Olympic Village were the most controversial topic. These beds, the first try in the history of the Olympic Games, were all made of recycled materials, which were put together like "paper boxes." These cardboard beds caused many doubts in terms of safety, price, and comfort. However, it is estimated that the total price of the whole set of bedding is 150,000-250,000 yen (US $1400-2300). Moreover, all medals of this Olympic Games were unprecedentedly made of recycled electronic waste. In 2017, based on the concept of environmental protection, the Japanese government launched the collection activities of used mobile phone appliances. In more than two years, nearly 79,000 tons of small household appliances and 6.21 million old mobile phones were collected from the whole country, from which about 32 kilograms of pure gold, about 3,500 kilograms of pure silver, and about 2,200 kilograms of copper were extracted. Finally, all the medals of Tokyo Olympic Games were made with these recycled and refined metals. Tokyo took pride in applying recycled electronic waste to make gold medals. However, the gold medals were painted off just after the Olympic Games.

5. Summary

5.1. In Most Cases, the Host City of the Olympic Games Is under Great Ecological Carrying Pressure, and Attention Should Be Paid to the ECC of the Host City. Because of the particularity of the Olympic Games, most of the Olympic Games, especially the Summer Olympic Games, are almost held in the world's megacities, and now the world's megacities are under the pressure of ecological environment overload without exception. The investment in the Olympic Games is huge, and the period from the bid to the competition is often as long as 5-10 years. During the competition, tens of thousands of athletes, journalists and spectators will flood into the host city and the surrounding areas of sports venues in a short period of time. The transportation, accommodation, and energy consumption during this period will generate huge carbon emissions, which will easily cause huge ecological pressure on the host city. During the competition, the ecological burden of the host city is often overloaded,

causing great difficulties for the postcompetition recovery. Therefore, at the beginning of the application, it is necessary to assess the ECC of the host city, make relevant plans, reduce carbon emissions, strive for carbon neutrality, and properly handle the problem of excessive ecological carrying pressure of the city caused by the competition.

5.2. The Sustainable Development of the Olympic Games Is an Important Issue in the Development of the Olympics, but the Sustainable Development Plan of the Olympics Is Still Being Explored. Sustainable development is an inevitable topic in the Olympics. In recent years, the Olympic Organizing Committee has issued a large number of documents on sustainable development. Whether it is the 2020 Tokyo Olympic Games or the 2022 Beijing Winter Olympics, the sustainable development plan is an important agenda. Relatively speaking, however, the sustainable development of the Olympics is still a new agenda, and there is still much room for improvement in terms of concept interpretation and practical operation. Especially in terms of frugality, it is necessary to avoid the appearance of "formal" frugality and "false" frugality. Starting from the purpose of hosting the Games and the actual situation of the host city, we should realistically introduce a scientific and achievable frugality scheme to further improve the sustainable development plan of the Olympic Games.

6. Suggestions

6.1. Full-Cycle Assessment of the Host City's ECC. The ecological and environmental problems faced by the host city in the process of hosting the Olympic Games put forward a severe test on the supporting power of resource consumption, the degree of environmental pollution, and the ability of maintaining a certain living standard population. Any events that exceed the ECC will seriously affect the sustainable development of the city. Therefore, the ECC is an important basis to measure whether the urban environment is in harmony with the competition activities. Therefore, before the competition, we should strengthen the evaluation of the ECC of the competition and at the same time build a multifactor urban ECC estimation model related to the soil, water, atmosphere, and sound environment related to the competition, so as to comprehensively and quantitatively estimate the urban ECC and provide technical support for the construction of the evaluation system of urban ECC. Strengthen the monitoring of the ecological environment of the host city. The process of hosting the Olympic Games involves the reception of foreign tourists, the transportation of personnel and goods, the holding of the Olympic Games, the maintenance of venues and auxiliary facilities, etc., so that the eco-environmental stress factors in the host cities of the Olympic Games are characterized by multisource heterogeneity, complexity and variability, wide spatial and temporal distribution, large regional span, etc. Therefore, the eco-environmental monitoring in the process of hosting the Olympic Games should be based on diversified business databases. Focusing on the demand of early warning information of eco-environmental risks in the host cities, the relevant information in the fields of eco-environmental risk sources, atmosphere, soil, water, sound environment, etc. in the process of hosting the events will be integrated to form an environmental information database, and a complete eco-environmental risk monitoring system will be built to dynamically monitor the eco-environment of the host cities during the events. After the Games, strengthen the restoration and compensation of the host city's ecological environment. After the Games, on the premise of following the principles of "ecological priority, sustainable development and equal rights and responsibilities" and according to the damage degree and present situation of the Olympic Games to the ecological environment, a reasonable ecological environment restoration scheme is formulated. Ecological compensation, as a benefit coordination and balance mechanism between the competition and the ecological environment, is the inevitable choice for the sustainable development of the Olympic Games and the urban ecological environment by constantly optimizing and adjusting the distribution relationship among stakeholders and realizing the mutually beneficial symbiosis among environmental protection actors.

6.2. Establish the Principle of Ecological Priority and Avoid the Overload Mode of Ecological Burden. To host the Olympic Games, the host cities generally put improving the ECC in the strategic height of sustainable development, which means that they should advocate green environmental protection, highlight green images, shape green brands, and establish the principle of ecological priority. The host cities should strictly enforce the environmental protection system, select the best control scheme, and control investment to reduce the air pollution around the city. It is also necessary to improve the quality of urban ecological environment and slow down the greenhouse effect and heat island effect in order to improve the natural environment and maintain the ecological balance. To host the Olympic Games, host cities need to avoid the overload mode evolved from the overload operation of bottleneck elements. Moreover, they can neither take the economic growth mode of excessive resource consumption and excessive environmental pollution nor stop or even sacrifice development to protect the resources and environment of the city. Instead, seeking the scientific, sustainable, and coordinated development is the only choice. Meanwhile, they should actively explore an effective development path in terms of improving the ECC of the city.

6.3. Strive to Achieve Carbon Neutrality during the Event. During the Olympic Games, the venues will gather a large number of people, producing all kinds of domestic garbage, leaving a variety of carbon footprints, and causing a heavy burden on the environment. At the same time, the venues will consume a lot of water, electricity, gas, and so on when emitting plenty of carbon. Facing these challenges, the host city can take carbon neutralization measures, such as energy saving and emission reduction technology, recycling, garbage sorting, etc., and strengthen the audience's awareness of carbon neutralization in order to realize carbon

neutralization in venues. Event organizers or venue managers should provide green travel, green catering, and other services as much as possible and reduce the carbon footprint during large-scale events by providing degradable products, using energy-saving and environmentally friendly and recyclable materials, reducing solid wastes and using disposable plastic products. The carbon neutrality of the competition can be understood as offsetting the carbon dioxide generated by the competition through energy saving and emission reduction technology or afforestation, so as to achieve the relative "zero emission" of carbon dioxide. For example, Beijing 2022 Winter Olympics and Winter Paralympics proposed to realize carbon neutrality and zero emission, and the concept of green and low carbon has been deeply integrated into the design, construction, and operation of venues, thus forming the accounting methodology of greenhouse gas emissions of Beijing Winter Olympics. The green and low carbon measures adopted will ensure the realization of carbon neutrality in the preparation and holding of the events. In the long run, the experience of carbon neutrality in Beijing 2022 Winter Olympics and Paralympic Winter Games will lead to the fulfillment of carbon neutrality.

6.4. Scientific Practice of Frugality in Running Competitions. Thrift is the guiding concept of the Olympic Games, and it cannot be rigidly required. As a large-scale public activity in modern society, sports events are held because of their great value. The objectives of the competition usually include political benefits, economic benefits, social benefits, etc. Focusing on these objectives, the host city should consider the integrity and coordination of resource management and form standards and scales for evaluating the efficiency of resource use, so as to measure the input and output effects of competition resources and implement frugal competition. This study draws a conclusion that thrifty competition should be started from the following three aspects: (1) Infrastructure construction and public facilities support. According to the idea of thrifty competition, the design of competition venues should adhere to the principles of practicality, intelligence, and green; optimize resource allocation by means of Internet and Internet of Things; and avoid budget overruns and environmental pollution. In terms of public facility support, the ideas of intelligence, green, and frugality should be followed, and modern logistics technology should be introduced to improve the operation efficiency of the transportation system with efficient, safe, timely, and reliable logistics operation. In terms of the scale and quantity of venue construction, it is necessary to transform and expand the existing stadium resources in the city and surrounding cities and gradually promote the preoperation concept of competition venues. Take Beijing Winter Olympic Games as an example. When bidding for the Winter Olympic Games, China has three major ideas, one of which is holding a thrifty Olympic Game. The most costly two aspects of the Beijing Winter Olympic Games are competition preparation (about US \$1.56 billion) and venue construction (about US \$1.51 billion), totaling about 3 billion US dollars, which is 1/5 of the 2018 PyeongChang Winter Olympics and 1/15 of the 2014 Sochi Winter Olympics. The biggest expense of

the Olympic Games credits to infrastructure and venue construction; the overspending of the Olympic Games in the past proves the fact. Among the 12 competition venues of the Beijing Winter Olympics, five of them were the old venues of the 2008 Olympic Games, including the Bird's Nest, the National Aquatics Center, and the Cadillac Arena, which can be directly transformed and reused. For example, the Bird's Nest was used for holding the opening ceremony of the Beijing Winter Olympics again, and the National Aquatics Center was transformed into the Ice Cube. The total value of these venues exceeds 700 million yuan. The strategy of replacing the old with the new has helped Beijing save half of the venue construction fee. In addition, some hardware of BOCOG is leased directly to enterprises on a rental basis, which not only saves the cost but also reduces the later expenses. Through calculation, the mode of renting and purchasing can save more than 30% of equipment cost. Moreover⊠Organizing Committee use items to get funds. 65% of the \$1.51 billion cost of venue construction comes from enterprise investment. For example, the Winter Olympic Village in the three major competition areas will be reused after the competition, in which Beijing and Zhangjiakou Olympic Village will be sold directly as commercial housing, while the Winter Olympic Village in Yanqing competition area will be transformed into a holiday hotel in scenic spots, as well as the National Alpine Ski Center and the National Ski Jumping Center, all of which will serve as tourist attractions after the competition. (2) Investment structure and operational efficiency. Investment structure and operation efficiency directly affect the benefit of running the competition. We should take advantage of the opportunity of the Olympic Games to guide the optimization and upgrading of the urban industrial structure, widen the width of the Olympic economy, arrange the Olympic investment reasonably, and promote the integration and development of the Olympic Games and cities. It is necessary to improve the operational efficiency of the Olympic Games; establish an all-round, multilevel, and multiechelon investment system; provide a good investment and financing environment; strengthen the supervision of funds; make overall arrangements for construction funds; optimize various forms of financing structures; strengthen project supervision; scientifically determine the scale of budget estimates; improve the scientificity of project design; improve the supervision and restraint mechanism; and ensure the clean and efficient preparation of the Olympic Games. For example, BOCOG's budget for expenses is confidential and strictly reduces the construction cost. BOCOG's budget for the preparation of events is based on the balance of payment strategy. The special funds of the IOC total 1.56 billion US dollars in sponsorship ticket revenue, brand authorization, and other income, just balancing the budget of 1.56 billion US dollars for the preparation of events. (3) Etiquette activity investment and personnel and organization control. Too much investment in etiquette activities, a huge number of staff and overstaffed organization have been bothering the organizers. Both the number of staff and organization of the Olympic Games and the input of the etiquette activities should under strict control. According to the actual needs of the events, we

Retraction

Retracted: Data Analysis and Optimization of Youth Physical Fitness Training Based on Deep Learning

Journal of Sensors

This article has been retracted by Hindawi following an investigation undertaken by the publisher [1]. This investigation has uncovered evidence of one or more of the following indicators of systematic manipulation of the publication process:

(1) Discrepancies in scope

(2) Discrepancies in the description of the research reported

(3) Discrepancies between the availability of data and the research described

(4) Inappropriate citations

(5) Incoherent, meaningless and/or irrelevant content included in the article

(6) Manipulated or compromised peer review

The presence of these indicators undermines our confidence in the integrity of the article's content and we cannot, therefore, vouch for its reliability. Please note that this notice is intended solely to alert readers that the content of this article is unreliable. We have not investigated whether authors were aware of or involved in the systematic manipulation of the publication process.

In addition, our investigation has also shown that one or more of the following human-subject reporting requirements has not been met in this article: ethical approval by an Institutional Review Board (IRB) committee or equivalent, patient/participant consent to participate, and/or agreement to publish patient/participant details (where relevant).

Wiley and Hindawi regrets that the usual quality checks did not identify these issues before publication and have since put additional measures in place to safeguard research integrity.

We wish to credit our own Research Integrity and Research Publishing teams and anonymous and named external researchers and research integrity experts for contributing to this investigation.

The corresponding author, as the representative of all authors, has been given the opportunity to register their agreement or disagreement to this retraction. We have kept a record of any response received.

References

[1] J. Pan, "Data Analysis and Optimization of Youth Physical Fitness Training Based on Deep Learning," *Journal of Sensors*, vol. 2022, Article ID 6778882, 9 pages, 2022.

Research Article

Data Analysis and Optimization of Youth Physical Fitness Training Based on Deep Learning

Juqian Pan ![ORCID]

School of Physical Education, Hechi University, Yizhou, Guangxi 546300, China

Correspondence should be addressed to Juqian Pan; 08013@hcnu.edu.cn

Adolescents are the future of national development, but according to effective surveys, it can be found that the health of the youth system in my country is in a state of decline. At present, the reasons for the decline of the youth system in our country are caused by many factors, such as poor sports awareness and too much academic stress. The main reason is lack of exercise. Based on the deep learning method, this paper analyzes the importance of physical fitness training for adolescents, and proposes to improve the service system of physical fitness training for adolescents, and promote the formation of a guarantee mechanism for physical fitness training for adolescents. The research results of the article are as follows: (1) Before receiving the training, the test results of various indicators of the experimental group and the control group were basically the same, and there was no major difference. The T test results showed that the P values of the two groups were both above 0.05. Explain that before training, the initial situation of the two groups can be regarded as the same. After receiving the special training, the general condition of the members of the conventional training group was slightly improved compared with the test before the training. Compared with the experimental group, they performed pull-ups, throwing a 2Kg medicine ball on the spot, running 30 meters, reaching a height on approach, moving half a meter, and repeating. The P values of the cross-test scores are all less than 0.05, indicating a large gap between the two. Among them, the P value of the 30-meter run is lower than 0.000, which has a very significant difference, while the P value of the fast clean and jerk 20 kg and the 60s double shake is greater than 0.05. It can be seen that there is no significant difference between the control group and the experimental group after these two assessments. The experimental results also show that the trainees who received the mode training method have been improved in various indicators of physical fitness, and the experimental results and the traditional mode training have been greatly optimized. (2) In the simulation test analysis experiment, the statistical average of exercise time is 5.784, which is the highest statistical average among the five variables, and the statistical average of physical fitness is 2.436, which is the lowest in the statistical results. There is no significant difference between the statistical average of the quality and the daily exercise situation. In the sensitivity test, the evaluation accuracy of the deep learning methods is the highest among all models. When the number of iterations reaches 50, the evaluation accuracy can reach 1. (3) After running on the test set, the article proposes that the accuracy rate of the physical training model based on the deep learning algorithm is 89.12%, and the improved accuracy rate can reach 92.46%, which is the one with the highest index value among the four models in the experiment. The AUC curve values of the article and the improved system are very stable. The AUC value before the improvement remains around 0.90, and the AUC value after the model improvement also remains at 0.97. After running on the mixed test set, the performance of the four methods has declined to a certain extent, but the performance of the model proposed in this article is still the highest among the four models, and the AUC curve values of the improved system are very stable. Yes, the AUC value has been maintained at 0.95, and the AUC value before the improvement is stable within the range of 0.90-095. The research data also show that the recognition accuracy of the physical training method of the deep learning algorithm is the highest.

1. Introduction

The development and progress of a nation depend on the physical and mental conditions of adolescents, and the physical fitness training of adolescents is an important factor affecting the healthy development of adolescents. With the support of today's highly advanced technology, the communication technology between governments is developing day by day. Sports and teaching activities have also become important conditions for the prosperity of the country. We should pay attention to sports health teaching, which not only designs the healthy growth of the youth system, but also affects the future of the nation and the development of the country. In middle and high schools with heavy academics, students should also have sufficient exercise time, and form a healthy lifestyle and cultural leisure. Literature [1] concluded that a certain amount of exercise can lead to a reduction in risk factors. Literature [2] analyzed the necessity of physical exercise in this age group of students. Reference [3] illustrates the importance of developing practical abilities in sports culture and sports. Literature [4] explains that the future life of each nation and the development of the country depend on the physical and mental conditions of the youth. Reference [5] illustrates that physical exercise and a positive attitude towards physical activity must be one of the basic areas of activity in higher education institutions. Literature [6] analyzes the use of special equipment in the current special physical training, and proposes the key elements and principles to be followed in the special physical training. Literature [7] analyzed exercise motivation and concluded that exercise can increase the motivation of students and students. Literature [8] analyzes the significance of physical training, the problems existing in physical training, and the characteristics of football. Literature [9] discusses the use of physical training as a substance abuse prevention intervention for youth in Illinois. Literature [10] conducted a historical survey of physical exercise activities in youth groups and found that there was no identifiable physical training program in early youth group activities. Literature [11], on the basis of analyzing the importance of youth physical exercise, proposed a service system to improve the quality of youth physical exercise. Literature [12] finds out the problems existing in the physical training of youth basketball players and proposes corresponding solutions through literature data, field investigation, and logical analysis. Reference [13] discusses the physical fitness training strategy of shooting athletes in the physical fitness training stage. The literature [14] promoted the change among adolescents' physical exercise and promoted the progress of physical exercise in China. Literature [15] studied whether the reaction time of intellectually disabled people could be improved through exercise program, and the experimental results showed that the reaction time of intellectually disabled youth could be improved through exercise program.

2. Analysis of Adolescent Physical Training

2.1. Analysis of the Importance of Physical Fitness Training for Adolescents.
"Physical training" is a popular word in the sports industry in recent years, and it is also the research direction of many experts in the field of sports. "Physical fitness" refers to the ability of the human body to adapt to the human living environment without external force [16]. In the process of physical growth, adolescents receive a certain degree of physical training, which will achieve a multiplier effect. In the process of youth physical training, scientific training can not only make the youth's physical quality surpass that of their peers, but also prolong the physical quality of high-level youth athletes [17]. The group of teenagers mainly includes primary and secondary school students. This is the golden stage of their physical growth and development. Physical training is very important to them. Only by insisting on scientific physical training methods can the body be in the process of physical training. Physical fitness is improved.

2.2. Build a Youth Physical Fitness Training Service System.
The youth physical training service system consists of 4 modules, namely, the application layer, the ability layer, the adaptation layer, and the physical layer. The application layer mainly includes four functional modules: physical fitness training, physical fitness testing, physical fitness self-checking, and physical fitness evaluation. The 4 molds are technically supported by the hybrid cloud security system and the hybrid cloud operation and maintenance system. The specific functional modules are shown in Figure 1.

2.3. Improve the Guarantee Mechanism of Physical Fitness Training for Young People.
At present, there are many reasons for the decline in physical health of young people in our country, such as insufficient physical activity, more social incentives, and weakening of concept and awareness, and the biggest reason is insufficient physical training. To clarify and improve the goals and tasks of youth physical fitness training to promote physical health, based on the actual situation of youth physical fitness training, to seek the core value of the construction of the guarantee mechanism of youth physical fitness training to promote physical health service system under the constraints of different regions and resources, is the realization of youth physical fitness training. It is a strategic measure to construct the system and mechanism of physical health service so as to maximize the effect of health service. It is suggested that youth physical fitness training to promote physical health services should be listed as the local sports development strategy, and incorporated into the local national economic and social development plan, improve the coordination mechanism, clarify the responsibilities of each department, and grasp the key points, difficulties, and phased goals of the operation mechanism. Combined with the local reality, strengthen the investment and guarantee for the weak links of the youth physical fitness training to promote the physical health service system, make overall planning and coordination, and continuously improve the level of the development of the physical health service for young students.
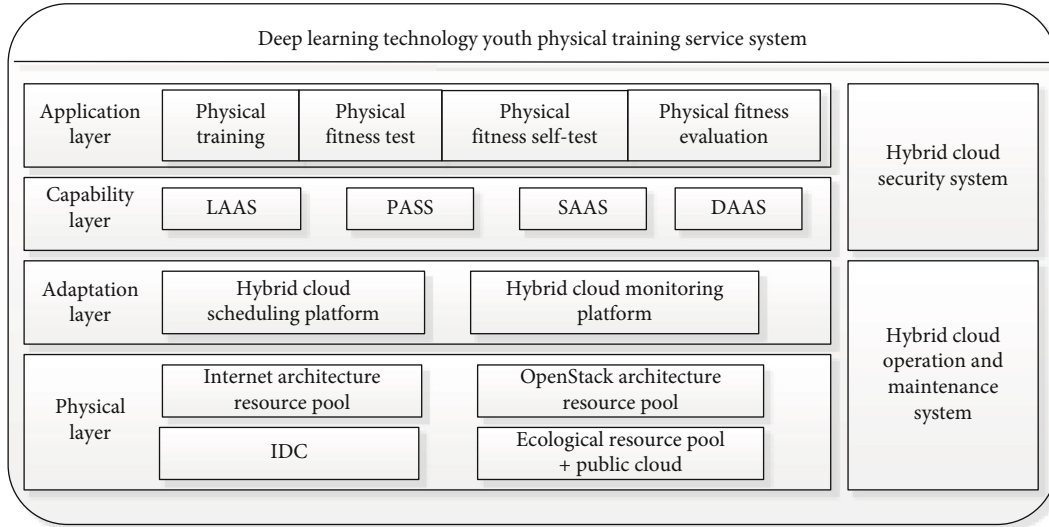
Figure 1: Adolescent physical training module diagram.

3. Construction of Youth Physical Training Model

3.1. Sampling of Sports Information for Young Athletes. The article divides the level 1 of the youth physical training effect evaluation into N levels, which are 2, namely:

$$X^{(0)} = \bigcup_{i=1}^{N} X^{(i)}. \tag{1}$$

Youth sports statistical function [18]:

$$\min F = R^2 + A \sum_i \varepsilon_i \tag{2}$$

$$s.t : \|\varnothing(x_i) - o\|^2 \le R^2 + \varepsilon_i \text{ and } \varepsilon_i \ge 0, i = 1, 2, \cdots$$

$$\max \sum_i \alpha_i K(X_i, X_i) - \sum_i \sum_j \alpha_i \alpha_j K(X_i, X_j) \tag{3}$$

$$s.t. : \sum_i \alpha_i \le 1 \text{ and } 0 \le \alpha_i \le A, i = 1, 2, \cdots$$

The correlation distribution of the constraint parameter sets R^N and X^N for establishing the evaluation of the effect of physical fitness training for adolescents is:

$$p(R^N = r_i) = p(X^N = X_i \| X_i | = |r_i|, \text{angle}(X_i)), \tag{4}$$

$$\{X(t_0 + i\Delta t), i = 0, 1, \cdots, N - 1. \tag{5}$$

Optimization set for teen training [19]:

$$X = [s_1, s_2, \cdots, s_k]_n = \left(X_n, X_{N-T}, \cdots, X_{n-(m-1)T}\right). \tag{6}$$

The expression for constructing a statistical analysis model for evaluating the effect of physical fitness training for adolescents:

$$\frac{dz(t)}{dt} = F(z), \tag{7}$$

make:

$$f(si) = (f(x_1), f(x_2, \cdots, f(x_n)). \tag{8}$$

Parametric distribution model [20]:

$$P(n_i) = \left\{ p_k \middle| pr_{kj} = 1, k = 1, 2, \cdots, m \right\}. \tag{9}$$

Distribution of mechanical characteristics of adolescent physical training:

$$\lambda = \frac{1}{1 + \alpha(\partial S/\partial t)^2}, \tag{10}$$

$$\widehat{k}_\mu(t+1) = \widehat{k}_\mu(t) + Q(t+1) \times \left[\frac{\partial \widehat{F}_\mu/Mg}{\partial t} - \frac{\partial S}{\partial t} \widehat{K}_\mu(t) \right], \tag{11}$$

in:

$$Q(t+1) = P(t+1) \frac{\partial S}{\partial t}, \tag{12}$$

$$P(t+1) = \frac{1}{\lambda} \left[P(t) - \frac{P^2(t)(\partial S/\partial t)^2}{\lambda + P(t)(\partial S/\partial t)^2} \right], \tag{13}$$

$$\frac{\partial S}{\partial t} = \frac{r}{V_c} \frac{\partial \omega_w}{\partial t}. \tag{14}$$

TABLE 1: Basic statistics of athletes.

	Control group	Experimental group	P value	T value
Height (cm)	184.0±2.00	184±1.41	0.974	-0.150
Weight (kg)	80.10±2.61	80.10±2.17	0.965	-0.087
Age	15.6±0.51	16±0.00	0.601	-2.049

Among them, λ represents the big data ambiguity distribution factor for the evaluation of adolescent physical fitness training effect, $\widehat{F}_\mu$ is the characteristic distribution amount of adolescent physical fitness training effect evaluation, and ω_w is the adaptive weighting coefficient.

3.2. Training Effect Evaluation Model Optimization. Let $X^{(0)} = (X^{(0)}(1), X^{(0)}(2), \cdots, X^{(0)}(n))$ be the original data and $X^{(1)} = (X^{(1)}(1), X^{(1)}(2), \cdots, X^{(1)}(n))$ be the one-time accumulated data sequence of the $X^{(0)}$-sequence, where:

$$X^{(1)}(1) = X^{(0)}(1), \tag{15}$$

$$x^{(1)}(k) = \sum_{i=1}^{k} x^{(0)} i. \tag{16}$$

The fuzzy scheduling function to obtain the evaluation of adolescent physical training effect is:

$$X_j(t+1) = p_j(t+1) \mp \beta \times |m\text{best}(t+1) - X_j(t)| \times \ln\left(\frac{1}{u_j(t+1)}\right). \tag{17}$$

Let $Z^{(1)}$ be the mean sequence of $X^{(1)}$:

$$Z^{(1)} = \left(Z^{(2)}(1), Z^{(1)}(3), \cdots Z^{(1)}(n)\right), \tag{18}$$

$$Z^{(1)}(K) = \frac{1}{2}\left(x^{(1)}(k) + x^{(1)}(k-1)\right). \tag{19}$$

Then, there are:

$$x^{(0)}(K) + az^{(1)}(k) = b. \tag{20}$$

Among them, a is the development coefficient, and b is the gray scale action.

Substitute the original data series $X^{(0)}$ into formula (20) to get:

$$\begin{aligned} x^{(0)}(2) + az^{(1)}(2) &= b, \\ x^{(0)}(3) + az^{(1)}(3) &= b, \\ &\cdots \\ x^{(0)}(n) + az^{(1)}(n) &= b. \end{aligned} \tag{21}$$
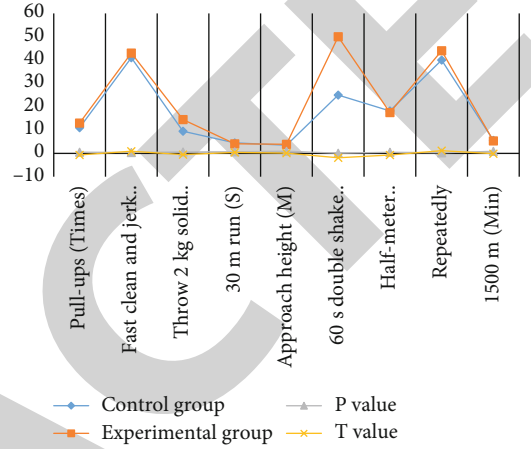

FIGURE 2: Statistics of physical fitness index evaluation results before training.

Formula (21) is the gray prediction GM (1,1) model, rewritten as a matrix equation of $Y = B \cdot A$, and the solution of the equation is [21]:

$$A = \begin{bmatrix} a \\ b \end{bmatrix} = \left(B^T B\right)^{-1} \cdot B^T Y. \tag{22}$$

Substitute the resulting a, b into (22) to get:

$$\widehat{x}^{(1)}(t+1) = \left[x^{(0)}(1) - \frac{b}{a}\right] \cdot \exp(-at) + \frac{b}{a} (t = 0, 1, 2, \cdots, n-1). \tag{23}$$

Quantitative relationships to obtain assessments of adolescent physical training effects:

$$\widehat{x}^{(0)}(i) = \widehat{x}^{(1)}(i) - \widehat{x}^{(1)}(i-1)(i = 1, 2, \cdots, n). \tag{24}$$

Define $\sigma(k)$ as the residual value [22]:

$$\sigma(k) = x^{(0)}(k) - \widehat{x}^{(0)}(k). \tag{25}$$

Definition $\varepsilon(k)$ is the residual relative difference [23]:

$$\varepsilon(K) = \frac{x^{(0)}(k) - \widehat{x}^{(0)}(k)}{x^{(0)}(k)} \times 100\%. \tag{26}$$

TABLE 2: Assessment results of physical fitness indicators of young athletes before training.

Test content	Control group	Experimental group	P value	T value
Pull-ups (times)	11.0	13.0	0.512	-0.673
Fast clean and jerk 20 kg (times)	41.0	43.0	0.378	0.911
Throw 2 kg solid ball (m) in place	9.5	14.5	0.611	-0.521
30 m run (s)	4.5	4.1	0.685	0.414
Approach height (m)	3.5	3.9	0.920	0.102
60s double shake (times)	25.0	50.0	0.081	-1.880
Half-meter movement (s)	18.2	17.5	0.495	-0.701
Repeatedly traverse (times)	40.0	44.0	0.262	1.168
1500 m (min)	5.59	5.35	0.887	-0.144

TABLE 3: Assessment results of physical fitness indicators of young athletes after training.

Test content	Control group	Experimental group	P value	T value
Pull-ups (times)	13.0	15.0	0.003	-3.578
Fast clean and jerk 20 kg (times)	42.0	44.0	0.192	-1.372
Throw 2 kg solid ball (m) in place	12.1	15.3	0.009	-3.026
30 m run (s)	4.1	3.9	0.001	5.062
Approach height (m)	3.7	4.2	0.028	-2.456
60s double shake (times)	44.0	52..0	0.086	-1.864
Half-meter movement (s)	18.9	17.1	0.018	2.677
Repeatedly traverse (times)	42.0	46.0	0.010	-2.973
1500 m (min)	5.4	5.36	0.335	0.998

Predictive function for evaluating the effect of physical training in adolescents:

$$p_{ij}^{(k)} = \frac{n_{ij}^{(k)}}{N_i}. \tag{27}$$

4. Simulation Experiments

4.1. Data Analysis. In order to study the specific data of youth physical training, the experiment selected 60 young male athletes for physical fitness test, and divided 60 young athletes into two methods, the control group received conventional training methods, the experimental group received model training methods. The evaluation results after a longer period of physical training were compared with the evaluation results without physical training, and the differences between the two comparison experiments were analyzed. The 60 athletes selected in the experiment are basically the same in height, weight, and age, and the P values are all greater than 0.06, indicating that the experiment can ensure that the conditions of the two groups are basically the same, so the experiment can exclude the error caused by the body and other elements in the experimental results. The basic information of the two teams is shown in Table 1 and Figure 2:

According to the experimental results in Table 2, we can know that before the training, the test results of various indicators of the members of the experimental group and the control group are basically the same, and there is no major difference. In the pull-up test, the control group can reach 11 times a minute, the experimental group can reach 13, the fast clean and jerk control group can reach 41, the experimental group can reach 43, and the 2 kg solid ball is thrown back in place. The control group can reach 9.5 meters, and the experimental group can reach 14.5 meters. 30 meters running in the control group for 4.5 seconds, for the experimental group for 4.1 seconds, for the run-up touch control group for 3.5 meters, for the experimental group for 3.9 meters, for the 60s double-shake control group for 25 times, for the experimental group for 50 times, for the half-meter movement control group for 18.2 seconds, 17.5 seconds in the experimental group, 40 times across the control group, 44 times in the experimental group, 5.59 minutes in the control group, and 5.35 minutes in the experimental group. The experiment conducted a T test on the control group and the experimental group. The results showed that the P values of the evaluation results of the two groups were both above 0.05. The experimental results showed that the initial conditions of the two groups could be regarded as the same before the training.

As can be seen from Table 3 and Figure 3, by analyzing the evaluation results between the control group and the experimental group, the overall situation of the members of the conventional training group was slightly improved compared with the test before training. 30-meter run, the P value of the run-up touch, the half-meter movement, and the repeated crossing test results are all less than 0.05,
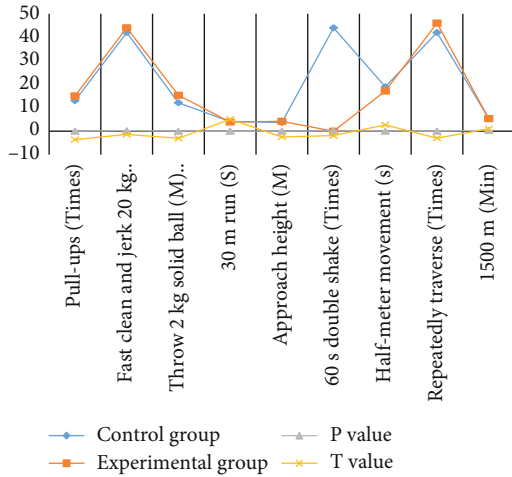
Figure 3: Statistics of physical fitness index evaluation results after training.

Table 4: Statistical analysis values of physical training effect evaluation for young athletes.

	Mean	Standard value	Minimum	Statistical mean
Exercise time	0.267	0.686	0.144	5.784
Physical fitness	0.365	0.544	0.368	2.436
Daily exercise	0.556	0.457	0.465	2.587
Training intensity	0.454	0.476	0.354	4.376
Correlation coefficient	0.425	0.546	0.424	3.655

indicating that the difference between the two is large. However, the P value of fast clean and jerk 20 kg and 60s double shake is greater than 0.05, which shows that there is no significant difference between the control group and the experimental group after these two evaluations. Combining the evaluation results of the two groups before the training, we can conclude that under the condition that the initial conditions are basically the same, and the training conditions and environment are basically the same, the trainees who have received the mode training method have obtained better physical fitness indicators. The improvement and the effect are greatly optimized compared with the mode training.

4.2. Simulation Test Analysis. In order to verify that the method proposed in the article can improve the performance of the physical training effect of young athletes, a series of statistical analysis software was used for simulation test analysis, and the data of the physical training effect of young athletes was counted. The statistical results are shown in Table 4:

According to Table 4 and Figure 4, the results of physical fitness evaluation of young athletes are analyzed. The statistical average of exercise time is 5.784, which is the highest statistical average among the five variables. The statistical average of physical fitness is 2.436, which is the highest in the statistical results. The lowest one, the statistical average
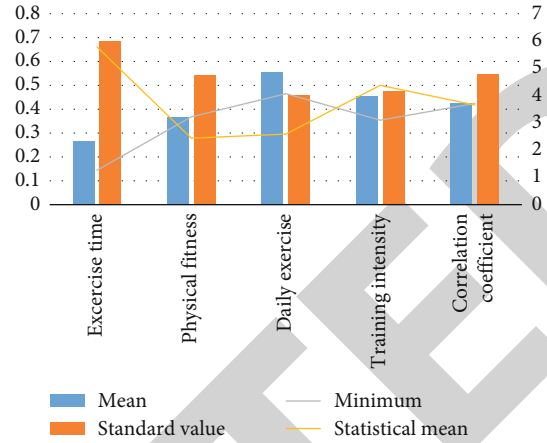

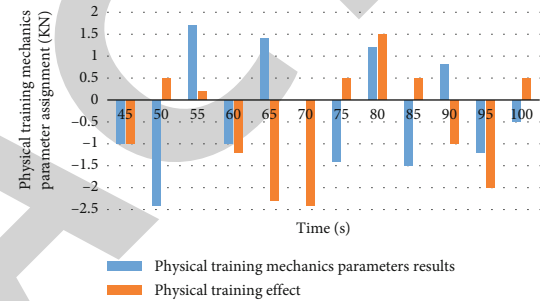Figure 4: Statistical chart of physical training effect.

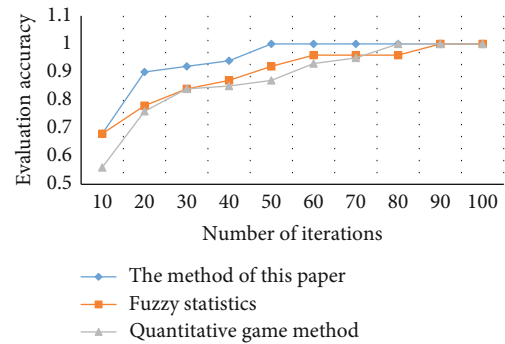Figure 5: Statistical graph of the output of physical training effect evaluation.

Figure 6: Evaluation accuracy comparison test.

of physical fitness and daily exercise situation, is not significantly different. According to the experimental results in Table 1, the statistical results of physical training parameters and physical training effect evaluation output of young athletes are calculated, and the statistical results are shown in Figure 5:

According to the experimental results in Figure 5, we can conclude that the method in this paper has higher accuracy in evaluating the training effect after youth physical training. The experiment also carried out a confidence test on the method proposed in the article, which is different from the fuzzy statistical method and the quantitative game method.

TABLE 5: Evaluation criteria table.

	Metrics	Formula
Accuracy	The accuracy rate measure is the ratio of the number of passes to the total number of passes. The larger the index value, the more accurate the detection result.	$Precision = hits_u/recset_u$
Recall	The recall rate criterion refers to the ratio of the number of detections to the theoretical maximum number of hits.	$Recall = hits_u/testset_u$
F1 measure	The F1 metric can effectively balance the precision and recall by biasing towards the side with the smaller value. The larger the index value, the more accurate the test result.	$F1 = 2 \times Precision \times Recall/Precision + Recall$

TABLE 6: The performance of each model on the test set.

Model	Accuracy	Precision	Recall	F1 score
Deep learning physical training model	89.12%	89.56%	90.10%	90.48%
Improved fitness training model	92.46%	93.27%	93.21%	93.45%
Fuzzy statistical model	85.45%	85.43%	86.12%	86.18%
Quantitative game model	75.14%	75.24%	75.46%	75.12%

TABLE 7: The performance of each system on the mixed test set.

Model	Accuracy	Precision	Recall	F1 score
Deep learning physical training model	87.25%	87.12%	88.10%	88.24%
Improved fitness training model	90.12%	90.24%	90.48%	90.29%
Fuzzy statistical model	82.14%	82.47%	82.27%	82.14%
Quantitative game model	72.28%	72.45%	72.89%	73.10%

For comparison, the comparison results are shown in Figure 6:

According to the experimental data in Figure 6, we can know that the evaluation accuracy of the method in this paper is the highest among the three methods. When the number of iterations reaches 50, the evaluation accuracy can reach 1. When the number of iterations of the fuzzy statistical method is 80, the evaluation accuracy can reach 0.95. When the number of iterations of the method is 90, the evaluation accuracy can reach 1.

4.3. Performance Test

4.3.1. Evaluation Criteria. Shown in Table 5.

4.3.2. Specific Tests. In order to test the superiority of the performance of the physical training model based on deep learning technology proposed in the article, after the model proposed in the article is improved, the fuzzy statistical model and the quantitative game model are run on the test set and the mixed test set, respectively. The test set is used to evaluate the generalization ability of the final model, and the mixed test set tunes the model's hyperparameters and is used to make an initial evaluation of the model's ability. The experimental results were recorded to verify the advantages of the three models for adolescent physical training, and the AUC curves were drawn based on the experimental results. AUC is a model evaluation metric in the field of machine learning. The larger the AUC value of the
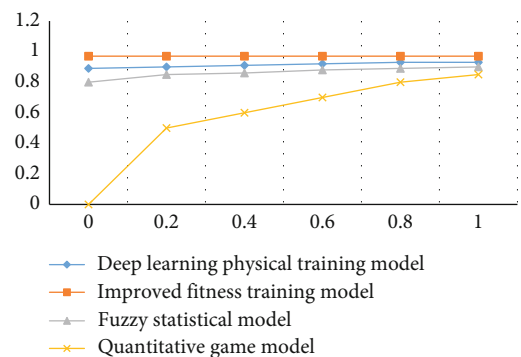

FIGURE 7: AUC curve on the test set.

classifier, the higher the accuracy rate. The experimental data of different models on the test set and the mixed test set are shown in Table 6 and Table 7:

According to the data in Table 6 and Figure 7, we can conclude that after running on the test set, the article proposes that the accuracy rate of the physical training model based on the deep learning algorithm is 89.12%, the accuracy rate can reach 89.56%, and the improved accuracy rate can reach 92.46%, and the accuracy rate can reach 93.27%, which is the one with the highest index value among the four experimental models. The accuracy rate of the quantitative game model is 75.14%, which is the lowest among the four systems, and the fuzzy statistical model is in the middle state.
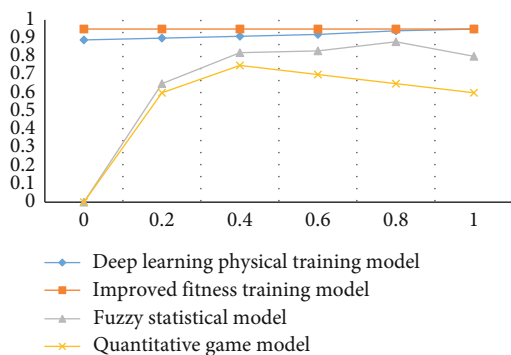
FIGURE 8: AUC curve on the mixed test set.

According to the AUC curves of the four algorithms, we can also see that the AUC curve values of the article and the improved system are very stable. 0.97, the AUC value of the fuzzy statistical model is low, the AUC curve of the quantitative game algorithm is more tortuous, and the AUC value is also low. The research data also show that the recognition accuracy of the physical training method of the deep learning algorithm is the highest.

According to the data in Table 7 and Figure 8, we can conclude that after running on the mixed test set, showing four models has decreased to a certain extent, but the performance of the model proposed in this article is still the highest among the four models. The accuracy of the model before improvement is 87.25%, and the accuracy of the improved model is 90.12%. According to the AUC curve diagrams of the four algorithms, we can also see that the AUC curve value of the improved system is very stable no matter in the test set or the mixed test set, stable within the range of 0.90-095. The AUC curves of the fuzzy statistical model and the quantitative game model are more tortuous, and the AUC values are also lower. The experimental results also show that the recognition accuracy of the physical training model of the deep learning algorithm is the highest.

5. Conclusion

Adolescents are the future of national development, and adolescent physical training is the most important basic condition for promoting the healthy development of the adolescent system. According to effective research, the physical quality of Chinese adolescents has continued to decline for more than 20 years, and many adolescents lack exercise. Physical fitness training for adolescents is an objective need for building a harmonious society, and is related to the strength of individuals and nations. Based on strengthening physical fitness training for adolescents, this paper studies a data analysis model of adolescent physical fitness based on deep learning algorithm. With the goal of improving the physical quality of adolescents, it will form an interactive synergy with the theoretical research on the health promotion of the adolescent system, and build a physical training method to promote the formation of the adolescent health system. In the future research work, in the growth process

of young people, we should not pay attention to their achievements, but should pay attention to their physical health, physical and mental health, and realize the all-round development of young people. The government should give sufficient financial support to ensure diversified development of adolescent health.

Data Availability

The experimental data used to support the findings of this study are available from the corresponding author upon request.

Conflicts of Interest

The author declared that he has no conflicts of interest regarding this work.

References

[1] G. E. Couto, S. A. Nunes, and O. De, "Oxidants, antioxidants, and the beneficial roles of exercise-induced production of reactive species," *Oxidative Medicine and Cellular Longevity*, vol. 2012, no. 6, 2012.

[2] I. Шеремет, "Physical Training in Social Sphere of Student Youth," in *The Scientific Issues of Ternopil Volodymyr Hnatiuk National Pedagogical University*, vol. 10 of Pedagogy, no. 12, pp. 52–64, 2015.

[3] L. Chen, J. J. Hou, and W. D. Wang, "Exploration of practical ability of scientific and technological education for biological normal students," *Journal of Hubei Normal University (Natural Science)*, vol. 38, no. 1, 2018.

[4] G. I. Honchar, "Moral priorities of students in the sphere of physical training and sport," *Pedagogics Psychology, Medical-Biological Problems of Physical Training and Sports*, vol. 3, pp. 34–39, 2012.

[5] L. K. Kozhevnikova, "Physical training as means of a healthy way of life and cultural leisure formation of student's youth," *Physical Education of Students*, vol. 10, no. 12, pp. 34–38, 2010.

[6] M. A. Yun-Feng, "Youth physical fitness training method for short track speed skaters," *China Winter Sports*, vol. 10, no. 12, pp. 21–32, 2018.

[7] N. M. Kulish, S. I. Horodinskiy, and N. M. Bukoros, "The low youth motivation for physical training or sports is the problem of healthy lifestyle forming," *Pedagogics, Psychology, Medical-Biological Problems of Physical Training and Sports*, vol. 14, no. 10, pp. 24–31, 2012.

[8] J. Zhang, "Youth football physical training method of study," *Contemporary Sports Technology*, vol. 10, no. 8, pp. 21–25, 2015.

[9] R. Collingwood, J. Sunderlin, R. Reynolds, and H. W. Kohl III, "Physical training as a substance abuse prevention intervention for youth," *Journal of Drug Education*, vol. 30, no. 4, pp. 435–451, 2000.

Retraction

Retracted: Analysis and Evaluation Research on the Construction of the Music Art Management Curriculum System Based on the Deep Learning Model

Journal of Sensors

This article has been retracted by Hindawi following an investigation undertaken by the publisher [1]. This investigation has uncovered evidence of one or more of the following indicators of systematic manipulation of the publication process:

(1) Discrepancies in scope

(2) Discrepancies in the description of the research reported

(3) Discrepancies between the availability of data and the research described

(4) Inappropriate citations

(5) Incoherent, meaningless and/or irrelevant content included in the article

(6) Manipulated or compromised peer review

The presence of these indicators undermines our confidence in the integrity of the article's content and we cannot, therefore, vouch for its reliability. Please note that this notice is intended solely to alert readers that the content of this article is unreliable. We have not investigated whether authors were aware of or involved in the systematic manipulation of the publication process.

In addition, our investigation has also shown that one or more of the following human-subject reporting requirements has not been met in this article: ethical approval by an Institutional Review Board (IRB) committee or equivalent, patient/participant consent to participate, and/or agreement to publish patient/participant details (where relevant).

Wiley and Hindawi regrets that the usual quality checks did not identify these issues before publication and have since put additional measures in place to safeguard research integrity.

We wish to credit our own Research Integrity and Research Publishing teams and anonymous and named external researchers and research integrity experts for contributing to this investigation.

The corresponding author, as the representative of all authors, has been given the opportunity to register their agreement or disagreement to this retraction. We have kept a record of any response received.

References

[1] S. Hu and L. Yang, "Analysis and Evaluation Research on the Construction of the Music Art Management Curriculum System Based on the Deep Learning Model," *Journal of Sensors*, vol. 2022, Article ID 5873218, 9 pages, 2022.

Research Article

Analysis and Evaluation Research on the Construction of the Music Art Management Curriculum System Based on the Deep Learning Model

Shichang Hu[1] and Lei Yang [2]

[1]College of Art, Hainan College of Vocation and Technique, Haikou, Hainan 570216, China
[2]College of Music, Hainan Normal University, Haikou, Hainan 571158, China

Correspondence should be addressed to Lei Yang; 100037@hainnu.edu.cn

In view of the fact that music courses are seldom offered in schools and lack of management, there are many problems in the management system of music and art. In order to improve the learning effect of students in music courses, this paper proposes to build a music art management curriculum system based on the in-depth learning model. This paper puts forward the requirements of in-depth learning in music and art curriculum indicators and puts forward the model framework of music and art learning. Through the combined application of music courses, first of all, the current music course model is compared with Ghostnet music course, Mobilenet music course, and traditional music course to verify that the current music course model has certain advantages in accuracy, precision, recall, and image recognition performance. This proves that the current music curriculum is more suitable for the construction of this model. Secondly, the proposed model has a high score through the comprehensive application of several indicators in the course. Finally, under the model constructed by deep learning, the opening of music courses in schools has also increased significantly and improves the interest point and the application of people on the music art course so as to achieve the final application effect.

1. Introduction

With the development of industrialization, the development of music art has become more and more rapid, but it is also accompanied by many chaos that are difficult to manage. Therefore, the music art market needs professional talents to manage, but professional managers have little understanding of music art, and it is difficult to guarantee music art, which affects the positioning of products; economic management requires all music products to be estimated, but music art cannot use quantitative costs to calculate the price, which requires very keen judgment and professionalism in art. Conversely, music art creators do not understand systematic economic management knowledge, and products cannot be converted either. How to better integrate and develop the two and cultivate talents with both music and art judgment and management ability, the music art man-

agement course came into being. Literature [1] indicated that because of the acceleration of my country's modernization process and the continuous deepening of education reform, music and art education have received more and more attention. In order to achieve the purpose of strengthening the management of music courses, it is necessary to use music art education to innovate student management, stimulate students' creative thinking, and cultivate students' music appreciation ability and aesthetic orientation. Literature [2] explains that art managers must master the basis of art-related knowledge and skills, and engaging in related cultural industries and undertakings is the purpose of comprehensive art schools to cultivate comprehensive art management talents. The mastery of basic music skills plays a huge role in understanding and evaluating related professional knowledge in the field of music. Literature [3] explains that an important research topic of colleges and

universities has added a new quality education of business origin. The start of quality education combined with the actual situation of the music major. Literature [4] shows that music and art education are important components of implementing and deepening comprehensive quality education in colleges and universities. Literature [5] describes that music appreciation is not only an important art education curriculum for universities but also one of the main goals of art education. Literature [6] is a key issue to improve the quality of students' music by paying attention to the teaching process for quality education. Literature [7] indicates that the intermittent nature of music and art enables the music appreciation course to strengthen students' understanding of different art courses and improve the development of professional standards. Literature [8] shows that music and art courses are one of the most important components of aesthetic education. Literature [9] indicates that the relationship between art curriculum and music curriculum is a necessary trend of music education reform for art curriculum. The literature [10] shows that music teachers should make speeches vigorously and vividly in the classroom, give full play to the leading role of teachers, and to stimulate the initiative of students in learning. Literature [11] helps students to establish a scientific music spirit by cultivating students' musical potential, which is the purpose of the new curriculum reform. Adopting the teaching principle of "lower, slower, higher and higher" is a powerful "weapon." Literature [12] indicates that music curriculum is the core value of the new curriculum. The concept of the new curriculum is how to stimulate students' creative thinking, how to improve the quality of problems, and maximize the potential of students in realizing basic music. Literature [13] shows that music and art education can promote the artistic cultivation of education, enrich emotions, and tap the potential of thinking. You can introduce music courses into common university courses and use different teaching materials and methods. Literature [14] indicates that the introduction of western art music meets the artistic requirements of public courses. This introductory course is called music appreciation and includes the study of musical elements. The evolution of classical music actively listening to music is an important part of it. Literature [15] explains that the experimental project of art education reform held by the Ministry of Education includes training of compound art teachers in higher normal colleges. The purpose is for more students to be exposed to art education. The abovementioned study of music curriculum is basically improved through teaching means and methods, and the traditional methods are inefficient in improving the art of music. It is necessary to make an in-depth analysis of the music and art curriculum through new technological means, and the goal of in-depth learning is to provide technical support for the learning community. In the model, there are mainly two learning subjects of teachers and students, both of which can use the optimized resources of the deep learning model to get the resources they pay more attention to. The learning community is divided into preclass resource application, in-class resource exchange, and postclass resource discussion, making full use of in-depth learning methods to achieve full opti-

mization. In order to improve the level of art management courses, the deep learning model is introduced in the article. In the deep learning model, students' art resources are managed according to the learning community of students and teachers in different systems of art management. Through in-depth learning, it can play a key role in the acquisition and evaluation of art management knowledge points and can enhance the learning effect of students. The use of the in-depth learning model can promote the efficiency and application scenarios of art course learning and has a better learning effect, which has important research significance for improving the application of the course.

2. Model Construction

2.1. Deep Learning-Related Concepts.
Deep learning is very helpful to the interpretation of information data. Let the machine have the ability to analyze and learn like humans. It is his ultimate goal to be able to recognize data such as text, images, and sounds. Deep learning is more complicated in machine learning algorithms, but his achievements far exceed previous related technologies [16].

Deep learning has achieved a lot of results in a variety of related fields. Deep learning is a machine that imitates human activities and solves many complex recognition problems, making artificial intelligence have made great progress in related aspects [17].

2.2. The Embodiment of Deep Learning in Music Courses.
Deep learning in music courses is reflected in many aspects: (1) teaching philosophy, adhere to student-oriented, (2) teaching goals, adhere to ability training, (3) teaching methods, adhere to changing methods, and (4) teaching practice, persist in active exploration, as shown in Table 1:

2.3. Constructing a Model of the Music Art Management Curriculum System.
In order to improve students' music ability, deep learning is used to construct a music art management curriculum model. The goal of deep learning is divided into three steps, as follows: before class, design standards and curriculum and preassessment; in class, create a positive learning culture, prepare and activate prior knowledge, and acquire new knowledge and deep processing knowledge; after class, evaluate students' learning.

The learning community includes teachers and students, who will interact online and offline: (1) communicate on the online platform before class: teachers publish teaching resources and tasks based on the analysis and evaluation of learners and the analysis of teaching objectives. Students learn independently through online guidance resources and carry out preclass exercises and learning feedback. (2) Face-to-face communication in class: after the teaching resources and tasks are released, the teacher needs to create a teaching situation, then ask the inquiry questions, then conduct personalized guidance, and finally make an evaluation. What students need to do is to actively explore the tasks issued by the teacher, then collaboratively study, then demonstrate and communicate, and finally evaluate them. (3) Online platform exchanges are also conducted after class:

TABLE 1: The embodiment of deep learning in music courses.

Index	Content
Teaching philosophy	Adhere to "student-oriented," in the classroom, there are more or less the phenomenon that some teachers only teach themselves and ignore the students' learning. Teachers only care about themselves in the classroom according to the books, regardless of whether the students accept the knowledge taught. Therefore, in teaching, we must give play to the main role of students, allowing students to learn actively and complete their learning tasks independently. In music courses, students are required to take the initiative to preview in advance, to independently complete the tasks assigned by the teacher when learning music, and to review in time after class.
Teaching objectives	Adhering to "capability training," in music teaching, we should not only be limited to the teaching of theoretical knowledge but also require students to practice, and turn knowledge to rely on ability when assessing. Always infiltrate ability training into music teaching classrooms, guiding students to discover music knowledge and evaluate the value of the process.
Teaching methods	Persist in "transformation methods," change the methods of teachers "teaching" and students "learning," advocate independent, cooperative, and inquiring learning methods in music classrooms, and transform from passive learning to active learning. Let students become the main body of teaching and help students grasp the essence of knowledge through in-depth processing.
Teaching practice	Adhering to "active exploration" requires learning design for each unit in the music curriculum, which is divided into unit learning topics, learning objectives, learning activities, and continuous evaluation. The relationship between these four is to first determine the unit learning theme, then set the learning goals, then carry out the learning activities, and finally continue to evaluate. Every process requires practical exploration of teaching.
Teaching philosophy	Adhere to "student-oriented," in the classroom, there are more or less the phenomenon that some teachers only teach themselves and ignore the students' learning. Teachers only care about themselves in the classroom according to the books, regardless of whether the students accept the knowledge taught. Therefore, in teaching, we must give play to the main role of students, allowing students to learn actively and complete their learning tasks independently. In music courses, students are required to take the initiative to preview in advance, to independently complete the tasks assigned by the teacher when learning music and to review in time after class.
Teaching objectives	Adhering to "capability training," in music teaching, we should not only be limited to the teaching of theoretical knowledge, but also require students to practice, and turn knowledge to rely on ability when assessing. Always infiltrate ability training into music teaching classrooms, guiding students to discover music knowledge, and evaluate the value of the process.
Teaching methods	Persist in "transformation methods," change the methods of teachers "teaching" and students "learning," advocate independent, cooperative, and inquiring learning methods in music classrooms, and transform from passive learning to active learning. Let students become the main body of teaching and help students grasp the essence of knowledge through in-depth processing.
Teaching practice	Adhering to "active exploration" requires learning design for each unit in the music curriculum, which is divided into unit learning topics, learning objectives, learning activities, and continuous evaluation. The relationship between these four is to first determine the unit learning theme, then set the learning goals, then carry out the learning activities, and finally continue to evaluate. Every process requires practical exploration of teaching.

teachers on the online communication platform will answer questions, discuss, and communicate with students, conduct individual counseling on the questions raised by the students, and finally reflect and summarize. Students have discussions, exchanges, and reflections, as shown in Figure 1.

3. Deep Learning and Music Learning Methods

3.1. Methods of Deep Learning. Input is as follows: values of x over a minibatch:

$$B = \{X_1, X_2, \cdots, \cdot Xm\}. \tag{1}$$

Parameters to be learned: γ, β.
Output is as follows:

$$\{y_i = BN_{\gamma,\beta}(x_i)\}, \tag{2}$$

$$\mu B \longleftarrow \frac{1}{m} \sum_{i=1}^{m} x_i //\text{mini} - \text{batch mean}, \tag{3}$$

$$\sigma_B^2 \longleftarrow \frac{1}{m} \sum_{i=1}^{m} (x_i - \mu B)^2 //\text{mini} - \text{batch variance}, \tag{4}$$

$$\widehat{x}_i \longleftarrow \frac{x_i - \mu B}{\sqrt{\sigma_B^2 + 1}} //\text{normalize}, \tag{5}$$

$$y_i \longleftarrow \gamma \widehat{x}_i + \beta \equiv BN_{\gamma,\beta}(x_i) //\text{scale and shift}. \tag{6}$$

3.1.1. Stochastic Gradient Descent. Stochastic gradient descent is mainly used to solve optimization problems. Summation form is as follows:
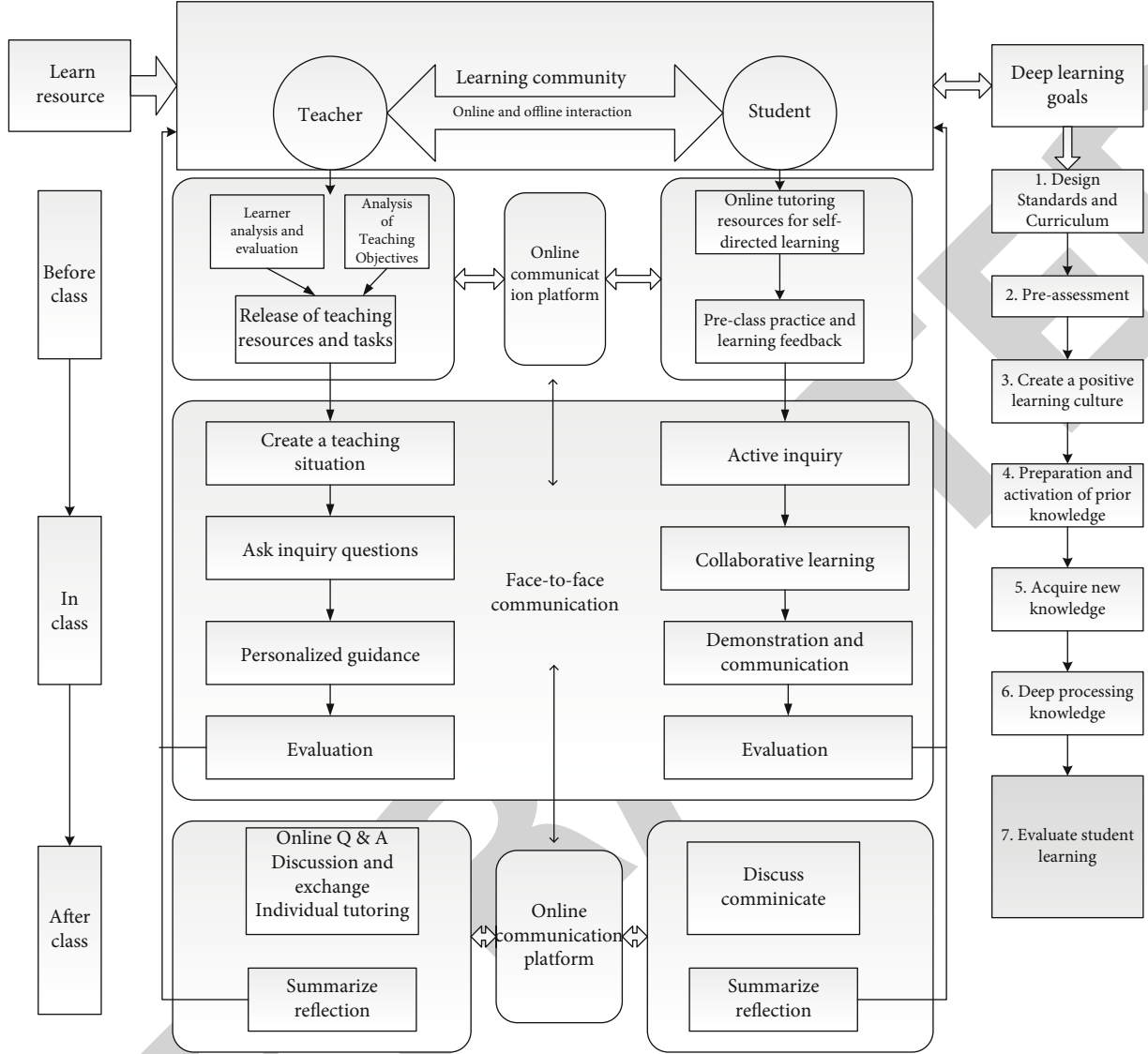
$$f(w) = \sum_{i=1}^{n} f_i(w, x_i, y_i). \tag{7}$$

Figure 1: Music curriculum model constructed.

Gradient descent method is as follows:

$$w_{t+1} = w_t - \eta_{t+1}\nabla f(w_t) = w_t - \eta_{t+1}\sum_{i=1}^{n}\nabla f_i(w_t, x_i, y_i). \quad (8)$$

3.2. Hypothetical Model of Deep Learning Process

3.2.1. Model Fit Index

(1) Chi-Square Degree of Freedom Ratio (χ^2/df). The chi-square value (χ^2) formula is

$$\chi^2 = (n-1)F\left(S;\widehat{\Sigma}\right), \quad (9)$$

$$F\left(S;\widehat{\Sigma}\right) = tr\left(S\widehat{\Sigma}^{\wedge}(-1)\right) + \lg\left|\widehat{\Sigma}\right| - \lg|S| - P, \quad (10)$$

where χ^2 will be affected by the number of variables and the data sample size.

(2) Asymptotic Residual Mean Square and Square Root (RESEA). The asymptotic residual mean square and square root formula is

$$\text{RMSEA} = \sqrt{\frac{F_0}{df}}, \quad (11)$$

where F_0 represents the value of the difference function, and df represents the degree of freedom.

(3) Fitting Index. GFI stands for fit index. AGFI represents the adjusted number of fits. The formula is

$$\text{GFI} = 1 - \frac{F\left(S;\widehat{\Sigma}\right)}{F\left(S;\widehat{\Sigma}(0)\right)}, \quad (12)$$

TABLE 2: Accuracy test.

Courses type	Accuracy	Exactness	Recall rate	Test accuracy
Current music courses	96.7%	94.8%	95.6%	81.2%
Ghostnet music course	85.1%	90.2%	87.4%	79.4%
Mobilenet music course	90.4%	89.2%	92.6%	78.6%
Traditional music course	94.2%	91.5%	90.8%	80.5%
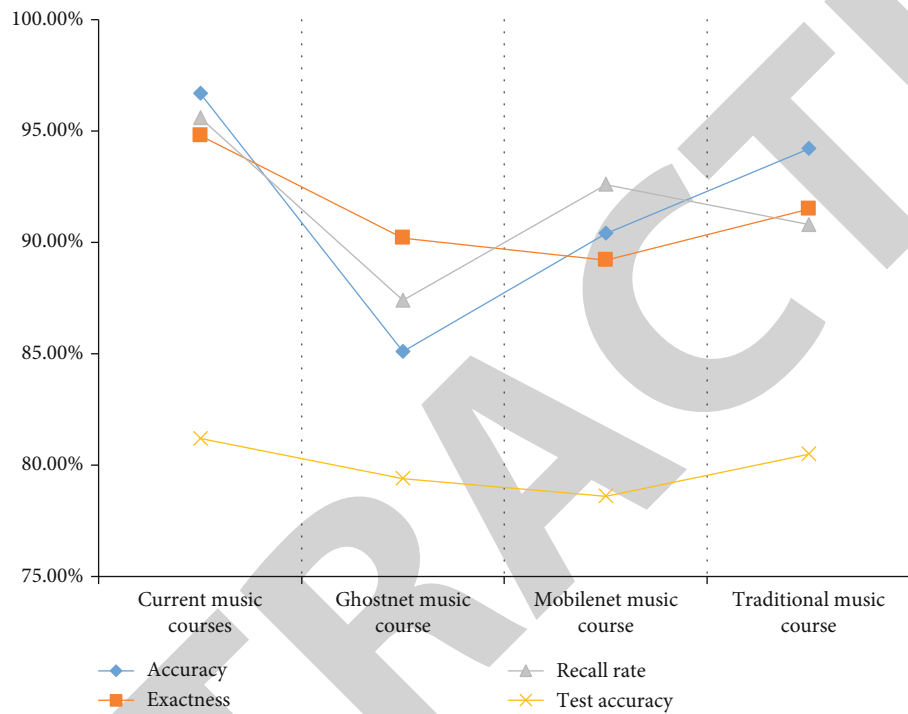
FIGURE 2: Accuracy comparison.

$$AGFI = 1 - (1 - GFI)\left[\frac{n(n+1)}{2df}\right]. \quad (13)$$

(4) Comparison of Fit Number (CFI). CFI refers to the degree of agreement between predicted results and actual data. The calculation formula of CFI is

$$CFI = 1 - \frac{MAX\left(\chi_T^2 - df_T, 0\right)}{MAX\left(\chi_N^2 - df_N, 0\right)}. \quad (14)$$

The data obtained by subtracting the chi-square value of the predicted result χ_T^2 minus the degree of freedom of the predicted result df_T divided by the chi-square value of the actual data χ_N^2 minus the degree of freedom of the actual data df_N is the predicted result. The degree of agreement is with the actual data.

3.3. CNN Structure and Model. The specific formula of convolutional neural network (CNN) is

$$H_i = W_i \cdot X + b_i, i = 1, \cdots \cdots k. \quad (15)$$

The CNN model structure can speed up the training speed and adjust the accuracy of the parameters through the two-way transmission of the learning signal in the neuron.

The main calculation formula of the residual network is

$$F(\chi_i) = \omega \cdot \chi_i + b, \quad (16)$$

$$y_i = R(F) + h(\chi_i), \quad (17)$$

$$\chi_{i+1} = R(y_i), \quad (18)$$

where the input is χ_i, the weight is ω, the bias is b, the sum of the two branch layers is y_i, the activation function is R, the convolution operation is $F(\chi_i)$, the input data is transformed into $h(\chi_i)$, and the residual module input is χ_{i+1}.

3.4. Music Art

3.4.1. Separation Algorithm. Harmonic sound components and impact sound components make up the music signal. According to the difference between the two sounds in the frequency spectrum, the original frequency spectrum W_{fJ}

TABLE 3: Performance test.

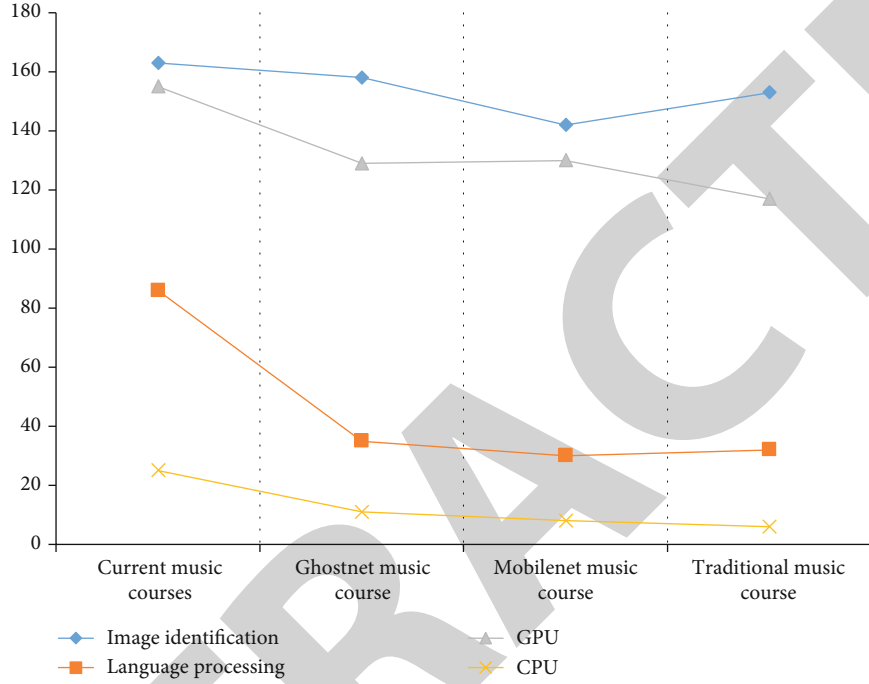| Courses type	Image identification	Language processing	GPU	CPU
Current music courses	163	86	155	25
Ghostnet music course	158	35	129	11
Mobilenet music course	142	30	130	8
Traditional music course	153	32	117	6

FIGURE 3: Performance test.

can be separated into the impact frequency spectrum P_{fJ} and the harmonic frequency spectrum H_{fJ}. The formula is

$$W_{fJ} = P_{fJ} + H_{fJ}, \tag{19}$$

where $P_{fJ} > 0$, $H_{fJ} > 0$.

The separation formula for realizing impact sound and spectrum sound is

$$
\begin{aligned}
Q\left(H^t, P^t, U^t, V^t\right) \\
= \frac{1}{\sigma_H^2} \sum_{fJ} \left\{ \left(H_{f,t-1}^t - U_{f,t}^t\right)^2 - \left(H_{f,t}^t - U_{f,t}^t\right)^2 \right\} \\
+ \frac{1}{\sigma_P^2} \sum_{fJ} \left\{ \left(P_{f,t-1}^t - V_{f,t}^t\right)^2 - \left(P_{f,t}^t - V_{f,t}^t\right)^2 \right\}.
\end{aligned}
\tag{20}
$$

Find the minimum value, the updated formula is

$$H_{f,J}^{t+1} = H_{fJ}^t + \Delta^t, \tag{21}$$

$$P_{f,J}^{t+1} = P_{fJ}^t + \Delta^t, \tag{22}$$

where

$$\Delta^t = \frac{\alpha}{4} \left(H_{fJ-1}^t - 2H_{ft+1}^t + H_{ft+1}^t\right) - \frac{1-\alpha}{4} \left(P_{fJ-1}^t - 2P_{ft+1}^t + P_{ft+1}^t\right), \tag{23}$$

$$\alpha = \frac{\sigma_\gamma^2}{\sigma_H^2 + \sigma_\gamma^2}. \tag{24}$$

3.5. Establishment of a Music Curriculum System Model. $f(x)$ and x represent the content and students learned in the music course, $df(x)/dx$ represents the learning effect of students, and the expression is as follows:

$$\frac{df(x)}{dx} = \lim_{h \longrightarrow 0} \frac{f(x+h) - f(x)}{h}. \tag{25}$$

4. Analysis and Research

4.1. Environment and Method Settings. According to the established model system, excluding external influence factors, we will verify the applicability of the model through experiments. In this experiment, 50 students and two teachers in a class are used as experimental research objects. In one semester, the two teachers will use the model we
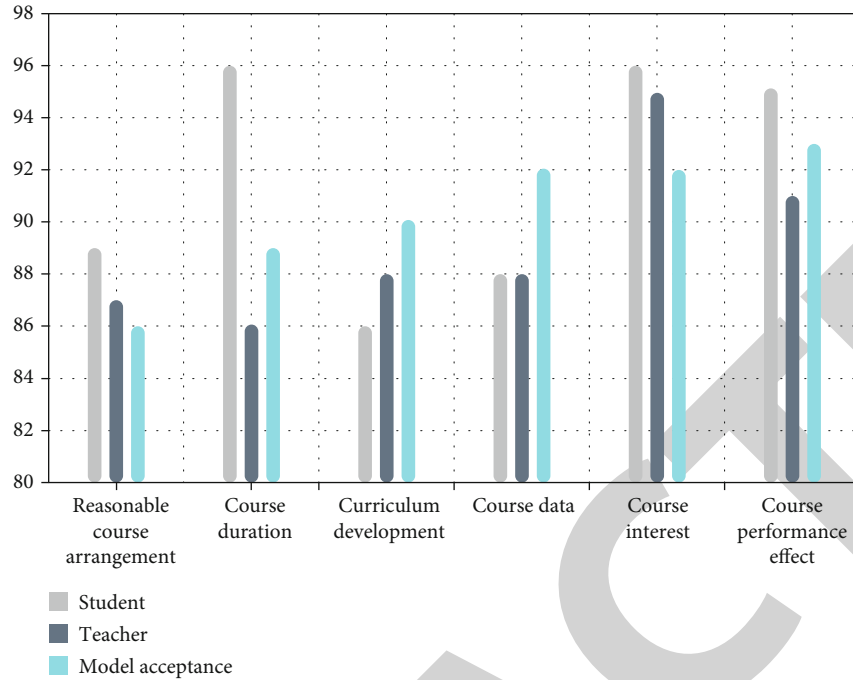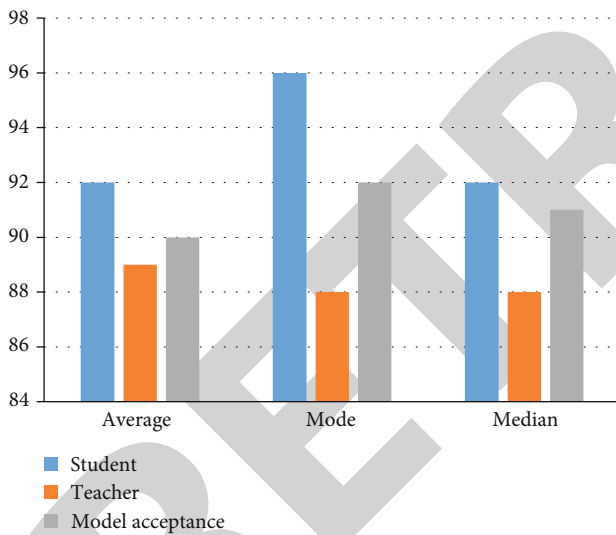
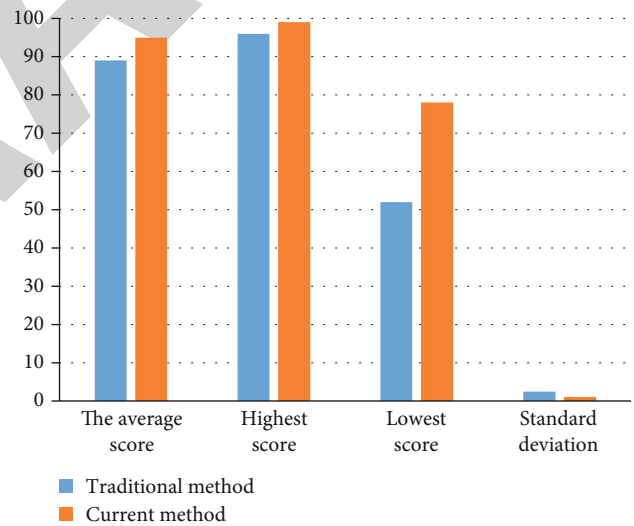Figure 4: Course evaluation.

Figure 5: Model acceptance.

Figure 6: Course score analysis.

constructed to teach students music courses and verify the superiority of this model through their test results after the end of teaching and their scoring and evaluation of the model.

4.2. Model Test. First of all, we need to compare the methods. We compare the accuracy and performance of the music course model constructed in this article with Ghostnet music courses, Mobilenet music courses, and traditional music courses through experiments, and the following results are obtained.

4.2.1. Accuracy Comparison. The accuracy test results are shown in Table 2:

By comparing the current music course model with Ghostnet music course, Mobilenet music course, and traditional music course, it can be concluded that deep learning is better than the other three methods in accuracy, precision, recall, and test accuracy. It is shown in Figure 2:

4.2.2. Performance Test. The results of the performance test are shown in Table 3:

Through the performance test of the above methods, it can be concluded that the performance of the current music course model in image recognition, language processing, GPU, and CPU is higher than other methods, as shown in Figure 3.
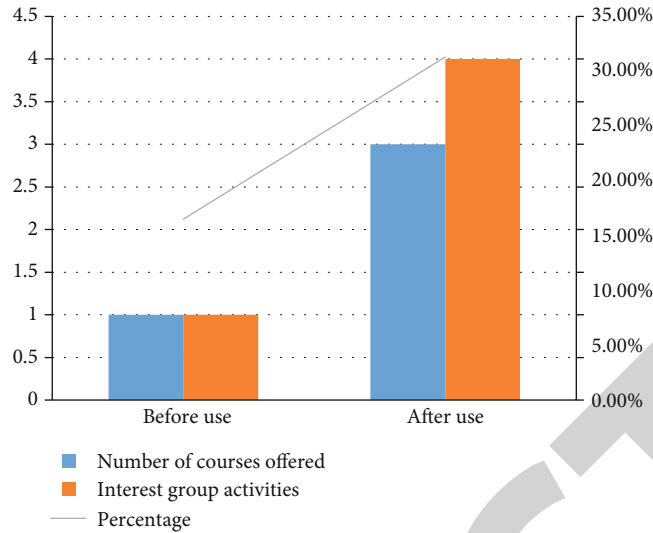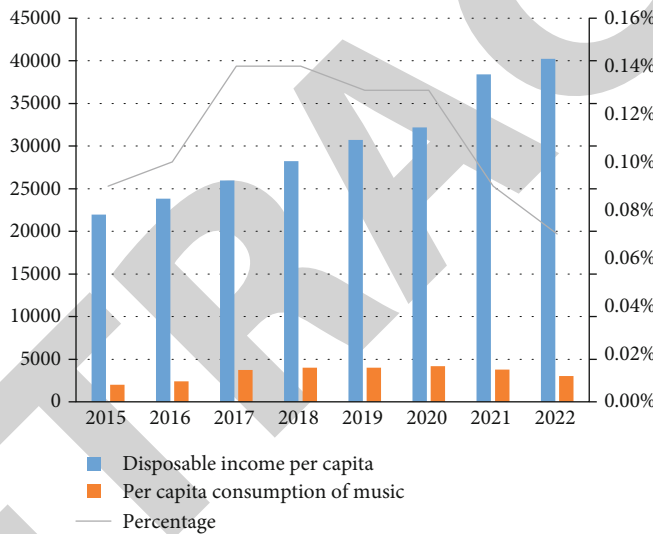
Figure 7: Comparison of curriculum.

Figure 8: The impact of the model on consumption.

4.3. Course Evaluation Scoring. Then, when using the model built by deep learning to conduct experiments, we also need to evaluate the model. After a semester of testing, students and teachers will evaluate the deep learning model. We will score and evaluate the curriculum development, curriculum data, curriculum interest, and curriculum achievement effects, as shown in Figure 4.

According to the scoring and evaluation of the model by teachers and classmates, we will summarize these data and calculate their average, mode, and median, combined with their statistics on the recognition of this model, as shown in Figure 5.

4.4. Course Grades and Course Settings

4.4.1. Course Results. After a semester of study under the model constructed by deep learning, the students have achieved significant improvement in their grades, and each index has shown an upward trend, especially in the lowest

score index. This shows that this model is well used in music art management courses, as shown in Figure 6.

4.4.2. Course Setting. After learning using the management curriculum model, the school has significantly increased the music curriculum and the number of interest group activities. The proportion of music in the curriculum has skyrocketed, as shown in Figure 7.

4.5. The Impact of Using This Model. After using the deep learning model, it also has an impact on our economy. Before using deep learning, people's consumption in music has increased year by year. After using this model, people's consumption of music is gradually reduced. This is because we can learn music knowledge that we spent a lot of money in the past in the deep learning model; so, we can reduce the consumption of music and spend money on it, where it is needed more, and we expect that the per capita consumption of music will decrease year by year, as shown in Figure 8.

Research Article

Intelligent Spraying Water Based on the Internet of Orchard Things and Fuzzy PID Algorithms

Pingchuan Zhang [ID],[1] **Sijie Wang** [ID],[1] **Menglong Bai,**[2] **Qiaoling Bai,**[1] **Zhao Chen** [ID],[1] **Xu Chen** [ID],[1] **Yanjun Hu,**[1] **Jianming Zhang** [ID],[1] **Yulin Li,**[1] **Xueqian Hu,**[1] **Yiran Shi,**[1] **and Jiajun Deng**[1]

[1]*School of Information Engineering, Henan Institute of Science and Technology, Xinxiang 453003, China*
[2]*College of Software, Zhengzhou University, Zhenghzou 451000, China*

Correspondence should be addressed to Pingchuan Zhang; 362764053@qq.com

During the fruit ripening period, the orchard temperature difference between day and night has a substantial impact on the fruit quality, and it is not easy to be controlled like that of in greenhouse, this paper designed the smart orchard Internet of Things (IoT), through the fuzzy PID (Proportion-Integration-Differentiation) algorithm to control the water spraying to adjust the temperature difference ΔT between day and night in the orchard, intelligently influenced the orchard energy conversion process, and promoted the fruit sugar accumulation. Experiments show that the maximum ΔT can reach 20℃, the intelligent energy regulation based on the IoT has a good effect, and a scheme to intervene the microclimate in farmland (quite different from the greenhouse environment) is provided.

1. Introduction

As we all know, the growth of crops is a process of energy transfer and transformation. Through photosynthesis, solar energy is converted into chemical energy and stored in crops and fruits. With the development of smart agriculture, artificial management of energy conversion conditions in the growth process of crops to promote crop better growth has always been a research focus. For example, promoting the improvement of fruit quality in orchards is worth exploring. The Internet of Things (IoT) is the fourth information revolution after computers, the Internet, and mobile communication technologies. Since 1999, the Massachusetts Institute of Technology introduced the concept to major countries in the world such as the United States. Smart Planet, the European Union made the Internet of Things

Action Plan in 2009, China proposed the sensing China and made the Internet of Things one of the strategic emerging industries [1–4].

At present, the Internet of Things has been applied to various fields such as transportation, medical treatment, industry, and military. In agriculture, various sensing terminals such as radio frequency identification (RFID), sensors, and visual devices have been used to comprehensively sense collection facilities, environmental information of production processes such as field planting, breeding, etc. to gradually achieve the optimal control, and intelligent management of agricultural production processes [5].

Among them, the Orchard Internet of Things mainly is used, detects and communicates related data such as soil, temperature, light, weather, and insect pests in the orchard environment, and can carry out independent

irrigation, integrated water and fertilizer management, and insect forecasting, which improves the orchard information level, management efficiency, and fruit yield [6–10].

Nowadays, fuzzy PID control technology has been widely used in orchards because of its fast response speed, no overshoot, almost no shock, and high control precision [11, 12]. First, aiming at pest control in orchards, it is used for chemical pesticide spray operation. Combined with precision target technology and variable air spray technology, it improves the precision of fruit trees' air spray and achieves the effect of precision application p [13–16]. Second, together with the orchard Internet of things to achieve intelligent irrigation, water saving effect [17, 18]. Third, it is used to control the intelligent lighting in orchard and improve the appearance quality of fruit [19, 20].

However, China as the biggest fruit production of the world, Chinese fruits also have problems such as low sugar content [21]. As for the sugar content of fruits, according to the literature [22–25], during fruit growth, carbohydrates are produced during the day of photosynthesis. Under the same conditions as water and fertilizer, high temperatures can enhance photosynthesis to produce more carbohydrates; these carbohydrates are converted into sugars at night. Temperature is the main factor affecting sugar conversion, which is the temperature difference between day and night. The greater the temperature difference between day and night, the more favourable the sugar conversion is, and the sweetness of the fruit is higher.

In the northern plains of China, popular fruits such as apples, strawberries, peaches, and pears generally start to accumulate sugar during the summer fruit ripening period, but the temperature difference in the northern plains is not as large as in Xinjiang and other regions.

Based on the key factors that affect the sugar content of fruit during the fruit growth process, this article proposed an IoT system with the function of regulating in the peach orchard during the ripening period, using fuzzy PID to control the mist sprayer to spray 16°C water to reduce the night temperature of the orchard, increase the temperature difference, and weaken the respiration of the fruit tree, which is beneficial to promote sugar conversion and fruit expansion and improve fruit quality. The expected contributions are as the following:

(1) The ambient temperature of the orchard at night can be effectively reduced, and the maximum temperature reduction range can reach 10°C so that the day-night temperature difference of the orchard on that day can reach 20°C. According to the literature [21], it can be known that the orchard's breathing effect can be better suppressed, which is beneficial to the orchard organic matter accumulation and sugar conversion, increasing the sugar content and dry matter content

(2) The misting operation increases the environmental humidity during the orchard fruit ripening period. According to the literature [26–30], it is helpful to promote fruit expansion and increase orchard yield

(3) The system can meet the actual needs of orchard data collection and control in terms of signal transmission quality, network stability, data collection timeliness, and system power consumption. Comparing with the literature [7], the development cost is reduced, and the orchard can be realized. Remote real-time monitoring

(4) Fuzzy PID algorithm effectively controls the intensity of mist and achieves water conservation. This system is of positive significance for promoting the informatization and development of orchards in temperate plains and improving fruit quality and yield

2. Materials and Methods

The materials and methods section should contain sufficient detail so that all procedures can be repeated. It may be divided into headed subsections if several methods are described.

2.1. Principle and Process of Temperature Difference Regulation in Orchard. Photosynthesis and respiration occur simultaneously in cells of green plants such as fruit trees. During the day, photosynthesis is the main process because the light intensity and the temperature are high. During the photosynthesis process, the chloroplast in the cell synthesizes solar energy, CO_2, H_2O, and other organic matter, stores energy, and releases O_2.

At night, the light intensity is small, and the respiration is stronger than photosynthesis. Cell mitochondria decompose organic matter produced by photosynthesis and release energy and oxygen. Respiratory effects include aerobic and anaerobic respiration.

Studies have shown that [21] photosynthetic intensity (also called photosynthetic rate) is affected by light intensity, temperature, CO_2 concentration, etc.; under light conditions, photosynthesis starts under enzyme catalysis, and temperature directly affects enzyme activity. General plants normally perform photosynthesis at 10°C to 35°C. The range of 10°C to 35°C gradually increases with increasing temperature. Photosynthetic enzyme activity decreases above 35°C, and photosynthesis begins to decline. Photosynthesis at 40°C to 50°C, effect is almost completely stopped; the main influencing factor of respiration is temperature. The higher the temperature, the stronger the respiration. Respiration is the strongest at the optimal temperature (25°C ~35°C); above the optimal temperature, the enzyme activity decreases, even degeneration and inactivation, and the breathing is suppressed; below the optimal temperature, the enzyme activity decreases and the breathing is suppressed.

In China, summer is the main period of fruit growth, high temperature during the day, strong photosynthesis, and produced more organic matter; the low temperature at night, weak respiration, and less organic matter decomposed. Therefore, more organic matter accumulated in the photosynthesis of plants than organic matter consumed by respiration, accumulated in the body, increase in organic matter results in particularly sweet fruits, so "where the
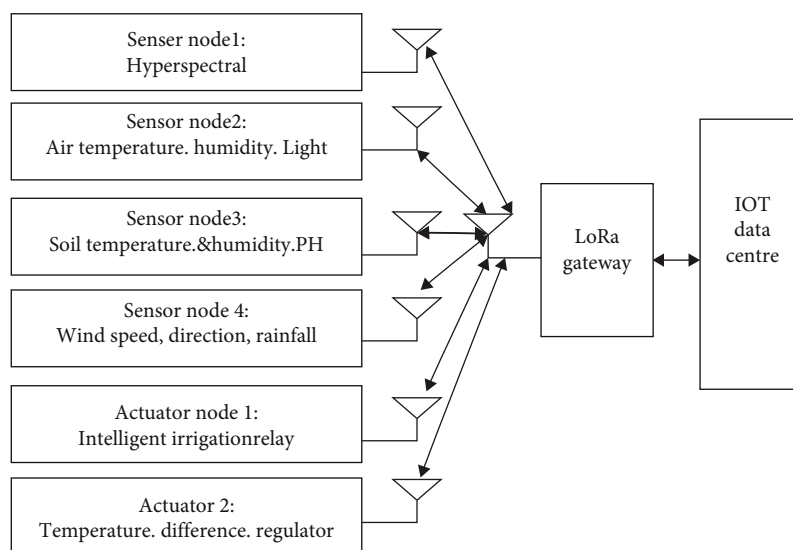
FIGURE 1: The Internet of orchard things system scheme.

temperature difference between day and night is particularly sweet and delicious," the scientific explanation is that photosynthesis will increase when the temperature is appropriately high, and the respiration will weaken and decompose when the temperature is low. Fewer organics are good for organics accumulation. It can be seen that increasing the temperature difference between day and night can increase the sugar content of fruits.

In the summer of temperate plains, temperatures are high during the day and fruits accumulate nutrients. At night, the ambient temperature drops, however, in general, declines less, and the decline rate is slower. Therefore, the mist cooling method can be used to accelerate the reduction of the ambient temperature. In summer, the sun enters the sunset point relatively late. To make full use of the photosynthesis of fruit trees after sunset, under nonrainfall conditions, it is generally chosen to spray the water misting in the orchard at 8 : 00 pm every day. According to the wind direction collected by the wind direction sensor, the data centre transmits the command to the sprayer node through LoRa, adjusts the direction of the sprayer nozzle, and sprays the water mist. The spray distance varies from 5 to 100 m, and the height is 2 meters above the fruit tree. Multiple mist dispensers form a mist of water covering the entire orchard. Misty time lasted until 4 : 00 in the morning. The water in the well is less affected by the ground temperature and is maintained at about 16°C throughout the year. The local summer temperature averages 30°C, so water mist can quickly reduce the ambient temperature of the orchard to below 20°C, which can reduce the night-time temperature of the orchard by 10°C in a short time.

2.2. Orchard IoT for Temperature Difference Regulation. The proposed orchard IoT scheme is shown in Figure 1. The basic functions include collection of orchard environmental information, soil temperature, soil pH, soil humidity, carbon dioxide, CO_2 concentration, air temperature and humidity, light intensity, wind speed and direction, rainfall,

etc.; monitoring fruit tree pests by hyperspectral sensors; and remote monitoring achieved on computer or smartphone device [6–8].

According to the three-layer basic architecture of the Internet of Things: the sensing layer, the transmission layer, and the application layer; the sensing layer contains 4 types of sensor nodes and 2 types of actuator nodes. The sensor node mainly implements the orchard information collection. Actuator node 1 completes automatic orchard irrigation. Actuator 2 reduces the ambient temperature of the orchard at night by spraying the mist and increases the temperature difference between day and night in the summer. Water mist is conducive to fruit expansion after the fruit enters the expansion stage [21].

The basic composition of a sensor node is a sensor, an ARM microcontroller, and LoRa module; the basic composition of an actuator node is a relay, ARM microcontroller, and LoRa module.

The ARM microcontroller is a low power, high-performance embedded system as the node control core. It is an MCU based on the STM32 F401 series ARM® Cortex™-M4. It has a 12-bit ADC and a 16-bit/32-bit timer. FPU (floating- point unit), communication peripheral interfaces (USART, SPI ,I2C,I2S) and audio PLL (Phased Locked Loop). The operating frequency reaches 84 MHz, 105 DMIPS/285 Core-Mark, the flash ROM capacity is 256 kB, the SRAM capacity is 64 KB, and the chip's operating voltage ranges from 1.7 to 3.6 V.

To reduce costs, each node is provided with several related sensors. To control the day and night temperature difference of the orchard, sensor node 2 collects four orchard meteorological parameters such as air temperature, humidity, CO_2, and light intensity, and actuator node 1 executes the relevant commands sent by the data centre. Sensors/ transducers utilized in the internet of orchard things are shown in Figures 2(a)–2(g).

Sensor node 2 can measure four parameters: air temperature, relative humidity, CO_2 concentration, and illumination.

(a) Hyperspectral

(b) Wind and illuminator

(c) CO2 sensor

(d) Air temperature and humidity

(e) Soil parametres sensors

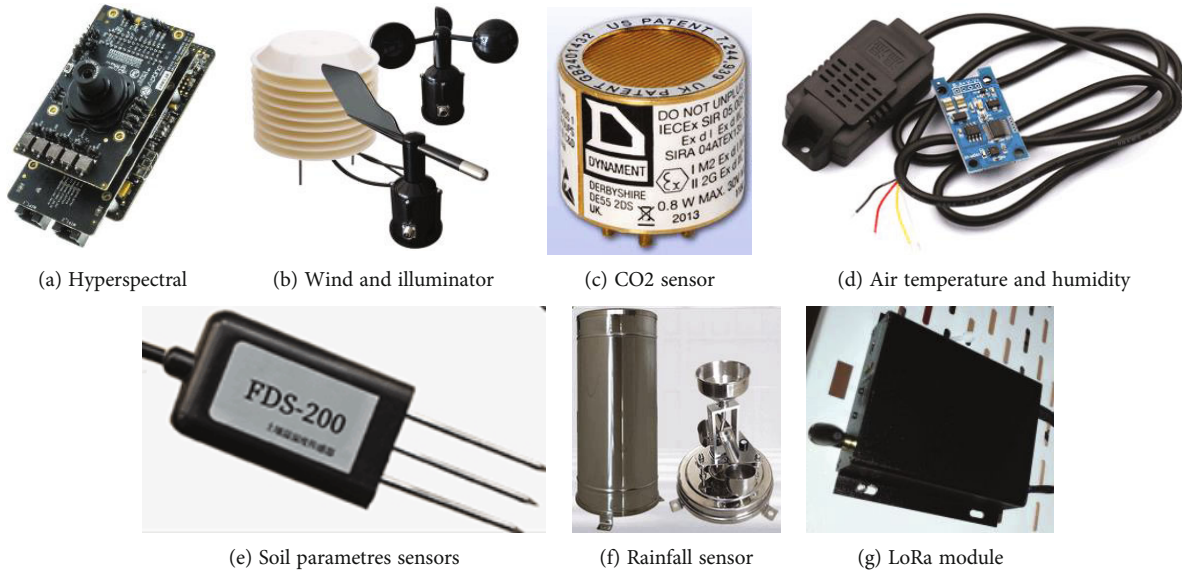(f) Rainfall sensor

(g) LoRa module

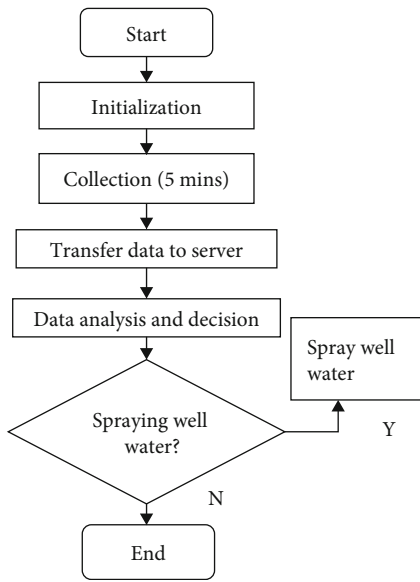FIGURE 2: Sensors/transducer utilized in the internet of orchard things.
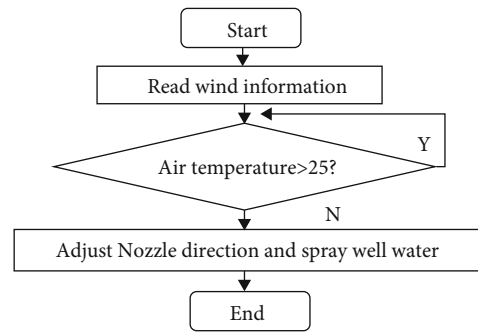

FIGURE 3: Data acquisition program flowchart.

FIGURE 4: Orchard mist operation process flow chart.

The measurement range and accuracy of the four parameters are air temperature $-30 \sim 70 \pm 0.2°C$; relative humidity, $0 \sim 100\%RH \pm 3\%RH$; carbon dioxide concentration $0 \sim 10000$ ppm (optional 2000, 5000 ppm) ± 20 ppm; and light intensity $0 \sim 200$ k lx (optional 2 k, 20 k lx and other ranges) $\pm 3\%$. In the North China Plain area, under normal conditions, the illuminance under strong sunlight in summer is $100,000$ lx (3 to 300,000 lx). It is 10,000 lx, and the intensity of sunrise and sunset lights is 300-400 lx. Sensor node 4 is used to collect wind speed/direction and rainfall and provides a decision basis for temperature difference control.

The wind sensor for collecting 16 directions including east, west, south, north, southeast, southwest, northeast, and northwest. The voltage signal output is $0 \sim 2$ V, and the comprehensive voltage accuracy is $\pm 2\%$. Three bulk sensor measurement. Measuring range: $0 \sim 30$ m/s, $0 \sim 60$ m/s, response time is less than 1S, start-up wind is $0.4 \sim 0.8$ m/s, and power supply voltage is 12~24 VDC.

A dump bucket rain sensor is used for detecting the rainfall, its range of rain intensity is 0.01 mm~4 mm/min (the maximum rain intensity allowed is 8 mm/min), and the measurement accuracy is $\leq \pm 3\%$.

The transmission layer is mainly composed of wireless transmission modules and gateways, and each sensor and actuator node contains a wireless transmission module LoRa (long range). Wireless transmission can avoid the difficulty of wired communication in the orchard and prevent the line from affecting the operation of the orchard. There are many wireless transmission methods. Commonly used ZigBee, Bluetooth, Wi-Fi, etc. and their transmission distances are relatively short. Orchard data centres are generally located in urban areas with good environmental conditions. For complex orchards in the field, WSN (wireless sensor network) has high cost and complicated networks.

In comprehensive consideration, the LoRa [16–18] was used because of its excellent performance of long-distance,
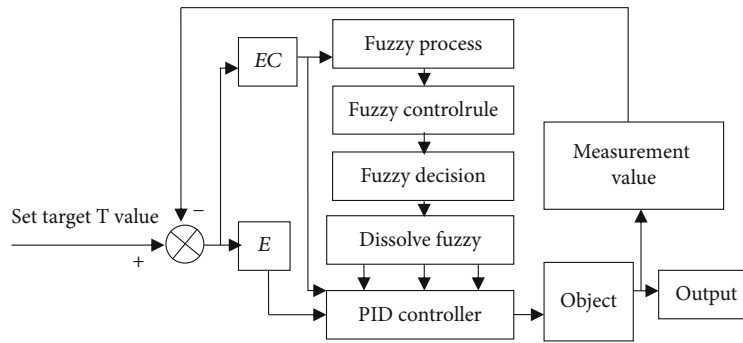
FIGURE 5: Fuzzy PID for spraying water mist.

(a) Pumping and pressure tanks

(b) Spraying nozzle

(c) Spraying at 10 MPa and 40 m

(d) Spraying at 40 MPa and 99.8 m

FIGURE 6: The spray water fog effect with different pressure and range.

large capacity, low power consumption, and other characteristics., which is one of the low power wide area networks LPWAN (low power wide area network) technology. Here, the LoRa module is SX1278 with 433 MHz and spread spectrum technology. Its communication interface is RS232/485, 9600 Baud (1200~115200 Baud), and 5W12V (10~28 V). Gateway LoRa and each node LoRa form a star topology, structure of the transmission network, and the transmission distance is up to 20 km, which meets the 12 km distance between the orchard and the data centre, reducing the data transmission costs.

The application layer is the data centre of the Internet of Orchard Things. The central database is configured with MySQL, which can store data, analyse, visualize, and make decisions. The data collected by the sensors is transmitted to the gateway through the LoRa wireless transmission module and sent to the data centre. The control command of the centre is passed to the LoRa module through the gateway and realizes automatic irrigation and fogging operations.

Various device nodes, such as sensor nodes, irrigation nodes, and spraying actuator nodes, all use LoRa's free networking technology, which can also easily implement single control and centralized management of each node of the system. At the same time, the convenience and practicability of LoRa free networking greatly save the development cycle and reduce the system development cost and difficulty.

3. System Software

Based on the function analysis of the orchard IoT, the system consists of 7 parts: parameter collection, irrigation, spraying, mist, insect analysis, data server, and mobile clients. The application layer uses Baidu Cloud Server as the cloud server with the open-source GNU/Linux operating system Ubuntu and the E-Chart visualization tools. The display can ensure the normal operation of the orchard's data access, data storage, and visual display programs;
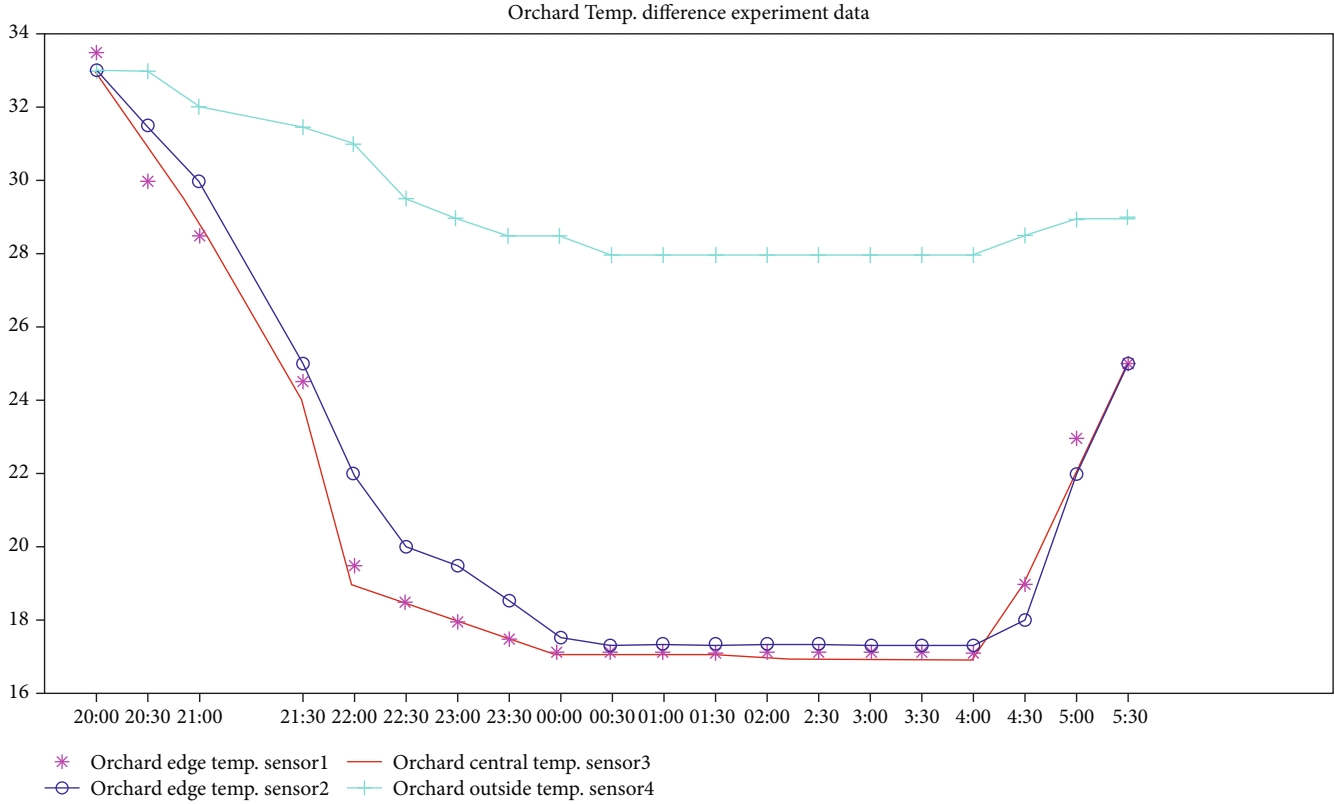
FIGURE 7: Control data of temperature difference.

the interactive platform uses the B/S (Brower/Server) mode.

3.1. The Flow Chart of the Sensor Collection. There are many types of sensors in this system. Here, only the basic process of temperature sensor collecting temperature is given, and the temperature data is mainly used to judge whether to carry out water spray. The flow chart of the sensor collection is shown in Figure 3.

3.2. Mist Spraying Operation Procedure. Spray subroutine is mainly used to control spraying water mist to realize orchard cooling. When the ambient temperature of the orchard is higher than 20 degrees, the spray will be started, and the direction of the nozzle can be adjusted according to the wind direction to achieve the optimal spray effect. Mist spraying operation procedure flow is shown in Figure 4.

3.3. Fuzzy PID Algorithm. To adjust the temperature difference according to the night temperature with high efficiency and save water, the algorithm of fuzzy PID for spraying is shown in Figure 5.

The fuzzy PID controller is mainly composed of a fuzzy controller and an adjustable PID controller. The input of the fuzzy controller is the deviation between the measured temperature value $t1$ of the sensor and the set target temperature value $t0$ and the deviation change rate. The output is the three input correction parameters of the PID controller

$$u(t) = K_p E(t) + K_i EC(t) \int_0^t E(t)dt + K_d \frac{dE(t)}{dt}, \quad (1)$$

where $u(t)$ is output of the system at time t; K_p is the proportional coefficient; K_i is the integral coefficient; K_d is the differential coefficient. The fuzzy PID control effect is better when set the K_p, K_i, K_d initial value as $\{K_{p0}, K_{i0}, K_{d0}\} = \{16, 0.4, 0.07\}$, and $K_p \in [10, 18], K_i \in [0, 1], K_d \in [0, 0.15]$.

4. Results and Discussion

The experiment site and conditions: WH Agricultural Fruit Planting Cooperative Peach Orchard, with an area of 1hm2, and an Internet of orchard Things. There is a self-use well in the orchard with a depth of 30 meters. The test time is summer 2018-07-20, and the weather conditions are sunny, temperature 37°C~28°C, south wind 3-4 level. The water temperature of the well is 16°C. Mist spraying machine parameters: electric high-pressure remote sprayer, rated flow: 30-40 L/min; adjustable working pressure: 10-40 MPa; horizontal range: up to 100 M. The spray apparatus and effect are shown in Figures 6(a)–6(c).

The pumping device draws water out of the well at a temperature of 16 degrees and then feeds it into a tank, which is pressurized and then sprayed from nozzles at different locations in the orchard, and the water mist could cover the whole orchard and cool it down.

TABLE 1

	P1	P2	P3	P4	P5	C1	C2	C3	C4	C5
Original size	41	46	39	45	50	47	52	46	43	44
1	48	52	47	51	56	52	58	54	50	51
2	57	59	56	58	64	58	63	59	56	56
3	65	67	66	67	71	65	68	67	63	67
4	74	73	76	75	80	72	74	72	72	73
5	89	88	87	83	91	81	83	79	78	78

TABLE 2: Sweetness data.

	P1	P2	P3	P4	P5	C1	C2	C3	C4	C5
Original value	7	7.1	6.7	6.5	6.8	6.7	6.5	6.4	7.1	7.2
1	7.2	7.4	7.1	6.8	7.1	6.9	6.8	6.6	7.2	7.3
2	7.5	7.7	7.4	7.4	7.4	7.2	7.2	6.8	7.3	7.5
3	7.9	8.1	7.8	7.9	7.9	7.4	7.5	7.3	7.5	7.8
4	8.4	8.6	8.5	8.5	8.7	7.7	7.9	7.7	7.8	8.1
5	8.9	9.3	9.4	9.8	9.5	8.1	8.2	8.2	8.4	8.5

TABLE 3: Data comparison results (average).

	Original size (mm)	Size after picking	Average size daily increasing	Original sweetness	Sweetness after picking	Sweetness daily increasing
Experiment peach	44.2	87.6	2.89	6.82	9.38	0.17
Comparing peach	46.4	79.8	2.23	6.78	8.28	0.1

There are five sprayers, one at each corner of the orchard and the centre. The plot according to the temperature data is shown in Figure 7.

It can be seen from Figure 7 that during the misting operation of the orchard, the ambient temperature in the orchard is reduced by a maximum of 10°C compared with the temperature outside the orchard, and the cooling effect is obvious. Compared with the maximum temperature of 37°C during the day, the temperature difference between day and night reaches 20°C. According to the literature, the respiration of the fruit, tree, leaves, and fruit in the orchard will be significantly weakened compared with that without misting operation, which is beneficial to the sugar conversion and organic matter accumulation of the fruit. There are differences in the data measured by the three sets of sensors, mainly due to the different installation locations. The south wind is not good for cooling the southern part of the orchard. The north side of the orchard is affected by the wind, the concentration of water mist is greater, and the temperature drop is slightly larger than the south. After finishing the misting operation at 4:30 in the morning, the temperature of the orchard began to rise.

NLE-AI800 development board and 5-million-pixel camera were used as image acquisition equipment to construct fruit size measuring instrument. The system supports Linux/Ubuntu-Server, and Ros system supports ROS-core. CPU: dual-core A73+ dual-core A53+ single-core A53; storage: 4 GB RAM, 32 GB storage space; AI computing unit: dual core NNIE@840 MHz, 4.0TFLOPTS computing power. HMI display device touch screen, camera: Python3.6.7 environment and PyCharm2020.1.1 VERSION of IDE, as well as plug-ins.

PAL-HIKARi 10 fruit nondestructive sugar meter (peach) was used to measure peach sweetness. The measuring range of the instrument is Brix 8.0 ~ 20.0%; the measurement accuracy is Brix ± 1.5%. Brix 0.1% resolution; the repeatability was Brix ± 1%.

In order to verify the fruit sweetness and expansion effect, one peach from each of the 5 peach trees in the experimental orchard was selected, with the numbers P1 ~ P5, respectively; at the same time, select 5 peach trees of the same variety in the nearby orchard, and numbered C1 ~ C5. Measure once every three days at 3:00 p.m. and for five consecutive times. The measured fruit size and sweetness data are shown in Tables 1 and 2, and Table 3 is for data comparison results.

It can be seen from Table 3 that there is little difference between the initial average sweetness and the size of the fruit. But after the experiment, there is a significant difference between the size and sweetness of the fruit, which verifies the effectiveness of the designed method.

5. Conclusions

The Internet of orchard Things was designed and implemented by comprehensively utilizing multiple types of

sensors and LoRa, and a temperature difference control experiment was carried out in the peach orchard. The fuzzy PID was used to perform spraying water of constant 16°C in a peach orchard in the ripening period. The main results are as follows:

(1) The ambient temperature of the orchard at night can be effectively reduced, and the maximum temperature reduction range can reach 10°C so that the day-night temperature difference of the orchard on that day can reach 20°C, which is beneficial to the orchard organic matter accumulation and sugar conversion, increasing the sugar content and dry matter content

(2) The misting operation is helpful to promote fruit expansion and increase orchard yield

(3) The system development cost is reduced, and the orchard can be realized. Remote real-time monitoring

(4) Fuzzy PID algorithm effectively controls the intensity of mist precisely for achieving water conservation, furthermore, useful for improving fruit quality and yield

Data Availability

The primary data of this article is in Figure 5.

Conflicts of Interest

The authors declare that there is no conflict of interest regarding the publication of this paper.

Acknowledgments

References

[1] M. Filippini and L. C. Hunt, "Energy demand and energy efficiency in the OECD countries: a stochastic demand frontier approach," *Energy Journal*, vol. 32, no. 2, pp. 59–80, 2011.

[2] M. Filippini and L. C. Hunt, "US residential energy demand and energy efficiency: a stochastic demand frontier approach," *Energy Economics*, vol. 34, no. 5, pp. 1484–1491, 2012.

[3] S. Hammoudi, Z. Aliouat, and S. Harous, "Challenges and research directions for internet of things," *Telecommunication Systems*, vol. 67, no. 2, pp. 367–385, 2018.

[4] Z. B. Zhou, K. F. Tsang, Z. F. Zhao, and W. Gaaloul, "Data intelligence on the internet of things," *Personal and Ubiquitous Computing*, vol. 20, no. 3, pp. 277–281, 2016.

[5] J. I. Shuqi, *The Internet of Things and the Transform of Social Production Mode*, LIAONING University, 2018.

[6] C. H. E. N. Weirong, W. A. N. G. Hu, and P. E. N. G. Zhiliang, "Development and application of orchard water and fertilizer integration control system based on internet technology," *Guizhou Agricultural sciences*, vol. 44, no. 8, pp. 140–143, 2018.

[7] Z. H. A. O. Wenxing, W. U. Zhijing, and L. I. U. Deli, "Design of orchard environmental intelligent monitoring system based on internet of agricultural things," *Jiangsu Agricultural Sciences*, vol. 45, no. 5, pp. 391–394, 2016.

[8] C. Y. Ren, P. C. Zhang, and M. R. Wang, "Orchard IoT system based on LoRa technology," *Internet of Things Technology*, vol. 11, no. 3, 2021.

[9] P. C. Zhang, Y. C. Liu, and Q. L. Bai, "Internet of things design for improving fruit quality in orchard based on night cooling at fruit ripening stage," *J Xinyang Normal University (Natural Science Edition)*, vol. 32, no. 4, pp. 659–663, 2019.

[10] Z. H. O. N. G. Yue, D. I. N. G. Hui, and Z. H. A. N. G. Jun, "Study on strawberry moisture content monitoring system based on Internet of things," *Information System Engineering*, vol. 7, pp. 64–66, 2017.

[11] H. Baogang and G. K. I. Mann, "New methodology for analytical and optimal design of fuzzy PID controllers," *IEEE Transactions on Fuzzy Systems*, vol. 7, no. 5, pp. 521–539, 1999.

[12] N. D. Phu, N. N. Hung, A. Ahmadian, and N. Senu, "A new fuzzy PID control system based on fuzzy PID controller and fuzzy control process," *International Journal of Fuzzy Systems*, vol. 22, no. 7, pp. 2163–2187, 2020.

[13] S. Wenfeng, L. Haiyang, and R. Wang, "Design and experiment of variable PID control system based on neural network tuning," *Transactions of the Chinese society for agricultural machinery*, vol. 51, no. 12, 2020.

[14] M. SHuli and H. A. O. Lei, "Design and experiment of agricultural intelligent spray control system based on fuzzy PID," *Agricultural Engineering*, vol. 9, no. 11, pp. 36–38, 2019.

[15] D. Kejun and L. Zaixin, "Research on agricultural greenhouse system based on fuzzy adaptive PID," *Southern agricultural machinery*, vol. 50, no. 19, pp. 7–9, 2019.

[16] C. Zhenzhao, Y. Xuejun, and W. Linhui, "Design and experiment of Uav adaptive variable spray system based on neural network PID," *Journal of south China agricultural university*, vol. 40, no. 4, pp. 100–108, 2019.

[17] S. Li, *Design and Study on Decision Control System of Water and Fertilizer Irrigation in Apple Orchard*, Xinjiang University, 2019.

[18] L. Xuelin, "Design and research of intelligent control system for water-saving irrigation based on fuzzy PID control," *Hebei Agricultural Machinery*, vol. 12, pp. 53–55, 2021.

[19] F. Q. Chen, *Research and Implementation of Greenhouse Monitoring and Control System Based on Adaptive Fuzzy Control*, Jiangsu University, 2019.

[20] J. Wang, *Research on Remote Intelligent Control System of Greenhouse Based on Fuzzy Control Strategy*, Jilin University, 2015.

[21] Z. Zhilong, *Fruit Culture Science*, China Agricultural Science and Technology Press, Beijing, 2012.

[22] M. Pessarakli, *Handbook of Photo Synthesis*, CRC Press, Florida, 3rd edition, 2016.

[23] P. Li-li, J. Wei-bing, and H. Jian, "Factors affecting night respiration of early-maturing peach leaf coloring differently,"

Jiangsu Journal of Agricultural Sciences, vol. 29, no. 5, pp. 1131–1135, 2013.

[24] S. Yi, Y. Wenwen, and X. Kai, "Effect of temperature stress on photosynthesis in Myrica rubra leaves," *Chinese Agricultural Science Bulletin*, vol. 25, no. 16, pp. 161–166, 2009.

[25] C. M. Coupland, *Estimating Daily Primary Production and Night-Time Respiration in Estuaries by an In-Situ Carbon Method*, University of Rhode Island, Kingston, 2015.

[26] D. Loka, *Effect of High Night Temperature on Cotton Respiration, ATP Content and Carbohydrate Accumulation*, University of Arkansas, Fayetteville, 2008.

[27] W. A. N. G. Jiulin, Z. H. A. O. Chengping, and Y. A. N. Hua, "Design and research of water saving irrigation system based on LoRa," *Water Saving Irrigation*, vol. 12, 2017.

[28] S. U. N. Tianzhu and D. A. I. Yawen, "Design of field information wireless acquisition scheme based on LoRa," *Computer Measurement & Control*, vol. 26, no. 8, pp. 208–212, 2018.

[29] H. Wang Zheng and S. T. Jing, "Design and implementation of farmland information collection system based on LoRa," *Electronic Engineering*, vol. 44, no. 3, pp. 53–57, 2018.

[30] Y. A. N. G. Yang, "Design of intelligent farm monitoring system based on LoRa technology," *Computer Measurement & Control*, vol. 26, no. 6, pp. 49–52, 2018.

Research Article

Responses of Urban Ecosystem Vulnerability and Restoration Assessment on Typhoon Disaster: A Case Study of Zhuhai City, China

Mengyuan Su ,[1] Jialong Wu ,[2] and Miaoling Feng[2]

[1]*Department of Geography, Durham University, Durham DH13LE, UK*
[2]*Land Development and Reclamation Center of Guangdong Province, Guangzhou 510635, China*

Correspondence should be addressed to Jialong Wu; jialongw003@163.com

With the frequent occurrence of extreme disasters and the development of urbanization, the ecological vulnerability of urban system has been seriously affected, which has become an important issue in urgent need of research. In this study, a comprehensive analysis method of exposure, sensitivity, responsiveness, and resilience was used to establish an ecological vulnerability assessment model based on the impact of typhoon. With the help of big data analysis and model, this paper explored the impact and response of typhoon Hato on Zhuhai's ecological vulnerability and restoration. Our results showed that under the influence of Hato, Jinwan district showed higher vulnerability, followed by Doumen district and Xiangzhou district. The lowest vulnerability of Xiangzhou district mainly for its coping capacity was significantly higher than the other two districts. Judging from the recovery situation shown by big data, Doumen and Xiangzhou districts recovered relatively quickly in terms of hydraulic and communication systems. The results of this study can provide a theoretical reference for vulnerability assessment, predisaster prevention, and postdisaster recovery of typhoon disaster risk areas.

1. Introduction

Typhoon, as a common natural disaster, has great destructive effect on human society with considerable economic losses, which exceeds other natural disasters such as earthquakes [1]. The average annual direct economic loss from tropical cyclone disasters in the world in the past ten years is about 55 billion U.S. dollars [2]. China is one of the countries that severely affected by typhoon [3, 4]. Because of the severe losses caused by typhoons, it is necessary to evaluate disasters and carry out disaster management. Therefore, research of tropical cyclone disaster risk assessment and management have received more and more attention from the scientific community [5, 6].

Disaster risk assessment is a quantitative analysis and assessment of the possibility and possible consequences of disasters with different intensities. The assessment is an important bridge to closely link the hazard factors and the vulnerability of the disaster-bearing body. As early as the end of the nineteenth century, the improvement of disaster observation technology and the development of risk mapping technology prompted the emergence of catastrophe models for the simulation and evaluation [7, 8]. Much attention has been paid on the assessment of storm surge disaster losses caused by typhoons, and the disaster losses have been quantitatively assessed by establishing a loss assessment model [9–13]. Loss assessment of typhoon is one of the hotspots and difficulties in disaster theory research. However, the lack of scientific norms for the investigation and assessment of natural disaster losses, coupled with the unpredictability of natural disasters, further increase the difficulty of data collection and assessment. With the "vulnerability of hazard-bearing bodies" put forward in the 1980s, the concept of vulnerability has gradually been widely used in many domains like nature, society, economy, and environment [14].

There are two main research methods for vulnerability assessment of disaster bearing body, including index system method and quantitative vulnerability curve. The index

system method is a semiquantitative calculation method, which mainly expresses the relative vulnerability of the evaluation unit by establishing the evaluation index system and calculating the vulnerability index of the disaster bearing body. At present, index system method has been widely used in the vulnerability assessment of a single disaster-bearing body [15], multiple disaster-bearing bodies [16], and disaster-bearing systems [17], but different studies have different understandings of the causes of disasters and the performance characteristics of disaster-bearing bodies, and the established index systems are different. In addition, the research on the vulnerability of disaster-bearing bodies is highly regional. Therefore, the process of using the index system method to assess the vulnerability of hazard-bearing bodies is artificially subjective. Moreover, the vulnerability curve is a quantitative vulnerability assessment method based on the relationship between the strength parameters of different hazards and the loss rate of the disaster-bearing body [18]. At present, most research focus on the construction of vulnerability curves between typhoon wind speed, submergence depth, earthquake intensity and other hazard factors, and the loss rate of disaster-bearing bodies, such as houses and crops [19]. This method does not involve the assessment of social, economic, and environmental vulnerability levels and emergency response capabilities to disasters. It only represents the vulnerability measurement of absolute physical parameters.

This paper will use the index system method to evaluate the impact of typhoon Hato on urban ecological vulnerability. And using big data makes the analysis method in this paper have strong universal adaptability. Recently, there are many applications for typhoon disaster risk assessments [20, 21]. However, most of the disaster mitigation work relies on the short-term forecast results of the meteorological department's typhoon model for the input of hazard factors (e.g., wind and rain), while the quantitative research on typhoon disaster vulnerability of specific disaster-bearing bodies remains blank. In terms of typhoon assessment methods, the current typhoon pre-assessment focuses on obtaining high-accuracy data [22], but the postdisaster vulnerability assessment still often lacks time-sensitive data with redundant computation process [23]. Therefore, it is concluded that the effective and accurate postdisaster vulnerability assessment is particularly necessary for disaster assessment. Moreover, research and practice have proved that the unique advantages of big data in feasibility, timeliness, and accuracy make it successfully applied in various fields [24, 25].

As such, based on the secondary data derived from the "octopus" network information resource picking software and data collected by traditional surveys, this paper establishes a social economic and ecological system to evaluate the impact of typhoons on urban ecological vulnerability. Zhuhai, a city often hit by the south subtropical monsoon, was selected as the study region. This study is to develop a conceptual model of aspects of exposure, sensitivity, resilience, and response to typhoon Hato; to explore how big data can provide input data to undertake a socioeconomic assessment of vulnerability, using "Octopus" software; to produce a socioecological vulnerability assessment tool; and to evaluate the methods and outputs from the socioecological vulnerability assessment tool. We consider that this study provides a theoretical reference for disaster prevention and reduction and the establishment of sustainable, resilient cities.

2. Data and Methodology

2.1. Study Site. Zhuhai (see Figure 1) is located between $21°48'-22°27'$ north latitude and $113°03'-114°19'$ east longitude. By 2020, Zhuhai City has a total land area of 1736.45 km^2 with three administrative districts, namely, Xiangzhou district, Doumen district, and Jinwan district, including 15 towns and 9 streets. Zhuhai City occupies the largest ocean area, the most islands, and the longest coastline in the Pearl River Delta. According to the seventh national census, the population of Zhuhai City is 2.44 million at the end of 2020 [26]. Typhoons usually occur from June to October, with an average of about four per year. Such disasters severely affecting Zhuhai City average about one a year, and there are about five periods of torrential rains [27]. Zhuhai land use data were derived from "Zhuhai Land Use Master Plan."

Hato was one of the strongest storms in the global range in 2017 [27], which landed at the coast of Jinwan district, Zhuhai City, at about 12:50 on August 23, 2017, causing considerable losses to Zhuhai, Hong Kong, Macau, and other regions [28–31]. In addition, the maximum wind force near the center of Hato is force 14 (45 m·s^{-1}), and the minimum pressure in the center is 950 HPa [30]. Monitoring showed that the Zhuhai National Weather Station observed an instantaneous gale of 51.9 m·s^{-1} (level 16) between 12:10 and 12:15. Moreover, Hato brought violent showers to Zhuhai City, causing two deaths and the collapse of 275 houses [27]. Some roads were blocked due to falling trees. The total direct economic loss was around 0.8 billion USD [27].

2.2. Data Collection. This study uses the big data analysis method to obtain the relevant data of indicators such as power, traffic, and telecommunications signal recovery speed. However, due to gap between the publication time and the occurrence of Hato, it is hard to quickly obtain the information of all affected points. Big data comes from Weibo software, a common social platform in China (like the twitter); such platform documents people's dynamics, thoughts, and locations. This study used the network information resource picking software, a program to automatically grab Internet information resources to understand the locations affected by the typhoon; the specific process is shown in Figure 2.

The relevant keyword selection parameters were shown in Table 1. The location information was derived from the location data of Weibo users. The duplicate data caused by forwarding or other reasons was deleted after manual review. Because typhoon Pakhar landed on August 27, 2017, and affected the west bank of the Pearl River and western Guangdong Province, the data on August 28, 2017, and
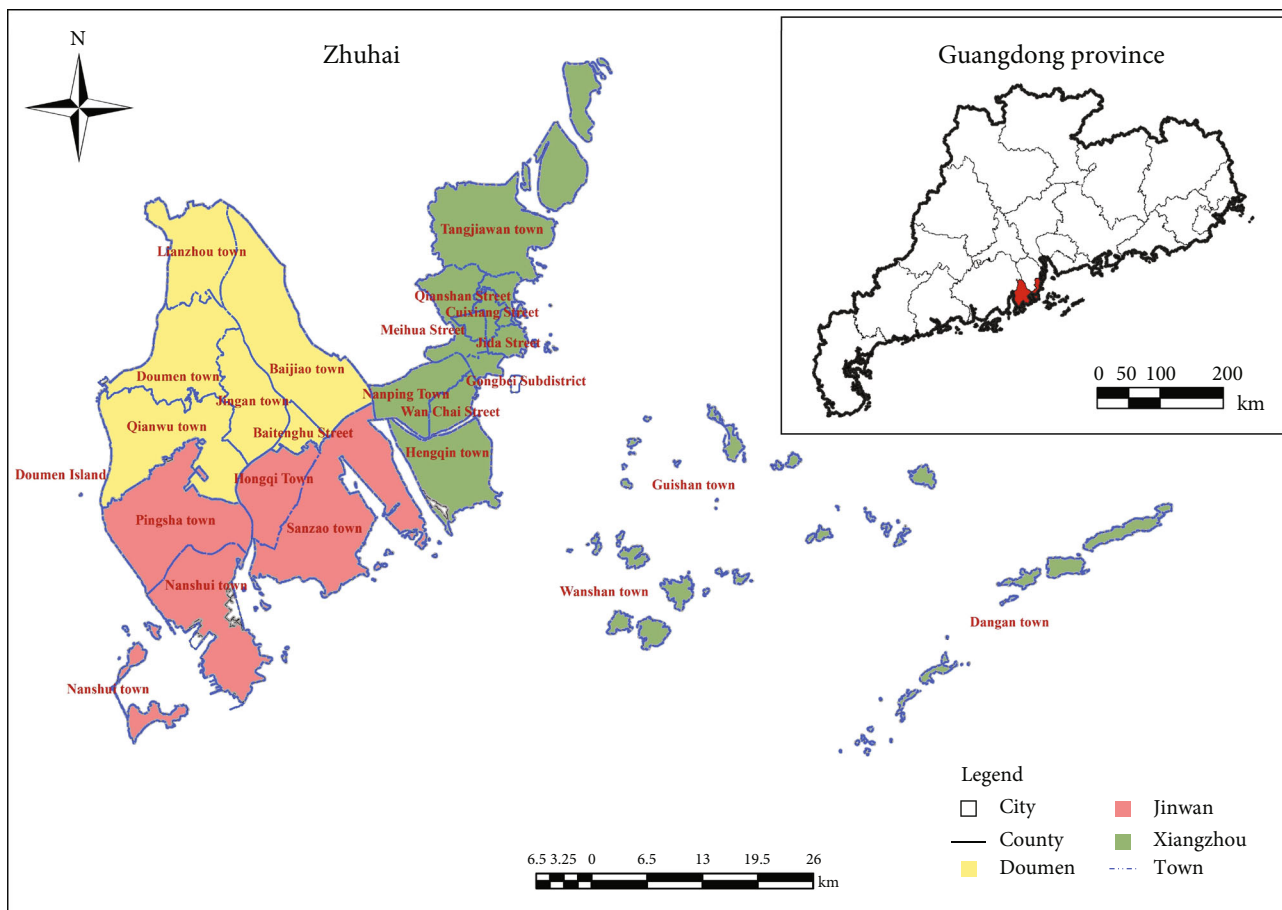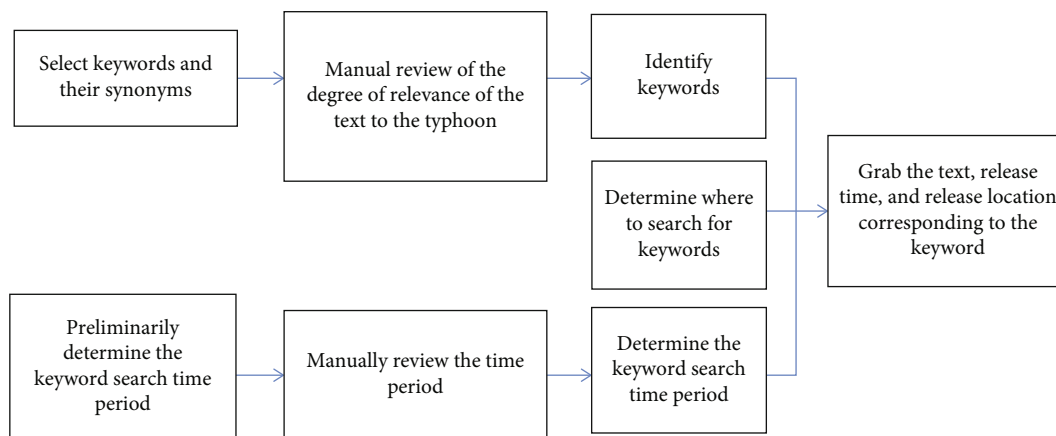
FIGURE 1: Zhuhai City administrative map.

FIGURE 2: Keyword selection flowchart for typhoon disaster information.

later were deleted in the analysis. In the end, it was determined to adopt the release volume of all keywords from August 23 to August 27, 2017. Then, data on recovery speed data of power, traffic, and telecommunication signals were obtained.

In order to obtain the data of exposure, response, and sensitivity of Zhuhai City, this paper adopted the data in the 2018 statistical yearbook published by this city. The data included district area, typhoon wind force, population den-

sity, proportion of primary industry, proportion of tertiary industry, ecological index, regional GDP, per capita disposable income of urban residents, general public service expenditure, and medical and health institution expenditure.

2.3. Methods

2.3.1. The Vulnerability Evaluation Index System. Vulnerability refers to the degree of self-change of the system after

Table 1: Vulnerability assessment index system of socioecological systems under the influence of typhoon disaster in Zhuhai City.

Primary indicators	Secondary indicators
Exposure	Land area
	Wind force
	Population density
Sensitivity	Proportion of primary industry
	Proportion of tertiary industry
	Ecological index
Response	Regional GDP
	Per capital disposable income of urban residents
	General public service expenditure
	Medical and health institutions expenditure
Resilience	Electricity restoration speed
	Traffic restoration speed
	Telecom signal recovery speed

being damaged by various pressures. The system is jointly determined by natural, social, economic, and environmental factors and processes [32]. For this paper, the natural and social systems in Xiangzhou district, Doumen district, and Jinwan district of Zhuhai City were selected as the disaster-bearing body on the basis of fully considering the research object and the characteristics of the typhoon disaster. This study summarized the main risk factors of climate change and the evaluation factors used by Sajjad et al. to evaluate the vulnerability of coastal cities [33]. These assessment factors were based on the principles of science, completeness, feasibility, and practicability, combined with the vulnerability caused by exposure. This study considered indicators from four aspects [34], sensitivity [35], resilience [35, 36], exposure, and response, respectively. A social-ecological system vulnerability index system was established for three districts in Zhuhai under the disaster of typhoon Hato, as shown in Table 1.

Firstly, in order to evaluate the degree of damage caused by the typhoon to different regions, we selected the land area, wind speed, and population density as indicators to evaluate the different conditions of each area exposed to the typhoon. Secondly, ground roughness characterizes the interaction between the surface and the atmosphere, reflecting the reduction of wind speed on the surface and the ground in areas with high ecological index. The roughness of a typhoon was high [37], so the ecological index and the intensity of typhoon landing were negatively correlated, i.e., the higher the vegetation coverage, the less the sensitivity. And since the Hato natured with extreme wind speeds, the primary and tertiary industries were relatively sensitive. Therefore, the proportion of the primary and tertiary industries and the vegetation coverage were selected for evaluation. Sensitivity starting from the socioeconomic conditions of different regions, two indicators representing the economic level of the region and residents, and two indicators representing

the perfection of the region's infrastructure and social security were selected to evaluate the region's ability to respond to typhoon disasters. Finally, based on the trend of big data changes, the perspective of affecting the recovery of residents' lives, the three indicators of power system, water supply system, and telecommunication system were selected for resilience evaluation.

2.3.2. Vulnerability Comprehensive Evaluation Model. Fuzzy comprehensive evaluation (FCE) is a decision-making method that can make a comprehensive evaluation affected by multiple factors [38]. In this study, FCE was employed as the basis of the vulnerability assessment for the various districts of Zhuhai under the typhoon Hato; the entropy weight (EW) was used to calculate the weights for every indicator. Firstly, the original data was standardized, and the EW was used to establish the weight set of all levels of indicators. Secondly, the membership function was used to combine the standardized values and the grading standards of the vulnerability comment set to construct an evaluation matrix. The comment set is an evaluation set established based on the evaluation indicators. In the vulnerability evaluation of hazard-bearing bodies, due to the difference in the importance of the selected evaluation factors, it is necessary to determine the weight. Entropy is a measure of uncertainty; the greater the amount of information, the smaller the uncertainty, and the smaller the entropy. Therefore, the information carried by the entropy value can be used for computing the weights for each factor, combined with the degree of variation of various indicators, and the tool of information entropy is used to calculate the weight of each indicator, which provides a basis for the comprehensive evaluation of multiple indicators. The weights established in this paper based on the entropy method are shown in Table 2.

Ecological vulnerability depends on four aspects: the exposure degree of the system, the sensitivity of the system to external interference, and the adaptability and recovery ability of the system. The degree of vulnerability represents the degree of vulnerability of each primary indicator. This paper divided the degree of vulnerability into three levels and used the median method and the average method to determine the grading standard of the comment set [39], that iss, the evaluation set V = {V1, V2, V3} = {Low Degree of vulnerability, moderate degree of vulnerability, high degree of vulnerability}. At the end of this paper, the evaluation matrix and the weight set were synthesized by matrix calculation. The value of the corresponding evaluation level of each primary indicator could be added to represent the comprehensive evaluation result of vulnerability.

3. Results

3.1. Analysis of Big Data Mining Results. Figure 3 reflected the restoration after typhoon Hato, as indicated by the change in search volume. Among the keywords, the search time span of five keywords and their synonyms, "power outage," "water outage," "tree," "injured," and "no signal," was long, and the data decreased with the passage of time. The

TABLE 2: Weight set of vulnerability assessment index system of socioecological systems under the influence of typhoon disaster in Zhuhai City.

Indicator	Weight
Land area	0.0844
Wind speed	0.1394
Population density	0.0792
Proportion of primary industry	0.1022
Proportion of tertiary industry	0.0615
Ecological index	0.0864
Regional GDP	0.0943
Per capita disposable income of urban residents	0.0654
General public service expenditure	0.0598
Medical and health institutions expenditure	0.0547
Electricity restoration speed	0.0662
Traffic restoration speed	0.0532
Telecom signal recovery speed	0.0532

FIGURE 3: Search volumes of Weibo keywords before and after typhoon Hato.

highest number of keywords posted on the day the typhoon landed in Zhuhai, August 23, 2017. Two days later, on August 25, the number of keywords posted dropped sharply and then showed a gentle downward trend over time. In the final data, the amount approaches zero. The search volume of "tree" and "injured" decreased rapidly on August 24, and then tended to zero on August 25 and August 26, respectively. Among the keywords related to the three vulnerability secondary indicators of "power outage", "water outage" and "outage of mobile phone signal," the search volume reached the smallest on August 27, August 26, and August 26, respectively. The release of keywords is closely related to the time of the typhoon and the disaster relief situation. Therefore, it can be explained that the recovery day of each system was the day when the search volume was the smallest in each district of Zhuhai City. According to the calculation, the recovery speed of power supply, water supply, and telecommunication signals were 0.2 day^{-1}, 0.25 day^{-1}, and 0.25 day^{-1}, respectively. This represents the rate of completion of the daily restoration of the city's power, hydraulic, and communication systems, which could be used to calculate the resilience of each district.

3.2. Analysis of Visualized Results of Urban Restoration. The release of all keywords peaked on the day of the typhoon landing and gradually decreased the next day. With the continuous development of postdisaster reconstruction, the locations of failures of power, hydraulic supply, and communication systems affected by the typhoon decreased. This chapter would explore the restoration of power, hydraulic supply, and communication systems under the influence of typhoon Hato. Figure 4 reflected the repair of the power system after Hato, as indicated by the change in search volume. On the day of Hato landing, a large number of power supply failures occurred in three districts of Zhuhai City, most of which were located within the construction land. Xiangzhou district is the city center of Zhuhai city, which has a large number of commercial land and residential areas with a high
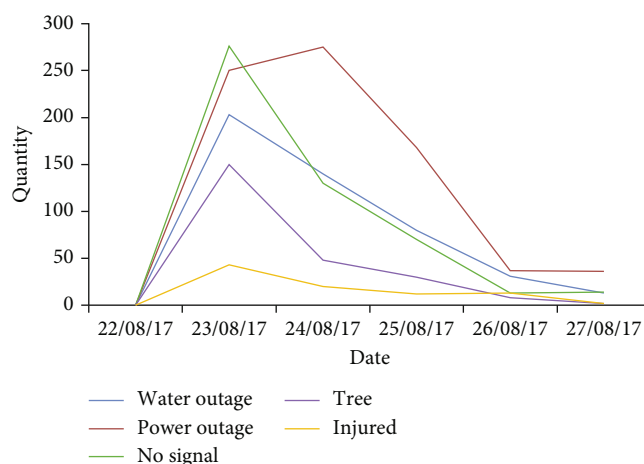
population density. Therefore, on August 23, the fault spots were concentrated in the city center, including Tangjiawan Town and Hengqin Island. By August 25, the power failure in the center of Zhuhai City was almost solved, but the power failure still existed in Tangjiawan Town and on Hengqin Island. By August 26, the power supply in Xiangzhou district was almost back to normal. The power outages in Doumen district affected mostly residential areas, such as Jingan Town and Doumen Town. As rescue and relief work continued, only sporadic areas in Doumen district were left with power supply problems on August 26. The power failure in Jinwan district was the most serious with a large number of occurrences in the whole area. As of August 27, the power supply system of coastal Sanzao Town and Nanshai Town, which were most seriously affected by the typhoon, has not been fully restored.

The repair of the hydraulic system after typhoon Hato, was shown by the change in search volume (Figure 5). On the day the typhoon landed, a large number of water supply faults occurred in the three districts of Zhuhai, most of which were located near the main roads and within the construction land. In Xiangzhou district on August 23, the breakdown points were concentrated in the city center, in Tangjiawan Town and on Hengqin Island. By August 24, the water supply had improved in the city center, but there was still a lack of water near the S32 provincial road and on Hengqin Island. By August 25, the water supply in Xiangzhou district was almost back to normal. However, water supply of Doumen district had almost cut off in residential areas and on main roads, such as Qianwu Town and the provincial road S32. With the rescue and relief work underway, only a few water supply faults remained in Doumen district near the main road by August 25. Water supply cutoff in Jinwan district was the most serious, which occurs on a large scale in the whole region. As of August 27, there were still hydraulic faults in the whole Jinwan district.

The repair of the communication system after typhoon Hato, was indicated by the change in search volume (see Figure 6). On the day of typhoon landing, a large number of communication faults occurred in three districts of
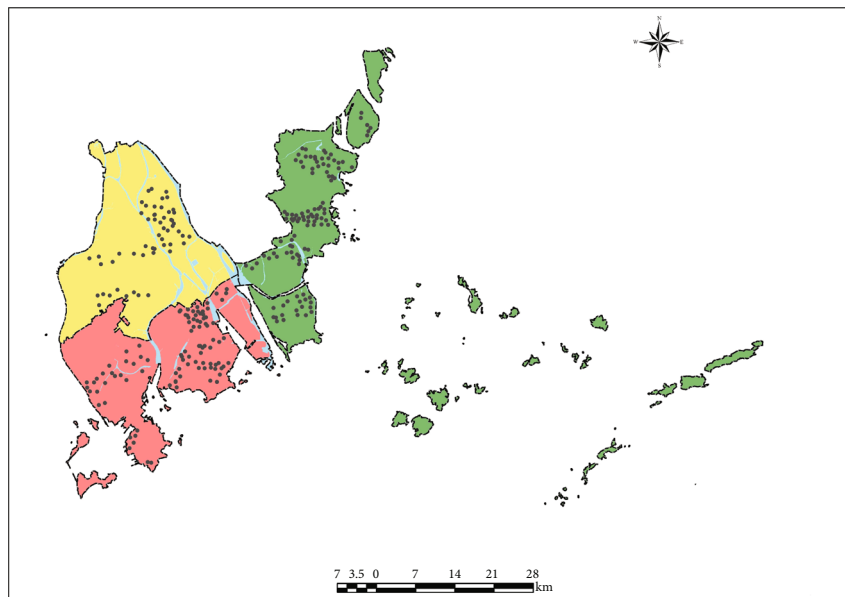
(a) August 23, 2017
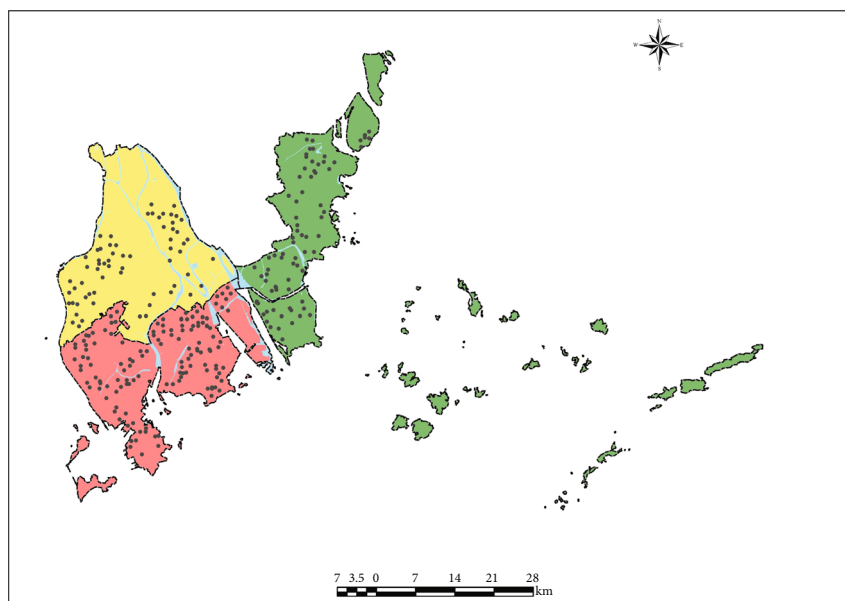
(b) August 24, 2017
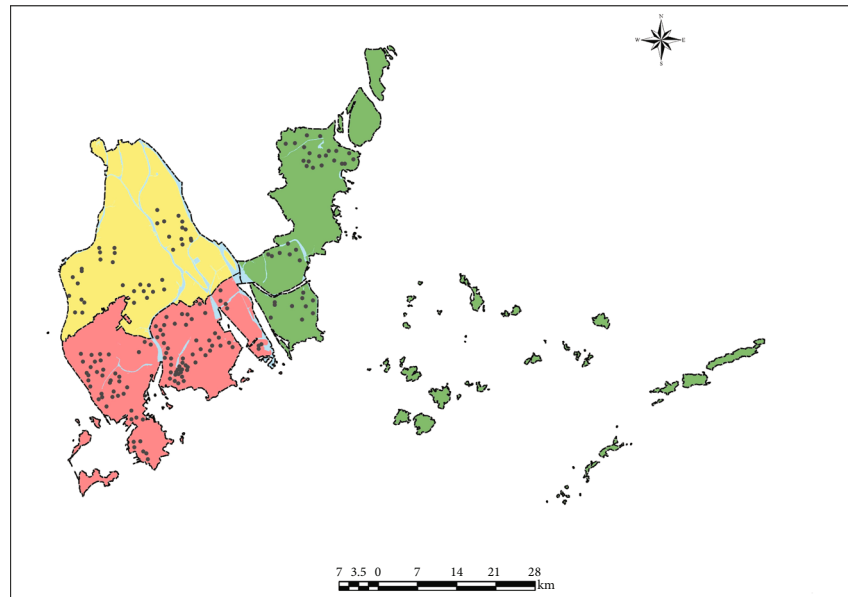
FIGURE 4: Continued.

Legend

● Power outage   ▮ Jinwan
---- County   ▮ Xiangzhou
-·-· City   ▮ River network
▮ Doumen

(c) August 25, 2017

Legend

● Power outage   ▮ Jinwan
---- County   ▮ Xiangzhou
-·-· City   ▮ River network
▮ Doumen
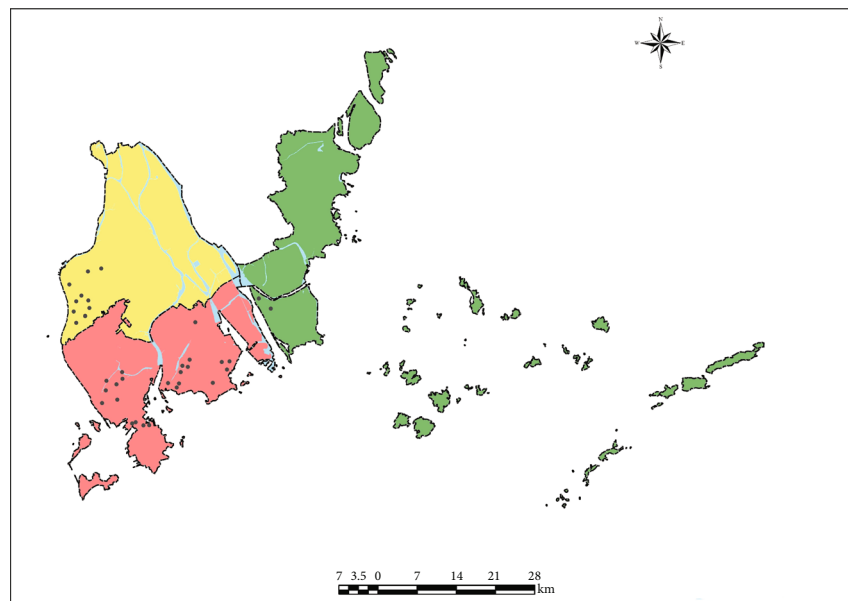
(d) August 26, 2017

FIGURE 4: Continued.

Legend

● Power outage | Jinwan
--- County | Xiangzhou
--- City | River network
Doumen
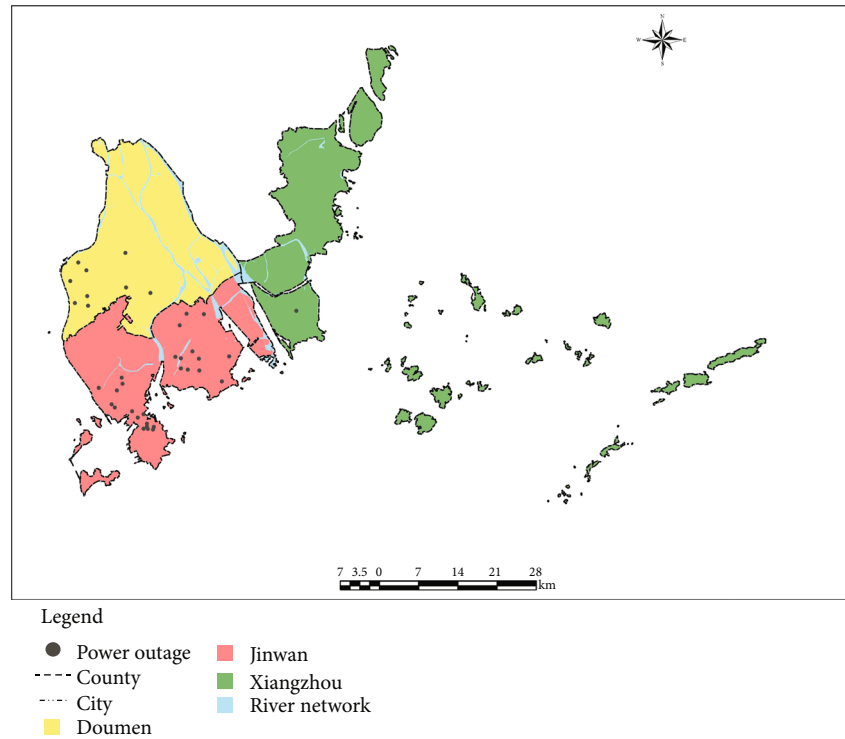
(e) August 27, 2017

Figure 4: The repair of power system after typhoon Hato.

Zhuhai City, and the fault points covered almost the whole city. In Xiangzhou district on August 23, the breakdown points were concentrated in densely populated commercial service center and residential areas, such as the city center, Tangjiawan Town, and Hengqin Island. By August 24, Tangjiawan Town was almost back to normal, but there were still a few communication problems in the city center and on Hengqin Island. By August 25, the communication system in Xiangzhou district was almost back to normal. The areas without signal in Doumen district were mostly residential areas, such as Qianwu Town, Doumen Town, and Jingan Town. As rescue and relief work began, only a few communication failures remained in the vicinity of Jingan Town on August 25. The communication failure was the most serious in Jinwan district, where it occurred in large numbers throughout the whole area. By August 27, the communication system had been mostly restored in the Jinwan district.

The spatial differences in the number of keywords posted effectively reveals the resilience of each district after the disaster. On August 23, the number of keywords in Jinwan district was greater than in both Doumen district and Xiangzhou district, and the number of keywords in Xiangzhou district was greater than in Doumen district. In the early days of the typhoon landing, Xiangzhou district was densely populated and had many Weibo users, making it more sensitive than other districts with a small population density. Therefore, the number of people affected was large, and correspondingly the number of keywords posted was also large.

In the postdisaster reconstruction stage, the number of keywords posted in Xiangzhou district and Doumen district dropped significantly, reflecting its stronger resilience. Jinwan district did not show a significant drop in the amount of data released for the keywords "power outage" and "water outage," indicating that its power system was weak in resilience and that the reconstruction after the disaster was not satisfactory. According to the changes in the search volume of the three keywords of "power outage," "water outage," and "no signal," the Xiangzhou and Doumen districts had basically resumed water supply and telecommunications signals on August 25. The water supply interruption in Jinwan district was still serious, and there were still many places where the water supply had not been restored. Compared with the restoration of the hydraulic system and the communication system, it was found that the power system was more affected and its restoration was slower than that of the other two supply systems. The power system in all districts was basically restored on August 27. It can be seen the resilience of hydropower and communication systems in Xiangzhou and Doumen districts after the disaster was significantly stronger than that in Jinwan district.

3.3. Analysis of Comprehensive Vulnerability Assessment Results of Typhoon Hato. After mining the big data of Weibo with keywords, the data of the resilience index of each district in Zhuhai was obtained, and a comprehensive vulnerability index data set was established for fuzzy comprehensive evaluation. The evaluation results are shown in Table 3.
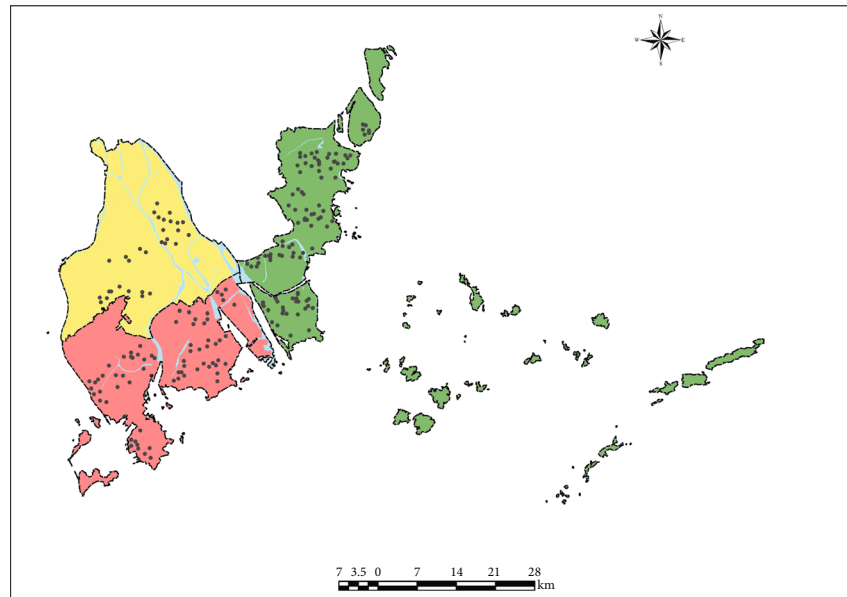
Legend

● Water outage
---- County
-·-· City
■ Doumen

■ Jinwan
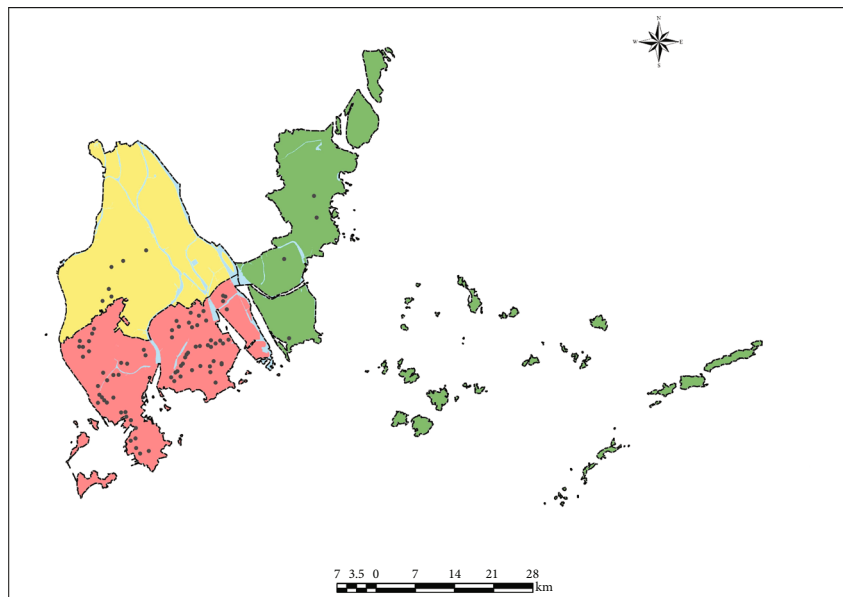■ Xiangzhou
■ River network

(a) August 23, 2017
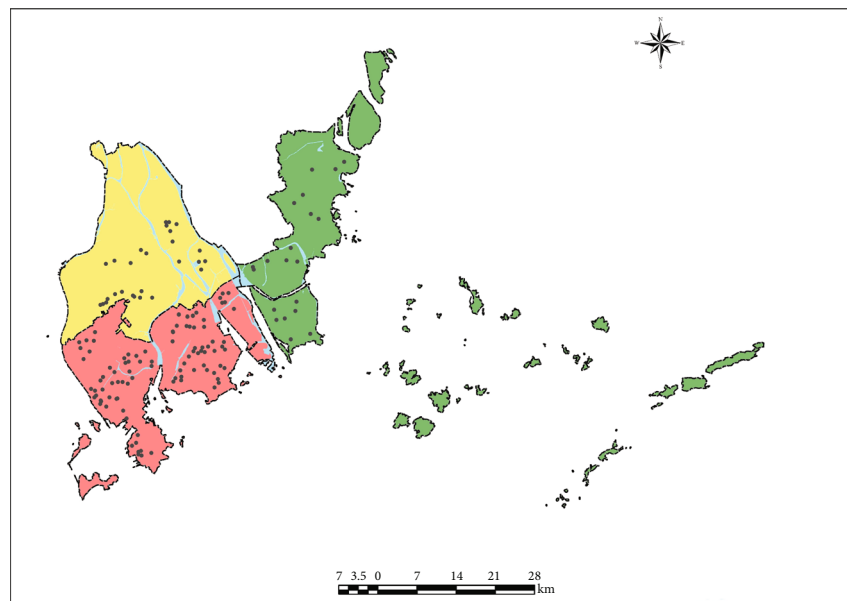
Legend

● Water outage
---- County
-·-· City
■ Doumen

■ Jinwan
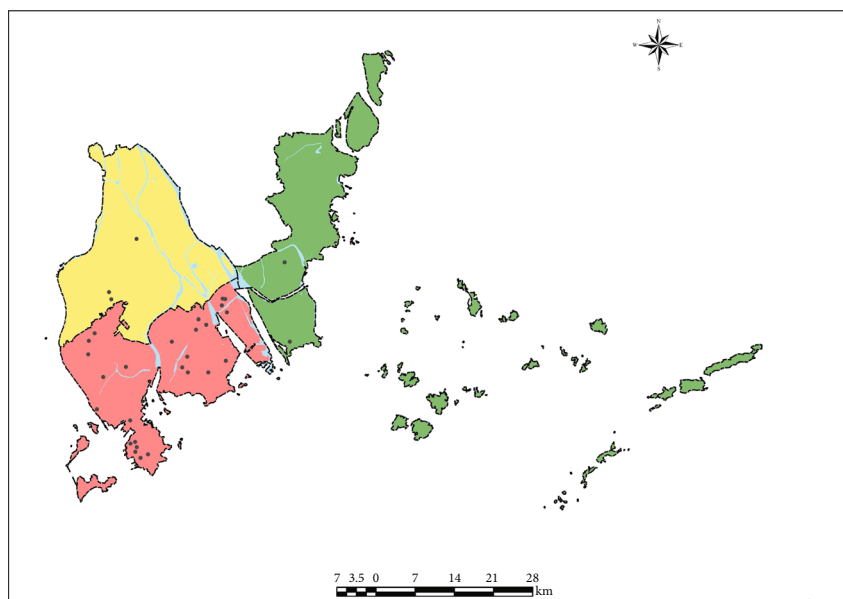■ Xiangzhou
■ River network

(b) August 24, 2017

Figure 5: Continued.

Legend

● Water outage
---- County
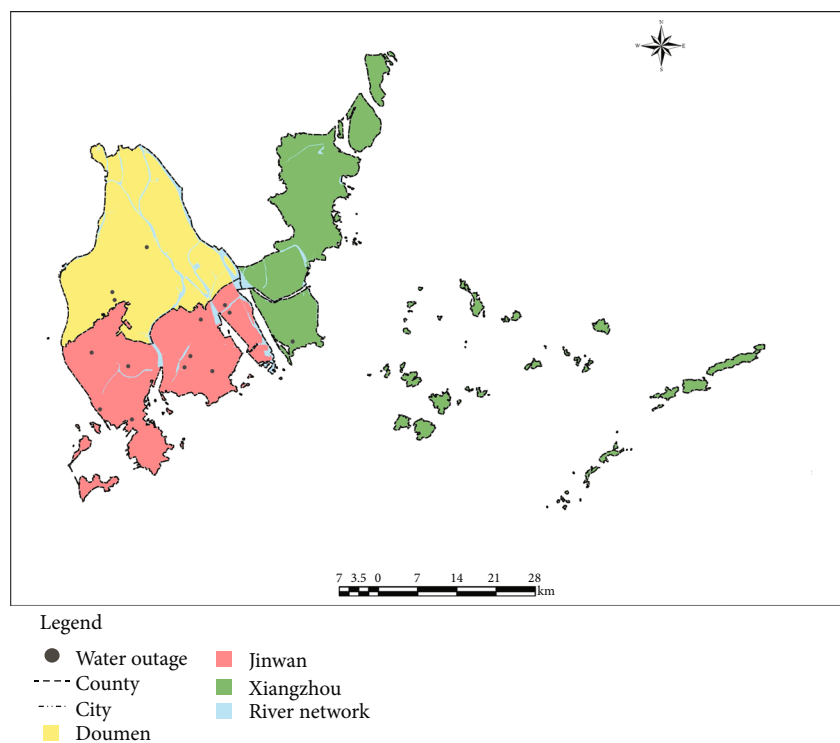-·- City
▮ Doumen
▮ Jinwan
▮ Xiangzhou
▮ River network

(c) August 25, 2017

Legend

● Water outage
---- County
-·- City
▮ Doumen
▮ Jinwan
▮ Xiangzhou
▮ River network

(d) August 26, 2017

FIGURE 5: Continued.

Legend

- ● Water outage
- --- County
- --- City
- ▮ Doumen
- ▮ Jinwan
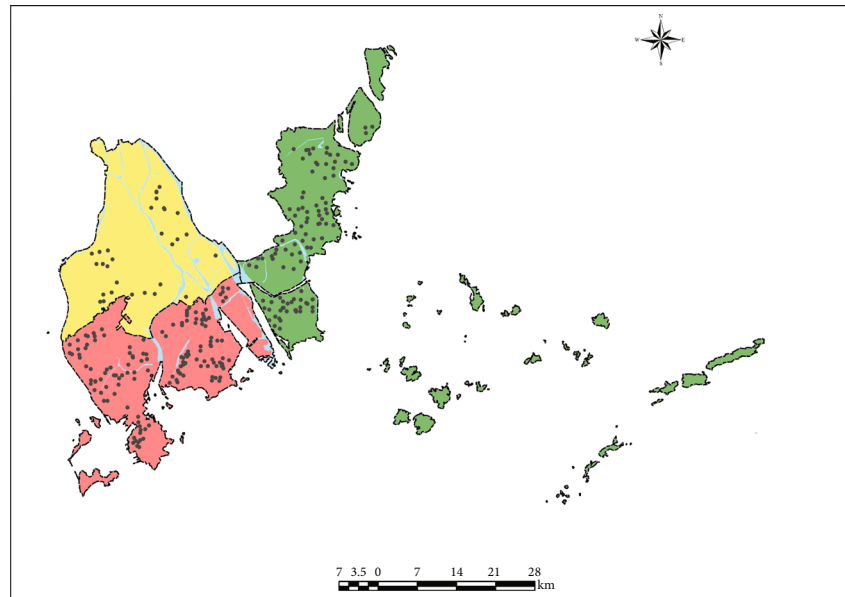- ▮ Xiangzhou
- ▮ River network

(e) August 27, 2017

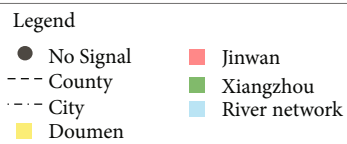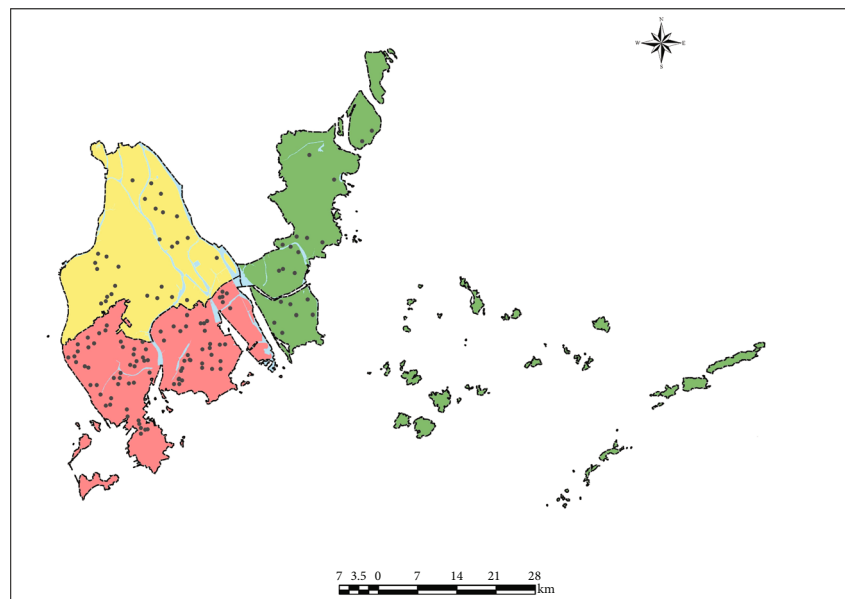FIGURE 5: The repair of the hydraulic system after typhoon Hato.

The vulnerabilities of three districts to typhoon Hato showed obvious regional differences. The overall result of vulnerability in Xiangzhou district and Doumen district was weaker, while that in Jinwan district was stronger. From the perspective of the primary indicators that affected vulnerability, the high ecological index and the low proportion of primary industry were the main reasons for the low vulnerability of the sensitivity index. The long failure time of the power supply system and the high wind speed were the indicators of resilience and exposure. The value of the rating results of exposure and response occupied two of the largest proportions in the comprehensive evaluation, which intuitively showed that the dominant factor for the different vulnerabilities of districts was the difference in coping ability and the geographical location of each districts. The general public service expenditure and per capital disposable income of Xiangzhou district and Doumen district were significantly higher than that of Jinwan district. The economy of Xiangzhou district and Doumen district were more developed, and public service investment was higher, so the response was relatively strong. Moreover, the typhoon made landfall in Jinwan district, and because Doumen district is located in the northern part of Jinwan district, Jinwan district was more affected by the typhoon. However, since the recovery speed was evaluated in several days, the differences in the results of recovery were not obvious, so further discussion and analysis should be combined with the search results of keywords.

4. Discussion

Usually, Guangdong is the province with the earliest typhoon landing time in the country and the longest typhoon impact (Local History Compilation Committee of Guangdong Province, 2001), and it had a large and rapidly developing national economy; the losses suffered were often serious. It was very important to evaluate the vulnerability of cities in Guangdong Province, which could reduce the search time in the early stage of rescue and relief work and improve the efficiency of disaster relief. By taking advantage of the immediacy, accuracy, and many users of big data, postdisaster assessment could be carried out quickly and accurately to solve the problems of inefficiency and inaccuracy in traditional assessment methods. The destruction of hydropower systems and communication systems was the most direct and obvious impact of the typhoon on the lives of people affected by the disaster. With the keyword information obtained by the comprehensive big data platform, it was clear that the public paid much more attention to water supply, power supply, and telecommunications signals than to other aspects, so the data information of hydropower and signal recovery is relatively accurate. With the help of big data, the destruction and recovery process of the hydropower system were displayed in the form of Weibo data, and its application to vulnerability assessment was beneficial to the recovery of the hydropower system. The positioning information obtained by the big data platform could clearly
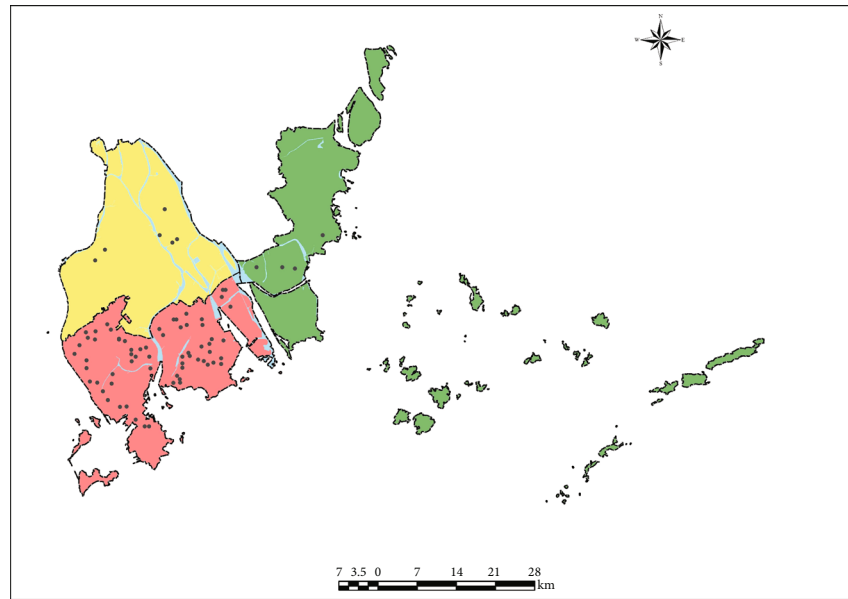
Legend

● No signal   ■ Jinwan
--- County   ■ Xiangzhou
-·- City   ■ River network
■ Doumen

(a) August 23, 2017

Legend

● No Signal   ■ Jinwan
--- County   ■ Xiangzhou
-·- City   ■ River network
■ Doumen

(b) August 24, 2017

Figure 6: Continued.

(c) August 25, 2017
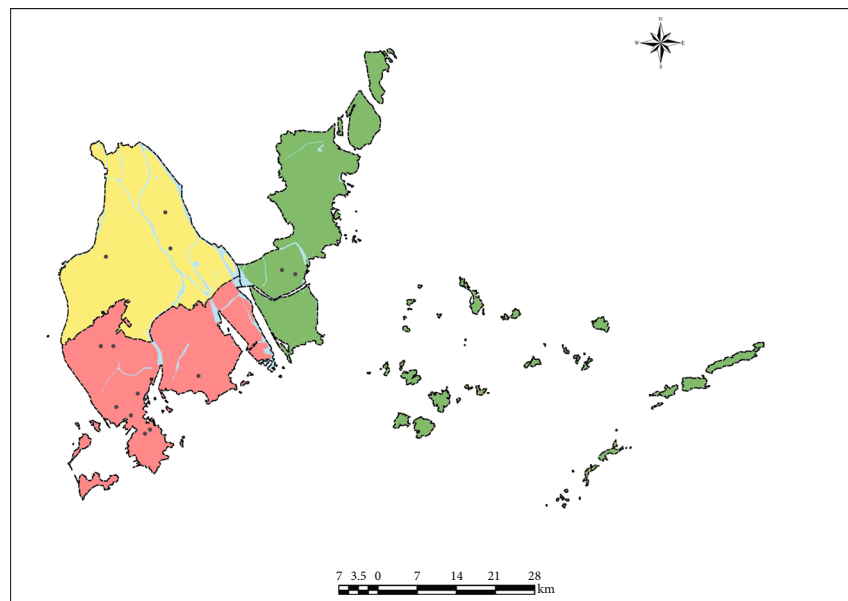
(d) August 26, 2017

FIGURE 6: Continued.
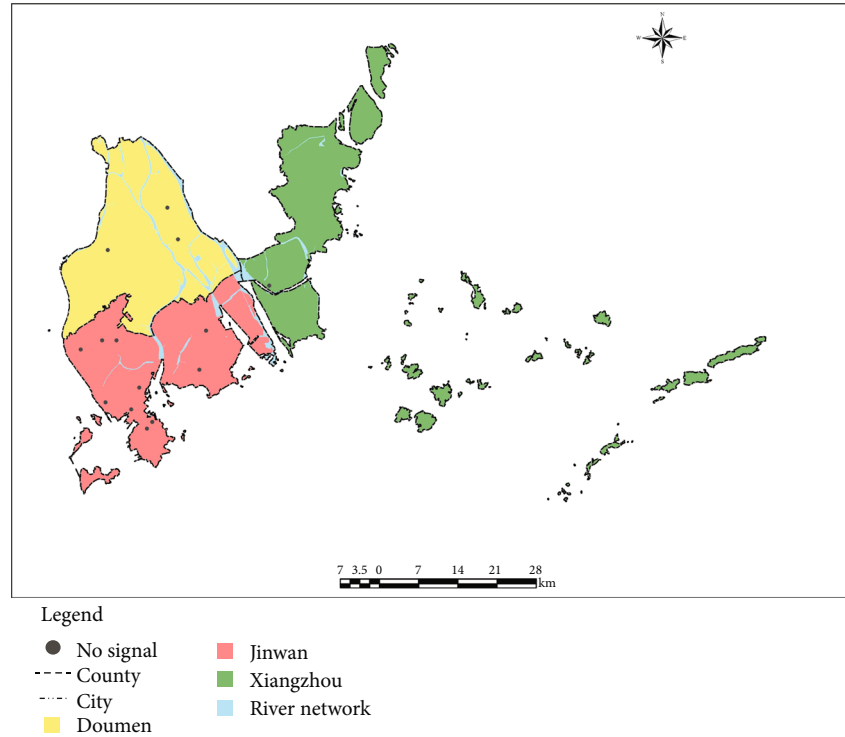
(e) August 27, 2017

FIGURE 6: The repair of the communication system after typhoon Hato.

TABLE 3: Results of socioecological systems vulnerability evaluation in Zhuhai City.

Area (districts)	Low vulnerability level V1	Medium vulnerability level V2	High vulnerability level V3	Rating level
Xiangzhou	0.7994	0.0598	0.1407	Low
Doumen	0.3603	0.3587	0.2809	Medium
Jinwan	0.1407	0.3809	0.4783	High

show the dynamic changes of hydropower recovery, realize the visualization of the disaster recovery capabilities of different locations, and more quickly and more accurately investigate the hydropower system in the disaster-stricken area, which was helpful in guiding the postdisaster recovery work. Due to the particularity of the data source of the resilience index of this study, the accuracy of the results could reach the street level in terms of geographic location. For postdisaster recovery, a relatively refined assessment could be carried out for each district.

At present, the comprehensive risk assessment of typhoon is based on the weighted index method of index system, which evaluates the risk zoning of typhoon hazard formative factors, sensitivity of inducing environment, vulnerability of hazard bearing body, and capacity of prevent disaster, respectively, and then combines the evaluation results of the three aspects. For example, Wang et al. analyzed the typhoon disaster risk in Anhui Province, China [40]. This method paid more attention to the natural condi-

tions of study area and lists the elevation, topographic relief, river network density, and its buffer area as indicators. Gao et al. analyzed the typhoon disaster risk in Zhuhai City, Guangdong Province, China [35]; evaluated the resilience, potential strength, and sensitivity of the typhoon, respectively; and then combined the evaluation results of the three aspects. The results of this study showed that Xiangzhou district was the strongest ecological vulnerability in Zhuhai, Doumen district was the second, and Jinwan district was the weakest, which were quite different from the results of our study, probably because the research objectives and indicators between the two studies were different. The disadvantage of the method of Gao et al. is the incompleteness of index selection. It ignored the government's response to disasters and underestimates the resilience of typhoons. The big data mining data used in this study overcame this shortcoming, because the recovery speed of the three systems reflected the efforts of the district governments for urban recovery. The government's response also reduced the harm of the typhoon to residents as much as possible, so as to improve the resilience of each district. Therefore, the system could more effectively and accurately assess the ecological vulnerability in the region. This advantage can also provide more targeted reference opinions for disaster recovery and more accurate early warning of potential urban, social, and ecological risk and even provide suggestions for urban planning.

In addition, the comprehensive evaluation results reflect the differences in small-scale vulnerabilities within cities. The overall vulnerability of Zhuhai City Centre (Xiangzhou

district) is lower than that of Jinwan district and Doumen district. This is the result of the combined effects of the three systems of society, economy, and ecology. Ecological and economic systems work together on sensitivity. The lower the ecological index, the greater the proportion of primary and tertiary industries, the higher the sensitivity, and the greater the overall vulnerability. At the same time, the economic system also plays a role in response capacity. The more developed the economy, the better the infrastructure construction, the more the government spends on people's livelihood expenditures, and the greater the response capacity, the smaller the overall vulnerability. In addition, the social system acts on resilience. The faster the recovery after a disaster, the stronger the resilience, and the smaller the overall vulnerability. According to the evaluation results, economic indicators play a greater role in response than in sensitivity, while ecological indicators have a smaller impact on overall vulnerability than other socioeconomic indicators. Therefore, socioeconomic indicators are the dominant factor affecting overall vulnerability. Since Xiangzhou district was superior to Doumen district and Jinwan district in terms of percentage of primary and tertiary industries, infrastructure construction, and postdisaster recovery speed, the vulnerability of Xiangzhou district was lower than that of other two districts.

This study mainly researched the impact of typhoons on urban socioecological vulnerability and lacks connection with government emergency work. The research methods in this article can be further combined with the government's emergency work, thereby improving the efficiency of responding to disasters. There are still many aspects to be improved. For example, the research methods are how to strengthen communication with the government, how to improve the accuracy and effectiveness of relevant data, and how to intensify the availability of data. These are the problems that need to be solved in further research.

5. Conclusions

This study, based on the statistical data and the recovery speed of power, hydraulic, and communication systems collected by big data, constructs an ecological vulnerability evaluation system including exposure, resilience, response, and sensitivity. The system can quickly show the disaster situation, realize the visualization of disaster situation, and more effectively show the ecological vulnerability in the study area. This paper, taken the severely hit Zhuhai city under the background of typhoon Hato as the research object, uses big data mining technology to track the disaster, establish a vulnerability assessment model to analyze the vulnerability characteristics and reasons of urban social ecosystems under typhoon disasters, and obtain the following main conclusions. China is one of the countries most affected by typhoon disasters; typhoon Hato had a serious impact on Zhuhai, wreaking damage on the entire social, economic, and ecological system. On the basis of ecological vulnerability assessment model for typhoon disaster established by this research, our results showed the areas with the highest postdisaster vulnerability, such as Jinwan district,

followed by Doumen and Xiangzhou districts. The response was the decisive factor leading to the significant differences in the vulnerability of typhoon disasters in each district. The areas with the lowest postdisaster vulnerability, such as Xiangzhou district, has a developed economy, higher regional GDP, more social security investment, and the strongest disaster response capacity. The hydropower and communication systems in Xiangzhou district and Doumen district recovered quickly. However, the recovery of hydropower in Jinwan district was relatively slow, and the ability there to withstand disasters needs to be enhanced.

Data Availability

The data are available upon request.

Conflicts of Interest

The authors declare that there is no conflict of interest regarding the publication of this paper.

Acknowledgments

References

[1] S. Schmidt, C. Kemfert, and P. Hoppe, "The impact of socio-economics and climate change on tropical cyclone losses in the USA," *Regional Environment Change*, vol. 10, no. 1, pp. 13–26, 2010.

[2] J. Ou, Z. Duan, and L. Chang, "Typhoon hazard analysis of key cities along the southeast coast of China," *Journal of Natural Disaster*, vol. 11, no. 4, pp. 9–17, 2002.

[3] W. Gray, "Summary of the eighth IMO lecture to be presented at twelfth congress (may/June, 1995)," *World Meteorological Organization Bulletin*, vol. 44, no. 2, pp. 115–118, 1995.

[4] F. Xiao and Z. Xiao, "Characteristics of tropical cyclones in China and their impacts analysis," *Natural Hazards*, vol. 54, no. 3, pp. 827–837, 2010.

[5] S. Raghavan and S. Rajesh, "Trends in tropical cyclone impact: a study in Andhra Pradesh, India," *Bulletin of the American Meteorological Society*, vol. 84, no. 5, pp. 635–644, 2003.

[6] Ippc, *Managing the Risks of Extreme Events and Disasters to Advance Climate Change Adaptation. A Special Report of the Intergovernmental Panel on Climate Change*, Cambridge University, Cambridge, UK, and New York, NY, USA, 2012.

[7] G. Walker, "Modelling the vulnerability of buildings to wind-a review," *Canadian Journal of Civil Engineering*, vol. 38, no. 9, pp. 1031–1039, 2011.

[8] K. Chen, "Disaster modeling and its major foreign developers," *Journal of Natural Disaster Science*, vol. 13, no. 2, pp. 1–8, 2004.

[9] W. Fang and X. Shi, "Summary of stochastic simulation of tropical cyclone path and intensity for disaster risk assessment," *Advances in Earth Sciences*, vol. 27, no. 8, pp. 866–875, 2012.

[10] W. Fang and W. Lin, "A review of research on typhoon wind field models for disaster risk assessment," *Advances in Geographical Sciences*, vol. 32, no. 6, pp. 852–867, 2013.

[11] G. Pita, J. Pinelli, and K. Gurley, "State of the art of hurricane vulnerability estimation methods: a review," *Natural Hazards Review*, vol. 16, no. 2, pp. 0401–4022, 2014.

[12] Z. Yin, *Urban Natural Disaster Risk Assessment and Empirical Research*, Shanghai: East China Normal University, 2009.

[13] C. Xie, *Typhoon Storm Surge Disaster Scenario Simulation and Risk Assessment in the Coastal Areas of Shanghai*, Shanghai: East China Normal University, 2010.

[14] Y. Zhang and H. Wang, "Review of risk assessment of typhoon storm surge disaster," *Marine Forecasts*, vol. 33, no. 2, pp. 81–88, 2016.

[15] R. Wang F. Lian et al., "Global typhoon disaster chain classification and regional characteristics analysis based on disaster pregnant environment," *Geographical Research*, vol. 35, no. 5, pp. 836–850, 2016.

[16] Y. Shi, S. Xu, and C. Shi, "Research progress on flood disaster vulnerability," *Advances in Geographical Sciences*, vol. 28, no. 1, pp. 41–46, 2009.

[17] J. Birkmann, *Measuring Vulnerability to Natural Hazards-Towards Disaster Resilient Societies*, UNU, New York, 2006.

[18] Y. Zhou and J. Wang, "Research progress on vulnerability curves of natural disasters," *Advances in Earth Science Exhibition*, vol. 27, no. 4, pp. 435–442, 2012.

[19] Z. Yin, S. Xu, and J. Yin, "Small-scale urban rainstorm and waterlogging disaster scenario simulation and risk assessment," *Acta Geographica Sinica*, vol. 65, no. 5, pp. 553–562, 2010.

[20] S. Maiti, S. Jha, S. Garai et al., "An assessment of social vulnerability to climate change among the districts of Arunachal Pradesh, India," *Ecological Indicators*, vol. 77, pp. 105–113, 2017.

[21] W. Lin and W. Fang, "Research on the regional characteristics of Holland B coefficient in the Northwest Pacific typhoon wind field model," *Tropical Geography*, vol. 33, no. 2, pp. 124–132, 2013.

[22] T. Li, P. Niu, and C. Gu, "Review of elastic city research framework," *Journal of urban planning*, vol. 5, pp. 23–31, 2014.

[23] J. Chambers, J. Fisher, H. Zeng, E. L. Chapman, D. B. Baker, and G. C. Hurtt, "Hurricane Katrina's carbon footprint on U.S. gulf coast forests," *Science*, vol. 318, no. 5853, pp. 1107–1107, 2007.

[24] M. Meekan, C. Duarte, J. Fernández-Gracia et al., "The Ecology of Human Mobility," *Trends in Ecology and Evolution*, vol. 32, no. 3, pp. 198–210, 2017.

[25] T. Lin, X. Liu, J. Song et al., "Urban waterlogging risk assessment based on internet open data: A case study in China," *Habitat International*, vol. 71, pp. 88–96, 2018.

[26] J. Ning and National Bureau of Statistics, *The main data of the seventh national census*, 2020, http://www.stats.gov.cn/tjsj/zxfb/202105/t20210510_1817176.html.

[27] Anonymous, "Typhoon Hato," *Cities and Disaster Reduction*, vol. 5, pp. 2-3, 2017.

[28] P. Net, *Typhoon Hato hits Macau severely, SAR government recommends multiple measures to rescue*, Last modified, 2017, http://env.people.com.cn/n1/2017/0825/c1010-29493720.html.

[29] L. Xinzhu, *National Meteorological Center of CMA, Typhoon Committee*, Typhoon Yearbook Report Column, 2017.

[30] "Typhoon CommitteeTyphoon committee 50th Annual Meeting," 2018.

[31] C. Shan, "Response and Enlightenment of typhoon Hato," *Labor Protection*, vol. 9, p. 4, 2019.

[32] K. Chen, D. Lan, W. Ke et al., "Research and implementation of Sina Weibo crawler based on Java," *Computer Technology and Development*, vol. 27, no. 9, pp. 191–196, 2017.

[33] M. Sajjad, Y. Li, Z. Tang, L. Cao, and X. Liu, "Assessing Hazard Vulnerability, Habitat Conservation, and Restoration for the Enhancement of Mainland China's Coastal Resilience," *Earth's Future*, vol. 6, no. 3, pp. 326–338, 2018.

[34] W. Wu J. Chen et al., "Vulnerability assessment of urban socio-ecological systems in coastal zones under the influence of typhoons: big data perspective," *Acta Ecologica Sinica*, vol. 39, no. 19, pp. 7079–7086, 2019.

[35] Z. Gao, R. Wan, Q. Ye et al., "Typhoon Disaster Risk Assessment Based on Emergy Theory: A Case Study of Zhuhai City, Guangdong Province, China," *Sustainability*, vol. 12, article 4212, 2020.

[36] S. Prybutok, G. Newman, K. Atoba, G. Sansom, and Z. Tao, "Combining co$ting nature and suitability modeling to identify high flood risk areas in need of nature-based services," *Land*, vol. 10, no. 8, p. article 853, 2021.

[37] J. Gu, *Dictionary of Atmospheric Sciences*, Meteorological Press, Beijing, 1994.

[38] Z. Meng, W. Zhang, and Y. Meng, "Comprehensive evaluation of environmental quality by fuzzy mathematics," *Environmental Protection*, vol. 8, pp. 28-29, 1993.

[39] J. Du, F. He, and P. Shi, "Comprehensive risk assessment of flood disasters in the Xiangjiang River basin," *Journal of Natural Disasters*, vol. 15, no. 6, pp. 38–44, 2006.

[40] S. Wang, H. Tian, and W. Xie, "GIS-based risk evaluation and zoning of typhoon disaster: a case study of Anhui province," *Journal of China Agricultural University*, vol. 17, no. 1, pp. 161–166, 2012.